The background of the cover is a photograph of a space shuttle launch. The shuttle is on the left, angled upwards, with its three main engines and boosters visible. A large, bright plume of white and orange smoke and fire trails behind it, filling the right and bottom portions of the frame. The overall color palette is dominated by the white and orange of the exhaust, with some dark grey and black from the shuttle's structure.

Digital Control of Dynamic Systems

THIRD EDITION

Gene F. Franklin

J. David Powell

Michael Workman

Ellis-Kagle Press eEdition-2

From the Back Cover (with updates for the eEdition-2)

This well-respected, market-leading text discusses the use of digital computers in the real-time control of dynamic systems. The emphasis is on the design of digital controls that achieve good dynamic response and small errors while using signals that are sampled in time and quantized in amplitude. Both transform-based and state-based classical and modern control methods are described and applied to illustrative examples. The strengths and limitations of each method are explored to help the reader develop solid designs with the least effort.

The third edition includes two chapters which offer a review of feedback control systems and an overview of digital control. The eEdition-2 version is the same, except the composition has been compressed in order to improve the quality of the typesetting, save pages, and reduce the memory storage required. Although the page numbering is now revised, the Table of Contents and the Index have been revised in order to reflect the correct pages.

MATLAB is thoroughly integrated throughout the text, in exposition and in problems, to offer readers a complete design picture. The 3rd e-Edition-2 has been updated to be fully compatible with current MATLAB versions as of 2022 and includes twice as many end-of-chapter problems as the previous 2nd print edition.

Gene F. Franklin was Professor Emeritus of Electrical Engineering at Stanford University where he served as Vice Chairman and Acting Chair of the department. In addition to directing research in feedback control, he has served as a consultant to several computer manufacturers on digital control of position mechanisms. He was a life Fellow of IEEE and delivered the IEEE Bode Lecture for 1994. He has been recognized for his work in the classroom with the American Automatic Control Council's Education Award. Sadly, he passed away in August, 2012.

J. David Powell is Professor(Emeritus), of Aeronautics and Astronautics and Mechanical Engineering at Stanford University. Professor Powell's most recent research focused on the use of GPS for air and ground navigation. In addition, he served as a consultant to the automotive industry, heavy equipment manufacturers, and aerospace companies on a wide range of controls problems . He is a Fellow of the AIAA and ASME.

Michael L. Workman was Vice President of Development Server/Subsystem Products for IBM's Storage Products Company. He was responsible for the worldwide development, launch, and support of SSD Hard Disk Drives for Server Product Families development. He then became the CEO of Pillar Data Systems, which became part of the Oracle Corporation. Mike recently retired from Oracle.

Also by **Gene Franklin** and **Dave Powell** (with **Abbas Emami-Naeini**),
Feedback Control of Dynamics Systems, Eighth Edition (2019), Pearson Education, Inc.

THIRD EDITION

Digital Control of Dynamic Systems

Gene F. Franklin
Stanford University

J. David Powell
Stanford University

Michael L. Workman
Oracle Corporation


Ellis-Kagle Press
Half Moon Bay, CA

ISBN-10: 0-9791226-3-5
ISBN-13: 978-0-9791226-3-7

Copyright ©1998, Franklin, Powell, and Workman

All rights reserved. This eEdition can not be sold to others in a print or electronic edition without permission from Ellis-Kagle Press. Translation in any language is prohibited without the permission of the copyright holders.

Printed in the United States of America

Library of Congress Cataloging-in-Publication Data

Franklin, Gene F,

Digital control of dynamic systems / Gene F. Franklin,
J. David Powell, Michael L. Workman, - 3rd ed.

p. cm.

Includes index.

1. Digital control systems, I. Powell, J. David, II Workman, Michael L. III Title.

TJ223.M53F73 1997

629.89 dc21

97-35994

Instructional Material Disclaimer: The programs presented in this book have been included for their instructional value. They have been tested with care but are not guaranteed for any particular purpose. Neither the publisher nor the authors offer any guarantee or representations, nor do they accept any liabilities with respect to the programs.

MATLAB and Simulink are registered trademarks of the MathWorks, Inc., Natick, MA.

All other trademarks or product names are the property of the owners.

Revised composition by Michael Sinner in 2022 with corrections.

Ellis-Kagle Press

1200 Pilarcitos Ave.

Half Moon Bay, CA 94019

EllisKagle@gmail.com

www.elliskaglepress.com

Tribute to Gene Franklin

It is with great personal sadness that we report the passing of Prof. Gene Franklin on August 9, 2012. Gene was a mentor, teacher and advisor to us. We had many meetings as we collaborated on the writing and publication of this textbook's editions over 35 years, and every single one of those meetings was friendly and enjoyable. We each have expressed different viewpoints over the years on various topics, but we were always able to encompass the views into the book in a friendly and collaborative manner. We learned control along with humor from Gene in grad school classes, and we benefited from his mentoring: in one case as a new Assistant Professor, and in the other as a PhD advisee. Collectively, we have collaborated on research, created new courses and laboratories, and written two textbooks over a period of 40 years. Gene always had a smile with a twinkle in his eye and was a pleasure to work with. We have lost a dear friend and colleague. Gene was a true gentleman.

J.D.P.
M.W.

*To Gertrude, David, Carole,
Valerie, Daisy, Annika, Dave,
Patti, Lauren, Max,
and to the memory of Lorna*

Contents

Preface	x
1 Introduction	1
1.1 Problem Definition	1
1.2 Overview of Design Approach	4
1.3 Computer-Aided Design	5
1.4 Suggestions for Further Reading	5
1.5 Summary	6
1.6 Problems	6
2 Review of Continuous Control	8
2.1 Dynamic Response	8
2.1.1 Differential Equations	8
2.1.2 Laplace Transforms and Transfer Functions	9
2.1.3 Output Time Histories	10
2.1.4 The Final Value Theorem	11
2.1.5 Block Diagrams	11
2.1.6 Response versus Pole Locations	11
2.1.7 Time-Domain Specifications	15
2.2 Basic Properties of Feedback	16
2.2.1 Stability	17
2.2.2 Steady-State Errors	17
2.2.3 PID Control	18
2.3 Root Locus	18
2.3.1 Problem Definition	18
2.3.2 Root Locus Drawing Rules	19
2.3.3 Computer-Aided Loci	21
2.4 Frequency Response Design	23
2.4.1 Specifications	24
2.4.2 Bode Plot Techniques	24
2.4.3 Steady-State Errors	26
2.4.4 Stability Margins	27
2.4.5 Bode's Gain-Phase Relationship	28
2.4.6 Design	28
2.5 Compensation	31
2.6 State-Space Design	32
2.6.1 Control Law	33
2.6.2 Estimator Design	35
2.6.3 Compensation: Combined Control and Estimation	37
2.6.4 Reference Input	37
2.6.5 Integral Control	38
2.7 Summary	39

2.8	Problems	40
3	Introductory Digital Control	44
3.1	Digitization	44
3.2	Effect of Sampling	48
3.3	PID Control	49
3.4	Summary	52
3.5	Problems	53
4	Discrete Systems Analysis	56
4.1	Linear Difference Equations	56
4.2	The Discrete Transfer Function	60
4.2.1	The z -Transform	60
4.2.2	The Transfer Function	61
4.2.3	Block Diagrams and State-Variable Descriptions	63
4.2.4	Relation of Transfer Function to Pulse Response	68
4.2.5	External Stability	71
4.3	Discrete Models of Sampled-Data Systems	73
4.3.1	Using the z -Transform	73
4.3.2	*Continuous Time Delay	76
4.3.3	State-Space Form	78
4.3.4	*State-Space Models for Systems with Delay	84
4.3.5	*Numerical Considerations in Computing Φ and Γ	88
4.3.6	*Nonlinear Models	89
4.4	Signal Analysis and Dynamic Response	91
4.4.1	The Unit Pulse	92
4.4.2	The Unit Step	92
4.4.3	Exponential	93
4.4.4	General Sinusoid	93
4.4.5	Correspondence with Continuous Signals	96
4.4.6	Step Response	98
4.5	Frequency Response	102
4.5.1	*The Discrete Fourier Transform (DFT)	103
4.6	Properties of the z -Transform	105
4.6.1	Essential Properties	105
4.6.2	*Convergence of z -Transform	109
4.6.3	*Another Derivation of the Transfer Function	112
4.7	Summary	113
4.8	Problems	114
5	Sampled-Data Systems	119
5.1	Analysis of the Sample and Hold	120
5.2	Spectrum of a Sampled Signal	123
5.3	Data Extrapolation	126
5.4	Block-Diagram Analysis of Sampled-Data Systems	130
5.5	Calculating the System Output Between Samples: The Ripple	139
5.6	Summary	140
5.7	Problems	140
5.8	Appendix	144

6	Discrete Equivalents	146
6.1	Design of Discrete Equivalents via Numerical Integration	147
6.2	Zero-Pole Matching Equivalents	156
6.3	Hold Equivalents	157
6.3.1	Zero-Order Hold Equivalent	158
6.3.2	A Non-Causal First-Order-Hold Equivalent: The Triangle-Hold Equivalent	159
6.4	Summary	161
6.5	Problems	163
7	Design Using Transform Techniques	165
7.1	System Specifications	166
7.2	Design by Emulation	167
7.2.1	Discrete Equivalent Controllers	168
7.2.2	Evaluation of the Design	171
7.3	Direct Design by Root Locus in the z -Plane	174
7.3.1	z -Plane Specifications	174
7.3.2	The Discrete Root Locus	178
7.4	Frequency Response Methods	183
7.4.1	Nyquist Stability Criterion	186
7.4.2	Design Specifications in the Frequency Domain	190
7.4.3	Low Frequency Gains and Error Coefficients	204
7.4.4	Compensator Design	205
7.5	Direct Design Method of Ragazzini	208
7.6	Summary	212
7.7	Problems	212
8	Design Using State-Space Methods	221
8.1	Control Law Design	222
8.1.1	Pole Placement	223
8.1.2	Controllability	225
8.1.3	Pole Placement Using CACSD	225
8.2	Estimator Design	228
8.2.1	Prediction Estimators	228
8.2.2	Observability	231
8.2.3	Pole Placement Using CACSD	232
8.2.4	Current Estimators	232
8.2.5	Reduced-Order Estimators	235
8.3	Regulator Design: Combined Control Law and Estimator	238
8.3.1	The Separation Principle	238
8.3.2	Guidelines for Pole Placement	243
8.4	Introduction of the Reference Input	244
8.4.1	Reference Inputs for Full-State Feedback	244
8.4.2	Reference Inputs with Estimators: The State-Command Structure	247
8.4.3	Output Error Command	250
8.4.4	A Comparison of the Estimator Structure and Classical Methods	251
8.5	Integral Control and Disturbance Estimation	253
8.5.1	Integral Control by State Augmentation	254
8.5.2	Disturbance Estimation	256
8.6	Effect of Delays	265
8.6.1	Sensor Delays	265
8.6.2	Actuator Delays	268
8.7	*Controllability and Observability	271
8.8	Summary	275

8.9	Problems	276
9	Multivariable and Optimal Control	283
9.1	Decoupling	283
9.2	Time-Varying Optimal Control	286
9.3	LQR Steady-State Optimal Control	292
9.3.1	Reciprocal Root Properties	293
9.3.2	Symmetric Root Locus	294
9.3.3	Eigenvector Decomposition	296
9.3.4	Cost Equivalents	298
9.3.5	Emulation by Equivalent Cost	300
9.4	Optimal Estimation	301
9.4.1	Least-Squares Estimation	301
9.4.2	The Kalman Filter	306
9.4.3	Steady-State Optimal Estimation	309
9.4.4	Noise Matrices and Discrete Equivalents	311
9.5	Multivariable Control Design	313
9.5.1	Selection of Weighting Matrices \mathbf{Q}_1 and \mathbf{Q}_2	313
9.5.2	Pincer Procedure	314
9.5.3	Paper-Machine Design Example	315
9.5.4	Magnetic-Tape-Drive Design Example	318
9.6	Summary	329
9.7	Problems	329
10	Quantization Effects	333
10.1	Analysis of Round-Off Error	333
10.2	Effects of Parameter Round-Off	342
10.3	Limit Cycles and Dither	344
10.4	Summary	348
10.5	Problems	348
11	Sample Rate Selection	352
11.1	The Sampling Theorem's Limit	353
11.2	Time Response and Smoothness	353
11.3	Errors Due to Random Plant Disturbances	355
11.4	Sensitivity to Parameter Variations	360
11.5	Measurement Noise and Antialiasing Filters	364
11.6	Multirate Sampling	367
11.7	Summary	371
11.8	Problems	372
12	System Identification	374
12.1	Defining the Model Set for Linear Systems	375
12.2	Identification of Nonparametric Models	377
12.3	Models and Criteria for Parametric Identification	386
12.3.1	Parameter Selection	386
12.3.2	Error Definition	388
12.4	Deterministic Estimation	391
12.4.1	Least Squares	391
12.4.2	Recursive Least Squares	394
12.5	Stochastic Least Squares	397
12.6	Maximum Likelihood	405
12.7	Numerical Search for the Maximum-Likelihood Estimate	409
12.8	Subspace Identification Methods	415
12.9	Summary	420

12.10 Problems	421
13 Nonlinear Control	424
13.1 Analysis Techniques	425
13.1.1 Simulation	425
13.1.2 Linearization	428
13.1.3 Describing Functions	436
13.1.4 Equivalent Gains	447
13.1.5 Circle Criterion	451
13.1.6 Lyapunov's Second Method	453
13.2 Nonlinear Control Structures: Design	455
13.2.1 Large Signal Linearization: Inverse Nonlinearities	455
13.2.2 Time-Optimal Servomechanisms	469
13.2.3 Extended PTOS for Flexible Structures	478
13.2.4 Introduction to Adaptive Control	481
13.3 Design with Nonlinear Cost Functions	496
13.3.1 Random Neighborhood Search	496
13.4 Summary	502
13.5 Problems	502
14 Design of a Disk Drive Servo: A Case Study	508
14.1 Overview of Disk Drives	508
14.1.1 High Performance Disk Drive Servo Profile	510
14.1.2 The Disk-Drive Servo	511
14.2 Components and Models	513
14.2.1 Voice Coil Motors	513
14.2.2 Shorted Turn	514
14.2.3 Power Amplifier Saturation	516
14.2.4 Actuator and HDA Dynamics	516
14.2.5 Position Measurement Sensor	518
14.2.6 Runout	519
14.3 Design Specifications	521
14.3.1 Plant Parameters for Case Study Design	521
14.3.2 Goals and Objectives	521
14.4 Disk Servo Design	523
14.4.1 Design of the Linear Response	524
14.4.2 Design by Random Numerical Search	526
14.4.3 Time-Domain Response of XPTOS Structure	531
14.4.4 Implementation Considerations	533
14.5 Summary	535
14.6 Problems	535
Appendix A Examples	538
A.1 Single-Axis Satellite Attitude Control	538
A.2 A Servomechanism for Antenna Azimuth Control	540
A.3 Temperature Control of Fluid in a Tank	542
A.4 Control Through a Flexible Structure	546
A.5 Control of a Pressurized Flow Box	548
Appendix B Tables	549
B.1 Properties of z -Transforms	549
B.2 Table of z -Transforms	550

Appendix C A Few Results from Matrix Analysis	552
C.1 Determinants and the Matrix Inverse	552
C.2 Eigenvalues and Eigenvectors	553
C.3 Similarity Transformations	555
C.4 The Cayley-Hamilton Theorem	556
Appendix D Summary of Facts from the Theory of Probability and Stochastic Processes	558
D.1 Random Variables	558
D.2 Expectation	560
D.3 More Than One Random Variable	562
D.4 Stochastic Processes	563
References	567
Index of MATLAB Functions	574
Index	575

Preface

This book is about the use of digital computers in the real-time control of dynamic systems such as servomechanisms, chemical processes, and vehicles that move over water, land, air, or space. The material requires some understanding of the Laplace transform and assumes that the reader has studied linear feedback controls. The special topics of discrete and sampled-data system analysis are introduced, and considerable emphasis is given to the z -transform and the close connections between the z -transform and the Laplace transform.

The book's emphasis is on designing digital controls to achieve good dynamic response and small errors while using signals that are sampled in time and quantized in amplitude. Both transform (classical control) and state-space (modern control) methods are described and applied to illustrative examples. The transform methods emphasized are the root-locus method of Evans and frequency response. The root-locus method can be used virtually unchanged for the discrete case; however, Bode's frequency response methods require modification for use with discrete systems. The state-space methods developed are the technique of pole assignment augmented by an estimator (observer) and optimal quadratic-loss control. The optimal control problems use the steady-state constant-gain solution; the results of the separation theorem in the presence of noise are stated but not proved.

Each of these design methods—classical and modern alike—has advantages and disadvantages, strengths and limitations. It is our philosophy that a designer must understand all of them to develop a satisfactory design with the least effort.

Closely related to the mainstream of ideas for designing linear systems that result in satisfactory dynamic response are the issues of sample-rate selection, model identification, and consideration of nonlinear phenomena. Sample-rate selection is discussed in the context of evaluating the increase in a least-squares performance measure as the sample rate is reduced. The topic of model making is treated as measurement of frequency response, as well as least-squares parameter estimation. Finally, every designer should be aware that all models are nonlinear and be familiar with the concepts of the describing functions of nonlinear systems, methods of studying stability of nonlinear systems, and the basic concepts of nonlinear design.

Material that may be new to the student is the treatment of signals which are discrete in time and amplitude and which must coexist with those that are continuous in both dimensions. The philosophy of presentation is that new material should be closely related to material already familiar, and yet, by the end, indicate a direction toward wider horizons. This approach leads us, for example, to relate the z -transform to the Laplace transform and to describe the implications of poles and zeros in the z -plane to the known meanings attached to poles and zeros in the s -plane. Also, in developing the design methods, we relate the digital control design methods to those of continuous systems. For more sophisticated methods, we present the elementary parts of quadratic-loss Gaussian design with minimal proofs to give some idea of how this powerful method is used and to motivate further study of its theory.

The use of computer-aided design (CAD) is universal for practicing engineers in this field, as in most other fields. We have recognized this fact and provided guidance to the reader so that learning the controls analysis material can be integrated with learning how to compute the answers with MATLAB, the most widely used CAD software package in universities. In many cases, especially in the earlier chapters, actual MATLAB scripts are included in the text to explain how to carry out a calculation. In other cases, the MATLAB routine is simply named for reference. All the routines given are tabulated in Appendix E for easy reference; therefore, this book can be used as a reference

for learning how to use MATLAB in control calculations as well as for control systems analysis. In short, we have tried to describe the entire process, from learning the concepts to computing the desired results. But we hasten to add that it is mandatory that the student retain the ability to compute simple answers by hand so that the computer's reasonableness can be judged. The First Law of Computers for engineers remains "Garbage In, Garbage Out." The code presented in this PDF version is up-to-date with current versions of MATLAB as of 2022. This is the main difference between this version and the print third edition.

Most of the graphical figures in this third edition were generated using MATLAB[®] supplied by The Mathworks, Inc. The files that created the figures are available from Ellis-Kagle Press at www.elliskaglepress.com. The reader is encouraged to use these MATLAB figure files as an additional guide in learning how to perform the various calculations.

To review the chapters briefly: Chapter 1 contains introductory comments. Chapters 2 and 3 are new to the third edition. Chapter 2 is a review of the prerequisite continuous control; Chapter 3 introduces the key effects of sampling in order to elucidate many of the topics that follow. Methods of linear analysis are presented in Chapters 4 through 6. Chapter 4 presents the z -transform. Chapter 5 introduces combined discrete and continuous systems, the sampling theorem, and the phenomenon of aliasing. Chapter 6 shows methods by which to generate discrete equations that will approximate continuous dynamics. The basic deterministic design methods are presented in Chapters 7 and 8—the root-locus and frequency response methods in Chapter 7 and pole placement and estimators in Chapter 8. The state-space material assumes no previous acquaintance with the phase plane or state space, and the necessary analysis is developed from the ground up. Some familiarity with simultaneous linear equations and matrix notation is expected, and a few unusual or more advanced topics such as eigenvalues, eigenvectors, and the Cayley-Hamilton theorem are presented in Appendix C. Chapter 9 introduces optimal quadratic-loss control: First the control by state feedback is presented and then the estimation of the state in the presence of system and measurement noise is developed, based on a recursive least-squares estimation derivation.

In Chapter 10 the nonlinear phenomenon of amplitude quantization and its effects on system error and system dynamic response are studied. Chapter 11 presents methods of analysis and design guidelines for the selection of, the sampling period in a digital control system. It utilizes the design methods discussed in Chapters 7, 8, and 9, in examples illustrating the effects of sample rate. Chapter 12 introduces both nonparametric and parametric identification. Nonparametric methods are based on spectral estimation. Parametric methods are introduced by starting with deterministic least squares, introducing random errors, and completing the solution with an algorithm for maximum likelihood. Sub-space methods are also introduced for estimating the state matrices directly. Nonlinear control is the subject of Chapter 13, including examples of plant nonlinearities and methods for the analysis and design of controllers for nonlinear models. Simulation, stability analysis, and performance enhancement by nonlinear controllers and by adaptive designs are also included in Chapter 13. The chapter ends with a nonlinear design optimization alternative to the techniques presented in Chapter 9. The final chapter, 14, is a detailed design example of a digital servo for a disk drive head.

For purposes of organizing a course, Fig. P.1 shows the dependence of material in each chapter on previous chapters. By following the solid lines, the reader will have all the background required to understand the material in a particular chapter, even if the path omits some chapters. Furthermore, sections with a star(*) are optional and may be skipped with no loss of continuity. Chapters may also be skipped, as suggested by the dashed lines, if the reader is willing to take some details on faith; however, the basic ideas of the later chapters will be understood along these paths.

The first seven chapters (skipping or quickly reviewing Chapter 2) constitute a comfortable one-quarter course that would follow a course in continuous linear control using a text such as Franklin, Powell, and Emami-Naeini (2019). For a one-semester course, the first eight chapters represent a comfortable load. The content of a second course has many possibilities. One possibility is to combine Chapters 8 and 9 with Chapter 10, 11, or 12. As can be seen from the figure, many options exist for including the material in the last five chapters. For a full-year course, all fourteen chapters can be covered. One of the changes made in this third edition is that the optimal control material no longer depends on the least-squares development in the system identification chapter, thus allowing for more flexibility in the sequence of teaching.

Chapter Title	3rd Edition Chapter Number	2nd Edition Chapter Number
Introduction	1	1
Review of Continuous Control	2	–
Introductory Digital Control	3	–
Discrete Analysis and the z -Transform	4	2
Sampled Data Systems	5	3
Discrete Equivalents	6	4
Design Using Transform Methods	7	5
Design Using State-Space Methods	8	6
Multivariable and Optimal Control	9	7
Quantization Effects	10	8
Sample-Rate Selection	11	9
System Identification	12	10
Nonlinear Control	13	11
Design of a Disk Drive Servo	14	12

Table P.1
Comparison of
the Table of
Contents

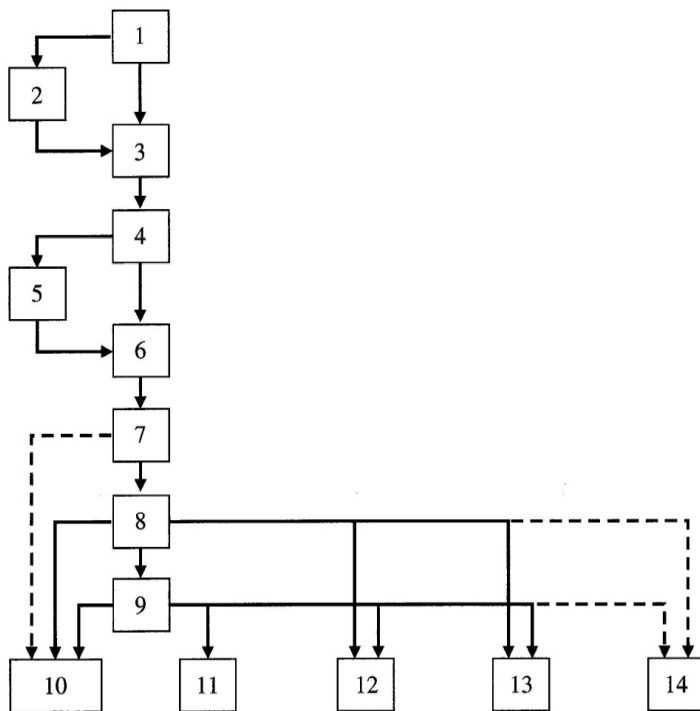


Figure P.1
Chapter
dependencies

It has been found at Stanford that it is very useful to supplement the lectures with laboratory work to enhance learning. A very satisfactory complement of laboratory equipment is a digital computer having an A/D and a D/A converter, an analog computer (or equivalent) with ten operational amplifiers, a digital storage scope, and a CAD package capable of performing the basic computations and plotting graphs as described in [Franklin, Powell (1989)].

There are many important topics in control that we have not been able to include in this book. There is, for example, no discussion of mu analysis or design, linear matrix inequalities, or convex optimization. It is our expectation, however, that careful study of this book will provide the student engineer with a sound basis for design of sampled-data controls and a foundation for the study of these and many other advanced topics in this most exciting field.

We wish to acknowledge the vast array of contributors on whose work our own presentation is based. The list of references gives some indication of those to whom we are in debt. On a more personal level, we wish to express our appreciation to Profs. S. Boyd, A. Bryson, R. Cannon, S. Citron, J. How, and S. Rock for their valuable suggestions for the book and especially to our long-time colleague, Prof. Dan DeBra, for his careful reading and many spirited suggestions. We also wish to express our appreciation for many valuable suggestions to the current and former students of E207 and E208, for whom this book was written. Furthermore, we wish to thank all the readers over the years who have forwarded corrections and clarifications, especially Prof. Lucy Pao.

In addition, we want to thank the following people for their helpful reviews of the manuscript: Fred Bailey, University of Minnesota; John Fleming, Texas A&M University; J.B. Pearson, Rice University; William Perkins, University of Illinois; James Carroll, Clarkson University; Walter Higgins, Jr., Arizona State University; Stanley Johnson, Lehigh University; Thomas Kurfess, Georgia Institute of Technology; Stephen Phillips, Case Western Reserve University; Chris Rahn, Clemson University; T. Srinivasan, Wilkes University; Hal Tharp, University of Arizona; Russell Trahan, Jr., University of New Orleans; and Gary Young, Oklahoma State University. We also wish to express our appreciation to Tom Robbins for his help with all the editions of the book, and to Laura Cheu, Emilie Bauer, and all the staff at Addison-Wesley for their quality production of this 3rd edition.

Stanford, California

*G.F.F.
J.D.P.
M.L.W.*

Chapter 1

Introduction

A Perspective on Digital Control

The control of physical systems with a digital computer or microcontroller is becoming more and more common. Examples of electromechanical servomechanisms exist in aircraft, automobiles, mass-transit vehicles, oil refineries, and paper-making machines. Furthermore, many new digital control applications are being stimulated by microprocessor technology including control of various aspects of automobiles and household appliances. Among the advantages of digital approaches for control are the increased flexibility of the control programs and the decision-making or logic capability of digital systems, which can be combined with the dynamic control function to meet other system requirements. In addition, one hardware design can be used with many different software variations on a broad range of products, thus simplifying and reducing the design time.

Chapter Overview

In Section 1.1, you will learn about what a digital control system is, what the typical structure is, and what the basic elements are. The key issues are discussed and an overview of where those issues are discussed in the book is given. Section 1.2 discusses the design approaches used for digital control systems and provides an overview of where the different design approaches appear in the book. Computer Aided Control System Design (CACSD) issues and how the book's authors have chosen to handle those issues are discussed in Section 1.3.

1.1 Problem Definition

The digital controls studied in this book are for closed-loop (feedback) systems in which the dynamic response of the process being controlled is a major consideration in the design. A typical structure of the elementary type of system that will occupy most of our attention is sketched schematically in Fig. 1.1. This figure will help to define our basic notation and to introduce several features that distinguish digital controls from those implemented with analog devices. The process to be controlled (sometimes referred to as the **plant**) may be any of the physical processes mentioned above whose satisfactory response requires control action.

By “satisfactory response” we mean that the plant output, $y(t)$, is to be forced to follow or track the reference input, $r(t)$, despite the presence of disturbance inputs to the plant [$w(t)$ in Fig. 1.1] and despite errors in the sensor [$v(t)$ in Fig. 1.1]. It is also essential that the tracking succeed even if the dynamics of the plant should change somewhat during the operation. The process of holding $y(t)$ close to $r(t)$, including the case where $r \equiv 0$, is referred to generally as the process of **regulation**. A system that has good regulation in the presence of disturbance signals is said to have good **disturbance rejection**. A system that has good regulation in the face of changes in the plant parameters is said to have low **sensitivity** to these parameters. A system that has both good disturbance rejection and low sensitivity we call **robust**.

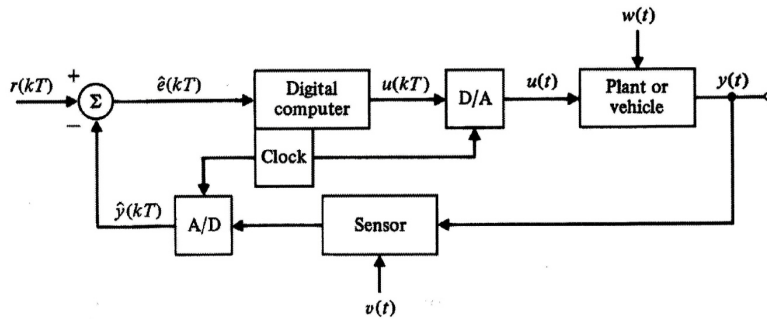


Figure 1.1
Block diagram of
a basic digital
control system

Notation:

- r = reference or command inputs
- u = control or actuator input signal
- y = controlled or output signal
- \hat{y} = instrument or sensor output, usually an approximation to or estimate of y . (For any variable, say θ , the notation $\hat{\theta}$ is now commonly taken from statistics to mean an estimate of θ .)
- \hat{e} = $r - \hat{y}$ = indicated error
- e = $r - y$ = system error
- w = disturbance input to the plant
- v = disturbance or noise in the sensor
- A/D = analog-to-digital converter
- D/A = digital-to-analog converter

The means by which robust regulation is to be accomplished is through the control inputs to the plant [$u(t)$ in Fig. 1.1]. It was discovered long ago¹ that a scheme of feedback wherein the plant output is measured (or sensed) and compared directly with the reference input has many advantages in the effort to design robust controls over systems that do not use such feedback. Much of our effort in later parts of this book will be devoted to illustrating this discovery and demonstrating how to exploit the advantages of feedback. However, the problem of control as discussed thus far is in no way restricted to digital control. For that we must consider the unique features of Fig. 1.1 introduced by the use of a digital device to generate the control action.

We consider first the action of the analog-to-digital (A/D) converter on a signal. This device acts on a physical variable, most commonly an electrical voltage, and converts it into a stream of numbers. In Fig. 1.1, the A/D converter acts on the sensor output and supplies numbers to the digital computer. It is common for the sensor output, \hat{y} , to be sampled and to have the error formed in the computer. We need to know the times at which these numbers arrive if we are to analyze the dynamics of this system.

In this book we will make the assumption that all the numbers arrive with the same fixed period T , called the **sample period**. In practice, digital control systems sometimes have varying sample periods and/or different periods in different feedback paths. Usually there is a clock as part of the computer logic which supplies a pulse or **interrupt** every T seconds, and the A/D converter sends a number to the computer each time the interrupt arrives. An alternative implementation is simply to access the A/D upon completion of each cycle of the code execution, a scheme often referred to as **free running**. A further alternative is to use some other device to determine a sample, such as an encoder on an engine crankshaft that supplies a pulse to trigger a computer cycle. This scheme is referred to as **event-based** sampling. In the first case the sample period is precisely fixed; in the second case the sample period is essentially fixed by the length of the code, providing no logic branches are present that could vary the amount of code executed; in the third case, the sample period varies with the engine speed. Thus in Fig. 1.1 we identify the sequence of numbers into the computer as $\hat{e}(kT)$. We conclude from the periodic sampling action of the A/D converter that some of the signals in the digital control system, like $\hat{e}(kT)$, are variable only at discrete times. We call these variables **discrete signals** to distinguish them from variables like w and y , which change continuously in time. A system having both discrete and continuous signals is called a **sampled-data** system.

¹See especially the book by Bode (1945).

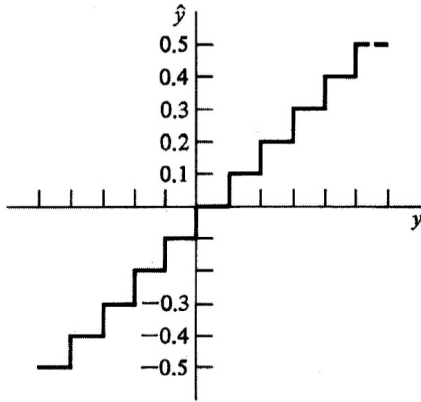


Figure 1.2
Plot of output
versus input
characteristics of
the A/D
converter

In addition to generating a discrete signal, however, the A/D converter also provides a **quantized** signal. By this we mean that the output of the A/D converter must be stored in digital logic composed of a finite number of digits. Most commonly, of course, the logic is based on binary digits (i.e., bits) composed of 0's and 1's, but the essential feature is that the representation has a finite number of digits. A common situation is that the conversion of y to \hat{y} is done so that \hat{y} can be thought of as a number with a fixed number of places of accuracy. If we plot the values of y versus the resulting values of \hat{y} we can obtain a plot like that shown in Fig. 1.2. We would say that \hat{y} has been truncated to one decimal place, or that \hat{y} is *quantized* with a q of 0.1, since \hat{y} changes only in fixed quanta of, in this case, 0.1 units. (We will use q for quantum size, in general.) Note that quantization is a nonlinear function. A signal that is both discrete and quantized is called a **digital signal**. Not surprisingly, digital computers in this book process digital signals.

In a real sense the problems of analysis and design of *digital controls* are concerned with taking account of the effects of the sampling period T and the quantization size q . If both T and q are extremely small (sampling frequency 30 or more times the system bandwidth with a 16-bit word size), digital signals are nearly continuous, and continuous methods of analysis and design can be used. The resulting design could then be converted to the digital format for implementation in a computer by using the simple methods described in Chapter 3 or the **emulation** method described in Chapter 7. We will be interested in this text in gaining an understanding of the effects of all sample rates, fast and slow, and the effects of quantization for large and small word sizes. Many systems are originally conceived with fast sample rates, and the computer is specified and frozen early in the design cycle; however, as the designs evolve, more demands are placed on the system, and the only way to accommodate the increased computer load is to slow down the sample rate. Furthermore, for cost-sensitive digital systems, the best design is the one with the lowest cost computer that will do the required job. That translates into being the computer with the slowest speed and the smallest word size. We will, however, treat the problems of varying T and q separately. We first consider q to be zero and study discrete and sampled-data (combined discrete and continuous) systems that are linear. In Chapter 10 we will analyze in more detail the source and the effects of quantization, and we will discuss in Chapters 7 and 11 specific effects of sample-rate selection.

Our approach to the design of digital controls is to assume a background in continuous systems and to relate the comparable digital problem to its continuous counterpart. We will develop the essential results, from the beginning, in the domain of discrete systems, but we will call upon previous experience in continuous-system analysis and in design to give alternative viewpoints and deeper understanding of the results. In order to make meaningful these references to a background in continuous-system design, we will review the concepts and define our notation in Chapter 2.

1.2 Overview of Design Approach

An overview of the path we plan to take toward the design of digital controls will be useful before we begin the specific details. As mentioned above, we place systems of interest in three categories according to the nature of the signals present. These are discrete systems, sampled-data systems, and digital systems.

In discrete systems all signals vary at discrete times only. We will analyze these in Chapter 4 and develop the z -transform of discrete signals and “pulse”-transfer functions for linear constant discrete systems. We also develop discrete transfer functions of continuous systems that are sampled, systems that are called sampled-data systems. We develop the equations and give examples using both transform methods and state-space descriptions. Having the discrete transfer functions, we consider the issue of the dynamic response of discrete systems.

A sampled-data system has both discrete and continuous signals, and often it is important to be able to compute the continuous time response. For example, with a slow sampling rate, there can be significant **ripple** between sample instants. Such situations are studied in Chapter 5. Here we are concerned with the question of data extrapolation to convert discrete signals as they might emerge from a digital computer into the continuous signals necessary for providing the input to one of the plants described above. This action typically occurs in conjunction with the D/A conversion. In addition to data extrapolation, we consider the analysis of sampled signals from the viewpoint of continuous analysis. For this purpose we introduce impulse modulation as a model of sampling, and we use Fourier analysis to give a clear picture for the ambiguity that can arise between continuous and discrete signals, also known as **aliasing**. The plain fact is that more than one continuous signal can result in exactly the same sample values. If a sinusoidal signal, y_1 , at frequency f_1 has the same samples as a sinusoid y_2 of a *different* frequency f_2 , y_1 is said to be an **alias** of y_2 . A corollary of aliasing is the **sampling theorem**, which specifies the conditions necessary if this ambiguity is to be removed and only one continuous signal allowed to correspond to a given set of samples.

As a special case of discrete systems and as the basis for the emulation design method, we consider discrete equivalents to continuous systems, which is one aspect of the field of **digital filters**. Digital filters are discrete systems designed to process discrete signals in such a fashion that the digital device (a digital computer, for example) can be used to replace a continuous filter. Our treatment in Chapter 6 will concentrate on the use of discrete filtering techniques to find discrete equivalents of continuous-control compensator transfer functions. Again, both transform methods and state-space methods are developed to help understanding and computation of particular cases of interest.

Once we have developed the tools of analysis for discrete and sampled systems we can begin the design of feedback controls. Here we divide our techniques into two categories: **transform**² and **state-space**³ methods. In Chapter 7 we study the transform methods of the root locus and the frequency response as they can be used to design digital control systems. The use of state-space techniques for design is introduced in Chapter 8. For purposes of understanding the design method, we rely mainly on **pole placement**, a scheme for forcing the closed-loop poles to be in desirable locations. We discuss the selection of the desired pole locations and point out the advantages of using the optimal control methods covered in Chapter 9. Chapter 8 includes control design using feedback of all the “state variables” as well as methods for estimating the state variables that do not have sensors directly on them. In Chapter 9 the topic of **optimal control** is introduced, with emphasis on the steady-state solution for linear constant discrete systems with quadratic loss functions. The results are a valuable part of the designer’s repertoire and are the only techniques presented here suitable for handling multivariable designs. A study of quantization effects in Chapter 10 introduces the idea of random signals in order to describe a method for treating the “average” effects of this important nonlinearity.

The last four chapters cover more advanced topics that are essential for most complete designs.

²Named because they use the Laplace or Fourier transform to represent systems.

³The state space is an extension of the space of displacement and velocity used in physics. Much that is called **modern control theory** uses differential equations in state-space form. We introduce this representation in Chapter 4 and use it extensively afterwards, especially in Chapters 8 and 9.

The first of these topics is sample rate selection, contained in Chapter 11. In our earlier analysis we develop methods for examining the effects of different sample rates, but in this chapter we consider for the first time the question of sample rate as a design parameter. In Chapter 12, we introduce **system identification**. Here the matter of model making is extended to the use of experimental data to verify and correct a theoretical model or to supply a dynamic description based only on input-output data. Only the most elementary of the concepts in this enormous field can be covered, of course. We present the method of least squares and some of the concepts of maximum likelihood.

In Chapter 13, an introduction to the most important issues and techniques for the analysis and design of nonlinear sampled-data systems is given. The analysis methods treated are the describing function, equivalent linearization, and Lyapunov's second method of stability analysis. Design techniques described are the use of inverse nonlinearity, optimal control (especially time-optimal control), and adaptive control. Chapter 14 includes a case study of a disk-drive design, and treatment of both implementation and manufacturing issues is discussed.

1.3 Computer-Aided Design

As with any engineering design method, design of control systems requires many computations that are greatly facilitated by a good library of well-documented computer programs. In designing practical digital control systems, and especially in iterating through the methods many times to meet essential specifications, an interactive computer-aided control system design (CACSD) package with simple access to plotting graphics is crucial. Many commercial control system CACSD packages are available which satisfy that need, MATLAB[®] and Python[™] being two very popular ones. Much of the discussion in the book assumes that a designer has access to one of the CACSD products. Specific MATLAB routines that can be used for performing calculations are indicated throughout the text and in some cases the full MATLAB command sequence is shown. All the graphical figures were developed using MATLAB and the files that created them are provided by the authors within the Digital Control Toolbox, freely available online at www.elliskaglepress.com. The files and code presented in the text have been verified using MATLAB version R2018b with the Control Systems Toolbox installed. A list of useful MATLAB commands can be found in the Index of MATLAB Functions.

CACSD support for a designer is universal; however, it is essential that the designer is able to work out very simple problems by hand in order to have some idea about the reasonableness of the computer's answers. Having the knowledge of doing the calculations by hand is also critical for identifying trends that guide the designer; the computer can identify problems but the designer must make intelligent choices in guiding the refinement of the computer design.

1.4 Suggestions for Further Reading

Several histories of feedback control are readily available, including a *Scientific American Book* (1955), and the study of Mayr (1970). A good discussion of the historical developments of control is given by Dorf (1980) and by Fortmann and Hitz (1977), and many other references are cited by these authors for the interested reader. One of the earliest published studies of control systems operating on discrete time data (sampled-data systems in our terminology) is given by Hurewicz in Chapter 5 of the book by James, Nichols, and Phillips (1947).

The ideas of tracking and robustness embody many elements of the objectives of control system design. The concept of tracking contains the requirements of system stability, good transient response, and good steady-state accuracy, all concepts fundamental to every control system. Robustness is a property essential to good performance in practical designs because real parameters are subject to change and because external, unwanted signals invade every system. Discussion of performance specifications of control systems is given in most books on introductory control, including Franklin, Powell, and Emami-Naeini (2019). We will study these matters in later chapters with particular reference to digital control design.

To obtain a firm understanding of dynamics, we suggest a comprehensive text by Cannon (1967). It is concerned with writing the equations of motion of physical systems in a form suitable for control studies.

1.5 Summary

- In a digital control system, the analog electronics used for compensation in a continuous system is replaced with a digital computer or microcontroller, an analog-to-digital (A/D) converter, and a digital-to-analog (D/A) converter.
- Design of a digital control system can be accomplished by transforming a continuous design, called emulation, or designing the digital system directly. Either method can be carried out using transform or state-space system description.
- The design of a digital control system includes determining the effect of the sample rate and selecting a rate that is sufficiently fast to meet all specifications.
- Most designs today are carried out using computer-based methods; however the designer needs to know the hand-based methods in order to intelligently guide the computer design as well as to have a sanity check on its results.

1.6 Problems

- 1.1 Suppose a radar search antenna at the San Francisco airport rotates at 6 rev/min, and data points corresponding to the position of flight 1081 are plotted on the controller's screen once per antenna revolution. Flight 1081 is traveling directly toward the airport at 540 mi/hr. A feedback control system is established through the controller who gives course corrections to the pilot. He wishes to do so each 9 mi of travel of the aircraft, and his instructions consist of course headings in integral degree values.
- (a) What is the sampling rate, in Hz, of the range signal plotted on the radar screen?
 - (b) What is the sampling rate, in Hz, of the controller's instructions?
 - (c) Identify the following signals as continuous, discrete, or digital:
 - i. the aircraft's range from the airport,
 - ii. the range data as plotted on the radar screen,
 - iii. the controller's instructions to the pilot,
 - iv. the pilot's actions on the aircraft control surfaces.
 - (d) Is this a continuous, sampled-data, or digital control system?
 - (e) Show that it is possible for the pilot of flight 1081 to fly a zigzag course which would show up as a straight line on the controller's screen. What is the (lowest) frequency of a sinusoidal zigzag course which will be hidden from the controller's radar?
- 1.2 If a signal varies between 0 and 10 volts (called the **dynamic range**) and it is required that the signal must be represented in the digital computer to the nearest 5 millivolts, that is, if the *resolution* must be 5 mv, determine how many bits the analog-to-digital converter must have.
- 1.3 Describe five digital control systems that you are familiar with. State what you think the advantages of the digital implementation are over an analog implementation.
- 1.4 Historically, house heating system thermostats were a bimetallic strip that would make or break the contact depending on temperature. Today, most thermostats are digital. Describe how you think they work and list some of their benefits.

- 1.5 Use MATLAB (obtain a copy of the Student Edition or use what's available to you) and plot y vs x for $x = 1$ to 10 where $y = x^2$. Label each axis and put a title on it.
- 1.6 Use MATLAB (obtain a copy of the Student Edition or use what's available to you) and make two plots (use MATLAB's `subplot`) of y vs x for $x = 1$ to 10 . Put a plot of $y = x^2$ on the top of the page and $y = \sqrt{x}$ on the bottom.

Chapter 2

Review of Continuous Control

A Perspective on the Review of Continuous Control

The purpose of this chapter is to provide a ready reference source of the material that you have already taken in a prerequisite course. The presentation is not sufficient to learn the material for the first time; rather, it is designed to state concisely the key relationships for your reference as you move to the new material in the ensuing chapters. For a more in-depth treatment of any of the topics, see an introductory control text such as *Feedback Control of Dynamic Systems*, by Franklin, Powell, and Emami-Naeini (2019).

Chapter Overview

The chapter reviews the topics normally covered in an introductory controls course: dynamic response, feedback properties, root-locus design, frequency response design, and state-space design.

2.1 Dynamic Response

In control system design, it is important to be able to predict how well a trial design matches the desired performance. We do this by analyzing the equations of the system model. The equations can be solved using linear analysis approximations or simulated via numerical methods. Linear analysis allows the designer to examine quickly many candidate solutions in the course of design iterations and is, therefore, a valuable tool. Numerical simulation allows the designer to check the final design more precisely including all known characteristics and is discussed in Section 13.2. The discussion below focuses on linear analysis.

2.1.1 Differential Equations

Linear dynamic systems can be described by their differential equations. Many systems involve coupling between one part of a system and another. Any set of differential equations of any order can be transformed into a coupled set of first-order equations called the **state-variable form**. So a general way of expressing the dynamics of a linear system is

$$\dot{\mathbf{x}} = \mathbf{F}\mathbf{x} + \mathbf{G}\mathbf{u} \quad (2.1)$$

$$\mathbf{y} = \mathbf{H}\mathbf{x} + \mathbf{J}\mathbf{u}. \quad (2.2)$$

where the column vector \mathbf{x} is called the **state** of the system and contains n elements for an n th-order system, \mathbf{u} is the $m \times 1$ input vector to the system, \mathbf{y} is the $p \times 1$ output vector, \mathbf{F} is an $n \times n$ system matrix, \mathbf{G} is an $n \times m$ input matrix, \mathbf{H} is a $p \times n$ output matrix, and \mathbf{J} is $p \times m$.¹ Until Chapter 9, all

¹It is also common to use $\mathbf{A}, \mathbf{B}, \mathbf{C}, \mathbf{D}$ in place of $\mathbf{F}, \mathbf{G}, \mathbf{H}, \mathbf{J}$ as MATLAB does throughout. We prefer to use $\mathbf{F}, \mathbf{G} \dots$ for a continuous plant description, $\mathbf{A}, \mathbf{B} \dots$ for compensation, and $\Phi, \Gamma \dots$ for the discrete plant description in order to delineate the various system equation usages.

systems will have a scalar input, u , and a scalar output y ; in this case, \mathbf{G} is $n \times 1$, \mathbf{H} is $1 \times n$, and J is a scalar.

Using this system description, we see that the second-order differential equation

$$\ddot{y} + 2\zeta\omega_o\dot{y} + \omega_o^2y = K_o u, \quad (2.3)$$

can be written in the state-variable form as

$$\begin{aligned} \begin{bmatrix} \dot{x}_1 \\ \dot{x}_2 \end{bmatrix} &= \begin{bmatrix} 0 & 1 \\ -\omega_o^2 & -2\zeta\omega_o \end{bmatrix} \begin{bmatrix} x_1 \\ x_2 \end{bmatrix} + \begin{bmatrix} 0 \\ K_o \end{bmatrix} u \\ y &= \begin{bmatrix} 1 & 0 \end{bmatrix} \begin{bmatrix} x_1 \\ x_2 \end{bmatrix}, \end{aligned} \quad (2.4)$$

where the state

$$\mathbf{x} = \begin{bmatrix} x_1 \\ x_2 \end{bmatrix} = \begin{bmatrix} y \\ \dot{y} \end{bmatrix}$$

state

is the vector of variables necessary to describe the future behavior of the system, given the initial conditions of those variables.

2.1.2 Laplace Transforms and Transfer Functions

The analysis of linear systems is facilitated by use of the Laplace transform. The most important property of the Laplace transform (with zero initial conditions) is the transform of the derivative of a signal.

$$\mathcal{L}\{\dot{f}(t)\} = sF(s). \quad (2.5)$$

This relation enables us to find easily the transfer function, $G(s)$, of a linear continuous system, given the differential equation of that system. So we see that Eq. (2.3) has the transform

$$(s^2 + 2\zeta\omega_o s + \omega_o^2)Y(s) = K_o U(s),$$

and, therefore, the transfer function, $G(s)$, is

$$G(s) = \frac{Y(s)}{U(s)} = \frac{K_o}{s^2 + 2\zeta\omega_o s + \omega_o^2}.$$

CACSD software typically accepts the specification of a system in either the state-variable form or the transfer function form. The quantities specifying the state-variable form (Eqs. 2.1 and 2.2) are \mathbf{F} , \mathbf{G} , \mathbf{H} , and J . This is referred to as the “ss” form in MATLAB. The transfer function is specified in a polynomial form (“tf”) or a factored zero-pole-gain form (“zpk”). The transfer function in polynomial form is

$$G(s) = \frac{b_1 s^m + b_2 s^{m-1} + \dots + b_{m+1}}{a_1 s^n + a_2 s^{n-1} + \dots + a_{n+1}}, \quad (2.6)$$

where the MATLAB quantity specifying the numerator is a $1 \times (m+1)$ matrix of the coefficients, for example

$$\text{num} = [b_1 \quad b_2 \quad \dots \quad b_{m+1}]$$

and the quantity specifying the denominator is a $1 \times (n+1)$ matrix, for example

$$\text{den} = [a_1 \quad a_2 \quad \dots \quad a_{n+1}].$$

In MATLAB (with the Control System Toolbox) the numerator and denominator are combined into one system specification with the statement

$$\text{sys} = \text{tf}(\text{num}, \text{den})$$

In the zero-pole-gain form, the transfer function is written as the ratio of two factored polynomials,

$$G(s) = K \frac{\prod_{i=1}^m (s - z_i)}{\prod_{i=1}^n (s - p_i)}, \quad (2.7)$$

and the quantities specifying the transfer function are an $m \times 1$ matrix of the zeros, an $n \times 1$ matrix of the poles, and a scalar gain, for example

$$\mathbf{z} = \begin{bmatrix} z_1 \\ z_2 \\ \dots \\ z_m \end{bmatrix}, \quad \mathbf{p} = \begin{bmatrix} p_1 \\ p_2 \\ \dots \\ p_n \end{bmatrix}, \quad k = K$$

and can be combined into a system description by

$$\text{sys} = \text{zpk}(\mathbf{z}, \mathbf{p}, k).$$

For the equations of motion of a system with second-order or higher equations, the easiest way to find the transfer function is to use Eq. (2.5) and do the math by hand. If the equations of motion are in the state-variable form and the transfer function is desired, the Laplace transform of Eqs. (2.1) and (2.2) yields

$$G(s) = \frac{y(s)}{u(s)} = \mathbf{H}(s\mathbf{I} - \mathbf{F})^{-1}\mathbf{G} + J.$$

In MATLAB, given \mathbf{F} , \mathbf{G} , \mathbf{H} , and J , one can find the polynomial transfer function form by the MATLAB script

$$\text{sys} = \text{tf}(\text{ss}(\mathbf{F}, \mathbf{G}, \mathbf{H}, J))$$

or the zero-pole-gain form by

$$\text{sys} = \text{zpk}(\text{ss}(\mathbf{F}, \mathbf{G}, \mathbf{H}, J)).$$

Likewise, one can find a state-space realization of a transfer function by

$$\text{sys} = \text{ss}(\text{tf}(\text{num}, \text{den})).$$

2.1.3 Output Time Histories

Given the transfer function and the input, $u(t)$, with the transform $U(s)$, the output is the product,

$$Y(s) = G(s)U(s). \quad (2.8)$$

The transform of a time function can be found by use of a table (See Appendix B.2); however, typical inputs considered in control system design are steps

$$u(t) = R_o 1(t), \quad \Rightarrow \quad U(s) = \frac{R_o}{s},$$

ramps

$$u(t) = V_o t 1(t), \quad \Rightarrow \quad U(s) = \frac{V_o}{s^2},$$

parabolas

$$u(t) = \frac{A_o t^2}{2} 1(t), \quad \Rightarrow \quad U(s) = \frac{A_o}{s^3},$$

and sinusoids

$$u(t) = B \sin(\omega t) 1(t), \quad \Rightarrow \quad U(s) = \frac{B\omega}{s^2 + \omega^2}.$$

Using Laplace transforms, the output $Y(s)$ from Eq. (2.8) is expanded into its elementary terms using partial fraction expansion, then the time function associated with each term is found by looking it up

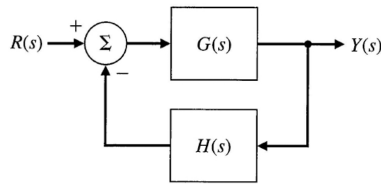


Figure 2.1
An elementary
feedback system

in the table. The total time function, $y(t)$, is the sum of these terms. In order to do the partial fraction expansion, it is necessary to factor the denominator. Typically, only the simplest cases are analyzed this way. Usually, system output time histories are solved numerically using computer based methods such as MATLAB's `step.m` for a step input or `lsim.m` for an arbitrary input time history. However, useful information about system behavior can be obtained by finding the individual factors without ever solving for the time history, a topic to be discussed later. These will be important because specifications for a control system are frequently given in terms of these time responses.

2.1.4 The Final Value Theorem

A key theorem involving the Laplace transform that is often used in control system analysis is the **final value theorem**. It states that, if the system is stable and has a final, constant value

$$\lim_{t \rightarrow \infty} x(t) = x_{ss} = \lim_{s \rightarrow 0} sX(s). \quad (2.9)$$

The theorem allows us to solve for that final value without solving for the system's entire response. This will be very useful when examining steady-state errors of control systems.

2.1.5 Block Diagrams

Manipulating block diagrams is useful in the study of feedback control systems. The most common and useful result is that the transfer function of the feedback system shown in Fig. 2.1 reduces to

$$\frac{Y(s)}{R(s)} = \frac{G(s)}{1 + H(s)G(s)}. \quad (2.10)$$

2.1.6 Response versus Pole Locations

Given the transfer function of a linear system,

$$H(s) = \frac{b(s)}{a(s)},$$

the values of s such that $a(s) = 0$ will be places where $H(s)$ is infinity, and these values of s are called **poles** of $H(s)$. On the other hand, values of s such that $b(s) = 0$ are places where $H(s)$ is zero, and the corresponding s locations are called **zeros**. Since the Laplace transform of an impulse is unity, the **impulse response** is given by the time function corresponding to the transfer function. Each pole location in the s -plane can be identified with a particular type of response. In other words, the poles identify the classes of signals contained in the impulse response, as may be seen by a partial fraction expansion of $H(s)$. For a first order pole

$$H(s) = \frac{1}{s + \sigma},$$

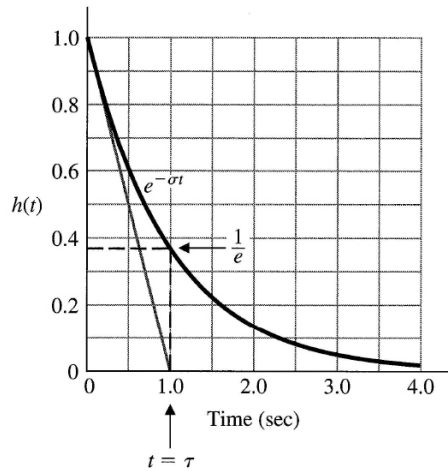


Figure 2.2
First-order
system response

Table B.2, Entry 8, indicates that the impulse response will be an exponential function; that is

$$h(t) = e^{-\sigma t} 1(t).$$

When $\sigma > 0$, the pole is located at $s < 0$, the exponential decays, and the system is said to be **stable**. stability

Likewise, if $\sigma < 0$, the pole is to the right of the origin, the exponential grows with time and is referred to as **unstable**. Figure 2.2 shows a typical response and the **time constant** time constant

$$\tau = \frac{1}{\sigma} \quad (2.11)$$

as the time when the response is $\frac{1}{e}$ times the initial value.

Complex poles can be described in terms of their real and imaginary parts, traditionally referred to as

$$s = -\sigma \pm j\omega_d.$$

This means that a pole has a negative real part if σ is positive. Since complex poles always come in complex conjugate pairs for real polynomials, the denominator corresponding to a complex pair will be

$$a(s) = (s + \sigma - j\omega_d)(s + \sigma + j\omega_d) = (s + \sigma)^2 + \omega_d^2. \quad (2.12)$$

When finding the transfer function from differential equations, we typically write the result in the polynomial form

$$H(s) = \frac{\omega_n^2}{s^2 + 2\zeta\omega_n s + \omega_n^2}. \quad (2.13)$$

By expanding the form given by Eq. (2.12) and comparing with the coefficients of the denominator of $H(s)$ in Eq. (2.13), we find the correspondence between the parameters to be

$$\sigma = \zeta\omega_n \quad \text{and} \quad \omega_d = \omega_n\sqrt{1 - \zeta^2}, \quad (2.14)$$

where the parameter ζ is called the **damping ratio**, and ω_n is called the **undamped natural frequency**. damping ratio The poles of this transfer function are located at a radius ω_n in the s -plane and at an angle $\theta = \sin^{-1}\zeta$, as shown in Fig. 2.3. Therefore, the damping ratio reflects the level of damping as a fraction of the critical damping value where the poles become real. In rectangular coordinates, the poles are at $s = -\sigma \pm j\omega_d$. When $\zeta = 0$ we have no damping, $\theta = 0$, and ω_d , the damped natural frequency, equals ω_n , the undamped natural frequency.

For the purpose of finding the time response corresponding to a complex transfer function from Table B.2, it is easiest to manipulate the $H(s)$ so that the complex poles fit the form of Eq. (2.12),

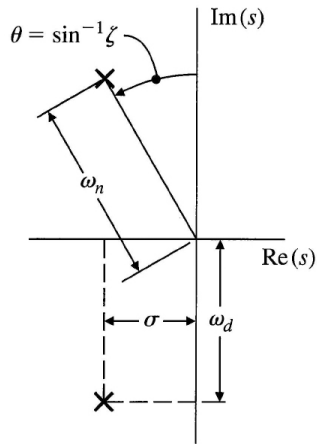


Figure 2.3
s-plane plot for a
pair of complex
poles

because then the time response can be found directly from the table. The $H(s)$ from Eq. (2.13) can be written as

$$H(s) = \frac{\omega_n^2}{(s + \zeta \omega_n)^2 + \omega_n^2(1 - \zeta^2)},$$

therefore, from Entry 21 in Table B.2 and the definitions in Eq. (2.14), we see that the impulse response is

$$h(t) = \omega_n e^{-\sigma t} \sin(\omega_d t) 1(t).$$

For $\omega_n = 3$ rad/sec and $\zeta = 0.2$, the impulse response time history could be obtained and plotted by the MATLAB statements:

```
Wn = 3;
Ze = 0.2;
s = tf('s');
sys=(Wn^2)/(s^2 + 2*Ze*Wn*s + Wn^2);
impulse(sys);
```

It is also interesting to examine the **step response** of $H(s)$, that is, the response of the system $H(s)$ to a unit step input $u = 1(t)$ where $U(s) = \frac{1}{s}$. The step response transform given by $Y(s) = H(s)U(s)$, contained in the tables in Entry 22, is

$$y(t) = 1 - e^{-\sigma t} \left(\cos \omega_d t + \frac{\sigma}{\omega_d} \sin \omega_d t \right), \quad (2.15)$$

where $\omega_d = \omega_n \sqrt{1 - \zeta^2}$ and $\sigma = \zeta \omega_n$. This could also be obtained by modifying the last line in the MATLAB description above for the impulse response to

```
step(sys)
```

Figure 2.4 is a plot of $y(t)$ for several values of ζ plotted with time normalized to the undamped natural frequency ω_n . Note that the actual frequency, ω_d , decreases slightly as the damping ratio increases. Also note that for very low damping the response is oscillatory, while for large damping (ζ near 1) the response shows no oscillation. A few step responses are sketched in Fig. 2.5 to show the effect of pole locations in the s -plane on the step responses. It is very useful for control designers to have the mental image of Fig. 2.5 committed to memory so that there is an instant understanding of how changes in pole locations influence the time response. The negative real part of the pole, σ , determines the decay rate of an exponential envelope that multiplies the sinusoid. Note that if σ is negative, the pole is in the right-half plane, the response will grow with time, and the system is said

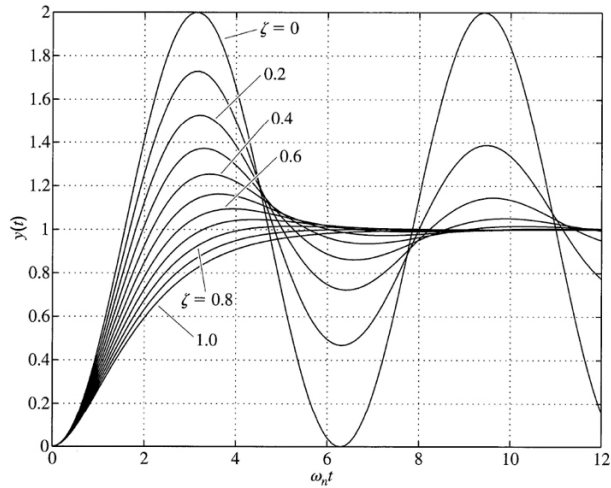


Figure 2.4
Step responses of second-order systems versus ζ

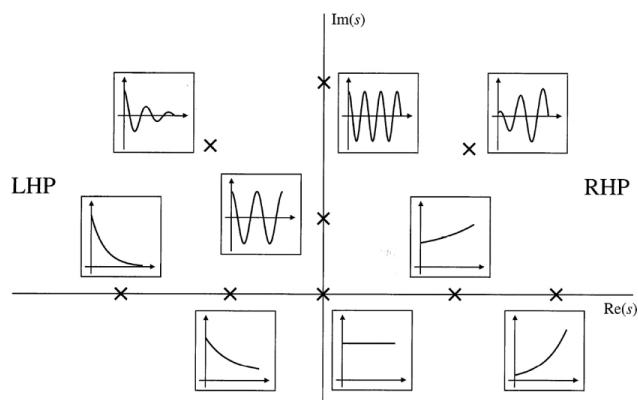


Figure 2.5
Time functions associated with points in the s -plane

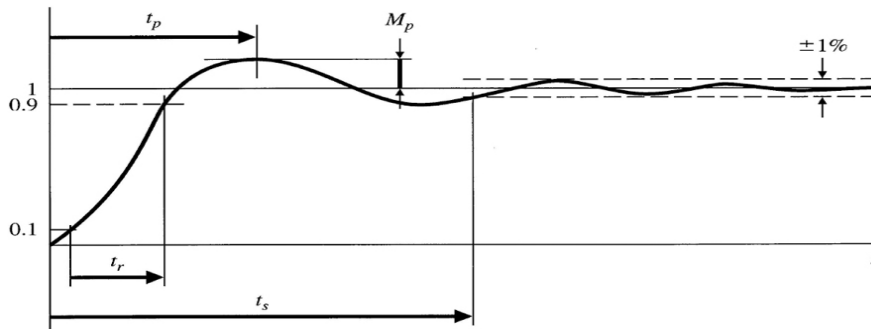


Figure 2.6
Definition of rise time t_r , settling time t_s , and overshoot M_p

to be unstable. If $\sigma = 0$, the response neither grows nor decays, so stability is a matter of definition. If σ is positive, the natural response decays and the system is said to be stable. Note that, as long as the damping is strictly positive, the system will eventually converge to the commanded value.

All these notions about the correspondence between pole locations and the time response pertained to the case of the step response of the system of Eq. (2.13), that is, a second-order system with no zeros. If there had been a zero, the effect would generally be an increased overshoot; the presence of an additional pole would generally cause the response to be slower. If there had been a zero in the right-half plane, the overshoot would be repressed and the response would likely go initially in the opposite direction to its final value. Nevertheless, the second-order system response is useful in guiding the designer during the iterations toward the final design, no matter how complex the system is.

2.1.7 Time-Domain Specifications

Specifications for a control system design often involve certain requirements associated with the time response of the system. The requirements for a step response are expressed in terms of the standard quantities illustrated in Fig. 2.6:

The **rise time** t_r is the time it takes the system to reach the vicinity of its new set point. t_r

The **settling time** t_s is the time it takes the system transients to decay. t_s

The **overshoot** M_p is the maximum amount that the system overshoots its final value divided by its final value (and often expressed as a percentage). M_p

For a second-order system, the time responses of Fig. 2.4 yield information about the specifications that is too complex to be remembered unless approximated. The commonly used approximations for the second-order case with no zeros are

$$t_r \approx \frac{1.8}{\omega_n} \quad (2.16)$$

$$t_s \approx \frac{4.6}{\zeta \omega_n} = \frac{4.6}{\sigma} \quad (2.17)$$

$$M_p \approx e^{-\pi\zeta/\sqrt{1-\zeta^2}} \quad 0 \leq \zeta < 1 \quad (2.18)$$

The overshoot M_p is plotted in Fig. 2.7. Two frequently used values from this curve are $M_p = 16\%$ for $\zeta = 0.5$ and $M_p = 5\%$ for $\zeta = 0.7$.

Equations (2.16)–(2.18) characterize the transient response of a system having no finite zeros and two complex poles with undamped natural frequency ω_n , damping ratio ζ , and negative real part σ .

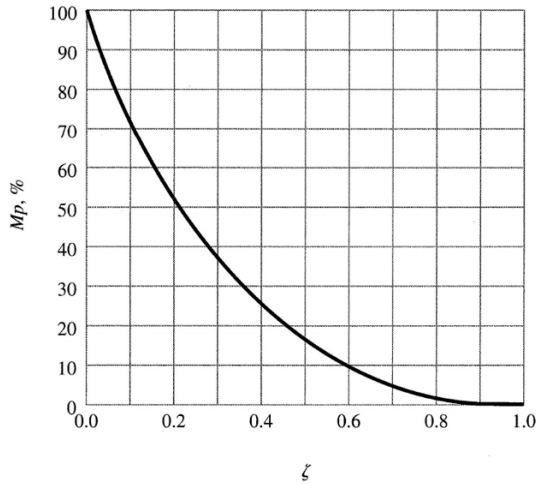


Figure 2.7
Plot of the peak overshoot M_p versus the damping ratio ζ for the second-order system

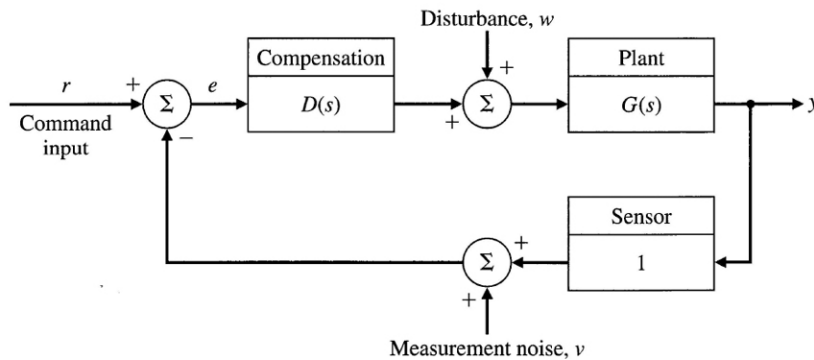


Figure 2.8
A unity feedback system

In analysis and design, they are used to obtain a rough estimate of rise time, overshoot, and settling time for just about any system. It is important to keep in mind, however, that they are qualitative guides and not precise design formulas. They are meant to provide a starting point for the design iteration and the time response should always be checked after the control design is complete by an exact calculation, usually by numerical simulation, to verify whether the time specifications are actually met. If they have not been met, another iteration of the design is required. For example, if the rise time of the system turns out to be longer than the specification, the target natural frequency would be increased and the design repeated.

2.2 Basic Properties of Feedback

An open-loop system described by the transfer function $G(s)$ can be improved by the addition of feedback including the dynamic compensation $D(s)$ as shown in Fig. 2.8. The feedback can be used to improve the stability, speed up the transient response, improve the steady-state error characteristics, provide disturbance rejection, and decrease the sensitivity to parameter variations.

2.2.1 Stability

The dynamic characteristics of the open-loop system are determined by the poles of $G(s)$ and $D(s)$, that is, the roots of the denominators of $G(s)$ and $D(s)$. Using Eq. (2.10), we can see that the transfer function of the closed-loop system in Fig. 2.8 is

$$\frac{Y(s)}{R(s)} = \frac{D(s)G(s)}{1 + D(s)G(s)} = \mathcal{T}(s), \quad (2.19)$$

sometimes referred to as the **complementary sensitivity**. In this case, the dynamic characteristics and stability are determined by the poles of the closed-loop transfer function, that is, the roots of

$$1 + D(s)G(s) = 0. \quad (2.20)$$

This equation is called the **characteristic equation** and is very important in feedback control analysis and design. The roots of the characteristic equation represent the types of motion that will be exhibited by the feedback system. It is clear from Eq. (2.20) that they can be altered at will by the designer via the selection of $D(s)$. characteristic equation

2.2.2 Steady-State Errors

The difference between the command input r (see Fig. 2.8) and the output y is called the system error, e . Using Eq. (2.10) for the case where the desired output is e , we find that

$$\frac{E(s)}{R(s)} = \frac{1}{1 + D(s)G(s)} = \mathcal{S}(s), \quad (2.21)$$

sometimes referred to as the **sensitivity**. For the case where $r(t)$ is a step input and the system is stable, the Final Value Theorem tells us that

$$e_{ss} = \frac{1}{1 + K_p}$$

where

$$K_p = \lim_{s \rightarrow 0} D(s)G(s)$$

and is called the **position-error constant**. If $D(s)G(s)$ has a denominator that does not have s as a factor, K_p and e_{ss} are finite. This kind of system is referred to as **type 0**. system type

These results can also be seen qualitatively by examining Fig. 2.8. In order for y to be at some desired value ($= r$), the higher the forward loop gain of DG (defined to be K_p), the lower the value of the error, e . An integrator has the property that a zero steady input can produce a finite output, thus producing an infinite gain. Therefore, if there is an integrator in D or G , the steady-state gain will be ∞ and the error will be zero.

Continuing, we define the **velocity constant** as

$$K_v = \lim_{s \rightarrow 0} sD(s)G(s)$$

and the **acceleration constant** as

$$K_a = \lim_{s \rightarrow 0} s^2 D(s)G(s).$$

When K_v is finite, we call the system **type 1**; likewise, when K_a is finite, we call the system **type 2**. For the unity feedback case, it is convenient to categorize the error characteristics for command inputs consisting of steps, ramps, and parabolas. Table 2.1 summarizes the results.

System type can also be defined with respect to the disturbance inputs w . The same ideas hold, but in this case the type is determined by the number of integrators in $D(s)$ only. Thus, if a system had a disturbance as shown in Fig. 2.8 which was constant, the steady-state error e_{ss} of the system would only be zero if $D(s)$ contained an integrator.

	Step	Ramp	Parabola
Type 0	$\frac{1}{(1+K_p)}$	∞	∞
Type 1	0	$\frac{1}{K_v}$	∞
Type 2	0	0	$\frac{1}{K_a}$

Table 2.1
Errors versus
system type for
unity feedback

2.2.3 PID Control

Proportional, integral, and derivative (PID) control contains three terms. They are proportional control

$$u(t) = Ke(t) \Rightarrow D(s) = K, \quad (2.22)$$

integral control

$$u(t) = \frac{K}{T_I} \int_0^t e(\eta) d\eta \Rightarrow D(s) = \frac{K}{T_I s}, \quad (2.23)$$

and derivative control

$$u(t) = KT_D \dot{e}(t) \Rightarrow D(s) = KT_D s. \quad (2.24)$$

T_I is called the integral (or reset) time, T_D the derivative time, and K the position feedback gain. Thus, the combined transfer function is

$$D(s) = \frac{u(s)}{e(s)} = K \left(1 + \frac{1}{T_I s} + T_D s \right). \quad (2.25)$$

Proportional feedback control can lead to reduced errors to disturbances but still has a small steady-state error. It can also increase the speed of response but typically at the cost of a larger transient overshoot. If the controller also includes a term proportional to the integral of the error, the error to a step can be eliminated as we saw in the previous section. However, there tends to be a further deterioration of the dynamic response. Finally, addition of a term proportional to the error derivative can add damping to the dynamic response. These three terms combined form the classical PID controller. It is widely used in the process industries and commercial controller hardware can be purchased where the user only need “tune” the gains on the three terms.

2.3 Root Locus

The **root locus** is a technique which shows how changes in the system’s open-loop characteristics influence the closed-loop dynamic characteristics. This technique allows us to plot the locus of the closed-loop roots in the s -plane as an open-loop parameter varies, thus producing a root locus. The root locus method is most commonly used to study the effect of the loop gain (K in Eq. (2.25)); however, the method is general and can be used to study the effect of any parameter in $D(s)$ or $G(s)$. In fact, the method can be used to study the roots of any polynomial versus parameters in that polynomial.

A key attribute of the technique is that it allows you to study the **closed-loop roots** while only knowing the factors (poles and zeros) of the **open-loop system**.

2.3.1 Problem Definition

The first step in creating a root locus is to put the polynomials in the **root locus form**

$$1 + K \frac{b(s)}{a(s)} = 0. \quad (2.26)$$

Typically, $Kb(s)/a(s)$ is the open loop transfer function $D(s)G(s)$ of a feedback system; however, this need not be the case. The root locus is the set of values of s for which Eq. (2.26) holds for

some real value of K . For the typical case, Eq. (2.26) represents the characteristic equation of the closed-loop system.

The purpose of the root locus is to show in a graphical form the general trend of the roots of a closed-loop system as we vary some parameter. Being able to do this by hand (1) gives the designer the ability to design simple systems without a computer, (2) helps the designer verify and understand computer-generated root loci, and (3) gives insight to the design process.

Equation (2.26) shows that, if K is real and positive, $b(s)/a(s)$ must be real and negative. In other words, if we arrange $b(s)/a(s)$ in polar form as magnitude and phase, then the phase of $b(s)/a(s)$ must be 180° . We thus define the root locus in terms of the phase condition as follows.

180° locus definition: The root locus of $b(s)/a(s)$ is the set of points in the s -plane where the phase of $b(s)/a(s)$ is 180° . root locus definition

Since the phase is unchanged if an integral multiple of 360° is added, we can express the definition as²

$$\angle \frac{b(s)}{a(s)} = 180^\circ + l360^\circ,$$

where l is any integer. The significance of the definition is that, while it is very difficult to solve a high-order polynomial, computation of phase is relatively easy. When K is positive, we call this the **positive or 180° locus**. When K is real and negative, $b(s)/a(s)$ must be real and positive for s to be on the locus. Therefore, the phase of $b(s)/a(s)$ must be 0° . This case is called the **0° or negative locus**.

2.3.2 Root Locus Drawing Rules

The steps in drawing a 180° root locus follow from the basic phase definition. They are

- STEP 1. On the s -plane, mark poles (roots of $a(s)$) by an \times and zeros (roots of $a(s)$) by a \circ . There will be a branch of the locus departing from every pole and a branch arriving at every zero.
- STEP 2. Draw the locus on the real axis to the left of an odd number of real poles plus zeros.
- STEP 3. Draw the asymptotes, centered at α and leaving at angles ϕ_l , where

$$\begin{aligned} n - m &= \text{number of asymptotes} \\ n &= \text{order of } a(s) \\ m &= \text{order of } b(s) \\ \alpha &= \frac{\sum p_i - \sum z_i}{n - m} = \frac{-a_1 + b_1}{n - m}; \\ \phi_l &= \frac{180^\circ + (l - 1)360^\circ}{n - m}, \quad l = 1, 2 \dots n - m. \end{aligned}$$

For $n - m > 0$, there will be a branch of the locus approaching each asymptote and departing to infinity. For $n - m < 0$, there will be a branch of the locus arriving from infinity along each asymptote.

- STEP 4. Compute locus departure angles from the poles and arrival angles at the zeros where

$$\begin{aligned} q\phi_{dep} &= \sum \psi_i - \sum \phi_i - 180^\circ - l360^\circ \\ q\psi_{arr} &= \sum \phi_i - \sum \psi_i + 180^\circ + l360^\circ \end{aligned}$$

where q is the order of the pole or zero and l takes on q integer values so that the angles are between $\pm 180^\circ$. ψ_i is the angle of the line going from the i_{th} pole to the pole or zero whose angle of departure or arrival is being computed. Similarly, ϕ_i is the angle of the line from the i_{th} zero.

² \angle refers to the phase of ().

- STEP 5. If further refinement is required at the stability boundary, assume $s_0 = j\omega_0$ and compute the point(s) where the locus crosses the imaginary axis for positive K .
- STEP 6. For the case of multiple roots, two loci come together at 180° and break away at $\pm 90^\circ$. Three loci segments approach each other at angles of 120° and depart at angles rotated by 60° .
- STEP 7. Complete the locus, using the facts developed in the previous steps and making reference to the illustrative loci for guidance. The loci branches start at poles and end at zeros or infinity.
- STEP 8. Select the desired point on the locus that meets the specifications (s_o), then use the magnitude condition from Eq. (2.26) to find that the value of K associated with that point is

$$K = \frac{1}{|b(s_o)/a(s_o)|}.$$

When K is negative, the definition of the root locus in terms of the phase relationship is

0° locus definition: The root locus of $b(s)/a(s)$ is the set of points in the s -plane where the phase of $b(s)/a(s)$ is 0° .

For this case, the Steps above are modified as follows

STEP 2. Draw the locus on the real axis to the left of an *even* number of real poles plus zeros.

STEP 3. The asymptotes depart at

$$\phi_l = \frac{(l-1)360^\circ}{n-m}, \quad l = 1, 2 \dots n-m.$$

STEP 4. The locus departure and arrival angles are modified to

$$\begin{aligned} q\phi_{dep} &= \sum \psi_i - \sum \phi_i - 1360^\circ \\ q\psi_{arr} &= \sum \phi_i - \sum \psi_i + 1360^\circ. \end{aligned}$$

Note that the 180° term has been removed.

Root Locus Sketch

Example 2.1

Sketch the root locus versus K (positive and negative) for the case where the open-loop system is given by

$$G(s) = K \frac{s}{s^2 + 1}.$$

Solution. First let's do the 180° locus.

STEP 1. There is a zero at $s = 0$ and poles at $s = \pm j\omega$.

STEP 2. There is a locus on the entire negative real axis.

STEP 3. $n - m = 1$, therefore, there is one asymptote and it departs at 180° ; that is, along the negative real axis.

STEP 4. The departure angle at the upper pole is calculated as

$$\phi_1 = 90^\circ - 90^\circ - 180^\circ = -180^\circ,$$

thus, the locus departs from the upper pole horizontally to the left. The departure angle from the lower pole also turns out to be -180° and that branch of the locus also departs horizontally to the left.

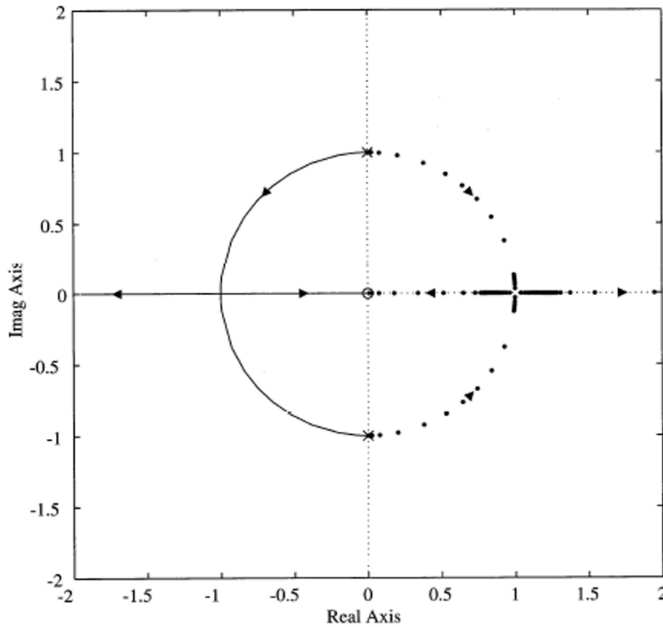


Figure 2.9
Example root
locus sketch

We know that there is a locus segment along the entire negative real axis; however, we also know that there is a locus branch moving to the right and arriving at the zero, and that there is a branch departing to infinity at the far left. Therefore, the two branches from the poles must join the real axis at some point and split in opposite directions. It turns out that the two complex branches form a semi-circle as they approach the real axis. The solid lines in Fig. 2.9 show the sketch of this 180° locus.

For the 0° locus, there is a segment along the positive real axis and the angles of departure are both 0° . The result is shown in the figure by the dotted lines.

2.3.3 Computer-Aided Loci

The most common approach to machine computation of the root locus is to cast the problem as a polynomial in the form $a(s) + Kb(s) = 0$, and, for a sequence of values of K varying from near zero to a large value, solve the polynomial for its n roots by any of many available numerical methods. A disadvantage of this method is that the resulting root locations are very unevenly distributed in the s -plane. For example, near a point of multiple roots, the sensitivity of the root locations to the parameter value is very great, and the roots just fly through such points, the plots appear to be irregular, and sometimes important features are missed. As a result, it is useful to have the root locus plotting rules in mind when interpreting computer plots. The polynomial is generally solved by transforming the problem to state-variable form and using the QR algorithm which solves for the eigenvalues of the closed-loop system matrix.

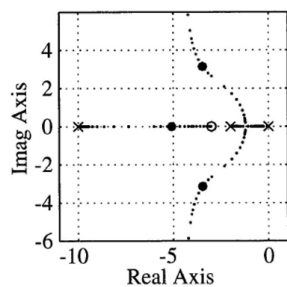
CACSD Root Locus

Example 2.2

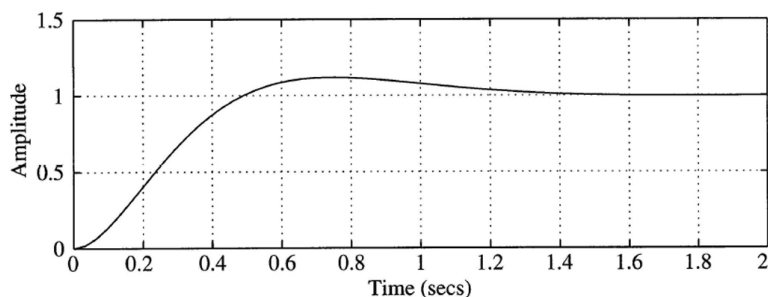
1. Plot the root locus using MATLAB for the open-loop system shown in Fig. 2.8 with

$$G(s) = \frac{10}{s(s+2)}, \quad \text{and} \quad D(s) = K \frac{s+3}{s+10}.$$

Figure 2.10
Example of
CACSD for (a)
root locus and
(b) step response



(a)



(b)

- Find the gain K for the given the compensator $D(s)$ associated with the point of maximum damping and plot the step response with that value of K .
- Reconcile the root locus plot with the hand plotting rules and compare the computer-based step response with the rules of thumb in Eqs. (2.16)–(2.18).

Solution.

- The MATLAB script following will generate the desired locus plot which is shown in Fig. 2.10(a).

```
s = tf('s')
sysG = 10/(s^2 + 2*s);
sysD = (s + 3)/(s + 10);
sys = sysG*sysD;
rlocus(sys)
```

- The statement

```
[K,p] = rlocfind(sys)
```

will place a cross-hair on the plot which can be moved with the mouse to the desired point on the locus in order to find the associated gain K and pole locations p . Given this value of K , ($\cong 3.7$) the script

```
K = 3.7
sysCL = feedback(K*sys,1)
step(sysCL)
```

produces the desired step response shown in Fig. 2.10(b).

3. The root locus in Fig. 2.10(a) has locus segments to the left of odd numbers of poles and zeros (Step 2); has two asymptotes departing at $\pm 90^\circ$ and centered at

$$\alpha = \frac{-2 + 3 - 10}{2} = -4.5,$$

(Step 3); and has branches departing the real axis at the multiple roots between the two poles at $\pm 90^\circ$ (Step 6). The gain associated with the desired root at $s = -3.5 \pm j3.1$ can be determined from Step 8 by

$$K = \frac{(4.7)(3.5)(7.2)}{(3.2)(10)} = 3.7$$

where 4.7 is the distance from the root to the pole at $s = 0$; 3.5 is the distance to the pole at $s = -2$; 7.2 is the distance to the pole at $s = -10$; 3.2 is the distance to the zero at $s = -3$; and 10 is from the gain of $G(s)$.

The step response shown in Fig. 2.10(b) has $t_r \cong 0.4$ sec, $t_s \cong 1.4$ sec, and $M_p \cong 10\%$. The closed-loop roots with $K = 3.7$ are at $s = -5.1, -3.5 \pm j3.1$; thus, for the complex roots, $\zeta = 0.74$, $\omega_n = 4.7$ rad/sec, and $\sigma = 3.5$. The rules of thumb given in Section 2.1.7 suggest that

$$\begin{aligned} t_r &\approx \frac{1.8}{\omega_n} = 0.38 \text{ sec} \\ t_s &\approx \frac{4.6}{\sigma} = 1.3 \text{ sec} \\ M_p &\approx e^{-\pi\zeta/\sqrt{1-\zeta^2}} = 4\% \quad (\text{Fig. 2.7}). \end{aligned}$$

The rule-of-thumb values based on the second order system with no zeros predict a t_r and t_s that are a little slow due to the presence of the extra pole. The predicted M_p is substantially too small due to the presence of the zero at $s = 3$.

2.4 Frequency Response Design

The response of a linear system to a sinusoidal input is referred to as the system's **frequency response**. A system described by

$$\frac{Y(s)}{U(s)} = G(s),$$

where the input $u(t)$ is a sine wave with an amplitude of U_o and frequency ω

$$u(t) = U_o \sin \omega_1 t,$$

which has a Laplace transform

$$U(s) = \frac{U_o \omega_1}{s^2 + \omega_1^2},$$

has a response with the transform,

$$Y(s) = G(s) \frac{U_o \omega_1}{s^2 + \omega_1^2}. \quad (2.27)$$

A partial fraction expansion of Eq. (2.27) will result in terms that represent the natural behavior of $G(s)$ and terms representing the sinusoidal input. Providing that all the natural behavior is stable, those terms will die out and the only terms left in the steady state are those due to the sinusoidal excitation, that is

$$Y(s) = \cdots + \frac{\alpha_o}{s + j\omega_1} + \frac{\alpha_o^*}{s - j\omega_1} \quad (2.28)$$

where α_o and α_o^* would be found by performing the partial fraction expansion. After the natural transients have died out, the time response is

$$y(t) = 2|\alpha_o| \sin(\omega_1 t + \phi) = U_o A \sin(\omega_1 t + \phi)$$

where

$$A = |G(j\omega_1)| = |G(s)| \Big|_{s=j\omega_1}, \quad (2.29)$$

$$\phi = \tan^{-1} \frac{\text{Im}[G(j\omega_1)]}{\text{Re}[G(j\omega_1)]} = \angle G(j\omega_1). \quad (2.30)$$

So, a stable linear system $G(s)$ excited by a sinusoid will eventually exhibit a sinusoidal output y with the same frequency as the input u . The **magnitude**, $A(\omega_1)$ of y with respect to the input, $= |G(j\omega_1)|$ and the **phase**, $\phi(\omega_1)$, is $\angle G(j\omega_1)$; that is, the magnitude and phase of $G(s)$ is evaluated by letting s take on values along the imaginary ($j\omega$) axis. In addition to the response to a sinusoid, the analysis of the frequency response of a system is very useful in the determination of stability of a closed-loop system given its open-loop transfer function.

A key reason that the frequency response is so valuable is that the designer can determine the frequency response experimentally with no prior knowledge of the system's model or transfer function. The system is excited by a sinusoid with varying frequency and the magnitude $A(\omega)$ is obtained by a measurement of the ratio of the output sinusoid to input sinusoid in the steady-state at each frequency. The phase $\phi(\omega)$ is the measured difference in phase between input and output signals. As an example, frequency responses of the second-order system

$$G(s) = \frac{1}{(s/\omega_n)^2 + 2\zeta(s/\omega_n) + 1}$$

are plotted for various values of ζ in Fig. 2.11 which is done by MATLAB with `bode(sys)`.

2.4.1 Specifications

A natural specification for system performance in terms of frequency response is the **bandwidth**, bandwidth defined to be the maximum frequency at which the output of a system will track an input sinusoid in a satisfactory manner. By convention, for the system shown in Fig. 2.12 with a sinusoidal input r , the bandwidth is the frequency of r at which the output y is attenuated to a factor of 0.707 times the input (or down 3 dB). Figure 2.13 depicts the idea graphically for the frequency response of the *closed-loop* transfer function (defined to be $\mathcal{T}(s)$ in Eq. (2.19))

$$\frac{Y(s)}{R(s)} = \mathcal{T}(s) = \frac{KG(s)}{1 + KG(s)}.$$

The plot is typical of most closed-loop systems in that 1) the output follows the input, $|\mathcal{T}| \cong 1$, at the lower excitation frequencies, and 2) the output ceases to follow the input, $|\mathcal{T}| < 1$, at the higher excitation frequencies.

The bandwidth ω_{BW} is a measure of the speed of response and is therefore similar to the time-domain measure of rise time t_r or the s -plane measure of natural frequency ω_n . In fact, it can be seen from Fig. 2.11 that the bandwidth will be equal to the natural frequency when $\zeta = 0.7$. For other damping ratios, the bandwidth is approximately equal to the natural frequency with an error typically less than a factor of 2.

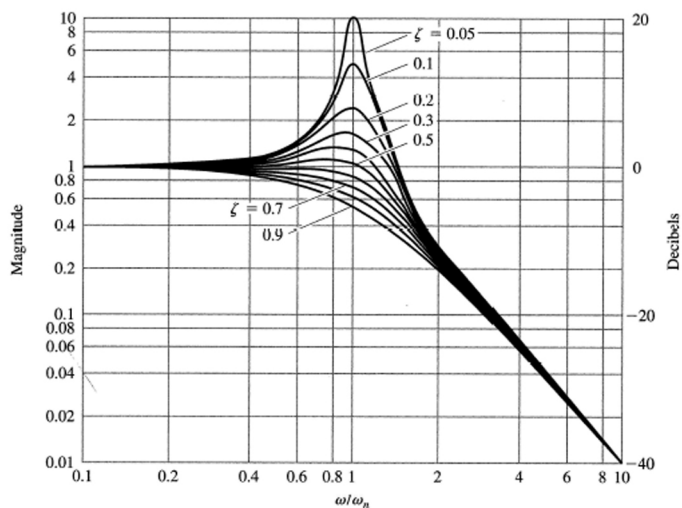
The resonant peak M_r is a measure of the damping, as evidenced by Fig. 2.11 where the peak is approximately the value at $\omega = \omega_n$, which is $\frac{1}{2\zeta}$ for $\zeta < 0.5$.

2.4.2 Bode Plot Techniques

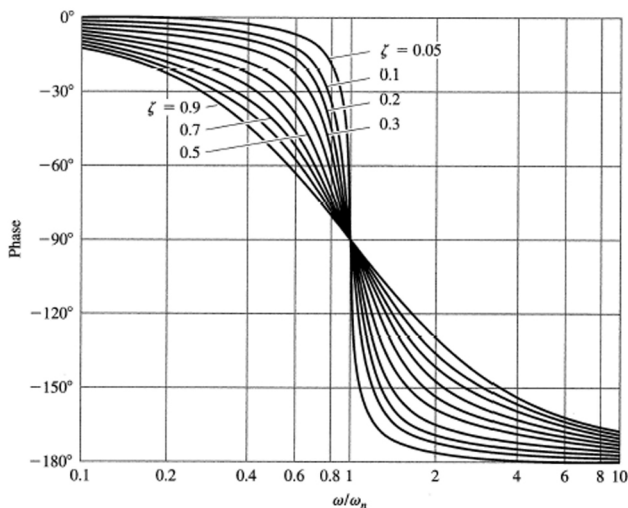
It is useful to be able to plot the frequency response of a system by hand in order to (a) design simple systems without the aid of a computer, (b) check computer-based results, and (c) understand the effect of compensation changes in design iterations. H. W. Bode developed plotting techniques in the 1930s that enabled quick hand plotting of the frequency response. His rules are:

STEP 1. Manipulate the transfer function into the **Bode form**

$$KG(j\omega) = K_o(j\omega)^n \frac{(j\omega\tau_1 + 1)(j\omega\tau_2 + 1) \cdots}{(j\omega\tau_a + 1)(j\omega\tau_b + 1) \cdots}$$



(a)



(b)

Figure 2.11
(a) Magnitude and (b) phase of a second-order system

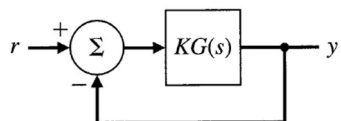


Figure 2.12
Simplified system definition

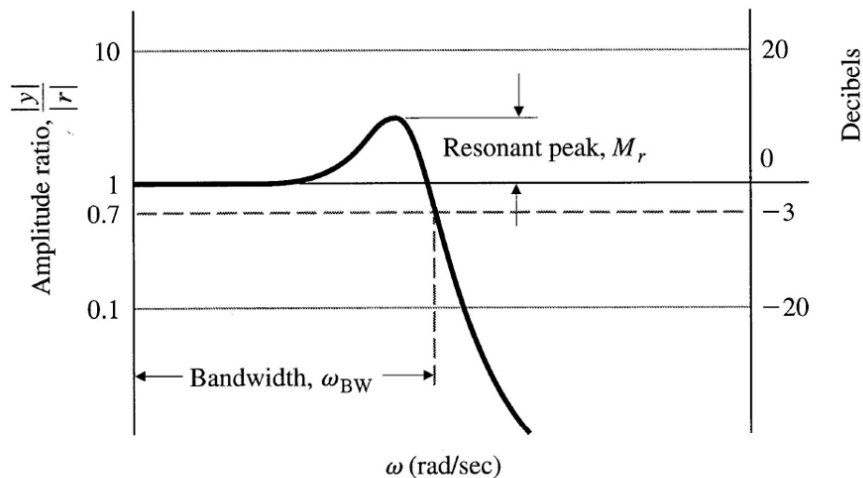


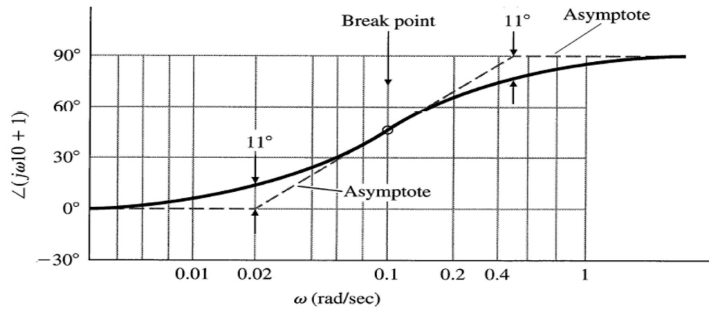
Figure 2.13
Definitions of
bandwidth and
resonant peak

- STEP 2. Determine the value of n for the $K_o(j\omega)^n$ term. Plot the low-frequency magnitude asymptote through the point K_o at $\omega = 1$ rad/sec with a slope of n (or $n \times 20$ dB per decade).
- STEP 3. Determine the **break points** where $\omega = 1/\tau_i$. Complete the composite magnitude asymptotes by extending the low frequency asymptote until the first frequency break point, then stepping the slope by ± 1 or ± 2 , depending on whether the break point is from a first or second order term in the numerator or denominator, and continuing through all break points in ascending order.
- STEP 4. Sketch in the approximate magnitude curve by increasing from the asymptote by a factor of 1.4 (+3 dB) at first order numerator breaks and decreasing it by a factor of 0.707 (−3 dB) at first order denominator breaks. At second order break points, sketch in the resonant peak (or valley) according to Fig. 2.11(a) using the relation that $|G(j\omega)| = 1/(2\zeta)$ at the break.
- STEP 5. Plot the low frequency asymptote of the phase curve, $\phi = n \times 90^\circ$.
- STEP 6. As a guide, sketch in the approximate phase curve by changing the phase gradually over two decades by $\pm 90^\circ$ or $\pm 180^\circ$ at each break point in ascending order. For first order terms in the numerator, the gradual change of phase is $+90^\circ$; in the denominator, the change is -90° . For second order terms, the change is $\pm 180^\circ$.
- STEP 7. Locate the asymptotes for each individual phase curve so that their phase change corresponds to the steps in the phase from the approximate curve indicated by Step 6. Sketch in each individual phase curve as indicated by Fig. 2.14 or Fig. 2.11(b).
- STEP 8. Graphically add each phase curve. Use dividers if an accuracy of about $\pm 5^\circ$ is desired. If lesser accuracy is acceptable, the composite curve can be done by eye, keeping in mind that the curve will start at the lowest frequency asymptote and end on the highest frequency asymptote, and will approach the intermediate asymptotes to an extent that is determined by the proximity of the break points to each other.

2.4.3 Steady-State Errors

Section 2.2.2 showed that the steady-state error of a feedback system decreases as the gain of the open loop transfer function increases. In plotting a composite magnitude curve, the low frequency

Figure 2.14
Phase plot for
 $j\omega\tau + 1$; $\tau = 0.1$



asymptote is given by

$$KG(j\omega) = K_o(j\omega)^n. \quad (2.31)$$

Therefore, we see that the larger the value of the magnitude on the low-frequency asymptote, the lower the steady-state errors will be for the closed loop system. This idea is very useful in designing compensation.

For a system with $n = 0$, (a type 0 system) the low frequency asymptote is a constant and the gain K_o of the open loop system is equal to the position error constant, K_p . For a system where $n = -1$, (a type 1 system) the low frequency asymptote has a slope of -1 and $K_v = K_o$.

The easiest way of determining the value of K_v in a type 1 system is to read the magnitude of the low frequency asymptote at a frequency low enough to be well below the any of the break points because $\frac{K_v}{\omega}$ equals the magnitude at these frequencies. In some cases, the lowest frequency break point will be below $\omega = 1$ rad/sec, therefore the asymptote can be extended to $\omega = 1$ rad/sec in order to read K_v directly.

2.4.4 Stability Margins

If the closed-loop transfer function of a system is known, the stability of the system can be determined by simply inspecting the denominator in factored form to observe whether the real parts are positive or negative. However, the closed-loop transfer function is not usually known; therefore, we would like to determine closed-loop stability by evaluating the frequency response of the *open-loop* transfer function $KG(j\omega)$ and then performing a simple test on that response. This can be done without a math model of the system by experimentally determining the open-loop frequency response.

We saw in Section 2.3.1 that all points on the root locus have the property that

$$|KG(s)| = 1 \quad \text{and} \quad \angle(KG(s)) = 180^\circ.$$

At the point of neutral stability we see that these root-locus conditions hold for $s = j\omega$, so

$$|KG(j\omega)| = 1 \quad \text{and} \quad \angle(KG(j\omega)) = 180^\circ. \quad (2.32)$$

Thus a Bode plot of a system that is neutrally stable (that is, with the value of K such that the closed-loop roots fall on the imaginary axis) will satisfy the conditions of Eq. (2.32). That means that the magnitude plot must equal 1 at the same frequency that the phase plot equals 180° . Typically, a system becomes less stable as the gain increases; therefore, we have the condition for stability

$$|KG(j\omega)| < 1 \quad \text{at} \quad \angle(KG(j\omega)) = -180^\circ. \quad (2.33)$$

This stability criterion holds for all systems where increasing gain leads to instability and $|KG(j\omega)|$ crosses the magnitude = 1 once, the most common situation. However, there are systems where an increasing gain can lead from instability to stability and in this case, the stability condition is

$$|KG(j\omega)| > 1 \quad \text{at} \quad \angle(KG(j\omega)) = -180^\circ.$$

One way that will frequently resolve the ambiguity is to perform a rough sketch of the root locus to resolve the question of whether increasing gain leads to stability or instability. The rigorous way to resolve the ambiguity is to use the Nyquist stability criterion, which is reviewed in Section 7.5.1 for continuous systems.

Two quantities that measure the stability margin of a system are directly related to the stability criterion of Eq. (2.33): gain margin and phase margin. The **gain margin** (GM) is the factor by which the gain is less than the neutral stability value when the phase = 180° . The **phase margin** (PM) is the amount by which the phase of $G(s)$ exceeds -180° when $|KG(j\omega)| = 1$. The two margins are alternate ways of measuring the degree to which the stability conditions of Eq. (2.33) are met.

The phase margin is generally related to the damping of a system. For a second-order system, the approximation that

$$\zeta \cong \frac{\text{PM}}{100}$$

is commonly used. Therefore, if it were known that a system was to be designed using frequency response methods, it would make sense to specify the speed of response of the system in terms of a required bandwidth and the stability of the system in terms of a required phase margin.

2.4.5 Bode's Gain-Phase Relationship

One of Bode's important contributions is his theorem that states

For any minimum phase system (that is, one with no time delays, RHP zeros or poles), the phase of $G(j\omega)$ is uniquely related to the integral of the magnitude of $G(j\omega)$.

When the slope of $|G(j\omega)|$ versus ω on a log-log scale persists at a constant value for nearly a decade of frequency, the relationship is particularly simple

$$\angle G(j\omega) \cong n \times 90^\circ, \quad (2.34)$$

where n is the slope of $|G(j\omega)|$ in units of decade of amplitude per decade of frequency.

Equation (2.34) is used as a guide to infer stability from $|G(j\omega)|$ alone. When $|KG(j\omega)| = 1$, the **crossover frequency**, the phase

$$\begin{aligned} \angle G(j\omega) &\cong -90^\circ && \text{if } n = -1, \\ \angle G(j\omega) &\cong -180^\circ && \text{if } n = -2. \end{aligned}$$

For stability we want $\angle G(j\omega) > -180^\circ$ for a PM > 0 . Therefore we adjust the $|KG(j\omega)|$ curve so that it has a slope of -1 at the crossover frequency. If the slope is -1 for a decade above and below the crossover frequency, the PM would be approximately 90° ; however, to ensure a reasonable PM, it is usually only necessary to insist on a -1 slope (-20 dB per decade) persisting for a decade in frequency that is centered at the crossover frequency.

2.4.6 Design

One of the very useful aspects of frequency-response design is the ease with which we can evaluate the effects of gain changes. In fact, we can determine the PM for any value of K without redrawing the magnitude or phase information. We need only indicate on the figure where $|KG(j\omega)| = 1$ for selected trial values of K since varying K has the effect of sliding the magnitude plot up or down.

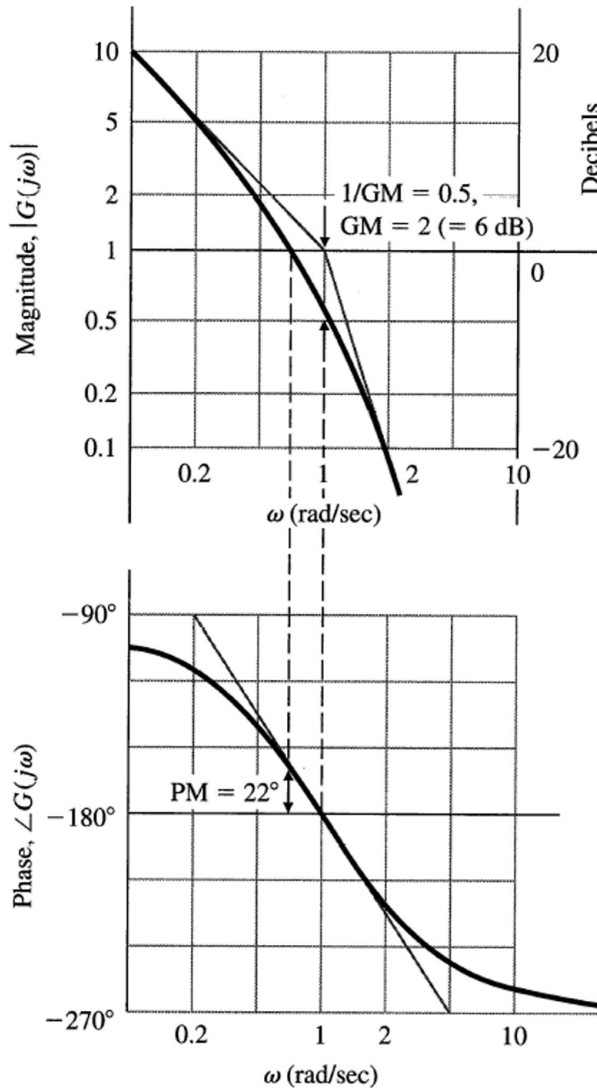


Figure 2.15
Magnitude and phase plots with PM and GM for $1/s(s+1)^2$

Frequency-Response Design

Example 2.3

For a plant given by

$$G(s) = K \frac{1}{s(s+1)^2},$$

determine the PM and GM for the system with unity feedback and (a) $K = 1$, (b) determine if the system is stable if $K = 5$, and (c) find what value of K is required to achieve a PM of (i) 45° , and (ii) 70° .

Solution. Using the hand plotting rules, we see that the low frequency asymptote has a slope of -1 and goes thru magnitude = 1 at $\omega = 1$ rad/sec. The slope changes to -3 at the break point ($\omega = 1$). We can then sketch in the actual magnitude curve, noting (STEP 4 in Section 2.4.2) that it will go below the asymptote intersection by -6 dB because there is a slope change of -2 at that break point. The curve is sketched in Fig. 2.15. The phase curve starts out at -90° and drops to -270° along the asymptote as sketched in the figure according to STEP 7.

Using MATLAB, the statements

```
num = 1, den = [1 2 1 0]
sys = tf(num,den)
```

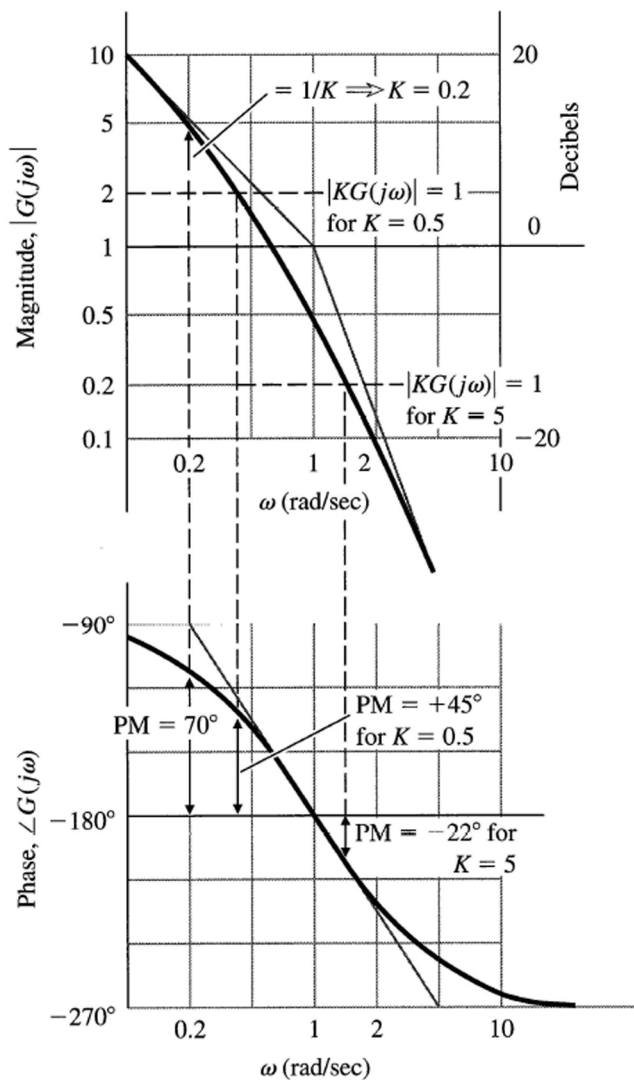


Figure 2.16
PM versus K for
 $1/(s+1)^2$

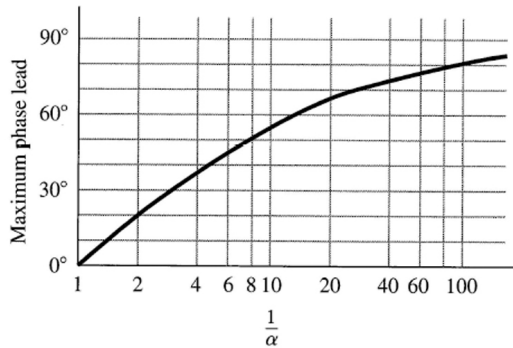


Figure 2.17
Maximum phase increase for lead compensation

bode(sys)

will also create the plots of magnitude and phase for this example. The curves are drawn in Fig. 2.15 showing the PM and GM for $K = 1$ and the same curves are drawn in Fig. 2.16 showing the PM's for $K = 5, 0.5, \& 0.2$.

- We can read the PM from Fig. 2.15 to be 22° .
- Fig. 2.16 shows that the system is unstable for $K = 5$.
- (i) PM = 45° when $K = 0.5$, and (ii) PM = 70° when $K = 0.2$

2.5 Compensation

If the plant dynamics are of such a nature that a satisfactory design cannot be achieved by adjustment of the feedback gain alone, then some modification or **compensation** must be made in the feedback to achieve the desired specifications. Typically, it takes the form

$$D(s) = K \frac{s+z}{s+p}$$

where it is called **lead compensation** if $z < p$ and **lag compensation** if $z > p$. Lead compensation approximates the addition of a derivative control term and tends to increase the bandwidth and the speed of response while decreasing the overshoot. Lag compensation approximates integral control and tends to improve the steady-state error.

The design of lead compensation typically entails placing the zero z at a frequency that is lower than the magnitude = 1 crossover frequency and the pole higher than the crossover frequency. Lead compensation provides an increased magnitude slope and an increased phase in the interval between these two break points; the maximum being halfway between the two break points on a logarithmic scale. The maximum phase increase is

$$\delta\phi = \sin^{-1} \frac{1-\alpha}{1+\alpha} \quad \text{where} \quad \alpha = \frac{z}{p}$$

and is plotted versus α in Fig. 2.17.

The design of lag compensation typically entails placing both break points well below the crossover frequency. Lag compensation decreases the phase in the vicinity of the two break points; therefore, z should be well below the crossover frequency in order to prevent the compensation from degrading the PM and the system stability. The primary role of lag compensation is to increase the gain (magnitude of the frequency response) at the low frequencies. As we saw in Section 2.4.3, this will decrease the steady-state error.

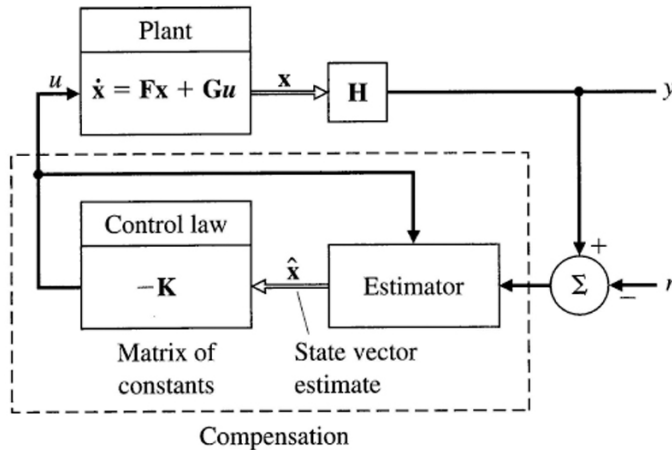


Figure 2.18
Schematic
diagram of
state-space
design elements

2.6 State-Space Design

We saw in Section 2.1.1 that equations of motion could be written in the state-variable form of Eqs. (2.1) and (2.2). The **state-space** design approach utilizes this way of describing the plant and arrives directly with feedback controllers (compensation) without the need to determine transforms. Advantages of state-space design are especially apparent when the system to be controlled has more than one control input or more than one sensed output, called multivariable or multi input-multi output (MIMO). However, we will review only the single input-single output (SISO) case here. For readers not familiar with state-space design, the material in this section is not required for comprehension of the remainder of the book. The basic ideas of state-space design are covered in detail in Chapter 8 for the discrete case and that chapter does not require that the reader be knowledgeable about continuous state-space design. Chapter 9 extends state-space design for discrete systems to optimal control design for the multivariable case.

One of the attractive features of the state-space design method is that it consists of a sequence of independent steps. The first step, discussed in Section 2.6.1, is to determine the control. The purpose of the control law is to allow us to design a set of pole locations for the closed-loop system that will correspond to satisfactory dynamic response in terms of rise-time, overshoot, or other measures of transient response.

The second step—necessary if the full state is not available—is to design an **estimator** (sometimes called an **observer**), which computes an estimate of the entire state vector when provided with the measurements of the system indicated by Eq. (2.2). We review estimator design in Section 2.6.2.

The third step consists of combining the control law and the estimator. Figure 2.18 shows how the control law and the estimator fit together and how the combination takes the place of what we have been previously referring to as compensation.

The fourth and final step is to introduce the reference input in such a way that the plant output will track external commands with acceptable rise-time, overshoot and settling time values. Figure 2.18 shows the command input r introduced in the same relative position as was done with the transform design methods; however, in Section 2.6.4 we will show how to introduce the reference input in a different way that results in a better system response.

2.6.1 Control Law

The first step is to find the control law as feedback of a linear combination of all the state variables—that is,

$$u = -\mathbf{K}\mathbf{x} = -[K_1 K_2 \cdots K_n] \begin{bmatrix} x_1 \\ x_2 \\ \vdots \\ x_n \end{bmatrix}. \quad (2.35)$$

We *assume* for design purposes that all the elements of the state vector are at our disposal, an infrequent situation for an actual system, but an expedient assumption for the time being.

pole placement

For an n th-order system there will be n feedback gains K_1, \dots, K_n , and since there are n roots (or *poles*) of the system, it is possible that there are enough degrees of freedom to select *arbitrarily* any desired root location by choosing the proper values of K_j .

Substituting the feedback law, Eq. (2.35) into the system described by Eq. (2.1) yields

$$\dot{\mathbf{x}} = \mathbf{F}\mathbf{x} - \mathbf{G}\mathbf{K}\mathbf{x}. \quad (2.36)$$

The characteristic equation of this closed-loop system is

$$\det[s\mathbf{I} - (\mathbf{F} - \mathbf{G}\mathbf{K})] = 0. \quad (2.37)$$

When evaluated, this yields an n th-order polynomial in s containing the gains K_1, \dots, K_n . The control-law design then consists of picking the gains \mathbf{K} so that the roots of Eq. (2.37) are in desirable locations. Selection of desirable locations for the roots is an inexact science and may require some iteration by the designer. For now, we will assume that the desired locations are known, say

$$s = s_1, s_2, \dots, s_n.$$

Then the corresponding desired (control) characteristic equation is

$$\alpha_c(s) = (s - s_1)(s - s_2) \cdots (s - s_n) = 0. \quad (2.38)$$

Hence the required elements of \mathbf{K} are obtained by matching coefficients in Eq. (2.37) and Eq. (2.38). This forces the system characteristic equation to be identical with the desired characteristic equation and the closed-loop poles to be placed at the desired locations.

The calculation of \mathbf{K} can be done providing the system is **controllable**. Systems that are not controllable have certain modes or subsystems that are unaffected by the control. This usually means that parts of the system are physically disconnected from the input. Although there is a mathematical test for controllability, it is good practice to insist on the stronger condition that the control input be as strongly coupled to the modes of interest as possible.

controllability

It is theoretically possible to solve for \mathbf{K} by hand with Eq. (2.37) and Eq. (2.38). In practice, this is almost never done. Ackermann's formula for this calculation has been implemented in MATLAB as the function `acker.m` and can be used for the design of SISO systems with a small (≤ 10) number of state variables. For more complex cases a more reliable formula is available, implemented in MATLAB as the function `place.m`. A modest limitation on `place` is that none of the desired closed-loop poles are repeated; i.e., that the poles are *distinct*, a requirement that does not apply to `acker`. Both `acker` and `place` require inputs consisting of the system description matrices, \mathbf{F} and \mathbf{G} , and a vector, \mathbf{p} , of n desired pole locations. Their output is the feedback gain \mathbf{K} . Thus the MATLAB statements

$$\mathbf{K} = \text{acker}(\mathbf{F}, \mathbf{G}, \mathbf{p}) \quad \text{or}$$

$$\mathbf{K} = \text{place}(\mathbf{F}, \mathbf{G}, \mathbf{P})$$

will provide the desired value of \mathbf{K} . When selecting the desired root locations, it is always useful to keep in mind that the control effort required is related to how far the open-loop poles are moved by the feedback. Furthermore, when a zero is near a pole, the system may be nearly uncontrollable and

moving such a pole may require large control effort. Therefore, a pole placement philosophy that aims to fix only the undesirable aspects of the open-loop response and avoids either large increases in bandwidth or efforts to move poles that are near zeros will typically allow smaller gains and thus smaller control actuators.

A method called the **linear quadratic regulator (LQR)** specifically addresses the issue of achieving a balance between good system response and the control effort required. The method consists of calculating the gain K that minimizes a **cost function**

LQR
optimal control

$$\mathcal{J} = \int_0^{\infty} [\mathbf{x}^T \mathbf{Q} \mathbf{x} + \mathbf{u}^T \mathbf{R} \mathbf{u}] dt \quad (2.39)$$

where \mathbf{Q} is an $n \times n$ state weighting matrix, \mathbf{R} is an $m \times m$ control weighting matrix, and m is the number of control inputs in a multi-input system. For the SISO systems that we are primarily concerned with here, $m = 1$ and \mathbf{R} is a scalar R . The weights \mathbf{Q} and R are picked by the designer by trial-and-error in order to arrive at the desired balance between state errors $\mathbf{x}^T \mathbf{x}$ and control usage u^2 , thus avoiding the necessity of picking desired pole locations that do not use excessive control. Generally, \mathbf{Q} is a diagonal matrix with a weighting factor on one or more of the state-vector elements while $R = 1$. It is perfectly acceptable to only weight one element, in fact, the element representing the system output is often the only element weighted. Rules of thumb that help in picking the weights are that (1) the bandwidth of the system increases as overall values in \mathbf{Q} increase, (2) the damping increases as the term in \mathbf{Q} that weights the velocity type state elements increase, and (3) a portion of a system can be made faster by increasing the weights on the state elements representing that portion of the system. The MATLAB statement

$$K = \text{lqr}(F, G, Q, R)$$

solves for the \mathbf{K} that minimizes the cost, \mathcal{J} .

State-Space Control Design

Example 2.4

For a plant given by

$$G(s) = \frac{1}{s^2},$$

- Find the feedback gain matrix \mathbf{K} that yields closed-loop roots with $\omega_n = 3$ rad/sec and $\zeta = 0.8$.
- Investigate the roots obtained by using LQR with

$$\mathbf{Q} = \begin{bmatrix} 1 & 0 \\ 0 & 0 \end{bmatrix}, \quad \begin{bmatrix} 100 & 0 \\ 0 & 0 \end{bmatrix}, \quad \text{and} \quad \begin{bmatrix} 100 & 0 \\ 0 & 5 \end{bmatrix}$$

and $R = 1$.

Solution. The state-variable description of $G(s)$ is (Eq. (2.4) with $\omega_o = 0$, $\zeta = 0$, and $K_o = 1$)

$$\mathbf{F} = \begin{bmatrix} 0 & 1 \\ 0 & 0 \end{bmatrix}, \quad \mathbf{G} = \begin{bmatrix} 0 \\ 1 \end{bmatrix}$$

$$\mathbf{H} = [1 \ 0], \quad J = 0.$$

- The desired characteristic equation is

$$\alpha_c(s) = s^2 + 2\zeta\omega_n s + \omega_n^2 = 0.$$

Therefore, the MATLAB script

$$F = [0 \ 1; 0 \ 0]$$

$$G = [0; 1]$$

```

Wn = 3
Ze = 0.8
p = roots([1 2*Wn*Ze Wn^2])
K = acker(F,G,p)

```

provides the answer

$$\mathbf{K} = [9 \quad 4.8].$$

(b) The scripts

```

Q = [1 0; 0 0],      [100 0; 0 0],      and      [100 0; 0 5]
R = 1
K = lqr(F,G,Q,R)
p = eig(F - G*K)
[Wn,Ze] = damp(p)

```

compute feedback gains of

$$\mathbf{K} = [1 \quad 1.4], \quad [10 \quad 4.5], \quad \text{and} \quad [10 \quad 5].$$

which produces natural frequencies of

$$\omega_n = 1, \quad 3.2, \quad \text{and} \quad 3.2 \text{ rad/sec}$$

and damping of

$$\zeta = 0.71, \quad 0.71, \quad \text{and} \quad 0.79.$$

For this simple example, use of `acker` is the easier way to find \mathbf{K} ; however, in more complex systems with higher order roots, it is easier to use `lqr` rather than iterate on the best value for all the roots.

2.6.2 Estimator Design

For a system described by Eqs. (2.1) and (2.2), an estimate, $\hat{\mathbf{x}}$, of the full state vector, \mathbf{x} , can be obtained based on measurements of the output, y , from

$$\dot{\hat{\mathbf{x}}} = \mathbf{F}\hat{\mathbf{x}} + \mathbf{G}u + \mathbf{L}(y - \mathbf{H}\hat{\mathbf{x}}). \quad (2.40)$$

Here \mathbf{L} is a proportional gain defined as

$$\mathbf{L} = [l_1, l_2, \dots, l_n]^T, \quad (2.41)$$

and is chosen to achieve satisfactory error characteristics. The dynamics of the error can be obtained by subtracting the estimate (Eq. 2.40) from the state (Eq. 2.1), to get the error equation

$$\dot{\tilde{\mathbf{x}}} = (\mathbf{F} - \mathbf{L}\mathbf{H})\tilde{\mathbf{x}}. \quad (2.42)$$

The characteristic equation of the error is now given by

$$\det[s\mathbf{I} - (\mathbf{F} - \mathbf{L}\mathbf{H})] = 0. \quad (2.43)$$

We choose \mathbf{L} so that $\mathbf{F} - \mathbf{L}\mathbf{H}$ has stable and reasonably fast eigenvalues, so $\tilde{\mathbf{x}}$ decays to zero, independent of the control $u(t)$ and the initial conditions. This means that $\hat{\mathbf{x}}(t)$ will converge to $\mathbf{x}(t)$.

Errors in the model of the plant (\mathbf{F} , \mathbf{G} , \mathbf{H}) cause additional errors to the state estimate from those predicted by Eq. (2.42). However, \mathbf{L} can typically be chosen so that the error is kept acceptably small. It is important to emphasize that the nature of the plant and the estimator are quite different. The plant is a physical system such as a chemical process or servomechanism whereas the estimator is usually an electronic unit computing the estimated state according to Eq. (2.40).

The selection of \mathbf{L} is approached in exactly the same fashion as \mathbf{K} is selected in the control-law design. If we specify the desired location of the estimator error poles as

$$s_i = \beta_1, \beta_2, \dots, \beta_n,$$

then the desired estimator characteristic equation is

$$\alpha_e(s) \triangleq (s - \beta_1)(s - \beta_2) \cdots (s - \beta_n). \quad (2.44)$$

We can solve for \mathbf{L} by comparing coefficients in Eq. (2.43) and Eq. (2.44).

As in the control case, this is almost never done by hand. Rather, the functions `acker.m` and `place.m` are used, but with a slight twist. The transpose of Eq. (2.43) is

$$\det[s\mathbf{I} - (\mathbf{F}^T - \mathbf{H}^T\mathbf{L}^T)] = 0, \quad (2.45)$$

and we now see that this is identical in form to Eq. (2.37) where \mathbf{K} and \mathbf{L}^T play the same role. Therefore, we compute \mathbf{L} to achieve estimator poles at the desired location, \mathbf{p} , by typing in MATLAB

```
L = acker(F',H',p) ' or
```

```
L = place(F',H',p) '
```

where \mathbf{F}^T is indicated in MATLAB as `F'`, etc.

There will be a unique solution for \mathbf{L} for a SISO system provided that the system is **observable**.
Roughly speaking, observability refers to our ability to deduce information about all the modes of the system by monitoring only the sensed outputs. Unobservability results when some mode or subsystem has no effect on the output. observability

The selection of the estimator poles that determine \mathbf{L} are generally chosen to be a factor of 2 to 6 faster than the controller poles. This ensures a faster decay of the estimator errors compared with the desired dynamics, thus causing the controller poles to dominate the total system response. If sensor noise is particularly large, it sometimes makes sense for the estimator poles to be slower than two times the controller poles, which would yield a system with lower bandwidth and more noise smoothing. On the other hand, the penalty in making the estimator poles too fast is that the system becomes more noise sensitive.

The tradeoff between fast and slow estimator roots can also be made using results from **optimal estimation theory**. First, let's consider that there is a random input affecting the plant, called **process noise**, w , that enters Eq. (2.1) as optimal estimation

$$\dot{\mathbf{x}} = \mathbf{F}\mathbf{x} + \mathbf{G}u + \mathbf{G}_1w, \quad (2.46)$$

and a random **sensor noise**, v entering Eq. (2.1) as

$$y = \mathbf{H}\mathbf{x} + v. \quad (2.47)$$

The estimator error equation with these additional inputs is

$$\dot{\tilde{\mathbf{x}}} = (\mathbf{F} - \mathbf{L}\mathbf{H})\tilde{\mathbf{x}} + \mathbf{G}_1w - \mathbf{L}v. \quad (2.48)$$

In Eq. (2.48) the sensor noise is multiplied by \mathbf{L} and the process noise is not. If \mathbf{L} is very small, then the effect of sensor noise is removed but the estimator's dynamic response will be "slow", so the error will not reject effects of w very well. The state of a low-gain estimator will not track uncertain plant inputs very well or plants with modeling errors. On the other hand, if \mathbf{L} is "large", then the estimator response will be fast and the disturbance or process noise will be rejected, but the sensor noise, multiplied by \mathbf{L} , results in large errors. Clearly, a balance between these two effects is required.

It turns out that the optimal solution to this balance can be found as a function of the process noise intensity, R_w , and the sensor noise intensity, R_v , both of which are scalars for the SISO case under consideration. Since the only quantity affecting the result is the ratio R_w/R_v , it makes sense to let $R_v = 1$ and vary R_w only. An important advantage of using the optimal solution is that only one parameter, R_w , needs to be varied by the designer rather than picking n estimator poles for an n^{th} -order system. The solution is calculated by MATLAB as

```
L = kalman(sys,Rw,Rv) .
```

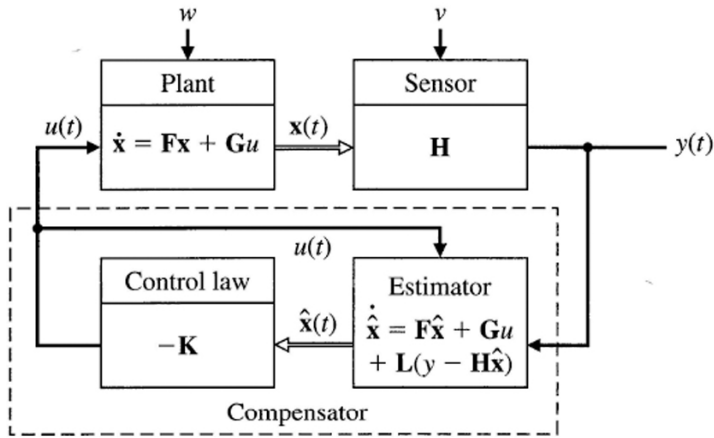


Figure 2.19
Estimator and
controller
mechanization

2.6.3 Compensation: Combined Control and Estimation

We now put all this together, ignoring for the time being the effect of a command input, r . If we take the control law (Eq. 2.35), combine it with the estimator (Eq. 2.40), and implement the control law using the estimated state elements, the design is complete and the equations describing the result are

$$\begin{aligned}\dot{\hat{x}} &= (\mathbf{F} - \mathbf{GK} - \mathbf{LH})\hat{x} + \mathbf{L}y, \\ u &= -\mathbf{K}\hat{x}.\end{aligned}\quad (2.49)$$

These equations describe what we previously called compensation; that is, the control, u , is calculated given the measured output, y . Figure 2.19 shows schematically how the pieces fit together. The roots of this new closed-loop system can be shown to consist of the chosen roots of the controller plus the chosen roots of the estimator that have been designed in separate procedures in Sections 2.6.1 and 2.6.2. The poles and zeros of the compensator alone could be obtained by examining the system described by Eq. (2.49); however, that step need not be carried out unless the designer is curious how the compensation from this approach compares with compensation obtained using a transform based design method.

2.6.4 Reference Input

One obvious way to introduce a command input is to subtract y from r in exactly the same way it has been done for the transform design methods discussed previously. This scheme is shown schematically in Fig. 2.20(b). Using this approach, a step command in r enters directly into the estimator, thus causing an estimation error that decays with the estimator dynamic characteristics in addition to the response corresponding to the control poles.

An alternative approach consists of entering the command r directly into the plant and estimator in an identical fashion as shown in Fig. 2.20(a). Since the command creates a step in u that affects the plant and estimator in an identical fashion, both respond identically, and no estimator error is induced. Therefore, there are no estimator error characteristics in the response and the total response consists of controller characteristics only. This approach is usually superior.

The feedforward gain, \bar{N} , can be computed so that no steady-state error exists. Its value is based on computing the steady-state value of the control, u_{ss} , and the steady-state values of the state, \mathbf{x}_{ss} , that result in no steady-state error, e . The result is

$$\bar{N} = N_u + \mathbf{K}\mathbf{N}_x \quad (2.50)$$

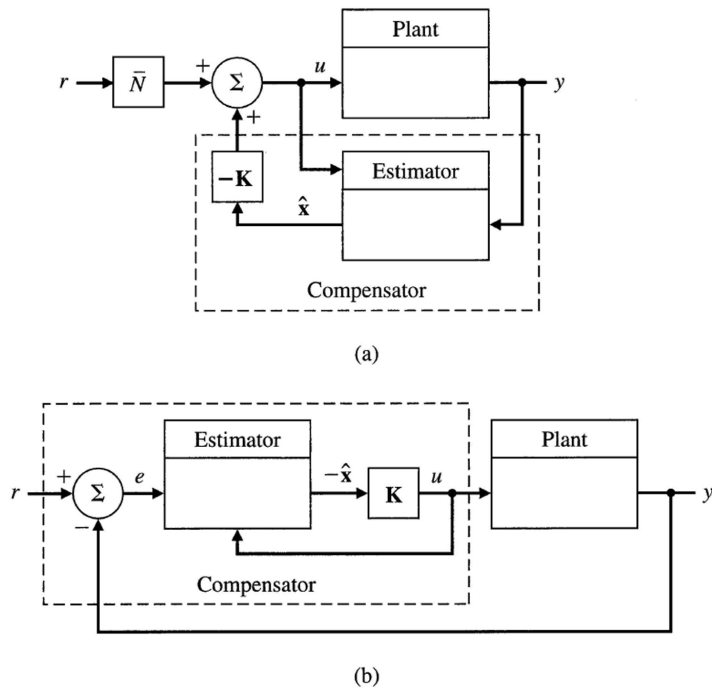


Figure 2.20
Possible locations for introducing the reference input:
(a) compensation in the feedback path,
(b) compensation in the feedforward path

where

$$\begin{bmatrix} N_x \\ N_u \end{bmatrix} = \begin{bmatrix} \mathbf{F} & \mathbf{G} \\ \mathbf{H} & J \end{bmatrix}^{-1} \begin{bmatrix} \mathbf{0} \\ 1 \end{bmatrix}.$$

2.6.5 Integral Control

In many cases, it is difficult to obtain an accurate value for the plant gain, in part because plants are typically nonlinear and the plant model is a linearization at a particular point. Therefore, the value of \bar{N} will not be accurate and steady-state errors will result even though the model is sufficiently accurate for good feedback control design. The solution is to incorporate an integral control term in the feedback similar to the integral control discussed in Section 2.2.3.

Integral control is accomplished using state-space design by augmenting the state vector with the desired integral x_I . It obeys the differential equation

$$\dot{x}_I = \mathbf{H}\mathbf{x} - r \quad (= e).$$

Thus

$$x_I = \int^t e dt.$$

This equation is augmented to the state equations (Eq. 2.1) and they become

$$\begin{bmatrix} \dot{x}_I \\ \dot{\mathbf{x}} \end{bmatrix} = \begin{bmatrix} 0 & \mathbf{H} \\ 0 & \mathbf{F} \end{bmatrix} \begin{bmatrix} x_I \\ \mathbf{x} \end{bmatrix} + \begin{bmatrix} 0 \\ \mathbf{G} \end{bmatrix} u - \begin{bmatrix} 1 \\ \mathbf{0} \end{bmatrix} r. \quad (2.51)$$

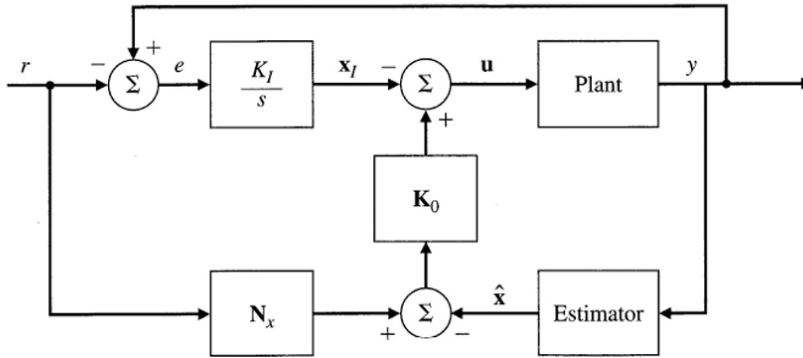
The feedback law is

$$u = - \begin{bmatrix} K_1 & \mathbf{K}_0 \end{bmatrix} \begin{bmatrix} x_I \\ \mathbf{x} \end{bmatrix},$$

or simply

$$u = -\mathbf{K} \begin{bmatrix} x_I \\ \mathbf{x} \end{bmatrix}.$$

Figure 2.21
Integral control
structure



With this revised definition of the system, the design techniques from Section 2.6.1 can be applied in a similar fashion. The elements of \mathbf{K} obtained are implemented as shown in Fig. 2.21.

2.7 Summary

- System dynamics can be represented by a state-space description, Eq. (2.1), or by a transfer function, Eqs. (2.6) or (2.7).
- The key property of the Laplace transform that allows solution of differential equations is Eq. (2.5)

$$\mathcal{L}\{\dot{f}(t)\} = sF(s).$$

- A system's output can be determined by the inverse Laplace transform for very simple cases or, more often the case, by numerical methods such as `impulse.m`, `step.m`, or `lsim.m` in MATLAB.
- If a system's output is described by $X(s)$ and is stable, the Final Value Theorem states that

$$\lim_{t \rightarrow \infty} x(t) = x_{ss} = \lim_{s \rightarrow 0} sX(s).$$

- One can associate certain time response behavior with pole locations in the s -plane as summarized in Fig. 2.5.
- Control system specifications are usually defined in terms of the rise time t_r , settling time t_s , and overshoot M_p which are defined by Eqs. (2.16)–(2.18).
- For an open loop system given by $D(s)G(s)$, the closed loop system as defined by Fig. 2.8 is given by Eq. (2.19)

$$\frac{Y(s)}{R(s)} = \frac{D(s)G(s)}{1 + D(s)G(s)} = \mathcal{T}(s).$$

- The basic types of feedback are proportional, integral, and derivative, and are defined by Eqs. (2.22)–(2.24).

- The root locus is a method to sketch the location of the closed-loop roots of a system vs. some parameter of interest, usually the feedback gain. It is based on phase considerations which can easily be determined graphically by hand, and are therefore very useful in checking computer based results.
- The frequency response of the open-loop transfer function of a system can be easily analyzed to determine the stability of the related closed-loop system. The open-loop transfer function can be determined experimentally or analytically.
- Design of control systems using the state space approach is carried out by specifying the desired closed-loop root location, called pole-placement, or by selecting weighting matrices in a cost function, called optimal or LQR control. Either method tends to reduce the design iterations required over root locus or frequency response design, especially for higher order systems and those with multiple inputs and/or outputs.
- State space design requires that all elements of the state vector are available for the control; therefore, they must be measured directly or estimated using measurements of a portion of the state vector. Pole placement or optimal methods can also be used to arrive at the best estimator for this purpose.

2.8 Problems

2.1 Design feedback with lead compensation for the open-loop system

$$G(s) = \frac{10}{s^2}.$$

The rise time should be 1 sec or less and the overshoot should be less than 10%.

2.2 Design feedback with lead compensation for the open-loop system

$$G(s) = \frac{5}{s^2}.$$

The bandwidth should be faster than 1 rad/sec and the phase margin should be better than 50°.

2.3 For the open-loop system

$$G(s) = \frac{2}{s^2},$$

- design feedback assuming you have access to all the state elements. Ensure that there are closed-loop system poles at $s = -3 \pm 3j$.
- Design an estimator for the system so that it has poles at $s = -6 \pm 6j$.
- Find the transfer function of the complete controller consisting of the control from part (a) and the estimator from part (b).

2.4 For the open-loop system

$$G(s) = \frac{1}{s(s+4)},$$

- design feedback assuming you have access to all the state elements. Ensure that there are closed-loop system poles that provide a natural frequency of $\omega_n = 3$ rad/sec with $\zeta = 0.5$.
- Design an estimator for the system so that it has poles that provide a natural frequency of $\omega_n = 6$ rad/sec with $\zeta = 0.5$.
- Find the transfer function of the complete controller consisting of the control from part (a) and the estimator from part (b).

2.5 Can you stabilize the system

$$G(s) = \frac{1}{s^2(s^2 + 25)}$$

with a single lead compensation? If you can, do it. If you can't, show why not.

2.6 For the open-loop system

$$G(s) = \frac{1}{s^2(s^2 + 25)},$$

- design feedback assuming you have access to all the state elements. Place the closed-loop system poles at $s = -1 \pm 1j, -0.5 \pm 5j$.
- Design an estimator for the system so that it has poles at $s = -2 \pm 2j, -2 \pm 8j$.
- Find the transfer function of the complete controller consisting of the control from part (a) and the estimator from part (b).

2.7 Consider a pendulum with control torque T_c and disturbance torque T_d whose differential equation is

$$\ddot{\theta} + 4\theta = T_c + T_d.$$

Assume there is a potentiometer at the pin that measures the output angle θ , that is, $y = \theta$.

- Design a lead compensation using a root locus that provides for an $M_p < 10\%$ and a rise time, $t_r < 1$ sec.
- Add an integral term to your controller so that there is no steady-state error in the presence of a constant disturbance, T_d , and modify the compensation so that the specifications are still met.

2.8 Consider a pendulum with control torque T_c and disturbance torque T_d whose differential equation is

$$\ddot{\theta} + 4\theta = T_c + T_d.$$

Assume there is a potentiometer at the pin that measures the output angle θ , that is, $y = \theta$.

- Design a lead compensation using frequency response that provides for a PM $> 50^\circ$ and a bandwidth, $\omega_{BW} > 1$ rad/sec.
- Add an integral term to your controller so that there is no steady-state error in the presence of a constant disturbance, T_d , and modify the compensation so that the specifications are still met.

2.9 Consider a pendulum with control torque T_c and disturbance torque T_d whose differential equation is

$$\ddot{\theta} + 4\theta = T_c + T_d.$$

Assume there is a potentiometer at the pin that measures the output angle θ , that is, $y = \theta$.

- Taking the state vector to be

$$\begin{bmatrix} \theta \\ \dot{\theta} \end{bmatrix},$$

write the system equations in state form. Give values for the matrices **F**, **G**, **H**.

- Show, using state-variable methods, that the characteristic equation of the model is $s^2 + 4 = 0$.
- Write the estimator equations for

$$\begin{bmatrix} \hat{\theta} \\ \hat{\dot{\theta}} \end{bmatrix}.$$

Pick estimator gains $[L_1, L_2]^T$ to place both roots of the estimator-error characteristic equation at $s = -10$.

- (d) Using state feedback of the estimated state variables θ and $\dot{\theta}$, derive a control law to place the closed-loop control poles at $s = -2 \pm 2j$.
- (e) Draw a block diagram of the system, that is, estimator, plant, and control law.
- (f) Demonstrate the performance of the system by plotting the step response to a reference command on (i) θ , and (ii) T_d .
- (g) Design a controller with an integral term and demonstrate its performance to the step inputs as in (f).

2.10 For the open-loop system

$$G(s) = \frac{3}{s^2 + 2s - 3},$$

determine

- (a) the final value to a unit step input.
- (b) Answer (a) for the case where

$$G(s) = \frac{3}{s^2 + 2s + 3}.$$

2.11 For the open-loop system

$$G(s) = \frac{3}{s^2 + 2s - 3},$$

assume there is a feedback with a proportional gain, K , and sketch a locus of the closed-loop roots vs. K . What is the minimum value of K to achieve a stable system?

2.12 For the open-loop system

$$G(s) = \frac{1}{s^2(s^2 + 2s + 100)},$$

use a single lead compensation in the feedback to achieve as fast a response as possible, keeping the damping of the resonant mode better than $\zeta = 0.05$.

2.13 Sketch the locus of roots vs. the parameter b for

$$s^2 + bs + b + 1 = 0.$$

2.14 Sketch the root locus with respect to K for the open-loop system

$$G(s) = \frac{K(s+3)}{s(s+2)(s+1)^2}.$$

After completing the hand sketch, verify your result using MATLAB.

2.15 Sketch the root locus with respect to K for the open-loop system

$$G(s) = \frac{K(s+2)}{s^4}.$$

After completing the hand sketch, verify your result using MATLAB.

2.16 Sketch the root locus with respect to K for the open-loop system

$$G(s) = \frac{K(s+2)}{s^4}.$$

After completing the hand sketch, verify your result using MATLAB.

2.17 Sketch the root locus with respect to K for the open-loop system

$$G(s) = \frac{K(s+1)}{s(s+2)(s^2+25)}.$$

After completing the hand sketch, verify your result using MATLAB.

2.18 Sketch a Bode plot for the open-loop system

$$G(s) = \frac{(s+0.1)}{s(s+1)(s^2+2s+100)}.$$

After completing the hand sketch, verify your result using MATLAB. With unity feedback, would the system be stable?

2.19 Sketch a Bode plot for the open-loop system

$$G(s) = \frac{100(s+1)}{s^2(s+10)}.$$

After completing the hand sketch, verify your result using MATLAB. With unity feedback, would the system be stable? What is the PM?

2.20 Sketch a Bode plot for the open-loop system

$$G(s) = \frac{5000(s+1)}{s^2(s+10)(s+50)}.$$

After completing the hand sketch, verify your result using MATLAB. With unity feedback, would the system be stable? If not, how would you stabilize it?

Chapter 3

Introductory Digital Control

A Perspective on Introductory Digital Control

The continuous controllers you have studied so far are built using analog electronics such as resistors, capacitors, and operational amplifiers. However, most control systems today use digital computers (usually microprocessors or microcontrollers) with the necessary input/output hardware to implement the controllers. The intent of this chapter is to show the very basic ideas of designing control laws that will be implemented in a digital computer. Unlike analog electronics, digital computers cannot integrate. Therefore, in order to solve a differential equation in a computer, the equation must be approximated by reducing it to an algebraic equation involving sums and products only. These approximation techniques are often referred to as **numerical integration**. This chapter shows a simple way to make these approximations as an introduction to digital control. Later chapters expand on various improvements to these approximations, show how to analyze them, and show that digital compensation may also be carried out directly without resorting to these approximations. In the final analysis, we will see that direct digital design provides the designer with the most accurate method and the most flexibility in selection of the sample rate.

From the material in this chapter, you should be able to design and implement a digital control system. The system would be expected to give adequate performance if the sample rate is at least 30 times faster than the bandwidth of the system.

Chapter Overview

In Section 3.1, you will learn how to approximate a continuous $D(s)$ with a set of difference equations, a design method sometimes referred to as **emulation**. Section 3.1 is sufficient to enable you to approximate a continuous feedback controller in a digital control system. Section 3.2 shows the basic effect of sampling on the performance of the system and a simple way to analyze that effect. Section 3.3 shows how to convert a continuous PID control law to the digital form.

3.1 Digitization

Figure 3.1(a) shows the topology of the typical continuous system. The computation of the error signal, e , and the dynamic compensation, $D(s)$, can all be accomplished in a digital computer as shown in Fig. 3.1(b). The fundamental differences between the two implementations are that the digital system operates on *samples* of the sensed plant output rather than on the continuous signal and that the dynamics represented by $D(s)$ are implemented by algebraic recursive equations called **difference equations**.

We consider first the action of the analog-to-digital (A/D) converter on a signal. This device acts on a physical variable, most commonly an electrical voltage, and converts it into a binary number that usually consists of 10 or 12 bits. A binary number with 10 bits can take on $2^{10} = 1024$ values; therefore, an A/D converter with 10 bits has a resolution of 0.1%. The conversion from the analog signal

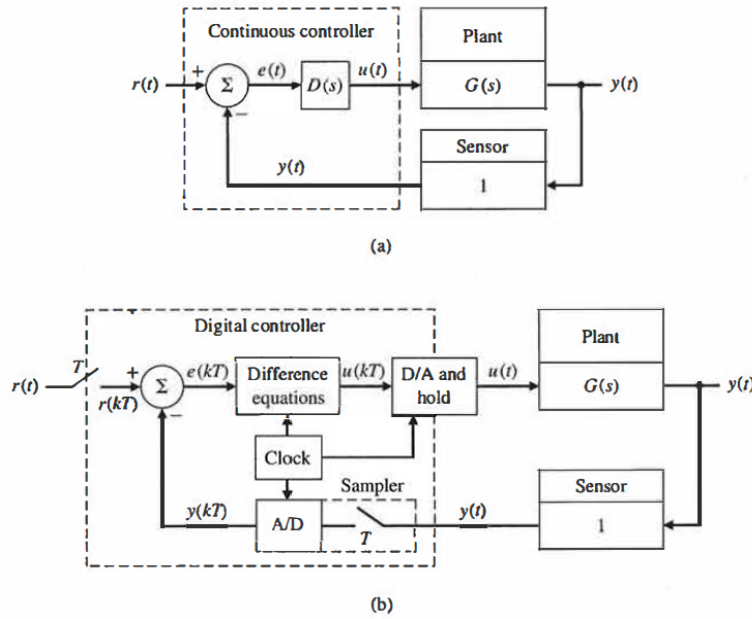


Figure 3.1
Basic control-system block diagrams: (a) continuous system, (b) with a digital computer

$y(t)$ occurs repetitively at instants of time that are T seconds apart. T is called the **sample period** and $1/T$ is the **sample rate** in cycles per second or Hz (also sometimes given in radians/second or $2\pi/T$). The sampled signal is $y(kT)$ where k can take on any integer value. It is often written simply as $y(k)$. We call this type of variable a **discrete signal** to distinguish it from a continuous variable like $y(t)$, which changes continuously in time. We make the assumption here that the sample period is fixed; however, it may vary depending on the implementation as discussed in Section 1.1.

There also may be a sampler and A/D converter for the input command, $r(t)$, producing the discrete $r(kT)$ from which the sensed $y(kT)$ would be subtracted to arrive at the discrete error signal, $e(kT)$. The differential equation of the continuous compensation is approximated by a difference equation which is the discrete approximation to the differential equation and can be made to duplicate the dynamic behavior of a $D(s)$ if the sample period is short enough. The result of the difference equation is a discrete $u(kT)$ at each sample instant. This signal is converted to a continuous $u(t)$ by the D/A and hold. The D/A converts the binary number to an analog voltage, and a **zero-order hold (ZOH)** maintains that same voltage throughout the sample period. The resulting $u(t)$ is then applied to the actuator in precisely the same manner as the continuous implementation.

One particularly simple way to make a digital computer approximate the real time solution of differential equations is to use Euler's method. It follows from the definition of a derivative that

$$\dot{x} = \lim_{\delta t \rightarrow 0} \frac{\delta x}{\delta t} \tag{3.1}$$

where δx is the change in x over a time interval δt . Even if δt is not quite equal to zero, this relationship will be approximately true, and

$$\dot{x}(k) \cong \frac{x(k+1) - x(k)}{T} \tag{3.2}$$

where

$$T = t_{k+1} - t_k \text{ (the sample interval in seconds),}$$

$$t_k = kT \text{ (for a constant sample interval),}$$

k is an integer,

$x(k)$ is the value of x at t_k , and

$x(k+1)$ is the value of x at t_{k+1} .

This approximation¹ can be used in place of all derivatives that appear in the controller differential equations to arrive at a set of equations that can be solved by a digital computer. These equations are called **difference equations** and are solved repetitively with time steps of length T . For systems having bandwidths of a few Hertz, sample rates are often on the order of 100 Hz, so that sample periods are on the order of 10 msec and errors from the approximation can be quite small.

Difference Equations Using Euler's Method

Example 3.1

Using Euler's method, find the difference equations to be programmed into the control computer in Fig. 3.1(b) for the case where the $D(s)$ in Fig. 3.1(a) is

$$D(s) = \frac{U(s)}{E(s)} = K_o \frac{s+a}{s+b}. \quad (3.3)$$

Solution. First find the differential equation that corresponds to $D(s)$. After cross multiplying Eq. (3.3) to obtain

$$(s+b)U(s) = K_o(s+a)E(s),$$

we can see by inspection that the corresponding differential equation is

$$\dot{u} + bu = K_o(\dot{e} + ae). \quad (3.4)$$

Using Euler's method to approximate Eq. (3.4) according to Eq. (3.2), we get the approximating difference equation

$$\frac{u(k+1) - u(k)}{T} + bu(k) = K_o \left[\frac{e(k+1) - e(k)}{T} + ae(k) \right]. \quad (3.5)$$

Rearranging Eq. (3.5) puts the difference equation in the desired form

$$u(k+1) = u(k) + T \left[-bu(k) + K_o \left(\frac{e(k+1) - e(k)}{T} + ae(k) \right) \right]. \quad (3.6)$$

Equation (3.6) shows how to compute the new value of the control, $u(k+1)$, given the past value of the control, $u(k)$, and the new and past values of the error signal, $e(k+1)$ and $e(k)$. For computational efficiency, it is convenient to re-arrange Eq. (3.6) to

$$u(k+1) = (1 - bT)u(k) + K_o(aT - 1)e(k) + K_o e(k+1). \quad (3.7)$$

In principle, the difference equation is evaluated initially with $k = 0$, then $k = 1, 2, 3, \dots$. However, there is usually no requirement that values for all times be saved in memory. Therefore, the computer need only have variables defined for the current and past values for this first-order difference equation. The instructions to the computer to implement the feedback loop in Fig. 3.1(b) with the difference equation from Eq. (3.7) would call for a continual looping through the code in Table 3.1. Note in the table that the calculations have been arranged so as to minimize the computations required between the reading of the A/D and the writing to the D/A, thus keeping the computation delay to a minimum.

The sample rate required depends on the closed-loop bandwidth of the system. Generally, sample rates should be faster than 30 times the bandwidth in order to assure that the digital controller can be made to closely match the performance of the continuous controller. Discrete design methods described in later chapters will show how to achieve this performance and the consequences of sampling even slower if that is required for the computer being used. However, when using the techniques

¹This particular version is called the **forward rectangular** rule. See Problem 3.2 for the **backward rectangular** version.

```

x = 0 (initialization of past values for first loop through)
Define constants:
 $\alpha_1 = 1 - bT$ 
 $\alpha_2 = K_o(aT - 1)$ 
READ A/D to obtain y and r
e = r - y
u = x + Koe
OUTPUT u to D/A and ZOH
now compute x for the next loop through
x =  $\alpha_1 u + \alpha_2 e$ 
go back to READ when T seconds have elapsed since last READ

```

Table 3.1
Real Time
Controller
Implementation

presented in this chapter, a good match to the continuous controller is obtained when the sample rate is greater than approximately 30 times the bandwidth.

Lead Compensation Using a Digital Computer

Example 3.2

Find digital controllers to implement the lead compensation

$$D(s) = 70 \frac{s+2}{s+10} \quad (3.8)$$

for the plant

$$G(s) = \frac{1}{s(s+1)}$$

using sample rates of 20 Hz and 40 Hz. Implement the control equations on an experimental laboratory facility like that depicted in Fig. 3.1, that is, one that includes a microprocessor for the control equations, a ZOH, and analog electronics for the plant. Compute the theoretical step response of the continuous system and compare that with the experimentally determined step response of the digitally controlled system.

Solution. Comparing the compensation transfer function in Eq. (3.8) with Eq. (3.3) shows that the values of the parameters in Eq. (3.6) are $a = 2$, $b = 10$, and $K_o = 70$. For a sample rate of 20 Hz, $T = 0.05$ sec and Eq. (3.6) can be simplified to

$$u(k+1) = 0.5u(k) + 70[e(k+1) - 0.9e(k)].$$

For a sample rate of 40 Hz, $T = 0.025$ sec and Eq. (3.6) simplifies to

$$u(k+1) = 0.75u(k) + 70[e(k+1) - 0.95e(k)].$$

The statements in MATLAB to compute the continuous step response is

```

numD = 70*[1 2]; denD = [1 10]
numG = 1; denG = [1 1 0]
sys1 = tf(numD,denD)*tf(numG,denG)
sysCL = feedback(sys1,1)
step(sysCL)

```

Figure 3.2 shows the step response of the two digital controllers compared to the continuous step response. Note that the 40 Hz sample rate (about $30 \times$ bandwidth) behaves essentially like the continuous case, whereas the 20 Hz sample rate (about $15 \times$ bandwidth) has a detectable increased overshoot signifying some degradation in the damping. The damping would degrade further if the sample rate were made any slower.

The MATLAB file that created Fig. 3.2 (`fig32.m`) computed the digital responses as well as the continuous response. You will learn how to compute the response of a digital system in Chapter 4.

In Chapter 6, you will see that there are several ways to approximate a continuous transfer function, each with different merits, and most with better qualities than the Euler method presented here.

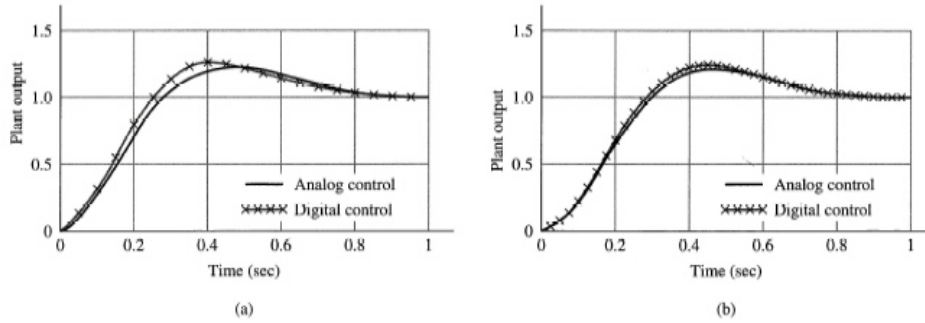


Figure 3.2 Continuous and digital step response using Euler’s method for discretization: (a) 20 Hz sample rate, (b) 40 Hz sample rate

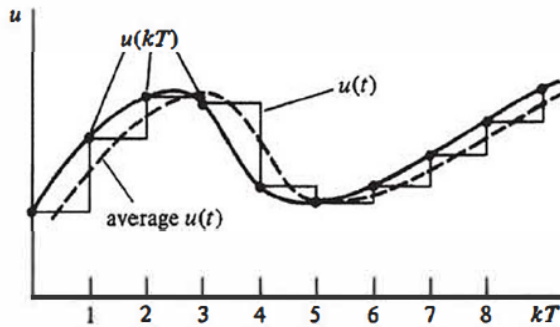


Figure 3.3 The delay due to the hold operation

In fact, MATLAB provides a function (`c2d.m`) that computes these approximations. However, before those methods can be examined, it will be necessary to understand discrete transfer functions, a topic covered in Chapter 4.

3.2 Effect of Sampling

It is worthy to note that *the single most important* impact of implementing a control system digitally is the delay associated with the hold. A delay in any feedback system degrades the stability and damping of the system. Because each value of $u(kT)$ in Fig. 3.1(b) is held constant until the next value is available from the computer, the continuous value of $u(t)$ consists of steps (see Fig. 3.3) that, on the average, lag $u(kT)$ by $T/2$, as shown by the dashed line in the figure. By incorporating a continuous approximation of this $T/2$ delay in a continuous analysis of the system, an assessment can be made of the effect of the delay in the digitally controlled system. The delay can be approximated by the method of Padé. The simplest first-order approximation is

$$G_h(s) = \frac{2/T}{s + 2/T}. \tag{3.9}$$

Figure 3.4 compares the responses from Fig. 3.2 with a continuous analysis that includes a delay approximation according to Eq. (3.9).

This linear approximation of the sampling delay (Eq. (3.9)) could also be used to determine the effect of a particular sample rate on the roots of a system via linear analysis, perhaps a locus of roots vs. T . Alternatively, the effect of a delay can be analyzed using frequency response techniques because a time delay of $T/2$ translates into a phase decrease of

$$\delta\phi = -\frac{\omega T}{2}. \tag{3.10}$$

Thus, we see that the loss of phase margin due to sampling can be estimated by invoking Eq. (3.10) with ω equal to the frequency where the magnitude equals one, that is, the “gain crossover frequency.”

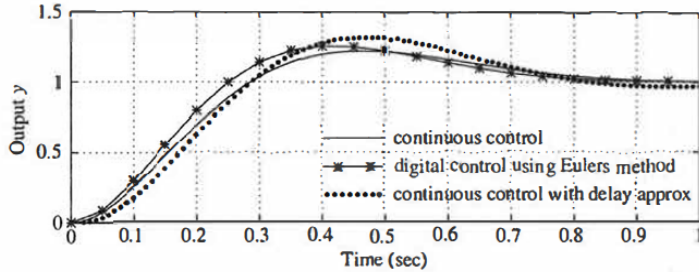


Figure 3.4
Continuous and digital step response at 20 Hz sample rate showing results with a $T/2$ delay approximation

Approximate Analysis of the Effect of Sampling

For the system in Example 3.2, determine the decrease in damping that would result from sampling at 10 Hz. Use both linear analysis and the frequency response method. Compare the time response of the continuous system with the discrete implementation to validate the analysis.

Solution. The damping of the system in Example 3.2 can be obtained from the MATLAB statement

```
damp(sysCL)
```

where `sysCL` is that computed in Example 3.2. The result is $\zeta = .56$.

The damping of the system with the simple delay approximation added (Eq. (3.9)) is obtained from

```
T = 1/10
numDL = 2/T; denDL = [1 2/T]
sys2 = tf(numDL,denDL)*sys1
sysCL = feedback(sys2,1)
damp(sysCL)
```

where `sys1` is that computed in Example 3.2. The result of this calculation is $\zeta = .33$.

The frequency response of the continuous system is shown by the solid line in Fig. 3.5 and shows that the crossover frequency is about 6 rad/sec and the PM is about 50° . The line of small circles shows the phase corrected by Eq. (3.10) and, therefore, that the PM decreases to about 30° . For more precision, the use of `margin.m` in MATLAB shows that the continuous system has a PM of 49.5° at a crossover frequency of 6.17 rad/sec. Equation (3.10) then indicates that the correction due to sampling should be 17.7° , thus the PM of the digital system would be 31.8° . Since the PM is approximately $100 \times \zeta$, this analysis shows that the ζ decreases from approximately 0.5 for the continuous system to 0.32 for the digital system.

Both analysis methods indicate a similar reduction in the damping of the system. One should, therefore, expect that the overshoot of the step response should increase. For the case with no zeros, Fig. 2.7 indicates that this decrease in ζ should result in the step response overshoot, M_p , going from 16% to 35% for a 2nd-order system with no zeros. The actual step responses in Fig. 3.6 have about 20% overshoot for the continuous system and about 30% for the digital case. So, we see that the approximate analysis was somewhat conservative in the prediction of the decreased damping and increased overshoot in the digital case. The trend that decreasing sample rate causes decreasing damping and stability will be analyzed more completely throughout the book.

3.3 PID Control

The notion of proportional, integral, and derivative (PID) control is reviewed in Section 2.2.3. Re-viewing again briefly, the three terms are proportional control

$$u(t) = Ke(t), \quad (3.11)$$

integral control

$$u(t) = \frac{K}{T_I} \int_0^t e(\eta) d\eta, \quad (3.12)$$

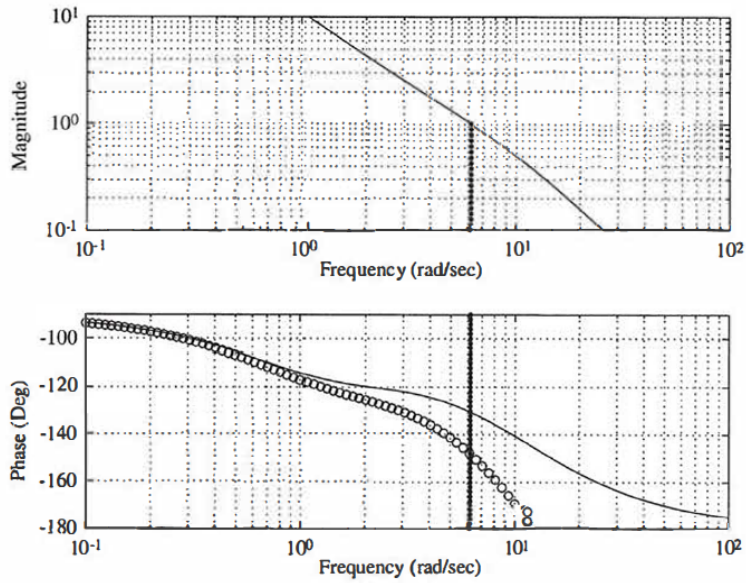


Figure 3.5
Frequency response for Example 3.3

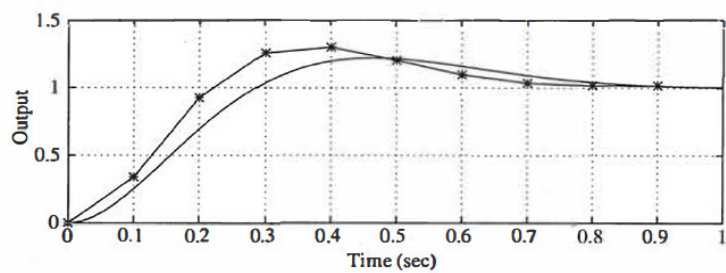


Figure 3.6
Continuous and digital responses for Example 3.3 (at 10 Hz sample rate)

and derivative control

$$u(t) = KT_D \dot{e}(t), \quad (3.13)$$

where K is called the proportional gain, T_I the integral time, and T_D the derivative time. These three constants define the control.

The approximations of these individual control terms to an algebraic equation that can be implemented in a digital computer are proportional control

$$u(k) = Ke(k), \quad (3.14)$$

integral control

$$u(k) = u(k-1) + \frac{K}{T_I} Te(k), \quad (3.15)$$

and derivative control

$$u(k) = \frac{KT_D}{T} [e(k) - e(k-1)]. \quad (3.16)$$

Equation (3.11) is already algebraic, therefore Eq. (3.14) follows directly while Eqs. (3.15) and (3.16) result from an application of Euler's method (Eq. (3.2)) to Eqs. (3.12) and (3.13). However, normally these terms are used together and, in this case, the combination needs to be done carefully. The combined continuous transfer function (Eq. 2.24) is

$$D(s) = \frac{u(s)}{e(s)} = K(1 + 1T_I s + T_D s).$$

Therefore, the differential equation relating $u(t)$ and $e(t)$ is

$$\dot{u} = K \left(\dot{e} + \frac{1}{T_I} e + T_D \ddot{e} \right)$$

and the use of Euler's method (twice for \ddot{e}) results in

$$u(k) = u(k-1) + K \left[\left(1 + \frac{T}{T_I} + \frac{T_D}{T} \right) e(k) - \left(1 + 2\frac{T_D}{T} \right) e(k-1) + \frac{T_D}{T} e(k-2) \right]. \quad (3.17)$$

Transforming a Continuous PID to a Digital Computer

Example 3.4

A micro-servo motor has a transfer function from the input applied voltage to the output speed (rad/sec),

$$G(s) = \frac{360000}{(s+60)(s+600)}. \quad (3.18)$$

It has been determined that PID control with $K = 5$, $T_D = 0.0008$ sec, and $T_I = 0.003$ sec gives satisfactory performance for the continuous case. Pick an appropriate sample rate, determine the corresponding digital control law, and implement on a digital system. Compare the digital step response with the calculated response of a continuous system. Also, separately investigate the effect of a higher sample rate and re-tuning the PID parameters on the ability of the digital system to match the continuous response.

Solution. The sample rate needs to be selected first. But before we can do that, we need to know how fast the system is or what its bandwidth is. The solid line in Fig. 3.7 shows the step response of the continuous system and indicates that the rise time is about 1 msec. Based on Eq. (2.16), this suggests that $\omega_n \cong 1800$ rad/sec, and so the bandwidth would be on the order of 2000 rad/sec or 320 Hz. Therefore, the sample rate would be about 3.2 kHz if 10 times bandwidth. So let's pick $T = 0.3$ msec. Use of Eq. (3.17) results in the difference equation

$$u(k) = u(k-1) + 5[3.7667e(k) - 6.3333e(k-1) + 2.6667e(k-2)]$$

which, when implemented in the digital computer results in the line with stars in Fig. 3.7. This implementation shows a considerably increased overshoot over the continuous case. The line with circles in the figure shows the improved performance obtained by increasing the sample rate to 10 kHz; i.e., a sample rate about 30 times

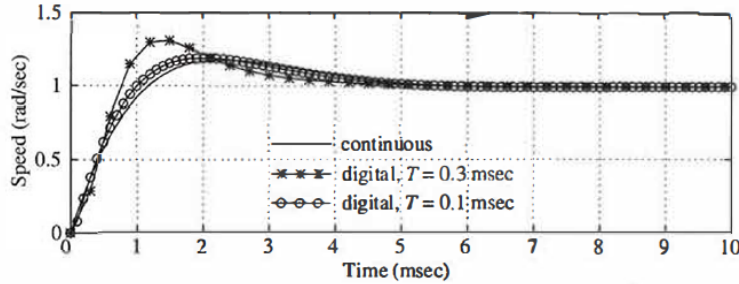


Figure 3.7
Step response of
a micro-motor,
Example 3.4,
same PID
parameters

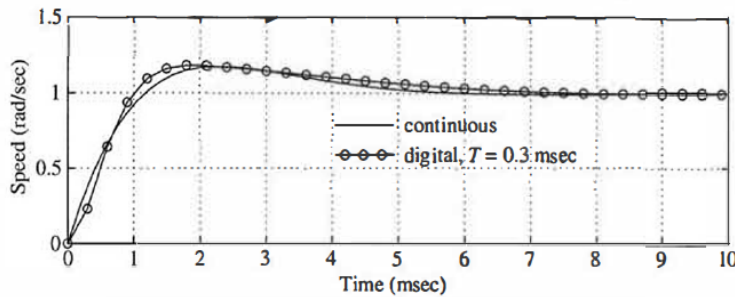


Figure 3.8
Effect of PID
tuning on the
digital response,
Example 3.4

bandwidth, while using the same PID parameters as before. It shows that the digital performance has improved to be essentially the same as the continuous case.

Increasing the sample rate, however, will increase the cost of the computer and the A/D converter; therefore, there will be a cost benefit by improving the performance while maintaining the 3.2 kHz sample rate. A look at Fig. 3.7 shows that the digital response ($T = 0.3$ msec) has a faster rise time and less damping than the continuous case. This suggests that the proportional gain, K , should be reduced to slow the system down and the derivative time, T_D , should be increased to increase the damping. Some trial and error, keeping these ideas in mind, produces the results in Fig. 3.8. The revised PID parameters that produced these results are $K = 3.2$ and $T_D = 0.0011$ sec. The integral reset time, T_I , was left unchanged.

This example once again showed the characteristics of a digital control system. The damping was degraded an increasing amount as the sample rate was reduced. Furthermore, it was possible to restore the damping with suitable adjustments to the control.

3.4 Summary

- Digitization methods allow the designer to convert a continuous compensation, $D(s)$, into a set of difference equations that can be programmed directly into a control computer.
- Euler's method can be used for the digitization

$$\dot{x}(k) \cong \frac{x(k+1) - x(k)}{T}. \quad (3.2)$$

- As long as the sample rate is on the order of $30 \times$ bandwidth or faster, the digitally controlled system will behave close to its continuous counterpart and the continuous analysis that has been the subject of your continuous control systems study will suffice.

- For sample rates on the order of 10 to 30 times the bandwidth, a first order analysis can be carried out by introducing a delay of $T/2$ in the continuous analysis to see how well the digital implementation matches the continuous analysis. A zero-pole approximation for this delay is

$$G_h(s) = \frac{2/T}{s + 2/T}. \quad (3.9)$$

The delay can be analyzed more accurately using frequency response where the phase from the continuous analysis should be decreased by

$$\delta\phi = \frac{\omega T}{2}. \quad (3.10)$$

- A continuous PID control law whose transfer function is

$$D(s) = \frac{u(s)}{e(s)} = K \left(1 + \frac{1}{T_I s} + T_D s \right)$$

can be implemented digitally using Eq. (3.17)

$$u(k) = u(k-1) + K \left[\left(1 + \frac{T}{T_I} + \frac{T_D}{T} \right) e(k) - \left(1 + 2\frac{T_D}{T} \right) e(k-1) + \frac{T_D}{T} e(k-2) \right].$$

The digital control system will behave reasonably close to the continuous system providing the sample rate is faster than 30 times the bandwidth.

- In order to analyze the system accurately for any sample rate, but especially for sample rates below about 30 times bandwidth, you will have to proceed on to the next chapters to learn about z-transforms and how to apply them to the study of discrete systems.
- For digital control systems with sample rates less than 30 times bandwidth, design is often carried out directly in the discrete domain, eliminating approximation errors.

3.5 Problems

3.1 Do the following:

- Design a continuous lead compensation for the satellite attitude control example ($G(s) = 1/s^2$) described in Appendix A.1 so that the complex roots are at approximately $s = -4.4 \pm j4.4$ rad/sec.
- Assuming the compensation is to be implemented digitally, approximate the effect of the digital implementation to be a delay of $T/2$ as given by

$$G_h(s) = \frac{2/T}{s + 2/T}$$

and determine the revised root locations for sample rates of $\omega_s = 5$ Hz, 10 Hz, and 20 Hz where $T = 1/\omega_s$ sec.

3.2 Repeat Example 3.1 from page 46, but use the approximation that

$$\dot{x}(k) \cong \frac{x(k) - x(k-1)}{T},$$

the **backward rectangular** version of Euler's method. Compare the resulting difference equations with the forward rectangular Euler method. Also compute the numerical value of the coefficients for both cases vs. sample rate for $\omega_s = 1 - 100$ Hz. Assume the continuous values from Eq. (3.8). Note that the coefficients of interest are given in Eq. (3.7) for the forward rectangular case as $(1 - bT)$ and $(aT - 1)$.

3.3 For the compensation

$$D(s) = 25 \frac{s+1}{s+15},$$

use Euler's forward rectangular method to determine the difference equations for a digital implementation with a sample rate of 80 Hz. Repeat the calculations using the backward rectangular method (see Problem 3.2) and compare the difference equation coefficients.

3.4 For the compensation

$$D(s) = 5 \frac{s+2}{s+20},$$

use Euler's forward rectangular method to determine the difference equations for a digital implementation with a sample rate of 80 Hz. Repeat the calculations using the backward rectangular method (see Problem 3.2) and compare the difference equation coefficients.

3.5 The read arm on a computer disk drive has the transfer function

$$G(s) = \frac{1000}{s^2}.$$

Design a digital PID controller that has a bandwidth of 100 Hz, a phase margin of 50° , and has no output error for a constant bias torque from the drive motor. Use a sample rate of 6 kHz.

3.6 The read arm on a computer disk drive has the transfer function

$$G(s) = \frac{1000}{s^2}.$$

Design a digital controller that has a bandwidth of 100 Hz and a phase margin of 50° . Use a sample rate of 6 kHz.

3.7 For

$$G(s) = \frac{1}{s^2},$$

- design a continuous compensation so that the closed-loop system has a rise time $t_r < 1$ sec and overshoot $M_p < 15\%$ to a step input command,
- revise the compensation so the specifications would still be met if the feedback was implemented digitally with a sample rate of 5 Hz, and
- find difference equations that will implement the compensation in the digital computer.

3.8 The read arm on a computer disk drive has the transfer function

$$G(s) = \frac{500}{s^2}.$$

Design a continuous lead compensation so that the closed-loop system has a bandwidth of 100 Hz and a phase margin of 50° . Modify the MATLAB file `fig32.m` so that you can evaluate the digital version of your lead compensation using Euler's forward rectangular method. Try different sample rates, and find the slowest one where the overshoot does not exceed 30%.

3.9 The antenna tracker has the transfer function

$$G(s) = \frac{10}{s(s+2)}.$$

Design a continuous lead compensation so that the closed-loop system has a rise time $t_r < 0.3$ sec and overshoot $M_p < 10\%$. Modify the MATLAB file `fig32.m` so that you can evaluate the digital version of your lead compensation using Euler's forward rectangular method. Try different sample rates, and find the slowest one where the overshoot does not exceed 20%.

3.10 The antenna tracker has the transfer function

$$G(s) = \frac{10}{s(s+2)}.$$

Design a continuous lead compensation so that the closed-loop system has a rise time $t_r < 0.3$ sec and overshoot $M_p < 10\%$. Approximate the effect of a digital implementation to be

$$G_h(s) = \frac{2/T}{s + 2/T},$$

and estimate M_p for a digital implementation with a sample rate of 10 Hz.

Chapter 4

Discrete Systems Analysis

A Perspective on Discrete Systems Analysis

The unique element in the structure of Fig. 3.1 is the digital computer. The fundamental character of the digital computer is that it takes a finite time to compute answers, and it does so at discrete steps in time. The purpose of this chapter is to develop tools of analysis necessary to understand and to guide the design of programs for a computer sampling at discrete times and acting as a linear, dynamic control component. Needless to say, digital computers can do many things other than control linear dynamic systems; it is our purpose in this chapter to examine their characteristics when doing this elementary control task and to develop the basic analysis tools needed to write programs for real-time computer control.

Chapter Overview

Section 4.1 restates the difference equations used by a computer to represent a dynamic system, a topic covered very briefly in Section 3.1. The tool for analyzing this sort of system, the z -transform, is introduced and developed in Section 4.2. Use of the z -transform is developed further in Section 4.3 to show how it applies to the combined system in Fig. 3.1. Furthermore, state-space models of discrete systems are developed in this section. Section 4.4 shows the correspondence between roots in the z -plane and time response characteristics while Section 4.5 discusses characteristics of the discrete frequency response. The last section, 4.6, derives properties of the z -transform.

4.1 Linear Difference Equations

We assume that the analog-to-digital converter (A/D) in Fig. 1.1 takes samples of the signal y at discrete times and passes them to the computer so that $\hat{y}(kT) = y(kT)$. The job of the computer is to take these sample values and compute in some fashion the signals to be put out through the digital-to-analog converter (D/A). The characteristics of the A/D and D/A converters will be discussed later. Here we consider the treatment of the data inside the computer. Suppose we call the input signals up to the k th sample $e_0, e_1, e_2, \dots, e_k$, and the output signals prior to that time $u_0, u_1, u_2, \dots, u_{k-1}$. Then, to get the next output, we have the machine compute some function, which we can express in symbolic form as

$$u_k = f(e_0, \dots, e_k; u_0, \dots, u_{k-1}). \quad (4.1)$$

Because we plan to emphasize the elementary and the dynamic possibilities, we assume that the function f in Eq. (4.1) is *linear* and depends on only a *finite* number of past e 's and u 's. Thus we write

$$u_k = -a_1 u_{k-1} - a_2 u_{k-2} - \dots - a_n u_{k-n} + b_0 e_k + b_1 e_{k-1} + \dots + b_m e_{k-m}. \quad (4.2)$$

Equation (4.2) is called a linear **recurrence equation** or **difference equation** and, as we shall see, has many similarities with a linear differential equation. The name "difference equation" derives

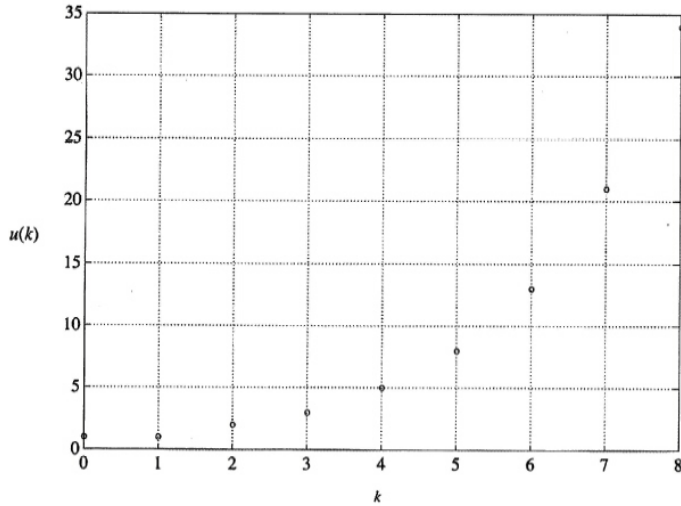


Figure 4.1
The Fibonacci
numbers

from the fact that we could write Eq. (4.2) using u_k plus the differences in u_k , which are defined as

$$\begin{aligned}\nabla u_k &= u_k - u_{k-1} \\ \nabla^2 u_k &= \nabla u_k - \nabla u_{k-1} \\ \nabla^n u_k &= \nabla^{n-1} u_k - \nabla^{n-1} u_{k-1}.\end{aligned}\quad (4.3)$$

If we solve Eq. (4.3) for the values of u_k , u_{k-1} , and u_{k-2} in terms of differences, we find

$$\begin{aligned}u_k &= u_k, \\ u_{k-1} &= u_k - \nabla u_k \\ u_{k-2} &= u_k - 2\nabla u_k + \nabla^2 u_k.\end{aligned}$$

Thus, for a second-order equation with coefficients a_1, a_2 , and b_0 (we let $b_1 = b_2 = 0$ for simplicity), we find the equivalent difference equation to be

$$a_2 \nabla^2 u_k - (a_1 + 2a_2) \nabla u_k + (a_2 + a_1 + 1) u_k = b_0 e_k.$$

Although the two forms are equivalent, the recurrence form of Eq. (4.2) is more convenient for computer implementation; we will drop the form using differences. We will continue, however, to refer to our equations as “difference equations.” If the a ’s and b ’s in Eq. (4.2) are constant, then the computer is solving a **constant-coefficient difference equation** (CCDE). We plan to demonstrate later that with such equations the computer can control linear constant dynamic systems and approximate most of the other tasks of linear, constant, dynamic systems, including performing the functions of electronic filters. To do so, it is necessary first to examine methods of obtaining solutions to Eq. (4.2) and to study the general properties of these solutions.

To solve a specific CCDE is an elementary matter. We need a starting time (k -value) and some initial conditions to characterize the contents of the computer memory at this time. For example, suppose we take the case

$$u_k = u_{k-1} + u_{k-2} \quad (4.4)$$

and start at $k = 2$. Here there are no input values, and to compute u_2 we need to know the (initial) values for u_0 and u_1 . Let us take them to be $u_0 = u_1 = 1$. The first nine values are 1, 1, 2, 3, 5, 8, 13, 21, 34, ... A plot of the values of u_k versus k is shown in Fig. 4.1.

The results, the **Fibonacci numbers**, are named after the thirteenth-century mathematician¹ who studied them. For example, Eq. (4.4) has been used to model the growth of rabbits in a protected environment². However that may be, the output of the system represented by Eq. (4.4) would seem to be growing, to say the least. If the response of a dynamic system to any finite initial conditions can grow without bound, we call the system **unstable**. We would like to be able to examine equations like Eq. (4.2) and, without having to solve them explicitly, see if they are stable or unstable and even understand the general shape of the solution.

One approach to solving this problem is to assume a form for the solution with unknown constants and to solve for the constants to match the given initial conditions. For continuous, ordinary, differential equations that are constant and linear, exponential solutions of the form e^{st} are used. In the case of linear, constant, difference equations, it turns out that solutions of the form z^k will do where z has the role of s and k is the discrete independent variable replacing time, t . Consider Eq. (4.4). If we assume that $u(k) = Az^k$, we get the equation

$$Az^k = Az^{k-1} + Az^{k-2}.$$

Now if we assume $z \neq 0$ and $A \neq 0$, we can divide by A and multiply by z^{-k} , with the result

$$1 = z^{-1} + z^{-2}$$

or

$$z^2 = z + 1.$$

This polynomial of second degree has two solutions, $z_{1,2} = 1/2 \pm \sqrt{5}/2$. Let's call these z_1 and z_2 . Since our equation is linear, a sum of the individual solutions will also be a solution. Thus, we have found that a solution to Eq. (4.4) is of the form

$$u(k) = A_1 z_1^k + A_2 z_2^k.$$

We can solve for the unknown constants by requiring that this general solution satisfy the specific initial conditions given. If we substitute $k = 0$ and $k = 1$, we obtain the simultaneous equations

$$\begin{aligned} 1 &= A_1 + A_2, \\ 1 &= A_1 z_1 + A_2 z_2. \end{aligned}$$

These equations are easily solved to give

$$\begin{aligned} A_1 &= \frac{\sqrt{5} + 1}{2\sqrt{5}}, \\ A_2 &= \frac{\sqrt{5} - 1}{2\sqrt{5}}. \end{aligned}$$

And now we have the complete solution of Eq. (4.4) in a closed form. Furthermore, we can see that since $z_1 = (1 + \sqrt{5})/2$ is greater than 1, the term in z_1^k will grow without bound as k grows, which confirms our suspicion that the equation represents an unstable system. We can generalize this result. The equation in z that we obtain after we substitute $u = z^k$ is a polynomial in z known as the **characteristic equation** of the difference equation. If any solution of this equation is outside the unit circle (has a magnitude greater than one), the corresponding difference equation is unstable in the specific sense that for some finite initial conditions the solution will grow without bound as time goes to infinity. If *all* the roots of the characteristic equation are *inside* the unit circle, the corresponding difference equation is stable.

Discrete Stability

Example 4.1

¹Leonardo Fibonacci of Pisa, who introduced Arabic notation to the Latin world about 1200 A.D.

²Wilde (1964). Assume that u_k represents pairs of rabbits and that babies are born in pairs. Assume that no rabbits die and that a new pair begin reproduction after one period. Thus at time k , we have all the old rabbits, u_{k-1} , plus the newborn pairs born to the mature rabbits, which are u_{k-2} .

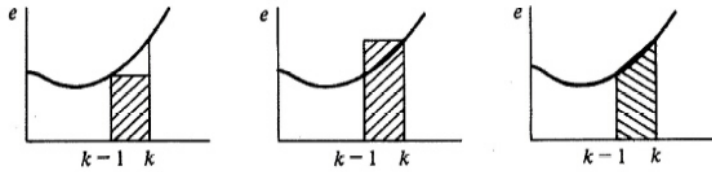


Figure 4.2
Plot of a function and alternative approximations to the area under the curve over a single time interval

Is the equation

$$u(k) = 0.9u(k-1) - 0.2u(k-2)$$

stable?

Solution. The characteristic equation is

$$z^2 - 0.9z + 0.2 = 0,$$

and the characteristic roots are $z = 0.5$ and $z = 0.4$. Since both these roots are inside the unit circle, the equation is stable.

As an example of the origins of a difference equation with an external input, we consider the discrete approximation to integration. Suppose we have a continuous signal, $e(t)$, of which a segment is sketched in Fig. 4.2, and we wish to compute an approximation to the integral

$$\mathcal{J} = \int_0^t e(t) dt, \quad (4.5)$$

using only the discrete values $e(0), \dots, e(t_{k-1}), e(t_k)$. We assume that we have an approximation for the integral from zero to the time t_{k-1} and we call it u_{k-1} . The problem is to obtain u_k from this information. Taking the view of the integral as the area under the curve $e(t)$, we see that this problem reduces to finding an approximation to the area under the curve between t_{k-1} and t_k . Three alternatives are sketched in Fig. 4.2. We can use the rectangle of height e_{k-1} , or the rectangle of height e_k , or the trapezoid formed by connecting e_{k-1} to e_k by a straight line. If we take the third choice, the area of the trapezoid is

$$A = \frac{t_k - t_{k-1}}{2} (e_k + e_{k-1}). \quad (4.6)$$

Finally, if we assume that the sampling period, $t_k - t_{k-1}$, is a constant, T , we are led to a simple formula for discrete integration called the **trapezoid rule**

trapezoid rule

$$u_k = u_{k-1} + \frac{T}{2} (e_k + e_{k-1}). \quad (4.7)$$

If $e(t) = t$, then $e_k = kT$ and substitution of $u_k = (T^2/2)k^2$ satisfies Eq. (4.7) and is exactly the integral of e . (It should be, because if $e(t)$ is a straight line, the trapezoid is the *exact* area.) If we approximate the area under the curve by the rectangle of height e_{k-1} , the result is called the **forward rectangular rule** (sometimes called Euler's method, as discussed in Chapter 3 for an approximation to differentiation) and is described by

$$u_k = u_{k-1} + Te_{k-1}.$$

The other possibility is the **backward rectangular rule**, given by

$$u_k = u_{k-1} + Te_k.$$

Each of these integration rules is a special case of our general difference equation Eq. (4.2). We will examine the properties of these rules later, in Chapter 6, while discussing means to obtain a difference equation that will be equivalent to a given differential equation.

Thus we see that difference equations can be evaluated directly by a digital computer and that they can represent models of physical processes and approximations to integration. It turns out that if the difference equations are linear with coefficients that are constant, we can describe the relation between u and e by a transfer function, and thereby gain a great aid to analysis and also to the design of linear, constant, discrete controls.

4.2 The Discrete Transfer Function

We will obtain the transfer function of linear, constant, discrete systems by the method of z -transform analysis. A logical alternative viewpoint that requires a bit more mathematics but has some appeal is given in Section 4.6.2. The results are the same. We also show how these same results can be expressed in the state space form in Section 4.2.3.

4.2.1 The z -Transform

If a signal has discrete values $e_0, e_1, \dots, e_k, \dots$ we define the z -transform of the signal as the function^{3,4}

$$\begin{aligned} E(z) &\triangleq \mathcal{Z}\{e(k)\} \\ &\triangleq \sum_{k=-\infty}^{\infty} e_k z^{-k}, \quad r_o < |z| < R_o, \end{aligned} \quad (4.8)$$

and we assume we can find values of r_0 and R_0 as bounds on the magnitude of the complex variable z for which the series Eq. (4.8) converges. A discussion of convergence is deferred until Section 4.6.

The z -Transform

Example 4.2

The data e_k are taken as samples from the time signal $e^{-at} 1(t)$ at sampling period T where $1(t)$ is the unit step function, zero for $t < 0$, and one for $t \geq 0$. Then $e_k = e^{-akT} 1(kT)$. Find the z -transform of this signal.

Solution. Applying Eq. (4.8), we find that

$$\begin{aligned} \sum_{k=-\infty}^{\infty} e_k z^{-k} &= \sum_0^{\infty} e^{-akT} z^{-k} \\ &= \sum_0^{\infty} (e^{-aT} z^{-1})^k \\ &= \frac{1}{1 - e^{-aT} z^{-1}} \\ &= \frac{z}{z - e^{-aT}} \quad |z| > e^{-aT}. \end{aligned}$$

We will return to the analysis of signals and development of a table of useful z -transforms in Section 4.4; we first examine the use of the transform to reduce difference equations to algebraic equations and techniques for representing these as block diagrams.

³We use the notation \triangleq to mean "is defined as."

⁴In Eq. (4.8) the lower limit is $-\infty$ so that values of e_k on both sides of $k = 0$ are included. The transform so defined is sometimes called the two-sided z -transform to distinguish it from the one-sided definition, which would be $\sum_0^{\infty} e_k z^{-k}$. For signals that are zero for $k < 0$, the transforms obviously give identical results. To take the one-sided transform of u_{k-1} , however, we must handle the value of u_{-1} , and thus are initial conditions introduced by the one-sided transform. Examination of this property and other features of the one-sided transform are invited by the problems. We select the two-sided transform because we need to consider signals that extend into negative time when we study random signals in Chapter 12.

4.2.2 The Transfer Function

The z -transform has the same role in discrete systems that the Laplace transform has in analysis of continuous systems. For example, the z -transforms for e_k and u_k in the difference equation (4.2) or in the trapezoid integration (4.7) are related in a simple way that permits the rapid solution of linear, constant, difference equations of this kind. To find the relation, we proceed by direct substitution. We take the definition given by Eq. (4.8) and, in the same way, we define the z -transform of the sequence $\{u_k\}$ as

$$U(z) = \sum_{k=-\infty}^{\infty} u_k z^{-k}. \quad (4.9)$$

Now we multiply Eq. (4.7) by z^{-k} and sum over k . We get

$$\sum_{k=-\infty}^{\infty} u_k z^{-k} = \sum_{k=-\infty}^{\infty} u_{k-1} z^{-k} + \frac{T}{2} \left(\sum_{k=-\infty}^{\infty} e_k z^{-k} + \sum_{k=-\infty}^{\infty} e_{k-1} z^{-k} \right). \quad (4.10)$$

From Eq. (4.9), we recognize the left-hand side as $U(z)$. In the first term on the right, we let $k-1 = j$ to obtain

$$\sum_{k=-\infty}^{\infty} u_{k-1} z^{-k} = \sum_{j=-\infty}^{\infty} u_j z^{-(j+1)} = z^{-1} U(z). \quad (4.11)$$

By similar operations on the third and fourth terms we can reduce Eq. (4.10) to

$$U(z) = z^{-1} U(z) + \frac{T}{2} [E(z) + z^{-1} E(z)]. \quad (4.12)$$

Equation (4.12) is now simply an algebraic equation in z and the functions U and E . Solving it we obtain

$$U(z) = \frac{T}{2} \frac{1+z^{-1}}{1-z^{-1}} E(z). \quad (4.13)$$

We *define* the ratio of the transform of the output to the transform of the input as the **transfer function**, $H(z)$. Thus, in this case, the transfer function for trapezoid-rule integration is

$$\frac{U(z)}{E(z)} \triangleq H(z) = \frac{T}{2} \frac{z+1}{z-1}. \quad (4.14)$$

For the more general relation given by Eq. (4.2), it is readily verified by the same techniques that

$$H(z) = \frac{b_0 + b_1 z^{-1} + \dots + b_m z^{-m}}{1 + a_1 z^{-1} + a_2 z^{-2} + \dots + a_n z^{-n}},$$

and if $n \geq m$, we can write this as a ratio of polynomials in z as

$$H(z) = \frac{b_0 z^n + b_1 z^{n-1} + \dots + b_m z^{n-m}}{z^n + a_1 z^{n-1} + a_2 z^{n-2} + \dots + a_n}. \quad (4.15)$$

or

$$H(z) = \frac{b(z)}{a(z)}.$$

This transfer function is represented in MATLAB in the `tf` form similarly to the continuous case as discussed after Eq. (2.6). The numerator of Eq. (4.15) would be specified in MATLAB as a $1 \times (n+1)$ matrix of the coefficients, for example, when $m = n$

$$\text{num} = [b_0 \quad b_1 \quad b_2 \quad \dots \quad b_m]$$

and when $n > m$, there would be $n - m$ zeros after b_m . The quantity specifying the denominator would be specified as a $1 \times (n+1)$ matrix, for example

$$\text{den} = [1 \quad a_1 \quad a_2 \quad \dots \quad a_n].$$



Figure 4.3
The unit delay

Note that $H(z)$ was assumed to be in the form given by Eq. (4.15), that is, with positive powers of z . The discrete system is specified as

$$\text{sys} = \text{tf}(\text{num}, \text{den}, T)$$

where T is the sample period.

The general input–output relation between transforms with linear, constant, difference equations is

$$U(z) = H(z)E(z). \quad (4.16)$$

Although we have developed the transfer function with the z -transform, it is also true that the transfer function is the ratio of the output to the input when both vary as z^k .

Because $H(z)$ is a rational function of a complex variable, we use the terminology of that subject. Suppose we call the numerator polynomial $b(z)$ and the denominator $a(z)$. The places in z where $b(z) = 0$ are **zeros** of the transfer function, and the places in z where $a(z) = 0$ are the **poles** of $H(z)$. If z_0 is a pole and $(z - z_0)^p H(z)$ has neither pole nor zero at z_0 , we say that $H(z)$ has a pole of order p at z_0 . If $p = 1$, the pole is simple. The transfer function Eq. (4.14) has a simple pole at $z = 1$ and a simple zero at $z = -1$. When completely factored, the transfer function would be

$$H(z) = K \frac{\prod_{i=1}^m (z - z_i)}{\prod_{i=1}^n (z - p_i)}, \quad (4.17)$$

and the quantities specifying the transfer function in the MATLAB `zpk` form are an $m \times 1$ matrix of the zeros, an $n \times 1$ matrix of the poles, and a scalar gain, for example

$$\mathbf{z} = \begin{bmatrix} z_1 \\ z_2 \\ \dots \\ z_m \end{bmatrix}, \quad \mathbf{p} = \begin{bmatrix} p_1 \\ p_2 \\ \dots \\ p_n \end{bmatrix}, \quad \mathbf{k} = K.$$

The system is then

$$\text{sys} = \text{zpk}(\mathbf{z}, \mathbf{p}, \mathbf{k}, T).$$

We can now give a physical meaning to the variable z . Suppose we let all coefficients in Eq. (4.15) be zero except b_1 and we take b_1 to be 1. Then $H(z) = z^{-1}$. But $H(z)$ represents the transform of Eq. (4.2), and with these coefficient values the difference equation reduces to

$$u_k = e_{k-1}. \quad (4.18)$$

The present value of the output, u_k , equals the input *delayed by one period*. Thus we see that a transfer function of z^{-1} is a *delay* of one time unit. We can picture the situation as in Fig. 4.3, where both time and transform relations are shown. z^{-1} and cycle delay

Since the relations of Eqs. (4.7), (4.14), (4.15) are all composed of delays, they can be expressed in terms of z^{-1} . Consider Eq. (4.7). In Fig. 4.4 we illustrate the difference equation (4.7) using the transfer function z^{-1} as the symbol for a unit delay.

We can follow the operations of the discrete integrator by tracing the signals through Fig. 4.4. For example, the present value of e_k is passed to the first summer, where it is added to the previous value e_{k-1} , and the sum is multiplied by $T/2$ to compute the area of the trapezoid between e_{k-1} and e_k . This is the signal marked a_k in Fig. 4.4. After this, there is another sum, where the previous output, u_{k-1} , is added to the new area to form the next value of the integral estimate, u_k . The discrete integration occurs in the loop with one delay, z^{-1} , and unity gain.

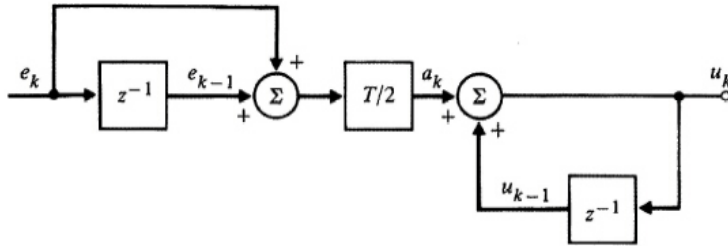


Figure 4.4
A block diagram of trapezoid integration as represented by Eq. (4.7)

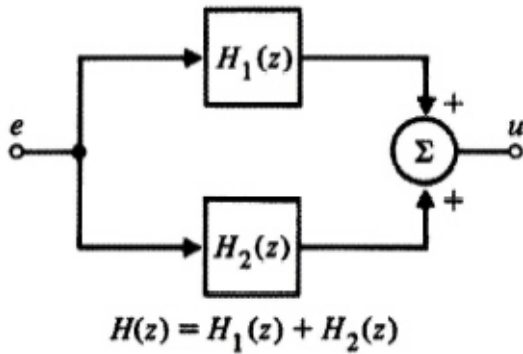


Figure 4.5
Block diagram of parallel blocks

4.2.3 Block Diagrams and State-Variable Descriptions

Because Eq. (4.16) is a linear algebraic relationship, a system of such relations is described by a system of linear equations. These can be solved by the methods of linear algebra or by the graphical methods of block diagrams in the same way as for continuous system transfer functions. To use block-diagram analysis to manipulate these discrete-transfer-function relationships, there are only four primitive cases:

1. The transfer function of paths in parallel is the sum of the single-path transfer functions (Fig. 4.5).
2. The transfer function of paths in series is the *product* of the path transfer functions (Fig. 4.6).
3. The transfer function of a single loop of paths is the transfer function of the forward path divided by one minus the loop transfer function (Fig. 4.7).
4. The transfer function of an arbitrary multipath diagram is given by combinations of these cases. Mason's rule⁵ can also be used.

For the general difference equation of (4.2), we already have the transfer function in Eq. (4.15). It is interesting to connect this case with a block diagram *using only simple delay forms for z* in order

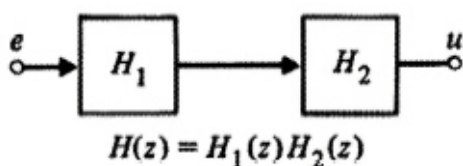


Figure 4.6
Block diagram of cascade blocks

⁵Mason (1956). See Franklin, Powell, and Emami-Naeini (2019) for a discussion.

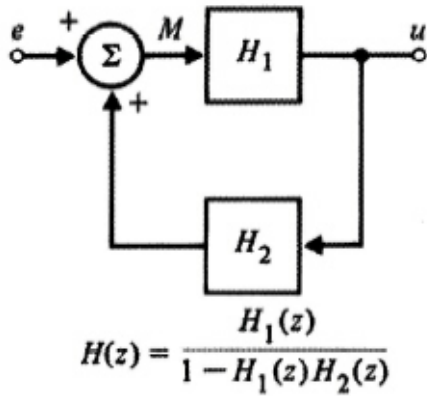


Figure 4.7
Feedback transfer function

to see several “canonical” block diagrams and to introduce the description of discrete systems using equations of state.

***Canonical Forms**

There are many ways to reduce the difference equation (4.2) to a block diagram involving z only as the delay operator, z^{-1} . The first one we will consider leads to the “**control**” **canonical form**. We begin with the transfer function as a ratio of polynomials

$$U(z) = H(z)E(z) = \frac{b(z)}{a(z)}E(z) = b(z)\xi,$$

where

$$\xi = \frac{E(z)}{a(z)}$$

and thus

$$a(z)\xi = E(z).$$

At this point we need to get specific; and rather than carry through with a system of arbitrary order, we will work out the details for the third-order case. In the development that follows, we will consider the variables u , e , and ξ as *time* variables and z as an advance operator such that $zu(k) = u(k+1)$ or $z^{-1}u(k) = u(k-1)$. With this convention (which is simply using the property of z derived earlier), consider the equations

$$(z^3 + a_1z^2 + a_2z + a_3)\xi = e, \tag{4.19}$$

$$(b_0z^3 + b_1z^2 + b_2z + b_3)\xi = u. \tag{4.20}$$

We can write Eq. (4.19) as

$$\begin{aligned} z^3\xi &= e - a_1z^2\xi - a_2z\xi - a_3\xi, \\ \xi(k+3) &= e(k) - a_1\xi(k+2) - a_2\xi(k+1) - a_3\xi(k). \end{aligned} \tag{4.21}$$

Now assume we have $z^3\xi$, which is to say that we have $\xi(k+3)$ because z^3 is an advance operator of three steps. If we operate on this with z^{-1} three times in a row, we will get back to $\xi(k)$, as shown in Fig. 4.8(a). From Eq. (4.21), we can now compute $z^3\xi$ from e and the lower powers of z and ξ given in the block diagram; the picture is now as given in Fig. 4.8(b). To complete the representation of Eqs. (4.19) and (4.20), we need only add the formation of the output u as a weighted sum of the variables $z^3\xi$, $z^2\xi$, $z\xi$, and ξ according to Eq. (4.20). The completed picture is shown in Fig. 4.8(c).

In Fig. 4.8(c), the internal variables have been named x_1 , x_2 , and x_3 . These variables comprise the *state* of this dynamic system in this form. Having the block diagram shown in Fig. 4.8(c), we can

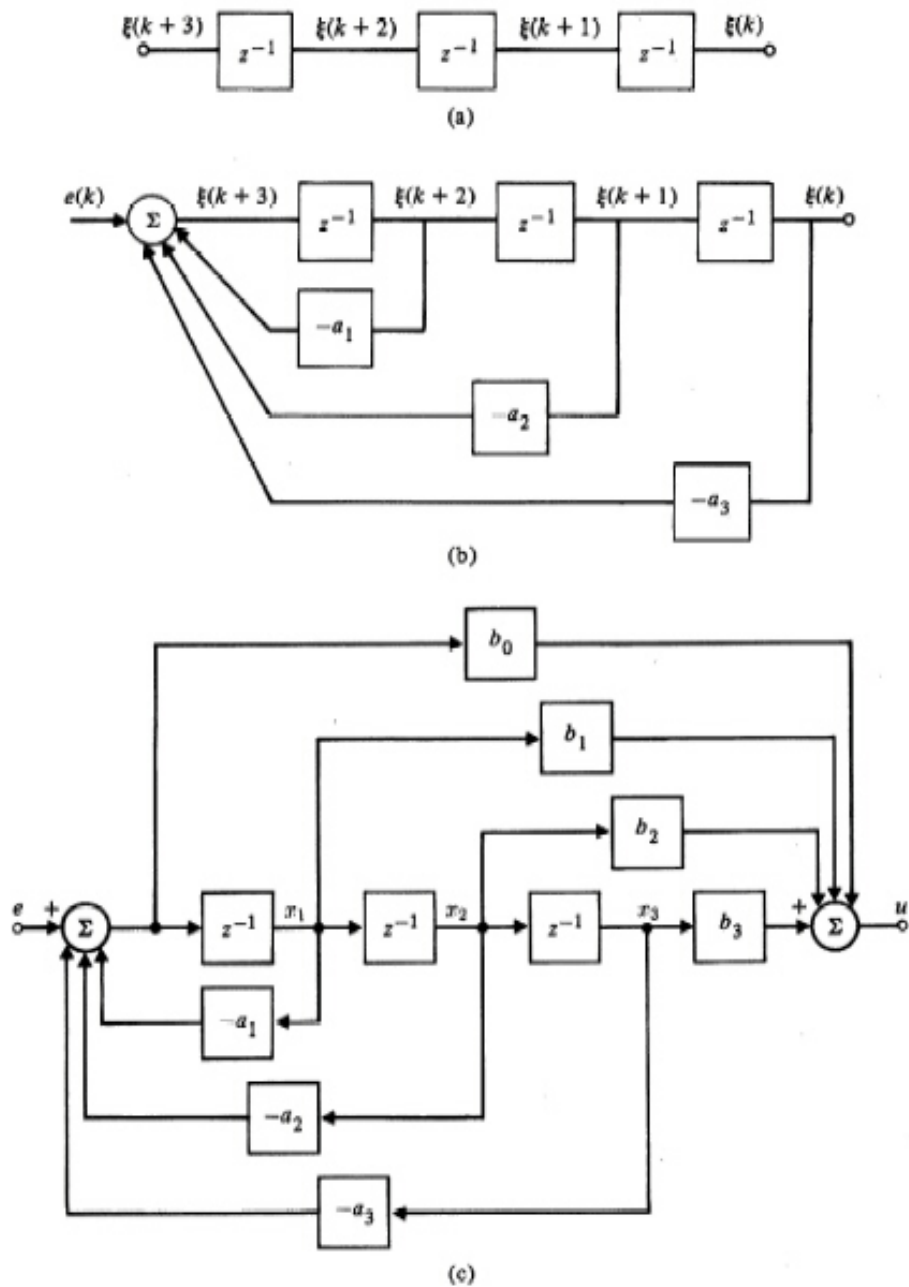


Figure 4.8
 Block diagram development of control canonical form: (a) Solving for $\xi(k)$; (b) solving for $\xi(k+3)$ from $e(k)$ and past ξ 's; (c) solving for $U(k)$ from ξ 's

write down, almost by inspection, the difference equations that describe the evolution of the state, again using the fact that the transfer function z^{-1} corresponds to a one-unit delay. For example, we see that $x_3(k+1) = x_2(k)$ and $x_2(k+1) = x_1(k)$. Finally, expressing the sum at the far left of the figure, we have

$$x_1(k+1) = -a_1x_1(k) - a_2x_2(k) - a_3x_3(k) + e(k).$$

We collect these three equations together in proper order, and we have

$$\begin{aligned} x_1(k+1) &= -a_1x_1(k) - a_2x_2(k) - a_3x_3(k) + e(k), \\ x_2(k+1) &= x_1(k), \\ x_3(k+1) &= x_2(k). \end{aligned} \quad (4.22)$$

Using vector-matrix notation,⁶ we can write this in the compact form

$$\mathbf{x}(k+1) = \mathbf{A}_c\mathbf{x}(k) + \mathbf{B}_c e(k),$$

where

$$\begin{aligned} \mathbf{x} &= \begin{bmatrix} x_1 \\ x_2 \\ x_3 \end{bmatrix} \\ \mathbf{A}_c &= \begin{bmatrix} -a_1 & -a_2 & -a_3 \\ 1 & 0 & 0 \\ 0 & 1 & 0 \end{bmatrix} \end{aligned} \quad (4.23)$$

and

$$\mathbf{B}_c = \begin{bmatrix} 1 \\ 0 \\ 0 \end{bmatrix}. \quad (4.24)$$

The output equation is also immediate except that we must watch to catch *all* paths by which the state variables combine in the output. The problem is caused by the b_0 term. If $b_0 = 0$, then $u = b_1x_1 + b_2x_2 + b_3x_3$, and the corresponding matrix form is immediate. However, if b_0 is not 0, x_1 for example not only reaches the output through b_1 but also by the parallel path with gain $-b_0a_1$. The complete equation is

$$u = (b_1 - a_1b_0)x_1 + (b_2 - a_2b_0)x_2 + (b_3 - a_3b_0)x_3 + b_0e.$$

In vector/matrix notation, we have

$$u = \mathbf{C}_c\mathbf{x} + \mathbf{D}_c e$$

where

$$\mathbf{C}_c = [b_1 - a_1b_0 \quad b_2 - a_2b_0 \quad b_3 - a_3b_0] \quad (4.25)$$

$$\mathbf{D}_c = b_0. \quad (4.26)$$

We can combine the equations for the state evolution and the output to give the very useful and most compact equations for the dynamic system,

$$\mathbf{x}(k+1) = \mathbf{A}_c\mathbf{x}(k) + \mathbf{B}_c e(k),$$

where \mathbf{A}_c and \mathbf{B}_c for this control canonical form are given by Eq. (4.23), and \mathbf{C}_c and \mathbf{D}_c are given by Eq. (4.25).

The other canonical form we want to illustrate is called the “**observer**” canonical form and is found by starting with the difference equations in operator/transform form as observer canonical form

$$z^3u + a_1z^2u + a_2zu + a_3u = b_0z^3e + b_1z^2e + b_2ze + b_3e.$$

⁶We assume the reader has some knowledge of matrices. The results we require and references to study material are given in Appendix C.

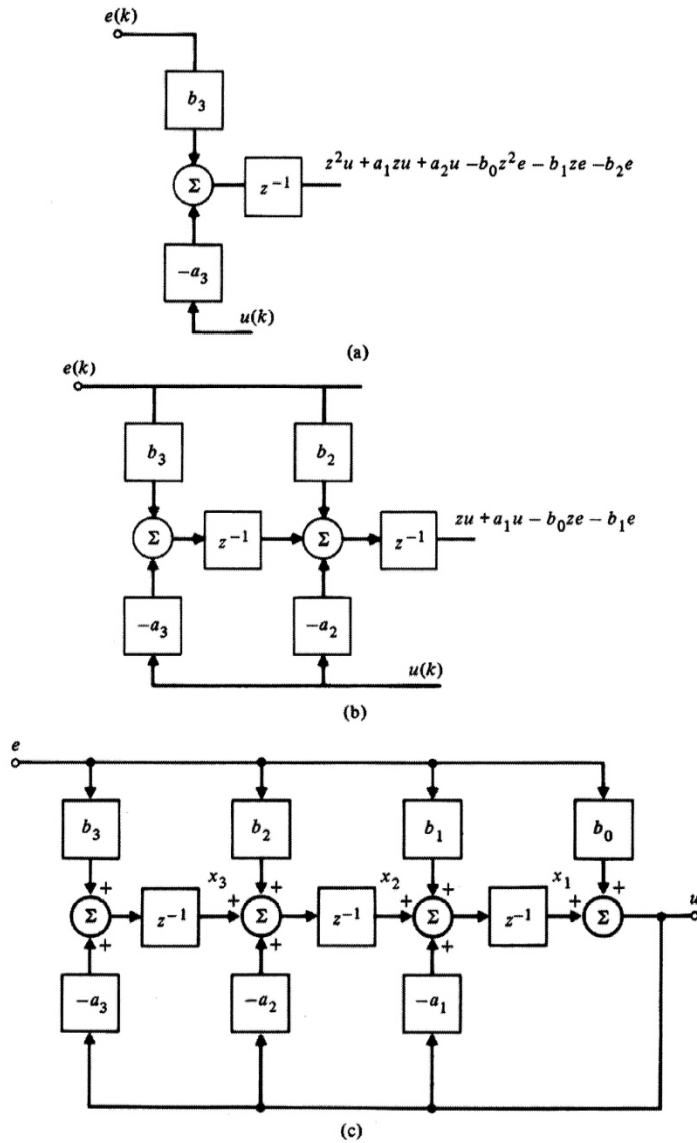


Figure 4.9
Block diagram development of observer canonical form: (a) the first partial sum and delay; (b) the second partial sum and delay; (c) the completion with the solution for $u(k)$

In this equation, the external input is $e(k)$, and the response is $u(k)$, which is the solution of this equation. The terms with factors of z are time-shifted toward the future with respect to k and must be eliminated in some way. To do this, we assume at the start that we have the $u(k)$, and of course the $e(k)$, and we rewrite the equation as

$$b_3e - a_3u = z^3u + a_1z^2u + a_2zu - b_0z^3e - b_1z^2e - b_2ze.$$

Here, every term on the right is multiplied by at least one power of z , and thus we can operate on the lot by z^{-1} as shown in the partial block diagram drawn in Fig. 4.9(a).

Now in this internal result there appear a_2u and $-b_2e$, which can be canceled by adding proper multiples of u and e , as shown in Fig. 4.9(b), and once they have been removed, the remainder can again be operated on by z^{-1} .

If we continue this process of subtracting out the terms at k and operating on the rest by z^{-1} , we finally arrive at the place where all that is left is u alone! But that is just what we assumed we had in the first place, so connecting this term back to the start finishes the block diagram, which is drawn in Fig. 4.9(c).

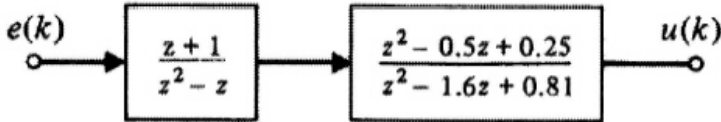


Figure 4.10
Block diagram of
a cascade
realization

A preferred choice of numbering for the state components is also shown in the figure. Following the technique used for the control form, we find that the matrix equations are given by

$$\begin{aligned}\mathbf{x}(k+1) &= \mathbf{A}_o \mathbf{x}(k) + \mathbf{B}_o e(k) \\ u(k) &= \mathbf{C}_o \mathbf{x}(k) + \mathbf{D}_o e(k).\end{aligned}\quad (4.27)$$

where

$$\begin{aligned}\mathbf{A}_o &= \begin{bmatrix} -a_1 & 1 & 0 \\ -a_2 & 0 & 1 \\ -a_3 & 0 & 0 \end{bmatrix} \\ \mathbf{B}_o &= \begin{bmatrix} b_1 - b_0 a_1 \\ b_2 - b_0 a_2 \\ b_3 - b_0 a_3 \end{bmatrix} \\ \mathbf{C}_o &= [1 \quad 0 \quad 0] \\ \mathbf{D}_o &= [b_0].\end{aligned}$$

The block diagrams of Figs. 4.8 and 4.9 are called **direct canonical form** realizations of the transfer function $H(z)$ because the gains of the realizations are coefficients in the transfer-function polynomials.

Another useful form is obtained if we realize a transfer function by placing several first- or second-order direct forms in series with each other, a **cascade canonical form**. In this case, the $H(z)$ is represented as a product of factors, and the poles and zeros of the transfer function are clearly represented in the coefficients.

For example, suppose we have a transfer function

$$\begin{aligned}H(z) &= \frac{z^3 + 0.5z^2 - 0.25z + 0.25}{z^4 - 2.6z^3 + 2.4z^2 - 0.8z} \\ &= \frac{(z+1)(z^2 - 0.5z + 0.25)}{(z^2 - z)(z^2 - 1.6z + 0.8)}.\end{aligned}$$

The zero factor $z+1$ can be associated with the pole factor $z^2 - z$ to form one second-order system, and the zero factor $z^2 - 0.5z + 0.25$ can be associated with the second-order pole factor $z^2 - 1.6z + 0.8$ to form another. The cascade factors, which could be realized in a direct form such as control or observer form, make a cascade form as shown in Fig. 4.10.

4.2.4 Relation of Transfer Function to Pulse Response

We have shown that a transfer function of z^{-1} is a unit delay in the time domain. We can also give a time-domain meaning to an arbitrary transfer function. Recall that the z -transform is defined by Eq. (4.8) to be $E(z) = \sum e_k z^{-k}$, and the transfer function is defined from Eq. (4.16) as $H(z)$ when the input and output are related by $U(z) = H(z)E(z)$. Now suppose we deliberately select $e(k)$ to be the

k	e_{k-1}	e_k	a_k	u_{k-1}	$u_k \equiv h_k$
0	0	1	$T/2$	0	$T/2$
1	1	0	$T/2$	$T/2$	T
2	0	0	0	T	T
3	0	0	0	T	T

Table 4.1
Step-by-step
construction of
the unit pulse
response for Fig.
4.4

unit discrete pulse defined by

$$e_k = \begin{cases} 1, & (k = 0), \\ 0, & (k \neq 0), \end{cases} \\ \cong \delta_k. \quad (4.28)$$

Then it follows that $E(z) = 1$ and therefore that

$$U(z) = H(z). \quad (4.29)$$

Thus the transfer function $H(z)$ is seen to be the *transform* of the response to a unit-pulse input. For example, let us look at the system of Fig. 4.4 and put a unit pulse in at the e_k -node (with no signals in the system beforehand).⁷ We can readily follow the pulse through the block and build Table 4.1.

Thus the unit-pulse response is zero for negative k , is $T/2$ at $k = 0$, and equals T thereafter. The z -transform of this sequence is

$$H(z) = \sum_{-\infty}^{\infty} u_k z^{-k} \cong \sum_{-\infty}^{\infty} h_k z^{-k}.$$

If we add $T/2$ to the z^0 -term and subtract $T/2$ from the whole series, we have a simpler sum, as follows

$$\begin{aligned} H(z) &= \sum_{k=0}^{\infty} T z^{-k} - \frac{T}{2} \\ &= \frac{T}{1-z^{-1}} - \frac{T}{2} \quad (1 < |z|) \\ &= \frac{2T - T(1-z^{-1})}{2(1-z^{-1})} \\ &= \frac{T + Tz^{-1}}{2(1-z^{-1})} \\ &= \frac{T}{2} \frac{z+1}{z-1} \quad (1 < |z|). \end{aligned} \quad (4.30)$$

Of course, this is the transfer function we obtained in Eq. (4.13) from direct analysis of the difference equation.

A final point of view useful in the interpretation of the discrete transfer function is obtained by multiplying the infinite polynomials of $E(z)$ and $H(z)$ as suggested in Eq. (4.16). For purposes of illustration, we will assume that the unit-pulse response, h_k , is zero for $k < 0$. Likewise, we will take $k = 0$ to be the starting time for e_k . Then the product that produces $U(z)$ is the polynomial product given in Fig. 4.11.

Since this product has been shown to be $U(z) = \sum u_k z^{-k}$, it must therefore follow that the coeffi-

⁷In this development we assume that Eq. (4.7) is intended to be used as a formula for computing values of u_k as k increases. There is no reason why we could not also solve for u_k as k takes on negative values. The direction of time comes from the application and not from the recurrence equation.

e_0	$+ e_1 z^{-1}$	$+ e_2 z^{-2}$	$+ e_3 z^{-3}$	$+ \dots$
h_0	$+ h_1 z^{-1}$	$+ h_2 z^{-2}$	$+ h_3 z^{-3}$	$+ \dots$
$e_0 h_0$	$+ e_1 h_0 z^{-1}$	$+ e_2 h_0 z^{-2}$	$+ e_3 h_0 z^{-3}$	
	$+ e_0 h_1 z^{-1}$	$+ e_1 h_1 z^{-2}$	$+ e_2 h_1 z^{-3}$	
		$+ e_0 h_2 z^{-2}$	$+ e_1 h_2 z^{-3}$	
			$+ e_0 h_3 z^{-3}$	
$e_0 h_0 + (e_0 h_1 + e_1 h_0) z^{-1} + (e_0 h_2 + e_1 h_1 + e_2 h_0) z^{-2} + (e_0 h_3 + e_1 h_2 + e_2 h_1 + e_3 h_0) z^{-3} + \dots$				

Figure 4.11
Representation of
the product
 $E(z)H(z)$ as a
product of
polynomials

cient of z^{-k} in the product is u_k . Listing these coefficients, we have the relations

$$\begin{aligned} u_0 &= e_0 h_0 \\ u_1 &= e_0 h_1 + e_1 h_0 \\ u_2 &= e_0 h_2 + e_1 h_1 + e_2 h_0 \\ u_3 &= e_0 h_3 + e_1 h_2 + e_2 h_1 + e_3 h_0. \end{aligned}$$

The extrapolation of this simple pattern gives the result

$$u_k = \sum_{j=0}^k e_j h_{k-j}.$$

By extension, we let the lower limit of the sum be $-\infty$ and the upper limit be $+\infty$:

$$u_k = \sum_{j=-\infty}^{\infty} e_j h_{k-j}. \quad (4.31)$$

Negative values of j in the sum correspond to inputs applied before time equals zero. Values for j greater than k occur if the unit-pulse response is nonzero for negative arguments. By definition, such a system, which responds *before* the input that causes it occurs, is called **noncausal**. This is the discrete **convolution** sum and is the analog of the convolution integral that relates input and impulse response to output in linear, constant, continuous systems.

To verify Eq. (4.31) we can take the z -transform of both sides

$$\sum_{k=-\infty}^{\infty} u_k z^{-k} = \sum_{k=-\infty}^{\infty} z^{-k} \sum_{j=-\infty}^{\infty} e_j h_{k-j}.$$

Interchanging the sum on j with the sum on k leads to

$$U(z) = \sum_{j=-\infty}^{\infty} e_j \sum_{k=-\infty}^{\infty} z^{-k} h_{k-j}.$$

Now let $k - j = l$ in the second sum

$$U(z) = \sum_{j=-\infty}^{\infty} e_j \sum_{l=-\infty}^{\infty} h_l z^{-(l+j)},$$

but $z^{-(l+j)} = z^{-l} z^{-j}$, which leads to

$$U(z) = \sum_{j=-\infty}^{\infty} e_j z^{-j} \sum_{l=-\infty}^{\infty} h_l z^{-l},$$

and we recognize these two separate sums as

$$U(z) = E(z)H(z).$$

We can also derive the convolution sum from the properties of linearity and stationarity. First we need more formal definitions of “linear” and “stationary.”

1. **Linearity:** A system with input e and output u is *linear* if superposition applies, which is to say, if $u_1(k)$ is the response to $e_1(k)$ and $u_2(k)$ is the response to $e_2(k)$, then the system is linear if and only if, for every scalar α and β , the response to $\alpha e_1 + \beta e_2$ is $\alpha u_1 + \beta u_2$.
2. **Stationarity:** A system is *stationary*, or time invariant, if a time shift in the input results in only a time shift in the output. For example, if we take the system at rest (no internal energy in the system) and apply a certain signal $e(k)$, suppose we observe a response $u(k)$. If we repeat this experiment at any later time when the system is again at rest and we apply the shifted input, $e(k - N)$, if we see $u(k - N)$, then the system is stationary. A constant coefficient difference equation is stationary and typically referred to as a constant system.

These properties can be used to derive the convolution in Eq. (4.31) as follows. If response to a unit pulse at $k = 0$ is $h(k)$, then response to a pulse of intensity e_0 is $e_0 h(k)$ if the system is linear. Furthermore, if the system is stationary then a delay of the input will delay the response. Thus, if

$$\begin{aligned} e &= e_l, & k &= l \\ &= 0, & k &\neq l. \end{aligned}$$

Finally, by linearity again, the total response at time k to a sequence of these pulses is the *sum* of the responses, namely,

$$u_k = e_0 h_k + e_1 h_{k-1} + \cdots + e_l h_{k-l} + \cdots + e_k h_0,$$

or

$$u_k = \sum_{l=0}^k e_l h_{k-l}.$$

Now note that if the input sequence began in the distant past, we must include terms for $l < 0$, perhaps back to $l = -\infty$. Similarly, if the system should be noncausal, future values of e where $l > k$ may also come in. The general case is thus (again)

$$u_k = \sum_{l=-\infty}^{\infty} e_l h_{k-l}. \quad (4.32)$$

4.2.5 External Stability

A very important qualitative property of a dynamic system is stability, and we can consider internal or external stability. Internal stability is concerned with the responses at all the internal variables such as those that appear at the delay elements in a canonical block diagram as in Fig. 4.8 or Fig. 4.9 (the state). Otherwise we can be satisfied to consider only the **external stability** as given by the study of the input–output relation described for the linear stationary case by the convolution Eq. (4.32). These differ in that some internal modes might not be connected to both the input and the output of a given system.

For external stability, the most common definition of *appropriate response* is that for every Bounded Input, we should have a Bounded Output. If this is true we say the system is BIBO stable.

A test for BIBO stability can be given directly in terms of the unit-pulse response, h_k . First we consider a sufficient condition. Suppose the input e_k is bounded, that is, there is an M such that

$$|e_l| \leq M < \infty \quad \text{for all } l. \quad (4.33)$$

If we consider the magnitude of the response given by Eq. (4.32), it is easy to see that

$$|u_k| \leq \left| \sum e_l h_{k-l} \right|,$$

which is surely less than the sum of the magnitudes as given by

$$\leq \sum_{-\infty}^{\infty} |e_l| |h_{k-l}|.$$

But, because we assume Eq. (4.33), this result is in turn bounded by

$$\leq M \sum_{l=-\infty}^{\infty} |h_{k-l}|. \quad (4.34)$$

Thus the output will be bounded for every bounded input if

$$\sum_{l=-\infty}^{\infty} |h_{k-l}| < \infty. \quad (4.35)$$

This condition is also necessary, for if we consider the bounded (by 1!) input

$$\begin{aligned} e_l &= \frac{h_{-l}}{|h_{-l}|} & (h_{-l} \neq 0) \\ &= 0 & (h_{-l} = 0) \end{aligned}$$

and apply it to Eq. (4.32), the output at $k = 0$ is

$$\begin{aligned} u_0 &= \sum_{l=-\infty}^{\infty} e_l h_{-l} \\ &= \sum_{l=-\infty}^{\infty} \frac{(h_{-l})^2}{|h_{-l}|} \\ &= \sum_{l=-\infty}^{\infty} |h_{-l}|. \end{aligned} \quad (4.36)$$

Thus, unless the condition given by Eq. (4.35) is true, the system is not BIBO stable.

Integration Stability

Example 4.3

Is the discrete approximation to integration (Eq. 4.7) BIBO stable?

Solution. The test given by Eq. (4.35) can be applied to the unit pulse response used to compute the u_k -column in Table 4.1. The result is

$$\begin{aligned} h_0 &= T/2 \\ h_k &= T, \quad k > 0 \\ \sum |h_k| &= T/2 + \sum_{k=1}^{\infty} T = \text{unbounded}. \end{aligned} \quad (4.37)$$

Therefore, this discrete approximation to integration is not BIBO stable!

General Difference Equation Stability

Example 4.4

Consider the difference equation (4.2) with all coefficients except a_1 and b_0 equal to zero

$$u_k = a_1 u_{k-1} + b_0 e_k. \quad (4.38)$$

Is this equation stable?

Solution. The unit-pulse response is easily developed from the first few terms to be

$$\begin{aligned} u_0 &= b_0, & u_1 &= a_1 b_0, & u_2 &= a_1^2 b_0, & \dots \\ u_k &= h_k = b_0 a_1^k, & k &\geq 0. \end{aligned} \quad (4.39)$$

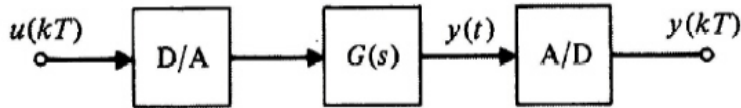


Figure 4.12
The prototype
sampled-data
system

Applying the test, we have

$$\begin{aligned} \sum_{l=-\infty}^{\infty} |h_l| &= \sum_{l=0}^{\infty} b_0 |a_1|^l = b_0 \frac{1}{1 - |a_1|} && (|a_1| < 1) \\ &= \text{unbounded} && (|a_1| \geq 1). \end{aligned}$$

Thus we conclude that the system described by this equation is BIBO stable if $|a_1| < 1$, and unstable otherwise.

For a more general rational transfer function with many simple poles, we can expand the function in partial fractions about its poles, and the corresponding pulse response will be a sum of respective terms. As we saw earlier, if a pole is inside the unit circle, the corresponding pulse response decays with time geometrically and is stable. Thus, if all poles are inside the unit circle, the system with rational transfer function is stable; if at least one pole is on or outside the unit circle, the corresponding system is not BIBO stable. With modern computer programs available, finding the poles of a particular transfer function is no big deal. Sometimes, however, we wish to test for stability of an entire class of systems; or, as in an adaptive control system, the potential poles are constantly changing and we wish to have a quick test for stability in terms of the literal polynomial coefficients. In the continuous case, such a test was provided by Routh; in the discrete case, the most convenient such test was worked out by Jury and Blanchard (1961).⁸

4.3 Discrete Models of Sampled-Data Systems

The systems and signals we have studied thus far have been defined in discrete time only. Most of the dynamic systems to be controlled, however, are continuous systems and, if linear, are described by continuous transfer functions in the Laplace variable s . The interface between the continuous and discrete domains are the A/D and the D/A converters as shown in Fig. 1.1. In this section we develop the analysis needed to compute the discrete transfer function between the samples that come from the digital computer to the D/A converter and the samples that are picked up by the A/D converter.⁹ The situation is drawn in Fig. 4.12.

4.3.1 Using the z -Transform

We wish to find the discrete transfer function from the input samples $u(kT)$ (which probably come from a computer of some kind) to the output samples $y(kT)$ picked up by the A/D converter. Although it is possibly confusing at first, we follow convention and call the discrete transfer function $G(z)$ when the continuous transfer function is $G(s)$. Although $G(z)$ and $G(s)$ are entirely different functions, they do describe the *same* plant, and the use of s for the continuous transform and z for the discrete transform is always maintained. To find $G(z)$ we need only observe that the $y(kT)$ are samples of the plant output when the input is from the D/A converter. As for the D/A converter, we assume that this device, commonly called a zero-order hold or ZOH, accepts a sample $u(kT)$ at $t = kT$ and holds its output constant at this value until the next sample is sent at $t = kT + T$. The piecewise constant output of the D/A is the signal, $u(t)$, that is applied to the plant.

⁸See Franklin, Powell, and Workman, 2nd edition, 1990, for a discussion of the Jury test.

⁹In Chapter 5, a comprehensive frequency analysis of sampled data systems is presented. Here we undertake only the special problem of finding the sample-to-sample discrete transfer function of a continuous system between a D/A and an A/D.

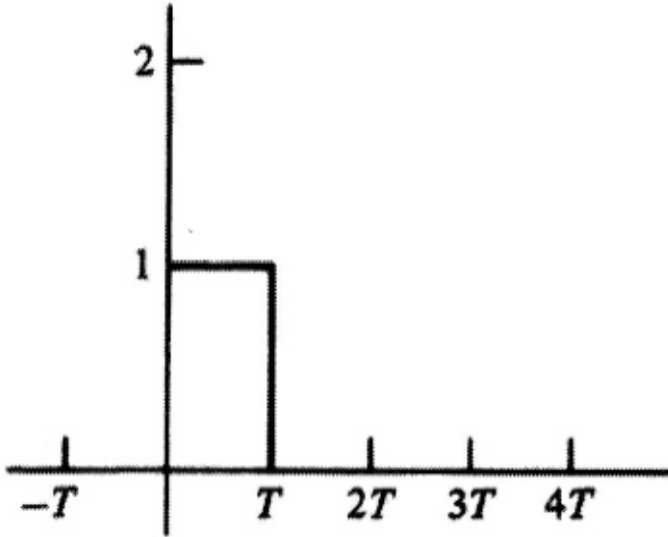


Figure 4.13
D/A output for
unit-pulse input

Our problem is now really quite simple because we have just seen that the discrete transfer function is the z -transform of the samples of the output when the input samples are the unit pulse at $k = 0$. If $u(kT) = 1$ for $k = 0$ and $u(kT) = 0$ for $k \neq 0$, the output of the D/A converter is a pulse of width T seconds and height 1, as sketched in Fig. 4.13. Mathematically, this pulse is given by $1(t) - 1(t - T)$. Let us call the particular output in response to the pulse shown in Fig. 4.13 $y_1(t)$. This response is the difference between the step response [to $1(t)$] and the delayed step response [to $1(t - T)$]. The Laplace transform of the step response is $G(s)/s$. Thus in the transform domain the unit pulse response of the plant is

$$Y_1(s) = (1 - e^{-Ts}) \frac{G(s)}{s}, \quad (4.40)$$

and the required transfer function is the z -transform of the samples of the inverse of $Y_1(s)$, which can be expressed as

$$\begin{aligned} G(z) &= \mathcal{Z}\{Y_1(kT)\} \\ &= \mathcal{Z}\{\mathcal{L}^{-1}\{Y_1(s)\}\} \cong \mathcal{Z}\{Y_1(s)\} \\ &= \mathcal{Z}\left\{(1 - e^{-Ts}) \frac{G(s)}{s}\right\}. \end{aligned}$$

This is the sum of two parts. The first part is $\mathcal{Z}\left\{\frac{G(s)}{s}\right\}$, and the second is

$$\mathcal{Z}\left\{e^{-Ts} \frac{G(s)}{s}\right\} = z^{-1} \mathcal{Z}\left\{\frac{G(s)}{s}\right\}$$

because e^{-Ts} is exactly a delay of one period. Thus the transfer function is

$$G(z) = (1 - z^{-1}) \mathcal{Z}\left\{\frac{G(s)}{s}\right\}. \quad (4.41)$$

What is the discrete transfer function of

$$G(s) = a/(s + a)$$

preceded by a ZOH?

Solution. We will apply the formula (4.41)

$$\frac{G(s)}{s} = \frac{a}{s(s+a)} = \frac{1}{s} - \frac{1}{s+a},$$

and the corresponding time function is

$$\mathcal{L}^{-1} \left\{ \frac{G(s)}{s} \right\} = 1(t) - e^{-at}1(t).$$

The samples of this signal are $1(kT) - e^{-akT}1(kT)$, and the z -transform of these samples is

$$\begin{aligned} \mathcal{Z} \left\{ \frac{G(s)}{s} \right\} &= \frac{z}{z-1} - \frac{z}{z-e^{-aT}} \\ &= \frac{z(1-e^{-aT})}{(z-1)(z-e^{-aT})}. \end{aligned}$$

We could have gone to the tables in Appendix B and found this result directly as Entry 12. Now we can compute the desired transform as

$$\begin{aligned} G(z) &= \frac{z-1}{z} \frac{z(1-e^{-aT})}{(z-1)(z-e^{-aT})} \\ &= \frac{1-e^{-aT}}{z-e^{-aT}}. \end{aligned} \quad (4.42)$$

Discrete Transfer Function of a $1/s^2$ Plant

Example 4.6

What is the discrete transfer function of

$$G(s) = \frac{1}{s^2}$$

preceded by a ZOH?

Solution. We have

$$G(z) = (1-z^{-1})\mathcal{Z} \left\{ \frac{1}{s^3} \right\}.$$

This time we refer to the tables in Appendix B and find that the z -transform associated with $1/s^3$ is

$$\frac{T^2}{2} \frac{z(z+1)}{(z-1)^3},$$

and therefore Eq. (4.41) shows that

$$G(z) = \frac{T^2(z+1)}{2(z-1)^2}. \quad (4.43)$$

The MATLAB function, `c2d.m` computes Eq. (4.41) (the ZOH method is the default) as well as other discrete equivalents discussed in Chapter 6. It is able to accept the system in any of the forms.

Discrete Transfer Function of a $1/s^2$ Plant Using MATLAB

Example 4.7

Use MATLAB to find the discrete transfer function of

$$G(s) = \frac{1}{s^2}$$

preceded by a ZOH, assuming the sample period is $T = 1$ sec.

Solution. The MATLAB script

```

T = 1;
s = tf('s');
sysC = 1/s^2;
sysD = c2d(sysC, T, 'zoh')

```

produces the result that

$$G(z) = \frac{0z^2 + 0.5z + 0.5}{z^2 - 2z + 1} = 0.5 \frac{z + 1}{(z - 1)^2}$$

which is the same as Eq. (4.43) with $T = 1$.

4.3.2 *Continuous Time Delay

We now consider computing the discrete transfer function of a continuous system preceded by a ZOH with pure time delay. The responses of many chemical process-control plants exhibit pure time delay because there is a finite time of transport of fluids or materials between the process and the controls and/or the sensors. Also, we must often consider finite computation time in the digital controller, and this is exactly the same as if the process had a pure time delay. With the techniques we have developed here, it is possible to obtain the discrete transfer function of such processes exactly, as Example 4.8 illustrates.

Discrete Transfer Function of 1st-Order System with Delay

Example 4.8

Find the discrete transfer function of the mixer in Appendix A.3 with $a = 1$, $T = 1$, and $\lambda = 1.5$.

Solution. The fluid mixer problem in Appendix A.3 is described by

$$G(s) = e^{-\lambda s} H(s).$$

The term $e^{-\lambda s}$ represents the delay of λ seconds, which includes both the process delay and the computation delay, if any. We assume that $H(s)$ is a rational transfer function. To prepare this function for computation of the z -transform, we first define an integer ℓ and a positive number m less than 1.0 such that $\lambda = \ell T - mT$. With these definitions we can write

$$\frac{G(s)}{s} = e^{-\ell T s} \frac{e^{mT s} H(s)}{s}.$$

Because ℓ is an integer, this term reduces to $z^{-\ell}$ when we take the z -transform. Because $m < 1$, the transform of the other term is quite direct. We select $H(s) = a/(s + a)$ and, after the partial fraction expansion of $H(s)/s$, we have

$$G(z) = \frac{z - 1}{z^{\ell + 1}} \mathcal{Z} \left\{ \frac{e^{mT s}}{s} - \frac{e^{mT s}}{s + a} \right\}.$$

To complete the transfer function, we need the z -transforms of the inverses of the terms in the braces. The first term is a unit step shifted left by mT seconds, and the second term is an exponential shifted left by the same amount. Because $m < 1$, these shifts are less than one full period, and no sample is picked up in negative time. The signals are sketched in Fig. 4.14.

The samples are given by $1(kT)$ and $e^{-aT(k+m)}1(kT)$. The corresponding z -transforms are $z/(z - 1)$ and $ze^{-amT}/(z - e^{-aT})$. Consequently the final transfer function is

$$\begin{aligned} G(z) &= \frac{z - 1}{z} \frac{1}{z^\ell} \left\{ \frac{z}{z - 1} - \frac{ze^{-amT}}{z - e^{-aT}} \right\} \\ &= \frac{z - 1}{z^\ell} \left\{ \frac{z - e^{-aT} - (z - 1)e^{-amT}}{(z - 1)(z - e^{-aT})} \right\} \\ &= (1 - e^{-amT}) \frac{z + \alpha}{z^\ell (z - e^{-aT})} \end{aligned}$$

where the zero position is at $-\alpha = -(e^{-amT} - e^{-aT})/(1 - e^{-amT})$. Notice that this zero is near the origin of the z -plane when m is near 1 and moves outside the unit circle to near $-\infty$ when m approaches 0. For specific

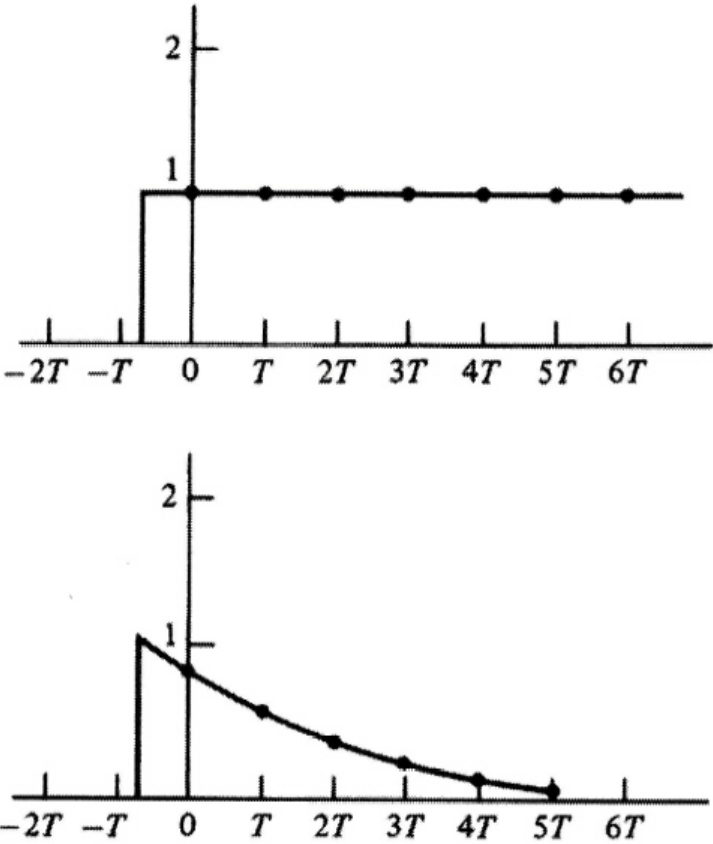


Figure 4.14
Sketch of the shifted signals showing sample points

values of the mixer, we take $a = 1$, $T = 1$, and $\lambda = 1.5$. Then we can compute that $\ell = 2$ and $m = 0.5$. For these values, we get

$$G(z) = \frac{0.3935(z + 0.6065)}{z^2(z - 0.3679)}. \quad (4.44)$$

In MATLAB, the transfer function for this system would be computed by

```
Td = 1.5;    a = 1;    T = 1
sysC = tf(a, [1    a], 'OutputDelay', Td)
sysD = c2d(sysC, T, 'zoh')
```

4.3.3 State-Space Form

Computing the z -transform using the Laplace transform as in Eq. (4.41) is a very tedious business that is unnecessary with the availability of computers. We will next develop a formula using state descriptions that moves the tedium to the computer. A continuous, linear, constant-coefficient system of differential equations was expressed in Eq. (2.1) as a set of first-order matrix differential equations. For a scalar input, it becomes

$$\dot{\mathbf{x}} = \mathbf{F}\mathbf{x} + \mathbf{G}u + \mathbf{G}_1w, \quad (4.45)$$

where u is the scalar control input to the system and w is a scalar disturbance input. The output was expressed in Eq. (2.2) as a linear combination of the state, \mathbf{x} , and the input, u , which becomes for scalar output

$$y = \mathbf{H}\mathbf{x} + Ju. \quad (4.46)$$

Often the sampled-data system being described is the plant of a control problem, and the parameter J in Eq. (4.46) is zero and will frequently be omitted.

State Representation of a $1/s^2$ Plant

Example 4.9

Apply Eqs. (4.45) and (4.46) to the double integrator plant of the satellite control problem in Appendix A.1

$$G(s) = \frac{1}{s^2}.$$

Solution. The satellite attitude-control example is shown in block diagram form in Fig. 4.15 and the attitude (θ) and attitude rate ($\dot{\theta}$) are defined to be x_1 and x_2 , respectively. Therefore, the equations of motion can be written as

$$\begin{aligned} \begin{bmatrix} \dot{x}_1 \\ \dot{x}_2 \end{bmatrix} &= \underbrace{\begin{bmatrix} 0 & 1 \\ 0 & 0 \end{bmatrix}}_{\mathbf{F}} \begin{bmatrix} x_1 \\ x_2 \end{bmatrix} + \underbrace{\begin{bmatrix} 0 \\ 1 \end{bmatrix}}_{\mathbf{G}} u, \\ \theta = y &= \underbrace{\begin{bmatrix} 1 & 0 \end{bmatrix}}_{\mathbf{H}} \begin{bmatrix} x_1 \\ x_2 \end{bmatrix} \end{aligned} \quad (4.47)$$

which, in this case, turns out to be a rather involved way of writing

$$\ddot{\theta} = u.$$

The representations given by Eqs. (4.45) and (4.46) are not unique. Given one state representation, any nonsingular linear transformation of that state such as $Bx = Tx$ is also an allowable alternative realization of the same system.

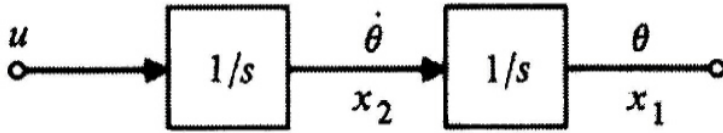


Figure 4.15
Satellite attitude control in classical representation



Figure 4.16
System definition with sampling operations shown

If we let $\xi = \mathbf{T}\mathbf{x}$ in Eqs. (4.45) and (4.46), we find

$$\begin{aligned}\dot{\xi} &= \mathbf{T}\dot{\mathbf{x}} = \mathbf{T}(\mathbf{F}\mathbf{x} + \mathbf{G}u + \mathbf{G}_1w) \\ &= \mathbf{T}\mathbf{F}\mathbf{x} + \mathbf{T}\mathbf{G}u + \mathbf{T}\mathbf{G}_1w, \\ \dot{\xi} &= \mathbf{T}\mathbf{F}\mathbf{T}^{-1}\xi + \mathbf{T}\mathbf{G}u + \mathbf{T}\mathbf{G}_1w, \\ y &= \mathbf{H}\mathbf{T}^{-1}\xi + Ju.\end{aligned}$$

If we designate the system matrices for the new state ξ as \mathbf{A} , \mathbf{B} , \mathbf{C} , and \mathbf{D} , then

$$\dot{\xi} = \mathbf{A}\xi + \mathbf{B}u + \mathbf{B}_1w, \quad y = \mathbf{C}\xi + \mathbf{D}u,$$

where

$$\mathbf{A} = \mathbf{T}\mathbf{F}\mathbf{T}^{-1}, \quad \mathbf{B} = \mathbf{T}\mathbf{G}, \quad \mathbf{B}_1 = \mathbf{T}\mathbf{G}_1, \quad \mathbf{C} = \mathbf{H}\mathbf{T}^{-1}, \quad \mathbf{D} = J.$$

State Transformation for $1/s^2$ Plant

Example 4.10

Find the state representation for the case with the state definitions of the previous example interchanged.

Solution. Let $\xi_1 = x_2$ and $\xi_2 = x_1$ in Eq. (4.47); or, in matrix notation, the transformation to interchange the states is

$$\mathbf{T} = \begin{bmatrix} 0 & 1 \\ 1 & 0 \end{bmatrix}.$$

In this case $\mathbf{T}^{-1} = \mathbf{T}$, and application of the transformation equations to the system matrices of Eq. (4.47) gives

$$\mathbf{A} = \begin{bmatrix} 0 & 0 \\ 1 & 0 \end{bmatrix} \quad \mathbf{B} = \begin{bmatrix} 1 \\ 0 \end{bmatrix} \quad \mathbf{C} = [0 \quad 1].$$

Most often, a change of state is made to bring the description matrices into a useful canonical form. We saw earlier how a single high-order difference equation could be represented by a state description in control or in observer canonical form. Also, there is a very useful state description corresponding to the partial-fraction expansion of a transfer function. State transformations can take a general description for either a continuous or a discrete system and, subject to some technical restrictions, convert it into a description in one or the other of these forms, as needed.

We wish to use the state description to establish a general method for obtaining the difference equations that represent the behavior of the continuous plant. Fig. 4.16 again depicts the portion of our system under consideration. Ultimately, the digital controller will take the samples $y(k)$, operate on that sequence by means of a difference equation, and put out a sequence of numbers, $u(k)$, which are the inputs to the plant. The loop will, therefore, be closed. To analyze the result, we must be able

to relate the samples of the output $y(k)$ to the samples of the control $u(k)$. To do this, we must solve Eq. (4.45).

We will solve the general equation in two steps. We begin by solving the equation with only initial conditions and no external input. This is the homogeneous equation

$$\dot{\mathbf{x}}_h = \mathbf{F}\mathbf{x}_h(t), \quad \mathbf{x}_h(t_0) = \mathbf{x}_0. \quad (4.48)$$

To solve this, we assume the solution is sufficiently smooth that a series expansion of the solution is possible

$$\mathbf{x}_h(t) = \mathbf{A}_0 + \mathbf{A}_1(t - t_0) + \mathbf{A}_2(t - t_0)^2 + \dots \quad (4.49)$$

If we let $t = t_0$, we find immediately that $\mathbf{A}_0 = \mathbf{x}_0$. If we differentiate Eq. (4.49) and substitute into Eq. (4.48), we have

$$\mathbf{A}_1 + 2\mathbf{A}_2(t - t_0) + 3\mathbf{A}_3(t - t_0)^2 + \dots = \mathbf{F}\mathbf{x}_h$$

and, at $t = t_0$, $\mathbf{A}_1 = \mathbf{F}\mathbf{x}_0$. Now we continue to differentiate the series and the differential equation and equate them at t_0 to arrive at the series

$$\mathbf{x}_h(t) = \left[\mathbf{I} + \mathbf{F}(t - t_0) + \frac{\mathbf{F}^2(t - t_0)^2}{2} + \frac{\mathbf{F}^3(t - t_0)^3}{6} + \dots \right] \mathbf{x}_0.$$

This series is defined as the matrix exponential and written

$$\mathbf{x}_h(t) = e^{\mathbf{F}(t-t_0)} \mathbf{x}(t_0), \quad (4.50)$$

where, by definition, the matrix exponential is

$$\begin{aligned} e^{\mathbf{F}(t-t_0)} &= \mathbf{I} + \mathbf{F}(t - t_0) + \mathbf{F}^2 \frac{(t - t_0)^2}{2!} + \mathbf{F}^3 \frac{(t - t_0)^3}{3!} + \dots \\ &= \sum_{k=0}^{\infty} \mathbf{F}^k \frac{(t - t_0)^k}{k!}. \end{aligned} \quad (4.51)$$

It can be shown that the solution given by Eq. (4.50) is unique, which leads to very interesting properties of the matrix exponential. For example, consider two values of t : t_1 and t_2 . We have

$$\mathbf{x}(t_1) = e^{\mathbf{F}(t_1-t_0)} \mathbf{x}(t_0)$$

and

$$\mathbf{x}(t_2) = e^{\mathbf{F}(t_2-t_0)} \mathbf{x}(t_0).$$

Because t_0 is arbitrary also, we can express $\mathbf{x}(t_2)$ as if the equation solution began at t_1 , for which

$$\mathbf{x}(t_2) = e^{\mathbf{F}(t_2-t_1)} \mathbf{x}(t_1).$$

Substituting for $\mathbf{x}(t_1)$ gives

$$\mathbf{x}(t_2) = e^{\mathbf{F}(t_2-t_1)} e^{\mathbf{F}(t_1-t_0)} \mathbf{x}(t_0).$$

We now have two separate expressions for $\mathbf{x}(t_2)$, and, if the solution is unique, these must be the same. Hence we conclude that

$$e^{\mathbf{F}(t_2-t_0)} = e^{\mathbf{F}(t_2-t_1)} e^{\mathbf{F}(t_1-t_0)} \quad (4.52)$$

for all t_2, t_1, t_0 . Note especially that if $t_2 = t_0$, then

$$\mathbf{I} = e^{-\mathbf{F}(t_1-t_0)} e^{\mathbf{F}(t_1-t_0)}.$$

Thus we can obtain the inverse of $e^{\mathbf{F}t}$ by merely changing the sign of t ! We will use this result in computing the particular solution to Eq. (4.45).

The particular solution when u is not zero is obtained by using the method of **variation of parameters**.¹⁰ We guess the solution to be in the form

$$\mathbf{x}_p(t) = e^{\mathbf{F}(t-t_0)}\mathbf{v}(t), \quad (4.53)$$

where $\mathbf{v}(t)$ is a vector of variable parameters to be determined [as contrasted to the constant parameters $\mathbf{x}(t_0)$ in Eq. (4.50)]. Substituting Eq. (4.53) into Eq. (4.45), we obtain

$$\mathbf{F}e^{\mathbf{F}(t-t_0)}\mathbf{v} + e^{\mathbf{F}(t-t_0)}\dot{\mathbf{v}} = \mathbf{F}e^{\mathbf{F}(t-t_0)}\mathbf{v} + \mathbf{G}u,$$

and, using the fact that the inverse is found by changing the sign of the exponent, we can solve for $\dot{\mathbf{v}}$ as

$$\dot{\mathbf{v}}(t) = e^{-\mathbf{F}(t-t_0)}\mathbf{G}u(t).$$

Assuming that the control $u(t)$ is zero for $t < t_0$, we can integrate $\dot{\mathbf{v}}$ from t_0 to t to obtain

$$\mathbf{v}(t) = \int_{t_0}^t e^{-\mathbf{F}(\tau-t_0)}\mathbf{G}u(\tau)d\tau.$$

Hence, from Eq. (4.53), we get

$$\mathbf{x}_p(t) = e^{\mathbf{F}(t-t_0)} \int_{t_0}^t e^{-\mathbf{F}(\tau-t_0)}\mathbf{G}u(\tau)d\tau,$$

and simplifying, using the results of Eq. (4.52), we obtain the particular solution (convolution)

$$\mathbf{x}_p(t) = \int_{t_0}^t e^{\mathbf{F}(t-\tau)}\mathbf{G}u(\tau)d\tau. \quad (4.54)$$

The total solution for $w = 0$ and $u \neq 0$ is the sum of Eqs. (4.50) and (4.54):

$$\mathbf{x}(t) = e^{\mathbf{F}(t-t_0)}\mathbf{x}(t_0) + \int_{t_0}^t e^{\mathbf{F}(t-\tau)}\mathbf{G}u(\tau)d\tau. \quad (4.55)$$

We wish to use this solution over one sample period to obtain a difference equation: hence we juggle the notation a bit (let $t = kT + T$ and $t_0 = kT$) and arrive at a particular version of Eq. (4.55):

$$\mathbf{x}(kT + T) = e^{\mathbf{F}T}\mathbf{x}(kT) + \int_{kT}^{kT+T} e^{\mathbf{F}(kT+T-\tau)}\mathbf{G}u(\tau)d\tau. \quad (4.56)$$

This result is not dependent on the type of hold because u is specified in terms of its continuous time history, $u(t)$, over the sample interval. A common and typically valid assumption is that of a zero-order hold (ZOH) with no delay, that is,

$$u(\tau) = u(kT), \quad kT \leq \tau < kT + T.$$

If some other hold is implemented or if there is a delay between the application of the control from the ZOH and the sample point, this fact can be accounted for in the evaluation of the integral in Eq. (4.56). The equations for a delayed ZOH will be given in the next subsection. To facilitate the solution of Eq. (4.56) for a ZOH with no delay, we change variables in the integral from τ to η such that

$$\eta = kT + T - \tau.$$

Then we have

$$\mathbf{x}(kT + T) = e^{\mathbf{F}T}\mathbf{x}(kT) + \int_0^T e^{\mathbf{F}\eta}d\eta\mathbf{G}u(kT). \quad (4.57)$$

¹⁰Due to Joseph Louis Lagrange, French mathematician (1736–1813). We assume $w = 0$, but because the equations are linear, the effect of w can be added later.

-
1. Select sampling period T and description matrices F and G .
 2. Matrix $\mathbf{I} \leftarrow$ Identity
 3. Matrix $\Psi \leftarrow \mathbf{I}$
 4. $k \leftarrow 11$ [We are using $N = 11$ in Eq. (4.62).]
 5. If $k = 1$, go to step 9.
 6. Matrix $\Psi \leftarrow \mathbf{I} + \frac{FT}{k}\Psi$
 7. $k \leftarrow k + 1$
 8. Go to step 5.
 9. Matrix $\Gamma \leftarrow T\Psi G$
 10. Matrix $\Phi \leftarrow \mathbf{I} + FT\Psi$
-

Table 4.2

Program logic to compute Φ and Γ from F, G , and T for simple cases. (The left arrow \leftarrow is read as "is replaced by.")

If we define

$$\begin{aligned}\Phi &= e^{FT} \\ \Gamma &= \int_0^T e^{F\eta} d\eta G,\end{aligned}\quad (4.58)$$

Eqs. (4.57) and (4.46) reduce to difference equations in standard form

$$\begin{aligned}\mathbf{x}(k+1) &= \Phi\mathbf{x}(k) + \Gamma u(k) + \Gamma_1 w(k), \\ y(k) &= \mathbf{H}\mathbf{x}(k),\end{aligned}\quad (4.59)$$

where we include the effect of an impulsive or piecewise constant disturbance, w , and assume that $J = 0$ in this case. If w is a constant, then Γ_1 is given by Eq. (4.58) with G replaced by G_1 . If w is an impulse, then $\Gamma_1 = G_1$.¹¹ The Φ series expansion

$$\Phi = e^{FT} = \mathbf{I} + FT + \frac{F^2 T^2}{2!} + \frac{F^3 T^3}{3!} + \dots,$$

can also be written

$$\Phi = \mathbf{I} + FT\Psi, \quad (4.60)$$

where

$$\Psi = \mathbf{I} + \frac{FT}{2!} + \frac{F^2 T^2}{3!} + \dots$$

The Γ integral in Eq. (4.58) can be evaluated term by term to give

$$\begin{aligned}\Gamma &= \sum_{k=0}^{\infty} \frac{F^k T^{k+1}}{(k+1)!} G \\ &= \sum_{k=0}^{\infty} \frac{F^k T^k}{(k+1)!} TG \\ &= \Psi TG.\end{aligned}\quad (4.61)$$

We evaluate Ψ by a series in the form

$$\Psi \approx \mathbf{I} + \frac{FT}{2} \left(\mathbf{I} + \frac{FT}{3} \left(\dots \frac{FT}{N-1} \left(\mathbf{I} + \frac{FT}{N} \right) \dots \right) \right), \quad (4.62)$$

which has better numerical properties than the direct series of powers. We then find Γ from Eq. (4.61) and Φ from Eq. (4.60). A discussion of the selection of N and a technique to compute Ψ for comparatively large T is given by Källström (1973), and a review of various methods is found in a classic paper by Moler and Van Loan (1978). The program logic for computation of Φ and Γ for simple cases

¹¹If $w(t)$ varies significantly between its sample values, then an integral like that of Eq. (4.56) is required to describe its influence on $\mathbf{x}(k+1)$. Random disturbances are treated in Chapter 9.

is given in Fig. 4.2. MATLAB's `c2d.m` and all control design packages that we know of compute Φ and Γ from the continuous matrices \mathbf{F} , \mathbf{G} , and the sample period T .

To compare this method of representing the plant with the discrete transfer functions, we can take the z -transform of Eq. (4.59) with $w = 0$ and obtain

$$\begin{aligned} [z\mathbf{I} - \Phi]\mathbf{X} &= \Gamma U(z), \\ Y(z) &= \mathbf{H}\mathbf{X}(z) \end{aligned} \quad (4.63)$$

therefore

$$\frac{Y(z)}{U(z)} = \mathbf{H}[z\mathbf{I} - \Phi]^{-1}\Gamma. \quad (4.64)$$

Φ and Γ Calculation

Example 4.11

By hand, calculate the Φ and Γ matrices for the satellite attitude-control system of Example 4.9.

Solution. Use Eqs. (4.60) and (4.61) and the values for \mathbf{F} and \mathbf{G} defined in Eq. (4.47). Since $\mathbf{F}^2 = 0$ in this case, we have

$$\begin{aligned} \Phi &= \mathbf{I} + \mathbf{F}T + \frac{\mathbf{F}^2 T^2}{2!} + \dots \\ &= \begin{bmatrix} 1 & 0 \\ 0 & 1 \end{bmatrix} + \begin{bmatrix} 0 & 1 \\ 0 & 0 \end{bmatrix} T = \begin{bmatrix} 1 & T \\ 0 & 1 \end{bmatrix} \\ \Gamma &= \left[\mathbf{I}T + \mathbf{F} \frac{T^2}{2!} + \frac{\mathbf{F}^2 T^3}{3!} \right] \mathbf{G} \\ &= \left\{ \begin{bmatrix} T & 0 \\ 0 & T \end{bmatrix} + \begin{bmatrix} 0 & 1 \\ 0 & 0 \end{bmatrix} \frac{T^2}{2} \right\} \begin{bmatrix} 0 \\ 1 \end{bmatrix} = \begin{bmatrix} T^2/2 \\ T \end{bmatrix}, \end{aligned}$$

hence, using Eq. (4.64), we obtain

$$\begin{aligned} \frac{Y(z)}{U(z)} &= [1 \quad 0] \left\{ z \begin{bmatrix} 1 & 0 \\ 0 & 1 \end{bmatrix} - \begin{bmatrix} 1 & T \\ 0 & 1 \end{bmatrix} \right\}^{-1} \begin{bmatrix} T^2/2 \\ T \end{bmatrix} \\ &= \frac{T^2}{2} \frac{(z+1)}{(z-1)^2}, \end{aligned}$$

which is the same result that would be obtained using Eq. (4.41) and the z -transform tables. Note that the values for Φ and Γ could have been obtained for a specific value of T by the MATLAB statements

```
sysC = ss(F,G,H,J)
sysD = c2d(sysC,T)
[phi,gam,h,J] = ssdata(sysD)
```

Note that to compute Y/U we find that the denominator is the determinant $\det(z\mathbf{I} - \Phi)$, which comes from the matrix inverse in Eq. (4.64). This determinant is the characteristic polynomial of the transfer function, and the zeros of the determinant are the poles of the plant. We have two poles at $z = 1$ in this case, corresponding to the two integrations in this plant's equations of motion.

We can explore further the question of poles and zeros and the state-space description by considering again the transform equations (4.63). An interpretation of transfer-function poles from the perspective of the corresponding difference equation is that a pole is a value of z such that the equation has a nontrivial solution when the forcing input is zero. From Eq. (4.63a), this implies that the linear eigenvalue equations

$$[z\mathbf{I} - \Phi]\mathbf{X}(z) = [\mathbf{0}]$$

have a nontrivial solution. From matrix algebra the well-known requirement for this is that $\det(z\mathbf{I} - \Phi) = 0$. Using the Φ from the previous example, we have

$$\begin{aligned}\det[z\mathbf{I} - \Phi] &= \det \left[\begin{bmatrix} z & 0 \\ 0 & z \end{bmatrix} - \begin{bmatrix} 1 & T \\ 0 & 1 \end{bmatrix} \right] \\ &= \det \begin{bmatrix} z-1 & -T \\ 0 & z-1 \end{bmatrix} \\ &= (z-1)^2 = 0,\end{aligned}$$

which is the characteristic equation, as we have seen. To compute the poles numerically when the matrices are given, one would use an eigenvalue routine. In MATLAB, the statement

```
lam = eig(phi)
```

will produce a vector, `lam`, of the poles of Φ .

Along the same line of reasoning, a system zero is a value of z such that the system output is zero even with a nonzero state-and-input combination. Thus if we are able to find a nontrivial solution for $X(z_0)$ and $U(z_0)$ such that $Y(z_0)$ is zero, then z_0 is a zero of the system. Combining the two parts of Eq. (4.59), we must satisfy the requirement

$$\begin{bmatrix} z\mathbf{I} - \Phi & -\Gamma \\ \mathbf{H} & 0 \end{bmatrix} \begin{bmatrix} X(z) \\ U(z) \end{bmatrix} = [\mathbf{0}]. \quad (4.65)$$

Once more the condition for the existence of nontrivial solutions is that the determinant of the square coefficient system matrix be zero.¹² For the satellite example, we have

$$\begin{aligned}\det \begin{bmatrix} z-1 & -T & -T^2/2 \\ 0 & z-1 & -T \\ 1 & 0 & 0 \end{bmatrix} &= 1 \cdot \det \begin{bmatrix} -T & -T^2/2 \\ z-1 & -T \end{bmatrix} \\ &= +T^2 + \left(\frac{T^2}{2}\right)(z-1) \\ &= +\frac{T^2}{2}z + \frac{T^2}{2} \\ &= +\frac{T^2}{2}(z+1).\end{aligned}$$

Thus we have a single zero at $z = -1$, as we have seen from the transfer function. These zeros are called **transmission zeros** and are easily computed using MATLAB's `tzero.m`.¹³ Using the discrete model `sysD` found in Example 4.11 the statement

```
zer = tzero(sysD)
```

produces the transmission zeros in the quantity `zer`.

4.3.4 *State-Space Models for Systems with Delay

Thus far we have discussed the calculation of discrete state models from continuous, ordinary differential equations of motion. Now we present the formulas for including a time delay in the model and also a time prediction up to one period which corresponds to the **modified z-transform** as defined by

¹²We do not consider here the case of different numbers of inputs and outputs.

¹³In using this function, one must be careful to account properly for the zeros that are at infinity; the function might return them as very large numbers that the user must remove to “uncover” the finite zeros; that is, to scale the finite numbers so they don't appear to be zero by the computer.

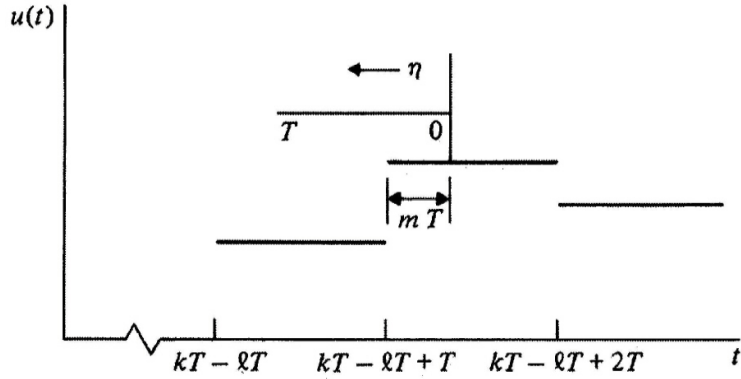


Figure 4.17
Sketch of a
piecewise input
and time axis for
a system with
time delay

Jury. We begin with a state-variable model that includes a delay in control action. The state equations are

$$\begin{aligned}\dot{\mathbf{x}}(t) &= \mathbf{F}\mathbf{x}(t) + \mathbf{G}u(t - \lambda), \\ y &= \mathbf{H}\mathbf{x}.\end{aligned}\quad (4.66)$$

The general solution to Eq. (4.66) is given by Eq. (4.55); it is

$$\mathbf{x}(t) = e^{\mathbf{F}(t-t_0)}\mathbf{x}(t_0) + \int_{t_0}^t e^{\mathbf{F}(t-\tau)}\mathbf{G}u(\tau - \lambda) d\tau.$$

If we let $t_0 = kT$ and $t = kT + T$, then

$$\mathbf{x}(kT + T) = e^{\mathbf{F}T}\mathbf{x}(kT) + \int_{kT}^{kT+T} e^{\mathbf{F}(kT+T-\tau)}\mathbf{G}u(\tau - \lambda) d\tau.$$

If we substitute $\eta = kT + T - \tau$ for τ in the integral, we find a modification of Eq. (4.57)

$$\begin{aligned}\mathbf{x}(kT + T) &= e^{\mathbf{F}T}\mathbf{x}(kT) + \int_T^0 e^{\mathbf{F}\eta}\mathbf{G}u(kT + T - \lambda - \eta)(-d\eta) \\ &= e^{\mathbf{F}T}\mathbf{x}(kT) + \int_0^T e^{\mathbf{F}\eta}\mathbf{G}u(kT + T - \lambda - \eta) d\eta.\end{aligned}$$

If we now separate the system delay λ into an integral number of sampling periods plus a fraction, we can define an integer ℓ and a positive number m less than one such that

$$\lambda = \ell T - mT, \quad (4.67)$$

and

$$\begin{aligned}\ell &\geq 0, \\ 0 &\leq m < 1.\end{aligned}$$

With this substitution, we find that the discrete system is described by

$$\mathbf{x}(kT + T) = e^{\mathbf{F}T}\mathbf{x}(kT) + \int_0^T e^{\mathbf{F}\eta}\mathbf{G}u(kT + T - \ell T + mT - \eta) d\eta. \quad (4.68)$$

If we sketch a segment of the time axis near $t = kT - \ell T$ (Fig. 4.17), the nature of the integral in Eq. (4.68) with respect to the variable η will become clear. The integral runs for η from 0 to T , which corresponds to t from $kT - \ell T + T + mT$ backward to $kT - \ell T + mT$. Over this period, the control, which we assume is piecewise constant, takes on first the value $u(kT - \ell T + T)$ and then the

value $u(kT - \ell T)$. Therefore, we can break the integral in (2.66) into two parts as follows

$$\begin{aligned} \mathbf{x}(kT + T) &= e^{\mathbf{F}T} \mathbf{x}(kT) + \int_0^{mT} e^{\mathbf{F}\eta} \mathbf{G} d\eta u(kT - \ell T + T) \\ &\quad + \int_{mT}^T e^{\mathbf{F}\eta} \mathbf{G} d\eta u(kT - \ell T) \\ &= \mathbf{\Phi} \mathbf{x}(kT) + \mathbf{\Gamma}_1 u(kT - \ell T) + \mathbf{\Gamma}_2 u(kT - \ell T + T). \end{aligned} \quad (4.69)$$

In Eq. (4.69) we defined

$$\mathbf{\Phi} = e^{\mathbf{F}T}, \quad \mathbf{\Gamma}_1 = \int_{mT}^T e^{\mathbf{F}\eta} \mathbf{G} d\eta, \quad \text{and} \quad \mathbf{\Gamma}_2 = \int_0^{mT} e^{\mathbf{F}\eta} \mathbf{G} d\eta. \quad (4.70)$$

To complete our analysis it is necessary to express Eq. (4.69) in standard state-space form. To do this we must consider separately the cases of $\ell = 0$, $\ell = 1$, and $\ell > 1$.

For $\ell = 0$, $\lambda = -mT$ according to Eq. (4.67), which implies not delay but prediction. Because mT is restricted to be less than T , however, the output will not show a sample before $k = 0$, and the discrete system will be causal. The result is that the discrete system computed with $\ell = 0$, $m \neq 0$ will show the response at $t = 0$, which the same system with $\ell = 0$, $m = 0$ would show at $t = mT$. In other words, by taking $\ell = 0$ and $m \neq 0$ we pick up the response values *between* the normal sampling instants. In z -transform theory, the transform of the system with $\ell = 0$, $m \neq 0$ is called the **modified z -transform**.¹⁴ The state-variable form requires that we evaluate the integrals in Eq. (4.70). To do so we first convert $\mathbf{\Gamma}_1$ to a form similar to the integral for $\mathbf{\Gamma}_2$. From Eq. (4.70) we factor out the constant matrix \mathbf{G} to obtain

$$\mathbf{\Gamma}_1 = \int_{mT}^T e^{\mathbf{F}\eta} d\eta \mathbf{G}.$$

If we set $\sigma = \eta - mT$ in this integral, we have

$$\begin{aligned} \mathbf{\Gamma}_1 &= \int_0^{T-mT} e^{\mathbf{F}(mT+\sigma)} d\sigma \mathbf{G} \\ &= e^{\mathbf{F}mT} \int_0^{T-mT} e^{\mathbf{F}\sigma} d\sigma \mathbf{G}. \end{aligned} \quad (4.71)$$

For notational purposes we will define, for any positive nonzero scalar number, a , the two matrices

$$\mathbf{\Phi}(a) = e^{\mathbf{F}a}, \quad \mathbf{\Psi}(a) = \frac{1}{a} \int_0^a e^{\mathbf{F}\sigma} d\sigma. \quad (4.72)$$

In terms of these matrices, we have

$$\begin{aligned} \mathbf{\Gamma}_1 &= (T - mT) \mathbf{\Phi}(mT) \mathbf{\Psi}, \\ \mathbf{\Gamma}_2 &= mT \mathbf{\Psi}. \end{aligned} \quad (4.73)$$

The definitions in Eqs. (4.72) are also useful from a computational point of view. If we recall the series definition of the matrix exponential

$$\mathbf{\Phi}(a) = e^{\mathbf{F}a} = \sum_{k=0}^{\infty} \frac{\mathbf{F}^k a^k}{k!},$$

then we get

$$\begin{aligned} \mathbf{\Psi}(a) &= \frac{1}{a} \int_0^a \sum_{k=0}^{\infty} \frac{\mathbf{F}^k \sigma^k}{k!} d\sigma \\ &= \frac{1}{a} \sum_{k=0}^{\infty} \frac{\mathbf{F}^k}{k!} \frac{a^{k+1}}{k+1} \\ &= \sum_{k=0}^{\infty} \frac{\mathbf{F}^k a^k}{(k+1)!}. \end{aligned} \quad (4.74)$$

¹⁴See Jury (1964) or Ogata (1987).

But now we note that the series for $\Phi(a)$ can be written as

$$\Phi(a) = \mathbf{I} + \sum_{k=1}^{\infty} \frac{\mathbf{F}^k a^k}{k!}.$$

If we let $k = j + 1$ in the sum, then, as in Eq. (4.60), we have

$$\begin{aligned} \Phi(a) &= \mathbf{I} + \sum_{j=0}^{\infty} \frac{\mathbf{F}^{j+1} a^{j+1}}{(j+1)!} \\ &= \mathbf{I} + \sum_{j=0}^{\infty} \frac{\mathbf{F}^j a^j}{(j+1)!} a\mathbf{F} \\ &= \mathbf{I} + a\mathbf{\Psi}(a)\mathbf{F}. \end{aligned} \quad (4.75)$$

The point of Eq. (4.75) is that only the series for $\mathbf{\Psi}(a)$ needs to be computed and from this single sum we can compute Φ and Γ .

If we return to the case $\ell = 0$, $m \neq 0$, the discrete state equations are

$$\mathbf{x}(k+1) = \Phi\mathbf{x}(k) + \Gamma_1 u(k) + \Gamma_2 u(k+1),$$

where Γ_1 and Γ_2 are given by Eq. (4.73). In order to put these equations in state-variable form, we must eliminate the term in $u(k+1)$. To do this, we define a new state, $\xi(k) = \mathbf{x}(k) - \Gamma_2 u(k)$. Then the equations are

$$\begin{aligned} \xi(k+1) &= \mathbf{x}(k+1) - \Gamma_2 u(k+1) \\ &= \Phi\mathbf{x}(k) + \Gamma_1 u(k) + \Gamma_2 u(k+1) - \Gamma_2 u(k+1), \\ \xi(k+1) &= \Phi[\xi(k) + \Gamma_2 u(k)] + \Gamma_1 u(k) \\ &= \Phi\xi(k) + (\Phi\Gamma_2 + \Gamma_1)u(k) \\ &= \Phi\xi(k) + \Gamma u(k). \end{aligned} \quad (4.76)$$

The output equation is

$$\begin{aligned} y(k) &= \mathbf{H}\mathbf{x}(k) \\ &= \mathbf{H}[\xi(k) + \Gamma_2 u(k)] \\ &= \mathbf{H}\xi(k) + \mathbf{H}\Gamma_2 u(k) \\ &= \mathbf{H}_d \xi(k) + J_d u(k). \end{aligned} \quad (4.77)$$

Thus for $\ell = 0$, the state equations are given by Eqs. (4.73), (4.76), and (4.77). Note especially that if $m = 0$, then $\Gamma_2 = 0$, and these equations reduce to the previous model with no delay.

Our next case is $\ell = 1$. From Eq. (4.69), the equations are given by

$$\mathbf{x}(k+1) = \Phi\mathbf{x}(k) + \Gamma_1 u(k-1) + \Gamma_2 u(k).$$

In this case, we must eliminate $u(k-1)$ from the right-hand side, which we do by defining a new state $x_{n+1}(k) = u(k-1)$. We have thus an increased dimension of the state, and the equations are

$$\begin{aligned} \begin{bmatrix} \mathbf{x}(k+1) \\ x_{n+1}(k+1) \end{bmatrix} &= \begin{bmatrix} \Phi & \Gamma_1 \\ 0 & 0 \end{bmatrix} \begin{bmatrix} \mathbf{x}(k) \\ x_{n+1}(k) \end{bmatrix} + \begin{bmatrix} \Gamma_2 \\ 1 \end{bmatrix} u(k) \\ y(k) &= \begin{bmatrix} \mathbf{H} & 0 \end{bmatrix} \begin{bmatrix} \mathbf{x} \\ x_{n+1} \end{bmatrix}. \end{aligned} \quad (4.78)$$

For our final case, we consider $\ell > 1$. In this case, the equations are

$$\mathbf{x}(k+1) = \Phi\mathbf{x}(k) + \Gamma_1 u(k-\ell) + \Gamma_2 u(k-\ell+1)$$

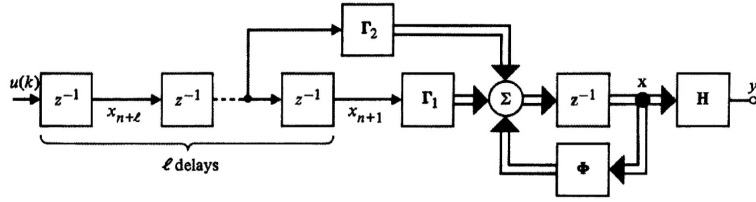


Figure 4.18
Block diagram of system with delay of more than one period. Double line indicates vector valued variables

and we must eliminate the past controls up to $u(k)$. To do this we introduce ℓ new variables such that

$$x_{n+1}(k) = u(k - \ell), \quad x_{n+2}(k) = u(k - \ell + 1), \quad \dots, \quad x_{n+\ell}(k) = u(k - 1).$$

The structure of the equations is

$$\begin{bmatrix} \mathbf{x}(k+1) \\ x_{n+1}(k+1) \\ x_{n+2}(k+1) \\ \vdots \\ x_{n+\ell}(k+1) \end{bmatrix} = \begin{bmatrix} \Phi & \Gamma_1 & \Gamma_2 & 0 & \dots & 0 \\ 0 & 0 & 1 & 0 & \dots & 0 \\ 0 & 0 & 0 & 1 & \dots & 0 \\ \vdots & \vdots & \vdots & \vdots & \ddots & \vdots \\ 0 & 0 & 0 & 0 & 0 & 1 \\ 0 & 0 & 0 & 0 & 0 & 0 \end{bmatrix} \begin{bmatrix} x(k) \\ x_{n+1}(k) \\ x_{n+2}(k) \\ x_{n+3}(k) \\ \vdots \\ x_{n+\ell}(k) \end{bmatrix} + \begin{bmatrix} 0 \\ 0 \\ 0 \\ 0 \\ \vdots \\ 1 \end{bmatrix} u(k)$$

$$y(k) = [\mathbf{H} \quad 0 \quad \dots \quad 0] \begin{bmatrix} \mathbf{x}(k) \\ x_{n+1}(k) \\ \vdots \\ x_{n+\ell}(k) \end{bmatrix}. \quad (4.79)$$

This final solution is easily visualized in terms of a block diagram, as shown in Fig. 4.18.

4.3.5 *Numerical Considerations in Computing Φ and Γ

The numerical considerations of these computations are centered in the approximation to the infinite sum for Ψ given by Eq. (4.74) or, for $a = T$, by Eq. (4.62). The problem is that if \mathbf{FT} is large, then $(\mathbf{FT})^N/N!$ becomes extremely large before it becomes small, and before acceptable accuracy is realized most computer number representations will overflow, destroying the value of the computation. Källström (1973) has analyzed a technique used by Kalman and Englar (1966), which has been found effective by Moler and Van Loan (1978). The basic idea comes from Eq. (4.52) with $t_2 - t_0 = 2T$ and $t_1 - t_0 = T$, namely

$$(e^{\mathbf{FT}})^2 = e^{\mathbf{FT}} e^{\mathbf{FT}} = e^{\mathbf{F}2T}. \quad (4.80)$$

Thus, if T is too large, we can compute the series for $T/2$ and square the result. If $T/2$ is too large, we compute the series for $T/4$, and so on, until we find a k such that $T/2^k$ is *not* too large. We need a test for deciding on the value of k . We propose to approximate the series for Ψ , which can be written

$$\Psi \left(\frac{T}{2^k} \right) = \sum_{j=0}^{N-1} \frac{[\mathbf{F}(T/2^k)]^j}{(j+1)!} + \sum_{j=N}^{\infty} \frac{(\mathbf{FT}/2^k)^j}{(j+1)!} = \hat{\Psi} + \mathbf{R}.$$

We will select k , the factor that decides how much the sample period is divided down, to yield a small remainder term \mathbf{R} . Källström suggests that we estimate the size of \mathbf{R} by the size of the first term ignored in $\hat{\Psi}$, namely,

$$\hat{\mathbf{R}} \cong (\mathbf{FT})^N / (N+1)! 2^{Nk}.$$

A simpler method is to select k such that the size of \mathbf{FT} divided by 2^k is less than 1. In this case, the series for $\mathbf{FT}/2^k$ will surely converge. The rule is to select k such that

$$2^k > \|\mathbf{FT}\| = \max_j \sum_{i=1}^n |F_{ij}| T.$$

-
1. Select \mathbf{F} and T .
 2. Comment: Compute $\|\mathbf{F}T\|$.
 3. $V \leftarrow \max_j \{\sum_i |F_{ij}|\} \times T$
 4. $k \leftarrow$ smallest nonnegative integer greater than $\log_2 V$.
 5. Comment: compute $\Psi(T/2^k)$.
 6. $T_1 \leftarrow T/2^k$
 7. $\mathbf{I} \leftarrow$ Identity
 8. $\Psi \leftarrow \mathbf{I}$
 9. $j \leftarrow 11$
 10. If $j = 1$, go to step 14.
 11. $\Psi \leftarrow \mathbf{I} + \frac{\mathbf{F}T_1}{j} \Psi$
 12. $j \leftarrow j - 1$
 13. Go to step 10.
 14. Comment: Now double Ψ k times.
 15. If $k = 0$, stop.
 16. $\Psi \leftarrow \left(\mathbf{I} + \frac{\mathbf{F}T}{2^{k+1}} \Psi \right) \Psi$
 17. $k \leftarrow k - 1$
 18. Go to step 15.
-

Table 4.3
Logic for a
program to
compute Ψ using
automatic time
scaling

Taking the log of both sides, we find

$$k > \log_2 \|\mathbf{F}T\|,$$

from which we select

$$k = \max(\lceil \log_2 \|\mathbf{F}T\|, 0), \quad (4.81)$$

where the symbol $\lceil x$ means the smallest integer greater than x . The maximum of this integer and zero is taken because it is possible that $\|\mathbf{F}T\|$ is already so small that its log is negative, in which case we want to select $k = 0$.

Having selected k , we now have the problem of computing $\hat{\Psi}(T)$ from $\hat{\Psi}(T/2^k)$. Our original concept was based on the series for Φ , which satisfied Eq. (4.80). To obtain the suitable formula for Ψ , we use the relation between Φ and Ψ given by Eq. (4.60) as follows to obtain the “doubling” formula for Ψ

$$\begin{aligned} \Phi(2T) &= \Phi(T)\Phi(T), \\ \mathbf{I} + 2T\mathbf{F}\Psi(2T) &= [\mathbf{I} + T\mathbf{F}\Psi(T)][\mathbf{I} + T\mathbf{F}\Psi(T)] \\ &= \mathbf{I} + 2T\mathbf{F}\Psi(T) + T^2\mathbf{F}^2\Psi^2(T); \end{aligned}$$

therefore

$$2T\mathbf{F}\Psi(2T) = 2T\mathbf{F}\Psi(T) + T^2\mathbf{F}^2\Psi^2(T).$$

This is equivalent to

$$\Psi(2T) = \left(\mathbf{I} + \frac{T\mathbf{F}}{2} \Psi(T) \right) \Psi(T),$$

which is the form to be used. The program logic for computing Ψ is shown in Fig. 4.3.¹⁵ This algorithm does not include the delay discussed in Section 4.3.4. For that, we must implement the logic shown in Fig. 4.18. In the Control Toolbox, the function `c2d.m` executes the logic with a delay if one is specified.

4.3.6 *Nonlinear Models

Contrary to the predominant developments in this book, models of dynamic systems are generally nonlinear. However, it is more difficult to apply analysis to nonlinear models and, thus, less insight

¹⁵Similar logic is used by MATLAB in `c2d.m`.

is gained if models are left in their nonlinear form throughout the entire design process. Controls engineers commonly use numerical simulation of nonlinear models to evaluate the performance of control systems, a technique that should always be a part of any control system design. To aid in the design synthesis of controllers and to gain insight into approximate behavior, it is often advantageous to linearize the system so the methods in this text can be utilized.

We begin with the assumption that our plant dynamics are adequately described by a set of ordinary differential equations in state-variable form as

$$\begin{aligned}
 \dot{x}_1 &= f_1(x_1, \dots, x_n, u_1, \dots, u_m, t), \\
 \dot{x}_2 &= f_2(x_1, \dots, x_n, u_1, \dots, u_m, t), \\
 &\vdots \\
 \dot{x}_n &= f_n(x_1, \dots, x_n, u_1, \dots, u_m, t), \\
 y_1 &= h_1(x_1, \dots, x_n, u_1, \dots, u_m, t), \\
 &\vdots \\
 y_p &= h_p(x_1, \dots, x_n, u_1, \dots, u_m, t),
 \end{aligned} \tag{4.82}$$

or, more compactly in matrix notation, we assume that our plant dynamics are described by

$$\begin{aligned}
 \dot{\mathbf{x}} &= \mathbf{f}(\mathbf{x}, \mathbf{u}, t), \\
 \mathbf{x}(t_0) &= \mathbf{x}_0, \\
 \mathbf{y} &= \mathbf{h}(\mathbf{x}, \mathbf{u}, t).
 \end{aligned} \tag{4.83}$$

One proceeds as follows with the process of linearization and small-signal approximations. We assume stationarity by the approximation that \mathbf{f} and \mathbf{h} do not change significantly from their initial values at t_0 . Thus we can set

$$\dot{\mathbf{x}} = \mathbf{f}(\mathbf{x}, \mathbf{u}, t_0)$$

or, simply

$$\dot{\mathbf{x}} = \mathbf{f}(\mathbf{x}, \mathbf{u}), \quad \mathbf{y} = \mathbf{h}(\mathbf{x}, \mathbf{u}). \tag{4.84}$$

The assumption of small signals can be reflected by taking \mathbf{x} and \mathbf{u} to be always close to their reference values \mathbf{x}_0 , \mathbf{u}_0 , and these values, furthermore, to be an equilibrium point of Eq. (4.82), where

$$\mathbf{f}(\mathbf{x}_0, \mathbf{u}_0) = \mathbf{0}. \tag{4.85}$$

Now, if \mathbf{x} and \mathbf{u} are “close” to \mathbf{x}_0 and \mathbf{u}_0 , they can be written as $\mathbf{x} = \mathbf{x}_0 + \delta\mathbf{x}$; $\mathbf{u} = \mathbf{u}_0 + \delta\mathbf{u}$, and these can be substituted into Eq. (4.84). The fact that $\delta\mathbf{x}$ and $\delta\mathbf{u}$ are small is now used to motivate an expansion of Eq. (4.84) about \mathbf{x}_0 and \mathbf{u}_0 and to suggest that the only terms in the first power of the small quantities $\delta\mathbf{x}$ and $\delta\mathbf{u}$ need to be retained. We thus have a vector equation and need the expansion of a vector-valued function of a vector variable,

$$\frac{d}{dt}(\mathbf{x}_0 + \delta\mathbf{x}) = \mathbf{f}(\mathbf{x}_0 + \delta\mathbf{x}, \mathbf{u}_0 + \delta\mathbf{u}). \tag{4.86}$$

If we go back to Eq. (4.82) and do the expansion of the components f_i one at a time, it is tedious but simple to verify that Eq. (4.86) can be written as¹⁶

$$\delta\dot{\mathbf{x}} = \mathbf{f}(\mathbf{x}_0, \mathbf{u}_0) + \mathbf{f}_{,\mathbf{x}}(\mathbf{x}_0, \mathbf{u}_0)\delta\mathbf{x} + \mathbf{f}_{,\mathbf{u}}(\mathbf{x}_0, \mathbf{u}_0)\delta\mathbf{u} + \dots \tag{4.87}$$

where we define the partial derivative of a scalar f_i with respect to the vector \mathbf{x} by a subscript notation:

$$f_{i,\mathbf{x}} \hat{=} \left(\frac{\partial f_i}{\partial x_1} \quad \dots \quad \frac{\partial f_i}{\partial x_n} \right). \tag{4.88}$$

¹⁶Note that $d\mathbf{x}_0/dt = 0$ because our “reference trajectory” \mathbf{x}_0 is a constant here.

The row vector in Eq. (4.88) is called the **gradient**

of the scalar f_1 with respect to the vector \mathbf{x} . If \mathbf{f} is a vector, we define its partial derivatives with respect to the vector \mathbf{x} as the matrix (called the **Jacobian**) composed of *rows* of gradients. In the subscript notation, if we mean to take the partial of *all* components, we omit the specific subscript such as 1 or 2 but hold its place by the use of a comma

$$\mathbf{f}_{,\mathbf{x}} = \begin{bmatrix} \frac{\partial f_1}{\partial \mathbf{x}} \\ \frac{\partial f_2}{\partial \mathbf{x}} \\ \vdots \\ \frac{\partial f_n}{\partial \mathbf{x}} \end{bmatrix}. \quad (4.89)$$

Now, to return to Eq. (4.87), we note that by Eq. (4.85) we chose $\mathbf{x}_0, \mathbf{u}_0$ to be an equilibrium point, so the first term on the right of Eq. (4.87) is zero, and because the terms beyond those shown depend on higher powers of the small signals $\delta \mathbf{x}$ and $\delta \mathbf{u}$, we are led to the approximation

$$\begin{aligned} \delta \dot{\mathbf{x}} &\approx \mathbf{f}_{,\mathbf{x}}(\mathbf{x}_0, \mathbf{u}_0) \delta \mathbf{x} + \mathbf{f}_{,\mathbf{u}}(\mathbf{x}_0, \mathbf{u}_0) \delta \mathbf{u}, \\ \delta \mathbf{y} &= \mathbf{h}_{,\mathbf{x}} \delta \mathbf{x} + \mathbf{h}_{,\mathbf{u}} \delta \mathbf{u}. \end{aligned} \quad (4.90)$$

But now the notation is overly clumsy, so we drop the $\delta \mathbf{x}$, $\delta \mathbf{u}$ and $\delta \mathbf{y}$ notation and simply call them \mathbf{x} , \mathbf{u} and \mathbf{y} and define the constant matrices

$$\begin{aligned} \mathbf{F} &= \mathbf{f}_{,\mathbf{x}}(\mathbf{x}_0, \mathbf{u}_0), & \mathbf{G} &= \mathbf{f}_{,\mathbf{u}}(\mathbf{x}_0, \mathbf{u}_0), \\ \mathbf{H} &= \mathbf{h}_{,\mathbf{x}}(\mathbf{x}_0, \mathbf{u}_0), & \mathbf{J} &= \mathbf{h}_{,\mathbf{u}}(\mathbf{x}_0, \mathbf{u}_0). \end{aligned}$$

This results in the form we used earlier in Section 2.1.1

$$\dot{\mathbf{x}} = \mathbf{F}\mathbf{x} + \mathbf{G}\mathbf{u}, \quad \mathbf{y} = \mathbf{H}\mathbf{x} + \mathbf{J}\mathbf{u}. \quad (4.91)$$

We go even further and restrict ourselves to the case of single input and single output and discrete time. We then write the model as

$$\begin{aligned} \mathbf{x}(k+1) &= \mathbf{\Phi}\mathbf{x}(k) + \mathbf{\Gamma}u(k), \\ y(k) &= \mathbf{H}\mathbf{x}(k) + Ju(k), \end{aligned} \quad (4.92)$$

from which the transfer function is

$$G(z) = Y(z)/U(z) = \mathbf{H}(z\mathbf{I} - \mathbf{\Phi})^{-1}\mathbf{\Gamma} + J. \quad (4.93)$$

Thus we see that nonlinear models can be approximated as linear state-space models or as transfer function models. The accuracy of the approximation varies with the problem, but is generally useful in designing the control system. The final design of the control system should always be checked via numerical simulation of the nonlinear equations.

4.4 Signal Analysis and Dynamic Response

In Section 4.2 we demonstrated that if two variables are related by a linear constant difference equation, then the ratio of the z -transform of the output signal to that of the input is a function of the system equation alone, and the ratio is called the transfer function. A method for study of linear constant discrete systems is thereby indicated, consisting of the following steps:

1. Compute the transfer function of the system $H(z)$.
2. Compute the transform of the input signal, $E(z)$.

3. Form the product, $E(z)H(z)$, which is the transform of the output signal, U .
4. Invert the transform to obtain $u(kT)$.

If the system description is available in difference-equation form, and if the input signal is elementary, then the first three steps of this process require very little effort or computation. The final step, however, is tedious if done by hand, and, because we will later be preoccupied with design of transfer functions to give desirable responses, we attach great benefit to gaining intuition for the kind of response to be expected from a transform without actually inverting it or numerically evaluating the response. Our approach to this problem is to present a repertoire of elementary signals with known features and to learn their representation in the transform or z -domain. Thus, when given an unknown transform, we will be able, by reference to these known solutions, to infer the major features of the time-domain signal and thus to determine whether the unknown is of sufficient interest to warrant the effort of detailed time-response computation. To begin this process of attaching a connection between the time domain and the z -transform domain, we compute the transforms of a few elementary signals.

4.4.1 The Unit Pulse

We have already seen that the unit pulse is defined by¹⁷

$$\begin{aligned} e_1(k) &= 1 & (k = 0) \\ &= 0 & (k \neq 0) \\ &\hat{=} \delta_k; \end{aligned}$$

therefore we have

$$E_1(z) = \sum_{-\infty}^{\infty} \delta_k z^{-k} = z^0 = 1. \quad (4.94)$$

This result is much like the continuous case, wherein the Laplace transform of the unit impulse is the constant 1.0.

The quantity $E_1(z)$ gives us an instantaneous method to relate signals to systems: To characterize the system $H(z)$, consider the signal $u(k)$, which is the unit pulse response; then $U(z) = H(z)$.

4.4.2 The Unit Step

Consider the unit step function defined by

$$\begin{aligned} e_2(k) &= 1 & (k \geq 0) \\ &= 0 & (k < 0) \\ &\hat{=} & & & 1(k). \end{aligned}$$

In this case, the z -transform is

$$\begin{aligned} E_2(z) &= \sum_{k=-\infty}^{\infty} e_2(k) z^{-k} = \sum_{k=0}^{\infty} z^{-k} \\ &= \frac{1}{1 - z^{-1}} & (|z^{-1}| < 1) \\ &= \frac{z}{z - 1} & (|z| > 1). \end{aligned} \quad (4.95)$$

Here the transform is characterized by a zero at $z = 0$ and a pole at $z = 1$. The significance of the convergence being restricted to $|z| > 1$ will be explored later when we consider the inverse transform operation. The Laplace transform of the unit step is $1/s$; we may thus keep in mind that a pole at

¹⁷We have shifted notation here to use $e(k)$ rather than e_k for the k th sample. We use subscripts to identify different signals.

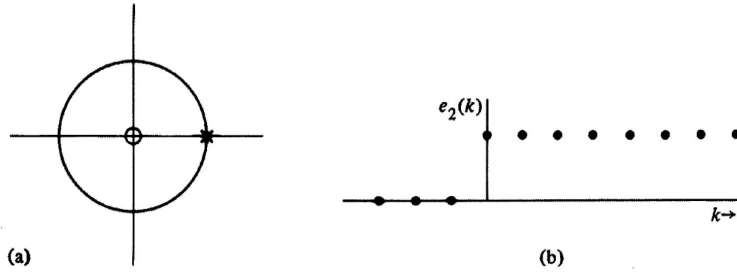


Figure 4.19
 (a) Pole and zero of $E_2(z)$ in the z -plane. The unit circle is shown for reference. (b) Plot of $e_2(k)$

$s = 0$ for a continuous signal corresponds in some way to a pole at $z = 1$ for discrete signals. We will explore this further later. In any event, we record that a pole at $z = 1$ with convergence outside the unit circle, $|z| = 1$, will correspond to a constant for positive time and zero for negative time.

To emphasize the connection between the time domain and the z -plane, we sketch in Fig. 4.19 the z -plane with the unit circle shown and the pole of $E_2(z)$ marked \times and the zero marked \circ . Beside the z -plane, we sketch the time plot of $e_2(k)$.

4.4.3 Exponential

The one-sided exponential in time is

$$\begin{aligned} e_3(k) &= r^k & (k \geq 0) \\ &= 0 & (k < 0) \end{aligned} \quad (4.96)$$

which is the same as $r^k 1(k)$, using the symbol $1(k)$ for the unit step function. Now we get

$$\begin{aligned} E_3(z) &= \sum_{k=0}^{\infty} r^k z^{-k} \\ &= \sum_{k=0}^{\infty} (rz^{-1})^k \\ &= \frac{1}{1 - rz^{-1}} \quad (|rz^{-1}| < 1) \\ &= \frac{z}{z - r} \quad (|z| > |r|). \end{aligned} \quad (4.97)$$

The pole of $E_3(z)$ is at $z = r$. From Eq. (4.96) we know that $e_3(k)$ grows without bound if $|r| > 1$. From Eq. (4.97) we conclude that a z -transform that converges for large z and has a real pole *outside* the circle $|z| = 1$ corresponds to a growing signal. If such a signal were the unit-pulse response of our system, such as our digital control program, we would say the program was *unstable* as we saw in Eq. (4.39). We plot in Fig. 4.20 the z -plane and the corresponding time history of $E_3(z)$ as $e_3(k)$ for the stable value, $r = 0.6$.

4.4.4 General Sinusoid

Our next example considers the modulated sinusoid $e_4(k) = [r^k \cos(k\theta)] 1(k)$, where we assume $r > 0$. Actually, we can decompose $e_4(k)$ into the sum of two complex exponentials as

$$e_4(k) = r^k \left(\frac{e^{jk\theta} + e^{-jk\theta}}{2} \right) 1(k),$$

and because the z -transform is linear,¹⁸ we need only compute the transform of each single complex exponential and add the results later. We thus take first

$$e_5(k) = r^k e^{jk\theta} 1(k) \quad (4.98)$$

¹⁸We have not shown this formally. The demonstration, using the definition of linearity given above, is simple and is given in Section 4.6.

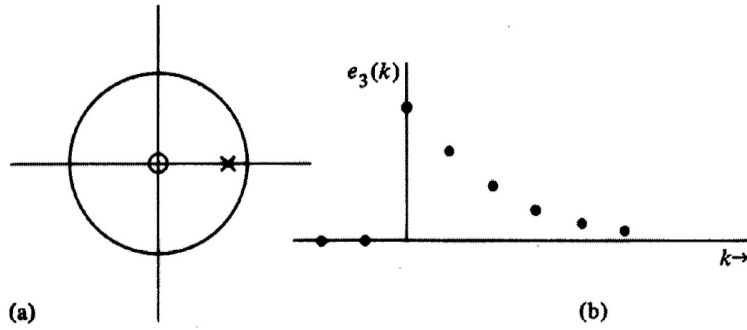


Figure 4.20
 (a) Pole and zero of $E_3(z)$ in the z -plane. (b) Plot of $e_3(k)$

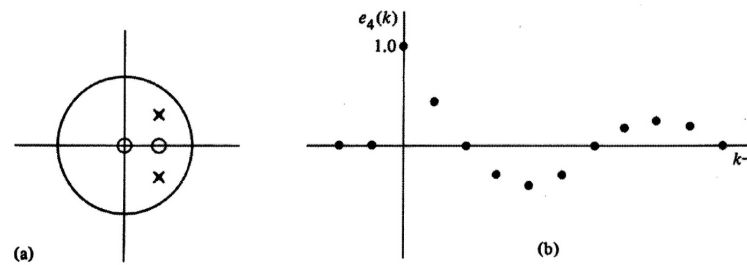


Figure 4.21
 (a) Poles and zeros of $E_4(z)$ for $\theta = 45^\circ$, $r = 0.7$ in the z -plane. (b) Plot of $e_4(k)$

and compute

$$\begin{aligned}
 E_5(z) &= \sum_{k=0}^{\infty} r^k e^{j\theta k} z^{-k} \\
 &= \sum_{k=0}^{\infty} (r e^{j\theta} z^{-1})^k \\
 &= \frac{1}{1 - r e^{j\theta} z^{-1}} \\
 &= \frac{z}{z - r e^{j\theta}} \quad (|z| > r).
 \end{aligned} \tag{4.99}$$

The signal $e_5(k)$ grows without bound as k gets large if and only if $r > 1$, and a system with this pulse response is BIBO stable if and only if $|r| < 1$. The boundary of stability is the unit circle. To complete the argument given before for $e_4(k) = r^k \cos k\theta 1(k)$, we see immediately that the other half is found by replacing θ by $-\theta$ in Eq. (4.99)

$$\mathcal{Z}\{r^k e^{-j\theta k} 1(k)\} = \frac{z}{z - r e^{-j\theta}} \quad (|z| > r), \tag{4.100}$$

and thus that

$$\begin{aligned}
 E_4(z) &= \frac{1}{2} \left\{ \frac{z}{z - r e^{j\theta}} + \frac{z}{z - r e^{-j\theta}} \right\} \\
 &= \frac{z(z - r \cos \theta)}{z^2 - 2r(\cos \theta)z + r^2} \quad (|z| > r).
 \end{aligned} \tag{4.101}$$

The z -plane pole-zero pattern of $E_4(z)$ and the time plot of $e_4(k)$ are shown in Fig. 4.21 for $r = 0.7$ and $\theta = 45^\circ$.

We note in passing that if $\theta = 0$, then e_4 reduces to e_3 and, with $r = 1$, to e_2 , so that three of our signals are special cases of e_4 . By exploiting the features of $E_4(z)$, we can draw a number of conclusions about the relation between pole locations in the z -plane and the time-domain signals to which the poles correspond. We collect these for later reference.

Pole Radius	Response Duration
r	N
0.9	43
0.8	21
0.6	9
0.4	5

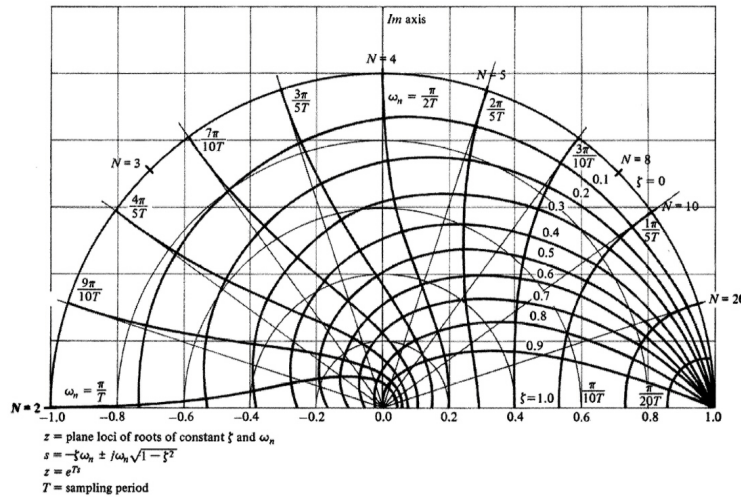


Figure 4.22
Sketch of the unit circle with angle θ marked in numbers of samples per cycle

- The settling time of a transient, defined as the time required for the signal to decay to one percent of its maximum value, is set mainly by the value of the radius, r , of the poles.
 - $r > 1$ corresponds to a growing signal that will not decay at all.
 - $r = 1$ corresponds to a signal with constant amplitude (which is *not* BIBO stable as a pulse response).
 - For $r < 1$, the closer r is to 0 the shorter the settling time. The corresponding system is BIBO stable. We can compute the settling time in samples, N , in terms of the pole radius, r .
 - A pole at $r = 0$ corresponds to a transient of finite duration.
- The number of samples per oscillation of a sinusoidal signal is determined by θ . If we require $\cos(\theta k) = \cos(\theta(k + N))$, we find that a period of 2π rad contains N samples, where

$$N = \frac{2\pi}{\theta} = \frac{360}{\theta_{\text{deg}}} \text{ samples/cycle.}$$

For $\theta_{\text{deg}} = 45^\circ$, we have $N = 8$, and the plot of $e_4(k)$ given in Fig. 4.21(b) shows the eight samples in the first cycle very clearly. A sketch of the unit circle with several points corresponding to various numbers of samples per cycle marked is drawn in Fig. 4.22 along with other contours that will be explained in the next section. The sampling frequency in Hertz is $1/T$, and the signal frequency is $f = 1/NT$ so that $N = f_s/f$ and $1/N$ is a *normalized* signal frequency. Since $\theta = (2\pi)/N$, θ is the normalized signal frequency in radians/sample. θ/T is the frequency in radians/second.

A compilation of signal responses versus their pole location in the z -plane is shown in Fig. 4.23. It demonstrates visually the features just summarized for the general sinusoid, which encompasses all possible signals.

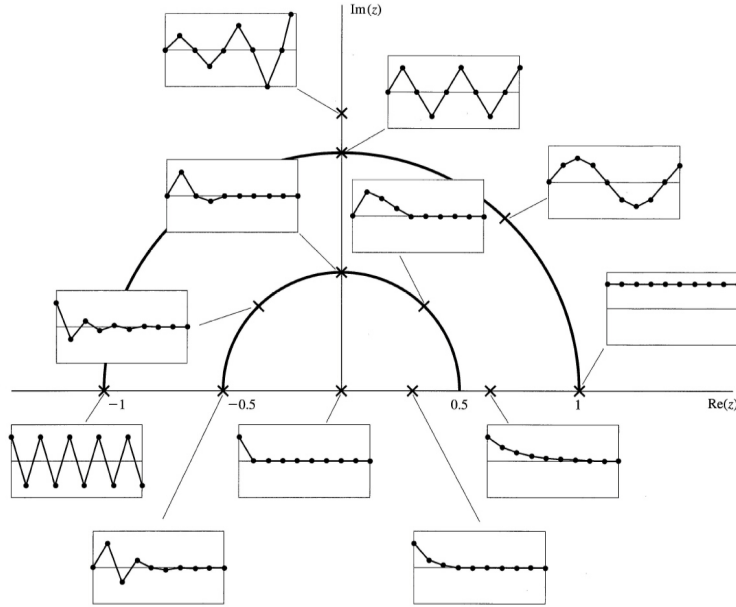


Figure 4.23
Time sequences
associated with
pole locations in
the z -plane

4.4.5 Correspondence with Continuous Signals

From the calculation of these few z -transforms, we have established that the duration of a time signal is related to the radius of the pole locations and the number of samples per cycle is related to the angle, θ . Another set of very useful relationships can be established by considering the signals to be samples from a continuous signal, $e(t)$, with Laplace transform $E(s)$. With this device we can exploit our knowledge of s -plane features by transferring them to equivalent z -plane properties. For the specific numbers represented in the illustration of e_4 , we take the continuous signal

$$y(t) = e^{-at} \cos bt \, 1(t) \quad (4.102)$$

with

$$\begin{aligned} aT &= 0.3567, \\ bT &= \pi/4. \end{aligned}$$

And, taking samples one second apart ($T = 1$), we have

$$\begin{aligned} y(kT) &= (e^{-0.3567})^k \cos \frac{\pi k}{4} \, 1(k) \\ &= (0.7)^k \cos \frac{\pi k}{4} \, 1(k) \\ &= e_4(k). \end{aligned}$$

The poles of the Laplace transform of $y(t)$ (in the s -plane) are at

$$s_{1,2} = -a + jb, -a - jb.$$

From Eq. (4.101), the z -transform of $E_4(z)$ has poles at

$$z_{1,2} = re^{j\theta}, re^{-j\theta},$$

but because $y(kT)$ equals $e_4(k)$, it follows that

$$\begin{aligned} r &= e^{-aT}, \quad \theta = bT \\ z_{1,2} &= e^{s_1 T}, e^{s_2 T}. \end{aligned}$$

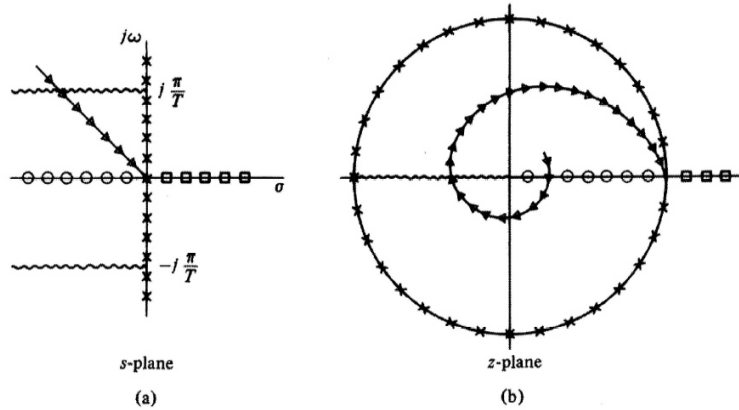


Figure 4.24
Corresponding lines in the s-plane and the z-plane according to $z = e^{sT}$

s-plane	Symbol	z-plane
$s = j\omega$ Real frequency axis $s = \sigma \geq 0$ $s = \sigma \leq 0$	$\times \times \times$ $\square \square \square$ $\bigcirc \bigcirc \bigcirc$	$ z = 1$ Unit circle $z = r \geq 1$ $z = r, 0 \leq r \leq 1$
$s = -\zeta\omega_n + j\omega_n\sqrt{1-\zeta^2}$ $= -a + jb$ Constant damping ratio if ζ is fixed and ω_n varies	$\triangle \triangle \triangle$	$z = re^{j\theta}$ where $r = \exp(-\zeta\omega_n T) = e^{-aT}$, $\theta = \omega_n T \sqrt{1-\zeta^2} = bT$ Logarithmic spiral
$s = \pm j(\pi/T) + \sigma, \sigma \leq 0$		$z = -r$

Table 4.4
Description of corresponding lines in s-plane and z-plane

If $E(z)$ is a ratio of polynomials in z , which will be the case if $e(k)$ is generated by a linear difference equation with constant coefficients, then by partial fraction expansion, $E(z)$ can be expressed as a sum of elementary terms like E_4 and E_3 .¹⁹ In all such cases, the discrete signal can be generated by samples from continuous signals where the relation between the s-plane poles and the corresponding z-plane poles is given by

$$z = e^{sT}. \tag{4.103}$$

If we know what it means to have a pole in a certain place in the s-plane, then Eq. (4.103) shows us where to look in the z-plane to find a representation of discrete samples having the *same time features*. It is useful to sketch several major features from the s-plane to the z-plane according to Eq. (4.103) to help fix these ideas. Such a sketch is shown in Fig. 4.24.

Each feature should be traced in the mind to obtain a good grasp of the relation. These features are given in Table 4.2. We note in passing that the map $z = e^{sT}$ of Eq. (4.103) is many-to-one. There are many values of s for each value of z . In fact, if

$$s_2 = s_1 + j\frac{2\pi}{T}N,$$

then $e^{s_1 T} = e^{s_2 T}$. The (great) significance of this fact will be explored in Chapter 5.

Lines of constant damping in the s-plane are mapped into the z-plane according to Eq. (4.103) for several values of ζ in Fig. 4.22. We often refer to the damping of a pole in the z-plane in terms of this **equivalent s-plane** damping, or sometimes we simply refer to the damping of a z-plane pole. Likewise, lines of constant natural frequency, ω_n , in the s-plane (semi-circles centered at the origin) are also mapped into the z-plane according to Eq. (4.103) for several values of ω_n in Fig. 4.22. It's

¹⁹Unless a pole of $E(z)$ is repeated. We have yet to compute the discrete version of a signal corresponding to a higher-order pole. The result is readily shown to be a polynomial in k multiplying $r^k e^{jk\theta}$.

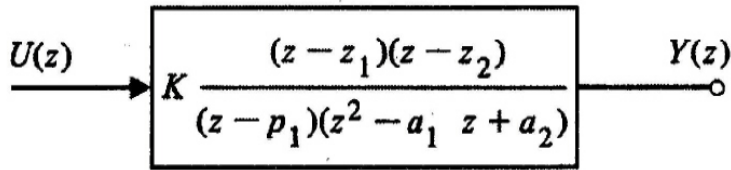


Figure 4.25
Definition of the parameters of the system whose step responses are to be catalogued

interesting to note that in the immediate vicinity of $z = +1$, the map of ζ and ω_n looks exactly like the s -plane in the vicinity of $s = 0$. Because of the usefulness of this mapping, the Control System Toolbox has the function `zgrid.m` that allows one to superimpose this mapping on various plots to help in the interpretation of the results. You will see its use in the figure files of discrete root loci in Chapter 7.

4.4.6 Step Response

Our eventual purpose, of course, is to design digital controls, and our interest in the relation between z -plane poles and zeros and time-domain response comes from our need to know how a proposed design will respond in a given dynamic situation. The generic dynamic test for controls is the step response, and we will conclude this discussion of discrete system dynamic response with an examination of the relationships between the pole-zero patterns of elementary systems and the corresponding step responses for a discrete transfer function from u to y of a hypothetical plant. Our attention will be restricted to the step responses of the discrete system shown in Fig. 4.25 for a selected set of values of the parameters.

Note that if $z_1 = p_1$, the members of the one pole-zero pair cancel out; and if at the same time $z_2 = r \cos(\theta)$, $a_1 = -2r \cos(\theta)$, and $a_2 = r^2$, the system response, $Y(z)$, to the input with transform $U(z) = 1$ (a unit pulse) is

$$Y(z) = \frac{z - r \cos \theta}{z^2 - 2r \cos \theta z + r^2}. \quad (4.104)$$

This transform, when compared with the transform $E_4(z)$ given in Eq. (4.101), is seen to be

$$Y(z) = z^{-1} E_4(z),$$

and we conclude that under these circumstances the system pulse response is a delayed version of $e_4(k)$, a typical second-order system pulse response.

For our first study we consider the effect of zero location. We let $z_1 = p_1$ and explore the effect of the (remaining) zero location, z_2 , on the step-response overshoot for three sets of values of a_1 and a_2 . We select a_1 and a_2 so that the poles of the system correspond to a response with an equivalent s -plane damping ratio $\zeta = 0.5$ and consider values of θ of 18, 45, and 72 degrees. In every case, we will take the gain K to be such that the steady-state output value equals the step size. The situation in the z -plane is sketched in Fig. 4.26 for $\theta = 18^\circ$. The curve for $\zeta = 0.5$ is also shown for reference. In addition to the two poles and one zero of $H(z)$, we show the pole at $z = 1$ and the zero at $z = 0$, which come from the transform of the input step, $U(z)$, given by $z/(z - 1)$.

The major effect of the zero z_2 on the step response $y(k)$ is to change the percent overshoot, as can be seen from the four step responses for this case plotted in Fig. 4.27. To summarize all these data, we plot the percent overshoot versus zero location in Fig. 4.28 for $\zeta = 0.5$ and in Fig. 4.29 for $\zeta = 0.707$. The major feature of these plots is that the zero has very little influence when on the negative axis, but its influence is dramatic as it comes near $+1$. Also included on the plots of Fig. 4.28 are overshoot figures for a zero in the unstable region on the positive real axis. These responses go in the *negative* direction at first, and for the zero very near $+1$, the negative peak is larger than 1!²⁰

²⁰Such systems are called nonminimum phase by Bode because the phase shift they impart to a sinusoidal input is greater than the phase of a system whose *magnitude* response is the same but that has a zero in the stable rather than the unstable region.

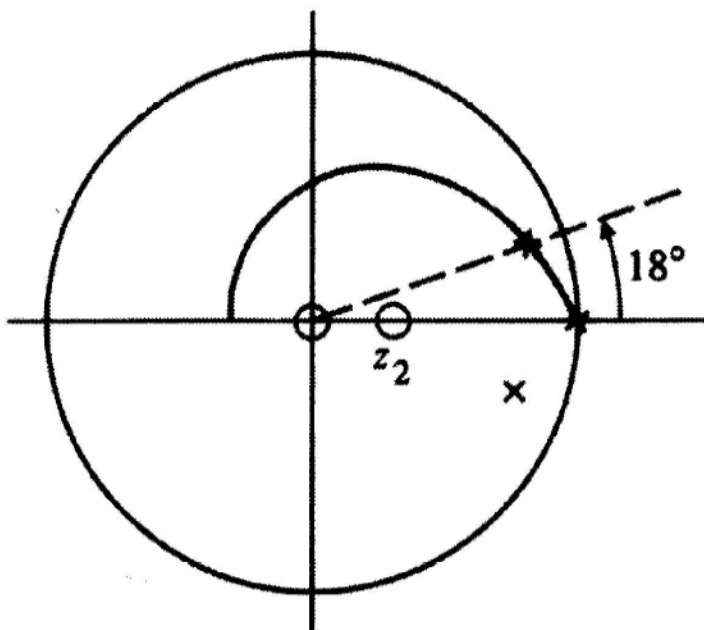


Figure 4.26
 Pole-zero pattern of $Y(z)$ for the system of Fig. 4.25, with $z_1 = p_1$, $U(z) = z/(z-1)$, a_1 and a_2 selected for $\theta = 18^\circ$, and $\zeta = 0.5$

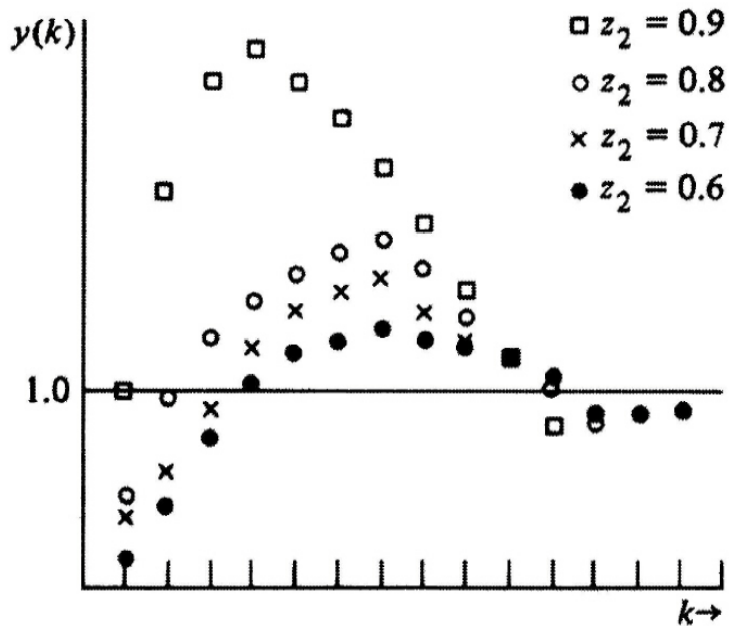


Figure 4.27
 Plot of step responses for a discrete plant described by the pole-zero pattern of Fig. 4.26 for various values of z_2

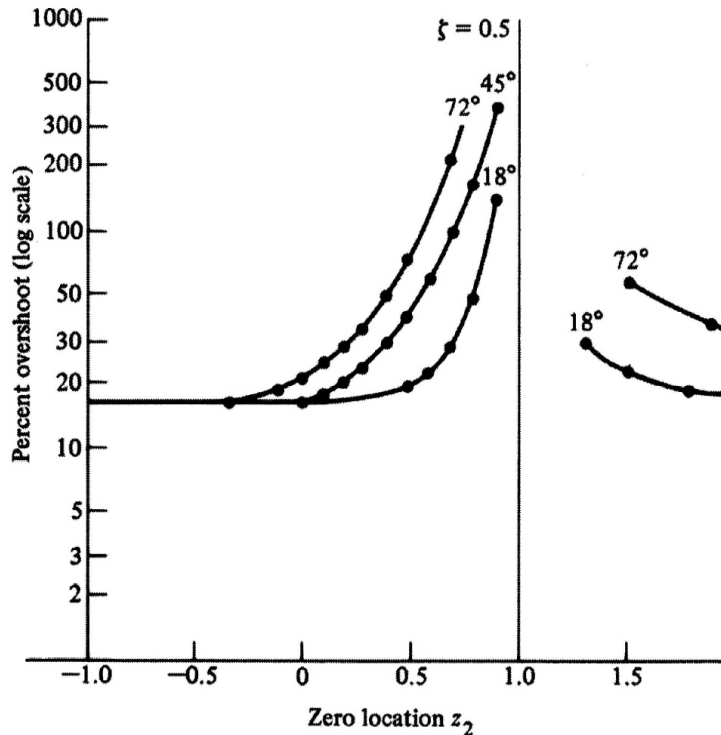


Figure 4.28
Effects of an extra zero on a discrete second-order system, $\zeta = 0.5$; $\theta = 18^\circ$, 45° , and 72°

Our second class of step responses corresponds to a study of the influence of a third pole on a basically second-order response. For this case we again consider the system of Fig. 4.25, but this time we fix $z_1 = z_2 = -1$ and let p_1 vary from near -1 to near $+1$. In this case, the major influence of the moving singularity is on the rise time of the step response. We plot this effect for $\theta = 18, 45$, and 72 degrees and $\zeta = 0.5$ on Fig. 4.30. In the figure we defined the rise time as the time required for the response to rise to 0.95, which is to 5% of its final value. We see here that the extra pole causes the rise time to get very much longer as the location of p_1 moves toward $z = +1$ and comes to dominate the response.

Our conclusions from these plots are that the addition of a pole or zero to a given system has only a small effect if the added singularities are in the range from 0 to -1 . However, a zero moving toward $z = +1$ greatly increases the system overshoot. A pole placed toward $z = +1$ causes the response to slow down and thus primarily affects the rise time, which is progressively increased.

The understanding of how poles and zeros affect the time response is very useful for the control system designer. The knowledge helps guide the iterative design process and helps the designer understand why a response is the way it is. Ultimately, however, the test of a design is typically the actual time response, either by numerical simulation or an experimental evaluation. Today, transform inversion would never be carried out. In MATLAB, the numerical simulation of the impulse response for a discrete system, `sysD` is accomplished by

```
y = impulse(sysD)
```

and the discrete step response by

```
y = step(sysD)
```

Invoked without a left-hand argument (`y =`), both functions result in a plot of the response on the screen.

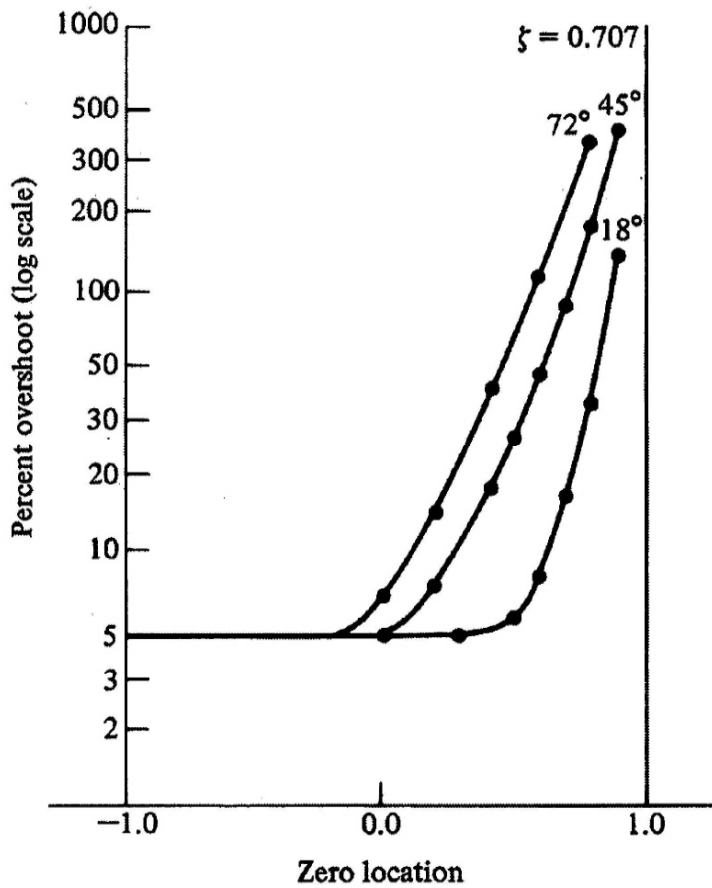


Figure 4.29
Effects of an extra zero on a discrete second-order system, $\zeta = 0.707$; $\theta = 18^\circ, 45^\circ,$ and 72° ; percent overshoot versus zero location

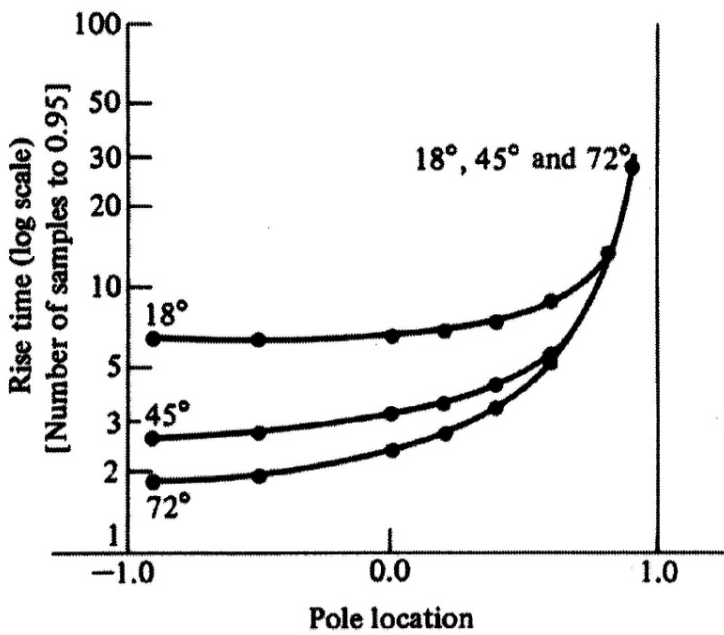


Figure 4.30
Effects of an extra pole on rise time for a discrete third-order system, two zeros at -1 , one zero at ∞ ; $\zeta = 0.5$; $\theta = 18^\circ, 45^\circ, 72^\circ$

4.5 Frequency Response

A very important concept in linear systems analysis is the frequency response. If a sinusoid at frequency ω_o is applied to a stable, linear, constant, continuous system, the response is a transient plus a sinusoidal steady state at the *same frequency*, ω_o , as the input. If the transfer function is written in gain-phase form as $H(j\omega) = A(\omega)e^{j\psi(\omega)}$, then the steady-state response to a unit-amplitude sinusoidal signal has amplitude $A(\omega_o)$ and phase $\psi(\omega_o)$ relative to the input signal.

We can say almost exactly the same respecting the frequency response of a stable, linear, constant, discrete system. If the system has a transfer function $H(z)$, we define its magnitude and phase for z taking on values around the unit circle by $H(e^{j\omega T}) = A(\omega T)e^{j\psi(\omega T)}$. If a unit-amplitude sinusoid is applied, then in the steady state, the response samples will be on a sinusoid of the same frequency with amplitude $A(\omega_o T)$ and phase $\psi(\omega_o T)$. It is worthwhile going through the calculations to fix ideas on this point.

From Eq. (4.16), the discrete response transform is

$$U(z) = H(z)E(z). \quad (4.105)$$

If $e(k) = \cos(\omega_o T k)1(k)$, then, from Eq. (4.101) with $r = 1$ and $\theta = \omega_o T$, we have

$$E(z) = \frac{1}{2} \left\{ \frac{z}{z - e^{j\omega_o T}} + \frac{z}{z - e^{-j\omega_o T}} \right\}. \quad (4.106)$$

If we substitute Eq. (4.106) into Eq. (4.105), we obtain

$$U(z) = \frac{1}{2} \left\{ \frac{zH(z)}{z - e^{j\omega_o T}} + \frac{zH(z)}{z - e^{-j\omega_o T}} \right\}. \quad (4.107)$$

The steady state of $u(kT)$ corresponds to the terms in the expansion of Eq. (4.107) associated with the two poles on the unit circle. If we expand $U(z)/z$ into partial fractions and multiply back by z , the steady state part can be found as

$$U_{ss}(z) = \frac{1}{2} \frac{H(e^{j\omega_o T})z}{z - e^{j\omega_o T}} + \frac{1}{2} \frac{H(e^{-j\omega_o T})z}{z - e^{-j\omega_o T}}.$$

If $H(e^{j\omega_o T}) = A(\omega_o T)e^{j\psi(\omega_o T)}$, then we have

$$U_{ss}(z) = \frac{A}{2} \frac{e^{j\psi} z}{z - e^{j\omega_o T}} + \frac{A}{2} \frac{e^{-j\psi} z}{z - e^{-j\omega_o T}}, \quad (4.108)$$

and the inverse transform of $U_{ss}(z)$ is

$$\begin{aligned} U_{ss}(kT) &= \frac{A}{2} e^{j\psi} e^{j\omega_o T k} + \frac{A}{2} e^{-j\psi} e^{-j\omega_o T k} \\ &= A \cos(\omega_o T k + \psi), \end{aligned} \quad (4.109)$$

which, of course, are samples at kT instants on a sinusoid of amplitude A , phase ψ , and frequency ω_o .

We will defer the plotting of particular frequency responses until later chapters (see, for example, Figs. 6.3, 6.8, 7.16, and 7.28). However, it should be noticed here that although a sinusoid of frequency ω_o could be passed through the samples of Eq. (4.109), there are other continuous sinusoids of frequency $\omega_o + \ell 2\pi/T$ for integer ℓ which also pass through these points. This is the phenomenon of aliasing, to which we will return in Chapter 5. Here, we define the discrete frequency response of a transfer function $H(z)$ to sinusoids of frequency ω_o as $H(e^{j\omega_o T})$ so that the amplitude A and phase ψ are

$$A = |H(e^{j\omega_o T})| \quad \text{and} \quad \psi = \angle(H(e^{j\omega_o T})) \quad (4.110)$$

which can be evaluated and plotted by MATLAB's `bode.m` with the scripts

	Time	Frequency
Fourier Series	periodic	discrete
z-transform	discrete	periodic

```
sysD = tf(num,den,T)
bode(sysD)
```

where amplitude is plotted in decibels (dB), or

```
[mag,phase,w] = bode(sysD)
subplot(2,1,1); loglog(w,squeeze(mag))
subplot(2,1,2); semilogx(w,squeeze(phase))
```

where amplitude is plotted as a ratio as in the figures in this text. If the system is described by the state-space matrices, the scripts above can be invoked with

```
sysD = ss(F,G,H,J,T).
```

4.5.1 *The Discrete Fourier Transform (DFT)

The analysis developed above based on the z -transform is adequate for considering the theoretical frequency response of a linear, constant system or the corresponding difference equation, but it is not the best for the analysis of real-time signals as they occur in the laboratory or in other experimental situations. For the analysis of real data, we need a transform defined over a finite data record, which can be computed quickly and accurately. The required formula is that of the **Discrete Fourier Transform**, the DFT, and its numerical cousin, the **Fast Fourier Transform**, the FFT. Implementation of a version of the FFT algorithm is contained in all signal-processing software and in most computer-aided control-design software. Fast Fourier Transform

To understand the DFT, it is useful to consider two properties of a signal and its Fourier transform that are complements of each other: the property of being periodic and the property of being discrete. In ordinary Fourier analysis, we have a signal that is neither periodic nor discrete and its Fourier transform is also neither discrete nor periodic. If, however, the time function $f(t)$ is periodic with period T_0 , then the appropriate form of the transform is the Fourier series, and the transform is defined only for the discrete frequencies $\omega = 2\pi n/T_0$. In other words, if the function in time is periodic, the function in frequency is discrete. The case where the properties are reversed is the z -transform we have just been studying. In this case, the time functions are discrete, being sampled, and the z -transform is periodic in ω ; for if $z = e^{j\omega T}$, corresponding to real frequencies, then replacing $\omega = \omega + 2\pi k/T$ leaves z unchanged. We can summarize these results with the following table:

Suppose we now have a time function that is both periodic and discrete. Based on what we have seen, we would expect the transform of this function also to be both periodic and discrete. And this is the case, which leads us to the finite discrete Fourier transform and its finite inverse. Let the time function in question be $f(kT) = f(kT + NT)$. Because the function is periodic, the transform can be defined as the finite sum

$$F\left(\frac{2\pi n}{NT}\right) = \sum_{k=0}^{N-1} f(kT)e^{-j2\pi(nkT)/(NT)}.$$

This is the same as the z -transform over one period evaluated at the discrete frequencies of a Fourier series $\omega = 2\pi n/NT$. It is standard practice to suppress all the arguments except the indices of time and frequency and write

$$F_n = \sum_{k=0}^{N-1} f_k e^{-j2\pi(nk)/N}. \quad (4.111)$$

To complete the DFT, we need the inverse transform, which, by analogy with the standard Fourier transform, we guess to be the sum

$$\sum_{n=0}^{N-1} F_n e^{j2\pi(nk)/N}.$$

If we substitute Eq. (4.111) with summation index ℓ into this, we find

$$\sum_{n=0}^{N-1} \left\{ \sum_{\ell=0}^{N-1} f_\ell e^{-j2\pi(n\ell)/N} \right\} e^{j2\pi(nk)/N}.$$

Interchanging the order of the summations gives

$$\sum_{\ell=0}^{N-1} f_\ell \left\{ \sum_{n=0}^{N-1} e^{j2\pi[n(k-\ell)]/N} \right\}.$$

The sum in the braces is a finite geometric series, which we can evaluate as follows

$$\begin{aligned} \sum_{n=0}^{N-1} e^{j2\pi[n(k-\ell)]/N} &= \frac{1 - e^{j2\pi(k-\ell)}}{1 - e^{j2\pi(k-\ell)/N}} \\ &= \begin{cases} N & k - \ell = 0 \\ 0 & k - \ell = 1, 2, \dots, N-1. \end{cases} \end{aligned}$$

The sum is periodic with period N . With this evaluation, we see that the sum we have been considering is Nf_k , and thus we have the inverse sum

$$f_k = \frac{1}{N} \sum_{n=0}^{N-1} F_n e^{j2\pi(nk)/N}. \quad (4.112)$$

Equations (4.111) and (4.112) comprise the DFT

$$\begin{aligned} F_n &= \sum_{k=0}^{N-1} f_k e^{-j2\pi(nk)/N}, \\ f_k &= \frac{1}{N} \sum_{n=0}^{N-1} F_n e^{j2\pi(nk)/N}. \end{aligned}$$

Because there are N terms in the sum in Eq. (4.111), it would appear that to compute the DFT for one frequency it will take on the order of N multiply and add operations; and to compute the DFT for all N frequencies, it would take on the order of N^2 multiply and add operations. However, several authors, especially Cooley and Tukey (1965), have showed how to take advantage of the circular nature of the exponential so that all N values of F_n can be computed with the order of $N \log(N)$ operations if N is a power of 2. For $N = 1024$, this is a saving of a factor of 100, a very large value. Their algorithm and related schemes are called the Fast Fourier Transform or FFT.

To use the DFT/FFT in evaluating frequency response, consider a system described by Eq. (4.105) and where the input is a sinusoid at frequency $\omega_\ell = 2\pi\ell/NT$ so that $e(kT) = A \sin(2\pi\ell kT/NT)$. We apply this input to the system *and wait until all transients have died away*. At this time, the output is given by $u(kT) = B \sin(2\pi\ell k/N + \psi)$. The DFT of $e(k)$ is

$$\begin{aligned} E_n &= \sum_{k=0}^{N-1} A \sin\left(\frac{2\pi\ell k}{N}\right) e^{-j(2\pi nk)/N} \\ &= \sum_{k=0}^{N-1} \frac{A}{2j} \left[e^{j(2\pi\ell k)/N} - e^{-j(2\pi\ell k)/N} \right] e^{-j(2\pi nk)/N} \\ &= \begin{cases} 0, & \ell \neq n \\ \frac{NA}{2j}, & \ell = n. \end{cases} \end{aligned}$$

The DFT of the output is

$$\begin{aligned} U_n &= \sum_{k=0}^{N-1} B \sin\left(\frac{2\pi\ell k}{N} + \psi\right) e^{-j(2\pi nk)/N} \\ &= \sum_{k=0}^{N-1} \frac{B}{2j} \left[e^{j\psi} e^{j(2\pi\ell k)/N} - e^{-j\psi} e^{-j(2\pi\ell k)/N} \right] e^{-j(2\pi nk)/N} \\ &= \begin{cases} 0, & \ell \neq n \\ \frac{NB}{2j} e^{j\psi}, & \ell = n. \end{cases} \end{aligned}$$

Dividing these results, we see that with sinusoidal input and output, the frequency response at the frequency $\omega = (2\pi\ell)/NT$ is given by

$$H\left(e^{j(2\pi\ell)/N}\right) = \frac{U_\ell}{E_\ell},$$

where $U_\ell = FFT(u_k)$ and $E_\ell = FFT(e_k)$, each evaluated at $n = \ell$. We will discuss in Chapter 12 the general problem of estimation of the total frequency response from experimental data using the DFT/FFT as well as other tools.

4.6 Properties of the z -Transform

We have used the z -transform to show that linear, constant, discrete systems can be described by a transfer function that is the z -transform of the system's unit-pulse response, and we have studied the relationship between the pole-zero patterns of transfer functions in the z -plane and the corresponding time responses. We began a table of z -transforms, and a more extensive table is given in Appendix B. In Section 4.6.1 we turn to consideration of some of the properties of the z -transform that are essential to the effective and correct use of this important tool. In Section 4.6.2 convergence issues concerning the z -transform are discussed and in Section 4.6.3 an alternate derivation of the transfer function is given.

4.6.1 Essential Properties

In order to make maximum use of a table of z -transforms, one must be able to use a few simple properties of the z -transform which follow directly from the definition. Some of these, such as linearity, we have already used without making a formal statement of it, and others, such as the transform of the convolution, we have previously derived. For reference, we will demonstrate a few properties here and collect them into Appendix B for future reference. In all the properties listed below, we assume that $F_i(z) = \mathcal{Z}\{f_i(kT)\}$.

1. *Linearity*: A function $f(x)$ is linear if $f(\alpha x_1 + \beta x_2) = \alpha f(x_1) + \beta f(x_2)$. Applying this result to the definition of the z -transform, we find immediately that

$$\begin{aligned} \mathcal{Z}\{\alpha f_1(kT) + \beta f_2(kT)\} &= \sum_{k=-\infty}^{\infty} \{\alpha f_1(k) + \beta f_2(k)\} z^{-k} \\ &= \alpha \mathcal{Z}\{f_1(k)\} + \beta \mathcal{Z}\{f_2(k)\} \\ &= \alpha F_1(z) + \beta F_2(z). \end{aligned}$$

Thus the z -transform is a linear function. It is the linearity of the transform that makes the partial-fraction technique work.

2. *Convolution of Time Sequences*:

$$\mathcal{Z}\left\{\sum_{l=-\infty}^{\infty} f_1(l)f_2(k-l)\right\} = F_1(z)F_2(z).$$

We have already developed this result in connection with Eq. (4.32). It is this result with linearity that makes the transform so useful in linear-constant-system analysis because the analysis of a combination of such dynamic systems can be done by linear algebra on the transfer functions.

3. *Time Shift:*

$$\mathcal{Z}\{f(k+n)\} = z^{+n}F(z). \quad (4.113)$$

We demonstrate this result also by direct calculation:

$$\mathcal{Z}\{f(k+n)\} = \sum_{k=-\infty}^{\infty} f(k+n)z^{-k}.$$

If we let $k+n = j$, then

$$\begin{aligned} \mathcal{Z}\{f(k+n)\} &= \sum_{j=-\infty}^{\infty} f(j)z^{-(j-n)} \\ &= z^n F(z). \quad \text{QED} \end{aligned}$$

This property is the essential tool in solving linear constant-coefficient difference equations by transforms. We should note here that the transform of the time shift is not the same for the one-sided transform because a shift can introduce terms with negative argument which are not included in the one-sided transform and must be treated separately. This effect causes initial conditions for the difference equation to be introduced when solution is done with the one-sided transform. See Problem 4.13.

4. *Scaling in the z -Plane:*

$$\mathcal{Z}\{r^{-k}f(k)\} = F(rz). \quad (4.114)$$

By direct substitution, we obtain

$$\begin{aligned} \mathcal{Z}\{r^{-k}f(k)\} &= \sum_{k=-\infty}^{\infty} r^{-k}f(k)z^{-k} \\ &= \sum_{k=-\infty}^{\infty} f(k)(rz)^{-k} \\ &= F(rz). \quad \text{QED} \end{aligned}$$

As an illustration of this property, we consider the z -transform of the unit step, $1(k)$, which we have computed before

$$\mathcal{Z}\{1(k)\} = \sum_{k=0}^{\infty} z^{-k} = \frac{z}{z-1}.$$

By property 4 we have immediately that

$$\mathcal{Z}\{r^{-k}1(k)\} = \frac{rz}{rz-1} = \frac{z}{z-(1/r)}.$$

As a more general example, if we have a polynomial $a(z) = z^2 + a_1z + a_2$ with roots $re^{\pm j\theta}$, then the scaled polynomial $\alpha^2 z^2 + a_1 \alpha z + a_2$ has roots $(r/\alpha)e^{\pm j\theta}$. This is an example of radial projection whereby the roots of a polynomial can be projected radially simply by changing the coefficients of the polynomial. The technique is sometimes used in pole-placement designs as described in Chapter 8, and sometimes used in adaptive control as described in Chapter 13.

5. *Final-Value Theorem:* If $F(z)$ converges for $|z| > 1$ and all poles of $(z-1)F(z)$ are inside the unit circle, then

$$\lim_{k \rightarrow \infty} f(k) = \lim_{z \rightarrow 1} (z-1)F(z). \quad (4.115)$$

The conditions on $F(z)$ assure that the only possible pole of $F(z)$ not strictly inside the unit circle is a simple pole at $z = 1$, which is removed in $(z - 1)F(z)$. Furthermore, the fact that $F(z)$ converges as the magnitude of z gets arbitrarily large ensures that $f(k)$ is zero for negative k . Therefore, all components of $f(k)$ tend to zero as k gets large, with the possible exception of the constant term due to the pole at $z = 1$. The size of this constant is given by the coefficient of $1/(z - 1)$ in the partial-fraction expansion of $F(z)$, namely

$$C = \lim_{z \rightarrow 1} (z - 1)F(z).$$

However, because all other terms in $f(k)$ tend to zero, the constant C is the final value of $f(k)$, and Eq. (4.115) results. QED

As an illustration of this property, we consider the signal whose transform is given by

$$U(z) = \frac{z}{z - 0.5} \frac{T}{2} \frac{z + 1}{z - 1}, \quad |z| > 1.$$

Because $U(z)$ satisfies the conditions of Eq. (4.115), we have

$$\begin{aligned} \lim_{k \rightarrow \infty} u(k) &= \lim_{z \rightarrow 1} (z - 1) \frac{z}{z - 0.5} \frac{T}{2} \frac{z + 1}{z - 1} \\ &= \lim_{z \rightarrow 1} \frac{z}{z - 0.5} \frac{T}{2} (z + 1) \\ &= \frac{1}{1 - 0.5} \frac{T}{2} (1 + 1) \\ &= 2T. \end{aligned}$$

This result can be checked against the closed form for $u(k)$ given by Eq. (4.121) below.

6. *Inversion:* As with the Laplace transform, the z -transform is actually one of a pair of transforms that connect functions of time to functions of the complex variable z . The z -transform computes a function of z from a sequence in k . (We identify the sequence number k with time in our analysis of dynamic systems, but there is nothing in the transform *per se* that requires this.) The inverse z -transform is a means to compute a sequence in k from a given function of z . We first examine two elementary schemes for inversion of a given $F(z)$ which can be used if we know beforehand that $F(z)$ is rational in z and converges as z approaches infinity. For a sequence $f(k)$, the z -transform has been defined as

$$F(z) = \sum_{k=-\infty}^{\infty} f(k)z^{-k}, \quad r_0 < |z| < R_0. \quad (4.116)$$

If any value of $f(k)$ for negative k is nonzero, then there will be a term in Eq. (4.116) with a positive power of z . This term will be unbounded if the magnitude of z is unbounded; and thus if $F(z)$ converges as $|z|$ approaches infinity, we know that $f(k)$ is zero for $k < 0$. In this case, Eq. (4.116) is one-sided, and we can write

$$F(z) = \sum_{k=0}^{\infty} f(k)z^{-k}, \quad r_0 < |z|. \quad (4.117)$$

The right-hand side of Eq. (4.117) is a series expansion of $F(z)$ about infinity or about $z^{-1} = 0$. Such an expansion is especially easy if $F(z)$ is the ratio of two polynomials in z^{-1} . We need only divide the numerator by the denominator in the correct way, and when the division is done, the coefficient of z^{-k} is automatically the sequence value $f(k)$. An example we have worked out before will illustrate the process.

*z-Transform Inversion by Long Division***Example 4.12**

The system for trapezoid-rule integration has the transfer function given by Eq. (4.14)

$$H(z) = \frac{T}{2} \frac{z+1}{z-1}, \quad |z| > 1.$$

Determine the output for an input which is the geometric series represented by $e_3(k)$ with $r = 0.5$. That is

$$E_3(z) = \frac{z}{z-0.5}, \quad |z| > 0.5.$$

Solution. The z -transform of the output is

$$\begin{aligned} U(z) &= E_3(z)H(z) \\ &= \frac{z}{z-0.5} \frac{T}{2} \frac{z+1}{z-1}, \quad |z| > 1. \end{aligned} \quad (4.118)$$

Equation (4.118) represents the transform of the system output, $u(k)$. Keeping out the factor of $T/2$, we write $U(z)$ as a ratio of polynomials in z^{-1}

$$U(z) = \frac{T}{2} \frac{1+z^{-1}}{1-1.5z^{-1}+0.5z^{-2}}, \quad (4.119)$$

and divide as follows

$$\begin{array}{r} \frac{T}{2} [1 + 2.5z^{-1} + 3.25z^{-2} + 3.625z^{-3} + \dots] \\ 1 - 1.5z^{-1} + 0.5z^{-2} \overline{) 1 + z^{-1}} \\ \underline{1 - 1.5z^{-1} + 0.5z^{-2}} \\ 2.5z^{-1} - 0.5z^{-2} \\ \underline{2.5z^{-1} - 3.75z^{-2} + 1.25z^{-3}} \\ 3.25z^{-2} - 1.25z^{-3} \\ \underline{3.25z^{-2} - 4.875z^{-3} + 1.625z^{-4}} \\ 3.625z^{-3} - 1.625z^{-4} \\ \underline{3.625z^{-3} - \dots} \end{array}$$

By direct comparison with $U(z) = \sum_0^\infty u(k)z^{-k}$, we conclude that

$$\begin{aligned} u_0 &= T/2, \\ u_1 &= (T/2)2.5, \\ u_2 &= (T/2)3.25, \\ &\vdots \end{aligned} \quad (4.120)$$

Clearly, the use of a computer will greatly aid the speed of this process in all but the simplest of cases. Some may prefer to use synthetic division and omit copying over all the extraneous z 's in the division. The process is identical to converting $F(z)$ to the equivalent difference equation and solving for the unit-pulse response.

The second special method for the inversion of z -transforms is to decompose $F(z)$ by partial-fraction expansion and look up the components of the sequence $f(k)$ in a previously prepared table.

*z-Transform Inversion by Partial Fraction Expansion***Example 4.13**

Repeat Example 4.12 using the partial fraction expansion method.

Solution. Consider again Eq. (4.118) and expand $U(z)$ as a function of z^{-1} as follows

$$U(z) = \frac{T}{2} \frac{1+z^{-1}}{1-z^{-1}} \frac{1}{1-0.5z^{-1}} = \frac{A}{1-z^{-1}} + \frac{B}{1-0.5z^{-1}}.$$

We multiply both sides by $1 - z^{-1}$, let $z^{-1} = 1$, and compute

$$A = \frac{T}{2} \frac{2}{0.5} = 2T.$$

Similarly, at $z^{-1} = 2$, we evaluate

$$B = \frac{T}{2} \frac{1+2}{1-2} = -\frac{3T}{2}.$$

Looking back now at e_2 and e_3 , which constitute our “table” for the moment, we can copy down that

$$\begin{aligned} u_k &= Ae_2(k) + Be_3(k) \\ &= 2Te_2(k) - \frac{3T}{2}e_3(k) \\ &= \left(2T - \frac{3T}{2} \left(\frac{1}{2} \right)^k \right) 1(k) \\ &= \frac{T}{2} \left[4 - \frac{3}{2^k} \right] 1(k). \end{aligned} \quad (4.121)$$

Evaluation of Eq. (4.121) for $k = 0, 1, 2, \dots$ will, naturally, give the same values for $u(k)$ as we found in Eq. (4.120).

4.6.2 *Convergence of z -Transform

We now examine more closely the role of the region of convergence of the z -transform and present the inverse-transform integral. We begin with another example. The sequence

$$f(k) = \begin{cases} -1 & k < 0 \\ 0 & k \geq 0 \end{cases}$$

has the transform

$$\begin{aligned} F(z) &= \sum_{k=-\infty}^{-1} -z^{-k} = - \left[\sum_0^{\infty} z^k - 1 \right] \\ &= \frac{z}{z-1}, \quad |z| < 1. \end{aligned}$$

This transform is exactly the same as the transform of the unit step $1(k)$, Eq. (4.95), except that this transform converges *inside* the unit circle and the transform of the $1(k)$ converges outside the unit circle. Knowledge of the region of convergence is obviously essential to the proper inversion of the transform to obtain the time sequence. The inverse z -transform is the closed, complex integral²¹

$$f(k) = \frac{1}{2\pi j} \oint F(z) z^k \frac{dz}{z}, \quad (4.122)$$

where the contour is a circle in the region of convergence of $F(z)$. To demonstrate the correctness of the integral and to use it to compute inverses, it is useful to apply Cauchy’s residue calculus [see Churchill and Brown (1984)]. Cauchy’s result is that a closed integral of a function of z which is analytic on and inside a closed contour C except at a finite number of isolated singularities z_i is given by

$$\frac{1}{2\pi j} \oint_C F(z) dz = \sum_i \text{Res}(z_i). \quad (4.123)$$

²¹If it is known that $f(k)$ is causal, that is, $f(k) = 0$ for $k < 0$, then the region of convergence is outside the smallest circle that contains all the poles of $F(z)$ for rational transforms. It is this property that permits inversion by partial-fraction expansion and long division.

In Eq. (4.123), $\text{Res}(z_i)$ means the residue of $F(z)$ at the singularity at z_i . We will be considering only rational functions, and these have only poles as singularities. If $F(z)$ has a pole of order n at z_1 , then $(z - z_1)^n F(z)$ is regular at z_1 and can be expanded in a Taylor series near z_1 as

$$(z - z_1)^n F(z) = A_{-n} + A_{-n+1}(z - z_1) + \cdots + A_{-1}(z - z_1)^{n-1} + A_0(z - z_1)^n + \cdots \quad (4.124)$$

The residue of $F(z)$ at z_1 is A_{-1} .

First we will use Cauchy's formula to verify Eq. (4.123). If $F(z)$ is the z -transform of $f(k)$, then we write

$$\mathcal{I} = \frac{1}{2\pi j} \oint \sum_{l=-\infty}^{\infty} f(l) z^{-l} z^k \frac{dz}{z}.$$

We assume that the series for $F(z)$ converges uniformly on the contour of integration, so the series can be integrated term by term. Thus we have

$$\mathcal{I} = \frac{1}{2\pi j} \sum_{l=-\infty}^{\infty} f(l) \oint z^{k-l} \frac{dz}{z}.$$

The argument of the integral has no pole inside the contour if $k - l \geq 1$, and it has zero residue at the pole at $z = 0$ if $k - l < 0$. Only if $k = l$ does the integral have a residue, and that is 1. By Eq. (4.123), the integral is zero if $k \neq l$ and is $2\pi j$ if $k = l$. Thus $\mathcal{I} = f(k)$, which demonstrates Eq. (4.122).

To illustrate the use of Eq. (4.123) to compute the inverse of a z -transform, we will use the function $z/(z - 1)$ and consider first the case of convergence for $|z| > 1$ and second the case of convergence for $|z| < 1$. For the first case

$$f_1(k) = \frac{1}{2\pi j} \oint_{|z|=R>1} \frac{z}{z-1} z^k \frac{dz}{z}, \quad (4.125)$$

where the contour is a circle of radius greater than 1. Suppose $k < 0$. In this case, the argument of the integral has two poles inside the contour: one at $z = 1$ with residue

$$\lim_{z \rightarrow 1} (z - 1) \frac{z^k}{z - 1} = 1,$$

and one pole at $z = 0$ with residue found as in (2.109) (if $k < 0$, then z^{-k} removes the pole)

$$\begin{aligned} z^{-k} \frac{z^k}{z - 1} &= \frac{-1}{z - 1} \\ &= -(1 + z^{-1} + z^{-2} + \cdots + z^{-k} + \cdots). \end{aligned}$$

The residue is thus -1 for all k , and the sum of the residues is zero, and

$$f_1(k) = 0, \quad k < 0. \quad (4.126)$$

For $k \geq 0$, the argument of the integral in Eq. (4.125) has only the pole at $z = 1$ with residue 1. Thus

$$f_1(k) = 1, \quad k \geq 0. \quad (4.127)$$

Equations (4.123) and (4.124) correspond to the unit-step function, as they should. We would write the inverse transform symbolically $\mathcal{Z}^{-1}\{.\}$ as, in this case

$$\mathcal{Z}^{-1} \left\{ \frac{z}{z-1} \right\} = 1(k) \quad (4.128)$$

when $z/(z - 1)$ converges for $|z| > 1$.

If, on the other hand, convergence is inside the unit circle, then for $k \geq 0$, there are no poles of the integrand contained in the contour, and

$$f_2(k) = 0, \quad k \geq 0.$$

At $k < 0$, there is a pole at the origin of z , and as before, the residue is equal to -1 there, so

$$f_2(k) = -1, \quad k < 0.$$

In symbols, corresponding to Eq. (4.128), we have

$$\mathcal{Z}^{-1} \left\{ \frac{z}{z-1} \right\} = 1(k) - 1$$

when $z/(z-1)$ converges for $|z| < 1$.

Although, as we have just seen, the inverse integral can be used to compute an expression for a sequence to which a transform corresponds, a more effective use of the integral is in more general manipulations. We consider one such case that will be of some interest later. First, we consider an expression for the transform of a product of two sequences. Suppose we have

$$f_3(k) = f_1(k)f_2(k),$$

and f_1 and f_2 are such that the transform of the product exists. An expression for $F_3(z)$ in terms of $F_1(z)$ and $F_2(z)$ can be developed as follows. By definition

$$F_3(z) = \sum_{k=-\infty}^{\infty} f_1(k)f_2(k)z^{-k}.$$

From the inversion integral, Eq. (4.122), we can replace $f_2(k)$ by an integral

$$F_3(z) = \sum_{k=-\infty}^{\infty} f_1(k)z^{-k} \frac{1}{2\pi j} \oint_{C_2} F_2(\zeta) \zeta^k \frac{d\zeta}{\zeta}.$$

We assume that we can find a region where we can exchange the summation with the integration. The contour will be called C_3 in this case

$$F_3(z) = \frac{1}{2\pi j} \oint_{C_3} F_2(\zeta) \sum_{k=-\infty}^{\infty} f_1(k) \left(\frac{z}{\zeta} \right)^{-k} \frac{d\zeta}{\zeta}.$$

The sum can now be recognized as $F_1(z/\zeta)$ and, when we substitute this,

$$F_3(z) = \frac{1}{2\pi j} \oint_{C_3} F_2(\zeta) F_1 \left(\frac{z}{\zeta} \right) \frac{d\zeta}{\zeta}, \quad (4.129)$$

the contour C_3 must be in the overlap of the convergence regions of $F_2(\zeta)$ and $F_1(z/\zeta)$. Then $F_3(z)$ will converge for the range of values of z for which C_3 can be found.

If we let $f_1 = f_2$ and $z = 1$ in Eq. (4.129), we have the discrete version of Parseval's theorem, where convergence is on the unit circle

$$F_3(1) = \sum_{k=-\infty}^{\infty} f_1^2 = \frac{1}{2\pi j} \oint_C F_1(\zeta) F_1 \left(\frac{1}{\zeta} \right) \frac{d\zeta}{\zeta}. \quad (4.130)$$

This particular theorem shows how we can compute the sum of squares of a time sequence by evaluating a complex integral in the z -domain. The result is useful in the design of systems by least squares.

4.6.3 *Another Derivation of the Transfer Function

Let \mathcal{D} be a discrete system which maps an input sequence, $\{e(k)\}$, into an output sequence $\{u(k)\}$.²² Then, expressing this as an operator on $e(k)$, we have

$$u(k) = \mathcal{D}\{e(k)\}.$$

If \mathcal{D} is linear, then

$$\mathcal{D}\{\alpha e_1(k) + \beta e_2(k)\} = \alpha \mathcal{D}\{e_1(k)\} + \beta \mathcal{D}\{e_2(k)\}. \quad (4.131)$$

If the system is time invariant, a shift in $e(k)$ to $e(k+j)$ must result in no other effects but a shift in the response, u . We write

$$\mathcal{D}\{e(k+j)\} = u(k+j) \quad \text{for all } j \quad (4.132)$$

if

$$\mathcal{D}\{e(k)\} = u(k).$$

Theorem

If \mathcal{D} is linear and time invariant and is given an input z^k for a value of z for which the output is finite at time k , then the output will be of the form $H(z)z^k$.

In general, if $e(k) = z^k$, then an arbitrary finite response can be written

$$u(k) = H(z, k)z^k.$$

Consider $e_2(k) = z^{k+j} = z^j z^k$ for some fixed j . From Eq. (4.131), if we let $\alpha = z^j$, it must follow that

$$\begin{aligned} u_2 &= z^j u(k) \\ &= z^j H(z, k)z^k \\ &= H(z, k)z^{k+j}. \end{aligned} \quad (4.133)$$

From Eq. (4.132), we must have

$$\begin{aligned} u_2(k) &= u(k+j) \\ &= H(z, j+k)z^{k+j} \quad \text{for all } j. \end{aligned} \quad (4.134)$$

From a comparison of Eqs. (4.133) and (4.134), it follows that

$$H(z, k) = H(z, k+j) \quad \text{for all } j$$

that is, H does not depend on the second argument and can be written $H(z)$. Thus for the elemental signal $e(k) = z^k$, we have a solution $u(k)$ of the same (exponential) shape but modulated by a ratio $H(z)$, $u(k) = H(z)z^k$.

Can we represent a general signal as a *linear sum* (integral) of such elements? We can, by the inverse integral derived above, as follows

$$e(k) = \frac{1}{2\pi j} \oint E(z) z^k \frac{dz}{z}, \quad (4.135)$$

where

$$E(z) = \sum_{-\infty}^{\infty} e(k) z^{-k}, \quad r < |z| < R, \quad (4.136)$$

for signals with $r < R$ for which Eq. (4.136) converges. We call $E(z)$ the z -transform of $e(k)$, and the (closed) path of integration is in the annular region of convergence of Eq. (4.136). If $e(k) = 0, k < 0$, then $R \rightarrow \infty$, and this region is the whole z -plane *outside* a circle of finite radius.

²²This derivation was suggested by L. A. Zadeh in 1952 at Columbia University.

The consequences of linearity are that the response to a sum of signals is the sum of the responses as given in Eq. (4.131). Although Eq. (4.135) is the limit of a sum, the result still holds, and we can write

$$u(k) = \frac{1}{2\pi j} \oint E(z) [\text{response to } z^k] \frac{dz}{z},$$

but, by the theorem, the response to z^k is $H(z)z^k$. Therefore we can write

$$\begin{aligned} u(k) &= \frac{1}{2\pi j} \oint E(z) [H(z)z^k] \frac{dz}{z} \\ &= \frac{1}{2\pi j} \oint H(z)E(z)z^k \frac{dz}{z}. \end{aligned} \quad (4.137)$$

We can define $U(z) = H(z)E(z)$ by comparison with Eq. (4.135) and note that

$$U(z) = \sum_{k=-\infty}^{\infty} u(k)z^{-k} = H(z)E(z). \quad (4.138)$$

Thus $H(z)$ is the *transfer function*, which is the ratio of the transforms of $e(k)$ and $u(k)$ as well as the amplitude response to inputs of the form z^k .

This derivation begins with linearity and stationarity and derives the z -transform as the natural tool of analysis from the fact that input signals in the form z^k produce an output that has the same shape.²³ It is somewhat more satisfying to derive the necessary transform than to start with the transform and see what systems it is good for. Better to start with the problem and find a tool than start with a tool and look for a problem. Unfortunately, the direct approach requires extensive use of the inversion integral and more sophisticated analysis to develop the main result, which is Eq. (4.138). *Chacun à son goût.*

4.7 Summary

- The z -transform can be used to solve discrete difference equations in the same way that the Laplace transform is used to solve continuous differential equations.
- The key property of the z -transform that allows solution of difference equations is

$$\mathcal{Z}\{f(k-1)\} = z^{-1}F(z). \quad (4.113)$$

- A system will be stable in the sense that a *Bounded Input* will yield a *Bounded Output* (BIBO stability) if

$$\sum_{l=-\infty}^{\infty} |h_{k-l}| < \infty. \quad (4.35)$$

- A discrete system can be defined by its transfer function (in z) or its state-space difference equation.
- The z -transform of the samples of a continuous system $G(s)$ preceded by a zero-order-hold (ZOH) is

$$G(z) = (1 - z^{-1})\mathcal{Z}\left\{\frac{G(s)}{s}\right\} \quad (4.41)$$

which is typically evaluated using MATLAB's `c2d.m`.

²³Because z^k is unchanged in shape by passage through the linear constant system, we say that z^k is an eigenfunction of such systems.

- For the continuous state-space model

$$\dot{\mathbf{x}} = \mathbf{F}\mathbf{x} + \mathbf{G}u, \quad (4.45)$$

$$y = \mathbf{H}\mathbf{x} + Ju, \quad (4.46)$$

preceded by a zero-order-hold, the discrete state-space difference equations are

$$\begin{aligned} \mathbf{x}(k+1) &= \mathbf{\Phi}\mathbf{x}(k) + \mathbf{\Gamma}u(k), \\ y(k) &= \mathbf{H}\mathbf{x}(k) + Ju(k), \end{aligned} \quad (4.59)$$

where

$$\begin{aligned} \mathbf{\Phi} &= e^{\mathbf{F}T} \\ \mathbf{\Gamma} &= \int_0^T e^{\mathbf{F}\eta} d\eta \mathbf{G}, \end{aligned} \quad (4.58)$$

which can be evaluated by MATLAB's `c2d.m`.

- The discrete transfer function in terms of the state-space matrices is

$$\frac{Y(z)}{U(z)} = \mathbf{H}[z\mathbf{I} - \mathbf{\Phi}]^{-1}\mathbf{\Gamma}, \quad (4.64)$$

which can be evaluated in MATLAB by the `tf` function.

- The characteristic behavior associated with poles in the z -plane is shown in Figs. 4.21 through 4.23 and summarized in Fig. 4.25. Responses are typically determined via MATLAB's `impz.m` or `step.m`.
- A system represented by $H(z)$ has a discrete frequency response to sinusoids at ω_o , given by an amplitude, A , and phase, ψ , as

$$A = |H(e^{j\omega_o T})| \quad \text{and} \quad \psi = \angle(H(e^{j\omega_o T})) \quad (4.110)$$

which can be evaluated by MATLAB's `bode.m`.

- The discrete Final Value Theorem, for an $F(z)$ that converges and has a final value, is given by

$$\lim_{k \rightarrow \infty} f(k) = \lim_{z \rightarrow 1} (z-1)F(z). \quad (4.115)$$

4.8 Problems

4.1 Check the following for stability:

(a) $u(k) = 0.5u(k-1) - 0.3u(k-2)$

(b) $u(k) = 1.6u(k-1) - u(k-2)$

(c) $u(k) = 0.8u(k-1) + 0.4u(k-2)$

- 4.2 (a) Derive the difference equation corresponding to the approximation of integration found by fitting a parabola to the points e_{k-2}, e_{k-1}, e_k and taking the area under this parabola between $t = kT - T$ and $t = kT$ as the approximation to the integral of $e(t)$ over this range.
- (b) Find the transfer function of the resulting discrete system and plot the poles and zeros in the z -plane.

4.3 Verify that the transfer function of the system of Fig. 4.8(c) is given by the same $H(z)$ as the system of Fig. 4.9(c).

- 4.4 (a) Compute and plot the unit-pulse response of the system derived in Problem 4.2.
 (b) Is this system BIBO stable?

4.5 Consider the difference equation

$$u(k+2) = 0.25u(k).$$

- (a) Assume a solution $u(k) = A_1 z_1^k$ and find the characteristic equation in z .
 (b) Find the characteristic roots z_1 and z_2 and decide if the equation solutions are stable or unstable.
 (c) Assume a general solution of the form

$$u(k) = A_1 z_1^k + A_2 z_2^k$$

and find A_1 and A_2 to match the initial conditions $u(0) = 0, u(1) = 1$.

- (d) Repeat parts (a), (b), and (c) for the equation

$$u(k+2) = -0.25u(k).$$

- (e) Repeat parts (a), (b), and (c) for the equation

$$u(k+2) = u(k+1) - 0.5u(k).$$

4.6 Show that the characteristic equation

$$z^2 - 2r \cos(\theta)z + r^2$$

has the roots

$$z_{1,2} = r e^{\pm j\theta}.$$

- 4.7 (a) Use the method of block-diagram reduction, applying Figs. 4.5, 4.6, and 4.7 to compute the transfer function of Fig. 4.8(c).
 (b) Repeat part (a) for the diagram of Fig. 4.9(c).

4.8 Use MATLAB to determine how many roots of the following are outside the unit circle.

- (a) $z^2 + 0.25 = 0$
 (b) $z^3 - 1.1z^2 + 0.01z + 0.405 = 0$
 (c) $z^3 - 3.6z^2 + 4z - 1.6 = 0$

4.9 Compute by hand and table look-up the discrete transfer function if the $G(s)$ in Fig. 4.12 is

- (a) $\frac{K}{s}$
 (b) $\frac{3}{s(s+3)}$
 (c) $\frac{3}{(s+1)(s+3)}$
 (d) $\frac{(s+1)}{s^2}$
 (e) $\frac{e^{sT/2}}{s^2}$
 (f) $\frac{(1-s)}{s^2}$
 (g) $\frac{3e^{-1.5Ts}}{(s+1)(s+3)}$

- (h) Repeat the calculation of these discrete transfer functions using MATLAB. Compute for the sampling period $T = 0.05$ and $T = 0.5$ and plot the location of the poles and zeros in the z -plane.

4.10 Use MATLAB to compute the discrete transfer function if the $G(s)$ in Fig. 4.12 is

- the two-mass system with the non-colocated actuator and sensor of Eq. (A.21) with sampling periods $T = 0.02$ and $T = 0.1$. Plot the zeros and poles of the results in the z -plane. Let $\omega_p = 5$, $\zeta_p = 0.01$.
- the two-mass system with the colocated actuator and sensor given by Eq. (A.23). Use $T = 0.02$ and $T = 0.1$. Plot the zeros and poles of the results in the z -plane. Let $\omega_p = 5$, $\omega_z = 3$, $\zeta_p = \zeta_z = 0$.
- the two-input–two-output paper machine described in Eq. (A.24). Let $T = 0.1$ and $T = 0.5$.

4.11 Consider the system described by the transfer function

$$\frac{Y(s)}{U(s)} = G(s) = \frac{3}{(s+1)(s+3)}.$$

- Draw the block diagram corresponding to this system in control canonical form, define the state vector, and give the corresponding description matrices **F**, **G**, **H**, **J**.
- Write $G(s)$ in partial fractions and draw the corresponding parallel block diagram with each component part in control canonical form. Define the state ξ and give the corresponding state description matrices **A**, **B**, **C**, **D**.
- By finding the transfer functions X_1/U and X_2/U of part (a) in partial fraction form, express x_1 and x_2 in terms of ξ_1 and ξ_2 . Write these relations as the two-by-two transformation **T** such that $\mathbf{x} = \mathbf{T}\xi$.
- Verify that the matrices you have found are related by the formulas

$$\begin{aligned}\mathbf{A} &= \mathbf{T}^{-1}\mathbf{FT}, \\ \mathbf{B} &= \mathbf{T}^{-1}\mathbf{G}, \\ \mathbf{C} &= \mathbf{HT}, \\ \mathbf{D} &= \mathbf{J}.\end{aligned}$$

4.12 The first-order system $(z - \alpha)/(1 - \alpha)z$ has a zero at $z = \alpha$.

- Plot the step response for this system for $\alpha = 0.8, 0.9, 1.1, 1.2, 2$.
- Plot the overshoot of this system on the same coordinates as those appearing in Fig. 4.28 for $-1 < \alpha < 1$.
- In what way is the step response of this system unusual for $\alpha > 1$?

4.13 The one-sided z -transform is defined as

$$F(z) = \sum_0^{\infty} f(k)z^{-k}.$$

- Show that the one-sided transform of $f(k+1)$ is

$$\mathcal{Z}\{f(k+1)\} = zF(z) - zf(0).$$

- Use the one-sided transform to solve for the transforms of the Fibonacci numbers by writing Eq. (4.4) as $u_{k+2} = u_{k+1} + u_k$. Let $u_0 = u_1 = 1$. [You will need to compute the transform of $f(k+2)$.]
- Compute the location of the poles of the transform of the Fibonacci numbers.
- Compute the inverse transform of the numbers.

- (e) Show that if u_k is the k th Fibonacci number, then the ratio u_{k+1}/u_k will go to $(1 + \sqrt{5})/2$, the golden ratio of the Greeks.
- (f) Show that if we add a forcing term, $e(k)$, to Eq. (4.4) we can generate the Fibonacci numbers by a system that can be analyzed by the two-sided transform; i.e., let $u_k = u_{k-1} + u_{k-2} + e_k$ and let $e_k = \delta_0(k)$ ($\delta_0(k) = 1$ at $k = 0$ and zero elsewhere). Take the two-sided transform and show the same $U(z)$ results as in part (b).

4.14 Substitute $u = Az^k$ and $e = Bz^k$ into Eqs. (4.2) and (4.7) and show that the transfer functions, Eqs. (4.15) and (4.14), can be found in this way.

4.15 Consider the transfer function

$$H(z) = \frac{(z+1)(z^2 - 1.3z + 0.81)}{(z^2 - 1.2z + 0.5)(z^2 - 1.4z + 0.81)}.$$

Draw a *cascade* realization, using observer canonical forms for second-order blocks and in such a way that the coefficients as shown in $H(z)$ above are the parameters of the block diagram.

- 4.16 (a) Write the $H(z)$ of Problem 4.15 in partial fractions in two terms of second order each, and draw a *parallel* realization, using the observer canonical form for each block and showing the coefficients of the partial-fraction expansion as the parameters of the realization.
- (b) Suppose the two factors in the denominator of $H(z)$ were identical (say we change the 1.4 to 1.2 and the 0.81 to 0.5). What would the parallel realization be in this case?
- 4.17 Show that the observer canonical form of the system equations shown in Fig. 4.9 can be written in the state-space form as given by Eq. (4.27).
- 4.18 Draw out each block of Fig. 4.10 in (a) control and (b) observer canonical form. Write out the state-description matrices in each case.
- 4.19 For a second-order system with damping ratio 0.5 and poles at an angle in the z -plane of $\theta = 30^\circ$, what percent overshoot to a step would you expect if the system had a zero at $z_2 = 0.6$?
- 4.20 Consider a signal with the transform (which converges for $|z| > 2$)

$$U(z) = \frac{z}{(z-1)(z-2)}.$$

- (a) What value is given by the formula (Final Value Theorem) of Eq. (4.115) applied to this $U(z)$?
- (b) Find the final value of $u(k)$ by taking the inverse transform of $U(z)$, using partial-fraction expansion and the tables.
- (c) Explain why the two results of (a) and (b) differ.
- 4.21 (a) Find the z -transform and be sure to give the region of convergence for the signal

$$u(k) = r^{+|k|}, \quad |r| < 1.$$

[Hint: Write u as the sum of two functions, one for $k \geq 0$ and one for $k < 0$, find the individual transforms, and determine values of z for which *both* terms converge.]

- (b) If a rational function $U(z)$ is known to converge on the unit circle $|z| = 1$, show how partial-fraction expansion can be used to compute the inverse transform. Apply your result to the transform you found in part (a).
- 4.22 Compute the inverse transform, $f(k)$, for each of the following transforms:

(a) $F(z) = \frac{1}{1+z^{-2}}, \quad |z| > 1;$

$$(b) F(z) = \frac{z(z-1)}{z^2-1.25z+0.25}, \quad |z| > 1;$$

$$(c) F(z) = \frac{z}{z^2-2z+1}, \quad |z| > 1;$$

$$(d) F(z) = \frac{z}{(z-\frac{1}{2})(z-2)}, \quad 1/2 < |z| < 2.$$

4.23 Use MATLAB to plot the time sequence associated with each of the transforms in Problem 4.22.

4.24 Use the z -transform to solve the difference equation

$$y(k) - 3y(k-1) + 2y(k-2) = 2u(k-1) - 2u(k-2),$$

$$u(k) = \begin{cases} k, & k \geq 0 \\ 0 & k < 0 \end{cases}$$

$$y(k) = 0, \quad k < 0.$$

4.25 For the difference equation in Problem 4.24, solve using MATLAB.

4.26 Compute by hand and table look-up the discrete transfer function if the $G(s)$ in Fig. 4.12 is

$$G(s) = \frac{10(s+1)}{s^2(s+10)}$$

and the sample period is $T = 10$ msec. Verify the calculation using MATLAB.

4.27 Find the discrete state-space model for the system in Problem 4.26.

4.28 Compute by hand and table look-up the discrete transfer function if the $G(s)$ in Fig. 4.12 is

$$G(s) = \frac{10(s+1)}{s^2+s+10}$$

and the sample period is $T = 10$ msec. Verify the calculation using MATLAB and find the DC gain of both the $G(s)$ and the $G(z)$.

4.29 Find the discrete state-space model for the system in Problem 4.28. Then compute the eigenvalues of Φ and the transmission zeros of the state-space model.

4.30 Find the state-space model for Fig. 4.12 with

$$G(s) = \frac{1}{s^2}$$

where there is a one cycle delay after the A/D converter.

Chapter 5

Sampled-Data Systems

A Perspective on Sampled-Data Systems

The use of digital logic or digital computers to calculate a control action for a continuous, dynamic system introduces the fundamental operation of sampling. Samples are taken from the continuous physical signals such as position, velocity, or temperature and these samples are used in the computer to calculate the controls to be applied. Systems where discrete signals appear in some places and continuous signals occur in other parts are called *sampled-data systems* because continuous data are sampled before being used. In many ways the analysis of a purely continuous system or of a purely discrete system is simpler than is that of sampled-data systems. The analysis of linear, time-invariant continuous systems can be done with the Laplace transform and the analysis of linear time-invariant discrete systems can be done with the z -transform alone. If one is willing to restrict attention to only the samples of all the signals in a digital control one can do much useful analysis and design on the system as a purely discrete system using the z -transform. However the physical reality is that the computer operations are on discrete signals while the plant signals are in the continuous world and in order to consider the behavior of the plant between sampling instants, it is necessary to consider both the discrete actions of the computer and the continuous response of the plant. Thus the role of sampling and the conversion from continuous to discrete and back from discrete to continuous are very important to the understanding of the complete response of digital control, and we must study the process of sampling and how to make mathematical models of analog-to-digital conversion and digital-to-analog conversion. This analysis requires careful treatment using the Fourier transform but the effort is well rewarded with the understanding it provides of sampled-data systems.

Chapter Overview

In this chapter, we introduce the analysis of the sampling process and describe both a time-domain and a frequency-domain representation. We also describe the companion process of data extrapolation or data holding to construct a continuous time signal from samples. As part of this analysis we show that a sampled-data system is made time varying by the introduction of sampling, and thus it is not possible to describe such systems exactly by a continuous-time transfer function. However, a continuous signal is recovered by the hold process and we can approximate the sinusoidal response of a sampler and hold by fitting another sinusoid of the same frequency to the complete response. We show how to compute this best-fit sinusoidal response analytically and use it to obtain a good approximation to a transfer function. For those familiar with the idea, this approach is equivalent to the use of the “describing function” that is used to approximate a transfer function for simple nonlinear systems. In Section 5.1 the analysis of the sample and hold operation is considered and in Section 5.2 the frequency analysis of a sampled signal is given. Here the important phenomenon of signal aliasing caused by sampling is introduced. In Section 5.3 the zero-order hold and some of its generalizations are considered. Analysis of sampled-data systems in the frequency domain is introduced

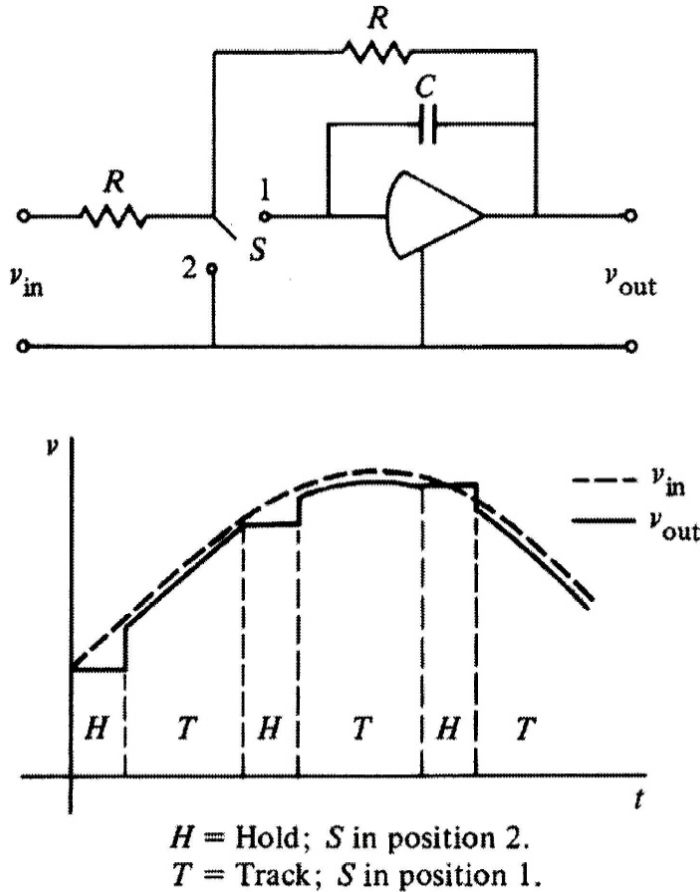


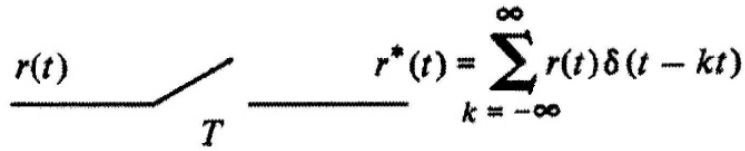
Figure 5.1
Analog-to-digital
converter with
sample and hold

in Section 5.4 including block diagram analysis of these combined systems. Finally in Section 5.5 computation of intersample ripple is discussed.

5.1 Analysis of the Sample and Hold

To get samples of a physical signal such as a position or a velocity into digital form, we typically have a sensor that produces a voltage proportional to the physical variable and an **analog-to-digital converter**, commonly called an **A/D converter** or ADC, that transforms the voltage into a digital number. The physical conversion always takes a non-zero time, and in many instances this time is significant with respect to the sample period of the control or with respect to the rate of change of the signal being sampled. In order to give the computer an accurate representation of the signal exactly at the sampling instants kT , the A/D converter is typically preceded by a **sample-and-hold circuit (SHC)**. A simple electronic schematic is sketched in Fig. 5.1, where the switch, S , is an electronic device driven by simple logic from a clock. Its operation is described in the following paragraph.

With the switch, S , in position 1, the amplifier output $v_{out}(t)$ tracks the input voltage $v_{in}(t)$ through the transfer function $1/(RCs + 1)$. The circuit bandwidth of the SHC, $1/RC$, is selected to be high compared to the input signal bandwidth. Typical values are $R = 1000$ ohms, $C = 30 \times 10^{-12}$ farads for a bandwidth of $f = 1/2\pi RC = 5.3$ MHz. During this “tracking time,” the ADC is turned off and ignores v_{out} . When a sample is to be taken at $t = kT$ the switch S is set to position 2 and the capacitor C holds the output of the operational amplifier frozen from that time at $v_{out}(kT) = v_{in}(kT)$. The ADC is now signaled to begin conversion of the constant input from the SHC into a digital number which will be a true representation of the input voltage at the sample instant. When the conversion



$$r^*(t) = \sum_{k=-\infty}^{\infty} r(t) \delta(t - kt)$$

Figure 5.2
The sampler

is completed, the digital number is presented to the computer at which time the calculations based on this sample value can begin. The SHC switch is now moved to position 1, and the circuit is again tracking, waiting for the next command to freeze a sample. The SHC needs only to hold the voltage for a short time on the order of microseconds in order for the conversion to be completed before it starts tracking again. The value converted is held inside the computer for the entire sampling period of the system, so the combination of the electronic SHC plus the ADC operate as a sample-and-hold for the sampling period, T , which may be many milliseconds long. The number obtained by the ADC is a quantized version of the signal represented in a finite number of bits, 12 being a typical number. As a result, the device is nonlinear. However, the signals are typically large with respect to the smallest quantum and the effect of this nonlinearity can be ignored in a first analysis. A detailed study of quantization is included in Chapter 10.

For the purpose of the analysis, we separate the sample and hold into two mathematical operations: a sampling operation represented by impulse modulation and a hold operation represented as a linear filter. The symbol or schematic of the ideal sampler is shown in Fig. 5.2; its role is to give a mathematical representation of the process of taking periodic samples from $r(t)$ to produce $r(kT)$ and to do this in such a way that we can include the sampled signals in the analysis of continuous signals using the Laplace transform.¹ The technique is to use *impulse modulation* as the mathematical representation of sampling. Thus, from Fig. 5.2, we picture the output of the sampler as a string of impulses

$$r^*(t) = \sum_{k=-\infty}^{\infty} r(t) \delta(t - kT). \quad (5.1)$$

The impulse can be visualized as the limit of a pulse of unit area that has growing amplitude and shrinking duration. The essential property of the impulse is the sifting property that

$$\int_{-\infty}^{\infty} f(t) \delta(t - a) dt = f(a) \quad (5.2)$$

for all functions f that are continuous at a . The integral of the impulse is the unit step

$$\int_{-\infty}^t \delta(\tau) d\tau = 1(t), \quad (5.3)$$

and the Laplace transform of the unit impulse is 1, because

$$\mathcal{L}\{\delta(t)\} = \int_{-\infty}^{\infty} \delta(\tau) e^{-s\tau} d\tau = 1. \quad (5.4)$$

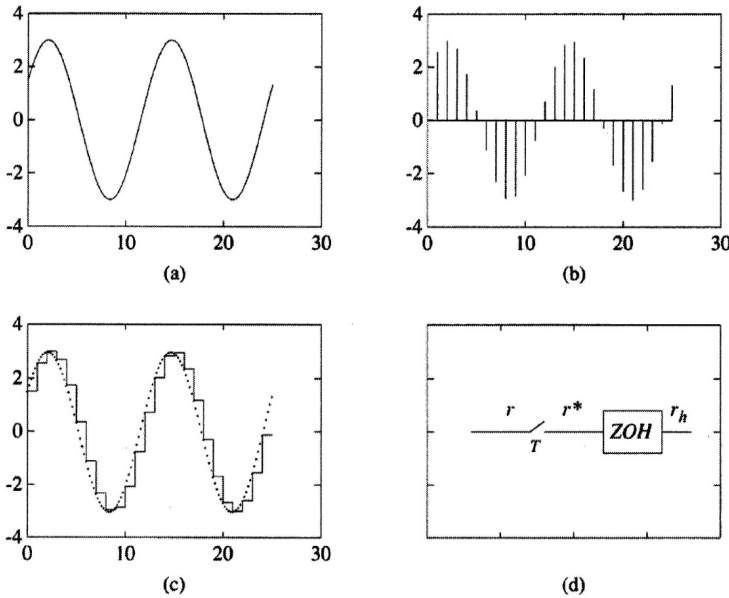
Using these properties we can see that $r^*(t)$, defined in Eq. (5.1), depends only on the discrete sample values $r(kT)$. The Laplace transform of $r^*(t)$ can be computed as follows

$$\mathcal{L}\{r^*(t)\} = \int_{-\infty}^{\infty} r^*(\tau) e^{-s\tau} d\tau.$$

If we substitute Eq. (5.1) for $r^*(t)$, we obtain

$$= \int_{-\infty}^{\infty} \sum_{k=-\infty}^{\infty} r(\tau) \delta(\tau - kT) e^{-s\tau} d\tau,$$

¹We assume that the reader has some familiarity with Fourier and Laplace transform analysis. A general reference is Bracewell (1978).

**Figure 5.3**

The sample and hold, showing typical signals. (a) Input signal r ; (b) sampled signal r^* ; (c) output signal r_h ; (d) sample and hold

and now, exchanging integration and summation and using Eq. (5.2), we have

$$R^*(s) = \sum_{k=-\infty}^{\infty} r(kT)e^{-skT}. \quad (5.5)$$

The notation $R^*(s)$ is used to symbolize the (Laplace) transform of $r^*(t)$, the sampled or impulse-modulated $r(t)$.² Notice that if the signal $r(t)$ in Eq. (5.1) is shifted a small amount then different samples will be selected by the sampling process for the output proving that sampling is not a time-invariant process. Consequently one must be very careful in using transform analysis in this context.

Having a model of the sampling operation as impulse modulation, we need to model the hold operation to complete the description of the physical sample-and-hold which will take the impulses that are produced by the mathematical sampler and produce the piecewise constant output of the device. Typical signals are sketched in Fig. 5.3.

Once the samples are taken, as represented by $r^*(t)$ in Eq. (5.1), the hold is defined as the means whereby these impulses are extrapolated to the piecewise constant signal $r_h(t)$, defined as

$$r_h(t) = r(kT) \quad kT \leq t < kT + T. \quad (5.6)$$

A general technique of data extrapolation from samples is to use a polynomial fit to the past samples. If the extrapolation is done by a constant, which is a zero-order polynomial, then the extrapolator is called a **zero-order hold**, and its transfer function is designated as $ZOH(s)$. We can compute $ZOH(s)$ as the transform of its impulse response.³ If $r^*(t) = \delta(t)$, then $r_h(t)$, which is now the

²It will be necessary, from time to time, to consider sampling a signal that is not continuous. The only case we will consider will be equivalent to applying a step function, $1(t)$, to a sampler. For the purposes of this book we will define the unit step to be continuous from the right and assume that the impulse, $\delta(t)$, picks up the full value of unity. By this convention and Eq. (5.1) we compute

$$1^*(t) = \sum_{k=0}^{\infty} \delta(t - kT), \quad (a)$$

and, using Eq. (5.2), we obtain

$$\mathcal{L}\{1^*(t)\} = 1/(1 - e^{-Ts}). \quad (b)$$

The reader should be warned that the Fourier integral converges to the *average* value of a function at a discontinuity and not the value approached from the right as we assume. Because our use of the transform theory is elementary and the convenience of equation (b) above is substantial, we have selected the continuous-from-the-right convention. In case of doubt, the discontinuous term should be separated and treated by special analysis, perhaps in the time domain.

³The hold filter in Fig. 5.3(d) will receive one unit-size impulse if the input signal is zero at every sample time except $t = 0$ and is equal to 1 there. That is, if $r(kT) = 0$, $k \neq 0$ and $r(0) = 1$.

impulse response of the *ZOH*, is a pulse of height 1 and duration T seconds. The mathematical representation of the impulse response is simply

$$p(t) = 1(t) - 1(t - T).$$

The required transfer function is the Laplace transform of $p(t)$ as

$$\begin{aligned} ZOH(s) &= \mathcal{L}\{p(t)\} \\ &= \int_0^{\infty} [1(t) - 1(t - T)]e^{-st} dt \\ &= (1 - e^{-sT})/s. \end{aligned} \quad (5.7)$$

Thus the linear behavior of an A/D converter with sample and hold can be modeled by Fig. 5.3. We must emphasize that the impulsive signal $r^*(t)$ in Fig. 5.3 is not expected to represent a physical signal in the A/D converter circuit; rather it is a hypothetical signal introduced to allow us to obtain a transfer-function model of the hold operation and to give an input-output model of the sample-and-hold suitable for transform and other linear systems analysis.

5.2 Spectrum of a Sampled Signal

We can get further insight into the process of sampling by an alternative representation of the transform of $r^*(t)$ using Fourier analysis. From Eq. (5.1) we see that $r^*(t)$ is a product of $r(t)$ and the train of impulses, $\sum \delta(t - kT)$. The latter series, being periodic, can be represented by a Fourier series

$$\sum_{k=-\infty}^{\infty} \delta(t - kT) = \sum_{n=-\infty}^{\infty} C_n e^{j(2\pi n/T)t},$$

where the Fourier coefficients, C_n , are given by the integral over one period as

$$C_n = \frac{1}{T} \int_{-T/2}^{T/2} \sum_{k=-\infty}^{\infty} \delta(t - kT) e^{-jn(2\pi t/T)} dt.$$

The only term in the sum of impulses that is in the range of the integral is the $\delta(t)$ at the origin, so the integral reduces to

$$C_n = \frac{1}{T} \int_{-T/2}^{T/2} \delta(t) e^{-jn(2\pi t/T)} dt;$$

but the sifting property from Eq. (5.2) makes this easy to integrate, with the result

$$C_n = \frac{1}{T}.$$

Thus we have derived the representation for the sum of impulses as a Fourier series

$$\sum_{k=-\infty}^{\infty} \delta(t - kT) = \frac{1}{T} \sum_{n=-\infty}^{\infty} e^{j(2\pi n/T)t}. \quad (5.8)$$

We define $\omega_s = 2\pi/T$ as the sampling frequency (in radians per second) and now substitute Eq. (5.8) into Eq. (5.1) using ω_s . We take the Laplace transform of the output of the mathematical sampler,

$$\mathcal{L}\{r^*(t)\} = \int_{-\infty}^{\infty} r(t) \left\{ \frac{1}{T} \sum_{n=-\infty}^{\infty} e^{jn\omega_s t} \right\} e^{-st} dt$$

and integrate the sum, term by term to obtain

$$R^*(s) = \frac{1}{T} \sum_{n=-\infty}^{\infty} \int_{-\infty}^{\infty} r(t) e^{jn\omega_s t} e^{-st} dt.$$

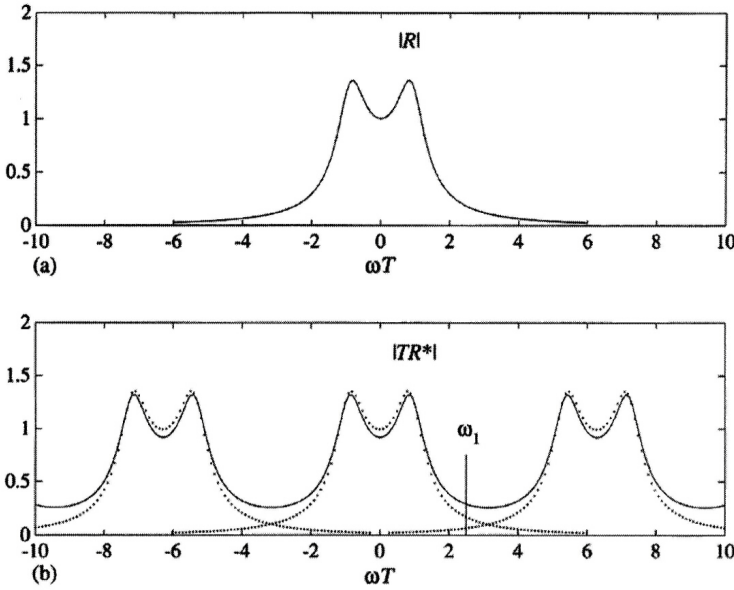


Figure 5.4
 (a) Sketch of a spectrum amplitude and
 (b) the components of the spectrum after sampling, showing aliasing

If we combine the exponentials in the integral, we get

$$R^*(s) = \frac{1}{T} \sum_{n=-\infty}^{\infty} \int_{-\infty}^{\infty} r(t) e^{-(s-jn\omega_s)t} dt.$$

The integral here is the Laplace transform of $r(t)$ with only a change of variable where the frequency goes. The result can therefore be written as

$$R^*(s) = \frac{1}{T} \sum_{n=-\infty}^{\infty} R(s - jn\omega_s), \tag{5.9}$$

where $R(s)$ is the transform of $r(t)$. In communication or radio engineering terms, Eq. (5.8) expresses the fact that the impulse train corresponds to an infinite sequence of carrier frequencies at integral values of $2\pi/T$, and Eq. (5.9) shows that when $r(t)$ modulates all these carriers, it produces a never-ending train of sidebands. A sketch of the elements in the sum given in Eq. (5.9) is shown in Fig. 5.4.

An important feature of sampling, shown in Fig. 5.4, is illustrated at the frequency marked ω_1 . Two curves are drawn representing two of the elements that enter into the sum given in Eq. (5.9). The value of the larger amplitude component located at the frequency ω_1 is the value of $R(j\omega_1)$. The smaller component shown at ω_1 comes from the spectrum centered at $2\pi/T$ and is $R(j\omega_0)$, where ω_0 is such that $\omega_0 = \omega_1 - 2\pi/T$. This signal at frequency ω_0 which produces a component at frequency ω_1 after sampling is called in the trade an “alias” of ω_1 ; the phenomenon is called **aliasing**.

aliasing

The phenomenon of aliasing has a clear meaning in time. Two continuous sinusoids of different frequencies appear at the same frequency when sampled. We cannot, therefore, distinguish between them based on their samples alone. Figure 5.5 shows a plot of a sinusoid at $\frac{1}{8}$ Hz and of a sinusoid at $\frac{7}{8}$ Hz. If we sample these waves at 1 Hz, as indicated by the dots, then we get the same sample values from both signals and would continue to get the same sample values for all time. Note that the sampling frequency is 1, and, if $f_1 = \frac{1}{8}$, then

$$f_0 = \frac{1}{8} - 1 = -\frac{7}{8}.$$

The significance of the negative frequency is that the $\frac{7}{8}$ -Hz sinusoid in Fig. 5.5 is a negative sine function.

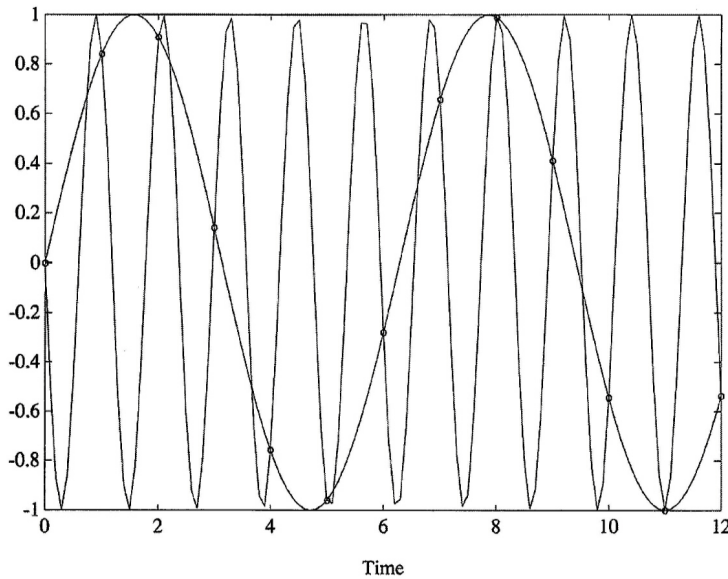


Figure 5.5
Plot of two sinusoids that have identical values at unit sampling intervals—an example of aliasing

Thus, as a direct result of the sampling operation, when data are sampled at frequency $2\pi/T$, the total harmonic content at a given frequency ω_1 is to be found not only from the original signal at ω_1 but also from all those frequencies that are aliases of ω_1 , namely, components from all frequencies $\omega_1 + n2\pi/T = \omega_1 + n\omega_s$ as shown in the formula of Eq. (5.9) and sketched in Fig. 5.4. The errors caused by aliasing can be very severe if a substantial quantity of high-frequency components is contained in the signal to be sampled. To minimize the error caused by this effect, it is standard practice to *precede* the sampling operation (such as the sample-and-hold circuit discussed earlier) by a low-pass antialias filter that will remove substantially all spectral content above the half-sampling frequency, i.e., above π/T . A sketch suggesting the result of an anti-aliasing filter is drawn in Fig. 5.6.

If all spectral content above the frequency π/T is removed, then no aliasing is introduced by sampling and the signal spectrum is not distorted, even though it is repeated endlessly, centered at $n2\pi/T$. The critical frequency, π/T , was first reported by H. Nyquist and is called the Nyquist frequency. Band-limited signals that have no components above the Nyquist frequency are represented unambiguously by their samples. A corollary to the aliasing issue is the **sampling theorem**. We have seen that if $R(j\omega)$ has components above the Nyquist frequency $\omega_s/2$ or π/T , then overlap and aliasing will occur. Conversely, we noticed that if $R(j\omega)$ is zero for $|\omega| \geq \pi/T$, then sampling at intervals of T sec. will produce no aliasing and the original spectrum can be recovered exactly from R^* , the spectrum of the samples. Once the spectrum is recovered by inverse transform, we can calculate the original signal itself. This is the sampling theorem: One can recover a signal from its samples if the sampling frequency ($\omega_s = 2\pi/T$) is *at least twice* the highest frequency (π/T) in the signal. Notice that the sampling theorem requires that $R(j\omega)$ is exactly zero for all frequencies above π/T .

A phenomenon somewhat related to aliasing is that of **hidden oscillations**. There is the possibility that a signal could contain some frequencies that the samples do not show *at all*. Such signals, when they occur in a digital control system, are called “hidden oscillations,” an example of which is shown in a design problem in Fig. 7.29. Hidden oscillations can only occur at multiples of the Nyquist frequency (π/T).

sampling theorem

hidden oscillations

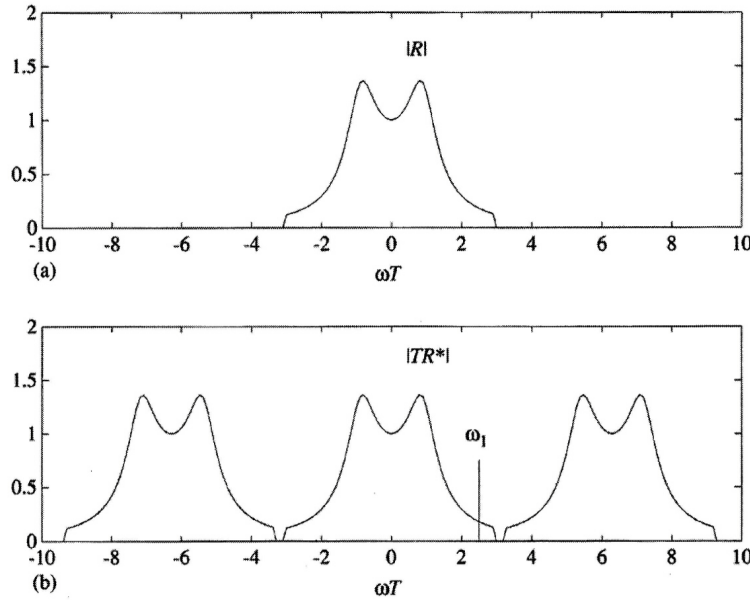


Figure 5.6
 (a) Sketch of a spectrum amplitude and
 (b) the components of the spectrum after sampling, showing removal of aliasing with an antialiasing filter

5.3 Data Extrapolation

The sampling theorem states that under the right conditions it is possible to recover a signal from its samples; we now consider a formula for doing so. From Fig. 5.6 we can see that the spectrum of $R(j\omega)$ is contained in the low-frequency part of $R^*(j\omega)$. Therefore, to recover $R(j\omega)$ we need only process $R^*(j\omega)$ through a low-pass filter and multiply by T . As a matter of fact, if $R(j\omega)$ has zero energy for frequencies in the bands above π/T (such an R is said to be band-limited), then an ideal low-pass filter with gain T for $-\pi/T \leq \omega \leq \pi/T$ and zero elsewhere would recover $R(j\omega)$ from $R^*(j\omega)$ exactly. Suppose we define this ideal low-pass filter characteristic as $L(j\omega)$. Then we have the result

$$R(j\omega) = L(j\omega)R^*(j\omega). \quad (5.10)$$

The signal $r(t)$ is the inverse transform of $R(j\omega)$, and because by Eq. (5.10) $R(j\omega)$ is the *product* of two transforms, its inverse transform $r(t)$ must be the convolution of the time functions $\ell(t)$ and $r^*(t)$. The form of the filter impulse response can be computed by using the definition of $L(j\omega)$ from which the inverse transform gives

$$\begin{aligned} \ell(t) &= \frac{1}{2\pi} \int_{-\pi/T}^{\pi/T} T e^{j\omega t} d\omega \\ &= \frac{T}{2\pi} \frac{e^{j\omega t}}{jt} \Big|_{-\pi/T}^{\pi/T} \\ &= \frac{T}{2\pi jt} (e^{j(\pi t/T)} - e^{-j(\pi t/T)}) \\ &= \frac{\sin(\pi t/T)}{\pi t/T} \\ &\triangleq \operatorname{sinc} \frac{\pi t}{T}. \end{aligned} \quad (5.11)$$

Using Eq. (5.1) for $r^*(t)$ and Eq. (5.11) for $\ell(t)$, we find that their convolution is

$$r(t) = \int_{-\infty}^{\infty} r(\tau) \sum_{k=-\infty}^{\infty} \delta(\tau - kT) \operatorname{sinc} \frac{\pi(t - \tau)}{T} d\tau.$$

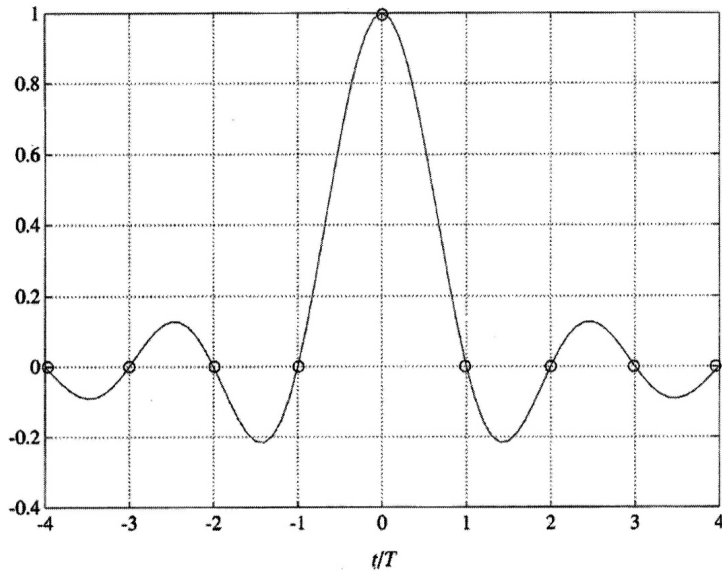


Figure 5.7
Plot of the
impulse response
of the ideal
low-pass filter

Using the sifting property of the impulse, we have

$$r(t) = \sum_{k=-\infty}^{\infty} r(kT) \operatorname{sinc} \frac{\pi(t - kT)}{T}. \quad (5.12)$$

Equation (5.12) is a constructive statement of the sampling theorem. It shows explicitly how to construct a band-limited function $r(t)$ from its samples. The sinc functions are the interpolators that fill in the time gaps between samples with a signal that has no frequencies above π/T . A plot of the impulse response of this “ideal” hold filter is drawn in Fig. 5.7 from the formula of Eq. (5.11).

There is one serious drawback to the extrapolating signal given by Eq. (5.11). Because $\ell(t)$ is the impulse response of the ideal low-pass filter $L(j\omega)$, it follows that this filter is *noncausal* because $\ell(t)$ is nonzero for $t < 0$. $\ell(t)$ starts at $t = -\infty$ while the impulse that triggers it does not occur until $t = 0$! In many communications problems the interpolated signal is not needed until well after the samples are acquired, and the noncausality can be overcome by adding a phase lag, $e^{-j\omega\lambda}$, to $L(j\omega)$, which adds a *delay* to the filter and to the signals processed through it. In feedback control systems, a large delay is usually disastrous for stability, so we avoid such approximations to this function and use something else, like the polynomial holds, of which the zero-order hold already mentioned in connection with the ADC is the most elementary and the most common.

In Section 5.2 we introduced the zero-order hold as a model for the storage register in an A/D converter that maintains a constant signal value between samples. We showed in Eq. (5.7) that it has the transfer function

$$\operatorname{ZOH}(j\omega) = \frac{1 - e^{-j\omega T}}{j\omega}. \quad (5.13)$$

We can discover the frequency properties of $\operatorname{ZOH}(j\omega)$ by expressing Eq. (5.13) in magnitude and phase form. To do this, we factor out $e^{-j\omega T/2}$ and multiply and divide by $2j$ to write the transfer function in the form

$$\operatorname{ZOH}(j\omega) = e^{-j\omega T/2} \left\{ \frac{e^{j\omega T/2} - e^{-j\omega T/2}}{2j} \right\} \frac{2j}{j\omega}.$$

The term in brackets is recognized as the sine, so this can be written

$$\operatorname{ZOH}(j\omega) = T e^{-j\omega T/2} \frac{\sin(\omega T/2)}{\omega T/2}$$

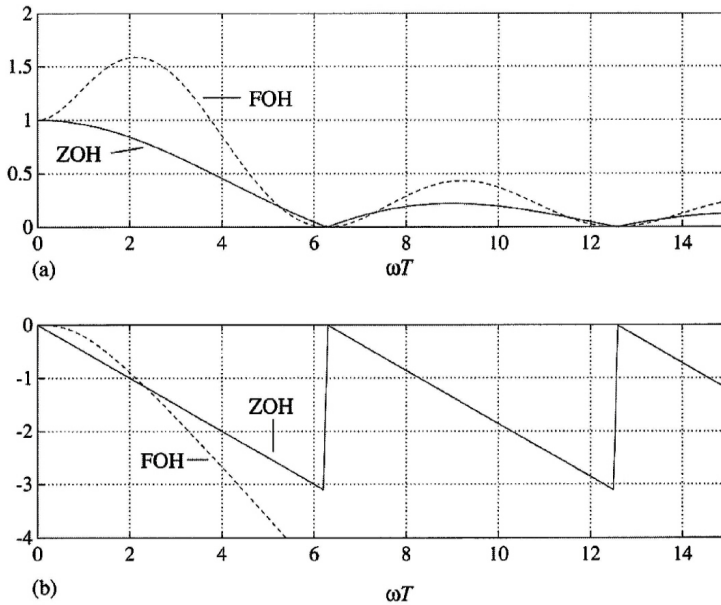


Figure 5.8
(a) Magnitude and (b) phase of polynomial hold filters

and, using the definition of the sinc function,

$$ZOH(j\omega) = e^{-j\omega T/2} T \operatorname{sinc}(\omega T/2). \quad (5.14)$$

Thus the effect of the zero-order hold is to introduce a phase shift of $\omega T/2$, which corresponds to a time delay of $T/2$ seconds, and to multiply the gain by a function with the magnitude of $\operatorname{sinc}(\omega T/2)$. A plot of the magnitude is shown in Fig. 5.8, which illustrates the fact that although the zero-order hold is a low-pass filter, it has a cut-off frequency well beyond the Nyquist frequency. The magnitude function is

$$|ZOH(j\omega)| = T \left| \operatorname{sinc} \frac{\omega T}{2} \right|, \quad (5.15)$$

which slowly gets smaller as ω gets larger until it is zero for the first time at $\omega = \omega_s = 2\pi/T$. The phase is

$$\angle ZOH(j\omega) = \frac{-\omega T}{2}, \quad (5.16)$$

plus the 180° shifts where the sinc function changes sign.

We can now give a complete analysis of the sample-and-hold circuit of Fig. 5.3(d) for a sinusoidal input $r(t)$ in both the time and the frequency domains. We consider first the time domain, which is simpler, being just an exercise in construction. For purposes of illustration, we will use $r(t) = 3 \sin(50t + \pi/6)$ as plotted in Fig. 5.9. If we sample $r(t)$ at the instants kT where the sampling frequency is $\omega_s = 2\pi/T = 200\pi$ and $T = 0.01$, then the plot of the resulting $r_h(kT)$ is as shown in Fig. 5.9. Notice that although the input is a single sinusoid, the output is clearly *not* sinusoidal. Thus it is not possible to describe this system by a transfer function, because the fundamental property of linear, time-invariant systems is that a sinusoid input produces an output that is a sinusoid of the same frequency and the relative amplitudes and phases determine the transfer function. The sample-and-hold system is linear but time varying. In the frequency domain, it is clear that the output $r_h(t)$ contains more than one frequency, and a complete analysis requires that we compute the amplitudes and phases of them all. However, in the application to control systems, the output of the hold will typically be applied to a dynamical system that is of low-pass character; thus the most important component in $r_h(t)$ is the fundamental harmonic, at $\omega_o = 50$ rad/sec in this case. The other harmonics are *impostors*, appearing as part of the output signal when they are really unwanted consequences of the sample-and-hold process. In any event, we can proceed to analyze $r_h(t)$ for all its harmonics and select out the fundamental component, either by analysis or by a low-pass smoothing filter.

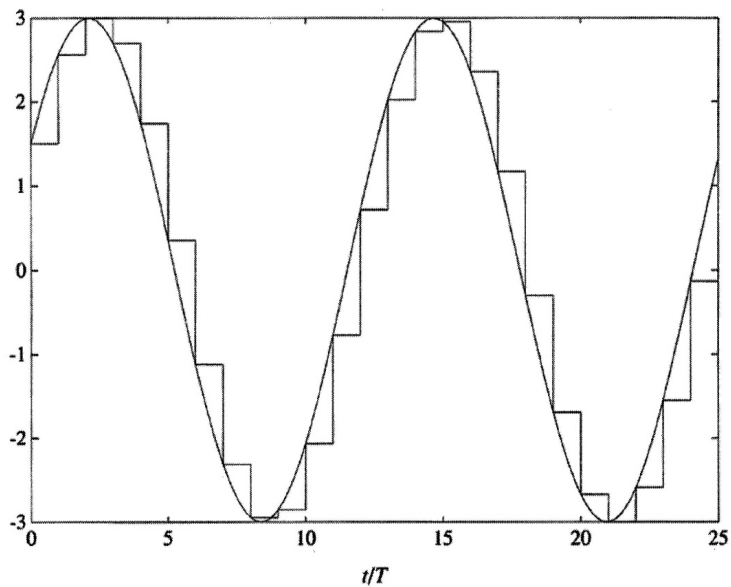


Figure 5.9
 Plot of $3 \sin(50t + \pi/6)$ and the output of a sample-and-hold with sample period $T = 0.01$

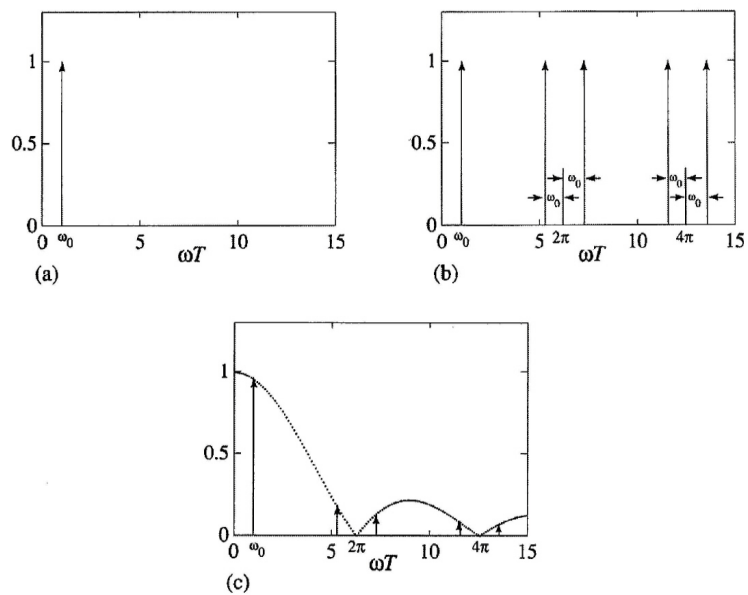


Figure 5.10
 Plot of the spectra of (a) R ; (b) R^* ; and (c) R_h

First, we need the spectrum of $r(t)$. Because a sinusoid can be decomposed into two exponentials, the spectrum of $r(t) = A \cos(\omega_o t + \phi)$ is given by two impulse functions at ω_o and $-\omega_o$ of intensity πA and phase ϕ and $-\phi$ as⁴

$$R(j\omega) = \pi A [e^{j\phi} \delta(\omega - \omega_o) + e^{-j\phi} \delta(\omega + \omega_o)].$$

A sketch of this spectrum is shown in Fig 5.10(a) for $A = 1/\pi$. We represent the impulses by arrows whose heights are proportional to the intensities of the impulses.

After sampling, as we saw in Eq. (5.9), the spectrum of R^* is directly derived from that of R as the sum of multiple copies of that of R shifted by $n2\pi/T$ for all integers n and multiplied by $1/T$. A plot of the result normalized by T is shown in Fig. 5.10(b). Finally, to find the spectrum of R_h , we need only multiply the spectrum of R^* by the transfer function $ZOH(j\omega)$, which is

$$ZOH(j\omega) = T e^{-j\omega T/2} \text{sinc}(\omega T/2).$$

Thus the spectrum of R_h is also a sum of an infinite number of terms, but now with intensities modified by the sinc function and phases shifted by the delay function $\omega T/2$. These intensities are plotted in Fig. 5.10(c). Naturally, when all the harmonics included in R_h are converted to their time functions and added, they sum to the piecewise-constant staircase function plotted earlier in Fig. 5.9.

If we want a best approximation to r_h using only one sinusoid, we need only take out the first or fundamental harmonic from the components of R^* . This component has phase shift ϕ and amplitude $A \text{sinc}(\omega T/2)$. In the time domain, the corresponding sinusoid is given by

$$v_1(t) = A [\text{sinc}(\omega T/2)] \sin[\omega_o(t - \frac{T}{2})]. \quad (5.17)$$

A plot of this approximation for the signal from Fig 5.9 is given in Fig. 5.11 along with both the original input and the sampled-and-held output to show the nature of the approximation. In control design, we can frequently achieve a satisfactory design for a sampled-data system by approximating the sample and hold with a continuous transfer function corresponding to the delay of $T/2$. The controller design is then done in the continuous domain but is implemented by computing a discrete equivalent. More discussion of this technique, sometimes called *emulation*, will be given in Chapter 6, where some examples illustrate the results.

5.4 Block-Diagram Analysis of Sampled-Data Systems

We have thus far talked mainly about discrete, continuous, and sampled signals. To analyze a feedback system that contains a digital computer, we need to be able to compute the transforms of output signals of systems that contain sampling operations in various places, including feedback loops, in the block diagram. The technique for doing this is a simple extension of the ideas of block-diagram analysis of systems that are all continuous or all discrete, but one or two rules need to be carefully observed to assure success. First, we should review the facts of sampled-signal analysis.

We represent the process of sampling a continuous signal and holding it by impulse modulation followed by low-pass filtering. For example, the system of Fig. 5.12 leads to

$$\begin{aligned} E(s) &= R^*(s)H(s), \\ U(s) &= E^*(s)G(s). \end{aligned} \quad (5.18)$$

Impulse modulation of continuous-time signals like $e(t)$ and $u(t)$ produces a series of sidebands as given in Eq. (5.9) and plotted in Fig. 5.4, which result in periodic functions of frequency. If the transform of the signal to be sampled is a product of a transform that is already periodic of period $2\pi/T$, and one that is not, as in $U(s) = E^*(s)G(s)$, where $E^*(s)$ is periodic and $G(s)$ is not, we

⁴See the appendix to this chapter for details.

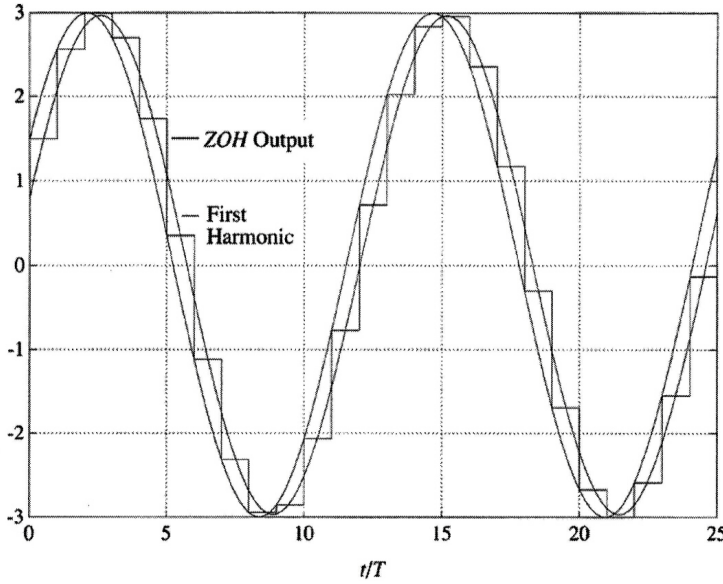


Figure 5.11
Plot of the output of the sample and hold and the first harmonic approximation

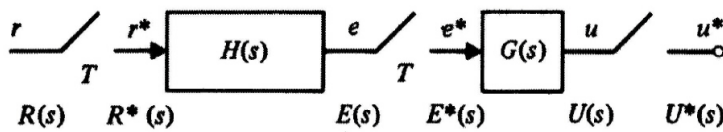


Figure 5.12
A cascade of samplers and filters

can show that $E^*(s)$ comes out as a factor of the result. This is the most important relation for the block-diagram analysis of sampled-data systems, namely⁵

$$U^*(s) = (E^*(s)G(s))^* = E^*(s)G^*(s). \quad (5.19)$$

We can prove Eq. (5.19) either in the frequency domain, using Eq. (5.9), or in the time domain, using Eq. (5.1) and convolution. We will use Eq. (5.9) here. If $U(s) = E^*(s)G(s)$, then by definition we have

$$U^*(s) = \frac{1}{T} \sum_{n=-\infty}^{\infty} E^*(s - jn\omega_s)G(s - jn\omega_s); \quad (5.20)$$

but $E^*(s)$ is

$$E^*(s) = \frac{1}{T} \sum_{k=-\infty}^{\infty} E(s - jk\omega_s),$$

so that

$$E^*(s - jn\omega_s) = \frac{1}{T} \sum_{k=-\infty}^{\infty} E(s - jk\omega_s - jn\omega_s). \quad (5.21)$$

Now in Eq. (5.21) we can let $k = \ell - n$ to get

$$\begin{aligned} E^*(s - jn\omega_s) &= \frac{1}{T} \sum_{\ell=-\infty}^{\infty} E(s - j\ell\omega_s) \\ &= E^*(s). \end{aligned} \quad (5.22)$$

⁵We of course assume the existence of $U^*(s)$, which is assured if $G(s)$ tends to zero as s tends to infinity at least as fast as $1/s$. We must be careful to avoid impulse modulation of impulses, for $\delta(t)\delta(t)$ is undefined.

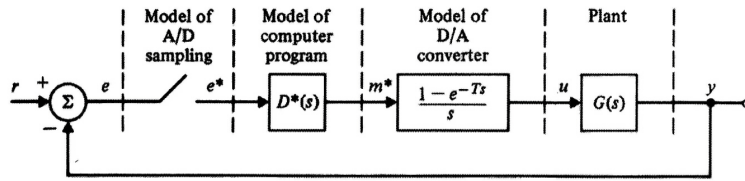


Figure 5.13
Block diagram of digital control as a sampled-data system

In other words, because E^* is already periodic, shifting it an integral number of periods leaves it unchanged. Substituting Eq. (5.22) into Eq. (5.20) yields

$$\begin{aligned} U^*(s) &= E^*(s) \frac{1}{T} \sum_{-\infty}^{\infty} G(s - jn\omega_s) \\ &= E^*(s)G^*(s). \quad \text{QED} \end{aligned} \quad (5.23)$$

Note especially what is *not* true. If $U(s) = E(s)G(s)$, then $U^*(s) \neq E^*(s)G^*(s)$ but rather $U^*(s) = (EG)^*(s)$. The periodic character of E^* in Eq. (5.19) is crucial.

The final result we require is that, given a sampled-signal transform such as $U^*(s)$, we can find the corresponding z -transform simply by letting $e^{sT} = z$ or

$$U(z) = U^*(s) \big|_{e^{sT}=z}. \quad (5.24)$$

There is an important time-domain reflection of Eq. (5.24). The inverse Laplace transform of $U^*(s)$ is the sequence of *impulses* with intensities given by $u(kT)$; the inverse z -transform of $U(z)$ is the sequence of values $u(kT)$. Conceptually, sequences of values and the corresponding z -transforms are easy to think about as being processed by a computer program, whereas the model of sampling as a sequence of impulses is what allows us to analyze a discrete system embedded in a continuous world (see Fig. 5.13). Of course, the impulse modulator must *always* be eventually followed by a low-pass circuit (hold circuit) in the physical world. Note that Eq. (5.24) can also be used in the other direction to obtain $U^*(s)$, the Laplace transform of the train of impulses, from a given $U(z)$.

Block Diagram Analysis

Example 5.1

Compute the transforms of Y^* and Y for the system block diagram of Fig. 5.13.

Solution. In Fig. 5.13 we have modeled the A/D converter plus computer program plus D/A converter as an impulse modulator [which takes the samples from $e(t)$], a computer program that processes these samples described by $D^*(s)$, and a zero-order hold that constructs the piecewise-constant output of the D/A converter from the impulses of m^* . In the actual computer we assume that the samples of $e(t)$ are manipulated by a difference equation whose input-output effect is described by the z -transform $D(z)$. These operations are represented in Fig. 5.13 *as if* they were performed on impulses, and hence the transfer function is $D^*(s)$ according to Eq. (5.24). Finally, the manipulated impulses, $m^*(t)$, are applied to the zero-order hold from which the piecewise-constant-control signal $u(t)$ comes. In reality, of course, the computer operates on the sample values of $e(t)$ and the piecewise-constant output is generated via a storage register and a D/A converter. The impulses provide us with a convenient, consistent, and effective model of the processes to which Laplace-transform methods can be applied. From the results given thus far, we can write relations among Laplace transforms as

$$\begin{aligned} E(s) &= R - Y, & (a) \\ M^*(s) &= E^*D^*, & (b) \\ U &= M^* \left[\frac{1 - e^{-Ts}}{s} \right], & (c) \\ Y &= GU. & (d) \end{aligned} \quad (5.25)$$

The usual idea is to relate the discrete output, Y^* , to the discrete input, R^* . Suppose we sample each of these

equations by using the results of Eq. (5.19) to “star” each transform. The equations are ⁶

$$\begin{aligned} E^* &= R^* - Y^*, & (a) \\ M^* &= E^* D^*, & (b) \\ U^* &= M^*, & (c) \\ Y^* &= [GU]^*. & (d) \end{aligned} \quad (5.26)$$

Now Eq. (5.26(d)) indicates that we need U , not U^* , to compute Y^* , so we must back up to substitute Eq. (5.25(c)) into Eq. (5.26(d)):

$$Y^* = \left[GM^* \left(\frac{1 - e^{-Ts}}{s} \right) \right]^*. \quad (5.27)$$

Taking out the periodic parts, which are those in which s appears only as e^{sT} [which include $M^*(s)$], we have

$$Y^* = (1 - e^{-Ts}) M^* \left(\frac{G}{s} \right)^*. \quad (5.28)$$

Substituting from Eq. (5.26(b)) for M^* gives

$$Y^* = (1 - e^{-Ts}) E^* D^* (G/s)^*. \quad (5.29)$$

And substituting Eq. (5.26(a)) for E^* yields

$$Y^* = (1 - e^{-Ts}) D^* (G/s)^* [R^* - Y^*]. \quad (5.30)$$

If we call

$$(1 - e^{-Ts}) D^* (G/s)^* = H^*, \quad (5.31)$$

then we can solve Eq. (5.30) for Y^* , obtaining

$$Y^* = \frac{H^*}{1 + H^*} R^*. \quad (5.32)$$

Analysis of a Specific Block Diagram

Example 5.2

Apply the results of Example 1 to compute Y^* and Y for the case where

$$G(s) = \frac{a}{s+a}, \quad (5.33)$$

and the sampling period T is such that $e^{-aT} = \frac{1}{2}$. The computer program corresponds to a discrete integrator

$$u(kT) = u(kT - T) + K_0 e(kT), \quad (5.34)$$

and the computer D/A holds the output constant so that the zero-order hold is the correct model.

Solution. We wish to compute the components of H^* given in Eq. (5.31). For the computer program we have the transfer function of Eq. (5.34), which in terms of z is

$$D(z) = \frac{U(z)}{E(z)} = \frac{K_0}{1 - z^{-1}} = \frac{K_0 z}{z - 1}.$$

Using Eq. (5.24), we get the Laplace-transform form

$$D^*(s) = \frac{K_0 e^{sT}}{e^{sT} - 1}. \quad (5.35)$$

⁶In sampling Eq. (5.25(c)) we obtain Eq. (5.26(c)) by use of the continuous-from-the-right convention for Eq. (5.5) for impulse modulation of discontinuous functions. From the time-domain operation of the zero-order hold, it is clear that the samples of u and m are the same, and then from this Eq. (5.26(c)) follows.

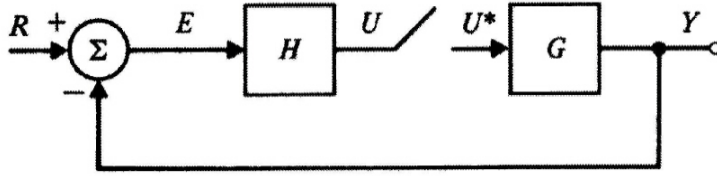


Figure 5.14
A simple system that does not have a transfer function

For the plant and zero-order-hold we require

$$\begin{aligned} (1 - e^{-Ts})(G(s)/s)^* &= (1 - e^{-Ts}) \left(\frac{a}{s(s+a)} \right)^* \\ &= (1 - e^{-Ts}) \left(\frac{1}{s} - \frac{1}{s+a} \right)^* . \end{aligned}$$

Using Eq. (5.5), we have

$$(1 - e^{-Ts})(G(s)/s)^* = (1 - e^{-Ts}) \left(\frac{1}{1 - e^{-Ts}} - \frac{1}{1 - e^{-aT} e^{-Ts}} \right) .$$

Because $e^{-aT} = \frac{1}{2}$, this reduces to

$$\begin{aligned} (1 - e^{-Ts})(G(s)/s)^* &= \frac{(1/2)e^{-Ts}}{1 - (1/2)e^{-Ts}} \\ &= \frac{1/2}{e^{Ts} - 1/2} . \end{aligned} \quad (5.36)$$

Combining Eq. (5.36) and Eq. (5.35) then, in this case, we obtain

$$H^*(s) = \frac{K_0}{2} \frac{e^{sT}}{(e^{sT} - 1)(e^{sT} - 1/2)} . \quad (5.37)$$

Equation (5.37) can now be used in Eq. (5.32) to find the closed-loop transfer function from which the dynamic and static responses can be studied, as a function of K_0 , the program gain. We note also that beginning with Eq. (5.25), we can readily calculate that

$$Y(s) = R^* \frac{D^*}{1 + H^*} \frac{(1 - e^{-Ts})}{s} G(s) . \quad (5.38)$$

Equation (5.38) shows how to compute the response of this system in between sampling instants. For a given $r(t)$, the starred terms in Eq. (5.38) and the $(1 - e^{-Ts})$ -term correspond to a train of impulses whose individual values can be computed by expanding in powers of e^{-Ts} . These impulses are applied to $G(s)/s$, which is the step response of the plant. Thus, between sampling instants, we will see segments of the plant step response.

With the exception of the odd-looking forward transfer function, Eq. (5.32) looks like the familiar feedback formula: forward-over-one-plus-feedback. Unfortunately, the sequence of equations by which Eq. (5.32) was computed was a bit haphazard, and such an effort might not always succeed. Another example will further illustrate the problem.

Another Block Diagram Analysis

Example 5.3

Compute Y^* and Y for the block diagram of Fig. 5.14.

Solution. The equations describing the system are (all symbols are Laplace transforms)

$$\begin{aligned} E &= R - Y, (a) \\ U &= HE, (b) \\ Y &= U^*G; (c) \end{aligned} \quad (5.39)$$

and after sampling, the equations are

$$\begin{aligned} E^* &= R^* - Y^*, (a) \\ U^* &= (HE)^*, (b) \\ Y^* &= U^*G^*. (c) \end{aligned} \quad (5.40)$$

How do we solve these? In Eq. (5.40(b)) we need E , not E^* . So we must go back to Eq. (5.39(a))

$$\begin{aligned} U^* &= (H(R - Y))^* \\ &= (HR)^* - (HY)^*. \end{aligned}$$

Using Eq. (5.39(c)) for Y , we have

$$U^* = (HR)^* - (HU^*G)^*.$$

Taking out the periodic U^* in the second term on the right gives

$$U^* = (HR)^* - U^*(HG)^*.$$

Solving, we get

$$U^* = \frac{(HR)^*}{1 + (HG)^*}. \quad (5.41)$$

From Eq. (5.40(c)), we can solve for Y^*

$$Y^* = \frac{(HR)^*}{1 + (HG)^*} G^*. \quad (5.42)$$

Equation (5.42) displays a curious fact. The transform of the input is bound up with $H(s)$ and *cannot* be divided out to give a transfer function! This system displays an important fact that with the manipulations of stars for sampling might be overlooked: A sampled-data system is *time varying*. The response depends on the time *relative to the sampling instants* at which the signal is applied. Only when the input samples *alone* are required to generate the output samples can we obtain a discrete transfer function. The time variation occurs on the taking of samples. In general, as in Fig. 5.14, the entire input signal $r(t)$ is involved in the system response, and the transfer-function concept fails. Even in the absence of a transfer function, however, the techniques developed here permit study of stability and response to specific inputs such as step, ramp, or sinusoidal signals.

We need to know the general rules of block-diagram analysis. In solving Fig. 5.14 we found ourselves working with U , the signal that was sampled. This is in fact the key to the problem. Given a block diagram with several samplers, *always select the variables at the inputs to the samplers as the unknowns*. Being sampled, these variables have periodic transforms that will always factor out after the sampling process and result in a set of equations in the sampled (starred) variables that can be solved.

Another Block Diagram Analysis

Example 5.4

Compute the transforms of Y^* and Y for the block diagram drawn in Fig. 5.15.

Solution. We select E and M as independent variables and write

$$\begin{aligned} E(s) &= R - M^*G_2, \\ M(s) &= E^*HG_1. \end{aligned} \quad (5.43)$$

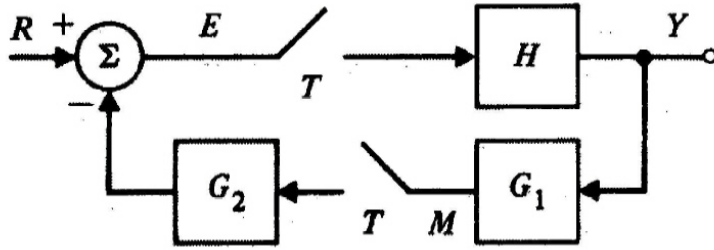


Figure 5.15
A final example for transfer-function analysis of sampled-data systems

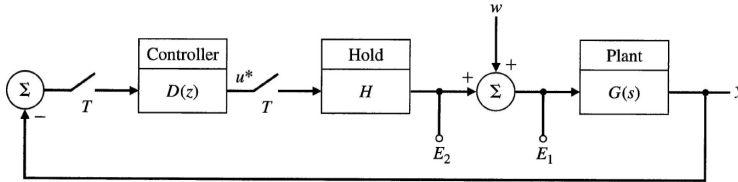


Figure 5.16
A block diagram for experimental measurement of a sampled-data transfer function

Next we sample these signals, and use the “if periodic, then out” rule from Eq. (5.19):

$$\begin{aligned} E^* &= R^* - M^* G_2^* \\ M^* &= E^* (HG_1)^* \end{aligned} \tag{5.44}$$

We solve these equations by substituting for M^* in Eq. (5.44) from Eq. (5.43)

$$\begin{aligned} E^* &= R^* - E^* (HG_1)^* G_2^* \\ &= \frac{R^*}{1 + (HG_1)^* G_2^*} \end{aligned} \tag{5.45}$$

To obtain Y we use the equation

$$\begin{aligned} Y &= E^* H \\ &= \frac{R^* H}{1 + (HG_1)^* G_2^*} \end{aligned} \tag{5.46}$$

and

$$Y^* = \frac{R^* H^*}{1 + (HG_1)^* G_2^*} \tag{5.47}$$

In this case we have a transfer function. Why? Because only the samples of the external input are used to cause the output. To obtain the z -transform of the samples of the output, we would let $e^{sT} = z$ in Eq. (5.47). From Eq. (5.46) we can solve for the continuous output, which consists of impulses applied to $H(s)$ in this case.

As a final example of analysis of sampled-data systems we consider a problem of experimental transfer function measurement in a sampled-data system.

Measuring the Transfer Function of a Sampled-Data System

Example 5.5

It has been proposed to use an experiment to measure the loop gain of a trial sampled-data design on the actual physical system using the setup of Figure 5.16. The proposal is to have zero reference input but to inject a sinusoid into the system at W and to measure the responses at that frequency at locations E_1 and E_2 . It is thought that the (complex) ratio of these signals will give the loop gain from which the gain and phase margins can be determined and with which a frequency response design can be worked out.

1. Compute the transforms of E_1 and E_2 for a general signal input at w .

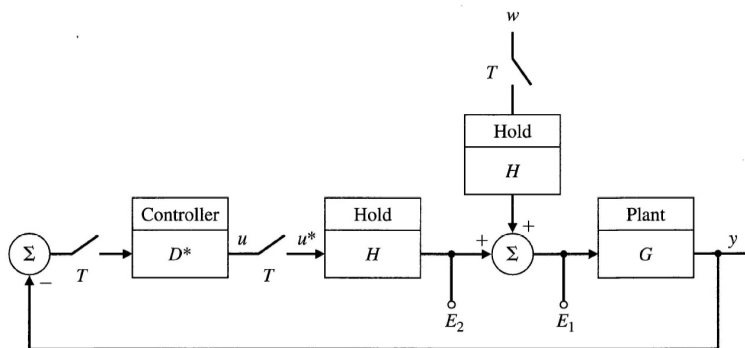


Figure 5.17
A block diagram for experimental measurement of a sampled-data transfer function with sampled input

2. Suppose that the signal w is a sinusoid of frequency ω_0 less than π/T (no aliasing). Plot the spectra of GW and $(GW)^*$ and show that $(GW)^* = \frac{1}{T}GW$ at the frequency ω_0 .
3. Use the results of 2) to get an expression for the complex ratio of the signals E_1 and E_2 when $\omega_0 < \pi/T$.
4. Repeat these calculations for the setup of Fig. 5.17 where the input signal is first sampled and held before being applied to the system.

Solution.

1. Following the procedure just given, we express the signals of interest in terms of sampled signals as follows

$$E_1 = W + U^*H \tag{5.48}$$

$$E_2 = U^*H \tag{5.49}$$

$$Y = WG + U^*HG \tag{5.50}$$

$$Y^* = (WG)^* + U^*(HG)^* \tag{5.51}$$

$$U^* = -D^*Y^* \tag{5.52}$$

Solving Eq. (5.52) for U^*

$$U^*(s) = -\frac{D^*(WG)^*}{1 + D^*(HG)^*} \tag{5.53}$$

If we now substitute this result into Eq. (5.48) and Eq. (5.49) we have the solution of this part as

$$\begin{aligned} E_1 &= W - \frac{D^*(WG)^*}{1 + D^*(HG)^*} H \\ E_2 &= -\frac{D^*(WG)^*}{1 + D^*(HG)^*} H \end{aligned} \quad (5.54)$$

Clearly we do not have a transfer function since the transform of the signal is imbedded in the signal transforms.

2. For the second part, we can consider the sinusoid one exponential at a time and consider $w = 2\pi\delta(\omega - \omega_0)$. Then

$$(GW)^* = \frac{1}{T} \sum_{k=-\infty}^{k=\infty} G(j\omega - jk\frac{2\pi}{T}) 2\pi\delta(\omega - \omega_0 - \frac{2\pi k}{T}).$$

The spectra involved are easily sketched. Since $\omega_0 < \pi/T$ there is no overlap and at ω_0 the signal is

$$\begin{aligned} (GW)^* &= \frac{1}{T} G(j\omega_0) 2\pi\delta(\omega - \omega_0) \\ &= \frac{1}{T} GW|_{\omega_0}. \end{aligned} \quad (5.55)$$

3. If we substitute Eq. (5.55) into Eq. (5.54) and take the ratio, we find the describing function

$$\frac{E_2}{E_1} = -\frac{\frac{1}{T} D^* GH}{1 + D^*(GH)^* - \frac{1}{T} D^* GH} \quad (5.56)$$

Notice that if $|G| = 0$ for $|\omega| > \pi/T$ so that $G^* = G$ for frequencies less than π/T , then Eq. (5.56) reduces to

$$\frac{E_2}{E_1} = -D^*(GH)^*,$$

which is the transfer function. Thus the proposed method works well if there is a good antialias filter in the loop.

4. With the input applied through a sample and hold as drawn in Fig. 5.17 the key expressions are given by

$$\begin{aligned} E_1 &= U^*H + W^*H \\ E_2 &= U^*H \\ U^* &= -D^*Y^* \\ Y &= U^*HG + W^*HG. \end{aligned} \quad (5.57)$$

These equations can be readily solved, after taking the “star” of Y to give

$$\begin{aligned} E_1 &= \frac{W^*H}{1 + D^*(HG)^*} \\ E_2 &= -\frac{D^*(HG)^*}{1 + D^*(HG)^*} W^*H. \end{aligned}$$

From these, the ratio gives the true discrete transfer function

$$\frac{E_2}{E_1} = -D^*(HG)^*.$$

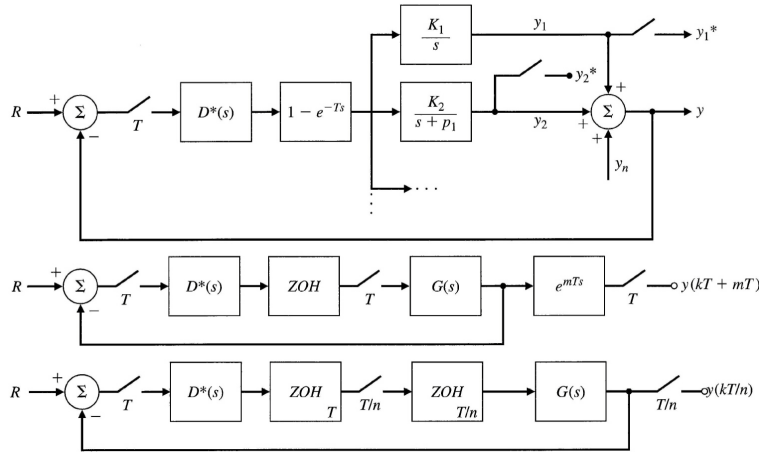


Figure 5.18
Three methods used to evaluate ripple. (Top) Partial fraction expansion; (Middle) Modified z-transform; (Bottom) Multi-rate sampling

5.5 Calculating the System Output Between Samples: The Ripple

In response to a particular input, the output of a sampled-data system at sampling instants can be computed by the z-transform, even in those cases where there is no transfer function. However, in many problems it is important to examine the response between sampling instants, a response that is called the “ripple” in the response. Often, for example, the maximum overshoot will not occur at a sampling instant but at some intermediate point. In other cases, hidden oscillations are present, oscillations that may or may not decay with time. The ripple is generated by the continuous-time part of the system at the output. For example, in the case drawn in Fig. 5.13, the ripple is given by the response of $G(s)/s$ between sampling instants. Three techniques have been suggested to compute ripple. The first, suggested by J. Sklansky, is based on the partial-fraction expansion of $G(s)/s$. The second, suggested by E. Jury, is based on introducing a time shift in the sampler at the output of the system. If this shift is less than a sample period, the new samples are taken between the system samples. The modified transform from input samples to shifted samples is called the *modified z-transform* of $G(s)/s$. The third technique, introduced by G. Kranc, is based on sampling the output at a faster rate than the feedback loop is updated. Block diagrams representing the three methods are given in Fig. 5.18.

In the partial-fraction method, shown in Fig. 5.18(a), the outputs of the several fractions are sampled and the values of $y_1(kT), y_2(kT), \dots$ are computed in the regular way with z-transforms or MATLAB statements. These values at the instant kT represent initial conditions for the several partial fraction continuous dynamics at time kT and from them the transient over the period from kT to $(k + 1)T$ can be computed. The total system output is the sum of these components. The method is somewhat tedious but gives an exact expression for the ripple during any given sample period from which, for example, the peak overshoot can be exactly computed.

The modified z-transform of the plant with zero-order hold is defined as

$$G(z, m) = (1 - z^{-1}) \mathcal{Z} \left\{ \frac{G(s)}{s} e^{mTs} \right\} \quad 0 \leq m < 1,$$

and represents samples taken at the times $kT + mT$. The modified transform of the output of the system shown in Fig. 5.18(b) is given by

$$Y(z, m) = \frac{D(z)G(z, m)}{1 + D(z)G(z)} R(z), \tag{5.58}$$

and its inverse will give samples at $kT + mT$. The modified operation is noncausal but is only being used as a computational device to obtain inter-sample ripple. For example, if $m = 0.5$ then use of

Eq. (5.58) will find sample values halfway between sample updates of the control. MATLAB only permits delays (causal models) and can be used to find the output of the modified plant delayed by one sample shown in the figure as $z^{-1}Y(z, m)$. If the plant is given in state form with description matrices $[F, G, H, J]$, then the representation of the delayed modified transform can be computed in MATLAB using

```
sys=ss(F,G,H,J)
```

The delay for sample period T and shift m is set by the command

```
set(sys, 'OutputDelay', (1-m)*T)
```

and finally, the discrete representation of the system which has a delayed modified z -transform is given by the standard conversion

```
sysd=c2d(sys,T)
```

The method of multi-rate sampling is shown in Fig. 5.18(c). The output of the controller is held for the full T seconds but this signal is again sampled at the rate T/n for some small n , such as 5. The plant output is also sampled at the rate T/n . The feedback loop is unchanged by these additional samplers but the output ripple is now available at n points in between the regular sample times. This technique is readily programmed in MATLAB and is regularly used in this book to compute the ripple. An interesting case is given in Fig. 7.14 where it can be seen that the maximum overshoot occurs in the ripple.

5.6 Summary

In this chapter we have considered the analysis of mixed systems that are partly discrete and partly continuous, taking the continuous point of view. These systems arise from digital control systems that include A/D and D/A converters. The important points of the chapter are

- The large-signal behavior of an A/D converter can be modeled as a linear impulse modulator followed by a zero-order-hold.
- D/A converter can be modeled as a zero-order-hold.
- The transform of a sampled signal is periodic with period $2\pi/T$ for sample period T .
- Sampling introduces aliasing, which may be interpreted in both the frequency and the time domains.
- The sampling theorem shows how a band-limited signal can be reconstructed from its samples.
- Interconnections of systems that include sampling can be analyzed by block-diagram analysis.
- If the input signal to a sampled-data system is not sampled, it is impossible to define a transfer function.
- The output of a sampled-data system between sampling instants can be computed using partial fraction expansion, using the modified z -transform, or by multi-rate sampling. With a computer, multi-rate sampling is the most practical method.

5.7 Problems

- 5.1 Sketch a signal that represents bounded hidden oscillations.
- 5.2 Show how to construct a signal of hidden oscillations that grows in an unstable fashion. Where in the s -plane are the poles of the transforms of your signal(s)?

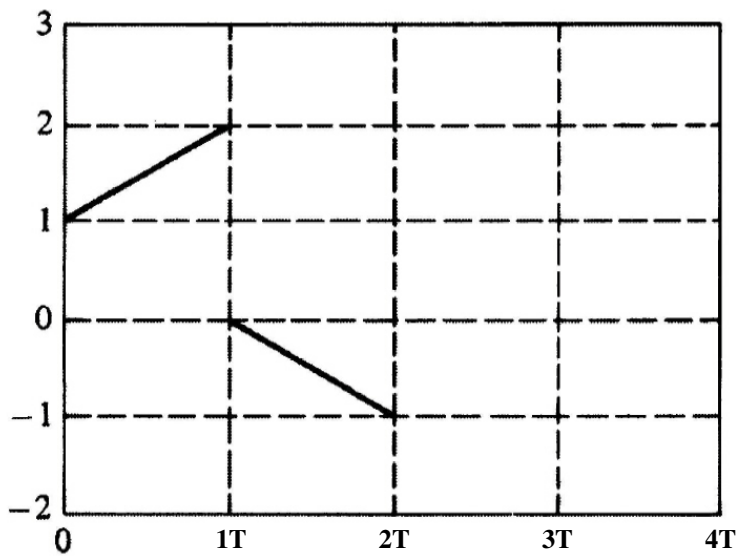


Figure 5.19
Impulse response
of a first-order
hold filter

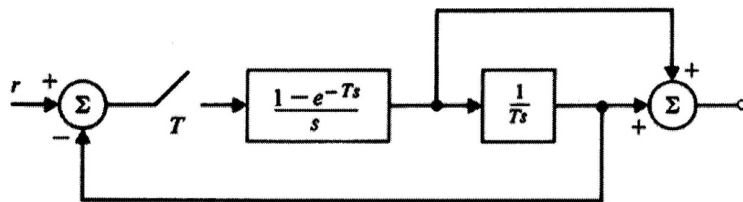


Figure 5.20
Block diagram of
a sample and
first-order hold

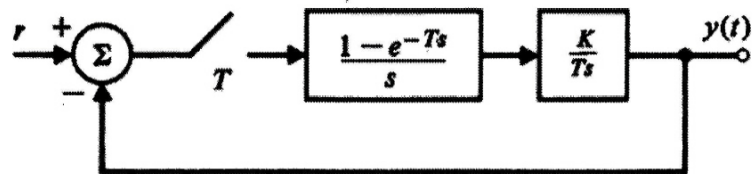


Figure 5.21
A sampled-data
system

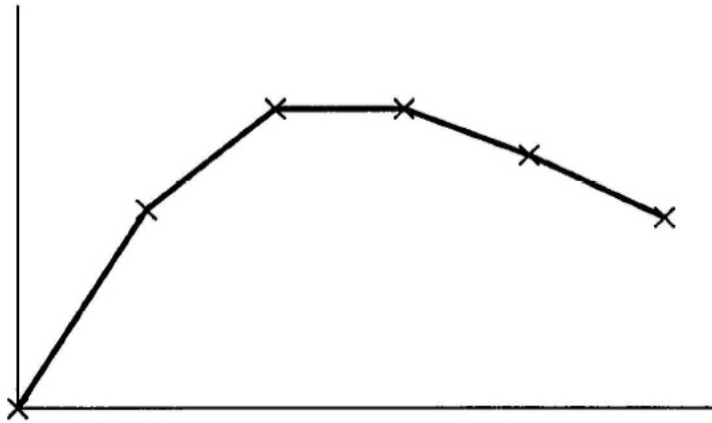


Figure 5.22
Response of a
sample and
triangle hold

- 5.3 A first-order hold is a device that extrapolates a line over the interval from kT to $(k+1)T$ with slope given by the samples $r(kT - T)$ and $r(kT)$ starting from $r(kT)$ as shown in Fig. 5.19. Compute the frequency response of the first-order hold.
- 5.4 Consider the circuit of Fig. 5.20. By plotting the response to a signal that is zero for all sample instants except $t = 0$ and that is 1.0 at $t = 0$, show that this circuit implements a first-order hold.
- 5.5 Sketch the step response $y(t)$ of the system shown in Fig. 5.21 for $K = \frac{1}{2}$, 1, and 2.
- 5.6 Sketch the response of a *second-order* hold circuit to a step unit. What might be the major disadvantage of this data extrapolator?
- 5.7 A triangle hold is a device that has an output, as sketched in Fig. 5.22 that connects the samples of an input with straight lines.
- Sketch the impulse response of the triangle hold. Notice that it is noncausal.
 - Compute the transfer function of the hold.
 - Use MATLAB to plot the frequency response of the triangle hold.
 - How would the frequency response be changed if the triangle hold is made to be causal by adding a delay of one sample period?
- 5.8 Sketch the output of a sample and zero-order hold to
- A step input.
 - A ramp input.
 - A sinusoid of frequency $\omega_s/10$.
- 5.9 Sketch the output of a sample and first-order hold to
- A step input.
 - A ramp input.
 - A sinusoid of frequency $\omega_s/10$.
- 5.10 Sketch the output of a sample and triangle hold to
- A step input.
 - A ramp input.

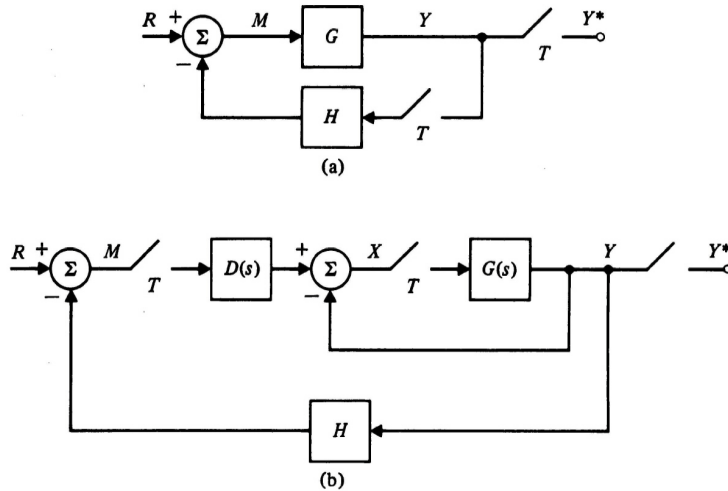


Figure 5.23
Block diagrams
of sampled data
systems.
(a) Single loop;
(b) multiple loop

(c) A sinusoid of frequency $\omega_s/10$.

5.11 Sketch the output of a sample and *causal* triangle hold to

- (a) A step input.
- (b) A ramp input.
- (c) A sinusoid of frequency $\omega_s/10$.

5.12 A sinusoid of frequency 11 rad/sec. is sampled at the frequency $\omega_s = 5 \text{ rad/sec}$.

- (a) Indicate the component frequencies up to $\omega = 20 \text{ rad/sec}$.
- (b) Indicate the relative amplitudes of the components up to 20 rad/sec . if the sampler is followed by a zero-hold.

5.13 A signal $r(t) = \sin(2t) + \sin(15t)$ is sampled at the frequency $\omega_s = 16$.

- (a) Indicate the frequency of the components in the sampled signal up to $\omega = 32$.
- (b) Indicate the relative amplitudes of the signals in the output if the signal is passed through the anti-aliasing filter with transfer function $\frac{1}{(\frac{s}{8}+1)^2}$ before sampling. You can use MATLAB to compute the filter gain.

5.14 Derive Eq. (5.38).

5.15 Find the transform of the output $Y(s)$ and its samples $Y^*(s)$ for the block diagrams shown in Fig. 5.23. Indicate whether a transfer function exists in each case.

5.16 Assume the following transfer functions are preceded by a sampler and zero-order hold and followed by a sampler. Compute the resulting discrete transfer functions.

- (a) $G_1(s) = 1/s^2$
- (b) $G_2(s) = e^{-1.5s}/(s+1)$
- (c) $G_3(s) = 1/s(s+1)$
- (d) $G_4(s) = e^{-1.5s}/s(s+1)$
- (e) $G_5(s) = 1/(s^2-1)$

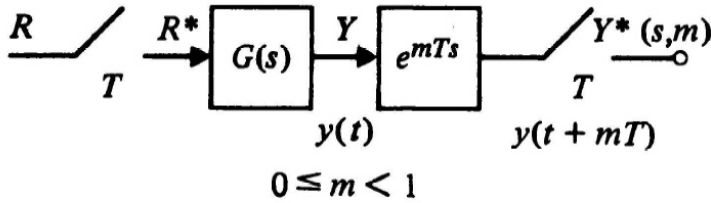


Figure 5.24
Block diagrams
showing the
modified
z-transform

5.17 One technique for examining the response of a sampled data system between sampling instants is to shift the response a fraction of a period to the left and to sample the result. The effect is as shown in the block diagram of Fig. 5.24 and described by the equation

$$Y^*(s, m) = R^*(s) \{G(s)e^{mTs}\}^*.$$

As a function of z , the equivalent equation is

$$Y(z) = R(z)G(z, m).$$

The function $G(z, m)$ is called the modified z -transform of $G(s)$. In the figure, let

$$G(s) = \frac{1}{(s+1)}, \quad R(s) = \frac{1}{s}, \quad \text{and} \quad T = 1.$$

- (a) Compute $y(t)$ by calculating $y(kT)$ from the ordinary z -transform and observing that between samples, the output $y(t)$ is an exponential decay with unit time constant. Sketch the response for five sample intervals. Notice that this technique is the essence of the partial-fraction method of obtaining the ripple.
- (b) Compute the modified z -transform for $m = \frac{1}{2}$ and compute the samples according to the equation for $Y(z, m)$. Plot these on the same plot as that of $y(t)$ and verify that you have found the values at the mid-points of the sampling pattern.

5.8 Appendix

To compute the transform of a sinusoid, we consider first the Fourier transform of $v(t) = e^{j\omega_0 t + j\phi}$. For this we have

$$V(j\omega) = \int_{-\infty}^{\infty} e^{(j\omega_0 t + j\phi)} e^{-j\omega t} dt. \quad (5.59)$$

This integral does not converge in any obvious way, but we can approach it from the back door, as it were. Consider again the impulse, $\delta(t)$. The direct transform of this object is easy, considering the sifting property, as follows

$$\int_{-\infty}^{\infty} \delta(t) e^{-j\omega t} dt = 1.$$

Now the general form of the inverse Fourier transform is given by

$$f(t) = \frac{1}{2\pi} \int_{-\infty}^{\infty} F(j\omega) e^{j\omega t} d\omega.$$

If we apply the inverse transform integral to the impulse and its transform, we take $f(t) = \delta(t)$ and $F(j\omega) = 1$ with the result

$$\delta(t) = \frac{1}{2\pi} \int_{-\infty}^{\infty} e^{j\omega t} d\omega.$$

However, except for notation and a simple change of variables, this is exactly the integral we needed to evaluate the spectrum of the single exponential. If we exchange t with ω the integral reads

$$\delta(\omega) = \frac{1}{2\pi} \int_{-\infty}^{\infty} e^{j\omega t} dt.$$

Eq. (5.59) is of this form

$$\begin{aligned} V(j\omega) &= \int_{-\infty}^{\infty} e^{(j\omega_o t + j\phi)} e^{-j\omega t} dt \\ &= e^{j\phi} \int_{-\infty}^{\infty} e^{jt(\omega_o - \omega)} dt \\ &= 2\pi e^{j\phi} \delta(\omega - \omega_o). \end{aligned}$$

At the last step in this development, the sign of the argument in the delta function was changed, which is legal because $\delta(t)$ is an even function and $\delta(t) = \delta(-t)$. The argument is more natural as $(\omega - \omega_o)$ rather than the opposite.

Chapter 6

Discrete Equivalents

A Perspective on Computing Discrete Equivalents

One of the exciting fields of application of digital systems¹ is in signal processing and digital filtering. A filter is a device designed to pass desirable signal components and to reject undesirable ones; in signal processing it is common to represent signals as a sum of sinusoids and to define the “desirable components” as those signals whose frequencies are in a specified band. Thus a radio receiver is designed to pass the band of frequencies transmitted by the station we want to hear and reject all others. We would call a filter which does this a **bandpass filter**. In electrocardiography it often happens that power-line frequency signals are strong and unwanted, so a filter is designed to pass signals between 1 and 500 Hz but to eliminate those at 60 Hz. The magnitude of the transfer function for this purpose may look like Fig. 6.1 on a log-frequency scale, where the amplitude response between 59.5 and 60.5 Hz might reach 10^{-3} . Here we have a band-reject filter with a 60-dB rejection ratio in a 1-Hz band centered at 60 Hz.

In long-distance telephony some filters play a conceptually different role. There the issue is that ideal transmission requires that all desired frequencies be treated equally but transmission media—wires or microwaves—introduce distortion in the amplitude and phase of the sinusoids that comprise the desired signal and this distortion must be removed. Filters to correct the distortion are called **equalizers**. Finally, the dynamic response of control systems requires modification in order for the complete system to have satisfactory dynamic response. We call the devices that make these changes **compensators**.

Whatever the name—filter, equalizer, or compensator—many fields have use for linear dynamic systems having a transfer function with specified characteristics of amplitude and phase. Increasingly the power and flexibility of digital processors makes it attractive to perform these functions by digital means. The design of continuous electronic filters is a well-established subject that includes not only very sophisticated techniques but also well-tested computer programs to carry out

¹Including microprocessors and special-purpose devices for digital signal processing, called DSP chips.

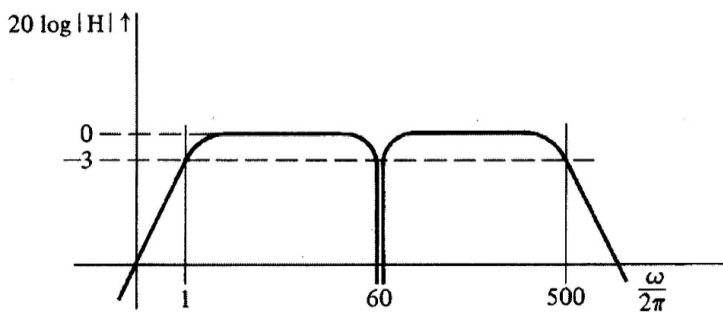


Figure 6.1
Magnitude of a low-frequency bandpass filter with a narrow rejection band

the designs [Van Valkenburg (1982)]. Consequently, an important approach to digital filter design is to start with a good analog design and construct a filter having a discrete frequency response that approximates that of the satisfactory design. For digital control systems we have much the same motivation: Continuous-control designs are well established and one can take advantage of a good continuous design by finding a discrete equivalent to the continuous compensator. This method of design is called **emulation**. Although much of our presentation in this book is oriented toward direct digital design and away from emulation of continuous designs with digital equivalents, it is important to understand the techniques of discrete equivalents both for purposes of comparison and because it is widely used by practicing engineers.

Chapter Overview

The specific problem of this chapter is to find a discrete transfer function that will have approximately the same characteristics over the frequency range of importance as a given transfer function, $H(s)$. Three approaches to this task are presented. The first method is based on *numerical integration* of the differential equations that describe the given design. While there are many techniques for numerical integration, only simple formulas based on rectangular and trapezoid rules are presented. The second approach is based on comparisons of the s and z domains. Note that the natural response of a continuous filter with a pole at some point $s = s_o$ will, when sampled with period T , represent the response of a discrete filter with a pole at $z = e^{s_o T}$. This formula can be used to map the poles and zeros of the given design into poles and zeros of an approximating discrete filter. This is called *pole and zero mapping*. The third and final approach is based on taking the samples of the input signal, extrapolating between samples to form an approximation to the signal, and passing this approximation through the given filter transfer function. This technique is called *hold equivalence*. The methods are compared with respect to the quality of the approximation in the frequency domain as well as the ease of computation of the designs.

6.1 Design of Discrete Equivalents via Numerical Integration

The topic of numerical integration of differential equations is quite complex, and only the most elementary techniques are presented here. For example, we only consider formulas of low complexity and fixed step-size. The fundamental concept is to represent the given filter transfer function $H(s)$ as a differential equation and to derive a difference equation whose solution is an approximation of the differential equation. For example, the system

$$\frac{U(s)}{E(s)} = H(s) = \frac{a}{s+a} \quad (6.1)$$

is equivalent to the differential equation

$$\dot{u} + au = ae. \quad (6.2)$$

Now, if we write Eq. (6.2) in integral form, we have a development much like that described in Chapter 4, except that the integral is more complex here

$$\begin{aligned} u(t) &= \int_0^t [-au(\tau) + ae(\tau)] d\tau, \\ u(kT) &= \int_0^{kT-T} [-au + ae] d\tau + \int_{kT-T}^{kT} [-au + ae] d\tau \\ &= u(kT - T) + \left\{ \begin{array}{l} \text{area of } -au + ae \\ \text{over } kT - T \leq \tau < kT. \end{array} \right. \end{aligned} \quad (6.3)$$

Many rules have been developed based on how the incremental area term is approximated. Three possibilities are sketched in Fig. 6.2. The first approximation leads to the **forward rectangular**

rule² wherein we approximate the area by the rectangle looking forward from $kT - T$ and take the amplitude of the rectangle to be the value of the integrand at $kT - T$. The width of the rectangle is T . The result is an equation in the first approximation, u_1

$$\begin{aligned} u_1(kT) &= u_1(kT - T) + T[-au_1(kT - T) + ae(kT - T)] \\ &= (1 - aT)u_1(kT - T) + aTe(kT - T). \end{aligned} \quad (6.4)$$

The transfer function corresponding to the forward rectangular rule in this case is

$$\begin{aligned} H_F(z) &= \frac{aTz^{-1}}{1 - (1 - aT)z^{-1}} \\ &= \frac{a}{(z - 1)/T + a} \quad (\text{forward rectangular rule}). \end{aligned} \quad (6.5)$$

A second rule follows from taking the amplitude of the approximating rectangle to be the value looking *backward* from kT toward $kT - T$, namely, $-au(kT) + ae(kT)$. The equation for u_2 , the second approximation,³ is

$$\begin{aligned} u_2(kT) &= u_2(kT - T) + T[-au_2(kT) + ae(kT)] \\ &= \frac{u_2(kT - T)}{1 + aT} + \frac{aT}{1 + aT}e(kT). \end{aligned} \quad (6.6)$$

Again we take the z -transform and compute the transfer function of the **backward rectangular rule**

$$\begin{aligned} H_B(z) &= \frac{aT}{1 + aT} \frac{1}{1 - z^{-1}/(1 + aT)} = \frac{aTz}{z(1 + aT) - 1} \\ &= \frac{a}{(z - 1)/Tz + a} \quad (\text{backward rectangular rule}). \end{aligned} \quad (6.7)$$

Our final version of integration rules is the **trapezoid rule** found by taking the area approximated in Eq. (6.3) to be that of the trapezoid formed by the average of the previously selected rectangles. The approximating difference equation is

$$\begin{aligned} u_3(kT) &= u_3(kT - T) + \frac{T}{2}[-au_3(kT - T) \\ &\quad + ae(kT - T) - au_3(kT) + ae(kT)] \\ &= \frac{1 - (aT/2)}{1 + (aT/2)}u_3(kT - T) + \frac{aT/2}{1 + (aT/2)}[e_3(kT - T) + e_3(kT)]. \end{aligned} \quad (6.8)$$

The corresponding transfer function from the trapezoid rule is

$$\begin{aligned} H_T(z) &= \frac{aT(z + 1)}{(2 + aT)z + aT - 2} \\ &= \frac{a}{(2/T)\{(z - 1)/(z + 1)\} + a} \quad (\text{trapezoid rule}). \end{aligned} \quad (6.9)$$

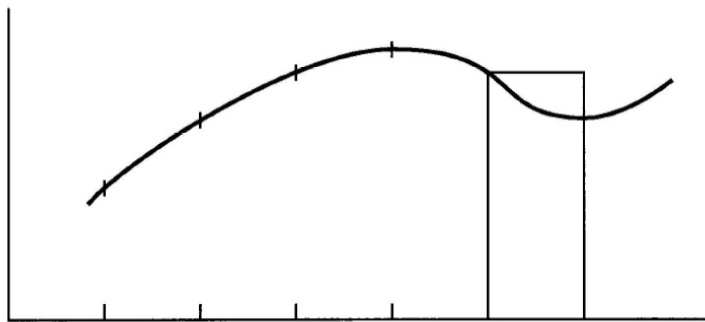
Suppose we tabulate our results obtained thus far.

$H(s)$	Method	Transfer function
$\frac{a}{s + a}$	Forward rule	$H_F = \frac{a}{(z - 1)/T + a}$
$\frac{a}{s + a}$	Backward rule	$H_B = \frac{a}{(z - 1)/Tz + a}$
$\frac{a}{s + a}$	Trapezoid rule	$H = \frac{a}{(2/T)\{(z - 1)/(z + 1)\} + a}$

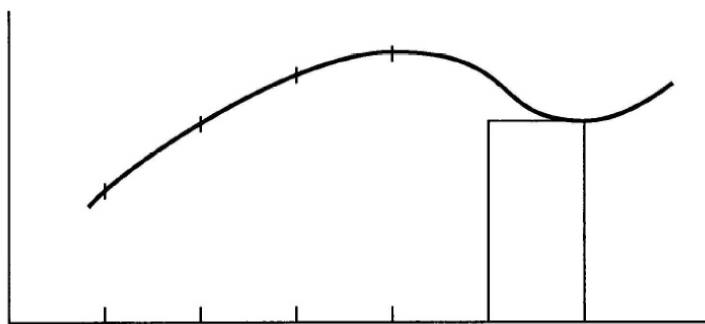
(6.10)

²Also known as *Euler's rule*.

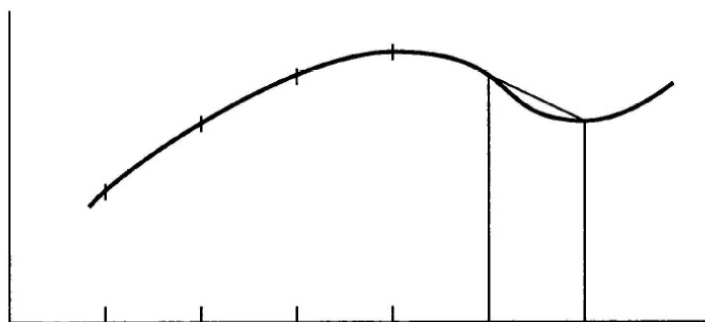
³It is worth noting that in order to solve for Eq. (6.6) we had to eliminate $u(kT)$ from the right-hand side where it entered from the integrand. Had Eq. (6.2) been nonlinear, the result would have been an implicit equation requiring an iterative solution. This topic is the subject of predictor-corrector rules, which are beyond our scope of interest. A discussion is found in most books on numerical analysis. See Golub and Van Loan (1983).



(a) Forward Rectangular Rule



(b) Backward Rectangular Rule



(c) Trapezoid Rule

Figure 6.2

Sketches of three ways the area under the curve from kT to $kT + T$ can be approximated: (a) forward rectangular rule, (b) backward rectangular rule, (c) trapezoid rule

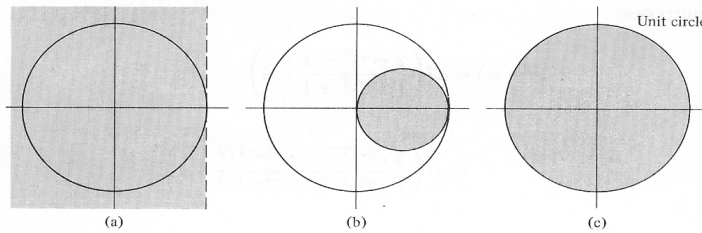


Figure 6.3 Maps of the left-half of the s -plane by the integration rules of Eq. (6.10) into the z -plane. Stable s -plane poles map into the shaded regions in the z -plane. The unit circle is shown for reference.
 (a) Forward rectangular rule.
 (b) Backward rectangular rule.
 (c) Trapezoid or bilinear rule

From direct comparison of $H(s)$ with the three approximations in this tabulation, we can see that the effect of each of our methods is to present a discrete transfer function that can be obtained from the given Laplace transfer function $H(s)$ by substitution of an approximation for the frequency variable as shown below

Method	Approximation	
Forward rule	$s \leftarrow \frac{z-1}{T}$	(6.11)
Backward Rule	$s \leftarrow \frac{z-1}{Tz}$	
Trapezoid Rule	$s \leftarrow \frac{2}{T} \frac{z-1}{z+1}$	

The trapezoid-rule substitution is also known, especially in digital and sampled-data control circles, as **Tustin’s method** [Tustin (1947)] after the British engineer whose work on nonlinear circuits stimulated a great deal of interest in this approach. The transformation is also called the **bilinear transformation** from consideration of its mathematical form. The design method can be summarized by stating the rule: Given a continuous transfer function (filter), $H(s)$, a discrete equivalent can be found by the substitution

$$H_T(z) = H(s) \Big|_{s=\frac{2}{T} \frac{z-1}{z+1}} \tag{6.12}$$

Each of the approximations given in Eq. (6.11) can be viewed as a map from the s -plane to the z -plane. A further understanding of the maps can be obtained by considering them graphically. For example, because the $(s = j\omega)$ -axis is the boundary between poles of stable systems and poles of unstable systems, it would be interesting to know how the $j\omega$ -axis is mapped by the three rules and where the left (stable) half of the s -plane appears in the z -plane. For this purpose we must solve the relations in Eq. (6.11) for z in terms of s . We find

$$\begin{aligned} \text{i) } z &= 1 + Ts, && \text{(forward rectangular rule).} \\ \text{ii) } z &= \frac{1}{1 - Ts}, && \text{(backward rectangular rule).} \\ \text{iii) } z &= \frac{1 + Ts/2}{1 - Ts/2}, && \text{(bilinear rule).} \end{aligned} \tag{6.13}$$

If we let $s = j\omega$ in these equations, we obtain the boundaries of the regions in the z -plane which originate from the stable portion of the s -plane. The shaded areas sketched in the z -plane in Fig. 6.3 are these stable regions for each case. To show that rule (ii) results in a circle, $\frac{1}{2}$ is added to and subtracted from the right-hand side to yield

$$\begin{aligned} z &= \frac{1}{2} + \left\{ \frac{1}{1 - Ts} - \frac{1}{2} \right\} \\ &= \frac{1}{2} - \frac{1}{2} \frac{1 + Ts}{1 - Ts}. \end{aligned} \tag{6.14}$$

Now it is easy to see that with $s = j\omega$, the magnitude of $z - \frac{1}{2}$ is constant

$$\left| z - \frac{1}{2} \right| = \frac{1}{2},$$

and the curve is thus a circle as drawn in Fig. 6.3(b). Because the unit circle is the stability boundary in the z -plane, it is apparent from Fig. 6.3 that the forward rectangular rule could cause a stable continuous filter to be mapped into an unstable digital filter.

It is especially interesting to notice that the bilinear rule maps the stable region of the s -plane exactly into the stable region of the z -plane although the entire $j\omega$ -axis of the s -plane is compressed into the 2π -length of the unit circle! Obviously a great deal of distortion takes place in the mapping in spite of the congruence of the stability regions. As our final rule deriving from numerical integration ideas, we discuss a formula that extends Tustin's rule one step in an attempt to correct for the inevitable distortion of real frequencies mapped by the rule. We begin with our elementary transfer function Eq. (6.1) and consider the bilinear rule approximation

$$H_T(z) = \frac{a}{(2/T)[(z-1)/(z+1)] + a}.$$

The original $H(s)$ had a pole at $s = -a$, and for real frequencies, $s = j\omega$, the magnitude of $H(j\omega)$ is given by

$$\begin{aligned} |H(j\omega)|^2 &= \frac{a^2}{\omega^2 + a^2} \\ &= \frac{1}{\omega^2/a^2 + 1}. \end{aligned}$$

Thus our reference filter has a half-power point, $|H|^2 = \frac{1}{2}$, at $\omega = a$. It will be interesting to know where $H_T(z)$ has a half-power point.

As we saw in Chapter 4, signals with poles on the imaginary axis in the s -plane (sinusoids) map into signals on the unit circle of the z -plane. A sinusoid of frequency ω_1 corresponds to $z_1 = e^{j\omega_1 T}$, and the response of $H_T(z)$ to a sinusoid of frequency ω_1 is $H_T(z_1)$. We consider now Eq. (6.8) for $H_T(z_1)$ and manipulate it into a more convenient form for our present purposes

$$\begin{aligned} H_T(z_1) &= a / \left(\frac{2}{T} \frac{e^{j\omega_1 T} - 1}{e^{j\omega_1 T} + 1} + a \right) \\ &= a / \left(\frac{2}{T} \frac{e^{j\omega_1 T/2} - e^{-j\omega_1 T/2}}{e^{j\omega_1 T/2} + e^{-j\omega_1 T/2}} + a \right) \\ &= a / \left(\frac{2}{T} j \tan \frac{\omega_1 T}{2} + a \right). \end{aligned} \quad (6.15)$$

The magnitude squared of H_T will be $\frac{1}{2}$ when

$$\frac{2}{T} \tan \frac{\omega_1 T}{2} = a$$

or

$$\tan \frac{\omega_1 T}{2} = \frac{aT}{2}. \quad (6.16)$$

Equation (6.16) is a measure of the frequency distortion or warping caused by Tustin's rule. Whereas we wanted to have a half-power point at $\omega = a$, we realized a half-power point at $\omega_1 = (2/T) \tan^{-1}(aT/2)$. ω_1 will be approximately correct only if $aT/2 \ll 1$ so that $\tan^{-1}(aT/2) \cong aT/2$, that is, if $\omega_s (= 2\pi/T) \gg a$ and the sample rate is much faster than the half-power frequency. We can turn our intentions around and suppose that we really want the half-power point to be at ω_1 . Equation (6.16) can be made into an equation of prewarping: If we select a according to Eq. (6.16), then, using Tustin's bilinear rule for the design, the half-power point will be at ω_1 . A statement of a complete set of rules for filter design via bilinear transformation with prewarping is

1. Write the desired filter characteristic with transform variable s and critical frequency ω_1 in the form $H(s/\omega_1)$.⁴
2. Replace ω_1 by a such that

$$a = \frac{2}{T} \tan \frac{\omega_1 T}{2},$$

and in place of $H(s/\omega_1)$, consider the prewarped function $H(s/a)$. For more complicated shapes, such as bandpass filters, the specification frequencies, such as band edges and center frequency, should be prewarped before the continuous design is done; and then the bilinear transformation will bring all these points to their correct frequencies in the digital filter.

3. Substitute

$$s = \frac{2}{T} \frac{z-1}{z+1}$$

in $H(s/a)$ to obtain the prewarped equivalent $H_p(z)$.

As a frequency substitution the result can be expressed as

$$H_p(z) = H\left(\frac{s}{\omega_1}\right) \Big|_{\frac{s}{\omega_1} = \frac{1}{\tan(\omega_1 T/2)} \frac{z-1}{z+1}}. \quad (6.17)$$

It is clear from Eq. (6.17) that when $\omega = \omega_1$, $H_p(z_1) = H(j1)$ and the discrete filter has exactly the same transmission at ω_1 as the continuous filter has at this frequency. This is the consequence of prewarping. We also note that as the sampling period gets small, $H_p(z)$ approaches $H(j\omega/\omega_1)$.

Computing a Discrete Equivalent

Example 6.1

The transfer function of a third order low-pass Butterworth filter⁵ designed to have unity pass bandwidth ($\omega_p = 1$) is

$$H(s) = \frac{1}{s^3 + 2s^2 + 2s + 1}.$$

A simple frequency scaling would of course translate the design to have any desired passband frequency. Compute the discrete equivalents and plot the frequency responses using the forward rectangular rule, the backward rectangular rule, the Tustin bilinear rule and the bilinear rule with prewarping at $\omega = 1$. Use sampling periods $T = 0.1$, $T = 1$, and $T = 2$.

Solution. Computation of the discrete equivalents is numerically tedious and the state-space algorithms described below were used in MATLAB to generate the transfer functions and the response curves plotted in Fig. 6.4. Fig 6.4(a) shows that at a high sample rate ($T = 0.1$), where the ratio of sampling frequency to passband frequency is $\omega_s/\omega_p \approx 63$, all the rules do reasonably well but the rectangular rules are already showing some deviation. From Fig. 6.4(b) we see that at $\omega_s/\omega_p = 2\pi$ the rectangular rules are useless (the forward rule is unstable). Finally, in Fig. 6.4(c) at very slow sampling frequency with $\omega_s/\omega_p = \pi$ corresponding to a sampling period of $T = 2$ sec, only with prewarping do we have a design that comes even close to the continuous response. In each case at the Nyquist frequency, $\omega = \pi/T$, the magnitude responses of the discrete filters start to repeat according to the periodic nature of discrete-transfer-function frequency responses. It can be seen that the magnitude and phase of the prewarped designs match those of the continuous filter exactly at the band edge, $\omega = 1$, for all these cases. This is no surprise, because such matching was the whole idea of prewarping.

The formulas for discrete equivalents are particularly simple and convenient when expressed in state-variable form and used with a computer-aided design package. For example, suppose we have

⁴The critical frequency need not be the band edge. We can use the band center of a bandpass filter or the crossover frequency of a Bode plot compensator. However, we must have $\omega_1 < \pi/T$ if a stable filter is to remain stable after warping.

⁵A description of the properties of Butterworth filters is given in most books on filter design and briefly in Franklin, Powell and Emami-Naeini (2019).

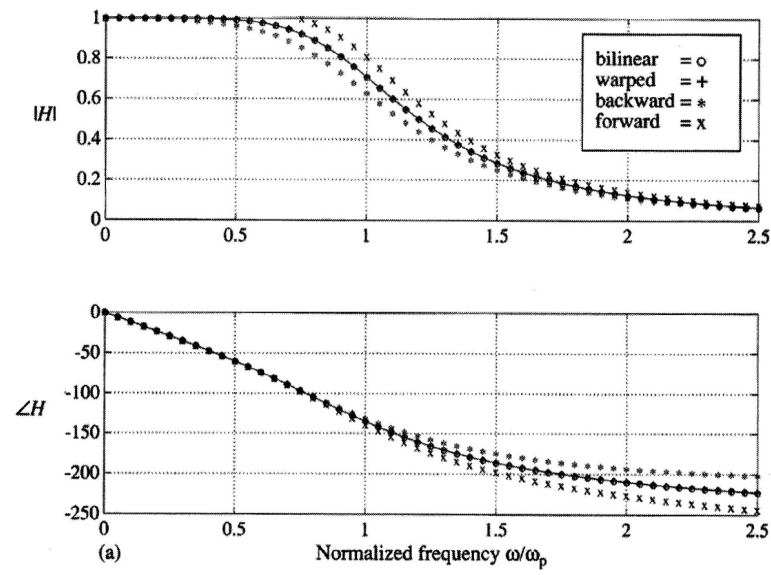
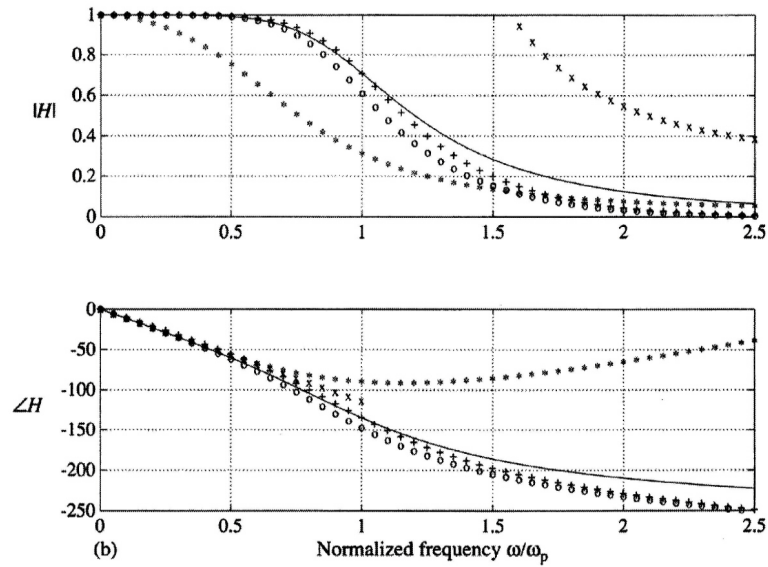
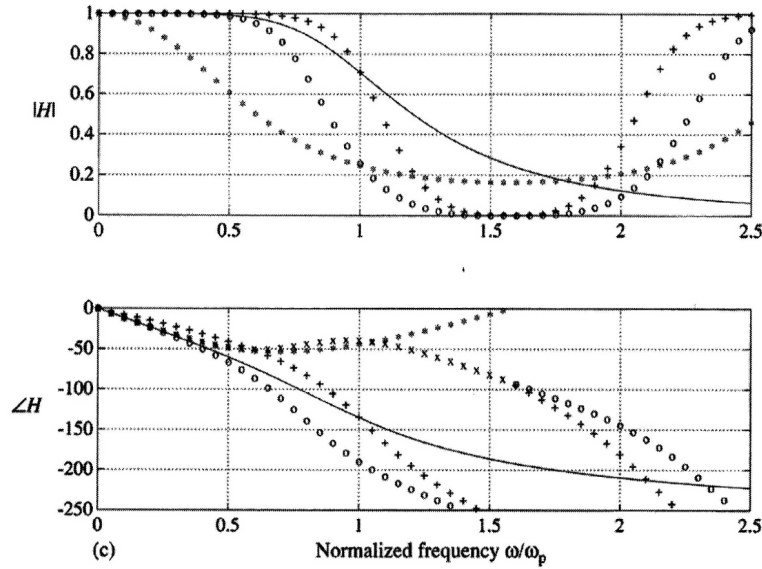


Figure 6.4

(a) Response of third-order lowpass filter and digital equivalents for $\omega_s/\omega_p = 20\pi$.
 (b) Response of third-order lowpass filter and digital equivalents for $\omega_s/\omega_p = 2\pi$.
 (c) Response of third-order lowpass filter and digital equivalents for $\omega_s/\omega_p = \pi$





a vector-matrix description of a continuous design in the form of the equations

$$\begin{aligned}\dot{\mathbf{x}} &= \mathbf{A}\mathbf{x} + \mathbf{B}e, \\ u &= \mathbf{C}\mathbf{x} + \mathbf{D}e.\end{aligned}\quad (6.18)$$

The Laplace transform of this equation is

$$\begin{aligned}s\mathbf{X} &= \mathbf{A}\mathbf{X} + \mathbf{B}E, \\ U &= \mathbf{C}\mathbf{X} + \mathbf{D}E.\end{aligned}\quad (6.19)$$

We can now substitute for s in Eq. (6.19) any of the forms in z corresponding to an integration rule. For example, the forward rectangular rule is to replace s with $(z-1)/T$ from Eq. (6.11)

$$\begin{aligned}\frac{z-1}{T}\mathbf{X} &= \mathbf{A}\mathbf{X} + \mathbf{B}E, \\ U &= \mathbf{C}\mathbf{X} + \mathbf{D}E.\end{aligned}\quad (6.20)$$

In the time domain, the operator z corresponds to forward shift; that is, $zx(k) = x(k+1)$. Thus the corresponding discrete equations in the time domain are

$$\begin{aligned}\mathbf{x}(k+1) - \mathbf{x}(k) &= T\mathbf{A}\mathbf{x}(k) + T\mathbf{B}e(k), \\ \mathbf{x}(k+1) &= (\mathbf{I} + T\mathbf{A})\mathbf{x}(k) + T\mathbf{B}e(k), \\ u &= \mathbf{C}\mathbf{x} + \mathbf{D}e.\end{aligned}\quad (6.21)$$

Equation (6.21) is a state-space formula for the forward rule equivalent.

For the backward rule, substitute $s \leftarrow (z-1)/zT$ with the result

$$\frac{z-1}{Tz}\mathbf{X} = \mathbf{A}\mathbf{X} + \mathbf{B}E,$$

which corresponds to the time domain equations

$$\mathbf{x}(k+1) - \mathbf{x}(k) = T\mathbf{A}\mathbf{x}(k+1) + T\mathbf{B}e(k+1).\quad (6.22)$$

In this equation, there are terms in $k+1$ on both the right- and left-hand sides. In order to get an equation with such terms only on the left, transpose all $k+1$ terms to the left and define them as a

new state vector

$$\mathbf{x}(k+1) - T\mathbf{A}\mathbf{x}(k+1) - T\mathbf{B}e(k+1) = \mathbf{x}(k) \triangleq \mathbf{w}(k+1). \quad (6.23)$$

From this equation, solving for \mathbf{x} in terms of \mathbf{w} and e

$$\begin{aligned} (\mathbf{I} - \mathbf{A}T)\mathbf{x} &= \mathbf{w} + T\mathbf{B}e \\ \mathbf{x} &= (\mathbf{I} - \mathbf{A}T)^{-1}\mathbf{w} + (\mathbf{I} - \mathbf{A}T)^{-1}T\mathbf{B}e. \end{aligned} \quad (6.24)$$

With this expression for \mathbf{x} , Eq. (6.23) can be put in standard form as

$$\mathbf{w}(k+1) = (\mathbf{I} - \mathbf{A}T)^{-1}\mathbf{w}(k) + (\mathbf{I} - \mathbf{A}T)^{-1}T\mathbf{B}e(k), \quad (6.25)$$

and the output equation is now

$$u(k) = \mathbf{C}(\mathbf{I} - \mathbf{A}T)^{-1}\mathbf{w} + \{\mathbf{D} + \mathbf{C}(\mathbf{I} - \mathbf{A}T)^{-1}T\mathbf{B}\}e. \quad (6.26)$$

Equation (6.25) plus Eq. (6.26) are a state-space description of the backward rule equivalent to Eq. (6.18).

Finally, for the trapezoid or bilinear rule, the z -transform equivalent is obtained from

$$\begin{aligned} \frac{2(z-1)}{T(z+1)}\mathbf{X} &= \mathbf{A}\mathbf{X} + \mathbf{B}E \\ (z-1)\mathbf{X} &= \frac{\mathbf{A}T}{2}(z+1)\mathbf{X} + \frac{\mathbf{B}T}{2}(z+1)E \\ U &= \mathbf{C}\mathbf{X} + \mathbf{D}E, \end{aligned} \quad (6.27)$$

and the time domain equation for the state is

$$\mathbf{x}(k+1) - \mathbf{x}(k) = \frac{\mathbf{A}T}{2}(\mathbf{x}(k+1) + \mathbf{x}(k)) + \frac{\mathbf{B}T}{2}(e(k+1) + e(k)). \quad (6.28)$$

Once more, collect all the $k+1$ terms onto the left and define these as $\mathbf{w}(k+1)$ as follows⁶

$$\begin{aligned} \mathbf{x}(k+1) - \frac{\mathbf{A}T}{2}\mathbf{x}(k+1) - \frac{\mathbf{B}T}{2}e(k+1) &= \mathbf{x}(k) + \frac{\mathbf{A}T}{2}\mathbf{x}(k) + \frac{\mathbf{B}T}{2}e(k) \\ &\triangleq \sqrt{T}\mathbf{w}(k+1). \end{aligned} \quad (6.29)$$

Writing the definition of \mathbf{w} at time k , solve for \mathbf{x} as before

$$\begin{aligned} \left(\mathbf{I} - \frac{\mathbf{A}T}{2}\right)\mathbf{x} &= \sqrt{T}\mathbf{w} + \frac{\mathbf{B}T}{2}e \\ \mathbf{x} &= \left(\mathbf{I} - \frac{\mathbf{A}T}{2}\right)^{-1}\sqrt{T}\mathbf{w} + \left(\mathbf{I} - \frac{\mathbf{A}T}{2}\right)^{-1}\frac{\mathbf{B}T}{2}e. \end{aligned} \quad (6.30)$$

Substituting Eq. (6.30) into Eq. (6.29), we obtain

$$\begin{aligned} \sqrt{T}\mathbf{w}(k+1) &= \left(\mathbf{I} + \frac{\mathbf{A}T}{2}\right)\left(\mathbf{I} - \frac{\mathbf{A}T}{2}\right)^{-1}\left\{\sqrt{T}\mathbf{w}(k) + \frac{\mathbf{B}T}{2}e\right\} + \frac{\mathbf{B}T}{2}e(k) \\ \mathbf{w}(k+1) &= \left(\mathbf{I} + \frac{\mathbf{A}T}{2}\right)\left(\mathbf{I} - \frac{\mathbf{A}T}{2}\right)^{-1}\mathbf{w}(k) \\ &\quad + \left\{\left(\mathbf{I} + \frac{\mathbf{A}T}{2}\right)\left(\mathbf{I} - \frac{\mathbf{A}T}{2}\right)^{-1} + \mathbf{I}\right\}\frac{\mathbf{B}\sqrt{T}}{2}e(k) \\ &= \left(\mathbf{I} + \frac{\mathbf{A}T}{2}\right)\left(\mathbf{I} - \frac{\mathbf{A}T}{2}\right)^{-1}\mathbf{w}(k) + \left(\mathbf{I} - \frac{\mathbf{A}T}{2}\right)^{-1}\mathbf{B}\sqrt{T}e(k). \end{aligned} \quad (6.31)$$

⁶The scale factor of \sqrt{T} is introduced so that the gain of the discrete equivalent will be balanced between input and output, a rather technical condition. See Al Saggaf and Franklin (1986) for many more details.

In following this algebra, it is useful to know that in deriving the last part of Eq. (6.31), we expressed the identity \mathbf{I} as $(\mathbf{I} - \frac{\mathbf{A}T}{2})(\mathbf{I} - \frac{\mathbf{A}T}{2})^{-1}$ and factored out $(\mathbf{I} - \frac{\mathbf{A}T}{2})^{-1}$ on the right.

To obtain the output equation for the bilinear equivalent, we substitute Eq. (6.30) into the second part of Eq. (6.27):

$$u(k) = \sqrt{T}\mathbf{C} \left(\mathbf{I} - \frac{\mathbf{A}T}{2} \right)^{-1} \mathbf{w}(k) + \left\{ \mathbf{D} + \mathbf{C} \left(\mathbf{I} - \frac{\mathbf{A}T}{2} \right)^{-1} \frac{\mathbf{B}T}{2} \right\} e(k).$$

These results can be tabulated for convenient reference. Suppose we have a continuous system described by

$$\begin{aligned} \dot{\mathbf{x}}(t) &= \mathbf{A}\mathbf{x}(t) + \mathbf{B}e(t), \\ u(t) &= \mathbf{C}\mathbf{x}(t) + \mathbf{D}e(t). \end{aligned}$$

Then a discrete equivalent at sampling period T will be described by the equations

$$\begin{aligned} \mathbf{w}(k+1) &= \Phi\mathbf{w}(k) + \Gamma e(k), \\ u(k) &= \mathbf{H}\mathbf{w}(k) + \mathbf{J}e(k), \end{aligned}$$

where Φ , Γ , \mathbf{H} , and \mathbf{J} are given respectively as follows:

	Forward	Backward	Bilinear
Φ	$\mathbf{I} + \mathbf{A}T$	$(\mathbf{I} - \mathbf{A}T)^{-1}$	$(\mathbf{I} + \frac{\mathbf{A}T}{2})(\mathbf{I} - \frac{\mathbf{A}T}{2})^{-1}$
Γ	$\mathbf{B}T$	$(\mathbf{I} - \mathbf{A}T)^{-1}\mathbf{B}T$	$(\mathbf{I} - \frac{\mathbf{A}T}{2})^{-1}\mathbf{B}\sqrt{T}$
\mathbf{H}	\mathbf{C}	$\mathbf{C}(\mathbf{I} - \mathbf{A}T)^{-1}$	$\sqrt{T}\mathbf{C}(\mathbf{I} - \frac{\mathbf{A}T}{2})^{-1}$
\mathbf{J}	\mathbf{D}	$\mathbf{D} + \mathbf{C}(\mathbf{I} - \mathbf{A}T)^{-1}\mathbf{B}T$	$\mathbf{D} + \mathbf{C}(\mathbf{I} - \frac{\mathbf{A}T}{2})^{-1}\mathbf{B}T/2$

The MATLAB Control Toolbox provides for the computation of Tustin bilinear equivalents with the function `c2d`. The syntax of computing the bilinear equivalent `sysd` of a continuous system `sys` at sampling period `Ts` is

```
sysd = c2d(sys,Ts,'tustin')
```

If 'tustin' is replaced with 'prewarp', the bilinear equivalent with prewarping is computed. When using the 'prewarp' method, the critical frequency ω_1 must also be supplied to `c2d`.

6.2 Zero-Pole Matching Equivalents

A very simple but effective method of obtaining a discrete equivalent to a continuous transfer function is to be found by extrapolation of the relation derived in Chapter 4 between the s - and z -planes. If we take the z -transform of samples of a continuous signal $e(t)$, then the poles of the discrete transform $E(z)$ are related to the poles of $E(s)$ according to $z = e^{sT}$. We must go through the z -transform process to locate the zeros of $E(z)$, however. The idea of the zero-pole matching technique is that the map $z = e^{sT}$ could reasonably be applied to the zeros also. The technique consists of a set of heuristic rules for locating the zeros and poles and setting the gain of a z -transform that will describe a discrete, equivalent transfer function that approximates the given $H(s)$. The rules are as follows:

1. All poles of $H(s)$ are mapped according to $z = e^{sT}$. If $H(s)$ has a pole at $s = -a$, then $H_{zp}(z)$ has a pole at $z = e^{-aT}$. If $H(s)$ has a pole at $-a + jb$, then $H_{zp}(z)$ has a pole at $re^{j\theta}$, where $r = e^{-aT}$ and $\theta = bT$.
2. All finite zeros are also mapped by $z = e^{sT}$. If $H(s)$ has a zero at $s = -a$, then $H_{zp}(z)$ has a zero at $z = e^{-aT}$, and so on.
3. The zeros of $H(s)$ at $s = \infty$ are mapped in $H_{zp}(z)$ to the point $z = -1$. The rationale behind this rule is that the map of real frequencies from $j\omega = 0$ to increasing ω is onto the unit circle

at $z = e^{j0} = 1$ until $z = e^{j\pi} = -1$. Thus the point $z = -1$ represents, in a real way, the highest frequency possible in the discrete transfer function, so it is appropriate that if $H(s)$ is zero at the highest (continuous) frequency, $|H_{zp}(z)|$ should be zero at $z = -1$, the highest frequency that can be processed by the digital filter.

- (a) If no delay in the discrete response is desired, all zeros at $s = \infty$ are mapped to $z = -1$.
 - (b) If one sample period delay is desired to give the computer time to complete the output calculation, then one of the zeros at $s = \infty$ is mapped to $z = \infty$ and the others mapped to $z = -1$. With this choice, $H_{zp}(z)$ is left with a number of finite zeros one fewer than the number of finite poles.
4. The gain of the digital filter is selected to match the gain of $H(s)$ at the band center or a similar critical point. In most control applications, the critical frequency is $s = 0$, and hence we typically select the gain so that

$$H(s)|_{s=0} = H_{zp}(z)|_{z=1}.$$

A Zero-pole Matching Equivalent

Example 6.2

Compute the discrete equivalent to

$$H(s) = \frac{a}{s+a}$$

by zero-pole matching.

Solution. The pole of $H(s)$ at $s = -a$ will map to a pole of $H(z)$ at e^{-aT} . The zero at $s = \infty$ will map to a zero at $z = -1$. The gain of $H(s)$ at $s = 0$ is 1. To match this gain in $H(z)$ at $z = 1$ requires gain of $\frac{1 - e^{-aT}}{2}$. The final function is given by

$$H_{zp}(z) = \frac{(z+1)(1 - e^{-aT})}{2(z - e^{-aT})}, \quad (6.33)$$

or, using rule 3(b), the result is

$$H_{zp}(z) = \frac{1 - e^{-aT}}{z - e^{-aT}}. \quad (6.34)$$

As with the rules based on numerical analysis, an algorithm to generate the matched zero-pole equivalent is also readily constructed. In MATLAB, a matched zero-pole equivalent, `sysd`, at sample period T_s to the continuous system, `sys`, is given by

```
sysd = c2d(sys, Ts, 'matched')
```

The frequency response of the matched zero-pole equivalent for the third-order Butterworth filter of Example 6.1 is plotted in Fig. 6.9 along with that of other equivalents for purposes of comparison.

6.3 Hold Equivalents

For this technique, we construct the situation sketched in Fig. 6.5. The samplers in Fig. 6.5(b) provide the samples at the input of $H_{ho}(z)$ and take samples at its output insuring that $H_{ho}(z)$ can be realized as a discrete transfer function. The philosophy of the design is the following. We are asked to design a discrete system that, with an input consisting of *samples* of $e(t)$, has an output that approximates the output of the continuous filter $H(s)$ whose input is the *continuous* $e(t)$. The discrete hold equivalent is constructed by first approximating $e(t)$ from the samples $e(k)$ with a hold filter and then putting this $e_h(t)$ through the given $H(s)$. There are many techniques for taking a sequence of samples and extrapolating or holding them to produce a continuous signal.⁷ Suppose we have the $e(t)$ as

⁷Some books on digital-signal processing suggest using no hold at all, using the equivalent $H(z) = \mathcal{Z}\{H(s)\}$. This choice is called the z -transform equivalent.

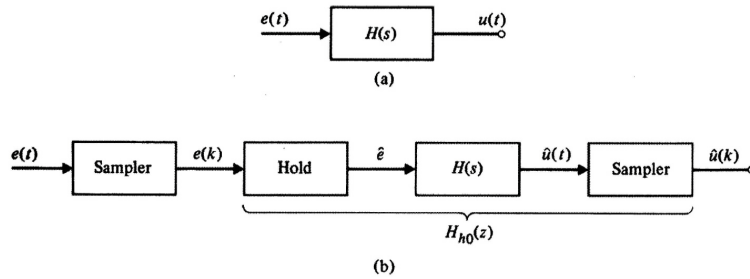


Figure 6.5
System construction for hold equivalents. (a) A continuous transfer function. (b) Block diagram of an equivalent system.

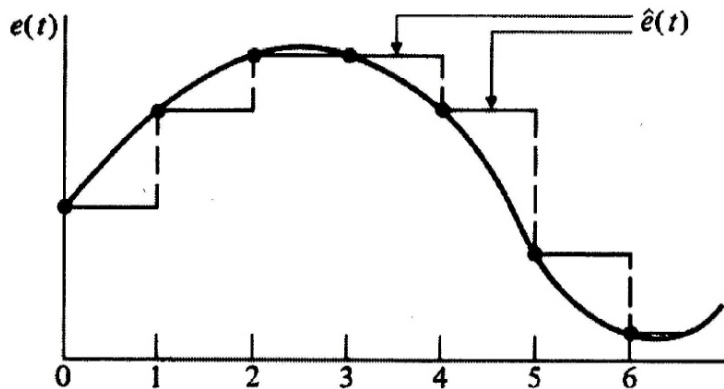


Figure 6.6
A signal, its samples, and its approximation by a zero-order hold

sketched in Fig. 6.6. This figure also shows a sketch of a piecewise constant approximation to $e(t)$ obtained by the operation of holding $e_h(t)$ constant at $e(k)$ over the interval from kT to $(k+1)T$. This operation is the *zero-order hold* (or ZOH) we've discussed before. If we use a first-order polynomial for extrapolation, we have a *first-order hold* (or FOH), and so on for higher-order holds.

6.3.1 Zero-Order Hold Equivalent

If the approximating hold is the zero-order hold, then we have for our approximation exactly the same situation that in Chapter 4 was analyzed as a sampled-data system.⁸ Therefore, the zero-order-hold equivalent to $H(s)$ is given by Eq. (4.41)

$$H_{h0}(z) = (1 - z^{-1}) \mathcal{Z} \left\{ \frac{H(s)}{s} \right\}. \tag{6.35}$$

A Hold Equivalent

Find the zero-order-hold equivalent to the first-order transfer function

$$H(s) = \frac{a}{s+a}.$$

Solution. The partial fraction expansion of the s -plane terms of Eq. (6.35) is

$$\frac{H(s)}{s} = \frac{a}{s(s+a)} = \frac{1}{s} - \frac{1}{s+a}$$

⁸Recall that we noticed in Chapter 4 that the signal \hat{e} is, on the average, delayed from e by $T/2$ sec. The size of this delay is one measure of the quality of the approximation and can be used as a guide to the selection of T .

Example 6.3

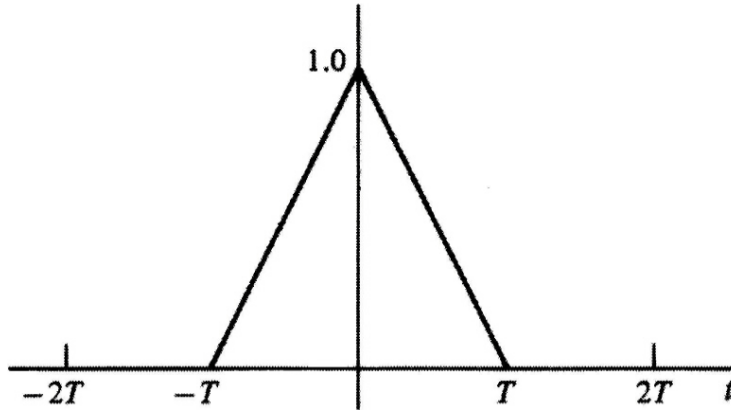


Figure 6.7
Impulse response
of the
extrapolation
filter for the
triangle hold

and the z -transform is

$$\mathcal{Z}\left\{\frac{H(s)}{s}\right\} = \mathcal{Z}\left\{\frac{1}{s}\right\} - \mathcal{Z}\left\{\frac{1}{s+a}\right\}, \quad (6.36)$$

and, by definition of the operation given in Eq. (6.36)

$$\begin{aligned} \mathcal{Z}\left\{\frac{H(s)}{s}\right\} &= \sum_0^{\infty} z^{-k} - \sum_0^{\infty} z^{-k} e^{-akT} \\ &= \frac{1}{1-z^{-1}} - \frac{1}{1-e^{-aT}z^{-1}} \\ &= \frac{(1-e^{-aT}z^{-1}) - (1-z^{-1})}{(1-z^{-1})(1-e^{-aT}z^{-1})}. \end{aligned} \quad (6.37)$$

Substituting Eq. (6.37) in Eq. (6.35), the zero-order-hold equivalent of $H(s)$ is found as

$$H_{h0}(z) = \frac{(1-e^{-aT})}{z-e^{-aT}}. \quad (6.38)$$

We note that for the trivial example given, the zero-order-hold equivalent of Eq. (6.38) is identical to the matched zero-pole equivalent given by Eq. (6.34). However, this is not generally true as is evident in the comparison with frequency responses of other equivalents for the third-order Butterworth filter example plotted in Fig. 6.9. Because a sample and zero-order hold is an exact model for the sample and hold with A/D converter used in the majority of discrete systems, we have already seen the computation of this equivalent in MATLAB as

```
sysd = c2d(sys, Ts, 'zoh')
```

where the continuous system is described by `sys` and the sample period is `Ts`.

6.3.2 A Non-Causal First-Order-Hold Equivalent: The Triangle-Hold Equivalent

An interesting hold equivalent can be constructed by imagining that we have a noncausal first-order-hold impulse response, as sketched in Fig. 6.7. The result is called the triangle-hold equivalent to distinguish it from the causal first-order hold. The effect of the triangle hold is to extrapolate the samples so as to connect sample to sample in a straight line. Although the continuous system that does this is noncausal, the resulting discrete equivalent is causal.

The Laplace transform of the extrapolation filter that follows the impulse sampling is

$$\frac{e^{Ts} - 2 + e^{-Ts}}{Ts^2}.$$

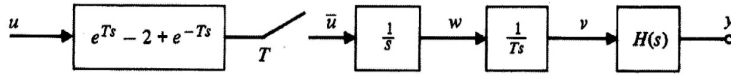


Figure 6.8
Block diagram of
the triangle-hold
equivalent

Therefore the discrete equivalent that corresponds to Eq. (6.35) is

$$H_{tri}(z) = \frac{(z-1)^2}{Tz} \mathcal{Z} \left\{ \frac{H(s)}{s^2} \right\}. \quad (6.39)$$

A Triangle-Hold Equivalent

Example 6.4

Compute the triangle-hold equivalent for $H(s) = 1/s^2$.

Solution. In this case, from the tables of z -transforms

$$\begin{aligned} \mathcal{Z} \left\{ \frac{H(s)}{s^2} \right\} &= \mathcal{Z} \left\{ \frac{1}{s^4} \right\} \\ &= \frac{T^3}{6} \frac{(z^2 + 4z + 1)z}{(z-1)^4}, \end{aligned} \quad (6.40)$$

and direct substitution into Eq. (6.39) results in

$$\begin{aligned} H_{tri}(z) &= \frac{(z-1)^2}{Tz} \frac{T^3}{6} \frac{(z^2 + 4z + 1)z}{(z-1)^4} \\ &= \frac{T^2}{6} \frac{z^2 + 4z + 1}{(z-1)^2}. \end{aligned} \quad (6.41)$$

An alternative, convenient way to compute the triangle-hold equivalent is again to consider the state-space formulation. The block diagram is shown in Fig. 6.8. The continuous equations are

$$\begin{aligned} \dot{\mathbf{x}} &= \mathbf{F}\mathbf{x} + \mathbf{G}v, \\ \dot{v} &= w/T, \\ \dot{w} &= u(t+T)\delta(t+T) - 2u(t)\delta(t) + u(t-T)\delta(t-T), \end{aligned} \quad (6.42)$$

and, in matrix form,

$$\begin{bmatrix} \dot{\mathbf{x}} \\ \dot{v} \\ \dot{w} \end{bmatrix} = \begin{bmatrix} \mathbf{F} & \mathbf{G} & \mathbf{0} \\ 0 & 0 & 1/T \\ 0 & 0 & 0 \end{bmatrix} \begin{bmatrix} \mathbf{x} \\ v \\ w \end{bmatrix} + \begin{bmatrix} \mathbf{0} \\ 0 \\ 1 \end{bmatrix} \bar{u} \quad (6.43)$$

where \bar{u} represents the input impulse functions. We define the large matrix in Eq. (6.43) as F_T , and the one-step solution to this equation is

$$\boldsymbol{\zeta}(kT+1) = e^{\mathbf{F}_T T} \boldsymbol{\zeta}(kT)$$

because \bar{u} consists only of impulses at the sampling instants. If we define

$$\exp(\mathbf{F}_T T) = \begin{bmatrix} \boldsymbol{\Phi} & \boldsymbol{\Gamma}_1 & \boldsymbol{\Gamma}_2 \\ 0 & 1 & 0 \\ 0 & 0 & 1 \end{bmatrix} \quad (6.44)$$

then the equation in \mathbf{x} becomes

$$\mathbf{x}(k+1) = \boldsymbol{\Phi}\mathbf{x}(k) - \boldsymbol{\Gamma}_1 v(k) + \boldsymbol{\Gamma}_2 w(k).$$

With care, the last two equations of Eq. (6.42) can be integrated to show that $v(k) = u(k)$ and that $w(k) = u(k+1) - u(k)$. If a new state is defined as $\xi(k) = \mathbf{x}(k) - \mathbf{\Gamma}_2 u(k)$, then the state equation for the triangle equivalent is

$$\begin{aligned}\xi(k+1) &= \Phi(\xi(k) + \mathbf{\Gamma}_2 u(k)) + (\mathbf{\Gamma}_1 - \mathbf{\Gamma}_2)u(k) \\ &= \Phi\xi(k) + (\mathbf{\Gamma}_1 + \Phi\mathbf{\Gamma}_2 - \mathbf{\Gamma}_2)u(k).\end{aligned}\quad (6.45)$$

The output equation is

$$\begin{aligned}y(k) &= \mathbf{H}\mathbf{x}(k) + \mathbf{J}u(k) \\ &= H(\xi(k) + \mathbf{\Gamma}_2 u(k)) + \mathbf{J}u(k) \\ &= \mathbf{H}\xi(k) + (\mathbf{J} + \mathbf{H}\mathbf{\Gamma}_2)u(k).\end{aligned}\quad (6.46)$$

Thus the triangle equivalent of a continuous system described by $[\mathbf{F}, \mathbf{G}, \mathbf{H}, \mathbf{J}]$ with sample period T is given by

$$\begin{aligned}\mathbf{A} &= \Phi, \\ \mathbf{B} &= \mathbf{\Gamma}_1 + \Phi\mathbf{\Gamma}_2 - \mathbf{\Gamma}_2, \\ \mathbf{C} &= \mathbf{H}, \\ \mathbf{D} &= \mathbf{J} + \mathbf{H}\mathbf{\Gamma}_2,\end{aligned}\quad (6.47)$$

where Φ , $\mathbf{\Gamma}_1$, and $\mathbf{\Gamma}_2$ are defined by Eq. (6.44). In the MATLAB Control Toolbox, the function `c2d` will compute the triangle-hold equivalent (referenced there as a first-order-hold equivalent) of continuous system `sys` by

```
sysd = c2d(sys, Ts, 'foh')
```

In Fig. 6.9 the frequency responses of the zero-pole, the zero-order hold, and the triangle-hold equivalents are compared again for the third-order Butterworth lowpass filter. Notice in particular that the triangle hold has excellent phase responses, even with the relatively long sampling period of $T = 2$, which corresponds to a sampling frequency to passband frequency ratio of only $\omega_s/\omega_p = \pi$.

6.4 Summary

In this chapter we have presented several techniques for the construction of discrete equivalents to continuous transfer functions so that known design methods for continuous systems can be used as a basis for the design of discrete systems. The methods presented were

1. *Numerical integration*
 - (a) Forward rectangular rule
 - (b) Backward rectangular rule
 - (c) Trapezoid, bilinear, or Tustin's rule
 - (d) Bilinear transformation with prewarping
2. *Zero-pole matching*
3. *Hold equivalents*
 - (a) Zero-order-hold equivalent
 - (b) Noncausal first-order- or triangle-hold equivalent

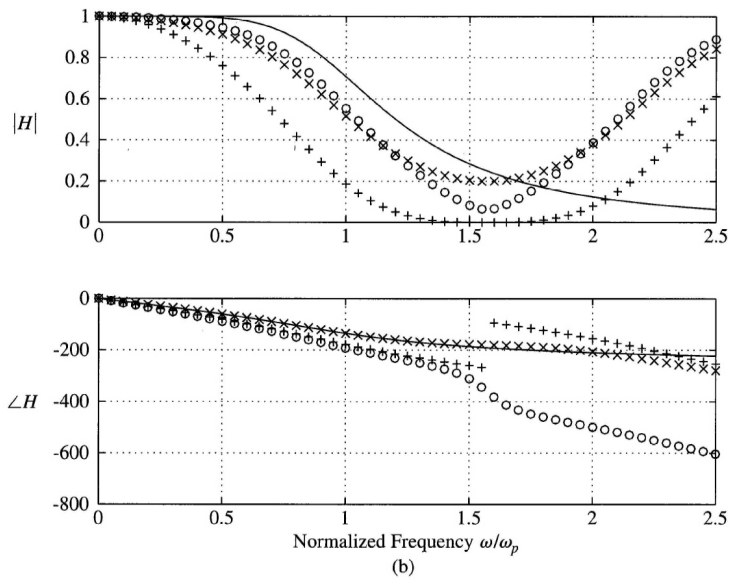
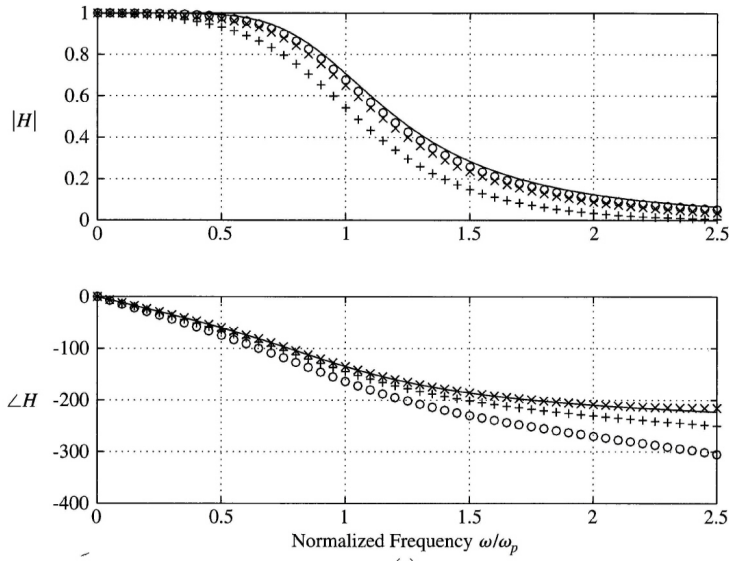


Figure 6.9
 Comparison of digital equivalents for sampling period (a) $T = 1$ and $\omega_s/\omega_p = 2\pi$ and (b) $T = 2$ and $\omega_s/\omega_n = \pi$ where ZOH = \circ , zero-pole = +, and triangle = \times

sysd	=	c2d(sys, Ts, method)	where
method	=	'zoh'	zero-order hold
method	=	'foh'	first-order hold (triangle hold)
method	=	'tustin'	Tustin's bilinear method
method	=	'prewarp'	bilinear with prewarping (requires critical frequency)
method	=	'matched'	zero-pole matching

All methods except the forward rectangular rule guarantee a stable discrete system from a stable continuous prototype with the provision that the warping frequency of the bilinear transformation with prewarping must be less than the Nyquist frequency of $\frac{\pi}{T}$ rad/sec. Zero-pole matching is the simplest method to apply computationally if the zeros and poles of the desired filter are known and takes advantage of the known relations between response and poles and zeros. This is one of the most effective methods in the context of an overall design problem and in later chapters the zero-pole matching method is frequently selected. With a reasonable computer-aided-design tool, the designer can select the method that best meets the requirements of the design. The MATLAB function `c2d` computes the discrete description for most of these discrete equivalents from a continuous system described by `SYS` with sample period T_s as follows.

6.5 Problems

- 6.1 Sketch the zone in the z -plane where poles corresponding to the left half of the s -plane will be mapped by the zero-pole mapping technique and the zero-order-hold technique.
- 6.2 Show that Eq. (6.15) is true.
- 6.3 The following transfer function is a lead network designed to add about 60° phase lead at $\omega_1 = 3$ rad/s

$$H(s) = \frac{s+1}{0.1s+1}.$$

- (a) For each of the following design methods compute and plot in the z -plane the pole and zero locations and compute the amount of phase lead given by the equivalent network at $z_1 = e^{j\omega_1 T}$ if $T = 0.25$ sec and the design is via
- Forward rectangular rule
 - Backward rectangular rule
 - Bilinear rule
 - Bilinear with prewarping (use ω_1 as the warping frequency)
 - Zero-pole mapping
 - Zero-order-hold equivalent
 - Triangular-hold equivalent
- (b) Plot over the frequency range $\omega_l = 0.1 \rightarrow \omega_h = 100$ the amplitude and phase Bode plots for each of the above equivalents.
- 6.4 The following transfer function is a lag network designed to increase K_v by a factor of 10 and have negligible phase lag at $\omega_1 = 3$ rad/s.

$$H(s) = 10 \frac{10s+1}{100s+1}.$$

- (a) For each of the following design methods, compute and plot on the z -plane the zero-pole patterns of the resulting discrete equivalents and give the phase lag at $z_1 = e^{j\omega_1 T}$ corresponding to $\omega_1 = 3$ rad/sec. Let $T = 0.25$ sec.
- Forward rectangular rule

- ii. Backward rectangular rule
 - iii. Bilinear rule
 - iv. Bilinear with prewarping (Use $\omega_1 = 3$ rad/s as the warping frequency)
 - v. Zero-pole matching
 - vi. Zero-order-hold equivalent
 - vii. Triangle-hold equivalent
- (b) For each case computed, plot the Bode amplitude and phase curves over the range $\omega_l = 0.01 \rightarrow \omega_h = 10$ rad/s.

Chapter 7

Design Using Transform Techniques

A Perspective on Design Using Transform Techniques

The idea of controlling processes that evolve in time is ubiquitous. Systems from airplanes to the national rate of unemployment, from unmanned space vehicles to human blood pressure, are considered fair targets for control. Over a period of three decades from about 1930 until 1960, a body of control theory was developed based on electronic feedback amplifier design modified for servomechanism problems. This theory was coupled with electronic technology suitable for implementing the required dynamic compensators to give a set of approaches to solve control problems now often called **classical techniques** to distinguish these methods from designs based on a state-space formulation which came to be called **modern techniques**. The landmark contributors to this “classical” theory are Evans (1950) [root locus] and Nyquist (1932) and Bode (1945) [frequency response]. For random inputs, the work of Wiener (1948) should be added. The unifying theme of these methods is the use of Fourier and Laplace transforms to represent signals and system dynamics and to describe the control specifications. Controller design is then carried out in the selected transform domain. From the perspective of the 90’s the terms “classical” and “modern” seem a bit pejorative and we prefer to classify the methods as **transform techniques** and **state-space techniques**.

The methods based on transforms were developed before computers were available and the engineer had to depend on hand calculations and careful hand plotting to achieve the design. The availability of computers and software such as MATLAB have made calculations and plotting simple, fast and accurate; and now the hand-plotting guidelines are used as verification of the automatic calculations and as a guide to design decisions. In this role, the understanding of the design process gained by the experience of doing a simple design by hand is well worth the effort spent in developing the required skills. The introduction of digital control and sampled data adds new constraints and new possibilities to the transform design methods. The z -transform is added to the Laplace and the Fourier transforms and poles and zeros have meaning relative to the unit circle rather than to the imaginary axis. The meaningful part of the frequency response is restricted to half the sampling frequency. Each of these developments must be understood in order to apply transform methods to digital control.

Chapter Overview

Building on previous understanding of the design of continuous systems, the first method for digital design is based on **emulation** of a continuous design. The continuous controller is simply replaced with a digital equivalent computed by using one of the techniques described in Chapter 6. The result may be evaluated in terms of poles and zeros in the z -plane, magnitude and phase in the frequency response, or transient response to step, impulse or other input.

The second method introduced is the **root locus** where it is demonstrated that the rules of the root locus are unchanged from the continuous case but the relations between pole location and time response must refer to the z -plane rather than the s -plane.

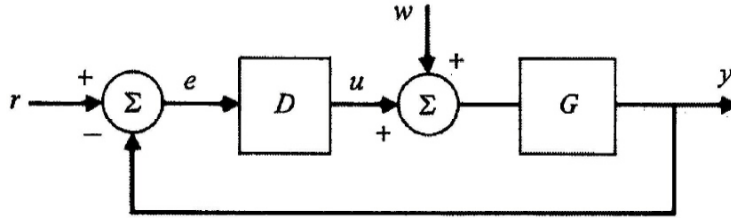


Figure 7.1
A unity feedback system

Finally, the Nyquist stability criterion for discrete systems is developed and Bode’s design methods for gain and phase margins are extended to discrete systems. In addition to the usual results, the concept of system sensitivity is developed to show how **frequency response** can be used to cause the system to be robust with respect to both stability and performance when the plant transfer function is subjected to bounded but unknown perturbations.

design by frequency response

7.1 System Specifications

We first consider the design specifications that the controller is expected to achieve. As reviewed in Chapter 2, the central concerns of controller design are for good transient and steady-state response and for sufficient robustness. Requirements on time response and robustness need to be expressed as constraints on *s*-plane pole and zero locations or on the shape of the frequency response in order to permit design in the transform domains. Dynamic performance in the time domain is defined in terms of parameters of system response to a step in command input. The most frequently used parameters are the rise time, t_r ; the settling time, t_s ; the percent overshoot, M_p ; and the steady-state error, e_{ss} . These parameters, which apply equally well to discrete control as to continuous control, are discussed in Section 4.1.7. The *s*-plane expressions of these requirements are summarized by the following guidelines:

- The requirement on natural frequency is

$$\omega_n \geq 1.8/t_r. \tag{7.1}$$

- The requirement on the magnitude of the real part of the pole is

$$|\text{Re}\{s_i\}| = \sigma = \zeta\omega_n \geq 4.6/t_s. \tag{7.2}$$

- The fractional overshoot, M_p , is given in terms of the damping ratio, ζ , by the plot of Fig. 2.7 which can be very crudely approximated by

$$\zeta \approx 0.6(1 - M_p). \tag{7.3}$$

The specifications on steady-state error to polynomial inputs is determined by the error constant appropriate for the case at hand as described in Section 4.2.2. The most common case is for systems of Type 1, which is to say, systems that have zero steady-state error to a step input and finite error to a ramp input of slope r_0 of size $e_{ss} = r_0/K_v$ where K_v is the velocity constant. For a single-loop system with *unity* feedback gain and forward transfer function $D(s)G(s)$ as shown in Fig. 7.1, the system is **Type 1** if DG has a simple pole at $s = 0$.

- The **velocity constant** is then given by

velocity constant

$$K_v = \frac{r_0}{e_{ss}} = \lim_{s \rightarrow 0} sD(s)G(s).$$

The fact that in discrete systems the control is applied as a piecewise constant signal causes a roughness in the response that is directly related to the sample frequency. A specification on roughness leads to a specification on sample period, T . This parameter is so important to the design of discrete controls that Chapter 11 is devoted to the decision. At this point, let it suffice to point out that the smaller the T , the better the approximation to continuous control and the smaller the roughness.

- A reasonable choice of T is one that results in at least 6 samples in the closed-loop rise time and better, smoother control results if there are more than 10 samples in the rise time.

Selection of Sample Period

Example 7.1

What is the relation between sampling frequency and system natural frequency if there are 10 samples in a rise time?

Solution. The sampling frequency in radians/sec is given by $\omega_s = 2\pi/T$ and we assume that rise time and natural frequency are related by Eq. (7.1) so that

$$\begin{aligned}\omega_n &= 1.8/t_r \\ &= \frac{1.8}{10T}.\end{aligned}$$

Substituting for T , we find that

$$\omega_n = \frac{0.18\omega_s}{2\pi}$$

or

$$\omega_n \approx \omega_s/35.$$

In other words, the sample rate, ω_s , should be 35 times faster than the natural frequency, ω_n .

From this example, we conclude that typically the sample frequency should be chosen to be 20 to 35 times the closed loop natural frequency. Slower sampling can be used but one would expect the resulting transients to be excessively rough.

Robustness is the property that the dynamic response (including stability of course) is satisfactory not only for the nominal plant transfer function used for the design but also for the entire class of transfer functions that express the uncertainty of the designer about the dynamic environment in which the real controller is expected to operate. A more comprehensive discussion of robustness will be given when design using frequency response is considered. For root locus design, the natural measure of robustness is, in effect, gain margin. One can readily compare the system gain at the desired operating point and at the point(s) of onset of instability to determine how much gain change is acceptable.

- A typical robustness requirement is that one should have gain margin of two so that the loop gain must double from the design value before reaching the stability boundary.

7.2 Design by Emulation

The elements of design by emulation have been covered already. Continuous control design is reviewed in Chapter 2, and in Chapter 6 the techniques of computing discrete equivalents are described. Control design by emulation is mainly a combination of these two ideas. A controller design is done as if the system is to be continuous and, after a sample period is selected, a discrete equivalent is computed and used in place of the continuous design. This discrete controller may then be simulated and tested in the discrete control loop and modifications made, if necessary.

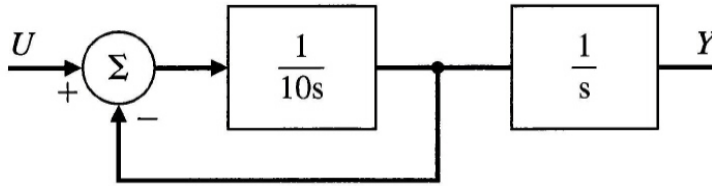


Figure 7.2
Block diagram of
the plant transfer
function

7.2.1 Discrete Equivalent Controllers

Techniques to compute discrete equivalents are described in general terms in Chapter 6, and their performance is illustrated on the basis of filter frequency responses. In this chapter, we are interested in controllers for feedback control and in performance comparisons on the basis of time responses. Any of the techniques from Chapter 6 can be used for the purpose; here we illustrate the use of the pole-zero mapping equivalent and explore the choice of sample period by example. An alternative approach that considers directly the performance for the discrete controller in the feedback context has been described by Anderson (1992). The method described in that reference leads to a multirate sampling problem of the sort which will be considered in Chapter 11.

Design of Antenna Servo Controller

Example 7.2

A block diagram of the plant for an antenna angle-tracker is drawn in Fig. 7.2. The transfer function is given by

$$G(s) = \frac{1}{s(10s+1)}.$$

The specifications for this system are

1. Overshoot to a step input less than 16%
2. Settling time to 1% to be less than 10 sec
3. Tracking error to a ramp input of slope 0.01 rad/sec to be less than 0.01 rad
4. Sampling time to give at least 10 samples in a rise-time

Design a controller for this system using the method of emulation.

Solution. From the specifications one can estimate the acceptable region in the s -plane for the closed loop poles. From the overshoot requirement, we conclude that the damping ratio must be $\zeta \geq 0.5$. From the settling time requirement, we conclude that the roots must have a real part of $\sigma \geq 4.6/10 = 0.46$. Finally, from the steady-state error requirement, we conclude that the velocity constant is constrained to be $K_v \geq \frac{0.01}{0.01} = 1.0$. Based on the limits on the damping ratio and the real-part of the poles, we can sketch the acceptable region for closed-loop poles in the s -plane as done in Fig. 7.3. Using lead compensation to cancel a plant pole, a first choice for controller might be

$$D(s) = \frac{10s+1}{s+1}. \quad (7.4)$$

The root locus for this choice is drawn in Fig. 7.4 using MATLAB commands to enter the plant as a system, `ant`, the compensation as `lead1`, and the product as the open loop system, `sysol`.

```
np = 1;
dp = [10 1 0];
ant = tf(np,dp);
nc = [10 1];
dc = [1 1];
lead1 = tf(nc,dc);
sysol = lead1*ant;
rlocus(sysol)
```

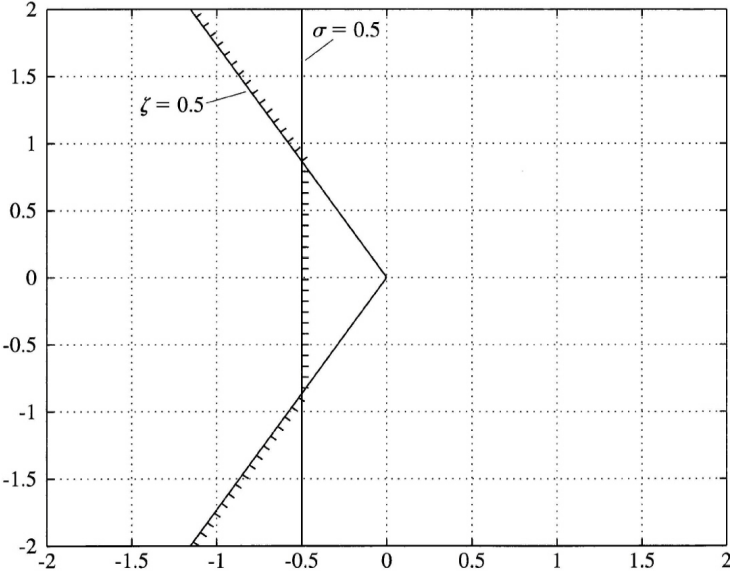


Figure 7.3
Acceptable pole locations for the antenna control

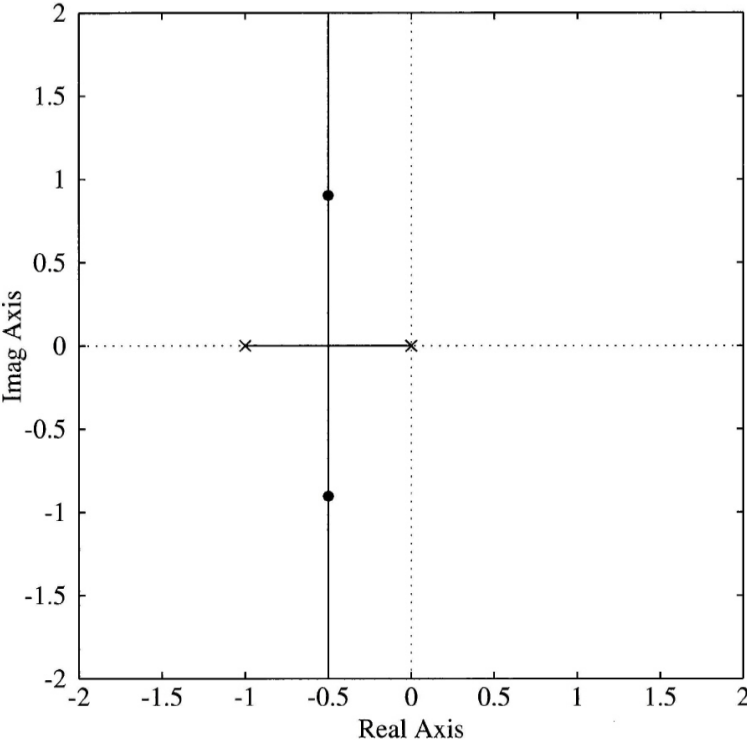


Figure 7.4
Root locus for compensated antenna model

The locations of the roots with $K = 1$ corresponding to a velocity constant of $K_v = 1$ are marked by the dots computed by

```
p = rlocus(sysol,1.0)
```

The natural frequency for the given pole locations is essentially $\omega_n = 1$, which corresponds to a rise time of $t_r = 1.8$ sec. The indicated sampling period is thus $T = t_r/10 = 0.18$. A value of $T = 0.2$ will be used for this example and a value of $T = 1.0$ illustrated later to dramatize the effects of the choice of T . The compensation, $D(s)$, given by Eq. (7.4), has two first-order factors; the zero is at $s = -0.1$, and the pole is at $s = -1$. The pole-zero mapping technique requires that each singularity is mapped according to $z = e^{sT}$; therefore, we take $D(z)$ of the form

$$D(z) = K \frac{z - z_1}{z - p_1},$$

and place a zero at

$$z_1 = e^{(-0.1)(0.2)} = 0.9802,$$

and a pole at

$$p_1 = e^{(-1)(0.2)} = 0.8187.$$

To make the dc gain of $D(z)$ and $D(s)$ be identical, we require that

$$\begin{aligned} \text{dc gain} &= \lim_{z \rightarrow 1} D(z) = \lim_{s \rightarrow 0} D(s) = 1 \\ &= K \frac{1 - 0.9802}{1 - 0.8187}. \end{aligned} \quad (7.5)$$

Solving for K we have

$$K = 9.15,$$

and the design of the discrete equivalent compensation has the transfer function

$$D(z) = 9.15 \frac{z - 0.9802}{z - 0.8187}. \quad (7.6)$$

To compute this result in MATLAB, the command is

```
lead1d = c2d(lead1,0.2,'matched')
```

Implementing the Controller

Example 7.3

Give the difference equation that corresponds to the $D(z)$ given by Eq. (7.6).

Solution. The transfer function is converted into a difference equation for implementation using the ideas developed in Chapter 4. Specifically, we first multiply top and bottom by z^{-1} to obtain

$$D(z) = \frac{U(z)}{E(z)} = 9.15 \frac{1 - 0.9802z^{-1}}{1 - 0.8187z^{-1}},$$

which can be restated as

$$(1 - 0.8187z^{-1})U(z) = 9.15(1 - 0.9802z^{-1})E(z).$$

The z -transform expression above is converted to the difference equation form by noting that z^{-1} represents a 1-cycle delay. Thus

$$u(k) = 0.8187u(k-1) + 9.15(e(k) - 0.9802e(k-1)).$$

This equation can be directly evaluated by a computer.

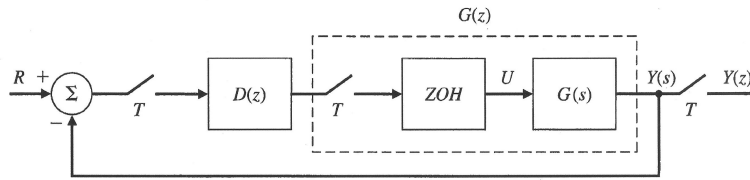


Figure 7.5
Block diagram of
sampled-data
system

7.2.2 Evaluation of the Design

A description of a digital controller that is expected to satisfy the specifications for the antenna controller is now complete. A block diagram of the sampled-data system with discrete controller is given in Fig. 7.5. To analyze the behavior of this compensation, we first determine the z -transform of the continuous plant (Fig. 7.2) preceded by a zero-order hold (ZOH).

$$G(z) = \frac{z-1}{z} \mathcal{Z} \left\{ \frac{a}{s^2(s+a)} \right\}, \quad (7.7)$$

which is

$$G(z) = \frac{z-1}{z} \mathcal{Z} \left\{ \frac{1}{s^2} - \frac{1}{as} + \frac{1}{a} \frac{1}{s+a} \right\}.$$

Using the tables in Appendix B, we find

$$\begin{aligned} G(z) &= \frac{z-1}{z} \left\{ \frac{Tz}{(z-1)^2} - \frac{z}{a(z-1)} + \frac{1}{a} \frac{z}{z-e^{-aT}} \right\} \\ &= \frac{Az+B}{a(z-1)(z-e^{-aT})}, \end{aligned}$$

where

$$A = e^{-aT} + aT - 1, \quad B = 1 - e^{-aT} - aTe^{-aT}.$$

For this example, with $T = 0.2$ and $a = 0.1$, this evaluates to

$$G(z) = 0.00199 \frac{z+0.9934}{(z-1)(z-0.9802)}. \quad (7.8)$$

Of course, this can be computed in MATLAB as the discrete model of the antenna by

```
antd = c2d(ant,0.2)
```

With the transfer function of the plant-plus-hold and the discrete controller, we can obtain the system difference equation and compute the step response, obviously most easily using a computer aided design package. The steps are

```
sysold = lead1d*antd
syscld = connect(sysold,[1 -1])
step(syscld)
```

In this case, the step response of the system with the discrete controller is shown in Fig. 7.6. The figure confirms that the discrete controller will perform satisfactorily, albeit with somewhat increased overshoot. This simulation was carried out using the linear, discrete model of the system. As mentioned earlier, simulations can be embellished with the important nonlinearities such as friction and with computation delays in order to assess their effects in addition to the effect of the discretization approximations.

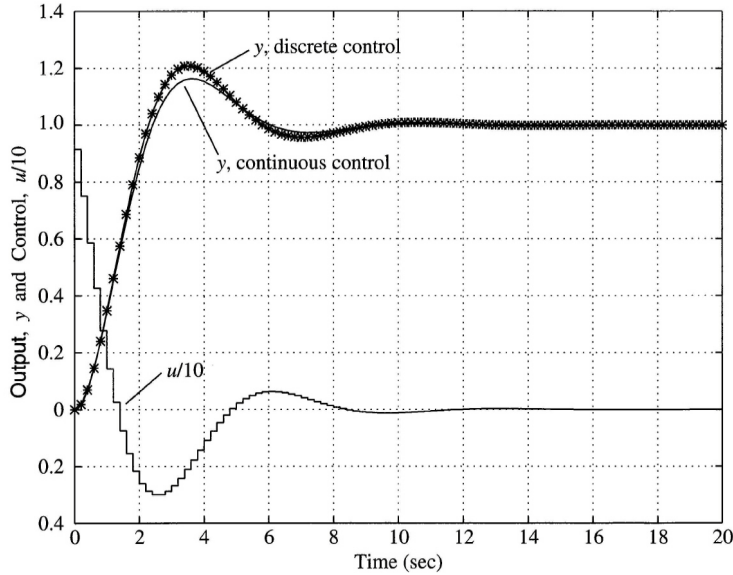


Figure 7.6
Step response of
the 5 Hz
controller

Antenna Servo with Slow Sampling

Example 7.4

Repeat the antenna design with a sample rate of 1 Hz ($T = 1$ sec); in this case the sample rate is approximately two samples per rise time.

Solution. Repeating the calculations as in Eq. (7.7) with $T = 1$ sec results in

$$G(z) = 0.0484 \frac{z + 0.9672}{(z - 1)(z - 0.9048)}. \quad (7.9)$$

Furthermore, repeating the calculations that led to Eq. (7.6) but with $T = 1$ sec, we obtain

$$D(z) = 6.64 \frac{z - 0.9048}{z - 0.3679}. \quad (7.10)$$

A plot of the step response of the resulting system is shown in Fig. 7.7 and shows substantial degradation of the response as a result of the slow sampling. A partial explanation of the extra overshoot can be obtained by looking at the Bode plot of the continuous design, computed with `bode(sysol)` and plotted in Fig. 7.8. The designed phase margin in the continuous system is seen to be 51.8° . As was indicated in Chapter 4, the sample and hold can be roughly approximated by a delay of $T/2$ sec. At the crossover frequency of $\omega_{cp} = 0.8$ rad, and with sampling at $T = 0.2$, this corresponds only to $\phi = \omega_{cp}T = 4.5^\circ$. However, at $T = 1.0$, the sample-hold delay corresponds to $\phi = 23^\circ$. Thus the effective phase margin with a sample and hold is reduced to $Pm = 51.8^\circ - 23^\circ = 28.8^\circ$. With this small phase margin, the effective damping ratio is about 0.29 and the overshoot is expected to be about 0.4 rather than 0.16 as designed. The step response shows the actual $M_p = 0.5$, so most of the extra overshoot is explained by the sample-hold delay.

The examples presented here illustrate only a small selection of the alternatives for design by emulation. An immediate improvement would be expected if the continuous design were to include at the outset the characteristic $T/2$ delay of the sample and zero-order hold. Other than this modification, the other algorithms for discrete equivalent design can be tried. These include the very simple Euler rectangular rules, the bilinear transformations, and the several hold-equivalent methods. The triangle hold equivalent appears to be especially promising.¹ There does not seem to be a dominant technique that is best for every case. The designer needs to explore alternatives based on the particular system, the required performance specifications and the practical constraints introduced by the

¹In the MATLAB Control Toolbox function `c2d`, the triangle hold is called a first-order hold in recognition of the fact that it is a first-order hold although it is *noncausal*.

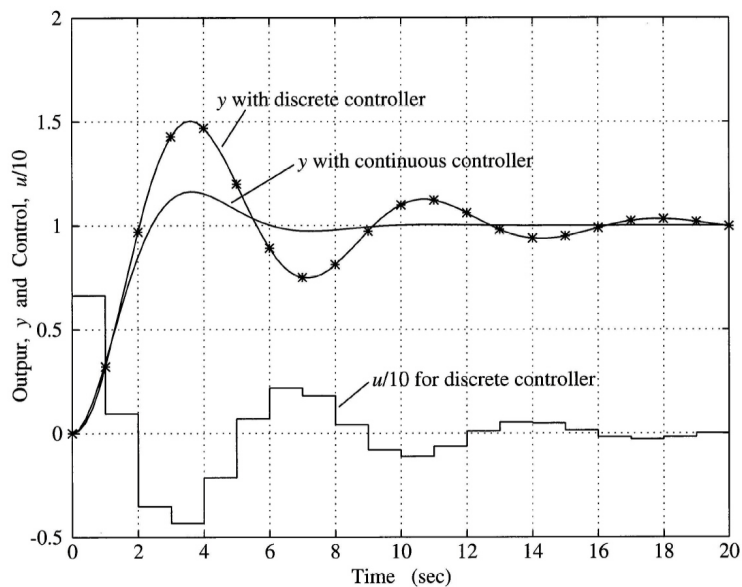


Figure 7.7
Step response of the 1-Hz controller

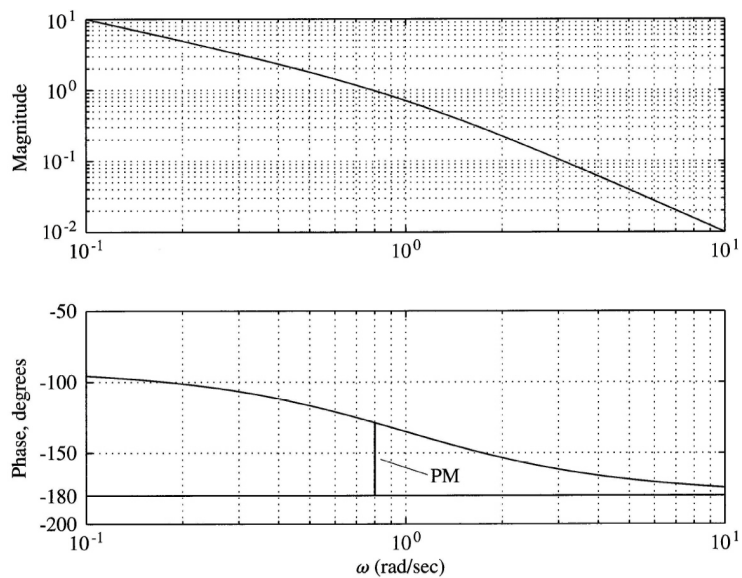


Figure 7.8
Bode plot of the continuous design for the antenna control

technology to be used for implementation to guide the final choice. Here we now turn to consider the direct discrete design methods, beginning with design by use of the root locus in the z -plane.

7.3 Direct Design by Root Locus in the z -Plane

The root locus introduced by W. Evans is based on graphical rules for plotting the roots of a polynomial as a parameter is varied. The most common root locus is a plot of the roots of a closed-loop characteristic polynomial in the s -plane as the loop gain is varied from 0 to ∞ . In linear discrete systems also the dynamic performance is largely determined by the roots of the closed-loop characteristic polynomial, in this case a polynomial in z with stability represented by having all roots inside the unit circle. The consequences for direct digital design are that one can use Evans' root locus rules unchanged, but that the performance specifications must first be translated into the z -plane.

7.3.1 z -Plane Specifications

Figure 4.26 is a map of the unit disk in the z -plane on which is superimposed discrete system time responses that correspond to several typical z -plane pole locations. These can be used to make the translation of dynamic response performance specifications to a region of acceptable pole locations. For example, we have seen that rise time of a continuous second-order system is found to be inversely proportional to natural frequency as given by Eq. (7.1). Since poles in the s -plane are mapped to $z = e^{sT}$, the natural frequency in s maps to the angle of the pole in polar coordinates in the z -plane as $\theta = \omega_d T$ where $\omega_d = \sqrt{1 - \zeta^2} \omega_n$. Settling time is found to be inversely proportional to the magnitude of the real part of a pole in the s -plane (σ) which maps to the *radius* of the pole in the z -plane as $r = e^{-\sigma T}$. The step response overshoot varies inversely with the damping ratio. Under the s -to- z mapping, lines of constant damping map into logarithmic spirals in the z -plane. With these guidelines, one can readily estimate the dynamic response parameters based on the pole-zero pattern for simple transfer functions and can derive useful guidelines for design of more complex systems. In summary, to get the specifications on acceptable pole locations in the z -plane

- Estimate the desired ω_n , ζ , and M_p from the continuous-time response specifications. Compute $\sigma = \zeta \omega_n$.
- Compute the radius $r = e^{-\sigma T}$.
- Obtain a plot of the z -plane showing lines of fixed damping and ω_n . The MATLAB command `zgrid` will do this, plotting ζ in steps of 0.1 from 0.1 to 0.9 and $\omega_n = N\pi/10T$ for integer N from 1 to 10. An example is shown in Fig. 7.9. The command `axis equal` will cause the unit circle to be plotted as a circle and the command `axis([-1 1 0 1])` will cause only the upper half of the circle to be plotted.
- Mark the region of acceptable closed-loop pole locations on the plane.

getting acceptable pole location in the z -plane

Z-Plane Specifications

Indicate on a z -plane map the region of acceptable closed-loop poles for the antenna design of Example 7.2.

Solution. The given specifications are that the system is to have a damping ratio of $\zeta \geq 0.5$, natural frequency of $\omega_n \geq 1$, and the real-parts of the roots are to be greater than 0.5. The standard grid of the z -plane shows the curve corresponding to $\zeta = 0.5$. With the requirement that the roots correspond to a natural frequency greater than $\omega_n = 1$, we need a plot on the standard grid corresponding to $N = 10T\omega_n/\pi = 2/\pi \approx 0.64$. The last requirement means that the roots in the z -plane must be inside a circle of radius $r \leq e^{-0.5T} = 0.9048$. The curves corresponding to these criteria are marked in Fig. 7.10.

Example 7.5

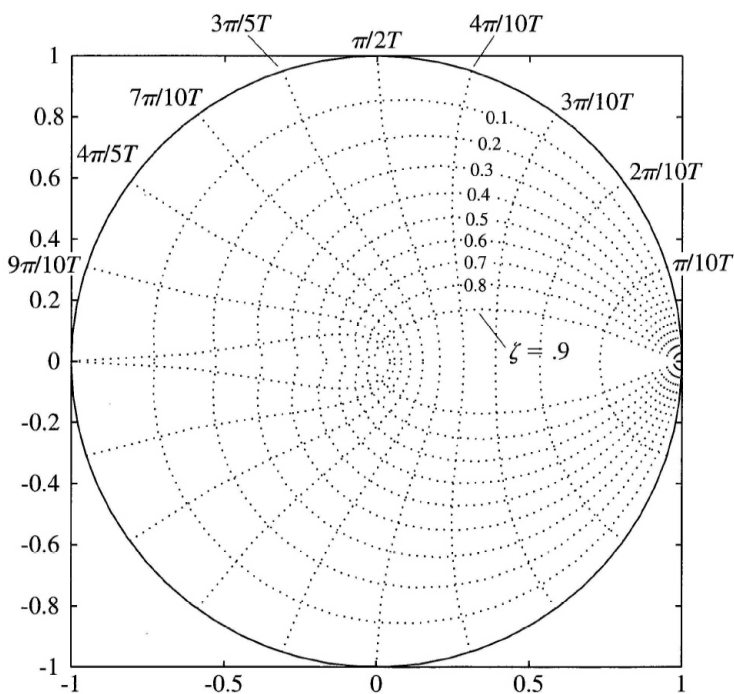


Figure 7.9
Lines of constant damping and natural frequency in the z -plane

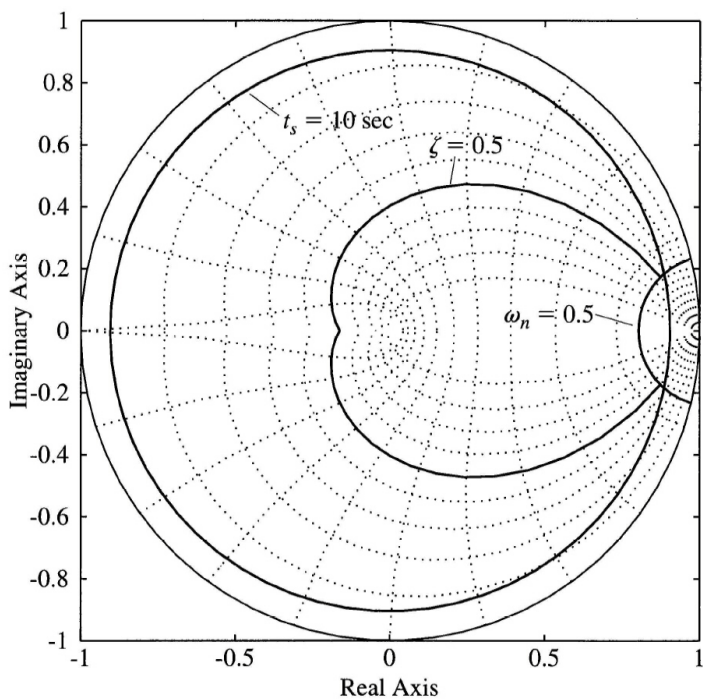


Figure 7.10
Plot of acceptable pole locations in the z -plane

The specification of steady-state error also follows the continuous case but transferred to the z -plane when the controller is implemented in a computer and represented by its discrete transfer function $D(z)$. The discrete transfer function of the plant is given by

$$G(z) = (1 - z^{-1})\mathcal{Z}\left\{\frac{G(s)}{s}\right\}. \quad (7.11)$$

The closed-loop system can now be represented in a purely discrete manner. The discrete transfer functions of the controller, $D(z)$, and the plant, $G(z)$, are combined as before according to Fig. 7.5, where it is now understood that the reference r and the disturbance w are sampled versions of their continuous counterparts. Proceeding as we did for the continuous system, suppose the input r is a step, $r(k) = 1(k)$, and the disturbance w is zero. The transform of the error is computed using the same block-diagram reduction tools that apply for continuous systems represented by their Laplace transforms, except that now we use $D(z)$ and $G(z)$. Doing this yields the transform of the error

$$\begin{aligned} E(z) &= \frac{R(z)}{1 + D(z)G(z)} \\ &= \frac{z}{z-1} \frac{1}{1 + D(z)G(z)}. \end{aligned}$$

The final value of $e(k)$, if the closed loop system is stable with all roots of $1 + DG = 0$ inside the unit circle, is, by Eq. (4.115) discrete time final value

$$\begin{aligned} e(\infty) &= \lim_{z \rightarrow 1} (z-1) \frac{z}{z-1} \frac{1}{1 + D(z)G(z)} \\ &= \frac{1}{1 + D(1)G(1)} \\ &= \frac{1}{1 + K_p}. \end{aligned} \quad (7.12)$$

Thus, $D(1)G(1)$ is the position error constant, K_p , of the Type 0 system in discrete time if the limit in Eq. (7.12) is finite. If DG has a pole at $z = 1$, then the error given by Eq. (7.12) is zero. Suppose there is a single pole at $z = 1$. Then we have a Type 1 system and we can compute the error to a unit ramp input, $r(kT) = kT1(kT)$ as discrete system type

$$E(z) = \frac{Tz}{(z-1)^2} \frac{1}{1 + D(z)G(z)}.$$

Now the steady-state error is

$$\begin{aligned} e(\infty) &= \lim_{z \rightarrow 1} (z-1) \frac{Tz}{(z-1)^2} \frac{1}{1 + DG} \\ &= \lim_{z \rightarrow 1} \frac{Tz}{(z-1)(1 + DG)} \\ &\triangleq \frac{1}{K_v}. \end{aligned} \quad (7.13)$$

Thus the **velocity constant** of a Type 1 discrete system with unity feedback (as shown in Fig. 7.5) is

$$K_v = \lim_{z \rightarrow 1} \frac{(z-1)(1 + D(z)G(z))}{Tz},$$

which simplifies to

$$K_v = \lim_{z \rightarrow 1} \frac{(z-1)D(z)G(z)}{Tz}. \quad (7.14)$$

Although it appears from Eq. (7.14) that K_v is inversely proportional to the sample period, this is not the case if comparing for the same $G(s)$. The reason is that the transfer function of $G(z)$

computed from Eq. (7.11) is typically proportional to the sample period. This proportionality is exact for the very simple case where $G(s) = 1/s$, as can be seen by using Eq. (7.11) and inspecting Entry 4 in Appendix B.2. For systems with a finite K_v and fast sample rates, this proportionality will be approximately correct. The result of this proportionality is that the dc gain of a continuous plant alone preceded by a ZOH is essentially the same as that of the continuous plant.

*Truxal's Rule, Discrete Case

Because systems of Type 1 occur frequently, it is useful to observe that the value of K_v is fixed by the *closed-loop* poles and zeros by a relation given, for the continuous case, by Truxal (1955). Suppose the overall transfer function Y/R is $H(z)$, and that $H(z)$ has poles p_i and zeros z_i . Then we can write

$$H(z) = K \frac{(z - z_1)(z - z_2) \cdots (z - z_n)}{(z - p_1)(z - p_2) \cdots (z - p_n)}. \quad (7.15)$$

Now suppose that $H(z)$ is the closed-loop transfer function that results from a Type 1 system, which implies that the steady-state error of this system to a step is zero and requires that

$$H(1) = 1. \quad (7.16)$$

Furthermore, by definition we can express the error to a ramp as

$$\begin{aligned} E(z) &= R(z)(1 - H(z)) \\ &= \frac{Tz}{(z-1)^2}(1 - H(z)), \end{aligned}$$

and the final value of this error is given by

$$e(\infty) = \lim_{z \rightarrow 1} (z-1) \frac{Tz}{(z-1)^2} (1 - H(z)) \triangleq \frac{1}{K_v};$$

therefore (omitting a factor of z in the numerator, which makes no difference in the result)

$$\frac{1}{TK_v} = \lim_{z \rightarrow 1} \frac{1 - H(z)}{z - 1}. \quad (7.17)$$

Because of Eq. (7.16), the limit in Eq. (7.17) is indeterminate, and so we can use L'Hôpital's rule

$$\begin{aligned} \frac{1}{TK_v} &= \lim_{z \rightarrow 1} \frac{(d/dz)(1 - H(z))}{(d/dz)(z - 1)} \\ &= \lim_{z \rightarrow 1} \left\{ -\frac{dH(z)}{dz} \right\}. \end{aligned}$$

However, note that by using Eq. (7.16) again, at $z = 1$, we have

$$\frac{d}{dz} \ln H(z) = \frac{1}{H} \frac{d}{dz} H(z) = \frac{d}{dz} H(z),$$

so that

$$\begin{aligned} \frac{1}{TK_v} &= \lim_{z \rightarrow 1} -\frac{d}{dz} \ln H(z) \\ &= \lim_{z \rightarrow 1} -\frac{d}{dz} \left\{ \ln K \frac{\prod(z - z_i)}{\prod(z - p_i)} \right\} \\ &= \lim_{z \rightarrow 1} -\frac{d}{dz} \left\{ \sum \ln(z - z_i) - \sum \ln(z - p_i) + \ln K \right\} \\ &= \lim_{z \rightarrow 1} \left\{ \sum \frac{1}{z - p_i} - \sum \frac{1}{z - z_i} \right\} \\ &= \sum_{i=1}^n \frac{1}{1 - p_i} - \sum_{i=1}^n \frac{1}{1 - z_i}. \end{aligned}$$

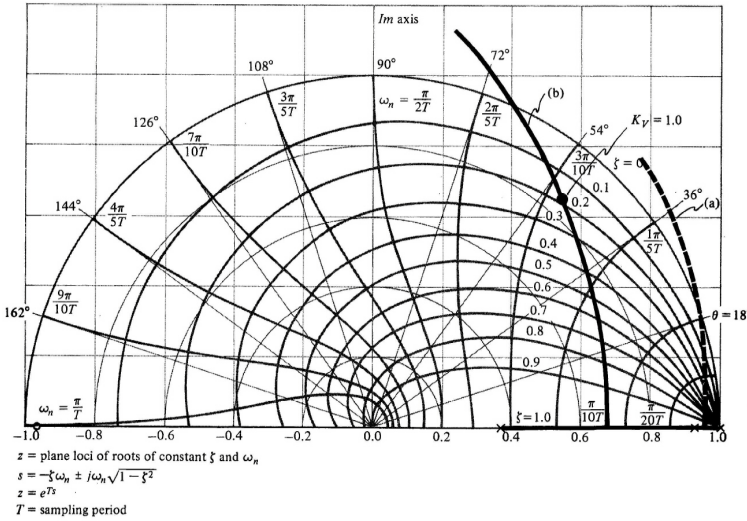


Figure 7.11
 Root loci for antenna design: (a) Uncompensated system; (b) Locus with $D(z)$ having the poles and zeros of Eq. (7.10)

We note especially that the farther the *poles* of the closed-loop system are from $z = 1$, the larger the velocity constant and the smaller the errors. Similarly, K_v can be increased and the errors decreased by *zeros close* to $z = 1$. From the results of Chapter 4 on dynamic response, we recall that a zero close to $z = 1$ usually yields large overshoot and poor dynamic response. Thus is expressed one of the classic trade-off situations: We must balance small steady-state errors against good transient response.

7.3.2 The Discrete Root Locus

The root locus is the locus of points where roots of a characteristic equation can be found as some real parameter varies from zero to large values. From Fig. 7.5 and block-diagram analysis, the characteristic equation of the single-loop system is

$$1 + D(z)G(z) = 0. \tag{7.18}$$

The significant thing about Eq. (7.18) is that this is exactly the same equation as that found for the s -plane root locus. The implication is that the *mechanics* of drawing the root loci are exactly the same in the z -plane as in the s -plane; the rules for the locus to be on the real axis, for asymptote construction, and for arrival/departure angles are all unchanged from those developed for the s -plane and reviewed in Chapter 2. As mentioned earlier, the difference lies in the interpretation of the results because the pole locations in the z -plane mean different things than pole locations in the s -plane when we come to interpret system stability and dynamic response.

Discrete Root Locus Design

Example 7.6

Design the antenna system for the slow sampling case with $T = 1$ sec. using the discrete root locus.

Solution. The exact discrete model of the plant plus hold is given by the $G(z)$ in Eq. (7.9). If the controller consisted simply of a proportional gain [$D(z) = K$], the locus of roots versus K can be found by solving the characteristic equation

$$1 + 0.0484K \frac{z + 0.9672}{(z - 1)(z - 0.9048)} = 0$$

for many values of K . The result computed by `rlocus(antd)` is shown in Fig. 7.11 as the dashed arc marked (a). From study of the root locus we should remember that this locus, with two poles and one zero, is a circle centered at the zero ($z = -0.9672$) and breaking away from the real axis between the two real poles.

From the root locus of the uncompensated system (Fig. 7.11(a)) it is clear that some dynamic compensation is required if we are to get satisfactory response from this system. The radius of the roots never gets less than

0.95, preventing the t_s specification from being met. The system goes unstable at $K \cong 19$ [where $K_v = 0.92$, as can be verified by using Eq. (7.14)], which means that there is no stable value of gain that meets the steady-state error specification with this compensation.

If we cancel the plant pole at 0.9048 with a zero and add a pole at 0.3679, we are using the lead compensation of Eq. (7.10). The root locus for this control versus the gain K [K was equal to 6.64 in Eq. (7.10)] computed with `rlocus(sysold)` is also sketched in Fig. 7.11 as the solid curve (b). The points, p , where $K = 6.64$ are computed with `p = rlocus(sysold,6.64)` and marked by dots. We can see that a damping ratio of about 0.2 is to be expected, as we have previously seen from the step response of Fig. 7.7. This gain, however, does result in the specified value of $K_v = 1$ because this criterion was used in arriving at Eq. (7.10). The locus shows that increasing the gain, K , would lower the damping ratio still further. Better damping could be achieved by decreasing the gain, but then the criterion of steady-state error would be violated. It is therefore clear that this choice of compensation pole and zero cannot meet the specifications.

A better choice of compensation can be expected if we transform the specifications into the z -plane and select the compensation so that the closed loop roots meet those values. The original specifications were $K_v \geq 1$, $t_s \leq 10$ sec, and $\zeta \geq 0.5$. If we transform the specifications to the z -plane we compute that the t_s specification requires that the roots be inside the radius $r = e^{-0.5} = 0.61$, and the overshoot requires that the roots are inside the $\zeta = 0.5$ spiral. The requirement that $K_v \geq 1$ applies in either plane but is computed by Eq. (7.14) for the z -plane.

It is typically advantageous to use the design obtained using emulation and to modify it using discrete design methods so that it is acceptable. The problem with the emulation-based design is that the damping is too low at the mandated gain, a situation that is typically remedied by adding more lead in the compensation. More lead is obtained in the s -plane by increasing the separation between the compensation's pole and zero; and the same holds true in the z -plane. Therefore, for a first try, let's keep the zero where it is (canceling the plant pole) and move the compensation pole to the left until the roots and K_v are acceptable. After a few trials, we find that there is no pole location that satisfies all the requirements! Although moving the pole to the left of $z \cong 0$ will produce acceptable z -plane pole locations, the gain K_v is not sufficiently high to meet the criterion for steady-state error. The only way to raise K_v and to meet the requirements for damping and settling time is to move the zero to the left also.

After some trial and error, we see that

$$D(z) = 6 \frac{z - 0.80}{z - 0.05} \quad (7.19)$$

meets the required z -plane constraints for the complex roots and has a $K_v = 1.26$. The root locus for Eq. (7.19) is shown in Fig. 7.12(a), and the roots corresponding to $K = 6$ are marked by squares. The fact that all requirements seem to be met is encouraging, but there is an additional real root at $z = 0.74$ and a zero at $z = 0.8$, which may degrade the actual response from that expected if it were a second-order system. The actual time history is shown in Fig. 7.12(b). It shows that the overshoot is 29% and the settling time is 15 sec. Therefore, further iteration is required to improve the damping and to prevent the real root from slowing down the response.

A compensation that achieves the desired result is

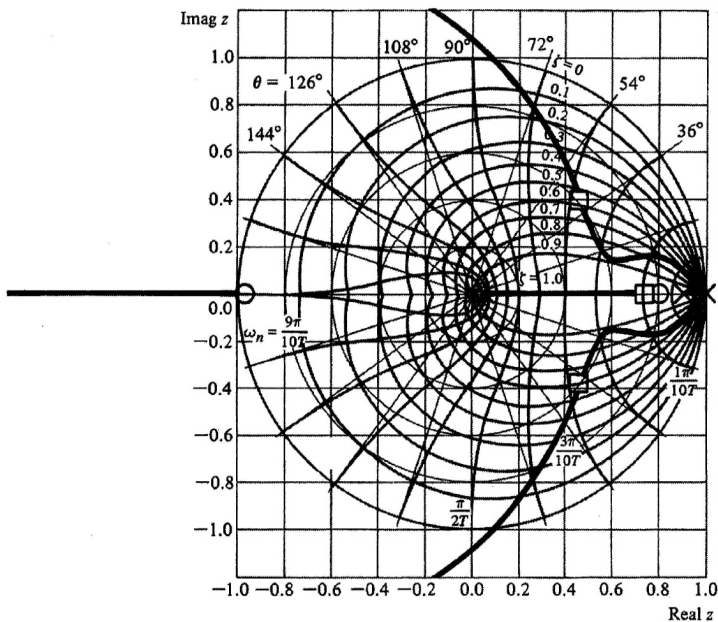
$$D(z) = 13 \frac{z - 0.88}{z + 0.5}. \quad (7.20)$$

The damping and radius of the complex roots substantially exceed the specified limits, and $K_v = 1.04$. Although the real root is slower than the previous design, it is very close to a zero that attenuates its contribution to the response. The root locus for all K 's is shown in Fig. 7.13(a) and the time response for $K = 13$ in Fig. 7.13(b).

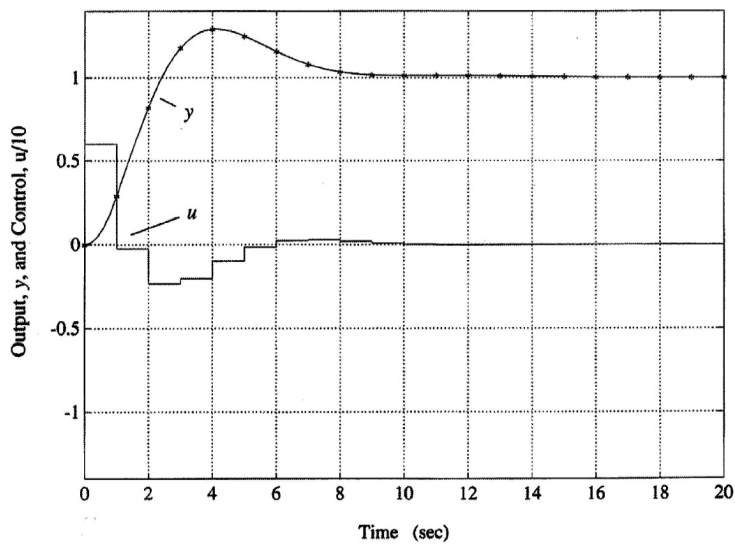
Note that the pole of Eq. (7.20) is on the negative real z -plane axis. In general, placement of poles on the negative real axis should be done with some caution. In this case, however, no adverse effects resulted because all roots were in well-damped locations. As an example of what could happen, consider the compensation

$$D(z) = 9 \frac{(z - 0.8)}{(z + 0.8)}. \quad (7.21)$$

The root locus versus K and the step response are shown in Fig. 7.14. All roots are real with one root at $z = -0.59$. But this negative real axis root has $\zeta = 0.2$ and represents a damped sinusoid with frequency of $\omega_s/2$. The output has very low overshoot, comes very close to meeting the settling time specification, and has $K_v = 1$; however, the control, u , has large oscillations with a damping and frequency consistent with the negative real root. This indicates that there are "hidden oscillations" or "intersample ripple" in the output that are only apparent by computing the continuous plant output between sample points as is done in Fig. 7.14. The computation of the intersample behavior was carried out by computing it at a much higher sample rate than the

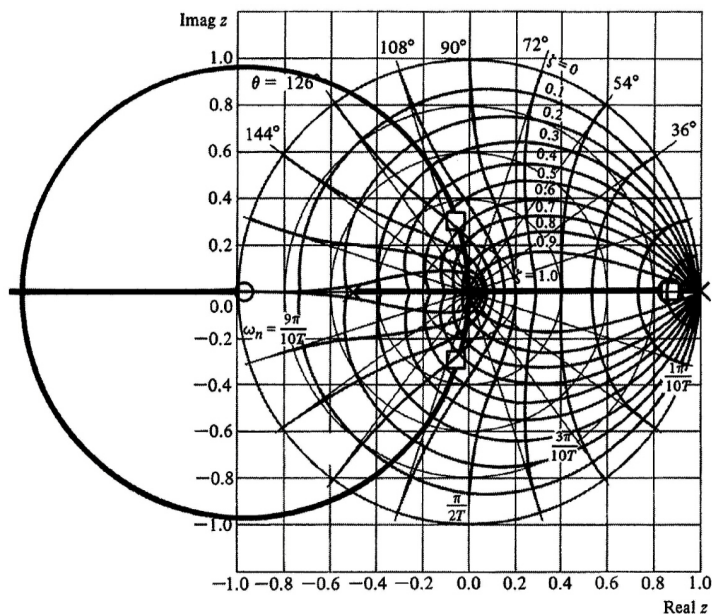


(a)

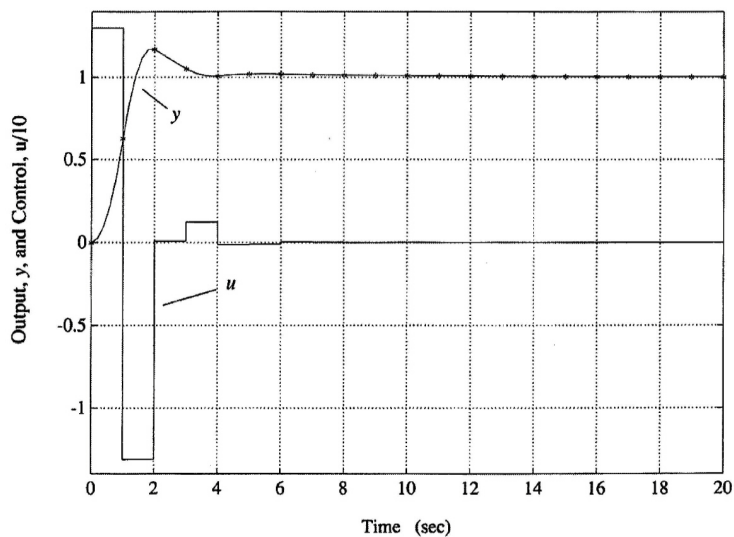


(b)

Figure 7.12
Antenna design
with $D(z)$ given
by Eq. (7.19):
(a) root locus,
(b) step response

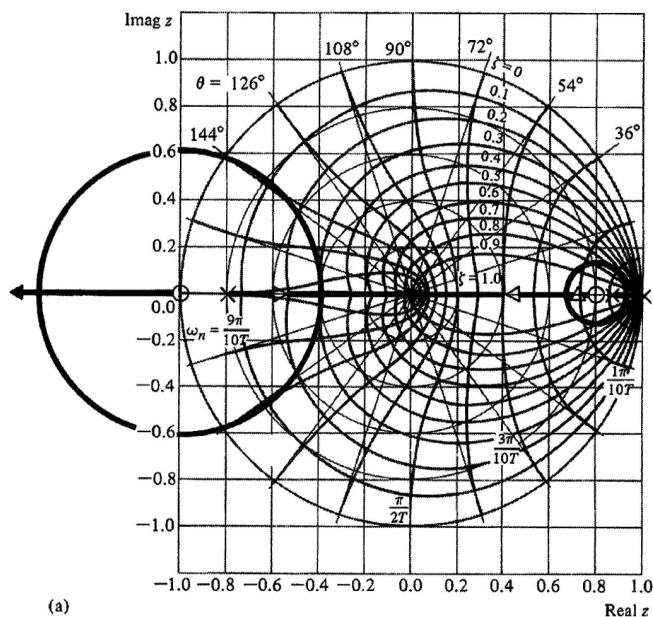


(a)

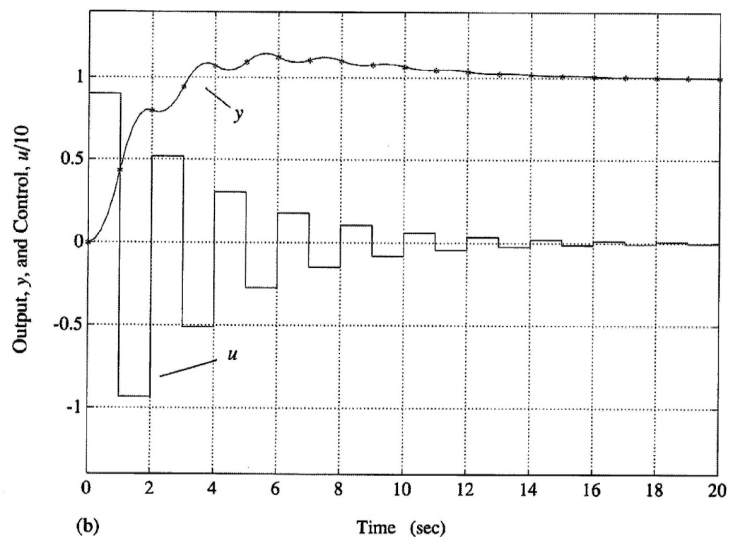


(b)

Figure 7.13
Antenna design with $D(z)$ given by Eq. (7.20):
(a) root locus,
(b) step response



(a)



(b)

Figure 7.14
Antenna design with $D(z)$ given by Eq. (7.21):
(a) root locus,
(b) step response

digital controller, taking care that the control value was constant throughout the controller sample period. The MATLAB function `ripple`, included in the Digital Control Toolbox, has been written to do these calculations. Note that if only the output at the sample points had been determined, the system would appear to have very good response. This design uses much more control effort than that shown in Fig. 7.13, a fact that is usually very undesirable. So we see that a compensation pole in a lightly damped location on the negative real axis could lead to a poorly damped system pole and undesirable performance.

In the design examples to this point, the computed output time histories have assumed that the control, $u(k)$, was available from the computer at the sample instant. However, in a real system this is not always true. In the control implementation example in Table 3.1, we see that some time must pass between the sample of $y(k)$ and the output of $u(k)$ for the computer to calculate the value of $u(k)$. This time delay is called **latency** and usually can be kept to a small fraction of the sample period with good programming and computer design. Its effect on performance can be evaluated precisely using the transform analysis of Section 4.4.2, the state-space analysis of Section 4.3.4, or the frequency response. The designer can usually determine the expected delay and account for it in the design. However, if not taken into account, the results can be serious as can be seen by an analysis using the root locus.

Because a one-cycle delay has a z -transform of z^{-1} , the effect of a full-cycle delay can be analyzed by adding z^{-1} to the numerator of the controller representation. This will result in an additional pole at the origin of the z -plane. If there is a delay of two cycles, two poles will be added to the z -plane origin, and so on.

Effect of Unexpected Delay

Add one cycle delay to the compensation of Eq. (7.21) and plot the resulting root locus and step response.

Solution. The new controller representation is

$$D(z) = 13 \frac{z - 0.88}{z(z + 0.5)}. \quad (7.22)$$

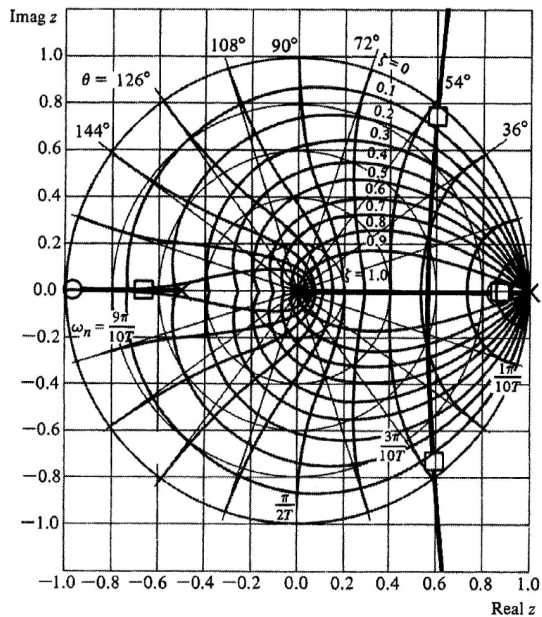
The root locus and time response are shown in Fig. 7.15, which are both substantially changed from the same controller without the delay as shown in Fig. 7.13. The only difference is the new pole at $z = 0$. The severity of the one-cycle delay is due to the fact that this controller is operating at a very slow sample rate (six times the closed loop bandwidth). This sensitivity to delays is one of many reasons why one would prefer to avoid sampling at this slow a rate.

Example 7.7

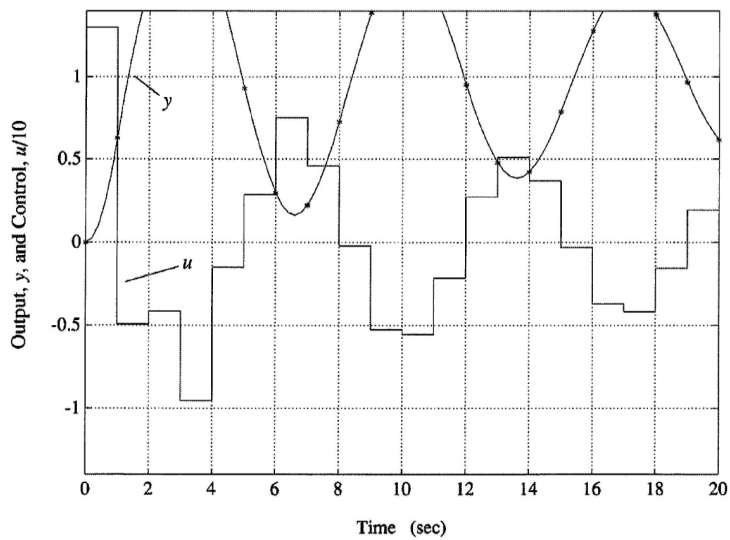
7.4 Frequency Response Methods

The frequency response methods for continuous control system design were developed from the original work of Bode (1945) on feedback-amplifier techniques. Their attractiveness for design of continuous linear feedback systems depends on several ideas.

1. The gain and phase curves for a rational transfer function can be easily plotted *by hand*.
2. If a physical realization of the system is available, the frequency response can be measured experimentally without the necessity of having a mathematical model at all.
3. Nyquist's stability criterion can be applied, and dynamic response specifications can be readily interpreted in terms of gain and phase margins, which are easily seen on the plot of log gain and phase-versus-log frequency.



(a)



(b)

Figure 7.15
One-cycle-delay antenna design with $D(z)$ given by Eq. (7.22):
(a) root locus,
(b) step response

4. The system error constants, mainly K_p or K_v , can be read directly from the low-frequency asymptote of the gain plot.
5. The corrections to the gain and phase curves (and thus the corrections in the gain and phase margins) introduced by a trial pole or zero of a compensator can be quickly and easily computed, *using the gain curve alone*.
6. The effect of pole, zero, or gain changes of a compensator on the speed of response (which is proportional to the crossover frequency) can be quickly and easily determined *using the gain curve alone*.

Use of the frequency response in the design of continuous systems has been reviewed in Chapter 2 and the idea of discrete frequency responses has been introduced in Chapter 4. In order to apply these concepts to the design of digital controls, the basic results on stability and performance must be translated to the discrete domain. The concepts are the same as for continuous systems, but plots of the magnitude and phase of a discrete transfer function, $H(z)$, are accomplished by letting z take on values around the unit circle, $z = e^{j\omega T}$, that is,

$$\begin{aligned} \text{magnitude} &= |H(z)|_{e^{j\omega T}}, \\ \text{phase} &= \angle H(z)|_{e^{j\omega T}}. \end{aligned}$$

Discrete Bode Plot

Example 7.8

Plot the discrete frequency response corresponding to the plant transfer function

$$G(s) = \frac{1}{s(s+1)} \quad (7.23)$$

sampling with a zero order hold at $T = 0.2, 1, \text{ and } 2$ seconds and compare with the continuous response.

Solution. The discrete transfer functions for the specified sampling periods are computed with `c2d.m` as

```
sysc = tf([1],[1 1 0])
sysd1 = c2d(sysc,0.2)
sysd2 = c2d(sysc,1)
sysd3 = c2d(sysc,2)
```

with transfer functions

$$\begin{aligned} G_1(z) &= 0.0187 \frac{z+0.9355}{(z-1)(z-0.8187)} \quad \text{for } T = 0.2 \text{ sec} \\ G_2(z) &= 0.368 \frac{z+0.718}{(z-1)(z-0.368)} \quad \text{for } T = 1 \text{ sec} \\ G_3(z) &= 1.135 \frac{z+0.523}{(z-1)(z-0.135)} \quad \text{for } T = 2 \text{ sec}. \end{aligned} \quad (7.24)$$

The frequency responses of Eq. (7.23) and Eq. (7.24) are plotted in Fig. 7.16 using the statement `bode(sysc,'-',sysd1,'-.',sysd2,':',sysd3,'-')`

It is clear that the curves for the discrete systems are nearly coincident with the continuous plot for low frequencies but deviate substantially as the frequency approaches π/T in each case. In particular, the amplitude plots do not approach the simple asymptotes used in the hand-plotting procedures developed by Bode, and his theorem relating the phase to the derivative of the magnitude curve on a log-log plot does not apply. The primary effect of sampling is to cause an additional phase lag.

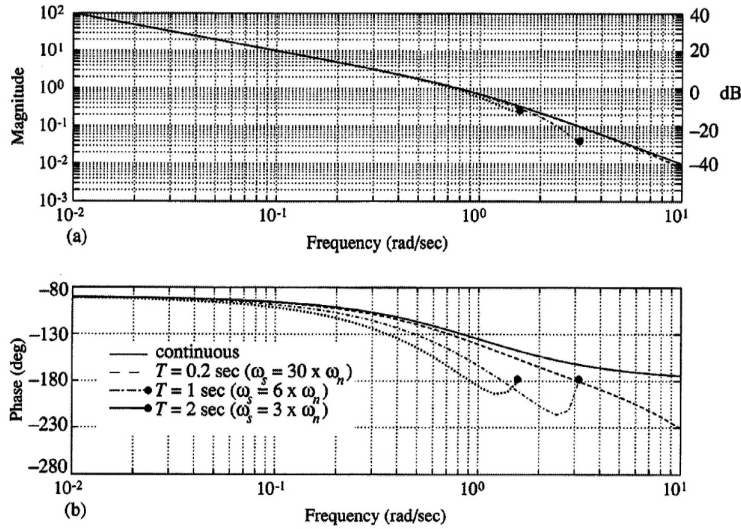


Figure 7.16
Frequency responses of continuous and discrete transfer functions

Fig. 7.17 shows this additional phase lag by plotting the phase difference, $\Delta\phi$, between the continuous case and the discrete cases. The approximation to the discrete phase lag given by

$$\Delta\phi = \frac{\omega T}{2} \tag{7.25}$$

is also shown and demonstrates the accuracy of this approximation for sample rates up to $\omega T = \pi/2$, which corresponds to frequencies up to 1/4 the sample rate. Crossover frequencies (where magnitude = 1) for designs will almost always be lower than 1/4 the sample rate; therefore, one can obtain a good estimate of the phase margin if a sample and hold is introduced into a continuous design by simply subtracting the factor $\omega T/2$ from the phase of the continuous design's phase margin.

The inability to use the standard plotting guidelines detracts from the ease with which a designer can predict the effect of pole and zero changes on the frequency response. Therefore, points 1, 5, and 6 above are less true for discrete frequency-response design using the z -transform than they are for continuous systems and we are more dependent on computer aids in the discrete case. With some care in the interpretations however, points 2, 3, and 4 are essentially unchanged. All these points will be discussed further in this chapter as they pertain to design using the *discrete* frequency response. We begin with the discrete form of the **Nyquist stability criterion** and follow with a discussion of specifications of performance and stability robustness as expressed in the frequency domain before we introduce the design techniques directly.

Nyquist stability criterion

7.4.1 Nyquist Stability Criterion

For continuous systems, the Nyquist stability criterion seeks to determine whether there are any zeros of the closed-loop characteristic equation

$$1 + KD(s)G(s) = 0 \tag{7.26}$$

in the right half-plane. The method establishes stability by determining the excess of zeros over poles of the characteristic equation in the right-half plane by plotting $KD(s)G(s)$ for s along the \mathcal{D} contour that encloses the entire right-hand side (unstable region) of the s -plane as sketched in Fig. 7.18(a).

It is assumed that the designer *knows* the number of (unstable) poles that are inside the contour and from the plot can then determine the number of zeros of Eq. (7.26) in the unstable region that is the same as the number of closed-loop system unstable poles. The entire contour evaluation is fixed by examining $KD(s)G(s)$ over $s = j\omega$ for $0 \leq \omega < \infty$, which is the frequency-response evaluation of the open-loop system. For experimental data, the plot is to be made for $\omega_{low} \leq \omega \leq \omega_{high}$, where

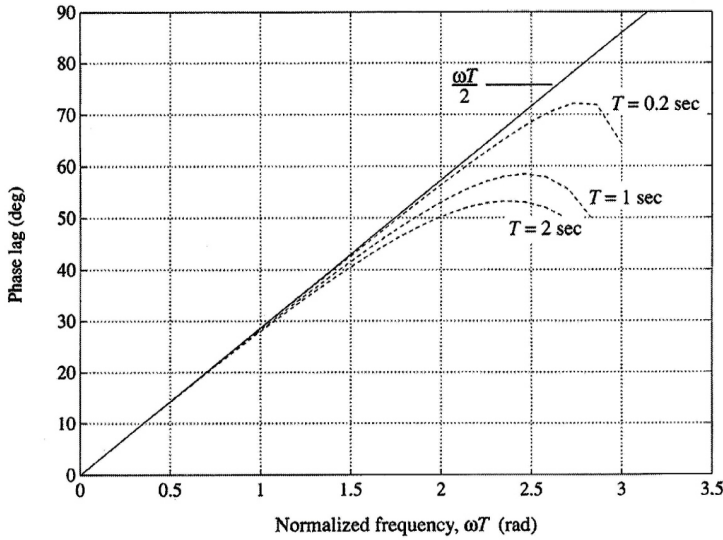


Figure 7.17
Phase lag due to
sampling

ω_{low} is small enough to allow the low-frequency behavior to be decided (usually the gain is very high at ω_{low} and the phase is approaching a fixed multiple of 90°), and where ω_{high} is taken to be high enough that it is known that the magnitude is much less than 1 for all higher frequencies. Fig. 7.18(a) shows the full \mathcal{D} contour and the portion of the contour for $\omega_{low} \leq \omega \leq \omega_{high}$. The indentation near $\omega = 0$ excludes the (known) poles of KDG at $s = 0$ from the unstable region; the map of this small semicircle is done analytically by letting $s = r^{j\phi}$ for $r \ll 1$, $-\frac{\pi}{2} \leq \phi \leq \frac{\pi}{2}$.

The specific statement of the Nyquist stability criterion for continuous systems is

$$Z = P + N, \quad (7.27)$$

where

- Z = the number of unstable zeros of Eq. (7.26) (that are unstable closed-loop poles). For stability, $Z = 0$.
- P = the number of unstable (open-loop) poles of $KD(s)G(s)$.
- N = the net number of encirclements of the -1 point for the contour evaluation of $KD(s)G(s)$ in the *same direction* as that taken by s along \mathcal{D} as shown in Fig 7.18(a). Usually s is taken clockwise around \mathcal{D} and therefore clockwise encirclements are taken as positive.

For the common case of a stable open-loop system ($P = 0$) the closed-loop system is stable if and only if the contour evaluation of $KD(s)G(s)$ does not encircle the -1 point. For unstable open-loop systems, the closed-loop system is stable if and only if the contour evaluation encircles the -1 point counter to the s direction as many times as there are unstable open-loop poles ($N = -P$ in Eq. (7.27)). The proof of this criterion relies on Cauchy's principle of the argument and is given in most introductory textbooks on continuous control systems. The elementary interpretation is based on the following points:

- If we take values of s on a contour in the s -plane that encloses the unstable region, we can plot the corresponding values of the function $1 + KD(s)G(s)$ in an image plane.
- If the s -plane contour encircles a *zero* of $1 + KD(s)G(s)$ in a certain direction, the image contour will encircle the origin in the *same* direction. In the s -plane, the angle of the vector from the zero to s on the contour goes through 360° .

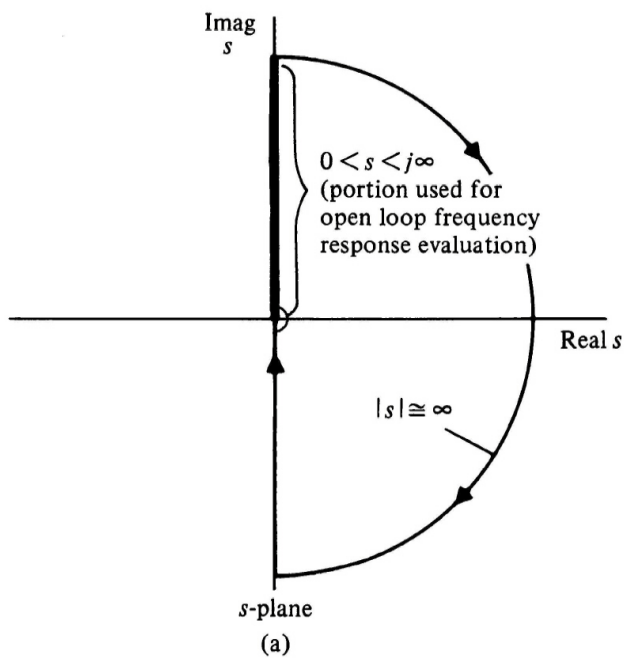
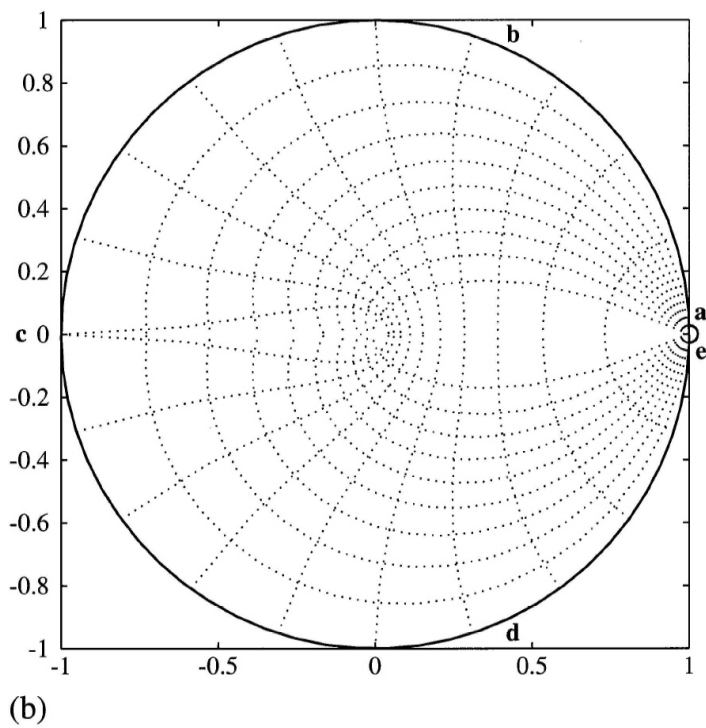


Figure 7.18
Contours used for Nyquist stability criterion: (a) In the s -plane; (b) In the z -plane



- If the s -plane contour encircles a *pole* of $1 + KDG$, the image contour will encircle the origin in the *opposite direction*. In this case, the s -plane vector angle also goes through 360° but the contribution to the image angle is a negative 360° .
- Thus the *net* number of same-direction encirclements, N , equals the difference $N = Z - P$.²
- The origin of the $1 + KDG$ plane is the same as the point $KDG = -1$ so we can plot KDG and count N as the encirclements of the -1 point just as well.³
- From all of this, Eq. (7.27) follows immediately.

For the discrete case, the ideas are identical; the only difference is that the unstable region of the z -plane is the *outside* of the unit circle and it is awkward to visualize a contour that encloses this region. The problem can be avoided by the simple device of considering the encirclement of the *stable* region and calculating the stability result from that. The characteristic equation of the discrete system is written as

$$1 + KD(z)G(z) = 0, \quad (7.28)$$

and, as in the continuous case, it is assumed that the number, P , of unstable poles of $KD(z)G(z)$, which are also unstable poles of $1 + KD(z)G(z)$, is known and we wish to determine the number, Z , of unstable zeros of Eq. (7.28), which are the unstable closed-loop poles. Examination of Eq. (7.28) reveals that the (possibly unknown) total number of stable plus unstable poles, n , is the same as the total number of zeros of Eq. (7.28). Thus the number of *stable* zeros is $n - Z$ and the number of *stable* poles is $n - P$. Following the mapping result used by Nyquist, the map of $1 + KD(z)G(z)$ for the z contour of Fig. 7.18(b) will encircle the origin N times where

$$\begin{aligned} N &= \{\text{number of stable zeros}\} - \{\text{number of stable poles}\} \\ &= \{n - Z\} - \{n - P\} \\ &= P - Z. \end{aligned}$$

Therefore, the Nyquist stability criterion for discrete systems is

$$Z = P - N. \quad (7.29)$$

In summary, the discrete Nyquist stability criterion is

- Determine the number, P , of unstable poles of KDG .
- Plot $KD(z)G(z)$ for the unit circle, $z = e^{j\omega T}$ and $0 \leq \omega T \leq 2\pi$. This is a counter-clockwise path around the unit circle. Points for the plot can be conveniently taken from a discrete Bode plot of KDG .
- Set N equal to the net number of counter-clockwise (same direction) encirclements of the point -1 on the plot.
- Compute $Z = P - N$. The system is stable if and only if $Z = 0$.

Nyquist Stability

Example 7.9

Evaluate the stability of the unity feedback discrete system with the plant transfer function

$$G(s) = \frac{1}{s(s+1)}, \quad (7.30)$$

with sampling at the rate of 1/2 Hz or $T = 2$ and zero-order hold. The controller is proportional discrete feedback [$KD(z) = K$].

²It is much easier to remember same-direction and opposite-direction encirclements than to keep clockwise and counter-clockwise distinguished.

³When the characteristic equation is written as $1 + KDG$, we can plot only DG and count encirclements of $DG = -\frac{1}{K}$ and thus easily consider the effects of K on stability and stability margins.

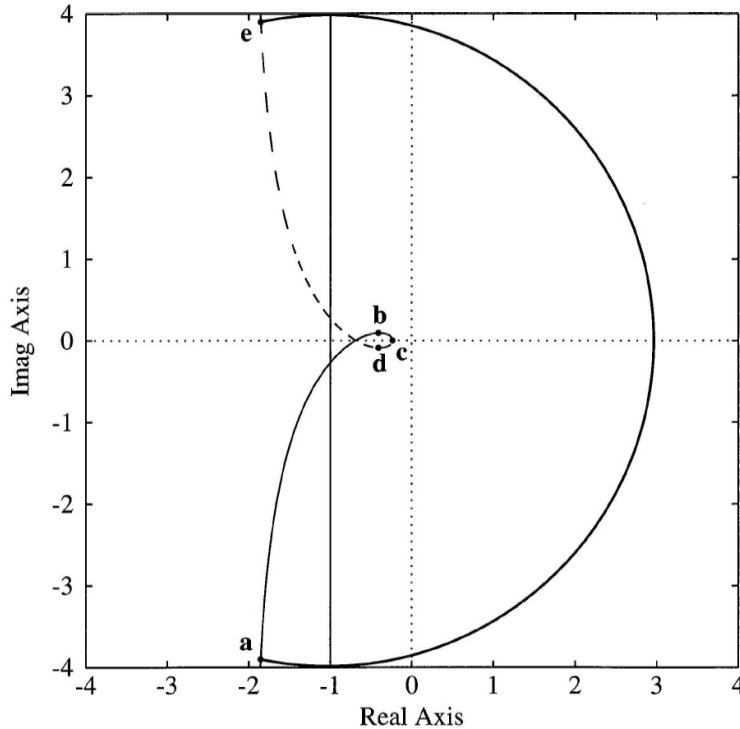


Figure 7.19
Nyquist plot of
Example 7.9

Solution. The discrete transfer function at the specified sampling rate and ZOH is given by `sysd3` of Example 7.8 with transfer function

$$G(z) = \frac{1.135(z+0.523)}{(z-1)(z-0.135)}, \quad (7.31)$$

and the plot of magnitude and phase of $G(z)$ for $z = e^{j\omega T}$ is included in Fig. 7.16 for $0 \leq \omega T \leq \pi$. Using the data from Fig. 7.16 for $T = 2$, the plot of $KD(z)G(z)$ can be drawn as shown in Fig. 7.19. The plot is marked with corresponding points from Fig. 7.18(b) to facilitate understanding the results. Note that the portion from $a \rightarrow b \rightarrow c$ is directly from Fig. 7.16, and the section from $c \rightarrow d \rightarrow e$ is the same information reflected about the real axis. The large semicircle from $e \rightarrow a$ is the analytically drawn map of the small semicircle about $z = 1$ drawn by letting $(z-1) = re^{j\phi}$ in Eq. (7.31) for $r \ll 1$ and $-\frac{\pi}{2} \leq \phi \leq \frac{\pi}{2}$. Because this system is open-loop stable and there are no -1 point encirclements, we conclude that the closed-loop system will be stable as plotted for $K = 1$. Note that all the necessary information to determine stability is contained in the Bode plot information from Fig. 7.16, which determines the portion from $a \rightarrow c$ in Fig. 7.19. Using MATLAB, the plot can be made by the statements

```
nyquist(sysd3)
axis equal
grid
```

The `axis` statement sets the x and y axes to have equal increments.

7.4.2 Design Specifications in the Frequency Domain

Gain and Phase Margins

The Nyquist plot shows the number of encirclements and thus the stability of the closed-loop system. Gain and phase margins are defined so as to provide a two-point measure of how close the Nyquist plot is to encircling the -1 point, and they are identical to the definitions developed for continuous systems. **Gain margin** (GM) is the factor by which the gain can be increased before causing the gain margin

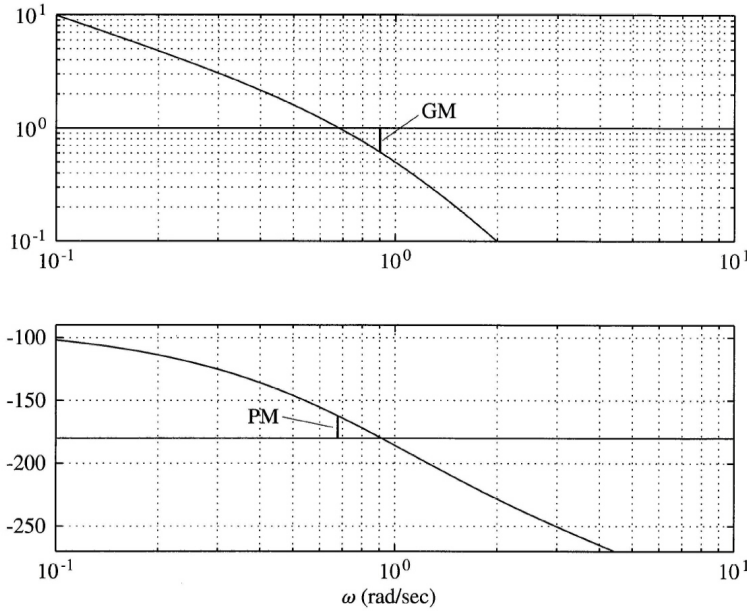


Figure 7.20
Gain and phase margins on a Bode plot for Example 7.10

system to go unstable, and is usually the inverse of the magnitude of $D(z)G(z)$ when its phase is 180° . The **phase margin (PM)** is the difference between -180° and the phase of $D(z)G(z)$ when its amplitude is 1. The PM is a measure of how much additional phase lag or time delay can be tolerated in the loop before instability results.

Stability Margins

Example 7.10

Consider the open-loop transfer function

$$G(s) = \frac{1}{s(s+1)^2},$$

with ZOH and sample rate of 5 Hz. The discrete transfer function is given by

$$G(z) = 0.0012 \frac{(z+3.38)(z+0.242)}{(z-1)(z-0.8187)^2}.$$

What are the gain and phase margins when in a loop with proportional discrete feedback ($D(z) = K = 1$)?

Solution. The discrete Bode plot is given in Fig. 7.20 and the portion of the Nyquist plot representing the frequency response in the vicinity of -1 is plotted in Fig. 7.21. Unlike Example 7 which had a very slow sample rate, the higher sample rate here causes the magnitude to be essentially zero at $\omega T = \pi$, and hence the Nyquist plot goes almost to the origin. The plot is very similar to what would result for a continuous controller. Furthermore, just as in the continuous case, there are no -1 point encirclements if $K = 1$ as plotted ($N = 0$), and since there are no unstable poles ($P = 0$), the system will be stable at this gain ($Z = 0$). If the Nyquist plot is multiplied by 1.8, then the plot will go through the -1 point. Thus the gain margin is $GM = 1.8$. For values of $K > 1.8$, the -1 point lies within the contour thus creating two encirclements ($N = 2$) and two unstable closed-loop poles ($Z = 2$). As indicated on the plot, the angle of the plot when the gain is 1 is 18° from the negative axis, so the phase margin is 18° .

For continuous systems, it has been observed that the phase margin, PM , is related to the damping ratio, ζ , for a second-order system by the approximate relation, $\zeta \cong PM/100$. This relationship is examined in Fig. 7.22 for the continuous case and for discrete systems with two values of the sample ratio

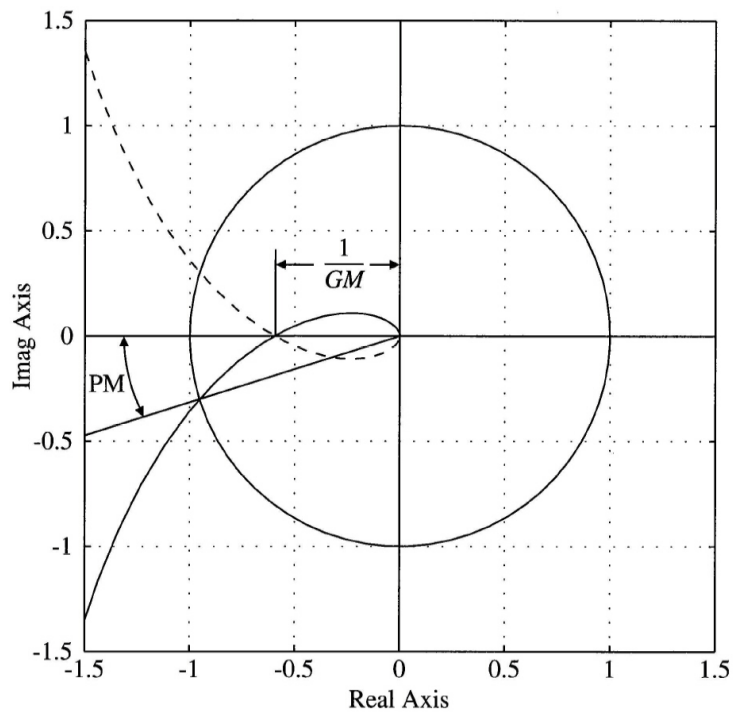


Figure 7.21
Gain and phase margins on a Nyquist plot for Example 7.10

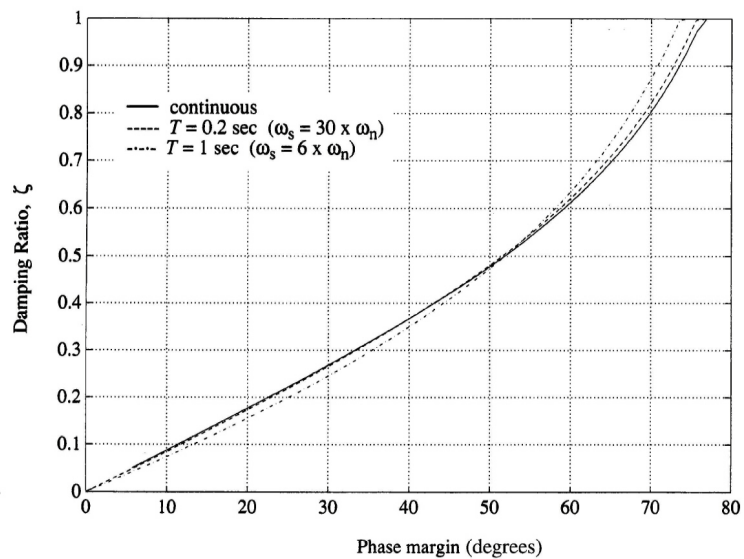


Figure 7.22
Damping ratio of a second-order system versus phase margin (PM)

rate. Figure 7.22 was generated by evaluating the damping ratio of the closed-loop system that resulted when discrete proportional feedback was used with the open-loop system

$$G(s) = \frac{1}{s(s+1)}.$$

A z -transform analysis of this system resulted in z -plane roots that were then transformed back to the s -plane via the inverse of $z = e^{sT}$. The ζ of the resulting s -plane roots are plotted in the figure. As the feedback gain was varied, the damping ratio and phase margin were related as shown in Fig. 7.22. The actual sample rates used in the figure are 1 Hz and 5 Hz, which represent 6 and 30 times the open-loop system pole at 1 rad/sec. The conclusion to be drawn from Fig. 7.22 is that the PM from a discrete z -plane frequency response analysis carries essentially the same implications about the damping ratio of the closed-loop system as it does for continuous systems. For second-order systems without zeros, the relationship between ζ and PM in the figure shows that the approximation of $\zeta \cong PM/100$ is equally valid for continuous and discrete systems with reasonably fast sampling. For higher-order systems, the damping of the individual modes needs to be determined using other methods.

Tracking Error in Terms of the Sensitivity Function

The gain and phase margins give useful information about the relative stability of nominal systems but can be very misleading as guides to the design of realistic control problems. A more accurate margin can be given in terms of the sensitivity function. For the unity feedback system drawn in Fig. 7.1, the error is given by

$$E(j\omega) = \frac{1}{1+DG}R \triangleq \mathcal{S}(j\omega)R, \quad (7.32)$$

where we have defined the **sensitivity function** \mathcal{S} . In addition to being a factor of the system error, the sensitivity function is also the reciprocal of the distance of the Nyquist curve, DG , from the critical point -1 . A large value for \mathcal{S} indicates a Nyquist plot that comes close to the point of instability. The maximum value of $|\mathcal{S}|$ is often a more accurate measure of stability margin than either gain or phase margin alone. For example, in Fig. 7.23 a Nyquist plot is sketched that is much closer to instability than either gain or phase margin would indicate. The **vector gain margin** (VGM) is defined as the gain margin in the direction of the worst possible phase. For example, if the Nyquist plot comes closest to -1 on the negative real axis, then the vector margin is the same as the standard gain margin. From the geometry of the Nyquist plot, the distance from the curve to -1 is $1 + DG = \frac{1}{\mathcal{S}}$ and with the definition that

$$S_\infty = \max_{\omega} |\mathcal{S}|,$$

it follows that the distance of the closest point on the Nyquist curve from -1 is $\frac{1}{S_\infty}$. If the Nyquist curve came this close to the -1 point on the real axis, it would pass through $1 - \frac{1}{S_\infty}$ and by definition, the product $VGM \times (1 - \frac{1}{S_\infty}) = 1$. Therefore we have that

$$VGM = \frac{S_\infty}{S_\infty - 1}. \quad (7.33)$$

The VGM and related geometry are marked on the Nyquist plot in Fig. 7.23.

We can express more complete frequency domain design specifications than any of these margins if we first give frequency descriptions for the external reference and disturbance signals. For example, we have described so far dynamic performance by the transient response to simple steps and ramps. A more realistic description of the actual complex input signals is to represent them as random processes with corresponding frequency spectra. A less sophisticated description which is adequate for our purposes is to assume that the signals can be represented as a sum of sinusoids with frequencies in a specified range. For example, we can usually describe the frequency content of the reference input as a sum of sinusoids with relative amplitudes given by a magnitude function $|R|$ such as that plotted in Fig. 7.24, which represents a signal with sinusoidal components each having about the same

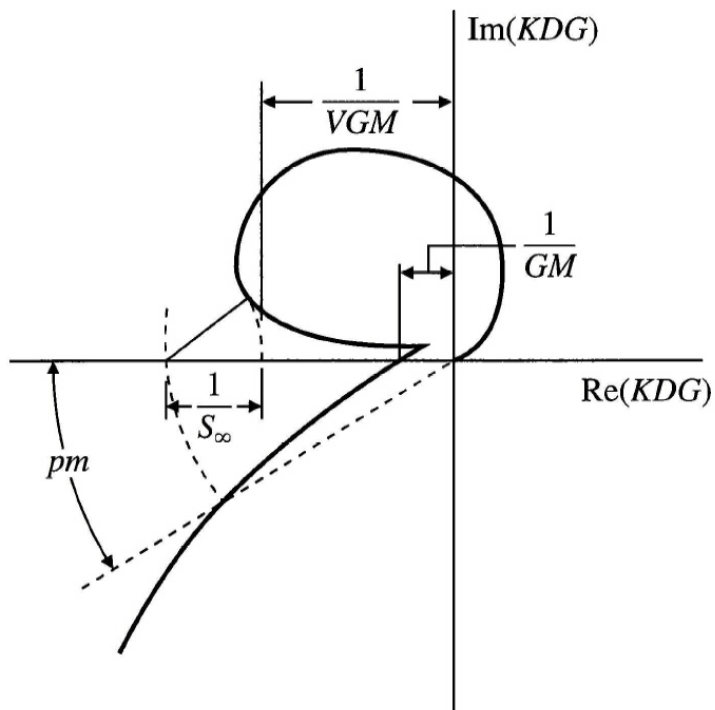


Figure 7.23
A Nyquist plot showing the vector gain margin

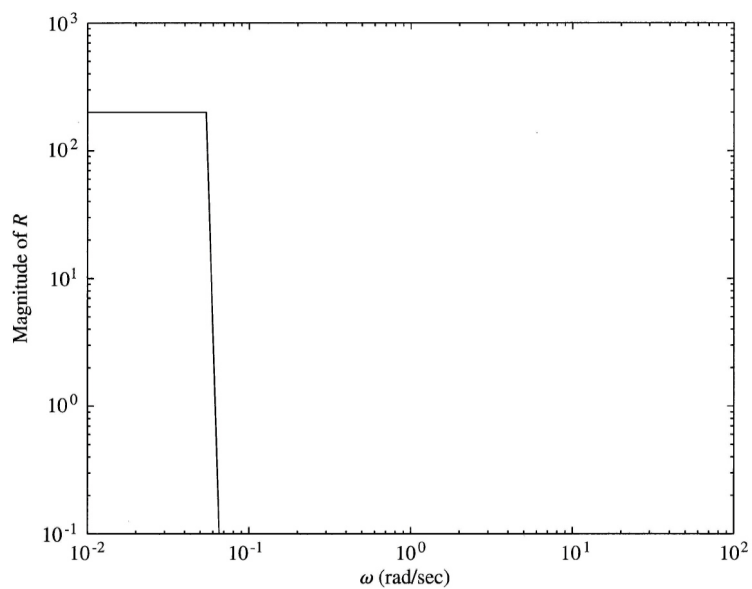


Figure 7.24
Sketch of typical specification of frequency content for reference input tracking

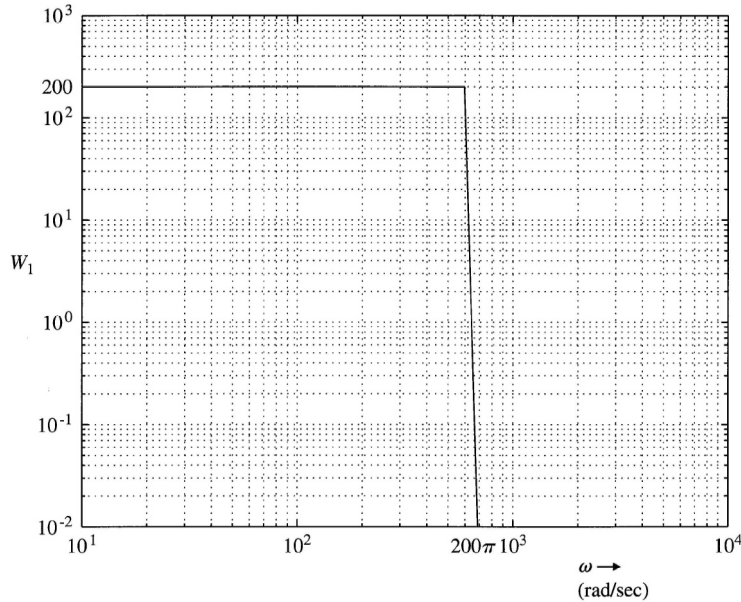


Figure 7.25
Plot of performance frequency function for Example 7.11

amplitude of 150 up to some value ω_1 and very small amplitudes for frequencies above that. With this assumption the response specification can be expressed by a statement such as “the magnitude of the system error is to be less than the bound e_b (a value such as 0.01 that defines the required tracking accuracy) for any sinusoid of frequency ω_o and of amplitude given by $|R(j\omega_o)|$.” We can now define the size of the error in terms of the sensitivity function and the amplitude of the input. Using Eq. (7.32), the frequency-based error specification can be expressed as $|E| = |S||R| \leq e_b$. In order to normalize the problem without defining both the spectrum R and the error bound each time, we define the real function of frequency $W_1(\omega) = |R|/e_b$ and the requirement can be written as

$$|S|W_1 \leq 1. \tag{7.34}$$

Performance Bound Function

Example 7.11

A unity feedback system is to have an error less than 0.005 for all unity amplitude sinusoids having frequency below 100 Hz. Draw the performance frequency function $W_1(\omega)$ for this design.

Solution. The spectrum, from the problem description, is unity for $0 \leq \omega \leq 200\pi$. Since $e_b = 0.005$, the required function is given by a rectangle of amplitude $1/0.005 = 200$ over the given range. The function is plotted in Fig. 7.25.

The expression in Eq. (7.34) can be translated to the more familiar Bode plot coordinates and given as a requirement on the open-loop gain, DG , by observing that over the frequency range when errors are small the loop gain is large. In that case $|S| \approx \frac{1}{|DG|}$ and the requirement is approximately

$$\begin{aligned} \frac{W_1}{|DG|} &\leq 1 \\ |DG| &\geq W_1. \end{aligned} \tag{7.35}$$

Stability Robustness in Terms of the Sensitivity Function

In addition to the requirements on dynamic performance, the designer is usually required to design for stability robustness. The models used for design are almost always only approximations to the real system. Many small effects are omitted, such as slight flexibility in structural members or parasitic electrical elements in an electronic circuit. Usually these effects influence the transfer function at frequencies above the control bandwidth and a nominal transfer function, G_o , is used for the design. However, while the design is done for the nominal plant transfer function, the actual system is expected to be stable for an entire class of transfer functions that represent the range of changes that are expected to be faced as all elements are included and as changes due to temperature, age, and other environmental factors vary the plant dynamics from the nominal case. A realistic way to express plant uncertainty is to describe the plant transfer function as having a multiplicative uncertainty as

$$G(j\omega) = G_o(j\omega)[1 + w_2(\omega)\Delta(j\omega)]. \quad (7.36)$$

In Eq. (7.36), $G_o(j\omega)$ is the nominal plant transfer function, and the real function, $w_2(\omega)$, is a magnitude function that expresses the size of changes as a function of frequency that the transfer function is expected to experience and is *known to be less than some upper bound* $W_2(\omega)$. The value of the bound W_2 is almost always very small for low frequencies (we know the model very well there) and increases substantially as we go to high frequencies where parasitic parameters come into play and unmodeled structural flexibility is common.

Model Uncertainty

Example 7.12

A magnetic memory read/write head assembly can be well modelled at low frequencies as

$$G_o(s) = \frac{K}{s^2}. \quad (7.37)$$

However, the arm supporting the read/write head has some lightly damped flexibility with uncertain resonant frequency. With scaling to place the resonant frequency at ω_o , and damping B , the more accurate model is represented as

$$G(s) = \frac{K}{s^2} \frac{B \frac{s}{\omega_o} + 1}{\left(\frac{s}{\omega_o}\right)^2 + B \frac{s}{\omega_o} + 1} \quad (7.38)$$

Compute the model uncertainty function for this case.

Solution. The model transfer function given by Eq. (7.38) can be written as

$$G(s) = \frac{K}{s^2} \left[1 + \frac{-\left(\frac{s}{\omega_o}\right)^2}{\left(\frac{s}{\omega_o}\right)^2 + B \frac{s}{\omega_o} + 1} \right]. \quad (7.39)$$

Comparing Eq. (7.39) with Eq. (7.36), the model uncertainty function is given by

$$w_2(\omega) = \left| \frac{-\left(\frac{s}{\omega_o}\right)^2}{\left(\frac{s}{\omega_o}\right)^2 + B \frac{s}{\omega_o} + 1} \right|_{s=j\omega}. \quad (7.40)$$

A plot of this function is given in Fig. 7.26 for $\omega_o = 1$ and $B = .03$.

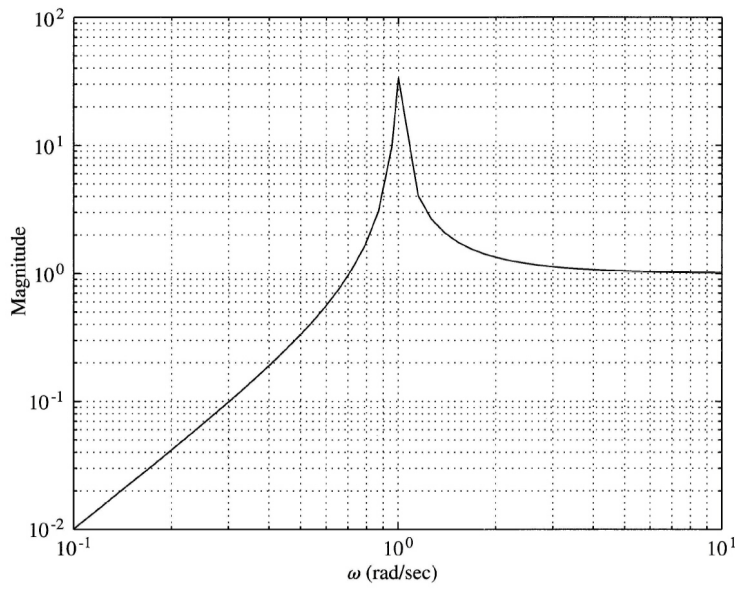


Figure 7.26
Plot of model uncertainty function for disk drive read/write head assembly

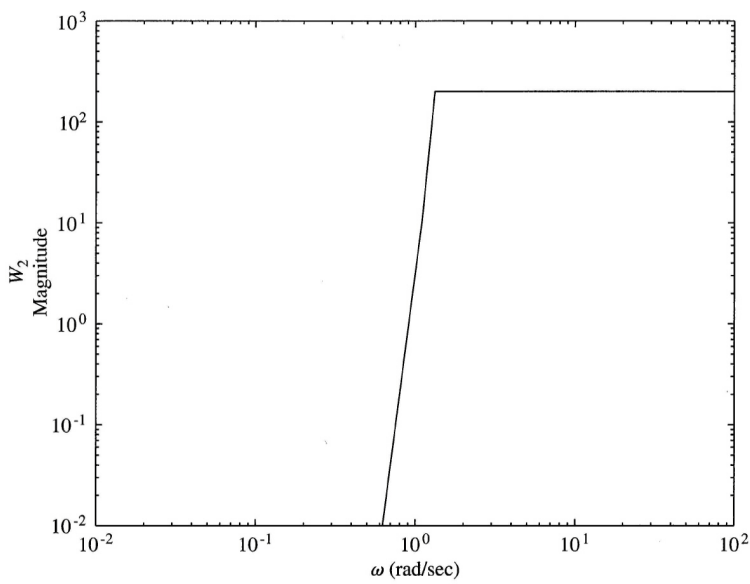


Figure 7.27
A plot of a typical plant uncertainty frequency function

In general, a model uncertainty bound is small for low frequencies and large for higher frequencies. A typical shape is sketched in Fig. 7.27. The complex function, $\Delta(j\omega)$, represents the uncertainty in phase and is restricted only by the constraint

$$|\Delta(j\omega)| \leq 1. \quad (7.41)$$

Stability robustness requires that we construct a control design for $G_o(s)$ which will result in a stable system for any transfer function described by Eq. (7.36). To derive the requirement, we begin with the assumption that the nominal design has been done and is stable so that the Nyquist plot of DG_o satisfies the Nyquist stability criterion. In this case, the equation $1 + D(j\omega)G_o(j\omega) = 0$ is never satisfied for any real frequency. If the system is to have stability robustness, the characteristic equation using the uncertain plant as described by Eq. (7.36) must not go to zero for any real frequency for any value of either W_2 or Δ . The requirement can be written as a function of $j\omega$ in the form

$$1 + DG \neq 0, \quad (7.42)$$

$$1 + DG_o[1 + w_2\Delta] \neq 0, \quad (7.43)$$

$$(1 + DG_o) \left(1 + \frac{DG_o}{1 + DG_o} w_2\Delta \right) \neq 0, \quad (7.44)$$

$$(1 + DG_o)(1 + \mathcal{T}w_2\Delta) \neq 0,$$

where the **complementary sensitivity function** is defined as $\mathcal{T}(j\omega) \triangleq \frac{DG_o}{(1 + DG_o) = 1 - \mathcal{S}}$. Because the nominal system is stable, the first term in Eq. (7.42), $(1 + D(j\omega)G_o(j\omega))$, is not zero for any ω . Thus, if Eq. (7.42) is not to be zero for any frequency, any $w_2 \leq W_2$, or for any phase function Δ , then it is necessary and sufficient that

$$\begin{aligned} |\mathcal{T}w_2\Delta| &< 1, \\ |\mathcal{T}| |w_2| |\Delta| &< 1, \end{aligned}$$

which reduces to

$$|\mathcal{T}| W_2 < 1, \quad (7.45)$$

making use of Eq. (7.41) and the fact that w_2 is bounded by W_2 . As with the performance specification, for single-input-single-output unity feedback systems this requirement can be approximated by a more convenient form. Over the range of high frequencies where there is significant model uncertainty and W_2 is non-negligible, DG_o is small. Therefore we can approximate $\mathcal{T} \approx DG_o$ and the constraint becomes

$$\begin{aligned} |DG_o| W_2 &< 1 \\ |DG_o| &< \frac{1}{W_2}. \end{aligned} \quad (7.46)$$

Stability Robustness Function

Example 7.13

The uncertainty in the model of a disk read/write head assembly is given in Example 12. Suppose it is known that the parameter B is restricted to the range $.03 \leq B \leq .3$ and that the resonant frequency ω_o is known to be no less than 1.0. Plot the stability robustness bound, $1/W_2$ for this problem.

Solution. The function $1/w_2(\omega)$ is plotted for $B = .03$ and $\omega = 1$ and $\omega = 6$ in Fig. 7.28 using bode. It is clear that if the resonant frequency can take on any value greater than 1.0, then the bound $1/W_2$ needs to be extended at the value .03 for all frequencies greater than 1.0. The boundary line is marked with hatching in Fig. 7.28.

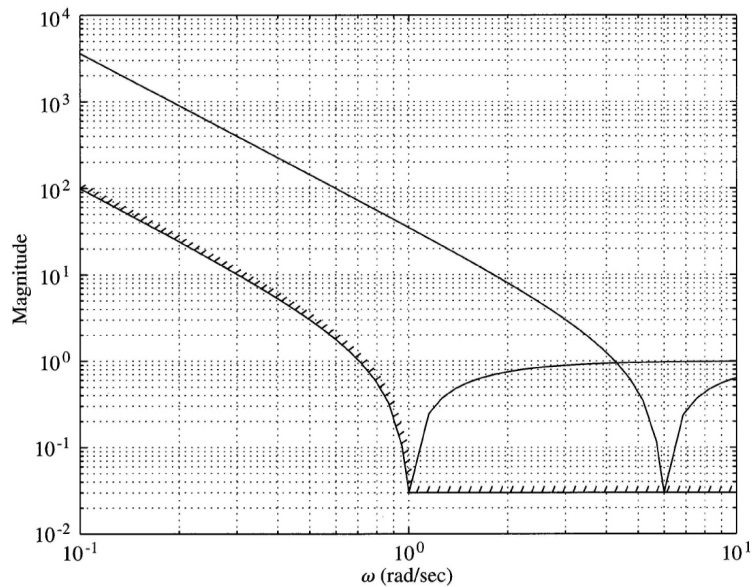


Figure 7.28
Plot of the stability robustness frequency function for disk read/write head assembly

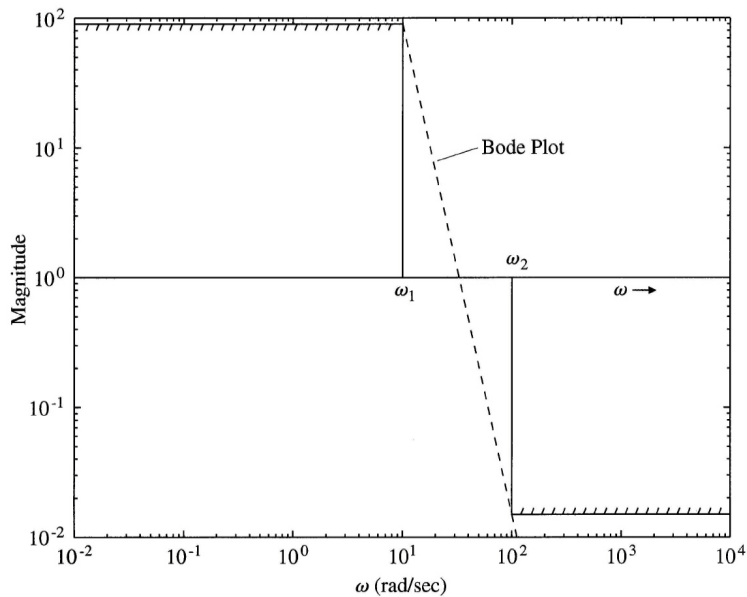


Figure 7.29
Typical design limitations as displayed on a Bode magnitude plot

In practice, the magnitude of the loop gain is plotted on log-log coordinates, and the constraints of Eq. (7.35) and Eq. (7.46) are included on the same plot. A typical sketch is drawn in Fig. 7.29. The designer is expected to construct a loop gain that will stay above W_1 for frequencies below ω_1 , cross over the magnitude-of-1 line ($\log(|DG|) = 0$) in the range $\omega_1 \leq \omega \leq \omega_2$ and stay below $1/W_2$ for frequencies above ω_2 . We have developed the design constraints Eq. (7.35) and Eq. (7.46) in terms of $j\omega$ as for continuous systems. The algebra and the equations are the same for the discrete case; one need only substitute the discrete transfer functions for the continuous ones and use the variable $e^{j\omega T}$.

Limitations on Design: Continuous Case

One of the major contributions of Bode was to derive important limitations on transfer functions that set limits on achievable design specifications. For example, we would like to have the system error kept small for the widest possible range of frequencies and yet to have a system that is stable in the presence of uncertainty in the plant transfer function. In terms of the plot in Fig. 7.29, we want W_1 and W_2 to be large in their respective frequency ranges and for ω_1 to be close to ω_2 . Thus the loop gain is expected to plunge with a large negative slope from being greater than W_1 to being less than $1/W_2$ in a short span, while maintaining stability which can be expressed as having a good phase margin. Bode showed that this is *impossible* with a linear controller by showing that the minimum possible phase is determined by an integral depending on the slope of the magnitude curve. A common form of the formula for phase is

Bode's gain-phase formula

Bode's gain-phase integral

$$\phi(\omega_o) = \frac{1}{\pi} \int_{-\infty}^{+\infty} \left(\frac{dM}{du} \right) \ln\left(\coth \left| \frac{u}{2} \right| \right) du, \tag{7.47}$$

where $M = \ln(|DG|)$ and $u = \ln(\frac{\omega}{\omega_o})$, and thus $\frac{dM}{du}$ is the magnitude slope on the log-log (Bode) plot. The weighting function in Eq. (7.47) is concentrated near ω_o , and if the slope is constant for a substantial range around ω_o , then the formula can be approximated by

$$\phi(\omega_o) \approx \frac{\pi}{2} \left. \frac{dM}{du} \right|_{u=0}.$$

If, for example, the phase is to be kept above -150° to maintain a 30° phase margin, then the magnitude slope is estimated to be

$$\begin{aligned} \frac{dM}{du} &\approx \frac{2}{\pi} \left(-150 \frac{\pi}{180} \right) \\ &\approx -1.667 \end{aligned}$$

in the neighborhood of crossover. If we try to make the average slope steeper (more negative) than this near crossover, we will lose the phase margin. From this condition there developed the design rule:

- The asymptotes of the Bode plot magnitude, which are restricted to be integral values for rational functions, should be made to crossover the magnitude 1 line at a slope of -1 over a frequency range of about one decade around the cross-over frequency.

Modifications to this rule need of course to be made in particular cases, but the limitation expressed by Eq. (7.47) is a hard limit that cannot be avoided.

In Freudenberg and Looze (1985) an extension to another of Bode's relations was derived. This is a constraint on the integral of the sensitivity function dependent on the presence of open-loop right-half plane poles. Suppose the loop gain DG_o has n_p poles, p_i , in the right-half plane and "rolls off" at high frequencies at a slope faster than -1 . For rational functions, this means that there is an excess of at least two more total poles than zeros. Then it can be shown that

sensitivity integral

$$\int_0^\infty \ln(|S|) d\omega = \pi \sum_{i=1}^{n_p} \text{Re}\{p_i\}. \tag{7.48}$$

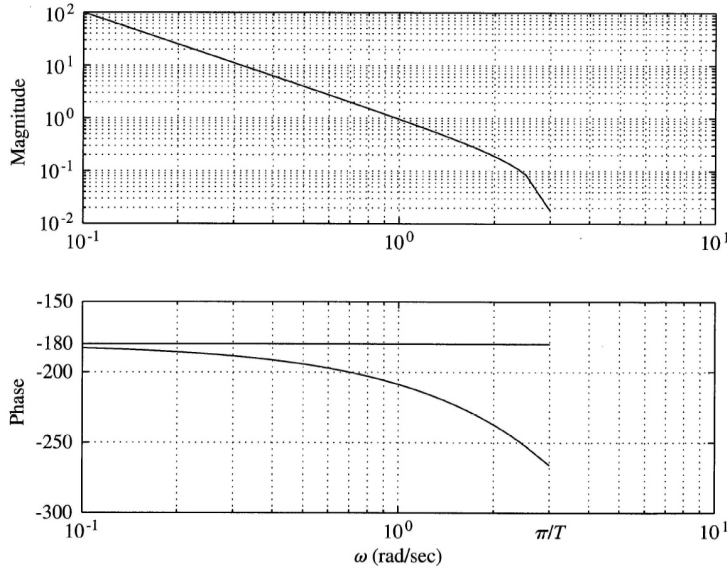


Figure 7.30
Discrete Bode
plot of $1/s^2$ plant
with zero-order
hold

If there are no right-half plane poles, then the integral is zero. This means that if we make the log of the sensitivity function very negative over some frequency band to reduce errors in that band, then *of necessity* $\ln|S|$ will be positive over another part of the band and errors will be amplified there. If there are unstable poles, the situation is worse because the positive area where sensitivity magnifies the error must exceed the negative area where the error is reduced by the feedback. There are also consequences if DG_o has any *zeros* in the right-half plane. If the open-loop system has no zeros in the right-half plane, then it is in principle possible to keep the magnitude of the sensitivity small by spreading the sensitivity increase over all positive frequencies to infinity but such a design requires an excessive bandwidth and is rarely practical. If a specific bandwidth is imposed, then the sensitivity function is constrained to take on a finite, possibly large, positive value at some point below the bandwidth and a large value of $|S|_\infty$ leads to a small VGM and generally an unsatisfactory design.

An alternative to Eq. (7.48) is also true if there is a (non-minimum-phase) zero of DG_o in the right-half plane. Suppose the zero is located at $z_o = \sigma_o + j\omega_o$, where $\sigma_o > 0$. Again we assume there are n_p right-half plane poles at locations p_i with conjugate values \bar{p}_i . Now the condition can be expressed as a two-sided weighted integral

constraint on
non-minimum
phase systems

$$\int_{-\infty}^{\infty} \ln(|S|) \frac{\sigma_o}{\sigma_o^2 + (\omega - \omega_o)^2} d\omega = \pi \sum_{i=1}^{n_p} \ln \left| \frac{\bar{p}_i + z_o}{p_i - z_o} \right|. \quad (7.49)$$

In this case, we do not have the “roll-off” restriction and there is no possibility of spreading the positive area over all high frequencies because the weighting function goes to zero with frequency. The important point about this integral is that if the non-minimum phase zero is close to a right-half plane pole, the right side of the integral can be very large and the excess of positive area is required to be correspondingly large. Based on this result, *one expects especially great difficulty meeting specifications on sensitivity with a system having right-half plane poles and zeros close together.*

Limitations on Design: Discrete Case

In the discrete case, the relation between gain slope and phase does not hold although it is approximately true for frequencies well below the Nyquist frequency. The situation is illustrated by the Bode plot in Fig. 7.30 for the plant $G = 1/s^2$. Notice that the phase is always slightly more negative than the -180° one would get for this plant in the continuous case and deviates more as we approach the Nyquist limit at π/T . The effect is approximated by the delay of $T/2$ due to the sample and ZOH.

From this example, one suspects that the restriction on phase due to gain slope is *more severe* in the discrete case than in the continuous case.

In Sung and Hara (1988) the discrete versions of these design limitations are derived. We consider the single-loop unity feedback structure and define the sensitivity function as $\mathcal{S} = \frac{1}{1+DG}$ as before. We also assume that the open-loop transfer function $D(z)G(z)$ has n_p poles outside the unit circle at $z_i = r_i e^{j\phi_i}$, $r_i > 1$. It can be shown that

$$\int_0^\pi \ln(|\mathcal{S}(e^{j\phi})|) d\phi = \pi \sum_{i=1}^{n_p} \ln(r_i). \quad (7.50)$$

The implications of Eq. (7.50) are the same as in the continuous case except for the fact that the integral in Eq. (7.50) is over a *finite* limit. If we require that sensitivity is small (negative log) over a given range of frequencies, there is only a finite frequency range over which we can spread the required sensitivity gain or “positive log” area. Again, unstable poles make the situation worse and the effect increases if the poles are located far from the unit circle. We can illustrate the implications of Eq. (7.50) by two simple examples. Consider a stable generic model of a chemical process and an unstable model of a magnetic levitation system. The two transfer functions are

$$G_1(s) = \frac{1}{(s+1)^2} \quad \text{chemical process,}$$

$$G_2(s) = \frac{1}{s^2-1} \quad \text{magnetic levitation.}$$

In each case we will include a zero-order hold and sample with $T = 0.2$ and in each case the controller transfer function is $D = 15 \frac{z-0.7}{z+0.5}$, selected to give approximately the same rise time and bandwidth. The step responses are shown in Fig. 7.31(a) and the sensitivity plots are shown in Fig. 7.31(b). Notice the substantially larger value of the sensitivity for the unstable plant compared to that of the stable one. The vector gain margin for G_1 is 5.4 while that for G_2 is 2.25, less than half as much. To plot the sensitivity magnitude, it is necessary to obtain a system having the transfer function of \mathcal{S} . This can be done using the feedback function if a representation of the open loop system DG is given as, for example, the open loop discrete system `sysold`. The expression `sysc1 = feedback(sys1,sys2)` generates the loop with forward system `sys1` and feedback system `sys2`. For sensitivity, DG is the feedback system, and we need to construct the dummy gain of 1 for the forward system. This can be done with the statement

```
sysf = ss(0,0,0,1,Ts)
```

Finally, the sensitivity is given by

```
sens = feedback(sysf,sysold)
```

The plot is given by the statements

```
[mag,ph,w] = bode(sens);
semilogy(w,squeeze(mag))
grid
```

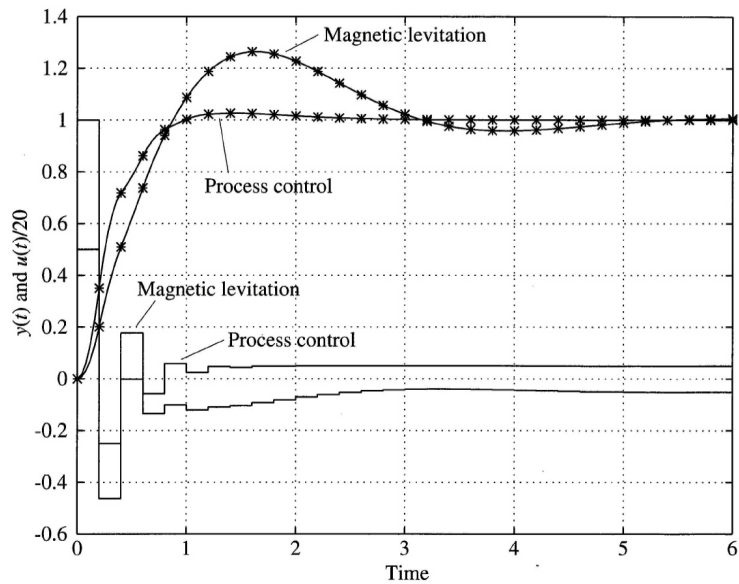
The weighted integral of the discrete sensitivity function is similar to that of the continuous case. We assume again that the system has n_p poles outside the unit circle at $\alpha_i = r_i e^{j\phi_i}$, $r_i > 1$, and conjugate $\bar{\alpha}_i$, and also has a zero outside the unit circle at $\beta_o = r_o e^{j\phi_o}$, $r_o > 1$. Then

$$\int_{-\pi}^{\pi} \ln(|\mathcal{S}(e^{j\phi})|) \frac{r_o^2 - 1}{r_o^2 - 2r_o \cos(\phi - \phi_o) + 1} d\phi = 2\pi \sum_{i=1}^{n_p} \ln \left| \frac{1 - \bar{\alpha}_i \beta_o}{\beta_o - \alpha_i} \right|. \quad (7.51)$$

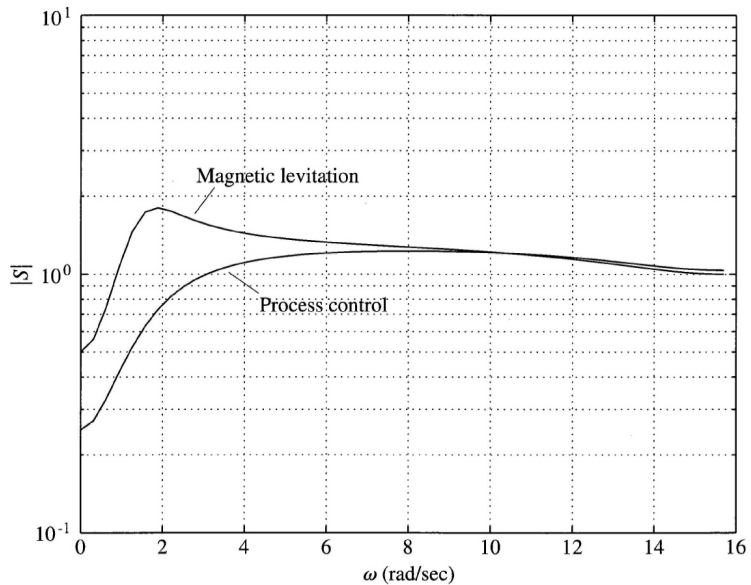
The main consequence of this constraint is that it expresses a limitation imposed by the non-minimum phase zero on the sensitivity function. The constraint is especially severe if there is a non-minimum phase zero near an unstable pole ($\beta_o \approx \alpha_i$).

discrete sensitiv-
ity integral

weighted integral
of the discrete
sensitivity func-
tion



(a)



(b)

Figure 7.31
Comparisons of a stable process control with an unstable magnetic levitation:
(a) step responses
(b) sensitivity plots

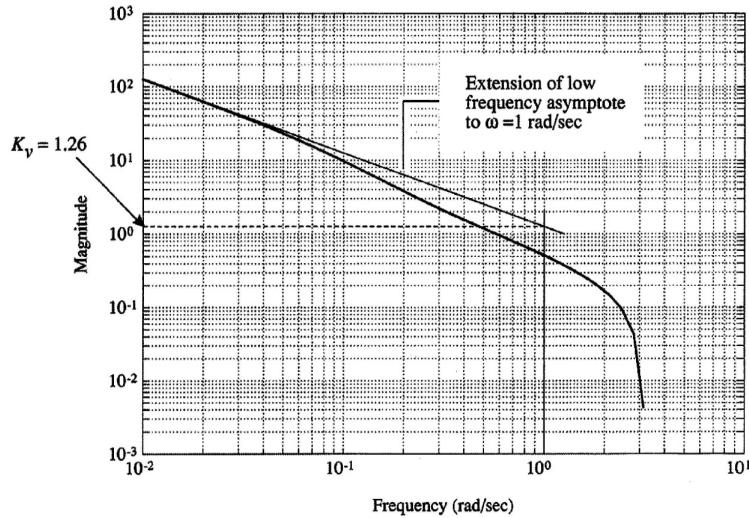


Figure 7.32
Determination of K_v from frequency response

7.4.3 Low Frequency Gains and Error Coefficients

The steady-state error constants for polynomial inputs for discrete systems were established in Section 7.2 and are given by

$$K_p = \lim_{z \rightarrow 1} D(z)G(z)$$

for a Type 0 system, and by

$$K_v = \lim_{z \rightarrow 1} \frac{(z-1)D(z)G(z)}{Tz}, \quad (7.52)$$

for a Type 1 system. In the frequency domain, for a Type 0 system, the procedure is identical to the continuous case. Since $z = e^{j\omega T}$, $z \rightarrow 1$ implies that $\omega T \rightarrow 0$, and the magnitude frequency-response plot will show a constant value on the low-frequency asymptote which is equal to K_p . For a Type 1 system, the procedure is again identical to the continuous case in that the magnitude of $D(z)G(z)$ at $\omega = 1$ on the low-frequency asymptote is equal to K_v . This can be seen from Eq. (7.52) if we note that for $\omega T \rightarrow 0$, $e^{j\omega T} \cong 1 + j\omega T$. Therefore

$$\lim_{z \rightarrow 1} \frac{(z-1)}{Tz} = \lim_{j\omega \rightarrow 0} \omega,$$

thus establishing the fact that evaluation of the low-frequency asymptote of $D(z)G(z)$ at $\omega = 1$ yields K_v . This fact is most easily used if the frequency-response magnitude is plotted versus ω in units of rad/sec so that $\omega = 1$ rad/sec is readily found. If the magnitude is plotted versus ω in units of Hz or versus ωT , one would need to perform a calculation to find the $\omega = 1$ rad/sec point. However, the error constants could be calculated directly with good software tools; therefore the issues in their calculation are of passing interest only. But no matter how the constants are found, the *fact remains for discrete and continuous frequency response alike, the higher the magnitude curve at low frequency, the lower the steady-state errors.*

Finding Velocity Constant on a Bode Plot

Example 7.14

Use the discrete Bode plot to determine the K_v for the antenna system of Example 6 with the compensation given by Eq. (7.19).

Solution. The open-loop discrete transfer function is

$$G(z)D(z) = (0.0484) \frac{z + 0.9672}{(z-1)(z-0.9048)} \stackrel{(6)}{=} \frac{z-0.80}{z-0.05},$$

which yields the magnitude versus frequency in Fig. 7.32. Evaluation of the magnitude of the low-frequency asymptote at $\omega = 1$ indicates that $K_v = 1.26$. Also note in the figure that the extension of the low-frequency asymptote reaches crossover at $\omega = 1.26$, thus indicating also that $K_v = 1.26$ since this Type 1 system has a low-frequency slope of -1 .

7.4.4 Compensator Design

The amplitude and phase curves can be used to determine the stability margins based on the Nyquist stability criterion for either continuous or discrete systems. In the continuous case with minimum-phase transfer functions, Bode showed that the phase is uniquely determined by an integral of the slope of the magnitude curve on a log-log plot as expressed by Eq. (7.47). If the function is rational, these slopes are readily and adequately approximated by constants! As a consequence the amplitude curve must cross unity gain (zero on a log scale) at a slope of -1 for a reasonable phase margin. The ability to predict stability from the amplitude curve alone in minimum phase systems is an important contributor to the ease with which designers can evaluate changes in compensator parameters in those cases.

Bode's relationship between the amplitude and phase curve is lost for discrete systems because the variable z takes on values around the unit circle in contrast to s traversing the imaginary axis as in continuous systems. Figure 7.16 illustrates the degree to which the relationship is lost and indicates that the error would be small for frequencies lower than 1/20th of the sample frequency. However, it is typically necessary to determine both magnitude and phase for discrete z -plane systems and not depend on magnitude alone for an accurate assessment of the stability. In carrying out direct digital designs, some intuition from continuous design can be used if the z -plane poles and zeros on the real axis are measured by their distance from $+1$. For example, the equivalent idea in the z -plane for the "breakpoint" in Bode's hand-plotting rules is that the magnitude will change slope at a frequency when ωT , the *angular* position on the unit circle in radians, has the same value as the fractional distance of the singularity on the real axis to $z = +1$. For example, a pole at $z = 0.9$ will produce a slope change at $\omega T = 0.1$ rad. This equivalence is very accurate for low angular values ($\omega T \leq 0.1$ rad, i.e., sampling at more than 60 times the frequency) and is a reasonable approximation for angular values less than 0.8 rad (i.e., sampling at more than 8 times the frequency). In order to arrive at trial compensations with potential for better *PM*, *GM*, steady-state errors, or crossover frequency, it is useful to understand how a pole or zero placement will affect the magnitude and phase curves. Because of the equivalence of the break-point concept between the continuous and discrete cases, this is accomplished for discrete systems using the ideas from the continuous Bode hand-plotting techniques, keeping in mind that their fidelity degrades as frequency approaches the Nyquist frequency. It is easiest to select compensator break points if the frequency-response magnitude and phase is plotted versus ωT so that the correspondence between those curves and the location of the compensation parameters is retained.

Design of the Antenna Servo Control

Example 7.15

Design a discrete controller for the antenna system with $T = 1$ using the frequency response. The specifications are as before: overshoot less than 16%, settling time less than 10 sec and $K_v \geq 1$.

Solution. The system transfer function is

$$G(z) = 0.0484 \frac{z + 0.9672}{(z - 1)(z - 0.9048)}. \quad (7.53)$$

The magnitude and phase of the uncompensated system $[G(z)]$ shown in Fig. 7.35 indicate that with a compensator gain of $K = 1$ the system has a *PM* of 8° and a gain crossover frequency (ω_{cg}) of 0.3 rad/sec. The 16% overshoot requirement translates into $\zeta \geq 0.5$, which translates in turn into the requirement that the *PM* be $\geq 50^\circ$ from Fig. 7.24. The specification for settling time translates into the requirement that $\omega_n \geq 0.92$.

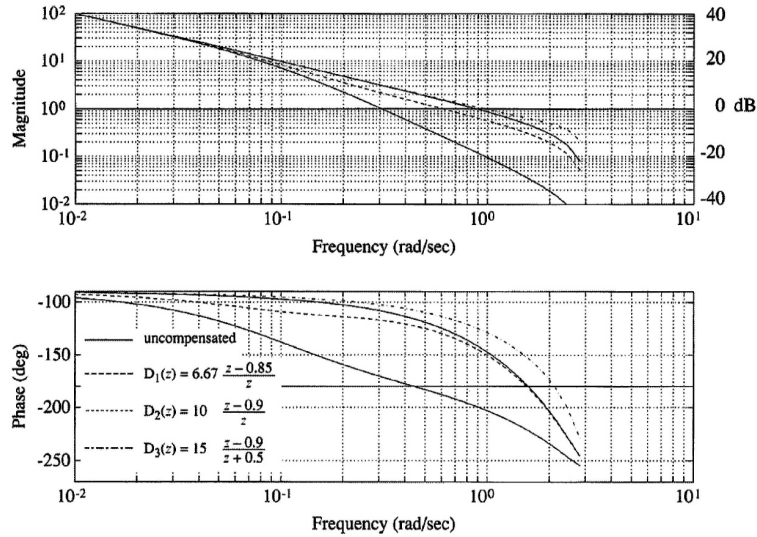


Figure 7.33
Frequency responses with D_1 , D_2 , and D_3 for Example 7.15

Because the gain of $(z-1)G(z)$ at $z=1$ is 1, and $T=1$, the compensated system will also have $K_v=1$ provided the DC gain of $D(z)=1$. In terms of the frequency response, this means that the extension of the low-frequency-magnitude asymptote should pass through the value 1 at $\omega=1$ for the uncompensated case (in Fig. 7.33), and the gain of this low-frequency asymptote should not be decreased with any candidate compensation. To maintain an acceptable K_v , we will evaluate only $D(z)$'s with a DC gain of 1. The uncompensated system's PM of 8° indicates poor damping, and the ω_{cg} of 0.3 rad/sec indicates that it will be too slow. Just as for continuous systems, ω_{cg} occurs approximately at the system bandwidth and dominant natural frequency; therefore, we should try to change the design so that it has a ω_{cg} of about 0.9 rad/sec in order to meet the $t_s \leq 10$ sec. Once we find a compensation that meets the guidelines of $PM=50^\circ$ and $\omega_{cg}=0.9$ rad/sec, we will need to check whether the settling time and overshoot specifications are actually met, because the design guidelines followed are only approximate.

Figure 7.33 shows several attempts to produce a design. The breakpoint of the first attempt ($D_1(z)$) in Fig. 7.33) was at 0.15 rad/sec⁴ and did not increase the slope of the magnitude curve at a low enough frequency to bring about the desired ω_{cg} . This was remedied in $D_2(z)$, where the breakpoint was lowered to 0.1 rad/sec (zero at $z=0.9$) causing a ω_{cg} of 0.9 rad/sec, but the resulting PM of 40° was still lower than desired. By moving the compensator pole out to $z=-0.5$ in $D_3(z)$, we had very little effect on the ω_{cg} but achieved an increase in the PM to 50° . Because both goals are met, $D_3(z)$ has a reasonable chance to meet the specifications; in fact, the calculation of a time history of the system response to a step input shows that the t_s is 7 sec, but, alas, the overshoot is 27%. The guidelines were not successful in meeting the specifications because the system is third order with a zero, whereas the rules were derived assuming a second-order system without a zero.

The necessary revisions to our design guidelines are clear; we want more than a 50° PM and do not require a 0.9 rad/sec ω_{cg} . Figure 7.34 shows the system frequency response using $D_3(z)$ along with two revisions of $D(z)$ that satisfy our revised goals. $D_4(z)$ has a 60° PM and a 0.6 rad/sec ω_{cg} , and $D_5(z)$ has a 58° PM and a 0.8 rad/sec ω_{cg} . The time history of the system response to a step using $D_5(z)$ in Fig. 7.35 shows that it exactly meets the requirements for 16% overshoot and $t_s=10$ sec. Furthermore, the design of the system imposed the constraint that $K_v=1$ and the design is complete.

It is interesting to look at the sensitivity functions for these designs, plotted in Fig. 7.36 as log of the sensitivity versus a linear frequency scale to illustrate the balance between positive and negative areas for such plots for stable systems. On this plot, one can see that controller D_3 results in the highest bandwidth and also the highest maximum of the sensitivity or lowest vector gain margin. Controller D_4 has improved robustness (lower maximum of the sensitivity) but also lower bandwidth. Finally, the design given by D_5 splits the difference and meets each specification.

⁴The zero at $z=0.85$ translates into a 0.15 rad/sec breakpoint only because the sample period, T , is 1 sec. For $T=0.1$ sec, a zero at $z=0.85$ would translate into a 1.5 rad/sec breakpoint, etc.

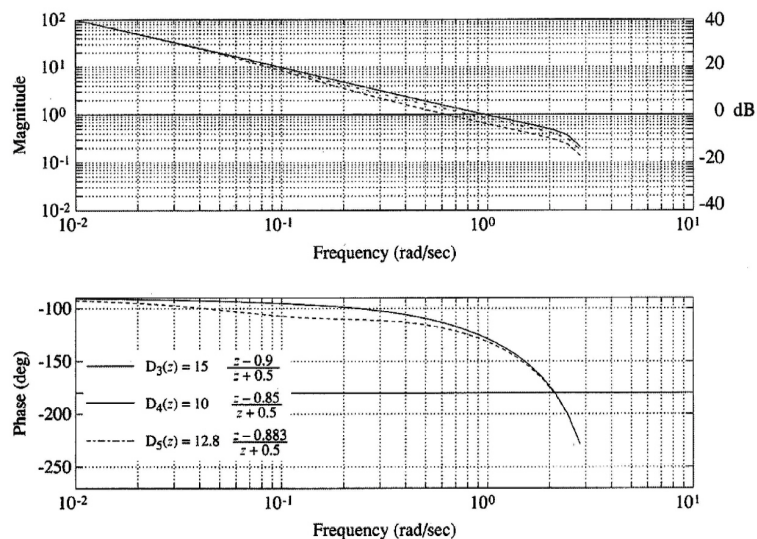


Figure 7.34
Bode plots of designs with controllers D_3 , D_4 , and D_5 for Example 7.15

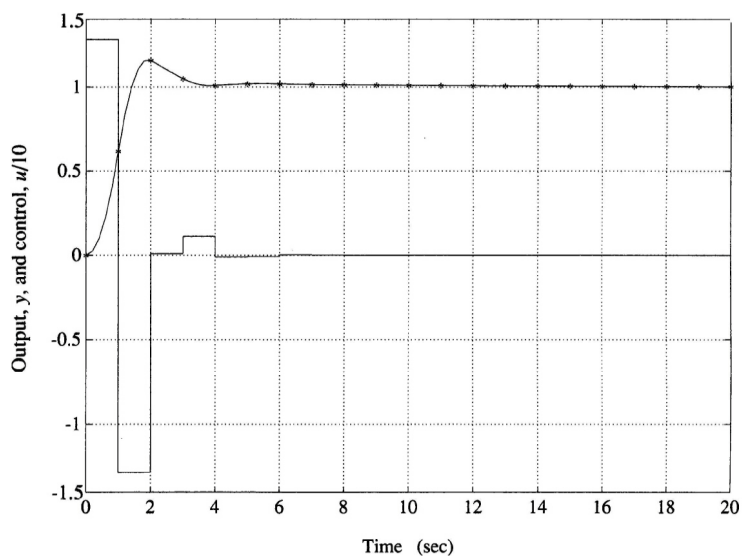


Figure 7.35
Step response of the system with controller D_5

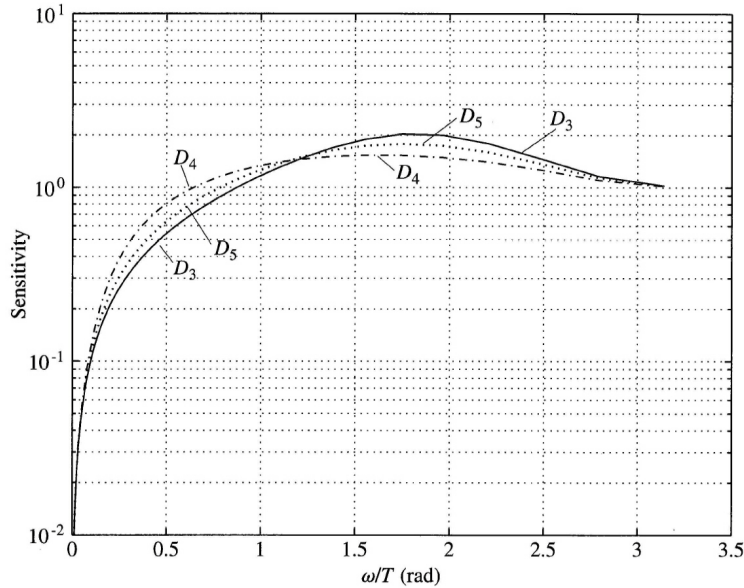


Figure 7.36
Sensitivity plots
of designs with
controllers D_3 ,
 D_4 , and D_5 for
Example 7.15

7.5 Direct Design Method of Ragazzini

Much of the style of the transform design techniques we have been discussing in this chapter grew out of the limitations of technology that was available for realization of continuous-time compensators with pneumatic components or electric networks and amplifiers. In particular, many constraints were imposed in order to assure the realization of electric compensator networks $D(s)$ consisting only of resistors and capacitors.⁵ With controllers realized by digital computer, such limitations on realization are, of course, not relevant and one can ignore these particular constraints. An alternative design method that ignores constraints of technology has been found to be useful in adaptive controls. Suppose we are given a discrete transfer function $G(z)$ of the plant (plus hold) and a desired transfer function $H(z)$ between reference R and output Y . The structure is assumed to be a unity feedback system and the design is to select the computer transfer function $D(z)$ to realize $H(z)$. The overall transfer function is given by the formula

$$H(z) = \frac{DG}{1 + DG},$$

from which we get the direct design formula

$$D(z) = \frac{1}{G(z)} \frac{H(z)}{1 - H(z)}. \quad (7.54)$$

From Eq. (7.54) we can see that this design calls for a $D(z)$ that will cancel the plant effects and add whatever is necessary to give the desired result. The problem is to discover and implement constraints on $H(z)$ so that we do not ask for the impossible.

First, the design must be causal. From z -transform theory we know that if $D(z)$ is to be causal, then as $z \rightarrow \infty$ its transfer function is bounded and does not have a pole at infinity. Looking at Eq. (7.54), we see that if $G(z)$ were to have a zero at infinity, then $D(z)$ would have a pole there unless we require an $H(z)$ that cancels it. Thus we have the constraint that for $D(z)$ to be causal

$$\begin{aligned} H(z) \text{ must have a zero at infinity of the same order} \\ \text{as the zero of } G(z) \text{ at infinity.} \end{aligned} \quad (7.55)$$

⁵In the book by Truxal (1955), where much of this theory is collected at about the height of its first stage of development, a chapter is devoted to RC network synthesis.

This requirement has an elementary interpretation in the time domain: A zero of order k at infinity in $G(z)$ corresponds to a delay of k samples in the pulse response of the plant. The causality requirement on $H(z)$ is that the closed-loop system must have at least as long a delay as the plant.

Considerations of stability add a second constraint. The roots of the characteristic equation of the closed-loop system are the roots of the equation

$$1 + D(z)G(z) = 0. \quad (7.56)$$

We can express Eq. (7.56) as a polynomial if D and G are rational and we identify $D = c(z)/d(z)$ and $G = b(z)/a(z)$ where a, b, c , and d are polynomials. Then the characteristic polynomial is

$$ad + bc = 0. \quad (7.57)$$

Now suppose there is a common factor in DG , as would result if $D(z)$ were called upon to cancel a pole or zero of $G(z)$. Let this factor be $z - \alpha$ and suppose it is a pole of $G(z)$, so we can write $a(z) = (z - \alpha)\bar{a}(z)$, and to cancel it we have $c(z) = (z - \alpha)\bar{c}(z)$. Then Eq. (7.57) becomes

$$\begin{aligned} (z - \alpha)\bar{a}(z)d(z) + b(z)(z - \alpha)\bar{c}(z) &= 0, \\ (z - \alpha)[\bar{a}d + b\bar{c}] &= 0. \end{aligned} \quad (7.58)$$

In other words—perhaps it was obvious from the start—a common factor *remains a factor of the characteristic polynomial*. If this factor is outside the unit circle, the system is unstable! How do we avoid such cancellation? Considering again Eq. (7.54), we see that if $D(z)$ is not to cancel a pole of $G(z)$, then that factor of $a(z)$ must also be a factor of $1 - H(z)$. Likewise, if $D(z)$ is not to cancel a zero of $G(z)$, such zeros must be factors of $H(z)$. Thus we write the constraints⁶

$$1 - H(z) \text{ must contain as zeros all the poles of } G(z) \text{ that are outside the unit circle,} \quad (7.59)$$

$$H(z) \text{ must contain as zeros all the zeros of } G(z) \text{ that are outside the unit circle.} \quad (7.60)$$

Consider finally the constraint of steady-state accuracy. Because $H(z)$ is the overall transfer function, the error transform is given by

$$E(z) = R(z)(1 - H(z)). \quad (7.61)$$

Thus if the system is to be Type 1 with velocity constant K_v , we must have zero steady-state error to a step and $1/K_v$ error to a unit ramp. The first requirement is

$$e(\infty) = \lim_{z \rightarrow 1} (z - 1) \frac{1}{z - 1} [1 - H(z)] = 0, \quad (7.62)$$

which implies

$$H(1) = 1. \quad (7.63)$$

The velocity constant requirement is that

$$e(\infty) = \lim_{z \rightarrow 1} (z - 1) \frac{Tz}{(z - 1)^2} [1 - H(z)] = \frac{1}{K_v}. \quad (7.64)$$

From Eq. (7.63) we know that $1 - H(z)$ is zero at $z = 1$, so that to evaluate the limit in Eq. (7.64), it is necessary to use L'Hôpital's rule with the result

$$-T \left. \frac{dH}{dz} \right|_{z=1} = \frac{1}{K_v}. \quad (7.65)$$

*Design by the Direct Method***Example 7.16**

Consider again the plant described by the transfer function of Eq. (7.53) and suppose we ask for a digital design that has the characteristic equation that is the discrete equivalent of the continuous characteristic equation

$$s^2 + s + 1 = 0,$$

with a sampling period $T = 1$ sec.

Solution. The discrete characteristic equation according to the specifications is

$$z^2 - 0.7859z + 0.36788 = 0. \quad (7.66)$$

Let us therefore ask for a design that is stable, has $K_v = 1$, and has poles at the roots of Eq. (7.66) plus, if necessary, additional poles at $z = 0$, where the transient is as short as possible. The form of $H(z)$ is thus

$$H(z) = \frac{b_0 + b_1z^{-1} + b_2z^{-2} + b_3z^{-3} + \dots}{1 - 0.7859z^{-1} + 0.3679z^{-2}}. \quad (7.67)$$

The causality design constraint, using Eq. (7.55) requires that

$$H(z)|_{z=\infty} = 0$$

or

$$b_0 = 0. \quad (7.68)$$

Equations (7.59) and (7.60) add no constraints because $G(z)$ has all poles and zeros inside the unit circle except for the single zero at ∞ , which is taken care of by Eq. (7.68). The steady-state error requirement leads to

$$\begin{aligned} H(1) &= 1 \\ &= \frac{b_1 + b_2 + b_3 + \dots}{1 - 0.7859 + 0.3679} = 1. \end{aligned} \quad (7.69)$$

Therefore

$$b_1 + b_2 + b_3 + \dots = 0.5820,$$

and

$$-T \left. \frac{dH}{dz} \right|_{z=1} = \frac{1}{K_v}.$$

Because in this case both T and K_v are 1, we use Eq. (7.69) and the derivative with respect to z^{-1} to obtain

$$\begin{aligned} 1 &= \frac{1}{K_v} = \left. \frac{dH}{dz^{-1}} \right|_{z=1} \\ &= \frac{(0.5820)[b_1 + 2b_2 + 3b_3 + \dots] - [0.5820][-0.7859 + 0.3679(2)]}{(0.5820)(0.5820)} \end{aligned}$$

or

$$\frac{b_1 + 2b_2 + 3b_3 + \dots - [-0.05014]}{0.5820} = 1. \quad (7.70)$$

Because we have only two equations to satisfy, we need only two unknowns and we can truncate $H(z)$ at b_2 . The resulting equations are

$$\begin{aligned} b_1 + b_2 &= 0.5820, \\ b_1 + 2b_2 &= 0.5318, \end{aligned}$$

which have the solution

$$b_1 = 0.6321, \quad (7.71)$$

$$b_2 = -0.05014. \quad (7.72)$$

Thus the final design gives an overall transfer function

$$H(z) = \frac{0.6321z - 0.05014}{z^2 - 0.7859z + 0.3679}. \quad (7.73)$$

⁶Roots on the unit circle are also unstable by some definitions, and good practice indicates that we should not cancel singularities outside the radius of desired settling time.

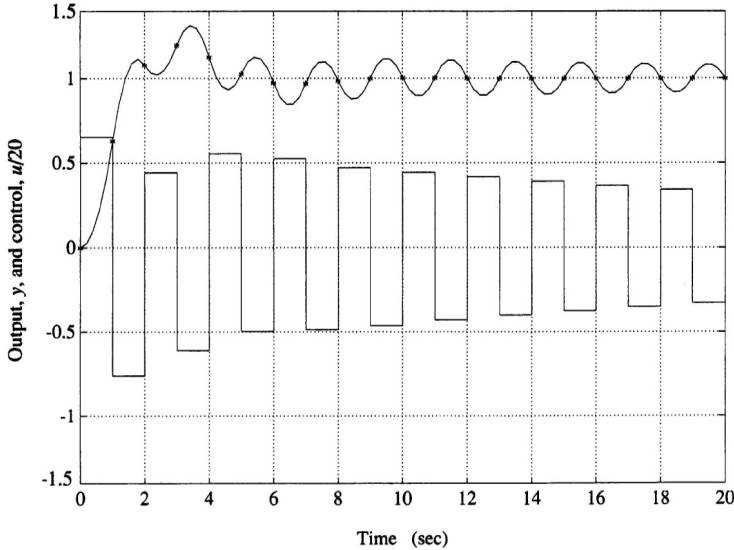


Figure 7.37
Step response of
antenna system
from direct
design

We shall also need

$$1 - H(z) = \frac{(z-1)(z-0.4180)}{z^2 - 0.7859z + 0.3679}. \quad (7.74)$$

We know that $H(1) = 1$ so that $1 - H(z)$ must have a zero at $z = 1$. Now, turning to the basic design formula, Eq. (7.54), we compute

$$\begin{aligned} D(z) &= \frac{(z-1)(z-0.9048)(0.6321)}{(0.04837)(z+0.9672)} \frac{(z-0.07932)}{(z-1)(z-0.4180)} \\ &= 13.07 \frac{(z-0.9048)(z-0.07932)}{(z+0.9672)(z-0.4180)}. \end{aligned}$$

A plot of the step response of the resulting design for this example is provided in Fig. 7.37 and verifies that the response samples behave as specified by $H(z)$. However, as can be seen also from the figure, large oscillations occur in the control that cause a large ripple in the system response between samples. How can this be for a system response transfer function,

$$\frac{Y(z)}{R(z)} = H(z) = \frac{DG}{1 + DG},$$

that is designed to have only two well-damped roots? The answer lies in the fact that the control response is determined from

$$\frac{U(z)}{R(z)} = \frac{D}{1 + DG} = \frac{H(z)}{G(z)},$$

which for this example is

$$\frac{U(z)}{R(z)} = 13.06 \frac{z-0.0793}{z^2 - 0.7859z + 0.3679} \frac{(z-1)(z-0.9048)}{z+0.9672}.$$

The pole at $z = -0.9672$, very near to the unit circle, is the source of the oscillation in the control response. The poor transient due to the pole did not show up in the output response because it was exactly canceled by a zero in the plant transfer function. The large control oscillation in turn causes the ripple in the output response. This pole was brought about because we allowed the controller to have a pole to cancel a plant zero at this position. The poor response that resulted could have been

avoided if this nearly unstable zero had been included in the stability constraint list. In that case we would introduce another term in $H(z)$, b_3z^{-3} , and require that $H(z)$ be zero at $z = -0.9672$, so this zero of $G(z)$ is not canceled by $D(z)$. The result will be a simpler $D(z)$ with a slightly more complicated $H(z)$.

7.6 Summary

In this chapter we have reviewed the philosophy and specifications of the design of control systems by transform techniques and discussed three such methods.

- Discrete controllers can be designed by emulation, root locus, or frequency response methods.
- Successful design by emulation typically requires a sampling frequency at least 30 times the expected closed-loop bandwidth.
- Expressions for steady-state error constants for discrete systems have been given in Eq. (7.12) and Eq. (7.14) in terms of open-loop transfer functions and in Eq. (7.18) in terms of closed-loop poles and zeros.
- Root locus rules for discrete system characteristic equations are shown to be the same as the rules for continuous system characteristic equations.
- Step response characteristics such as rise time and overshoot can be correlated with regions of acceptable pole locations in the z -plane as sketched in Fig. 7.10.
- Asymptotes as used in continuous system frequency response plots *do not apply* for discrete frequency response.
- Nyquist's stability criterion and gain and phase margins were developed for discrete systems.
- The sensitivity function was shown to be useful to develop specifications on performance robustness as expressed in Eq. (7.34).
- Stability robustness in terms of the overall transfer function, the complementary sensitivity function, is expressed in Eq. (7.47).
- Limitations on the frequency response of closed-loop discrete designs are made more severe by poles and zeros outside the unit circle as expressed by Eq. (7.50) and Eq. (7.51).
- Lead and lag compensation can be used to improve the steady-state and transient response of discrete systems.
- The direct design method of Ragazzini can be used to realize a closed-loop transfer function limited only by causality and stability constraints.

7.7 Problems

- 7.1 Use the $z = e^{sT}$ mapping function and prove that the curve of constant ζ in s is a logarithmic spiral in z .
- 7.2 A servomechanism system is expected to have a rise-time of no more than 10 milliseconds and an overshoot of no more than 5%.
- (a) Plot in the s -plane the corresponding region of acceptable closed-loop pole locations.
 - (b) What is the estimated Bode gain crossover frequency (rad/sec)?
 - (c) What is the estimated phase margin in degrees?

- (d) What is the sample period, T , if the estimated phase shift due to the sample and hold is to be no more than 10° at the gain crossover?
- (e) What is the sample period T if there are to be 8 samples per rise time?

7.3 *Root locus review.* The following root loci illustrate important features of the root locus technique. All are capable of being sketched by hand, and it is recommended that they be done that way in order to develop skills in verifying a computer's output. Once sketched roughly by hand, it is useful to fill in the details with a computer.

- (a) The locus for

$$1 + K \frac{s+1}{s^2(s+p_1)} = 0$$

is typical of the behavior near $s = 0$ of a double integrator with lead compensation or a single integration with a lag network and one additional real pole. Sketch the locus versus K for values of p_1 of 5, 9, and 20. Pay close attention to the real axis break-in and break-away points.

- (b) The locus for

$$1 + K \frac{1}{s(s+1)((s+a)^2+4)} = 0$$

is a typical locus that includes complex poles and shows the value of departure angles. Plot the locus for $a = 0, 1, \text{ and } 2$. Be sure to note the departure angles from the complex poles in each case.

- (c) The locus for

$$1 + K \frac{(s+1)^2 + \omega_o^2}{s(s^2+4)} = 0$$

illustrates the use of complex zeros to compensate for the presence of complex poles due to structural flexibility. Be sure to estimate the angles of departure and arrival. Sketch the loci for $\omega_o = 1$ and $\omega_o = 3$. Which case is unconditionally stable (stable for all positive K less than the design value)?

- (d) For

$$1 + K \frac{s}{(s-p_1)(s-p_2)} = 0$$

show that the locus is a circle of radius $\sqrt{p_1 p_2}$ centered at the origin (location of the zero). Can this result be translated to the case of two poles and a zero on the negative real axis?

7.4 The basic transfer function of a satellite attitude control is $G(s) = \frac{1}{s^2}$.

- (a) Design a continuous lead network compensation so as to give closed-loop poles corresponding to $\zeta = 0.5$ and natural frequency $\omega_n = 1.0$. The ratio of pole to zero of the lead is to be no more than 10.
- Plot the step response of the design and note the rise time and the percent overshoot.
 - What is the system type and corresponding error constant?
- (b) Select a sampling period to give 10 samples in a rise time and compute the discrete equivalent to the lead using the Tustin bilinear transformation. Plot the step response of the discrete system and compare the rise time and overshoot to those of the continuous design.
- (c) Select a sampling period that will give 5 samples per rise time, compute the discrete equivalent using Tustin's method, and compare rise time and overshoot of this design with the continuous case.

- 7.5 Repeat the design for the satellite attitude control of Problem 4, including method of choosing sampling periods but using the matched pole-zero method to obtain the discrete compensations.
- 7.6 Repeat the design of the satellite attitude control of Problem 4 including method of choice of sampling period but using the triangle hold equivalent (noncausal first-order hold) to design the discrete compensations.
- 7.7 Repeat the design for the satellite attitude control of Problem 4 but augment the plant with a Pade approximation to the delay of $T/2$ which is to say, multiply the plant transfer function by

$$P(s) = \frac{1 - \frac{sT}{4}}{1 + \frac{sT}{4}}$$

before doing the continuous design. Once the design of the lead compensation is completed, continue with the discrete equivalents as in Problem 4, including the method of choosing sampling periods. Use the matched pole-zero method to obtain the discrete compensations. Compare the design with the continuous case.

- 7.8 Design a discrete compensation for the antenna control system as specified in Example 7.2 with a sample period of $T = 0.1$ using a matched pole-zero equivalent for the discrete compensation. Plot the step response and compare rise time and overshoot with those of the continuous design.
- 7.9 Design the antenna control system as specified in Example 7.2 with a sample period of $T = 0.5$ sec.
- Use the zero-pole mapping equivalent emulation method.
 - Augment the plant model with an approximation of the sample-hold delay consisting of

$$P(s) = \frac{2/T}{s + 2/T},$$

then redesign $D(s)$ and find the discrete equivalent with the matched pole-zero equivalent emulation method. Plot the step response and compare with the continuous design done on the unaugmented plant.

- Compare the degradation of the equivalent damping ratio ζ due to sampling for both design methods.
- 7.10 For the satellite with transfer function $1/s^2$, design a lead compensation to give closed-loop poles with damping $\zeta = 0.5$ and natural frequency $\omega_n = 1.0$. The pole-to-zero ratio of the compensation should not be more than 10. Plot the step response of the closed loop and note the rise time and overshoot.
- Let sampling period be $T_s = 0.5$ sec and compute the discrete model of the plant with a sample and zero-order hold. Using this model, design a discrete lead compensation with pole at $z = -0.5$ and a zero so as to give closed loop poles at the mapped place from the continuous poles, $\zeta = 0.5$ and $\omega_n = 1.0$. What is the ratio of ω_s/ω_n for this problem? How many samples do you expect to find per rise time? Plot the step response and compare result with expectation. Compare the discrete design with the continuous design.
 - Repeat the discrete design with sampling period $T_s = 1.2$ sec, plot the step response, and compare rise time and overshoot with the continuous case.
- 7.11 Sketch the region in the z -plane of discrete pole locations corresponding to $\zeta \geq 0.5$ and
- $\omega_n \leq \omega_s/30$.
 - $\omega_n \leq \omega_s/10$.

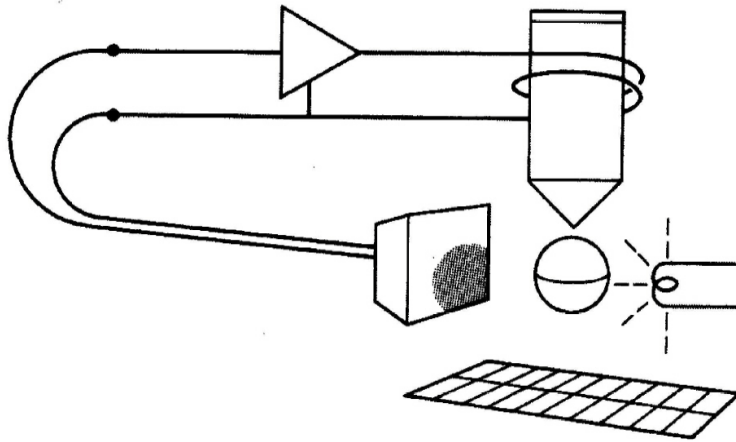


Figure 7.38
A steel ball
balanced by an
electromagnet

(c) $\omega_n \leq \omega_s/5$.

7.12 The plant transfer function

$$G(s) = \frac{1}{(s+0.1)(s+3)}$$

is to be controlled with a digital controller using a sample period of $T = 0.1$ sec.

- Design compensation using the z -plane root locus that will respond to a step with a rise time of ≤ 1 sec and an overshoot $\leq 5\%$. Plot the step response and verify that the response meets the specifications.
- What is the system type and corresponding error constant? What can be done to reduce the steady-state error to a step input?
- Design a discrete lag compensation that will cut the steady-state error in half. Plot the step response and compare the complete response to the transient and steady-state error specifications.

7.13 It is possible to suspend a steel ball bearing by means of an electromagnet whose current is controlled by the position of the mass [Woodson and Melcher (1968)]. A schematic of a possible setup is shown in Fig. 7.38. The equations of motion are

$$m\ddot{X} = -mg + f(X, I),$$

where the force on the ball due to the electromagnet is given by $f(X, I)$. It is found that the magnet force balances the gravity force when the magnet current is I_0 and the ball at X_0 . If we write $I = I_0 + i$ and $X = X_0 + x$ and expand f about $X = X_0$ and $I = I_0$, and then neglect higher-order terms, we obtain a linear approximation

$$m\ddot{x} = k_1x + k_2i.$$

Values measured for a particular device in the Stanford Controls Laboratory are $m = 0.02$ kg, $k_1 = 20$ N/m, $k_2 = 0.4$ N/A.

- Compute the transfer function from i to x and draw the (continuous) root locus for proportional feedback $i = -Kx$.
- Let the sample period be $T = 0.02$ sec and compute the plant discrete transfer function when used with a sample and zero-order hold.

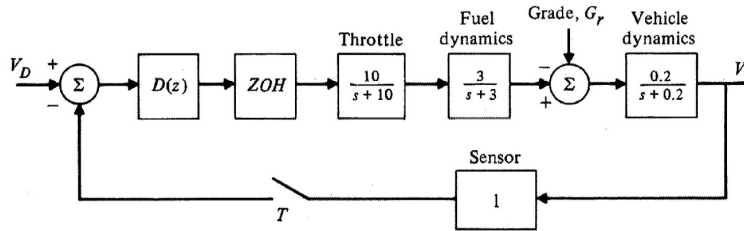


Figure 7.39
An automotive cruise-control system

- (c) Design a digital control for the magnetic levitation to meet the specifications $t_r \leq 0.1$ sec, $t_s \leq 0.4$ sec, and overshoot $\leq 20\%$.
- (d) Plot a root locus of your design versus m and discuss the possibility of balancing balls of various masses.
- (e) Plot a step response of your design to an initial disturbance displacement on the ball and show both x and the control current i . If the sensor can measure x over a range of only $\pm \frac{1}{2}$ cm, and if the amplifier can provide a maximum current of 1A, what is the *maximum* initial displacement, $x(0)_{\max}$ that will keep the variables within these limits, using $m = 0.02$ kg?

7.14 A discrete transfer function for approximate derivative control is

$$D(z) = K_p T_D \frac{z-1}{Tz},$$

where the pole at $z = 0$ adds some destabilizing phase lag. It therefore seems that it would be advantageous to remove it and to use derivative control of the form

$$D(z) = K_p T_D \frac{(z-1)}{T}.$$

Can this be done? Support your answer with the difference equation that would be required and discuss the requirements to implement it.

7.15 For the automotive cruise-control system shown in Fig. 7.39, the sample period is $T = 0.5$ sec.

- (a) Design a PD controller to achieve a t_r of 5 sec with no overshoot.
- (b) Determine the speed error on a 3% grade (i.e., $G_r = 3$ in Fig. 7.39).
- (c) Design a PID controller to meet the same specifications as in part (a) and that has zero steady-state error on constant grades. What is the velocity constant of your design?

7.16 For the disk drive read/write head assembly described in Fig. 7.40, you are to design a compensation that will result in a closed-loop settling time $t_s = 20$ msec and with overshoot to a step input $M_p \leq 20\%$.

- (a) Assume no sampling and use a continuous compensation. Plot the step response and verify that your design meets the specifications.
- (b) Assume a sampling period $T = 1$ msec and use matched pole-zero emulation. If you wish, you can include a Pade approximation to the delay and do a redesign of the continuous compensation before computing the discrete equivalent. Plot the step response and compare it with the continuous design's response.
- (c) Do a z -plane design for the same specifications and plot its step response. Compare these three designs with respect to meeting the transient performance.

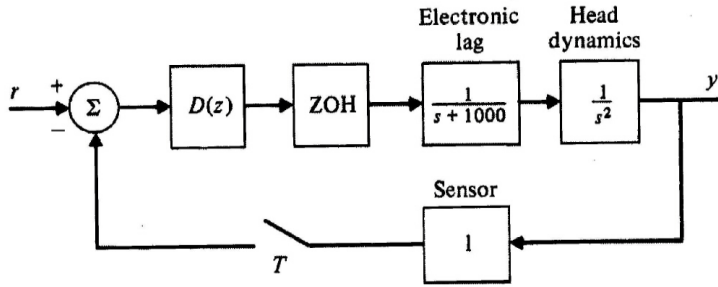


Figure 7.40
A disk drive
read/write head
assembly

7.17 The tethered satellite system shown in Fig. 7.41 has a moveable tether attachment point so that torques can be produced for attitude control. The block diagram of the system is shown in Fig. 7.42. Note that the integrator in the actuator block indicates that a constant-voltage command to the servomotor will produce a constant velocity of the attachment point.

- Is it possible to stabilize this system with θ feedback to a PID controller? Support your answer with a root locus argument.
- Suppose it is possible to measure δ , and $\dot{\theta}$ as well as θ . Select the variable(s) on which you would like to place a sensor(s) to augment the θ feedback.
- Design compensation for the system using the sensor(s) that you selected in part (b) so that it has a 2-sec rise time and equivalent closed loop damping of $\zeta = 0.5$.

7.18 The excavator shown in Fig. 7.43 has a sensor measuring the angle of the stick as part of a control system to control automatically the motion of the bucket through the earth. The sensed stick angle is to be used to determine the control signal to the hydraulic actuator moving the stick. The schematic diagram for this control system is shown in Fig 7.44, where $G(s)$ is the system transfer function given by

$$G(s) = \frac{1000}{s(s+10)(s^2+1.2s+144)}.$$

The compensation is implemented in a control computer sampling at $f_s = 50$ Hz and is of the form $D(z) = K(1 + K_1(1 - z^{-1}) + K_2(1 - 2z^{-1} + z^{-2}))$. The oscillatory roots in $G(s)$ arise from the compressibility of the hydraulic fluid (with some entrained air) and is often referred to as the *oil-mass resonance*.

- Show that the steady-state error, $\varepsilon (= \theta_r - \theta)$, is

$$\varepsilon(\infty) = \frac{1.44}{K},$$

when θ_r is a unit ramp.

- Determine the highest K possible (i.e., at the stability boundary) for proportional control ($K_1 = K_2 = 0$).
- Determine the highest K possible (i.e., at the stability boundary) for PD ($K_2 = 0$) control.
- Determine the highest K possible (i.e., at the stability boundary) for PD plus acceleration ($K_2 \neq 0$) control.⁷

7.19 For the excavator described in Problem 7.18 with transfer function

$$G(s) = \frac{1000}{s(s+10)(s^2+1.2s+144)},$$

plot the Bode plot and measure the gain and phase margins with just unity feedback.

⁷For further reading on damping the oil-mass resonance of hydraulic systems, see Viersma (1980).

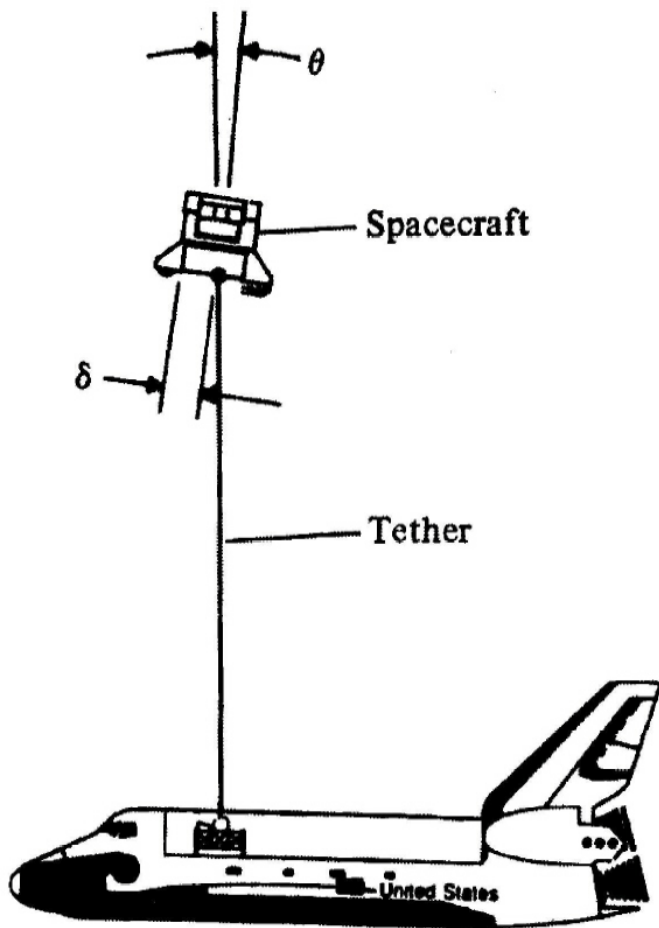
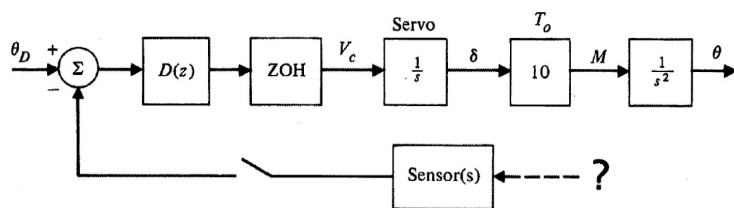


Figure 7.41
A tethered satellite system



δ = displacement of tether attachment point
 T_o = tether tension
 M = moment on satellite
 θ = satellite attitude

Figure 7.42
Block diagram for the tethered satellite system



Figure 7.43
An excavator with an automatic control system

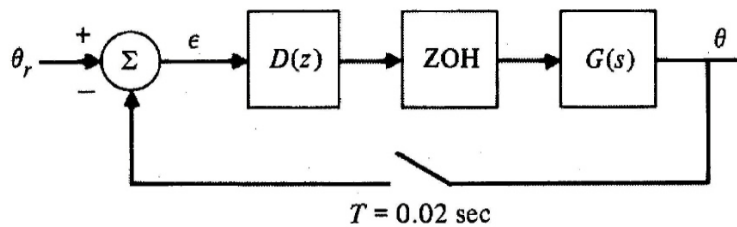


Figure 7.44
Schematic diagram for the control system of the excavator

- Design a compensation that will give a phase margin of 50° , a gain margin *as measured at the resonance peak* of at least 2 and a crossover of at least $\omega_{cg} \geq 1.0$. Plot the step response of the resulting design and note the rise time and the overshoot.
- With sample frequency $f_s = 50\text{Hz}$, design a discrete controller to meet the same specifications given for the continuous case. Plot the Bode plot of the design and verify that the specifications are met.

7.20 A simple model of a satellite attitude control has the transfer function $1/s^2$.

- Plot the Bode plot for this system and design a lead compensation to have a phase margin of 50° and a crossover ω_{cg} of 1.0 rad/sec. Plot the step response and note the rise time and overshoot.
- With sample period of $T = 0.2$ sec, design a discrete compensation to give 50° phase margin and crossover $\omega_{cg} = 1.0$. Plot the step response and compare rise time and overshoot with the continuous design.
- With sample period $T = 0.5$ sec, design a discrete compensation to give 50° phase margin and crossover $\omega_{cg} = 1.0$. Plot the step response and compare rise time and overshoot with the continuous design.

7.21 For a system given by

$$G(s) = \frac{a}{s(s+a)},$$

determine the conditions under which the K_v of the continuous system is approximately equal to the K_v of the system preceded by a ZOH and represented by its discrete transfer function.

7.22 Design a digital controller for

$$G(s) = \frac{1}{s(s+0.4)}$$

preceded by a ZOH so that the response has a rise time of approximately 0.5 sec, overshoot $< 25\%$, and zero steady-state error to a step command. [*Hint*: Cancel the plant pole at $s = 0.4$ with a compensator zero; a second-order closed-loop system will result, making the transient response comparison between experiment and theory much easier.]

- (a) Determine a $D(z)$ using emulation with the matched pole-zero mapping technique. Do two designs, one for $T = 100$ msec and one for $T = 250$ msec.
- (b) Repeat part (a) using the z -plane root locus method for the two sample periods.
- (c) Simulate the closed-loop system response to a unit step with the $D(z)$'s obtained in parts (a) and (b). Use the discrete equivalent of the plant in your calculations. Compare the four digitally controlled responses with the original specifications. Explain any differences that you find.

7.23 A generic mechanical control problem is that of two masses coupled by a lightly damped flexible structure. With amplitude and time scaling, the model can be reduced to

$$G(s) = K \frac{Bs + 1}{s^2(s^2 + Bs + 1)}.$$

For the parameters $K = 0.05$ and $B = 0.1$, plot the Bode plot and indicate the gain and phase margins. For performance tracking, the open loop gain for frequencies below $\omega = 0.005$ must be above 50 and the gain for frequencies above $\omega = 1$ must be below 0.5. The phase margin must be at least 35° .

- (a) Design a continuous compensation to meet the specifications. If possible, keep the phase above -180° so the system will not be conditionally stable.
- (b) Design a discrete compensation for the system with the lowest sampling frequency possible. A prize will be given to the student who obtains the lowest sampling frequency with a design that meets the specifications.
- (c) Plot the sensitivity of the digital design and compute the vector gain margin.

Chapter 8

Design Using State-Space Methods

A Perspective on State-Space Design Methods

In Chapter 7, we discussed how to design digital controllers using transform techniques, methods now commonly designated as “classical design.” The goal of this chapter is to solve the identical problem using the state-space formulation. The difference in the two approaches is entirely in the design method; the end result, a set of difference equations providing control, is identical.

Advantages of the state-space formulation are especially apparent when designing controllers for multi-input, multi-output (MIMO) systems, that is, those with more than one control input and/or sensed output. However, state-space methods are also an aid in the design of controllers for single-input, single-output (SISO) systems because of the widespread use of computer-aided control system design (CACSD) tools, which often rely heavily on this system representation. Chapters 4 and 5 have already demonstrated the advantages of the state-space formulation in using CACSD packages for the computation of discrete equivalents. State-space methods also offer advantages in the structure for command inputs and disturbance estimation. In this chapter, we will limit our state-space design efforts to SISO controllers, similar to those found in Chapter 7 with classical methods. Techniques for MIMO design are discussed in Chapter 9.

In Chapter 7, two basic methods were described: *emulation* and *direct digital design*. The same two methods apply to the state-space formulation as well. Using emulation, one would design a continuous controller using state-space methods, then transform the controller to a discrete form by using one of the discrete equivalents from Chapter 6. The discussion of the method and its accuracy in Chapter 7 applies equally well here. Furthermore, the development in Chapter 6 used both classical and state-space system descriptions in the computation of the equivalents. Therefore, no further discussion of emulation is required, and we will concentrate solely on the direct digital design method.

Chapter Overview

As for the continuous case reviewed in Section 2.6, design using state-space involves separate design of the control assuming all state elements are available, then design of an estimator to reconstruct the state given a partial measurement of it. Section 8.1 covers the discrete control design while Section 8.2 covers the discrete estimator design. Section 8.3 puts it together into what is called the **regulator** and Section 8.4 discusses the relative merits of the various ways of introducing the reference input command. Section 8.5 presents how a designer builds an integral control feature or disturbance estimation, and how they accomplish similar goals. Section 8.6 discusses the limitations imposed by delays in the system and how to minimize their effect. The chapter concludes in Section 8.7 with a discussion of observability and controllability, the required conditions for the design to be possible.

8.1 Control Law Design

In Chapter 2, we saw that the state-space description of a continuous system is given by Eq. (2.1)

$$\dot{\mathbf{x}} = \mathbf{F}\mathbf{x} + \mathbf{G}u, \quad (8.1)$$

and Eq. (2.2)

$$y = \mathbf{H}\mathbf{x} + Ju. \quad (8.2)$$

We assume the control is applied from the computer through a ZOH as shown in Fig. 1.1. Therefore, Eqs. (8.1, and (8.2) have an exact discrete representation as given by Eq. (4.59)

$$\begin{aligned} \mathbf{x}(k+1) &= \mathbf{\Phi}\mathbf{x}(k) + \mathbf{\Gamma}u(k), \\ y(k) &= \mathbf{H}\mathbf{x}(k) + Ju(k), \end{aligned} \quad (8.3)$$

where

$$\begin{aligned} \mathbf{\Phi} &= e^{\mathbf{F}T}, \\ \mathbf{\Gamma} &= \int_0^T e^{\mathbf{F}\eta} d\eta \mathbf{G}. \end{aligned} \quad (8.4)$$

We can easily transform between the classical transfer function of a continuous system, $G(s)$ (represented by `sysTF` in MATLAB), to the state-space continuous description by the MATLAB script¹

```
sysC = ss(sysTF)
```

where `sysC` contains $\mathbf{F}, \mathbf{G}, \mathbf{H}, J$. Provided the continuous system is preceded by a ZOH, we can transform to the discrete model, $\mathbf{\Phi}, \mathbf{\Gamma}, \mathbf{H}, J$, (or `sysD`) with a sample period T , using the MATLAB script

```
sysD = c2d(sysC, T)
```

One of the attractive features of state-space design methods is that the procedure consists of two independent steps. The first step *assumes* that we have all the state elements at our disposal for feedback purposes. In general, of course, this would not be a good assumption; a practical engineer would not, as a rule, find it necessary to purchase such a large number of sensors, especially because he or she knows that they would not be needed using classical design methods. The assumption that all states are available merely allows us to proceed with the first design step, namely, the control law. The remaining step is to design an “estimator” (or “observer”²), which estimates the entire state vector, given measurements of the portion of the state provided by Eq. (8.2). The final control algorithm will consist of a combination of the control law and the estimator with the control-law calculations based on the estimated states rather than on the actual states. In Section 8.3 we show that this substitution is reasonable and that the combined control law and estimator can give closed-loop dynamic characteristics that are unchanged from those assumed in designing the control law and estimator separately. The dynamic system we obtain from the combined control law and estimator is the same that has been previously referred to as compensation.

As for the continuous case, the control law is simply the feedback of a linear combination of all the state elements, that is

$$u = -\mathbf{K}\mathbf{x} = - \begin{bmatrix} K_1 & K_2 & \cdots \end{bmatrix} \begin{bmatrix} x_1 \\ x_2 \\ \vdots \end{bmatrix}. \quad (8.5)$$

Note that this structure does not allow for a reference input to the system. The topology that we used all through Chapter 7 (Fig. 7.5) always included a reference input, r . The control law, Eq. (8.5),

¹In MATLAB 4, $G(s)$ would be represented by `[num,den]` and the `tf2ss` function would be invoked. See Appendix F.

²The literature [Luenberger (1960)] commonly refers to these devices as “observers”; however, we feel that the term “estimator” is much more descriptive of their function because “observe” implies a direct measurement. In this book the term “estimator” is used but the reader can think of the terms interchangeably.

assumes that $r = 0$ and is, therefore, usually referred to as a **regulator**. Section 8.4 will discuss how one introduces reference inputs.

Substituting Eq. (8.5) in Eq. (8.3), we have

$$\mathbf{x}(k+1) = \mathbf{\Phi}\mathbf{x}(k) - \mathbf{\Gamma}\mathbf{K}\mathbf{x}(k). \quad (8.6)$$

Therefore the z -transform of Eq. (8.6) is

$$(z\mathbf{I} - \mathbf{\Phi} + \mathbf{\Gamma}\mathbf{K})\mathbf{X}(z) = 0,$$

and the characteristic equation of the system with the hypothetical control law is

$$|z\mathbf{I} - \mathbf{\Phi} + \mathbf{\Gamma}\mathbf{K}| = 0. \quad (8.7)$$

8.1.1 Pole Placement

The approach we wish to take at this point is pole placement; that is, having picked a control law with enough parameters to influence all the closed-loop poles, we will arbitrarily select the desired pole locations of the closed-loop system and see if the approach will work. Although this approach can often lead to trouble in the design of complex systems (see the discussion in Sections 2.6 and 8.3), we use it here to illustrate the power of full state feedback. In Chapter 9, we will build on this idea to arrive at a more practical design methodology.

The control-law design, then, consists of finding the elements of \mathbf{K} so that the roots of Eq. (8.7), that is, the poles of the closed-loop system, are in the desired locations. Unlike classical design, where we iterated on parameters in the compensator (hoping) to find acceptable closed-loop root locations, the full state feedback, pole-placement approach guarantees success and allows us to arbitrarily pick any pole location, providing that n poles are specified for an n th-order system.

Given desired pole locations,³ say

$$z_i = \beta_1, \beta_2, \beta_3, \dots, \beta_n,$$

the desired control-characteristic equation is

$$\alpha_c(z) = (z - \beta_1)(z - \beta_2) \cdots (z - \beta_n) = 0. \quad (8.8)$$

Equations (8.7) and (8.8) are both the characteristic equation of the controlled system; therefore, they must be identical, term by term. Thus we see that the required elements of \mathbf{K} are obtained by matching the coefficients of each power of z in Eq. (8.7) and Eq. (8.8), and there will be n equations for an n th-order system.

Pole Placement for Satellite Attitude Control

Example 8.1

Design a control law for the satellite attitude-control system described by Eq. (4.47). Pick the z -plane roots of the closed-loop characteristic equation so that the equivalent s -plane roots have a damping ratio of $\zeta = 0.5$ and real part of $s = -1.8$ rad/sec (i.e., $s = -1.8 \pm j3.12$ rad/sec). Use a sample period of $T = 0.1$ sec.

Solution. Example 4.11 showed that the discrete model for this system is

$$\mathbf{\Phi} = \begin{bmatrix} 1 & T \\ 0 & 1 \end{bmatrix} \quad \text{and} \quad \mathbf{\Gamma} = \begin{bmatrix} T^2/2 \\ T \end{bmatrix}.$$

Using $z = e^{sT}$ with a sample period of $T = 0.1$ sec, we find that $s = -1.8 \pm j3.12$ rad/sec translates to $z = 0.8 \pm j0.25$, as shown in Fig. 8.1. The desired characteristic equation is then

$$z^2 - 1.6z + 0.70 = 0, \quad (8.9)$$

³Discussion of how one selects pole locations was reviewed in Section 2.6 for the continuous case and will occur through the following examples and in Section 8.3 for the discrete case. The results of the specification discussion in Chapter 7 can also be used to specify poles.

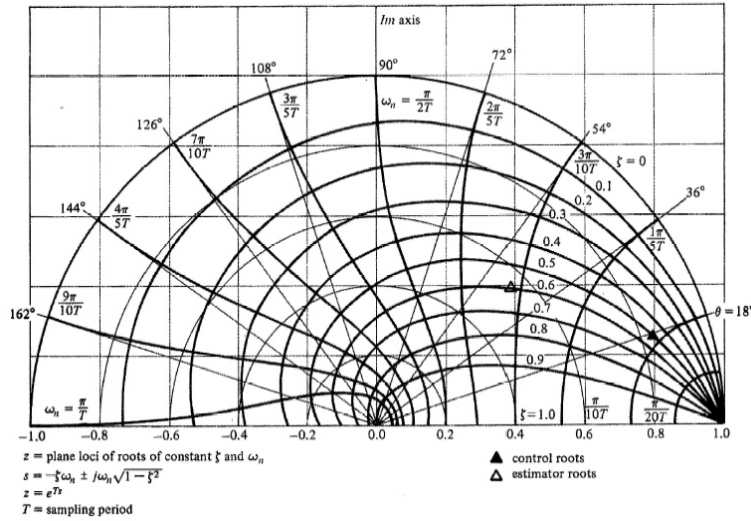


Figure 8.1
Desired root locations for satellite attitude-control system of Examples 8.1 and 8.4

and the evaluation of Eq. (8.7) for any control law \mathbf{K} leads to

$$\left| z \begin{bmatrix} 1 & 0 \\ 0 & 1 \end{bmatrix} - \begin{bmatrix} 1 & T \\ 0 & 1 \end{bmatrix} + \begin{bmatrix} T^2/2 \\ T \end{bmatrix} \begin{bmatrix} K_1 & K_2 \end{bmatrix} \right| = 0$$

or

$$z^2 + (TK_2 + (T^2/2)K_1 - 2)z + (T^2/2)K_1 - TK_2 + 1 = 0. \tag{8.10}$$

Equating coefficients in Eqs. (8.9) and (8.10) with like powers of z , we obtain two simultaneous equations in the two unknown elements of \mathbf{K}

$$\begin{aligned} TK_2 + (T^2/2)K_1 - 2 &= -1.6, \\ (T^2/2)K_1 - TK_2 + 1 &= 0.70, \end{aligned}$$

which are easily solved for the coefficients and evaluated for $T = 0.1$ sec

$$K_1 = \frac{0.10}{T^2} = 10, \quad K_2 = \frac{0.35}{T} = 3.5.$$

The calculation of the gains using the method illustrated in the previous example becomes rather tedious when the order of the system (and therefore the order of the determinant to be evaluated) is greater than 2. A computer does not solve the tedium unless it is used to perform the algebraic manipulations necessary in expanding the determinant in Eq. (8.7) to obtain the characteristic equation. Therefore, other approaches have been developed to provide convenient computer-based solutions to this problem.

The algebra for finding the specific value of \mathbf{K} is especially simple if the system matrices happen to be in the form associated with the block diagram of Fig. 4.8(c). This structure is called “control canonical form” because it is so useful in control law design. Referring to that figure and taking the state elements as the outputs of the delays (z^{-1} blocks), numbered from the left, we get (assuming $b_0 = 0$ for this case)

$$\Phi_c = \begin{bmatrix} -a_1 & -a_2 & -a_3 \\ 1 & 0 & 0 \\ 0 & 1 & 0 \end{bmatrix}, \quad \Gamma_c = \begin{bmatrix} 1 \\ 0 \\ 0 \end{bmatrix}, \quad \mathbf{H}_c = [b_1 \quad b_2 \quad b_3]. \tag{8.11}$$

Note that from Eq. (4.15), the characteristic polynomial of this system is $a(z) = z^3 + a_1z^2 + a_2z + a_3$. The key idea here is that the elements of the first row of Φ_c are exactly the coefficients of the

characteristic polynomial of the system. If we now form the closed-loop system matrix $\Phi_c - \Gamma_c \mathbf{K}$, we find

$$\Phi_c - \Gamma_c \mathbf{K} = \begin{bmatrix} -a_1 - K_1 & -a_2 - K_2 & -a_3 - K_3 \\ 1 & 0 & 0 \\ 0 & 1 & 0 \end{bmatrix}. \quad (8.12)$$

By inspection, we find that the characteristic equation of Eq. (8.12) is

$$z^3 + (a_1 + K_1)z^2 + (a_2 + K_2)z + (a_3 + K_3) = 0.$$

Thus, if the desired pole locations result in the characteristic equation

$$z^3 + \alpha_1 z^2 + \alpha_2 z + \alpha_3 = 0,$$

then the necessary values for control gains are

$$K_1 = \alpha_1 - a_1, \quad K_2 = \alpha_2 - a_2, \quad K_3 = \alpha_3 - a_3. \quad (8.13)$$

Conceptually, then, we have the canonical-form design method: Given an arbitrary (Φ, Γ) and a desired characteristic equation $\alpha(z) = 0$, we convert (by redefinition of the state) (Φ, Γ) to control form (Φ_c, Γ_c) and solve for the gain by Eq. (8.13). Because this gain is for the state in the control form, we must, finally, express the result back in terms of the original state elements. This method is sometimes used by CACSD packages because of the numerical advantages; however, the transformation is transparent to the designer, who generally prefers to use a state definition that is related to the physical system's characteristics.

8.1.2 Controllability

The first question this process raises is existence: Is it always possible to find an equivalent (Φ_c, Γ_c) for arbitrary (Φ, Γ) ? The answer is almost always “yes.” The exception occurs in certain pathological systems, dubbed “uncontrollable,” for which no control will give arbitrary pole locations. These systems have certain modes or subsystems that are unaffected by the control. Uncontrollability is best exhibited by a realization (selection of state elements) where each state element represents a natural mode of the system. If all the roots of the open-loop characteristic equation

$$|z\mathbf{I} - \Phi| = 0$$

are distinct, then Eq. (8.3) written in this way (normal mode or “Jordan canonical form”) becomes

$$\mathbf{x}(k+1) = \begin{bmatrix} \lambda_1 & 0 & \cdots & 0 \\ 0 & \lambda_2 & \cdots & 0 \\ 0 & 0 & \ddots & 0 \\ 0 & 0 & \cdots & \lambda_n \end{bmatrix} \mathbf{x}(k) + \begin{bmatrix} \Gamma_1 \\ \Gamma_2 \\ \vdots \\ \Gamma_n \end{bmatrix} u(k), \quad (8.14)$$

and explicitly exhibits the criterion for controllability: No element in Γ can be zero. If any Γ element was zero, the control would not influence that normal mode, and the associated state would remain uncontrolled. A good physical understanding of the system being controlled usually prevents any attempt to design a controller for an uncontrollable system; however, there is a mathematical test for controllability applicable to any system description, which may be an additional aid in discovering this condition; a discussion of this test is contained in Section 8.7.

8.1.3 Pole Placement Using CACSD

MATLAB has two functions that perform the calculation of `K` `place.m` and `acker.m`. `Acker` is based on Ackermann's formula [Ackermann (1972)] and is satisfactory for SISO systems of order less than 10 and can handle systems with repeated roots. The relation is

$$\mathbf{K} = [0 \quad \cdots \quad 1] [\Gamma \quad \Phi\Gamma \quad \Phi^2\Gamma \quad \cdots \quad \Phi^{n-1}\Gamma]^{-1} \alpha_c(\Phi) \quad (8.15)$$

where $\mathcal{C} = [\mathbf{\Gamma} \quad \mathbf{\Phi}\mathbf{\Gamma} \dots]$ is called the **controllability matrix**, n is the order of the system or number of state elements, and we substitute $\mathbf{\Phi}$ for z in $\alpha_c(z)$ to form controllability matrix

$$\alpha_c(\mathbf{\Phi}) = \mathbf{\Phi}^n + \alpha_1 \mathbf{\Phi}^{n-1} + \alpha_2 \mathbf{\Phi}^{n-2} + \dots + \alpha_n \mathbf{I}, \quad (8.16)$$

where the α_i 's are the coefficients of the desired characteristic equation, that is,

$$\alpha_c(z) = |z\mathbf{I} - \mathbf{\Phi} + \mathbf{\Gamma}\mathbf{K}| = z^n + \alpha_1 z^{n-1} + \dots + \alpha_n. \quad (8.17)$$

The controllability matrix, \mathcal{C} , must be full rank for the matrix to be invertible and for the system to be controllable.

`place` [Kautsky, Nichols, and Van Dooren (1985)] is best for higher order systems and can handle MIMO systems, but will not handle systems where the desired roots are repeated.

Note that these functions are used for both the continuous and discrete cases because they solve the same mathematical problems given by Eqs. (2.37) and (8.7). The only difference is that the desired root locations are in substantially different locations for the s -plane and z -plane and that \mathbf{F} , \mathbf{G} have been replaced by $\mathbf{\Phi}$ and $\mathbf{\Gamma}$.

Control Law Pole Placement with MATLAB

Example 8.2

Design a control law for the satellite attitude-control system as in Example 8.1. Place the z -plane closed-loop poles at $z = 0.8 \pm j0.25$.

Solution. The MATLAB statements

```
T = .1
Phi = [1 T; 0 1]
Gam = [T^2/2; T]
p = [.8+i*.25; .8-i*.25]
K = acker(Phi, Gam, p)
```

result in $\mathbf{K} = [10.25 \quad 3.4875]$. The difference between these values and those shown in Example 8.1 are due to round-off error in the hand calculation. `place` would have given the same answer.

A more complex system demonstrates the kind of difficulty you might encounter in using the pole placement approach. The specific difficulty is brought about by the necessity to pick n desired pole locations. Where should the higher frequency poles be picked? The system specifications typically help the designer pick only two of the desired poles. As discussed in Section 2.6, it is helpful to move poles as little as possible in order to minimize the required amount of control effort and to avoid exciting the system any more than necessary. The following example specifically illustrates how a poor choice of desired poles can cause an undesirable response, and how a wise choice of desired poles can drastically improve the situation.

Pole Placement for a 4th-Order System with MATLAB

Example 8.3

Design a control law for the double mass-spring system in Appendix A.4 using d as the measurement. This system is representative of many systems where there is some flexibility between the measured output and control input. Assume the resonant mode has a frequency $\omega_n = 1$ rad/sec and damping $\zeta = 0.02$ and select a 10:1 ratio of the two masses. The parameters that provide these characteristics are: $M = 1$ kg, $m = 0.1$ kg, $b = 0.0036$ N-sec/m, and $k = 0.091$ N/m. Pick the sample rate to be 15 times faster than the resonance and show the free response to an initial condition of $d = 1$ m for two cases:

- (a) Pick all the poles at $z = 0.9$.
- (b) Pick the poles at $z = 0.9 \pm j0.05, 0.8 \pm j0.4$.

Discuss why the response is better for case (b).

Solution. From Eq. (A.17) we can write the state-space description as

$$x = [d \quad \dot{d} \quad y \quad \dot{y}]^T$$

$$\mathbf{H} = \begin{bmatrix} 1 & 0 & 0 & 0 \\ 0 & 1 & 0 & 0 \\ 0 & 0 & 1 & 0 \\ 0 & 0 & 0 & 1 \end{bmatrix}$$

$$\mathbf{F} = \begin{bmatrix} 0 & 1 & 0 & 0 \\ -0.91 & -0.036 & 0.91 & 0.036 \\ 0 & 0 & 0 & 1 \\ 0.091 & 0.0036 & -0.091 & -0.0036 \end{bmatrix}$$

$$\mathbf{G} = \begin{bmatrix} 0 \\ 0 \\ 0 \\ 1 \end{bmatrix}, \quad J = 0.$$

The sample rate should be 15 rad/sec which translates to approximately $T = 0.4$ secs.

- (a) All poles at $z = 0.9$, the MATLAB script

```
sysC = ss(F,G,H,J)
sysD = c2d(sysC,T,'zoh')
p = [.9;.9;.9;.9]
[phi,gam,H,J] = ssdata(sysD)
K=acker(phi,gam,p)
```

results in the feedback gain

$$\mathbf{K} = [0.650 \quad -0.651 \quad -0.645 \quad 0.718]. \quad (8.18)$$

`place` cannot be used for case (a) because of the repeated roots. For the response to an initial condition, the script

```
sysCL = feedback(sysD,K)
Xo = [1;0;0;0]
d = initial(sysCL,Xo)
```

produces the closed-loop response for $d(0) = 1$ m, shown in Fig. 8.2(a). It exhibits a response that is *much* larger than that of the initial condition, but the time characteristics are consistent with the selected poles.

- (b) For the desired poles at $z = 0.9 \pm j0.05, 0.8 \pm j0.4$, we modify the script above with

```
p = [.9+i*.05;.9-i*.05;.8+i*.4;.8-i*.4]
```

and this results in the feedback gain

$$\mathbf{K} = [-0.458 \quad -0.249 \quad 0.568 \quad 0.968], \quad (8.19)$$

which produces the response to an initial condition, $d = 1$ m, shown in Fig. 8.2(b). It exhibits *much* less response of d with no increase in control effort, although the resonant mode oscillations did influence the response with damping consistent with the poles selected. The primary reason for the superior response is that the oscillatory mode was not changed substantially by the control. Two of the selected poles ($z = 0.8 \pm j0.4$) have a natural frequency $\omega_n = 1$ rad/sec with a damping $\zeta \cong 0.2$. Therefore, the control is not attempting to change the natural frequency of the resonant mode at all; rather, the only task for the control in modifying this pole is to increase its damping from $\zeta = 0.02$ to $\zeta \cong 0.2$. Since the mode remains lightly damped, its oscillations are still visible on the output. The selected poles at $z = 0.9 \pm j0.05$ affect the overall motion of the system and their placement is less critical. Generally, pole selections with a damping $\zeta \cong 0.7$ give a better balance between system response and control usage. The control is clearly much more effective with these desired pole locations.

So we see that the mechanics of computing the control law are easy, once the desired pole locations are known. The trick is to pick a good set of poles! The designer should iterate between pole selections and some other system evaluation to determine when the design is complete. System evaluation might consist of an initial-condition time response as shown in the example, a step response, steady-state errors, gain and phase margins, or the entire frequency-response shape. Pole placement by itself leaves something to be desired. But it is useful as a design tool to be used in conjunction with the other design methods discussed in Chapter 7 or as a part of an optimal design process that will be discussed in Chapter 9.

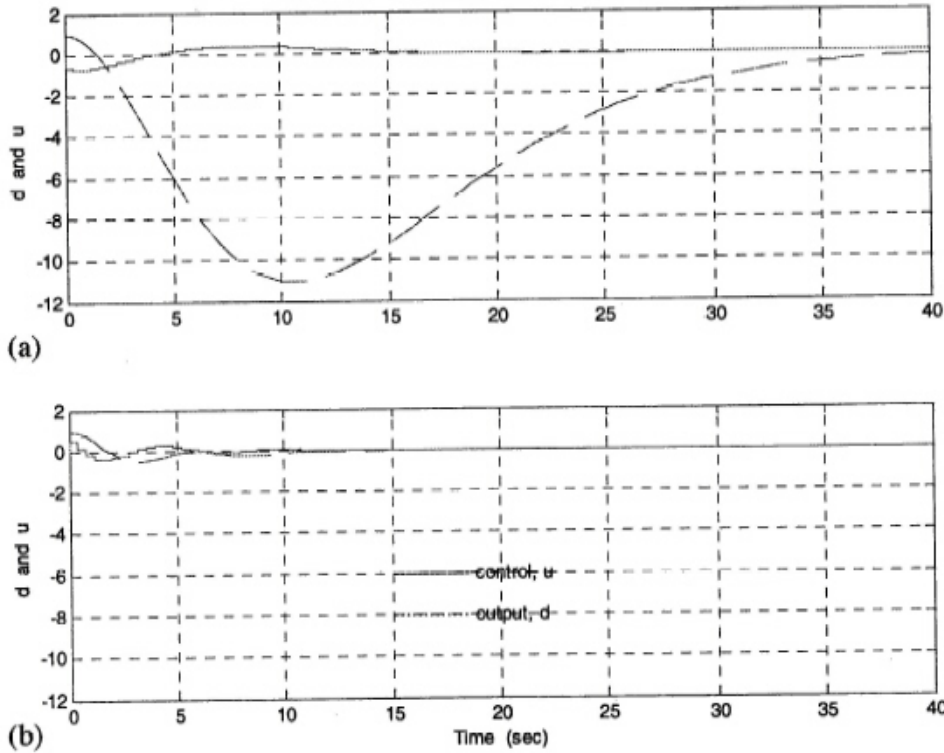


Figure 8.2
Initial condition
response for
Example 8.3;
(a) desired poles
all at $z = 0.9$, and
(b) desired poles
at $z = 0.9 \pm$
 $j0.05, 0.8 \pm j0.4$

8.2 Estimator Design

The control law designed in the last section assumed that all state elements were available for feedback. Typically, not all elements are measured; therefore, the missing portion of the state needs to be reconstructed for use in the control law. We will first discuss methods to obtain an estimate of the entire state given a measurement of one of the state elements. This will provide the missing elements as well as provide a smoothed value of the measurement, which is often contaminated with random errors or “noise.” There are two basic kinds of estimates of the state, $\mathbf{x}(k)$: We call it the **current** estimate, $\hat{\mathbf{x}}(k)$, if based on measurements $y(k)$ up to and including the k th instant; and we call it the **predictor** estimate, $\bar{\mathbf{x}}(k)$, if based on measurements up to $y(k-1)$. The idea eventually will be to let $u = -\mathbf{K}\hat{\mathbf{x}}$ or $u = -\mathbf{K}\bar{\mathbf{x}}$, replacing the true state used in Eq. (8.5) by its estimate.

8.2.1 Prediction Estimators

One method of estimating the state vector which might come to mind is to construct a model of the plant dynamics,

$$\bar{\mathbf{x}}(k+1) = \Phi\bar{\mathbf{x}}(k) + \Gamma u(k). \quad (8.20)$$

We know Φ , Γ , and $u(k)$, and hence this estimator should work if we can obtain the correct $\mathbf{x}(0)$ and set $\bar{\mathbf{x}}(0)$ equal to it. Figure 8.3 depicts this “open-loop” estimator. If we define the error in the estimate as

$$\tilde{\mathbf{x}} = \mathbf{x} - \bar{\mathbf{x}}, \quad (8.21)$$

and substitute Eqs. (8.3) and (8.20) into Eq. (8.21), we find that the dynamics of the resulting system are described by the estimator-error equation

$$\tilde{\mathbf{x}}(k+1) = \Phi\tilde{\mathbf{x}}(k). \quad (8.22)$$

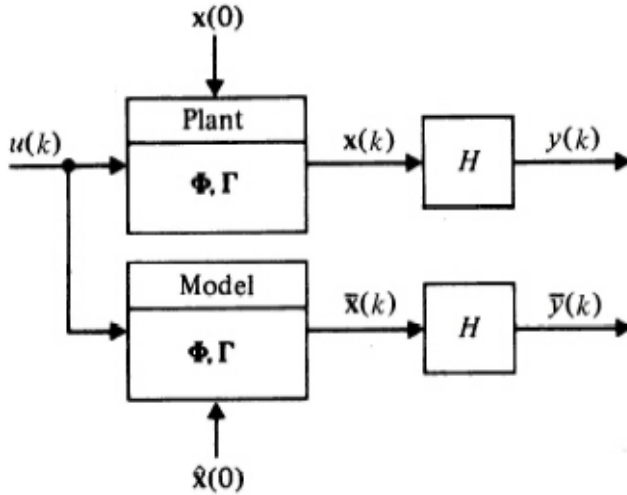


Figure 8.3
Open-loop
estimator

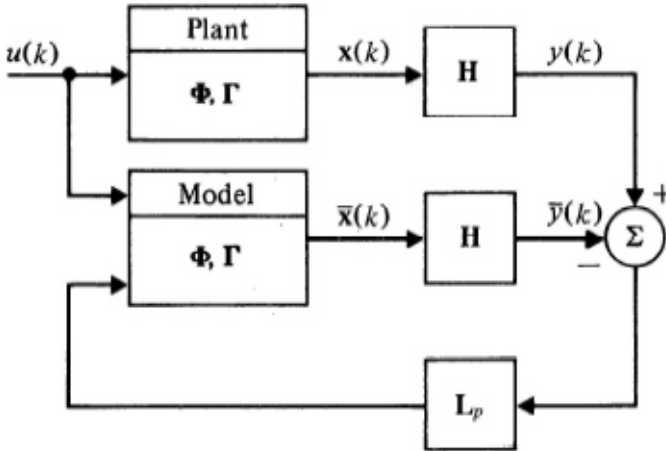


Figure 8.4
Closed-loop
estimator

Thus, if the initial value of $\bar{\mathbf{x}}$ is off, the dynamics of the estimate error are those of the uncompensated plant, Φ . For a marginally stable or unstable plant, the error will never decrease from the initial value. For an asymptotically stable plant, an initial error will decrease only because the plant and estimate will both approach zero. Basically, the estimator is running open loop and not utilizing any continuing measurements of the system's behavior, and we would expect that it would diverge from the truth. However, if we feed back the difference between the measured output and the estimated output and constantly correct the model with this error signal, the divergence should be minimized. The idea is to construct a feedback system around the open-loop estimator with the estimated output error as the feedback. This scheme is shown in Fig. 8.4; the equation for it is

$$\bar{\mathbf{x}}(k+1) = \Phi \bar{\mathbf{x}}(k) + \Gamma u(k) + \mathbf{L}_p [y(k) - H \bar{\mathbf{x}}(k)], \quad (8.23)$$

where \mathbf{L}_p is the feedback gain matrix. We call this a **prediction estimator** because a measurement at time k results in an estimate of the state vector that is valid at time $k+1$; that is, the estimate has been predicted one cycle in the future.

A difference equation describing the behavior of the estimation errors is obtained by subtracting

Eq. (8.23) from Eq. (8.3). The result is

$$\bar{\mathbf{x}}(k+1) = [\Phi - \mathbf{L}_p \mathbf{H}] \bar{\mathbf{x}}(k). \quad (8.24)$$

This is a homogeneous equation, but the dynamics are given by $[\Phi - \mathbf{L}_p \mathbf{H}]$; and if this system matrix represents an asymptotically stable system, $\bar{\mathbf{x}}$ will converge to zero for any value of $\bar{\mathbf{x}}(0)$. In other words, $\bar{\mathbf{x}}(k)$ will converge toward $\mathbf{x}(k)$ regardless of the value of $\bar{\mathbf{x}}(0)$ and could do so faster than the normal (open-loop) motion of $\mathbf{x}(k)$ if the estimator gain, \mathbf{L}_p , were large enough so that the roots of $\Phi - \mathbf{L}_p \mathbf{H}$ are sufficiently fast. In an actual implementation, $\bar{\mathbf{x}}(k)$ will not equal $\mathbf{x}(k)$ because the model is not perfect, there are unmodelled disturbances, and the sensor has some errors and added noise. However, typically the sensed quantity and \mathbf{L}_p can be chosen so that the system is stable and the error is acceptably small.

To find the value of \mathbf{L}_p , we take the same approach that we did when designing the control law. First, specify the desired estimator pole locations in the z -plane to obtain the desired estimator characteristic equation,

$$(z - \beta_1)(z - \beta_2) \cdots (z - \beta_n) = 0, \quad (8.25)$$

where the β 's are the desired estimator pole locations⁴ and represent how fast the estimator state vector converges toward the plant state vector. Then form the characteristic equation from the estimator-error equation (8.24),

$$|z\mathbf{I} - \Phi + \mathbf{L}_p \mathbf{H}| = 0. \quad (8.26)$$

Equations (8.25) and (8.26) must be identical. Therefore, the coefficient of each power of z must be the same, and, just as in the control case, we obtain n equations in n unknown elements of \mathbf{L}_p for an n th-order system.

Estimator Design for Satellite Attitude

Example 8.4

Construct an estimator for the same case as in Example 8.1, where the measurement is the position state element, x_1 , so that $\mathbf{H} = [1 \ 0]$ as given by Eq. (4.47). Pick the desired poles of the estimator to be at $z = 0.4 \pm j0.4$ so that the s -plane poles have $\zeta \cong 0.6$ and ω_n is about three times faster than the selected control poles (see Fig. 8.1).

Solution. The desired characteristic equation is then (approximately)

$$z^2 - 0.8z + 0.32 = 0, \quad (8.27)$$

and the evaluation of Eq. (8.26) for any estimator gain \mathbf{L}_p leads to

$$\left| z \begin{bmatrix} 1 & 0 \\ 0 & 1 \end{bmatrix} - \begin{bmatrix} 1 & T \\ 0 & 1 \end{bmatrix} + \begin{bmatrix} L_{p1} \\ L_{p2} \end{bmatrix} \begin{bmatrix} 1 & 0 \end{bmatrix} \right| = 0$$

or

$$z^2 + (L_{p1} - 2)z + TL_{p2} + 1 - L_{p1} = 0. \quad (8.28)$$

Equating coefficients in Eqs. (8.27) and (8.28) with like powers of z , we obtain two simultaneous equations in the two unknown elements of \mathbf{L}_p

$$\begin{aligned} L_{p1} - 2 &= -0.8 \\ TL_{p2} + 1 - L_{p1} &= 0.32, \end{aligned}$$

which are easily solved for the coefficients and evaluated for $T = 0.1$ sec

$$L_{p1} = 1.2, \quad L_{p2} = \frac{0.52}{T} = 5.2. \quad (8.29)$$

Thus the estimator algorithm would be Eq. (8.23) with L_p given by Eq. (8.29), and the equations to be coded in the computer are

$$\begin{aligned} \bar{x}_1(k+1) &= \bar{x}_1(k) + 0.1\bar{x}_2(k) + 0.005u(k) + 1.2[y(k) - \bar{x}_1(k)] \\ \bar{x}_2(k+1) &= \bar{x}_2(k) + 0.1u(k) + 5.2[y(k) - \bar{x}_1(k)]. \end{aligned}$$

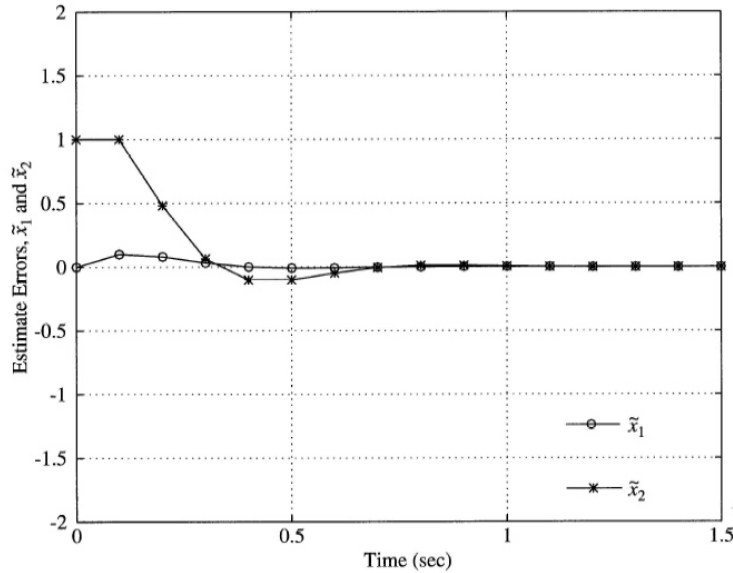


Figure 8.5
Time history of
the prediction
estimator error

Figure 8.5 shows the time history of the estimator error from Eq. (8.24) for the gains in Eq. (8.29) and with an initial error of 0 for the position estimate and 1 rad/sec for the velocity estimate.

The transient settling in \tilde{x}_2 could be hastened by higher values of the gains, \mathbf{L}_p , that would result by selecting faster estimator poles, but this would occur at the expense of more response of both \tilde{x}_1 and \tilde{x}_2 to measurement noise.

It is important to note that an initial estimator transient or, equivalently, the occurrence of an unmodelled input to the plant, can be a rare event. If the problem is one of regulation, the initial transient might be unimportant compared to the long-term performance of the estimator in the presence of noisy measurements. In the regulator case with very small plant disturbances, very slow poles (maybe even slower than the control poles) and their associated low estimator gains would give smaller estimate errors. Optimal selection of estimator gains based on the system's noise characteristics will be discussed in Chapter 9.

8.2.2 Observability

Given a desired set of estimator poles, is \mathbf{L}_p uniquely determined? It is, provided y is a scalar and the system is “observable.” We might have an unobservable system if some of its modes do not appear at the given measurement. For example, if only derivatives of certain states are measured and these states do not affect the dynamics, a constant of integration is obscured. This situation occurs with a $1/s^2$ plant if only velocity is measured, for then it is impossible to deduce the initial condition of the position. For an oscillator, a velocity measurement is sufficient to estimate position because the acceleration, and consequently the velocity, observed are affected by position. A system with cycle delays can also be unobservable because the state elements representing the delays have no influence on the measurement and can therefore not be reconstructed by the measurements. A mathematical test for observability is stated in the next section as a necessary condition for the solution of Ackermann's formula; its proof is given in Section 8.7.

⁴The following sections discuss how one should select these poles in relation to the control poles and how both sets of poles appear in the combined system. The issue was also discussed for the continuous case in Section 2.6.2.

8.2.3 Pole Placement Using CACSD

If we take the transpose of the error-equation system matrix from Eq. (8.24)

$$[\Phi - \mathbf{L}_p \mathbf{H}]^T = \Phi^T - \mathbf{H}^T \mathbf{L}_p^T,$$

we see that the result is the same form as the system matrix $\Phi - \Gamma \mathbf{K}$ of the control problem from Eq. (8.6), and the mathematics of the solution is the same. Therefore, to solve the problem, we substitute Φ^T for Φ , \mathbf{H}^T for Γ and \mathbf{L}_p^T for \mathbf{K} , and use the control-design results. Making the substitutions in Eq. (8.15) results in Ackermann's estimator formula

$$\mathbf{L}_p = \alpha_e(\Phi) \begin{bmatrix} \mathbf{H} \\ \mathbf{H}\Phi \\ \mathbf{H}\Phi^2 \\ \vdots \\ \mathbf{H}\Phi^{n-1} \end{bmatrix}^{-1} \begin{bmatrix} 0 \\ 0 \\ \vdots \\ 0 \\ 1 \end{bmatrix}, \quad (8.30)$$

where

$$\alpha_e(\Phi) = \Phi^n + \alpha_1 \Phi^{n-1} + \alpha_2 \Phi^{n-2} + \cdots + \alpha_n \mathbf{I}, \quad (8.31) \quad \begin{array}{l} \text{observability} \\ \text{matrix} \end{array}$$

and the α_i 's are the coefficients of the desired characteristic equation, that is

$$\alpha_e(z) = (z - \beta_1)(z - \beta_2) \cdots (z - \beta_n) = z^n + \alpha_1 z^{n-1} + \cdots + \alpha_n. \quad (8.32)$$

The coefficient matrix with rows $\mathbf{H}\Phi^j$ is called the **observability matrix** and must be full rank for the matrix to be invertible and for the system to be observable.

For calculation of \mathbf{L}_p with MATLAB, either `acker` or `place` can be used by invoking the substitutions above. The same restrictions apply that existed for the control problem.

Predictor Estimator Pole Placement with MATLAB

Example 8.5

Design an estimator for the satellite attitude-control system as in Example 8.4. Place the z -plane poles at $z = 0.4 \pm j0.4$.

Solution. The MATLAB statements

```
T = .1
Phi = [1 T; 0 1]
H = [1 0]
p = [.4+i*.4; .4-i*.4]
Lp = acker(Phi', H', p)
```

result in

$$\mathbf{L}_p = \begin{bmatrix} 1.2 \\ 5.2 \end{bmatrix}.$$

`place` would have given the same answer.

8.2.4 Current Estimators

As was already noted, the previous form of the estimator equation (8.23) arrives at the state vector estimate $\bar{\mathbf{x}}$ after receiving measurements up through $y(k-1)$. This means that the current value of control⁵ does not depend on the most current value of the observation and thus might not be as accurate as it could be. For high-order systems controlled with a slow computer or any time the sample periods are comparable to the computation time, this delay between the observation instant

⁵We plan to use $u(k) = -\mathbf{K}\bar{\mathbf{x}}$ in place of $u(k) = -\mathbf{K}\mathbf{x}$.

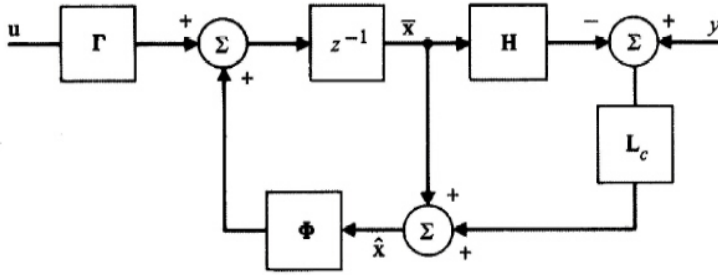


Figure 8.6
Estimator block
diagram

and the validity time of the control output can be a blessing because it allows time for the computer to complete the calculations. In many systems, however, the computation time required to evaluate Eq. (8.23) is quite short compared to the sample period, and the delay of almost a cycle between the measurement and the proper time to apply the resulting control calculation represents an unnecessary waste. Therefore, it is useful to construct an alternative estimator formulation that provides a current estimate $\hat{\mathbf{x}}$ based on the current measurement $y(k)$.⁶ Modifying Eq. (8.23) to yield this feature, we obtain

$$\hat{\mathbf{x}}(k) = \bar{\mathbf{x}}(k) + \mathbf{L}_c[y(k) - \mathbf{H}\bar{\mathbf{x}}(k)], \quad (8.33)$$

where $\bar{\mathbf{x}}(k)$ is the predicted estimate based on a model prediction from the previous time estimate, that is

$$\bar{\mathbf{x}}(k) = \Phi\hat{\mathbf{x}}(k-1) + \Gamma u(k-1). \quad (8.34)$$

Control from this estimator cannot be implemented exactly because it is impossible to sample, perform calculations, and output with absolutely no time elapsed. However, the calculation of $u(k)$ based on Eq. (8.33) can be arranged to minimize computational delays by performing all calculations before the sample instant that do not directly depend on the $y(k)$ measurement. In Chapter 3, we also had a $u(k)$ that was dependent on $y(k)$ (see Table 3.1); and here, too, we organized the calculations to minimize the delay. If this latency in the implementation causes significant errors in the performance of the system compared to the analysis, it could be modeled and accounted for in the estimator equations by using the results of Section 4.3.4.

To help understand the difference between the prediction and current form of estimation—that is, Equations (8.23) and (8.33)—it is useful to substitute Eq. (8.33) into Eq. (8.34). This results in

$$\bar{\mathbf{x}}(k+1) = \Phi\bar{\mathbf{x}}(k) + \Gamma u(k) + \Phi\mathbf{L}_c[y(k) - \mathbf{H}\bar{\mathbf{x}}(k)]. \quad (8.35)$$

Furthermore, the estimation-error equation for $\bar{\mathbf{x}}(k)$, obtained by subtracting Eq. (8.3) from Eq. (8.35), is

$$\bar{\mathbf{x}}(k+1) = [\Phi - \Phi\mathbf{L}_c\mathbf{H}]\bar{\mathbf{x}}(k). \quad (8.36)$$

By comparing Eqs. (8.35) with (8.23) and (8.36) with (8.24), we can conclude that $\bar{\mathbf{x}}$ in the current estimator equation, (8.33), is the same quantity as $\bar{\mathbf{x}}$ in the predictor estimator equation, (8.23), and that the estimator gain matrices are related by

$$\mathbf{L}_p = \Phi\mathbf{L}_c. \quad (8.37)$$

The relationship between the two estimates is further illuminated by writing Eqs. (8.33) and (8.34) as a block diagram, as in Fig. 8.6. It shows that $\hat{\mathbf{x}}$ and $\bar{\mathbf{x}}$ represent different outputs of the same estimator system.

We can also determine the estimator-error equation for $\hat{\mathbf{x}}$ by subtracting Eq. (8.33) from (8.3). The result is⁷

$$\hat{\mathbf{x}}(k+1) = [\Phi - \mathbf{L}_c\mathbf{H}\Phi]\hat{\mathbf{x}}(k). \quad (8.38)$$

⁶This form of the equations is used in the Kalman filter, which is discussed in Chapter 9.

⁷Equation (8.21) defines $\tilde{\mathbf{x}}$ to be $\mathbf{x} - \bar{\mathbf{x}}$; however, we use $\tilde{\mathbf{x}}$ here to be $\mathbf{x} - \hat{\mathbf{x}}$. In both cases, $\tilde{\mathbf{x}}$ refers to the estimator error.

The two error equations, (8.36) and (8.38), can be shown to have the same roots, as should be the case because they simply represent the dynamics of different outputs of the same system. Therefore, we could use either form as the basis for computing the estimator gain, \mathbf{L}_c . Using Eq. (8.38), we note that it is similar to Eq. (8.24) except that $\mathbf{H}\Phi$ appears instead of \mathbf{H} . To use Ackermann's formula for \mathbf{L}_c , we use Eq. (8.30) with \mathbf{H} replaced by $\mathbf{H}\Phi$ and find

$$\mathbf{L}_c = \alpha_e(\Phi) \begin{bmatrix} \mathbf{H}\Phi \\ \mathbf{H}\Phi^2 \\ \mathbf{H}\Phi^3 \\ \vdots \\ \mathbf{H}\Phi^n \end{bmatrix}^{-1} \begin{bmatrix} 0 \\ 0 \\ 0 \\ \vdots \\ 1 \end{bmatrix}, \quad (8.39)$$

where $\alpha_e(\Phi)$ is based on the desired root locations and is given by Eqs. (8.31) and (8.32). To use the control form of Ackermann's formula to perform the calculations, we take the transpose of $\Phi - \mathbf{L}_c \mathbf{H}\Phi$ and get $\Phi^T - \Phi^T \mathbf{H}^T \mathbf{L}_c^T$, which is the same form as the system matrix $\Phi - \mathbf{G}\mathbf{K}$ of the control problem. Therefore substitutions Φ^T for Φ and $\Phi^T \mathbf{H}^T$ for $\mathbf{G}\mathbf{K}$ yield \mathbf{L}_c instead of \mathbf{K} . Alternatively, we could compute \mathbf{L}_p using Eq. (8.30) and then compute \mathbf{L}_c using Eq.(8.37); that is

$$\mathbf{L}_c = \Phi^{-1} \mathbf{L}_p. \quad (8.40)$$

Current Estimator Pole Placement with MATLAB

Example 8.6

Design a current estimator for the satellite attitude-control system as in Examples 8.4 and 8.5. Place the z -plane poles at $z = 0.4 \pm j0.4$ and compare the error response to an initial error in the velocity with that obtained in Example 8.4.

Solution. The MATLAB statements

```
T = .1
Phi = [1 T; 0 1]
H = [1 0]
p = [.4+i*.4; .4-i*.4]
Lc = acker(Phi',Phi'*H',p)'
```

result in

$$\mathbf{L}_c = \begin{bmatrix} 0.68 \\ 5.2 \end{bmatrix}.$$

Therefore, the estimator implementation using Eq. (8.33) in a way that reduces the computation delay as much as possible is, before sampling

$$\begin{aligned} \bar{x}_1(k) &= \hat{x}_1(k-1) + 0.005u(k-1) + 0.1\hat{x}_2(k-1), \\ \bar{x}_2(k) &= \hat{x}_2(k-1) + 0.1u(k-1), \\ x'_1 &= (1 - 0.68)\bar{x}_1(k), \\ x'_2 &= (1 - 5.2)\bar{x}_1(k) + \bar{x}_2, \end{aligned}$$

and after sampling $y(k)$

$$\begin{aligned} \hat{x}_1(k) &= x'_1 + 0.68y(k), \\ \hat{x}_2(k) &= x'_2 + 5.2y(k), \end{aligned}$$

at which time the state vector estimate is available for the calculation of the control $u(k)$.

Figure 8.7 shows the time history of the estimator error equation from Eq. (8.38), again with an initial error of 0 for the position estimate and 1 rad/sec for the velocity estimate. The figure shows very similar results compared to the prediction estimator in Fig. 8.5; however, the current estimator implementation exhibits a response which is about a cycle faster.

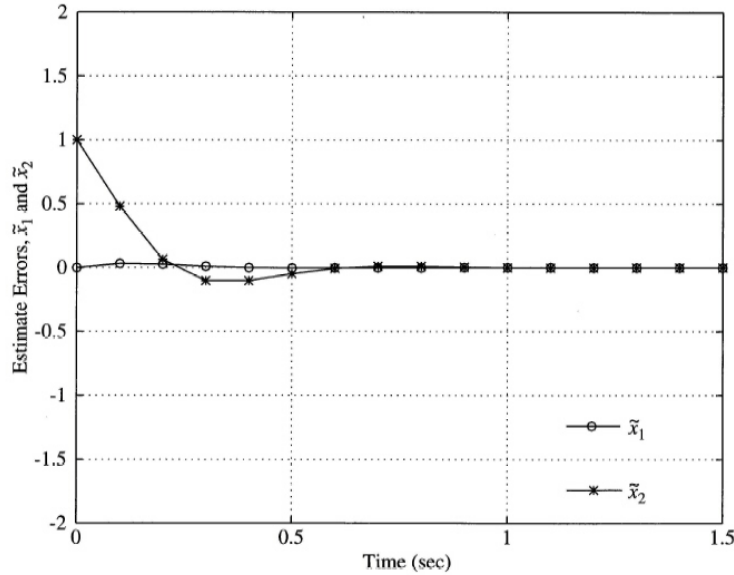


Figure 8.7
Time history of
current estimator
error

If Φ is singular, as can happen with systems having time delays, neither Eqs. (8.39) nor (8.40) can be used. However, estimators can be designed for these systems as discussed in Section 8.6.

Note that we now have two estimates that could be used for control purposes, the predicted estimate $[\hat{\mathbf{x}}(k)$ from Eq. (8.23)] and the current estimate $[\hat{\mathbf{x}}(k)$ from Eq. (8.33)]. The current estimate is the obvious choice because it is based on the most current value of the measurement, y . Its disadvantage is that it is out of date before the computer can complete the computation of Eqs. (8.33) and (8.5), thus creating a delay that is not accounted for in the design process, which will cause less damping in the implemented system than specified by the desired poles. The use of the predicted estimate for control eliminates the modeling error from the latency because it can be calculated using the measurement, $y(k-1)$, thus providing an entire sample period to complete the necessary calculations of $u(k)$ before its value is required. Generally, however, one should use the current estimate because it provides the fastest response to unknown disturbances or measurement errors and thus better regulation of the desired output. Any deficiencies in the system response due to the latency from the computation lag that is found by simulation or experiment can be patched up with additional iterations on the desired pole locations or accounted for exactly by including computation delay in the plant model.

8.2.5 Reduced-Order Estimators

The estimators discussed so far are designed to reconstruct the entire state vector, given measurements of some of the state elements.⁸ One might therefore ask: Why bother to reconstruct the state elements that are measured directly? The answer is: You don't have to, although, when there is significant noise on the measurements, the estimator for the full state vector provides smoothing of the measured elements as well as reconstruction of the unmeasured state elements.

To pursue an estimator for only the unmeasured part of the state vector, let us partition the state vector into two parts: \mathbf{x}_a is the portion directly measured, which is y , and \mathbf{x}_b is the remaining portion

⁸Reduced-order estimators (or observers) were originally proposed by Luenberger (1964). This development follows Gopinath (1971).

to be estimated. The complete system description, like Eq. (8.3), becomes

$$\begin{bmatrix} x_a(k+1) \\ \mathbf{x}_b(k+1) \end{bmatrix} = \begin{bmatrix} \Phi_{aa} & \Phi_{ab} \\ \Phi_{ba} & \Phi_{bb} \end{bmatrix} \begin{bmatrix} x_a(k) \\ \mathbf{x}_b(k) \end{bmatrix} + \begin{bmatrix} \Gamma_a \\ \Gamma_b \end{bmatrix} u(k), \quad (8.41)$$

$$y(k) = [I \quad 0] \begin{bmatrix} x_a(k) \\ \mathbf{x}_b(k) \end{bmatrix} \quad (8.42)$$

and the portion describing the dynamics of the unmeasured state elements is

$$\mathbf{x}_b(k+1) = \Phi_{bb}\mathbf{x}_b(k) + \underbrace{\Phi_{ba}x_a(k) + \Gamma_b u(k)}_{\text{known "input"}}, \quad (8.43)$$

where the right-hand two terms are known and can be considered as an input into the \mathbf{x}_b dynamics. If we reorder the x_a portion of Eq. (8.41), we obtain

$$\underbrace{x_a(k+1) - \Phi_{aa}x_a(k) - \Gamma_a u(k)}_{\text{known "measurements"}} = \Phi_{ab}\mathbf{x}_b(k). \quad (8.44)$$

Note that this is a relationship between a measured quantity on the left and the unknown state vector on the right. Therefore, Eqs. (8.43) and (8.44) have the same relationship to the state vector \mathbf{x}_b that the original equation, (8.3), had to the entire state vector \mathbf{x} . Following this reasoning, we arrive at the desired estimator by making the following substitutions

$$\begin{aligned} \mathbf{x} &\leftarrow \mathbf{x}_b, \\ \Phi &\leftarrow \Phi_{bb}, \\ \Gamma u(k) &\leftarrow \Phi_{ba}x_a(k) + \Gamma_b u(k), \\ y(k) &\leftarrow x_a(k+1) - \Phi_{aa}x_a(k) - \Gamma_a u(k), \\ \mathbf{H} &\leftarrow \Phi_{ab}, \end{aligned}$$

into the prediction estimator equations (8.23). Thus the reduced-order estimator equations are

$$\begin{aligned} \hat{\mathbf{x}}_b(k+1) &= \Phi_{bb}\hat{\mathbf{x}}_b(k) + \Phi_{ba}x_a(k) + \Gamma_b u(k) \\ &+ \mathbf{L}_r [x_a(k+1) - \Phi_{aa}x_a(k) - \Gamma_a u(k) - \Phi_{ab}\hat{\mathbf{x}}_b(k)]. \end{aligned} \quad (8.45)$$

Subtracting Eq. (8.45) from (8.43) yields the error equation

$$\tilde{\mathbf{x}}_b(k+1) = [\Phi_{bb} - \mathbf{L}_r \Phi_{ab}] \tilde{\mathbf{x}}_b(k), \quad (8.46)$$

and therefore \mathbf{L}_r is selected exactly as before, that is, (a) by picking roots of

$$|z\mathbf{I} - \Phi_{bb} + \mathbf{L}_r \Phi_{ab}| = \alpha_e(z) = 0 \quad (8.47)$$

to be in desirable locations, or (b) using Ackermann's formula

$$\mathbf{L}_r = \alpha_e(\Phi_{bb}) \begin{bmatrix} \Phi_{ab} \\ \Phi_{ab}\Phi_{bb} \\ \Phi_{ab}\Phi_{bb}^2 \\ \vdots \\ \Phi_{ab}\Phi_{bb}^{n-2} \end{bmatrix}^{-1} \begin{bmatrix} 0 \\ 0 \\ \vdots \\ 0 \\ 1 \end{bmatrix}. \quad (8.48)$$

We note here that Gopinath (1971) proved that if a full-order estimator as given by Eq. (8.23) exists, then the reduced-order estimator given by Eq. (8.45) also exists; that is, we can place the roots of Eq. (8.47) anywhere we choose by choice of \mathbf{L}_r .

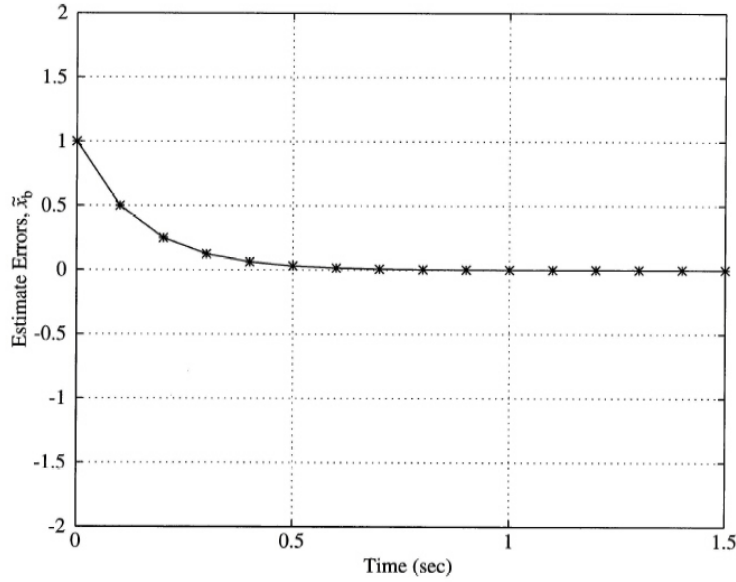


Figure 8.8
Time history of
reduced-order
estimator error

Reduced-Order Estimator for Satellite Attitude

Example 8.7

Determine a reduced-order estimator for the same case as in Examples 8.4 and 8.5.

Solution. We start out by partitioning the plant equations to fit the mold of Eqs. (8.41) and (8.42). This results in

$$\begin{bmatrix} \Phi_{aa} & \Phi_{ab} \\ \Phi_{ba} & \Phi_{bb} \end{bmatrix} = \begin{bmatrix} 1 & T \\ 0 & 1 \end{bmatrix}, \quad \begin{bmatrix} \Gamma_a \\ \Gamma_b \end{bmatrix} = \begin{bmatrix} T^2/2 \\ T \end{bmatrix} = \begin{bmatrix} 0.005 \\ 0.1 \end{bmatrix}$$

$$\begin{bmatrix} x_1 \\ x_2 \end{bmatrix} = \begin{bmatrix} \text{the measured position state } y, \\ \text{the velocity to be estimated} \end{bmatrix}, \quad (8.49)$$

where Φ_{aa} , and so on, are all scalars. Therefore L_r is a scalar also, and there is only one estimator pole to pick, the pole corresponding to the speed at which the estimate of scalar velocity converges. From Eq. (8.47) we pick L_r from

$$z - 1 + L_r T = 0.$$

For this estimator to be about the same speed as the two previous estimator examples, which had two poles at $z = 0.4 \pm j0.4$, we will pick the pole at $z = 0.5$; therefore $L_r T - 1 = -0.5$ and $L_r = 5$. The estimator equation, (8.45), is

$$\begin{aligned} \hat{x}_b(k) &= \hat{x}_b(k-1) + 0.1 u(k-1) \\ &\quad + 5.0 [y(k) - y(k-1) - 0.005 u(k-1) - (0.1) \hat{x}_b(k-1)]. \end{aligned} \quad (8.50)$$

The implementation in a control computer would, before sampling, look something like

$$x' = 0.5 \hat{x}_b(k-1) + 0.075 u(k-1) - 5 y(k-1),$$

and after sampling

$$\hat{x}_b(k) = x' + 5 y(k).$$

Figure 8.8 shows the time history of the estimator-error equation (8.46) with an initial (velocity) estimate error of 1 rad/sec. The figure shows very similar results compared to the velocity element estimates in Figs. 8.5 and 8.7. Of course, there is no position estimate because this formulation assumes that the measurement is used directly without smoothing.

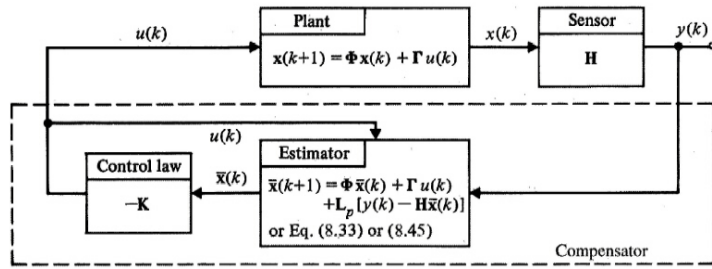


Figure 8.9
Estimator and
controller
mechanization

8.3 Regulator Design: Combined Control Law and Estimator

If we take the control law (Section 8.1) and implement it, using an estimated state vector (Section 8.2), the control system can be completed. A schematic of such a system is shown in Fig. 8.9. However, because we designed the control law assuming that the true state, \mathbf{x} , was fed back instead of $\hat{\mathbf{x}}$ or $\bar{\mathbf{x}}$, it is of interest to examine what effect this has on the system dynamics. We will see that it has no effect! The poles of the complete system consisting of the estimator feeding the control law will have the same poles as the two cases analyzed separately.

8.3.1 The Separation Principle

The control is now

$$u(k) = -\mathbf{K} \bar{\mathbf{x}}(k)$$

and the controlled plant equation (8.6) becomes

$$\mathbf{x}(k+1) = \Phi \mathbf{x}(k) - \Gamma \mathbf{K} \bar{\mathbf{x}}(k), \quad (8.51)$$

which can also be written in terms of the estimator error using Eq. (8.21)

$$\mathbf{x}(k+1) = \Phi \mathbf{x}(k) - \Gamma \mathbf{K} (\mathbf{x}(k) - \bar{\mathbf{x}}(k)). \quad (8.52)$$

Combining this with the estimator-error equation (8.24)⁹ we obtain two coupled equations that describe the behavior of the complete system¹⁰

$$\begin{bmatrix} \bar{\mathbf{x}}(k+1) \\ \mathbf{x}(k+1) \end{bmatrix} = \begin{bmatrix} \Phi - L_p H & 0 \\ \Gamma \mathbf{K} & \Phi - \Gamma \mathbf{K} \end{bmatrix} \begin{bmatrix} \bar{\mathbf{x}}(k) \\ \mathbf{x}(k) \end{bmatrix}. \quad (8.53)$$

The characteristic equation is

$$\begin{vmatrix} z\mathbf{I} - \Phi + L_p H & 0 \\ \Gamma \mathbf{K} & z\mathbf{I} - \Phi + \Gamma \mathbf{K} \end{vmatrix} = 0 \quad (8.54)$$

which, because of the zero matrix in the upper right, can be written as

$$|z\mathbf{I} - \Phi + L_p H| |z\mathbf{I} - \Phi + \Gamma \mathbf{K}| = \alpha_c(z) \alpha_e(z) = 0. \quad (8.55)$$

In other words, the characteristic poles of the complete system consist of the combination of the estimator poles and the control poles that are unchanged from those obtained assuming actual state feedback. The fact that the combined control-estimator system has the same poles as those of the control alone and the estimator alone is a special case of the separation principle by which control and estimation can be designed separately yet used together.

To compare this method of design to the methods discussed in Chapter 7, we note from Fig. 8.9 that the portion within the dashed line corresponds to classical compensation. The difference equation for this system or “state-space designed compensator” is obtained by including the control feedback (because it is part of the compensation) in the estimator equations. Using Eq. (8.23) yields for the prediction estimator

$$\begin{aligned}\bar{\mathbf{x}}(k) &= [\Phi - \Gamma\mathbf{K} - \mathbf{L}_p\mathbf{H}]\bar{\mathbf{x}}(k-1) + \mathbf{L}_p y(k-1), \\ u(k) &= -\mathbf{K}\bar{\mathbf{x}}(k),\end{aligned}\quad (8.56)$$

and using Eq. (8.33) yields for the current estimator

$$\begin{aligned}\hat{\mathbf{x}}(k) &= [\Phi - \Gamma\mathbf{K} - \mathbf{L}_c\mathbf{H}\Phi + \mathbf{L}_c\mathbf{H}\Gamma\mathbf{K}]\hat{\mathbf{x}}(k-1) + \mathbf{L}_c y(k), \\ u(k) &= -\mathbf{K}\hat{\mathbf{x}}(k).\end{aligned}\quad (8.57)$$

The poles of the compensators above are obtained from, for Eq. (8.56),

$$|z\mathbf{I} - \Phi + \Gamma\mathbf{K} + \mathbf{L}_p\mathbf{H}| = 0 \quad (8.58)$$

and, for Eq. (8.57),

$$|z\mathbf{I} - \Phi + \Gamma\mathbf{K} + \mathbf{L}_c\mathbf{H}\Phi - \mathbf{L}_c\mathbf{H}\Gamma\mathbf{K}| = 0, \quad (8.59)$$

and are *neither* the control law poles, Eq. (8.8), nor the estimator poles, Eq. (8.25). These poles need not be determined during a state-space design effort, but can be of interest for comparison with compensators designed using the transform methods of Chapter 7.

If desired, Eq. (8.56) can be converted to transfer function-form using the same steps that were used in arriving at Eq. (4.64). This results in what was called compensation in Chapter 7 and usually referred to as $D(z)$. For the prediction estimator, we find

$$\frac{U(z)}{Y(z)} = D_p(z) = -\mathbf{K}[z\mathbf{I} - \Phi + \Gamma\mathbf{K} + \mathbf{L}_p\mathbf{H}]^{-1}\mathbf{L}_p. \quad (8.60)$$

The $D(z)$ could also be found from Eq. (8.56) by using `tf.m` in MATLAB or, for the current estimator, from Eq. (8.57). Likewise, the transfer function for the reduced-order compensator is found by using the measured part of the state, x_a , directly in the control law and the estimated part, $\hat{\mathbf{x}}_b(k)$, for the remainder. Thus, the control gain \mathbf{K} needs to be partitioned, so that

$$u(k) = [K_a \quad K_b] \begin{bmatrix} x_a \\ \mathbf{x}_b \end{bmatrix} \quad \text{where } \mathbf{K} = [K_a \quad K_b]. \quad (8.61)$$

In the previous sections, we developed techniques to compute \mathbf{K} and \mathbf{L}_p (which define the compensation), given the desired locations of the roots of the characteristic equations of the control and the estimator. We now know that these desired root locations will be the closed-loop system poles. The same meter sticks that applied to the classical design and were discussed in Section 7.2 also apply to picking these poles. In practice, when measurement noise is not an issue, it is convenient to pick the control poles to satisfy the performance specifications and actuator limitations, and then to pick the estimator poles somewhat faster (by a factor of 2 to 4) so that the total response is dominated by the response due to the slower control poles. It does not cost anything in terms of actuator hardware to increase the estimator gains (and hence speed of response) because they appear only in the estimator pole selection computer. The upper limit to estimator speed of response is based on the behavior of sensor-noise rejection, which is the subject of Chapter 9.

In order to evaluate the full system response with the estimator in the loop, it is necessary to simulate both the real system and the estimator system as was formulated in Eq. (8.53). However, it

⁹We show only the prediction estimator case. The other estimators lead to identical conclusions.

¹⁰This description of the entire system does not apply if the estimator model is imperfect; see Section 11.5 for an analysis of that case.

is easier to see what is going on by using $\bar{\mathbf{x}}$ or $\hat{\mathbf{x}}$ in place of $\tilde{\mathbf{x}}$. The result for the predictor case using Eq. (8.56) is

$$\begin{bmatrix} \mathbf{x}(k+1) \\ \bar{\mathbf{x}}(k+1) \end{bmatrix} = \begin{bmatrix} \Phi & -\Gamma\mathbf{K} \\ \mathbf{L}_p\mathbf{H} & \Phi - \Gamma\mathbf{K} - \mathbf{L}_p\mathbf{H} \end{bmatrix} \begin{bmatrix} \mathbf{x}(k) \\ \bar{\mathbf{x}}(k) \end{bmatrix}, \quad (8.62)$$

the result for the current estimator using Eq. (8.57) is

$$\begin{bmatrix} \mathbf{x}(k+1) \\ \hat{\mathbf{x}}(k+1) \end{bmatrix} = \begin{bmatrix} \Phi & -\Gamma\mathbf{K} \\ \mathbf{L}_c\mathbf{H}\Phi & \Phi - \Gamma\mathbf{K} - \mathbf{L}_c\mathbf{H}\Phi \end{bmatrix} \begin{bmatrix} \mathbf{x}(k) \\ \hat{\mathbf{x}}(k) \end{bmatrix}, \quad (8.63)$$

and the result for the reduced-order estimator using Eq. (8.45) is

$$\begin{bmatrix} \mathbf{x}(k+1) \\ \hat{\mathbf{x}}_b(k+1) \end{bmatrix} = \begin{bmatrix} \Phi - \Gamma \begin{bmatrix} K_a & 0 \end{bmatrix} & -\Gamma\mathbf{K}_b \\ \mathbf{A} & \mathbf{B} \end{bmatrix} \begin{bmatrix} \mathbf{x}(k) \\ \hat{\mathbf{x}}_b(k) \end{bmatrix}, \quad (8.64)$$

where

$$\mathbf{A} = \mathbf{L}_r\mathbf{H}\Phi + \Phi_{ba}\mathbf{H} - \Gamma_b\mathbf{K}_a\mathbf{H} - \mathbf{L}_r\Phi_{aa}\mathbf{H}$$

and

$$\mathbf{B} = \Phi_{bb} - \Gamma_b\mathbf{K}_b - \mathbf{L}_r\Phi_{ab}$$

and where K_a and \mathbf{K}_b are partitions of \mathbf{K} according to the dimensions of x_a and \mathbf{x}_b .

Compensation Based on the Predictor Estimator

Example 8.8

Put together the full feedback control system based on the calculations already done in Examples 8.1 and 8.4, that is, using the prediction estimator. Use the control gain, $\mathbf{K} = [10 \ 3.5]$, and the estimator gain, $\mathbf{L}_p^T = [1.2 \ 5.2]$. Determine the $D(z)$ for comparison with a classical lead compensation. Plot the response of the system variables for an initial plant velocity of -1 rad/sec and zero for all other initial conditions. Comment on whether the responses are consistent with your expectations.

Solution. The compensation equations consist of Eq. (8.56) with the values of \mathbf{K} and \mathbf{L}_p plugged in and, being in difference-equation form, can be coded directly in a control computer. To find the transfer function form, we use `zp.m` (or Eq. (8.60)), to find that¹¹

$$D_p(z) = -30.4 \frac{z - 0.825}{z - 0.2 \pm j0.557}. \quad (8.65)$$

There is a compensator zero near the two plant poles at $z = +1$ and there are two compensator poles considerably to the left. This is very similar to a classical lead compensator except that it has two poles instead of one. State-space design using a full-order estimator will always produce compensation that is the same order as the plant. Note that the difference equation that results from this $D(z)$ will have a one cycle delay between the input and output.

Figure 8.10 shows the response of the system and controller to the initial conditions. This could be thought of as a condition that would result from a sudden disturbance on the system. Note the estimator error at the beginning which decays in about 0.7 sec, consistent with the estimator poles. The overall system response is slower and has a settling time of about 2.5 sec, consistent with the control poles.

Compensation Based on the Current Estimator

Example 8.9

Put together the full feedback control system based on the calculations already done in Examples 8.1 and 8.5, that is, using the current estimator. Use the control gain, $\mathbf{K} = [10 \ 3.5]$, and the estimator gain, $\mathbf{L}_c^T = [0.68 \ 5.2]$. Determine the $D(z)$ for comparison with a classical lead compensation. Plot the response of the

¹¹Equation (8.60) includes a minus sign because it is the transfer function from $Y(s)$ to $U(s)$ rather than from $E(s)$, as is the normal convention used in Chapter 7.

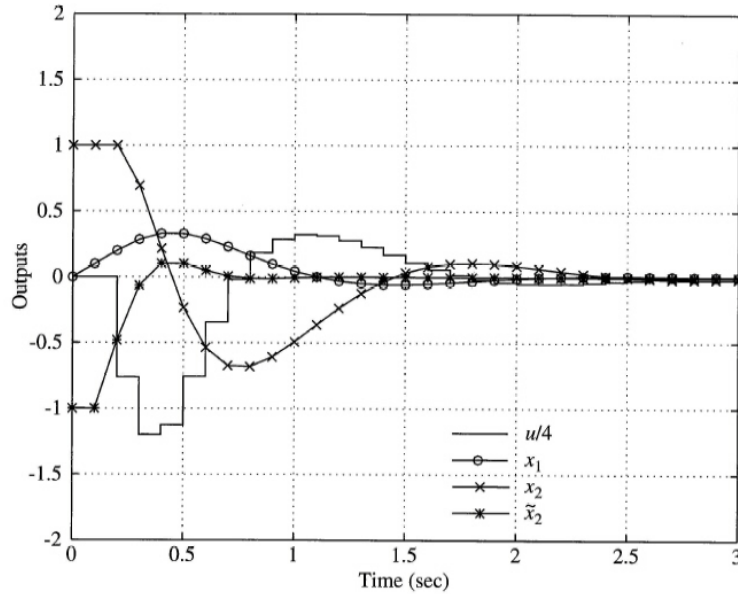


Figure 8.10
Time histories of controlled system with prediction estimator, Example 8.8

system variables for an initial plant velocity of -1 rad/sec and zero for all other initial conditions. Comment on whether the responses are consistent with your expectations.

Solution. The compensation equations consist of Eq. (8.57) and, with the values of \mathbf{K} and \mathbf{L}_c plugged in, we find that

$$D_c(z) = -25.1 \frac{z(z-0.792)}{z-0.265 \pm j0.394}. \quad (8.66)$$

This compensation is very much like that from the prediction estimator; however, because of the extra z in the numerator, there is no 1 cycle delay between input and output. This faster cycle response required less lead from the compensation, as exhibited by the zero being further from $z = 1$.

Figure 8.11 shows the response of the controlled system to the initial conditions. Note the somewhat faster response as compared to Fig. 8.10 due to the more immediate use of the measured signal.

Compensation Based on the Reduced-Order Estimator

Example 8.10

Put together the full feedback control system based on the calculations already done in Examples 8.1 and 8.6, that is, using the reduced-order estimator. Use the control gain, $\mathbf{K} = [10 \ 3.5]$, and the estimator gain, $\mathbf{L}_r^T = 5$. Determine the $D(z)$ for comparison with a classical lead compensation. Plot the response of the system variables for an initial plant velocity of -1 rad/sec and zero for all other initial conditions. Comment on whether the responses are consistent with your expectations.

Also, use the $D(z)$ to construct a root locus for this system and show where the desired root locations for the control and estimation lie on the locus.

Solution. The compensation equations consist of Eqs. (8.50) and (8.61). With the values of \mathbf{K} and \mathbf{L}_r plugged in, we find after much algebra that

$$D_r(z) = -27.7 \frac{z-0.8182}{z-0.2375}. \quad (8.67)$$

Figure 8.12 shows the response of the system to the initial conditions. It is very similar to that of Example 8.9; the only notable difference is the first-order response of the estimator error, which slightly reduced the control usage.

This compensation now looks exactly like the classic lead compensation that was used often in Chapter 7 and would typically be used for a $1/s^2$ plant. A sketch of a root locus vs. K is given in Fig. 8.13. For this design a gain of 27.7 is now the variable K .

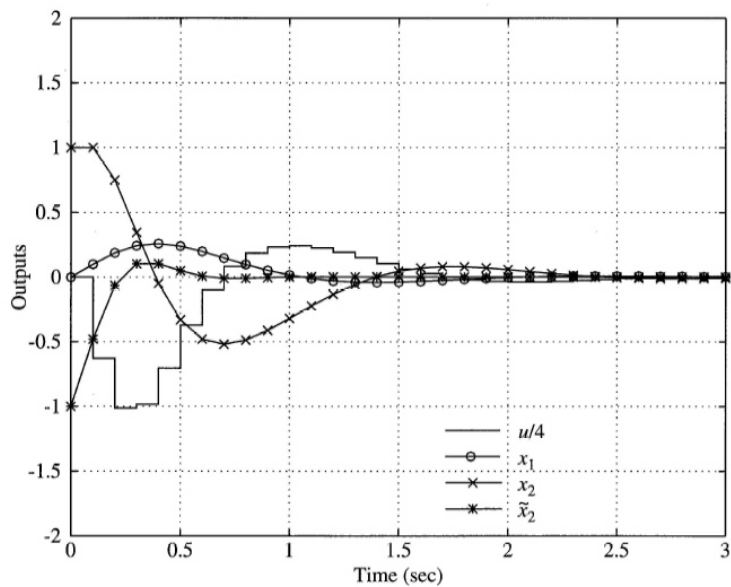


Figure 8.11
Time histories of controlled system with current estimator, Example 8.9

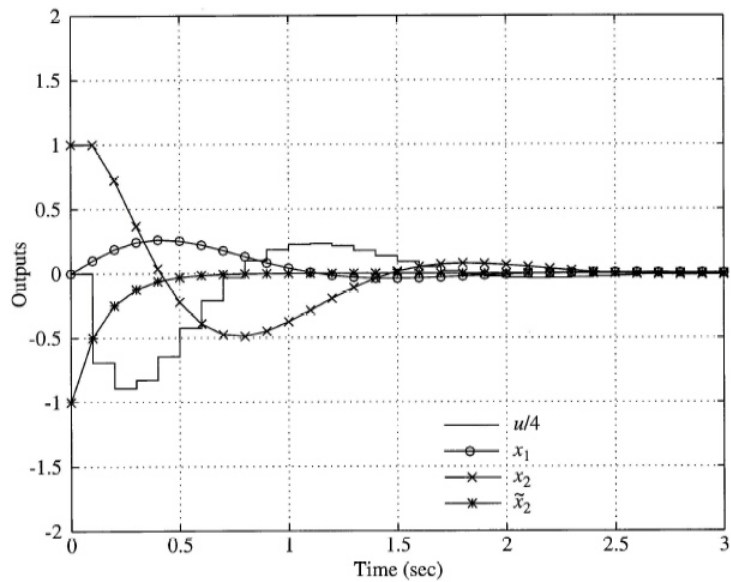


Figure 8.12
Time histories of system with reduced-order estimator, Example 8.10

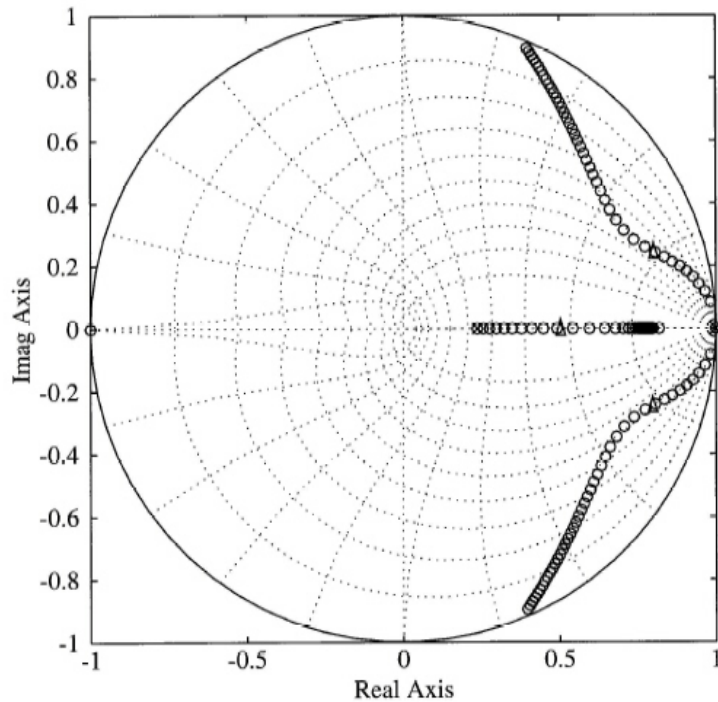


Figure 8.13
Sketch of the
root locus for
Example 8.10

The closed-loop root locations corresponding to $K = 27.7$ are indicated by the triangles and lie on the two control roots at $z = 0.8 \pm j0.25$ and on the one estimator root at $z = 0.5$, as they should.

The higher order compensators that resulted in Examples 8.8 and 8.9 have the benefit of more attenuation at high frequencies, thus reducing the sensitivity to measurement noise. This also follows from the fact that they provided a smoothed value of the measured output as well as reconstructing the velocity state variable. Full order estimators are also easier to implement because of the simpler matrix equations that result using $u = -\mathbf{K}\hat{\mathbf{x}}$ rather than the partitioned Eq. (8.61). As a result, reduced-order estimation is not often used in practice.

8.3.2 Guidelines for Pole Placement

The selection criteria of the closed-loop control and estimator poles (or roots) have been encountered throughout the examples in Chapter 8 to this point. Also see the review of state-space design for continuous systems in Section 2.6 as well as Franklin, Powell, and Emami-Naeini (2019), Sections 7.4 and 7.5.3. The key idea for control-pole selection is that one needs to pick the poles so that the design specifications are met while the use of control is kept to a level that is no more than needed to meet the specifications. This pole-selection criterion will keep the actuator sizes to a minimum, which helps to minimize the cost and weight of the control system. The relationships between various system specifications developed in Section 7.1 can be used as an aid in the pole-selection process. For high-order systems, it is sometimes helpful to use the ITAE or Bessel prototype design root locations as discussed in Section 7.6 in Franklin, Powell, and Emami-Naeini (2019). For the case where there is a lightly damped open-loop mode, a technique that minimizes control usage is simply to add damping with little or no change in frequency, a technique called **radial projection** that was demonstrated in Example 8.3.

The optimal design methods discussed in Chapter 9 can also be used to select pole locations. They are based on minimizing a cost function that consists of the weighted sum of squares of the state errors and control. The relative weightings between the state errors and control are varied by the

designer in order to meet all the system specifications with the minimum control. Optimal methods can be applied to the SISO systems, which are the subject of this chapter, or to MIMO systems.

Estimator-error pole selection is a similar kind of design process to the control-pole selection process; however, the design trade-off is somewhat different. Fast poles in an estimator do not carry the penalty of a large actuator like they do in the control case because the large signals exist only in the computer. The penalty associated with fast estimator poles is that they create an increased sensitivity between sensor errors and estimation errors.

The key idea for estimator-error pole selection is that the estimation errors should be minimized with respect to the prevailing system disturbances and sensor noise. It is also convenient to keep the estimator poles faster than the control poles in order that the total system response is dominated by the control poles. Typically, we select well-damped estimator poles that are two to six times faster than the control poles in order to provide a response dominated by the control poles. For cases where this criterion produces estimation errors due to sensor noise that are unacceptably large, the poles can be slowed down to be less than two times the control poles; however, in this case the total response could be strongly influenced by the location of the estimator poles, thus coupling the estimator design with the control design and complicating the process.

In the optimal estimation discussion in Chapter 9 we will see that the optimal estimator error poles are proportional to the ratio between the plant model errors and the sensor errors. For an accurate plant model with small disturbances but large sensor errors, the optimal estimation is achieved with very low estimator gains (slow response) because the estimator is best served by relying primarily on the plant model. On the other hand, a system with a plant model that includes the possibility of large disturbances but with an accurate sensor achieves the best estimation by using a large estimator gain (fast response) in order to use the sensed information to correct the model errors as quickly as possible.

8.4 Introduction of the Reference Input

The compensation obtained by combining the control law studied in Section 8.1 with any of the estimators of Section 8.2 is a regulator design in that the goal was to drive all states to zero. We designed the characteristic equations of the control and the estimator to give satisfactory natural mode transients to initial conditions or disturbances, but no mention was made of how to structure a reference input or of the considerations necessary to obtain good transient response to reference inputs. To study these matters we will consider first how one introduces a reference input to the full-state feedback case, and then we will proceed to the case with estimators. We then turn to a discussion of output error command, a structure that occurs when the sensor is capable of providing only an error signal, for example, an attitude error from a gyro or the pointing error from a radar signal. The output error structure is also the one that results if one is designing the compensation using transfer-function methods and the reference input is structured according to Fig. 7.5, the typical case. It is, therefore, of interest to study this structure in order to understand the impact of its use on the dynamic response of the system. In conclusion, we will discuss the implications of this section's results and compare the relative advantages of the structure made possible by the state-space control/estimation approach with the classical approach.

8.4.1 Reference Inputs for Full-State Feedback

Let us first consider a reference input for a full-state feedback system as in Eq. (8.5). The structure is shown in Fig. 8.14 and consists of a state command matrix \mathbf{N}_x that defines the desired value of the state, \mathbf{x}_r . We wish to find \mathbf{N}_x so that some system output, $\mathbf{y}_r = \mathbf{H}_r \mathbf{x}$, is at a desired reference value. This desired output, \mathbf{y}_r , might not be the same quantity that we sense and feed to an estimator that has been called y and determined by \mathbf{H} in the previous two sections.

Although so far in this book we have only considered systems with a single control input and single output (SISO), Chapter 9 considers the case of more than one input and output (MIMO), and, therefore, we will allow for that in the development here and in the following subsection. We will,

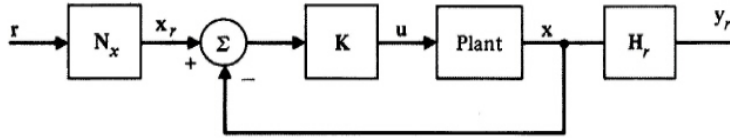


Figure 8.14
Block diagram for full-state feedback with reference input

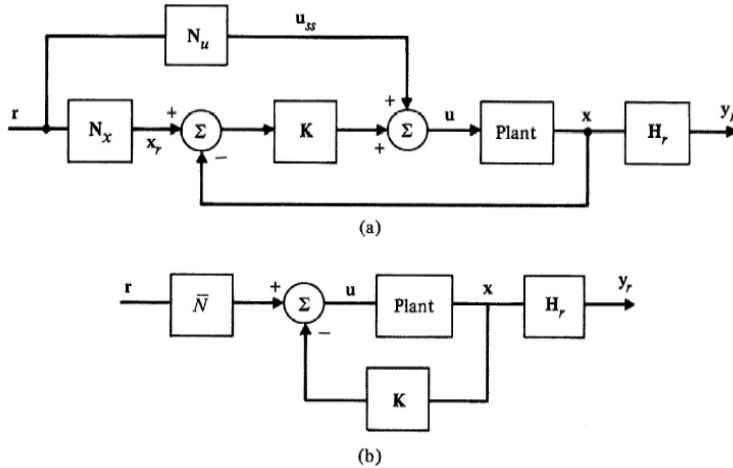


Figure 8.15
(a) Block diagram and (b) modified block diagram for full-state feedback with reference input and feedforward

however, require that the number of inputs in \mathbf{u} and desired outputs in \mathbf{y}_r be the same.¹² The basic idea in determining \mathbf{N}_x is that it should transform the reference input, \mathbf{r} , to a reference state that is an equilibrium one for that \mathbf{r} . For example, for a step command to Example 8.1, $\mathbf{N}_x^T = [1 \ 0]$; that is, we wish to command the position state element, but the velocity state element will be zero in steady state. For the double mass-spring system of Example 8.3, if we desire that $d = r$ —that is, that $\mathbf{H}_r = [1 \ 0 \ 0 \ 0]$ —then we should set $\mathbf{N}_x^T = [1 \ 0 \ 1 \ 0]$ because that provides a state reference, \mathbf{x}_r , that, if matched by the actual state, is at equilibrium for the desired output.

More specifically, we have defined \mathbf{N}_x so that

$$\mathbf{N}_x \mathbf{r} = \mathbf{x}_r \quad \text{and} \quad \mathbf{u} = -\mathbf{K}(\mathbf{x} - \mathbf{x}_r). \tag{8.68}$$

If the system is Type 1 or higher and \mathbf{r} is a step, there will be no steady-state error, and the final state

$$\mathbf{x}(\infty) = \mathbf{x}_{ss} = \mathbf{x}_r.$$

For Type 0 systems, there will be an error because some control is required to maintain the system at the desired \mathbf{x}_r .

Often the designer has sufficient knowledge of the plant to know what the equilibrium state is for the desired output, in which case the determination of \mathbf{N}_x is complete. For complex plants, however, this can be difficult. In these cases, it is useful to solve for the equilibrium condition that satisfies $\mathbf{y}_r = \mathbf{r}$.¹³

In order for the solution to be valid for all system types, whether they require a steady-state control input or not, we will include the possibility of a steady-state control term that is proportional to the reference input step, that is,

$$\mathbf{u}_{ss} = \mathbf{N}_u \mathbf{r}, \tag{8.69}$$

as shown in Fig. 8.15(a). The proportionality constant, \mathbf{N}_u , will be solved for in the formulation.

¹²This is the only case that has a unique and exact answer, although other situations have been studied.

¹³See Trankle and Bryson (1978) for a more complete discussion and extensions of the ideas to inputs other than steps, often called “model following.”

If the resulting \mathbf{u}_{ss} is actually computed and implemented in the reference input structure, we refer to it as “feedforward,” but the feedforward component of the input is often not used. Instead, the preferred method of providing for zero steady-state error is through integral control or bias estimation, which essentially replaces the \mathbf{u}_{ss} in Fig. 8.15(a) with an integral that is an estimate of the steady-state control, a topic that is the subject of Section 8.5. In some cases, it is difficult to achieve a high enough bandwidth when replacing feedforward with integral control; therefore, feedforward is sometimes used to reduce the demands on the integral so that it need only provide the error in the feedforward control, thus speeding up the system response. On the other hand, if the system is Type 1 or higher, the steady-state value of control for a step will be zero, and the solution will simply give us $\mathbf{N}_u = 0$ and \mathbf{N}_x , which defines the desired value of the state, \mathbf{x}_r .

Continuing on then, the steady state requirements for the system are that

$$\begin{aligned}\mathbf{N}_x \mathbf{r} &= \mathbf{x}_r = \mathbf{x}_{ss}, \\ \mathbf{H}_r \mathbf{x}_{ss} &= \mathbf{y}_r = \mathbf{r},\end{aligned}\quad (8.70)$$

which reduce to

$$\mathbf{H}_r \mathbf{N}_x \mathbf{r} = \mathbf{r} \quad \text{and} \quad \mathbf{H}_r \mathbf{N}_x = \mathbf{I}. \quad (8.71)$$

Furthermore, we are assuming the system is at steady state; therefore,

$$\mathbf{x}(k+1) = \Phi \mathbf{x}(k) + \Gamma \mathbf{u}(k) \Rightarrow \mathbf{x}_{ss} = \Phi \mathbf{x}_{ss} + \Gamma \mathbf{u}_{ss}$$

or

$$(\Phi - \mathbf{I}) \mathbf{x}_{ss} + \Gamma \mathbf{u}_{ss} = \mathbf{0};$$

and, from Eqs. (8.69) and (8.70)

$$(\Phi - \mathbf{I}) \mathbf{N}_x \mathbf{r} + \Gamma \mathbf{N}_u \mathbf{r} = \mathbf{0},$$

which reduces to

$$(\Phi - \mathbf{I}) \mathbf{N}_x + \Gamma \mathbf{N}_u = \mathbf{0}. \quad (8.72)$$

Collecting Eqs. (8.71) and (8.72) into one matrix equation

$$\begin{bmatrix} \Phi - \mathbf{I} & \Gamma \\ \mathbf{H}_r & \mathbf{0} \end{bmatrix} \begin{bmatrix} \mathbf{N}_x \\ \mathbf{N}_u \end{bmatrix} = \begin{bmatrix} \mathbf{0} \\ \mathbf{I} \end{bmatrix}$$

yields the desired result¹⁴

$$\begin{bmatrix} \mathbf{N}_x \\ \mathbf{N}_u \end{bmatrix} = \begin{bmatrix} \Phi - \mathbf{I} & \Gamma \\ \mathbf{H}_r & \mathbf{0} \end{bmatrix}^{-1} \begin{bmatrix} \mathbf{0} \\ \mathbf{I} \end{bmatrix}. \quad (8.73)$$

It is also possible to enter the reference input after the gain multiplication according to Fig. 8.15(b) by combining \mathbf{N}_x and \mathbf{N}_u according to

$$\bar{\mathbf{N}} = \mathbf{N}_u + \mathbf{K} \mathbf{N}_x. \quad (8.74)$$

Calculation of \mathbf{N}_x and \mathbf{N}_u can be carried out by the MATLAB function `refi.m` contained in the Digital Control Toolbox.

Reference Input for the Mass-Spring System

Example 8.11

Compute the reference input quantities for the system of Example 8.3 where it is desired to command d to a new value. Compare the two structures (a) and (b) in Fig. 8.15.

Solution. The state was defined to be $\mathbf{x} = [d \quad \dot{d} \quad y \quad \dot{y}]^T$. Therefore, to command a desired value of d , $\mathbf{H}_r = [1 \quad 0 \quad 0 \quad 0]$, and the evaluation of Eq. (8.73) leads to $\mathbf{N}_x^T = [1 \quad 0 \quad 1 \quad 0]$ and $\mathbf{N}_u = 0$, as expected by inspecting the physical system shown in Fig. A.8. The fact that $\mathbf{N}_u = 0$ makes sense because this system is in

¹⁴This cannot be solved if the plant has a zero at $z = 1$.

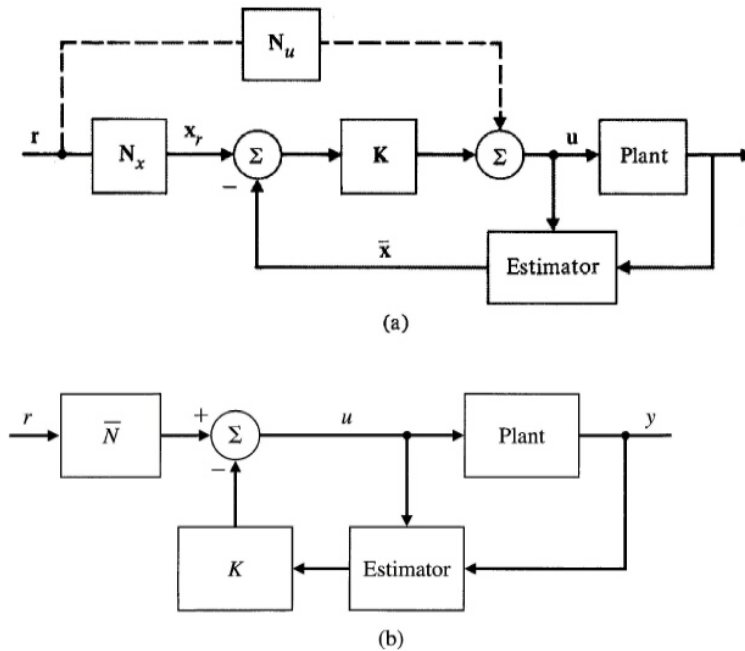


Figure 8.16
Block diagrams
for the best
reference input
structure with
estimators: the
state command
structure. (a) as
derived,
(b) simplified

equilibrium without the need of any control as long as $d = y$, which is ensured by the resulting value of \mathbf{N}_x . In fact, N_u will be zero for any system of Type 1 or higher, as already discussed. The elements of \mathbf{N}_x do not depend on specific values of any parameters in the plant and are therefore not sensitive to modeling errors of the plant.

Use of Eq. (8.74) leads to $\bar{N} = 0.005$ using the \mathbf{K} from Eq. (8.18) and $\bar{N} = 0.011$ using the \mathbf{K} from Eq. (8.19). However, note that this input structure can be very sensitive to errors in \mathbf{K} . In this particular example, \bar{N} is the result of a difference of two numbers (K_1 and K_3) that are close to each other in absolute value, extremely close for the first case (which also exhibited poor response), thus producing an extreme sensitivity. Specifically, if one of the elements of \mathbf{K} in Eq. (8.18) were in error by 1%, the resulting error in \bar{N} would be 120%! To avoid the high sensitivity for cases like this, it is advisable to structure the reference input as in Fig. 8.15(a).

This example shows that there are some systems where it is better to use the structure of Fig. 8.15(a). However, most cases do not exhibit this sensitivity and Fig. 8.15(b) is preferred due to its simplicity.

If the system in the example had been Type 0, we would have found that N_u was nonzero and that its value was inversely proportional to the plant gain. However, the plant gain can vary considerably in practice; therefore, designers usually choose not to use any feedforward for Type 0 systems, relying instead on the feedback to keep errors acceptably small or by implementing integral control as discussed in Section 8.5. If this is the desired action for a control design using state space, the designer can simply ignore the computed value of N_u and solely rely on \mathbf{N}_x for guidance on how to command the state vector to the desired values.

8.4.2 Reference Inputs with Estimators: The State-Command Structure

The same ideas can be applied to the case where the estimator is used to supply a state estimate for control in place of the actual state feedback. However, it is important to structure the system so that the control \mathbf{u} that is applied to the plant is also applied to the estimator as shown in Fig. 8.16. This means that Eqs. (8.56) and (8.57) should *not* be used in the estimator box in Fig. 8.16 because they were based on control feedback that did not include the reference input. The basic idea of the estimator that resulted in the structure of Fig. 8.4 is to drive the plant model in the estimator with the *same* inputs that are applied to the actual plant, thus minimizing estimation errors. Therefore, the

form of the estimator given by Eq. (8.23) should be used with $\mathbf{u}(k)$ as shown by Fig. 8.16, that is

$$\mathbf{u}(k) = -\mathbf{K}(\bar{\mathbf{x}}(k) - \mathbf{x}_r) + \mathbf{N}_u \mathbf{r} = -\mathbf{K}\bar{\mathbf{x}}(k) + \bar{\mathbf{N}}\mathbf{r}, \quad (8.75)$$

or, with the current estimator, Eq. (8.33) is used with

$$\mathbf{u}(k) = -\mathbf{K}(\hat{\mathbf{x}}(k) - \mathbf{x}_r) + \mathbf{N}_u \mathbf{r} = -\mathbf{K}\hat{\mathbf{x}}(k) + \bar{\mathbf{N}}\mathbf{r}, \quad (8.76)$$

or, for the reduced-order estimator, Eq. (8.45) should be used with

$$\mathbf{u}(k) = -[\mathbf{K}_a \quad \mathbf{K}_b] \begin{bmatrix} x_a \\ \hat{\mathbf{x}}_b \end{bmatrix} - \mathbf{x}_r + \mathbf{N}_u \mathbf{r} = -[\mathbf{K}_a \quad \mathbf{K}_b] \begin{bmatrix} x_a \\ \hat{\mathbf{x}}_b \end{bmatrix} + \bar{\mathbf{N}}\mathbf{r}. \quad (8.77)$$

Under ideal conditions where the model in the estimator is perfect and the input \mathbf{u} applied to plant and estimator is identical, no estimator error will be excited. We use the feedback to the estimator through y only to correct for imperfections in the estimator model, input scale factor errors, and unknown plant disturbances.

To analyze the response of a system, we must combine the estimator equations with the model of the system to be controlled. It is often useful to analyze the effect of disturbances, so the system equations (8.3) are augmented to include the disturbance, w , as

$$\begin{aligned} \mathbf{x}(k+1) &= \Phi \mathbf{x}(k) + \Gamma u(k) + \Gamma_1 w(k), \\ y(k) &= \mathbf{H}\mathbf{x}(k) + Ju(k). \end{aligned} \quad (8.78)$$

For the predictor estimator, Eq. (8.62) is augmented with the input command and disturbance as follows:

$$\begin{bmatrix} \mathbf{x} \\ \bar{\mathbf{x}} \end{bmatrix}_{k+1} = \begin{bmatrix} \Phi & -\Gamma\mathbf{K} \\ \mathbf{L}_p\mathbf{H} & \Phi - \Gamma\mathbf{K} - \mathbf{L}_p\mathbf{H} \end{bmatrix} \begin{bmatrix} \mathbf{x} \\ \bar{\mathbf{x}} \end{bmatrix}_k + \begin{bmatrix} \Gamma\bar{\mathbf{N}} \\ \Gamma\bar{\mathbf{N}} \end{bmatrix} r(k) + \begin{bmatrix} \Gamma_1 \\ 0 \end{bmatrix} w(k). \quad (8.79)$$

Note that the term on the right with r introduces the command input in an identical way to both the plant and estimator equations. The term on the right with w introduces the disturbance into the plant only; the estimator is unaware of it.

It may be useful to inspect the performance of the system in terms of the desired output y_r , the control u , and the estimator error $\bar{\mathbf{x}}$. This can be accomplished with the output equation

$$\begin{bmatrix} y_r(k) \\ u(k) \\ \bar{\mathbf{x}}(k) \end{bmatrix} = \begin{bmatrix} \mathbf{H}_r & 0 \\ 0 & -\mathbf{K} \\ \mathbf{I} & -\mathbf{I} \end{bmatrix} \begin{bmatrix} \mathbf{x}(k) \\ \bar{\mathbf{x}}(k) \end{bmatrix}. \quad (8.80)$$

For the current estimator, the system equations are found by combining Eqs. (8.57) and (8.78), which yields

$$\begin{aligned} \begin{bmatrix} \mathbf{x} \\ \hat{\mathbf{x}} \end{bmatrix}_{k+1} &= \begin{bmatrix} \Phi & -\Gamma\mathbf{K} \\ \mathbf{L}_c\mathbf{H}\Phi & \Phi - \Gamma\mathbf{K} - \mathbf{L}_c\mathbf{H}\Phi \end{bmatrix} \begin{bmatrix} \mathbf{x} \\ \hat{\mathbf{x}} \end{bmatrix}_k \\ &+ \begin{bmatrix} \Gamma\bar{\mathbf{N}} \\ \Gamma\bar{\mathbf{N}} + \mathbf{L}_c\mathbf{H}\Gamma\bar{\mathbf{N}} \end{bmatrix} r(k) + \begin{bmatrix} \Gamma_1 \\ \mathbf{L}_c\mathbf{H}\Gamma_1 \end{bmatrix} w(k). \end{aligned} \quad (8.81)$$

Reference Input Command to Satellite Attitude

Example 8.12

Determine the state-command structure for the system whose regulator was found in Example 8.8 and verify that its step response does not excite an estimator error.

Solution. Evaluation of Eq. (8.73) yields $\mathbf{N}_x = [1 \ 0]^T$ and $N_u = 0$. Therefore, $\bar{\mathbf{N}} = \mathbf{K}_1$. The desired response of the system is obtained from Eqs. (8.79) and (8.80). Using `step` in MATLAB yields the unit step

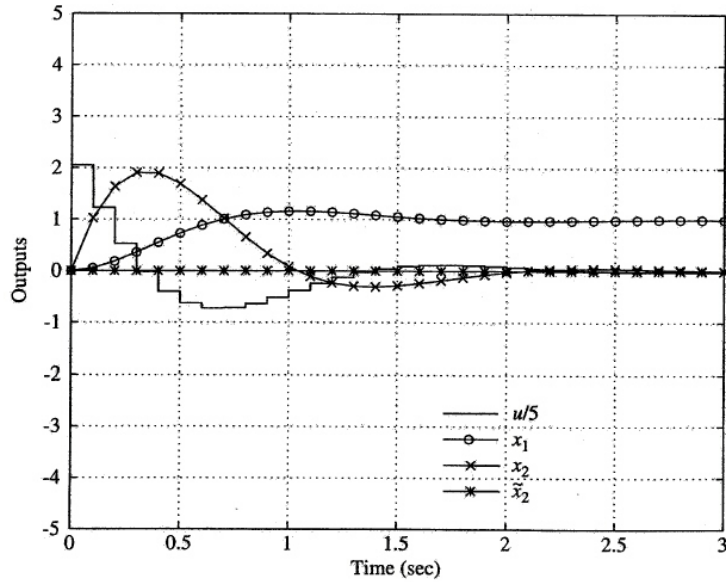


Figure 8.17
Step-response
time histories for
Example 8.12

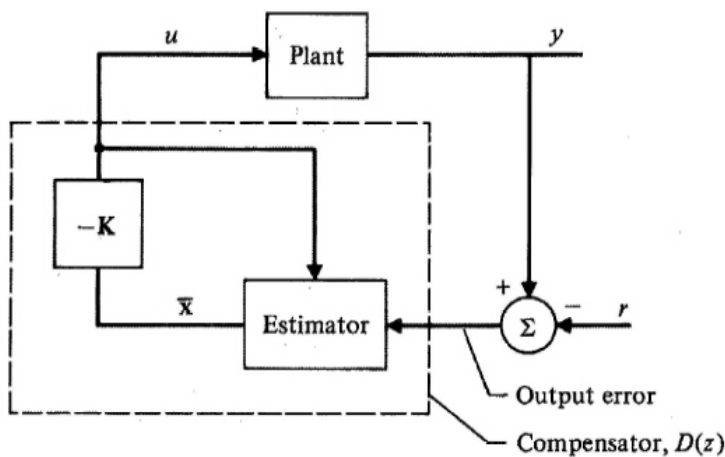


Figure 8.18
Reference input
as an
output-error
command

responses shown in Fig. 8.17. Note that the estimator error remains zero; thus the response is exactly the same as if no estimator were present. Note also that the structure shown in Fig. 8.16(b) does not allow us to represent the system in a simple, classical manner with the $D_p(z)$ from Example 8.8 placed in the upper path as in Fig. 7.5, nor does it allow us to place $D_p(z)$ in the lower feedback path. Rather, it is best to stay with the state-space description and enter the equations in the control computer based on Fig. 8.16. The response in Fig. 8.17 would also have resulted if using no estimator, a current estimator, or a reduced-order estimator.

It is worthwhile to reflect on the fact that the combined system has poles that consist of the control *and* the estimator poles, as given by Eq. (8.55). The fact that the system response to an input structured as in Fig. 8.16(b) did not excite the estimator response means that the transfer function of this system had zeros that canceled the estimator poles. The determination of the structure in which the reference command is entered into a system can be viewed as one of “zero placement” and, in fact, it has been shown that it is possible to place the zeros of the closed loop transfer function at any arbitrary location [(Emami-Naeini and Franklin (1982)].

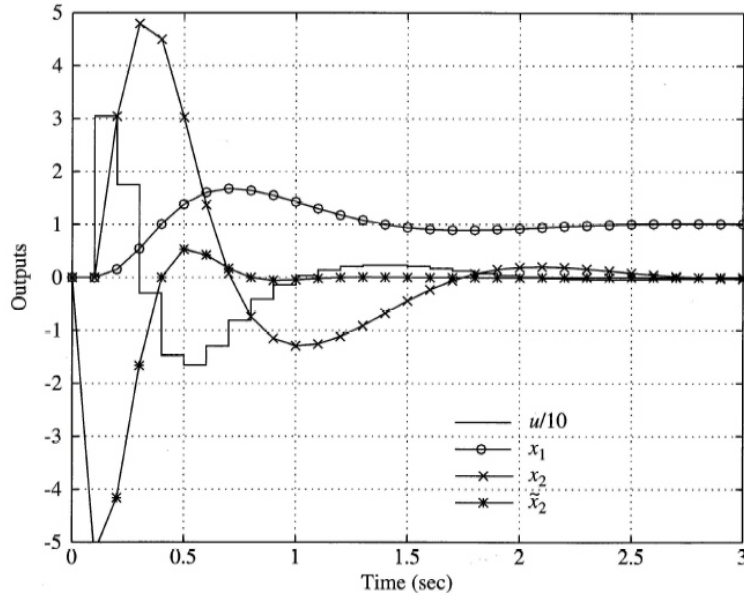


Figure 8.19
Output time histories for prediction estimator with output command, Example 8.13

8.4.3 Output Error Command

Another approach to the reference-input structure is to introduce the command only at the measured estimator input, as shown in Fig. 8.18. This solution is sometimes forced on the control designer because the sensor measures only the error. For example, many thermostats have an output that is the difference between the temperature to be controlled and the reference, or set-point, temperature. No absolute indication of the reference temperature is available to the controller. Likewise, some radar tracking systems have a reading that is proportional to the pointing error, and this signal alone must be used for control. In this case, the estimator equation (8.56) becomes

$$\bar{x}(k + 1) = (\Phi - \Gamma K - L_p H)\bar{x} + L_p(y - r),$$

and the system response can be determined by solving

$$\begin{bmatrix} \mathbf{x} \\ \bar{x} \end{bmatrix}_{k+1} = \begin{bmatrix} \Phi & -\Gamma K \\ L_p H & \Phi - \Gamma K - L_p H \end{bmatrix} \begin{bmatrix} \mathbf{x} \\ \bar{x} \end{bmatrix}_k + \begin{bmatrix} \mathbf{0} \\ -L_p \end{bmatrix} r(k) + \begin{bmatrix} \Gamma_1 \\ \mathbf{0} \end{bmatrix} w(k). \quad (8.82)$$

Note that the command input r only enters the estimator; therefore, the plant and estimator do not see the same command and an estimator error will be excited.

Output Command Structure with a Predictor Estimator

Example 8.13

Analyze the performance of Example 8.12 when using the output-command structure, specifically looking at the step response of the estimator error.

Solution. The system is analyzed using Eq. (8.82) and the output Eq. (8.80). The result is shown in Fig. 8.19. Note the estimator error response and that it causes a substantial increase in overshoot as compared to that of Fig. 8.17 (about 70% rather than 20%) and an increased use of control. Although this degradation could be reduced with faster estimator-error roots, there are limits due to the adverse effect on the estimator’s sensitivity to measurement noise. Some of the degradation can be reduced by using a current or reduced order estimator because of their quicker response from the immediate use of the measured signal.

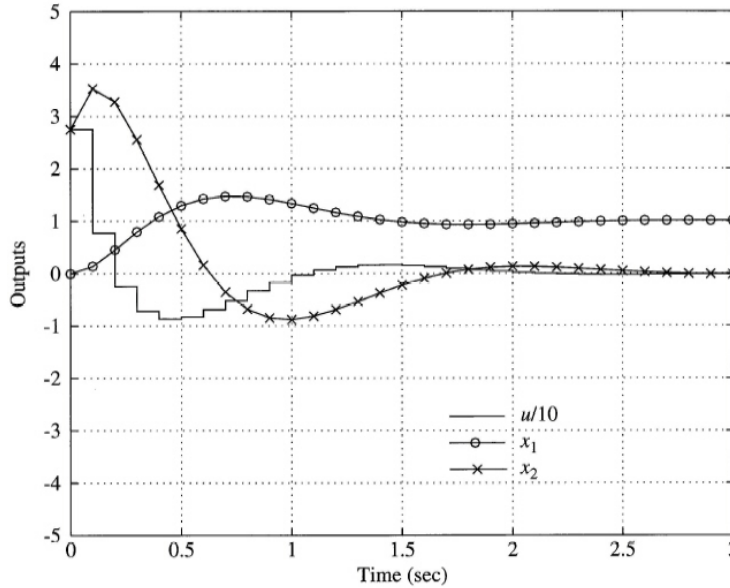


Figure 8.20
Output time histories for reduced-order estimator with output command, Example 8.14

Output Command Structure with a Reduced-Order Estimator

Example 8.14

Analyze the performance of Example 8.13 when using the output-command structure and a reduced-order estimator.

Solution. The easiest way to analyze this system is by transform methods. The plant transfer function was analyzed in Section 4.3.1 and found to be

$$G(z) = \frac{T^2 (z+1)}{2 (z-1)^2},$$

and the transfer function that arose from the reduced-order estimator is given by Eq. (8.67). The output time histories using these transfer functions are shown in Fig. 8.20. Note again that there is more overshoot (about 50%) than shown in Fig. 8.17 but not as much as the prediction estimator. The control usage for this case is also less than in Fig. 8.19, and it starts at the first cycle rather than being delayed by one cycle, as was the case in Fig. 8.19. This result produced a settling time for the reduced-order case that is about one sample period faster than the prediction estimator. A current estimator would produce results similar to this case because it, too, shares the feature of an immediate response to the measured output.

8.4.4 A Comparison of the Estimator Structure and Classical Methods

This section has demonstrated a key result: The controller structure based on state-space design of the control and estimator exposes a methodology for the introduction of the reference input in a way that produces a better response than that typically used with transfer-function design. The state-command input shown in Fig. 8.16 provides a faster response with less control usage than the output-error-command scheme shown in Fig. 8.18, which is the typical transfer function structure. The reason for the advantage is that the state-command structure provides an immediate input to the plant and does not excite any modes of the compensator that degrade the response. Although this result has been specifically shown only for a simple second-order system, it applies to more complicated systems as well. In fact, for higher-order plants, higher-order compensators are often required with more modes for potential excitation.

It is not mandatory that the state-space representation and the state-estimator design approach be used in order to determine a structure that does not excite compensator modes. However, the

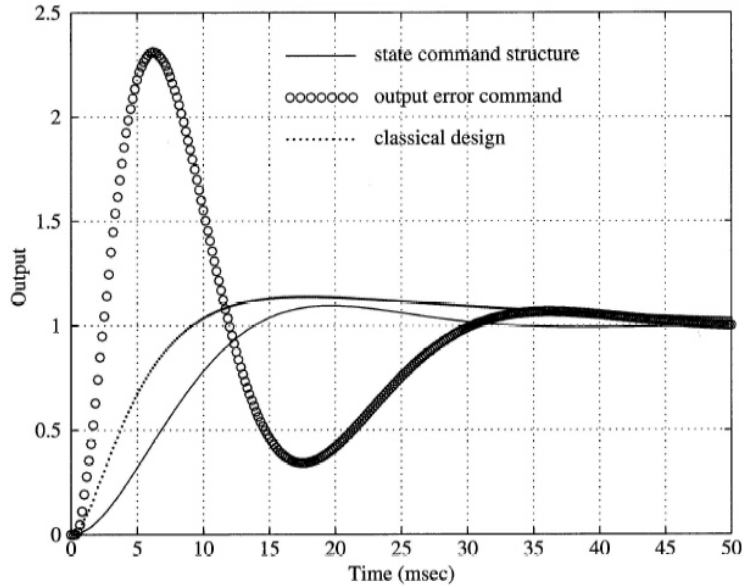


Figure 8.21
Disk read head
response,
Example 8.15

determination is difficult using the transfer-function approach, especially in the MIMO case.

The advantages of using the transfer-function representation are that high-order systems are easier to trouble shoot, the designs are made robust with less effort, and experimental frequency-response data can be used to close a loop quickly without a time-consuming modeling effort. These advantages might not always warrant transforming to the state-space form in order to achieve easily the better reference input structure.

Although not discussed in this section using linear systems, the state-command structure allows for superior response of systems with nonlinear control characteristics, for example, saturation or on-off actuators. Whatever nonlinearity is present in the plant can usually be modeled to some degree in the estimator as well, thus reducing errors that would otherwise be excited by the nonlinearity.

Compensation Design for a System with a Resonance

Example 8.15

A computer disk drive has a control system that commands the read head to move to specific tracks on the disk. One such system is described in Chapter 14. Although the dynamics between the torquer and the head motion are primarily $G(s) = 1/s^2$, there are typically several resonances due to the arm's flexibility that limit the performance of the servo system. Here we wish to limit the flexibility to one resonance mode for simplicity. The transfer function is the same as the mass-spring system shown in Appendix A.4, although the derivation of it would involve rotational dynamics rather than the linear dynamics in Appendix A.4. (See Franklin, Powell, and Emami-Naeini (2019), Chapter 2, for more details.)

The system transfer function is

$$G(s) = \frac{1 \times 10^8}{s^2(s^2 + 2\zeta_r \omega_r s + \omega_r^2)}$$

where the resonance frequency $\omega_r = 1$ kHz and the damping $\zeta_r = 0.05$. Use a sample rate of 6 kHz and design control systems that have a rise time of 10 msec with an overshoot less than 15%.

- Do the design using a state estimator and the state command structure,
- evaluate the \mathbf{K} and \mathbf{L} from (a) using the output error structure whether or not they meet the specifications, and
- do a classical design with a lead compensator.

Iterate on whatever design parameters are appropriate for (a) and (c) to meet the design specifications.

Solution. Equation (2.16) indicates that a $t_r < 10$ msec would be met if $\omega_n > 180$ rad/sec and the $M_p < 15\%$ would be met if $\zeta > 0.5$.

- (a) For the state space design, a good starting point would be with two of the desired poles at $\omega_n = 200$ rad/sec and $\zeta = 0.6$. Two more poles also need to be selected for this 4th order system; so let's pick them at $\omega = 1$ kHz and $\zeta = 0.06$. As discussed in Section 2.6, it is not wise to move poles any more than you have to. In this case, we have retained the same natural frequency and increased the damping slightly. For the estimator, a good starting point is to pick the natural frequencies twice those of the controller, that is, at 400 rad/sec and 2 kHz. The damping was selected to be 0.7 for both sets of poles in the estimator. The selected poles were converted to their discrete equivalents and used with `acker` to find **K** and **L**. Evaluation of the response for the state command structure is found using Eq. (8.79) in `step` and is shown in Fig. 8.21. We see that the rise time and overshoot specifications were met for this case and that the system settles to its final value at about 35 msec.
- (b) Using Eq. (8.82) shows the response of the system with the same **K** and **L** for the output error command case and it is shown in the figure also. Note that the estimator excitation for this case caused an overshoot of 130% rather than the desired 15% and the system appears to be lightly damped even though its poles are in precisely the same place as case (a). It is interesting that the large overshoot was, in part, caused by using desired poles that increased the resonant mode damping from $\zeta = 0.05$ to 0.06. Had the damping been kept at 0.05, the overshoot would have been about 50% which is still excessive but significantly less. This illustrates the sensitivity of the system to the pole placement when using the output error command structure.
- (c) For the classical design, we note that the sample rate of 6 kHz is over 100 times faster than the desired closed loop natural frequency (200 rad/sec \cong 30 Hz). Therefore, the most expedient design method is to use the s -plane and convert the result to the discrete case when through. Furthermore, since the resonance frequency is significantly faster than the desired bandwidth (\cong 200 rad/sec), we can ignore the resonance for the first cut at the design and simply find a compensation for a $1/s^2$ system. Using frequency response ideas, we know that a lead compensation with a ratio of 25 between the zero and pole will yield a maximum increase in phase of about 60° (Fig. 2.17). We also know that a 60° *PM* (Section 2.4.4) will translate to a damping ratio of about 0.6 which will meet the overshoot specification. For a $1/s^2$ plant, the phase is 180° everywhere; therefore, the desired *PM* will be obtained if we place the lead compensation so that the maximum phase lead is at the desired crossover point (\cong 200 rad/sec). This is accomplished by placing the zero a factor of 5 below 200 (at 40 rad/sec) and the pole a factor of 5 above 200 (at 1000 rad/sec), thus producing

$$D(s) = K \frac{s + 40}{s + 1000}.$$

Using this with the $G(s)$ above in a Bode plot shows that the resonant mode does not affect the design significantly, the *PM* is met, and the desired crossover is achieved when $K = 8000$. To convert to the digital form, we invoke `c2d` using the matched pole-zero approach and find that

$$D(z) = 7394 \frac{z + 0.9934}{z + 0.8465}.$$

The closed loop step response with $D(z)$ in the forward path is found using `step` and shown in Fig. 8.21. It also meets the specifications, but a slow compensator mode was excited and the settling time of this system is considerably longer than the state command structure. The advantage of this approach is that the compensator is first order while the estimator approach (a) required a 4th order compensation.

8.5 Integral Control and Disturbance Estimation

Integral control is useful in eliminating the steady-state errors due to constant disturbances or reference input commands. Furthermore, most actual control systems are nonlinear and the input gain Γ and the state matrix Φ vary with time and/or the set point. The linear analysis which is the subject of this book pertains to perturbations about a set point of the nonlinear plant and the control u is a perturbation from a nominal value. The use of integral control eliminates the need to catalog nominal values or to reset the control. Rather, the integral term can be thought of as constantly calculating the value of the control required at the set point to cause the error to go to zero. For these reasons, some form of integral control is typically included in most control systems. More generally, the external

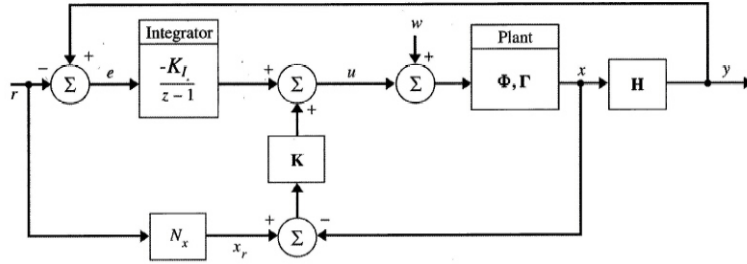


Figure 8.22
Block diagram for integral control with full-state feedback

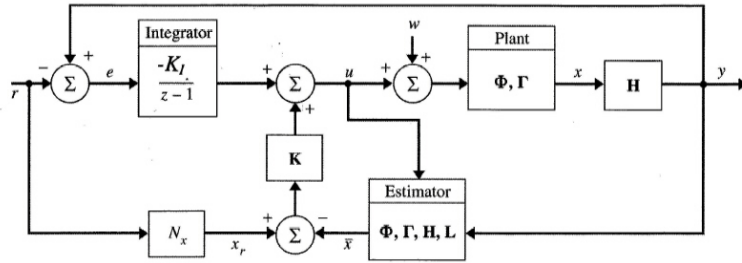


Figure 8.23
Block diagram for integral control with state estimation

signals frequently include persistent deterministic components and the control engineer is required to design a controller which will force the steady-state error to be zero in the presence of such signals. A particular case is that of the disk drive servo required to follow a data track that is slightly off center so the reference signal is sinusoidal.

In the state-space design methods discussed so far, no mention has been made of integral control; nor have any of the design examples produced a compensation with an integral kind of behavior. In fact, state-space designs will not produce an integral action unless special steps are taken. There are two basic methods to force zero steady-state error in the presence of persistent signals: state augmentation also called internal signal model control and disturbance estimation. The idea of state augmentation for constant commands or disturbances was discussed for continuous systems in Section 2.6.5 and is essentially the same as the addition of an integral term that was discussed for transform design in Section 2.2.3. The generalization augments the state in a way that achieves zero steady-state error for a general class of reference and disturbance signals. Disturbance estimation provides the same effect based on estimation of the state of a model which could generate the external signals. We begin with the heuristic introduction of integral control.

8.5.1 Integral Control by State Augmentation

The idea is to add an integrator so as to obtain an integral of the error signal. This integrator will be physically implemented as part of the controller equations. We then feed back that integral along with the estimated or measured state as shown in Figs. 8.22 and 8.23 in a similar manner as before. To accomplish the design of the feedback gains for both the integral and the original state vector, we augment the model of the plant with an integrator, thus adding an error integral output to the existing plant state output. This augmented model is then used as before to calculate the feedback control gains for the augmented state. More specifically, to the standard system

$$\begin{aligned} \mathbf{x}(k+1) &= \Phi \mathbf{x}(k) + \Gamma u(k) + \Gamma_1 w(k), \\ y(k) &= \mathbf{H} \mathbf{x}(k), \end{aligned}$$

we augment the state with x_I , the integral of the error, $e = y - r$. The discrete integral is simply a summation of all past values of $e(k)$ (Eq. 3.15), which results in the difference equation

$$x_I(k+1) = x_I(k) + e(k) = x_I(k) + \mathbf{H} \mathbf{x}(k) - r(k), \tag{8.83}$$

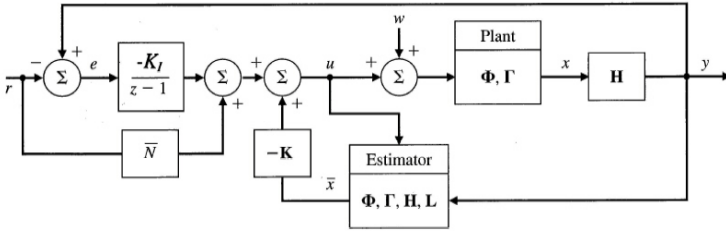


Figure 8.24
Block diagram for integral control with full-state feedback and an added zero

therefore arriving at the augmented plant model

$$\begin{bmatrix} x_I(k+1) \\ \mathbf{x}(k+1) \end{bmatrix} = \begin{bmatrix} 1 & \mathbf{H} \\ 0 & \Phi \end{bmatrix} \begin{bmatrix} x_I(k) \\ \mathbf{x}(k) \end{bmatrix} + \begin{bmatrix} 0 \\ \Gamma \end{bmatrix} u(k) - \begin{bmatrix} 1 \\ \mathbf{0} \end{bmatrix} r(k). \quad (8.84)$$

The control law, following Eq. (8.75), is

$$u(k) = -[K_I \quad \mathbf{K}] \begin{bmatrix} x_I(k) \\ \mathbf{x}(k) \end{bmatrix} + \mathbf{K}\mathbf{N}_x r(k).$$

With this revised definition of the system, the design techniques already developed can be used directly for the control law design. Following Figs. 8.15(a) and 8.16(a), it would be implemented as shown in Fig. 8.22 for the full-state feedback case and as shown in Fig. 8.23 for the case where an estimator is used to provide $\bar{\mathbf{x}}$. The integral is replacing the feedforward term, N_u , and has the additional role of eliminating errors due to w .

The estimator is based on the unaugmented model and is used to reconstruct the unaugmented state. It will be n th-order, where n is the order of the original system and requires the placement of n poles. On the other hand, the design of $[K_I \quad \mathbf{K}]$ requires the augmented system matrices (Eq. 8.84); therefore, there will be $n + 1$ poles to be selected for this portion of the design.

If implemented as in Fig. 8.23, the addition of the extra pole for the integrator state element will typically lead to a deteriorated command input response compared to that obtained without integral control. While it is possible to iterate on the $n + 1$ selected control poles until a satisfactory response is obtained, it is also possible to retain the reference response obtained from a non-integral-control design by placing a zero in the controller as shown in Fig. 8.24 so that it cancels the extra pole from the integrator. Note that the feedforward N_x term in Fig. 8.22 has been replaced by \bar{N} which introduces a zero at $z_I = 1 - \frac{K_I}{\bar{N}}$ ¹⁵. Using the zero to cancel the closed-loop pole that was added for the integral state element cancels the excitation of that pole by command inputs. Note that this does not cancel the integral action, it merely eliminates the excitation of the extra root by command inputs. A change in the disturbance, w , will also excite the integral dynamics and the steady-state errors due to either constant disturbances or constant command inputs are eliminated. As always, the integrator output changes until its input, which is constructed to be the system error, is zero. The configuration of Fig. 8.24 can be changed to replace the feedforward of r to additional feedforward of e and modified feedback of y .

integrator pole cancellation

Integral Control for the Satellite Attitude Case

Example 8.16

Determine the integral control structure and gains for the satellite attitude control problem using full state feedback. Place the control poles at $z = 0.8 \pm j0.25, 0.9$ and use a sample period of $T = 0.1$ sec. Compute the time responses for a unit step in r at $t = 0$ sec and a step disturbance of 5 deg/sec^2 at $t = 2$ sec for (a) no integral control, (b) integral control as in Fig. 8.22, and (c) integral control as in Fig. 8.24 with the added zero at $z = +0.9$.

Solution.

¹⁵In fact, the system of Fig. 8.22 has a zero at $1 - \frac{K_I}{\mathbf{K}\mathbf{N}_x}$, so the selection of the zero location corresponds to a particular selection of N_x .

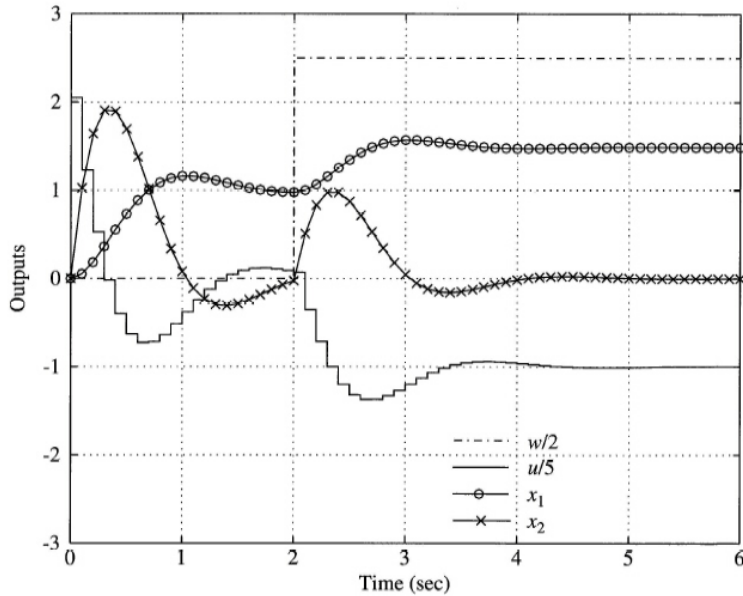


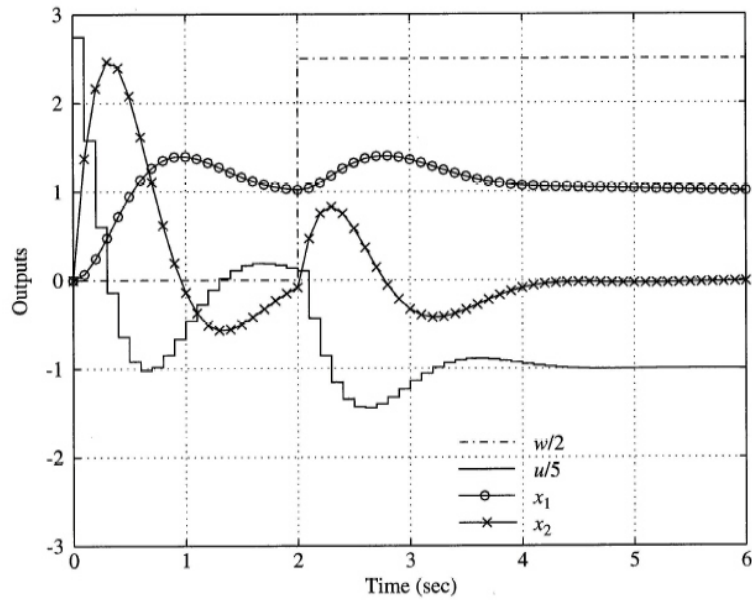
Figure 8.25
Response of satellite example to a unit reference input at $t = 0$ and a step disturbance at $t = 2$ sec with no integral control action, Example 8.16

- (a) This case is the same controller as used in Example 8.12. The only difference is that there is a step in the disturbance at 2 sec. Therefore, `lsim` must be used in order to allow the multiple inputs, the step in r at $t = 0$ and the disturbance step in w starting at 2 sec. The result is shown in Fig. 8.25. We see that the system responds identically to Fig. 8.17 for the first 2 sec, then there is a steady-state error in the output, x_1 , after the transients from the disturbance die out. The output error can be shown via the final value theorem to be $w/K_1 = 0.5$, thus the final value of x_1 is 1.5 instead of the commanded value of 1.
- (b) A steady-state error resulting from a disturbance is a classic motivation for the addition of integral control. The system model from Example 8.1 is augmented according to Eq. (8.84) and used with `acker` to obtain the augmented feedback gain matrix, $[K_I \ K] = [1.025 \ 13.74 \ 4.313]$ by asking for control roots at $z = 0.8 \pm j0.25, 0.9$. We saw from Example 8.12 that $\mathbf{N}_x = [1 \ 0]^T$; therefore, the system design is complete and can be implemented according to Fig. 8.22. Use of `lsim` produces the response in Fig. 8.26(a). Note that the desired result has been obtained in that there is no longer a steady-state error in the output, x_1 . However, also note that it has come with a price; the behavior before the disturbance step has been degraded. More control was used, and the initial overshoot has increased from the original 20% to about 40% because of the additional root at $z = 0.9$.
- (c) The implementation is structured as shown in Fig. 8.24 which produces a zero at $z = 0.9$. All other parameters are the same as (b). Note that the resulting response in Fig. 8.26(b) before 2 sec is now identical to the case in Example 8.12 with no integral control; yet, the integral action successfully eliminates the steady-state error.

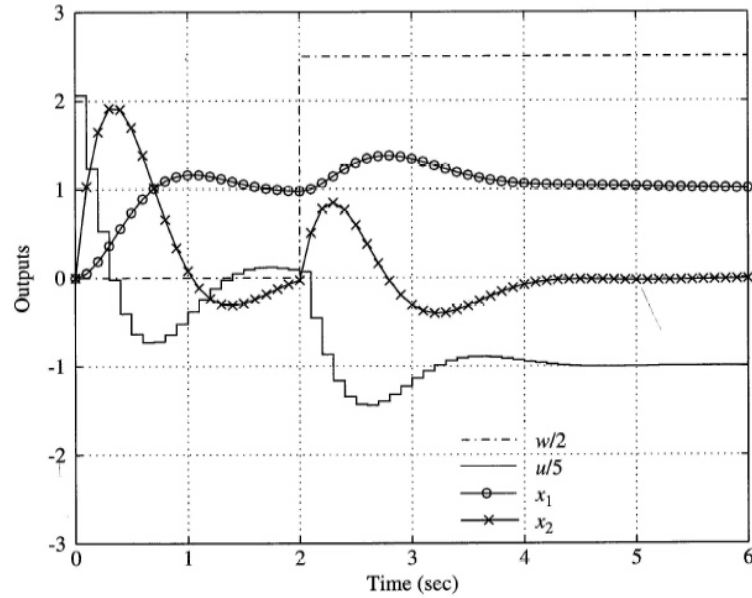
It should be clear from the discussion and the example that the preferred implementation of integral control is given by Fig. 8.24 where the zero cancels the integrator closed-loop root.

8.5.2 Disturbance Estimation

An alternate approach to state augmentation is to estimate the disturbance signal in the estimator and then to use that estimate in the control law so as to force the error to zero as shown in Fig. 8.27. This is called **disturbance rejection**. This approach yields results that are equivalent to integral control disturbance rejection when the disturbance is a constant. After the estimate, \hat{w} , converges, the feedback of its value as shown in Fig. 8.27 will cancel the actual disturbance, w , and the system will behave in the steady state as if no disturbance were present. Therefore, the system will have no steady-state error, assuming, of course, that the steady-state error was due to a disturbance described by the assumed equation



(a)



(b)

Figure 8.26
Response of satellite attitude to a unit step input at $t = 0$ and a step disturbance at $t = 2$ sec with integral control, Example 8.16. (a) As in Fig. 8.22, (b) with an added zero as in Fig. 8.24

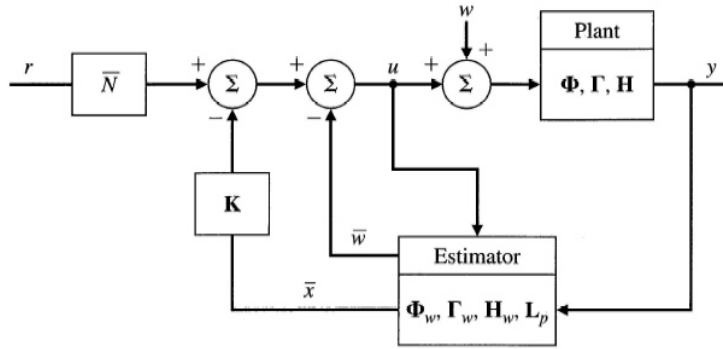


Figure 8.27
Block diagram for
input disturbance
rejection

used in the estimator. It is important to notice that while a disturbance may, in general, appear at any point in the plant equations, the control can apply a signal to cancel it only at the control input. To reconcile these facts, we introduce the “input equivalent” disturbance. This is a virtual signal applied at the control input which would produce the *same steady state output* at y as the actual disturbance does. Then, when the control applies the negative of the virtual disturbance, the effect of the real disturbance at the output is cancelled and the error is driven to zero. To obtain an estimate of the virtual disturbance, we build the estimator with the equations of the virtual disturbance included.

Disturbances other than constant biases can be modeled, included in the estimator equations, disturbance estimated along with the plant state, and their effect on errors eliminated in steady-state. If we modeling assume the disturbance is a constant, the continuous model is quite simple:

$$\dot{w} = 0.$$

A sinusoidal disturbance would have the model

$$\ddot{w} = -\omega_o^2 w,$$

or, in general, we could say that the disturbance obeys

$$\begin{aligned}\dot{\mathbf{x}}_d &= \mathbf{F}_d \mathbf{x}_d \\ w &= \mathbf{H}_d \mathbf{x}_d.\end{aligned}$$

and the discrete model is given by

$$\mathbf{x}_d(k+1) = \Phi_d \mathbf{x}_d(k) \quad (8.85)$$

$$w(k) = \mathbf{H}_d \mathbf{x}_d(k) \quad (8.86)$$

where $\Phi_d = e^{\mathbf{F}_d T}$. For purposes of disturbance estimation, we augment the system model with the disturbance model, so Eqs. (8.85) and (8.86) become

$$\begin{bmatrix} \mathbf{x}(k+1) \\ \mathbf{x}_d(k+1) \end{bmatrix} = \begin{bmatrix} \Phi & \Gamma_1 \mathbf{H}_d \\ \mathbf{0} & \Phi_d \end{bmatrix} \begin{bmatrix} \mathbf{x}(k) \\ \mathbf{x}_d(k) \end{bmatrix} + \begin{bmatrix} \Gamma \\ \mathbf{0} \end{bmatrix} u(k). \quad (8.87)$$

$$y = \begin{bmatrix} \mathbf{H} & \mathbf{0} \end{bmatrix} \begin{bmatrix} \mathbf{x} \\ \mathbf{x}_d \end{bmatrix}, \quad (8.88)$$

which can be written as

$$\begin{aligned}\begin{bmatrix} \mathbf{x}(k+1) \\ \mathbf{x}_d(k+1) \end{bmatrix} &= \Phi_w \begin{bmatrix} \mathbf{x}(k) \\ \mathbf{x}_d(k) \end{bmatrix} + \Gamma_w u(k) \\ y(k) &= \mathbf{H}_w \begin{bmatrix} \mathbf{x}(k) \\ \mathbf{x}_d(k) \end{bmatrix}\end{aligned}$$

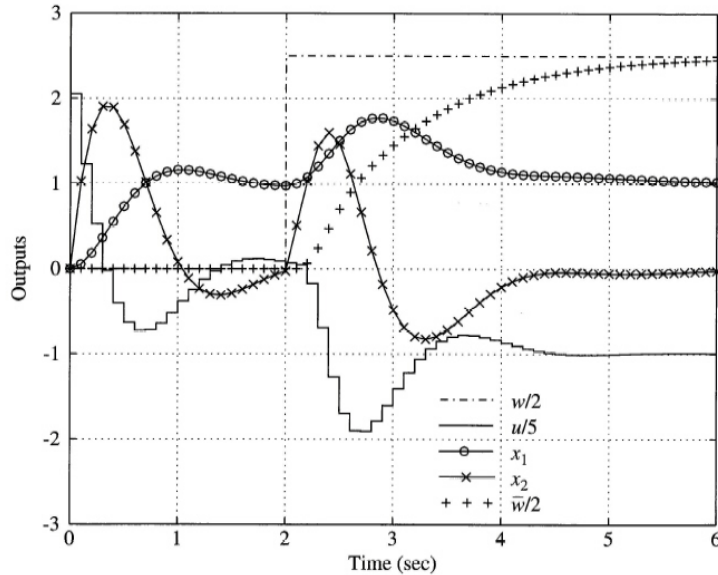


Figure 8.28
Response of satellite example to a unit reference input at $t = 0$ and a step disturbance at $t = 2$ sec with bias estimation as in Fig. 8.27, Example 8.17

In the particular case where the disturbance is a constant, these equations reduce to

$$\begin{bmatrix} x(k+1) \\ w(k+1) \end{bmatrix} = \begin{bmatrix} \Phi & \Gamma_1 \\ 0 & 1 \end{bmatrix} \begin{bmatrix} \mathbf{x}(k) \\ w(k) \end{bmatrix} + \begin{bmatrix} \Gamma \\ 0 \end{bmatrix} u(k). \quad (8.89)$$

$$y(k) = \begin{bmatrix} \mathbf{H} & 0 \end{bmatrix} \begin{bmatrix} \mathbf{x}(k) \\ w(k) \end{bmatrix}. \quad (8.90)$$

All the ideas of state estimation in Section 8.2 still apply, and any of the estimation methods can be used to reconstruct the state consisting of \mathbf{x} and \mathbf{x}_d , provided the system is observable.¹⁶ The computation of the required estimator gains is exactly as given in Section 8.2, the only change being that the system model is the augmented one given above by Φ_w and \mathbf{H}_w . Note from Fig. 8.27, however, that the control gain matrix, \mathbf{K} , is *not* obtained using the augmented model. Rather, it is obtained using the Φ and Γ associated with the unaugmented \mathbf{F} and \mathbf{G} . In fact, the augmented system described by $[\Phi_w, \mathbf{H}_w]$ will always be uncontrollable! We have no influence over the value of w by means of the control input, u , and must live with whatever value nature deals us; hence, the augmented system is uncontrollable. Our plan is not to control w , but to use the estimated value of w in a feedforward control scheme to eliminate its effect on steady-state errors. This basic idea works if w is a constant, a sinusoid, or any combination of functions that can be generated by a linear model. It works regardless of where the actual disturbance acts since the design is based on the virtual disturbance. The only constraint is that the disturbance state, \mathbf{x}_d , be observable.

Bias Estimation and Rejection for the Satellite Attitude Case

Example 8.17

Determine the bias rejection control structure and gains for the satellite attitude control problem. Place the control poles at $z = 0.8 \pm j0.25$ and use a sample period of $T = 0.1$ sec. Use a predictor estimator and place the estimator poles at $z = 0.4 \pm j0.4, 0.9$. Compute the time responses for a unit step in r at $t = 0$ sec and a step disturbance of 5 Deg/sec^2 at $t = 2$ sec and compare the results with the integral control in Example 8.16.

Solution. For purposes of finding the control gain, we use the unaugmented model as in Example 8.1 and, therefore, find the same value of $\mathbf{K} = [10.25 \quad 3.49]$. For purposes of designing the estimator, we augment the plant model according to Eqs. (8.89) and (8.90) and find that the desired poles yield $\mathbf{L}_p^T = [1.3 \quad 6.14 \quad 5.2]$.

¹⁶Observability requires that the virtual disturbance is “seen” at the plant output. Thus, if the disturbance is a constant, then the plant cannot have a zero from u to y at $z = 1$.

Structuring the control as in Fig. 8.27 and applying the inputs as specified above, `lsim` yields the response as shown in Fig. 8.28. Note the similarity to Example 8.16 shown in Figs. 8.26(a) and (b). The disturbance rejection approach also eliminates the steady-state error. But also note the early response to the reference input: There is no increased overshoot as in Fig. 8.26(a); in fact, the response is identical to Fig. 8.26(b) up until the disturbance enters at $t = 2$ sec. Note further that the disturbance estimate, \bar{w} , approaches the actual disturbance value asymptotically. Notice that in this case the steady state error due to the reference input is made to be zero by the calculation of \bar{N} and is not robust to small parameter changes in the way provided by integral control.

Example 8.17 shows that disturbance estimation can be used to estimate a constant disturbance input and then to use that estimate so as to reject the effect of the disturbance on steady-state errors. When the disturbance is a constant, this approach essentially duplicates the function of integral control. The following example shows how disturbance estimation can be used to estimate the value of the disturbance when it is a sinusoid. The estimate is used to cancel the effect of the disturbance, thus creating disturbance rejection.

Disturbance Torque Rejection for a Spinning Satellite

Example 8.18

For a spinning satellite, a disturbance torque from solar pressure acts on the system as a sinusoid at the spin frequency. The attitude dynamics become 4th order as the two axes are now coupled; however, for slow spin rates, the dynamics may be approximated to be $1/s^2$ as in Example 8.17.

Determine the disturbance rejection control structure and gains for the attitude control with a disturbance torque from solar pressure of 2 deg/sec^2 where the satellite is spinning at 15 rpm. Place the control poles at $z = 0.8 \pm j0.25$ and use a sample period of $T = 0.1$ sec, as before. Use a predictor estimator and place the estimator poles at $z = 0.4 \pm j0.4, 0.9 \pm j0.1$. The location of the estimator poles corresponding to the disturbance can be selected at a relatively slow frequency as above if the sinusoidal disturbance is known to be relatively stable in magnitude and phase. By picking those estimator poles at a slow frequency, the disturbance estimate will not respond much to other higher frequency disturbances.

Plot the time history of the disturbance, the estimate of the disturbance, and the system output to verify that, in steady-state, there is no error remaining from the disturbance. Put in a step command of 1° at $t = 5$ sec to verify that the input will not excite any unwanted estimator errors. Examine the roots of the 8th order system and explain what each of them represent.

Solution. The feedback for the unaugmented system is computed as in Example 8.17 to be

$$\mathbf{K} = [10.25 \quad 3.49].$$

The disturbance acts at the control input so there is no need for the concept of the virtual disturbance. It is modeled by choosing

$$\mathbf{F}_d = \begin{bmatrix} 0 & 1 \\ -\omega_o^2 & 0 \end{bmatrix}, \quad \mathbf{\Gamma}_1 = \mathbf{\Gamma} \quad \text{and} \quad \mathbf{H}_d = [1 \quad 0]$$

in Eqs. (8.87) and (8.88). Use of `acker` with Φ_w and \mathbf{H}_w and the desired poles results in

$$\mathbf{L}_p^T = [1.375 \quad 6.807 \quad 8.391 \quad -6.374].$$

The time response of the system described by Fig. 8.27 is found by use of `lsim` where the state of the complete system consists of the augmented state as well as the estimate of the augmented state, an 8th order system. The feedback of \bar{w} can be accomplished by using an augmented feedback gain $\mathbf{K}' = [\mathbf{K} \quad 1 \quad 0]$. Figure 8.29 shows the results. Note in the figure that the estimate takes about 4 sec to converge to the correct value and that there is a noticeable error in the output due to the disturbance until that time. The step at 5 sec has no effect on the estimate quality and therefore the response to the step is precisely as it was originally designed. Without the disturbance rejection, there would have been a steady sinusoidal error of about 0.2° superimposed on the output.

The roots of the closed loop 8th order system are:

$$z = 0.8 \pm 0.25j, \quad 0.4 \pm 0.4j, \quad 0.9 \pm 0.1j, \quad 0.988 \pm 0.156j.$$

The first 6 roots represent those selected in the control and estimation design. The last two represent the discrete equivalent of the pure oscillation at 15 rpm, which are unchanged by the feedback.

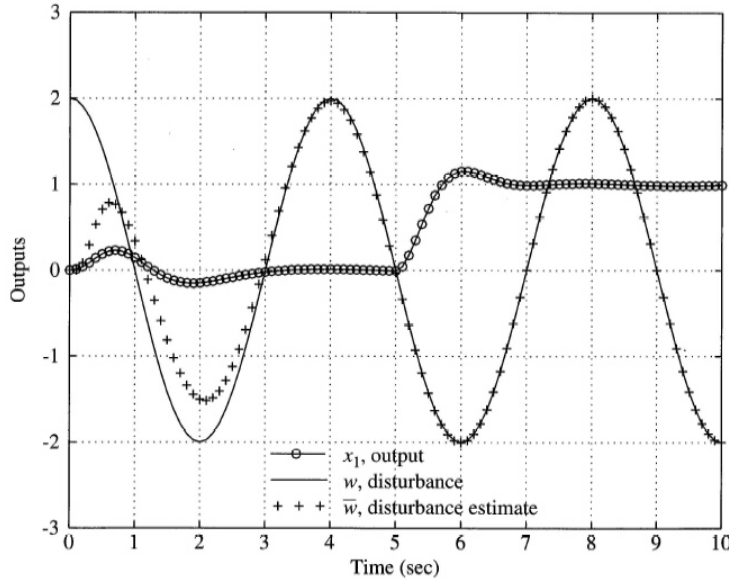


Figure 8.29
Response of satellite to a sinusoidal input disturbance with disturbance rejection as in Fig. 8.27, Example 8.18

The previous example had a sinusoidal disturbance torque acting on the input to the system. It is also possible to have a measurement or sensor error that is sinusoidal in nature that one would like to eliminate as a source of error to the control system. The role of the estimator in this case is to use the contaminated measurement to reconstruct the error-free state for use in the control. The estimate of the sensor error is ignored by the controller.

Satellite Attitude Control with Sinusoidal Sensor Disturbance Rejection

Example 8.19

When an attitude sensor on a spinning satellite is misaligned from a principal axis of inertia, the sensed attitude will have a sinusoidal component as the satellite naturally spins about its principal axis. Typically, it is desirable to spin about the principal axis; therefore, it is useful to estimate the magnitude and phase of the misalignment and to reject that component of the measurement.

Repeat the design from Example 8.18, but replace the sinusoidal disturbance torque with a sinusoidal measurement error of 0.3° at 15 rpm. Again include a step command of 1° at $t = 5$ sec. Place the control poles at $z = 0.8 \pm j0.25$, as in Example 8.18, and use a sample period of $T = 0.1$ sec. Use a predictor estimator and place the estimator poles at $z = 0.8 \pm j0.2, 0.95 \pm j0.05$.

Solution. As in Example 8.18, the feedback for the unaugmented system is $\mathbf{K} = [10.25 \ 3.49]$. The output disturbance is modeled by augmenting the continuous plant with the matrices

$$\mathbf{F}_d = \begin{bmatrix} 0 & 1 \\ -\omega_0^2 & 0 \end{bmatrix}, \quad \mathbf{\Gamma}_1 = \begin{bmatrix} 0 \\ 0 \end{bmatrix} \quad \text{and} \quad \mathbf{H}_d = [1 \ 0]$$

and the augmented continuous system is

$$\begin{aligned} \dot{\mathbf{x}} &= \mathbf{F}\mathbf{x} + \mathbf{G}u \\ \dot{\mathbf{x}}_d &= \mathbf{F}_d\mathbf{x}_d \\ y &= [\mathbf{H} \ \mathbf{H}_d]\mathbf{x} \end{aligned} \quad (8.91)$$

From these matrices, use of `c2d` will compute the discrete matrices Φ_w and \mathbf{H}_w from which, with the desired poles the estimator gain is computed as

$$\mathbf{L}_p^T = [0.3899 \ 0.1624 \ 0.0855 \ 0.7378].$$

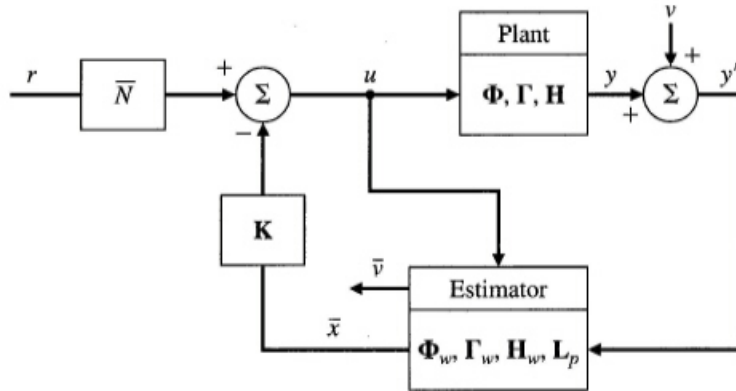


Figure 8.30
Block diagram
for sensor
disturbance
rejection

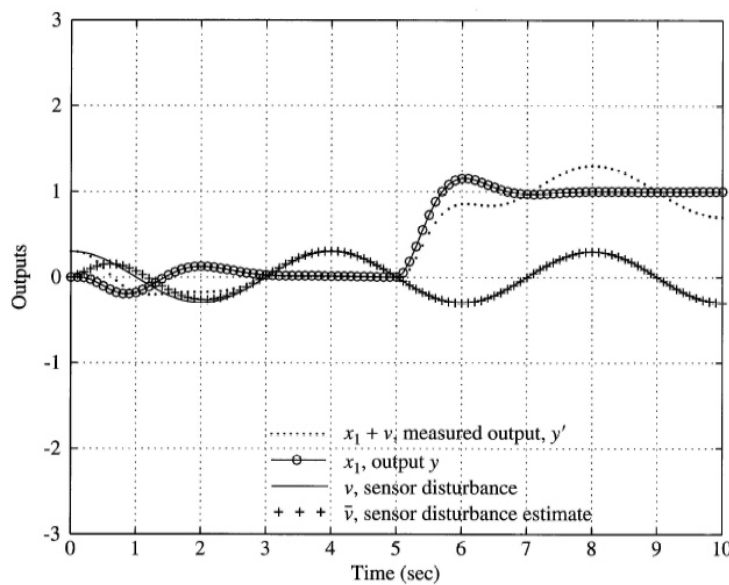


Figure 8.31
Response of
satellite to a
sinusoidal sensor
disturbance with
disturbance
rejection as in
Fig. 8.30,
Example 8.19

The time response of the system described by Fig. 8.30 is found by use of `lsim` where the state of the complete system consists of the augmented state as well as the estimate of the augmented state, an 8th order system. The estimate of \bar{v} is ignored. Figure 8.31 shows the results. Note in the figure that the estimate takes about 3 sec to converge to the correct value and that there is a noticeable error in the output due to the measurement error until that time. The step at 5 sec has no effect on the estimate quality and therefore the response to the step is precisely as it was originally designed. Without the disturbance rejection, there would have been a steady sinusoidal error of about 0.2° as the controller attempted to follow the sinusoidal measurement.

A final example of the use of the estimator to achieve zero steady state error arises when it is desirable to track a reference signal with as little error as possible and it is known that the signal follows some persistent pattern. Since it would usually take some control effort to follow such a signal, the system would normally exhibit a following error of sufficient magnitude to produce the required control effort. This following error can be eliminated if the systematic pattern can be modeled and estimated, then used in a feedforward manner to produce the desired control effort. This is called **reference following**. The idea is the same as with disturbance rejection except that the error is now not the output only but the difference between the reference and the output. The idea again is

to construct a virtual reference, ρ , at the control input which would produce the system error at the plant output, as shown in Figure 8.32(a). The feedback gain \mathbf{K} is designed using the unaugmented plant described by Φ and Γ , but the feedback signal is the system error e .

By estimating ρ and feeding that estimate into the plant with the control as shown in Fig. 8.32(a), the effect of ρ is eliminated in this virtual model and $e \equiv 0$ in steady state. The actual situation that is implemented is shown in Fig. 8.32(b) where the reference is subtracted from the output to form the error, e , and the estimate of the virtual reference, $\bar{\rho}$, is subtracted from the control. Therefore, e will behave as if ρ was canceled, so that in steady state, $e \equiv 0$, implying that y is following r .

Sinusoidal Sensor Disturbance Following of a Disk Drive

Example 8.20

A computer disk drive read head must follow tracks on the disk. Typically, there is a small offset between the center of the tracks and the rotational center of the disk, thus producing a wobble in the tracks that the read head must follow. Assume the transfer function between the input command and the read head response is

$$G(s) = \frac{1000}{s^2}$$

and the disk spins at 5000 rpm. Design a control system that follows tracks on the disk with no error even though they may be off center by some small amount. Pick the gains so that the system has a rise time better than 3 msec and no more than a 15% overshoot. Use a sample rate of 2 kHz.

Solution. The disk head system is described by

$$\mathbf{F} = \begin{bmatrix} 0 & 1 \\ 0 & 0 \end{bmatrix}, \quad \mathbf{G} = \begin{bmatrix} 0 \\ 1000 \end{bmatrix}, \quad \text{and} \quad \mathbf{H} = [1 \ 0].$$

We pretend that the disturbance is the same as in Example 8.18, that is

$$\mathbf{F}_d = \begin{bmatrix} 0 & 1 \\ -\omega_o^2 & 0 \end{bmatrix}, \quad \text{and} \quad \mathbf{H}_d = [1 \ 0]$$

where $\omega_o = 5000$ rpm or 523.6 rad/sec. The difference here compared to Example 8.18 is that the actual reference is being subtracted from the output and we wish to eliminate its effect on e . In other words, we want y to follow r in Fig. 8.32(b).

Using \mathbf{F} and \mathbf{G} with `c2d` yields Φ and Γ for the disk head dynamics. To meet the rise time and overshoot specifications, a few iterations show that poles with a natural frequency of 1000 rad/sec and a 0.6 damping ratio, converted to the digital domain, produce the desired response. The resulting feedback gain is

$$\mathbf{K} = [736.54 \ 1.0865].$$

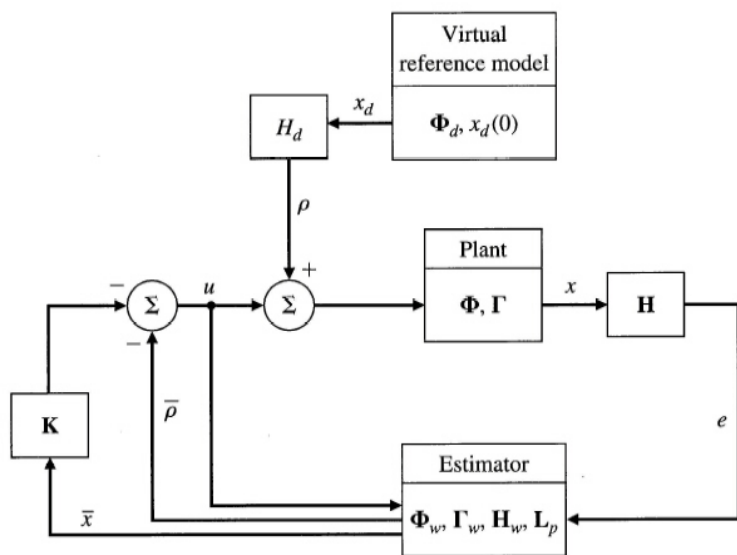
But we wish to include the virtual reference in the control as

$$u = \mathbf{K}\mathbf{x} - \rho.$$

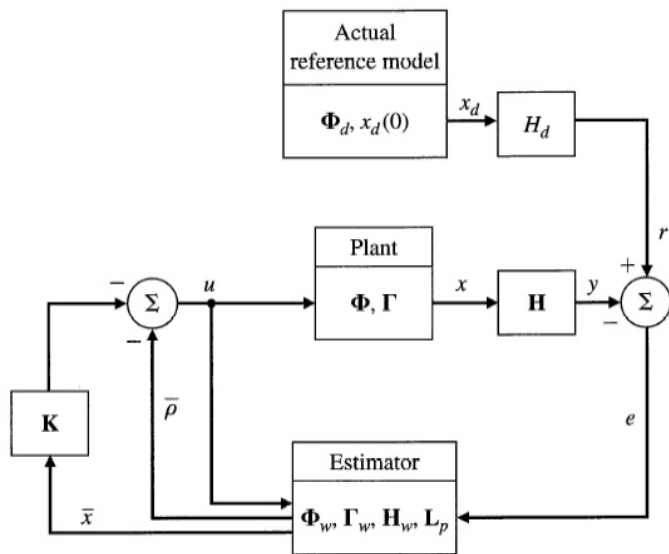
The estimator is constructed using the augmented system. A satisfactory design was found with equivalent s -plane poles that had natural frequencies of 1000 and 1200 rad/sec, both sets with $\zeta = 0.9$. Use of `acker` with Φ_w and \mathbf{H}_w results in $\mathbf{L}_p^T = [3.9 \ 1012.9 \ -2.4 \ 553.0]$.

The time response of the system described by Fig. 8.32(b) is found by use of `lsim` where the state consists of the augmented state as well as the estimate of the augmented state, an 8th order system.

The purpose of the feedforward is to provide a control that will produce $y = r$ and thus $e_{ss} \equiv 0$. Since we have an estimate of an input, $\bar{\rho}$, that will produce the track wobble which is the tracking reference, r , feedforward of $-\bar{\rho}$ causes $y = -r$. This produces the time response marked by small circles in Fig. 8.33. Note that, once $\bar{\rho}$ has converged, there is no noticeable following error.



(a)



(b)

Figure 8.32
Block diagram for sensor disturbance following:
(a) The pretend model, and
(b) the implementation model

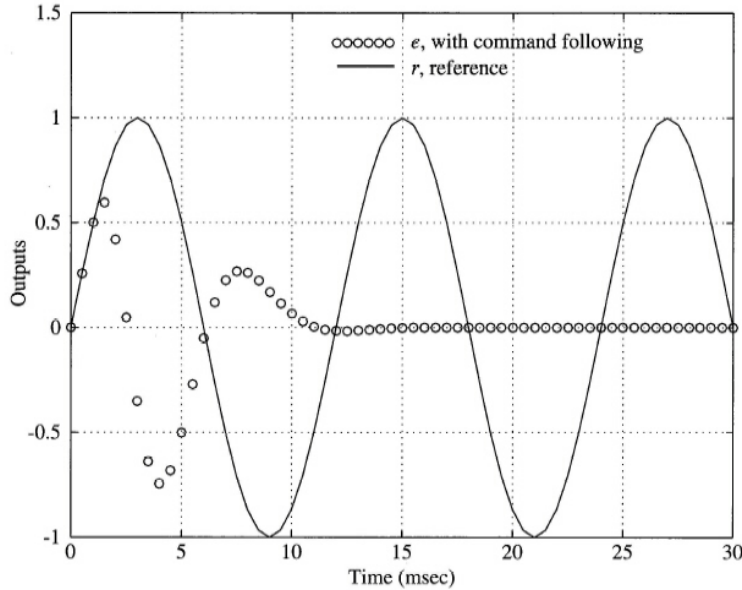


Figure 8.33
Response of disk drive to sinusoidal reference following as in Fig. 8.32, Example 8.20

8.6 Effect of Delays

Many feedback control systems have a pure time delay, λ , imbedded in some part of the loop. A one cycle delay was analyzed in Section 7.3.2 by adding a z^{-1} to the system model and using the root locus method to show that the stability of the system was decreased when no change to the compensation was made. We can also analyze the effect of delays with frequency response methods as in Section 7.4 by reducing the phase by $\omega\lambda$. This analysis easily shows that, if no changes are made to the compensation, the phase margin and hence stability will be reduced. Either design method can be used to modify the compensation so the response is improved.

For state-space design, we saw in Section 4.3.4 that, for an actuator delay, one state element must be added to the model for each cycle of delay or fraction thereof. In other words, a delay of $0 < \lambda \leq T$ will require an increase in the order of the system model by 1, a delay of $T < \lambda \leq 2T$ will increase the order by 2, and so on. Using the pole placement approach, we can assign any desired pole locations to the system. Therefore, we are able to achieve the same closed-loop poles in a system with delays as one without delays; however, there are extra poles in the system with delays. Those extra poles can slow down the response even if they are selected as fast as possible, that is, at $z = 0$. The response of the system to command inputs and disturbances is also affected by the location of the delays, that is, whether they are part of the control actuator or the sensor. Figure 8.34 shows systems with the delays in the two locations.

8.6.1 Sensor Delays

For the sensor delay, Fig. 8.34(a), an estimator can be used to reconstruct the entire state; therefore, the undelayed state is available for control. The system can be made to respond to command inputs, r , in exactly the same way that a system would respond without a sensor delay because the estimator sees the command through the feedforward of u and does not depend on the delayed output to detect it. Therefore, no estimator error is excited and the undelayed state estimate is accurate. On the other hand, a disturbance input, w , will not usually be seen by the estimator until the output, y_d , responds; therefore, the estimator error will be increased by the delay.

delay model

The model of a one cycle delay of a quantity y is

$$y_{1d}(k+1) = y(k), \tag{8.92}$$

where y_{1d} is the delayed version of y and is an additional state element that is added to the system

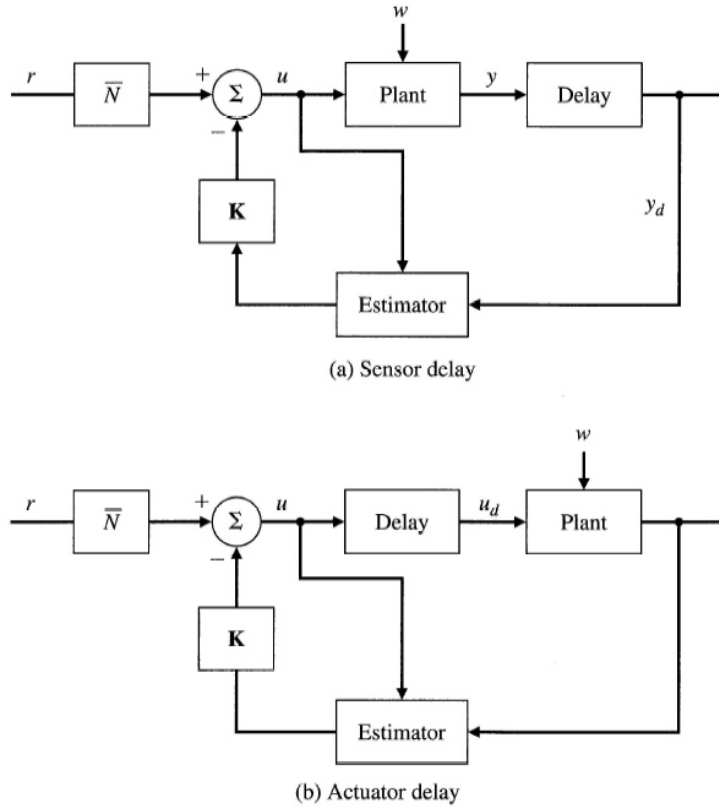


Figure 8.34
System with delays, (a) sensor delay, (b) actuator delay

model. The model for more than one cycle can be obtained by adding more similar equations and state elements. So, for two cycles of delay, we would add

$$y_{2d}(k+1) = y_{1d}(k), \tag{8.93}$$

to Eq. (8.92), where y_{2d} is one more state element and is the value of y that is delayed by two cycles. Therefore, for a system given by

$$\begin{aligned} \mathbf{x}(k+1) &= \mathbf{\Phi}\mathbf{x}(k) + \mathbf{\Gamma}u(k) \\ y(k) &= \mathbf{H}\mathbf{x}(k), \end{aligned}$$

the system model including a two-cycle sensor delay is

$$\begin{bmatrix} \mathbf{x}(k+1) \\ y_{1d}(k+1) \\ y_{2d}(k+1) \end{bmatrix} = \begin{bmatrix} \mathbf{\Phi} & \mathbf{0} & \mathbf{0} \\ \mathbf{H} & \mathbf{0} & \mathbf{0} \\ \mathbf{0} & \mathbf{1} & \mathbf{0} \end{bmatrix} \begin{bmatrix} \mathbf{x}(k) \\ y_{1d}(k) \\ y_{2d}(k) \end{bmatrix} + \begin{bmatrix} \mathbf{\Gamma} \\ \mathbf{0} \\ \mathbf{0} \end{bmatrix} u(k), \tag{8.94}$$

$$y_d(k) = \begin{bmatrix} \mathbf{0} & \mathbf{0} & \mathbf{1} \end{bmatrix} \begin{bmatrix} \mathbf{x}(k) \\ y_{1d}(k) \\ y_{2d}(k) \end{bmatrix}, \tag{8.95}$$

where y_d is the output y delayed by two cycles. Any number of cycles of delay can be achieved easily by using this scheme.

If a sensor had delay that was not an integer number of cycles, it would not influence the sampled value until the next sample instance. Therefore, sensor delays must be an integer number of samples.

Note that, due to the column of zeros, the augmented system matrix, $\mathbf{\Phi}_a$ in Eq. (8.94) will always be singular, a fact that will cause difficulties when calculating gains for a current estimator using `acker` in MATLAB.¹⁷

¹⁷We will see in Chapter 9 that a singular $\mathbf{\Phi}$ matrix will also cause difficulty with `d1qr`.

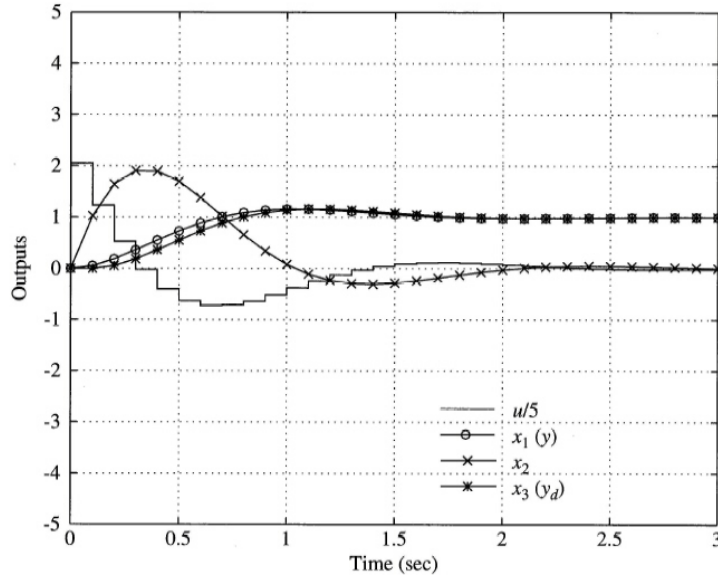


Figure 8.35
Step response for
input command
for Example 8.21

Effect of a Sensor Delay on the Satellite Attitude Response

Example 8.21

Examine the step response to a command input r of the satellite attitude control with one cycle of delay at the sensor. Place two of the control poles at $z = 0.8 \pm 0.25j$, as was the case for Examples 8.2 and 8.12, and the additional pole for the delay state at $z = 0$. Place the poles for a prediction estimator at $z = 0.4 \pm 0.4j$, as was the case for Examples 8.5 and 8.12, and the additional pole for the delay state at $z = 0$. Compare the results with Example 8.12, the same system step response without a delay.

Solution. The state-space equations for this system are (from Eqs. 8.94 and 8.95)

$$\begin{bmatrix} x_1(k+1) \\ x_2(k+1) \\ y_{1d}(k+1) \end{bmatrix} = \begin{bmatrix} 1 & T & 0 \\ 0 & 1 & 0 \\ 1 & 0 & 0 \end{bmatrix} \begin{bmatrix} x_1(k) \\ x_2(k) \\ y_{1d}(k) \end{bmatrix} + \begin{bmatrix} T^2/2 \\ T \\ 0 \end{bmatrix} u(k),$$

$$y_d(k) = \begin{bmatrix} 0 & 0 & 1 \end{bmatrix} \begin{bmatrix} x_1(k) \\ x_2(k) \\ y_{1d}(k) \end{bmatrix}.$$

Use of `acker` in MATLAB with the augmented Φ and Γ matrices as defined above with the desired control pole locations yields

$$K = [10.25 \quad 3.4875 \quad 0].$$

The first two elements are the exact same values that were obtained in Examples 8.2 and 8.12, and the zero third element means that the delayed state element is ignored. Thus the sensor delay has no effect on the controller.

Use of `acker` in MATLAB with the augmented Φ and H matrices as defined above with the desired estimator pole locations yields

$$L_p = \begin{bmatrix} 1.72 \\ 5.2 \\ 1.2 \end{bmatrix}.$$

In evaluating the step response according to Eq. (8.79), \bar{N} needs to be evaluated with the new values of N_x and N_u . In this case, Eq. (8.73) shows that

$$N_x = \begin{bmatrix} 1 \\ 0 \\ 1 \end{bmatrix}, \quad N_u = 0, \quad \text{and} \quad \bar{N} = 10.25.$$

The use of `step` with the system defined by Eq. (8.79) produces the step response shown in Fig. 8.35. It includes the output y and the delayed output y_d . Note that the response of y is precisely the same as the response

for Example 8.12 in Fig. 8.17 even though the only quantity fed back was the delayed output. This result follows because the current value of the state was estimated correctly due to the feedforward from the command input and the current value of the state was used by the controller.

It is remarkable that a system with a sensor delay can respond to a command input in precisely the same way that the undelayed system would respond. This implies that the system closed-loop transfer function was such that the pole at $z = 0$ was not excited. The ability to design such a control system is enhanced by the state-space controller/estimator approach. It is important to note, however, that if the system had a disturbance, w , that was not fed into the estimator in the feedforward path, the delayed output measurement would cause a delayed estimator response and, thus, a degraded response of the system to that disturbance.

An example of a system in common use with a sensor delay is the fuel injection control for an automobile engine. Here, the sensed value of the fuel-air ratio in the exhaust is delayed by the piston motion and the time for the exhaust stream to reach the sensor. The primary disturbance is the motion of the throttle by the driver's foot; however, this motion can be sensed and used as feedforward to the estimator. Thus the estimator structure is capable of instantaneous rejection of the throttle disturbance in spite of the significant delay of the exhaust sensor. (See Fekete, 1995.)

application to engine control

8.6.2 Actuator Delays

The model for an actuator delay is derived in Section 4.3.4. The result is Eq. (4.79), which allows for any length delay, fractional or whole cycles. The poles of a system with actuator delays can be placed arbitrarily, just like the sensor delay case, and it makes sense to add a pole at $z = 0$ for each added delay state element. However, for input commands or disturbance inputs, the extra poles at $z = 0$ will be excited and the system response will be delayed by the actuator delay. This fact can be understood by examining Fig. 8.34(b). There is no way that the input r can influence the plant without passing through the delay. A disturbance w will influence the plant without delay; however, the feedback through the estimator will be delayed before it can counteract the disturbance, thus causing an increased sensitivity to disturbances.

Effect of an Actuator Delay on an Engine Speed Governor

Example 8.22

An engine speed governor consists of an rpm sensor, usually a device that counts the time between the passage of teeth on a gear, and logic to determine the input to the fuel injector (diesel engines) or to the throttle actuator or spark advance (gasoline engines). Figure 8.36 shows the block diagram including the engine model, which is a simple first order lag with a time constant of around 3 sec so that $a = 0.3$. Fig. 8.36(a) shows the system without any delay, the ideal case. The actuator delay shown in Fig. 8.36(b) varies from engine to engine. For a gasoline engine with a throttle actuator, it is typically around a half engine cycle due to the piston motion (100 msec at 600 rpm). For diesel engines the actuator can be made to act more quickly; however, some manufacturers use injectors that have a full engine cycle delay (200 msec at 600 rpm). For this example, we will use a sample time of $T = 200$ msec and a one cycle actuator delay.

Investigate the response of the system for step input commands, r , and impulsive disturbances, w . Compare the results for control systems structured as in the three cases in Fig. 8.36. Pick the control gain so that the poles are at $z = 0.4$ for the ideal case and the estimator gain (if there is one) so that its pole is at $z = 0.2$. Select \bar{N} so that there is no steady-state error.

Solution. The step responses are shown in Fig. 8.37. For the ideal case (Fig. 8.36(a)), the gains were found to be

$$K = 9.303 \quad \text{and} \quad \bar{N} = 10.303.$$

The step response for $r = 1$ is shown in Fig. 8.37(a) and was obtained using `step`.

The model of the system with the delay in Fig. 8.36(b) can be accomplished with the aid of Eq. (4.79). For

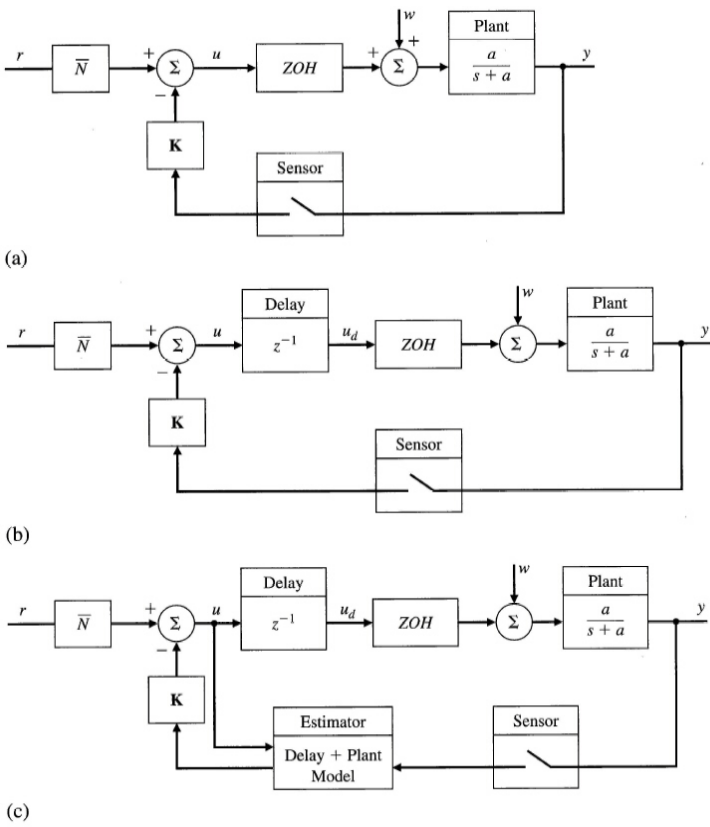


Figure 8.36 Engine speed control block diagrams, (a) the ideal feedback system without a delay and without an estimator, (b) the classical feedback with an actuator delay, (c) the estimator structure with an actuator delay

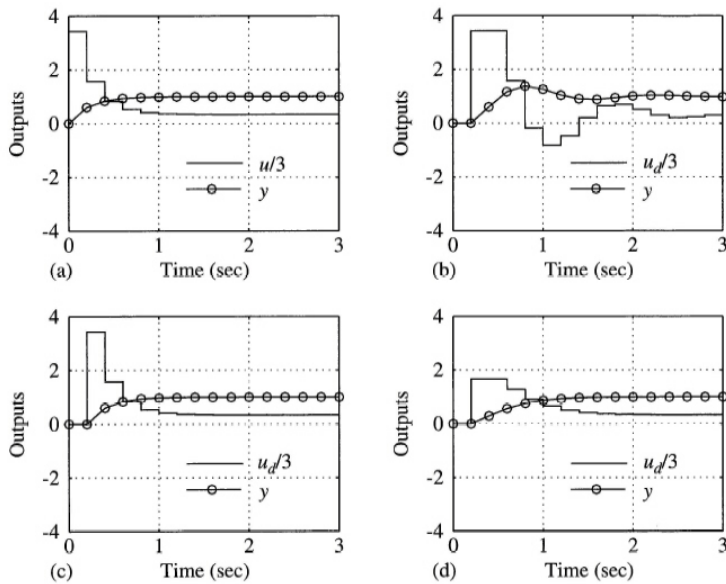


Figure 8.37 Responses to a step input, r , for Example 8.22. (a) Ideal case, no delay ($K = 9.3$), (b) classical feedback with delay ($K = 9.3$), (c) predictor estimator with delay, (d) classical feedback with delay ($K = 4.0$)

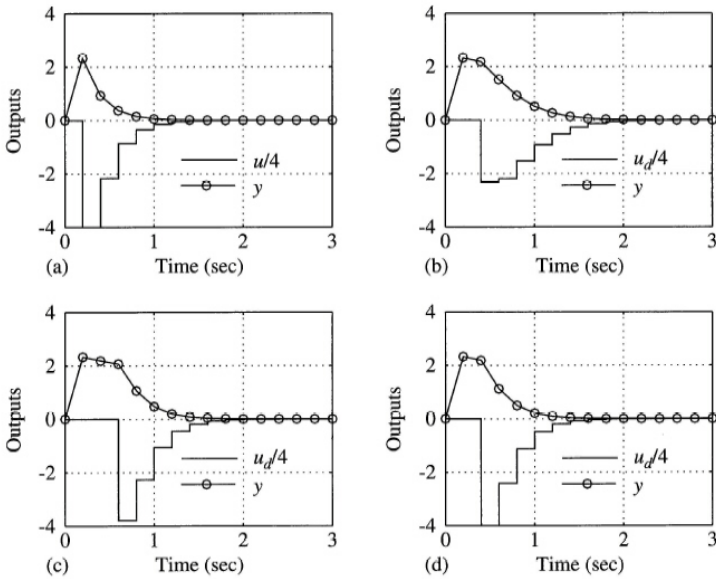


Figure 8.38
Responses to impulsive disturbance, w , for Example 8.22. (a) Ideal case, no delay ($K = 9.3$), (b) classical feedback with delay ($K = 4$), (c) predictor estimator w /delay ($K = 9.3$), (d) current estimator w /delay ($K = 9.3$)

this system it reduces to

$$\begin{bmatrix} x(k+1) \\ u_d(k+1) \end{bmatrix} = \begin{bmatrix} \Phi & \Gamma \\ 0 & 0 \end{bmatrix} \begin{bmatrix} x(k) \\ u_d(k) \end{bmatrix} + \begin{bmatrix} 0 \\ 1 \end{bmatrix} u(k) + \begin{bmatrix} \Gamma \\ 0 \end{bmatrix} w(k),$$

$$y(k) = \begin{bmatrix} 1 & 0 \end{bmatrix} \begin{bmatrix} x(k) \\ u_d(k) \end{bmatrix},$$

where Φ and Γ can be found using MATLAB's `c2d`, but can also be computed easily for this first order case to be

$$\Phi = e^{-aT} \quad \text{and} \quad \Gamma = 1 - e^{-aT}.$$

Figure 8.37(b) shows the response of this system with the classical feedback as shown in Fig. 8.36(b) using the same gains as in (a). Not only is the response delayed by a cycle, but it has become oscillatory. A z -plane analysis of this system explains why: the roots are at $z = 0.47 \pm 0.57j$, which yield an equivalent s -plane damping of $\zeta = 0.33$.

Figure 8.37(c) shows the response of the system with the estimator structure as shown in Fig. 8.36(c) using the desired control pole locations of $z = 0.4, 0$. This yielded gains of

$$K = [8.76 \quad 0.54] \quad \text{and} \quad \bar{N} = 10.303.$$

The estimator poles were placed at $z = 0.2, 0$, which yielded an estimator gain of

$$L_p = \begin{bmatrix} 0.742 \\ 0 \end{bmatrix}.$$

The response was obtained using Eq. (8.79) and is identical to the ideal case; however, it is delayed by one cycle. As previously discussed, this delay cannot be reduced if its source is due to the actuator.

The oscillatory response shown in Fig. 8.37(b) also can be eliminated by reducing the gain in the classical structure of Fig. 8.36(b), an easier solution than adding an estimator. Reducing the gain, K , from 9.3 to 4.0 produced the response in Fig. 8.37(d). While the oscillations have been removed, the response has slowed down. There is no value of gain in this simple structure that will duplicate the quality of the response obtained from the estimator system, although the difference is not large for this example.

Three of the cases were analyzed for an impulsive disturbance, w and shown in Fig. 8.38(a, b, and c). Qualitatively, the same kind of responses were obtained; however, the predictor estimator had an extra cycle of delay compared to the classical feedback system; therefore, there is little difference between the responses in Figs. 8.38(b) and 8.38(c). A current estimator formulation eliminates the extra delay and improves the response, which was obtained by evaluating Eq. (8.81) and is shown in Fig. 8.38(d).

Example 8.22 shows that an actuator delay will effect the response to a command input or a disturbance regardless of the control implementation. This is an inherent characteristic of an actuator delay for any system. However, use of an estimator including the delay minimizes its effect. Use of a current estimator provides the best response to a disturbance.

8.7 *Controllability and Observability

Controllability and observability are properties that describe structural features of a dynamic system.¹⁸ These concepts were explicitly identified and studied by Kalman (1960) and Kalman, Ho, and Narendra (1961). We will discuss only a few of the known results for linear, constant systems that have one input and one output.

We have encountered these concepts already in connection with design of control laws and estimator gains. We suggested in Section 8.1.3 that if the matrix \mathcal{C} given by

$$\mathcal{C} = [\mathbf{\Gamma}; \mathbf{\Phi}\mathbf{\Gamma}; \dots; \mathbf{\Phi}^{n-1}\mathbf{\Gamma}]$$

is nonsingular, then by a transformation of the state we can convert the given description into the control canonical form and construct a control law such that the closed-loop characteristic equation can be given arbitrary (real) coefficients. We begin our discussion of controllability by making the definition (the first of three):

I. The system $(\mathbf{\Phi}, \mathbf{\Gamma})$ is controllable if for every n th-order polynomial $\alpha_c(z)$, there exists a control law $u = -\mathbf{K}\mathbf{x}$ such that the characteristic polynomial of $\mathbf{\Phi} - \mathbf{\Gamma}\mathbf{K}$ is $\alpha_c(z)$.

And, from the results of Section 8.1.3, we have the test:

The pair $(\mathbf{\Phi}, \mathbf{\Gamma})$ is controllable if and only if the rank of $\mathcal{C} = [\mathbf{\Gamma}; \mathbf{\Phi}\mathbf{\Gamma}; \dots; \mathbf{\Phi}^{n-1}\mathbf{\Gamma}]$ is n .

The idea of pole placement that is used above to define controllability is essentially a z -transform concept. A time-domain definition is the following:

II. The system $(\mathbf{\Phi}, \mathbf{\Gamma})$ is controllable if for every \mathbf{x}_0 and \mathbf{x}_1 there is a finite N and a sequence of controls $u(0), u(1), \dots, u(N)$ such that if the system has state \mathbf{x}_0 at $k = 0$, it is forced to state \mathbf{x}_1 at $k = N$.

In this definition we are considering the direct action of the control u on the state \mathbf{x} and are not concerned explicitly with modes or characteristic equations. Let us develop a test for controllability for definition **II**. The system equations are

$$\mathbf{x}(k+1) = \mathbf{\Phi}\mathbf{x}(k) + \mathbf{\Gamma}u(k),$$

and, solving for a few steps, we find that if $\mathbf{x}(0) = \mathbf{x}_0$, then

$$\begin{aligned} \mathbf{x}(1) &= \mathbf{\Phi}\mathbf{x}_0 + \mathbf{\Gamma}u(0), \\ \mathbf{x}(2) &= \mathbf{\Phi}\mathbf{x}(1) + \mathbf{\Gamma}u(1) \\ &= \mathbf{\Phi}^2\mathbf{x}_0 + \mathbf{\Phi}\mathbf{\Gamma}u(0) + \mathbf{\Gamma}u(1), \\ &\vdots \\ \mathbf{x}(N) &= \mathbf{\Phi}^N\mathbf{x}_0 + \sum_{j=0}^{N-1} \mathbf{\Phi}^{N-1-j}\mathbf{\Gamma}u(j) \\ &= \mathbf{\Phi}^N\mathbf{x}_0 + [\mathbf{\Gamma}; \mathbf{\Phi}\mathbf{\Gamma}; \dots; \mathbf{\Phi}^{N-1}\mathbf{\Gamma}] \begin{bmatrix} u(N-1) \\ \vdots \\ u(0) \end{bmatrix}. \end{aligned}$$

¹⁸This section contains material that may be omitted without loss of continuity.

controllability
definitions

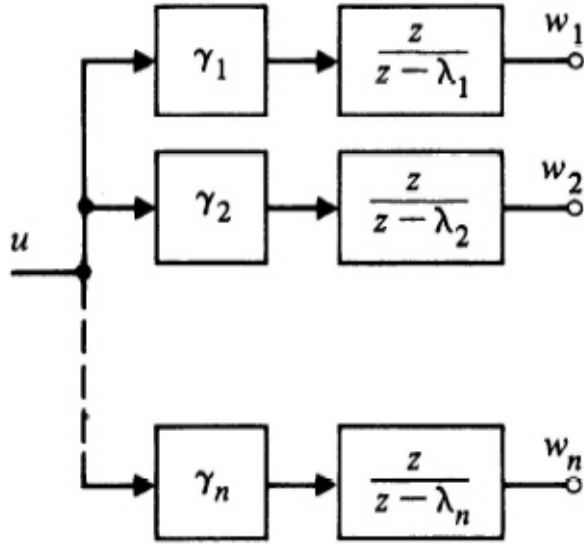


Figure 8.39
Block diagram
for a system with
a diagonal
 Φ -matrix

If $\mathbf{x}(N)$ is to equal \mathbf{x}_1 , then we must be able to solve the equations

$$[\Gamma : \Phi\Gamma : \dots : \Phi^{N-1}\Gamma] \begin{bmatrix} u(N-1) \\ u(N-2) \\ \vdots \\ u(0) \end{bmatrix} = \mathbf{x}_1 - \Phi^N \mathbf{x}_0.$$

We have assumed that the dimension of the state, and hence the number of rows of the coefficient matrix of these equations, is n ; the number of columns is N . If N is less than n , we cannot possibly find a solution for every \mathbf{x}_1 . If, on the other hand, N is greater than n , we will add a column $\Phi^n \Gamma$, and so on. But, by the Cayley-Hamilton theorem, (see Appendix C), Φ^n is a linear combination of lower powers of Φ , and the new columns add no new rank. Therefore we have a solution, and our system is controllable by definition II if and only if the rank of C is n , exactly the same condition as we found for pole assignment!

Our final definition is closest to the structural character of controllability.

III. The system (Φ, Γ) is controllable if every mode in Φ is connected to the control input.

Because of the generality of modes, we will treat only the case of systems for which Φ can be transformed to diagonal form. (The double-integrator model for the satellite does *not* qualify.) Suppose we have a diagonal Φ_λ matrix and corresponding input matrix Γ_λ with elements γ_i . Then the structure is as shown in Fig. 8.39. By the definition, the input must be connected to each mode so that no γ_i is zero. However, this is not enough if the roots λ_i are not distinct. Suppose, for instance, $\lambda_1 = \lambda_2$. Then the equations in the first two states are

$$\begin{aligned} w_1(k+1) &= \lambda_1 w_1(k) + \gamma_1 u, \\ w_2(k+1) &= \lambda_1 w_2(k) + \gamma_2 u. \end{aligned}$$

If we now define $\xi = \gamma_2 w_1 - \gamma_1 w_2$, the equation in ξ is

$$\gamma_2 w_1(k+1) - \gamma_1 w_2(k+1) = \lambda_1 \gamma_2 w_1(k) - \lambda_1 \gamma_1 w_2(k) + \gamma_1 \gamma_2 u - \gamma_1 \gamma_2 u,$$

which is the same as

$$\xi(k+1) = \lambda_1 \xi(k).$$

The point is that if two characteristic roots are equal in a diagonal Φ_λ system with only one input, we effectively have a hidden mode that is not connected to the control, and the system is not controllable. Therefore, even in this simple case, we have two conditions for controllability:

1. All characteristic values of Φ_λ are distinct, and
2. No element of Γ_λ is zero.

Now let us consider the controllability matrix of this diagonal system. By direct computation, we obtain

$$\begin{aligned} \mathcal{C} &= \begin{bmatrix} \gamma_1 & \gamma_1 \lambda_1 & \gamma_1 \lambda_1^{n-1} \\ \vdots & \gamma_2 \lambda_2 & \cdots & \vdots \\ \gamma_n & \gamma_n \lambda_n & \gamma_n \lambda_n^{n-1} \end{bmatrix} \\ &= \begin{bmatrix} \gamma_1 & 0 & 0 \\ 0 & \gamma_2 & \\ & \ddots & \\ 0 & +\gamma_n & \end{bmatrix} \begin{bmatrix} 1 & \lambda_1 & \lambda_1^2 & \cdots & \lambda_1^{n-1} \\ 1 & \lambda_2 & \lambda_2^2 & & \\ \vdots & \vdots & \vdots & \vdots & \\ 1 & \lambda_n & \lambda_n^2 & \cdots & \lambda_n^{n-1} \end{bmatrix}. \end{aligned}$$

The controllability matrix is a product of two terms, and \mathcal{C} is nonsingular if and only if each factor is nonsingular. The first term has a determinant that is the product of the γ_i , and the second term is nonsingular if and only if the λ_i are distinct! So once again we find that our definition of controllability leads to the same test: The matrix \mathcal{C} must be nonsingular. If \mathcal{C} is nonsingular, then we can assign the system poles by state feedback, we can drive the state to any part of the space in finite time, and we know that every mode is connected to the input.¹⁹

As our final remark on the topic of controllability we present a test that is an alternative to testing the rank (or determinant) of \mathcal{C} . This is the Rosenbrock-Hautus-Popov (RHP) test [see Rosenbrock (1970), Kailath (1979)]. The system (Φ, Γ) is controllable if the system of equations

$$\mathbf{v}'[z\mathbf{I} - \Phi : \Gamma] = \mathbf{0}'$$

has only the trivial solution $\mathbf{v}' = \mathbf{0}'$, or, equivalently

$$\text{rank}[z\mathbf{I} - \Phi : \Gamma] = n,$$

or there is *no* nonzero \mathbf{v}' such that

$$(i) \quad \mathbf{v}'\Phi = z\mathbf{v}', \quad (ii) \quad \mathbf{v}'\Gamma = 0.$$

This test is equivalent to the rank-of- \mathcal{C} test. It is easy to show that if such a \mathbf{v} exists, then \mathcal{C} is singular. For if a nonzero \mathbf{v} exists such that $\mathbf{v}'\Gamma = 0$ by (i), then, multiplying (i) by Γ on the right, we find

$$\mathbf{v}'\Phi\Gamma = z\mathbf{v}'\Gamma = 0.$$

Then, multiplying by $\Phi\Gamma$, we find

$$\mathbf{v}'\Phi^2\Gamma = z\mathbf{v}'\Phi\Gamma = 0,$$

and so on. Thus we derive $\mathbf{v}'\mathcal{C} = \mathbf{0}'$ has a nontrivial solution, \mathcal{C} is singular, and the system is not controllable. To show that a nontrivial \mathbf{v}' exists if \mathcal{C} is singular requires a bit more work and is omitted. See Kailath (1979).

We have given two pictures of an uncontrollable system. Either the input is not connected to a dynamic part physically or else two parallel parts have identical characteristic roots. The engineer should be aware of the existence of a third simple situation, illustrated in Fig. 8.40. Here the problem is that the mode at $z = \frac{1}{2}$ appears to be connected to the input but is masked by the zero in the

¹⁹Of course, we showed this only for Φ that can be made diagonal. The result is true for general Φ .

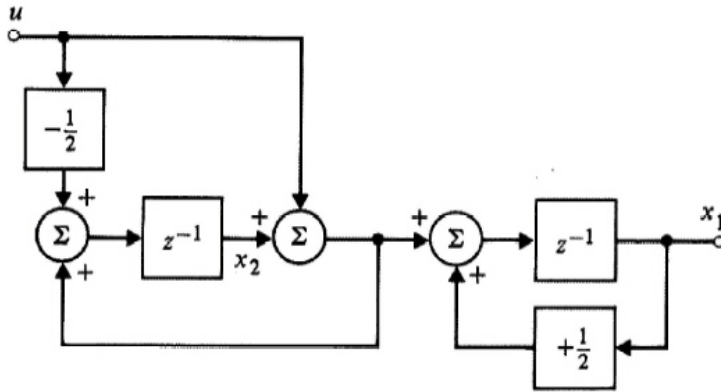


Figure 8.40
Block diagram of a simple uncontrollable system

preceding member; the result is an uncontrollable system. First we will confirm this allegation by computing the determinant of the controllability matrix. The system matrices are

$$\Phi = \begin{bmatrix} +\frac{1}{2} & 1 \\ 0 & 1 \end{bmatrix}, \quad \Gamma = \begin{bmatrix} 1 \\ \frac{1}{2} \end{bmatrix},$$

and

$$\mathcal{C} = [\Gamma \quad \Phi\Gamma] = \begin{bmatrix} 1 & 1 \\ \frac{1}{2} & \frac{1}{2} \end{bmatrix},$$

which is clearly singular. If we compute the transfer function from u to x_1 , we find

$$H(z) = \frac{z - \frac{1}{2}}{z - 1} \frac{1}{z - \frac{1}{2}} \tag{8.96}$$

$$= \frac{1}{z - 1}. \tag{8.97}$$

Because the natural mode at $z = \frac{1}{2}$ disappears, it is not connected to the input. Finally, if we consider the RHP test,

$$[z\mathbf{I} - \Phi \quad \Gamma] = \begin{bmatrix} z - \frac{1}{2} & -1 & 1 \\ 0 & z - 1 & \frac{1}{2} \end{bmatrix},$$

and let $z = \frac{1}{2}$, then we must test the rank of

$$\begin{bmatrix} 0 & -1 & 1 \\ 0 & -\frac{1}{2} & \frac{1}{2} \end{bmatrix},$$

which is clearly less than two, which means, again, uncontrollable. In conclusion, we have three definitions of controllability: pole assignment, state reachability, and mode coupling to the input. The definitions are equivalent, and the tests for any of these properties are found in the rank of the controllability matrix or in the rank of the input system matrix $[z\mathbf{I} - \Phi \quad \Gamma]$.

We have thus far discussed only controllability. The concept of observability is parallel to that of controllability, and most of the results thus far discussed can be transferred to statements about observability by the simple expedient of substituting the transposes Φ^T for Φ and \mathbf{H}^T for Γ . The result of these substitutions is a “dual” system. We have already seen an application of duality when we noticed that the conditions for the ability to select an observer gain \mathbf{L} to give the state-error dynamics an arbitrary characteristic equation were that (Φ^T, \mathbf{H}^T) must be controllable—and we were able to use the same Ackermann formula for estimator gain that we used for control gain. The other properties that are dual to controllability are

observability
observability
definitions

- OI.** The system (Φ, \mathbf{H}) is observable if for any n th-order polynomial $\alpha_e(z)$, there exists an estimator gain \mathbf{L} such that the characteristic equation of the state error of the estimator is $\alpha_e(z)$.
- OII.** The system (Φ, \mathbf{H}) is observable if for any $\mathbf{x}(0)$, there is a finite N such that $\mathbf{x}(0)$ can be computed from observation of $y(0), y(1), \dots, y(N-1)$.
- OIII.** The system (Φ, \mathbf{H}) is observable if every dynamic mode in Φ is connected to the output y via \mathbf{H} .

We will consider the development of a test for observability according to definition **OII**. The system is described by²⁰

$$\begin{aligned}\mathbf{x}(k+1) &= \Phi \mathbf{x}(k), & \mathbf{x}(0) &= \mathbf{x}_0, \\ y(k) &= \mathbf{H} \mathbf{x}(k);\end{aligned}$$

and successive outputs from $k = 0$ are

$$\begin{aligned}y(0) &= \mathbf{H} \mathbf{x}_0, \\ y(1) &= \mathbf{H} \mathbf{x}(1) = \mathbf{H} \Phi \mathbf{x}_0, \\ y(2) &= \mathbf{H} \mathbf{x}(2) = \mathbf{H} \Phi \mathbf{x}(1) = \mathbf{H} \Phi^2 \mathbf{x}_0, \\ &\vdots \\ y(N-1) &= \mathbf{H} \Phi^{N-1} \mathbf{x}_0.\end{aligned}$$

In matrix form, these equations are

$$\begin{bmatrix} y(0) \\ \vdots \\ y(N-1) \end{bmatrix} = \begin{bmatrix} \mathbf{H} \\ \mathbf{H} \Phi \\ \vdots \\ \mathbf{H} \Phi^{N-1} \end{bmatrix} \mathbf{x}_0.$$

As we saw in the discussion of state controllability, new rows in these equations cannot be independent of previous rows if $N > n$ because of the Cayley-Hamilton theorem. Thus the test for observability is that the matrix

$$\mathcal{O} = \begin{bmatrix} \mathbf{H} \\ \mathbf{H} \Phi \\ \vdots \\ \mathbf{H} \Phi^{n-1} \end{bmatrix}$$

must be nonsingular. If we take the transpose of \mathcal{O} and let $\mathbf{H}^T = \mathbf{\Gamma}$ and $\Phi^T = \Phi$, then we find the controllability matrix of $(\Phi, \mathbf{\Gamma})$, another manifestation of duality.

8.8 Summary

- For any controllable system $(\Phi, \mathbf{\Gamma})$ of order n , there exists a discrete full state feedback control law (\mathbf{K}) that will place the n closed-loop poles at arbitrary locations. `acker.m` or `place.m` using $\Phi, \mathbf{\Gamma}$ perform this function.
- $\mathcal{C} = [\mathbf{\Gamma} \quad \Phi \mathbf{\Gamma} \dots]$, the **controllability matrix**, must be of rank n , the order of the system, for the system to be controllable. `ctrb.m` performs this calculation.
- The general rule in selecting the desired pole locations is to move existing open-loop poles as little as possible in order to meet the system specifications.

²⁰Clearly the input is irrelevant here *if* we assume that all values of $u(k)$ are available in the computation of \mathbf{x}_0 . If some inputs, such as a disturbance w , are not available, we have a very different problem.

- For any observable system (Φ, \mathbf{H}) of order n , there exists a discrete estimator with gain \mathbf{L} that will place the n estimator error equation poles at arbitrary locations. `acker.m` or `place.m` using Φ^T, \mathbf{H}^T calculates \mathbf{L} .
- $\mathcal{O} = [\mathbf{H} \ \mathbf{H}\Phi \ \dots]$, the **observability matrix**, must be of rank n , the order of the system, for the system to be observable. `obsv.m` performs this calculation.
- Feedback via \mathbf{K} using the estimated state elements results in system poles that consist of the n control poles plus the n estimator poles.
- Estimator poles are usually selected to be approximately twice as fast as the controller poles in order for the response to be dominated by the control design. However, in order to smooth the effects of measurement noise, it is sometimes useful to select estimator poles as slow or slower than the control poles.
- Calculation of \mathbf{N}_x and N_u via `refi.m` and their usage with the structure in Figs. 8.15 or 8.16, the **state command structure**, provides the best response to command inputs.
- **Integral control** is achieved by implementing the desired error integral and including this as part of an augmented plant model in calculating \mathbf{K} . The estimator is based on the non-augmented model. Integral control eliminates steady state errors due to command inputs and input disturbances.
- Disturbance estimation is accomplished by augmenting the model used in the estimator to include the unknown disturbance as a state element. The disturbance could be an unknown constant or a sinusoid with unknown magnitude and phase. The disturbance estimate can then be used in the control law to reject its effect, called **disturbance rejection** or to cause the system to track the disturbance with no error, called **disturbance following**.
- Delays in the actuator or sensor can be modeled in the estimator so that no estimation errors occur. **Sensor delays** will cause a delay in the response to a disturbance but there need not be any delay in the response to command inputs. However, **actuator delays** will cause a delayed response from command inputs and disturbances.

8.9 Problems

8.1 For the open-loop system

$$G(s) = \frac{y(s)}{u(s)} = \frac{1}{s^2 + 0.2s + 1},$$

- Find the discrete state-space representation assuming there is a ZOH and the sample period $T = 0.5$ sec.
- Find the full state digital feedback that provides equivalent s -plane poles at $\omega_n = 2$ rad/sec with $\zeta = 0.5$.
- Examine the response of the closed-loop system to an initial value of y and verify that the response is consistent with the desired poles.

8.2 For the open-loop system

$$\Phi = \begin{bmatrix} 1 & 1 \\ 0 & 1 \end{bmatrix}, \quad \Gamma = \begin{bmatrix} \frac{1}{2} \\ 1 \end{bmatrix},$$

compute \mathbf{K} by hand so that the poles of the closed-loop system with full state feedback are at $z = 0.9 \pm j0.1$.

8.3 For the open-loop system

$$G(s) = \frac{y(s)}{u(s)} = \frac{1}{s^2(s+2)},$$

- (a) Find the discrete state-space model, assuming there is a ZOH and the sample rate is $T = 100$ msec.
- (b) Pick poles so that the settling time $t_s < 1$ sec and find the \mathbf{K} that will produce those poles with full state feedback.
- (c) Verify that t_s is satisfied by plotting the response to an initial value of y .

8.4 For the system in Problem 8.2, find the estimator equations and the value of the gain \mathbf{L} by hand so that $z_{\text{des}} = 0.6 \pm j0.3$ for

- (a) a predictor estimator,
- (b) a current estimator, and
- (c) a reduced-order estimator ($z_{\text{des}} = 0.6$).

8.5 For the system in Problem 8.3,

- (a) Find the predictor estimator equations and the value of the gain \mathbf{L}_p so that the estimator $t_s < 0.5$ sec.
- (b) Verify that t_s is satisfied by plotting the response of $\tilde{x}_1 (= \tilde{y})$ to an initial value.

8.6 For the open-loop system

$$G(s) = \frac{y(s)}{u(s)} = \frac{1}{s^2}$$

preceded by a ZOH and a sample rate of 20 Hz,

- (a) Find the feedback gain \mathbf{K} so that the control poles have an equivalent s -plane $\omega_n = 10$ rad/sec and $\zeta = 0.7$.
 - (b) Find the estimator gain \mathbf{L}_p so that the estimator poles have an equivalent s -plane $\omega_n = 20$ rad/sec and $\zeta = 0.7$.
 - (c) Determine the discrete transfer function of the compensation.
 - (d) Design a lead compensation using transform techniques so that the equivalent s -plane natural frequency $\omega_n \cong 10$ rad/sec and $\zeta \cong 0.7$. Use either root locus or frequency response.
 - (e) Compare the compensation transfer functions from (c) and (d) and discuss the differences.
- 8.7 For the system in Problem 8.6, design the controller and estimator so that the closed-loop unit step response to a command input has a rise time $t_r < 200$ msec and an overshoot $M_p < 15\%$ when using:
- (a) the state command structure,
 - (b) the output error command structure.

For both cases, check that the specifications are met by plotting the step response.

8.8 For the open-loop system

$$G(s) = \frac{y(s)}{u(s)} = \frac{1}{s^2(s^2 + 400)},$$

design the controller and estimator so that the closed-loop unit step response to a command input has a rise time $t_r < 200$ msec and an overshoot $M_p < 15\%$ when using the state command structure. Check that the specifications are met by plotting the step response.

8.9 Compute $G(z)$ from Eq. (4.64) for

$$\Phi = \begin{bmatrix} -a_1 & -a_2 & -a_3 \\ 1 & 0 & 0 \\ 0 & 1 & 0 \end{bmatrix}, \quad \Gamma = \begin{bmatrix} 1 \\ 0 \\ 0 \end{bmatrix}, \quad \mathbf{H} = [b_1 \quad b_2 \quad b_3].$$

Why is this form for Φ and Γ called control canonical form?

8.10 (a) For

$$\Phi = \begin{bmatrix} 1 & T \\ 0 & 1 \end{bmatrix}, \quad \Gamma = \begin{bmatrix} T^2/2 \\ T \end{bmatrix},$$

find a transform matrix \mathbf{T} so that if $\mathbf{x} = \mathbf{T}\mathbf{w}$, then the equations in \mathbf{w} will be in control canonical form.

(b) Compute \mathbf{K}_w , the gain, such that if $u = -\mathbf{K}_w\mathbf{w}$, the characteristic equation will be $\alpha_c(z) = z^2 - 1.6z + 0.7$.

(c) Use \mathbf{T} from part (a) to compute \mathbf{K}_x , the gain in the \mathbf{x} -states.

8.11 (a) Show that the equations for the current estimator can be written in standard state form

$$\xi_{k+1} = \mathbf{A}\xi_k + \mathbf{B}y_k, \quad u = \mathbf{C}\xi_k + D y_k,$$

where $\xi_k = \hat{\mathbf{x}}_k - \mathbf{L}_c y_k$, $\mathbf{A} = (\mathbf{I} - \mathbf{L}_c \mathbf{H})(\Phi - \Gamma \mathbf{K})$, $\mathbf{B} = \mathbf{A} \mathbf{L}_c$, $\mathbf{C} = -\mathbf{K}$, and $D = -\mathbf{K} \mathbf{L}_c$.

(b) Use the results of Eq. (4.65) to show that the controller based on a current estimator always has a zero at $z = 0$ for any choice of control law \mathbf{K} or estimator law \mathbf{L}_c .

8.12 For the open-loop system

$$\Phi = \begin{bmatrix} 1 & 1 \\ 0 & 1 \end{bmatrix}, \quad \Gamma = \begin{bmatrix} \frac{1}{2} \\ 1 \end{bmatrix},$$

check the observability for:

(a) $\mathbf{H} = [0 \quad 1]$.

(b) $\mathbf{H} = [1 \quad 0]$.

(c) Rationalize your results to (a) and (b), stating why the observability or lack of it occurred.

8.13 Design the antenna in Appendix A.2 by state-variable pole assignment.

(a) Write the equations in state form with $x_1 = y$ and $x_2 = \dot{y}$. Give the matrices \mathbf{F} , \mathbf{G} , and \mathbf{H} . Let $a = 0.1$.

(b) Let $T = 1$ and design \mathbf{K} for equivalent poles at $s = -1/2 \pm j(\sqrt{3}/2)$. Plot the step response of the resulting design.

(c) Design a prediction estimator with \mathbf{L}_p selected so that $\alpha_e(z) = z^2$; that is, both poles are at the origin.

(d) Use the estimated states for computing the control and introduce the reference input so as to leave the state estimate undisturbed. Plot the unit step response from this reference input and from a wind gust (step) disturbance that acts on the antenna just like the control force (but not on the estimator).

(e) Plot the root locus of the closed-loop system with respect to the plant gain and mark the locations of the closed-loop poles.

8.14 In Problem 7.8 we described an experiment in magnetic levitation described by the equations

$$\ddot{x} = 1000x + 20u.$$

Let the sampling time, T , be 10 msec.

- Use pole placement to design this system to meet the specifications that settling time is less than 0.25 sec and overshoot to an initial offset in x is less than 20%.
- Design a reduced-order estimator for \dot{x} for this system such that the error-settling time will be less than 0.08 sec.
- Plot step responses of x, \dot{x} , and u for an initial x displacement.
- Plot the root locus for changes in the plant gain and mark the design pole locations.
- Introduce a command reference with feedforward so that the estimate of \dot{x} is not forced by r . Measure or compute the frequency response from r to system error $r - x$ and give the highest frequency for which the error amplitude is less than 20% of the command amplitude.

8.15 Derive Eq. (8.63) from Eq. (8.57).

8.16 For the open-loop system

$$G(z) = \frac{y(z)}{u(z)} = \frac{y(z)}{w(z)} = \frac{0.1185(z+0.9669)}{z^2 - 1.6718z + 0.9048},$$

- Find the control feedback \mathbf{K} and estimator gain \mathbf{L}_p that will place control poles at $z = 0.8 \pm j0.2$ and estimator poles at $z = 0.6 \pm j0.3$.
- Plot the response of $y(k)$ for a unit step input (r) command using the state command structure. Would there be a steady-state error if $N_u = 0$? (See Fig. 8.16(a).)
- Determine what the steady state value of $y(k)$ would be if there was an input disturbance, w .
- Determine an integral control gain and show the system block diagram with the integral control term included. Set the extra control pole at $z = 0.9$.
- Demonstrate that the system will have no steady state error for a disturbance, w , or an input command, u , even when $N_u = 0$.

8.17 For the open-loop system

$$\Phi = \begin{bmatrix} 0.8815 & 0.4562 \\ -0.4562 & 0.7903 \end{bmatrix}, \quad \Gamma = \Gamma_1 = \begin{bmatrix} 0.1185 \\ 0.4562 \end{bmatrix}, \quad \mathbf{H} = [1 \quad 0],$$

- Find the control feedback \mathbf{K} and estimator gain \mathbf{L}_p that will place control poles at $z = 0.6 \pm j0.3$ and estimator poles at $z = 0.3 \pm j0.3$.
- Plot the response of $y(k)$ for a unit step of the disturbance (w).
- Determine an integral control gain and show the system block diagram with the integral control term included. Set the extra control pole at $z = 0.9$.
- Demonstrate that the system will have no steady-state error for a disturbance, w .

8.18 For the open-loop system from Problem 8.17

- Assuming w takes on some unknown but constant value, construct an estimator that includes an estimate of that disturbance. Place poles of the system as in Problem 8.17, except place the extra estimator pole at $z = 0.9$. Determine values of \mathbf{K} and \mathbf{L}_p and sketch the block diagram showing how the various quantities are used in the control. Include the command input r in the diagram using the state command structure.
- Plot the response of y and \bar{w} to a unit step in w with $r \equiv 0$. State whether the responses meet your expectations.
- Plot the response of y and \bar{w} to a unit step in r with $w \equiv 0$. State whether the responses meet your expectations.

8.19 A disk drive read head²¹ has the open-loop transfer function

$$G(s) = \frac{y(s)}{u(s)} = \frac{y(s)}{w(s)} = \frac{1000\omega_r^2}{s^2(s^2 + 2\zeta_r\omega_r s + \omega_r^2)}$$

where $\omega_r = 6000$ rad/sec and $\zeta_r = 0.02$.

- Design a digital compensation so that there is no steady state error to an input command nor to a constant disturbance w . The plant gain of 1000 is not known precisely, so it is not acceptable to assume the steady state error due to input commands can be eliminated via feedforward with an N_u term. The specifications are that the rise time t_r must be less than 2 msec and the overshoot $M_p < 10\%$. Use a sample rate of 3 kHz.
- The disk spins at 3000 rpm. There is typically a small offset between the center of the circular tracks on the disk and the center of rotation, thus producing a wobble in the location of the tracks that should be followed by the read head. Determine the track following error due to this wobble. Express the answer as a percentage of the wobble magnitude.
- Embellish your design from (a) so that the error due to the wobble is eliminated as best you can. Plot the frequency response of the tracking error (e in Fig. 8.32) where the input to the system is the track wobble. Mark the frequency that represents the spin rpm.

8.20 A pendulum with a torquer at its hinge is described by

$$\begin{bmatrix} \dot{x}_1 \\ \dot{x}_2 \end{bmatrix} = \begin{bmatrix} 0 & 1 \\ -1 & 0 \end{bmatrix} \begin{bmatrix} x_1 \\ x_2 \end{bmatrix} + \begin{bmatrix} 0 \\ 1 \end{bmatrix} u + \begin{bmatrix} 0 \\ 1 \end{bmatrix} w,$$

$$y = [1 \quad 0] \begin{bmatrix} x_1 \\ x_2 \end{bmatrix} + b$$

where $\mathbf{x}^T = [\theta \quad \dot{\theta}]$, θ = angle of the pendulum from vertical, u = torque, w = torque bias, and b = measurement bias. Answer the questions below assuming the output is sampled with $T = 100$ msec and the control ($u + w$) is applied through a ZOH.

- With no torque bias ($w = 0$), augment the system model so that the measurement bias is a state element. Is this system observable?
 - With no measurement bias ($b = 0$), augment the system model so that the torque bias is a state element. Is this system observable?
 - Augment the system model so that both biases are state elements. Is this system observable?
- 8.21 Design a controller (control plus estimator) for the same system as in Example 8.12, except add a delay of two sample periods between the system output and when the measurement is available to the computer.
- Compute \mathbf{K} for $z_{\text{des}} = 0.8 \pm j0.25, 0, 0$.
 - Is the system observable? Check for predictor and current estimators.
 - Compute \mathbf{L}_p with $z_{\text{des}} = 0.4 \pm j0.4, 0, 0$.
 - Compute \mathbf{L}_c with z_{des} as in part (c) and with $z_{\text{des}} = 0.4 \pm j0.4, 0.1, 0$.
 - Plot the unit step response to an input command using the predictor estimator showing the plant output as well as the delayed sensor output.

8.22 Determine the state-command input structure for a feedback system with the Type 0 plant

$$G(s) = \frac{10}{s^2 + 0.18s + 9}$$

²¹See Franklin, Powell, and Emami (1994), Example 2.4.

- (a) Convert the system to discrete state-space form with $T = 0.1$ sec.
- (b) Find \mathbf{K} to obtain equivalent s -plane control poles at $\zeta = 0.5$ and $\omega_n = 4$ rad/sec.
- (c) Find \mathbf{L}_p to obtain equivalent s -plane estimator poles at $\zeta = 0.5$ and $\omega_n = 8$ rad/sec.
- (d) Determine N_u and \mathbf{N}_x , then sketch a block diagram specifying the controller equations including the reference input.
- (e) Do you expect there will be a steady-state error for this system for a step input?
- (f) Plot the step response and confirm your answer to (e).

8.23 Repeat the design of the controller (control and estimator) for Examples 8.4 and 8.8, but place all four desired poles at $z = 0$. (This is often referred to as a *finite settling time* or *deadbeat* design because the system will settle in a finite number of sample periods.)

- (a) Using your \mathbf{K} and \mathbf{L}_p , determine the time response of the system to a unit-step input using the state-command input structure.
- (b) Determine the compensation in transfer function form, $D_p(z)$, and construct a root locus vs. the dc gain of $D_p(z)$. Mark the roots where the gain corresponds to the values computed for \mathbf{K} and \mathbf{L}_p .

8.24 The double mass–spring device described in Appendix A.4 is representative of many devices that have some structural resonances. Placing the sensor so that it measures y is called the *colocated* case, whereas placing it so that it measures d is called the *noncolocated* case. Often, the designer is not aware initially that a resonance exists in the system, a situation that is addressed by this problem.

For $M = 20$ kg, $m = 1$ kg, $k = 25$ N/m, and $b = 0.2$ N-sec/m, we obtain a resonance frequency of 5 rad/sec with a damping ratio, $\zeta = 0.02$.

- (a) To represent the case where the designer did not know about the resonance, assume the coupling is rigid, that is, k is infinite. The transfer function is then

$$G_1(s) = \frac{d(s)}{u(s)} = \frac{y(s)}{u(s)} = \frac{1}{(m+M)s^2}.$$

Design a digital controller (\mathbf{K} and \mathbf{L}_p) with $T = 200$ msec, control poles at $z = 0.75 \pm j0.2$, and estimator poles at $z = 0.3 \pm j0.3$. Verify by simulation that it provides a response to a unit-step command using the state-command input structure that is consistent with the selected poles.

- (b) Use the controller (\mathbf{K} and \mathbf{L}_p) obtained in part (a) in a simulation of the system where the infinite spring is replaced with the flexible one and the output is d , that is, a fourth-order plant with second-order controller. Examine the response and compare it qualitatively with an analysis of the closed-loop roots of this combined system.
- (c) Repeat part (b), but replace the plant output, d , with y .
- (d) Analyze where the roots of the system would be if you measured y and \dot{y} directly (no estimator) and fed them back using your \mathbf{K} from part (a).
- (e) Design a fourth-order controller with control poles at $z = 0.75 \pm j0.2, 0.4 \pm j0.6$, and estimator poles at $z = 0.3 \pm j0.3, 0 \pm j0.4$ with d as the measurement. Again, verify by simulation that it provides the correct response to a unit-step command using the state-command input structure.
- (f) Plot the frequency response of the compensation (control plus estimator) from part (e). State why you think this kind of compensation is usually referred to as a *notch filter*.
- (g) Plot the z -plane root locus of the system (plant plus controller) and comment on the sensitivity of this design to changes in the overall loop gain.

8.25 A heat exchanger²² has the transfer function

$$G(s) = \frac{e^{-5s}}{(10s + 1)(60s + 1)}.$$

where the delay is due to the sensor.

- (a) Write state equations for this system.
- (b) Compute the zero-order-hold model with a sample period of 5 sec.
- (c) Design the compensation including the command input with the control poles at $0.8 \pm j0.25$ and the estimator poles at $0.4 \pm j0.4, 0$.
- (d) Compute the step response to a reference input step and to a disturbance input at the control. Verify that there is no delay for the command input.

²²See Franklin, Powell, and Emami-Naeini (2019), Example 2.18.

Chapter 9

Multivariable and Optimal Control

A Perspective on Multivariable and Optimal Control

The control-design procedures described in Chapters 7 and 8 were applied to systems with a single input and single output (SISO). The transfer-function approach in Chapter 7 is best suited to SISO systems; the state-space methods of Chapter 8 were limited to SISO in order to simplify the procedures. In fact, if we try to apply the pole-placement approach of Chapter 8 to a multivariable (multi-input, multi-output, or MIMO) system, we find that the gains, \mathbf{K} or \mathbf{L} , are not uniquely determined by the resulting equations. Therefore, a design approach is required which intelligently uses this extra freedom for MIMO systems. In addition, we saw in Example 8.3 that the selection of desired pole locations for SISO systems can be tricky business. Some sort of systematic guidance for the selection of control and estimator pole locations seems highly desirable. The material in this chapter provides a tool that meets both these needs.

The subject of this chapter is the use of optimal control techniques as a tool in the design of control systems. It is important that the designer have no illusions that some true “optimal” design is being achieved; rather, the idea is to transfer the designer’s iteration on pole locations as used in Chapter 8, or compensation parameters as used in Chapter 7, to iterations on elements in a cost function, \mathcal{J} . The method will determine the control law that minimizes \mathcal{J} , but because the parameters in \mathcal{J} are arbitrarily selected, the design is at best only partially optimal. However, these designs will achieve some compromise between the use of control effort and the speed of response and will guarantee a stable system, no small feat. Therefore, each iteration on the parameters in \mathcal{J} produces a candidate design that should be evaluated in the light of the design specifications.

Chapter Overview

The chapter starts out in Section 9.1 by discussing some of the steps that might be taken in order to convert a MIMO system into a SISO one. Although this cannot always be done, it can help to clarify the key control issues in a complex system so that the later optimization of the whole system will be better understood. Section 9.2 derives the time-varying optimal control solution that results directly from the optimal control problem statement. Section 9.3 shows how to find the steady-state value of the optimal feedback gain that is significantly easier to implement and is the one typically used in control implementations. Section 9.4 derives the companion optimal estimation problem. As for the control case, the time-varying gain solution is found first, then we find the steady-state gain case that is typically the one implemented. The final section, 9.5, shows how to use these results in the design of MIMO control systems.

9.1 Decoupling

The first step in any multivariable design should be an attempt either to find an approximate model consisting of two or more single input–output models or else to decouple the control gain matrix \mathbf{K}

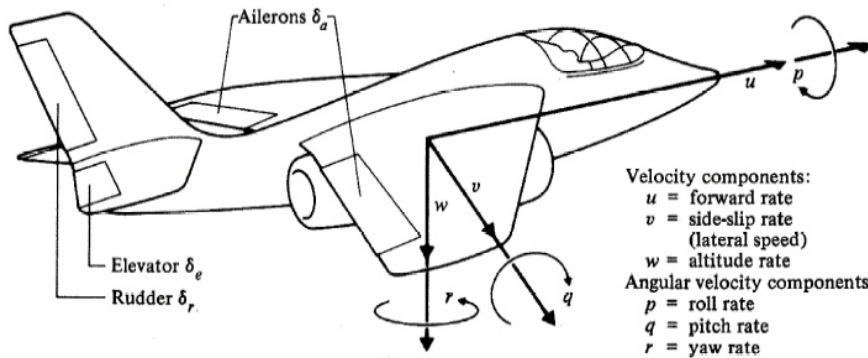


Figure 9.1
Schematic of an aircraft showing variable definitions

and the estimator gain matrix \mathbf{L} . This step will give better physical insight into the important feedback variables and can lead to a plant description that is substantially simpler for design purposes and yet yields no significant degradation from an analysis based on the full multivariable system.

For example, the linearized equations of motion of an aircraft (Fig. 9.1) are of eighth order but are almost always separated into two fourth-order sets representing longitudinal motion (w, u, q) and lateral motion (p, r, v). The elevator control surfaces affect longitudinal motion; the aileron and rudder primarily affect lateral motion. Although there is a small amount of coupling of lateral motion into longitudinal motion, this is ignored with no serious consequences when the control, or “stability-augmentation,” systems are designed independently for the two fourth-order systems.

Further decoupling of the equations is also possible.

Control Decoupling

Example 9.1

Decouple the lateral aircraft fourth-order equations into two second-order equations and show how to design the control.

Solution. The aircraft lateral equations are multivariable and of the form

$$\mathbf{x}(k+1) = \Phi \mathbf{x}(k) + \Gamma \mathbf{u}(k), \quad (9.1)$$

where

$$\mathbf{u} = \begin{bmatrix} \delta_r \\ \delta_a \end{bmatrix}, \quad \mathbf{x} = \begin{bmatrix} v \\ r \\ \phi_p \\ p \end{bmatrix}, \quad \text{and} \quad p = \dot{\phi}_p.$$

A control law of the standard form

$$\begin{bmatrix} \delta_r \\ \delta_a \end{bmatrix} = - \begin{bmatrix} K_{11} & K_{12} & K_{13} & K_{14} \\ K_{21} & K_{22} & K_{23} & K_{24} \end{bmatrix} \begin{bmatrix} v \\ r \\ \phi_p \\ p \end{bmatrix} \quad (9.2)$$

shows that there are eight elements in the gain matrix to be selected, and the specification of four closed-loop roots clearly causes the problem to be underdetermined and will leave many possible values of \mathbf{K} that will meet the specifications. This shows that the pole-placement approach to multivariable system design poses difficulties and additional criteria need to be introduced.

A decoupling that removes the ambiguity is to restrict the control law to

$$\begin{bmatrix} \delta_r \\ \delta_a \end{bmatrix} = - \begin{bmatrix} K_{11} & K_{12} & 0 & 0 \\ 0 & 0 & K_{23} & K_{24} \end{bmatrix} \begin{bmatrix} v \\ r \\ \phi_p \\ p \end{bmatrix}. \quad (9.3)$$

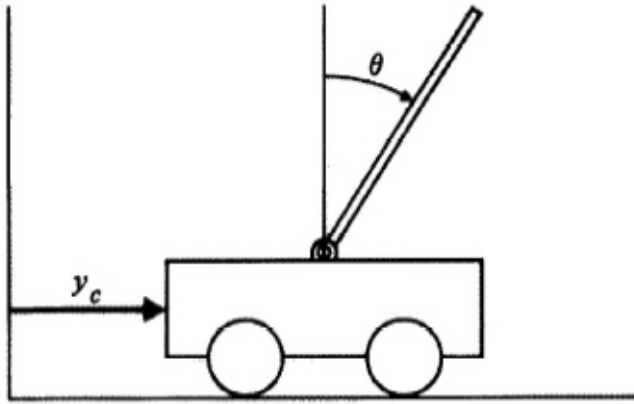


Figure 9.2
Hinged stick and
motorized cart

This makes good physical sense because the rudder primarily yaws the aircraft about a vertical axis (r -motion), thus directly causing sideslip (v), and the ailerons primarily roll the aircraft about an axis through the nose, thus causing changes in the roll angle, ϕ_p , and the roll rate, p . Given an achievable set of desired pole locations, there are unique values of the four nonzero components of \mathbf{K} ; however, the governing equations cannot be cast in the same form as in Eq. (8.5) and therefore can be difficult to solve.

A further decoupling that would permit an easy gain calculation is to assume that Eq. (9.1) is of the form

$$\begin{bmatrix} v \\ r \\ \phi_p \\ p \end{bmatrix}_{k+1} = \begin{bmatrix} \phi_{11} & \phi_{12} & 0 & 0 \\ \phi_{21} & \phi_{22} & 0 & 0 \\ 0 & 0 & \phi_{33} & \phi_{34} \\ 0 & 0 & \phi_{43} & \phi_{44} \end{bmatrix} \begin{bmatrix} v \\ r \\ \phi_p \\ p \end{bmatrix}_k + \begin{bmatrix} \Gamma_{11} & 0 \\ \Gamma_{21} & 0 \\ 0 & \Gamma_{32} \\ 0 & \Gamma_{42} \end{bmatrix} \begin{bmatrix} \delta_r \\ \delta_a \end{bmatrix}_k \quad (9.4)$$

and that the control law is given by Eq. (9.3).

This makes some physical sense but ignores important coupling between the two aircraft modes. It does, however, decouple the system into second-order systems for which the methods of Chapter 8 can be applied directly to obtain the gains. The resulting closed-loop characteristic roots of the full lateral equations can be checked by calculating the eigenvalues of the closed loop matrix: (see `eig.m` in MATLAB)

$$\Phi_{\text{closed loop}} = \begin{bmatrix} \phi_{11} - \Gamma_{11}\mathbf{K}_{11} & \phi_{12} - \Gamma_{11}\mathbf{K}_{12} & \phi_{13} - \Gamma_{12}\mathbf{K}_{23} & \phi_{14} - \Gamma_{12}\mathbf{K}_{24} \\ \phi_{21} - \Gamma_{21}\mathbf{K}_{11} & \phi_{22} - \Gamma_{21}\mathbf{K}_{12} & \phi_{23} - \Gamma_{22}\mathbf{K}_{23} & \phi_{24} - \Gamma_{22}\mathbf{K}_{24} \\ \phi_{31} - \Gamma_{31}\mathbf{K}_{11} & \phi_{32} - \Gamma_{31}\mathbf{K}_{12} & \phi_{33} - \Gamma_{32}\mathbf{K}_{23} & \phi_{34} - \Gamma_{32}\mathbf{K}_{24} \\ \phi_{41} - \Gamma_{41}\mathbf{K}_{11} & \phi_{42} - \Gamma_{41}\mathbf{K}_{12} & \phi_{43} - \Gamma_{42}\mathbf{K}_{23} & \phi_{44} - \Gamma_{42}\mathbf{K}_{24} \end{bmatrix}, \quad (9.5)$$

which results from combining Eq. (9.3) and (9.4).

If the plant coupling that was ignored in the gain computation is important, the roots obtained from Eq. (9.5) will differ from those used to compute the gains using Eqs. (9.3) and (9.4). In many cases, the method will be accurate enough and one need look no further. In other cases, one could revise the “desired” root locations and iterate until the correct roots from Eq. (9.5) are satisfactory or else turn to the methods of optimal control to be described in the following sections.

The same ideas apply equally well to the decoupling of the estimator into SISO parts.

Estimator Decoupling

Decouple the estimator for the inverted pendulum on a motorized cart (Fig. 9.2).

Example 9.2

Solution. The equations of motion can be written as

$$\begin{bmatrix} \mathbf{x}_c \\ \mathbf{x}_s \end{bmatrix}_{k+1} = \begin{bmatrix} \phi_{cc} & \phi_{cs} \\ \phi_{sc} & \phi_{ss} \end{bmatrix} \begin{bmatrix} \mathbf{x}_c \\ \mathbf{x}_s \end{bmatrix}_k + \begin{bmatrix} \mathbf{\Gamma}_c \\ \mathbf{\Gamma}_s \end{bmatrix} u(k), \quad (9.6)$$

where

$$\begin{aligned} \mathbf{x}_c &= \begin{bmatrix} y_c \\ \dot{y}_c \end{bmatrix} \text{ cart position and velocity,} \\ \mathbf{x}_s &= \begin{bmatrix} \theta \\ \dot{\theta} \end{bmatrix} \text{ stick angle and angular rate,} \end{aligned}$$

and the available measurements are

$$\begin{bmatrix} y \\ \theta \end{bmatrix} = \begin{bmatrix} 1 & 0 & 0 & 0 \\ 0 & 0 & 1 & 0 \end{bmatrix} \begin{bmatrix} y_c \\ \dot{y}_c \\ \theta \\ \dot{\theta} \end{bmatrix}. \quad (9.7)$$

The stick pictured in Fig. 9.2 is substantially lighter than the cart. This means that stick motion has a small dynamic effect on cart motion, which in turn implies that $\phi_{cs} \cong \mathbf{0}$. This does not imply that $\phi_{sc} = 0$; in fact, cart motion is the mechanism for influencing stick motion and hence stabilizing it.

An estimator for the system described by Eq. (9.6) and Eq. (9.7) requires the determination of eight elements of an estimator gain matrix, \mathbf{L} . Hence, specifying the four estimator roots and using the methods of Chapter 8 would not determine this \mathbf{L} uniquely—another example of an underdetermined system caused by the multivariable nature of the problem.

But because we can assume that $\phi_{cs} = \mathbf{0}$, the cart equation in Eq. (9.6) uncouples from the stick equation, and we simply design an estimator for

$$\begin{aligned} \mathbf{x}_c(k+1) &= \phi_{cc}\mathbf{x}_c(k) + \mathbf{\Gamma}_c u, \\ y_c &= [1 \quad 0] \begin{bmatrix} y_c \\ \dot{y}_c \end{bmatrix}, \end{aligned} \quad (9.8)$$

which can be done with the methods described in Chapter 8. There is one-way coupling into the stick equation, but this just acts like an additional control input and can be ignored in the calculation of the stick estimator gain matrix, \mathbf{L}_s , using the pole-placement methods of Chapter 8. However, the ϕ_{sc} coupling should not be ignored in the estimator equations, and there is no reason to ignore the weak coupling, ϕ_{cs} . The final (predictor) estimator would be of the form

$$\begin{aligned} \bar{\mathbf{x}}_c(k+1) &= \phi_{cc}\bar{\mathbf{x}}_c(k) + \phi_{cs}\bar{\mathbf{x}}_s(k) + \mathbf{\Gamma}_c u(k) + \mathbf{L}_c(y_c(k) - \bar{y}_c(k)), \\ \bar{\mathbf{x}}_s(k+1) &= \phi_{sc}\bar{\mathbf{x}}_c(k) + \phi_{ss}\bar{\mathbf{x}}_s(k) + \mathbf{\Gamma}_s u(k) + \mathbf{L}_s(\theta(k) - \bar{\theta}(k)), \end{aligned}$$

where \mathbf{L}_c and \mathbf{L}_s are both 2×1 matrices.

Even without the very weak one-way coupling in $\mathbf{\Phi}_{cs}$ that was obvious for this example, one could assume this to be the case, then check the resulting full-system characteristic roots using a method similar to the previous airplane example. Note that ignoring the coupling only causes approximations in the gain-matrix calculation and thus the root locations. There is no approximation in the system model used in the estimator; therefore, the estimation errors will still approach zero for stable estimator roots.

In short, it is often useful to apply your knowledge of the physical aspects of the system at hand to break the design into simpler and more tractable subsets. With luck, the whole job can be finished this way. At worst, insight will be gained that will aid in the design procedures to follow and in the implementation and checkout of the control system.

9.2 Time-Varying Optimal Control

Optimal control methods are attractive because they handle MIMO systems easily and aid in the selection of the desired pole locations for SISO systems. They also allow the designer to determine many good candidate values of the feedback gain, \mathbf{K} , using very efficient computation tools. We will

develop the time-varying optimal control solution first and then reduce it to a steady-state solution in the following section. The result amounts to another method of computing \mathbf{K} in the control law Eq. (8.5)

$$\mathbf{u} = -\mathbf{K}\mathbf{x} \quad (9.9)$$

that was used in Chapter 8 and illustrated by Eq. (9.2) in Example 9.1.

Given a discrete plant

$$\mathbf{x}(k+1) = \mathbf{\Phi}\mathbf{x}(k) + \mathbf{\Gamma}\mathbf{u}(k), \quad (9.10)$$

we wish to pick $\mathbf{u}(k)$ so that a **cost function**

cost function

$$\mathcal{J} = \frac{1}{2} \sum_{k=0}^N [\mathbf{x}^T(k)\mathbf{Q}_1\mathbf{x}(k) + \mathbf{u}^T(k)\mathbf{Q}_2\mathbf{u}(k)] \quad (9.11)$$

is minimized. \mathbf{Q}_1 and \mathbf{Q}_2 are symmetric weighting matrices to be selected by the designer, who bases the choice on the relative importance of the various states and controls. Some weight will almost always be selected for the control ($|\mathbf{Q}_2| \neq 0$); otherwise the solution will include large components in the control gains, and the states would be driven to zero at a very fast rate, which could saturate the actuator device.¹ The \mathbf{Q} 's must also be **nonnegative definite**,² which is most easily accomplished by picking the \mathbf{Q} 's to be diagonal with all diagonal elements positive or zero.

Another way of stating the problem given by Eqs. (9.10) and (9.11) is that we wish to minimize

$$\mathcal{J} = \frac{1}{2} \sum_{k=0}^N [\mathbf{x}^T(k)\mathbf{Q}_1\mathbf{x}(k) + \mathbf{u}^T(k)\mathbf{Q}_2\mathbf{u}(k)] \quad [9.11]$$

subject to the constraint that

$$-\mathbf{x}(k+1) + \mathbf{\Phi}\mathbf{x}(k) + \mathbf{\Gamma}\mathbf{u}(k) = 0, \quad k = 0, 1, \dots, N. \quad [9.10]$$

This is a standard constrained-minima problem which can be solved using the method of **Lagrange multipliers**. There will be one Lagrange multiplier vector, which we will call $\boldsymbol{\lambda}(k+1)$, for each value of k . The procedure is to rewrite Eqs. (9.10) and (9.11) as

Lagrange multipliers

$$\begin{aligned} \mathcal{J}' = \sum_{k=0}^N \left[\frac{1}{2} \mathbf{x}^T(k)\mathbf{Q}_1\mathbf{x}(k) + \frac{1}{2} \mathbf{u}^T(k)\mathbf{Q}_2\mathbf{u}(k) \right. \\ \left. + \boldsymbol{\Lambda}^T(k+1)(-\mathbf{x}(k+1) + \mathbf{\Phi}\mathbf{x}(k) + \mathbf{\Gamma}\mathbf{u}(k)) \right], \end{aligned} \quad (9.12)$$

and find the minimum of \mathcal{J}' with respect to $\mathbf{x}(k)$, $\mathbf{u}(k)$, and $\boldsymbol{\Lambda}(k)$. Note that for an optimal $\mathbf{u}(k)$ that obeys Eq. (9.10), the two cost functions, \mathcal{J}' and \mathcal{J} , are identical in magnitude. The index on $\boldsymbol{\Lambda}$ is arbitrary conceptually, but we let it be $k+1$ because this choice will yield a particularly easy form of the equations later on.

Proceeding with the minimization leads to

$$\begin{aligned} \frac{\partial \mathcal{J}'}{\partial \mathbf{u}(k)} = \mathbf{u}^T(k)\mathbf{Q}_2 + \boldsymbol{\Lambda}^T(k+1)\mathbf{\Gamma} = 0, \quad \text{control equations,} \\ \frac{\partial \mathcal{J}'}{\partial \boldsymbol{\Lambda}(k+1)} = -\mathbf{x}(k+1) + \mathbf{\Phi}\mathbf{x}(k) + \mathbf{\Gamma}\mathbf{u}(k) = 0, \quad \text{state equations,} \end{aligned} \quad (9.13)$$

and [9.10], the adjoint equations,

$$\frac{\partial \mathcal{J}'}{\partial \mathbf{x}(k)} = \mathbf{x}^T(k)\mathbf{Q}_1 - \boldsymbol{\Lambda}^T(k) + \boldsymbol{\Lambda}^T(k+1)\mathbf{\Phi} = 0. \quad (9.14)$$

The last set of the equations, the **adjoint equations**, can be written as the backward difference equa- adjoint equations

¹If the sampling rate, T , is long, however, a control that moves the state along as rapidly as possible might be feasible. Such controls are called "dead-beat" because they beat the state to a dead stop in at most n steps. They correspond to placement of all poles at $z = 0$. See Problem 8.23.

²Matrix equivalent of a nonnegative number; it ensures that $\mathbf{x}^T\mathbf{Q}_1\mathbf{x}$ and $\mathbf{u}^T\mathbf{Q}_2\mathbf{u}$ are nonnegative for all possible \mathbf{x} and \mathbf{u} .

tion

$$\mathbf{\Lambda}(k) = \mathbf{\Phi}^T \mathbf{\Lambda}(k+1) + \mathbf{Q}_1 \mathbf{x}(k). \quad (9.15)$$

Restating the results in more convenient forms, we have from Eq. (9.10)

$$\mathbf{x}(k+1) = \mathbf{\Phi} \mathbf{x}(k) + \mathbf{\Gamma} \mathbf{u}(k), \quad (9.16)$$

where, using Eq. (9.13)

$$\mathbf{u}(k) = -\mathbf{Q}_2^{-1} \mathbf{\Gamma}^T \mathbf{\Lambda}(k+1), \quad (9.17)$$

and from Eq. (9.15) we can describe $\mathbf{\Lambda}(k+1)$ in the forward difference equation form

$$\mathbf{\Lambda}(k+1) = \mathbf{\Phi}^{-T} \mathbf{\Lambda}(k) - \mathbf{\Phi}^{-T} \mathbf{Q}_1 \mathbf{x}(k). \quad (9.18)$$

Equations (9.16), (9.17), and either (9.15) or (9.18) are a set of coupled difference equations defining the optimal solution of $\mathbf{x}(k)$, $\mathbf{\Lambda}(k)$, and $\mathbf{u}(k)$, provided the initial (or final) conditions are known. The initial conditions on $\mathbf{x}(k)$ must be given; however, usually $\lambda(0)$ would not be known, and we are led to the endpoint to establish a boundary condition for $\mathbf{\Lambda}$. From Eq. (9.11) we see that $\mathbf{u}(N)$ should be zero in order to minimize \mathcal{J} because $\mathbf{u}(N)$ has no effect on $\mathbf{x}(N)$ [see Eq. (9.10)]. Thus Eq. (9.13) suggests that $\mathbf{\Lambda}(N+1) = \mathbf{0}$, and Eq. (9.14) thus shows that a suitable boundary condition is

$$\mathbf{\Lambda}(N) = \mathbf{Q}_1 \mathbf{x}(N). \quad (9.19)$$

A set of equations describing the solution to the optimal control problem is now completely specified. It consists of the two difference equations (9.16) and (9.15) with \mathbf{u} given by Eq. (9.17), the final condition on $\mathbf{\Lambda}$ given by Eq. (9.19), and the initial condition on \mathbf{x} would be given in the problem statement. The solution to this two-point boundary-value problem is not easy.

One method, called the **sweep method** by Bryson and Ho (1975), is to assume

sweep method

$$\mathbf{\Lambda}(k) = \mathbf{S}(k) \mathbf{x}(k). \quad (9.20)$$

This definition allows the transformation of the two-point boundary-value problem in \mathbf{x} and $\mathbf{\Lambda}$ to one in \mathbf{S} with a single-point boundary condition. With the definition Eq. (9.20), the control Eq. (9.13) becomes

$$\begin{aligned} \mathbf{Q}_2 \mathbf{u}(k) &= -\mathbf{\Gamma}^T \mathbf{S}(k+1) \mathbf{x}(k+1) \\ &= -\mathbf{\Gamma}^T \mathbf{S}(k+1) (\mathbf{\Phi} \mathbf{x}(k) + \mathbf{\Gamma} \mathbf{u}(k)). \end{aligned}$$

Solving for $\mathbf{u}(k)$, we obtain

$$\begin{aligned} \mathbf{u}(k) &= -(\mathbf{Q}_2 + \mathbf{\Gamma}^T \mathbf{S}(k+1) \mathbf{\Gamma})^{-1} \mathbf{\Gamma}^T \mathbf{S}(k+1) \mathbf{\Phi} \mathbf{x}(k) \\ &= -\mathbf{R}^{-1} \mathbf{\Gamma}^T \mathbf{S}(k+1) \mathbf{\Phi} \mathbf{x}(k). \end{aligned} \quad (9.21)$$

In Eq. (9.21) we have defined

$$\mathbf{R} = \mathbf{Q}_2 + \mathbf{\Gamma}^T \mathbf{S}(k+1) \mathbf{\Gamma}$$

for convenience. If we now substitute Eq. (9.20) into Eq. (9.15) for $\mathbf{\Lambda}(k)$ and $\mathbf{\Lambda}(k+1)$, we eliminate $\mathbf{\Lambda}$. Then we substitute Eq. (9.21) into Eq. (9.16) to eliminate $\mathbf{x}(k+1)$ as follows. From Eq. (9.15), we have

$$\mathbf{\Lambda}(k) = \mathbf{\Phi}^T \mathbf{\Lambda}(k+1) + \mathbf{Q}_1 \mathbf{x}(k),$$

and substituting Eq. (9.20), we have

$$\mathbf{S}(k) \mathbf{x}(k) = \mathbf{\Phi}^T \mathbf{S}(k+1) \mathbf{x}(k+1) + \mathbf{Q}_1 \mathbf{x}(k).$$

Now we use Eq. (9.16) for $\mathbf{x}(k+1)$

$$\mathbf{S}(k) \mathbf{x}(k) = \mathbf{\Phi}^T \mathbf{S}(k+1) (\mathbf{\Phi} \mathbf{x}(k) + \mathbf{\Gamma} \mathbf{u}(k)) + \mathbf{Q}_1 \mathbf{x}(k).$$

Next we use Eq. (9.21) for $\mathbf{u}(k)$ in the above

$$\mathbf{S}(k)\mathbf{x}(k) = \Phi^T \mathbf{S}(k+1) [\Phi \mathbf{x}(k) - \Gamma \mathbf{R}^{-1} \Gamma^T \mathbf{S}(k+1) \Phi \mathbf{x}(k)] + \mathbf{Q}_1 \mathbf{x}(k),$$

and collect all terms on one side

$$[\mathbf{S}(k) - \Phi^T \mathbf{S}(k+1) \Phi + \Phi^T \mathbf{S}(k+1) \Gamma \mathbf{R}^{-1} \Gamma^T \mathbf{S}(k+1) \Phi - \mathbf{Q}_1] \mathbf{x}(k) = 0. \quad (9.22)$$

Because Eq. (9.22) must hold for any $\mathbf{x}(k)$, the coefficient matrix must be identically zero, from which follows a backward difference equation describing the solution of $\mathbf{S}(k)$

Riccati equation

$$\mathbf{S}(k) = \Phi^T [\mathbf{S}(k+1) - \mathbf{S}(k+1) \Gamma \mathbf{R}^{-1} \Gamma^T \mathbf{S}(k+1)] \Phi + \mathbf{Q}_1, \quad (9.23)$$

which is often rewritten as

$$\mathbf{S}(k) = \Phi^T \mathbf{M}(k+1) \Phi + \mathbf{Q}_1, \quad (9.24)$$

where

$$\mathbf{M}(k+1) = \mathbf{S}(k+1) - \mathbf{S}(k+1) \Gamma [\mathbf{Q}_2 + \Gamma^T \mathbf{S}(k+1) \Gamma]^{-1} \Gamma^T \mathbf{S}(k+1). \quad (9.25)$$

Equation (9.23) is called the discrete **Riccati equation**. It is not easy to solve because it is nonlinear in \mathbf{S} . But note that the matrix to be inverted in Eq. (9.25) \mathbf{R} , has the same dimension as the number of controls, which is usually less than the number of states.

The boundary condition on the recursion relationship for $\mathbf{S}(k+1)$ is obtained from Eq. (9.19) and Eq. (9.20); thus

$$\mathbf{S}(N) = \mathbf{Q}_1, \quad (9.26)$$

and we see now that the problem has been transformed so that the solution is described by the recursion relations Eq. (9.24) and Eq. (9.25) with the single boundary condition given by Eq. (9.26). The recursion equations must be solved backwards because the boundary condition is given at the endpoint. To solve for $\mathbf{u}(k)$, we use Eq. (9.21) to obtain

$$\mathbf{u}(k) = -\mathbf{K}(k)\mathbf{x}(k), \quad (9.27)$$

where

$$\mathbf{K}(k) = [\mathbf{Q}_2 + \Gamma^T \mathbf{S}(k+1) \Gamma]^{-1} \Gamma^T \mathbf{S}(k+1) \Phi \quad (9.28)$$

and is the desired “optimal” time-varying feedback gain.

Let us now summarize the entire procedure:

1. Let $\mathbf{S}(N) = \mathbf{Q}_1$ and $\mathbf{K}(N) = \mathbf{0}$.
2. Let $k = N$.
3. Let $\mathbf{M}(k) = \mathbf{S}(k) - \mathbf{S}(k) \Gamma [\mathbf{Q}_2 + \Gamma^T \mathbf{S}(k) \Gamma]^{-1} \Gamma^T \mathbf{S}(k)$.
4. Let $\mathbf{K}(k-1) = [\mathbf{Q}_2 + \Gamma^T \mathbf{S}(k) \Gamma]^{-1} \Gamma^T \mathbf{S}(k) \Phi$.
5. Store $\mathbf{K}(k-1)$.
6. Let $\mathbf{S}(k-1) = \Phi^T \mathbf{M}(k) \Phi + \mathbf{Q}_1$.
7. Let $k = k - 1$.
8. Go to step 3.

For any given initial condition for \mathbf{x} , to apply the control, we use the stored gains $\mathbf{K}(k)$ and

$$\mathbf{x}(k+1) = \Phi \mathbf{x}(k) + \Gamma \mathbf{u}(k), \quad (9.16)$$

where

$$\mathbf{u}(k) = -\mathbf{K}(k)\mathbf{x}(k). \quad (9.27)$$

Note that the optimal gain, $\mathbf{K}(k)$, changes at each time step but can be precomputed and stored for later use as long as the length, N , of the problem is known. This is so because no knowledge of the initial state $\mathbf{x}(0)$ is required for computation of the control gain $\mathbf{K}(k)$.

Time-Varying Nature of Control Gains

Example 9.3

Solve for the time history of \mathbf{K} for the satellite attitude-control example described in Appendix A.1. Choose the state weighting matrix to be

$$Q_1 = \begin{bmatrix} 1 & 0 \\ 0 & 0 \end{bmatrix}, \quad (9.29)$$

which means that the angle state is weighted but not the angular velocity. Choose the control weighting matrix, a scalar in this case because there is a single control input, to have three values

$$Q_2 = 0.01, \quad 0.1, \quad \text{and} \quad 1.0, \quad (9.30)$$

and plot the resulting time histories of \mathbf{K} .

Solution. Equations (9.24) through (9.28) need to be solved for the system transfer function $G(s) = 1/s^2$. The problem length for purposes of defining \mathcal{J} was chosen to be 51 steps, which, with the sample period of $T = 0.1$ sec, means that the total time was 5.1 sec. This time was chosen long enough so that it was apparent that the gains were essentially constant over the initial time period.

Figure 9.3 contains the resulting gain time histories plotted by the computer. We see from the figure that the problem length affects only the values of K near the end, and in fact, the first portions of all cases show constant values of the gains. If the problem length had been chosen to be longer, the end characteristics would have been identical, and the early constant gain portion would have existed for a longer time.

The fact that the gain over the first portion of the example was constant is typical of the optimal gains for all constant coefficient systems, provided that the problem time is long enough. This means that the optimal controller over the early, constant-gain portion is identical to the constant-gain cases discussed in Chapter 8 and Section 9.1 except that the values of the constant gain, \mathbf{K} , are based on the minimization of a cost function rather than a computation based on specified root locations. We could also view this result as a method to find a “good” set of pole locations because the constant, optimal \mathbf{K} during the early portion of the solution determines a set of closed-loop roots.

For MIMO problems, the time-varying gains act exactly as in the preceding example. The next section develops a method to compute the constant value of the optimal gains so that they can be used in place of the time-varying values, thus yielding a much simpler implementation. The only region where the gains are not optimal is during the transient region near the end. In fact, many control systems are turned on and left to run for very long times; for example, a satellite-attitude control system might run for years. This kind of problem is treated mathematically as if it runs for an infinite time, and therefore the constant-gain portion of the time-varying optimal solution *is* the true optimal.

Before we leave the time-varying case it is informative to evaluate the optimal cost function \mathcal{J} in terms of $\mathbf{\Lambda}$ and \mathbf{S} . If we substitute Eqs. (9.13) and (9.14) for $\mathbf{\Lambda}^T(k+1)\mathbf{\Gamma}$ and $\mathbf{\Lambda}^T(k+1)\mathbf{\Phi}$ in Eq. (9.12), we find

$$\begin{aligned} \mathcal{J}' &= \frac{1}{2} \sum_{k=0}^N [\mathbf{x}^T(k)\mathbf{Q}_1\mathbf{x}(k) + \mathbf{u}^T(k)\mathbf{Q}_2\mathbf{u}(k) - \mathbf{\Lambda}^T(k+1)\mathbf{x}(k+1) \\ &\quad + (\mathbf{\Lambda}^T(k) - \mathbf{x}^T(k)\mathbf{Q}_1)\mathbf{x}(k) + (-\mathbf{u}^T(k)\mathbf{Q}_2)\mathbf{u}(k)] \\ &= \frac{1}{2} \sum_{k=0}^N [\mathbf{\Lambda}^T(k)\mathbf{x}(k) - \mathbf{\Lambda}^T(k+1)\mathbf{x}(k+1)] \\ &= \frac{1}{2} \mathbf{\Lambda}^T(0)\mathbf{x}(0) - \frac{1}{2} \mathbf{\Lambda}^T(N+1)\mathbf{x}(N+1). \end{aligned}$$

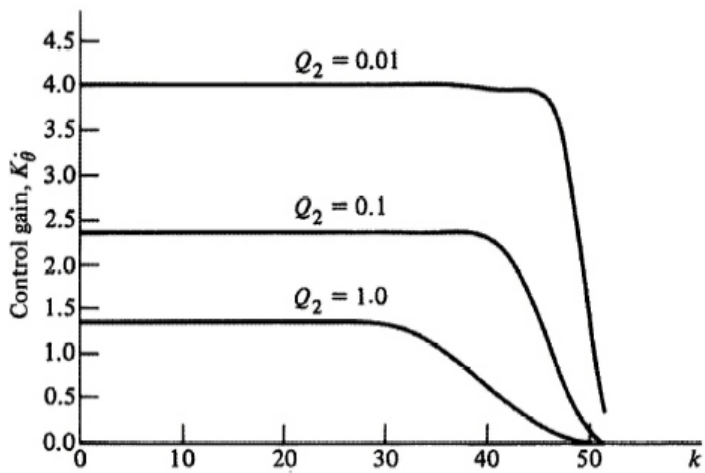
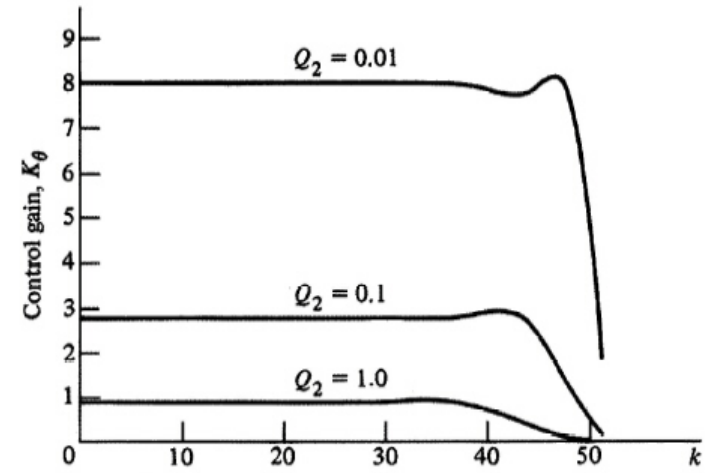


Figure 9.3
Example of control gains
versus time,
Example 9.3

However, from Eq. (9.19), $\mathbf{\Lambda}(N+1) = \mathbf{0}$, and thus, using Eq. (9.20), we find

$$\begin{aligned}\mathcal{J}' = \mathcal{J} &= \frac{1}{2} \mathbf{\Lambda}^T(0) \mathbf{x}(0) \\ &= \frac{1}{2} \mathbf{x}^T(0) \mathbf{S}(0) \mathbf{x}(0).\end{aligned}\quad (9.31)$$

Thus we see that having computed \mathbf{S} , we can immediately evaluate the cost associated with the control. Although the cost could be used in evaluating different candidate designs, in fact, it is not very useful because the weighting matrices, \mathbf{Q}_1 and \mathbf{Q}_2 , are arbitrary quantities that change with the different designs. Furthermore, the value of the discrete cost as defined by Eq. (9.11) is roughly proportional to the sample rate, thus eliminating any usefulness in evaluating the performance for different sample rates. Typically a designer would evaluate different designs by looking at the traditional measures that have been discussed in Chapter 7 or possibly by evaluating quadratic performance measures that are independent of the \mathbf{Q} 's and the sample rate. We will show in Section 9.3.4 how to remove the effect of sample rate on the value of the cost.

9.3 LQR Steady-State Optimal Control

The previous section developed the optimal control gain that minimized the cost in Eq. (9.11). We saw that the result was a time-varying gain, $\mathbf{K}(k)$, but that there would usually be a portion of the solution that produced a constant gain, \mathbf{K}_∞ , which would be much easier to implement in a control system. In fact, for the infinite time problem, called the **regulator** case, the constant-gain solution is the optimum. We call this solution the **linear quadratic regulator**, or LQR, because it applies to *linear* systems, the cost is *quadratic*, and it applies to the *regulator* case. This section will discuss how one finds the LQR solution and various properties of the solution.

One obvious method to compute the value of \mathbf{K} during the early, constant portion of a problem is to compute \mathbf{S} backward in time until it reaches a steady value, \mathbf{S}_∞ , then use Eq. (9.28) to compute \mathbf{K}_∞ . This has been done in some software packages and gives reliable answers. Its drawback is that it requires substantially more computation than the alternate methods.

Another method is to look for steady-state solutions of the Riccati equation. In steady state, $\mathbf{S}(k)$ becomes equal to $\mathbf{S}(k+1)$ (we'll call them both \mathbf{S}_∞) and the Riccati Eq. (9.23) reduces to

$$\mathbf{S}_\infty = \mathbf{\Phi}^T [\mathbf{S}_\infty - \mathbf{S}_\infty \mathbf{\Gamma} \mathbf{R}^{-1} \mathbf{\Gamma}^T \mathbf{S}_\infty] \mathbf{\Phi} + \mathbf{Q}_1, \quad (9.32)$$

which is usually referred to as the **algebraic Riccati equation**. Because of the quadratic appearance of \mathbf{S}_∞ , there is more than one solution, and one needs to know that \mathbf{S} must be positive definite to select the correct one. The fact that \mathbf{S} is positive definite follows by inspection of Eq. (9.31) and that \mathcal{J} must be positive. For extremely simple problems, one is sometimes able to use Eq. (9.32) to find an analytical solution for \mathbf{S}_∞ , but in most cases this is impossible, and a numerical solution is required.

Most software packages use variations on a method called **eigenvector decomposition** due to its superior computational efficiency compared to the methods above. It is based on the linear description of the combined state and adjoint equations given by Eqs. (9.16), (9.17), and (9.18), which describe the time-varying solution. We can combine these equations into a set of difference equations in standard form in \mathbf{x} and $\mathbf{\Lambda}$ if we assume that \mathbf{Q}_2 and $\mathbf{\Phi}$ are nonsingular.³ These equations are called **Hamilton's equations** or the **Euler-Lagrange equations**

$$\begin{bmatrix} \mathbf{x} \\ \mathbf{\Lambda} \end{bmatrix}_{k+1} = \begin{bmatrix} \mathbf{\Phi} + \mathbf{\Gamma} \mathbf{Q}_2^{-1} \mathbf{\Gamma}^T \mathbf{\Phi}^{-T} \mathbf{Q}_1 & -\mathbf{\Gamma} \mathbf{Q}_2^{-1} \mathbf{\Gamma}^T \mathbf{\Phi}^{-T} \\ -\mathbf{\Phi}^{-T} \mathbf{Q}_1 & \mathbf{\Phi}^{-T} \end{bmatrix} \begin{bmatrix} \mathbf{x} \\ \mathbf{\Lambda} \end{bmatrix}_k, \quad (9.33)$$

and their system matrix is called the control **Hamiltonian** matrix

$$\mathcal{H}_c = \begin{bmatrix} \mathbf{\Phi} + \mathbf{\Gamma} \mathbf{Q}_2^{-1} \mathbf{\Gamma}^T \mathbf{\Phi}^{-T} \mathbf{Q}_1 & -\mathbf{\Gamma} \mathbf{Q}_2^{-1} \mathbf{\Gamma}^T \mathbf{\Phi}^{-T} \\ -\mathbf{\Phi}^{-T} \mathbf{Q}_1 & \mathbf{\Phi}^{-T} \end{bmatrix}. \quad (9.34)$$

³For systems with a pure time delay that is greater than the sampling period, T , $\mathbf{\Phi}$ is singular and the following development would fail. Software packages usually have features in their formulations that circumvent this difficulty.

Because the system described by Eq. (9.33) is linear and the Hamiltonian matrix is constant, we can solve for the eigenvalues of Eq. (9.34) [or roots of Eq. (9.33)] using standard techniques (see `eig.m` in MATLAB). For an n th order system, there will be $2n$ eigenvalues. We will show in the next section that n of the roots are stable and the other n are unstable. In fact, the n unstable roots are the reciprocals of the n stable roots. Furthermore, the n stable roots are the roots of the optimal, constant-gain, closed-loop system! If we were trying to find the optimal \mathbf{K} for a SISO system, the problem would now be complete, because knowing the optimal roots allows us to use Ackermann's formula to find \mathbf{K} . But we want the optimal \mathbf{K} for MIMO systems, too, so it's not that simple. We will return to the eigenvector decomposition solution after establishing the characteristics of the roots just stated.

9.3.1 Reciprocal Root Properties

Let us turn to the question of the reciprocal nature of the roots of Eq. (9.33). If we take the z -transforms of Eqs. (9.16), (9.17), and (9.15), we obtain

$$z\mathbf{X}(z) = \Phi\mathbf{X}(z) + \Gamma\mathbf{U}(z), \quad (9.35)$$

$$\mathbf{U}(z) = -z\mathbf{Q}_2^{-1}\Gamma^T\Lambda(z), \quad (9.36)$$

$$\Lambda(z) = \mathbf{Q}_1\mathbf{X}(z) + z\Phi^T\Lambda(z). \quad (9.37)$$

If we substitute Eq. (9.36) into Eq. (9.35) and write the remaining two equations in terms of the variables $\mathbf{X}(z)$ and $z\Lambda(z)$, we find, in matrix form

$$\begin{bmatrix} z\mathbf{I} - \Phi & \Gamma\mathbf{Q}_2^{-1}\Gamma^T \\ -\mathbf{Q}_1 & z^{-1}\mathbf{I} - \Phi^T \end{bmatrix} \begin{bmatrix} \mathbf{X}(z) \\ z\Lambda(z) \end{bmatrix} = \mathbf{0}.$$

Thus the roots of the Hamiltonian system are those values of z for which

$$\det \begin{bmatrix} z\mathbf{I} - \Phi & \Gamma\mathbf{Q}_2^{-1}\Gamma^T \\ -\mathbf{Q}_1 & z^{-1}\mathbf{I} - \Phi^T \end{bmatrix} = 0.$$

If we now reduce the term $-\mathbf{Q}_1$ to zero by adding $\mathbf{Q}_1(z\mathbf{I} - \Phi)^{-1}$ times the first rows to the second rows, we have

$$\det \begin{bmatrix} z\mathbf{I} - \Phi & \Gamma\mathbf{Q}_2^{-1}\Gamma^T \\ 0 & z^{-1}\mathbf{I} - \Phi^T + \mathbf{Q}_1(z\mathbf{I} - \Phi)^{-1}\Gamma\mathbf{Q}_2^{-1}\Gamma^T \end{bmatrix} = 0.$$

Because this matrix is blockwise triangular, we have

$$\det(z\mathbf{I} - \Phi)\det\{z^{-1}\mathbf{I} - \Phi^T + \mathbf{Q}_1(z\mathbf{I} - \Phi)^{-1}\Gamma\mathbf{Q}_2^{-1}\Gamma^T\} = 0.$$

Now we factor the term $z^{-1}\mathbf{I} - \Phi^T$ from the second term to find

$$\det(z\mathbf{I} - \Phi)\det\{(z^{-1}\mathbf{I} - \Phi^T)\{\mathbf{I} + (z^{-1}\mathbf{I} - \Phi^T)^{-1}\mathbf{Q}_1(z\mathbf{I} - \Phi)^{-1}\Gamma\mathbf{Q}_2^{-1}\Gamma^T\}\} = 0.$$

To simplify the notation, we note that $\det(z\mathbf{I} - \Phi) = a(z)$, the plant characteristic polynomial, and $\det(z^{-1}\mathbf{I} - \Phi^T) = a(z^{-1})$. Thus, using the fact that $\det \mathbf{A}\mathbf{B} = \det \mathbf{A} \det \mathbf{B}$, we find that the Hamiltonian characteristic equation is

$$a(z)a(z^{-1})\det\{\mathbf{I} + \rho(z^{-1}\mathbf{I} - \Phi^T)^{-1}\mathbf{H}^T\mathbf{H}(z\mathbf{I} - \Phi)^{-1}\overline{\Gamma\Gamma}^T\} = 0. \quad (9.38)$$

where $\mathbf{Q}_1 = \rho\mathbf{H}^T\mathbf{H}$ and $\Gamma\mathbf{Q}_2^{-1}\Gamma^T = \overline{\Gamma\Gamma}^T$. Now we use the result (Eq. C.3) from Appendix C for the determinant of a sum of \mathbf{I} and a matrix product $\mathbf{A}\mathbf{B}$, choosing $\mathbf{A} = (z^{-1}\mathbf{I} - \Phi^T)^{-1}\mathbf{H}^T$ to write

$$a(z)a(z^{-1})\det[1 + \rho\mathbf{H}(z\mathbf{I} - \Phi)^{-1}\overline{\Gamma\Gamma}^T(z^{-1}\mathbf{I} - \Phi^T)^{-1}\mathbf{H}^T] = 0. \quad (9.39)$$

If we replace z by z^{-1} in Eq. (9.39), the result is unchanged because $\det A^T = \det A$. Therefore, if z_i is a characteristic root of the optimal system, so is the reciprocal z_i^{-1} , and the desired relationship has been established.

These $2n$ roots are those of the coupled \mathbf{x} , \mathbf{A} system described by Eq. (9.33), which describes the solution of the time-varying gain case. But the time-varying gain solution includes the portion where the gains are constant. Furthermore, during the constant-gain portion, the system can be described by Eq. (9.16) with

$$\mathbf{u}(k) = -\mathbf{K}_\infty \mathbf{x}(k),$$

and the roots of this simplified n th order description must be n of the $2n$ roots of Eq. (9.33). But which ones are they? The answer must be the n stable ones, because if any unstable roots were included, the value of \mathcal{J} would be approaching infinity and would be far from optimal.

Therefore we see that once the roots of Eq. (9.33) are found, the n stable ones are the roots of the optimal *constant-gain* case.

9.3.2 Symmetric Root Locus

An interesting special case of Eq. (9.39) occurs for SISO systems. In this case, the cost function \mathcal{J} can be written as $\mathcal{J} = \rho y^2 + u^2$ where $y = \mathbf{H}\mathbf{x}$ and \mathbf{Q}_2 was set equal to 1. Therefore, $\bar{\mathbf{\Gamma}} = \mathbf{\Gamma}$ and we see that $\mathbf{H}(z\mathbf{I} - \mathbf{\Phi})^{-1}\mathbf{\Gamma}$ is the plant transfer function $G(z)$. Eq. (9.39) reduces to

$$1 + \rho G(z^{-1})G(z) = 0, \quad (9.40)$$

and is the characteristic equation for SISO optimal control. It is an equation in root-locus form with respect to ρ , the parameter that reflects the relative weighting on output error y and control u . If ρ is small, the optimal roots are near the poles of the plant (or the stable reflections of the poles if $G(z)$ is unstable), and as ρ gets large, the roots go toward the zeros of $G(z^{-1})G(z)$, which are inside the unit circle.

Symmetric Root Locus for Satellite Attitude Control

Example 9.4

Draw the symmetric root locus for the satellite attitude-control problem in Example 4.11 for $T = 1.4$ sec. Comment on the damping of the optimal controller vs. ρ .

Solution. The discrete transfer function from Example 4.11 is

$$G(z) = \frac{(z+1)}{(z-1)^2}.$$

Replacing all the z 's with z^{-1} and multiplying top and bottom by z^2 results in

$$G(z^{-1}) = \frac{z(z+1)}{(z-1)^2}.$$

Therefore, the locus of optimal root locations versus the parameter ρ is determined by substituting the two G 's into Eq. (9.40) to arrive at

$$1 + \rho \frac{z(z+1)^2}{(z-1)^4} = 0.$$

The locus is drawn in Fig. 9.4. Note how the stable locus segments start from the open-loop poles and terminate at the zeros. Also note that, for each stable root, there is an unstable one that is its reciprocal.

The optimal damping ratio for *any* ρ is $\zeta \cong 0.7$. Designers have always known that picking $\zeta \cong 0.7$ produced a good compromise between speed of response, overshoot, and use of control; it also turns out, for this example, to be the *optimal* solution. This result makes sense because the optimal formulation is attempting to do the same thing that designers have always tried to do, that is, find the roots that achieve a good balance between the output error and the use of control.

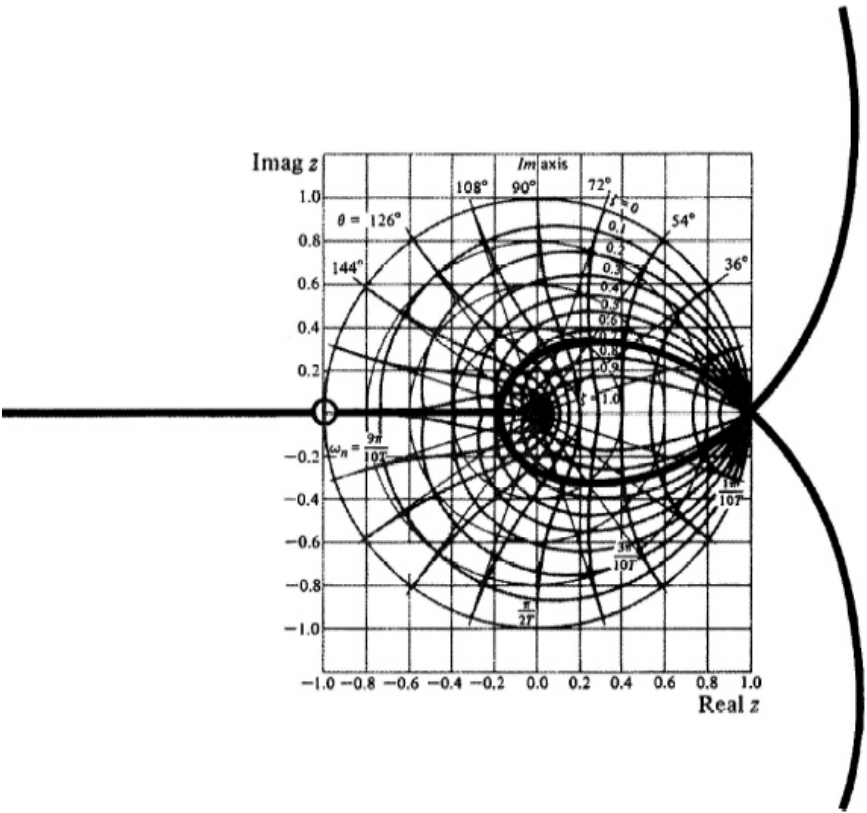


Figure 9.4
Symmetric root locus of Example 9.4

9.3.3 Eigenvector Decomposition

Now let us return to the optimal constant-gain solution for the general case. We can solve Eq. (9.33) by transforming to a new state that has a diagonal system matrix, and from this solution we can obtain the steady-state optimal control. Just as before, the eigenvalues of this matrix are such that the reciprocal of every eigenvalue is also an eigenvalue. Therefore, half the roots of the characteristic equation must be inside the unit circle and half must be outside. In this case, therefore, \mathcal{H}_c can be diagonalized to the form⁴

$$\mathcal{H}_c^* = \begin{bmatrix} \mathbf{E}^{-1} & \mathbf{0} \\ \mathbf{0} & \mathbf{E} \end{bmatrix},$$

where \mathbf{E} is a diagonal matrix of the unstable roots ($|z| > 1$) and \mathbf{E}^{-1} is a diagonal matrix of the stable roots ($|z| < 1$). \mathcal{H}_c^* is obtained by the similarity transformation

$$\mathcal{H}_c^* = \mathbf{W}^{-1} \mathcal{H}_c \mathbf{W},$$

where \mathbf{W} is the matrix of eigenvectors of \mathcal{H}_c and can be written in block form as

$$\mathbf{W} = \begin{bmatrix} \mathbf{X}_I & \mathbf{X}_0 \\ \mathbf{\Lambda}_I & \mathbf{\Lambda}_0 \end{bmatrix},$$

where

$$\begin{bmatrix} \mathbf{X}_0 \\ \mathbf{\Lambda}_0 \end{bmatrix}$$

is the matrix of eigenvectors associated with the eigenvalues (roots) outside the unit circle and

$$\begin{bmatrix} \mathbf{X}_I \\ \mathbf{\Lambda}_I \end{bmatrix}$$

is the matrix of eigenvectors associated with the eigenvalues of \mathcal{H}_c that are inside the unit circle.

This same transformation matrix, \mathbf{W} , can be used to transform \mathbf{x} and $\mathbf{\Lambda}$ to the normal modes of the system, that is,

$$\begin{bmatrix} \mathbf{x}^* \\ \mathbf{\Lambda}^* \end{bmatrix} = \mathbf{W}^{-1} \begin{bmatrix} \mathbf{x} \\ \mathbf{\Lambda} \end{bmatrix},$$

where \mathbf{x}^* and $\mathbf{\Lambda}^*$ are the normal modes. Conversely, we also have

$$\begin{bmatrix} \mathbf{x} \\ \mathbf{\Lambda} \end{bmatrix} = \mathbf{W} \begin{bmatrix} \mathbf{x}^* \\ \mathbf{\Lambda}^* \end{bmatrix} = \begin{bmatrix} \mathbf{X}_I & \mathbf{X}_0 \\ \mathbf{\Lambda}_I & \mathbf{\Lambda}_0 \end{bmatrix} \begin{bmatrix} \mathbf{x}^* \\ \mathbf{\Lambda}^* \end{bmatrix}. \quad (9.41)$$

The solution to the coupled set of difference equations Eq. (9.33) can be simply stated in terms of the initial and final conditions and the normal modes, because the solution for the normal modes is given by

$$\begin{bmatrix} \mathbf{x}^* \\ \mathbf{\Lambda}^* \end{bmatrix}_N = \begin{bmatrix} \mathbf{E}^{-N} & \mathbf{0} \\ \mathbf{0} & \mathbf{E}^N \end{bmatrix} \begin{bmatrix} \mathbf{x}^* \\ \mathbf{\Lambda}^* \end{bmatrix}_0. \quad (9.42)$$

To obtain the steady state, we let N go to infinity; therefore $\mathbf{x}^*(N)$ goes to zero and, in general, $\mathbf{\Lambda}^*(N)$ would go to infinity because each element of \mathbf{E} is greater than one. So we see that the only sensible solution for the steady-state ($N \rightarrow \infty$) case is for $\mathbf{\Lambda}^*(0) = \mathbf{0}$ and therefore $\mathbf{\Lambda}^*(k) = \mathbf{0}$ for all k .⁵

From Eqs. (9.41) and (9.42) with $\mathbf{\Lambda}^*(k) \equiv \mathbf{0}$, we have

$$\mathbf{x}(k) = \mathbf{X}_I \mathbf{x}^*(k) = \mathbf{X}_I \mathbf{E}^{-k} \mathbf{x}^*(0), \quad (9.43)$$

$$\mathbf{\Lambda}(k) = \mathbf{\Lambda}_I \mathbf{x}^*(k) = \mathbf{\Lambda}_I \mathbf{E}^{-k} \mathbf{x}^*(0). \quad (9.44)$$

⁴In rare cases, \mathcal{H}_c will have repeated roots and cannot be made diagonal by a change of variables. In those cases, a small change in \mathbf{Q}_1 or \mathbf{Q}_2 will remove the problem, or else we must compute the Jordan form for \mathcal{H}_c^* [see Strang (1976)].

⁵From Eq. (9.41) we see that if $\mathbf{\Lambda}^*$ is not zero then the state \mathbf{x} will grow in time and the system will be unstable. However, if the system is controllable we know that a control exists which will make the system stable and give a finite value to \mathcal{J} . Because we have the optimal control in Eq. (9.33), it must follow that the optimal system is stable and $\mathbf{\Lambda}^* \equiv \mathbf{0}$ if \mathbf{Q}_1 is such that all the states affect \mathcal{J} .

Therefore Eq. (9.43) leads to

$$\mathbf{x}^*(0) = \mathbf{E}^k \mathbf{X}_I^{-1} \mathbf{x}(k). \quad (9.45)$$

Thus, from Eqs. (9.44) and (9.45)

$$\mathbf{\Lambda}(k) = \mathbf{\Lambda}_I \mathbf{X}_I^{-1} \mathbf{x}(k) = \mathbf{S}_\infty \mathbf{x}(k),$$

which is the same form as our assumption Eq. (9.20) for the sweep method, so we conclude that

$$\mathbf{S}_\infty = \mathbf{\Lambda}_I \mathbf{X}_I^{-1} \quad (9.46)$$

is the steady-state solution to (9.23), and that the control law for this system corresponding to \mathcal{J} with $N \rightarrow \infty$ is

$$\mathbf{u}(k) = -\mathbf{K}_\infty \mathbf{x}(k), \quad (9.47)$$

where, from Eqs. (9.46) and (9.28),

$$\mathbf{K}_\infty = (\mathbf{Q}_2 + \mathbf{\Gamma}^T \mathbf{S}_\infty \mathbf{\Gamma})^{-1} \mathbf{\Gamma}^T \mathbf{S}_\infty \mathbf{\Phi}. \quad (9.48)$$

Furthermore, from Eq. (9.31), the cost associated with using this control law is

$$\mathcal{J}_\infty = \frac{1}{2} \mathbf{x}^T(0) \mathbf{S}_\infty \mathbf{x}(0).$$

In summary, the complete computational procedure is:

1. Compute eigenvalues of the system matrix \mathcal{H}_c defined by Eq. (9.34).
2. Compute eigenvectors associated with the stable ($|z| < 1$) eigenvalues of \mathcal{H}_c and call them

$$\begin{bmatrix} \mathbf{X}_I \\ \mathbf{\Lambda}_I \end{bmatrix}.$$

3. Compute control gain \mathbf{K}_∞ from Eq. (9.48) with \mathbf{S}_∞ given by Eq. (9.46).

We have already seen that the stable eigenvalues from Step 1 above are the resulting system closed-loop roots with constant gain \mathbf{K}_∞ from Step 3. We can also show that the matrix \mathbf{X}_I of Eq. (9.41) is the matrix of eigenvectors of the optimal steady-state closed-loop system.

Most software packages (see MATLAB's `d1qr.m` for the discrete case as developed here or `lqr.m` for the continuous case) use algorithms for these calculations that are closely related to the procedure above. In some cases the software gives the user a choice of the particular method to be used in the solution. Although it is possible to find the LQR gain \mathbf{K}_∞ for a SISO system by picking optimal roots from a symmetric root locus and then using Ackermann's formula, it is easier to use the general `lqr` routines in MATLAB for either SISO or MIMO systems. If a locus of the optimal roots is desired, `d1qr.m` can be used repetitively for varying values of elements in \mathbf{Q}_1 or \mathbf{Q}_2 .

Optimal Root Locus for the Double Mass-Spring System

Example 9.5

Examine the optimal locus for the double mass-spring system of Appendix A.4 and comment on the relative merits of this approach vs. the pole-placement approach used in Example 8.3 for this system.

Solution. Using the same model and sample period as in Example 8.3, we find values for $\mathbf{\Phi}, \mathbf{\Gamma}$ which are then used with `d1qr.m` to solve for the closed-loop roots for various values of the weighting matrix \mathbf{Q}_1 . Because the output d is the only quantity of interest, it makes sense to use weighting on that state element only, that is

$$\mathbf{Q}_1 = \begin{bmatrix} q_{11} & 0 & 0 & 0 \\ 0 & 0 & 0 & 0 \\ 0 & 0 & 0 & 0 \\ 0 & 0 & 0 & 0 \end{bmatrix},$$

and \mathbf{Q}_2 is arbitrarily selected to be 1. The locus is determined by varying the value of q_{11} . The MATLAB script

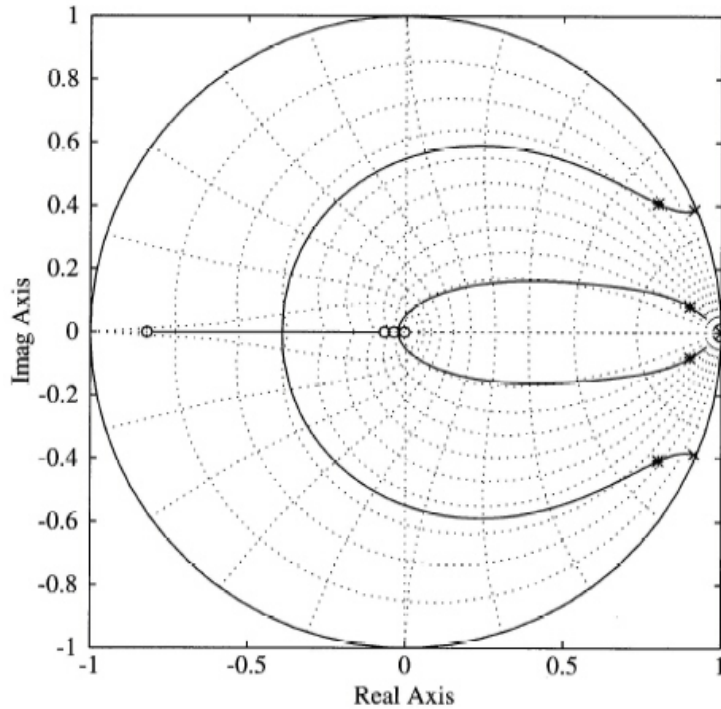


Figure 9.5
Locus of optimal
roots of Example
9.5

```

q = logspace(-3,9,300);   Q2=1
for i=1:100
    Q1=diag([q(i);0;0;0]);
    [k,s,e]=dlqr(phi,gam,Q1,Q2);
end

```

produced a series of values of the closed-loop system roots (e above) which were plotted on the z -plane in Fig. 9.5. Note that the roots selected in Example 8.3 that gave the best results lie at the points marked by stars on the stable portion of the locus. So we see that the optimal solution provides guidance on where to pick the oscillatory poles. In fact, the results from this design led to the selection of the pole locations for the second case in Example 8.3 that yielded the superior response.

9.3.4 Cost Equivalents

It is sometimes useful to be able to find the discrete cost function defined by Eq. (9.11), which is the equivalent to an analog cost function of the form

$$\mathcal{J}_c = \frac{1}{2} \int_0^{NT} (\mathbf{x}^T \mathbf{Q}_{c1} \mathbf{x} + \mathbf{u}^T \mathbf{Q}_{c2} \mathbf{u}) d\tau. \quad (9.49)$$

Having this equivalence relationship will allow us to compute the \mathcal{J}_c of two discrete designs implemented with different sample periods and, therefore, will provide a fair basis for comparison. It will also provide a method for finding a discrete implementation of an optimal, continuous design—an “optimal” version of the emulation design method discussed in Section 7.2. In this section, we will develop the cost equivalence, and the use of it for an emulation design will be discussed in Section 9.3.5.

The integration of the cost in Eq. (9.49) can be broken into sample periods according to

$$\mathcal{J}_c = \sum_{k=0}^{N-1} \frac{1}{2} \int_{kT}^{(k+1)T} (\mathbf{x}^T \mathbf{Q}_{c1} \mathbf{x} + \mathbf{u}^T \mathbf{Q}_{c2} \mathbf{u}) d\tau, \quad (9.50)$$

and because

$$\mathbf{x}(kT + \tau) = \mathbf{\Phi}(\tau) \mathbf{x}(kT) + \mathbf{\Gamma}(\tau) \mathbf{u}(kT), \quad (9.51)$$

where

$$\mathbf{\Phi}(\tau) = e^{\mathbf{F}\tau} \quad \mathbf{\Gamma}(\tau) = \int_0^\tau e^{\mathbf{F}\eta} d\eta \mathbf{G}$$

as indicated by Eq. (4.58), substitution of Eq. (9.51) into (9.50) yields

$$\mathcal{J}_c = \frac{1}{2} \sum_{k=0}^{N-1} [(\mathbf{x}^T(k) \mathbf{u}^T(k)) \begin{bmatrix} \mathbf{Q}_{11} & \mathbf{Q}_{12} \\ \mathbf{Q}_{21} & \mathbf{Q}_{22} \end{bmatrix} \begin{bmatrix} \mathbf{x}(k) \\ \mathbf{u}(k) \end{bmatrix}], \quad (9.52)$$

where

$$\begin{bmatrix} \mathbf{Q}_{11} & \mathbf{Q}_{12} \\ \mathbf{Q}_{21} & \mathbf{Q}_{22} \end{bmatrix} = \int_0^T \begin{bmatrix} \mathbf{\Phi}^T(\tau) & \mathbf{0} \\ \mathbf{\Gamma}^T(\tau) & \mathbf{I} \end{bmatrix} \begin{bmatrix} \mathbf{Q}_{c1} & \mathbf{0} \\ \mathbf{0} & \mathbf{Q}_{c2} \end{bmatrix} \begin{bmatrix} \mathbf{\Phi}(\tau) & \mathbf{\Gamma}(\tau) \\ \mathbf{0} & \mathbf{I} \end{bmatrix} d\tau. \quad (9.53)$$

Equation (9.53) is a relationship for the desired equivalent, discrete weighting matrices; however, we see that a complication has arisen in that there are now cross terms that weight the product of \mathbf{x} and \mathbf{u} . This can be circumvented by transforming the control to include a linear combination of the state, as we will show below; however, it is also possible to formulate the LQR solution so that it can account for the cross terms.

A method for computing the equivalent gains in Eq. (9.53), due to Van Loan (1978), is to form the matrix exponential⁶

$$\exp \begin{bmatrix} -\mathbf{F}^T & \mathbf{0} & \mathbf{Q}_{c1} & \mathbf{0} \\ -\mathbf{G}^T & \mathbf{0} & \mathbf{0} & \mathbf{Q}_{c2} \\ \mathbf{0} & \mathbf{0} & \mathbf{F} & \mathbf{G} \\ \mathbf{0} & \mathbf{0} & \mathbf{0} & \mathbf{0} \end{bmatrix} T \cong \begin{bmatrix} \mathbf{\Phi}_{11} & \mathbf{\Phi}_{12} \\ \mathbf{0} & \mathbf{\Phi}_{22} \end{bmatrix}. \quad (9.54)$$

It will turn out that

$$\mathbf{\Phi}_{22} = \begin{bmatrix} \mathbf{\Phi} & \mathbf{\Gamma} \\ \mathbf{0} & \mathbf{I} \end{bmatrix}$$

$$\mathbf{\Phi}_{11}^{-1} = \mathbf{\Phi}_{22}^T;$$

however, one needs to calculate the matrix exponential Eq. (9.54) in order to find $\mathbf{\Phi}_{12}$. Because

$$\mathbf{\Phi}_{12} = \mathbf{\Phi}_{11} \begin{bmatrix} \mathbf{Q}_{11} & \mathbf{Q}_{12} \\ \mathbf{Q}_{21} & \mathbf{Q}_{22} \end{bmatrix},$$

we have the desired result

$$\begin{bmatrix} \mathbf{Q}_{11} & \mathbf{Q}_{12} \\ \mathbf{Q}_{21} & \mathbf{Q}_{22} \end{bmatrix} = \mathbf{\Phi}_{22}^T \mathbf{\Phi}_{12}. \quad (9.55)$$

Routines to calculate the discrete equivalent of a continuous cost are available in some of the CAD control design packages (see `jdequiv.m` in the Digital Control Toolbox). Furthermore, MATLAB has an LQR routine (called `lqrd.m`) that finds the discrete controller for a continuous cost and computes the necessary discrete cost in the process.

In summary, the continuous cost function \mathcal{J}_c in Eq. (9.49) can be computed from discrete samples of the state and control by transforming the continuous weighting matrices, \mathbf{Q}_c 's, according to Eq. (9.55). The resulting discrete weighting matrices include cross terms that weight the product of \mathbf{x} and \mathbf{u} . The ability to compute the continuous cost from discrete samples of the state and control is useful for comparing digital controllers of a system with different sample rates and will also be useful in the emulation design method in the next section.

⁶Note that superscript ()^T denotes transpose, whereas the entire matrix is multiplied by the sample period, T .

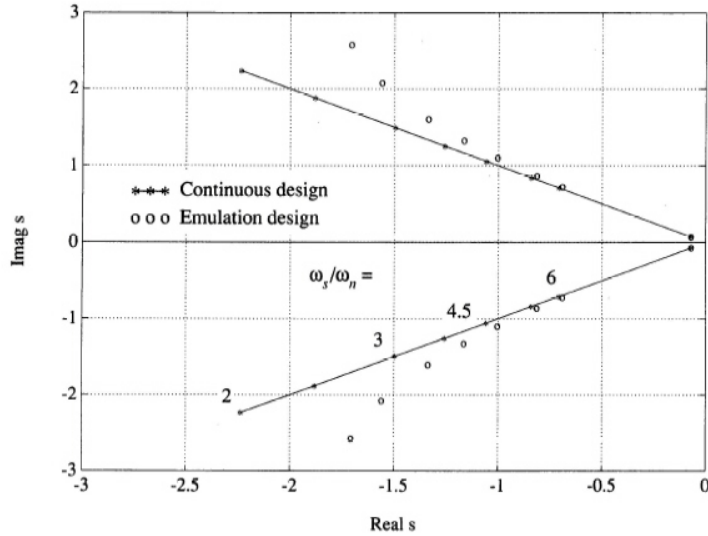


Figure 9.6
Degrations of s -plane root location for the optimal emulation method, Example 9.6

9.3.5 Emulation by Equivalent Cost

The emulation design method discussed in Section 7.2 took the approach that the design of the compensation be done in the continuous domain and the resulting $D(s)$ then be approximated using the digital filtering ideas of Chapter 6. This same approach can be applied when using optimal design methods [see Parsons (1982)]. First, an optimal design iteration is carried out in the continuous domain until the desired specifications are met. The discrete approximation is then obtained by calculating the discrete equivalent of the continuous cost function via Eq. (9.55), and then using that cost in the discrete LQR computation of Table 9.1, with modifications to account for the cross terms in the weighting matrices. These steps are all accomplished by MATLAB's `lqrd.m`.

Design by Equivalent Cost

Example 9.6

Examine the accuracy of the equivalent cost emulation method for the satellite attitude control example.

Solution. The continuous representation of the system is specified by \mathbf{F} and \mathbf{G} from Eq. (4.47). Use of a continuous LQR calculation (`lqr.m` in MATLAB) with

$$\mathbf{Q}_{c1} = \begin{bmatrix} 1 & 0 \\ 0 & 0 \end{bmatrix}$$

and

$$\mathbf{Q}_{c2} = [10000, 1, 0.5, 0.2, 0.1, 0.05, 0.02, 0.01]$$

results in s -plane roots exactly at $\zeta = 0.7$ as shown by the line in Fig. 9.6. Use of the `lqrd.m` function computes the discrete controller that minimizes the same continuous cost, thus arriving at an emulation of the continuous design. The equivalent s -plane roots of these digital controllers are also plotted in Fig. 9.6. The figure shows that very little change in root locations occur by this emulation method. In fact the change in root locations is about 1% when sampling at six times the closed-loop natural frequency ($\omega_s/\omega_n = 6$) and increases to about 10% for $\omega_s/\omega_n = 3$. The accuracy of the zero-pole mapping emulation method was evaluated in Example 7.3; its calculations for a similar example showed that $\omega_s/\omega_n = 30$ resulted in a 10% change in root location, and $\omega_s/\omega_n = 6$ resulted in a 60% reduction in damping.

In general, use of the optimal emulation method will result in a digital controller whose performance will match the continuous design much closer than any of the emulation design methods

discussed in Section 7.2 and Chapter 6. A requirement to use the method, however, is that the original continuous design be done using optimal methods so that the continuous weighting matrices \mathbf{Q}_{c1} and \mathbf{Q}_{c2} are available for the conversion because they are the parameters that define the design.

As discussed in Chapter 7, emulation design is attractive because it allows for the design process to be carried out before specifying the sample rate. Sampling degrades the performance of any system to varying degrees, and it is satisfying to be able to answer how good the control system can be in terms of disturbance rejection, steady-state errors, and so on, before the sampling degradation is introduced. Once the characteristics of a reasonable continuous design are known, the designer is better equipped to select a sample rate with full knowledge of how that selection will affect performance. emulation advantages

We acknowledge that the scenario just presented is not the reality of the typical digital design process. Usually, due to the pressure of schedules, the computer and sample rate are specified long before the controls engineers have a firm grasp on the controller algorithm. Given that reality, the most expedient path is to perform the design directly in the discrete domain and obtain the best possible with that constraint. Furthermore, many design exercises are relatively minor modifications to previous designs. In these cases, too, the most expedient path is to work directly in the discrete domain.

But we maintain that the most desirable design scenario is to gain knowledge of the effects of sampling by first performing the design in the continuous domain, then performing discrete designs. In this case, the emulation method described here is a useful tool to obtain quickly a controller to be implemented digitally or to use as a basis for further refinement in the discrete domain.

9.4 Optimal Estimation

Optimal estimation methods are attractive because they handle multi-output systems easily and allow a designer quickly to determine many good candidate designs of the estimator gain matrix, \mathbf{L} . We will first develop the least squares estimation solution for the static case as it is the basis for optimal estimation, then we will extend that to the time-varying optimal estimation solution (commonly known as the “Kalman filter”), and finally show the correspondence between the Kalman filter and the time-varying optimal control solution. Following the same route that we did for the optimal control solution, we will then develop the optimal estimation solution with a steady-state \mathbf{L} -matrix. In the end, this amounts to another method of computing the \mathbf{L} -matrix in the equations for the current estimator, Eqs. (8.33) and (8.34), which are

$$\hat{\mathbf{x}}(k) = \bar{\mathbf{x}}(k) + \mathbf{L}(y(k) - \bar{y}(k)), \quad (9.56)$$

where

$$\bar{\mathbf{x}}(k+1) = \Phi\hat{\mathbf{x}}(k) + \Gamma\mathbf{u}(k);$$

however, now \mathbf{L} will be based on minimizing estimation errors rather than picking dynamic characteristics of the estimator error equation.

9.4.1 Least-Squares Estimation

Suppose we have a linear static process given by

$$\mathbf{y} = \mathbf{H}\mathbf{x} + \mathbf{v}, \quad (9.57)$$

where \mathbf{y} is a $p \times 1$ measurement vector, \mathbf{x} is an $n \times 1$ unknown vector, \mathbf{v} is a $p \times 1$ measurement error vector, and \mathbf{H} is the matrix relating the measurements to the unknowns. We want to determine the best estimate of \mathbf{x} given the measurements \mathbf{y} . Often, the system is overdetermined; that is, there are more measurements in \mathbf{y} than the unknown vector, \mathbf{x} . A good way to find the best estimate of \mathbf{x} is to minimize the sum of the squares of \mathbf{v} , the fit error. This is called the **least squares** solution. This is both sensible and very convenient analytically. Proceeding, the sum of squares can be written as

$$\mathcal{J} = \frac{1}{2}\mathbf{v}^T\mathbf{v} = \frac{1}{2}(\mathbf{y} - \mathbf{H}\mathbf{x})^T(\mathbf{y} - \mathbf{H}\mathbf{x}) \quad (9.58)$$

and, in order to minimize this expression, we take the derivative with respect to the unknown, that is

$$\frac{\partial \mathcal{J}}{\partial \mathbf{x}} = (\mathbf{y} - \mathbf{H}\mathbf{x})^T (-\mathbf{H}) = 0 \quad (9.59)$$

which results in

$$\mathbf{H}^T \mathbf{y} = \mathbf{H}^T \mathbf{H} \mathbf{x},$$

so that

$$\hat{\mathbf{x}} = [\mathbf{H}^T \mathbf{H}]^{-1} \mathbf{H}^T \mathbf{y} \quad (9.60) \quad \text{least squares estimate}$$

where $\hat{\mathbf{x}}$ designates the “best estimate” of \mathbf{x} . Note that the matrix to be inverted is $n \times n$ and that p must be $\geq n$ for it to be full rank and the inverse to exist. If there are fewer measurements than unknowns ($p < n$), there are too few measurements to determine a unique value of \mathbf{x} .

The difference between the estimate and the actual value of \mathbf{x} is

$$\begin{aligned} \hat{\mathbf{x}} - \mathbf{x} &= [\mathbf{H}^T \mathbf{H}]^{-1} \mathbf{H}^T (\mathbf{H}\mathbf{x} + \mathbf{v}) - \mathbf{x} \\ &= [\mathbf{H}^T \mathbf{H}]^{-1} \mathbf{H}^T \mathbf{v}. \end{aligned} \quad (9.61)$$

Equation (9.61) shows that, if \mathbf{v} has zero mean, the error in the estimate, $\hat{\mathbf{x}} - \mathbf{x}$, will also be zero mean, sometimes referred to as an **unbiased estimate**. estimate accuracy

The **covariance** of the estimate error, \mathbf{P} , is defined to be

$$\begin{aligned} \mathbf{P} &= \mathcal{E}\{(\hat{\mathbf{x}} - \mathbf{x})(\hat{\mathbf{x}} - \mathbf{x})^T\} \\ &= \mathcal{E}\{(\mathbf{H}^T \mathbf{H})^{-1} \mathbf{H}^T \mathbf{v} \mathbf{v}^T \mathbf{H} (\mathbf{H}^T \mathbf{H})^{-1}\} \\ &= (\mathbf{H}^T \mathbf{H})^{-1} \mathbf{H}^T \mathcal{E}\{\mathbf{v} \mathbf{v}^T\} \mathbf{H} (\mathbf{H}^T \mathbf{H})^{-1}. \end{aligned} \quad (9.62)$$

If the elements in the noise vector, \mathbf{v} , are uncorrelated with one another, $\mathcal{E}\{\mathbf{v} \mathbf{v}^T\}$ ⁷

is a diagonal matrix, which we shall call \mathbf{R} . Furthermore, if all the elements of \mathbf{v} have the same uncertainty, then all the diagonal elements of \mathbf{R} are identical, and

$$\mathcal{E}\{\mathbf{v} \mathbf{v}^T\} = \mathbf{R} = \mathbf{I} \sigma^2, \quad (9.63)$$

where σ is the rms value of each element in \mathbf{v} . In this case, Eq. (9.62) can be written as

$$\mathbf{P} = (\mathbf{H}^T \mathbf{H})^{-1} \sigma^2 \quad (9.64)$$

and is a measure of how well we can estimate the unknown \mathbf{x} . The square root of the diagonal elements of \mathbf{P} represent the rms values of the errors in each element in \mathbf{x} .

Least-Squares Fit

Example 9.7

The monthly sales (in thousands \$) for the first year of the Mewisham Co. are given by

$$\mathbf{y}^T = [0.2 \ 0.5 \ 1.1 \ 1.2 \ 1.1 \ 1.3 \ 1.1 \ 1.2 \ 2.0 \ 1.2 \ 2.2 \ 4.0].$$

Find the least-squares fit parabola to this data and use that to predict what the monthly sales will be during the second year. Also state what the predicted accuracy of the parabolic coefficients are, assuming that the rms accuracy of the data is \$700.

Solution. The solution is obtained using Eq. (9.60), where \mathbf{H} contains the parabolic function to be fit. Each month’s sales obeys

$$y_i = a_0 + a_1 t_i + a_2 t_i^2 + v_i,$$

so that, in vector form

$$\begin{bmatrix} y_1 \\ y_2 \\ y_3 \\ \vdots \end{bmatrix} = \begin{bmatrix} 1 & t_1 & t_1^2 \\ 1 & t_2 & t_2^2 \\ 1 & t_3 & t_3^2 \\ \vdots & \vdots & \vdots \end{bmatrix} \begin{bmatrix} a_0 \\ a_1 \\ a_2 \end{bmatrix} + \begin{bmatrix} v_1 \\ v_2 \\ v_3 \\ \vdots \end{bmatrix},$$

⁷ \mathcal{E} is called the **expectation** and effectively means the average of the quantity in { }.

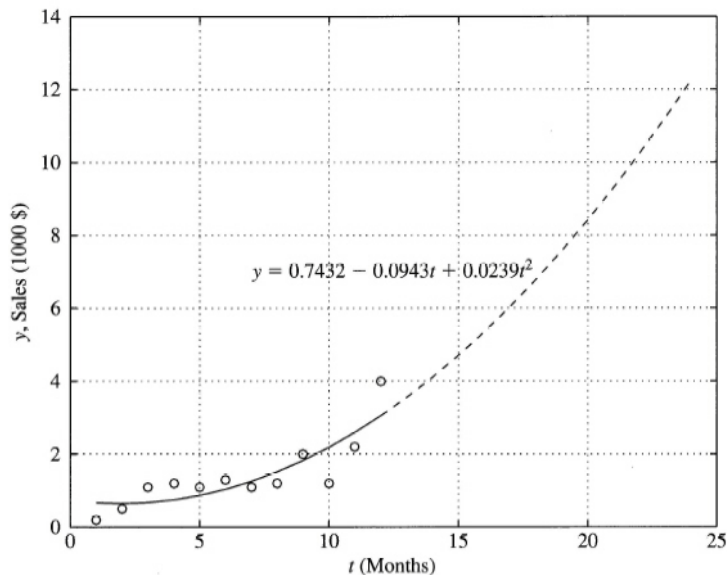


Figure 9.7
Least-squares fit
of parabola to
data in Example
9.7

and we see that

$$\mathbf{H} = \begin{bmatrix} 1 & t_1 & t_1^2 \\ 1 & t_2 & t_2^2 \\ 1 & t_3 & t_3^2 \\ \vdots & \vdots & \vdots \end{bmatrix} \quad t_i = i, \quad i = 1, 12$$

and

$$\mathbf{x} = \begin{bmatrix} a_0 \\ a_1 \\ a_2 \end{bmatrix}.$$

Evaluation of Eq. (9.60) produces an estimate of \mathbf{x}

$$\hat{\mathbf{x}} = \begin{bmatrix} 0.7432 \\ -0.0943 \\ 0.0239 \end{bmatrix}$$

which is used to plot the “best fit” parabola along with the raw data in Fig. 9.7. The data used to determine the parabola only occurred during the first 12 months, after that the parabola is an extrapolation.

Equation (9.64), with \mathbf{H} as above and $\sigma^2 = 0.49$ (σ was given to be 0.7), shows that

$$\mathbf{P} = \begin{bmatrix} 0.5234 & -0.1670 & 0.0111 \\ -0.1670 & 0.0655 & -0.0048 \\ 0.0111 & -0.0048 & 0.0004 \end{bmatrix},$$

which means that the rms accuracy of the coefficients are

$$\sigma_{a_0} = \sqrt{0.5234} = 0.7235$$

$$\sigma_{a_1} = \sqrt{0.0655} = 0.2559$$

$$\sigma_{a_2} = \sqrt{0.0004} = 0.0192.$$

Weighted Least Squares

In many cases, we know *a priori* that some measurements are more accurate than others so that all the diagonal elements in \mathbf{R} are *not* the same. In this case, it makes sense to weight the measurement errors higher for those measurements known to be more accurate because that will cause those measurements to have a bigger influence on the cost minimization. In other words, the cost function in Eq. (9.58) needs to be modified to

$$\mathcal{J} = \frac{1}{2} \mathbf{v}^T \mathbf{W} \mathbf{v}, \quad (9.65)$$

where \mathbf{W} is a diagonal weighting matrix whose elements are in some way inversely related to the uncertainty of the corresponding element of \mathbf{v} . Performing the same algebra as for the unweighted case above, we find that the best **weighted least squares** solution is given by

$$\hat{\mathbf{x}} = [\mathbf{H}^T \mathbf{W} \mathbf{H}]^{-1} \mathbf{H}^T \mathbf{W} \mathbf{y}. \quad (9.66)$$

The covariance of this estimate also directly follows the development of Eq. (9.62) and results in

$$\mathbf{P} = (\mathbf{H}^T \mathbf{W} \mathbf{H})^{-1} \mathbf{H}^T \mathbf{W} \mathcal{E}\{\mathbf{v} \mathbf{v}^T\} \mathbf{W} \mathbf{H} (\mathbf{H}^T \mathbf{W} \mathbf{H})^{-1}. \quad (9.67)$$

A logical choice for \mathbf{W} is to let it be inversely proportional to \mathbf{R} , thus weighting the square of the measurement errors exactly in proportion to the inverse of their *a priori* mean square error, that is, let

$$\mathbf{W} = \mathbf{R}^{-1}, \quad (9.68)$$

This choice of weighting matrix is proven in Section 12.7 to minimize the trace of \mathbf{P} and is called the **best linear unbiased estimate**. With this choice, Eq. (9.66) becomes

$$\hat{\mathbf{x}} = [\mathbf{H}^T \mathbf{R}^{-1} \mathbf{H}]^{-1} \mathbf{H}^T \mathbf{R}^{-1} \mathbf{y}, \quad (9.69)$$

and Eq. (9.67) reduces to

$$\mathbf{P} = (\mathbf{H}^T \mathbf{R}^{-1} \mathbf{H})^{-1}. \quad (9.70)$$

Recursive Least Squares

The two least-squares algorithms above, Eqs. (9.60) and (9.69), are both **batch** algorithms in that all the data is obtained and then processed in one calculation. For an estimation problem that runs for a long time, the measurement vector would become very large, and one would have to wait until the problem was complete in order to calculate the estimate. The recursive formulation solves both these difficulties by performing the calculation in small time steps. The ideas are precisely the same, that is, a weighted least squares calculation is being performed. But now we break the problem into old data, for which we already found $\hat{\mathbf{x}}$, and new data, for which we want a correction to $\hat{\mathbf{x}}$, so that the overall new $\hat{\mathbf{x}}$, is adjusted for the newly acquired data.

The problem is stated as

$$\begin{bmatrix} \mathbf{y}_o \\ \mathbf{y}_n \end{bmatrix} = \begin{bmatrix} \mathbf{H}_o \\ \mathbf{H}_n \end{bmatrix} \mathbf{x} + \begin{bmatrix} \mathbf{v}_o \\ \mathbf{v}_n \end{bmatrix}, \quad (9.71)$$

where the subscript o represents old data and n represents new data. The best estimate of \mathbf{x} given all the data follows directly from Eq. (9.69) and can be written as

$$\begin{bmatrix} \mathbf{H}_o \\ \mathbf{H}_n \end{bmatrix}^T \begin{bmatrix} \mathbf{R}_o^{-1} & \mathbf{0} \\ \mathbf{0} & \mathbf{R}_n^{-1} \end{bmatrix} \begin{bmatrix} \mathbf{H}_o \\ \mathbf{H}_n \end{bmatrix} \hat{\mathbf{x}} = \begin{bmatrix} \mathbf{H}_o \\ \mathbf{H}_n \end{bmatrix}^T \begin{bmatrix} \mathbf{R}_o^{-1} & \mathbf{0} \\ \mathbf{0} & \mathbf{R}_n^{-1} \end{bmatrix} \begin{bmatrix} \mathbf{y}_o \\ \mathbf{y}_n \end{bmatrix}, \quad (9.72)$$

where $\hat{\mathbf{x}}$ is the best estimate of \mathbf{x} given all the data, old and new. Let's define $\hat{\mathbf{x}}$ as

$$\hat{\mathbf{x}} = \hat{\mathbf{x}}_o + \delta \hat{\mathbf{x}}, \quad (9.73)$$

where $\hat{\mathbf{x}}_o$ is the best estimate given only the old data, \mathbf{y}_o . We want to find an expression for the correction to this estimate, $\delta \hat{\mathbf{x}}$, given the new data. Since $\hat{\mathbf{x}}_o$ was the best estimate given the old data, it satisfies

$$[\mathbf{H}_o^T \mathbf{R}_o^{-1} \mathbf{H}_o] \hat{\mathbf{x}}_o = \mathbf{H}_o^T \mathbf{R}_o^{-1} \mathbf{y}_o. \quad (9.74)$$

Expanding out the terms in Eq. (9.72) and using Eqs. (9.73) and (9.74) yields

$$\mathbf{H}_n^T \mathbf{R}_n^{-1} \mathbf{H}_n \hat{\mathbf{x}}_o + [\mathbf{H}_o^T \mathbf{R}_o^{-1} \mathbf{H}_o + \mathbf{H}_n^T \mathbf{R}_n^{-1} \mathbf{H}_n] \delta \hat{\mathbf{x}} = \mathbf{H}_n^T \mathbf{R}_n^{-1} \mathbf{y}_n, \quad (9.75)$$

which can be solved for the desired result

$$\delta \hat{\mathbf{x}} = [\mathbf{H}_o^T \mathbf{R}_o^{-1} \mathbf{H}_o + \mathbf{H}_n^T \mathbf{R}_n^{-1} \mathbf{H}_n]^{-1} \mathbf{H}_n^T \mathbf{R}_n^{-1} (\mathbf{y}_n - \mathbf{H}_n \mathbf{x}_o). \quad (9.76)$$

Equation (9.70) defined the covariance of the estimate, and in terms of the old data would be written as

$$\mathbf{P}_o = (\mathbf{H}_o^T \mathbf{R}_o^{-1} \mathbf{H}_o)^{-1}, \quad (9.77)$$

so that Eq. (9.76) reduces to

$$\delta \hat{\mathbf{x}} = [\mathbf{P}_o^{-1} + \mathbf{H}_n^T \mathbf{R}_n^{-1} \mathbf{H}_n]^{-1} \mathbf{H}_n^T \mathbf{R}_n^{-1} (\mathbf{y}_n - \mathbf{H}_n \hat{\mathbf{x}}_o), \quad (9.78)$$

and we see that the correction to the old estimate can be determined if we simply know the old estimate and its covariance. Note that the correction to \mathbf{x} is proportional to the *difference* between the new data \mathbf{y}_n and the estimate of the new data $\mathbf{H}_n \hat{\mathbf{x}}_o$ based on the old \mathbf{x} .

By analogy with the weighted least squares, the covariance of the new estimate is

$$\mathbf{P}_n = [\mathbf{P}_o^{-1} + \mathbf{H}_n^T \mathbf{R}_n^{-1} \mathbf{H}_n]^{-1}. \quad (9.79)$$

Note here that it is no longer necessary for there to be more new measurements than the elements in \mathbf{x} . The only requirement is that \mathbf{P}_n be full rank, which could be satisfied by virtue of \mathbf{P}_o being full rank. In other words, in Example 9.7 it would have been possible to start the process with the first three months of sales, then recursively update the parabolic coefficients using one month's additional sales at a time. In fact, we will see in the Kalman filter that it is typical for the new \mathbf{y} to have fewer elements than \mathbf{x} .

To summarize the procedure, we start by assuming that \mathbf{x}_o and \mathbf{P}_o are available from previous calculations.

recursive least-square procedure

- Compute the new covariance from Eq. (9.79)

$$\mathbf{P}_n = [\mathbf{P}_o^{-1} + \mathbf{H}_n^T \mathbf{R}_n^{-1} \mathbf{H}_n]^{-1}.$$

- Compute the new value of $\hat{\mathbf{x}}$ using Eqs. (9.73), (9.78), and (9.79)

$$\hat{\mathbf{x}} = \hat{\mathbf{x}}_o + \mathbf{P}_n \mathbf{H}_n^T \mathbf{R}_n^{-1} (\mathbf{y}_n - \mathbf{H}_n \hat{\mathbf{x}}_o). \quad (9.80)$$

- Take new data and repeat the process.

This algorithm assigns relative weighting to the old $\hat{\mathbf{x}}$ vs. new data based on their relative accuracies, similarly to the weighted least squares. For example, if the old data produced an extremely accurate estimate so that \mathbf{P}_o was almost zero, then Eq. (9.79) shows that \mathbf{P}_n is $\cong 0$ and Eq. (9.80) shows that the new estimate will essentially ignore the new data. On the other hand, if the old estimates are very poor, that is, \mathbf{P}_o is very large, Eq. (9.79) shows that

$$\mathbf{P}_n \cong [\mathbf{H}_n^T \mathbf{R}_n^{-1} \mathbf{H}_n]^{-1},$$

and Eq. (9.80) shows that

$$\hat{\mathbf{x}} \cong [\mathbf{H}_n^T \mathbf{R}_n^{-1} \mathbf{H}_n]^{-1} \mathbf{H}_n^T \mathbf{R}_n^{-1} \mathbf{y}_n,$$

which ignores the old data. Most cases are somewhere between these two extremes, but the fact remains that this recursive-weighted-least-squares algorithm weights the old and new data according to the associated covariance.

9.4.2 The Kalman Filter

Now consider a discrete dynamic plant

$$\mathbf{x}(k+1) = \mathbf{\Phi}\mathbf{x}(k) + \mathbf{\Gamma}\mathbf{u}(k) + \mathbf{\Gamma}_1\mathbf{w}(k) \quad (9.81)$$

with measurements

$$\mathbf{y}(k) = \mathbf{H}\mathbf{x}(k) + \mathbf{v}(k), \quad (9.82)$$

where the **process noise** $\mathbf{w}(k)$ and **measurement noise** $\mathbf{v}(k)$ are random sequences with zero mean, that is

$$\mathcal{E}\{\mathbf{w}(k)\} = \mathcal{E}\{\mathbf{v}(k)\} = \mathbf{0},$$

have no time correlation or are “white” noise, that is

$$\mathcal{E}\{\mathbf{w}(i)\mathbf{w}^T(j)\} = \mathcal{E}\{\mathbf{v}(i)\mathbf{v}^T(j)\} = 0 \quad \text{if } i \neq j,$$

and have covariances or mean square “noise levels” defined by

$$\mathcal{E}\{\mathbf{w}(k)\mathbf{w}^T(k)\} = \mathbf{R}_w, \quad \mathcal{E}\{\mathbf{v}(k)\mathbf{v}^T(k)\} = \mathbf{R}_v.$$

We allow \mathbf{L} in Eq. (9.56) to vary with the time step, and we wish to pick $\mathbf{L}(k)$ so that the estimate of $\mathbf{x}(k)$, given all the data up to and including time k , is optimal.

Let us pretend temporarily that without using the current measurement $\mathbf{y}(k)$, we already have a prior estimate of the state at the time of a measurement, which we will call $\bar{\mathbf{x}}(k)$. The problem at this point is to update this old estimate based on the current new measurement.

Comparing this problem to the recursive least squares, we see that the estimation measurement equation Eq. (9.82) relates the new measurements to \mathbf{x} just as the lower row in Eq. (9.71) does; hence the optimal state estimation solution is given by Eq. (9.80), where \mathbf{x}_o takes the role of $\bar{\mathbf{x}}(k)$, $\mathbf{P}_n = \mathbf{P}(k)$, $\mathbf{H}_n = \mathbf{H}$, and $\mathbf{R}_n = \mathbf{R}_v$. The solution equations are

$$\hat{\mathbf{x}}(k) = \bar{\mathbf{x}}(k) + \mathbf{L}(k)(\mathbf{y}(k) - \mathbf{H}\bar{\mathbf{x}}(k)), \quad (9.83)$$

where,

$$\mathbf{L}(k) = \mathbf{P}(k)\mathbf{H}^T\mathbf{R}_v^{-1}. \quad (9.84)$$

Equation (9.79) is used to find $\mathbf{P}(k)$, where we now call the old covariance $\mathbf{M}(k)$ instead of \mathbf{P}_o , thus

$$\mathbf{P}(k) = [\mathbf{M}^{-1} + \mathbf{H}^T\mathbf{R}_v^{-1}\mathbf{H}]^{-1}. \quad (9.85)$$

The size of the matrix to be inverted in Eq. (9.85) is $n \times n$, where n is the dimension of \mathbf{x} . For the Kalman filter, \mathbf{y} usually has fewer elements than \mathbf{x} , and it is more efficient to use the matrix inversion lemma (See Eq. (C.6) in Appendix C) to convert Eq. (9.85) to

$$\mathbf{P}(k) = \mathbf{M}(k) - \mathbf{M}(k)\mathbf{H}^T(\mathbf{H}\mathbf{M}(k)\mathbf{H}^T + \mathbf{R}_v)^{-1}\mathbf{H}\mathbf{M}(k). \quad (9.86)$$

$\mathbf{M}(k)$ is the covariance (or expected mean square error) of the state estimate, $\bar{\mathbf{x}}(k)$, before the measurement. The state estimate after the measurement, $\hat{\mathbf{x}}(k)$, has an error covariance $\mathbf{P}(k)$.

The idea of combining the previous estimate with the current measurement based on the relative accuracy of the two quantities—the recursive least-squares concept—was the genesis for the relationships in Eq. (9.83) and Eq. (9.85) and is one of the basic ideas of the Kalman filter. The other key idea has to do with using the known dynamics of \mathbf{x} to predict its behavior between samples, an idea that was discussed in the development of the estimator in Chapter 8.

Use of dynamics in the propagation of the estimate of \mathbf{x} between $k-1$ and k did not come up in the static least-squares estimation, but here this issue needs to be addressed. The state estimate at $k-1$, given data up through $k-1$, is called $\hat{\mathbf{x}}(k-1)$, whereas we defined $\bar{\mathbf{x}}(k)$ to be the estimate at k given the same data up through $k-1$. In the static least squares, these two quantities were identical and both called \mathbf{x}_o because it was presumed to be a constant; but here the estimates differ due to the fact that the state will change according to the system dynamics as time passes. Specifically, the

estimate $\bar{\mathbf{x}}(k)$ is found from $\hat{\mathbf{x}}(k-1)$ by using Eq. (9.81) with $\mathbf{w}(k-1) = 0$, because we know that this is the expected value of $\mathbf{x}(k)$ since the expected value of the plant noise, $\mathcal{E}\{\mathbf{w}(k-1)\}$ is zero. Thus

$$\bar{\mathbf{x}}(k) = \Phi \hat{\mathbf{x}}(k-1) + \Gamma \mathbf{u}(k-1). \quad (9.87)$$

The change in estimate from $\hat{\mathbf{x}}(k-1)$ to $\bar{\mathbf{x}}(k)$ is called a “time update,” whereas the change in the estimate from $\bar{\mathbf{x}}(k)$ to $\hat{\mathbf{x}}(k)$ as given by Eq. (9.83) is a “measurement update,” which occurs at the fixed time k but expresses the improvement in the estimate due to the measurement $\mathbf{y}(k)$. The same kind of time and measurement updates apply to the estimate covariances, \mathbf{P} and \mathbf{M} : \mathbf{P} represents the estimate accuracy immediately after a measurement, whereas \mathbf{M} is the propagated value of \mathbf{P} and is valid just before measurements. From Eq. (9.81) and Eq. (9.87) we see that

$$\mathbf{x}(k+1) - \bar{\mathbf{x}}(k+1) = \Phi(\mathbf{x}(k) - \hat{\mathbf{x}}(k)) + \Gamma_1 \mathbf{w}(k), \quad (9.88)$$

which we will use to find the covariance of the state at time $k+1$ before taking $\mathbf{y}(k+1)$ into account

$$\mathbf{M}(k+1) = \mathcal{E}[(\mathbf{x}(k+1) - \bar{\mathbf{x}}(k+1))(\mathbf{x}(k+1) - \bar{\mathbf{x}}(k+1))^T].$$

If the measurement noise, \mathbf{v} , and the process noise, \mathbf{w} , are uncorrelated so that $\mathbf{x}(k)$ and $\mathbf{w}(k)$ are also uncorrelated, the cross product terms vanish and we find that

$$\mathbf{M}(k+1) = \mathcal{E}[\Phi(\mathbf{x}(k) - \hat{\mathbf{x}}(k))(\mathbf{x}(k) - \hat{\mathbf{x}}(k))^T \Phi^T + \Gamma_1 \mathbf{w}(k) \mathbf{w}^T(k) \Gamma_1^T]. \quad (9.89)$$

But because

$$\mathbf{P}(k) = \mathcal{E}\{(\mathbf{x}(k) - \hat{\mathbf{x}}(k))(\mathbf{x}(k) - \hat{\mathbf{x}}(k))^T\} \quad \text{and} \quad \mathbf{R}_w = \mathcal{E}\{\mathbf{w}(k) \mathbf{w}^T(k)\},$$

Eq. (9.89) reduces to

$$\mathbf{M}(k+1) = \Phi \mathbf{P}(k) \Phi^T + \Gamma_1 \mathbf{R}_w \Gamma_1^T. \quad (9.90)$$

This completes the required relations for the optimal, time-varying gain, state estimation, commonly referred to as the Kalman filter. A summary of the required relations is:

- *At the measurement time* (measurement update)

$$\hat{\mathbf{x}}(k) = \bar{\mathbf{x}}(k) + \mathbf{P}(k) \mathbf{H}^T \mathbf{R}_v^{-1} (\mathbf{y}(k) - \mathbf{H} \bar{\mathbf{x}}(k)), \quad (9.91)$$

Kalman filter equations

where

$$\mathbf{P}(k) = \mathbf{M}(k) - \mathbf{M}(k) \mathbf{H}^T (\mathbf{H} \mathbf{M}(k) \mathbf{H}^T + \mathbf{R}_v)^{-1} \mathbf{H} \mathbf{M}(k). \quad (9.92)$$

- *Between measurements* (time update)

$$\bar{\mathbf{x}}(k+1) = \Phi \hat{\mathbf{x}}(k) + \Gamma \mathbf{u}(k) \quad (9.93)$$

and

$$\mathbf{M}(k+1) = \Phi \mathbf{P}(k) \Phi^T + \Gamma_1 \mathbf{R}_w \Gamma_1^T, \quad (9.94)$$

where the initial conditions for $\bar{\mathbf{x}}(0)$ and $\mathbf{M}(0) = \mathcal{E}\{\tilde{\mathbf{x}}(0) \tilde{\mathbf{x}}^T(0)\}$ must be assumed to be some value for initialization.

Because \mathbf{M} is time-varying, so will be the estimator gain, \mathbf{L} , given by Eq. (9.84). Furthermore, we see that the structure of the estimation process is exactly the same as the current estimator given by Eq. (9.56), the difference being that \mathbf{L} is time varying and determined so as to provide the minimum estimation errors, given *a priori* knowledge of the process noise magnitude, \mathbf{R}_w , the measurement noise magnitude, \mathbf{R}_v , and the covariance initial condition, $\mathbf{M}(0)$.

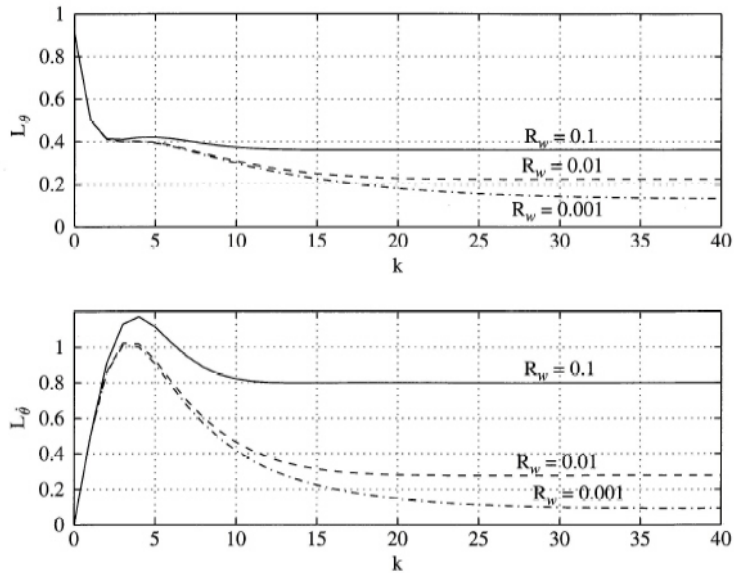


Figure 9.8
Example of
estimator gains
versus time

Solve for $\mathbf{L}(k)$ for the satellite attitude control problem in Example 9.3 assuming the angle, θ , is sensed with a measurement noise covariance

$$R_v = 0.1 \text{ deg}^2.$$

Assume the process noise is due to disturbance torques acting on the spacecraft with the disturbance-input distribution matrix

$$\mathbf{G}_1 = \begin{bmatrix} 0 \\ 1 \end{bmatrix},$$

and assume several values for the mean square magnitude of this disturbance:

$$\mathbf{R}_w = 0.001, 0.01, 0.1 \text{ (deg}^2/\text{sec}^4\text{)}.$$

Solution. Because only θ is directly sensed, we have from Eq. (4.47)

$$H = [1 \quad 0].$$

The time varying estimator gain, $\mathbf{L}(k)$, is found by evaluating Eqs. (9.84), (9.92), and (9.94). In order to start these recursive equations, some value for $\mathbf{M}(0)$ is required. Although somewhat arbitrary, a value of

$$\mathbf{M}(0) = \begin{bmatrix} 1 & 0 \\ 0 & 1 \end{bmatrix}$$

was selected in order to indicate that the initial rms uncertainty in θ was 1° and $\dot{\theta}$ was $1^\circ/\text{sec}$. The gain time histories are sensitive to this initial condition estimate during the initial transient, but the steady final values are not affected.

Figure 9.8 shows the time history of the \mathbf{L} 's for the values given above. We see from the figure that after an initial settling time, the estimator gains essentially reach a steady state. Just as for the control problem, where the feedback gain reached a steady value early in the problem time, the eventual steady value for \mathbf{L} occurs for all linear constant coefficient systems. The subject of the next section is a method to compute the value of this steady-state gain matrix so that it can be used in place of the time-varying one, thus eliminating the need to go through the rather lengthy recursive computation of Eq. (9.92) and Eq. (9.94).

Given an actual design problem, one can often assign a meaningful value to \mathbf{R}_v , which is based on the sensor accuracy. The same cannot be said for \mathbf{R}_w . The assumption of white process noise is often a mathematical artifice that is used because of the ease of solving the resulting optimization problem.

Physically, \mathbf{R}_w is crudely accounting for unknown disturbances, whether they be steps, white noise, or somewhere in between, and for imperfections in the plant model.

If there is a random disturbance that is time correlated—that is, **colored noise**—it can be accurately modeled by augmenting Φ with a coloring filter that converts a white-noise input into time-correlated noise, thus Eq. (9.81) can also be made to describe nonwhite disturbances. In practice, however, this is often not done due to the complexity. Instead, the disturbances are assumed white, and the noise intensity is adjusted to give acceptable results in the presence of expected disturbances, whether time-correlated or not.

If \mathbf{R}_w was chosen to be zero due to a lack of knowledge of a precise noise model, the estimator gain would eventually go to zero. This is so because the optimal thing to do in the idealistic situation of *no* disturbances and a *perfect* plant model is to estimate open loop after the initial condition errors have *completely* died out; after all, the very best filter for the noisy measurements is to totally ignore them. In practice, this will not work because there are always some disturbances and the plant model is never perfect; thus, the filter with zero gain will drift away from reality and is referred to as a **divergent filter**.⁸ If an estimator mode with zero gain was also naturally unstable, the estimator error would diverge from reality very quickly and likely result in saturation of the computer. We therefore are often forced to pick values of \mathbf{R}_w and sometimes Γ_1 “out of a hat” in the design process in order to assure that no modes of the estimator are without feedback and that the estimator will track all modes of the actual system. The disturbance noise model should be selected to approximate that of the actual known disturbances when practical, but the designer often settles on acceptable values based on the quality of the estimation that results in subsequent simulations including all known disturbances, white and otherwise.

It is possible to include a nonzero process noise input in the plant model and yet still end up with a divergent filter [Bryson (1978)]. This can arise when the process noise is modeled so that it does not affect some of the modes of the system. Bryson showed that the filter will not be divergent if you select Γ_1 so that the system, (Φ, Γ_1) , is *controllable* and all diagonal elements of \mathbf{R}_w are nonzero.

For an implementation of a time-varying filter, initial conditions for \mathbf{M} and $\bar{\mathbf{x}}$ are also required. Physically, they represent the *a priori* estimate of the accuracy of $\bar{\mathbf{x}}(0)$, which in turn represents the *a priori* estimate of the state. In some cases, there might be test data of some kind to support their intelligent choice; however, that is not typical. In lieu of any better information, one could logically assume that the components of $\bar{\mathbf{x}}(0)$ contained in \mathbf{y} are equal to the first measurement, and the remaining components are equal to zero. Similarly, the components in \mathbf{M} that represent a measured component could be logically set to \mathbf{R}_v and the remaining components set to a high value.

In obtaining the values of \mathbf{L} in Fig. 9.8, it was necessary to solve for the time history of \mathbf{P} . Because \mathbf{P} is the covariance of the estimation errors, we can sometimes use \mathbf{P} as an indicator of estimation accuracy, provided that the values of \mathbf{R}_v and \mathbf{R}_w are based on some knowledge of the actual noise characteristics and that \mathbf{w} and \mathbf{v} are approximately white.

The intent of this section and example is to give some insight into the nature of the solution so as to motivate and provide a basis for the following section. Readers interested in the application of Kalman filters are encouraged to review works devoted to that subject, such as Bryson and Ho (1975), Anderson and Moore (1979), and Stengel (1986).

9.4.3 Steady-State Optimal Estimation

As shown by Example 9.8, the estimator gains will eventually reach a steady-state value if enough time passes. This is so because the values of \mathbf{M} and \mathbf{P} reach a steady value. Because of the substantial simplification in the controller afforded by a constant estimator gain matrix, it is often desirable to determine the constant gain during the design process and to implement that constant value in the controller. As discussed in Section 9.2, many control systems run for very long times and can be treated mathematically as if they run for an infinite time. In this case the constant gain is the optimal because the early transient period has no significant effect. Whatever the motivation, a constant-gain

⁸A filter with one or more modes that is running open loop is sometimes dubbed “oblivious” or “fat, dumb, and happy” because it ignores the measurements. It is somewhat analogous to the person whose mind is made up and not interested in facts.

Control	Estimation
Φ	Φ^T
\mathbf{M}	\mathbf{P}
\mathbf{S}	\mathbf{M}
\mathbf{Q}_1	$\Gamma_1 \mathbf{R}_w \Gamma_1^T$
Γ	\mathbf{H}^T
\mathbf{Q}_2	\mathbf{R}_v

Table 9.1
Control and
Estimation
Duality

Kalman filter is identical in structure to the estimator discussed in Chapter 8, the only difference being that the gain, \mathbf{L} , is determined so that the estimate errors are minimized for the assumed level of process and measurement noise. This approach replaces the pole-placement method of finding the estimator gain and has the highly desirable feature that it can be applied to MIMO systems.

The equations to be solved that determine \mathbf{M} and \mathbf{P} are Eq. (9.92) and Eq. (9.94). Repeated, they are

$$\mathbf{P}(k) = \mathbf{M}(k) - \mathbf{M}(k)\mathbf{H}^T(\mathbf{H}\mathbf{M}(k)\mathbf{H}^T + \mathbf{R}_v)^{-1}\mathbf{H}\mathbf{M}(k), \quad (9.92)$$

$$\mathbf{M}(k+1) = \Phi\mathbf{P}(k)\Phi^T + \Gamma_1\mathbf{R}_w\Gamma_1^T \quad (9.94)$$

Comparing Eqs. (9.92) and (9.94) to the optimal *control* recursion relationships, Eq. (9.24) and Eq. (9.25)

$$\mathbf{M}(k) = \mathbf{S}(k) - \mathbf{S}(k)\Gamma[\mathbf{Q}_2 + \Gamma^T\mathbf{S}(k)\Gamma]^{-1}\Gamma^T\mathbf{S}(k), \quad (9.25)$$

$$\mathbf{S}(k) = \Phi^T\mathbf{M}(k+1)\Phi + \mathbf{Q}_1, \quad (9.24)$$

we see that they are precisely of the same form! The only exception is that Eq. (9.94) goes forward instead of backward as Eq. (9.24) does. Therefore, we can simply change variables and directly use the steady-state solution of the control problem as the desired steady-state solution to the estimation problem, even though the equations are solved in opposite directions in time.

Table 9.1 lists the correspondences that result by direct comparison of the control and estimation recursion relations: Eq. (9.25) with Eq. (9.92) and Eq. (9.24) with Eq. (9.94).

By analogy with the control problem, Eqs. (9.92) and (9.94) must have arisen from two coupled equations with the same form as Eq. (9.33). Using the correspondences in Table 9.1, the control Hamiltonian in Eq. (9.34) becomes the estimation Hamiltonian

$$\mathcal{H}_e = \begin{bmatrix} \Phi^T + \mathbf{H}^T\mathbf{R}_v^{-1}\mathbf{H}\Phi^{-1}\Gamma_1\mathbf{R}_w\Gamma_1^T & -\mathbf{H}^T\mathbf{R}_v^{-1}\mathbf{H}\Phi^{-1} \\ -\Phi^{-1}\Gamma_1\mathbf{R}_w\Gamma_1^T & \Phi^{-1} \end{bmatrix}. \quad (9.95)$$

Therefore, the steady-state value of \mathbf{M} is deduced by comparison with Eq. (9.46) and is

$$\mathbf{M}_\infty = \Lambda_I \mathbf{X}_I^{-1}, \quad (9.96)$$

where

$$\begin{bmatrix} \mathbf{X}_I \\ \Lambda_I \end{bmatrix}$$

are the eigenvectors of \mathcal{H}_e associated with its stable eigenvalues. Hence, from Eqs. (9.92) and (9.84) after some manipulation we find the steady state Kalman-filter gain to be⁹

$$\mathbf{L}_\infty = \mathbf{M}_\infty \mathbf{H}^T (\mathbf{H}\mathbf{M}_\infty \mathbf{H}^T + \mathbf{R}_v)^{-1}. \quad (9.97)$$

This is a standard calculation in MATLAB's `kalman.m`. Sometimes this solution is referred to as the **linear quadratic Gaussian (LQG)** problem because it is often assumed in the derivation that the noise has a Gaussian distribution. As can be seen from the development here, this assumption is not

⁹In the steady state, the filter has constant coefficients and, for the assumed model, is the same as the Wiener filter.

necessary. However, with this assumption, one can show that the estimate is not only the one that minimizes the error squared, but also the one that is statistically “most likely.” In this derivation, the result is referred to as the **maximum likelihood** estimate.

Because Eq. (9.34) and Eq. (9.95) are the same form, the eigenvalues have the same reciprocal properties in both cases. Furthermore, for systems with a single output and a single process noise input, the symmetric root locus follows by analogy with Eq. (9.40) and the use of Table 9.1. Specifically, the characteristic equation becomes

$$1 + qG_e(z^{-1})G_e(z) = 0, \quad (9.98)$$

where $q = R_w/R_v$ and

$$G_e(z) = \mathbf{H}(z\mathbf{I} - \mathbf{\Phi})^{-1}\mathbf{\Gamma}_1.$$

Therefore, for systems where the process noise is additive with the control input—that is, $\mathbf{\Gamma} = \mathbf{\Gamma}_1$ —the control and estimation optimal root loci are identical, and the control and estimation roots could be selected from the same loci. For example, the loci in Figs. 9.4 and 9.5 could be used to select estimator roots as well as the control roots.

9.4.4 Noise Matrices and Discrete Equivalents

The quantities defining the noise magnitude, the covariance matrices \mathbf{R}_w and \mathbf{R}_v , were defined in Section 9.4.2 as

$$\mathbf{R}_w = \mathcal{E}\{\mathbf{w}(k)\mathbf{w}^T(k)\} \quad \text{and} \quad \mathbf{R}_v = \mathcal{E}\{\mathbf{v}(k)\mathbf{v}^T(k)\}.$$

Typically, if there is more than one process or measurement noise component, one has no information on the cross-correlation of the noise elements and therefore \mathbf{R}_w and \mathbf{R}_v are selected as diagonal matrices. The magnitudes of the diagonal elements are the variances of the noise components.

Process Noise, \mathbf{R}_w

The process noise acts on the continuous portion of the system and, assuming that it is a white continuous process, varies widely throughout one sample period. Its effect over the sample period, therefore, cannot be determined as it was for Eq. (9.90); instead, it needs to be integrated. From Eqs. (4.55) and (4.56), we see that the effect of continuous noise input over one sample period is

$$\mathbf{x}(k+1) = \mathbf{\Phi}\mathbf{x}(k) + \int_0^T e^{\mathbf{F}(\eta)}\mathbf{G}_1\mathbf{w}(\eta)d\eta,$$

where \mathbf{G}_1 is defined by Eq. (4.45). Repeating the derivation¹⁰ of Eq. (9.90) with the integral above replacing $\mathbf{\Gamma}_1\mathbf{w}(k)$ in Eq. (9.88), we find that Eq. (9.90) becomes

$$\mathbf{M}(k+1) = \mathbf{\Phi}P(k)\mathbf{\Phi}^T + \int_0^T \int_0^T \mathbf{\Phi}(\eta)\mathbf{G}_1\mathcal{E}[\mathbf{w}(\eta)\mathbf{w}^T(\tau)]\mathbf{G}_1^T\mathbf{\Phi}^T(\tau)d\tau d\eta. \quad (9.99)$$

But the white noise model for \mathbf{w} means that

$$\mathcal{E}[\mathbf{w}(\eta)\mathbf{w}^T(\tau)] = \mathbf{R}_{w\text{psd}}\delta(\eta - \tau),$$

where $\mathbf{R}_{w\text{psd}}$ is called the power spectral density, or mean-square spectral density, of the continuous white noise. Therefore, Eq. (9.99) reduces to

$$\mathbf{M}(k+1) = \mathbf{\Phi}P(k)\mathbf{\Phi}^T + \mathbf{C}_d,$$

where

$$\mathbf{C}_d = \int_0^T \mathbf{\Phi}(\tau)\mathbf{G}_1\mathbf{R}_{w\text{psd}}\mathbf{G}_1^T\mathbf{\Phi}^T(\tau)d\tau. \quad (9.100)$$

¹⁰See Stengel (1986), p. 327.

Calculation of this integral (see `disrw.m` in the Digital Control Toolbox) can be carried out using a similar exponential form due to Van Loan (1978), as in Eq. (9.54). If T is very short compared to the system time constants, that is

$$\Phi \cong \mathbf{I} \quad \text{and} \quad \Gamma_1 \cong \mathbf{G}_1 T,$$

then the integral is approximately

$$\mathbf{C}_d \cong T \mathbf{G}_1 \mathbf{R}_{\text{wpsd}} \mathbf{G}_1^T,$$

which can also be written¹¹

$$\mathbf{C}_d \cong \Gamma_1 \frac{\mathbf{R}_{\text{wpsd}}}{T} \Gamma_1^T.$$

Therefore, one can apply the discrete covariance update Eq. (9.94) to the case where \mathbf{w} is continuous noise by using the approximation that

$$\mathbf{R}_w \cong \frac{\mathbf{R}_{\text{wpsd}}}{T}, \quad (9.101)$$

as long as T is much shorter than the system time constants. If this assumption is not valid, one must revert to the integral in Eq. (9.100).

In reality, however, there is no such thing as white continuous noise. A pure white-noise disturbance would have equal magnitude content at all frequencies from 0 to ∞ . Translated, that means that the correlation time of the random signal is precisely zero. The only requirement for our use of the white-noise model in discrete systems is that the disturbance have a correlation time that is short compared to the sample period. If the correlation time is on the same order or longer than the sample period, the correct methodology entails adding the colored-noise model to the plant model and estimating the random disturbance along with the original state. In fact, if the correlation time is extremely long, the disturbance acts much like a bias, and we have already discussed its estimation in Section 8.5.2. In practice, disturbances are often assumed to be either white or a bias, because the improved accuracy possible by modeling a random disturbance with a time constant on the same order as the sample period is not deemed worth the extra complexity.

The determination of the appropriate value of \mathbf{R}_{wpsd} that represents a physical process is aided by the realization that pure white noise does not exist in nature. Disturbances all have a nonzero correlation time, the only question being: How short? Assuming that the time correlation is exponential with a correlation time τ_c , and that $\tau_c \ll$ system time constants, the relation between the power spectral density and the mean square of the signal is¹²

$$R_{\text{wpsd}} \cong 2\tau_c \mathcal{E}\{w^2(t)\}. \quad (9.102)$$

Typically, one can measure the mean square value, $\mathcal{E}\{w^2(t)\}$, and can either measure or estimate its correlation time, τ_c , thus allowing the computation of each diagonal element of \mathbf{R}_{wpsd} . However, the desired result for our purposes is the discrete equivalent noise, \mathbf{R}_w . It can be computed from Eq. (9.101) and Eq. (9.102), where each diagonal element, $[\mathbf{R}_w]_i$, is related to the mean square and correlation time of the i th disturbance according to

$$[\mathbf{R}_w]_i = \frac{2}{T} [\tau_c \mathcal{E}\{w^2(t)\}]_i. \quad (9.103)$$

Note from Eq. (9.103) that \mathbf{R}_w and $\mathcal{E}\{w^2(t)\}$ are not the same quantities. Specifically, the diagonal elements of \mathbf{R}_w are the mean square values of the discrete noise, $w(k)$, that produces a response from the discrete model given by Eq. (9.90) that matches the response of the continuous system acted on by a $w(t)$ with $\mathcal{E}\{w^2(t)\}$ and τ_c . Note also that it has been assumed that the noise is white compared to the sample period, that is, $\tau_c \ll T$ and that $T \ll$ any system time constants. Under these conditions the discrete equivalent mean square value is less than the continuous signal mean square because the continuous random signal acting on the continuous system is averaged over the sample period. If τ_c is not $\ll T$, then the noise is not white and Eq. (9.100) is not valid; thus calculation of \mathbf{R}_w is not relevant.

¹¹By computing Γ_1 exactly according to Eq. (4.58), the approximation that follows for \mathbf{C}_d is substantially more accurate than the approximation using \mathbf{G}_1 .

¹²Bryson and Ho (1975), p. 331.

Sensor Noise, \mathbf{R}_v

The pertinent information given by the manufacturer of a sensor product would be the rms “jitter” error level (or some other similar name), which can usually be interpreted as the random component and assumed to be white, that is, uncorrelated from one sample to the next. The rms value is simply squared to arrive at the diagonal elements of $\mathcal{E}\{v^2(t)\}$. Unlike the process noise case these values are used directly, that is

$$[\mathbf{R}_v]_i = [\mathcal{E}\{v^2(t)\}]_i. \quad (9.104)$$

The assumption of no time correlation is consistent with the development of the optimal estimator that was discussed in Section 9.4.2. If the correlation time of a sensor is longer than the sample period, the assumption is not correct, and an accurate treatment of the noise requires that its “coloring” model be included with the plant model and the measurement noise error estimated along with the rest of the state.¹³ One could also ignore this complication and proceed as if the noise were white, with the knowledge that the effect of the measurement noise is in error and that skepticism is required in the interpretation of estimate error predictions based on \mathbf{P} . Furthermore, one could no longer claim that the filter was optimal.

Sensor manufacturers typically list bias errors also. This component should at least be evaluated to determine the sensitivity of the system to the bias, and if the effect is not negligible, the bias should be modeled, augmented to the state, and estimated using the ideas of Section 8.5.2.

Note that neither the sample period nor the correlation time of the sensor error has an impact on \mathbf{R}_v if \mathbf{v} is white. Although the rms value of \mathbf{v} is not affected by the sampling, sampling at a higher rate will cause more measurements to be averaged in arriving at the state estimate, and the estimator accuracy will improve with sample rate.

In some cases, the designer wishes to know how the sensor noise will affect an estimator that is implemented with analog electronics. Although this can be done in principle, in practice it is rarely done because of the low cost of digital implementations. The value of analyzing the continuous case is that the knowledge can be useful in selecting a sample rate. Furthermore, the designer is sometimes interested in creating a digital implementation whose roots match that of a continuous design, and finding the discrete equivalent noise is a method to approximate that design goal. Whatever the reason, the continuous filter can be evaluated digitally, with the appropriate value of \mathbf{R}_v being the one that provides the discrete equivalent to the continuous process, the same situation that was examined for the process noise. Therefore, the proper relation in this special case is from Eq. (9.101) or (9.103)

$$\mathbf{R}_v = \frac{\mathbf{R}_{vpsd}}{T} \quad \text{or} \quad [\mathbf{R}_v]_i = \frac{2}{T} [\tau_c \mathcal{E}\{v^2(t)\}]_i, \quad (9.105)$$

where $\mathcal{E}\{v^2(t)\}$ is the mean square value of the sensor noise and τ_c is its correlation time. Alternatively, if one desires only the continuous filter performance for a baseline, one can use a pure continuous analysis of the filter,¹⁴ which requires only \mathbf{R}_{vpsd} .

9.5 Multivariable Control Design

The elements of the design process of a MIMO system have been discussed in the preceding sections. This section discusses some of the issues in design and provides two examples of the process.

9.5.1 Selection of Weighting Matrices \mathbf{Q}_1 and \mathbf{Q}_2

As can be seen from the discussion in Sections 9.2 and 9.3, the selection of \mathbf{Q}_1 and \mathbf{Q}_2 is only weakly connected to the performance specifications, and a certain amount of trial and error is usually required with an interactive computer program before a satisfactory design results. There are, however, a few guidelines that can be employed. For example, Bryson and Ho (1975) and Kwakernaak and Sivan (1972) suggest essentially the same approach. This is to take $\mathbf{Q}_1 = \mathbf{H}^T \bar{\mathbf{Q}}_1 \mathbf{H}$ so that the states enter

¹³See Stengel (1986) or Bryson and Ho (1975).

¹⁴See Bryson and Ho (1975).

the cost via the important outputs (which may lead to $\mathbf{H} = \mathbf{I}$ if all states are to be kept under close regulation) and to select $\bar{\mathbf{Q}}_1$ and \mathbf{Q}_2 to be diagonal with entries so selected that a fixed percentage change of each variable makes an equal contribution to the cost.¹⁵ For example, suppose we have three outputs with maximum deviations $m_1, m_2,$ and m_3 . The cost for diagonal $\bar{\mathbf{Q}}_1$ is

$$\bar{q}_{11}y_1^2 + \bar{q}_{22}y_2^2 + \bar{q}_{33}y_3^2.$$

The rule is that if $y_1 = \alpha m_1, y_2 = \alpha m_2,$ and $y_3 = \alpha m_3,$ then

Bryson's rules

$$\bar{q}_{11}y_1^2 = \bar{q}_{22}y_2^2 = \bar{q}_{33}y_3^2;$$

thus

$$\bar{q}_{11}\alpha^2 m_1^2 = \bar{q}_{22}\alpha^2 m_2^2 = \bar{q}_{33}\alpha^2 m_3^2.$$

A satisfactory solution for elements of $\bar{\mathbf{Q}}_1$ is then¹⁶

$$\bar{Q}_{1,11} = 1/m_1^2, \bar{Q}_{1,22} = 1/m_2^2, \bar{Q}_{1,33} = 1/m_3^2. \quad (9.106)$$

Similarly, for \mathbf{Q}_2 we select a matrix with diagonal elements

$$Q_{2,11} = 1/u_{1\max}^2, Q_{2,22} = 1/u_{2\max}^2. \quad (9.107)$$

There remains a scalar ratio between the state and the control terms, which we will call ρ . Thus the total cost is

$$\mathcal{J} = \rho \mathbf{x}^T \mathbf{H}^T \bar{\mathbf{Q}}_1 \mathbf{H} \mathbf{x} + \mathbf{u}^T \mathbf{Q}_2 \mathbf{u}, \quad (9.108)$$

where $\bar{\mathbf{Q}}_1$ and \mathbf{Q}_2 are given by Eq. (9.106), and Eq. (9.107), and ρ is to be selected by trial and error. A computer-interactive procedure that allows examination of root locations and transient response for selected values of $\bar{\mathbf{Q}}_1$ and \mathbf{Q}_2 expedites this process considerably.

9.5.2 Pincer Procedure

The designer can introduce another degree of freedom into this problem by requiring that all the closed-loop poles be inside a circle of radius $1/\alpha$, where $\alpha \geq 1$. If we do this, then the magnitude of every transient in the closed loop will decay at least as fast as $1/\alpha^k$, which forms pincers around the transients and allows a degree of direct control over the settling time. We can introduce this effect in the following way.

Suppose that as a modification to the performance criterion of Eq. (9.11), we consider

$$\mathcal{J}_\alpha = \sum_{k=0}^{\infty} [\mathbf{x}^T \mathbf{Q}_1 \mathbf{x} + \mathbf{u}^T \mathbf{Q}_2 \mathbf{u}] \alpha^{2k}. \quad (9.109)$$

We can distribute the scalar term α^{2k} in Eq. (9.109) as $\alpha^k \alpha^k$ and write it as

$$\begin{aligned} \mathcal{J}_\alpha &= \sum_{k=0}^{\infty} [(\alpha^k \mathbf{x})^T \mathbf{Q}_1 (\alpha^k \mathbf{x}) + (\alpha^k \mathbf{u})^T \mathbf{Q}_2 (\alpha^k \mathbf{u})] \\ &= \sum_{k=0}^{\infty} [\mathbf{z}^T \mathbf{Q}_1 \mathbf{z} + \mathbf{v}^T \mathbf{Q}_2 \mathbf{v}], \end{aligned} \quad (9.110)$$

where

$$\mathbf{z}(k) = \alpha^k \mathbf{x}(k), \quad \mathbf{v}(k) = \alpha^k \mathbf{u}(k). \quad (9.111)$$

The equations in \mathbf{z} and \mathbf{v} are readily found. Consider

$$\mathbf{z}(k+1) = \alpha^{k+1} \mathbf{x}(k+1).$$

¹⁵Kwakernaak and Sivan (1972) suggest using a percentage change from nominal values; Bryson and Ho use percentage change from the maximum values.

¹⁶Sometimes called Bryson's rules.

From Eq. (9.10) we have the state equations for $\mathbf{x}(k+1)$, so that

$$\mathbf{z}(k+1) = \alpha^{k+1}[\Phi\mathbf{x}(k) + \Gamma\mathbf{u}(k)].$$

If we multiply through by the α^{k+1} -term, we can write this as

$$\mathbf{z}(k+1) = \alpha\Phi(\alpha^k\mathbf{x}(k)) + \alpha\Gamma(\alpha^k\mathbf{u}(k)),$$

but from the definitions in Eq. (9.111), this is the same as

$$\mathbf{z}(k+1) = \alpha\Phi\mathbf{z}(k) + \alpha\Gamma\mathbf{v}(k). \quad (9.112)$$

The performance function Eq. (9.110) and the equations of motion Eq. (9.112) define a new problem in optimal control for which the solution is a control law

$$\mathbf{v} = -\mathbf{K}\mathbf{z},$$

which, if we work backward, is

$$\alpha^k\mathbf{u}(k) = -\mathbf{K}(\alpha^k\mathbf{x}(k))$$

or

$$\mathbf{u}(k) = -\mathbf{K}\mathbf{x}(k). \quad (9.113)$$

We conclude from all this that if we use the control law Eq. (9.113) in the state equations (9.10), then a trajectory results that is optimal for the performance \mathcal{J}_α given by Eq. (9.109). Furthermore, the state trajectory satisfies Eq. (9.111), where $\mathbf{z}(k)$ is a stable vector so that $\mathbf{x}(k)$ must decay *at least* as fast as $1/\alpha^k$, or else $\mathbf{z}(k)$ could not be guaranteed to be stable.

To apply the pincers we need to relate the settling time to the value of α . Suppose we define settling time of x_j as that time t_s such that if $x_j(0) = 1$ and all other states are zero at $k = 0$, then the transients in x_j are less than 0.01 (1% of the maximum) for all times greater than t_s . If we approximate the transient in x_j as

$$x_j(k) \approx x_j(0)(1/\alpha)^k,$$

then when $kT = t_s$, we must have

$$x_j(kT) \leq 0.01x_j(0),$$

which will be satisfied if α is such that

$$(1/\alpha)^k \leq 0.01 = \frac{1}{100},$$

or

$$\alpha > 100^{1/k} = 100^{T/t_s}. \quad (9.114)$$

In summary, application of the pincer procedure requires that the designer select the settling time, t_s , within which all states should settle to less than 1%. Equation (9.114) is then used to compute α and, according to Eq. (9.112), the revised system $\alpha\Phi$ and $\alpha\Gamma$ for use in an LQR computation for the feedback gain matrix \mathbf{K} . Use of \mathbf{K} with the original system, Φ , will produce a response of all states that settle within the prescribed t_s .

9.5.3 Paper-Machine Design Example

As an illustration of a multivariable control using optimal control techniques, we will consider control of the paper-machine head box described in Appendix A.5. The continuous equations of motion are given by

$$\dot{\mathbf{x}} = \begin{bmatrix} -0.2 & 0.1 & 1 \\ -0.05 & 0 & 0 \\ 0 & 0 & -1 \end{bmatrix} \mathbf{x} + \begin{bmatrix} 0 & 1 \\ 0 & 0.7 \\ 1 & 0 \end{bmatrix} \mathbf{u}. \quad (9.115)$$

We assume the designer has the following specifications on the responses of this system:

1. The maximum sampling frequency is 5 Hz ($T = 0.2$ sec).
2. The 1% settling time to demands on x_1 (= total head) should be less than 2.4 sec (12 periods).
3. The settling time to demands on x_2 (= liquid level) should be less than 8 sec (40 periods).
4. The units on the states have been selected so that the maximum permissible deviation on total head, x_1 , is 2.0 units and the liquid level, x_2 , is 1.0.
5. The units on control have been selected so that the maximum permissible deviation on u_1 (air control) is 5 units and that of u_2 (stock control) is 10 units.

First let us apply the pincer procedure to ensure that the settling times are met. We have asked that the settling times be 2.4 sec for x_1 and 8 sec for x_2 . If, for purposes of illustration, we select the more stringent of these and in Eq. (9.114) set $t_s = 2.4$ for which $t_s/T = 12$, then

$$\alpha > 100^{1/12} = 1.47.$$

Now let us select the cost matrices. Based on the specifications and the discussion in Section 9.5.1, we can conclude that $m_1 = 2$ and $m_2 = 1$, and thus

$$\bar{\mathbf{Q}}_1 = \begin{bmatrix} 0.25 & 0 \\ 0 & 1 \end{bmatrix}.$$

Because we are interested only in x_1 and x_2 , the output matrix \mathbf{H} in Eq. (9.108) is

$$\mathbf{H} = \begin{bmatrix} 1 & 0 & 0 \\ 0 & 1 & 0 \end{bmatrix}$$

and

$$\mathbf{Q}_1 = \begin{bmatrix} 0.25 & 0 & 0 \\ 0 & 1 & 0 \\ 0 & 0 & 0 \end{bmatrix}.$$

Furthermore, because $u_{1\max} = 5$ and $u_{2\max} = 10$

$$\mathbf{Q}_2 = \begin{bmatrix} 0.04 & 0 \\ 0 & 0.01 \end{bmatrix}.$$

Conversion of the continuous system in Eq. (9.115) to a discrete one ($T = 0.2$ sec) yields

$$\Phi = \begin{bmatrix} 0.9607 & 0.0196 & 0.1776 \\ -0.0098 & 0.9999 & -0.0009 \\ 0 & 0 & 0.8187 \end{bmatrix} \quad \text{and} \quad \Gamma = \begin{bmatrix} 0.0185 & 0.1974 \\ -0.0001 & 0.1390 \\ 0.1813 & 0 \end{bmatrix}.$$

These two matrices are then multiplied by the scalar 1.47 ($= \alpha$) and used in MATLAB's `dlqr.m` with the preceding \mathbf{Q}_1 and \mathbf{Q}_2 .

The LQR calculation gives a control gain

$$\mathbf{K} = \begin{bmatrix} 6.81 & -9.79 & 3.79 \\ 0.95 & 4.94 & 0.10 \end{bmatrix},$$

and closed-loop poles at

$$z = 0.108, 0.491 \pm j0.068,$$

which are well within $1/1.47 = 0.68$. Fig. 9.9(a) shows the transient response to unit-state initial conditions on x_1 , and Fig. 9.9(b) shows the same for initial conditions on x_2 . Examination of these results shows that the requirement on settling time has been substantially exceeded because x_1 settles to within 1% by 1.8 sec, and x_2 settles within 1% by 1.6 sec for both cases. However, the control effort on u_1 is larger than its specification for both initial condition cases, and further iteration on the

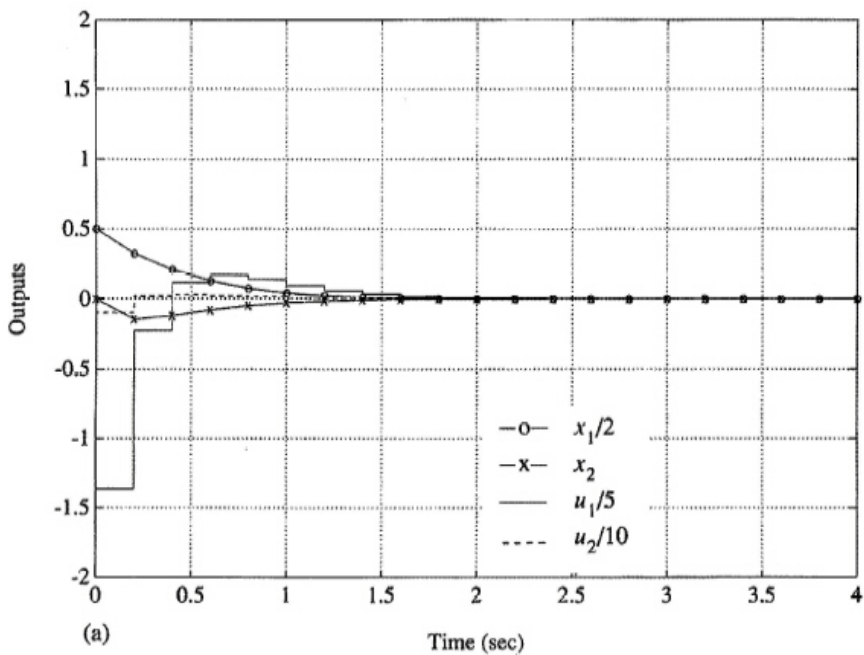
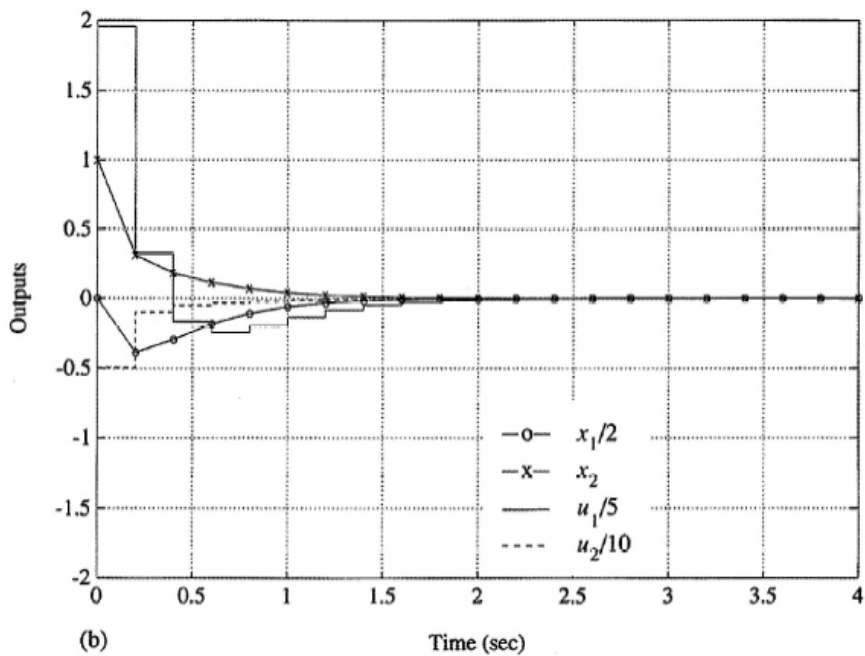


Figure 9.9
 Response of
 paper-machine
 closed-loop
 control to:
 (a) initial state
 $\mathbf{x}^T(0) =$
 $[1 \ 0 \ 0]$;
 (b) initial state
 $\mathbf{x}^T(0) = [0 \ 1 \ 0]$



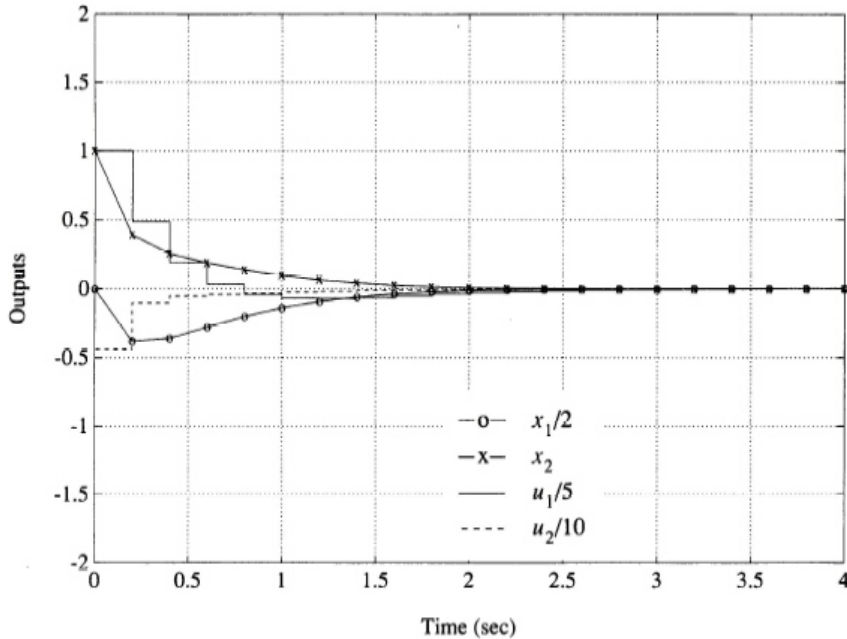


Figure 9.10
Response of
paper-machine
closed-loop
control to initial
state
 $\mathbf{x}^T(0) = [0 \ 1 \ 0]$
with t_s
lengthened to
5 sec

design is required. To correct this situation, the designer should be led by the fast response to relax the demands on response time in order to lower the overall need for control. Figure 9.10 shows the response with t_s in Eq. (9.114) selected to be 5 sec for the case with $\mathbf{x}(0) = [010]^T$. The control u_1 is just within the specification, and the response time of x_1 is 2.3 sec and that of x_2 is 2.0 sec. All specifications are now met.

It is possible to improve the design still further by noting that the response of x_2 beats its specified maximum value and settling time by a substantial margin. To capitalize on this observation, let us try relaxing the cost on x_2 . After some iteration (see Problem 9.7), we find that *no* cost on x_2 , that is

$$\mathbf{Q}_1 = \begin{bmatrix} 0.25 & 0 & 0 \\ 0 & 0 & 0 \\ 0 & 0 & 0 \end{bmatrix},$$

results in a design that still meets all specifications and substantially reduces the use of both controls. Its response to $\mathbf{x}(0) = [010]^T$ is shown in Figure 9.11.

9.5.4 Magnetic-Tape-Drive Design Example

As a further illustration of MIMO design, we will now apply the ideas to an example that includes integral control and estimation. The system is shown in Fig. 9.12. There is an independently controllable drive motor on each end of the tape; therefore, it is possible to control the tape position over the read head, x_3 , as well as the tension in the tape. We have modeled the tape to be a linear spring with a small amount of viscous damping. Although the figure shows the tape head to the left of the spring, in fact, the springiness is distributed along the full length of the tape as shown by the equations below. The goal of the control system is to enable commanding the tape to specific positions over the read head while maintaining a specified tension in the tape at all times. We will carry out the design using MIMO techniques applied to the full system equations and conclude the discussion by illustrating how one could perform the design using a decoupled model and SISO techniques.

The specifications are that we wish to provide a step change in position of the tape head, x_3 , of 1 mm with a 1% settling time of 250 msec with overshoot less than 20%. Initial and final velocity of x_3 is to be zero. The tape tension, T_e , should be controlled to 2 N with the constraint that $0 < T_e < 4$ N. The current is limited to 1 A at each drive motor.

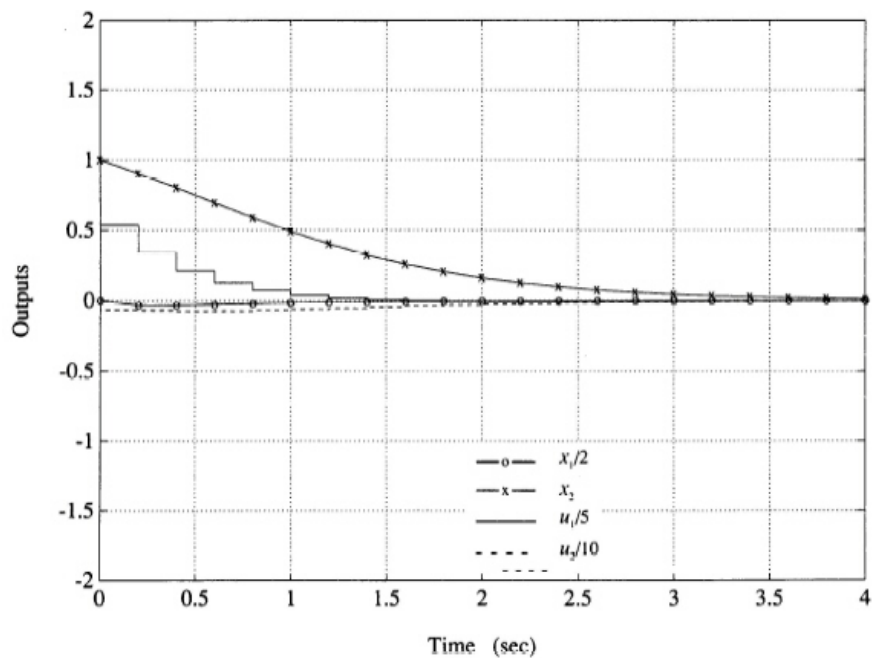


Figure 9.11
Response of paper-machine closed-loop control to initial state $\mathbf{x}^T(0) = [0 \ 1 \ 0]$ with t_s lengthened to 5 sec and no weight on x_2

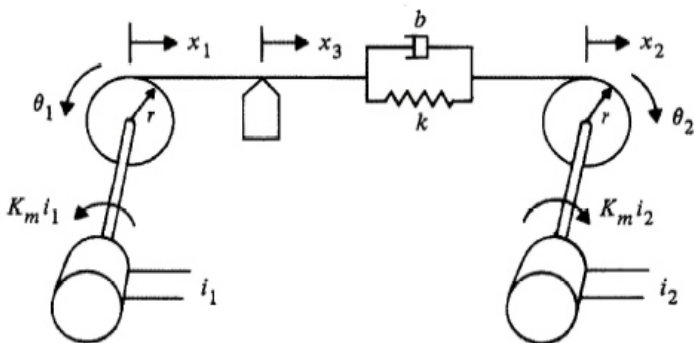


Figure 9.12
Magnetic-tape-drive design example

The equations of motion of the system are

$$\begin{aligned} J\ddot{\theta}_1 &= -T_e r + K_m i_1, \\ J\ddot{\theta}_2 &= -T_e r + K_m i_2, \\ T_e &= k(x_2 - x_1) + b(\dot{x}_2 - \dot{x}_1), \\ x_3 &= (x_1 + x_2)/2, \end{aligned} \quad (9.116)$$

where

$$\begin{aligned} i_1, i_2 &= \text{current into drive motors 1 and 2, respectively (A),} \\ T_e &= \text{tension in tape (N),} \\ \theta_1, \theta_2 &= \text{angular position of motor/capstan assembly (radians),} \\ x_1, x_2 &= \text{position of tape at capstan (mm),} \\ x_3 &= \text{position of tape over read head (mm),} \\ J &= 0.006375 \text{ kg} \cdot \text{m}^2, \text{ motor and capstan inertia,} \\ r &= 0.1 \text{ m, capstan radius,} \\ K_m &= 0.544 \text{ N} \cdot \text{m/A, motor torque constant,} \\ k &= 2113 \text{ N/m, tape spring constant, and} \\ b &= 3.75 \text{ N} \cdot \text{sec/m, tape damping constant.} \end{aligned}$$

In order to be able to simulate a control system design on inexpensive equipment where the system has time constants much faster than 1 sec, it is often useful to time-scale the equations so that the simulation runs slower in the laboratory than it would on the actual system.¹⁷ We have chosen to time-scale the equations above so they run a factor of 10 slower than the actual system. Therefore, the settling time specifications become 2.5 sec instead of 250 msec for the actual system. The numerical equations below and all the following discussion pertain to the time-scaled system. Incorporating the parameter values and writing the time-scaled equations in state form results in

$$\begin{aligned} \begin{bmatrix} \dot{x}_1 \\ \dot{x}_2 \\ \dot{\omega}_1 \\ \dot{\omega}_2 \end{bmatrix} &= \begin{bmatrix} 0 & 0 & -10 & 0 \\ 0 & 0 & 0 & 10 \\ 3.315 & -3.315 & -0.5882 & -0.5882 \\ 3.315 & -3.315 & -0.5882 & -0.5882 \end{bmatrix} \begin{bmatrix} x_1 \\ x_2 \\ \omega_1 \\ \omega_2 \end{bmatrix} \\ &+ \begin{bmatrix} 0 & 0 \\ 0 & 0 \\ 8.533 & 0 \\ 0 & 8.533 \end{bmatrix} \begin{bmatrix} i_1 \\ i_2 \end{bmatrix}, \end{aligned} \quad (9.117)$$

where the desired outputs are

$$\begin{bmatrix} x_3 \\ T_e \end{bmatrix} = \begin{bmatrix} 0.5 & 0.5 & 0 & 0 \\ -2.113 & 2.113 & 0.375 & 0.375 \end{bmatrix} \begin{bmatrix} x_1 \\ x_2 \\ \omega_1 \\ \omega_2 \end{bmatrix}, \quad (9.118)$$

where

$$\omega_1, \omega_2 = \text{angular rates of motor/capstan assembly, } \dot{\theta}_i \text{ (rad/sec).}$$

The eigenvalues of the system matrix in Eq. (9.117) are

$$s \cong 0, 0, \pm j8 \text{ rad/sec,}$$

where the oscillatory roots are from the spring–mass system consisting of the tape and the motor/capstan inertias. This open-loop resonance has a higher frequency than the required closed-loop roots to meet the settling time specifications; therefore, it would be wise to sample at $15\times$ the open-loop resonance at 8 rad/sec. A sample rate of $T = 0.05$ sec results.

¹⁷See Franklin, Powell, and Emami-Naeini (2019) for a discussion of time-scaling.

Full State Feedback

As a first step in the design, let's try state feedback of all four states in Eq. (9.117). We will address the state estimation in a few pages.

The output quantities to be controlled are x_3 and T_e so that it is logical to weight those quantities in the cost $\bar{\mathbf{Q}}_1$. According to the guidelines in Eq. (9.106), we should pick

$$\bar{\mathbf{Q}}_1 = \begin{bmatrix} 1 & 0 \\ 0 & \frac{1}{4} \end{bmatrix},$$

and because we expect each control to be used equally

$$\mathbf{Q}_2 = \begin{bmatrix} 1 & 0 \\ 0 & 1 \end{bmatrix}.$$

Although these weightings gave an acceptable result, a somewhat more desirable result was found by modifying these weightings to

$$\bar{\mathbf{Q}}_1 = \begin{bmatrix} 1 & 0 & 0 \\ 0 & 1 & 0 \\ 0 & 0 & 1 \end{bmatrix} \quad \text{and} \quad \mathbf{Q}_2 = \begin{bmatrix} 1 & 0 \\ 0 & 1 \end{bmatrix},$$

where a third output has been added to that of Eq. (9.118), which represents \dot{T}_e in order to obtain better damping of the tension. Thus we obtain the weighting matrix from

$$\mathbf{Q}_1 = \mathbf{H}_w^T \bar{\mathbf{Q}}_1 \mathbf{H}_w, \quad (9.119)$$

where

$$\mathbf{H}_w = \begin{bmatrix} 0.5 & 0.5 & 0 & 0 \\ -2.113 & 2.113 & 0.375 & 0.375 \\ 0 & 0 & 0.5 & 0.5 \end{bmatrix}. \quad (9.120)$$

Use of the \mathbf{Q}_1 and \mathbf{Q}_2 with the discrete equivalent of Eq. (9.117) in MATLAB's `d1qr.m` results in the feedback gain matrix

$$\mathbf{K} = \begin{bmatrix} -0.823 & 0.286 & 1.441 & 0.311 \\ -0.286 & 0.823 & 0.311 & 1.441 \end{bmatrix},$$

which can be used to form the closed-loop system for evaluation. Calculation of the eigenvalues of the discrete system and transformation of them to their discrete equivalent by $z = e^{sT}$ results in closed-loop roots at

$$s = -5.5 \pm j5.5, -10.4 \pm j12.4 \text{ sec}^{-1}.$$

To bring the system to the desired values of T_e and x_3 , we use the state command structure described in Section 8.4.2. Let us first try without the feedforward value of steady-state control, u_{ss} . Calculation of the reference state, \mathbf{x}_r , can be carried out from the physical relationships that must exist at the desired values of $x_3 = 1 \text{ mm}$ and $T_e = 2 \text{ N}$

$$\begin{aligned} x_1 + x_2 &= 2x_3 = 2, \\ x_2 - x_1 &= \frac{T_e}{k} = \frac{2}{2113} = 0.000947 \text{ m} = 0.947 \text{ mm}. \end{aligned}$$

Solving these two equations and adding the zero velocities results in

$$\mathbf{x}_r = \begin{bmatrix} 0.527 \\ 1.473 \\ 0 \\ 0 \end{bmatrix}.$$

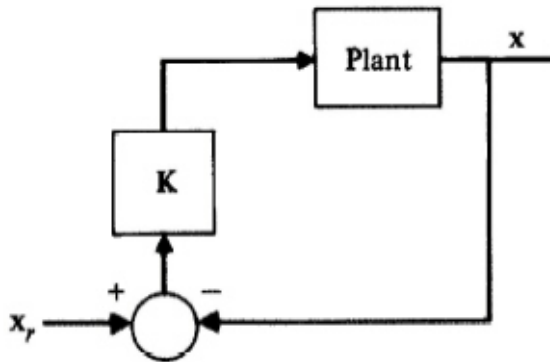


Figure 9.13
Reference input
structure used for
Fig. 9.14

Evaluation of the time response using the structure in Fig. 9.13 (from Fig. 8.14) shows that the input current limits are violated and results in a settling time of 1 sec, which is significantly faster than required. In order to slow down the response and thus reduce the control usage, we should lower \bar{Q}_1 . Revising the weightings to

$$\bar{Q}_1 = \begin{bmatrix} 0.1 & 0 & 0 \\ 0 & 0.1 & 0 \\ 0 & 0 & 0.1 \end{bmatrix} \quad \text{and} \quad Q_2 = \begin{bmatrix} 1 & 0 \\ 0 & 1 \end{bmatrix} \quad (9.121)$$

results in

$$K = \begin{bmatrix} -0.210 & 0.018 & 0.744 & 0.074 \\ -0.018 & 0.210 & 0.074 & 0.744 \end{bmatrix},$$

which produces a closed-loop system whose roots transform to

$$s = -3.1 \pm j3.1, -4.5 \pm j9.2 \text{ sec}^{-1},$$

and produces the response shown in Fig. 9.14. The figure shows that x_3 has a settling time of about 2 sec with an overshoot less than 20% while the control currents are within their limits; however, the tension did not go to the desired 2 N. The steady-state tension error of the system is substantial, and so we shall proceed to correct it.

As discussed in Section 8.4.2, we can provide a feedforward of the required steady-state value of the control input that eliminates steady-state errors. Evaluation of Eq. (8.73) (see `refi.m` in the Digital Control Toolbox) using H from Eq. (9.118) and Φ, Γ from Eq. (9.117) leads to

$$N_x = \begin{bmatrix} 1 & -0.2366 \\ 1 & +0.2366 \\ 0 & 0 \\ 0 & 0 \end{bmatrix} \quad \text{and} \quad N_u = \begin{bmatrix} 0 & 0.1839 \\ 0 & 0.1839 \end{bmatrix},$$

which can be used to command the system as in Fig. 8.15(a) with $r = [1 \text{ mm} \quad 2 \text{ N}]^T$. Note that $N_x r = x_r = [0.527 \quad 1.473 \quad 0 \quad 0]^T$ as already computed above, and we now have the steady state control, $u_{ss} = N_u r = [0.368 \quad 0.368]^T$, that should eliminate the tension error. The response of the system with this modification is shown in Fig. 9.15. It verifies the elimination of the tension error and that all other specifications are met.

Normally, designers prefer to avoid the use of feedforward of u_{ss} alone because its value depends on accurate knowledge of the plant gain. The preferred method of reducing steady-state errors is to use integral control or possibly to combine integral control with feedforward. In the latter case, the integral's function is simply to provide a correction for a possible error in the feedforward and thus can be designed to have less of an impact on the system bandwidth. So let's design an integral control to replace the u_{ss} feedforward.

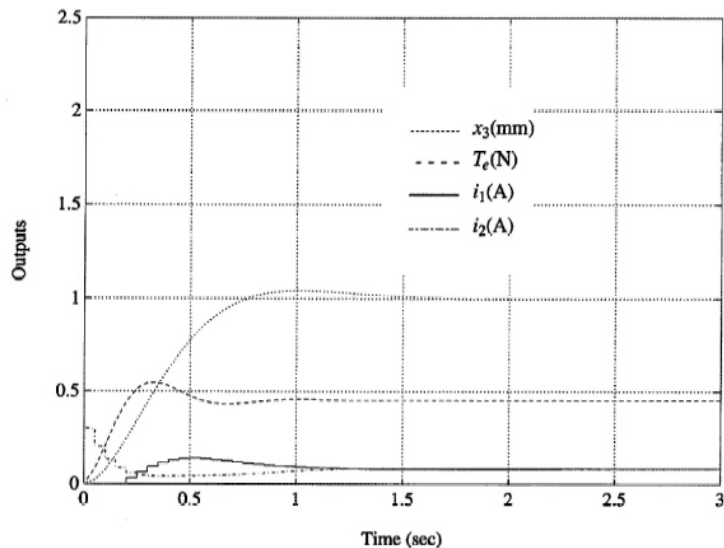


Figure 9.14
Time response
using Eq. (9.121)

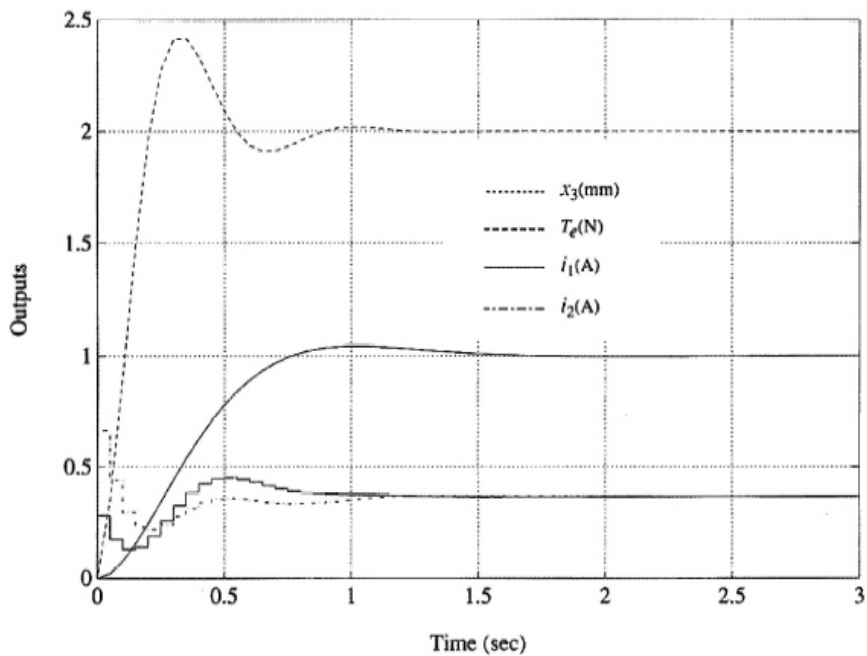


Figure 9.15
Time response
using Eq. (9.121)
and feedforward
of u_{ss}

Because the tension was the only quantity with the error, the integral control need only correct that. Therefore, we will integrate a measurement of the tension and use it to augment the feedback. We start out by augmenting the state with the integral of T_e according to Eq. (8.83) so that

$$\begin{bmatrix} x_I \\ \mathbf{x} \end{bmatrix}_{k+1} = \begin{bmatrix} 1 & \mathbf{H}_I \\ \mathbf{0} & \mathbf{\Phi} \end{bmatrix} \begin{bmatrix} x_I \\ \mathbf{x} \end{bmatrix}_k + \begin{bmatrix} 0 \\ \mathbf{\Gamma} \end{bmatrix} u(k), \quad (9.122)$$

where, from Eq. (9.118)

$$\mathbf{H}_I = [-2.113 \quad 2.113 \quad 0.375 \quad 0.375].$$

We will use the augmented system matrices ($\mathbf{\Phi}_a, \mathbf{\Gamma}_a$) from Eq. (9.122) in an LQR computation with a revised \mathbf{Q}_1 that also weights the integral state variable. This is most easily accomplished by forming a revised \mathbf{H}_w from Eq. (9.120) that includes a fourth output consisting of the tension integral, x_I , and that is used with the augmented state defined by Eq. (9.122). The result is

$$\mathbf{H}_w = \begin{bmatrix} 0 & 0.5 & 0.5 & 0 & 0 \\ 0 & -2.113 & 2.113 & 0.375 & 0.375 \\ 0 & 0 & 0 & 0.5 & 0.5 \\ 1 & 0 & 0 & 0 & 0 \end{bmatrix}. \quad (9.123)$$

The revised weighting matrices are then obtained by the use of Eq. (9.119) with an additional diagonal term in $\bar{\mathbf{Q}}_1$ corresponding to an equal weight on x_I , that is

$$\bar{\mathbf{Q}}_1 = \begin{bmatrix} 0.1 & 0 & 0 & 0 \\ 0 & 0.1 & 0 & 0 \\ 0 & 0 & 0.1 & 0 \\ 0 & 0 & 0 & 0.1 \end{bmatrix} \quad \text{and} \quad \mathbf{Q}_2 = \begin{bmatrix} 1 & 0 \\ 0 & 1 \end{bmatrix}. \quad (9.124)$$

Performing the calculations results in an augmented feedback gain matrix

$$\mathbf{K}_a = \begin{bmatrix} 0.137 & -0.926 & 0.734 & 1.26 & 0.585 \\ 0.137 & -0.734 & 0.926 & 0.585 & 1.26 \end{bmatrix}, \quad (9.125)$$

which can be partitioned into two gains, one for the integral and one for the original state

$$\mathbf{K}_I = \begin{bmatrix} 0.137 \\ 0.137 \end{bmatrix} \quad \text{and} \quad \mathbf{K} = \begin{bmatrix} -0.926 & 0.734 & 1.26 & 0.585 \\ -0.734 & 0.926 & 0.585 & 1.26 \end{bmatrix}. \quad (9.126)$$

These feedback gain matrices are then used to control the system as shown in Fig. 9.16, which is based on the ideas from Fig. 8.23. Essentially, the only difference between this implementation and the previous one is that we have replaced the \mathbf{u}_{ss} feedforward with an integral of the tension error.

The roots of the closed-loop system transformed to the s -plane are

$$s = -9.3, -3.1 \pm j3.1, -5.8 \pm j11.8 \text{ sec}^{-1},$$

and the time response of the system is shown in Fig. 9.17. Again, the tension goes to the desired 2 N, as it should, and all other specifications are met.

Add the Estimator

The only unfinished business now is to replace the full state feedback with an estimated state. We will assume there are two measurements, the tension, T_e , and tape position, x_3 . Although measurements of θ_1 and θ_2 would possibly be easier to make, it is typically best to measure directly the quantities that one is interested in controlling. Therefore, for purposes of estimation, our measurement matrix is

$$\mathbf{H}_e = \begin{bmatrix} 0.5 & 0.5 & 0 & 0 \\ -2.113 & 2.113 & 0.375 & 0.375 \end{bmatrix}. \quad (9.127)$$

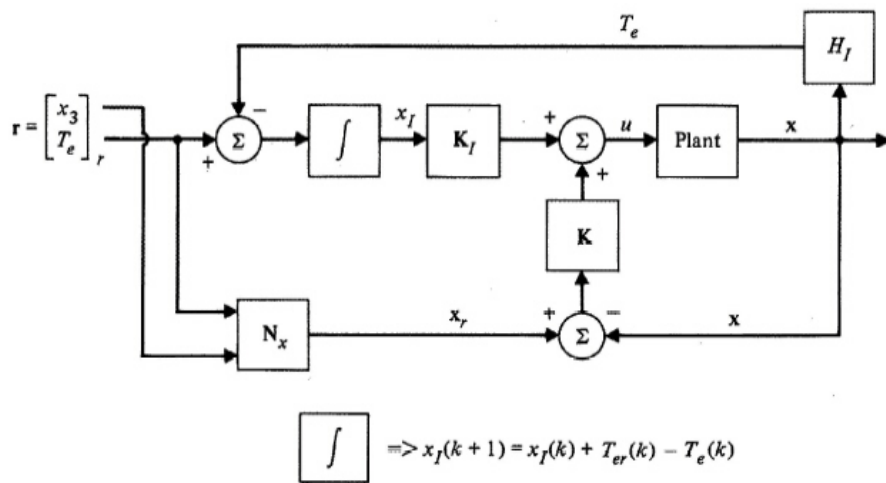


Figure 9.16
Integral control implementation with reference input and full state feedback

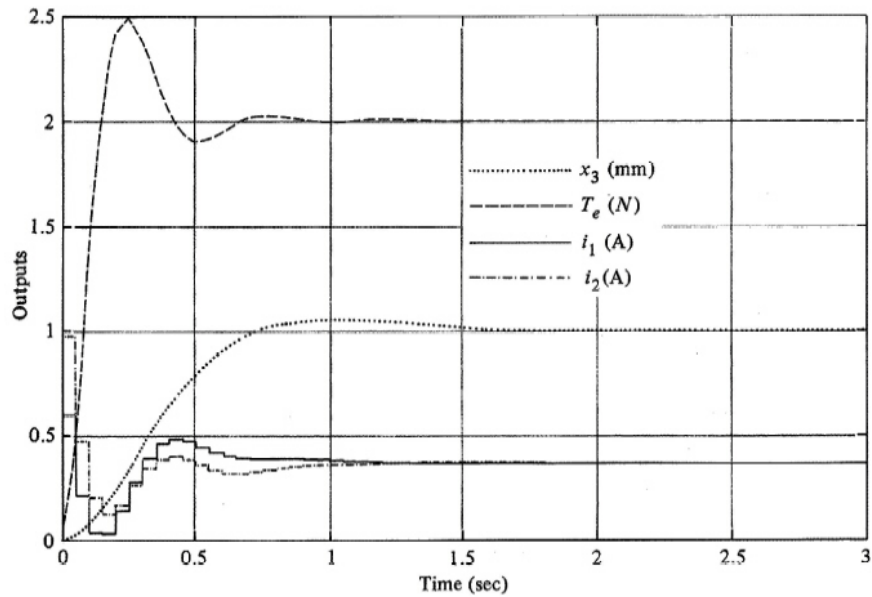


Figure 9.17
Time response using Eq. (9.126) and integral control as in Fig. 9.16

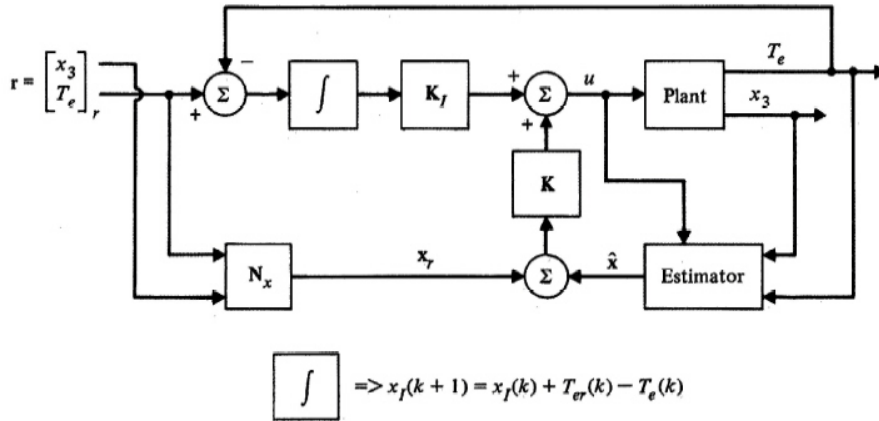


Figure 9.18
Integral control implementation with reference input and estimated state feedback

Let us suppose that the rms accuracy of the tape position measurement is 0.02 mm. According to Eq. (9.104), the first diagonal element of the \mathbf{R}_v matrix is therefore $0.02^2 = 0.0004$. Let us also suppose that the rms accuracy of the tension measurement is 0.01 N. This results in

$$\mathbf{R}_v = \begin{bmatrix} 0.0004 & 0 \\ 0 & 0.0001 \end{bmatrix}. \quad (9.128)$$

Determining values for the process-noise matrix, \mathbf{R}_w , is typically not based on the same degree of certainty as that possible for \mathbf{R}_v . We will assume that the process noise enters the system identically to i_1 and i_2 ; therefore, $\mathbf{\Gamma}_1 = \mathbf{\Gamma}$ in Eq. (9.81). We could make measurements of the magnitude and spectrum of the input-current noise to determine \mathbf{R}_w via Eqs. (9.101) and (9.102). However, other disturbances and modeling errors typically also affect the system and would need to be quantified in order to arrive at a truly optimal estimator. Instead, we will somewhat arbitrarily pick

$$\mathbf{R}_w = \begin{bmatrix} 0.0001 & 0 \\ 0 & 0.0001 \end{bmatrix}, \quad (9.129)$$

compute the estimator gains and resulting roots, then modify \mathbf{R}_w based on the estimator performance in simulations including measurement noise and plausible disturbances. Proceeding, we use the unaugmented $\mathbf{\Phi}$ and $\mathbf{\Gamma}_1$ based on Eq. (9.117) in MATLAB's `kalman.m` with \mathbf{H}_e from Eq. (9.127) and the noise matrices from Eqs. (9.128) and (9.129) to find that

$$\mathbf{L} = \begin{bmatrix} 0.321 & -0.120 \\ 0.321 & 0.120 \\ -0.124 & 0.142 \\ 0.124 & 0.142 \end{bmatrix}, \quad (9.130)$$

which results in estimator error roots that transform to

$$s = -3.0 \pm j4.5, -4.1 \pm j15.4 \text{ sec}^{-1}. \quad (9.131)$$

If implemented using the state command structure as in Fig. 9.18, which has the same reference input structure as in Fig. 9.16, the response will be identical to Fig. 9.17. This follows because the estimator model receives the same control input that the plant does and thus no estimator error is excited. In order to evaluate the estimator, we need to add measurement noise and/or some plant disturbance that is not seen by the estimator. Figure 9.19 shows the system response to the same reference input as Fig. 9.17; but zero mean random noise with an rms of 0.02 mm has been added to the x_3 measurement, noise with an rms of 0.01 N has been added to the T_e measurement, and a step disturbance of 0.01 A has been added to the i_1 entering the plant¹⁸ at 1.5 sec. Note in the figure that

¹⁸Only the plant, not the estimator.

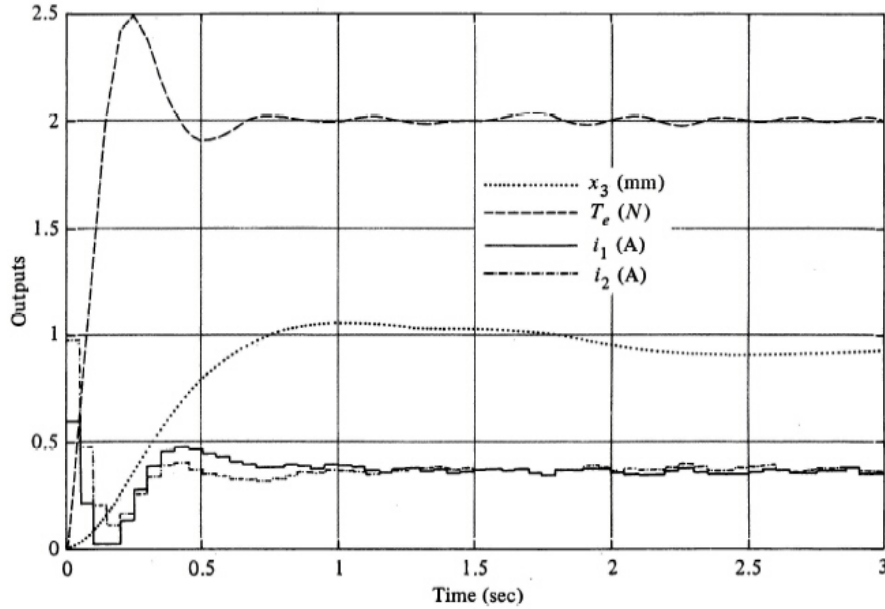


Figure 9.19
Time response with integral control and an estimator with L from Eq. (9.130) including measurement noise and a disturbance at 1.5 sec

there is some noise on T_e and the input currents, and that the disturbance on i_1 caused a steady-state error in x_3 .

This result can be modified by changing the estimator. Let us suppose that we wish to reduce the steady-state error on x_3 and we can tolerate increased noise effects.¹⁹ So let us increase the assumption for the process noise Eq. (9.129) to

$$\mathbf{R}_w = \begin{bmatrix} 0.001 & 0 \\ 0 & 0.001 \end{bmatrix}.$$

By increasing the process noise, we are essentially saying that the knowledge of the plant model is less precise; therefore, the optimal filter will pay more attention to the measurements by increasing the estimator gains and speeding up the estimator. Higher estimator gains should reduce the steady-state estimation errors and their effect on x_3 , but at the cost of increased sensitivity to measurement noise. Carrying out the calculations yields

$$\mathbf{L} = \begin{bmatrix} 0.497 & -0.143 \\ 0.497 & 0.143 \\ -0.338 & 0.329 \\ 0.338 & 0.329 \end{bmatrix}, \quad (9.132)$$

which is larger in every term than the previous gain in Eq. (9.130). Using the gain to form the estimator error equation and transforming its roots to the s -plane results in

$$s = -4.0 \pm j8.2, -2.1 \pm j20.6 \text{ sec}^{-1},$$

which are faster than the previous roots in Eq. (9.131). Evaluation of the same case as in Fig. 9.19 with everything identical except for the estimator gains results in Fig. 9.20. Note that the actual magnitude of the measurement noise and disturbance was *not* changed in generating the figure. The value of \mathbf{R}_w was changed in order to produce higher values in the gain matrix. The figure shows the expected result: larger sensitivity to the measurement noise but reduced sensitivity to the disturbance.

¹⁹We could also add a second integral control loop on x_3 to kill the error, but it is preferable to reduce errors with high control and estimator gains in order to have a robust system for all kinds of errors, if the gains can be tolerated.

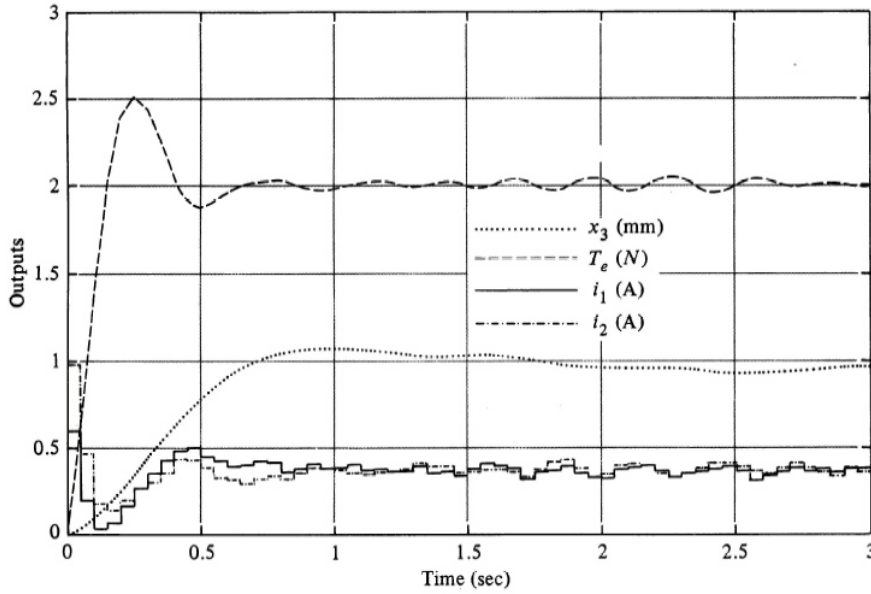


Figure 9.20
Time response with integral control and an estimator with L from Eq. (9.132) including measurement noise and a disturbance at 1.5 sec

Decoupled Design

As a final comment, we note that the plant can be uncoupled and designed as two independent second-order systems, one for x_3 and one for T_e . The key idea to accomplish the uncoupling is to note that equal commands on the two current inputs will cause an increase in tension with no change in x_3 , whereas equal and opposite current commands will cause a change in x_3 with no effect on tension. We therefore transform the control accordingly

$$\mathbf{u}_d = \begin{bmatrix} u_3 \\ u_t \end{bmatrix} = \begin{bmatrix} -1 & 1 \\ 1 & 1 \end{bmatrix} \begin{bmatrix} i_1 \\ i_2 \end{bmatrix} \Rightarrow \mathbf{T}_u = \begin{bmatrix} -1 & 1 \\ 1 & 1 \end{bmatrix}. \quad (9.133)$$

We also define a new state

$$\mathbf{x}_d = \begin{bmatrix} x_3 \\ \dot{x}_3 \\ T_e \\ \dot{T}_e \end{bmatrix} = \begin{bmatrix} \mathbf{H}_3 \\ \mathbf{H}_3\mathbf{F} \\ \mathbf{H}_t \\ \mathbf{H}_t\mathbf{F} \end{bmatrix} \mathbf{x} = \mathbf{T}_d\mathbf{x}, \quad (9.134)$$

where \mathbf{H}_3 and \mathbf{H}_t are the partitions of \mathbf{H}_e in Eq. (9.127) and \mathbf{F} is the system matrix from Eq. (9.117). Following the state transformation ideas in Section 4.3.3, we can write that

$$\dot{\mathbf{x}}_d = \mathbf{F}_d\mathbf{x}_d + \mathbf{G}_d\mathbf{u}_d, \quad (9.135)$$

where

$$\mathbf{F}_d = \mathbf{T}_d\mathbf{F}\mathbf{T}_d^{-1} \quad \text{and} \quad \mathbf{G}_d = \mathbf{T}_d\mathbf{G}\mathbf{T}_u^{-1}. \quad (9.136)$$

Performing these calculations yields

$$\mathbf{F}_d = \begin{bmatrix} 0 & 1 & 0 & 0 \\ 0 & 0 & 0 & 0 \\ 0 & 0 & 0 & 1 \\ 0 & 0 & -66.3 & -1.18 \end{bmatrix} \quad \text{and} \quad \mathbf{G}_d = \begin{bmatrix} 0 & 0 \\ 42.7 & 0 \\ 0 & 3.2 \\ 0 & 176.5 \end{bmatrix}. \quad (9.137)$$

Therefore, we see that there is a decoupling that results in two separate systems,

$$\begin{bmatrix} \dot{x}_3 \\ \ddot{x}_3 \end{bmatrix} = \begin{bmatrix} 0 & 1 \\ 0 & 0 \end{bmatrix} \begin{bmatrix} x_3 \\ \dot{x}_3 \end{bmatrix} + \begin{bmatrix} 0 \\ 42.7 \end{bmatrix} u_3, \quad (9.138)$$

and

$$\begin{bmatrix} \dot{T}_e \\ \ddot{T}_e \end{bmatrix} = \begin{bmatrix} 0 & 1 \\ -66.3 & -1.18 \end{bmatrix} \begin{bmatrix} T_e \\ \dot{T}_e \end{bmatrix} + \begin{bmatrix} 3.2 \\ 176.5 \end{bmatrix} u_t. \quad (9.139)$$

The two system equations, (9.138) and (9.139), can then be used to design two control systems using SISO methods. The resulting controls, u_3 and u_t , can then be “unscrambled” via \mathbf{T}_u to arrive at the desired i_1 and i_2 , that is,

$$\begin{bmatrix} i_1 \\ i_2 \end{bmatrix} = \mathbf{T}_u^{-1} \begin{bmatrix} u_3 \\ u_t \end{bmatrix}.$$

The perfect uncoupling was due to the perfect symmetry of the problem: motors and capstan inertias identical, motor constants identical, and tape read head exactly in the middle of the capstans. In an actual system, there would be differences and some coupling would be present. Due to the simplicity of the uncoupled design and its implementation, however, it can be worthwhile to evaluate the performance of a decoupled design to see if its errors warranted the full MIMO design.

9.6 Summary

- An optimal controller is one that minimizes a quadratic cost function where weighting matrices are selected by the designer to achieve a “good” design. Criteria for evaluation of the design are based on all the same factors that have been discussed throughout the book.
- Optimal control methods are useful in designing SISO systems because they help the designer place the pole locations.
- Optimal control methods are essential in designing MIMO systems as they reduce the degrees of freedom in the design iteration down to a manageable few.
- Generally, for linear, stationary systems, the steady-state optimal control solution is satisfactory and far more practical than the true optimal time-varying gain solution.
- The most accurate discrete emulation method is based on finding the discrete equivalent of a continuous cost function and solving for the discrete optimal control system with that cost.
- An optimal estimator is based on achieving the minimum mean square estimation error for a given level of process and measurement noise acting on the system.
- Generally, for linear, stationary systems, the steady-state optimal estimator is satisfactory and far more practical than the true optimal time-varying gain solution (Kalman filter).
- Optimal estimators are useful for SISO system design and essential for MIMO system design.
- The optimization procedures provide a technique for which many good design candidates can be generated which can then be evaluated to ascertain whether they meet all the design goals. The procedures do not eliminate trial-and-error methods; rather, they transfer iteration on classical compensation parameters to iteration on optimal cost-function parameters or assumed system noise characteristics.

9.7 Problems

9.1 Optimal control derivation:

- Derive Eq. (9.33) and hence verify the control Hamiltonian as given by Eq. (9.34).
- Demonstrate that if \mathbf{W} is a transformation that brings \mathcal{H}_c to diagonal form, then the first n columns of \mathbf{W} are eigenvectors of \mathcal{H}_c associated with stable eigenvalues.

- (c) Demonstrate that if the optimal steady-state control, \mathbf{K}_∞ , given by Eq. (9.47) is used in the plant equation Eq. (9.10), then the matrix in the upper left corner of \mathbf{W} , which is \mathbf{X}_I , has columns that are eigenvectors of the closed-loop system.

9.2 Symmetric root locus:

- (a) Compute the closed-loop pole locations of the satellite design problem, using the steady-state gains given by Fig. 9.3.
- (b) Take the discrete transfer function from u to θ for the satellite design problem (Appendix A) and form the symmetric root locus. Plot the locus and locate the values of ρ corresponding to the selections of Q_2 given in Eq. (9.30).
- (c) Show that for a system with one control it is always possible to construct a symmetric root locus corresponding to the optimal steady-state control. [Hint: Show that if $\mathbf{Q}_1 = \mathbf{H}\mathbf{H}^T$ and $\mathbf{G}(z)$ is a column-matrix transfer function given by $\mathbf{H}(z\mathbf{I} - \mathbf{\Phi})^{-1}\mathbf{\Gamma}$, then the roots of the optimal control are given by $1 + \rho\mathbf{G}^T(z^{-1})\mathbf{G}(z) = 0$, which is a scalar symmetric root-locus problem and which can be put in the form $1 + \rho G_1(z^{-1})G_1(z) = 0$. Use Eq. (9.38).]
- (d) Give the equivalent scalar plant transfer function $G_1(z)$, if we have the satellite control problem and use $\mathbf{Q}_1 = \mathbf{I}$, the 2×2 identity. Draw the symmetric root locus for this case.

9.3 Compute the location of the closed-loop poles of the optimal filter for the satellite problem for each of the values of R_w given by the steady final values of the curves of Fig. 9.8.

9.4 For the antenna example in Appendix A.2,

- (a) Design an optimal controller corresponding to the cost function $\mathcal{J}(y, u) = u^2 + \rho y^2$ for $\rho = 0.01, 0.1$, and 1 . Use $T = 0.2$ sec. Plot the step response of the closed loop system for initial errors in y and \dot{y} in each case. Which value of ρ most nearly meets the step-response specification given in Chapter 7?
- (b) Draw the symmetric root locus corresponding to the design of part (a).
- (c) Design an optimal steady-state filter for the antenna. Assume that the receiver noise has a variance $R_v = 10^{-6}\text{rad}^2$ and that the wind gust noise, w_d , is white, and we want three cases corresponding to $R_{wpsd} = 10^{-2}, 10^{-4}$, and 10^{-6} .
- (d) Plot the step response of the complete system with control law corresponding to $\rho = 0.1$ and filter corresponding to $R_{wpsd} = 10^{-4}$.

9.5 The lateral equations of motion for the B-767 in cruise are approximately

$$\begin{bmatrix} \dot{v} \\ \dot{r} \\ \dot{\phi}_p \\ \dot{p} \end{bmatrix} = \begin{bmatrix} -0.0868 & -1 & -0.0391 & 0 \\ 2.14 & -0.228 & 0 & -0.0204 \\ 0 & 0 & 0 & 1 \\ -4.41 & 0.334 & 0 & -1.181 \end{bmatrix} \begin{bmatrix} v \\ r \\ \phi_p \\ p \end{bmatrix} + \begin{bmatrix} 0.0222 & 0 \\ -1.165 & -0.065 \\ 0 & 0 \\ 0.549 & -2.11 \end{bmatrix} \begin{bmatrix} \delta_r \\ \delta_a \end{bmatrix}$$

- (a) Design two second-order controllers by ignoring the cross-coupling terms. Pick roots at $s = -1 \pm j1.5$ rad/sec for the yaw mode (v and r) and $s = -2, -0.1$ for the roll mode (ϕ_p and p). Use a sample period of $T = 0.05$ sec.
- (b) Determine the root locations that result when the cross-coupling terms are included. (Use `eig.m` in MATLAB.)
- (c) Assuming one can measure r and ϕ_p , design two second-order estimators by ignoring the cross-coupling terms. Place all poles at $s = -2$ rad/sec.

- (d) Determine the root locations that result from (c) when the cross-coupling terms are included.

9.6 The equations of motion for a stick balancer (Fig. 9.2) are given by

$$\begin{bmatrix} \dot{\theta} \\ \dot{\omega} \\ \dot{x} \\ \dot{v} \end{bmatrix} = \begin{bmatrix} 0 & 1 & 0 & 0 \\ 21 & 0 & 0 & 0.8 \\ 0 & 0 & 0 & 1 \\ 0 & 0 & 0 & -0.4 \end{bmatrix} \begin{bmatrix} \theta \\ \omega \\ x \\ v \end{bmatrix} + \begin{bmatrix} 0 \\ -2 \\ 0 \\ 1 \end{bmatrix} u,$$

$$\begin{bmatrix} y_1 \\ y_2 \end{bmatrix} = \begin{bmatrix} 1 & 0 & 0 & 0 \\ 0 & 0 & 1 & 0 \end{bmatrix} \begin{bmatrix} \theta \\ \omega \\ x \\ v \end{bmatrix}.$$

Design two second-order estimators, one for the stick (θ, ω) and one for the cart (x, v). Verify that the one-way coupling (cart to stick only) causes the full fourth-order estimator to have the same roots as the separate second-order designs.

- 9.7 Starting with the paper-machine design in Section 9.5.3 whose output is shown in Fig. 9.11, perform design iterations on \mathbf{Q}_1 , \mathbf{Q}_2 , and t_s to find the lowest possible value of u_1 that still meets the state specifications on maximum value and settling time. [Hint: The routines FIG99.M, FIG910.M and FIG911.M from the Digital Control Toolbox will be useful to you.]
- 9.8 For the double mass-spring system in Example 9.5, investigate the effect of different \mathbf{Q} 's on the closed-loop poles of the system. In particular, determine a \mathbf{Q} that will yield an equivalent damping of the oscillatory poles that is greater than $\zeta = 0.5$. [Hint: FIG95.M from the Digital Control Toolbox will be useful to you.]
- 9.9 For the double mass-spring system in Example 9.5, design a controller and estimator that uses a measurement of d . It should respond to a command input for d with a rise time of 2 sec with an overshoot less than 20%.
- 9.10 For the double mass-spring system in Example 9.5, design a controller and estimator that uses a measurement of d . It should respond to a command input for d with a rise time of 3 sec with an overshoot less than 15%. Plot the frequency response of your compensation (control plus estimator) and qualitatively describe the features of the compensation.
- 9.11 A simplified model of a disk drive is

$$G(s) = \frac{10^6 \omega_r^2}{s^2(s^2 + 2\zeta \omega_r s + \omega_r^2)},$$

where $\omega_r = 19,000$ rad/sec ($\cong 3$ KHz) and $\zeta = 0.05$. This is the transfer function between the torque applied to the disk head arm and the motion of the read head on the end of the arm. Note this is also the same generic model as the double mass-spring system in Eq. (A.20). The system has the capability to measure where the heads are with respect to the data tracks on the disk. The two biggest disturbances are due to an actuator bias (w_d) and track wobble (y_d) from an off center disk mounting. A schematic diagram of the system to be controlled is shown in Fig. 9.21.

Since the disk is rotating at 3822 rpm (400 rad/sec), an offset causes a sinusoidal y_d to be added to the output of the transfer function above. The purpose of the servo is to follow the data tracks as closely as possible, whether the disk is slightly off center or not because that allows higher data densities on the disk. It is also desirable for the servo to settle on a new track as quickly as possible because the disk access time is directly related to this settling time and is a major selling point for disk drives.

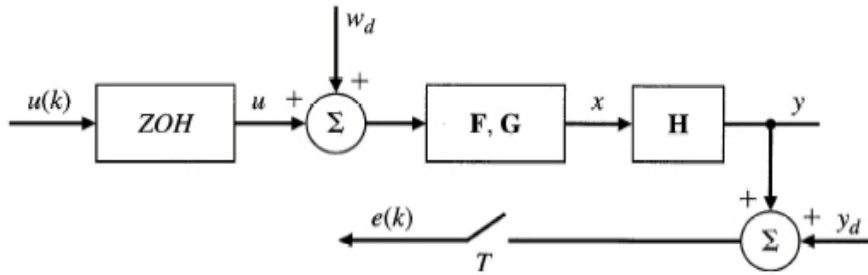


Figure 9.21
Disk drive
closed-loop
system for
Problems 9.11
and 9.12

Design a discrete compensator with a sample rate no faster than 8 kHz that has an overshoot to a step command no greater than 20%, does not allow steady state tracking errors due to the actuator bias, and has a settling time (to within 5% of the final value) to a step input less than 5 msec. The system should be robust with respect to variations in the resonance frequency as this can change by $\pm 2\%$ due to temperature changes. Plot the closed-loop frequency response of the error, e , in order to evaluate how well your system attenuates the disturbance response in the vicinity of 400 rad/sec (3822 rpm).

- 9.12 Design a compensator for the disk drive servo specified in Problem 9.11 so that it provides the minimum possible error due to the disturbance at 3822 rpm. Since the spin rate drifts some, define the error to be the average of that from: the nominal spin rate of 3822 rpm, $+1\%$ of the nominal, and -1% of the nominal. (*Hint*: Review Section 8.5.)

- 9.13 For

$$G(s) = \frac{1}{s^2},$$

use optimal control and estimation to design compensation that provides a 10 msec rise time with less than a 10% overshoot to a command. Determine the closed-loop system bandwidth and the system phase margin.

- 9.14 The MATLAB code below will generate some noisy data from an oscillator driven by a square wave

```
F=[0 1;-1 0];G=[0;1];H=[1 0];J=0;T=0.5;
sysC = ss(F,G,H,J)
sysD=c2d(sysC,T)
Un=[ones(1,10) zeros(1,10) ones(1,10) zeros(1,11)];
U=Un+0.1*randn(size(Un));
Yn=lsim(sysD,U);
Ym=Yn+0.2*randn(size(Yn))
```

The measurement noise is zero mean and normally distributed with $R_v = 0.2^2$ while the process noise is zero mean and normally distributed with $R_w = 0.1^2$. Assume the initial value of the state has a covariance matrix

$$\mathbf{M} = \begin{bmatrix} 1 & 0 \\ 0 & 1 \end{bmatrix},$$

and use a time-varying Kalman filter to reconstruct the state. Compare the resulting time history of the optimal state estimate with that from a constant gain Kalman filter. [*Hint*: FIG98.M from the Digital Control Toolbox will be useful to you.]

- 9.15 Repeat Example 9.7, but fit the best straight line to the data. [*Hint*: FIG97.M from the Digital Control Toolbox will be useful to you.]

Chapter 10

Quantization Effects

A Perspective on Quantization

In Chapter 13 we will consider the analysis of systems having general nonlinearities; but first, in this chapter, we will consider the special nonlinearity of digital control: Numbers in the computer must be forced to fit in digital words that are defined by a finite number of bits, usually 8, 16, 32, or 64 bits. Thus far we have considered the use of the digital computer as a linear, discrete-time device for implementing control designs. Now we turn to consideration of the fact that numbers in the computer are taken in, stored, calculated, and put out with finite accuracy. The technique of representing a real number by a digital value of finite accuracy affects digital control in two principal ways. First, the variable values such as e , u , and the internal state variables, \mathbf{x} , used in the difference equations are not exact, and thus errors are introduced into the output of the computer. As we shall see, these errors can often be analyzed as if there were noise sources in the computer. Second, the coefficients such as a_i and b_i of the difference equations, which must be stored in the computer, cannot be arbitrary real numbers but must be realizable by a finite number of bits. This can cause the machine to solve a slightly different equation than it was designed to do and has the potential to result in instability. Our purpose in this chapter is to explore methods that can be used for the analysis of these two effects: quantization of variables and quantization of coefficient parameters. The effect of quantization when the microprocessor has 32 bits is typically not noticeable. However, some products are very cost sensitive and it is desirable to use an 8 bit computer, if possible. The material in this chapter is primarily directed toward the design of such systems.

Chapter Overview

The random error model for the round-off process is first developed in Section 10.1. This section also develops several analysis methods for such random processes that are useful for quantization and then applies the random process analysis methods from Chapter 9 to the quantization case. Section 10.2 examines the deterministic problem of parameter storage quantization errors and demonstrates the sensitivity of the errors to the structure of the difference equation mechanization. The last section, 10.3, describes some of the consequences of round-off errors and what steps can be taken to alleviate them.

10.1 Analysis of Round-Off Error

In our first analysis of finite accuracy we will assume that the computer represents each number with a fixed location for the equivalent of the decimal point, or **fixed point** representation. Although for any given number the point is fixed, considerations of amplitude scaling and dynamic range often require that different numbers in the same program have their decimal points in different locations. The consequence is that different magnitudes of errors are introduced at different locations as the results of calculations being fitted into the proper computer number format. Fixed point representation

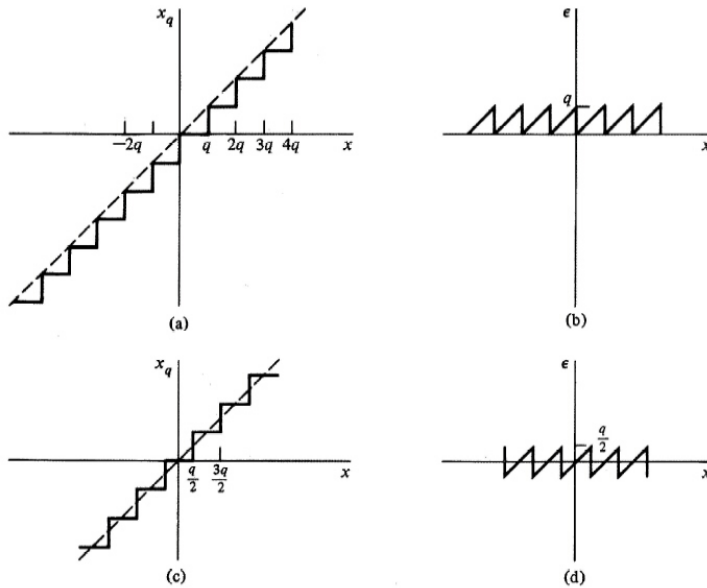


Figure 10.1
 Plot of effects of number truncation. (a) Plot of variable versus truncated values. (b) Plot of error due to truncation. (c) Plot of variable versus rounded values. (d) Round-off error

is typical in real-time control computers; however, in scientific calculations done in higher-level languages such as BASIC, MATLAB, or C, **floating point** representations are mainly used, wherein the number representation has both a mantissa (magnitude and sign information) and an exponent that causes the location of the decimal point to float. With fixed-point arithmetic, addition and subtraction are done without error except that the sum can overflow the limits of the representation. Overflow must be avoided by proper amplitude scaling or analyzed as a major nonlinearity. For control- or signal-processing applications, the logic is arranged so that the result of overflow is a saturation effect, a nonlinearity that will be treated in Chapter 13. In the case of multiplication, however, a double-length product is produced and the machine must reduce the number of bits in the product to fit it into the standard word size, a process we generally call **quantization**. One way to perform quantization is by ignoring the least significant half of the product, a process called **truncation**. If we assume that the numbers are represented with base 2 and that ℓ binary digits (bits) are to the right of the point (for the fractional part), the least significant bit kept represents the magnitude $2^{-\ell}$. The result of truncation will be accurate to this value (the part thrown away could be almost as large as $2^{-\ell}$). Thus a plot of the “true” value of a variable x versus the quantized value, x_q , would look like Fig. 10.1(a), where the error (shown in (b)) is decided by the quantum size, q (which is $2^{-\ell}$ under the conditions mentioned above). It is common practice in control computers to use **round-off** rather than truncation. With round-off, the result is the same as truncation if the first bit lost is a 0, but the result is increased by $2^{-\ell}$ if the first bit lost is a 1. The process is the same as is common with ordinary base 10 numbers where, for example, 5.125 is rounded to 5.13, but 5.124 becomes 5.12 to two (decimal) places of accuracy. An input–output plot of rounding is shown in Fig. 10.1(c), and the corresponding error is shown in 10.1(d).¹ Notice that the maximum error with roundoff is half that resulting from truncation. The value of ℓ in a particular case depends on the word size of the particular computer in use. For control implementations the choice is based on the required accuracy and dynamic range and is limited by the expense. At this time (1997), microprocessors are readily available with word sizes of 8, 16, and 32 bits, with a cost premium on the larger sizes. One of the goals of this chapter is to analyze the effect of ℓ and thus of word size on the stability and on the errors due to quantization’s effects so the designer can select the smallest word size consistent with the required performance.

¹The plots in Fig. 10.1 assume that the numbers are represented in two’s complement code.

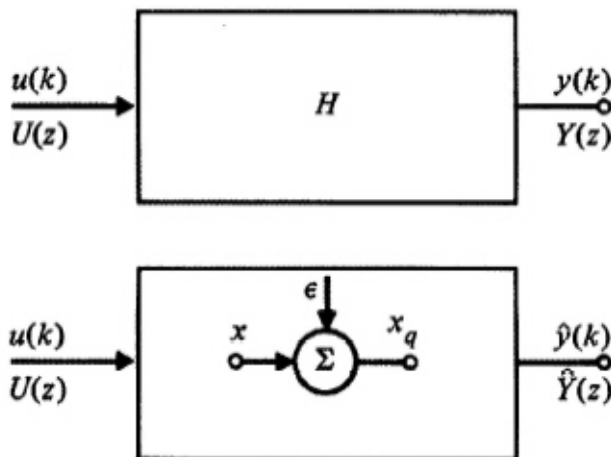


Figure 10.2
A linear system and the introduction of one source of round-off errors

We can represent either truncation or round-off by the equation

$$x = x_q + \varepsilon, \quad (10.1)$$

where ε is the error caused by the truncation or round-off of x into the digital representation x_q . Because the error due to truncation equals a constant plus round-off error, we will assume round-off in our analysis unless otherwise stated and assume that analysis of the effects of the additional constant bias when truncation is used (which is rare) can be treated separately. Clearly the process of analog-to-digital conversion also introduces a similar effect, although often with still another value for q than those resulting from round-off during arithmetic in the microprocessor.

The analysis of the effects of round-off depends on the model we take for ε . We will analyze three such models, which we can classify as (a) worst case, for which we will bound the error due to round-off; (b) steady-state worst case, for which we will compute the largest output possible if the system reaches a constant steady state; and (c) stochastic, for which we will present a model of the round-off error as a random process and compute the root-mean-square of the output error due to round-off.

quantization models

The Worst-Case Error Bound

The worst-case analysis is due to Bertram (1958). His analysis takes the pessimistic view that the round-off occurs in such a way as to cause the maximum harm, and his analysis bounds the maximum error that can possibly result from round-off. First we consider the case shown in Fig. 10.2, in which a single case of quantization is assumed to occur somewhere in an otherwise linear constant system.

Bertram bound

There is a transfer function from the point of round-off to the output, which we will call $H_1(z)$, and we can describe the situation by the equations

$$\begin{aligned} Y(z) &= H(z)U(z), \\ \hat{Y}(z) &= H(z)U(z) - H_1(z)E_1(z;x), \\ Y - \hat{Y} = \tilde{Y} &= H_1(z)E_1(z;x). \end{aligned} \quad (10.2)$$

We write E_1 as a function of the state variable x to emphasize that Eq. (10.2) is *not* linear because we do not know how to compute E_1 until we have the values of x . However, we are not looking for the exact value of \tilde{Y} but an upper bound on the time error, $\tilde{y}(k)$.

Because we wish to find a bound on the time signal $\tilde{y}(k)$, we need the time domain equivalent of

Eq. (10.2), which is the convolution sum given by

$$\tilde{y}(n) = \sum_{k=0}^n h_1(k) \varepsilon_1(n-k; x). \quad (10.3)$$

If we examine Fig. 10.1(d), we can see that whatever the exact values of ε_1 may be, its magnitude is bounded by $q_1/2$, where q_1 is the quantum value for the operation which introduces the quantization being analyzed. We can use this information to determine in short steps the bound on \tilde{y} as we did in Chapter 4 in the discussion of BIBO (bounded input, bounded output) stability. Taking the magnitudes of both sides on Eq. (10.3), we get

$$|\tilde{y}| = \left| \sum_0^n h_1 \varepsilon_1 \right|.$$

Because the sum is bounded by the sum of the magnitudes of each term, we have the inequality

$$\leq \sum_0^n |h_1 \varepsilon_1|,$$

which is the same as

$$\leq \sum_0^n |h_1| |\varepsilon_1|;$$

but by Fig. 10.1(d), the error magnitude is always less than $q_1/2$, so the output error is bounded by

$$\leq \sum_0^n |h_1| \frac{q_1}{2}.$$

Finally, the sum can only get larger if we increase the number of terms

$$|\tilde{y}(n)| \leq \sum_0^\infty |h_1| \frac{q_1}{2}. \quad (10.4)$$

Equation (10.4) is Bertram's worst-case bound. The function `qwc.m`² computes it. By comparison with the condition for BIBO stability, we can conclude that if the linear system is BIBO stable in response to inputs applied at the point of the quantization, then introduction of the quantization will not cause the system to be unstable in the BIBO sense.³ As we will see later, the system with quantization can have an output error that is nonzero either as a constant or as an oscillation; so the system may not be asymptotically stable but the output error will not grow beyond the bound given by Eq. (10.4).

Bertram Bound Application

Example 10.1

For the first-order system

$$y(k+1) = \alpha y(k) + u(k), \quad (10.5)$$

compute Bertram's bound, assuming that the round-off occurs in the computation of the product αy .

Solution. Using Eq. (10.4), we have

$$\hat{y}(k+1) = \alpha \hat{y}(k) + \varepsilon(k) + u(k), \quad (10.6)$$

and thus

$$\tilde{y}(k+1) = \alpha \tilde{y}(k) - \varepsilon(k). \quad (10.7)$$

²In the Digital Control Toolbox.

³We assume that there is no saturation of the quantizer during the transient.

For the error system, the unit pulse response is $h_1(k) = \alpha^k$, and Eq. (10.4) is easily computed as follows for $|\alpha| < 1$

$$|\bar{y}| \leq \frac{q}{2} \sum_{k=0}^{\infty} |\alpha|^k \leq \frac{q}{2} \frac{1}{1-|\alpha|}. \quad (10.8)$$

For this example, if $\alpha > 0$, the error due to quantization at any particular time is bounded by the DC gain from the quantizer to the output times $q/2$. This bound is only likely to be approached when a system has a constant input and has settled to its steady-state value.

The Steady-State Worst Case

The steady-state worst case was analyzed by Slaughter (1964) in the context of digital control, and by Blackman (1965) in the context of digital filters. For this analysis, we view the round-off to cause some stable, transient errors of no special concern, and we assume that all variables eventually, in the steady state, become constants. We wish to know how large this steady-state error can be as a result of round-off. We consider again the situation shown in Fig. 10.2 and thus Eq. (10.3). In this case, however, we assume that Eq. (10.3) reaches a steady state, at which time ε is constant and in the range $-q/2 \leq \varepsilon_{ss} \leq q/2$. Then Eq. (10.3) reduces to

$$\tilde{y}_{ss}(\infty) = \sum_0^{\infty} h_1(n) \varepsilon_{ss}.$$

The worst steady-state error is the magnitude of this signal with $\varepsilon_{ss} = q/2$, which is

$$|\tilde{y}_{ss}(\infty)| \leq \left| \sum_0^{\infty} h_1(n) \right| \frac{q}{2}. \quad (10.9)$$

There is one nice thing about Eq. (10.9): The sum is the value of the transfer function $H_1(z)$ at $z = 1$, and we can write⁴

$$|\tilde{y}_{ss}(\infty)| \leq |H_1(1)| \frac{q}{2}. \quad (10.10)$$

Worst Case Steady-State Bound

Example 10.2

Use the worst case analysis to compute the error bound for the first-order system given by Eq. (10.5).

Solution. In this case, the transfer function is

$$H_1(z) = 1/(z - \alpha).$$

From Eq. (10.10), we find that the bound is

$$|\tilde{y}_{ss}| \leq \frac{q}{2} \frac{1}{1-\alpha}. \quad (10.11)$$

This is the same as the Bertram worst-case bound if $\alpha > 0$.

So we see that this steady-state worst case yields the general result that the error is bounded by $q/2 \times$ dc gain from the quantization source to the output.

Equations (10.4) and (10.9) or (10.10) express the consequences of round-off from one source. For multiple sources, these equations can be extended in an obvious way. For example, if we have K

⁴A function to compute the quantization steady-state error is given by `qss.m` in the Digital Control Toolbox.

sources of round-off, each with possibly different quantization levels q_j , then Eq. (10.4) becomes

$$\begin{aligned} |\tilde{y}| &\leq \left\{ \sum_{n=0}^{\infty} |h_1(n)| \frac{q_1}{2} + \sum_{n=0}^{\infty} |h_2(n)| \frac{q_2}{2} + \dots \right\} \\ &\leq \sum_{j=1}^K \sum_{n=0}^{\infty} |h_j(n)| \frac{q_j}{2}. \end{aligned} \quad (10.12)$$

If all the quanta should be equal, the error bound is

$$\begin{aligned} |\tilde{y}| &\leq \left\{ \sum_{n=0}^{\infty} |h_1(n)| + \sum_{n=0}^{\infty} |h_2(n)| + \dots \right\} \frac{q}{2} \\ &\leq \sum_{j=1}^K \sum_{n=0}^{\infty} |h_j(n)| \frac{q}{2}. \end{aligned}$$

And likewise for multiple sources, Eq. (10.10) is extended to

$$|y_{ss}(\infty)| \leq [|H_1(1)| \frac{q_1}{2} + |H_2(1)| \frac{q_2}{2} + \dots + |H_K(1)| \frac{q_K}{2}]. \quad (10.13)$$

It is easily possible to express Eq. (10.10) in terms of a state-variable formulation of the equations of motion. Suppose the equations from the point of the quantization to the output are given by

$$\begin{aligned} \mathbf{x}(k+1) &= \mathbf{\Phi}\mathbf{x}(k) + \mathbf{\Gamma}_1 \varepsilon_1(k), \\ \tilde{y}(k) &= \mathbf{H}\mathbf{x}(k) + J\varepsilon_1(k). \end{aligned} \quad (10.14)$$

The assumptions of the steady-state worst-case error are that $\mathbf{x}(k+1) = \mathbf{x}(k) = \mathbf{x}_{ss}$ and $\varepsilon_1(k) = \varepsilon_{1,ss}$. Then

$$\mathbf{x}_{ss} = \mathbf{\Phi}\mathbf{x}_{ss} + \mathbf{\Gamma}_1 \varepsilon_{1,ss}, \quad \tilde{y} = \mathbf{H}\mathbf{x}_{ss} + J\varepsilon_{1,ss}. \quad (10.15)$$

Solving for \tilde{y} , we find

$$\tilde{y} = [\mathbf{H}[\mathbf{I} - \mathbf{\Phi}]^{-1} \mathbf{\Gamma}_1 + J] \varepsilon_{1,ss},$$

which is bounded by

$$|\tilde{y}| \leq |[\mathbf{H}[\mathbf{I} - \mathbf{\Phi}]^{-1} \mathbf{\Gamma}_1 + J]| \frac{q_1}{2}. \quad (10.16)$$

The major advantage of the steady-state result is the vastly simpler forms of Eqs. (10.13) and (10.16) as compared to (10.12). Unfortunately, Eq. (10.13) does not always hold because of the assumption of a constant quantization error of $q/2$ in the steady state,⁵ and yet the worst-case upper bound given by Eq. (10.12) is often excessively pessimistic. However, in some cases there is great expense due to distortion of the data should a signal overflow, and the absolute bound can be used to select q so that no overflow is possible. An example of the use of Bertram's bound in the design of a spectrum analyzer is given in Schmidt (1978).

Stochastic Analysis of Round-Off Error

The third model for round-off error is that of a stochastic variable. The analysis will follow Widrow (1956) and has two parts: development of a stochastic model for $\varepsilon(k)$ and analysis of the response of a linear system to a stochastic process that has the given characteristics. Because the development of the model requires use of somewhat sophisticated concepts of stochastic processes, and because the model can be given a very reasonable heuristic justification without this mathematical apparatus, we develop the model heuristically and proceed with an analysis of the response. A review of the necessary facts from the theory of probability and stochastic processes is to be found in Appendix D.

⁵Note that Eqs. (10.13) and (10.16) are *not* bounds on the error. They do, however, give a valuable estimate on error size, which is easy to compute for complex systems.

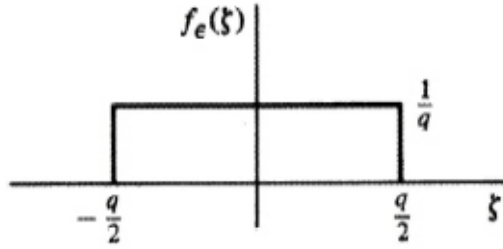


Figure 10.3
Plot of the
uniform density
function

First, then, we give a heuristic argument for a stochastic model of round-off error. We begin with examination of Fig. 10.1, where we have a plot of the output versus the input of the round-off operation and a sketch of error versus amplitude of the input signal x . If we imagine that $x(n)$ is a random variable that takes values at successive sampling instants in a scattered way across the scale of values, then it seems reasonable to suppose that the sequence of errors $\varepsilon(n)$ would be scattered over the entire range of possible values, which is to say, over the range from $-q/2$ to $q/2$. Furthermore, because the “teeth” in the saw like plot of ε versus x are linear and contain no flat places that would signal a preference for one value of ε over another, it seems reasonable that the values of $\varepsilon(n)$ are equally likely to be anywhere in the range $-q/2 \leq \varepsilon \leq q/2$. Furthermore, if the signal into the quantizer typically moves several quanta during one sample period, it seems reasonable to assume that the values of error at one sample time will not be correlated with errors at other times; that is, its spectrum would be expected to be flat, which we characterize as “white.”⁶ The reflection of this argument in terms of stochastic processes is to assert that we can model $\varepsilon(k)$ as a white random process having a uniform probability density from $-q/2$ to $q/2$. A plot of the uniform density is shown in Fig. 10.3.

From this density we can immediately compute the mean and variance of ε as follows

$$\mu_{\varepsilon} = \mathcal{E}\{\varepsilon\} = \int_{-\infty}^{\infty} \xi f_{\varepsilon}(\xi) d\xi = \int_{-q/2}^{q/2} \xi \frac{1}{q} d\xi = \frac{1}{q} \left. \frac{\xi^2}{2} \right|_{-q/2}^{q/2} = 0, \quad (10.17)$$

quantization
variance

and

$$\begin{aligned} \sigma_{\varepsilon}^2 &= \mathcal{E}\{(\varepsilon - \mu_{\varepsilon})^2\} = \int_{-\infty}^{\infty} (\xi - 0)^2 f_{\varepsilon}(\xi) d\xi = \int_{-q/2}^{q/2} (\xi)^2 \frac{1}{q} d\xi \\ &= \frac{1}{q} \left. \frac{(\xi)^3}{3} \right|_{-q/2}^{q/2} = \frac{1}{q} \left[\frac{1}{3} (q/2)^3 - \frac{1}{3} (-q/2)^3 \right] \\ &= \frac{1}{3q} \left[\frac{q^3}{8} + \frac{q^3}{8} \right] = \frac{q^2}{12}. \end{aligned} \quad (10.18)$$

Thus we assume the following white-noise model for $\varepsilon(n)$ for the case of round-off error as sketched in Fig. 10.1(d)

$$\varepsilon(n) = w(n), \quad (10.19)$$

where $w(n)$ has the autocorrelation function (defined in Appendix D)

$$\begin{aligned} R_w(n) &= \mathcal{E}\{w(k)w(k+n)\} = q^2/12 \quad (n=0) \\ &= 0 \quad (n \neq 0), \end{aligned} \quad (10.20)$$

and the mean value μ_{ε} is zero.

⁶If the input to the quantizer is a deterministic signal such as a square wave, a constant, or a sine wave, this argument is clearly wrong. It is also approximate if the input is a random signal with strong correlation over a time equal to a sampling period. A careful analysis is given in Clavier, et al. (1947). If the input is a sine wave, the error spectrum typically has a number of large spikes, far from flat or white.

With the model given by Eqs. (10.19) and (10.20) we can compute the mean and variance of the system error due to round-off using state-space methods. Again, we observe that analysis of the response to any constant nonzero mean μ_ε can be computed separately from the response to the white-noise component $w(n)$.

In order to analyze the effect of the random part of the quantization noise, let's review (see also Section 9.5) the general problem of finding the effect of zero-mean noise, w , on a linear system

$$\begin{aligned} \mathbf{x}(k+1) &= \Phi_1 \mathbf{x}(k) + \Gamma_1 w(k) \\ \tilde{y}(k) &= \mathbf{H}_1 \mathbf{x}(k) + J_1 w(k). \end{aligned} \quad (10.21)$$

We define the covariance of the state as

$$\mathbf{R}_x(k) = \mathcal{E}\{\mathbf{x}(k)\mathbf{x}^T(k)\}, \quad (10.22)$$

and, at $k+1$,

$$\begin{aligned} \mathbf{R}_x(k+1) &= \mathcal{E}\{\mathbf{x}(k+1)\mathbf{x}^T(k+1)\} \\ &= \mathcal{E}\{(\Phi_1 \mathbf{x}(k) + \Gamma_1 w(k))(\Phi_1 \mathbf{x}(k) + \Gamma_1 w(k))^T\} \\ &= \Phi_1 \mathbf{R}_x(k) \Phi_1^T + \Gamma_1 R_w \Gamma_1^T. \end{aligned} \quad (10.23)$$

covariance prop-
agation

Equation (10.23) can be used with an initial value (typically zero) of \mathbf{R}_x to compute the transient development of state covariance toward the steady state. Typically, we are only interested in the steady state, which is obtained by letting $\mathbf{R}_x(k+1) = \mathbf{R}_x(k) = \mathbf{R}_x(\infty)$. In this case, Eq. (10.23) reduces to the equation (called the discrete Lyapunov equation for its occurrence in Lyapunov's stability studies)

$$\mathbf{R}_x(\infty) = \Phi_1 \mathbf{R}_x(\infty) \Phi_1^T + \Gamma_1 R_w \Gamma_1^T. \quad (10.24)$$

Lyapunov equa-
tion

Several numerical methods for the solution of Eq. (10.24) have been developed, some based on solving Eq. (10.23) until \mathbf{R}_x no longer changes, and others based on converting Eq. (10.24) into a set of linear equations in the coefficients of \mathbf{R}_x and solving these equations by numerical linear algebra as done by `dlyap.m` in MATLAB.

Random Quantization Error for a First-Order System

Example 10.3

Determine the output of the first-order system of Eq. (10.5) for the case where the multiplication, $\alpha x(k)$, is rounded with a quantum level q .

Solution. The first-order system of Eq. (10.5), with the rounding error represented by ε is

$$x(k+1) = \alpha x(k) + \varepsilon(k),$$

and thus

$$\Phi = \alpha \quad \text{and} \quad \Gamma_1 = 1$$

and from Eq. (10.18), we see that

$$R_w = \frac{q^2}{12},$$

so that Eq. (10.24) is

$$\begin{aligned} R_x &= \alpha R_x \alpha + (1) \frac{q^2}{12} (1), \\ R_x &= \frac{q^2}{12} \frac{1}{1 - \alpha^2} \end{aligned} \quad (10.25)$$

Taking the square root, we find that

$$\sigma_x = \sqrt{R_x} = \frac{q}{2} \sqrt{\frac{1}{3(1 - \alpha^2)}}. \quad (10.26)$$

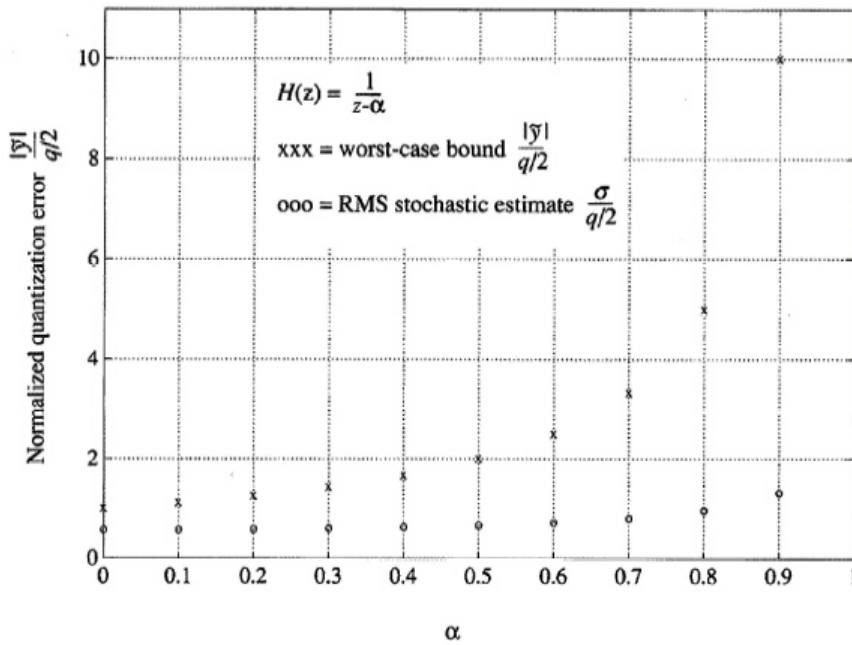


Figure 10.4
Error estimates
and error bounds

A plot of Eq. (10.26) along with the value of the worst-case bound from Eqs. (10.8) and (10.11) is shown in Fig. 10.4.

In some cases, the output of a system is not one of the state elements. In other words,

$$\tilde{y} = \mathbf{H}_1 \mathbf{x} + J_1 w,$$

and, therefore,

$$\mathcal{E}(\tilde{y}\tilde{y}^T) = \mathcal{E}\{(\mathbf{H}_1 \mathbf{x} + J_1 w)(\mathbf{H}_1 \mathbf{x} + J_1 w)^T\},$$

which is to say

$$\mathbf{R}_y = \mathbf{H}_1 \mathbf{R}_x \mathbf{H}_1^T + J_1 \mathbf{R}_w J_1^T. \quad (10.27)$$

Note that we can use Eq. (10.23) and (10.24) to compute the covariance of the state due to round-off error at several locations simply by taking \mathbf{w} to be a column matrix and \mathbf{R}_w to be a square diagonal matrix of covariances of the components of \mathbf{w} . In the multiple-source case, $\mathbf{\Gamma}_1$ is a matrix of dimension $n \times p$, where there are n states and p sources.

Random Quantization Error for a Second-Order System

Example 10.4

Determine the quantization error of the second-order system

$$y(k+2) + a_1 y(k+1) + a_2 y(k) = \frac{1+a_1+a_2}{2} (u(k) + u(k-1)),$$

in terms of the random root-mean-square response and compare it with the worst-case bounds.

Solution. The gain of the system has been set to be unity at frequency 0, and the parameters are related to the pole locations according to $a_1 = -2r\cos(\theta)$ and $a_2 = r^2$. In order to study the role of the frequency of the pole, given in normalized terms by the angle θ , we have computed the estimated errors according to Eqs. (10.4), (10.16), and (10.27) for several values of θ and plotted them in Fig 10.5. For the random-noise case, the square

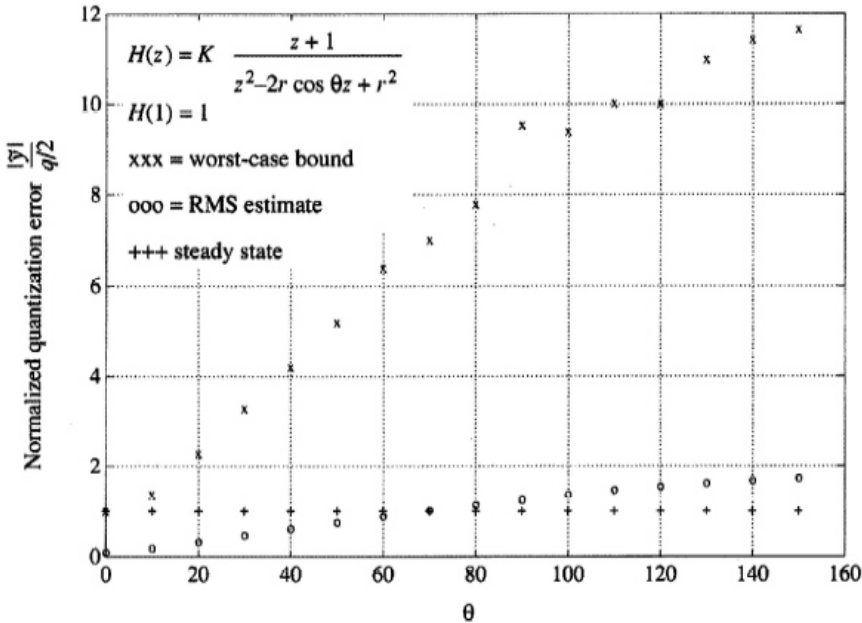


Figure 10.5
Error estimates and error bound with quantization input to a second-order system, where $r = 0.9$

root of the result of Eq. (10.27) is plotted. From the plot, it is clear that the worst-case bound is quite large compared to the other two computations for most of the range of angles. Experiments in the laboratory with random inputs to the system give results that compare very favorably with the numbers given by the random model.

10.2 Effects of Parameter Round-Off

We have thus far analyzed the effects of round-off on the variables such as y and u in Eq. (10.5). However, to do the calculations for a controller, the computer must also store the equation coefficients, and if the machine uses fixed point arithmetic, the parameter values must also be truncated or rounded off to the accuracy of the machine. This means that although we might design the program to solve

$$y(k+1) = \alpha y(k) + u(k),$$

it will actually solve

$$\hat{y}(k+1) = (\alpha + \delta\alpha)\hat{y}(k) + u(k) + \varepsilon(k). \quad (10.28)$$

In this section, we give methods for the analysis of the effects of the parameter error $\delta\alpha$.

The principal concern with parameter variations is that the dynamic response and especially the stability of the system will be altered when the parameters are altered. One way to study this problem is to look at the characteristic equation and ask what effect a parameter change has on the characteristic roots. For example, for the first-order system described by Eq. (10.28), the perturbed characteristic equation is

$$z - (\alpha + \delta\alpha) = 0;$$

and it is immediately obvious that if we want a pole at $z = 0.995$, it will be necessary to store α to three decimal places and that the limit on $\delta\alpha$ for stability is 0.005 because a variation of this magnitude results in a pole on the unit circle. Note, however, that if we structure the α term as $\alpha = 1 - \beta$ and add the 1-term separately then $\beta = 1 - \alpha = 0.005$, and the relative accuracy requirements on β are much less than those on α . Thus we see that the details of the architecture of a realization

can have a major impact on the robustness of the design to parameter value quantization. It is also the case that different canonical forms realized with a given parameter accuracy (word size) will be able to realize a different set of pole locations. It is often possible to select the realization structure in such a way that the desired dynamics are almost exactly realized with the available word length.

To study these matters, we consider the characteristic equation and ask how a particular root changes when a particular parameter changes. The general study of root variation with parameter change is the root locus; however, we can obtain results of some value by a linearized sensitivity analysis. We can compare the direct and the cascade realizations of Chapter 4, for example, to see which is to be preferred from a sensitivity point of view. In the direct realization, the characteristic equation is

$$z^n + \alpha_1 z^{n-1} + \dots + \alpha_n = 0. \quad (10.29)$$

This equation has roots at $\lambda_1, \lambda_2, \dots, \lambda_n$, where $\lambda_i = r_i e^{j\theta_i}$. We assume that one of the α 's, say α_k , is subject to error $\delta\alpha_k$, and we wish to compute the effect this has on λ_j and especially the effect on r_j so that stability can be checked. For this purpose, we can conveniently write Eq. (10.29) as a polynomial $P(z, \alpha)$ that depends on z and α_k . At $z = \lambda_j$, the polynomial is zero, so we have

$$P(\lambda_j, \alpha_k) = 0. \quad (10.30)$$

If α_k is changed to $\alpha_k + \delta\alpha_k$, then λ_j also changes, and the new polynomial is

$$\begin{aligned} P(\lambda_j + \delta\lambda_j, \alpha_k + \delta\alpha_k) &= P(\lambda_j, \alpha_k) + \left. \frac{\partial P}{\partial z} \right|_{z=\lambda_j} \delta\lambda_j + \frac{\partial P}{\partial \alpha_k} \delta\alpha_k + \dots \\ &= 0, \end{aligned} \quad (10.31)$$

where the dots represent terms of higher order in $\delta\lambda$ and $\delta\alpha$. By Eq. (10.30) we see that the first term on the right-hand side of Eq. (10.31) is zero. If $\delta\lambda_j$ and $\delta\alpha_k$ are both small, then the higher-order terms are also negligible. Thus the change in λ_j is given to first order by

root sensitivity

$$\delta\lambda_j \cong - \left. \frac{\partial P / \partial \alpha_k}{\partial P / \partial z} \right|_{z=\lambda_j} \delta\alpha_k. \quad (10.32)$$

We can evaluate the partial derivatives in Eq. (10.32) from Eq. (10.29) and the equivalent form

$$P(z, \alpha_k) = (z - \lambda_1)(z - \lambda_2) \cdots (z - \lambda_n). \quad (10.33)$$

First, using Eq. (10.29), we compute

$$\left. \frac{\partial P}{\partial \alpha_k} \right|_{z=\lambda_j} = \lambda_j^{n-k}, \quad (10.34)$$

and next, using Eq. (10.33), we compute⁷

$$\left. \frac{\partial P}{\partial z} \right|_{z=\lambda_j} = \prod_{\ell \neq j} (\lambda_j - \lambda_\ell). \quad (10.35)$$

Thus Eq. (10.32) reduces to

$$\delta\lambda_j = - \frac{\lambda_j^{n-k}}{\prod_{\ell \neq j} (\lambda_j - \lambda_\ell)} \delta\alpha_k. \quad (10.36)$$

We can say things about root sensitivity by examining Eq. (10.36). The numerator term varies with the index number of the parameter whose variation we are considering. Because we are dealing with a stable system, the magnitude of λ_j is less than one, so the larger the power of λ_j^{n-k} the smaller the variation. We conclude that the most sensitive parameter is α_n , the constant term in Eq. (10.29).

⁷This is true if $P(z)$ has only one root at λ_j . At a multiple root, this derivative is zero and the coefficient of $\delta\alpha_k$ in Eq. (10.36) is not bounded.

However, for values of λ_j near the unit circle, the relative sensitivity decreases slowly as k gets smaller. The denominator of Eq. (10.36) is the product of vectors from the characteristic roots to λ_j . This means that if all the roots are in a cluster, then the sensitivity is high, and if possible, the roots should be kept far apart. For example, if we wish to construct a digital low-pass filter with a narrow-pass band and sharp cutoff, then the system will have many poles in a cluster near $z = 1$. If we implement such a filter in the control canonical form (Fig. 4.8c), then the sensitivity given by Eq. (10.36) will have many factors in the denominator, all small. However, if we implement the *same* filter in the cascade or parallel forms, then the sensitivity factor will have only one term. Mantey (1968) studies these issues and quotes an example of a narrow-bandpass filter of six poles for which the parallel realization was less sensitive by a factor of 10^{-5} . In other words, it would take 17 bits of additional accuracy to implement this example in direct form over that required for the parallel or cascade form! The papers collected by Rabiner and Rader (1972) contain many other interesting results in this area.

Illustration of Parameter Storage Errors

Example 10.5

Compare the sensitivity of a fourth-order controller in cascade form

$$D(z) = \frac{(z+1)^3}{(z-0.9)(z-0.85)(z-0.8)(z-0.75)}$$

versus the same controller in direct form

$$D(z) = \frac{z^3 + 3z^2 + 3z + 1}{z^4 - 3.3000z^3 + 4.0775z^2 - 2.2358z + 0.4590}$$

Solution. If the transfer function is realized as a cascade of the first-order terms, then it is clear that the pole nearest to the unit circle is at $z = 0.9$, and a change in the coefficient by 0.1 will move this pole to the unit circle and lead to instability. This is a percent change of $(0.1/0.9)100 = 11.1\%$. On the other hand, if the controller is realized in one of the direct forms—either control or observer canonical form—then the coefficients used are those in the polynomial form. In this case, by numerical experimentation it is found that a change of a_4 from 0.4590 to 0.4580, a root is moved to the unit circle. This is a change of only $(0.001/0.4590)100 = 0.22\%$. Thus we see that the cascade form is more robust to parameter changes by a factor of almost 50 over the direct forms!

10.3 Limit Cycles and Dither

As a final study of the effects of finite word length in the realization of digital filters and compensators we present a view of the quantizer as a signal-dependent gain and analyze more closely the motions permitted by this nonlinearity. One type of motion is an output that persists in spite of there being no input and that eventually becomes periodic: Such a motion is called a **limit cycle**.

To analyze a nonlinear system we must develop new tools because superposition and transforms do not apply. One such tool is to use graphic methods to solve the equations. For example, suppose we have the first-order equation

$$y(k+1) = Q\{\alpha y(k)\}. \quad (10.37)$$

If we plot y versus αy as in Fig. 10.6, we can also plot the function $Q(\alpha y)$ and trace the trajectory of the solution beginning at the point a on the y -axis. Across from a at point b , we plot the value αy from the line with slope $1/\alpha$. Below b at c is the quantization of αy , and hence the next value of y , shown as d . We thus conclude that the trajectory can be found by starting with a point on the $(1/\alpha)$ -line, dropping to the $Q\{\cdot\}$ staircase, projecting left to the $(1/\alpha)$ -line again, dropping again, and so on, as shown by the dashed lines and arrowheads. Note that the path will always end on the segment of zero amplitude where $\alpha y \leq q$. Now, however, suppose the initial value of y is negative. The trajectory is plotted in Fig. 10.7, where projection is up to Q and to the right to the $(1/\alpha)$ -line.

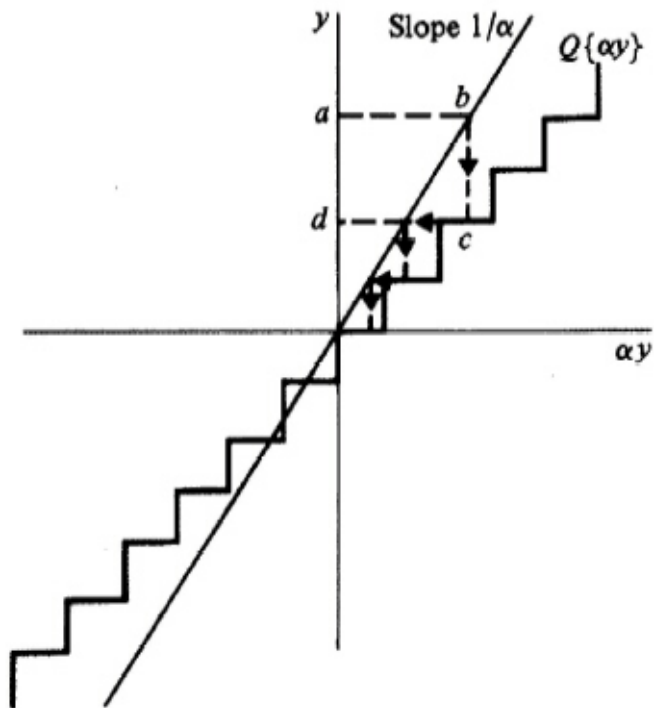


Figure 10.6
Trajectory of a first-order system with truncation quantization

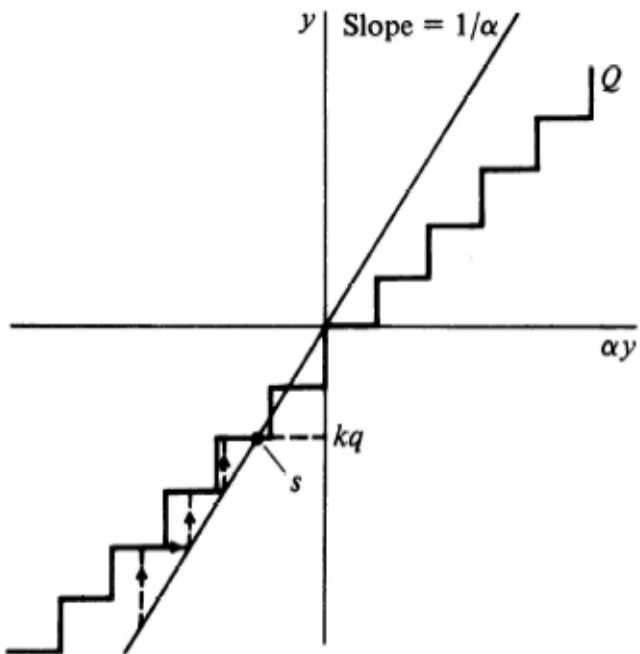


Figure 10.7
Trajectory of a first-order system with truncation quantization and negative initial condition

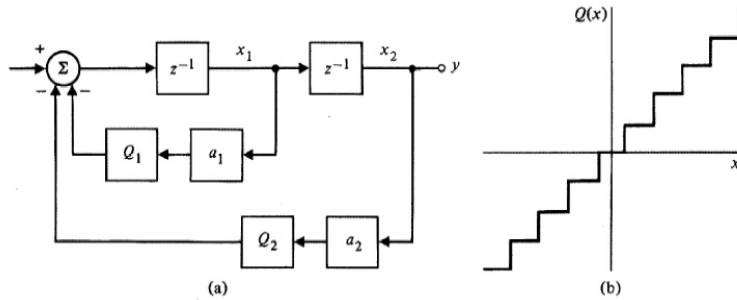


Figure 10.8
A second-order system in control canonical form and the quantizer characteristic corresponding to round-off

Note that this time the trajectory gets stuck at the point s , and the response does *not* go to zero. The point s is an equilibrium or stationary point of the equation. If the initial value of y had a magnitude smaller than s , then the motion would have moved down to the next equilibrium where the $(1/\alpha)$ -line and $Q\{\cdot\}$ intersect. It is clear that s represents the largest value of y that is at equilibrium and that this value depends on α . We should be able to find a relation between kq , the largest value of y at equilibrium, and α , the time constant of the filter. In fact, from inspection of Fig. 10.7 we see that the largest value of y at a stationary point is a value $y = -kq$ such that

$$\begin{aligned}
 -kq\alpha < -kq + q, & \quad \text{or} & \quad k\alpha > k - 1, & \quad \text{or} \\
 k < \frac{1}{1 - \alpha}, & \quad \text{or} & \quad |y| < q \frac{1}{1 - \alpha}. & \quad (10.38)
 \end{aligned}$$

The last result is the same as the worst-case bound that would be found from Eq. (10.8) with the maximum value of error q for truncation rather than $q/2$ as is the case for round-off. Thus we find in the first-order system that the worst case is rather likely to be realized.

In order to extrapolate these results to a higher-order system we must find a more subtle way to look at them. Such a viewpoint is provided by the observation that at the equilibrium points of Fig. 10.7 the gain of the quantizer is exactly $1/\alpha$. If we consider the quantizer as a variable gain, then the equilibrium occurs at those points where the combined gain of quantizer and parameter α are unity, which, for a linear system, would correspond to a pole at $z = 1$. The extrapolation of this idea to higher-order systems is to examine the range of possible **equivalent gains** of the quantizers and to conjecture that the limiting motion will be no larger than the largest signal for which the linear system with the resulting equivalent gain(s) has a pole on the unit circle.

We will illustrate the conjecture by means of the second-order control canonical form shown in Fig. 10.8(a) with the quantizer characteristic shown in Fig. 10.8(b) corresponding to round-off rather than truncation. Note from Fig. 10.8(b) that the staircase of this quantizer is centered about the line of slope 1.0 passing through the origin. The characteristic equation for this system, if quantization is ignored, is

$$\begin{aligned}
 z^2 + a_1z + a_2 &= 0, \\
 z^2 - 2r\cos \theta z + r^2 &= 0,
 \end{aligned}$$

where we assume that $0 < a_2 < 1$ and a_1 corresponds to a real angle. Thus we see that the system will have complex roots on the unit circle only if the action of the quantizer is to make the effective value of $a_2 = r^2 = 1.0$. Thus the condition for an oscillation is that $Q(a_2y) \geq y$. Following an analysis similar to Eq. (10.38), the property of the quantizer is that $Q(x - q/2) \leq q/2$. If we let $a_2y = kq - q/2$, then the oscillation condition becomes

$$kq \geq \frac{kq - q/2}{a_2},$$

from which the amplitude is predicted to be less than

$$kq < \frac{1}{2} \frac{q}{1 - |a_2|}. \quad (10.39)$$

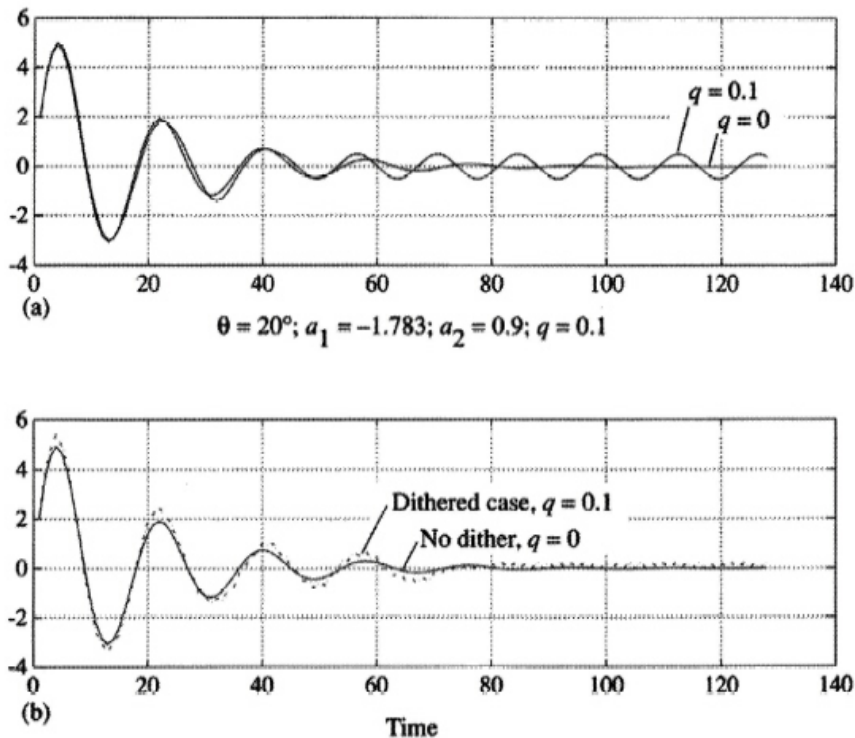


Figure 10.9
 (a) Second-order response with and without quantization showing limit cycle.
 (b) Second-order response with quantization $q = 0.1$ and dither $= 4q$

The effect of quantization on the a_1 -term influences only the frequency of the oscillations in this model. For this purpose, because the equivalent radius is 1, the equation for the digital frequency is $\theta = \cos^{-1}(-a_1/2)$.

Another benefit of the view of quantization as a variable gain is the idea that a second signal of high frequency and constant amplitude added to the input of the quantizer can destroy the limit cycle. Such a signal is called a **dither**, and its purpose is to make the effective gain of the quantizer 1.0 rather than something greater than 1. Consider again the situation sketched in Fig. 10.7 with the signal stuck at s . If an outside high-frequency signal of amplitude $3q$ is added to y , then one can expect that although the output would contain a fluctuating component, the average value would drift toward zero rather than remain stuck at s . If the frequency of the dither is outside the desired pass band of the device, then the result is improved response; that is, a large constant bias or else a high-amplitude, low-frequency, self-sustained, limit-cycle oscillation can sometimes be removed this way at the cost of a low-amplitude, high-frequency noise that causes very low amplitude errors at the system output.

Quantization-Caused Limit Cycles and Effect of Dither

Example 10.6

For the system in Fig. 10.8 with $a_1 = -1.78$ and $a_2 = 0.9$,

- determine the response to the initial condition of $x_1 = 2$ and $x_2 = 0$ with $q = 0$ and $q = 0.1$. Compare the results to that predicted by Eq. (10.39).
- Determine a dither signal that improves the response.

Solution. A simulation of the system of Fig. 10.8 with and without quantization is shown in Fig. 10.9(a). The limit cycle is clearly visible for the $q = 0.1$ case. The system parameters correspond to roots at a radius of 0.95 at an angle of 20° . The quantization level was set at 0.1. The response with quantization clearly shows the limit cycle with an amplitude of 0.5, which is exactly the value given by Eq. (10.39) with $a_2 = 0.9$. The period of the limit cycle can be seen from the figure to be approximately 14 samples. If we compute the frequency

corresponding to the value of $a_1 = -1.78$ with the radius taken as 1 in order to reflect the fact that the system is oscillating, we find $\theta = \cos^{-1}(-a_1/2) = 27^\circ$. This angle corresponds to an oscillation with a period of 13.2 samples, an estimate that is quite good, considering that the true period must be an integral number of sample periods.

In Fig. 10.9(b) are plotted the response with $q = 0$ and the response with $q = 0.1$ with dither added. In this case, after some experimentation, it was found that a square-wave dither at the Nyquist frequency worked quite well at an amplitude of $4q$. In that case the steady-state response has been reduced in amplitude from 0.5 to 0.1 and the frequency has been increased from that having a period of 14 to that having a period of 2, namely the Nyquist frequency. The experiments found that dither of less amplitude did not remove the natural limit cycle and dither of higher amplitude gave a larger steady-state error response. A random dither was also tried, which was found to be much less effective than the Nyquist frequency square wave. Unfortunately, the selection of the amplitude and signal shape of an effective dither remains more a matter for experimentation than theory.

10.4 Summary

- Multiplication round-off errors are bounded, in steady-state, according to

$$|\tilde{y}_{ss}(\infty)| \leq |H_1(1)| \frac{q}{2}, \quad (10.10)$$

where H_1 is the transfer function between the quantization error and the output; and $|H_1(1)|$ is the dc gain of H_1 .

- Multiplication round-off errors can be analyzed under most conditions by considering them to be an additional *random* input at each multiplication. The distribution of the random input is flat, its mean is 0, its variance is $R_x = q^2/12$, and it can be considered to be white (no time correlation).
- The effect of the random multiplication round-off error is analyzed by using the discrete Lyapunov equation

$$\mathbf{R}_x(\infty) = \Phi_1 \mathbf{R}_x(\infty) \Phi_1^T + \Gamma_1 R_w \Gamma_1^T, \quad (10.24)$$

which is evaluated via MATLAB using `dlyap.m` or `qrms.m` (in the Digital Control Toolbox). For 16 and 32 bit computers, these errors are usually negligible. They could be significant using a computer with 8 bits or less, as will be shown in Fig. 11.6.

- The effect of parameter round-off (or parameter storage error) is systematic and has the capability to render an otherwise stable system unstable. It was shown that a parallel or cascade implementation of the difference equations significantly reduces the sensitivity to this type of error as does the use of a large number of bits to represent the parameters being stored.
- Under certain conditions (usually lightly damped systems), uncommanded oscillations will occur due to quantization called **limit cycles** which can be alleviated by the addition of low amplitude oscillations called **dither**.

10.5 Problems

- 10.1 For the system from Eq. (10.5) with $\alpha = 0.9$ and $q = .01$, what is the rms of the quantization error of y that you expect for random input, $u(k)$?
- 10.2 Verify Fig. 10.4 by simulating the response of the system from Eq. (10.5) to $u(k) = 1$ with and without quantization of the αy multiplication. Use $\alpha = 0.9$, $q = .02$, and compute the response from $k = 0$ to $k = 100$, repeating the simulation 20 or more times. Compute σ of the difference between the case with and without quantization at $k = 5$ and $k = 95$ and compare with Fig. 10.4. Comment on the match you found and discuss any discrepancies.

10.3 A digital lowpass filter is described by the equation

$$y(k) = Q_2[\alpha y(k-1)] + Q_1[(1-\alpha)u(k-1)].$$

Assume that $\alpha > 0$ and that the input, $u(k)$, is a slowly varying signal that, for the purpose of this analysis, can be approximated by a constant. The magnitude of the input is restricted to be less than 0.99.

- If both quantizers operate with ℓ bits to the right of the point, what is the value of the quantum q for this case?
 - Give an expression in terms of α for the minimum value that ℓ must have to guarantee that quantization error cannot cause y to exceed 1.0.
 - Evaluate your expression in part (b) and give the necessary bit count if $\alpha = 0.9, 0.98, 0.995$.
 - Suppose the input A/D quantizer Q_1 is fixed at 12 bits with 11 bits to the right of the fixed point. At what value of α can the quantization error alone cause the input to Q_2 to equal unity?
- 10.4 A digital filter with the structure of Fig. 10.8 is preceded by an A/D converter having 12 bits of accuracy, with 11 bits to the right of the fixed point. The quantizer Q_1 is a 16-bit word length scaled to have 3 bits to the left of the point. The quantizer Q_2 is scaled to have only 1 (sign) bit to the left of the point in a 16-bit word length. Let $a_1 = -1.6$ and $a_2 = 0.81$.
- Give the quantum sizes q_i for the converter and each internal round-off quantizer.
 - Give the relevant transfer functions necessary to compute the output quantization error.
 - Compute the steady-state worst error at the output due to quantization.
 - Use MATLAB to compute the worst-case bound on output quantization error.
 - Use MATLAB to compute the rms error due to quantization using the white-noise model.

10.5 For the second-order observer canonical form shown in Fig. 10.10,

- compute the transfer functions from the quantizers to the output, y . Note carefully how many need to be computed.
- If $b_1 = b_2 = 1$, $a_1 = -1.6$, $a_2 = 0.81$, what is the maximum steady-state error due to equal rounding quanta of $\pm q/2$?
- Show that the stochastic state-transition model to use Eq. (10.24) on this system has

$$\Phi = \begin{bmatrix} 1.6 & 1 \\ -0.81 & 0 \end{bmatrix}, \quad \Gamma_1 = \begin{bmatrix} 1 & 0 \\ 0 & 1 \end{bmatrix}, \quad R_w(\infty) = \frac{q^2}{6}, \quad \mathbf{H} = [1 \quad 0].$$

- Assume that

$$\mathbf{R} = \begin{bmatrix} a & b \\ b & c \end{bmatrix},$$

solve Eq. (10.24) for this case, and compute $R_y(0)$ from Eq. (10.27).

- 10.6 Solve for the rms output due to round-off for the system of Fig. 10.8 using computer tools if $a_1 = -1.6$ and $a_2 = 0.81$.
- 10.7 The filter shown in Fig. 10.10 has input from an A/D converter that has 10 bits, 9 bits to the right of the fixed point. The input magnitude is restricted to 1. The four quantizers are based on 16-bit words scaled to have, respectively, 12, 12, 9, and 13 bits to the right of the points (i.e., Q_3 has 9 bits to the right). The parameters are $a_1 = -1.6$, $a_2 = 0.81$, and $b_1 = b_2 = 1$.

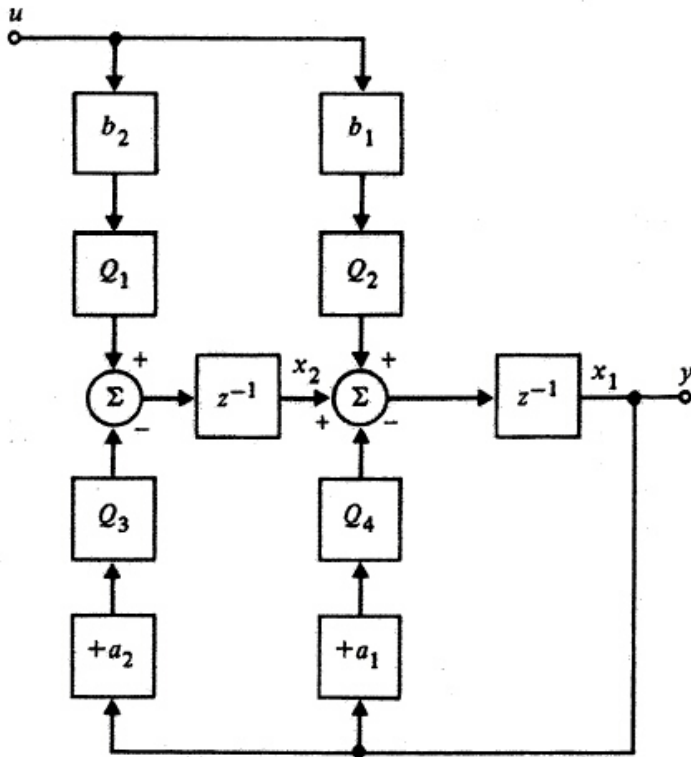


Figure 10.10
A second-order
system with
quantization

- Give the quanta q_i for each quantization location.
- Give the respective transfer functions from each quantizer to the output.
- Use MATLAB to compute the worst-case error bound on the output quantization error.
- Use MATLAB to compute the rms output error for this system based on the white-noise model of quantization error.

10.8 Consider the discrete compensation whose transfer function is

$$D(z) = \frac{z^3}{(z-0.5)(z-0.55)(z-0.6)(z-0.65)}.$$

- If implemented as a cascade of first-order filters with coefficients stored to finite accuracy, what is the smallest gain perturbation that could cause instability? Which parameter would be most sensitive?
- Draw an implementation of $D(z)$ in control canonical form with parameters a_1 , a_2 , a_3 , and a_4 . Compute the first-order sensitivities of these parameters according to Eq. (10.36). Which parameter is most sensitive? Compare the sensitivities of root locations for the cascade and the control forms for these nominal root positions.
- Using the root locus, find the maximum deviations possible for the parameters of the control canonical form and compare with the results of part (b).

10.9 For the equivalent-gain hypothesis of limit-cycle behavior,

- Show that the equivalent gain of the round-off quantizer is given by

$$G_q \leq \frac{2k}{2k-1}, \quad k = 1, 2, \dots$$

for a signal of amplitude greater than or equal to $kq - q/2$.

- (b) What is the largest-amplitude limit cycle you would expect for a second-order control canonical form system with complex roots at a radius of 0.9 and a quantization level of 0.01?
1. For the system of Fig. 10.8,
 - (a) Use MATLAB to simulate the response to the initial conditions $x_1 = 2$ and $x_2 = 0$ with zero input. Use $a_1 = -\sqrt{2}a_2$ and $a_2 = 0.8, 0.9, 0.95$, and 0.98 . Compare the amplitudes and frequencies of the limit cycles (if any) with the values predicted.
 - (b) Add dither at the Nyquist frequency to the quantizer of a_2y with amplitude A and find the dither amplitude that minimizes the peak output in the steady state.
 2. Repeat Example 10.6, but assume the design full scale is ± 20 units and the system is being implemented with an 8 bit cpu. Find the amplitude and frequency of the limit cycle, compare with the theory, and find a dither that improves the situation as much as possible. [*Hint*: FIG109.M in the Digital Control Toolbox will be useful.]
 3. For the system of Example 10.6, assuming the design full scale is ± 20 units, find the number of bits required in the cpu to eliminate the limit cycle without any dither. [*Hint*: FIG109.M in the Digital Control Toolbox will be useful.]
 4. For a system structured as in Example 10.6 with the same initial conditions, but with the coefficients selected so that the equivalent damping is $\zeta = 0.05$, assume the design full scale is ± 20 units and find the number of bits required in the cpu to eliminate the limit cycle without any dither. [*Hint*: FIG109.M in the Digital Control Toolbox will be useful.]
 5. For the discrete system

$$D(z) = \frac{z^3 + 3z^2 + 3z + 1}{z^4 - 3.3000z^3 + 4.0775z^2 - 2.2358z + 0.4590}$$

how many bits are required for parameter storage in order to keep errors in the pole locations to be less than 0.01 in the z -plane in either the real or complex directions? Assume the system is to be implemented in the direct form.

Chapter 11

Sample Rate Selection

A Perspective on Sample Rate Selection

The selection of the best sample rate (or rates) for a digital control system is a compromise. Generally, the performance of a digital controller improves with increasing sample rate, but cost may also increase with faster sampling. A decrease in sample rate means more time is available for the control calculations; hence slower computers are possible for a given control function, or more control capability is available for a given computer. Either result lowers the cost per function. For systems with A/D converters, slower sampling means less conversion speed is required, which will also lower cost. Furthermore, we will see that faster sampling can sometimes require a larger word size, which would also increase cost. All these arguments suggest that the best choice when considering the unit product cost is the slowest sample rate that meets all performance specifications.

On the other hand, digital controllers are often designed and built for systems where a very small number will be built. In this case, the cost of the design effort can be more than the unit product costs, and the savings in design time that are realized with very fast ($\geq 40\times$ bandwidth) sampling dictates that a higher rate is the best choice.

This chapter will discuss the influence of the sample rate on system performance in order to give some insight into how to reconcile the issues for a given design.

Chapter Overview

Section 11.1 examines the fundamental limit on the sample rate imposed by the sampling theorem; Section 11.2 covers the effect on the time response, smoothness, and time lags; Section 11.3 examines the regulation effectiveness as measured by the response errors from random disturbances; Section 11.4 looks at the effect of sample rate on the sensitivity to plant parameter variations; and Section 11.5 examines how sample rate affects the error due to the measurement noise and the influence of analog prefilters or antialiasing filters on this error. Since there are often conflicts in selecting the sample rate for different functions in a controller, some designers elect to have more than one sample rate (a “multirate system”) and this topic is discussed in Section 11.6.

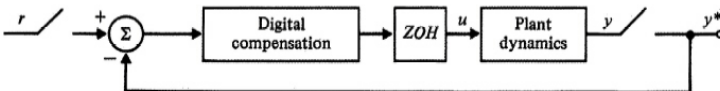


Figure 11.1
Digital control
system schematic

11.1 The Sampling Theorem's Limit

An absolute lower bound for the sample rate would be set if there is a specification to track certain command or reference input signals. This bound has a theoretical basis from the sampling theorem discussed in Section 5.2. Assuming we can represent our digital control system by a single-loop structure as depicted in Fig. 11.1, we can specify the tracking performance in terms of the frequency response from r to y . The sampling theorem states that in order to reconstruct an unknown band-limited continuous signal from samples of that signal, one must use a sample rate at least twice as fast as the highest frequency contained in the unknown signal. This theorem applies to a feedback controller like the one illustrated in Fig. 11.1, because r is an unknown signal that must be followed by the plant output y . If we want the system to track r up to a certain closed-loop bandwidth, ω_b , it follows that r will have spectral content up to that frequency. Based on the sampling theorem therefore, the sample rate must be at least twice the required closed-loop bandwidth of the system, that is

$$\frac{\omega_s}{\omega_b} > 2. \quad (11.1)$$

If a designer were to specify a certain value of the closed-loop bandwidth and then pick a sample rate that violated Eq. (11.1), the result would be that the sampled values of r would be aliased as discussed in Section 5.2, and the result would be a system response that was unstable or considerably slower than specified.

A similar argument can be made with regard to the closed-loop roots of a system, which typically would be slightly slower than the bandwidth. If a designer specified a closed-loop root by its s -plane location and failed to sample at twice its frequency, the actual root realized will be aliased and can have little resemblance to that specified. In practice, no designer would consider such a low sample rate; we bring it up only because it marks the theoretical lower limit of possibilities.

11.2 Time Response and Smoothness

Equation (11.1) provides the fundamental lower bound on the sample rate. In practice, however, this theoretical lower bound would be judged far too slow for an acceptable time response. For a system with a rise time on the order of 1 sec (which translates to a closed-loop bandwidth on the order of 0.5 Hz), it would be typical to choose a sample rate of 10 to 20 Hz in order to provide some smoothness in the response and to limit the magnitude of the control steps. This means that the desired sampling *multiple* ($= \omega_s/\omega_b$) for a reasonably smooth time response is

$$20 < \frac{\omega_s}{\omega_b} < 40. \quad (11.2)$$

Double Integrator Control Smoothness vs. Sample Rate

Example 11.1

Compute the unit step response of the double integrator control problem as developed in Example 8.1 and plot the output x_1 , its rate x_2 , and control u time histories. Find the feedback gains for sample rates of 4, 8, 20, and 40 times the bandwidth, ω_b , so that the responses all have closed-loop roots in the z -plane that are equivalent to $s = 0.5 \omega_b(1 \pm j)$. Discuss your results.

Solution. The four responses are shown in Fig. 11.2. The gains were computed using pole placement where the z -plane poles were computed using $z = e^{sT}$. Note that the relation $s = 0.5 \omega_b(1 \pm j)$ is approximate in that the actual bandwidth of the closed-loop frequency response may be slightly different.

It is interesting to note that the x_1 response was smooth for all cases, including the one with $\omega_s/\omega_b = 4$; however, the acceleration had large discontinuities and would have had a strong tendency to excite any flexible modes and produce high stresses in the actuator and its surrounding structure. In turn, these acceleration steps produced noticeable changes of slope in the velocity. A sampling multiple of $\omega_s/\omega_b \geq 20$ appears necessary for a reasonable smoothness.

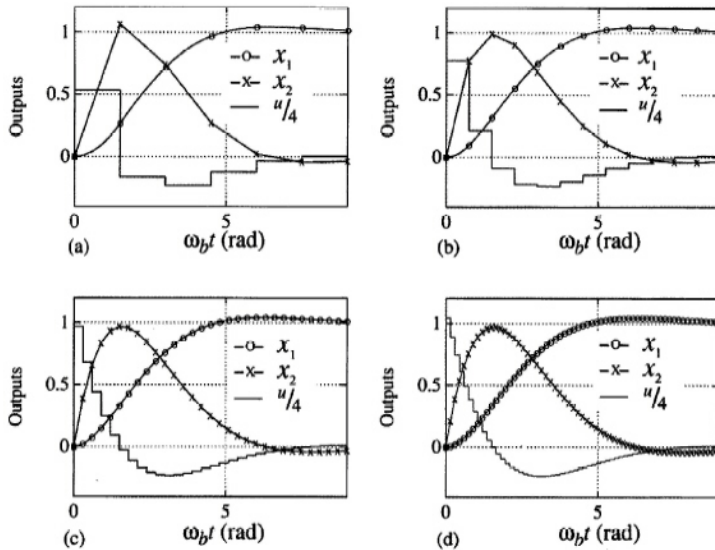


Figure 11.2
Double integrator step response for the sampling multiple with ω_s/ω_b equal to (a) 4, (b) 8, (c) 20, and (d) 40

The degree of smoothness required in a particular design depends on the application and is highly subjective. The commands issued to an electric motor can have large discontinuities, whereas the commands issued to hydraulic actuators are best kept fairly smooth.¹ The tolerance to roughness in the response also depends on the application; for example, if a person is being affected by the controller, a smooth ride is likely desirable. An unmanned satellite controller can be rough; however, slow sampling contributes to increased pointing errors from disturbances, a topic that is discussed in the following section.

In addition to the smoothness issue, it is sometimes important to reduce the delay between a command input and the system response to the command input. A command input can occur at any time throughout a sample period; therefore, there can be a delay of up to a full sample period before the digital controller is aware of a change in the command input. All the responses in Fig. 11.2 assumed that the controller was aware of the command input at time zero and that, therefore, all the attitude responses, x_1 , responded in a similar fashion. For systems with human input commands where the system response is critical (such as fly-by-wire flight control), the time delay alone suggests that the sample period be kept to a small fraction of the rise time. A pilot flying an airplane with digital fly-by-wire flight control will complain if the sampling delay is on the order of a tenth of a second from input action to the beginning of the response. Assuming we wish to keep the time delay to be 10% of the rise time, a 10-Hz sample frequency should be used for 1 sec rise time or, in terms of the nondimensional sampling multiple

time delay

$$\frac{\omega_s}{\omega_b} \geq 20. \tag{11.3}$$

Double Integrator Response vs. Sample Rate

Example 11.2

Repeat Example 11.1, but add a one cycle delay between the input command and the start of the control input in order to assess the worst case phasing of the input. Discuss the impact of this issue.

¹Sometimes lowpass filters are placed between the ZOH output and the actuators to soften the discontinuities, but the filters must be taken into account during design and compensated for.

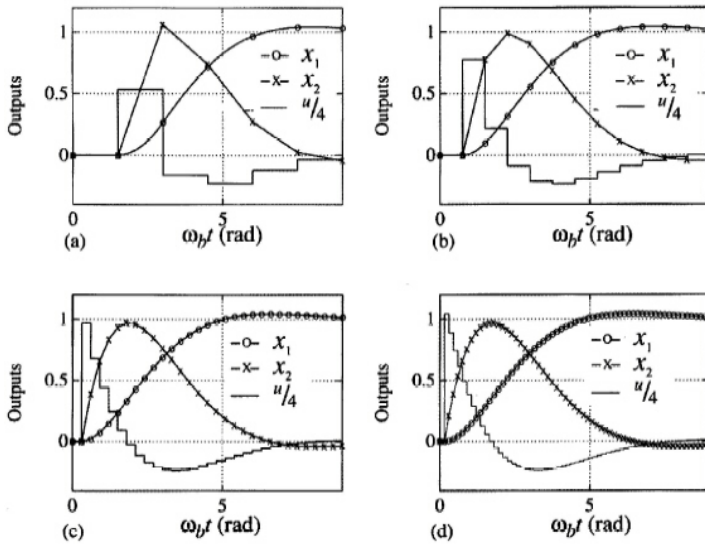


Figure 11.3
Double integrator
step response
with worst case
phasing between
command input
and the sampler
with ω_s/ω_b equal
to (a) 4, (b) 8,
(c) 20, (d) 40

Solution. The result is shown in Fig. 11.3. It demonstrates the noticeable impact on the response for the two slower cases. The overshoot is unchanged because the controller was adjusted in each case to maintain the same z -plane roots, but the extra delay affected the rise time substantially as measured from the instant of the input command.

11.3 Errors Due to Random Plant Disturbances

Disturbance rejection is an important aspect of any control system and, in many cases, is the most important one. In fact, Berman and Gran (1974) suggest that the sample rate for aircraft autopilots should be selected primarily on the basis of its effect on disturbance rejection. Indeed, this is the case for many control applications, although there are multitudes of applications with widely varying conditions where other factors are more important.

Disturbances enter a system with various characteristics ranging from steps to white noise. For determining the sample rate, the higher frequency random disturbances are the most influential; therefore, we will concentrate on their effect. In other words, we will look at disturbances that are fast compared to the plant and the sample rate, that is, where the plant noise can be considered to be white.

The ability of the control system to reject disturbances with a good continuous controller represents a lower bound on the magnitude of the error response that can be hoped for when implementing the controller digitally. In fact, some degradation over the continuous design must occur because the sampled values are slightly out of date at all times except at the very moment of sampling. In order to analyze the degradation of the digital controller as compared to the continuous controller, it is important to consider the effect of the noise [w in Eq. (4.45)] consistently, with both the continuous and the digital controllers.

The block diagram in Fig. 11.4 shows the situation. The plant noise, generally a vector quantity, w , is continuous in nature and acts on the continuous part of the system independently of whether the controller is continuous or discrete. Furthermore, we are at liberty to analyze the effect of w with a certain power spectral density regardless of what values of \mathbf{R}_w or \mathbf{R}_v were used in computing the estimator gains, \mathbf{L} , and regardless of whether an estimator was used. Proceeding then, we have a continuous system represented by

$$\dot{\mathbf{x}} = \mathbf{F}\mathbf{x} + \mathbf{G}u + \mathbf{G}_1 w, \quad (11.4)$$

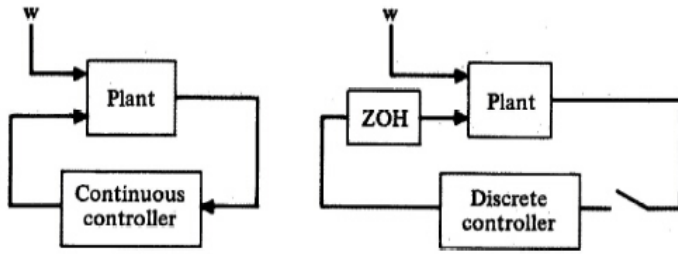


Figure 11.4
Block diagrams
of the systems for
disturbance
analysis

where the power spectral density of \mathbf{w} is \mathbf{R}_{wpsd} (alternatively referred to as the “white-noise intensity” or “mean-square spectral density”) so that the covariance of \mathbf{w} is

$$E[\mathbf{w}(t)\mathbf{w}^T(t+\tau)] = \mathbf{R}_{\text{wpsd}}\delta(\tau).$$

The steady-state value of the covariance of \mathbf{x} is given by the Lyapunov equation²

$$\mathbf{F}\mathbf{X} + \mathbf{X}\mathbf{F}^T + \mathbf{G}_1\mathbf{R}_{\text{wpsd}}\mathbf{G}_1^T = 0. \quad (11.5)$$

The solution to this equation, \mathbf{X} , ($= E[\mathbf{x}(t)\mathbf{x}(t)^T]$) represents the amplitude of the random response of the state due to the excitation from \mathbf{w} . It will be used to establish a baseline against which discrete controllers are compared. Note that the system matrices, \mathbf{F} and \mathbf{G} , can represent a closed-loop system including a continuous controller. The solution is obtained by `lyap.m` in MATLAB.

It is also necessary to evaluate \mathbf{X} when the system has a digital controller for the identical excitation applied to the plant. In order to do this, the entire system must be transferred to its discrete equivalent as given by Eq. (9.81) and discussed in Section 4.3. The discrete equivalent of Eq. (11.5) is given by Eqs. (9.90), (10.24), and (D.34) in slightly different contexts. The desired result for our purposes here, called the discrete Lyapunov equation (see `dlyap.m` in MATLAB) is

$$\Phi\mathbf{X}\Phi^T + \mathbf{C}_d = \mathbf{X}, \quad (11.6)$$

where

$$\mathbf{C}_d = \int_0^T \Phi(\tau)\mathbf{G}_1\mathbf{R}_{\text{wpsd}}\mathbf{G}_1^T\Phi^T(\tau)d\tau. \quad (11.7)$$

As discussed in Section 9.4.4, this integral can be approximated if T is shorter than all system time constants by

$$\mathbf{C}_d \cong \Gamma_1\mathbf{R}_w\Gamma_1^T, \quad \text{where} \quad \mathbf{R}_w = \frac{\mathbf{R}_{\text{wpsd}}}{T}. \quad (11.8)$$

When the approximation is not valid, it is necessary to evaluate Eq. (11.7) exactly using Van Loan’s (1978) algorithm, which can easily be done using `disrw.m` in the Digital Control Toolbox. Therefore, in order to evaluate the effect of sample rate on the performance of a controller in the presence of white plant disturbances, we first evaluate Eq. (11.5) to find the baseline covariance (\mathbf{X}) and then repeatedly evaluate Eq. (11.6) with varying sample rates to establish the degradation versus sampling. It usually suffices to examine the diagonal elements for a performance measure and to compute their square roots to find the rms value, the quantity that is typically measured.

Double Integrator Disturbance Response vs. Sample Rate

Example 11.3

Examine the effect of sample rate on the performance of a digital control system compared to a continuous control system for the double integrator plant used in Examples 11.1 and 11.2.

²See Kwakernaak and Sivan (1972).

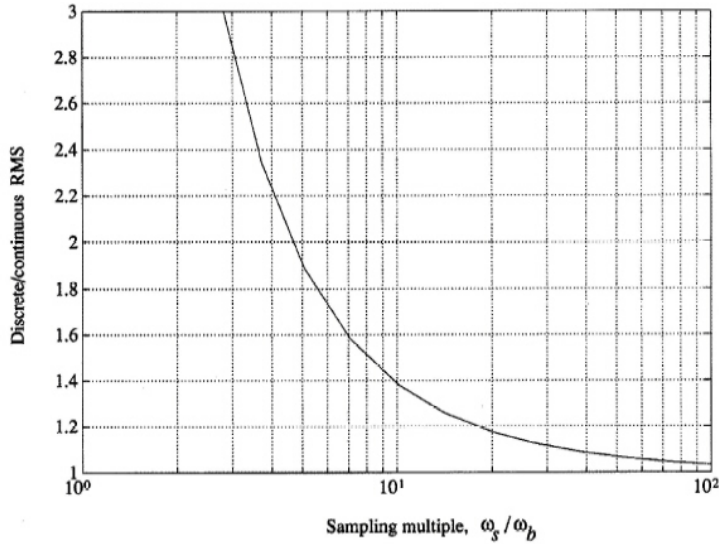


Figure 11.5
Discrete controller degradation versus sample rate for full state feedback and driven by a white disturbance, Example 11.3

- Assume the plant is driven by white noise entering in the same way as the control input with $\mathbf{R}_{\text{wpsd}} = 1$ and assume the use of full-state feedback.
- Assume the same plant noise, but now use an estimator with only x_1 measured with additive noise with $\mathbf{R}_v = 1$. Repeat this case assuming there is quantization in the estimator equivalent to 7, 8, and 9 bit word size.

Solution.

- The open loop \mathbf{F} , \mathbf{G} , and \mathbf{H} are given by Eq. (4.47). The control gain, \mathbf{K} , was determined by selecting optimal weighting matrices so that the closed-loop system had roots at $s = 0.5 \omega_b(1 \pm j)$ ($\zeta = 0.7$) and we assume that $\omega_b = \sqrt{2}\omega_n$. With full-state feedback the closed-loop continuous system matrix is given by $\mathbf{F}_c = \mathbf{F} - \mathbf{G}\mathbf{K}$. The plant disturbance noise enters the plant in precisely the same way that the control does, that is, $\mathbf{G}_1 = \mathbf{G}$. Therefore the response of a hypothetical continuous controller is found by solving Eq. (11.5) with \mathbf{F} replaced with \mathbf{F}_c and \mathbf{G}_1 as stated. Because we wish to illustrate only the degradation of the discrete controller compared to the continuous one, the choice of $\mathbf{R}_{\text{wpsd}} = 1$ has no effect on the results.

The family of discrete controllers with different sample periods were all designed to the same continuous cost function according to the method of Section 9.3.5, the idea being that all the discrete controllers should be trying to do the same thing. Each discrete design resulted in a unique \mathbf{K} and system matrix $\Phi_c (= \Phi - \mathbf{G}\mathbf{K})$, which was used in Eq. (11.6) to evaluate \mathbf{X} . Because this example had no dynamic characteristics that were faster than the slowest sample period, the approximation for the plant noise given by Eq. (11.8) could have been used, although the exact calculation of Eq. (11.7) was actually used. The result shown in Fig. 11.5 is the ratio of the rms values for the discrete case to the continuous case. The specific curve shown is for the rms of the x_1 variable; however, both rms ratios are essentially identical.

If white plant disturbances were the dominant source of error in the system, one could conclude from this example that a sampling multiple of

$$\frac{\omega_s}{\omega_b} \cong 20 \quad (11.9)$$

would be a good choice. The relative errors grow quickly when sampling slower than this multiple, whereas the gain by sampling faster is simply to reduce the degradation from about 20% downward.

- We can analyze the disturbance response of the system when the controller includes an estimator in a similar manner to that above. In this case, the system matrix Φ in Eq. (11.6) is defined by Eq. (8.62). Note that Φ now includes the plant dynamics as well as the estimator dynamics. The continuous control roots are in the same location as for part (a) and the continuous estimator roots were selected twice as fast as the control roots. The family of discrete controllers were found by using pole placement so that the discrete control and estimator roots were related to the continuous roots by $z = e^{sT}$. The lowest curve in Fig. 11.6 shows the discrete to continuous rms ratio and, compared to Fig. 11.5, is slightly higher. This

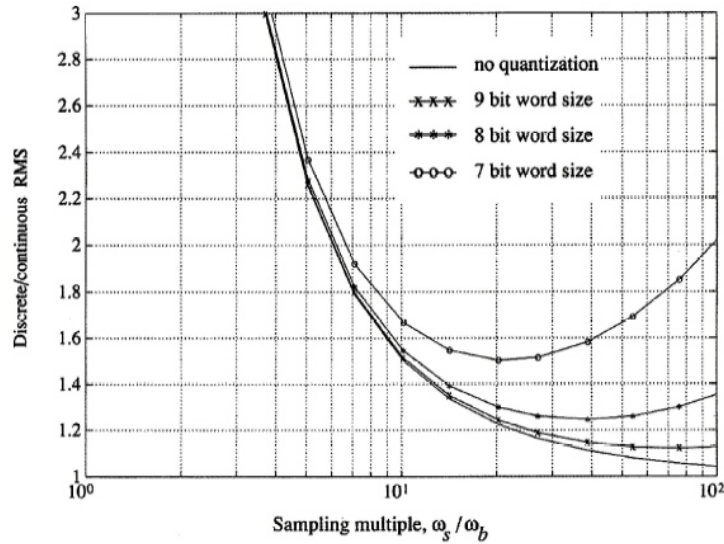


Figure 11.6
Discrete controller degradation versus sample rate for the case with an estimator with quantization errors and a white disturbance, Example 11.3.

is to be expected because the velocity information is now being estimated from a position measurement and the greater sensitivity to disturbances is the result of the approximate differentiation that is occurring. Although the curve is generally higher at all sample rates, the conclusion concerning sample rate selection for the case where disturbances are the dominant consideration is the same; that is, sample at 20 times the bandwidth or higher.

The addition of the random noise from quantization shows that there are limits to the improving noise response as the sampling rate increases. Figure 11.6 also includes quantization noise added according to the discussion in Section 10.1. Quantization is usually important only with a fixed-point implementation of the control equations, and an assumption was therefore required as to the scaling of the signals for this analysis. In Fig. 11.6 it is assumed that the controller was scaled so that the continuous rms error due to the plant disturbance is 2% of full scale, a somewhat arbitrary assumption. But the point is not the specific magnitude as much as the notion that there is a limit, and that if a designer is dealing with a microprocessor with fewer than 12 bits, it can be useful to perform a similar analysis to determine whether the word-size errors are sufficiently large to impact selection of sample rate. With 16- and 32-bit microprocessors and a parallel or cascade realization, the increase in rms errors due to quantization at the fast sample rates is typically so small that word size is not an issue and no practical upper limit to the sample rate exists. However, if using an 8-bit microprocessor, it may be counterproductive to use too high a sample rate.

quantization

The example, although on a very simple plant, shows the basic trend that usually results when a white disturbance acts on the plant: The degradation due to the discrete nature of the control over that possible with a continuous control is significant when sampling slower than 10 times the bandwidth. Except for controllers with small word sizes (8 bits or less), the performance continues to improve as the sample rate is increased, although diminishing returns tend to occur for sampling faster than 40 times the bandwidth.

Whether the rms errors due to plant disturbances are the primary criterion for selecting the sample rate is another matter. If cost was of primary importance and the errors in the system from all sources were acceptable with a sample rate at three times bandwidth, nothing encountered so far in this chapter would necessarily prevent the selection of such a slow sample rate.

On the other hand, resonances in the plant that are faster than the bandwidth sometimes can have a major impact on sample rate selection. Although they do not change the fundamental limit discussed in Section 11.1, they can introduce unacceptable sensitivities to plant disturbances. The analysis is identical to that used in the example above, except that it is mandatory in this case that an accurate evaluation of the integral in Eq. (11.7) be used because there are some plant dynamics that are faster

resonances

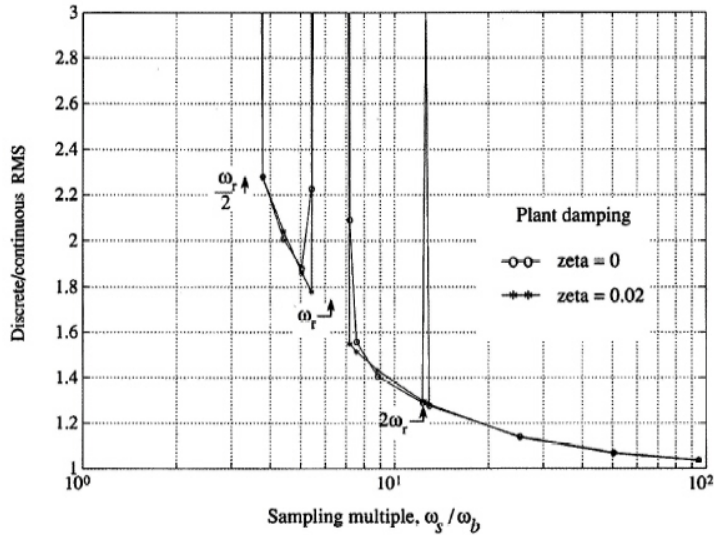


Figure 11.7
Discrete controller degradation for the double mass–spring system using full state feedback, Example 11.4

than the sample period.

Double Mass-Spring Disturbance Response vs. Sample Rate

Example 11.4

Repeat Example 11.3 for the double mass–spring system that was used in Examples 8.3 and 9.5 and described in Appendix A.4. Do part (a) for full-state feedback and part (b) for an estimator based on a measurement of d , that is, the noncolocated case where the resonance is between the sensor and the actuator.

Solution. The parameter values used are as given in Example 8.3, except that we will consider the case with no natural damping as well as the lightly damped ($\zeta = 0.02$) case used previously. The optimal continuous design was carried out in order to achieve a 6:1 ratio between the resonant mode frequency, ω_r , and the system bandwidth, ω_b . Weighting factors were applied to d and y , which provided good damping of the rigid body mode and increased slightly the damping of the resonance mode. The family of discrete designs were found by using pole placement so that the discrete roots were related to the continuous roots by $z = e^{sT}$. The result for the full state feedback case is shown in Fig. 11.7. The general shape of the curves is amazingly similar to the previous example, but there are three highly sensitive sample rates at $2\omega_r$, ω_r , and $\omega_r/2$. Note that these are *not* resonances in the traditional sense. The curves represent the ratio of the response of the discrete system compared to the continuous, so that large spikes mean that the discrete controller at that sample rate exhibits poor disturbance rejection compared to the continuous controller. The excitation is broad band for both controllers at all sample rates. Also note that there is *no* peak at $2\omega_r$ for the case with $\zeta = 0.02$.

The origin of the sensitivity peak at exactly ω_r is that the controller has no information about the resonance at these critical sample rates. The sampled resonance value will be constant no matter what the phase relationship between sampler and the resonant mode, thus producing an unobservable system.³ The additional peak at $2\omega_r$ arises from a similar unobservability, except that in this case the unobservability occurs only when the phasing is such that the samples are at the zero crossings. This peak is significantly less likely to occur and vanishes with a small amount of natural plant damping.

Figure 11.8 shows the sensitivity of the discrete controller to disturbance noise for the more realistic case where the full state feedback has been replaced with an estimator using the measurement of d (essentially a notch filter). As might be expected, the sensitivity peaks have become more serious. The figure shows a wider sample rate band of high sensitivity about each of the previous trouble points and additional peaks at $2\omega_r$ and $\frac{2}{3}\omega_r$. So we now see that there are sensitive sample rates at all integer fractions of $2\omega_r$ due to both unobservabilities noted above.

³The phenomenon was noted and discussed by Katz (1974) and analyzed by Hirata (1989).

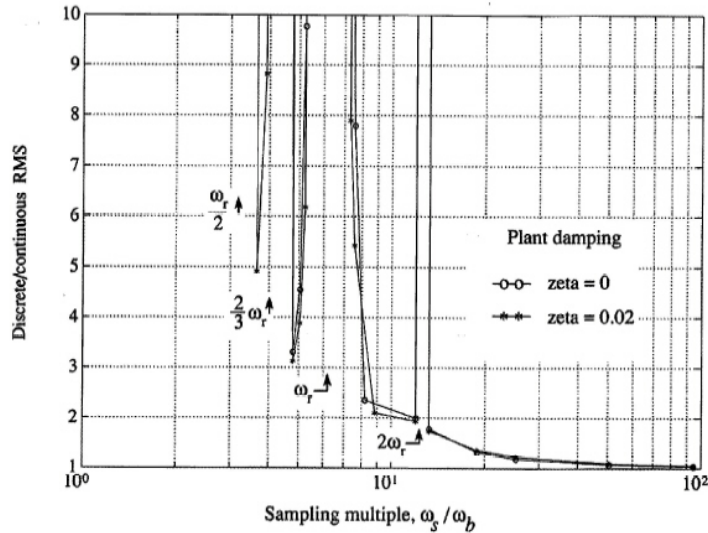


Figure 11.8
Discrete controller degradation for the double mass–spring system using an estimator with the measurement from d , Example 11.4

Example 11.4 demonstrates that, in some cases, a digital controller with sample rates centered about $2\omega_r$ or integer fractions of that value has difficulty and amplifies the effect of random disturbances acting on the plant. Factors that influence whether these sensitive sample rates exist have been studied by Hirata (1989) and generally show that the amount of damping added by the controller is the key aspect. Had more damping been added to the resonant modes by the controller than shown by the example, the sensitivity peaks would have been more pronounced because use of the mode information by the controllers would have been more critical to the performance. Furthermore, use of a collocated sensor and actuator—that is, using the measurement of y instead of d —produces results that are very little different than those shown for the noncollocated case, provided that the controller is adding some damping to the resonant mode.

The impact of this is that, for systems where the controller is adding some damping to a lightly damped mode, the only safe place to select a sample rate is faster than twice the resonant frequency, that is

$$\omega_s > 2\omega_r. \quad (11.10)$$

There is a possibility to pick the sample rate in one of the “valleys” in Fig. 11.8; however, resonant frequencies can often vary considerably, thus rendering this approach unreliable, and would cause this system to lack “robustness.” For systems with high-frequency resonant modes with adequate natural damping and to which the controller adds no damping, there are typically no sensitive sample rates related to the resonant mode, and these considerations can be ignored when selecting the sample rate. Note that these resonant modes may be considerably faster than the system bandwidth and, therefore, sampling faster than 20 times bandwidth may be advisable in order to eliminate the possibility of these sensitive sample rates.

In summary, the sample rate has a major impact on how well a digital controller performs in the presence of plant disturbances. Performance approaching that of a continuous controller can be achieved providing the sample rate is 20 or more times faster than the bandwidth for systems with no significant dynamics faster than the bandwidth. For systems where the controller is adding some damping to a lightly damped mode that is faster than the bandwidth, the sample rate should also be at least twice that resonant frequency.

11.4 Sensitivity to Parameter Variations

Any control design relies to some extent on a knowledge of the parameters representing plant dynamics. Discrete systems generally exhibit an increasing sensitivity to parameter errors for a decreasing

ω_s . The determination of the degree of sensitivity as a function of sample rate can be carried out by accounting for the fact that the model of the plant in the estimator (or compensation) is different from the actual plant.

In Section 8.3.1, we assumed that the actual plant and the model of the plant used in the estimator were precisely the same. This resulted in the separation principle, by which we found that the control and estimation roots designed independently remained unchanged when the feedback was based on the estimated state. We will now proceed to revise that analysis to allow for the case where the parameters representing the plant model in the estimator are different from those of the actual plant.

Let us suppose the plant is described as

$$\begin{aligned} \mathbf{x}(k+1) &= \mathbf{\Phi}_p \mathbf{x}(k) + \mathbf{\Gamma}_p \mathbf{u}(k), \\ \mathbf{y}(k) &= \mathbf{H} \mathbf{x}(k), \end{aligned} \quad (11.11)$$

and the current estimator and controller as

$$\begin{aligned} \hat{\mathbf{x}}(k) &= \bar{\mathbf{x}}(k) + \mathbf{L}(\mathbf{y}(k) - \mathbf{H}\bar{\mathbf{x}}(k)), \\ \bar{\mathbf{x}}(k+1) &= \mathbf{\Phi}_e \hat{\mathbf{x}}(k) + \mathbf{\Gamma}_e \mathbf{u}(k), \\ \mathbf{u}(k) &= -\mathbf{K}\hat{\mathbf{x}}(k). \end{aligned} \quad (11.12)$$

In the ideal case, $\mathbf{\Phi}_p = \mathbf{\Phi}_e (= \mathbf{\Phi})$ and $\mathbf{\Gamma}_p = \mathbf{\Gamma}_e (= \mathbf{\Gamma})$, and the system closed-loop roots are given by the controller and the estimator roots designed separately; that is, they are the roots of the characteristic equation [similar to Eq. (8.55)]

$$|z\mathbf{I} - [\mathbf{\Phi} - \mathbf{\Gamma}\mathbf{K}]| |z\mathbf{I} - (\mathbf{\Phi} - \mathbf{L}\mathbf{H}\mathbf{\Phi})| = 0. \quad (11.13)$$

If we allow $\mathbf{\Phi}_e \neq \mathbf{\Phi}_p$ and $\mathbf{\Gamma}_e \neq \mathbf{\Gamma}_p$, the roots do not separate, and the system characteristic equation is obtained from the full $2n \times 2n$ determinant that results from Eqs. (11.11) and (11.12)

$$\begin{vmatrix} \mathbf{\Phi}_p - \mathbf{I}z & -\mathbf{\Gamma}_p \mathbf{K} \\ \mathbf{L}\mathbf{H}\mathbf{\Phi}_p & (\mathbf{I} - \mathbf{L}\mathbf{H})(\mathbf{\Phi}_e - \mathbf{\Gamma}_e \mathbf{K}) - \mathbf{L}\mathbf{H}\mathbf{\Gamma}_p \mathbf{K} - \mathbf{I}z \end{vmatrix}. \quad (11.14)$$

Either the pole-placement approach of Chapter 8 or the steady-state, optimal, discrete design method of Chapter 9 could be used to arrive at the \mathbf{K} - and \mathbf{L} -matrices. In both cases, the root sensitivity is obtained by assuming some error in $\mathbf{\Phi}$ or $\mathbf{\Gamma}$ (thus $\mathbf{\Phi}_e \neq \mathbf{\Phi}_p$ and $\mathbf{\Gamma}_e \neq \mathbf{\Gamma}_p$) and comparing the resulting roots from Eq. (11.14) with the ideal case of Eq. (11.13).

If a system has been designed using the methods of Chapter 7, root sensitivity is obtained by repeating the closed-loop root analysis with a perturbed plant or, if one parameter is particularly troublesome, an analysis of a root locus versus that parameter might be worthwhile.

Robustness vs. Sample Rate

Example 11.5

The equations of pitch motion of a high-performance aircraft where there is some fuselage bending are⁴

$$\begin{aligned} \dot{x}_1 &= M_q q + M_\alpha x_2 + M_{\delta_e} \delta_e, \\ \dot{x}_2 &= q + Z_\alpha + Z_{\delta_e} \delta_e, \\ \dot{x}_3 &= \omega_r x_4, \\ \dot{x}_4 &= -\omega_r x_3 - 2\zeta_r \omega_r x_4 + \omega_r K_1 Z_{\delta_e} \delta_e + K_2 \omega_r Z_\alpha x_2, \end{aligned} \quad (11.15)$$

⁴This example is due to Katz (1974).

where

- x_1 = pitch rate,
- x_2 = angle of attack,
- x_3, x_4 = position and velocity of bending mode,
- δ_e = elevator control surface,
- $M's, Z's$ = aircraft stability derivatives,
- ζ_r = bending-mode damping,
- ω_r = bending-mode frequency, and
- K_1, K_2 = quantities depending on the specific aircraft shape and mass distribution.

In the flight condition chosen for analysis (zero altitude, Mach 1.2), the open-loop rigid-body poles are located at $s = -2 \pm j13.5$ rad/sec, and the bending mode is lightly damped ($\zeta_r = 0.01$) with a natural frequency of 25 rad/sec (4 Hz). The control system consists of a sensor for x_1 (a rate gyro), an estimator to reconstruct the remainder of the state, and a feedback to the elevator to be added to the pilot input. The purpose is to change the natural characteristics of the aircraft so that it is easier to fly, sometimes referred to as **stability augmentation**.

The closed-loop poles of the rigid body were located by optimal discrete synthesis to $s = -16 \pm j10$ rad/sec with essentially no change in the bending-mode root locations. The optimal compensator (control law plus estimator) generates a very deep and narrow notch filter that filters out the unwanted bending frequencies. The width of the notch filter is directly related to the low damping of the bending mode and the noise properties of the system. Furthermore, the optimal estimator gains for the bending mode are very low, causing low damping in this estimation error mode. If the bending frequency of the vehicle varies from the assumed frequency, the components of the incoming signal to the estimator due to the bending miss the notch and are transmitted as a positive feedback to the elevator.

Examine the sensitivity to errors in the bending frequency versus the sample rate.

Solution. Figure 11.9 shows the closed-loop bending mode damping ζ_r as a function of the ratio of the sample rate ω_s to bending mode frequency ω_r . Note the insensitivity to sample rate when knowledge of the bending mode is perfect (no error in ω_r) and the strong influence of sample rate for the case where the bending mode has a 10% error. For this example, the bending mode was unstable ($\zeta_r < 0$) for all sample rates with a 10% ω_r error, indicating a very sensitive system and totally unsatisfactory design if ω_r is subject to some error or change from flight conditions.

The sensitivity of the controlled system to errors in ω_r can be reduced using any one of many methods for sensitivity reduction, which are often referred to as **robust design** methods. One particularly simple method entails increasing the weighting term in \mathbf{Q}_1 which applies to the bending mode. The effect of this approach is to increase the width of the notch in the controller frequency response, thus making the controller more tolerant to changes in the bending-mode frequency. Figure 11.10 shows the effect on ζ_r as a function of the fourth element in \mathbf{Q}_1 , which we will refer to as the bending-mode weighting factor $Q_{1,44}$. It demonstrates a substantial increase in robustness. Note that it is theoretically possible to have $\zeta_r > 0.05$ with a 10% ω_r error and a sample rate only 20% faster than the bending mode; however, this ignores the disturbance-noise amplification that will occur at $\omega_s \cong 2\omega_r$ discussed in the previous section. With a sufficiently high value of $Q_{1,44}$, the example becomes “robust” in the sense that it is stable for a 10% ω_r error, but it continues to show an increasing sensitivity to the ω_r error for decreasing sample rate.

In summary, for the ideal case where the plant parameters are known exactly, there is no effect of sample rate on bending-mode damping or any other closed-loop dynamic characteristic. On the other hand, if there is some error between the plant parameters used for the controller design and the actual plant parameters, there will be an error in the desired closed-loop characteristics that increases with the sample period. In most cases, the use of reduced performance requirements or of robust design practice such as shown by the example can reduce the error to acceptable levels and thus does not impose extra criteria on the sample rate. However, sensitivity of the system to off-nominal parameters should be evaluated, and in some cases it might be necessary to design specifically for better robustness and, in rare cases, to increase the sample rate over that suggested by other considerations.

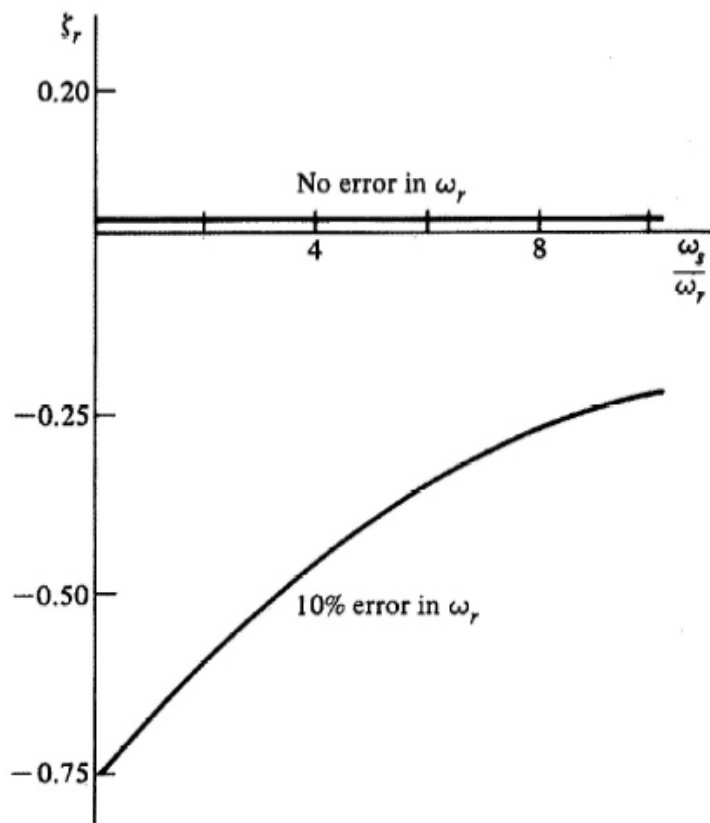


Figure 11.9
Closed-loop bending-mode damping of Example 11.5 versus ω_s

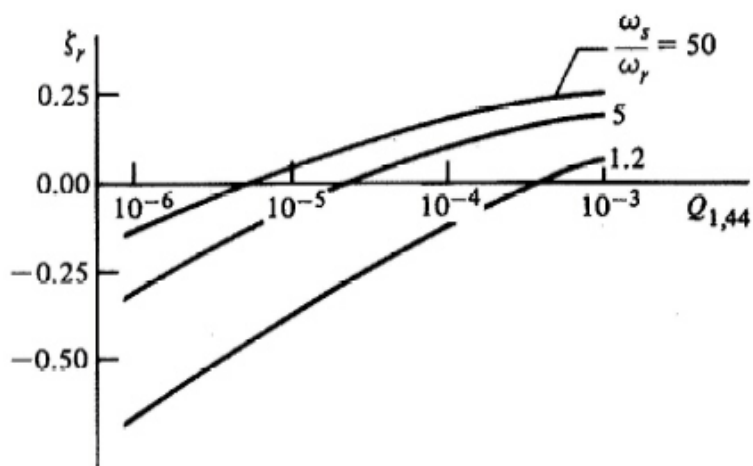


Figure 11.10
Closed-loop bending-mode damping versus $Q_{1,44}$ for Example 11.5 with a 10% ω_r error

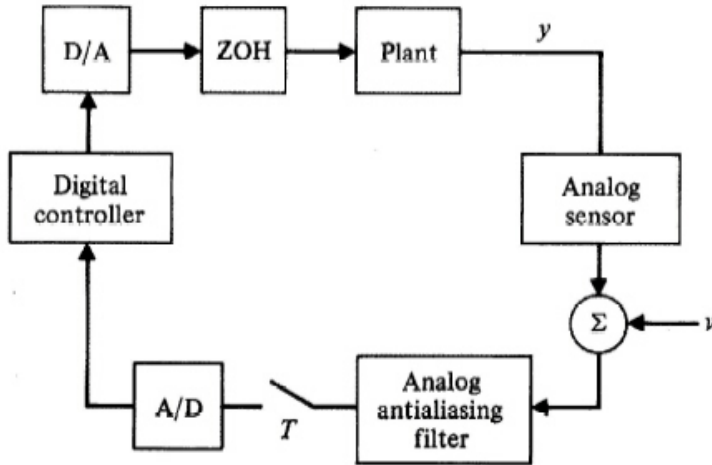


Figure 11.11
Block diagram showing the location of the antialiasing filter

11.5 Measurement Noise and Antialiasing Filters

In addition to the random plant disturbances, \mathbf{w} , that were evaluated in Section 11.3, there are usually some errors in the measurement or unmodeled bending mode oscillations as indicated by \mathbf{v} in Eq. (9.82). In this section, we wish to examine the effect of the sample rate on the response of the system to measurement errors. These errors are affected significantly by the presence of analog filters (called **antialiasing filters** or **prefilters**), which are typically placed between an analog sensor and the sampler in order to reduce aliasing of high-frequency components of the signal. Therefore, we will discuss antialiasing filters as well.

Figure 11.11 depicts the typical arrangement of the antialiasing filter. Digital control systems are arranged this way for many cases in order to prevent the aliasing of the higher-frequency components of \mathbf{v} . Exceptions are those cases where the sensor is fundamentally digital so that there is no analog signal that can contain high frequency noise; for example, an optical encoder provides a digitized signal directly. Antialiasing filters are low pass, and the simplest transfer function is⁵

$$G_p(s) = \frac{\omega_p}{s + \omega_p}, \quad (11.16)$$

so that the noise above the prefilter breakpoint $[\omega_p$ in Eq. (11.16)] is attenuated. The design goal is to provide enough attenuation at half the sample rate ($\omega_s/2$) so that the noise above $\omega_s/2$, when aliased into lower frequencies by the sampler, will not be detrimental to the control-system performance. The basic idea of aliasing was discussed in Section 5.2 and shown to be capable of transforming a very-high-frequency noise into a frequency that is well within the bandwidth of the control system, thus allowing the system to respond to it.

Effect of Prefiltering on Aliasing

Example 11.6

For a 1-Hz sine wave with a 60-Hz sine wave superimposed to represent noise, find a prefilter that will eliminate distortions when sampled at 28 Hz. Demonstrate the effect of the prefilter, and lack of one, by plotting the signals over 2 cycles.

Solution. Figure 11.12(a) shows the 1-Hz sine wave with a 60-Hz sine wave superimposed to represent measurement noise. If this analog signal is sampled as is, the high-frequency noise will be aliased; Fig. 11.12(b)

⁵Higher-order filters are also used in order to obtain better high-frequency attenuation with minimal low-frequency phase lag; common filter types are Bessel, Butterworth, and ITAE. See Franklin, Powell, and Emami-Naeini (2019) or Åström and Wittenmark (1997) for details.

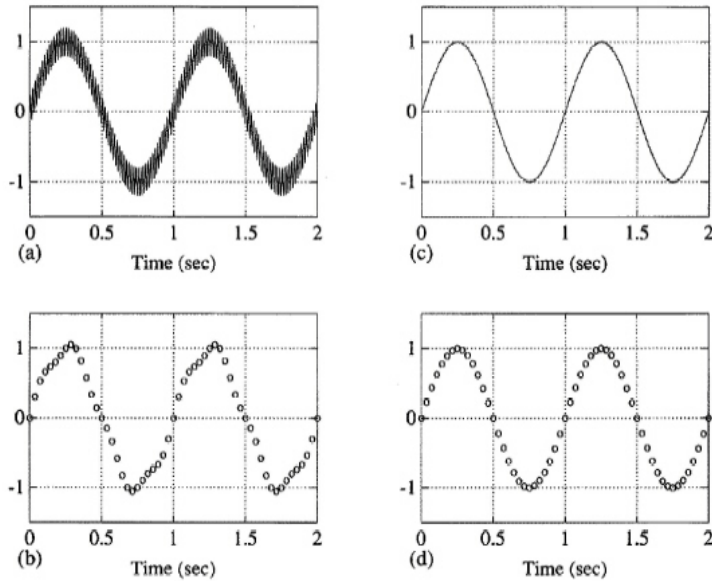


Figure 11.12
 Demonstration of the effects of an antialiasing filter or prefilter, Example 11.6. (a) Signal plus noise; (b) samples of (a) at $\omega_s = 28 \text{ Hz}$; (c) signal in (a) passed through antialiasing filter; (d) sampling of signal in (c)

shows the results for sampling at $\omega_s = 28 \text{ Hz}$ and we see that the 60-Hz noise has been changed to a much lower frequency and appears as a distortion of the original sine wave. Fig. 11.12(c) shows the results of passing the noisy signal in (a) through a first order antialiasing filter with a breakpoint, $\omega_p = 20 \text{ rad/sec}$ (3.2 Hz). The breakpoint was picked considerably below the noise frequency so there is a large attenuation of the noise; and yet sufficiently above the 1-Hz signal so it was not attenuated. Sampling this clean signal results in the faithful reproduction of the signal shown in Fig. 11.12(d).

For an analog control system with a bandwidth on the order of 1 Hz, the 60-Hz noise would be too fast for the system to respond, and the noise would not be apparent on the system output. For a 1-Hz bandwidth digital control system without an analog prefilter, aliasing of the noise to a lower frequency as shown in Fig. 11.12(b) would allow the system to respond, thus producing sensitivity to errors that do not exist for analog controllers. Thus we see the reason for using antialiasing filters.

To study the effect of sensor noise on sample-rate selection, we use the same analysis procedures that were used for the random plant disturbances. Equation (11.5) is used to determine the system output errors due to continuous-measurement noise acting on a continuous controller for comparison purposes, and then Eq. (11.6) is used to determine the degradation for digital controllers with various sample rates. The only difference from the cases examined in Section 11.3 is that the noise to be examined enters on the plant output instead of on the plant input. A complication arises, however, because the prefilter breakpoint, ω_p , is a design variable whose selection is intimately connected with the sample rate. It is therefore necessary to examine both quantities simultaneously.

A conservative design procedure is to select the breakpoint and ω_s sufficiently higher than the system bandwidth so that the phase lag from the prefilter does not significantly alter the system stability; thus the prefilter can be ignored in the basic control system design. Furthermore, for a good reduction in the high-frequency noise at $\omega_s/2$, the sample rate should be selected about five times higher than the prefilter breakpoint. The implication of this prefilter design procedure is that sample rates need to be on the order of 30 to 50 times faster than the system bandwidth. This kind of conservative prefilter and sample-rate design procedure is likely to suggest that the sample rate needs to be higher than the other factors discussed in this chapter.

An alternative design procedure, due to Peled (1978), is to allow significant phase lag from the prefilter at the system bandwidth and thus to require that the control design be carried out with the analog prefilter characteristics included. Furthermore, the analysis procedure described above is

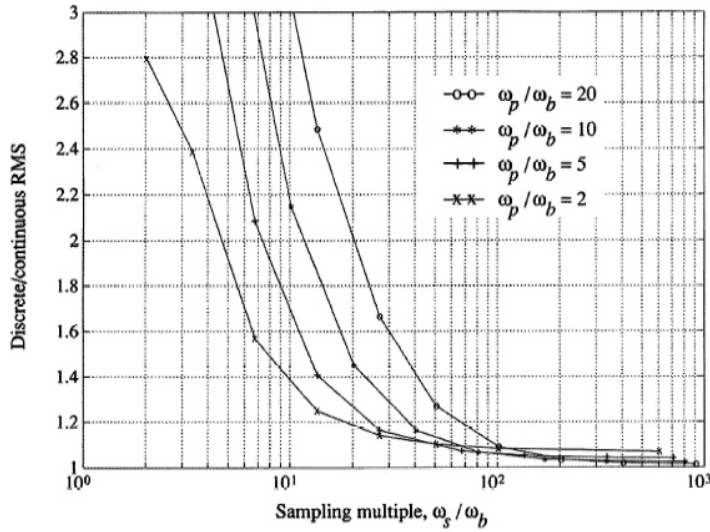


Figure 11.13
Root mean square response of Example 11.7 to white sensor noise showing effects of prefiltering, ω_p , and sampling, ω_s

carried out to determine more precisely what the effect of sampling is on the system performance. This procedure allows us to use sample rates as low as 10 to 30 times the system bandwidth, but at the expense of increased complexity in the design procedure. In addition, some cases can require increased complexity in the control implementation to maintain sufficient stability in the presence of prefilter phase lag; that is, the existence of the prefilter might, itself, lead to a more complex digital control algorithm.

Measurement Noise Effects vs. Sample Rate and Prefilter Breakpoint

Example 11.7

Use the double integrator plant as in Examples 11.1, 11.2, and 11.3 to demonstrate the degradation of the digital system response vs. the continuous control for various sample rates and prefilter breakpoints. Assume that only x_1 is available for measurement and use an estimator to reconstruct the state. Use the antialiasing filter as shown in Eq. (11.16).

Solution. The results of the digital controllers with the various prefilter breakpoints, ω_p , were all normalized to the results from a continuous controller with no prefilter. The exact evaluation of the integral in Eq. (11.7) was required because the sample rate was on the same order as ω_p for some sample rates studied. The continuous system was designed using the LQR and LQE methods of Chapter 9 so that the control roots were at $s = -1.5 \pm j1.5$ rad/sec and the estimator roots were at $s = -3.3 \pm j3.3$ rad/sec. All the digital controllers had roots at the discrete equivalent of those s -plane locations by using $z = e^{sT}$. The results of the normalized rms values of the output error due to white continuous-measurement noise entering the system as shown in Fig. 11.11 are shown in Fig. 11.13 for four different values of the prefilter breakpoint.

Note in the figure that, for sampling multiples below $\omega_s/\omega_b = 40$, the performance improves as the prefilter breakpoint decreases, even though it includes the case where the breakpoint is only twice the bandwidth. If a system is dominated by measurement noise as in this example and the designer chooses to limit the discrete degradation to 20% compared to the continuous case, the figure shows that a sampling multiple of

$$\omega_s/\omega_b \geq 25 \quad (11.17)$$

is adequate providing the prefilter breakpoint ratio $\omega_p/\omega_b \leq 5$, whereas a sampling multiple of $\omega_s/\omega_b = 40$ is required if the more conservative prefilter breakpoint ratio of $\omega_p/\omega_b = 10$ is used. An even slower sample rate would be adequate if a slower breakpoint was acceptable.

Also note in the figure at the very fast sample rates ($\omega_s/\omega_b > 200$) that the rms response decreased as the prefilter breakpoint increased, the opposite trend to that at the lower sample rates. This observation has little effect on the overall design because all values were within 10% of the continuous case for all the fast sample rates. However, there are detrimental effects of prefilters that can be more serious (see Hirata, 1989), and their

influence on random plant disturbances should also be evaluated according to Section 11.3 before a design is finalized.

In summary, there are two main conclusions. The first is that prefilters for removing high frequency measurement noise are effective and a methodology has been presented for their design. The second is that the bandwidth of the prefilter should be selected primarily for the reduction of sensor noise effects, and values approaching the system closed-loop bandwidth ($\omega_p/\omega_b \cong 2$) should be considered even though their phase lag needs to be adjusted for in the controller design. An exception to this would occur if the prefilter lag was sufficient to require a more complicated controller, because this increase in computation could offset any cost gains from slower sampling.

11.6 Multirate Sampling

In multi-input, multi-output (MIMO) systems, it is sometimes useful to use different sample rates on the various measurements and control variables. For example, in the tape-drive design in Chapter 9, one could logically sample the tension measurement, T_e in Fig. 9.18, faster than the tape position measurement, x_3 , because the tension results from faster natural dynamics than the tape positioning. For MIMO systems with significant time constant differences in some natural modes or control loops, improvements in performance can be realized by sampling at different rates; such a system is referred to as a **multirate** (MR) system. In this section we will address the issues of analysis of an MR system and selection of the sample rates.

The z -transform method that is presented in Chapter 4 and is the basis for the analysis of discrete systems throughout this book does not apply to MR systems. Considerable research on the subject was carried out in the 1950s and resulted in the “switch decomposition” method, which has been reviewed by Ragazzini and Franklin (1958) and Amit (1980) and extended to multivariable systems by Whitbeck and Didaleusky (1980). The key idea in this method is that it is possible to analyze an MR system by reducing it to an equivalent single-rate system operating at the longest sample period of the system. The “Kranc” operator⁶ facilitates this transformation.

Another approach uses a state-space description due to Kalman and Bertram (1959). The difference equations have coefficients in Φ and Γ that change periodically at the longest sample period. An MR analysis procedure with this approach is contained in Berg, Amit, and Powell (1988) and, similarly to switch decomposition, reduces the MR system to an equivalent single-rate system where conventional methods can be employed. The computational burden for both the switch-decomposition and the state-space MR analysis is substantial; therefore, digital control designers typically opt for design methods during the synthesis process which bypass the need for using one of the exact MR analysis techniques.

An analysis method often used is called **successive loop closure** (SLC). It requires that the system initially be decoupled into two or more single-rate subsystems along the lines discussed in Section 9.1 and as shown in Fig. 11.14. The dashed lines in the figure show the cross-coupling between $G_f(s)$ and $G_s(s)$, which is ignored in the decoupling process. The controller for the subsystem with the highest frequencies (and fastest sample rate) is designed first with the sample rate selected according to the ideas in this chapter. This digitally controlled subsystem is then converted back to a continuous system (see `d2c.m` in MATLAB), which makes it possible to meld it into the slow portion of the plant. This transformation is the inverse of Eqs. (4.41) or (4.58) and is exact in the sense that the continuous model outputs will match the discrete system at the sample times. A discrete representation at the slow sample rate of the entire plant, including the previously ignored cross-coupling and the fast controller, can now be obtained using conventional techniques. This enables design of a digital controller for the slow loop using the resulting discrete model. This model is exact provided the fast sample rate is an integer multiple of the slow rate.

The approximation made during the design of the inner (fast) loop is the elimination of the cross-coupling; however, the model of the system at the slow sample rate will accurately predict any inner-

⁶See Kranc (1957).

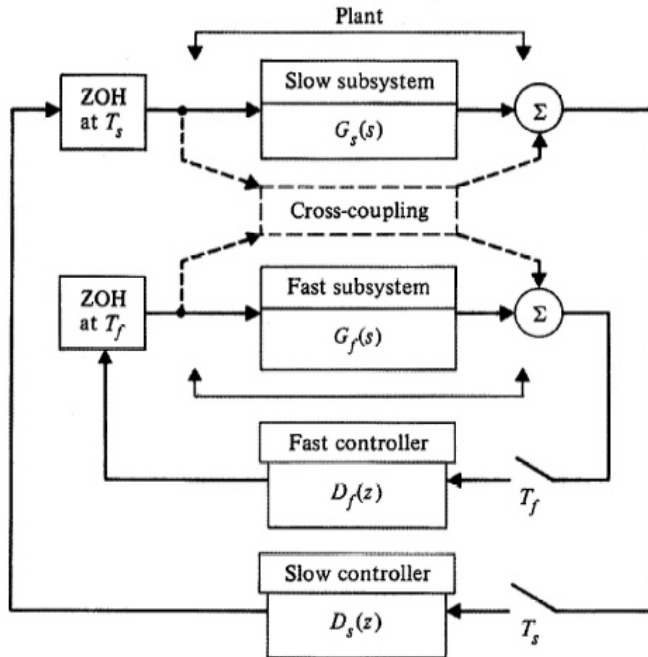


Figure 11.14
Block diagram of a MIMO system showing methodology for multirate analysis using successive loop closure

loop root migration due to the approximation and can be corrected by a second design iteration, if needed. Therefore, we see that the final design of the MR system should perform according to that predicted by linear analysis. The effect of the approximations made for design of the inner loop serve only to produce an inner-loop controller that may be somewhat inferior to that which could be obtained with an accurate MR analysis and optimal design of the entire system together as described by Berg, Amit, and Powell (1988).

For systems with three or more identifiable loops where it is desirable to have three or more different sample rates, the same ideas are invoked. The innermost (fastest) loop is closed first, transformed to a continuous model followed by transformation to a discrete model at the next slower sample rate, and so on until the final (slowest) loop is closed, encompassing the entire system.

The sample-rate selection for an MR system designed using SLC is carried out using the considerations discussed in Sections 11.1 through 11.5. Note that this does not imply that the same sampling multiple, ω_s/ω_b , be used for all loops. The appropriate sampling multiple is a function of the plant disturbance and sensor noise acting on that portion of the system which may be quite different for the different loops. Ignoring noise effects leads one to pick the same sampling multiple for all loops; that is, the sample rates for each loop are in the same proportion as the bandwidth for each loop.

Advantage of MR Sampling for the Double Mass-Spring System

Example 11.8

Investigate the merits of multirate sampling in terms of rms response to plant noise for the double mass-spring system.⁷ Compare the rms response of an MR controller with that of a single rate (SR) controller that uses the same amount of computation effort.

Solution. The double mass-spring system with control applied to both masses is shown in Fig. 11.15. We have defined x_1 as the absolute position of the large mass, whereas x_2 is the position of the small mass with respect to the large mass. The inner loop consists of the measurement of x_2 and its feedback through a controller to u_2 . The effect of the coupling from x_1 motion is ignored; so the dynamics are that of a simple mass-spring system. The inner (fast) loop was designed using pole-placement for full state feedback so that its open-loop

⁷This example is from Berg, Amit, and Powell (1988).

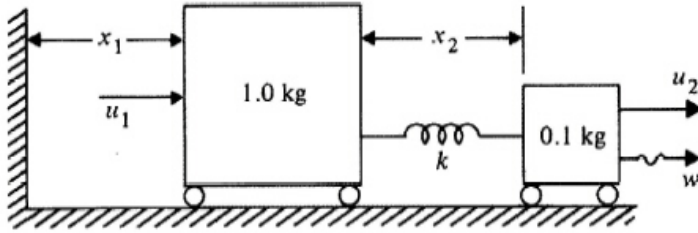


Figure 11.15
MIMO double
mass-spring
system used in
Example 11.8

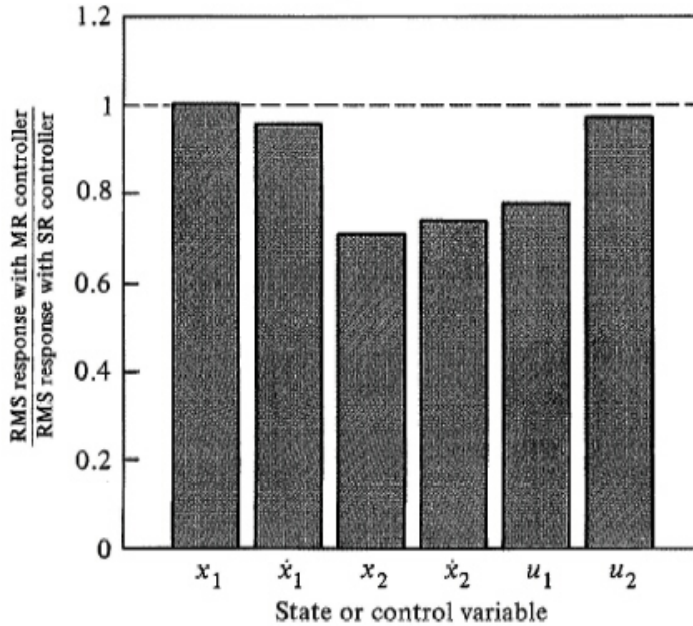


Figure 11.16
Relative rms
state and control
responses for
Example 11.8
with w applied to
the small mass

resonant frequency of 4 Hz was changed to a closed-loop frequency of 8 Hz, and the damping improved from $\zeta = 0$ to $\zeta = 0.7$. The sample rate was chosen to be 71 Hz, nine times faster than the closed-loop root.

A continuous model of this fast inner loop was then obtained via `d2c.m` in MATLAB and added to the dynamics of the large mass, including the coupling between the two masses. The entire system was then discretized at the slow rate. The outer loop was designed using feedback from the slow sampled states so that the rigid-body open-loop roots at $s = 0$ were changed to 1 Hz with a damping of $\zeta = 0.7$. The sample rate for this loop was chosen to be 9 Hz, also nine times the closed-loop root. The effect of the dynamics of the large mass and its coupling to the small mass along with the outer-loop feedback caused an insignificant movement of the closed-loop inner roots. If the inner roots had moved an unacceptable amount, it would have been necessary to return to the inner-loop design and revise the design so that it resulted in acceptable dynamics *after* the second loop closure.

For evaluation of the MR controller, its performance in the presence of plant disturbance noise, w , applied to the small mass as shown in Fig. 11.15 will be compared against the performance of a single-rate controller. The sample rate of the single-rate controller was selected to be 40 Hz, a value that required approximately the same amount of computer computation time as the MR controller, thus yielding a fair comparison. Fig. 11.16 shows the relative rms responses for the two cases and generally shows the superiority of the MR case in that its small mass response was approximately 30% less than the single-rate case, whereas the large mass response was approximately the same. One could say that, for this configuration, it pays to assign a large fraction of the computer power on the control of the small mass by employing a faster sample rate for the small mass feedback. This follows because the bandwidth of the inner loop was faster and the plant disturbance noise was applied to this mass.

To analyze the situation further, let us change the plant disturbance noise configuration from the small mass to the large mass and keep the controller described above. The same comparison of relative rms responses is

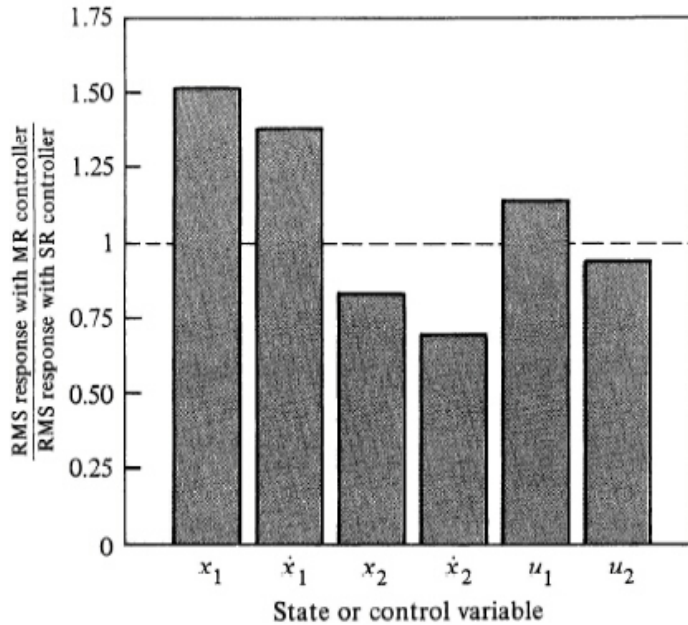


Figure 11.17
Relative rms
state and control
responses for
Example 11.8
with w applied to
the large mass

shown in Fig. 11.17 and indicates a different conclusion. The degradation of the large mass response with the MR controller is more than the improvement of the small mass; therefore, one could conclude that the single-rate controller was superior in this configuration. The reason is that the noise applied to the large mass (slow mode) produced a situation where the overall system response was improved by shifting more computer power to the slow mode compared to the previous configuration. The net result was that an equal sample rate on the two loops was best in spite of the fact that the roots of the two loops differed by a ratio of 8:1.

The significant benefit of the MR sampling shown in Fig. 11.16 is partially due to the fact that both sample rates were relatively slow, that is, nine times their respective closed-loop root. Had the sample rates been faster, the advantage would have been less pronounced. The reason for this is that the effect of disturbance noise versus sample rate is basically a quadratic function, with the errors growing quickly as sampling multiples fall below about 20. If all rates had been faster, the system performance would be less sensitive to both sample rates and thus less sensitive to the allocation of computer power to the fast or slow loop.

In summary, we see that multirate sampling allows for the assignment of available computer power to the control modes that can most benefit, thus improving system response. The design of multirate systems can usually be carried out using a successive loop closure method that employs analytical techniques, which are considerably simpler than exact MR techniques. The resulting design is typically acceptable.

Multirate sampling is not necessary in the majority of digital control systems. In the usual case, sufficient computer speed is available so that one sample rate based primarily on the fastest mode can be selected even though one or more of the slower modes will be sampled faster than necessary. This is a better overall design because it avoids the complication of multirate sampling, even though it could be claimed that computer power is being wasted on some of the slower modes.

11.7 Summary

- For a control system with a specified closed-loop bandwidth, ω_b , the theoretical lower bound on the sample rate to bandwidth multiple is

$$\omega_s/\omega_b > 2.$$

Other considerations usually dictate that the sample rate be considerably faster than 2 times the closed-loop bandwidth.

- In order to provide a “reasonably smooth” control response, a sampling multiple of

$$\omega_s/\omega_b > 20$$

is often judged desirable. This is a subjective issue and depends heavily on the specific application, with slower rates often acceptable.

- There is potentially a full sample period delay between command input and the system response. In order to limit the possible delay to be 10% of the rise time, a sampling multiple of

$$\omega_s/\omega_b > 20$$

is required.

- The primary purpose of many feedback control systems is to limit the response to random plant disturbances. In comparison to a continuous control system with the same equivalent s -plane roots, a digital control system degrades as the sample rate decreases. This degradation is shown by the bottom curve in Fig. 11.6 for a double integrator plant. In order to keep the degradation to be within 20% of a continuous controller, a sampling multiple of

$$\omega_s/\omega_b > 20$$

is required.

- For a system with a resonance at ω_r that is being damped or stabilized by the controller, it is prudent to select a sample rate

$$\omega_s > 2\omega_r.$$

- For a system with a resonance at ω_r that is being damped or stabilized by the controller, it may be useful for robustness purposes to sample considerably faster than $2\omega_r$.

- **Analog prefilters** or **antialiasing filters** are typically required to attenuate the effect of measurement noise at frequencies greater than $\omega_s/2$.

- Selection of the prefilter breakpoint, ω_p , is a complex design step that involves interactions with the sample rate and control system bandwidth. Generally, the further the breakpoint is below $\omega_s/2$, the better the measurement noise attenuation. It is also convenient to maintain the prefilter breakpoint above the control system bandwidth; however, this is of lessor importance. The tradeoffs for a double integrator plant are depicted in Fig. 11.13. It shows that a sampling multiple of

$$\omega_s/\omega_b > 25$$

is required for a breakpoint ratio of $\omega_p/\omega_b = 5$ if the designer wishes to limit the discrete noise degradation to 20% over that from the continuous case. Faster antialiasing filters require faster sample rates. Slower antialiasing filters reduce the effect of measurement noise, but more phase lag is introduced into the feedback and, if excessive, may necessitate extra lead in the controller.

- When using a small word size microprocessor (e.g., 8 bits), sampling multiples greater than 50 were shown in Fig. 11.6 to be counterproductive.

- The performance of a digital control system can sometimes be enhanced by using more than one sample rate for different loops in the system. The z -transform does not apply directly to this case and a successive loop closure design method for such systems was described in Section 11.6.
- The cost of a digital control system increases with sample rate due to the microprocessor cost and A/D cost. Therefore, for high volume products where the unit hardware costs dominate, picking the slowest sample rate that meets the requirements is the logical choice. For a low volume product, the labor cost to design the controller far outweighs the extra cost of a fast computer; therefore the logical choice of the sampling multiple is on the order of 40 or more so that the extra complexity of digital design methods is not required.

11.8 Problems

11.1 Find discrete compensation for a plant given by

$$G(s) = \frac{0.8}{s(s+0.8)}.$$

Use s -plane design techniques followed by the pole-zero mapping methods of Chapter 6 to obtain a discrete equivalent. Select compensation so that the resulting undamped natural frequency (ω_n) is 4 rad/sec and the damping ratio (ζ) is 0.5. Do the design for two sample periods: 100 ms and 600 ms. Now use an exact z -plane analysis of the resulting discrete systems and examine the resulting root locations. What do you conclude concerning the applicability of these design techniques versus sample rate?

11.2 The satellite attitude-control transfer function (Appendix A) is

$$G_1(z) = \frac{T^2(z+1)}{2(z-1)^2}.$$

Determine the lead network (pole, zero, and gain) that yields dominant poles at $\zeta = 0.5$ and $\omega_n = 2$ rad/sec for $\omega_s = 1, 2,$ and 4 Hz. Plot the control and output time histories for the first 5 sec and compare for the different sample rates.

11.3 Consider the satellite design problem of Appendix A.

- Design full state feedback controllers with both roots at $z = 0$ for $T = 0.01, 0.1,$ and 1 sec.
- Plot the closed-loop magnitude frequency response of θ for the three sample rates and determine the closed-loop bandwidth for each case.
- Plot the step response for the three sample rates and determine the rise time. Compare these values against that predicted by the relation in Section 2.1.7, $t_r \cong 1.8/\omega_n$.

11.4 Following the satellite design problem used for Example 11.3, evaluate the rms errors versus sample rate due to plant disturbance noise, using the case where only the attitude, θ , is measured and used by an estimator to reconstruct the state for control. Base all discrete control gains on z -plane roots that are equivalent to $\zeta = 0.7$ and $\omega_n = 3$ rad/sec and estimator gains on z -plane roots equivalent to $\zeta = 0.7$ and $\omega_n = 6$ rad/sec. Assume the torque disturbance has a power spectral density of $R_{\text{wpsd}} = 1 \text{ N}^2\text{-m}^2/\text{sec}$ as was done for Example 11.3. Plot the error for $\omega_s = 6, 10, 20, 40, 80,$ and 200 rad/sec and comment on the selection of T for disturbance rejection in this case.

11.5 In Appendix A, Section A.4, we discuss a plant consisting of two coupled masses. Assume $M = 20 \text{ kg}, m = 1 \text{ kg}, k = 144 \text{ N/m}, b = 0.5 \text{ N-sec/m},$ and $T = 0.15 \text{ sec}.$

- (a) Design an optimal discrete control for this system with quadratic cost $\mathcal{J} = y^2 + u^2$. Plot the resulting step response.
- (b) Design an optimal discrete filter based on measurements of d with $R_v = 0.1 \text{ m}^2$ and a disturbing noise in the form of a force on the main mass M with $R_w = 0.001 \text{ N}^2$.
- (c) Combine the control and estimation into a controller and plot its frequency response from d to u .
- (d) Simulate the response of the system designed above to a step input command and, leaving the controller coefficients unchanged, vary the value of the damping coefficient b in the plant. Qualitatively note the sensitivity of the design to this parameter.
- (e) Repeat steps (a) to (d) for $T = 0.25 \text{ sec}$.

11.6 For each design in Problem 11.2, increase the gain by 20% and determine the change in the system damping.

11.7 Consider a plant consisting of a diverging exponential, that is,

$$\frac{x(s)}{u(s)} = \frac{a}{s-a}.$$

Controlled discretely with a ZOH, this yields a difference equation, namely,

$$x(k+1) = e^{aT}x(k) + [e^{aT} - 1]u(k).$$

Assume proportional feedback,

$$u(k) = -Kx(k),$$

and compute the gain K that yields a z -plane root at $z = e^{-bT}$. Assume $a = 1 \text{ sec}^{-1}$, $b = 2 \text{ sec}^{-1}$, and do the problem for $T = 0.1, 1.0, 2, 5 \text{ sec}$. Is there an upper limit on the sample period that will stabilize this system? Compute the percent error in K that will result in an unstable system for $T = 2$ and 5 sec . Do you judge that the case when $T = 5 \text{ sec}$ is practical? Defend your answer.

11.8 In the disk drive servo design (Problem 9.11 in Chapter 9), the sample rate is often selected to be twice the resonance ($\omega_s = 6 \text{ kHz}$ in this case) so that the notch at the Nyquist rate ($\omega_s/2$) coincides with the resonance in order to alleviate the destabilizing effect of the resonance. Under what conditions would this be a bad idea?

11.9 For the MIMO system shown in Fig. 11.15, let $k = 10 \text{ N/m}$. Design an MR sampling controller where the fast sampling rate on the x_2 to u_2 loop is 10 Hz ($T = 100 \text{ msec}$) and the slow sampling on the x_1 to u_1 loop is 2 Hz ($T = 500 \text{ msec}$). Pick the fast poles at 1.5 Hz with $\zeta = 0.4$ and the slow poles at 0.3 Hz with $\zeta = 0.7$.

10.00

11.10 For your design in Problem 11.9, evaluate the steady state rms noise response of x_1 and x_2 for an rms value of $w = 0.1 \text{ N}$. Repeat the design with the same pole locations, for two cases:

- (a) fast sample period $T_{fast} = 50 \text{ msec}$, and slow sample period $T_{slow} = 500 \text{ msec}$,
- (b) fast sample period $T_{fast} = 100 \text{ msec}$, and slow sample period $T_{slow} = 250 \text{ msec}$, and evaluate the rms response in both cases. If extra computational capability existed, where should it be used? In other words, which sample rate should be increased?

11.11 Replot the information in the lower curve in Fig. 11.6 (that is, no quantization noise) for three cases: (a) process noise and no measurement noise (the case already plotted), (b) process noise and measurement noise with an rms = 1, and (c) measurement noise with an rms = 1 and no process noise. Use exactly the same controller and estimator as the current plot. Note that FIG116.M assumes $R_v = 1$ for purposes of computing the continuous estimator gains; however, in computing the rms response, no measurement noise was included.

Chapter 12

System Identification

A Perspective on System Identification

In order to design controls for a dynamic system it is necessary to have a model that will adequately describe the system's motion. The information available to the designer for this purpose is typically of two kinds. First, there is the knowledge of physics, chemistry, biology, and the other sciences which have over the years developed equations of motion to explain the dynamic response of rigid and flexible bodies, electric circuits and motors, fluids, chemical reactions, and many other constituents of systems to be controlled. However, it is often the case that for extremely complex physical phenomena the laws of science are not adequate to give a satisfactory description of the dynamic plant that we wish to control. Examples include the force on a moving airplane caused by a control surface mounted on a wing and the heat of combustion of a fossil fuel of uncertain composition. In these circumstances, the designer turns to data taken from experiments directly conducted to excite the plant and measure its response. The process of constructing models from experimental data is called **system identification**. In identifying models for control, our motivation is very different from that of modeling as practiced in the sciences. In science, one seeks to develop models of nature as it is; in control one seeks to develop models of the plant dynamics that will be adequate for the design of a controller that will cause the actual dynamics to be stable and to give good performance.

The initial design of a control system typically considers a small signal analysis and is based on models that are linear and time-invariant. Having accepted that the model is to be linear, we still must choose between several alternative descriptions of linear systems. If we examine the design methods described in the earlier chapters, we find that the required plant models may be grouped in two categories: parametric and nonparametric. For design via root locus or pole assignment, we require a parametric description such as a transfer function or a state-variable description from which we can obtain the poles and zeros of the plant. These equivalent models are completely described by the numbers that specify the coefficients of the polynomials, the elements of the state-description matrices, or the numbers that specify the poles and zeros. In either case we call these numbers the *parameters* of the model, and the category of such models is a **parametric description** of the plant model.

parametric
model

In contrast to parametric models, the frequency-response methods of Nyquist, Bode, and Nichols require the curves of amplitude and phase of the transfer function $G(e^{j\omega T}) = Y(j\omega)/U(j\omega)$ as functions of ω . Clearly, if we happen to have a parametric description of the system, we can compute the transfer function and the corresponding frequency response. However if we are given the frequency response or its inverse transform, the impulse response, without parameters (perhaps obtained from experimental data) we have all we need to design a lead, lag, notch, or other compensation to achieve a desired bandwidth, phase margin, or other frequency response performance objective without ever knowing what the parameters are. We call the functional curves of $G(e^{j\omega T})$ a **nonparametric** model because in principle there is no finite set of numbers that describes it exactly.

nonparametric
model

In addition to the selection of the type of model desired, one must define the error to be minimized by the model estimate. For transfer functions, if we assume the true value is $G(e^{j\omega T})$ and the model is given by $\hat{G}(e^{j\omega T})$, then one possible measure is $\int (G(e^{j\omega T}) - \hat{G}(e^{j\omega T}))^2 d\omega$. Clearly other

measures are also possible and can be considered. For discrete-time parametric models a standard form assumes that the output is generated by the discrete equation

$$a(z)y = b(z)u + c(z)v, \quad (12.1)$$

where a , b , and c are polynomials in the shift operator¹ z , y is the output, u is the input, and v is the error and assumed to be a random process independent of u . If $c(z) = a(z)$, then v is called the output error, for in that case Eq. (12.1) becomes $y = [b(z)/a(z)] u + v$, and v is noise added to the output of the system. If $c(z) = 1$ then v is called the equation error, for it is the error by which the data y and u fail to satisfy the equation given by $a(z)y = b(z)u$. Finally, if $c(z)$ is a general polynomial, then Eq. (12.1) is equivalent to a Kalman filter and v is called the prediction error.

The data used in system identification consist mainly of the records of input, $u(k)$, and output, $y(k)$ and assumptions about the error. However, in addition to these records there is usually very important information about the physical plant that must be used to get the best results. For example, the plant transfer function may have a known number of poles at $z = 1$ corresponding to rigid body motion. If there are such known components, the data can be filtered so that the identification needs only estimate the unknown part. Also typically it is known that the important features of the transfer function are contained in a known frequency range and that data outside that range is only noise. It is important to filter the raw data to remove these components in so far as possible without distorting important features to prevent the algorithm from distorting the estimated model in a futile effort to explain this noise. The important conclusion is that all *a priori* information be used fully to get the best results from the computations.

In summary, identification is the process by which a model is constructed from prior knowledge plus experimental data and includes four basic components: the data, the model set, the criterion by which one proposed model is to be compared with another and the process of validation by which the model is confirmed to mimic the plant on data not used to construct the model. Because of the large data records necessary to obtain effective models and the complexity of many of the algorithms used, the use of computer aids is essential in identification. Developments such as the MATLAB System Identification Toolbox are enormous aids to the practical use of the techniques described in this chapter.

Chapter Overview

In this chapter, we consider several of the most common and effective approaches to identification of linear models. In Section 1 we consider the development of linear models as used in identification. In Section 2 the construction of nonparametric models is considered. Data taken by single sinusoidal signal inputs as well as data in response to a complex signal are considered. Also presented is the concept of including prior knowledge of the plant response, including the possibility of known pole locations for rigid body cases. In Section 3 techniques for identification of parametric linear models based on equation error are introduced with the selection of parameters and definition of the error. Algorithms for batch least squares are given in Section 4, recursive least squares in Section 5, and stochastic least squares in Section 6. It is shown that bias is encountered when the equation error is not a white noise process in each of the techniques. In Section 7 the method of maximum likelihood is introduced as a method that can overcome the bias considering the prediction error. Finally, in Section 8 the estimation of state description matrices based on subspace methods is described.

12.1 Defining the Model Set for Linear Systems

Formally, one proceeds as follows with the process of linearization and small-signal approximations. We begin with the assumption that our plant dynamics are adequately described by a set of ordinary

¹Some authors use the variable q as the shift operator to avoid confusion with z as the variable of the \mathcal{Z} transform. It is expected that the rare use of z as an operator will not cause confusion here.

differential equations in state-variable form as discussed in Section 4.3.6

$$\begin{aligned}
 \dot{x}_1 &= f_1(x_1, \dots, x_n, u_1, \dots, u_m, t), \\
 \dot{x}_2 &= f_2(x_1, \dots, x_n, u_1, \dots, u_m, t), \\
 &\vdots \\
 \dot{x}_n &= f_n(x_1, \dots, x_n, u_1, \dots, u_m, t), \\
 y_1 &= h_1(x_1, \dots, x_n, u_1, \dots, u_m, t), \\
 &\vdots \\
 y_p &= h_p(x_1, \dots, x_n, u_1, \dots, u_m, t),
 \end{aligned} \tag{12.2}$$

or, more compactly in matrix notation, we assume that our plant dynamics are described by

$$\begin{aligned}
 \dot{\mathbf{x}} &= \mathbf{f}(\mathbf{x}, \mathbf{u}, t), & \mathbf{x}(t_0) &= \mathbf{x}_0, \\
 \mathbf{y} &= \mathbf{h}(\mathbf{x}, \mathbf{u}, t).
 \end{aligned} \tag{12.3}$$

The assumption of stationarity is here reflected by the approximation that \mathbf{f} and \mathbf{h} do not change significantly from their initial values at t_0 . Thus we can set

$$\dot{\mathbf{x}} = \mathbf{f}(\mathbf{x}, \mathbf{u}, t_0)$$

or, simply,

$$\begin{aligned}
 \dot{\mathbf{x}} &= \mathbf{f}(\mathbf{x}, \mathbf{u}), \\
 \mathbf{y} &= \mathbf{h}(\mathbf{x}, \mathbf{u}).
 \end{aligned} \tag{12.4}$$

The assumption of small signals can be reflected by taking \mathbf{x} and \mathbf{u} to be always close to their reference values \mathbf{x}_0 , \mathbf{u}_0 , and these values, furthermore, to be a solution of Eq. (12.4), as

$$\dot{\mathbf{x}}_0 = \mathbf{f}(\mathbf{x}_0, \mathbf{u}_0) \tag{12.5}$$

Now, if \mathbf{x} and \mathbf{u} are close to \mathbf{x}_0 and \mathbf{u}_0 , they can be written as $\mathbf{x} = \mathbf{x}_0 + \delta\mathbf{x}$; $\mathbf{u} = \mathbf{u}_0 + \delta\mathbf{u}$, and these can be substituted into Eq. (12.4). The fact that $\delta\mathbf{x}$ and $\delta\mathbf{u}$ are small is now used to motivate an expansion of Eq. (12.4) about \mathbf{x}_0 and \mathbf{u}_0 and to suggest that only the terms in the first power of the small quantities $\delta\mathbf{x}$ and $\delta\mathbf{u}$ need to be retained. We thus have a vector equation and need the expansion of a vector-valued function of a vector variable

$$\frac{d}{dt}(\mathbf{x}_0 + \delta\mathbf{x}) = \mathbf{f}(\mathbf{x}_0 + \delta\mathbf{x}, \mathbf{u}_0 + \delta\mathbf{u}). \tag{12.6}$$

If we go back to Eq. (12.2) and do the expansion of the components f_i one at a time, it is tedious but simple to verify that Eq. (12.6) can be written as

$$\dot{\mathbf{x}}_0 + \delta\dot{\mathbf{x}} = \mathbf{f}(\mathbf{x}_0, \mathbf{u}_0) + \mathbf{f}_{\mathbf{x}}(\mathbf{x}_0, \mathbf{u}_0)\delta\mathbf{x} + \mathbf{f}_{\mathbf{u}}(\mathbf{x}_0, \mathbf{u}_0)\delta\mathbf{u} + \dots \tag{12.7}$$

where we define the partial derivative of a scalar f_i with respect to the vector \mathbf{x} by a subscript notation

$$f_{i,\mathbf{x}} \triangleq \left(\frac{\partial f_i}{\partial x_1} \quad \dots \quad \frac{\partial f_i}{\partial x_n} \right). \tag{12.8}$$

The row vector in Eq. (12.8) is called the *gradient* of the scalar f_i with respect to the vector \mathbf{x} . If \mathbf{f} is a vector, we define its partial derivatives with respect to the vector \mathbf{x} as the matrix (called the Jacobean) composed of *rows* of gradients. In the subscript notation, if we mean to take the partial of *all* components, we use the bold vector as the subscript

$$\mathbf{f}_{\mathbf{x}} = \begin{bmatrix} \frac{\partial f_1}{\partial \mathbf{x}} \\ \frac{\partial f_2}{\partial \mathbf{x}} \\ \vdots \\ \frac{\partial f_n}{\partial \mathbf{x}} \end{bmatrix}. \tag{12.9}$$

Now, to return to Eq. (12.7), we note that by Eq. (12.5) we chose $\mathbf{x}_0, \mathbf{u}_0$ to be a solution so the first terms of Eq. (12.7) balance, and, because the terms beyond those shown depend on higher powers of the small signals $\delta\mathbf{x}$ and $\delta\mathbf{u}$, we are led to the approximation

$$\begin{aligned} \dot{\delta\mathbf{x}} &\approx, & \mathbf{f}_{\mathbf{x}}(\mathbf{x}_0, \mathbf{u}_0)\delta\mathbf{x} + \mathbf{f}_{\mathbf{u}}(\mathbf{x}_0, \mathbf{u}_0)\delta\mathbf{u} \\ \delta\mathbf{y} &= \mathbf{h}_{\mathbf{x}}\delta\mathbf{x} + \mathbf{h}_{\mathbf{u}}\delta\mathbf{u}. \end{aligned} \quad (12.10)$$

Now the notation is overly clumsy and we drop the δ -parts and define the constant matrices

$$\begin{aligned} \mathbf{F} &= \mathbf{f}_{\mathbf{x}}(\mathbf{x}_0, \mathbf{u}_0), & \mathbf{G} &= \mathbf{f}_{\mathbf{u}}(\mathbf{x}_0, \mathbf{u}_0) \\ \mathbf{H} &= \mathbf{h}_{\mathbf{x}}(\mathbf{x}_0, \mathbf{u}_0) & \mathbf{J} &= \mathbf{h}_{\mathbf{u}}(\mathbf{x}_0, \mathbf{u}_0) \end{aligned}$$

to obtain the form we have used in earlier chapters

$$\dot{\mathbf{x}} = \mathbf{F}\mathbf{x} + \mathbf{G}\mathbf{u}, \quad \mathbf{y} = \mathbf{H}\mathbf{x} + \mathbf{J}\mathbf{u}. \quad (12.11)$$

We will go even further in this chapter and restrict ourselves to the case of single input and single output and discrete time. We write the model as

$$\begin{aligned} \mathbf{x}(k+1) &= \mathbf{\Phi}\mathbf{x}(k) + \mathbf{\Gamma}u(k), \\ y(k) &= \mathbf{H}\mathbf{x}(k) + Ju(k), \end{aligned} \quad (12.12)$$

from which the transfer function is

$$G(z) = Y(z)/U(z) = \mathbf{H}(z\mathbf{I} - \mathbf{\Phi})^{-1}\mathbf{\Gamma} + J, \quad (12.13)$$

and the unit pulse response is

$$g(0) = J \quad g(k) = \mathbf{H}\mathbf{\Phi}^{k-1}\mathbf{\Gamma} \quad k = 1, \dots \quad (12.14)$$

The System Identification Toolbox includes the multivariable case, and multivariable theory is covered in a number of advanced texts devoted to identification, including Ljung (1987).

12.2 Identification of Nonparametric Models

One of the important reasons that design by frequency-response methods is so widely used is that it is so often feasible to obtain the frequency response from experimental data. Furthermore, reliable experimental estimates of the frequency response can be obtained when noise is present and when the system is weakly nonlinear. Models based on such frequency-response data can then be used effectively in control system design using, for example, the methods of Bode. The presence of nonlinearity leads to the concept of the “describing function,” a topic that will be considered in Chapter 13. Here we will introduce and illustrate experimental measurement of the frequency response in the case of linear, constant, stable models, including the possibility of unmeasured noise inputs to the system.

The situation to be considered is described by the transform equations

$$Y(z) = G(z)U(z) + H(z)W(z). \quad (12.15)$$

In this equation, Y is the plant output, U is the known plant control input, and W is the unmeasured noise (which might or might not be random). G is thus the plant transfer function and H is the unknown but stable transfer function from the noise to the system output. The frequency response of this system, as was discussed in Chapter 2, is the evaluation of $G(z)$ for z on the unit circle. If the noise is zero and the input $u(k)$ is a sinusoid of amplitude A and frequency ω_0 , then $u(k)$ is given by

$$u(kT) = A \sin(\omega_0 kT), \quad (12.16)$$

and the output samples, in the steady state, can be described by

$$y(kT) = B \sin(\omega_0 kT + \phi_0), \quad (12.17)$$

where

$$\begin{aligned} B/A &= |G(e^{j\omega_0 T})| \\ \phi_0 &= \angle G(e^{j\omega_0 T}). \end{aligned} \quad (12.18)$$

Given the situation described by Eq. (12.15), there are two basic schemes for obtaining a non-parametric estimate of $G(e^{j\omega T})$. The first of these can be described as the one-frequency-at-a-time method and the other as the spectral estimate method. We will describe these in turn. In each case we will require the computation of Fourier transforms using finite records of data; and for this the discrete Fourier transform (DFT) described in Chapter 4 is used, especially in its computationally optimized form, the fast Fourier transform (FFT).

identification,
one-frequency-
at-a-time

The Method of One Frequency at a Time

We assume that we have a system as described in Eq. (12.15) and that the input is a sinusoid of the form of Eq. (12.16). The input and the output are recorded for N samples, and we wish to find the amplitude B and the phase ϕ_0 , from which one point on the frequency response can be computed according to Eq. (12.18). We then increment the frequency to $\omega_1 = \omega_0 + \delta\omega$ and repeat until the entire range of frequencies of interest is covered with the desired resolution. The accuracy of the estimate at any one point is a function of the number of points taken, the relative intensity of the noise, and the extent to which system transients have been allowed to decay before the recordings are started. We will describe the calculations in an ideal environment and discuss briefly the consequences of other situations.

Consider an output of the form of Eq. (12.17) but with unknown amplitude and phase. Recognizing that the experimental data might reflect some nonlinear effects and contain some noise component, a reasonable computational approach is to find that amplitude B and phase ϕ_0 which best fit the given data. We define the estimate of the output as

$$\begin{aligned} \hat{y}(kT) &= B \sin(\omega_0 kT + \phi_0) \\ &= B_c \cos(\omega_0 kT) + B_s \sin(\omega_0 kT), \end{aligned}$$

where $B_c = B \sin(\phi_0)$ and $B_s = B \cos(\phi_0)$. Once we have computed B_c and B_s we can compute the values of B and ϕ_0 as

$$\begin{aligned} B &= \sqrt{(B_c^2 + B_s^2)}, \\ \phi_0 &= \arctan \frac{B_c}{B_s}. \end{aligned} \quad (12.19)$$

To find the best fit of \hat{y} to the data, we form the quadratic cost in the error between y and \hat{y} as

$$\begin{aligned} \mathcal{J} &= \frac{1}{N} \sum_{k=0}^{N-1} (y(kT) - \hat{y}(kT))^2 \\ &= \frac{1}{N} \sum_{k=0}^{N-1} (y(kT) - B_c \cos(\omega_0 kT) - B_s \sin(\omega_0 kT))^2. \end{aligned}$$

Keep in mind that $y(kT)$ is the measured output and $\hat{y}(kT)$ is the computed estimate of the output. We wish to compute B_c and B_s so as to make \mathcal{J} as small as possible. To do this, we set the derivative of \mathcal{J} with respect to B_c and B_s equal to zero. Consider B_c first

$$\frac{\partial \mathcal{J}}{\partial B_c} = \frac{1}{N} \sum_{k=0}^{N-1} 2(y(kT) - B_c \cos(\omega_0 kT) - B_s \sin(\omega_0 kT))(-\cos(\omega_0 kT)) = 0.$$

If we use elementary trigonometric identities for the product of sine and cosine, and collect terms of the sum, this expression is equivalent to

$$\begin{aligned} \frac{1}{N} \sum_{k=0}^{N-1} y(kT) \cos(\omega_0 kT) - \frac{B_c}{2} - \frac{B_c}{2N} \sum_{k=0}^{N-1} \cos(2\omega_0 kT) \\ - \frac{B_s}{2N} \sum_{k=0}^{N-1} \sin(2\omega_0 kT) = 0. \end{aligned} \quad (12.20)$$

Generally, we would expect the last two terms in Eq. (12.20) to be small because the sinusoids alternate in sign and have zero average value. They will be *exactly* zero if we select the test frequencies carefully. Consider the following identity (which also played an important role in the development of the DFT in Chapter 4)

$$\frac{1}{N} \sum_{k=0}^{N-1} z^{-k} = \frac{1 - z^{-N}}{N(1 - z^{-1})}.$$

If we select integers ℓ and N and let $z = e^{j2\pi\ell/N}$, corresponding to $\omega = 2\pi\ell/N$, then

$$\begin{aligned} \frac{1}{N} \sum_{k=0}^{N-1} e^{-j2\pi\ell k/N} &= \frac{1 - e^{-j2\pi\ell}}{1 - e^{-j2\pi\ell/N}} \\ &= \begin{cases} 1, & \ell = rN \\ 0 & \text{elsewhere} \end{cases} \end{aligned} \quad (12.21)$$

If we substitute Euler's formula, $e^{-j2\pi\ell k/N} = \cos(2\pi\ell k/N) - j\sin(2\pi\ell k/N)$, into the left side of Eq. (12.21) and equate real and imaginary parts, we find that

$$\frac{1}{N} \sum_{k=0}^{N-1} \cos(2\pi\ell k/N) = \begin{cases} 1 & \ell = rN \\ 0 & \text{elsewhere} \end{cases}$$

and also

$$\frac{1}{N} \sum_{k=0}^{N-1} \sin(2\pi\ell k/N) = 0.$$

If we now select our test frequencies to be $\omega_0 = 2\pi\ell/NT$, for integer ℓ , then Eq. (12.20) reduces to

$$B_c = \frac{2}{N} \sum_{k=0}^{N-1} y(kT) \cos(2\pi\ell k/N). \quad (12.22)$$

In similar fashion, for this choice of input frequency, one can show that

$$B_s = \frac{2}{N} \sum_{k=0}^{N-1} y(kT) \sin(2\pi\ell k/N). \quad (12.23)$$

Thus Eq. (12.22) and Eq. (12.23) give us formulas for computing the values of B_c and B_s , and Eq. (12.19) gives us the formulas for the gain and phase that describe the output data $y(kT)$. The transfer function from which the output was measured is then given by Eq. (12.18).

Equation (12.22) is closely related to the DFT of y derived in Section 4.5. In fact, if we assume that $y(kT)$ is a sinusoid of frequency $\omega_\ell = 2\pi\ell/NT$ and consider the DFT of y

$$\begin{aligned} DFT[y(kT)] &= \sum_{k=0}^{N-1} y(kT) e^{-j2\pi kn/N} \\ &= \sum_{k=0}^{N-1} y(kT) [\cos(2\pi kn/N) - j\sin(2\pi kn/N)] \\ &= \begin{cases} \frac{N}{2} [B_c - jB_s], & n = \ell \\ 0 & n \neq \ell \end{cases} \end{aligned}$$

Likewise, the DFT of the sinusoidal input of the same frequency is given by

$$\begin{aligned}
 DFT[u(kT)] &= \sum_{k=0}^{N-1} A \sin(2\pi\ell k/N) e^{-j2\pi\ell k/N} \\
 &= \frac{A}{2j} \sum_{k=0}^{N-1} [e^{j2\pi\ell k/N} - e^{-j2\pi\ell k/N}] e^{-j2\pi n k/N} \\
 &= \frac{NA}{2j}, \quad (n = \ell) \\
 &= 0, \quad \text{elsewhere.}
 \end{aligned} \tag{12.24}$$

Thus, for $n = \ell$, the ratio of the DFT of y to that of u is

$$\begin{aligned}
 \frac{DFT(y)}{DFT(u)} &= \frac{(N/2)(B_c - jB_s)}{NA/2j} \\
 &= \frac{B_s + jB_c}{A} \\
 &= |G|e^{j\phi_0},
 \end{aligned} \tag{12.25}$$

which is the result found in Section 4.5. Of course, using the DFT or the FFT on $y(kT)$ and $u(kT)$ just for one point on the transfer function is unnecessarily complicated, but because the DFT automatically computes the best fit of a sinusoid to the output in the least-squares sense, the result is very accurate and, with the use of the FFT, it is fast.

It is possible to take advantage of Eq. (12.25) to evaluate the transfer function at several frequencies at once by using an input that is nonzero over a band of frequencies and computing the ratio of output to input at each nonzero value. To illustrate this technique, we will use an input known as a *chirp*, which is a modulated sinusoidal function with a frequency that grows from an initial value to a final value so as to cover the desired range. An example of a chirp is given by the formulas

$$\begin{aligned}
 u(kT) &= A_0 + w(k) \sin(\omega_k kT), \quad 0 \leq k \leq N-1, \\
 w(k) &= A \text{ sat}(k/0.1N) \text{ sat}((N-k)/0.1N), \\
 \omega_k &= \omega_{\text{start}} + \frac{k}{N} (\omega_{\text{end}} - \omega_{\text{start}}).
 \end{aligned} \tag{12.26}$$

In this expression, $w(k)$ is a weighting or window function that causes the input to start at zero, ramp up to amplitude A , and ramp down to zero at the end. The “sat” is the saturation function, which is linear from -1 to $+1$ and saturates at -1 for arguments less than -1 and at $+1$ for arguments greater than $+1$. The constant A_0 is added to make the input have zero average value.

A Chirp Signal

Example 12.1

Plot a chirp of maximum amplitude 1.0, starting frequency $\omega T = 0.1$ rad and ending frequency $\omega T = 0.75$ rad. Use 256 points. Also plot the magnitude of the transform of the signal.

Solution. From Eq. (12.26) we have $A = 1$, $T\omega_{\text{start}} = 0.1$, $T\omega_{\text{end}} = 0.75$, and $N = 256$. The constant A_0 was computed as the negative of the average of the basic signal, using MATLAB. The transform was computed using `fft.m`. The results are plotted in Fig. 12.1, parts (a) and (b). Notice that the actual spectrum is very flat between 0.3 and 1.0 rad and has non-negligible energy over the wider range between 0.1 and 1.5 rad. The energy above $T\omega_{\text{end}} = 0.75$ rad is the result of the fact that the chirp is really a frequency modulated signal and many sidebands are present.

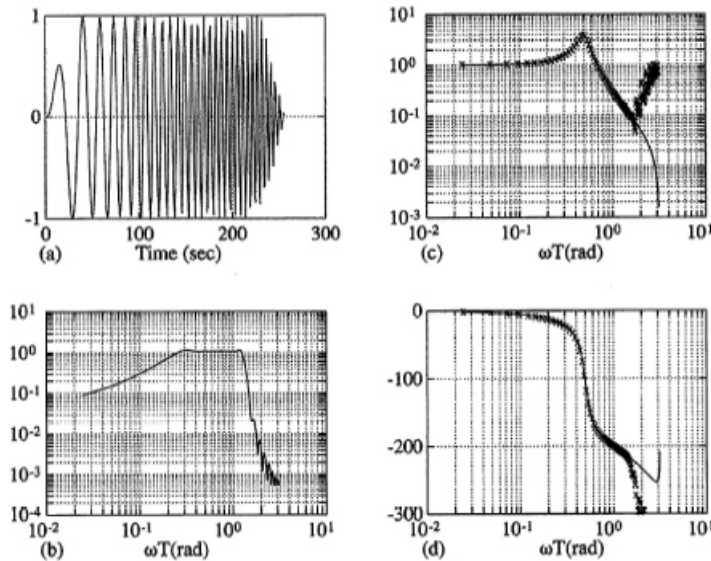


Figure 12.1
Estimation of transfer function using a chirp signal: (a) the chirp, (b) the chirp's spectrum, (c) the transfer function and its magnitude estimate, (d) the true and estimated phase

Computing a Transfer Function

Apply the chirp signal of Example 12.1 to a system obtained as the zero order hold equivalent of $1/(s^2 + 0.25s + 1)$ with $T = 0.5$. Compute the estimate of the transfer function using Eq. (12.25).

Solution. The results of the application of Eq. (12.25) to this data are plotted in Fig. 12.1, parts (c) and (d). The true frequency response is plotted as a solid line and the experimental transfer function estimate is plotted as x 's on the same graphs. As can be seen, the estimate is a very accurate measure for frequencies up to 1.8 rad, after which the estimate deviates badly from the true magnitude and phase curves. This deviation coincides with the frequencies where the input has little energy and leads us to conclude that one should not trust the result of Eq. (12.25) unless the input has significant energy at the computed frequency.

Example 12.2

Data Conditioning

As illustrated by Example 12.1, a signal can be constructed to have energy only in a certain band, and with its use the transfer function can be accurately estimated in this band. This observation is a particular case of an extremely important principle in system identification:

Use all available prior knowledge
to reduce the uncertainty in the estimate.

In the case of Example 12.1, we were able to use the fact that the important features of the unknown transfer function are in the digital frequency range $0.1 \leq \omega T \leq 1.5$ to design a chirp signal that would provide energy in that range only. Another situation, which was developed by Clary (1984), occurs when part of the transfer function is already known. This is common in the control of mechanical devices, such as robot mechanisms or space structures, where one knows that the transfer function has two poles at the origin in the s -plane and thus two poles at $z = 1$ in the z -plane. We may also know how fast the transfer function goes to zero for high frequencies and from this knowledge assign zeros of the transfer function at $z = -1$ to correspond to these. This assumption is not exact, because zeros at infinity in the s -plane do not map to any fixed point in the z -plane; however, in almost all cases, they result in z -plane zeros that are often well outside the unit circle so that they have almost no influence on the frequency response over the important band and are very difficult to

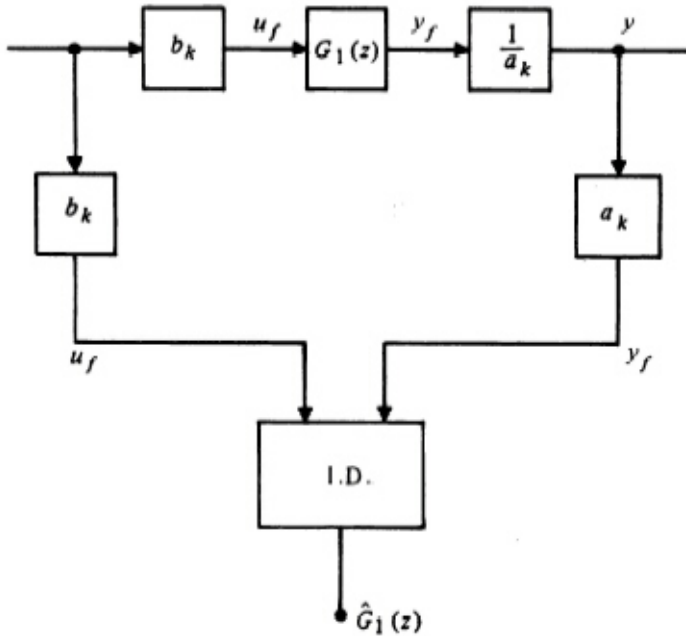


Figure 12.2
Block diagram of
identification of a
partially known
transfer function

identify accurately. It is for this reason that known s -plane zeros at infinity can be assigned to $z = -1$ and used to reduce the uncertainty in the discrete transfer-function estimation.

To illustrate Clary's procedure, suppose we model the known poles as the roots of the polynomial $a_k(z)$ and model the known zeros as the roots of $b_k(z)$. Then the overall transfer function can be factored into known and unknown parts in the form Clary's method

$$G(z) = \frac{b_k(z)}{a_k(z)} G_1(z). \quad (12.27)$$

In block-diagram form, the situation can be arranged as shown in Fig. 12.2. In this case, once the simpler unknown $G_1(z)$ is estimated from the filtered data u_f and y_f , the overall transfer function $G(z)$ can be reconstructed from Eq. (12.27).

Using Known Components

Example 12.3

Consider the system formed by multiplying the plant of Example 12.2 by $1/s^2$. Identify the corresponding discrete system by Clary's method.

Solution. The resulting fourth-order discrete system has two poles at $z = 1$ and zeros at $z = -9.5$, $z = -0.98$, and $z = -0.1$. If the same chirp signal used in Example 12.2 is used to identify this transfer function from its input and output, the results are shown in Fig. 12.3(a) and (b). Clearly the estimates, shown by x 's on the plots, are very poor in both magnitude and phase. However, if u is filtered by $(1 + z^{-1})^2$ and y is filtered by $(1 - z^{-1})^2$, then the transfer function G_1 can be estimated from these signals. Afterward, the estimated frequency responses are multiplied by the known frequency responses according to Eq. (12.27) and the total frequency response is plotted in Fig. 12.3(c) and (d). Now an excellent estimate of the transfer function results.

Our final example of the use of prior information in identification occurs when it is known what the important frequency range is and, furthermore, that significant sensor noise appears in the plant output outside this range. Such noise is almost always present in experimental data and typically

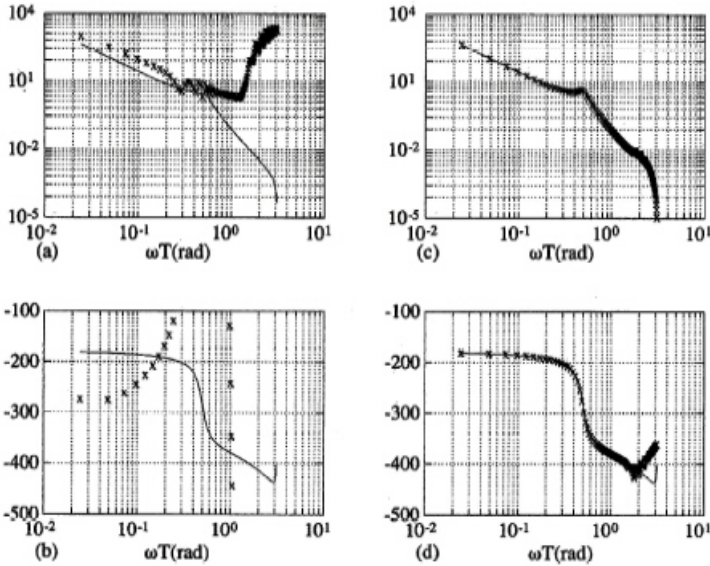


Figure 12.3
Transfer function estimates for a fourth-order system without filtering (a) and (b) and with filtering of the data, (c) and (d)

includes both noise from physical sources and noise that can be attributed to the quantization of A/D conversion. In this case, we observe that the identification of $G(z)$ is the same as the identification of $F(z)G(z)F(z)^{-1}$ because the filter transfer function F cancels. However, suppose that we filter both u and y through F . Although this has no influence on the relation between u and y , it can suppress the noise significantly. The equations that illustrate this effect are

$$\begin{aligned} y &= Gu + v, \\ Fy &= GFu + Fv, \\ y_f &= Gu_f + Fv. \end{aligned} \quad (12.28)$$

Therefore, we have succeeded in replacing the noise input v with the filtered noise Fv while keeping the same relation between the signal input and the output as before. If the noise includes significant energy at frequencies that are not important to the signal response, then F can be shaped to remove these components and greatly improve the transfer-function estimates. Most commonly, F is a lowpass filter such as a Butterworth characteristic with a cutoff frequency just above the range of important frequencies for the plant model. In the case of nonparametric estimation, the effect of the lowpass filter can be achieved simply by ignoring the estimates outside the desired range, as could be seen from Fig. 12.1. However, when we come to parametric estimation, the use of such filters will be found to be essential.

Stochastic Spectral Estimation

The deterministic methods just described require a high signal-to-noise ratio in the important band of the transfer function to be estimated. If this is not available, as frequently occurs, an alternative based on averaging or statistical estimation is available. The necessary equations are easily derived from the results on stochastic processes given in Appendix D. Suppose we describe the plant dynamics with the convolution

$$y(n) = \sum_{k=-\infty}^{\infty} g(k)u(n-k) \quad (12.29)$$

and assume that u and therefore y are zero mean stochastic processes. If we multiply Eq. (12.29) on both sides by $u(n - \ell)$ and take expected values, we obtain

$$\begin{aligned} \mathcal{E}y(n)u(n - \ell) &= \mathcal{E} \sum_{k=-\infty}^{\infty} g(k)u(n - k)u(n - \ell), \\ R_{yu}(\ell) &= \sum_{k=-\infty}^{\infty} g(k)R_{uu}(\ell - k), \end{aligned} \quad (12.30)$$

where $R_{yu}(\ell)$ is the cross-correlation between the y process and the u process and $R_{uu}(\ell - k)$ is the autocorrelation of the u process. If we take the z -transform of Eq. (12.30), it is clear, because this is a convolution, that

$$S_{yu}(z) = G(z)S_{uu}(z)$$

and thus that

$$G(z) = \frac{S_{yu}(z)}{S_{uu}(z)}, \quad (12.31)$$

where $S_{yu}(z)$, called the cross-power spectrum between the y and the u processes, is the z -transform of $R_{yu}(\ell)$ and $S_{uu}(z)$, the z -transform of $R_{uu}(\ell)$, is called the power spectrum of the u process.

With these equations, the estimation of the transfer function $G(z)$ has been converted to the estimation of the correlation functions R_{yu} and R_{uu} or, equivalently, to the estimation of the spectra S_{yu} and S_{uu} from the data records of $y(k)$ and $u(k)$. This topic, spectral estimation, is covered by a vast literature going back to the 1930's at least, and we will indicate only some of the important results relevant to the identification problem here. In the first place, our estimation of the correlation functions depends upon the ergodic assumption that the stochastic expectations can be computed as time averages according to ²

$$R_{yu}(\ell) = \lim_{N \rightarrow \infty} \frac{1}{2N + 1} \sum_{n=-N}^N y(n)u(n - \ell). \quad (12.32)$$

In order to use Eq. (12.32) with experimental data, we must consider that the data are finite. Suppose we have N points of input and N points of output data. Then we can write

$$\hat{R}_{yu}(\ell) = \frac{1}{N} \sum_{n=0}^N y(n)u(n - \ell), \quad (12.33)$$

where it is understood that $y(k)$ and $u(k)$ are zero outside the range $0 \leq k \leq N - 1$. The number of data values used to compose $R_{yu}(\ell)$ in Eq. (12.33) is $N - \ell$. Clearly, as ℓ gets near to N , this number gets small and very little averaging is involved. We conclude that the estimate of R from Eq. (12.33) can be expected to be very poor for $|\ell|$ near N , and we normally stop the sum for $|\ell| > L/2$, where we might take $L = N/8$, for example. The resulting estimate is a complicated function of the exact number of points used, and typically, in identification, the number to be used is determined by experience and experimentation. Another feature of Eq. (12.33) is the fact that in taking a finite number of points in the sum, it is as if we had multiplied the result, for any given ℓ , by a window of finite duration. The transform reflection of such a product is to convolve the true spectrum (transform) with the transform of the window, and the rectangular window obtained by simply truncating the series is particularly poor for this purpose. Rather, another window is normally introduced that has better spectral smoothing properties, such as the Hamming or the Kaiser window. To illustrate some of the properties of windows, a Hamming window of length 64 and its magnitude spectrum are plotted in Fig. 12.4. It should be recalled that convolution of a function with an impulse returns exactly the same function. Convolution with a bandpass filter of finite width has the effect of averaging the function over the width of the pass band. Fig. 12.4 shows that the Hamming window of length 64 has a spectrum with a main lobe of width about $8/128$, or 6.25% of the Nyquist frequency. A longer window would have a more narrow pass band, and a shorter window would have a wider spectral

²The MATLAB function `xcorr` computes $R_{yu}(-\ell) = R_{uy}(\ell)$.

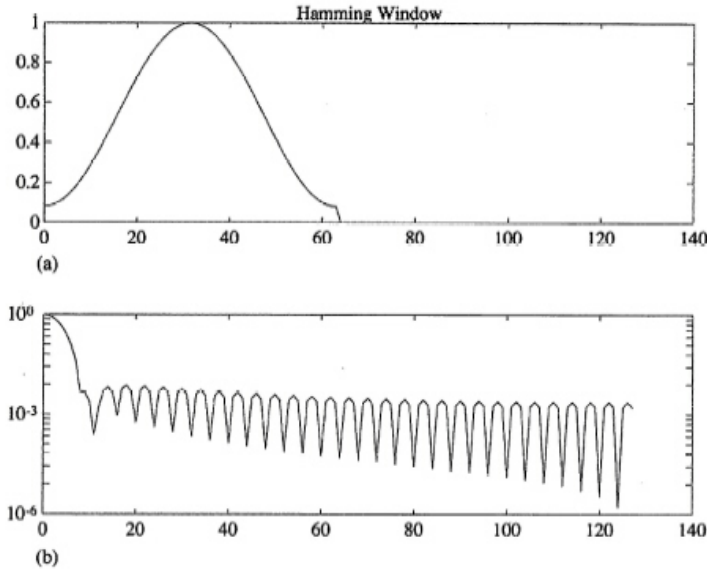


Figure 12.4
Hamming window:
(a) weighting
function, and (b)
spectrum

lobe and consequently more averaging of the spectrum in computing the estimate by Eq. (12.33). The engineer must use judgement to select a window function length that will balance noise reduction, for which a short window is wanted, against average spectrum accuracy, for which a long window is wanted.

From these considerations, a practical formula for spectrum estimation is derived as

$$\hat{S}_{yu}(z) = \sum_{\ell=-L/2}^{L/2} w(\ell) \hat{R}_{yu}(\ell) z^{-\ell}. \quad (12.34)$$

Stochastic Estimate of a Transfer Function

Example 12.4

Apply a random input signal to the second-order system of Example 12.2 and estimate the transfer function using Eq. (12.31) with the estimates according to Eq. (12.34). Repeat, with 20% random noise added to the output.

Solution. The system was excited with a 256-point random input of zero mean, and the autocorrelation and the cross-correlation were computed for all 512 points for the output with no noise and for the output with 20% noise. That is, the input to the system had a root-mean-square value of one, and the output had a noise added whose root-mean-square value was 0.2. A Hamming window of width 256 was used and the spectra computed for the system with no noise and for the system with output noise. The resulting transfer functions computed according to Eq. (12.31) are plotted in Fig. 12.5.

As can be seen from parts (a) and (b) of Fig. 12.5, the estimate when there is no noise is excellent. However, with the noise, as seen in parts (c) and (d), there is serious deviation of the estimate from the true transfer function, especially at the higher frequencies. In a real situation, serious consideration would be given to using a shorter window, perhaps as short as 100 or even less. As the window is shortened, however, the details of the resonant peak, as discussed, will be smeared out. The engineer's judgement and knowledge of the system under investigation must be used to balance the random fluctuations against the systematic errors.

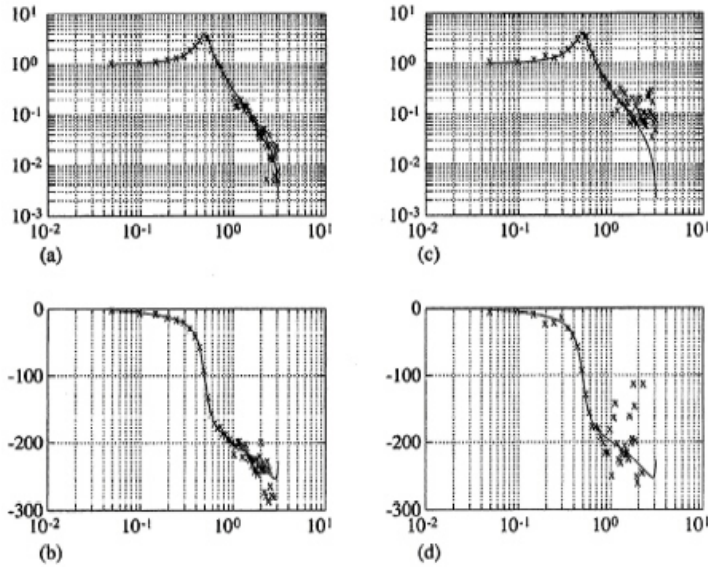


Figure 12.5
Estimation of transfer function with random input using spectral estimation: (a) and (b) no noise, (c) and (d) 20% noise

12.3 Models and Criteria for Parametric Identification

Because several design techniques including design by root locus and design by pole placement require a parametric model, it is important to understand how such models can be constructed. This is particularly important for adaptive control where the design must be implemented on-line and either the plant parameters or the controller parameters are to be estimated. To formulate a problem for parametric identification, it is necessary to select the parameters that are to be estimated and a criterion by which they are to be evaluated.

12.3.1 Parameter Selection

For example, suppose we have a transfer function that is the ratio of two polynomials in z . We can select the coefficients of these polynomials as the parameters. For the third-order case

$$G(z, \theta) = \frac{b_1 z^2 + b_2 z + b_3}{z^3 + a_1 z^2 + a_2 z + a_3}, \quad (12.35)$$

and the parameter vector θ is taken as

$$\theta = (a_1 \ a_2 \ a_3 \ b_1 \ b_2 \ b_3)^T. \quad (12.36)$$

We imagine that we observe a set of input sample values $[u(k)]$ and a set of corresponding output sample values $[y(k)]$, and that these come from a plant that can be described by the transfer function Eq. (12.35) for some “true” value of the parameters, θ^o . Our task, the parametric identification problem, is to compute from these $[u(k)]$ and $[y(k)]$ an estimate $\hat{\theta}$ that is a “good” approximation to θ^o .³

To repeat the formulations from a different point of view, suppose we postulate a (discrete) state-variable description of the plant and take the parameters to be the elements of the matrices Φ , Γ , \mathbf{H} . We assume $J = 0$. Then we have

$$\begin{aligned} \mathbf{x}(k+1) &= \Phi(\theta_1) \mathbf{x}(k) + \Gamma(\theta_1) u(k), \\ y(k) &= \mathbf{H}(\theta_1) \mathbf{x}(k). \end{aligned} \quad (12.37)$$

³For the moment, we assume that we know the number of states required to describe the plant. Estimation of n will be considered later.

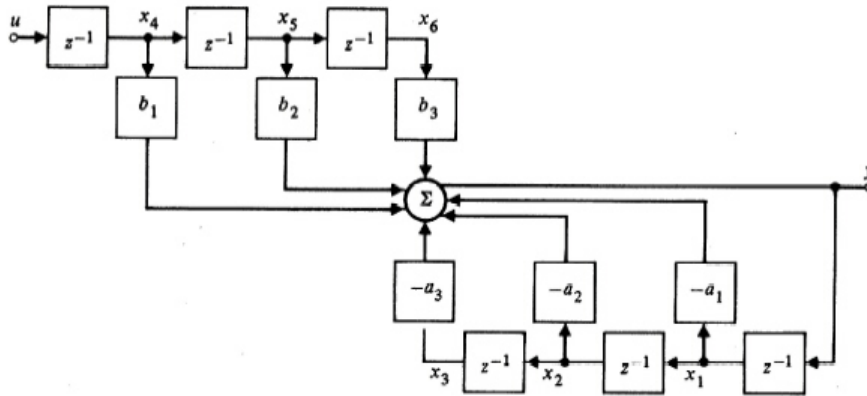


Figure 12.6
Block diagram of
the ARMA
realization of
 $G(z)$

For the third-order model, there are nine elements in Φ and three elements each in Γ and \mathbf{H} , for a total of fifteen parameters in Eq. (12.37), where six were enough in Eq. (12.35) for an equivalent description. If the six-element θ in Eq. (12.36) and the fifteen-element θ_1 in Eq. (12.37) describe the same transfer function, then we say they are *equivalent* parameters. Any set of $u(k)$ and $y(k)$ generated by one can be generated by the other, so, as far as control of y based on input u is concerned, there is no difference between θ and θ_1 even though they have very different elements. This means, of course, that the state-variable description has nine parameters that are in some sense redundant and can be chosen rather arbitrarily. In fact, we have already seen in Chapter 4 that the definition of the state is not unique and that if we were to change the state in Eq. (12.37) by the substitution $\xi = \mathbf{T}x$, we would have the same transfer function $G(z)$. It is exactly the nine elements of \mathbf{T} which represent the excess parameters in Eq. (12.37); we should select these in a way that makes our task as easy as possible. The standard, even obvious, way to do this is to *define* our state so that Φ, Γ, \mathbf{H} are in accordance with one of the *canonical* forms of Chapter 2 for transfer functions. For example, in observer canonical form we would have

$$\Phi = \begin{bmatrix} -a_1 & 1 & 0 \\ -a_2 & 0 & 1 \\ -a_3 & 0 & 0 \end{bmatrix} \quad \Gamma = \begin{bmatrix} b_1 \\ b_2 \\ b_3 \end{bmatrix}, \quad \mathbf{H} = [1 \quad 0 \quad 0], \quad (12.38)$$

and we see immediately that these matrices are just functions of the θ of Eq. (12.36), and the equivalence of θ_1 to θ is obvious.

But now let us repeat, in this context, the comments made earlier about the difference between identification for control and modelling for science. In taking the canonical form represented by Eq. (12.38), we have almost surely scrambled into the a_i and b_i a jumble of the *physical* parameters of masses, lengths, spring constants, coefficients of friction, and so on. Although the *physical* nature of the problem can be best described and understood in terms of these numbers, it is the a_i and b_i that best serve our purpose of control, and it is with these that we will be concerned here.

Before leaving the matter of canonical forms, it is appropriate at this point to introduce another form called, in digital signal processing, the ARMA⁴ model; this model has one feature especially appropriate for identification. A block diagram of the ARMA realization of $G(z)$ is shown in Fig. 12.6. Elementary calculations left to the reader will show that the transfer function of this block diagram is given by Eq. (12.35). The state equations are more interesting. Here we find six states and the

parameters of the
ARMA model

⁴ARMA, an acronym for AutoRegressive Moving Average, comes from study of random processes generated by white noise filtered through the transfer function $G(z)$ of Eq. (12.35). We will have more to say about this after the element of randomness is introduced.

matrices

$$\Phi = \begin{bmatrix} -a_1 & -a_2 & -a_3 & b_1 & b_2 & b_3 \\ 1 & 0 & 0 & 0 & 0 & 0 \\ 0 & 1 & 0 & 0 & 0 & 0 \\ 0 & 0 & 0 & 0 & 0 & 0 \\ 0 & 0 & 0 & 1 & 0 & 0 \\ 0 & 0 & 0 & 0 & 1 & 0 \end{bmatrix}, \quad \Gamma = \begin{bmatrix} 0 \\ 0 \\ 0 \\ 1 \\ 0 \\ 0 \end{bmatrix}$$

$$\mathbf{H} = \begin{bmatrix} -a_1 & -a_2 & -a_3 & b_1 & b_2 & b_3 \end{bmatrix}. \quad (12.39)$$

From the point of view of state-space analysis, the system described by Eq. (12.39) is seen to have six states to describe a third-order transfer function and thus to be “non-minimal.” In fact, the Φ matrix can be shown to have three poles at $z = 0$ that are *not observable* for any values of a_i or b_i . However, the system does have one remarkable property: The state is given by

$$\mathbf{x}(k) = [y(k-1) \quad y(k-2) \quad y(k-3) \quad u(k-1) \quad u(k-2) \quad u(k-3)]^T. \quad (12.40)$$

In other words, the state is exactly given by the past inputs and outputs so that, if we have the set of $[u(k)]$ and $[y(k)]$, we have the state also, since it is merely a listing of six members of the set.

All the action, as it were, takes place in the output equation, which is

$$\begin{aligned} y(k) &= \mathbf{H}\mathbf{x}(k) \\ &= -a_1y(k-1) - a_2y(k-2) - a_3y(k-3) \\ &\quad + b_1u(k-1) + b_2u(k-2) + b_3u(k-3). \end{aligned} \quad (12.41)$$

There is no need to carry any other equation along because the state equations are trivially related to this output equation. We will use the ARMA model in some of our later formulations for identification.

Thus we conclude that within the class of discrete parametric models we wish to select a model that has the fewest number of parameters and yet will be equivalent to the assumed plant description. A model whose parameters are uniquely determined by the observed data is highly desirable; a model that will make subsequent control design simple is also often selected.

12.3.2 Error Definition

Having selected the class of models described by our assumed plant description, we now turn to the techniques for selecting the particular estimate, $\hat{\boldsymbol{\theta}}$, that best represents the given data. For this we require some idea of goodness of fit of a proposed value of $\boldsymbol{\theta}$ to the true $\boldsymbol{\theta}^\circ$. Because, by the very nature of the problem, $\boldsymbol{\theta}^\circ$ is unknown, it is unrealistic to define a direct parameter error between $\boldsymbol{\theta}$ and $\boldsymbol{\theta}^\circ$. We must define the error in a way that can be computed from $[u(k)]$ and $[y(k)]$. Three definitions that have been proposed and studied extensively are *equation error*, *output error*, and *prediction error*.

Equation Error

For the equation error, we need complete equations of motion as given, for example, by a state-variable description. To be just a bit general for the moment, suppose we have a nonlinear continuous time description with parameter vector $\boldsymbol{\theta}$, which we can write as

$$\dot{\mathbf{x}} = \mathbf{f}(\mathbf{x}, \mathbf{u}; \boldsymbol{\theta}).$$

We assume, first, that we know the form of the vector functions \mathbf{f} but not the particular parameters $\boldsymbol{\theta}^\circ$ that describe the plant. We assume, second, that we are able to measure not only the controls \mathbf{u} but also the state \mathbf{x} and the state derivative $\dot{\mathbf{x}}$. We thus know *everything* about the equations but the particular parameter values. We can, therefore, form an error comprised of the extent to which these

equations of motion fail to be true for a specific value of $\boldsymbol{\theta}$ when used with the specific actual data \mathbf{x}_a , $\dot{\mathbf{x}}_a$, and \mathbf{u}_a . We write

$$\dot{\mathbf{x}}_a - \mathbf{f}(\mathbf{x}_a, \mathbf{u}_a; \boldsymbol{\theta}) = \mathbf{e}(t; \boldsymbol{\theta}),$$

and we assume that there is a vector of true parameters $\boldsymbol{\theta}^\circ$ such that $\mathbf{e}(t; \boldsymbol{\theta}^\circ) = \mathbf{0}$. The vector $\mathbf{e}(t; \boldsymbol{\theta})$ is defined as the **equation error**. The idea is that we would form some non-negative function of the equation error such as

$$\mathcal{J}(\boldsymbol{\theta}) = \int_0^T \mathbf{e}^T(t, \boldsymbol{\theta}) \mathbf{e}(t, \boldsymbol{\theta}) dt, \quad (12.42)$$

and search over $\boldsymbol{\theta}$ until we find $\hat{\boldsymbol{\theta}}$ such that $\mathcal{J}(\boldsymbol{\theta})$ is a minimum, at which time we will have a parameter set $\hat{\boldsymbol{\theta}}$ that is an estimate of $\boldsymbol{\theta}^\circ$. If we had an exact set of equations and selected a unique parameterization, then only one parameter set will make $\mathbf{e}(t; \boldsymbol{\theta}^\circ) = \mathbf{0}$, and so we will have $\hat{\boldsymbol{\theta}} = \boldsymbol{\theta}^\circ$. If noise is present in the equations of motion, then the error will not be zero at $\hat{\boldsymbol{\theta}} = \boldsymbol{\theta}^\circ$, but \mathcal{J} will be minimized at that point.⁵

The assumption that we have enough sensors to measure the total state and all state derivatives is a strong assumption and often not realistic in continuous model identification. However, in discrete linear models there is one case where it is immediate, and that is the case of an ARMA model. The reason for this is not hard to find: In an ARMA model the state is no more than recent values of input and output! To be explicit about it, let us write the linear, discrete model equation error, which is

$$\mathbf{x}_a(k+1) - \boldsymbol{\Phi} \mathbf{x}_a(k) - \boldsymbol{\Gamma} u_a(k) = \mathbf{e}(k; \boldsymbol{\theta}), \quad (12.43)$$

where $\boldsymbol{\Phi}$ and $\boldsymbol{\Gamma}$ are functions of the parameters $\boldsymbol{\theta}$. Now let us substitute the values from Eq. (12.39), the ARMA model

$$\begin{bmatrix} x_1(k+1) \\ x_2(k+1) \\ x_3(k+1) \\ x_4(k+1) \\ x_5(k+1) \\ x_6(k+1) \end{bmatrix} - \begin{bmatrix} -a_1 & -a_2 & -a_3 & b_1 & b_2 & b_3 \\ 1 & 0 & 0 & 0 & 0 & 0 \\ 0 & 1 & 0 & 0 & 0 & 0 \\ 0 & 0 & 0 & 0 & 0 & 0 \\ 0 & 0 & 0 & 1 & 0 & 0 \\ 0 & 0 & 0 & 0 & 1 & 0 \end{bmatrix} \begin{bmatrix} x_1(k) \\ x_2(k) \\ x_3(k) \\ x_4(k) \\ x_5(k) \\ x_6(k) \end{bmatrix} - \begin{bmatrix} 0 \\ 0 \\ 0 \\ 1 \\ 0 \\ 0 \end{bmatrix} u(k) = \begin{bmatrix} e_1(k) \\ e_2(k) \\ e_3(k) \\ e_4(k) \\ e_5(k) \\ e_6(k) \end{bmatrix}. \quad (12.44)$$

When we make the substitution from Eq. (12.40) we find that, for any $\boldsymbol{\theta}$ (which is to say, for any values of a_i and b_i) the elements of equation error are *all zero* except e_1 , and this element of error is given by

$$x_1(k+1) - b_1 x_4(k) - b_2 x_5(k) - b_3 x_6(k) = e_1(k; \boldsymbol{\theta}) + a_1 x_1(k) + a_2 x_2(k) + a_3 x_3(k)$$

or

$$y_a(k) + a_1 y_a(k-1) + a_2 y_a(k-2) + a_3 y_a(k-3) - b_1 u_a(k-1) - b_2 u_a(k-2) - b_3 u_a(k-3) = e_1(k; \boldsymbol{\theta}). \quad (12.45)$$

The performance measure Eq. (12.42) becomes

$$\mathcal{J}(\boldsymbol{\theta}) = \sum_{k=0}^N e_1^2(k; \boldsymbol{\theta}). \quad (12.46)$$

Again, we place the subscript a on the observed data to emphasize the fact that these are *actual* data that were produced via the plant with (we assume) parameter values $\boldsymbol{\theta}^\circ = [a_1^\circ \ a_2^\circ \ a_3^\circ \ b_1^\circ \ b_2^\circ \ b_3^\circ]$, and in Eq. (12.45) and Eq. (12.46) an error results because $\boldsymbol{\theta}$ differs from $\boldsymbol{\theta}^\circ$.

⁵Methods to search for the minimizing $\hat{\boldsymbol{\theta}}$ are the subject of nonlinear programming, which is discussed in Luenberger (1973). We give a brief discussion later in this chapter connected with maximum likelihood estimates.

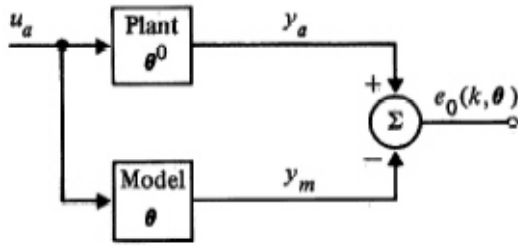


Figure 12.7
Block diagram
showing the
formulation of
output error

Output Error

As we have seen, the general case of equation error requires measurement of all elements of state and state derivatives. In order to avoid these assumptions a criterion based on output error can be used. This error is formulated in Fig. 12.7. Here we see that no attempt is made to measure the entire state of the plant, but rather the estimated parameter θ is used in a model to produce the model output $y_m(k)$, which is a function, therefore, of θ in the same way that the actual output is a function of the true parameter value θ° . In the scalar output case the output error e_o will be a scalar and we can form the criterion function

$$\mathcal{J}(\theta) = \sum_{k=0}^N e_o^2(k; \theta) \quad (12.47)$$

and search for that $\hat{\theta}$ which makes $\mathcal{J}(\hat{\theta})$ as small as possible. To illustrate the difference between output error and equation error in one case, consider again the ARMA model for which we have

$$\begin{aligned} y_m(k) = & -a_1 y_m(k-1) - a_2 y_m(k-2) - a_3 y_m(k-3) \\ & + b_1 u_a(k-1) + b_2 u_a(k-2) + b_3 u_a(k-3) \end{aligned}$$

and then the output error

$$\begin{aligned} e_o(k; \theta) = & y_a(k) - y_m(k) \\ = & y_a(k) + a_1 y_m(k-1) + a_2 y_m(k-2) + a_3 y_m(k-3) \\ & - b_1 u_a(k-1) - b_2 u_a(k-2) - b_3 u_a(k-3). \end{aligned} \quad (12.48)$$

If we compare Eq. (12.48) with Eq. (12.45) we see that the equation error formulation has past values of the *actual* output, and the output error formulation uses past values of the *model* output. Presumably the equation error is in some way better because it takes more knowledge into account, but we are not well situated to study the matter at this point.

Prediction Error

The third approach to developing an error signal by which a parameter search can be structured is the prediction error. When we discussed observers in Chapter 8 we made the point that a simple model is not a good basis for an observer because the equations of motion of the errors cannot be controlled. When we add random effects into our data-collection scheme, as we are about to do, much the same complaint can be raised about the generation of output errors. Instead of working with a simple model, with output $y_m(k)$, we are led to consider an output *predictor* that, within the confines of known structures, will do the best possible job of *predicting* $y(k)$ based on previous observations. We will see that in one special circumstance the ARMA model error as given by Eq. (12.45) has the least prediction error, but this is not true in general. Following our development of the observer, we might suspect that a *corrected* model would be appropriate, but we must delay any results in that area until further developments. For the moment, and for the purpose of displaying the output prediction error formulation, we have the situation pictured in Fig. 12.8.

prediction error

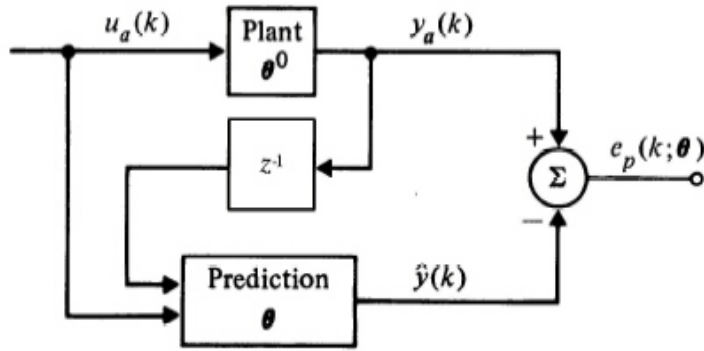


Figure 12.8
Block diagram
showing the
generation of
prediction error

12.4 Deterministic Estimation

Having defined an error that depends on θ , we can formulate a performance criterion and search for that $\hat{\theta}$ which is the best estimate of θ° within the context of the defined performance. To illustrate this use of error we have already defined a $\mathcal{J}(\theta)$ in Eq. (12.42), Eq. (12.46), and Eq. (12.47), in each case a sum of squares. The choice of a performance criterion is guided both by the computational difficulties it imposes in the effort to obtain $\hat{\theta}$ and by the properties of the estimate that results, that is, by how hard $\hat{\theta}$ is to find and how good it is when found. Among the criteria most widely used are:

1. least-squares estimate (LS),
2. best linear unbiased estimate (BLUE), and
3. maximum likelihood estimate (MLE)

The last two criteria require a stochastic element to be introduced into the model, and our understanding of least squares is enhanced by a stochastic perspective. However, before we introduce random noise into the picture, it is informative to consider deterministic least squares. Thus we will discuss least squares first, then introduce random noise and discuss the formulation of random errors, and finally define and discuss the BLUE and the MLE, their calculation and their properties.

12.4.1 Least Squares

To begin our discussion of least squares, we will take the ARMA model and equation error, which leads us to Eq. (12.45), repeated below for the n th-order case, where the subscript a is understood but omitted

$$y(k) + a_1y(k-1) + a_2y(k-2) + \cdots + a_ny(k-n) - b_1u(k-1) - \cdots - b_nu(k-n) = e(k; \theta). \quad (12.49)$$

We assume that we observe the set of outputs and inputs

$$\{-y(0), -y(1), \dots, -y(N), u(0), u(1), \dots, u(N)\}$$

and wish to compute values for

$$\theta = [a_1 \cdots a_n \ b_1 \cdots b_n]^T,$$

which will best fit the observed data. Because $y(k)$ depends on past data back to n periods earlier, the first error we can form is $e(n; \theta)$. Suppose we define the *vector* of errors by writing Eq. (12.49) over

and over for $k = n, n + 1, \dots, N$. The results would be

$$\begin{aligned} y(n) &= \Phi^T(n)\boldsymbol{\theta} + e(n; \boldsymbol{\theta}), \\ y(n+1) &= \Phi^T(n+1)\boldsymbol{\theta} + e(n+1; \boldsymbol{\theta}), \\ &\vdots \\ y(N) &= \Phi^T(N)\boldsymbol{\theta} + e(N; \boldsymbol{\theta}), \end{aligned} \quad (12.50)$$

where we have used the fact that the state of the ARMA model is⁶

$$\Phi(k) = [-y(k-1) - y(k-2) \cdots u(k-1) \cdots u(k-n)]^T.$$

To make the error even more compact, we introduce another level of matrix notation and define

$$\begin{aligned} \mathbf{Y}(N) &= [y(n) \cdots y(N)]^T, \\ \Phi(N) &= [\Phi(n) \Phi(n+1) \cdots \Phi(N)]^T, \\ \boldsymbol{\varepsilon}(N; \boldsymbol{\theta}) &= [e(n) \cdots e(N)]^T, \\ \boldsymbol{\theta} &= [a_1 \cdots a_n \ b_1 \cdots b_n]^T. \end{aligned} \quad (12.51)$$

Note that $\Phi(N)$ is a *matrix* with $2n$ columns and $N - n + 1$ rows. In terms of these, we can write the equation errors as

$$\mathbf{Y} = \Phi\boldsymbol{\theta} + \boldsymbol{\varepsilon}(N; \boldsymbol{\theta}). \quad (12.52)$$

Least squares is a prescription that one should take that value of $\boldsymbol{\theta}$ which makes the sum of the squares of the $e(k)$ as small as possible. In terms of Eq. (12.50), we define

$$\mathcal{J}(\boldsymbol{\theta}) = \sum_{k=n}^N e^2(k; \boldsymbol{\theta}), \quad (12.53)$$

and in terms of Eq. (12.52), this is

$$\mathcal{J}(\boldsymbol{\theta}) = \boldsymbol{\varepsilon}^T(N; \boldsymbol{\theta})\boldsymbol{\varepsilon}(N; \boldsymbol{\theta}). \quad (12.54)$$

We want to find $\hat{\boldsymbol{\theta}}_{\text{LS}}$, the least-squares estimate of $\boldsymbol{\theta}^0$, which is that $\boldsymbol{\theta}$ having the property

$$\mathcal{J}(\hat{\boldsymbol{\theta}}_{\text{LS}}) \leq \mathcal{J}(\boldsymbol{\theta}). \quad (12.55)$$

But $\mathcal{J}(\boldsymbol{\theta})$ is a quadratic function of the $2n$ parameters in $\boldsymbol{\theta}$, and from calculus we take the result that a necessary condition on $\hat{\boldsymbol{\theta}}_{\text{LS}}$ is that the partial derivatives of \mathcal{J} with respect to $\boldsymbol{\theta}$ at $\boldsymbol{\theta} = \hat{\boldsymbol{\theta}}_{\text{LS}}$ should be zero. This we do as follows

$$\begin{aligned} \mathcal{J}_{\boldsymbol{\theta}} &= \boldsymbol{\varepsilon}^T \boldsymbol{\varepsilon} \\ &= (\mathbf{Y} - \Phi\boldsymbol{\theta})^T (\mathbf{Y} - \Phi\boldsymbol{\theta}) \\ &= \mathbf{Y}^T \mathbf{Y} - \boldsymbol{\theta}^T \Phi^T \mathbf{Y} - \mathbf{Y}^T \Phi \boldsymbol{\theta} + \boldsymbol{\theta}^T \Phi^T \Phi \boldsymbol{\theta}; \end{aligned}$$

and applying the rules developed above for derivatives of scalars with respect to vectors⁷ we obtain

$$\mathcal{J}_{\boldsymbol{\theta}} = \left[\frac{\partial \mathcal{J}}{\partial \boldsymbol{\theta}_i} \right] = -2\mathbf{Y}^T \Phi + 2\boldsymbol{\theta}^T \Phi^T \Phi. \quad (12.56)$$

If we take the transpose of Eq. (12.56) and let $\boldsymbol{\theta} = \hat{\boldsymbol{\theta}}_{\text{LS}}$, we must get zero; thus

$$\Phi^T \Phi \hat{\boldsymbol{\theta}}_{\text{LS}} = \Phi^T \mathbf{Y}. \quad (12.57)$$

⁶We use Φ for the state here rather than \mathbf{x} as in Eq. (12.44) because we will soon be developing equations for the evolution of $\boldsymbol{\theta}(k)$, estimates of the parameters, which will be the state of our identification dynamic system.

⁷The reader who has not done so before should write out $\mathbf{a}^T \mathbf{Q} \mathbf{a}$ for a 3×3 case and verify that $\partial \mathbf{a}^T \mathbf{Q} \mathbf{a} / \partial \mathbf{a} = 2\mathbf{a}^T \mathbf{Q}$.

These equations are called the *normal equations* of the problem, and their solution will provide us with the least-squares estimate $\hat{\boldsymbol{\theta}}_{\text{LS}}$.

Do the equations have a unique solution? The answer depends mainly on how $\boldsymbol{\theta}$ was selected and what input signals $\{u(k)\}$ were used. Recall that earlier we saw that a general third-order state model had fifteen parameters, but that only six of these were needed to completely describe the input–output dependency. If we stayed with the fifteen-element $\boldsymbol{\theta}$, the resulting normal equations could not have a unique solution. To obtain a unique parameter set, we must select a canonical form having a minimal number of parameters, such as the observer or ARMA forms. By way of definition, a parameter $\boldsymbol{\theta}$ having the property that one and only one value of $\boldsymbol{\theta}$ makes $\mathcal{J}(\boldsymbol{\theta})$ a minimum is said to be “identifiable.” Two parameters having the property that $\mathcal{J}(\boldsymbol{\theta}_1) = \mathcal{J}(\boldsymbol{\theta}_2)$ are said to be “equivalent.”

As to the selection of the inputs $u(k)$, let us consider an absurd case. Suppose $u(k) \equiv c$ for all k — a step function input. Now suppose we look at Eq. (12.50) again for the third-order case to be specific. The errors are

$$\begin{aligned} y(3) &= -a_1y(2) - a_2y(1) - a_3y(0) + b_1c + b_2c + b_3c + e(3), \\ &\vdots \\ y(N) &= -a_1y(N-1) - a_2(N-2) - a_3(N-3) + b_1c + b_2c + b_3c + e(N). \end{aligned} \quad (12.58)$$

It is obvious that in Eq. (12.58) the parameters b_1, b_2 , and b_3 always appear as the sum $b_1 + b_2 + b_3$ and that separation of them is not possible when a constant input is used. Somehow the constant u fails to “excite” all the dynamics of the plant. This problem has been studied extensively, and the property of “persistently exciting” has been defined to describe a sequence $\{u(k)\}$ that fluctuates enough to avoid the possibility that only linear combinations of elements of $\boldsymbol{\theta}$ will show up in the error and hence in the normal equations [Ljung(1987)]. Without being more specific at this point, we can say that an input is *persistently exciting of order n* if the lower right $(n \times n)$ -matrix component of $\boldsymbol{\Phi}^T \boldsymbol{\Phi}$ [which depends only on $\{u(k)\}$] is nonsingular. It can be shown that a signal is persistently exciting of order n if its discrete spectrum has at least n nonzero points over the range $0 \leq \omega T < \pi$. White noise and a pseudo-random binary signal are examples of frequently used persistently exciting input signals.

For the moment, then, we will *assume* that the $u(k)$ are persistently exciting and that the $\boldsymbol{\theta}$ are identifiable and consequently that $\boldsymbol{\Phi}^T \boldsymbol{\Phi}$ is nonsingular. We can then write the explicit solution

$$\hat{\boldsymbol{\theta}}_{\text{LS}} = (\boldsymbol{\Phi}^T \boldsymbol{\Phi})^{-1} \boldsymbol{\Phi}^T \mathbf{Y}. \quad (12.59)$$

It should be especially noted that although we are here mainly interested in identification of parameters to describe dynamic systems, the solution Eq. (12.59) derives entirely from the error equations Eq. (12.52) and the sum of squares criterion Eq. (12.54). Least squares is used for all manner of curve fitting, including nonlinear least squares when the error is a nonlinear function of the parameters. Numerical methods for solving for the least-squares solution to Eq. (12.57) without ever explicitly forming the product $\boldsymbol{\Phi}^T \boldsymbol{\Phi}$ have been extensively studied [see Golub (1965) and Strang (1976)].

The performance measure Eq. (12.53) is essentially based on the view that all the errors are equally important. This is not necessarily so, and a very simple modification can take account of known differences in the errors. We might know, for example, that data taken later in the experiment were much more in error than data taken early on, and it would seem reasonable to weight the errors accordingly. Such a scheme is referred to as weighted least squares and is based on the performance criterion

$$\mathcal{J}(\boldsymbol{\theta}) = \sum_{k=n}^N w(k) e^2(k; \boldsymbol{\theta}) = \boldsymbol{\varepsilon}^T \mathbf{W} \boldsymbol{\varepsilon}. \quad (12.60)$$

In Eq. (12.60) we take the weighting function $w(k)$ to be positive and, presumably, to be small where the errors are expected to be large, and vice versa. In any event, derivation of the normal equations from Eq. (12.60) follows at once and gives

$$\boldsymbol{\Phi}^T \mathbf{W} \boldsymbol{\Phi} \hat{\boldsymbol{\theta}}_{\text{WLS}} = \boldsymbol{\Phi}^T \mathbf{W} \mathbf{Y},$$

and, subject to the coefficient matrix being nonsingular, we have

$$\hat{\boldsymbol{\theta}}_{\text{WLS}} = (\boldsymbol{\Phi}^T \mathbf{W} \boldsymbol{\Phi})^{-1} \boldsymbol{\Phi}^T \mathbf{W} \mathbf{Y}. \quad (12.61)$$

We note that Eq. (12.61) reduces to ordinary least squares when $\mathbf{W} = \mathbf{I}$, the identity matrix. Another common choice for $w(k)$ in Eq. (12.60) is $w(k) = (1 - \gamma)\gamma^{N-k}$ for $\gamma < 1$. This choice weights the recent (k near N) observations more than the past (k near n) ones and corresponds to a first-order filter operating on the squared error. The factor $1 - \gamma$ causes the gain of the equivalent filter to be 1 for constant errors. As γ nears 1, the filter memory becomes long, and noise effects are reduced; whereas for smaller γ , the memory is short, and the estimate can track changes that can occur in $\boldsymbol{\theta}$ if the computation is done over and over as N increases. The past is weighted geometrically with weighting γ , but a rough estimate of the memory length is given by $1/(1 - \gamma)$; so, for example, a $\gamma = 0.99$ corresponds to a memory of about 100 samples. The choice is a compromise between a short memory which permits tracking changing parameters and a long memory which incorporates a lot of averaging and reduces the noise variance.

12.4.2 Recursive Least Squares

The weighted least-squares calculation for $\hat{\boldsymbol{\theta}}_{\text{WLS}}$ given in Eq. (12.61) is referred to as a “batch” calculation, because by the definition of the several entries, the formula presumes that one has a batch of data of length N from which the matrices \mathbf{Y} and $\boldsymbol{\Phi}$ are composed according to the definitions in Eq. (12.51), and from which, with the addition of the weighting matrix \mathbf{W} , the normal equations are solved. There are times when the data are acquired sequentially rather than in a batch, and other times when one wishes to examine the nature of the solution as more data are included to see whether perhaps some improvement in the parameter estimates continues to be made or whether any surprises occur such as a sudden change in $\boldsymbol{\theta}$ or a persistent drift in one or more of the parameters. In short, one wishes sometimes to do a visual or experimental examination of the new estimates as one or several more data points are included in the computed values of $\hat{\boldsymbol{\theta}}_{\text{WLS}}$.

The equations of Eq. (12.61) can be put into a form for sequential processing of the type described. We begin with Eq. (12.61) as solved for N data points and consider the consequences of taking one more observation. We need to consider the structure of $\boldsymbol{\Phi}^T \mathbf{W} \boldsymbol{\Phi}$ and $\boldsymbol{\Phi}^T \mathbf{W} \mathbf{Y}$ as one more datum is added. Consider first $\boldsymbol{\Phi}^T \mathbf{W} \boldsymbol{\Phi}$. To be specific about the weights, we will assume $w = a\gamma^{N-k}$. Then, if $a = 1$ and $\gamma = 1$, we have ordinary least squares; and if $a = 1 - \gamma$, we have exponentially weighted least squares. From Eq. (12.51) we have, for data up to time $N + 1$

$$\boldsymbol{\Phi}^T = [\boldsymbol{\Phi}(n) \cdots \boldsymbol{\Phi}(N) \phi(N + 1)]$$

and

$$\boldsymbol{\Phi}^T \mathbf{W} \boldsymbol{\Phi} = \sum_{k=n}^{N+1} \boldsymbol{\Phi}(k) w(k) \boldsymbol{\Phi}^T(k) = \sum_{k=n}^{N+1} \boldsymbol{\Phi}(k) a \gamma^{N+1-k} \boldsymbol{\Phi}^T(k),$$

which can be written in two terms as

$$\begin{aligned} \boldsymbol{\Phi}^T \mathbf{W} \boldsymbol{\Phi} &= \sum_{k=n}^N \boldsymbol{\Phi}(k) a \gamma^{N-k} \boldsymbol{\Phi}^T(k) + \boldsymbol{\Phi}(N + 1) a \phi^T(N + 1) \\ &= \gamma \boldsymbol{\Phi}^T(N) \mathbf{W}(N) \boldsymbol{\Phi}(N) + \phi(N + 1) a \phi^T(N + 1). \end{aligned} \quad (12.62)$$

From the solution Eq. (12.61) we see that the inverse of the matrix in Eq. (12.62) will be required,⁸ and for convenience and by convention we *define* the $2n \times 2n$ matrix \mathbf{P} as

$$\mathbf{P}(N + 1) = [\boldsymbol{\Phi}^T(N + 1) \mathbf{W} \boldsymbol{\Phi}(N + 1)]^{-1}. \quad (12.63)$$

Then we see that Eq. (12.62) can be written as

$$\mathbf{P}(N + 1) = [\gamma \mathbf{P}^{-1}(N) + \boldsymbol{\Phi}(N + 1) a \phi^T(N + 1)]^{-1}, \quad (12.64)$$

⁸We assume for this discussion the existence of the inverse which assumes inputs that are persistently exciting and parameters that are identifiable.

and we need the inverse of a sum of two matrices. This is a well-known problem, and a formula attributed to Householder (1964) known as the *matrix inversion lemma* is

$$(\mathbf{A} + \mathbf{BCD})^{-1} = \mathbf{A}^{-1} - \mathbf{A}^{-1}\mathbf{B}(\mathbf{C}^{-1} + \mathbf{DA}^{-1}\mathbf{B})^{-1}\mathbf{DA}^{-1}. \quad (12.65)$$

To apply Eq. (12.65) to Eq. (12.62) we make the associations

$$\begin{aligned} \mathbf{A} &= \gamma\mathbf{P}^{-1}(N), \\ \mathbf{B} &= \Phi(N+1) \equiv \Phi, \\ \mathbf{C} &= w(N+1) \equiv a, \\ \mathbf{D} &= \Phi^T(N+1) \equiv \Phi^T, \end{aligned}$$

and we find at once that

$$\mathbf{P}(N+1) = \frac{\mathbf{P}(N)}{\gamma} - \frac{\mathbf{P}(N)}{\gamma} \Phi \left(\frac{1}{a} + \Phi^T \frac{\mathbf{P}(N)}{\gamma} \Phi \right)^{-1} \Phi^T \frac{\mathbf{P}(N)}{\gamma}. \quad (12.66)$$

In the solution we also need $\Phi^T \mathbf{WY}$, which we write as

$$\Phi^T \mathbf{WY} = \begin{bmatrix} \Phi(n) & \cdots & \Phi(N) & \Phi(N+1) \end{bmatrix} \begin{bmatrix} a\gamma^{N+1-n} & & & \circ \\ & \ddots & & \\ & & a\gamma & \\ \circ & & & a \end{bmatrix} \begin{bmatrix} y(n) \\ \vdots \\ y(N) \\ y(N+1) \end{bmatrix}, \quad (12.67)$$

which can be expressed in two terms as

$$\Phi^T \mathbf{WY}(N+1) = \gamma\Phi^T \mathbf{WY}(N) + \Phi(N+1)ay(N+1). \quad (12.68)$$

If we now substitute the expression for $\mathbf{P}(N+1)$ from Eq. (12.66) and for $\Phi^T \mathbf{WY}(N+1)$ from Eq. (12.68) into Eq. (12.61), we find [letting $\mathbf{P}(N) = \mathbf{P}$, $\Phi(N+1) = \Phi$, and $y(N+1) = y$ for notational convenience]

$$\hat{\boldsymbol{\theta}}_{\text{WLS}}(N+1) = \left[\frac{\mathbf{P}}{\gamma} - \frac{\mathbf{P}}{\gamma} \Phi \left(\frac{1}{a} + \Phi^T \frac{\mathbf{P}}{\gamma} \Phi \right)^{-1} \Phi^T \frac{\mathbf{P}}{\gamma} \right] [\gamma\Phi^T \mathbf{WY}(N) + \Phi ay]. \quad (12.69)$$

When we multiply the factors in Eq. (12.69), we see that the term $\mathbf{P}\Phi^T \mathbf{WY}(N) = \hat{\boldsymbol{\theta}}_{\text{WLS}}(N)$, so that Eq. (12.69) reduces to

$$\begin{aligned} \hat{\boldsymbol{\theta}}_{\text{WLS}}(N+1) &= \hat{\boldsymbol{\theta}}_{\text{WLS}}(N) + \frac{\mathbf{P}}{\gamma} \Phi ay - \frac{\mathbf{P}}{\gamma} \Phi \left(\frac{1}{a} + \Phi^T \frac{\mathbf{P}}{\gamma} \Phi \right)^{-1} \Phi^T \hat{\boldsymbol{\theta}}_{\text{WLS}} \\ &\quad - \frac{\mathbf{P}}{\gamma} \Phi \left(\frac{1}{a} + \Phi^T \frac{\mathbf{P}}{\gamma} \Phi \right)^{-1} \Phi^T \frac{\mathbf{P}}{\gamma} \Phi ay. \end{aligned} \quad (12.70)$$

If we now insert the identity

$$\left(\frac{1}{a} + \Phi^T \frac{\mathbf{P}}{\gamma} \Phi \right)^{-1} \left(\frac{1}{a} + \Phi^T \frac{\mathbf{P}}{\gamma} \Phi \right)$$

between the Φ and the a in the second term on the right of Eq. (12.70), we can combine the two terms which multiply y to reduce Eq. (12.70) to

$$\hat{\boldsymbol{\theta}}_{\text{WLS}}(N+1) = \hat{\boldsymbol{\theta}}_{\text{WLS}}(N) + \mathbf{L}(N+1)(y(N+1) - \Phi^T \hat{\boldsymbol{\theta}}_{\text{WLS}}(N)), \quad (12.71)$$

where we have defined

$$\mathbf{L}(N+1) = \frac{\mathbf{P}}{\gamma} \Phi \left(\frac{1}{a} + \frac{\Phi^T \mathbf{P} \Phi}{\gamma} \right)^{-1}. \quad (12.72)$$

Equations (12.66), (12.71), and (12.72) can be combined into a set of steps that constitute an algorithm for computing $\hat{\boldsymbol{\theta}}$ recursively. To collect these, we proceed as follows:

1. Select a , γ , and N .
2. Comment: $a = \gamma = 1$ is ordinary least squares; $a = 1 - \gamma$ and $0 < \gamma < 1$ is exponentially weighted least squares.
3. Select initial values for $\mathbf{P}(N)$ and $\hat{\boldsymbol{\theta}}(N)$. *Comment:* See discussion below.
4. Collect $y(0), \dots, y(N)$ and $u(0), \dots, u(N)$ and form $\boldsymbol{\Phi}^T(N+1)$.
5. Let $k \leftarrow N$.
6. $\mathbf{L}(k+1) \leftarrow \frac{\mathbf{P}(k)}{\gamma} \boldsymbol{\Phi}(k+1) \left(\frac{1}{a} + \boldsymbol{\Phi}^T(k+1) \frac{\mathbf{P}(k)}{\gamma} \boldsymbol{\Phi}(k+1) \right)^{-1}$
7. Collect $y(k+1)$ and $u(k+1)$.
8. $\hat{\boldsymbol{\theta}}(k+1) \leftarrow \hat{\boldsymbol{\theta}}(k) + \mathbf{L}(k+1)(y(k+1) - \boldsymbol{\Phi}^T(k+1)\hat{\boldsymbol{\theta}}(k))$
9. $\mathbf{P}(k+1) \leftarrow \frac{1}{\gamma} [\mathbf{I} - \mathbf{L}(k+1)\boldsymbol{\Phi}^T(k+1)]\mathbf{P}(k)$
10. Form $\boldsymbol{\Phi}(k+2)$.
11. Let $k \leftarrow k+1$.
12. Go to Step 6.

Especially pleasing is the form of Step 8, the “update” formula for the next value of the estimate. We see that the term $\boldsymbol{\Phi}^T \hat{\boldsymbol{\theta}}(N)$ is the output to be expected at the time $N+1$ based on the previous data, $\boldsymbol{\Phi}(N+1)$, and the previous estimate, $\hat{\boldsymbol{\theta}}(N)$. Thus the next estimate of $\boldsymbol{\theta}$ is given by the old estimate corrected by a term linear in the error between the observed output, $y(N+1)$, and the predicted output, $\boldsymbol{\Phi}^T \hat{\boldsymbol{\theta}}(N)$. The gain of the correction, $\mathbf{L}(N+1)$, is given by Eq. (12.71) and Eq. (12.72). Note especially that in Eq. (12.71) no matrix inversion is required but only division by the scalar

$$\frac{1}{a} + \boldsymbol{\Phi}^T \frac{\mathbf{P}}{\gamma} \boldsymbol{\Phi}.$$

However, one should not take the implication that Eq. (12.71) is without numerical difficulties, but their study is beyond the scope of this text.

We still have the question of initial conditions to resolve. Two possibilities are commonly recommended:

1. Collect a batch of $N > 2n$ data values and solve the batch formula Eq. (12.61) once for $\mathbf{P}(N)$, $\mathbf{L}(N+1)$, and $\hat{\boldsymbol{\theta}}(N)$, and enter these values at Step 3.
2. Set $\hat{\boldsymbol{\theta}}(N) = \mathbf{0}$, $\mathbf{P}(N) = \alpha \mathbf{I}$, where α is a large scalar. The suggestion has been made that an estimate of a suitable α is [Soderstrom, Ljung, and Gustavsson (1974)]

$$\alpha = (10) \frac{1}{N+1} \sum_{i=0}^N y^2(i).$$

The steps in the table update the least-squares estimate of the parameters $\boldsymbol{\theta}$ when one more pair of data points u and y are taken. With only modest effort we can extend these formulas to include the case of vector or multivariable observations wherein the data $\mathbf{y}(k)$ are a vector of p simultaneous observations. We assume that parameters $\boldsymbol{\theta}$ have been defined such that the system can be described by

$$\mathbf{y}(k) = \boldsymbol{\Phi}^T(k)\boldsymbol{\theta} + \boldsymbol{\varepsilon}(k; \boldsymbol{\theta}). \quad (12.73)$$

One such set of parameters is defined by the multivariable ARMA model

$$\mathbf{y}(k) = - \sum_{i=1}^n a_i \mathbf{y}(k-i) + \sum_{i=1}^n \mathbf{B}_i \mathbf{u}(k-i), \quad (12.74)$$

where the a_i are scalars, the \mathbf{B}_i are $p \times m$ matrices, $\boldsymbol{\theta}$ is $(n + nmp) \times 1$, and the $\boldsymbol{\Phi}(k)$ are now $(n + nmp) \times p$ matrices. If we define $\boldsymbol{\Phi}$, \mathbf{Y} , and $\boldsymbol{\varepsilon}$ as in Eq. (12.51), the remainder of the batch formula development proceeds exactly as before, leading to Eq. (12.59) for the least-squares estimates and Eq. (12.61) for the weighted least-squares estimates with little more than a change in the definition of the elements in the equations. We need to modify Eq. (12.60) to $\mathcal{J} = \boldsymbol{\Sigma} \boldsymbol{\varepsilon}^T \mathbf{w} \boldsymbol{\varepsilon}$, reflecting the fact that $\boldsymbol{\varepsilon}(k)$ is now also a $p \times 1$ vector and the $\mathbf{w}(k)$ are $p \times p$ nonsingular matrices.

To compute the recursive estimate equations, we need to repeat Eq. (12.62) and the development following Eq. (12.62) with the new definitions. Only minor changes are required. For example, in Eq. (12.66) we must replace $1/a$ by \mathbf{a}^{-1} . The resulting equations are, in the format of Eq. (12.71)

$$\mathbf{L}(N+1) = \frac{\mathbf{P}}{\gamma} \boldsymbol{\Phi} \left(\mathbf{a}^{-1} + \boldsymbol{\Phi}^T \frac{\mathbf{P}}{\gamma} \boldsymbol{\phi} \right)^{-1}, \quad (a)$$

$$\mathbf{P}(N+1) = \frac{1}{\gamma} (\mathbf{I} - \mathbf{L}(N+1) \boldsymbol{\Phi}^T) \mathbf{P}, \quad (b)$$

$$\hat{\boldsymbol{\theta}}_{\text{WLS}}(N+1) = \hat{\boldsymbol{\theta}}_{\text{WLS}} + \mathbf{L}(N+1) [\mathbf{y}(N+1) - \boldsymbol{\Phi}^T \hat{\boldsymbol{\theta}}_{\text{WLS}}(N)]. \quad (c) \quad (12.75)$$

12.5 Stochastic Least Squares

Thus far we have presented the least-squares method with no comment about the possibility that the data might in fact be subject to random effects. Because such effects are very common and often are the best available vehicle for describing the differences between an ideal model and real-plant signal observations, it is essential that some account of such effects be included in our calculations. We will begin with an analysis of the most elementary of cases and add realism (and difficulties) as we go along. Appendix D provides a brief catalog of results we will need from probability, statistics, and stochastic processes.

As a start, we consider the case of a deterministic model with random errors in the data. We consider the equations that generate the data to be⁹

$$y(k) = \mathbf{a}^T \boldsymbol{\theta}^0 + v(k), \quad (12.76)$$

which, in matrix notation, becomes

$$\mathbf{Y} = \mathbf{A} \boldsymbol{\theta}^0 + \mathbf{V}. \quad (12.77)$$

The $v(k)$ in Eq. (12.76) are assumed to be random variables with zero mean (one can always subtract a known mean) and known covariance. In particular, we assume that the actual data are generated from Eq. (12.77) with $\boldsymbol{\theta} = \boldsymbol{\theta}^0$ and

$$\begin{aligned} \mathcal{E}v(k) &= 0, \\ \mathcal{E}v(k)v(j) &= \sigma^2 \delta_{kj} = \begin{cases} 0 & (k \neq j) \\ \sigma^2 & (k = j) \end{cases} \end{aligned} \quad (12.78)$$

or

$$\mathcal{E} \mathbf{V} \mathbf{V}^T = \sigma^2 \mathbf{I}.$$

As an example of the type considered here, suppose we have a physics experiment in which observations are made of the positions of a mass that moves without forces but with unknown initial position and velocity. We assume then that the motion will be a line, which may be written as

$$y(t) = a^0 + b^0 t + n(t). \quad (12.79)$$

If we take observations at times $t_0, t_1, t_2, \dots, t_N$, then

$$\mathbf{Y} = [y(t_0) \dots y(t_N)]^T, \quad \mathbf{A} = \begin{pmatrix} t_0 & t_1 & \dots & t_N \\ 1 & 1 & \dots & 1 \end{pmatrix}^T,$$

⁹There is no connection between the \mathbf{a} in (12.76) and the a used as part of the weights in Section 12.4.

the unknown parameters are

$$\boldsymbol{\theta} = [a \quad b]^T,$$

and the noise is

$$v(k) = n(t_k).$$

We assume that the observations are without systematic bias—that is, the noise has zero average value—and that we can estimate the noise “intensity,” or mean-square value, σ^2 . We assume zero error in the clock times, t_k , so \mathbf{A} is known.

The (stochastic) least-squares problem is to find $\hat{\boldsymbol{\theta}}$ which will minimize

$$\begin{aligned} \mathcal{J}(\boldsymbol{\theta}) &= (\mathbf{Y} - \mathbf{A}\boldsymbol{\theta})^T (\mathbf{Y} - \mathbf{A}\boldsymbol{\theta}) \\ &= \sum_{k=0}^N e^2(k; \boldsymbol{\theta}). \end{aligned} \quad (12.80)$$

Note that the errors, $e(k; \boldsymbol{\theta})$, depend both on the random noise and on the choice of $\boldsymbol{\theta}$, and $e(k; \boldsymbol{\theta}^0) = v(k)$. Now the solution will be a random variable because the data, \mathbf{Y} , on which it is based, is random. However, for specific actual data, Eq. (12.80) represents the same quadratic function of $\boldsymbol{\theta}$ we have seen before; and the same form of the solution results, save only the substitution of \mathbf{A} for Φ , namely

$$\hat{\boldsymbol{\theta}}_{LS} = (\mathbf{A}^T \mathbf{A})^{-1} \mathbf{A}^T \mathbf{Y}. \quad (12.81)$$

Now, however, we should not expect to find zero for the sum of the errors given by Eq. (12.80), even if we should determine $\hat{\boldsymbol{\theta}} = \boldsymbol{\theta}^0$ exactly (which of course we won't). Because of the random effects, then, we must generalize our concepts of what constitutes a “good” estimate. We will use three features of a stochastic estimate. The first of these is consistency.

An estimate $\hat{\boldsymbol{\theta}}$ of a parameter $\boldsymbol{\theta}^0$ is said to be *consistent* if, in the long run, the difference between $\hat{\boldsymbol{\theta}}$ and $\boldsymbol{\theta}^0$ becomes negligible. In statistics and probability, there are several formal ways by which one can define a negligible difference. For our purposes we will use the mean-square criterion, by which we measure the difference between $\hat{\boldsymbol{\theta}}$ and $\boldsymbol{\theta}^0$ by the sum of the squares of the parameter error, $\hat{\boldsymbol{\theta}} - \boldsymbol{\theta}^0$. We make explicit the dependence of $\hat{\boldsymbol{\theta}}$ on the length of the data by writing $\hat{\boldsymbol{\theta}}(N)$ and say that an estimate is consistent if¹⁰

$$\begin{aligned} \lim_{N \rightarrow \infty} \mathcal{E}(\hat{\boldsymbol{\theta}}(N) - \boldsymbol{\theta}^0)^T (\hat{\boldsymbol{\theta}}(N) - \boldsymbol{\theta}^0) &= 0, \\ \lim_{N \rightarrow \infty} \text{tr} \mathcal{E}(\hat{\boldsymbol{\theta}}(N) - \boldsymbol{\theta}^0)(\hat{\boldsymbol{\theta}}(N) - \boldsymbol{\theta}^0)^T &= 0. \end{aligned} \quad (12.82)$$

If Eq. (12.82) is true, we say that $\hat{\boldsymbol{\theta}}(N)$ converges to $\boldsymbol{\theta}^0$ in the mean-square sense as N approaches infinity. The expression in Eq. (12.82) can be made more explicit in the case of the least-squares estimate of Eq. (12.81). We have

$$\begin{aligned} \hat{\boldsymbol{\theta}}_{LS} - \boldsymbol{\theta}^0 &= (\mathbf{A}^T \mathbf{A})^{-1} \mathbf{A}^T (\mathbf{A}\boldsymbol{\theta}^0 + \mathbf{V}) - \boldsymbol{\theta}^0 \\ &= \boldsymbol{\theta}^0 + (\mathbf{A}^T \mathbf{A})^{-1} \mathbf{A}^T \mathbf{V} - \boldsymbol{\theta}^0 \\ &= (\mathbf{A}^T \mathbf{A})^{-1} \mathbf{A}^T \mathbf{V} \end{aligned}$$

and

$$\begin{aligned} \mathcal{E}(\hat{\boldsymbol{\theta}}_{LS} - \boldsymbol{\theta}^0)(\hat{\boldsymbol{\theta}}_{LS} - \boldsymbol{\theta}^0)^T &= \mathcal{E}\{(\mathbf{A}^T \mathbf{A})^{-1} \mathbf{A}^T \mathbf{V} \mathbf{V}^T \mathbf{A} (\mathbf{A}^T \mathbf{A})^{-1}\} \\ &= (\mathbf{A}^T \mathbf{A})^{-1} \mathbf{A}^T \mathcal{E} \mathbf{V} \mathbf{V}^T \mathbf{A} (\mathbf{A}^T \mathbf{A})^{-1} \\ &= \sigma^2 (\mathbf{A}^T \mathbf{A})^{-1}. \end{aligned} \quad (12.83)$$

In making the reductions shown in the development of Eq. (12.83) we have used the facts that \mathbf{A} is a known matrix (not random) and that $\mathcal{E} \mathbf{V} \mathbf{V}^T = \sigma^2 \mathbf{I}$. Continuing then with consideration of the least-squares estimate, we see that $\hat{\boldsymbol{\theta}}_{LS}$ is consistent if

$$\lim_{N \rightarrow \infty} \text{tr} \sigma^2 (\mathbf{A}^T \mathbf{A})^{-1} = 0. \quad (12.84)$$

¹⁰The trace (tr) of a matrix \mathbf{A} with elements a_{ij} is the sum of the diagonal elements, or trace $\mathbf{A} = \sum_{i=1}^n a_{ii}$.

As an example of consistency, we consider the most simple of problems, the observation of a constant. Perhaps we have the mass of the earlier problem, but with zero velocity. Thus

$$y(k) = a^0 + v(k), \quad k = 0, 1, \dots, N, \quad (12.85)$$

and

$$\mathbf{A} = [1 \quad 1 \dots 1]^T, \quad \boldsymbol{\theta}^0 = a^0, \\ \mathbf{A}^T \mathbf{A} = \sum_{k=0}^N 1 = N + 1, \quad \mathbf{A}^T \mathbf{Y} = \sum_{k=0}^N y(k);$$

then

$$\hat{\boldsymbol{\theta}}_{\text{LS}}(N) = (N + 1)^{-1} \sum_{k=0}^N y(k), \quad (12.86)$$

which is the sample average.

Now, if we apply Eq. (12.84), we find

$$\lim_{N \rightarrow \infty} \text{tr} \boldsymbol{\sigma}^2 (N + 1)^{-1} = \lim_{N \rightarrow \infty} \frac{\boldsymbol{\sigma}^2}{N + 1} = 0, \quad (12.87)$$

and we conclude that this estimate Eq. (12.86) is a *consistent* estimate of a^0 . If we keep taking observations according to Eq. (12.85) and calculating the sum according to Eq. (12.86), we will eventually have a value that differs from a^0 by a negligible amount in the mean-square sense.

The estimate given by Eq. (12.86) is a batch calculation. It can be informative to apply the recursive algorithm of Eq. (12.52) to this trivial case just to see how the equations will look. Suppose we agree to start the equations with one stage of “batch” on, say, two observations, $y(0)$ and $y(1)$. We thus have $a = \gamma = 1$, for least squares, and

$$\left. \begin{array}{l} P(1) = (A^T A)^{-1} = \frac{1}{2}, \\ \Phi(N) = 1, \\ \hat{\boldsymbol{\theta}}(1) = \frac{1}{2}(y(0) + y(1)), \\ \mathbf{W} = 1. \end{array} \right\} \text{initial conditions} \quad (12.88)$$

The iteration in P is given by (because $\Phi \equiv 1$)

$$P(N + 1) = P(N) - \frac{P(N)(1)(1)P(N)}{1 + (1)P(N)(1)} \\ = \frac{P(N)}{1 + P(N)}.$$

Thus the entire iteration is given by the initial conditions of Eq. (12.88) plus:

1. Let $N = 1$.

$$2. P(N + 1) = \frac{P(N)}{1 + P(N)}. \quad (12.89)$$

$$3. L(N + 1) = \frac{P(N)}{1 + P(N)}.$$

$$4. \hat{\boldsymbol{\theta}}(N + 1) = \hat{\boldsymbol{\theta}}(N) + L(N + 1)(y(N + 1) - \hat{\boldsymbol{\theta}}(N)).$$

5. Let N be replaced by $N + 1$.

6. Go to Step 2.

The reader can verify that in this simple case, $\mathbf{P}(N) = 1/(N+1)$, and Step 4 of the recursive equations gives the same (consistent) estimate as the batch formula Eq. (4.60). We also note that the matrix \mathbf{P} is proportional to the variance in the error of the parameter estimate as expressed in Eq. (12.83).

Although consistency is the first property one should expect of an estimate, it is, after all, an asymptotic property that describes a feature of $\hat{\boldsymbol{\theta}}$ as N grows without bound. A second property that can be evaluated is that of “bias.” If $\hat{\boldsymbol{\theta}}$ is an estimate of $\boldsymbol{\theta}^0$, the bias in the estimate is the difference between the mean value of $\hat{\boldsymbol{\theta}}$ and the true value, $\boldsymbol{\theta}^0$. We have

$$\mathcal{E}\hat{\boldsymbol{\theta}}(N) - \boldsymbol{\theta}^0 = \mathbf{b} \quad (12.90)$$

If $\mathbf{b} = \mathbf{0}$ for all N , the estimate is said to be *unbiased*. The least-squares estimate given by Eq. (12.59) is unbiased, which we can prove by direct calculation as follows. If we return to the development of the mean-square error in $\hat{\boldsymbol{\theta}}_{\text{LS}}$ given by Eq. (12.83) we find that

$$\hat{\boldsymbol{\theta}}_{\text{LS}} - \boldsymbol{\theta}^0 = (\mathbf{A}^T \mathbf{A})^{-1} \mathbf{A}^T \mathbf{V}, \quad (12.91)$$

and the bias is

$$\begin{aligned} \mathcal{E}\hat{\boldsymbol{\theta}}_{\text{LS}} - \boldsymbol{\theta}^0 &= \mathcal{E}(\mathbf{A}^T \mathbf{A})^{-1} \mathbf{A}^T \mathbf{V} \\ &= (\mathbf{A}^T \mathbf{A})^{-1} \mathbf{A}^T \mathcal{E}\mathbf{V} \\ &= \mathbf{0}. \end{aligned} \quad (12.92)$$

Actually, we would really like to have $\hat{\boldsymbol{\theta}}(N)$ be “close” to $\boldsymbol{\theta}^0$ for finite values of N and would, as a third property, like to treat the mean-square parameter error for finite numbers of samples. Unfortunately, it is difficult to obtain an estimate that has a minimum for the square of $\hat{\boldsymbol{\theta}} - \boldsymbol{\theta}^0$ without involving the value of $\boldsymbol{\theta}^0$ directly, which we do not know, else there is no point in estimating it. We can, however, find an estimate that is the best (in the sense of mean-square parameter error) estimate which is also linear in \mathbf{Y} and unbiased. The result is called a Best Linear Unbiased Estimate, or BLUE.

The development proceeds as follows. Because the estimate is to be a linear function of the data, we write¹¹

$$\hat{\boldsymbol{\theta}} = \mathbf{L} \cdot \mathbf{Y}. \quad (12.93)$$

Because the estimate is to be unbiased, we require

$$\mathcal{E}\hat{\boldsymbol{\theta}} = \boldsymbol{\theta}^0,$$

or

$$\mathcal{E}\mathbf{L}\mathbf{Y} = \mathcal{E}\mathbf{L}(\mathbf{A}\boldsymbol{\theta}^0 + \mathbf{V}) = \boldsymbol{\theta}^0.$$

Thus

$$\mathbf{L}\mathbf{A}\boldsymbol{\theta}^0 = \boldsymbol{\theta}^0,$$

or

$$\mathbf{L}\mathbf{A} = \mathbf{I}. \quad (12.94)$$

We wish to find \mathbf{L} so that an estimate of the form Eq. (12.93), subject to the constraint Eq. (12.94), makes the mean-square error

$$\mathcal{J}(\mathbf{L}) = \text{tr} \mathcal{E}(\hat{\boldsymbol{\theta}} - \boldsymbol{\theta}^0)(\hat{\boldsymbol{\theta}} - \boldsymbol{\theta}^0)^T \quad (12.95)$$

as small as possible. Using Eq. (12.93) in Eq. (12.95), we have

$$\mathcal{J}(\mathbf{L}) = \text{tr} \mathcal{E}\{(\mathbf{L}\mathbf{Y} - \boldsymbol{\theta}^0)(\mathbf{L}\mathbf{Y} - \boldsymbol{\theta}^0)^T\},$$

¹¹The matrix \mathbf{L} used here for a linear dependence has no connection to the gain matrix used in the recursive estimate equation (12.72).

and using Eq. (12.77) for \mathbf{Y}

$$\mathcal{J}(\mathbf{L}) = \text{tr} \mathcal{E}(\mathbf{L}\mathbf{A}\boldsymbol{\theta}^0 + \mathbf{L}\mathbf{V} - \boldsymbol{\theta}^0)(\mathbf{L}\mathbf{A}\boldsymbol{\theta}^0 + \mathbf{L}\mathbf{V} - \boldsymbol{\theta}^0)^T.$$

But from Eq. (12.94), this reduces to

$$\begin{aligned} \mathcal{J}(\mathbf{L}) &= \text{tr} \mathcal{E}(\mathbf{L}\mathbf{V})(\mathbf{L}\mathbf{V})^T \\ &= \text{tr} \mathbf{L}\mathbf{R}\mathbf{L}^T, \end{aligned} \quad (12.96)$$

where we take the covariance for the noise to be

$$\mathcal{E}\mathbf{V}\mathbf{V}^T = \mathbf{R}.$$

We now have the entirely deterministic problem of finding that \mathbf{L} subject to Eq. (12.94) which makes Eq. (12.96) as small as possible. We solve the problem in an indirect way: We first find \mathbf{L} when $\boldsymbol{\theta}^0$ is a scalar and there is no trace operation (\mathbf{L} is a single row). From this scalar solution we *conjecture* what the multiparameter solution might be and demonstrate that it is in fact correct. First, we consider the case when \mathbf{L} is a row. We must introduce the constraint Eq. (12.94), and we do this by a Lagrange multiplier as in calculus and are led to find \mathbf{L} such that

$$\mathcal{J}(\mathbf{L}) = \mathbf{L}\mathbf{R}\mathbf{L}^T + \lambda(\mathbf{A}^T\mathbf{L}^T - \mathbf{I}) \quad (12.97)$$

is a minimum. The λ are the Lagrange multipliers. The necessary conditions on the elements of \mathbf{L} are that $\partial\mathcal{J}/\partial\mathbf{L}^T$ be zero. (We use \mathbf{L}^T , which is a column, to retain notation that is consistent with our earlier discussion of vector-matrix derivatives.) We have

$$\left. \frac{\partial\mathcal{J}}{\partial\mathbf{L}^T} \right|_{\mathbf{L}=\hat{\mathbf{L}}} = 2\hat{\mathbf{L}}\mathbf{R} + \lambda\mathbf{A}^T = 0.$$

Thus the best value for \mathbf{L} is given by

$$\begin{aligned} 2\hat{\mathbf{L}}\mathbf{R} &= -\lambda\mathbf{A}^T, \\ \hat{\mathbf{L}} &= -\frac{1}{2}\lambda\mathbf{A}^T\mathbf{R}^{-1}. \end{aligned} \quad (12.98)$$

Because the constraint Eq. (12.94) must be satisfied, $\hat{\mathbf{L}}$ must be such that

$$\hat{\mathbf{L}}\mathbf{A} = \mathbf{I},$$

or

$$-\frac{1}{2}\lambda\mathbf{A}^T\mathbf{R}^{-1}\mathbf{A} = \mathbf{I}.$$

From this we conclude that

$$\lambda = -2(\mathbf{A}^T\mathbf{R}^{-1}\mathbf{A})^{-1}, \quad (12.99)$$

and substituting Eq. (12.99) back again in Eq. (12.98), we have, finally, that

$$\hat{\mathbf{L}} = (\mathbf{A}^T\mathbf{R}^{-1}\mathbf{A})^{-1}\mathbf{A}^T\mathbf{R}^{-1}, \quad (12.100)$$

and the BLUE is

$$\hat{\boldsymbol{\theta}}_B = \hat{\mathbf{L}}\mathbf{Y} = (\mathbf{A}^T\mathbf{R}^{-1}\mathbf{A})^{-1}\mathbf{A}^T\mathbf{R}^{-1}\mathbf{Y}. \quad (12.101)$$

best linear unbiased estimate (BLUE)

If we look at Eq. (12.61), we immediately see that this is exactly weighted least squares with $\mathbf{W} = \mathbf{R}^{-1}$. What we have done, in effect, is give a reasonable—best linear unbiased—criterion for selection of the weights. If, as we assumed earlier, $\mathbf{R} = \sigma^2\mathbf{I}$, then the ordinary least-squares estimate is also the BLUE.

But we have jumped ahead of ourselves; we have yet to show that Eq. (12.100) or Eq. (12.101) is true for a matrix \mathbf{L} . Suppose we have another linear unbiased estimate, $\bar{\boldsymbol{\theta}}$. We can write, without loss of generality

$$\bar{\boldsymbol{\theta}} = \mathbf{L}\mathbf{Y} = (\hat{\mathbf{L}} + \bar{\mathbf{L}})\mathbf{Y},$$

where $\hat{\mathbf{L}}$ is given by Eq. (12.100). Because $\bar{\boldsymbol{\theta}}$ is required to be unbiased, Eq. (12.94) requires that

$$\begin{aligned} \mathbf{L}\mathbf{A} = \mathbf{I}, \quad (\hat{\mathbf{L}} + \bar{\mathbf{L}})\mathbf{A} = \mathbf{I}, \quad \hat{\mathbf{L}}\mathbf{A} + \bar{\mathbf{L}}\mathbf{A} = \mathbf{I}, \\ \mathbf{I} + \bar{\mathbf{L}}\mathbf{A} = \mathbf{I}, \quad \bar{\mathbf{L}}\mathbf{A} = \bar{\mathbf{0}}. \end{aligned} \quad (12.102)$$

Now the mean-square error using $\bar{\boldsymbol{\theta}}$ is

$$\mathcal{J}(\bar{\boldsymbol{\theta}}) = \text{tr} \mathcal{E}(\bar{\boldsymbol{\theta}} - \boldsymbol{\theta}^0)(\bar{\boldsymbol{\theta}} - \boldsymbol{\theta}^0)^T,$$

which can be written as

$$\begin{aligned} \mathcal{J}(\bar{\boldsymbol{\theta}}) &= \text{tr} \mathcal{E}(\bar{\boldsymbol{\theta}} - \hat{\boldsymbol{\theta}} + \hat{\boldsymbol{\theta}} - \boldsymbol{\theta}^0)(\bar{\boldsymbol{\theta}} - \hat{\boldsymbol{\theta}} + \hat{\boldsymbol{\theta}} - \boldsymbol{\theta}^0)^T \\ &= \text{tr} \{ \mathcal{E}(\bar{\boldsymbol{\theta}} - \hat{\boldsymbol{\theta}})(\bar{\boldsymbol{\theta}} - \hat{\boldsymbol{\theta}})^T + 2\mathcal{E}(\bar{\boldsymbol{\theta}} - \hat{\boldsymbol{\theta}})(\hat{\boldsymbol{\theta}} - \boldsymbol{\theta}^0)^T + \mathcal{E}(\hat{\boldsymbol{\theta}} - \boldsymbol{\theta}^0)(\hat{\boldsymbol{\theta}} - \boldsymbol{\theta}^0)^T \}. \end{aligned} \quad (12.103)$$

We note that the trace of a sum is the sum of the traces of the components, and the trace of the last term is, by definition, $\mathcal{J}(\hat{\mathbf{L}})$. Let us consider the second term of Eq. (12.103), namely

$$\begin{aligned} \text{term2} &= \text{tr} \mathcal{E}(\bar{\boldsymbol{\theta}} - \hat{\boldsymbol{\theta}})(\hat{\boldsymbol{\theta}} - \boldsymbol{\theta}^0)^T = \text{tr} \mathcal{E}(\mathbf{L}\mathbf{Y} - \hat{\mathbf{L}}\mathbf{Y})(\hat{\mathbf{L}}\mathbf{Y} - \boldsymbol{\theta}^0)^T \\ &= \text{tr} \mathcal{E}(\hat{\mathbf{L}}\mathbf{Y} + \bar{\mathbf{L}}\mathbf{Y} - \hat{\mathbf{L}}\mathbf{Y})(\hat{\mathbf{L}}\mathbf{Y} - \boldsymbol{\theta}^0) \\ &= \text{tr} \mathcal{E}(\bar{\mathbf{L}}\mathbf{Y})(\hat{\mathbf{L}}\mathbf{Y} - \boldsymbol{\theta}^0) \\ &= \text{tr} \mathcal{E}(\bar{\mathbf{L}}(\mathbf{A}\boldsymbol{\theta}^0 + \mathbf{V}))(\hat{\mathbf{L}}(\mathbf{A}\boldsymbol{\theta}^0 + \mathbf{V}) - \boldsymbol{\theta}^0)^T. \end{aligned}$$

Now we use Eq. (12.102) to eliminate one term and Eq. (12.94) to eliminate another to the effect that

$$\begin{aligned} \text{term2} &= \text{tr} \mathcal{E}(\bar{\mathbf{L}}\mathbf{V})(\hat{\mathbf{L}}\mathbf{V})^T \\ &= \text{tr} \bar{\mathbf{L}}\mathbf{R}\hat{\mathbf{L}}^T, \end{aligned}$$

and using Eq. (12.100) for $\hat{\mathbf{L}}$, we have

$$\begin{aligned} \text{term2} &= \text{tr} \bar{\mathbf{L}}\mathbf{R}\{\mathbf{R}^{-1}\mathbf{A}(\mathbf{A}^T\mathbf{R}^{-1}\mathbf{A})^{-1}\} \\ &= \text{tr} \bar{\mathbf{L}}\mathbf{A}(\mathbf{A}^T\mathbf{R}^{-1}\mathbf{A})^{-1}, \end{aligned}$$

but now from Eq. (12.102) we see that the term is zero. Thus we reduce Eq. (12.103) to

$$\mathcal{J}(\bar{\boldsymbol{\theta}}) = \text{tr} \mathcal{E}(\bar{\boldsymbol{\theta}} - \hat{\boldsymbol{\theta}})(\bar{\boldsymbol{\theta}} - \hat{\boldsymbol{\theta}})^T + \mathcal{J}(\hat{\boldsymbol{\theta}}).$$

Because the first term on the right is the sum of expected values of squares, it is zero or positive. Thus $\mathcal{J}(\bar{\boldsymbol{\theta}}) \geq \mathcal{J}(\hat{\boldsymbol{\theta}})$, and we have proved that Eq. (12.101) is really and truly BLUE.

To conclude this section on stochastic least squares, we summarize our findings as follows. If the data are described by

$$\mathbf{Y} = \mathbf{A}\boldsymbol{\theta}^0 + \mathbf{V},$$

and

$$\mathcal{E}\mathbf{V} = 0, \quad \mathcal{E}\mathbf{V}\mathbf{V}^T = \mathbf{R},$$

then the least-squares estimate of $\boldsymbol{\theta}^0$ is given by

$$\hat{\boldsymbol{\theta}}_{LS} = (\mathbf{A}^T\mathbf{A})^{-1}\mathbf{A}^T\mathbf{Y}, \quad (12.104)$$

which is unbiased. If $\mathbf{R} = \sigma^2\mathbf{I}$, then the variance of $\hat{\boldsymbol{\theta}}_{LS}$, which is defined as $\mathcal{E}(\hat{\boldsymbol{\theta}}_{LS} - \boldsymbol{\theta}^0)(\hat{\boldsymbol{\theta}}_{LS} - \boldsymbol{\theta}^0)^T$, is

$$\text{var}(\hat{\boldsymbol{\theta}}_{LS}) = \sigma^2(\mathbf{A}^T\mathbf{A})^{-1}. \quad (12.105)$$

From this we showed that the least-squares estimation of a constant in noise is not only unbiased but also consistent.

Furthermore, if we insist that the estimate be both a linear function of the data and unbiased, we showed that the BLUE is a weighted least squares given by

$$\hat{\boldsymbol{\theta}}_B = (\mathbf{A}^T \mathbf{R}^{-1} \mathbf{A})^{-1} \mathbf{A}^T \mathbf{R}^{-1} \mathbf{Y}. \quad (12.106)$$

The variance of $\hat{\boldsymbol{\theta}}_B$ is

$$\begin{aligned} \text{var}(\hat{\boldsymbol{\theta}}_B) &= \mathcal{E}(\hat{\boldsymbol{\theta}}_B - \boldsymbol{\theta}^0)(\hat{\boldsymbol{\theta}}_B - \boldsymbol{\theta}^0)^T \\ &= (\mathbf{A}^T \mathbf{R}^{-1} \mathbf{A})^{-1}. \end{aligned} \quad (12.107)$$

Thus, if $\mathbf{R} = \sigma^2 \mathbf{I}$, then the least-squares estimate is also the BLUE.

As another comment on the BLUE, we note that in a recursive formulation we take, according to Eq. (12.63)

$$\mathbf{P} = (\mathbf{A}^T \mathbf{R}^{-1} \mathbf{A})^{-1},$$

and so the matrix \mathbf{P} is the variance of the estimate $\hat{\boldsymbol{\theta}}_B$. In the recursive equations given for vector measurements in Eq. (12.75), the weight matrix a becomes \mathbf{R}_v^{-1} , the inverse of the covariance of the single time measurement noise vector and, of course, $\gamma = 1$. Thus the BLUE version of Eq. (12.75) is

$$\mathbf{L}(N+1) = \mathbf{P}\boldsymbol{\Phi}(\mathbf{R}_v + \boldsymbol{\Phi}^T \mathbf{P}\boldsymbol{\Phi})^{-1}.$$

Thus far we have considered only the least-squares estimation where \mathbf{A} , the coefficient of the unknown parameter, is known. However, as we have seen earlier, in the true identification problem, the coefficient of $\boldsymbol{\theta}$ is $\boldsymbol{\Phi}$, the state of the plant model; and if random noise is present, the elements of $\boldsymbol{\Phi}$ will be random variables also. Analysis in this case is complex, and the best we will be able to do is to quote results on consistency and bias before turning to the method of maximum likelihood. We can, however, illustrate the major features and the major difficulty of least-squares identification by analysis of a very simple case. Suppose we consider a first-order model with no control. The equations are taken to be

$$\begin{aligned} y(k) &= a^0 y(k-1) + v(k) + cv(k-1), \\ \mathcal{E}v(k) &= 0, \\ \mathcal{E}v(k)v(j) &= \begin{cases} \sigma^2 & k = j \\ 0 & k \neq j. \end{cases} \end{aligned} \quad (12.108)$$

In general, we would not know either the constant c or the noise intensity σ^2 . We will estimate them later. For the moment, we wish to consider the effects of the noise on the least-squares estimation of the constant a^0 . Thus we take

$$\begin{aligned} \mathbf{Y} &= [y(1) \cdots y(N)]^T, \\ \boldsymbol{\Phi} &= [y(0) \cdots y(N-1)]^T, \\ \boldsymbol{\theta} &= a. \end{aligned}$$

Then we have the simple sums

$$\boldsymbol{\Phi}^T \boldsymbol{\Phi} = \sum_{k=1}^N y(k-1)y(k-1), \quad \boldsymbol{\Phi}^T \mathbf{Y} = \sum_{k=1}^N y(k-1)y(k),$$

and the normal equations tell us that $\hat{\boldsymbol{\theta}}$ must satisfy

$$\left[\sum_{k=1}^N y^2(k-1) \right] \hat{\boldsymbol{\theta}} = \sum_{k=1}^N y(k-1)y(k). \quad (12.109)$$

Now we must quote a result from statistics (see Appendix D). For signals such as $y(k)$ that are generated by white noise of zero mean having finite intensity passed through a stationary filter, we can define the autocorrelation function

$$R_y(j) = \mathcal{E}y(k)y(k+j) \quad (12.110)$$

and (in a suitable sense of convergence)

$$\lim_{N \rightarrow \infty} \frac{1}{N} \sum_{k=1}^N y(k)y(k+j) = R_y(j). \quad (12.111)$$

Thus, while the properties of $\hat{\theta}$ for finite N are difficult, we can say that the asymptotic least-squares estimate is given by the solution to

$$\lim_{N \rightarrow \infty} \left(\frac{1}{N} \sum_{k=1}^N y^2(k-1) \right) \hat{\theta} = \lim_{N \rightarrow \infty} \frac{1}{N} \sum_{k=1}^N y(k-1)y(k),$$

which is

$$\begin{aligned} R_y(0)\hat{\theta} &= R_y(1), \\ \hat{\theta} &= R_y(1)/R_y(0). \end{aligned} \quad (12.112)$$

If we now return to the model from which we assume $y(k)$ to be generated, values for $R_y(0)$ and $R_y(1)$ can be obtained. For example, if we multiply Eq. (12.108) by $y(k-1)$ and take the expected value, we find

$$\begin{aligned} \mathcal{E}y(k-1)y(k) &= \mathcal{E}a^0y(k-1)y(k-1) + \mathcal{E}v(k)y(k-1) \\ &\quad + c\mathcal{E}v(k-1)y(k-1), \\ R_y(1) &= a^0R_y(0) + c\mathcal{E}v(k-1)y(k-1). \end{aligned} \quad (12.113)$$

We set $\mathcal{E}v(k)y(k-1) = 0$ because $y(k-1)$ is generated by $v(j)$ occurring at or before time $k-1$ and y is independent of (uncorrelated with) the noise $v(j)$, which is in the future. However, we still need to compute $\mathcal{E}v(k-1)y(k-1)$. For this, we write Eq. (12.108) for $k-1$ as

$$y(k-1) = a^0y(k-2) + v(k-1) + cv(k-2)$$

and multiply by $v(k-1)$ and take expected values,

$$\begin{aligned} \mathcal{E}y(k-1)v(k-1) &= \mathcal{E}a^0y(k-2)v(k-1) + \mathcal{E}v^2(k-1) + c\mathcal{E}v(k-2)v(k-1) \\ &= \sigma^2. \end{aligned}$$

We have, then,

$$R_y(1) = a^0R_y(0) + c\sigma^2. \quad (12.114)$$

Now we can substitute these values into Eq. (12.112) to obtain

$$\begin{aligned} \hat{\theta}(\infty) &= \frac{R_y(1)}{R_y(0)} \\ &= a^0 + c \frac{\sigma^2}{R_y(0)}. \end{aligned} \quad (12.115)$$

If $c = 0$, then $\hat{\theta}(\infty) = a^0$, and we can say that the least-squares estimate is asymptotically unbiased. However, if $c \neq 0$, Eq. (12.115) shows that even in this simple case the least-squares estimate is asymptotically biased and cannot be consistent.¹² Primarily because of the bias introduced when the ARMA model has noise terms correlated from one equation to the next, as in Eq. (12.108) when $c \neq 0$, least squares is not a good scheme for constructing parameter estimates of dynamic models that include noise. Many alternatives have been studied, among the most successful being those based on maximum likelihood.

¹²Clearly, if the constant c is known we can subtract out the bias term, but such corrections are not very pleasing because the essential nature of noise is its unknown dependencies. In some instances it is possible to construct a term that asymptotically cancels the bias term as discussed in Mendel (1973).

12.6 Maximum Likelihood

The method of maximum likelihood requires that we introduce a probability density function for the random variables involved. Here we consider only the normal or Gaussian distribution; the method is not restricted to the form of the density function in any way, however. A scalar random variable x is said to have a normal distribution if it has a density function given by

$$f_x(\boldsymbol{\xi}) = \frac{1}{\sqrt{2\pi}\sigma} \exp\left[-\frac{1}{2} \frac{(\boldsymbol{\xi} - \boldsymbol{\mu})^2}{\sigma^2}\right]. \quad (12.116)$$

It can be readily verified, perhaps by use of a table of definite integrals, that

$$\begin{aligned} \int_{-\infty}^{\infty} f_x(\boldsymbol{\xi}) d\boldsymbol{\xi} &= 1, \\ \mathcal{E}x &= \int_{-\infty}^{\infty} \boldsymbol{\xi} f_x(\boldsymbol{\xi}) d\boldsymbol{\xi} = \boldsymbol{\mu}, \\ \mathcal{E}(x - \boldsymbol{\mu})^2 &= \int_{-\infty}^{\infty} (\boldsymbol{\xi} - \boldsymbol{\mu})^2 f_x(\boldsymbol{\xi}) d\boldsymbol{\xi} = \sigma^2. \end{aligned} \quad (12.117)$$

The number σ^2 is called the variance of x , written $\text{var}(x)$, and σ is the standard deviation. For the case of a vector-valued set of n random variables with a joint distribution that is normal, we find that if we define the mean vector $\boldsymbol{\mu}$ and the (nonsingular) covariance matrix \mathbf{R} as

$$\begin{aligned} \mathcal{E}\mathbf{x} &= \boldsymbol{\mu}, \\ \mathcal{E}(\mathbf{x} - \boldsymbol{\mu})(\mathbf{x} - \boldsymbol{\mu})^T &= \mathbf{R}, \end{aligned}$$

then

$$f_x(\boldsymbol{\xi}) = \frac{1}{[(2\pi)^n \det \mathbf{R}]^{1/2}} \exp\left[-\frac{1}{2} (\boldsymbol{\xi} - \boldsymbol{\mu})^T \mathbf{R}^{-1} (\boldsymbol{\xi} - \boldsymbol{\mu})\right]. \quad (12.118)$$

If the elements of the vector \mathbf{x} are mutually uncorrelated and have identical means $\boldsymbol{\mu}$ and variances σ^2 , then $\mathbf{R} = \sigma^2 \mathbf{I}$, $\det \mathbf{R} = (\sigma^2)^n$, and Eq. (12.118) can be written as

$$f_x(\boldsymbol{\xi}) = \frac{1}{(2\pi\sigma^2)^{n/2}} \exp\left[-\frac{1}{2\sigma^2} \sum_{i=1}^n (\xi_i - \boldsymbol{\mu})^2\right]. \quad (12.119)$$

Because the normal distribution is completely determined by the vector of means $\boldsymbol{\mu}$ and the covariance matrix \mathbf{R} , we often use the notation $\mathcal{N}(\boldsymbol{\mu}, \mathbf{R})$ to designate the density Eq. (12.118).

The maximum-likelihood estimate is calculated on the basis of an assumed structure for the probability density function of the available observations. Suppose, for example, that the data consist of a set of observations having a density given by Eq. (12.119), but having an *unknown* mean value. The parameter is therefore $\boldsymbol{\theta}^0 = \boldsymbol{\mu}$.

The function¹³

$$f_x(\boldsymbol{\xi} | \boldsymbol{\theta}) = (2\pi\sigma^2)^{-n/2} \exp\left[-\frac{1}{2} \sum_{i=1}^n \frac{(\xi_i - \boldsymbol{\theta})^2}{\sigma^2}\right] \quad (12.120)$$

can be presented as a function of $\boldsymbol{\theta}$, as giving the density of a set of x_i for any value of the population mean $\boldsymbol{\theta}$. Because the probability that a particular x_i is in the range $a \leq x_i \leq b$ is given by

$$\Pr\{a \leq x_i \leq b\} = \int_a^b f_{x_i}(\xi_i | \boldsymbol{\theta}) d\xi_i,$$

the density function is seen to be a measure of the “likelihood” for a particular value; when f is large in a neighborhood \mathbf{x}^0 , we would expect to find many samples from the population with values near \mathbf{x}^0 . As a function of the parameters, $\boldsymbol{\theta}$, the density function $f_x(\boldsymbol{\xi} | \boldsymbol{\theta})$ is called the *likelihood function*. If the actual data come from a population with the density $f_x(\boldsymbol{\xi} | \boldsymbol{\theta}^0)$, then one might expect the samples

¹³We read $f_x(\boldsymbol{\xi} | \boldsymbol{\theta})$ as “the probability density of $\boldsymbol{\xi}$ given $\boldsymbol{\theta}$.”

to reflect this fact and that a good estimate for $\boldsymbol{\theta}^0$ given the observations $\mathbf{x} = \{x_1, \dots, x_n\}^T$ would be $\boldsymbol{\theta} = \hat{\boldsymbol{\theta}}$, where $\hat{\boldsymbol{\theta}}$ is such that the likelihood function $f_x(\mathbf{x} | \boldsymbol{\theta})$ is as large as possible. Such an estimate is called the maximum-likelihood estimate, $\hat{\boldsymbol{\theta}}_{\text{ML}}$. Formally, $\hat{\boldsymbol{\theta}}_{\text{ML}}$ is such that

$$f_x(\mathbf{x} | \hat{\boldsymbol{\theta}}_{\text{ML}}) \geq f_x(\mathbf{x} | \boldsymbol{\theta}). \quad (12.121)$$

From Eq. (12.120) we can immediately compute $\hat{\boldsymbol{\theta}}_{\text{ML}}$ for the mean μ , by setting the derivative of $f_x(\mathbf{x} | \boldsymbol{\theta})$ with respect to $\boldsymbol{\theta}$ equal to zero. First, we note that

$$\frac{d}{d\boldsymbol{\theta}} \log f = \frac{1}{f} \frac{df}{d\boldsymbol{\theta}}, \quad (12.122)$$

so that the derivative of the log of f is zero when $df/d\boldsymbol{\theta}$ is zero.¹⁴ Because the (natural) log of the normal density is a simpler function than the density itself, we will often deal with the log of f . In fact, the negative of the log of f is used so much, we will call it the log-likelihood function and give it the functional designation

$$-\log f_x(\mathbf{x} | \boldsymbol{\theta}) = \ell(\mathbf{x} | \boldsymbol{\theta}).$$

Thus, from Eq. (12.120), for the scalar parameter μ , we have

$$\ell(\mathbf{x} | \boldsymbol{\theta}) = +\frac{n}{2} \log(2\pi\sigma^2) + \frac{1}{2} \sum_{i=1}^n \frac{(x_i - \boldsymbol{\theta})^2}{\sigma^2} \quad (12.123)$$

and

$$\begin{aligned} \frac{\partial \ell}{\partial \boldsymbol{\theta}} &= -\frac{1}{2\sigma^2} \sum_{i=1}^n 2(x_i - \boldsymbol{\theta}) \\ &= -\frac{1}{\sigma^2} \left\{ \sum_{i=1}^n x_i - n\boldsymbol{\theta} \right\}. \end{aligned} \quad (12.124)$$

If we now set $\partial \ell / \partial \boldsymbol{\theta} = 0$, we have

$$\sum_{i=1}^n x_i - n\hat{\boldsymbol{\theta}}_{\text{ML}} = 0$$

or

$$\hat{\boldsymbol{\theta}}_{\text{ML}} = \frac{1}{n} \sum_{i=1}^n x_i. \quad (12.125)$$

We thus find that for an unknown mean of a normal distribution, the maximum-likelihood estimate is the sample mean, which is also least squares, unbiased, consistent, and BLUE. We have studied this estimate before. However, we can go on to apply the principle of maximum likelihood to the problem of dynamic system identification.

Consider next the ARMA model with simple white-noise disturbances for which we write

$$\begin{aligned} y(k) &= -a_1 y(k-1) - \dots - a_n y(k-n) \\ &\quad + b_1 u(k-1) + \dots + b_n u(k-n) + v(k), \end{aligned} \quad (12.126)$$

and we assume that the distribution of $\mathbf{V} = [v(n) \dots v(N)]^T$ is $N(0, \sigma^2 \mathbf{I})$. Thus we are assuming that the $v(k)$ are each normally distributed with zero mean and variance σ^2 and furthermore that the covariance between $v(k)$ and $v(j)$ is zero for $k \neq j$. Suppose, now, that a sequence of the $y(k)$ are observed and that we wish to estimate from them the a_i, b_i , and σ^2 by the method of maximum likelihood. We require the probability-density function of the observed $y(k)$ for known values of the parameters. From a look at Eq. (12.126), it is apparent that if we assume that y, u, a_i , and b_i are all known, then we can compute $v(k)$ from these observed y and u and assumed (true) a_i and b_i , and the

¹⁴It is not possible for f to be zero in the neighborhood of its maximum.

distribution of y is immediately determined by the distribution of v . Using the earlier notation, we define

$$\begin{aligned}\mathbf{V}(N) &= [v(n) \dots v(N)]^T, \\ \mathbf{Y}(N) &= [y(n) \dots y(N)]^T, \\ \Phi(k) &= [-y(k-1) \dots -y(k-n)u(k-1) \dots u(k-n)]^T, \\ \Phi(N) &= [\Phi(n) \dots \Phi(N)]^T, \\ \boldsymbol{\theta}^0 &= [a_1 \dots a_n b_1 \dots b_n]^T.\end{aligned}\quad (12.127)$$

Then Eq. (12.126) implies, again for the true parameters, that

$$\mathbf{Y}(N) = \Phi \boldsymbol{\theta}^0 + \mathbf{V}(N). \quad (12.128)$$

Equation (12.128) is an expression of the input–output relation of our plant equations of motion. To obtain the probability-density function $f(\mathbf{Y} | \boldsymbol{\theta}^0)$ as required for the method of maximum likelihood, we need only be able to compute the $v(k)$ or in batch form, the $\mathbf{V}(N)$, from the $y(k)$ or $\mathbf{Y}(N)$ because we are given the probability density of \mathbf{V} . To compute \mathbf{V} from \mathbf{Y} requires the *inverse* model of our plant, which in this case is so trivial as to be almost missed;¹⁵ namely, we solve Eq. (12.128) for \mathbf{V} to obtain

$$\mathbf{V}(N) = \mathbf{Y}(N) - \Phi(N)\boldsymbol{\theta}^0. \quad (12.129)$$

Because we have assumed that the density function of \mathbf{V} is $\mathcal{N}(0, \sigma^2 \mathbf{I})$, we can write instantly

$$f(\mathbf{Y} | \boldsymbol{\theta}^0) = (2\pi\sigma^2)^{-m/2} \exp \left[-\frac{1}{2} \frac{(\mathbf{Y} - \Phi \boldsymbol{\theta}^0)^T (\mathbf{Y} - \Phi \boldsymbol{\theta}^0)}{\sigma^2} \right], \quad (12.130)$$

where $m = N - n + 1$, the number of samples in Y .

The likelihood function is by definition $f(\mathbf{Y} | \boldsymbol{\theta})$, which is to say, Eq. (12.130) with the $\boldsymbol{\theta}^0$ dropped and replaced by a general $\boldsymbol{\theta}$. As in the elementary example discussed above, we will consider the negative of the log of f as follows

$$\begin{aligned}\ell(\mathbf{Y} | \boldsymbol{\theta}) &= -\log (2\pi\sigma^2)^{-m/2} - \log \left\{ \exp \left[-\frac{1}{2} \frac{(\mathbf{Y} - \Phi \boldsymbol{\theta})^T (\mathbf{Y} - \Phi \boldsymbol{\theta})}{\sigma^2} \right] \right\} \\ &= +\frac{m}{2} \log 2\pi + \frac{m}{2} \log \sigma^2 + \frac{1}{2} \frac{(\mathbf{Y} - \Phi \boldsymbol{\theta})^T (\mathbf{Y} - \Phi \boldsymbol{\theta})}{\sigma^2}.\end{aligned}\quad (12.131)$$

Our estimates, $\hat{\boldsymbol{\theta}}_{\text{ML}}$ and $\hat{\sigma}_{\text{ML}}^2$, are those values of $\boldsymbol{\theta}$ and σ^2 which make $\ell(\mathbf{Y} | \boldsymbol{\theta})$ as small as possible. We find these estimates by setting to zero the partial derivatives of ℓ with respect to $\boldsymbol{\theta}$ and σ^2 . These derivatives are (following our earlier treatment of taking partial derivatives)

$$\begin{aligned}\frac{\partial \ell}{\partial \boldsymbol{\theta}} &= \frac{1}{\sigma^2} [\Phi^T \Phi \hat{\boldsymbol{\theta}}_{\text{ML}} - \Phi^T \mathbf{Y}] = \mathbf{0}, \quad (a) \\ \frac{\partial \ell}{\partial \sigma^2} &= \frac{m}{2\hat{\sigma}_{\text{ML}}^2} - \frac{\mathbf{Q}}{2\hat{\sigma}_{\text{ML}}^4} = 0, \quad (b)\end{aligned}\quad (12.132)$$

where the quadratic term \mathbf{Q} is defined as

$$\mathbf{Q} = (\mathbf{Y} - \Phi \hat{\boldsymbol{\theta}}_{\text{ML}})^T (\mathbf{Y} - \Phi \hat{\boldsymbol{\theta}}_{\text{ML}}). \quad (c)$$

We see immediately that Eq. (12.132) is the identical “normal” equation of the least-squares method so that $\hat{\boldsymbol{\theta}}_{\text{ML}} = \hat{\boldsymbol{\theta}}_{\text{LS}}$ in this case. We thus know that $\hat{\boldsymbol{\theta}}_{\text{ML}}$ is asymptotically unbiased and consistent.

¹⁵We deliberately formulated our problem so that this inverse would be trivial. If we add plant and independent sensor noise to a state-variable description, the inverse requires a Kalman filter. Because $v(k)$ is independent of all past u and y , for any $\boldsymbol{\theta}$, $e(k)$ is the prediction error.

The equations for $\hat{\sigma}_{\text{ML}}^2$ decouple from those for $\hat{\boldsymbol{\theta}}_{\text{ML}}$, and solving Eq. (12.132(b)), we obtain (again using earlier notation)

$$\begin{aligned}\hat{\sigma}_{\text{ML}}^2 &= \frac{\mathbf{Q}}{m} = \frac{1}{m}(\mathbf{Y} - \Phi\hat{\boldsymbol{\theta}})^T(\mathbf{Y} - \Phi\hat{\boldsymbol{\theta}}) \\ &= \frac{1}{N-n+1} \sum_{k=n}^N e^2(k; \hat{\boldsymbol{\theta}}_{\text{ML}}).\end{aligned}\quad (12.133)$$

Thus far we have no new solutions except the estimate for σ^2 given in Eq. (12.133), but we have shown that the method of maximum likelihood gives the same solution for $\hat{\boldsymbol{\theta}}$ as the least-squares method for the model of Eq. (12.126). Now let us consider the general model given by

$$y(k) = -\sum_{i=1}^n a_i y(k-i) + \sum_{i=1}^n b_i u(k-i) + \sum_{i=1}^n c_i v(k-i) + v(k); \quad (12.134)$$

the distribution of $\mathbf{V}(N) = [v(n) \dots v(N)]^T$ is again taken to be normal, and \mathbf{V} is distributed according to the $N(0, \sigma^2 \mathbf{I})$ density. The difference between Eq. (12.134) and Eq. (12.126), of course, is that in Eq. (12.134) we find past values of the noise $v(k)$ weighted by the c_i and, as we saw in Eq. (12.115), the least-squares estimate is biased if the c_i are nonzero.

Consider first the special case where of the c 's only c_1 is nonzero, and write the terms in Eq. (12.134) that depend on noise $v(k)$ on one side and define $z(k)$ as follows

$$\begin{aligned}v(k) + c_1 v(k-1) &= y(k) + \sum_{i=1}^n a_i y(k-i) - \sum_{i=1}^n b_i u(k-i) \\ &= z(k).\end{aligned}\quad (12.135)$$

Now let the reduced parameter vector be $\bar{\boldsymbol{\theta}} = [a_1 \dots a_n \quad b_1 \dots b_n]^T$, composed of the a and b parameters but not including the c_i . In a natural way, we can write

$$\mathbf{Z}(N) = \mathbf{Y}(N) - \Phi \bar{\boldsymbol{\theta}}^0. \quad (12.136)$$

However, because $z(k)$ is a sum of two random variables $v(k)$ and $v(k-1)$, each of which has a normal distribution, we know that \mathbf{Z} is also normally distributed. Furthermore, we can easily compute the mean and covariance of z

$$\begin{aligned}\mathcal{E}z(k) &= \mathcal{E}(v(k) + c_1 v(k-1)) = 0 \quad \text{for all } k, \\ \mathcal{E}z(k)z(j) &= \mathcal{E}(v(k) + c_1 v(k-1))(v(j) + c_1 v(j-1)) \\ &= \sigma^2(1 + c_1^2) \quad (k=j) \\ &= \sigma^2 c_1 \quad (k=j-1) \\ &= \sigma^2 c_1 \quad (k=j+1) \\ &= 0 \quad \text{elsewhere.}\end{aligned}$$

Thus the structure of the covariance of $\mathbf{Z}(N)$ is

$$\begin{aligned}\mathbf{R} &= \mathcal{E}\mathbf{Z}(N)\mathbf{Z}^T(N) \\ &= \begin{bmatrix} 1 + c_1^2 & c_1 & 0 & 0 & 0 \\ c_1 & 1 + c_1^2 & c_1 & 0 & 0 \\ 0 & c_1 & 1 + c_1^2 & \ddots & \vdots \\ 0 & 0 & \ddots & \ddots & c_1 \\ 0 & 0 & \cdots & c_1 & 1 + c_1^2 \end{bmatrix} \sigma^2,\end{aligned}\quad (12.137)$$

and, with the mean and covariance in hand, we can write the probability density of $\mathbf{Z}(N)$ as

$$g(\mathbf{Z}(N) | \boldsymbol{\theta}^0) = ((2\pi)^m \det \mathbf{R})^{-1/2} \exp\left(-\frac{1}{2} \mathbf{Z}^T \mathbf{R}^{-1} \mathbf{Z}\right), \quad (12.138)$$

where $m = N - n + 1$. But from (12.136) this is the likelihood function if we substitute for \mathbf{Z} and $\boldsymbol{\theta}$ as follows:

$$f(\mathbf{Y} | \boldsymbol{\theta}) = [(2\pi)^m \det \mathbf{R}]^{-1/2} \exp\left[-\frac{1}{2}(\mathbf{Y} - \Phi\bar{\boldsymbol{\theta}})^T \mathbf{R}^{-1}(\mathbf{Y} - \Phi\bar{\boldsymbol{\theta}})\right]. \quad (12.139)$$

The negative of the log of f is again similar in form to previous results

$$\ell(\mathbf{Y} | \boldsymbol{\theta}) = \frac{m}{2} \log 2\pi + \frac{1}{2} \log(\det \mathbf{R}) + \frac{1}{2}(\mathbf{Y} - \Phi\bar{\boldsymbol{\theta}})^T \mathbf{R}^{-1}(\mathbf{Y} - \Phi\bar{\boldsymbol{\theta}}). \quad (12.140)$$

The major point to be made about Eq. (12.140) is that the log likelihood function depends on the a 's and b 's through $\bar{\boldsymbol{\theta}}$ and is thus *quadratic* in these parameters, but it depends on the c 's (c_1 only in this special case) through both \mathbf{R} and $\det \mathbf{R}$, a dependence that is definitely not quadratic. An explicit formula for the maximum-likelihood estimate is thus not possible, and we must retreat to a numerical algorithm to compute $\hat{\boldsymbol{\theta}}_{ML}$ in this case.

12.7 Numerical Search for the Maximum-Likelihood Estimate

Being unable to give a closed-form expression for the maximum-likelihood estimate, we turn to an algorithm that can be used for the numerical search for $\hat{\boldsymbol{\theta}}_{ML}$. We first formulate the problem from the assumed ARMA model of Eq. (12.134), once again forming the inverse system as

$$v(k) = y(k) + \sum_{i=1}^n a_i v(k-i) - \sum_{i=1}^n b_i u(k-i) - \sum_{i=1}^n c_i v(k-i). \quad (12.141)$$

By assumption, $v(k)$ has a normal distribution with zero mean and unknown (scalar) variance R_v . As before, we define the successive outputs of this inverse as

$$\mathbf{V}(N) = [v(n) \quad v(n+1) \quad \cdots \quad v(N)]^T. \quad (12.142)$$

This multivariable random vector also has a normal distribution with zero mean and covariance

$$\begin{aligned} \mathbf{R} &= R_v \mathbf{I}_m \\ &= \mathcal{E} \mathbf{V} \mathbf{V}^T, \end{aligned} \quad (12.143)$$

where \mathbf{I}_m is the $m \times m$ identity matrix, and $m = N - n + 1$ is the number of elements in \mathbf{V} . Thus we can immediately write the density function as a function of the true parameters $\boldsymbol{\theta}^0 = [a_1 \ a_2 \ \dots \ a_n \ b_1 \ \dots \ b_n \ c_1 \ \dots \ c_n]^T$ as

$$f(\mathbf{V} | \boldsymbol{\theta}) = ((2\pi)^m R_v^m)^{-1/2} \exp\left[-\frac{1}{2} \sum_{k=n}^N \frac{v^2(k)}{R_v}\right]. \quad (12.144)$$

The (log) likelihood function is found by substituting arbitrary parameters, $\boldsymbol{\theta}$, in Eq. (12.144) and using $e(k)$ as the output of Eq. (12.141) when $\boldsymbol{\theta} \neq \boldsymbol{\theta}^0$, then taking the log which gives the result

$$\ell(\mathbf{E} | \boldsymbol{\theta}) = \frac{m}{2} \log 2\pi + \frac{m}{2} \log \hat{R}_v + \frac{1}{2\hat{R}_v} \sum_{k=n}^N e^2(k). \quad (12.145)$$

As with Eq. (12.134) we can compute the estimate of \hat{R}_v by calculation of

$$\partial \ell / \partial \hat{R}_v = 0,$$

which gives

$$\hat{R}_v = \frac{1}{N - n + 1} \sum_{k=n}^N e^2(k). \quad (12.146)$$

To compute the values for the a_i , b_i , and c_i , we need to construct a numerical algorithm that will be suitable for minimizing $\ell(\mathbf{E} | \boldsymbol{\theta})$. The study of such algorithms is extensive;¹⁶ we will be content

¹⁶See Luenberger (1973) for a lucid account of minimizing algorithms.

to present a frequently used one, based on a method of Newton. The essential concept is that given the K th estimate of $\hat{\boldsymbol{\theta}}$, we wish to find a $(K+1)$ st estimate that will make $\ell(\mathbf{E}|\hat{\boldsymbol{\theta}}(K+1))$ smaller than $\ell(\mathbf{E}|\hat{\boldsymbol{\theta}}(K))$. The method is to expand ℓ about $\hat{\boldsymbol{\theta}}(K)$ and choose $\hat{\boldsymbol{\theta}}(K+1)$ so that the quadratic terms—the first three terms in the expansion of ℓ —are minimized. Formally, we proceed as follows: Let $\hat{\boldsymbol{\theta}}(K+1) = \hat{\boldsymbol{\theta}}(K) + \delta\hat{\boldsymbol{\theta}}$. Then

$$\begin{aligned}\ell(\mathbf{E}|\hat{\boldsymbol{\theta}}(K+1)) &= \ell(\mathbf{E}|\hat{\boldsymbol{\theta}}(K) + \delta\hat{\boldsymbol{\theta}}) \\ &= c + \mathbf{g}^T \delta\hat{\boldsymbol{\theta}} + \frac{1}{2} \delta\hat{\boldsymbol{\theta}}^T \mathbf{Q} \delta\hat{\boldsymbol{\theta}} + \dots,\end{aligned}\quad (12.147)$$

where

$$c = \ell(\mathbf{E}|\hat{\boldsymbol{\theta}}(K)), \quad \mathbf{g}^T = \left. \frac{\partial \ell}{\partial \boldsymbol{\theta}} \right|_{\boldsymbol{\theta}=\hat{\boldsymbol{\theta}}(K)}, \quad \mathbf{Q} = \left. \frac{\partial^2 \ell}{\partial \boldsymbol{\theta} \partial \boldsymbol{\theta}} \right|_{\boldsymbol{\theta}=\hat{\boldsymbol{\theta}}(K)}.$$
 (12.148)

We must return later to the computation of \mathbf{g}^T and \mathbf{Q} , but let us first construct the algorithm. We would like to select $\delta\hat{\boldsymbol{\theta}}$ so that the quadratic approximation to ℓ is as small as possible. The analytic condition for ℓ to be a minimum is that $\partial\ell/\partial\delta\hat{\boldsymbol{\theta}} = 0$. We thus differentiate Eq. (12.147) and set the derivative to zero with the result (ignoring the higher-order terms in $\delta\hat{\boldsymbol{\theta}}$)

$$\begin{aligned}\frac{\partial \ell}{\partial \delta\hat{\boldsymbol{\theta}}} &= \mathbf{g}^T + \delta\hat{\boldsymbol{\theta}}^T \mathbf{Q} \\ &= 0.\end{aligned}\quad (12.149)$$

Solving Eq. (12.149) for $\delta\hat{\boldsymbol{\theta}}$ we find

$$\delta\hat{\boldsymbol{\theta}} = -\mathbf{Q}^{-1}\mathbf{g}.$$
 (12.150)

We now use the $\delta\hat{\boldsymbol{\theta}}$ found in Eq. (12.150) to compute $\hat{\boldsymbol{\theta}}(K+1)$ as

$$\hat{\boldsymbol{\theta}}(K+1) = \hat{\boldsymbol{\theta}}(K) - \mathbf{Q}^{-1}\mathbf{g}.$$

In terms of ℓ as given in Eq. (12.148), the algorithm can be written as

$$\hat{\boldsymbol{\theta}}(K+1) = \hat{\boldsymbol{\theta}}(K) - \left(\frac{\partial^2 \ell}{\partial \boldsymbol{\theta} \partial \boldsymbol{\theta}} \right)^{-1} \left(\frac{\partial \ell}{\partial \boldsymbol{\theta}} \right)^T.$$
 (12.151)

Our final task is to express the partial derivatives in Eq. (12.151) in terms of the observed signals y and u . To do this, we return to Eq. (12.145) and proceed formally, as follows, taking $\hat{\mathbf{R}}_v$ to be a constant because $\hat{\mathbf{R}}_v$ is given by Eq. (12.146)

$$\begin{aligned}\frac{\partial \ell(\mathbf{E}|\boldsymbol{\theta})}{\partial \boldsymbol{\theta}} &= \frac{\partial}{\partial \boldsymbol{\theta}} \left\{ \frac{m}{2} \log 2\pi + \frac{m}{2} \log \hat{\mathbf{R}}_v + \frac{1}{2\hat{\mathbf{R}}_v} \sum_{k=n}^N e^2(k) \right\} \\ &= \frac{1}{\hat{\mathbf{R}}_v} \sum_{k=n}^N e(k) \frac{\partial e(k)}{\partial \boldsymbol{\theta}},\end{aligned}\quad (12.152)$$

$$\begin{aligned}\frac{\partial^2 \ell}{\partial \boldsymbol{\theta} \partial \boldsymbol{\theta}} &= \frac{\partial}{\partial \boldsymbol{\theta}} \left(\frac{1}{\hat{\mathbf{R}}_v} \sum_{k=n}^N e(k) \frac{\partial e(k)}{\partial \boldsymbol{\theta}} \right) \\ &= \frac{1}{\hat{\mathbf{R}}_v} \sum_{k=n}^N \left(\frac{\partial e(k)}{\partial \boldsymbol{\theta}} \right)^T \frac{\partial e(k)}{\partial \boldsymbol{\theta}} + \frac{1}{\hat{\mathbf{R}}_v} \sum_{k=n}^N e(k) \frac{\partial^2 e(k)}{\partial \boldsymbol{\theta} \partial \boldsymbol{\theta}}.\end{aligned}\quad (12.153)$$

We note that Eq. (12.152) and the first term in Eq. (12.153) depend only on the derivative of e with respect to $\boldsymbol{\theta}$. Because our algorithm is expected to produce an improvement only in $\hat{\boldsymbol{\theta}}$, and because, near the minimum, we would expect the first derivative terms in Eq. (12.153) to dominate, we will simplify the algorithm to include only the first term in Eq. (12.153). Thus we need only compute

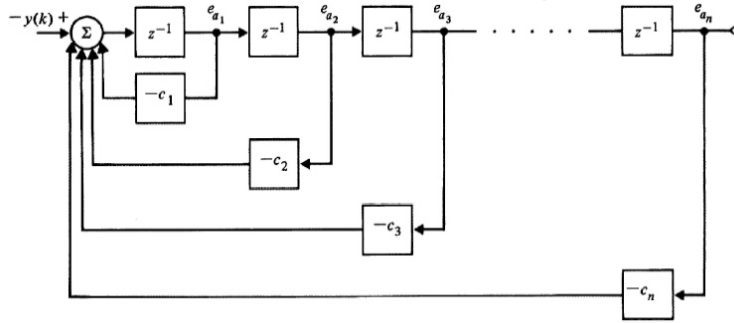


Figure 12.9
Block diagram of dynamic system whose states are the sensitivities of e with respect to a_i

$\partial e(k)/\partial \theta$. It is standard terminology to refer to these partial derivatives as the *sensitivities* of e with respect to θ .

We turn to the difference equations for $v(k)$ Eq. (12.139), substitute $e(k)$ for $v(k)$, and compute the sensitivities as follows:

$$\frac{\partial e(k)}{\partial a_i} = y(k-i) - \sum_{j=1}^n c_j \frac{\partial e(k-j)}{\partial a_i} \quad (a)$$

$$\frac{\partial e(k)}{\partial b_i} = -u(k-i) - \sum_{j=1}^n c_j \frac{\partial e(k-j)}{\partial b_i}, \quad (b)$$

$$\frac{\partial e(k)}{\partial c_i} = -e(k-i) - \sum_{j=1}^n c_j \frac{\partial e(k-j)}{\partial c_i}. \quad (c) \quad (12.154)$$

If we consider Eq. (12.154(a)) for the moment for fixed i , we see that this is a constant-coefficient difference equation in the variable $\partial e(k)/\partial a_i$ with $y(k-i)$ as a forcing function. If we take the z -transform of this system and call $\partial e/\partial a_i \triangleq e_a$, then we find

$$E_{a_i}(z) = z^{-i}Y(z) - \sum_{j=1}^n c_j z^{-j} E_{a_i}(z)$$

or

$$E_{a_i}(z) = \frac{z^{-i}}{1 + \sum_{j=1}^n c_j z^{-j}} Y(z).$$

Thus the derivative of e with respect to a_2 is simply z^{-1} times the partial derivative of e with respect to a_1 , and so on. In fact, we can realize all of these partial derivatives via the structure shown in Fig. 12.9.

In exactly analogous fashion, dynamic systems, whose states are the sensitivities of e with respect to b_i and c_i , can be constructed. With these then, we have all the elements of an explicit algorithm that can be used to compute improvements in θ . The steps can be summarized as follows:

1. Select an initial parameter estimate, $\hat{\theta}(0)$, based on analysis of the physical situation, the system step and frequency responses, cross-correlation of input and output, and/or least squares.
2. Construct (compute) $e(k)$ from Eq. (12.139) with e substituted for v ; compute the sensitivities from Eq. (12.154) using three structures as shown in Fig. 12.9; and simultaneously compute $\hat{R}_v \partial \ell / \partial \theta$ from Eq. (12.152) and the first term of $\hat{R}_v \partial^2 \ell / \partial \theta \partial \theta$ from Eq. (12.153).
3. Compute \hat{R}_v from Eq. (12.146) and solve for \mathbf{g} and \mathbf{Q} .
4. Compute $\hat{\theta}(K+1) = \hat{\theta}(K) - \mathbf{Q}^{-1} \mathbf{g}$.
5. If $[\hat{R}_v(k+1) - \hat{R}_v(K)] / \hat{R}_v(K) < 10^{-4}$, stop. Else go back to Step 2.

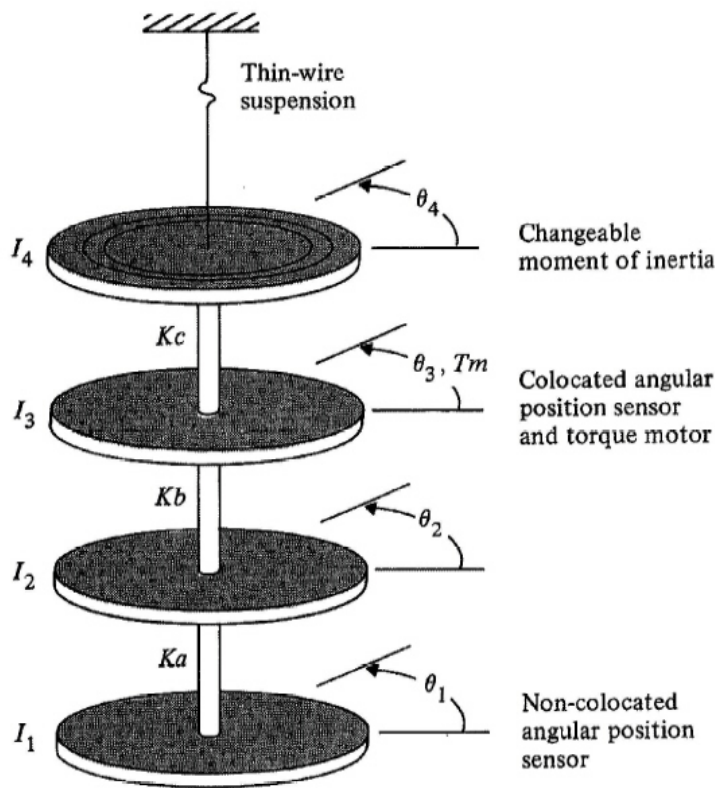


Figure 12.10
A four disk
system, from
Sidman (1986)

Note: Bearing assemblies around the torsion rod at each disk constrain motion to rotational modes.

In Step 5 of this algorithm it is suggested that when the sum of squares of the prediction errors, as given by \hat{R}_v , fails to be reduced by more than a relative amount of 10^{-4} , we should stop. This number, 10^{-4} , is suggested by a statistical test of the significance of the reduction. A discussion of such tests is beyond our scope here but can be found in Astrom and Eykhoff (1971), and Kendal and Stuart (1967). If the order of the system, n , is not known, this entire process can be done for $n = 1, 2, 3, \dots$, and a test similar to that of Step 5 can be used to decide when further increases in n are not significant.

Identification of the Four Disk System

Example 12.5

To illustrate parameter identification with a non-trivial example, we consider the four disk mechanical setup sketched in Fig 12.10 as studied by M. D. Sidman (1986). This is a representation of a physical system constructed in the Aeronautic Robotics Laboratory at Stanford University as part of a continuing study of the control of flexible mechanisms. In this case, the assembly has a torque motor coupled to disk 3 and angle sensors at disk 3 and at disk 1. The sensor at disk 3 is therefore collocated with the torque source and the sensor at disk 1 is non-collocated with the torque. All disks have the same inertia but, to permit parameter changes, provision is made to reduce the inertia of disk 4 by a factor of 0.5 or 0.25. Careful measurement of the transfer function by a one-frequency-at-a-time technique for each of the inertias of the disk was done and the magnitudes are plotted in Fig. 12.11. The problem is to estimate the transfer function by stochastic least squares.

Solution. If we write the $\theta_1(z)/U(z)$ transfer function as a ratio of two eight-degree polynomials, excite the system with a random signal, compute the least squares estimates of these parameters, and plot the resulting experimental frequency response, we obtain the curves shown in Fig. 12.12.

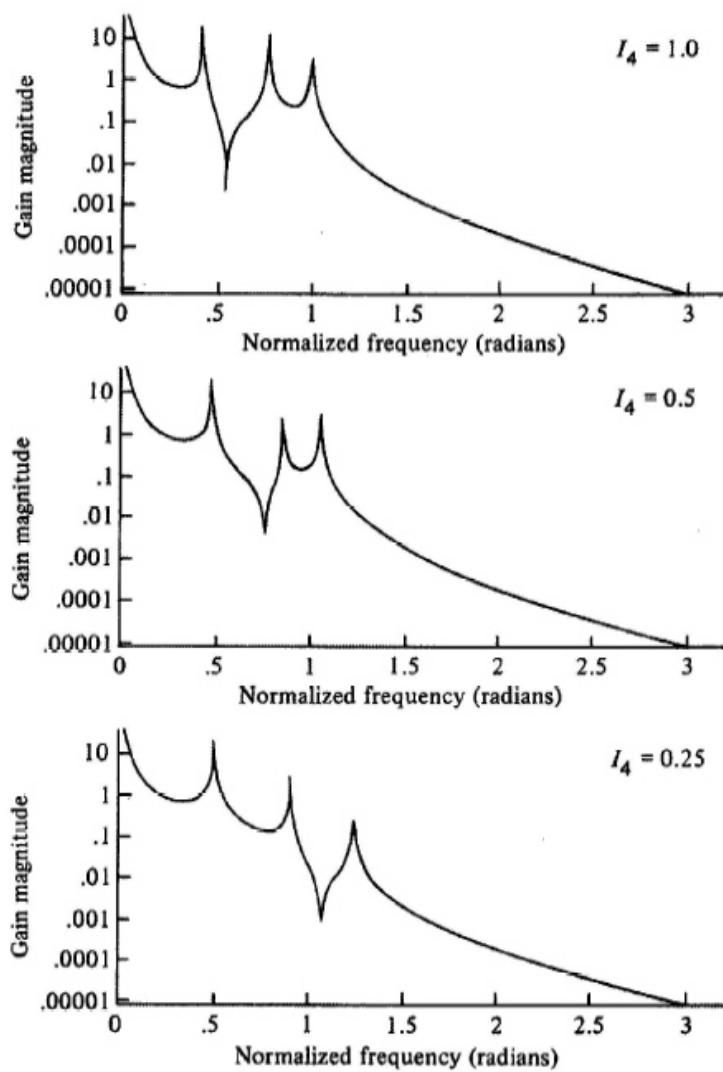


Figure 12.11
Frequency response for the four disk system measured with no noise and non-collocated signals, from Sidman (1986)

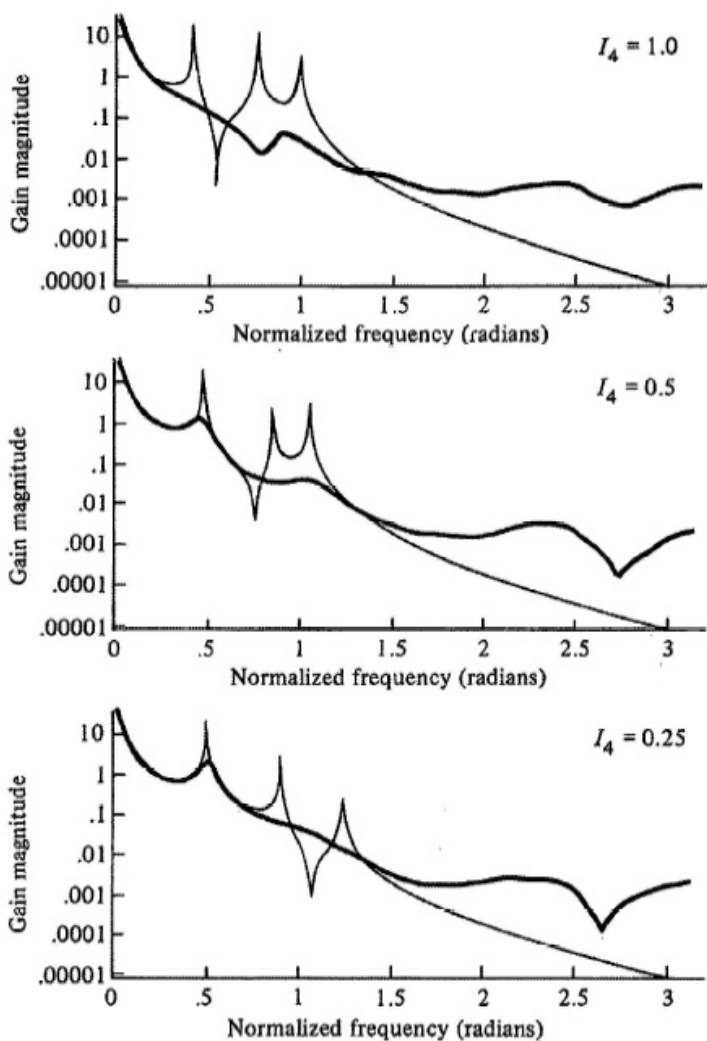


Figure 12.12
Frequency response of the four disk system found by least squares, from Sidman (1986)

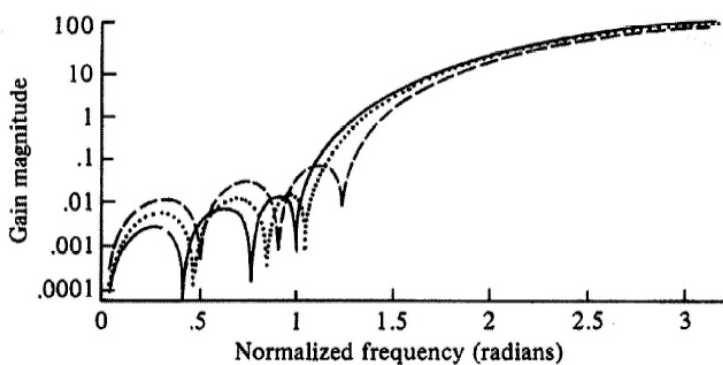


Figure 12.13
Frequency weighting caused by the system denominator, $a(z)$, from Sidman (1986)

The poor fit obtained by using least squares in the presence of very small data converter quantization noise, W_a , at the plant output is obvious in Fig. 12.12. Because the flexible modes are not successfully identified, the estimates are worthless for the purpose of designing a controller that actively dampens these modes. The poor performance of least squares in this situation is caused by the fact that the equation error is not white. It is colored by the characteristic polynomial of the plant, $a(z)$. Suppose we write the transfer function

$$Y(z) = \frac{b(z)}{a(z)}U(z) + W_a \quad (12.155)$$

Then the equation error is

$$a(z)Y(z) - b(z)U(z) = a(z)W_a. \quad (12.156)$$

Because $a(z)$ is typically large at high frequencies, and amplifies the noise, the parameter estimates will be greatly distorted by the least squares identification. This has the effect of corrupting the frequency response estimates as shown in Fig. 12.12. In the present case, a plot of the true $a(z)$ is shown in Fig. 12.13. If we filter the data with $a(z)$ as suggested by Eq. (12.156), we obtain the excellent results shown in Fig. 12.14. However, this polynomial is not known and cannot be used to reduce the high frequency distortion.

To reduce this effect, Sidman (1986) modified Clary's method and introduced the known parts and filtered the data with the structure shown in Fig. 12.15. The plant is divided into known and unknown parts, multiplied on both sides of Eq. (12.156) by the filter transfer function, F , and the new variables defined as

$$U_f(z) = U(z) \frac{b_k(z)}{a_k(z)} F(z), \quad (12.157)$$

$$Y_f(z) = Y(z) F(z). \quad (12.158)$$

Then the filtered least-squares formulation

$$a_u(z)[a_k(z)Y_f(z)] - b_u(z)[b_k(z)U_f(z)] = a_k(z)a_u(z)W_a \quad (12.159)$$

reduces to the modified formulation

$$a_u(z)Y_f(z) - b_u(z)U_f(z) = a_u(z)F(z)W_a \quad (12.160)$$

From these equations, one estimates the transfer function polynomials a_u and b_u of the unknown plant. However, as can be seen by comparing the right-hand sides of Eq. (12.159) and Eq. (12.160), this eliminates the coloration of the equation error due to the known a_k and introduces a filtering of the noise that can be used to reduce the weighting due to a_u in the estimates. In this example, a_k is a very significant cause of coloration at high frequencies since it includes the action of two roots at $z = 1$ corresponding to the plant's rigid body poles.

The bandpass filter $F(z)$ is selected to have a passband that brackets the region where the resonances are known to exist. This frequency constraint prefilter further reduces the effect of high and low frequency noise and disturbances including broadband quantization noise, DC bias in the sensor and actuator, low-frequency torque disturbances, as well as excited unmodeled dynamics above the frequency band of interest. The high pass portion of the bandpass filter may be chosen to have its zeros at $z = 1$. This leads to a stable, simple combined prefilter that lacks undesirable low frequency behavior. In this example, b_k consists of real zeros located on the negative real axis. The contribution to the system response due to the zeros of b_k is very insensitive to changes in the inertia or torsional stiffness in the plant. Thus, the identification need only estimate one complex zero pair and three complex pole pairs of the four disk system.

With the suggested pre-processing of the input and output data, the results of Fig. 12.16 are obtained. This model is quite suitable for use in control or in adaptive control schemes.

12.8 Subspace Identification Methods

The identification methods described thus far have been based on transfer function models. The nonparametric methods estimate the transfer function directly as a function of frequency and the parametric methods are based on representing the input-output relation as a rational function with unknown coefficients for the numerator and denominator polynomials. An alternative formulation of the identification problem is to express the input-state-output relationships in state space form with unknown description matrices Φ , Γ , \mathbf{H} , and J . In addition to these matrices, the (unknown) state

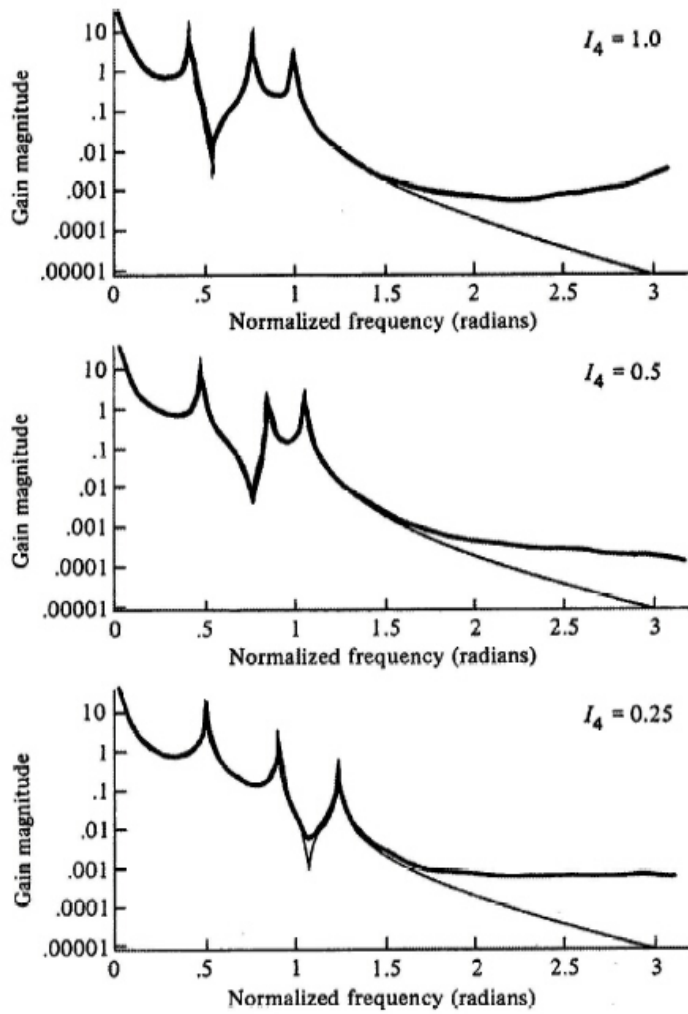


Figure 12.14
Frequency response using filtered least squares, from Sidman (1986)

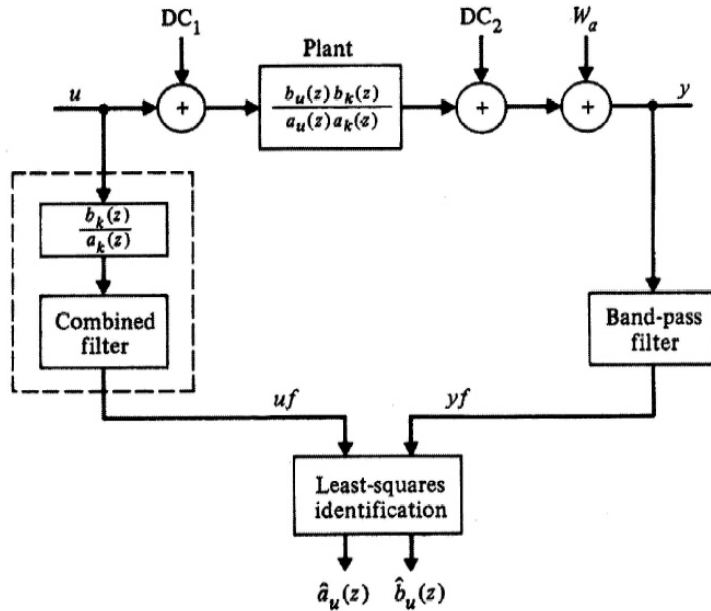


Figure 12.15
Structure of modified filtered least squares with frequency constraint prefiltering, from Sidman (1986)

sequence, $\mathbf{x}(k)$, is introduced as well. At first blush, it would seem that this structure greatly complicates the problem as there are many more parameters to be considered as compared to the transfer function model. The approach is to express the data in an *expanded* space guaranteed to contain the state description and to extract the *subspace* consistent with the state equations using reliable and robust methods of numerical linear algebra. The methods have been shown to have very desirable statistical properties and, perhaps most important, to be directly applicable to multivariable systems with vector inputs and outputs. The subspace-based methods have their origins in the early work toward finding a state realization from a deterministic impulse response as described in Ho (1966). A unification of the field has been given in Overshee (1995) where the method described here (based on Cho (1993)) is called a prediction method.

The method begins with a collection of input and output data $u(k)$ and $y(k)$ that we assume are scalars but could just as well be vectors for this method. To motivate the development of the algorithm, it is assumed that this data comes from a noise-free underlying state system given by equations of the form

$$\begin{aligned}\mathbf{x}(k+1) &= \Phi\mathbf{x}(k) + \Gamma u(k) \\ y(k) &= \mathbf{H}\mathbf{x}(k) + Ju(k)\end{aligned}\quad (12.161)$$

where the (unknown) dimension of the state is n . In order to express the constraints imposed on the input and output sequences by Eq. (12.161), a number, M , known to be larger than the state dimension but much smaller than the data length, is selected and the data are organized into the matrices \mathbf{Y} and

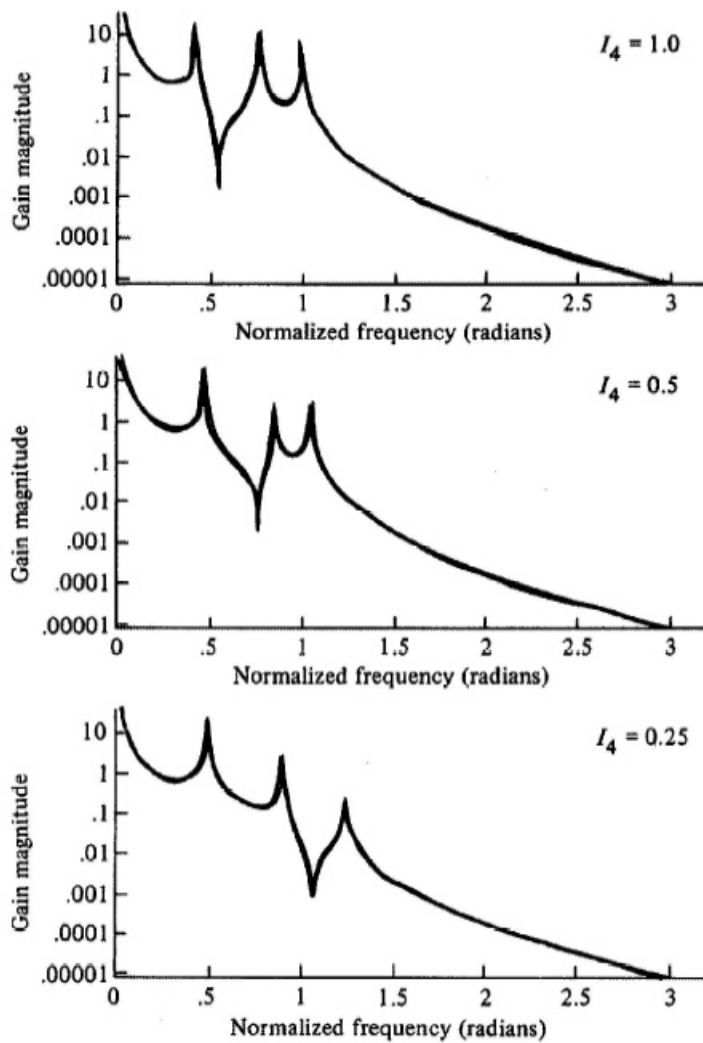


Figure 12.16
Frequency response of four disk system using least squares with low-pass filters and known factors, from Sidman (1986)

\mathbf{U} of size $M \times N$ as follows

$$\mathbf{Y} = \begin{bmatrix} y_0 & y_1 & \cdots & y_{N-1} \\ y_1 & y_2 & \cdots & y_N \\ \vdots & \vdots & \vdots & \vdots \\ y_{M-1} & y_M & \cdots & y_{N+M-2} \end{bmatrix}. \quad (12.162)$$

and

$$\mathbf{U} = \begin{bmatrix} u_0 & u_1 & \cdots & u_{N-1} \\ u_1 & u_2 & \cdots & u_N \\ \vdots & \vdots & \vdots & \vdots \\ u_{M-1} & u_M & \cdots & u_{N+M-2} \end{bmatrix}. \quad (12.163)$$

We assume that the input signals are “exciting” in the sense that $u(k)$ contains many frequencies and, in consequence, the matrix \mathbf{U} has full rank $= M$. To these data matrices we add the $n \times N$ matrix of states

$$\mathbf{X} = [\mathbf{x}_0 \quad \cdots \quad \mathbf{x}_{N-1}] \quad (12.164)$$

Finally, we define composite matrices made from the description matrices as

$$\mathcal{O}_x = \begin{bmatrix} \mathbf{H} \\ \mathbf{H}\Phi \\ \vdots \\ \mathbf{H}\Phi^{M-1} \end{bmatrix} \quad (12.165)$$

and

$$\mathcal{H} = \begin{bmatrix} J & 0 & 0 & 0 & 0 \\ \mathbf{H}\Gamma & J & 0 & 0 & 0 \\ \mathbf{H}\Phi\Gamma & \mathbf{H}\Gamma & J & 0 & 0 \\ \vdots & \cdots & \cdots & \ddots & \vdots \\ \mathbf{H}\Phi^{M-2}\Gamma & \mathbf{H}\Phi^{M-1}\Gamma & \cdots & \cdots & J \end{bmatrix}. \quad (12.166)$$

The $M \times n$ matrix \mathcal{O}_x is the observability matrix with n independent columns and the $M \times M$ matrix \mathcal{H} is an impulse response matrix. With these constructions of the data and definitions of matrices, the input-state-output relations can be compactly expressed as

$$\mathbf{Y} = \mathcal{O}_x \mathbf{X} + \mathcal{H} \mathbf{U}, \quad (12.167)$$

and the unknown model is contained in the matrices \mathcal{O}_x and \mathcal{H} .

The next step is to remove the term in \mathcal{H} by multiplying on the right by a matrix that is perpendicular to \mathbf{U} , which can be found by computing the **singular-value decomposition** (SVD) of \mathbf{U} partitioned as follows

$$\mathbf{U} = [\mathbf{P}_{u1} \quad \mathbf{P}_{u2}] [\boldsymbol{\Sigma}_u \quad \mathbf{0}] \begin{bmatrix} \mathbf{Q}_{u1}^T \\ \mathbf{Q}_{u2}^T \end{bmatrix} = \mathbf{P}_u \boldsymbol{\Sigma}_u \mathbf{Q}_{u1}^T. \quad (12.168)$$

It is a property of the SVD that the matrices \mathbf{P}_u and \mathbf{Q}_u are orthogonal matrices and consequently that the product $\mathbf{Q}_{u1}^T \mathbf{Q}_{u2} = \mathbf{0}$. Thus if we multiply Eq. (12.167) on the right by \mathbf{Q}_{u2} it is reduced to

$$\mathbf{Y} \mathbf{Q}_{u2} = \mathcal{O}_x \mathbf{X} \mathbf{Q}_{u2}. \quad (12.169)$$

The matrix on the right side of Eq. (12.169) is a combination of the columns of the observability matrix in the space of the state \mathbf{x} and has n independent columns. These can be identified by again taking an SVD, this time of $\mathbf{Y} \mathbf{Q}_{u2}$ by computing matrices \mathbf{P} , \mathbf{S} , and \mathbf{Q} so that

$$\mathbf{Y} \mathbf{Q}_{u2} = \mathbf{P} \mathbf{S} \mathbf{Q}^T = [\mathbf{P}_1 \quad \mathbf{P}_2] \begin{bmatrix} \boldsymbol{\Sigma} & \mathbf{0} \\ \mathbf{0} & \mathbf{0} \end{bmatrix} \begin{bmatrix} \mathbf{Q}_1^T \\ \mathbf{Q}_2^T \end{bmatrix}. \quad (12.170)$$

The number of independent columns in this product are the columns of \mathbf{P}_1 and equals the number of nonzero singular values in \mathbf{S} which is the size of $\mathbf{\Sigma}$ which is therefore by definition $n \times n$. Comparing this result with Eq. (12.169) means that we can take $\mathbf{P}_1 = \mathcal{O}_x$ from which we can solve for \mathbf{H} and Φ . If we wish to consider another state than \mathbf{x} via a transformation \mathbf{T} according to $\mathbf{x} = \mathbf{Tz}$ we would have $\mathcal{O}_z = \mathcal{O}_x \mathbf{T}$ and $\mathbf{P}_1 = \mathcal{O}_z \mathbf{T}^{-1}$.

With \mathcal{O}_x given by Eq. (12.164), the matrix \mathbf{H} is the first row.¹⁷ We next solve for Φ using the properties of \mathcal{O}_x given by Eq. (12.164). If we drop the last row of \mathcal{O}_x and call that reduced matrix $\overline{\mathcal{O}}_x$ and drop the first row and call that $\underline{\mathcal{O}}_x$ then it is clear that $\underline{\mathcal{O}}_x = \overline{\mathcal{O}}_x \Phi$ from which we can solve for

$$\Phi = [\overline{\mathcal{O}}_x]^\dagger \underline{\mathcal{O}}_x, \quad (12.171)$$

where $[\cdot]^\dagger$ represents the pseudo inverse and computes a least squares solution.¹⁸

Having \mathbf{H} and Φ , we now turn to computing $\mathbf{\Gamma}$ and J by operating on Eq. (12.167) to isolate \mathcal{H} . To do this we multiply Eq. (12.167) on the right by the pseudo inverse \mathbf{U}^\dagger (which is readily found from Eq. (12.168)) and on the left by \mathbf{P}_{u2}^T . Since by definition $\mathbf{U}\mathbf{U}^\dagger = \mathbf{I}$ and $\mathbf{P}_{u2}^T \mathcal{O}_x = \mathbf{P}_{u2}^T \mathbf{P}_{u1} = \mathbf{0}$, these operations reduce the equation to

$$\mathbf{P}_{u2}^T \mathbf{Y} \mathbf{U}^\dagger = \mathbf{P}_{u2}^T \mathcal{H}. \quad (12.172)$$

Because $\mathbf{\Gamma}$ and J appear on the right in \mathcal{H} in a linear fashion, we can solve for them by rearranging the terms in the equation. We partition the matrices in this equation consistent with \mathcal{H} and write it as

$$[K_1 \ K_2 \ \cdots \ K_M] = [p_1 \ p_2 \ \cdots \ p_M] \begin{bmatrix} J & 0 & \cdots & 0 \\ \mathbf{H}\mathbf{\Gamma} & J & \cdots & 0 \\ \vdots & \vdots & \ddots & \vdots \\ \mathbf{H}\Phi^{M-2}\mathbf{\Gamma} & \cdots & \mathbf{H}\mathbf{\Gamma} & J \end{bmatrix}. \quad (12.173)$$

To isolate the unknowns J and $\mathbf{\Gamma}$ these equations can be reorganized and written as

$$\begin{bmatrix} K_1 \\ K_2 \\ \vdots \\ K_M \end{bmatrix} = \begin{bmatrix} p_1 & p_2 & \cdots & p_M \\ p_2 & \cdots & p_M & 0 \\ \vdots & \cdots & 0 & \vdots \\ p_M & 0 & \cdots & 0 \end{bmatrix} \begin{bmatrix} 1 & 0 \\ 0 & \underline{\mathcal{O}}_x \end{bmatrix} \begin{bmatrix} J \\ \mathbf{\Gamma} \end{bmatrix}. \quad (12.174)$$

From this equation, one can solve for J and $\mathbf{\Gamma}$ by, for example, least squares again. This completes one variation of the prediction subspace identification algorithm. Clearly there are a substantial number of choices the engineer needs to make, including the selection of M and the selection of least squares or total least squares to solve Eq. (12.171) for Φ and Eq. (12.174) for $\mathbf{\Gamma}$ and J . Perhaps more important than these decisions is the choice of n from Eq. (12.170). As given, we have ignored the possibility of noise which is always present in any practical case. Thus in practice the dimension of $\mathbf{\Sigma}$ in Eq. (12.170) is not obvious but must be selected as that value such that the *significant* singular values are kept and the negligible singular values are dropped. How clearly this choice depends on the particular case and the other choices made in the algorithm and can be quite difficult. In important cases, models based on the prediction error method as well as one based on subspace methods are frequently computed and tested against new data and physical knowledge to guide final model selection.

12.9 Summary

In this chapter we have introduced some of the concepts of identification of dynamic systems for the purposes of control design. The main points were

¹⁷In the multivariable case, we'd take \mathbf{H} as the first n_i rows.

¹⁸Some authors suggest using total least squares rather than ordinary least squares, as both $\underline{\mathcal{O}}_x$ and $\overline{\mathcal{O}}_x$ are subject to noise and uncertainty in real cases.

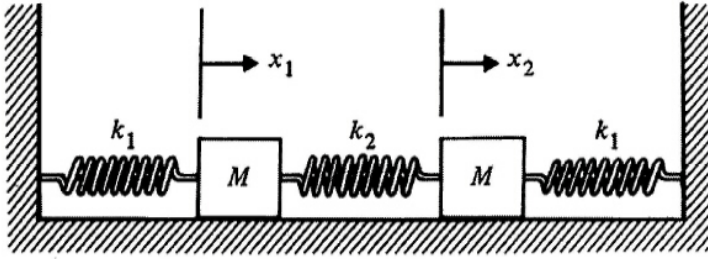


Figure 12.17
A mechanical system used in Problem 12.2

- Data to be used for identification should be filtered to reduce noise and to remove known components of the transfer function.
- A good frequency response model can be computed using sinusoidal inputs, one frequency at a time.
- A chirp signal input coupled with the FFT permits one to obtain a frequency response model in one pass.
- Either batch or recursive least squares gives a good model when the equation error is an independent white noise process.
- Prediction error methods based on the maximum likelihood are among the best general methods for identification.
- State subspace-based methods estimate state realizations directly and are especially effective for multi-input-multi-output systems.

12.10 Problems

12.1 Data from a mass moving in a plane (x, y) without force are given as

0	-0.426	1.501
1	0.884	1.777
2	2.414	2.530
3	2.964	3.441
4	3.550	3.762
5	5.270	4.328
6	5.625	4.016
7	7.188	5.368
8	8.129	5.736
9	9.225	6.499
10	10.388	6.233

Plot the points and use least squares to estimate the initial value of x , the initial value of y , and the velocity of the mass in x and in y . Draw the curve (line) that corresponds to your estimates.

12.2 A simple mechanical system without friction is sketched in Fig. 12.17.

(a) Show that this system is described by the equations

$$\begin{aligned} M\ddot{x}_1 + k_1x_1 + k_2(x_1 - x_2) &= 0, & x_1(0) &= x_{10}, \\ M\ddot{x}_2 + k_1x_2 + k_2(x_2 - x_1) &= 0, & x_2(0) &= x_{20}. \end{aligned}$$

- (b) We wish to estimate the parameters k_1, k_2 , and M from measurements of $x_1(t)$. However, note from (a) that if we divide by M in each equation the only identifiable parameters are $k_1/M = K_1$ and $k_2/M = K_2$. Give an intuitive argument to the effect that, if $x_{10} = x_{20}$ or if $x_{10} = -x_{20}$, it is impossible to estimate both K_1 and K_2 from $x_1(t)$. (*Hint*: Rewrite the equations using $y = x_1 - x_2$ and $z = x_1 + x_2$ as the position variables.) Show that if $x_{10} = 1$ and $x_{20} = 0$, it should be possible to estimate both K_1 and K_2 from $x_1(t)$. What do you conclude makes a “good” initial condition?
- (c) Compute a discrete equivalent system for sampling at 0.5 sec with an input that can set an initial condition on x_1 . Select $K_1 = 0.4$ and $K_2 = 0.6$. Compute the transform of X_1 if $x_{10} = 1$

$$X_1(z) = \frac{b_0z^4 + b_1z^3 + b_2z^2 + b_3z + b_4}{z^4 + a_1z^3 + a_2z^2 + a_3z + a_4},$$

where the parameters a_i are functions of K_1, K_2 , and sampling period T .

- (d) Formulate the least-squares problem to estimate the a_i from noisy measurements of $x_1(kT)$. Set up the problem so that it is possible to ignore the b_i .
- (e) Simulate the equations of part (a) for $K_1 = 0.4$ and $K_2 = 0.6$, sample x_1 at a rate of 0.5 sec for 30 samples, and compute $\hat{\boldsymbol{\theta}} = [\hat{a}_1 \ \hat{a}_2 \ \hat{a}_3 \ \hat{a}_4]^T$. Assume all the noise comes from an A/D converter operating at 10 bits including sign. If the simulation is done on a digital computer, add the appropriate noise according to the noise model of quantization discussed in Chapter 10. Compute the predicted variance in the estimate of $\hat{\boldsymbol{\theta}}$.
- (f) Deliberately add additional noise of known variance to your data, recompute $\hat{\boldsymbol{\theta}}$ 50 times from different runs of noisy data, and compare the sample variance of $\hat{\boldsymbol{\theta}}$ to the theoretical value based on P .
- (g) Keep the number of samples fixed at 30 but vary the sample rate from 0.1 sec to 1 sec in 0.1 steps and compute

$$\frac{1}{4} \sum_{k=1}^4 \left| \frac{\hat{\boldsymbol{\theta}}_k - \boldsymbol{\theta}_k^0}{\boldsymbol{\theta}_k^0} \right|$$

for each sample period as a measure of total estimate accuracy. What do you conclude respecting selection of sample period for identification?

- (h) Keep the sample period fixed at 0.5 sec, but compute the estimate for varying numbers of samples. Consider at least 5, 10, 30, 100, and 300 samples. Compare the same criterion used in part (g) and give an explanation of the results.

12.3 Program the recursive least-squares algorithm of Eq. (12.73) for no weighting. Use the algorithm to estimate the parameters of the system of Problem 12.2(h). Use $\hat{\boldsymbol{\theta}}(5) = \mathbf{0}$ and $P(5) = \mathbf{I}$ for your initial conditions. If available, use the Identification Toolbox to repeat the exercise.

12.4 Give the transfer function $H(z)$ of the filter that corresponds to exponentially weighted least squares as a function of a and γ . Prove that $H(1) = 1$ if $a = 1 - \gamma$.

12.5 In Eq. (12.84) we showed that the variance in the least-squares estimate is $(A^T A)^{-1} A^T R A (A^T A)^{-1}$ and, in Eq. (12.108), we showed that the variance of the BLUE is $(A^T R^{-1} A)^{-1}$. Use the development of the proof of the BLUE following Eq. (12.103) to devise an expression for the excess variance of least squares over BLUE.

12.6 (Contributed by N. Gupta.) Show that the least-squares estimate $\hat{\boldsymbol{\theta}} = (\mathbf{A}^T \mathbf{A})^{-1} \mathbf{A}^T \mathbf{Y}$ results in the error squared $\mathcal{E}(\mathbf{Y} - \mathbf{A}\hat{\boldsymbol{\theta}})^T (\mathbf{Y} - \mathbf{A}\hat{\boldsymbol{\theta}}) = (m - n)\sigma^2$, where $\mathcal{E}e^2 = \sigma^2$, \mathbf{Y} has m components, and $\hat{\boldsymbol{\theta}}$ has n components. What estimate of σ^2 does this result suggest? *Hint*: If $\mathbf{M} = \mathbf{I} - \mathbf{A}(\mathbf{A}^T \mathbf{A})^{-1} \mathbf{A}^T$, then $\mathbf{M}^2 = \mathbf{M} = \mathbf{M}^T$.

12.7 In Eq. (12.134) we showed that the maximum likelihood estimate of σ^2 is

$$(Y - A\hat{\boldsymbol{\theta}})^T (Y - A\hat{\boldsymbol{\theta}}) / m.$$

Show that this estimate is biased.

12.8 Write a computer program to implement the search for the maximum likelihood estimate following the method of Section 12.8.

12.9 Simulate the system [described in Astrom and Eykhoff (1971)]

- (a) $y_{k+1} = -a_1 y_k + b_1 u_k + v_{k+1} + c_1 v_k$, where u_k and v_k are independent sequences of unit variances and $a_1 = -0.5$, $b_1 = 1.0$, $c_1 = 0.1$.
- (b) Compute the least-squares estimate of a_1 and b_1 from observation of 5, 50, and 500 samples. Compare variance and bias to the theory in each case.
- (c) Compute the maximum-likelihood estimates of a_1, b_1, c_1 , and σ_v^2 from 5, 50, and 500 samples, and compare the estimates to the known true values.

12.10 Suppose we wish to identify a plant that is operating in a closed loop as

$$\begin{aligned} y_{k+1} &= ay_k + bu_k + e_k, \\ u_k &= -Ky_k, \end{aligned}$$

where e_k is white noise. Show that we cannot identify a and b from observation of y and u , even if K is known.

Chapter 13

Nonlinear Control

Perspective on Nonlinear Control

Every physical system is nonlinear for large signals, and many systems have important nonlinearities such as friction that cannot be ignored even for small signals. Furthermore, optimal control of many systems requires a nonlinear controller. Because the variety of nonlinear systems is so vast, it is only possible here to give an introduction to the most important issues and concepts.¹ The first concern is stability, and the most important stability theory is that of Lyapunov. It is this theory that justifies the enormous attention paid to the linear case by providing the proof that, for most nonlinear systems, stability of the small signal linear approximation implies a region of stability of the nonlinear system. Beyond this result, Lyapunov theory gives us a tool that can be used to determine further regions of stability and also can guide the design of purposely nonlinear controllers in a process called Lyapunov redesign. Unfortunately, application of Lyapunov theory is often difficult and can be very frustrating. Alternative approaches, including computer simulation, heuristic methods such as the describing function, and the frequency-response-based circle criterion are also important techniques.

Design of controls for nonlinear systems may be placed in several categories. The most primitive method is to obtain a linear approximation, design a linear controller, and use computer simulation and perhaps a stability theory such as Lyapunov's to explore nonlinear behavior. In an approach known as **Lyapunov redesign** the engineer constructs a tentative Lyapunov function and deliberately designs the controller to force the system to realize the function which automatically provides a proof that the system is stable. Another widely used approach is to use feedback to reduce the equations to a linear form and continue as in the first case. This method is known in the field of robotics as the method of **computed torque**. A combination of Lyapunov redesign and computed torque that extends both has recently been developed as **backstepping**. Another approach to nonlinear design is to apply the concepts of optimal control to obtain a controller that minimizes a performance measure. A well-known case is that of minimal time control of a linear system subject to bounded controls. A practical approximation to minimal time control has been developed as **proximate time optimal systems (PTOS)**. Finally, a widely used concept is that of **adaptive control**. The fundamental idea of adaptive control is that the controller is redesigned on-line to maintain good performance in the face of a changing environment that includes major changes in the plant dynamics. Sub-categories of adaptive control are **gain scheduling**, the **model-reference adaptive control (MRAC)**, and the **self-tuning regulator (STR)**.

Chapter Overview

In this chapter, we first consider computer simulation and the heuristic analysis methods of equivalent gain and the describing function. For stability, the main analysis technique presented is the second method of Lyapunov, but also discussed are the circle criterion and the small gain theorem. An

¹In this text we assume that the model equations have unique solutions and do not exhibit the astonishing behavior of Chaos (Gleick, 1987).

important design technique uses linear design methods based on a linear approximation to the plant model. As we will see, this approach is known as Lyapunov's first method. In Section 13.2 we consider two approaches to design by nonlinear feedback. The first is the proximate time optimal system (PTOS) design for linear systems having only saturation of the actuator as the nonlinearity, and the second is the self-tuning regulator approach to adaptive control. PTOS control is especially appropriate for motion control and adaptive control is widely used in chemical process control. In the last section of the chapter, several important approaches to computer-aided design of nonlinear systems are introduced.

13.1 Analysis Techniques

Final design of a controller contains two phases: performance analysis and design improvement. The **performance analysis** phase includes examination of a particular fixed structure to determine such properties as stability, signal sizes, and dynamic response to see if the performance specifications are met. The techniques available for analysis of nonlinear systems include computer simulation, study of a linear approximation, describing functions, equivalent gains, the circle theorem, and Lyapunov's second method. The **design improvement** phase consists of finding a structure and parameter set which achieve an improved trade-off among the goals and the constraints that define a satisfactory system. Approaches to obtaining design improvements will be covered in Section 13.2.

13.1.1 Simulation

Simulation is the process of constructing a mathematical model of a proposed or actual system and using a numerical solution of the model equations to estimate the behavior of the system. In control engineering, the models are most often a collection of integro-differential equations, the solution to which represents the response of the system to specific environmental conditions and inputs. Computer models vary in complexity from a few first-order differential equations to systems with thousands of state variables such as a model of the space shuttle. Increasingly, control models of sophisticated systems are hybrids of differential equations interacting with dynamic digital logic. For such systems simulation is essential to study the possible responses.

Simulation is one of the most valuable assets to the field of control engineering and is the only general method of analysis able to find solutions to arbitrary nonlinear differential and difference equations. Of course simulation finds only *particular* solutions, that is, solutions to the equations with specific inputs, initial conditions, and parameters. It is for that reason that simulation does not supplant other forms of analysis. Important properties such as stability or conditional stability cannot be *proven* with simulations. In the case of a nonlinear system, even if we have no proof or guarantee of stability, simulation can give us confidence that under the operating conditions expected the system is almost surely stable. Although a proof of stability is always desirable, sometimes we must rely on extensive simulation alone to decide that the complete system is satisfactory.

Many general purpose computer simulation tools have been developed in the last 50 years. Electronic analog computers based on operational amplifiers were used in the 1940s and 1950s. These were followed by combined digital-analog machines and then by completely digital simulations starting in the 1960s. More recently, software packages have been developed with user-friendly interfaces that have greatly enhanced the effectiveness of digital simulation. Although completely digital simulation is the most common technique used today, there are still some applications for digital-analog simulations, especially when one wishes to test a physical component imbedded in an otherwise computer simulation. Given the description of a system by differential equations such as Eq. (13.1), along with the initial conditions $\mathbf{x}(t_0)$ and the external inputs to the system $\mathbf{u}(t)$, a simulation program will find the time histories of all the system variables

$$\dot{\mathbf{x}}(t) = f(\mathbf{x}, \mathbf{u}, t). \quad (13.1)$$

A simple example will demonstrate the value of simulation.

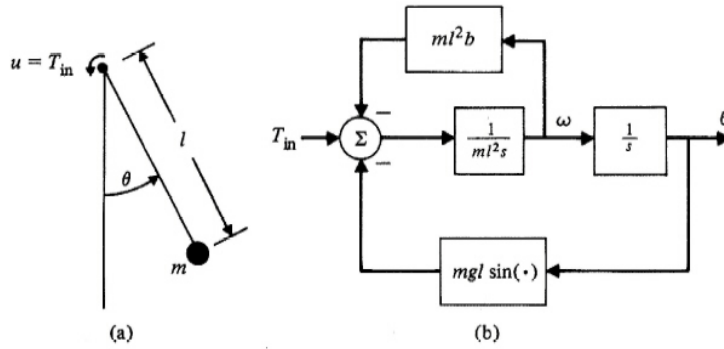


Figure 13.1
A simple pendulum
(a) schematic
(b) block diagram of pendulum dynamics

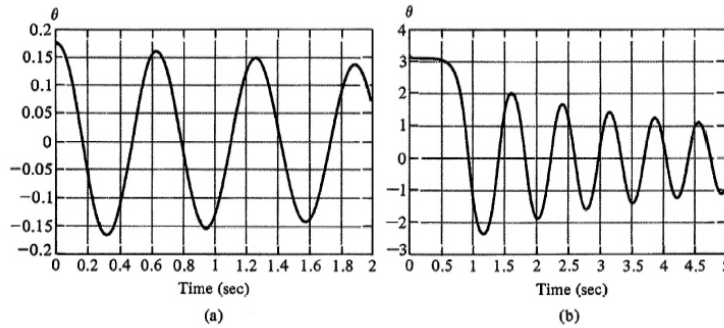


Figure 13.2
Response of the pendulum for
(a) small initial conditions
(b) large initial conditions

Response of a Nonlinear System

Example 13.1

The equations of motion for the simple forced pendulum shown in Figure 13.1 are given by

$$\dot{\omega} = -b\omega - \Omega^2 \sin \theta + \frac{1}{ml^2} T_{in} \tag{13.2}$$

$$\dot{\theta} = \omega, \tag{13.3}$$

where b is the coefficient of drag (or viscous friction) and $\Omega = \sqrt{g/l}$ is the oscillation frequency for “small” initial conditions (near $\theta = 0$). Find and plot the response of this system for initial conditions corresponding to $\theta(0) \approx 0$ and $\theta(0) \approx \pi$. Also plot the response to a piecewise constant input of sampled white noise. Use the parameters $b = 0.25$, $\Omega^2 = 100$, and $ml^2 = 1.00$.

Solution. It is a fact that for even such a simple, common system, the closed-form solution is very difficult to obtain. The homogeneous solution ($T_{in} = 0$) is a complicated Bessel series, while closed-form solutions to arbitrary inputs are impossible. Using simulation we can find the response of the system to arbitrary inputs easily. The time histories for the angular position and velocity of the pendulum are shown in Fig. 13.2 as obtained by the MATLAB/SIMULINK block diagram drawn in Fig. 13.3. One can see from this example how the computer software has been constructed to allow one to setup the simulation in a very intuitive way from the equations. As a matter of fact, the SIMULINK block diagram is essentially the same as would have been used years ago to set up an analog simulation where the $1/s$ factors would have been op-amp integrators. For “small” motions where $\sin \theta \approx \theta$ and with no input torque, the system appears to be linear. It is clear however that for an inverted pendulum ($\theta \approx \pi$) the system is anything but linear as it hangs up near the initial θ at the start. Figure 13.4 illustrates the response with a complex input torque T_{in} representing a random wind force acting on the pendulum. Simulation allows us to find this response, whereas a closed-form solution would be impossible. A reasonable intuition is that if this simple second-order system is difficult to solve analytically, then closed solutions for higher-order systems with even one nonlinearity will be very difficult if not impossible to find.

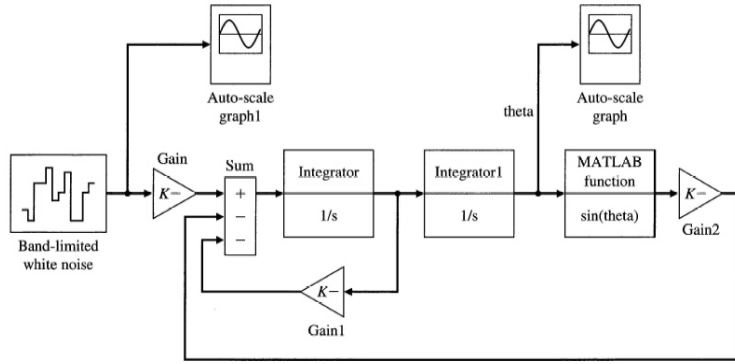


Figure 13.3
Simulation block diagram for solving the pendulum equations

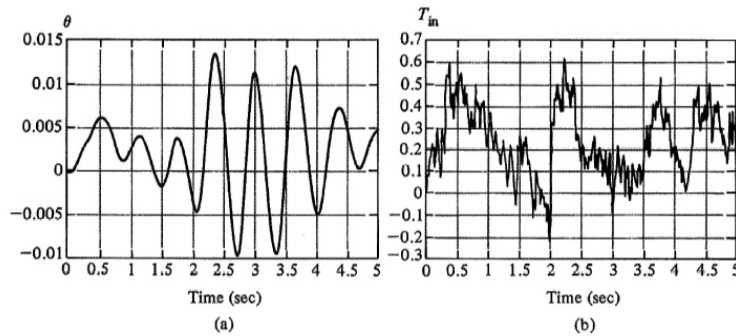


Figure 13.4
Response of the pendulum to an external input (a) pendulum angle (b) external torque

To perform a simulation of the forced pendulum in Example 13.1, the equations of motion are numerically integrated. Many general integration schemes have been developed to perform the task. For a system described in Eq. (13.1), the numerical solution is obtained by first expressing the model as the integral equation

$$\mathbf{x}(t) = \mathbf{x}(t-T) + \int_{t-T}^t f(\mathbf{x}, \mathbf{u}(\tau), \tau) d\tau. \quad (13.4)$$

This equation could be integrated if the function f is constant or linear. Difficulties arise when $f(\mathbf{x}, \mathbf{u}(\tau), \tau)$ is a nonlinear function of its arguments over the integration interval, $t - T \rightarrow t$. Two broad categories of numerical integration schemes are used for these cases: single-step and multi-step. Single-step methods (e.g., Runge-Kutta) approximate the integral by evaluating $f(\mathbf{x}, \mathbf{u}(\tau), \tau)$ at $t - T$, t , and various intermediate values, in an effort to arrive at an accurate approximation to $f(\mathbf{x}, \mathbf{u}(\tau), \tau)$ over the interval which can then be integrated. Multi-step methods (e.g., Adams-Moulton) rely on past values of the derivative, $f(\mathbf{x}, \mathbf{u}(\tau), \tau)$, and assume a certain degree of smoothness to predict future behavior. Multi-step methods generally don't perform well in the presence of discontinuities such as steps or static friction since the extrapolation may miss the point where the discontinuity occurs. The integration algorithm used in Example 13.1 was a fifth-order Runge-Kutta. Most simulation packages allow the user to choose from a large selection of integration routines.²

An important issue of any simulation is how do we determine if the answers produced are correct? As has been pointed out, when using simulation we usually do not have an analytic solution before we start. Several important techniques are employed to check simulation accuracy. First, the simulations of a given system with varying methods of integration, various integration error limitation tolerances and step sizes should produce results which are very close to each other. Using some metric such as the largest absolute value of the difference between two simulations' state variable trajectories, the measure of the difference should be insignificant to the designer. Drastically different results point to some numerical sensitivities which are causing one or both of the simu-

²Simulink, Symnon, ACSL, Easy 5, and XMath all have this capability.

lations to be incorrect. Second, in most situations the designer knows basic properties the system should have, such as the signs of derivatives, and steady state values. When simulations fail basic sanity checks such as these, there is something wrong. For instance, the pendulum example should behave like a linear harmonic oscillator near $\theta = 0$. It should never oscillate faster than this frequency (unforced). The pendulum should come to rest at zero angle and angular velocity and remain vertical for exact initial conditions of $[\pi \ 0]$. A quick examination of Fig. 13.2 reveals that these conditions are met (steady state solutions can be verified with a very long simulation time).

A partial list of issues for any simulation used for control system analysis or design is as follows:

1. Accuracy.
2. Run time.
3. Flexibility of integration routines.
4. Ability to simulate hybrid systems which contain logic, sampled, and continuous parts.
5. Ease of use including block-diagram support for system definition.
6. Graphics support for inputs and outputs.
7. Portability indicating how easily the simulation can be run on different computers.
8. Operating system and host computer requirements (memory, disk storage, etc.).

In this section we noted the nonlinearity of the simple pendulum and the ease with which a simulation package enabled us to find particular solutions for the system. The ability to solve differential equations of high order, complicated nonlinearity, and time-variable coefficients makes simulation an invaluable tool for control engineers.

As was noted earlier, in Fig. 13.2 the system appeared linear near $\theta = 0$, and in fact can be approximated as a linear system in that region. This approximation is known as **linearization**, and is an important tool in the analysis and design of nonlinear control systems.

13.1.2 Linearization

Linearization is the procedure in which a set of nonlinear differential equations is *approximated* by a linear set. There are two main reasons for the importance of linearization. First, there are many good design and analysis tools for linear systems; and second, Lyapunov proved that if the small-signal linear model of a system is stable, then there will exist a region, which may be small, within which the nonlinear system will be stable. Thus, almost always, the first technique of nonlinear system analysis and design is to obtain a linear approximation and design a controller for it. Simulation can then be used to explore the quality of this design when used with the nonlinear system model.

The “small signal” approach to linearization was discussed in Chapter 4. Although based on expansion for infinitesimal signals, the technique is by no means limited to infinitesimal deviations about the operating point. The relative sizes of the deviations from the operating point where the linear approximation is good are governed by two primary factors: first, the nature of the nonlinearity (how rapidly it deviates from being linear), and second, the accuracy with which we wish our model to match the true system. The definition of “small” is very much dependent on the particular problem.

The Small-Signal Approximation

Example 13.2

For the first example of linearization we return to the pendulum as described by Eq. (13.2) and Eq. (13.3). Assume that the system has a position sensor for the angle θ , and that the goal is to keep the pendulum perfectly vertical (pointed down) while the pivot point is subject to (small) horizontal accelerations as might occur in a hanging crane. Find the linear equations of motion.

Table 13.1

Parameter	Value
$m\ell^2$	1.00
b	0.25
Ω^2	100

Solution. Using the notation of Chapter 4 for state equations, the motion is described by the equations

$$\begin{aligned}\dot{\omega} &= f_1(\theta, \omega, T_{in}) \\ &= -b\omega - \Omega^2 \sin \theta - T_{in} \frac{1}{m\ell^2} \\ \dot{\theta} &= f_2(\theta, \omega, T_{in}) \\ &= \omega.\end{aligned}$$

With the definition of the state

$$\mathbf{x} \triangleq \begin{bmatrix} \omega \\ \theta \end{bmatrix},$$

we can linearize about the point (ω_0, θ_0) yielding

$$\begin{aligned}\frac{\partial f_1}{\partial \omega} &= -b \\ \frac{\partial f_2}{\partial \omega} &= 1 \\ \frac{\partial f_1}{\partial \theta} &= -\Omega^2 \cos \theta_0 \\ \frac{\partial f_2}{\partial \theta} &= 0 \\ \frac{\partial f_1}{\partial T_{in}} &= \frac{1}{m\ell^2} \\ \frac{\partial f_2}{\partial T_{in}} &= 0.\end{aligned}$$

Thus the complete linearized state equations are then given by

$$\dot{\mathbf{x}} = \begin{bmatrix} -b & -\Omega^2 \cos \theta_0 \\ 1 & 0 \end{bmatrix} \mathbf{x} + \begin{bmatrix} -\frac{1}{m\ell^2} \\ 0 \end{bmatrix} T_{in}, \quad (13.5)$$

and the output measurement is given by

$$y = \begin{bmatrix} 0 & 1 \end{bmatrix} \mathbf{x}. \quad (13.6)$$

To explore the properties of the linearized model let us use the system parameters as given in Table 13.1.

Substituting these parameters into the continuous system model linearized about $\omega_0 = 0$, and $\theta_0 = 0$, allows us to compute a discrete system model (for discrete time control). For illustrative purposes, we will assume a 10 millisecond sampling interval has already been chosen based on a desired control bandwidth of 2 Hz. Finding a discrete time model with a 10 millisecond sample interval yields the following equation

$$\mathbf{x}_{k+1} = \begin{bmatrix} .9925 & -.9971 \\ .0100 & .9950 \end{bmatrix} \mathbf{x}_k + \begin{bmatrix} 0.01 \\ 0.00 \end{bmatrix} T_{in}, \quad (13.7)$$

and the output measurement is given by

$$y = \begin{bmatrix} 0 & 1 \end{bmatrix} \mathbf{x}_k. \quad (13.8)$$

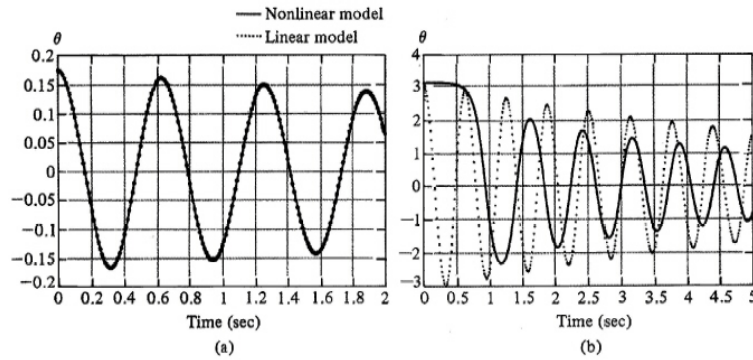


Figure 13.5
Comparison of linearized model and nonlinear model of the pendulum
(a) small initial conditions
(b) large initial conditions

The obvious question is, “How well does this model predict the system behavior?” Qualitatively we can see from Fig. 13.5(a) that for angles near $\theta_0 = 0$, the linear and nonlinear models are extremely close. However, Fig. 13.5(b) shows that a gross violation from the conditions under which the linearization was done $\theta_0 = \pi$ (inverted pendulum) yields results seriously in error.

Another very important point should be repeated here: the accuracy requirements for the model are a function of the application of the model. For open-loop prediction as in Fig. 13.5, the model may have to be extremely accurate if predictions are going to be made for long time intervals. However, if, as is usually the case in control systems, the linearized model is to be used in a state estimator, the accuracy of the model is much less critical because measurement updates in the state estimator are used to correct the model estimates (at each sample interval). In fact, modeling errors which produce time-domain errors well below the bandwidth of the state estimator can be easily tolerated, whereas modeling errors producing higher frequency errors are more likely to require reduction since they are beyond the bandwidth of the state estimator. Using this reasoning it is easy to get a feel for which type of modeling errors are permissible and which are not. All models contain errors, and there is always a trade-off between model complexity and computation time, so model simplification should be considered in any design. One of the simplest ways to test models is through simulation and examination of the resulting estimation errors and the overall system performance. The simulation should contain a **plant** model with a high degree of detail, and then estimator models based on differing levels of approximation can be studied. In this manner the accuracy required of the approximation can be determined through estimator error and performance analysis.

Before proceeding, let’s look at **piecewise linearization** as a simple simulation alternative for the system defined by Eq. (13.2) and Eq. (13.3).

Equations (13.2) and (13.3) can be rewritten as

$$\dot{\mathbf{x}} = \begin{bmatrix} -b & -\Omega^2 \frac{\sin \theta_k}{\theta_k} \\ 1 & 0 \end{bmatrix} \mathbf{x} + \begin{bmatrix} 1 \\ 0 \end{bmatrix} T_{in}, \quad (13.9)$$

and the output measurement remains as before

$$y = \begin{bmatrix} 0 & 1 \end{bmatrix} \mathbf{x}.$$

In this form, we can approximate the system matrix as constant over a small interval of time, thereby allowing us to compute a linear discrete time model for the system over that interval. Using a constant time interval, the state equations become

$$\mathbf{x}_{k+1} = \Phi(\theta_k) \mathbf{x}_k + \Gamma(\theta_k) u_k. \quad (13.10)$$

For discrete time control it is of course necessary to compute the corresponding discrete transition matrix $\Phi(\theta_k)$ and input matrix $\Gamma(\theta_k)$ at each sampling interval. To save computation time, the matrices can be computed over the expected range of θ_k and stored in tables as actual values or coefficients

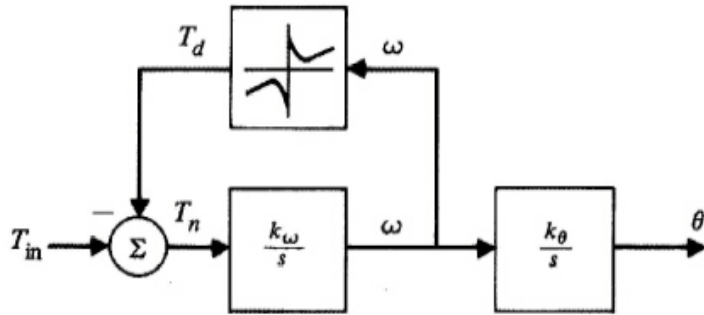


Figure 13.6
Spindle motor
model including
nonlinear stiction
and coulomb
friction

of some curve fit equations. Choosing the sample interval clearly will have an effect on the accuracy of this technique since the error in calculating the next sample is related to the maximum change of the state variable θ during the interval: the smaller the change, the closer the approximation. In a simulation of the pendulum, the size of the time step—and therefore the accuracy of the solution—would be traded off against the execution time of the simulation. For discrete time control, if the sample interval does not yield good enough model accuracy then it may be necessary to compute Eq. (13.10) more than once per sample interval.

Design Based on a Linear Approximation

Example 13.3

The use of linearization for design can be illustrated by design of a spindle speed controller for a compact disk player. The block diagram of the plant which uses a direct drive spindle motor is shown in Fig. 13.6. The total drag torque applied to the inertial load is given by

$$T_d(\omega) = k_{vf}\omega + k_{cf} \operatorname{sgn}(\omega) + k_{sf} \operatorname{sgn}(\omega) p(\omega), \quad (13.11)$$

with the following definitions

$$\begin{aligned} T_{in} &= \text{applied input torque [N-m]} \\ T_d &= \text{drag torque from friction components [N-m]} \\ T_n &= \text{net input torque causing acceleration [N-m]} \\ k_{\omega} &= \text{reciprocal of the load inertia [sec}^{-2}\text{/N-m]} \\ k_{\theta} &= \text{sensor gain} \\ k_{vf} &= \text{linear viscous friction coefficient [N-m-sec-rad}^{-1}\text{]} \\ k_{cf} &= \text{coulomb friction torque [Newton-meters]} \\ k_{sf} &= \text{static friction or "break away" torque [Newton-meters]} \\ \sigma &= \text{static friction velocity constant [rad-sec}^{-1}\text{]} \\ p(\omega) &= e^{-|\omega/\sigma|} \end{aligned}$$

where the signum function is defined as

$$\operatorname{sgn}(\sigma) = \begin{cases} +1 & \sigma > 1 \\ 0 & \sigma = 0 \\ -1 & \sigma < 1. \end{cases} \quad (13.12)$$

Construct a piecewise linear model for this system.

Solution. Clearly, the net torque applied to the spindle given by Eq. (13.11) is a highly nonlinear function. In this case the linearization as described in Chapter 4 fails if the “operating point” is at $\omega = 0$ because the partial derivative of the signum function does not exist at zero. This is one case where obtaining a linear discrete equivalent model would be extremely difficult, and cannot be handled by linearization with high accuracy. However, if we are after a spindle speed controller which has a nonzero lower bound on the desired operating

speeds, then we can linearize this plant. A reasonable assumption is that during operation the spindle speed will be in a restricted range as

$$0 < \omega_{min} \leq \omega \leq \omega_{max}. \quad (13.13)$$

During start-up (zero spindle speed) the conditions given by Eq. (13.13) will be violated, but the speed controller will only be expected to perform well once the speed is in the operating range.³

The nonlinear differential equations describing the spindle motor are given by

$$\begin{aligned} \dot{\omega} &= f_1(\theta, \omega, T_{in}) \\ \dot{\theta} &= f_2(\theta, \omega, T_{in}), \end{aligned}$$

where

$$\begin{aligned} f_1(\theta, \omega, T_{in}) &= k_{\omega}(-T_d(\omega) + T_{in}) \\ f_2(\theta, \omega, T_{in}) &= k_{\theta}\omega. \end{aligned}$$

Computing the partial derivatives yields

$$\begin{aligned} \frac{\partial f_1}{\partial \omega} &= -k_{\omega} \frac{\partial T_d(\omega)}{\partial \omega} + 0 = -k_{\omega} k_{vf} \\ \frac{\partial f_2}{\partial \omega} &= k_{\theta} \\ \frac{\partial f_1}{\partial \theta} &= 0 \\ \frac{\partial f_2}{\partial \theta} &= 0 \\ \frac{\partial f_1}{\partial T_{in}} &= k_{\omega} \\ \frac{\partial f_2}{\partial T_{in}} &= 0. \end{aligned}$$

We see that there is no dependence on the operating point. The state-space model is then given by

$$\begin{bmatrix} \dot{\omega} \\ \dot{\theta} \end{bmatrix} = \begin{bmatrix} -k_{\omega} k_{vf} & 0 \\ k_{\theta} & 0 \end{bmatrix} \begin{bmatrix} \omega \\ \theta \end{bmatrix} + \begin{bmatrix} k_{\omega} \\ 0 \end{bmatrix} T_{in} + \begin{bmatrix} k_{\omega} \\ 0 \end{bmatrix} T_{bias}, \quad (13.14)$$

where

$$T_{bias} = -k_{cf} \operatorname{sgn}(\omega).$$

The block diagram of the linearized system is shown in Fig. 13.7. Note that all the variables are still in absolute terms, but there is a dependence of T_{bias} on the sign of the rotational velocity ω . Note that if Eq. (13.14) is used to model the system in simulation, the bias torque should be set to zero at $\omega = 0$.

Besides the difficulty of the unbounded derivative of the signum function at zero, several other points can be illustrated with this example. It is not always necessary that the “operating point” be a constant value. In this example θ is increasing with time because ω remains positive after start-up. If the model outputs did not require angular position, we could simply drop θ from the state. However, if other parts of the overall system might require an angular position, input θ cannot be dropped. In any case, since neither f_1 nor f_2 are functions of θ , it is not necessary that θ remain constant. Although the states, inputs, and outputs can sometimes be conveniently described as deviations from the operating point, this is not necessary either. In the case of the spindle model, we can add a bias or “disturbance input” into the model and allow all of the state variables to represent the absolute variables as in a standard model. It should be clear that nonzero terms in the nonlinear system must be accounted for, as was done in this example, by adding T_{bias} to the state equations. It should be clear that the control function in this problem will have to provide at least a constant bias torque to overcome bearing friction and aerodynamic drag. Thus either feedforward, integral control, or bias estimation should be employed.

From the linear continuous time model of Eq. (13.14), we can use the method of Chapter 6 to find a discrete equivalent. Since the designer has found a way to approximate the nonlinear model by

³The only requirement for start-up would be initially overcoming the static friction force and obtaining operating speed within a specified maximum time.

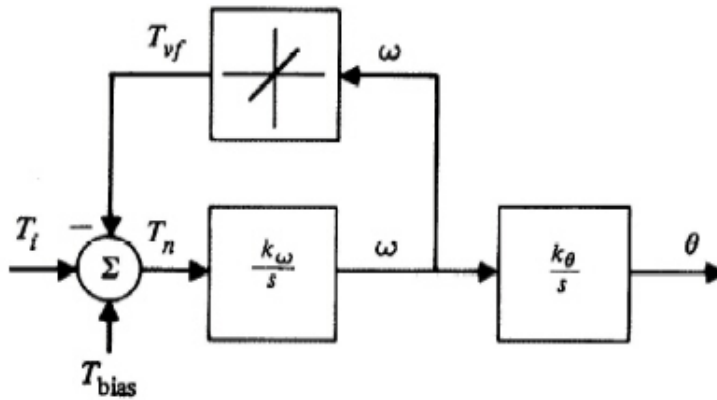


Figure 13.7
Linearized model
of the spindle
motor

a linear one, he or she can now proceed with linear design tools. Thus the goal of linearization is to obtain a linear model which is valid over an appropriate region of operation such that we can use the familiar and powerful linear systems analysis to understand the control system.

Many physical systems such as the spindle motor can be modeled very accurately by lumped parameter (finite order) linear models in the expected regions of operation. Although some nonlinear models can be linearized by hand, many are complex enough to require some sort of computer software assistance. Physical structures such as beams, buildings, bridges, loudspeakers, and missiles all have highly nonlinear dynamic behavior under reasonable operating conditions. Linearizing models for such common systems is greatly facilitated by computer programs.

Structural Analysis

Many systems include a flexible physical structure which is part of the plant to be controlled. The structure may be a simple pendulum as in the read/write assembly of a magnetic disk data storage system or it may contain an extremely complex structure such as that of the airframe and actuators of a jet aircraft. In all but the most trivial systems, analysis of the structural dynamics of such a plant are greatly facilitated by computer programs which turn physical descriptions of structures into linear dynamic models. One such program is NASTRAN (NAsa STRuctural ANalysis) (see Strang (1986)). The analysis or modeling technique employed by most such structural analysis programs is finite element analysis in which a structure is modeled as a joining of many simple elements drawn as geometrical shapes such as cubes, pyramids, or rhomboids. Properties of the material such as stiffness and damping determine the dynamical properties of each of the elements and their interconnections. An example of how NASTRAN is employed in control system design follows.

Example of Finite-Element Analysis

Example 13.4

A beam with a frictionless pivot at one end and a load mass at the other is shown in Fig. 13.8. This is a structure typical of those found in robots, disk read/write head assembly, and many other examples of motion control. Demonstrate the computation of a model of the motion using NASTRAN.

Solution. Both the beam and the load mass have been divided into elements for modeling. The motion in a horizontal plane (no gravity)—assuming in-plane motions only and a rigid beam—is just that of an inertia, and the basic response is just that of a double integration of input torque to produce the output angle θ as shown in part (a) of Fig. 13.5 (rigid body mode). The rigid body model is fine until the input torque starts to significantly excite the bending modes of the beam and load, which move as shown in parts (b–d) of Fig. 13.9 as computed by the program. The lowest frequency mode is the first bending mode of the pendulum beam which is at 157 Hz. The designer of a pendulum angle control system with a bandwidth less than one tenth of this resonant frequency could neglect this mode altogether, along with those of higher frequencies. Since the magnitude of the frequency

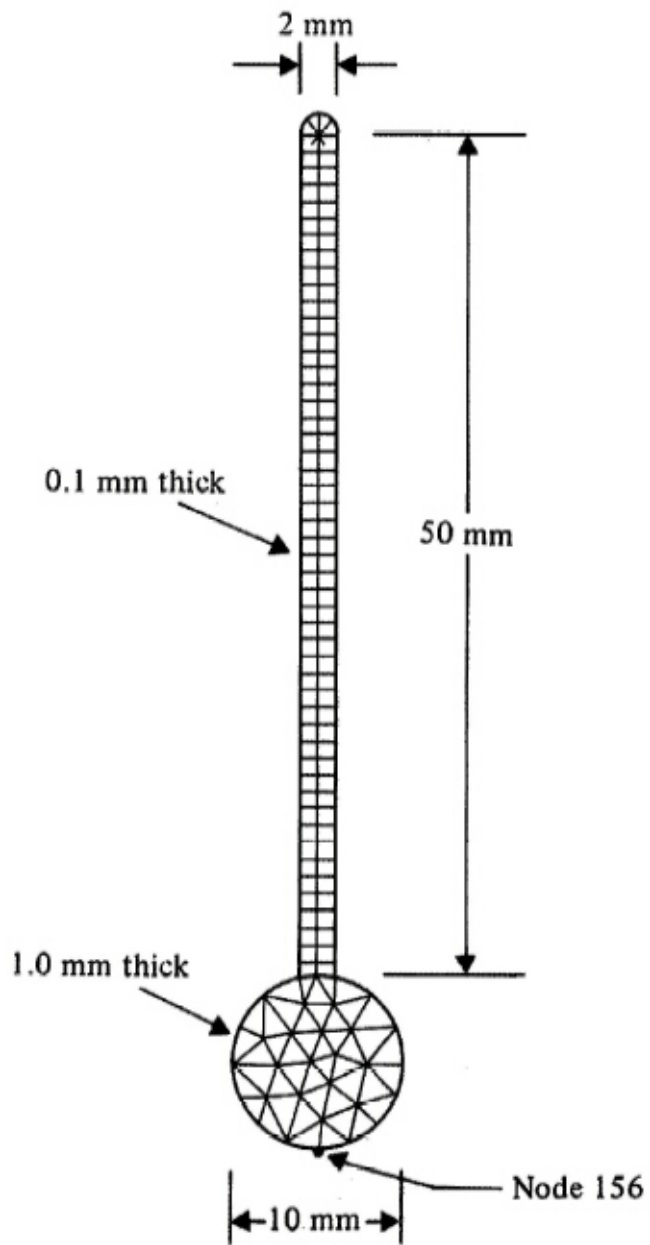


Figure 13.8
Simple pendulum
model for
structural
analysis by the
finite element
method

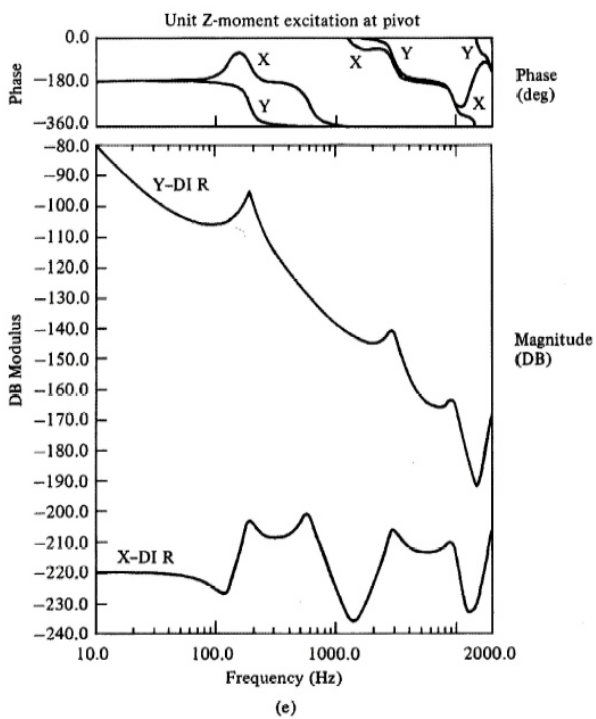
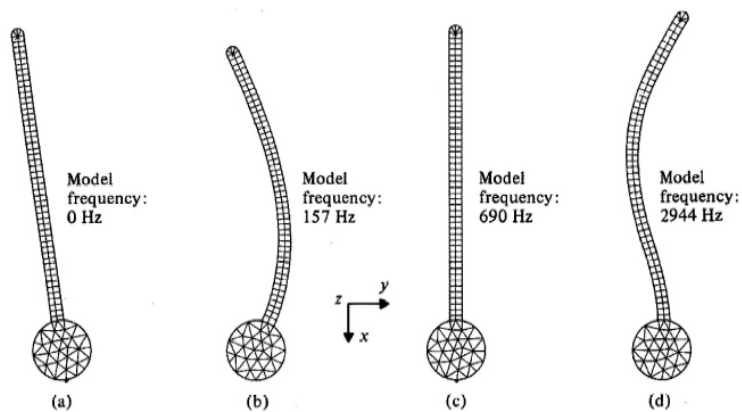


Figure 13.9
 Pendulum mode shapes determined by NASTRAN (a) rigid body, (b) first bending mode, (c) first extension mode, (d) second bending mode, and (e) frequency response from input torque to x and y deflections

response caused by the first mode resonance rises a factor of 10 (20 dB) above the baseline frequency response as defined by the $1/s^2$ inertial model, neglecting this bending mode of the pendulum will restrict control designs to have a bandwidth no higher than about 16 Hz.

For physical systems even of the complexity of the simple pendulum in the last example (and this is as simple as one could practically imagine), mechanical engineers and control designers find finite element analysis of the plant structures to be very advantageous. After entering a geometrical description of the physical system into an input file, along with information characterizing the materials the system is comprised of, a program such as NASTRAN can find a linear model that can match the physical system very closely. NASTRAN output can be used directly as part of the dynamic model used in the control design. Such models can be made far more accurately than normal hand analysis models. It should be noted that finite element analysis can also provide information about stress in the material under various loading conditions, weight, inertia, and mode *shapes* in addition to the dynamic response which is of primary interest to the control system designer.

13.1.3 Describing Functions

In many cases linearization of a nonlinear system or subsystem by small signal analysis is not possible or is not adequate to describe the system. The describing function is based on the fact that a linear stationary system responds to a sinusoid with another sinusoid of the same frequency but modified amplitude and phase. In 1950 R. J. Kochenburger proposed to represent a nonlinear element by the **transfer function** of the (fictitious) linear stationary system which would produce as its output a signal equal to the fundamental component of the nonlinear system's complete output. Higher order harmonics were to be ignored as negligible. Notice that this describing function is *not* a transfer function and in fact usually depends on both the amplitude and the frequency of the input. Describing function analysis assumes that only the fundamental component of the output is important. Thus, for an input $x(t) = A \sin \omega t$ to the nonlinear function, it is assumed that the output can be expressed as a Fourier series as follows⁴

$$\begin{aligned} y(t) &= A_0 + \sum_{n=1}^{\infty} (A_n \cos n\omega t + B_n \sin n\omega t) \\ &= A_0 + \sum_{n=1}^{\infty} Y_n \sin (n\omega t + \phi_n), \end{aligned}$$

where

$$A_n = \frac{1}{\pi} \int_0^{2\pi} y(t) \cos n\omega t d(n\omega t) \quad (13.15)$$

$$B_n = \frac{1}{\pi} \int_0^{2\pi} y(t) \sin n\omega t d(n\omega t) \quad (13.16)$$

$$Y_n = \sqrt{A_n^2 + B_n^2} \quad (13.17)$$

$$\phi_n = \arctan \frac{A_n}{B_n}. \quad (13.18)$$

A constant offset will be present in the output if the nonlinearity is not symmetric ($A_0 \neq 0$). Since the describing function is the complex ratio of the magnitude and phase of the first harmonic in the output to the magnitude and phase of the input, we are only interested in the first terms of the Fourier series representing the output. Thus the describing function is

$$N(A, \omega) = \frac{Y_1}{A} \angle \phi_1 = \frac{\sqrt{A_1^2 + B_1^2}}{A} \angle \arctan \frac{A_1}{B_1}. \quad (13.19)$$

⁴Some nonlinear systems have subharmonics in their outputs, while others display chaotic behavior. These cannot be analyzed by describing function methods.

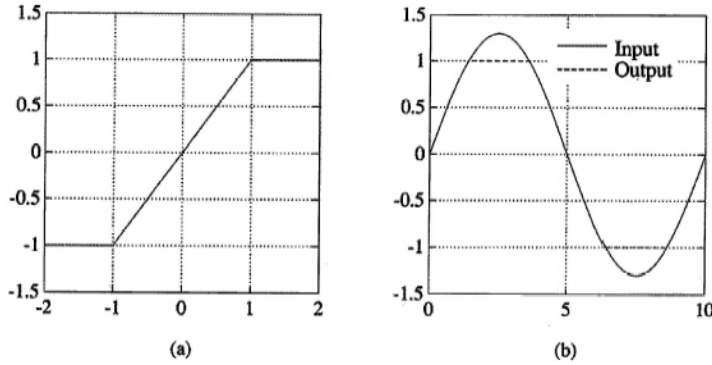


Figure 13.10
Saturation nonlinearity and signals used for the describing function
(a) saturation characteristic
(b) input and output signals used for the calculation

In the case of a memoryless nonlinearity which is an odd function ($f(-\sigma) = -f(\sigma)$), the Fourier series cosine coefficients will be zero and the describing function becomes

$$N(A) = \frac{B_1}{A} \angle 0, \quad (13.20)$$

that is also independent of ω . This is the most common case in control. If the nonlinearity has memory that is independent of time, as with hysteresis, then the describing function will be complex but independent of frequency.

Computation of a Describing Function

Example 13.5

Use Eq. (13.20) to calculate the describing function for saturation which is shown in Fig. 13.10(a) with example input and output in Fig. 13.10(b). Saturation is one of the most common nonlinearities in control systems. The general saturation function is expressed in terms of the basic saturation function defined by

$$\text{sat}(x) \triangleq \begin{cases} +1 & x > 1 \\ x & |x| \leq 1 \\ -1 & x < -1. \end{cases} \quad (13.21)$$

If the linear region slope or gain is k and the final saturated value is m , then the function is

$$y = m \text{sat}(kx/m). \quad (13.22)$$

Solution. A brief examination of Fig. 13.10 can simplify the task. For an input $x = A \sin \omega t$ with amplitude $A < m/k$, the describing function is just 1.0, a gain of 1. With $A \geq m/k$ we want to find the fundamental harmonic amplitude and phase at the output y given by Eq. (13.22). Because the saturation function is an odd function, the coefficients of the cosine terms, A_n in Eq. (13.15), will all be zero (hence the phase will also be zero). The describing function N given by Eq. (13.20) is then

$$N(A) = \frac{B_1}{A},$$

where A is the amplitude of the input sinusoid. Since we are only interested in the amplitude of the fundamental in y , we need to calculate the integral Eq. (13.16) for $n = 1$

$$B_1 = \frac{1}{\pi} \int_0^{\omega t = 2\pi} m \text{sat}\left(\frac{Ak}{m} \sin \omega t\right) \sin \omega t d(\omega t). \quad (13.23)$$

The integral for the coefficient B_1 over the interval $\omega t = [0, 2\pi]$ is just four times that over the quarter cycle $\omega t = [0, \pi/2]$

$$B_1 = \frac{4m}{\pi} \int_0^{\omega t = \pi/2} \text{sat}\left(\frac{Ak}{m} \sin \omega t\right) \sin \omega t d(\omega t). \quad (13.24)$$

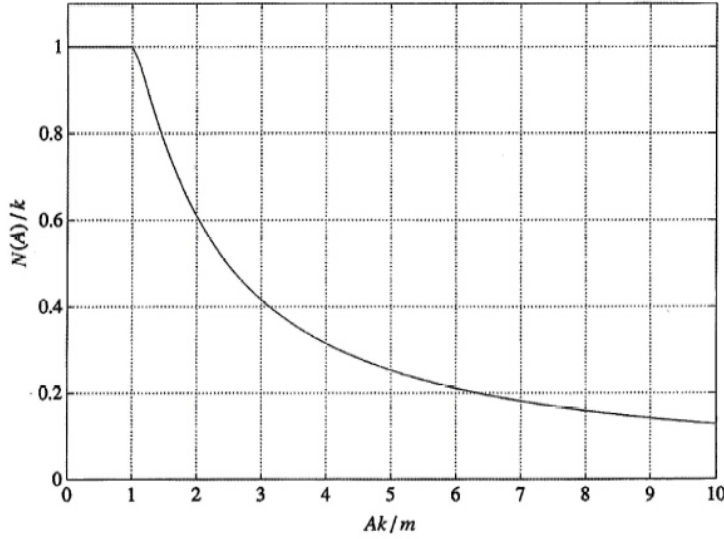


Figure 13.11
Describing
function for
saturation

The integral can be broken into two parts, before and after saturation. We define the point of saturation as occurring at time t_s , where

$$t_s = \frac{1}{\omega} \arcsin \frac{m}{Ak} \quad \text{or} \quad \omega t_s = \arcsin \frac{m}{Ak}.$$

Breaking Eq. (13.24) into two parts yields

$$\begin{aligned} N &= \frac{4m\omega}{A\pi} \left(\int_0^{\omega t_s} \text{sat} \left(\frac{Ak}{m} \sin \omega t \right) \sin \omega t \, dt + \int_{\omega t_s}^{\pi/2} \sin \omega t \, dt \right) \\ &= \frac{4m\omega}{A\pi} \left(\int_0^{\omega t_s} \frac{Ak}{m} \sin^2 \omega t \, dt + \int_{\omega t_s}^{\pi/2} \sin \omega t \, dt \right) \\ &= \frac{4m\omega}{A\pi} \left(\int_0^{\omega t_s} \frac{Ak}{2m} (1 - \cos 2\omega t) \, dt + \int_{\omega t_s}^{\pi/2} \sin \omega t \, dt \right) \\ &= \frac{4m\omega}{A\pi} \left(\frac{Ak}{2m} t \Big|_0^{t_s} - \frac{Ak}{4m\omega} \sin 2\omega t \Big|_0^{\omega t_s} - \frac{1}{\omega} \cos \omega t \Big|_{\omega t_s}^{\pi/2} \right) \\ &= \frac{4m\omega}{A\pi} \left(\frac{Ak}{2m} t_s - \frac{Ak}{4m\omega} 2 \sin \omega t_s \cos \omega t_s - \frac{1}{\omega} (\cos \pi/2 - \cos \omega t_s) \right). \end{aligned}$$

Using $\omega t_s = \arcsin [m/(Ak)]$, we have

$$\sin \omega t_s = \frac{m}{Ak} \quad \text{and} \quad \cos \omega t_s = \sqrt{1 - \left(\frac{m}{Ak} \right)^2},$$

thus we have

$$N(A) = \begin{cases} \frac{2k}{\pi} \arcsin \frac{m}{Ak} + \frac{2m}{A\pi} \sqrt{1 - \left(\frac{m}{Ak} \right)^2} & Ak/m > 1 \\ k & Ak/m \leq 1. \end{cases} \quad (13.25)$$

Fig. 13.11 shows the value of N/k as a function of Ak/m . As the input amplitude A increases, the value of $N(A)$ decreases because the amplitude of the fundamental approaches a constant, that of a unit magnitude square wave $2m/\pi$. Hence, normalized to the amplitude A , N decays as the inverse of A .

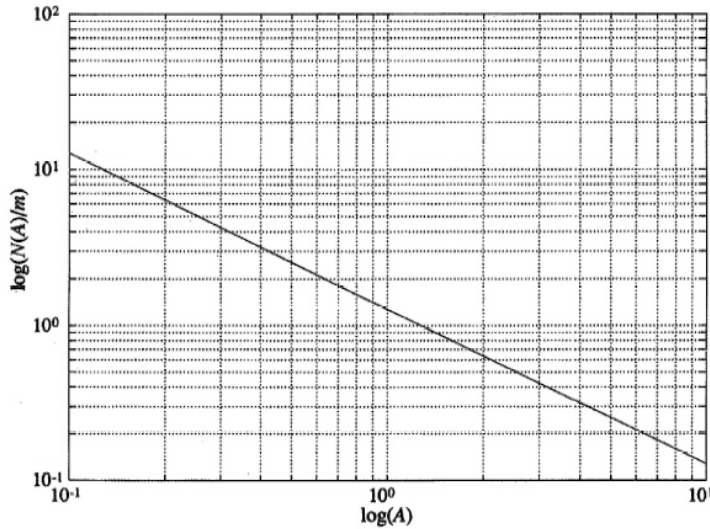


Figure 13.12
Describing function for the signum function

Compute the describing function of the signum function given in Eq. (13.12) with output multiplied by gain m .

Solution. For any nonzero input $x = A \sin \omega t$, the output, $y(t) = m \operatorname{sgn} x(t)$ is a square wave of the same fundamental frequency and phase. Calculating the first coefficients of the Fourier series we have $A_1 = 0$ and

$$\begin{aligned} B_1 &= \frac{4m}{\pi} \int_0^{\omega t = \pi/2} 1 \, d(\omega t) \\ &= \frac{4m}{\pi} \end{aligned}$$

from which the describing function of the signum function is

$$N(A) = \frac{4m}{\pi A} \tag{13.26}$$

for all $A \neq 0$. Eq. (13.26) is plotted in Fig. 13.12.

Describing Function for the Signum Function with Hysteresis

Example 13.7

Consider a signum function with hysteresis h as shown in Fig. 13.13 and compute its describing function.

Solution. As seen in the figure, the function with hysteresis exhibits the tendency to remain in its current state. Until the input to the signum function with hysteresis is past the value h , it is not possible to determine the output uniquely without knowing its past history which implies that this nonlinearity has memory. It is clear that the output is again a square wave with amplitude of one, as long as the input amplitude A is greater than the hysteresis level h ($A > h$, otherwise the output is a constant ± 1). Note from Fig. 13.13(b) that the square wave lags the input sine wave in time. The lag time can be calculated as

$$A \sin \omega t = h \quad \text{or} \quad \omega t = \arcsin \frac{h}{A} \tag{13.27}$$

Because the phase lag is given by Eq. (13.27) directly for all ω , we have

$$N(A) = \frac{4}{\pi A} \angle -\arcsin \frac{h}{A} \tag{13.28}$$

which is plotted in Fig. 13.14. It is interesting to note from this figure that when the input sine wave magnitude is just slightly larger than the hysteresis h , the phase angle is -90° , which corresponds to the output square wave being shifted to the peak of the input sine wave.

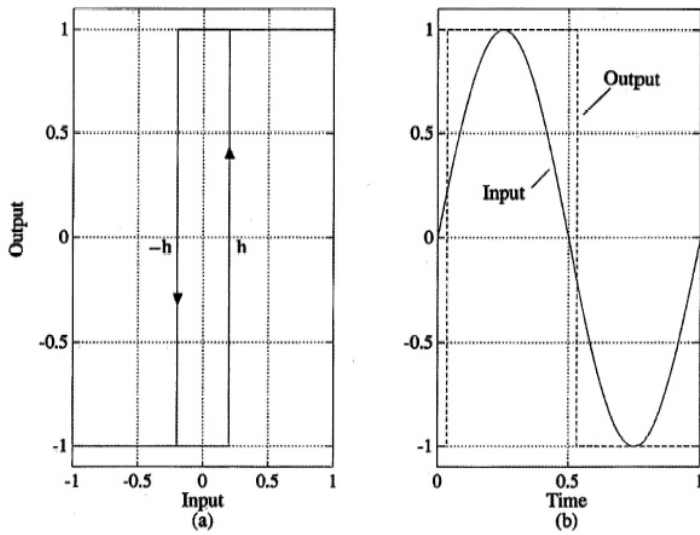


Figure 13.13
Computing the describing function for the signum function with hysteresis
(a) characteristic
(b) input and output signals

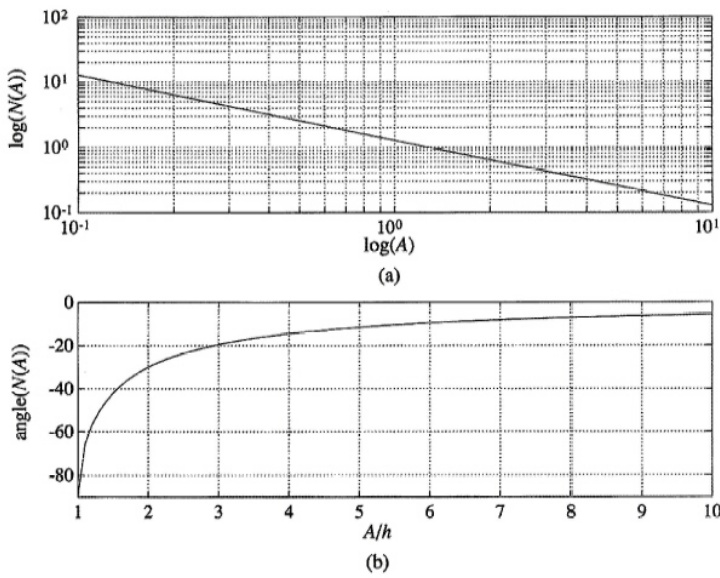


Figure 13.14
Plot of the describing function for the signum function with hysteresis

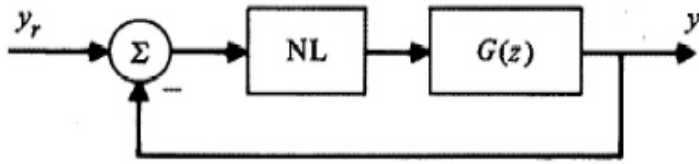


Figure 13.15
A discrete-time
system with one
series nonlinearity

Stability Analysis with Describing Functions

The method of stability analysis using describing functions is an extension of the Nyquist criterion for linear systems. If a linear system has characteristic equation $1 + KD(s)G(s) = 0$, the standard Nyquist stability analysis plots DG and examines the encirclements of $-\frac{1}{K}$. If K is known to be in a range $K_1 < K < K_2$ then we can mark the line segment from $-\frac{1}{K_1}$ to $-\frac{1}{K_2}$, and if the encirclements of the entire segment are counted and the stability criterion applied, we can decide if the system will be stable with any fixed gain in the given range. The describing function applies this concept by replacing the line segment with the plot of the function $\frac{-1}{N(A)}$. If the curve of $D(j\omega)G(j\omega)$ intersects the curve of $\frac{-1}{N(A)}$, the inference is that the system will oscillate at the corresponding frequency and amplitude. If the encirclement count corresponds to that of a stable system if it were linear, the inference is that the nonlinear system will be stable and unstable if the encirclements correspond to that of an unstable linear system. These inferences are not proven to be true but result in useful conclusions in many cases.

Figure 13.15 shows the block diagram of a system having a single nonlinearity in an otherwise linear feedback loop. Instead of plotting the open-loop transfer function in the complex plane and looking for encirclements of the $(-1, 0)$ point, the linear part of the transfer function is plotted on the same graph as the negative reciprocal of the describing function of the nonlinear part. Any intersection represents a possible instability in the closed-loop system. In effect, the single $(-1, 0)$ critical point is replaced by a locus of critical points as given by the describing function. It should be noted that nonlinearities can have a beneficial effect on a system in that in some cases they limit the amplitude of an instability. Periodic, finite-amplitude, steady-state motions are referred to as **limit cycles**. Although a limit-cycling system can be considered unstable, such motion is sometimes benign in that there is a finite region of state-space which contains the trajectory of the limit cycle; and if this region is within the allowable error, then the system may be satisfactory. The system does not have **asymptotic** stability which defines a system which comes to rest at the origin of the state space. One value of describing function analysis is in finding the conditions under which the system may become unstable or exhibit a limit cycle. Once those conditions are identified, the exact nature of the instability or the limit cycle is most accurately revealed via simulation. Also, choosing a remedy for the instability can often be done with describing function analysis, which can yield clues on how to minimize or eliminate the instability.

Analysis Using the Describing Function

Example 13.8

Consider the feedback control system of Fig. 13.16 where the continuous time linear transfer function $G(s)$ is given by

$$G(s) = \frac{3s^2 + 2s + 1}{s^3}. \quad (13.29)$$

The D/A can be modeled as a saturation with gain 1.0 and limits ± 1 followed by a zero-order hold, the z -

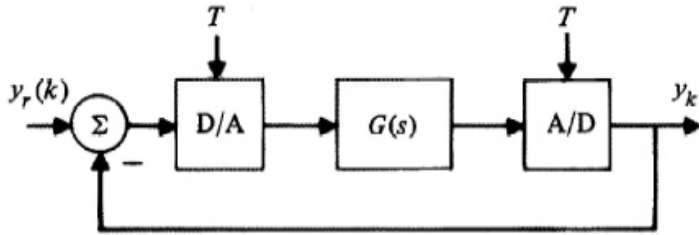


Figure 13.16
A discrete-time system with simple error feedback

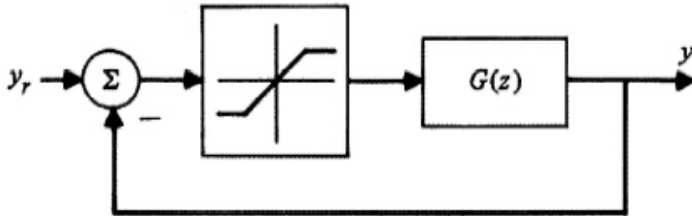


Figure 13.17
A discrete-time system with a saturation nonlinearity

transform of the open-loop system with $T = 0.1$ is

$$G(z) = \frac{0.3102z^2 - 0.5993z + 0.2902}{(z-1)^3}. \quad (13.30)$$

The nonlinear discrete-time system model is shown in Fig. 13.17. Using a describing function description for the saturation, predict the large signal behavior of the system.

Solution. Even in this simple example there are actually multiple nonlinearities present, caused by the saturation as well as the data quantization in the A/D and D/A. However, in this case we assume small quantization levels and that the effect of quantization will mainly be a small signal effect that can be ignored for a large signal analysis. This intuitive observation can be substantiated by examining the properties of the quantizer as will be done in the next section.

We have derived the describing function for the saturation function in Eq. (13.25). For the assumptions of the problem, the parameters m and k are both equal to one. A plot of the Nyquist diagram and of $-1/N(A)$ is shown in Figure 13.18. Because Eq. (13.25) has zero phase angle, $-1/N(A)$ lies strictly on the negative real axis of the Nyquist plot to the left from -1 . The two curves intersect at $|G(e^{j\omega T})| = 5.814$, where $\omega T = 0.058$ and the heuristics of the describing function predict a possible limit cycle at a frequency of $f = 0.058 / (.1 * 2 * \pi) = 0.0923$. The cycle may or may not be stable. In this case, from Fig. 13.11, a value of $N(A) = 1/5.814 = 0.172$ corresponds to an amplitude of approximately $A = 7$. To determine the stability of the limit cycle, a perturbation check is done. Assume that the system is operating at exactly the point represented by the intersection of the two curves. If the amplitude A is reduced slightly, $N(A)$ increases. The critical point shifts to the right, a position where the function $G(z)$ has no net encirclements, and the amplitude will decrease further moving away from the point of instability. On the other hand, assume that the amplitude is increased slightly, $N(A)$ is reduced, and $-1/N(A)$ is moved to the left from the point of intersection. The new critical point is now encircled twice, and the amplitude will increase still further. Thus we predict an unstable limit cycle with the use of a describing function. Figure 13.19 shows a simulation of this system. Note that small step inputs are responded to in a stable and reasonable fashion. As the step amplitude increases, the response gets more and more oscillatory until, at steps larger than 11.5, the output diverges. Note the approximate period of the oscillatory behavior is 12 seconds, which is near the $1/f = 10.8$ seconds predicted using the describing function. Another feature of Fig. 13.19 can be seen in comparing the size of the response to the magnitude of the reference (step) input: the input to the saturation nonlinearity is the controller error, or the difference between the command and the response. Until the error signal reaches an initial amplitude of 11.5, followed by a larger peak amplitude due to the following overshoot, the system remains stable. We calculate that the amplitude required to yield a small enough describing function is about 7, smaller than that required for the step input. If we have $k = 1$ and let

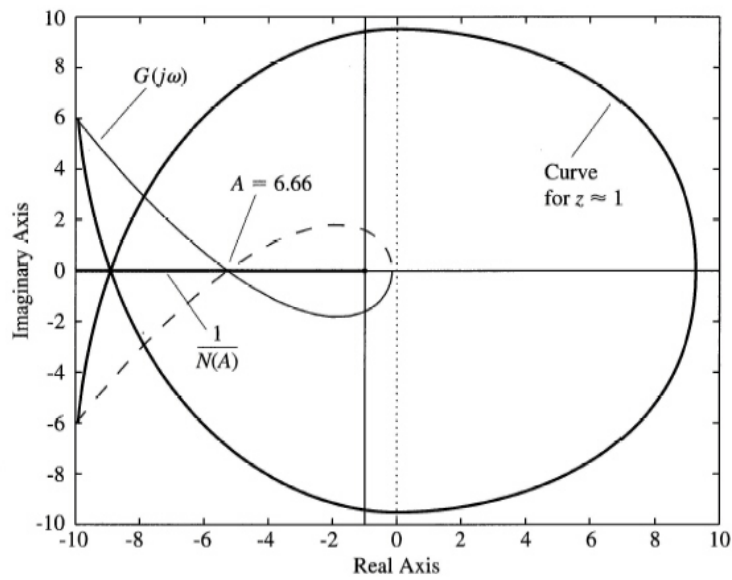


Figure 13.18
The Nyquist plot for the system of Eq. (13.30)

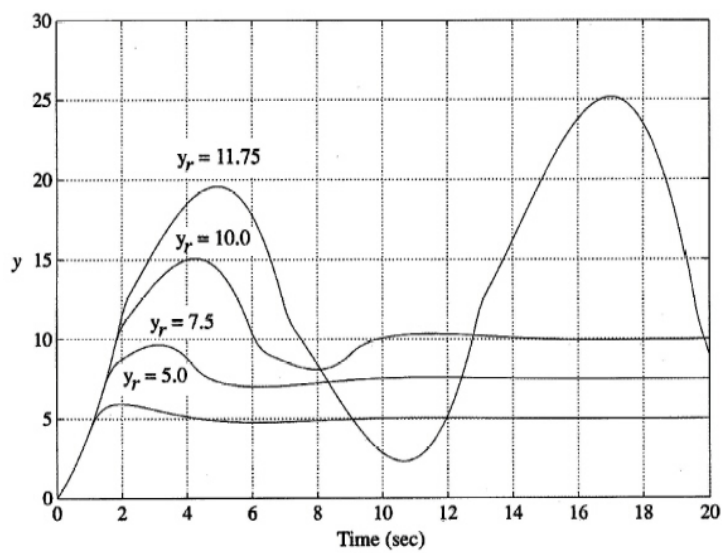


Figure 13.19
Step responses of the system of Fig. 13.17

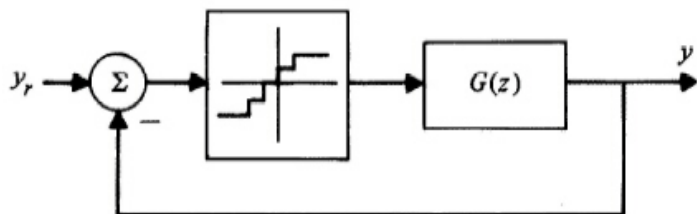


Figure 13.20
A discrete-time system with a quantizer nonlinearity

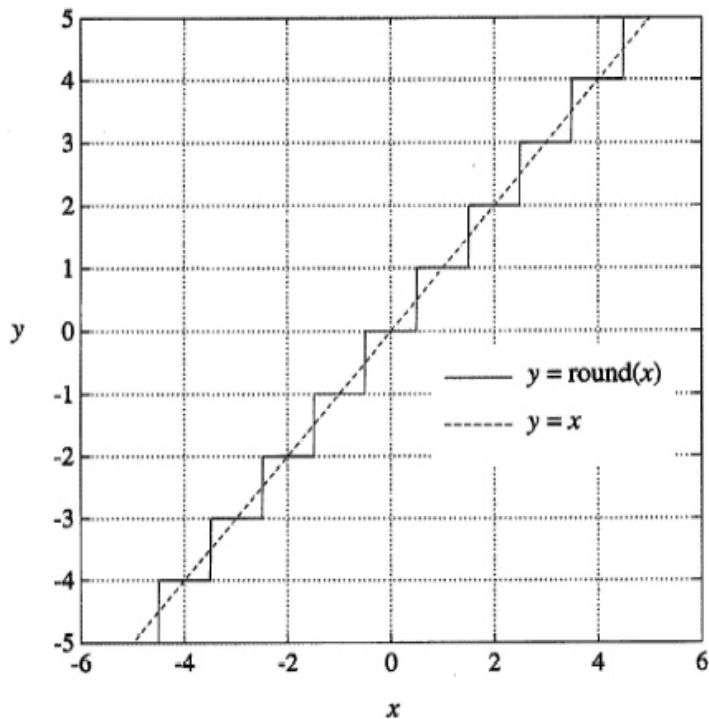


Figure 13.21
Characteristic of the round-off quantizer

$m \rightarrow \infty$, the nonlinearity becomes linear and the locus of points $-1/N(A)$ collapses to the standard $(-1, 0)$ point of Nyquist stability analysis.

Quantizer Nonlinearity

Example 13.9

Examine the small signal characteristics of the system of Example 13.8 with the quantizer nonlinearity instead of saturation. The system is shown in Fig. 13.20.

Solution. The input-output characteristic of the quantizer with a quantization level of q is given by

$$Q(\sigma) = q \text{round}(\sigma/q), \tag{13.31}$$

where the “round” function is the round-off function described in Chapter 10, and shown in Fig. 13.21 for convenience. The describing function for this nonlinearity is not hard to find (consider the addition of signum-

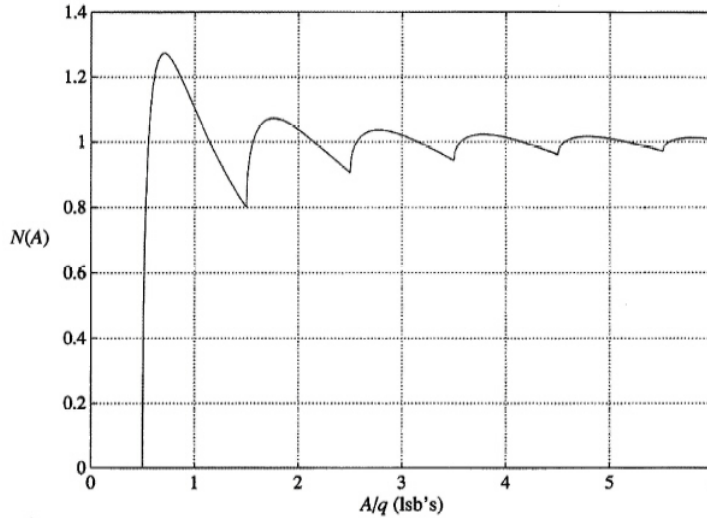


Figure 13.22
The describing
function of the
round-off
quantizer
characteristic

with-deadzone functions), and is given by

$$N(A) = \begin{cases} 0 & 0 < A < \frac{q}{2} \\ \frac{4q}{\pi A} \sum_{i=1}^n \sqrt{1 - \left(\frac{2i-1}{2A}q\right)^2} & \frac{2n-1}{2}q < A < \frac{2n+1}{2}q, \end{cases} \quad (13.32)$$

which is plotted versus A/q in Fig. 13.22. Although it is not obvious from the equation, it can be seen from Fig. 13.22 that Eq. (13.32) is not a monotonic function of A as was the saturation describing function. Hence an intersection of $-1/N(A)$ with $G(e^{j\omega T})$ does not always uniquely determine an amplitude, but this is not a problem in this case.

Analysis with a Describing Function

Example 13.10

With the transfer function given by Eq. (13.30) and quantization corresponding to a D/A of 12 bits over ± 1 volt accuracy, predict the small signal behavior of the system drawn in Fig. 13.20 based on the describing function. The plant transfer function is given by Eq. (13.30).

Solution. Since we know that the transfer function and the reciprocal of the describing function will intersect on the negative real axis of the Nyquist plot, we can simplify matters by plotting $-1/N(A)$ and the magnitude of $G(e^{j\omega T})$ when $\angle G(e^{j\omega T}) = -180$, which is 5.814, as shown in Fig. 13.23. The quantization from using a 12-bit DAC over an output voltage range of ± 1.0 Volt, yields

$$q = \frac{2V}{2^{12}} = \frac{V}{2^{11}} = 0.00048828 \text{ V/lsb},$$

where V is the abbreviation for Volts, and lsb is the abbreviation for least significant bit. The intersection of the two curves predicts a stable limit cycle with an amplitude of essentially $q/2 = 0.000244$ and a period of roughly 10.8 seconds (0.1 Hz). Note that the limit cycle will always be in the range of 1 lsb peak to peak in amplitude for systems of reasonably high gain at the first 180 degree crossover frequency. It should also be clear that there is nothing the designer can do about the amplitude of the limit cycle short of getting a better (higher resolution) D/A converter. Moreover, since the crossover gain is usually determined by more important considerations such as closed-loop bandwidth, rise time, and root locations, the frequency of the quantization induced limit cycle may also be fixed. Fig. 13.24 shows the system transient response to zero input with an initial output error of 0.001 units. It is important to note that the large signal response of the system with quantization plotted in

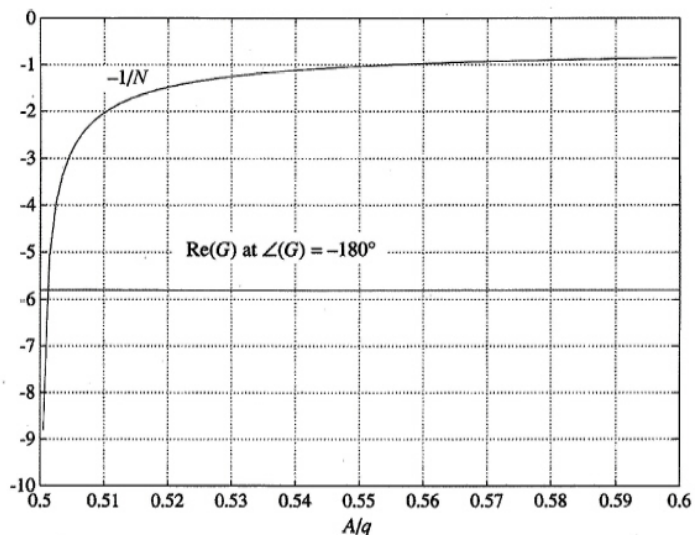


Figure 13.23
Plot of the negative reciprocal of the describing function intersecting with the plant gain at phase crossover

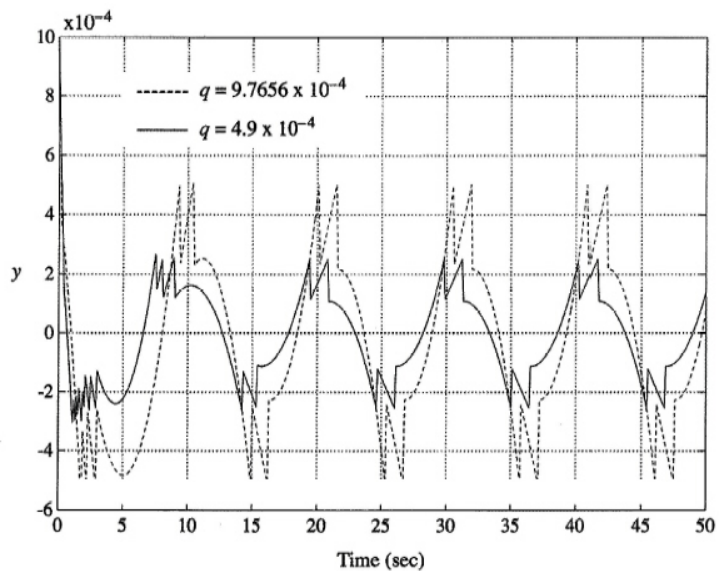


Figure 13.24
Small signal responses of the system of Fig. 13.20 with an 11 bit and a 12 bit quantizer, showing limit cycles

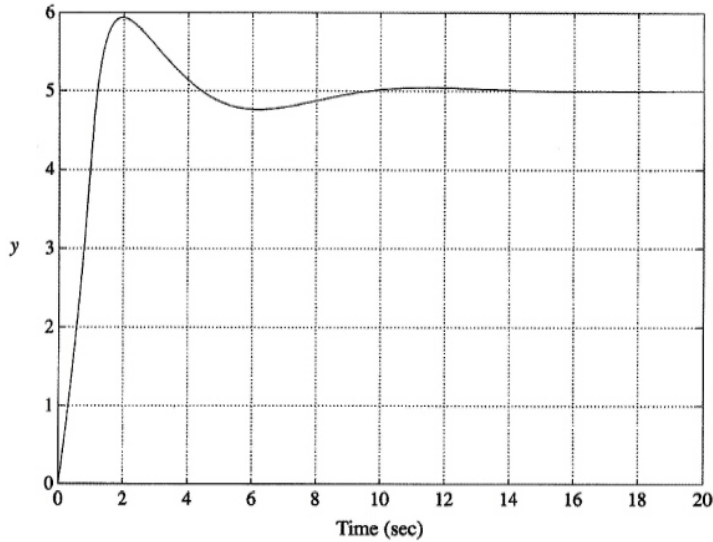


Figure 13.25
Response of the system of Fig. 13.20 with both saturation and quantization to a step of moderate size

Fig. 13.25 is again nearly identical to that of the unquantized system, indicating that analyzing the effect of the two nonlinearities separately was valid.

As a final note on stability analysis with describing functions, the nature of the intersection of $-1/N(A)$ and the open-loop transfer function $G(e^{j\omega T})$ can give information about the expected accuracy of the describing function analysis: nearly right angle crossings in the complex plane indicate a fairly high accuracy prediction. As the angle of intersection becomes smaller, higher degrees of uncertainty in the approximation are cause to suspect predicted limit cycles or instability. A simple sensitivity analysis explains the reason for uncertainty: The intersection point of lines which are nearly parallel will move large amounts along both lines for even minute changes in the position of either. In addition, the relative degree of uncertainty is dependent on the magnitude of higher harmonics (beyond fundamental component) in the output of the nonlinearity. Smaller harmonic content usually implies greater accuracy. Since the method of describing functions is an approximation of the nonlinearity, representing the output as a single gain and phase shifted version of a sinusoidal input, the accuracy of the method improves as the harmonic content in the output decreases. As such, plants with a low-pass frequency response tend to lend themselves to stability analysis using describing functions. Fortunately, most control systems, especially servomechanisms, have low-pass plants.

Furthermore, since describing functions utilize Fourier analysis, steady state sinusoidal conditions are implicitly assumed. Transient analysis is not facilitated with describing functions. However, the examples used in this section to illustrate stability analysis using describing functions employed step responses to excite the systems: better correlation between analysis and simulated responses could be attained using sinusoidal excitation of varying amplitude.

13.1.4 Equivalent Gains

The method of equivalent gains is another heuristic technique where a memoryless nonlinearity is replaced by an equivalent gain, and a root locus is done versus the equivalent gain. For a range of amplitudes the equivalent gain will take on a range of values, and the roots of the system are examined in this range as if the gain were fixed. For unstable roots, amplitudes will grow, and a new equivalent gain is examined. The process is repeated until a clear indication is obtained as to the ultimate system behavior. Before proceeding, it must be pointed out that although this analysis technique is *practical*, it is not by any means rigorous, and can be shown by counter-example to be false in some cases. First

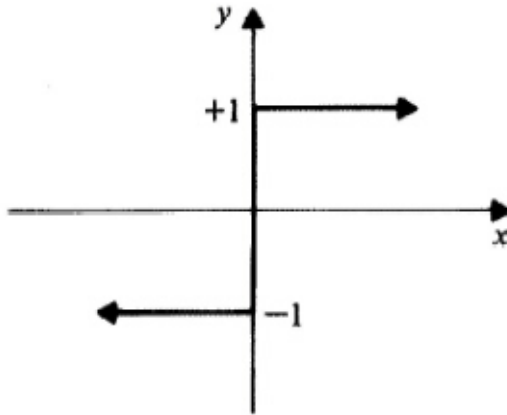


Figure 13.26
The characteristic
of the signum
function

we will begin by defining the sector condition for memoryless nonlinearities.

Sector Conditions

Suppose a function $\phi(x)$ has a scalar input and a scalar output. We say that $\phi(x)$ belongs to the sector $[k_1, k_2]$ if for all inputs x

$$k_1 x^2 \leq \phi(x)x \leq k_2 x^2.$$

In this definition k_1 or k_2 are allowed to be $-\infty$ or $+\infty$. Note that k_1 and k_2 *do not* necessarily represent the minimum and maximum *slopes* of the function $\phi(x)$. In most cases, they are smaller than the minimum and maximum slopes. The following three examples should help clarify how k_1 and k_2 are found.

Computation of a Sector

Example 13.11

What sector contains the signum function $y = \text{sgn}(x)$ shown in Fig. 13.26?

Solution. Since $\text{sgn}(0) = 0$, we know that the only line (through the origin) which bounds the signum function from above is the y -axis or a line through the origin with a slope of infinity. The line (through the origin) with the largest slope which bounds the signum function from below has a slope of 0. Therefore, we can say that the signum function is in sector $[0, \infty]$. In this case, k_1 and k_2 are the minimum and maximum slopes of the signum function.

The last example's signum function had a minimum and maximum slope which equaled its sector limits, which is not usual. Next, we will look at a more typical case.

Sector Analysis

Example 13.12

The transfer characteristic of an A/D converter that uses round-off is drawn in Fig. 13.27. If the A/D converter has unity gain, what sector is the transfer characteristic in?

Solution. The answer is computed by looking at the first part of the round-off function, a signum function of height q and a dead zone of $q/2$, as shown in Fig. 13.27. This signum with dead zone is bounded from above by a line with slope 2, and from below by a line with slope zero, thus the A/D has a transfer characteristic in sector $[0, 2]$.

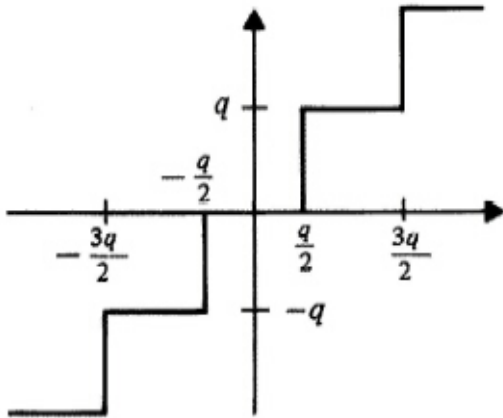


Figure 13.27
Transfer characteristic of the round-off A/D converter

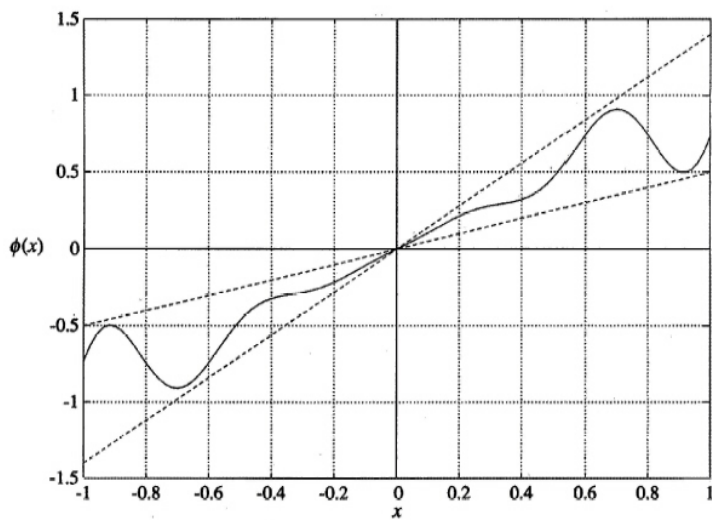


Figure 13.28
A general function contained in a simple sector

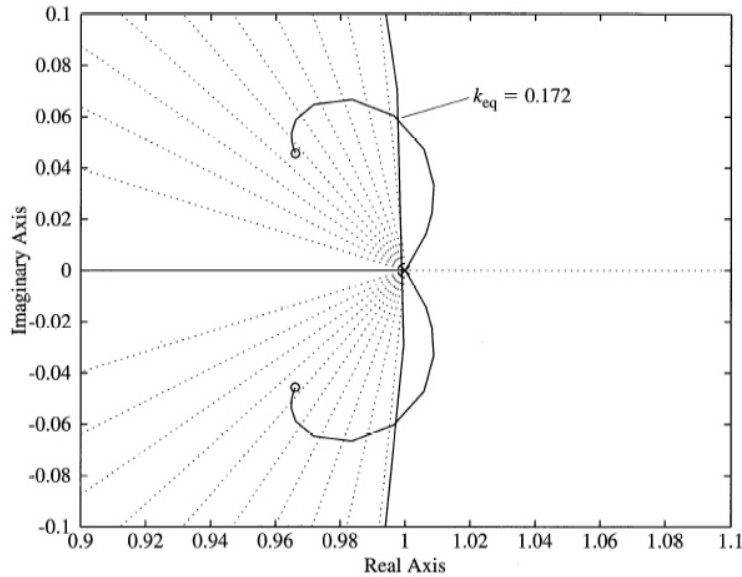


Figure 13.29
Root locus of the
system of
Fig. 13.20 as a
function of the
equivalent gain

A graphical example of a nonlinearity contained in the sector $(0.5, 1.4)$ is shown in Fig. 13.28. The minimum and maximum equivalent gains can be computed graphically from the figure by finding the sector which the function $\phi(x)$ is in. Two lines which bound the function $\phi(x)$ are shown in Fig. 13.28, one which bounds it from above (for positive x) with a slope of about 1.4, and the other with a slope of about 0.5 which bounds it from below. Since the function is symmetric we need only inspect the first and fourth quadrants of its graph. For asymmetric functions, all four quadrants must be considered. Sector conditions are used in many forms of stability analysis. When a function is in sector $[0, \infty]$, it is said to be *passive*. A function in sector $[k_1, \infty]$, with $k_1 > 0$, is said to be *strictly passive*. The quantizer of Example 13.13 is thus passive, whereas the function $\phi(x)$ shown in Fig. 13.28 is strictly passive.

Stability Analysis Using Equivalent Gains

Stability analysis using equivalent gains consists of replacing the nonlinearity in the analysis of the system with a linear gain which can range between k_1 and k_2 , and doing a stability analysis for the system at each point in the interval (k_1, k_2) .

Stability Based on a Variable Gain

Example 13.13

Consider the system of Example 13.8 of the last section and examine the stability by replacing the saturation characteristic with a variable gain.

Solution. For unsaturated signals the gain is one, and as the signal amplitude into the saturation function is increased, the gain decreases. The saturation function is in sector $[0, 1]$, thus the equivalent gain will range from one to zero as the signal gets larger and larger. The root locus of the system is examined in the range $0 \leq k_{eq} \leq 1$. Note that the input to the describing function must tend toward infinity to obtain an equivalent gain of zero ($k_{eq} = 0$) for the saturation function. Solving the characteristic equation

$$(z - 1)^3 + k_{eq}(0.3102z^2 - 0.5993z + 0.2902) = 0 \quad (13.33)$$

for root locations with k_{eq} in the interval $[0, 1]$ gives the root locus diagram of Fig. 13.29. It can be seen from Fig. 13.29 that when the input signal to the saturation block remains small (less than 1) the roots of the system are stable ($k_{eq} = 1$). However, as indicated by the describing function analysis, for equivalent gains less than 0.172 the system roots are unstable growing. From the describing function analysis of Example 13.8, growing signals

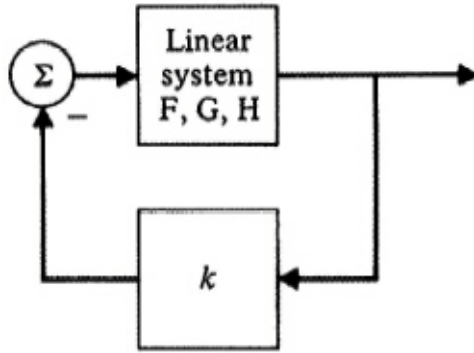


Figure 13.30
Block diagram of a linear system in series with a linear gain

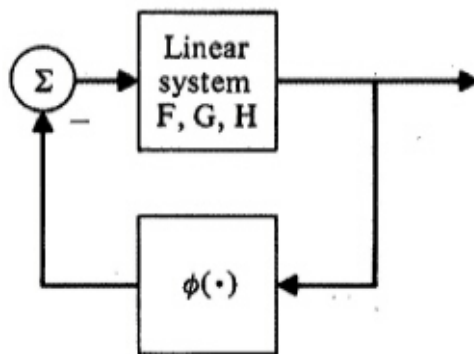


Figure 13.31
Block diagram of a linear system in series with a nonlinear sector function

cause smaller gain and move the roots further into the unstable region. We conclude that the system becomes unstable. With the describing function analysis we also predict the system will be unstable when the amplitude is such that the describing function gain will be 0.172. Thus for inputs or initial conditions large enough, the system will be unstable. Using the describing function method of stability analysis allows us to predict stability including limit cycle amplitude and frequency. Root locations can give an insight as to the frequency of the limit cycle as well, as in this case the roots move outside the unit circle at an angle of about 0.0095 radians, or about 0.095 Hz with a 10 Hz sampling rate.

The equivalent gains analysis and the describing function analysis yield equivalent results. If we take the equivalent gain to be the gain of the describing function, the results are the same and the amplitude of instability is predicted as before. Although equivalent to describing function analysis for nonlinearities whose describing function is real, the technique of equivalent gains is limited to nonlinearities in which there is no phase shift from input to output. Since this type of nonlinearity is common, the equivalent gains technique is a good one to remember.

13.1.5 Circle Criterion

In 1949, the Soviet scientist M. A. Aizermann put forth a rather famous conjecture: If a single-loop *continuous-time* feedback system shown in Fig. 13.30 with a linear forward path ($\{\mathbf{F}, \mathbf{G}, \mathbf{H}\}$) is stable for all linear fixed feedback gains k in the range $[\alpha, \beta]$, such that the resultant closed-loop system matrix $\mathbf{F} - \mathbf{G}\mathbf{H}k$ is stable, then the nonlinear system shown in Fig. 13.31, a combination of the same linear forward path and a memoryless nonlinear feedback term $\phi(\cdot)$ in sector $[\alpha, \beta]$, is also stable.

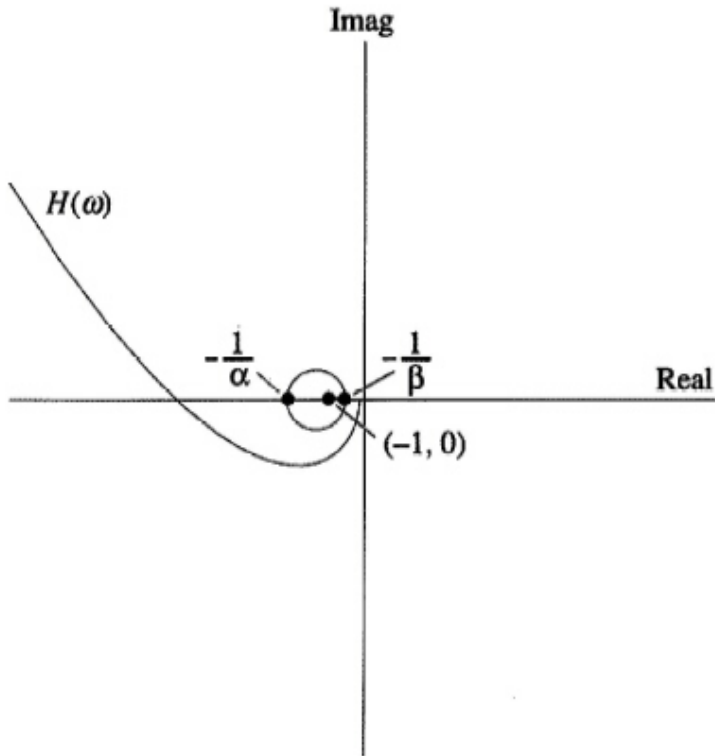


Figure 13.32
Nyquist diagram
with the stability
circle

Aizermann's conjecture is *false*. A variation of Aizermann's conjecture is true: The nonlinear system described is stable given that

1. $\phi(\cdot)$ lies in sector $[\alpha, \beta]$ where $0 < \alpha < \beta$ and
2. The Nyquist plot of the linear transfer function $H(\omega) = \mathbf{H}(e^{j\omega T} \mathbf{I} - \mathbf{F})^{-1} \mathbf{G}$ does not intersect or encircle the disk (or circle) which is centered on the real axis and passes through the points $(-1/\alpha, 0j)$ and $(-1/\beta, 0j)$ ($\alpha > 0$).

This result is known as the **Circle Theorem** or **Circle criterion** and is due to Sandberg and Zames. It can be very useful for proving the stability of nonlinear systems. These conditions are *sufficient* but not necessary because intersection of the transfer function $H(\omega)$ and the disk as defined does not prove instability.

Stability Based on the Circle Criterion

Example 13.14

Apply the circle criterion to the discrete-time system of Example 13.8, if the plant is in series with a nonlinearity as drawn in Fig. 13.28. Consider an enlarged sector, $(k_1, 1.4)$, and find the smallest value of k_1 for which the circle criterion will guarantee stability.

Solution. The Nyquist plot of the linear system transfer function is plotted in Fig. 13.32 along with circle defined according to the circle theorem for the nonlinear feedback function $\phi(\cdot)$ as given by Fig. 13.28. Since the graph of the transfer function $H(j\omega)$ ($= G(j\omega)$ in Example 13.10) does not intersect or encircle the disk passing through the points $(-2, 0j)$ and $(0.7143, 0j)$, the system is stable. If the function $\phi(\cdot)$ lies in sector $(k_1, 1.40)$, we can determine the minimum value of k_1 for which we can guarantee stability using the circle theorem by finding the largest circle passing through the points $(-1/k_1, 0j)$ and $(0.7143, 0j)$ that does not intersect the Nyquist plot of $G(z)$. As shown in Fig. 13.33, any value of $k_1 < 0.25$ causes the $G(z)$ plot to intersect the circle after which stability can no longer be guaranteed.

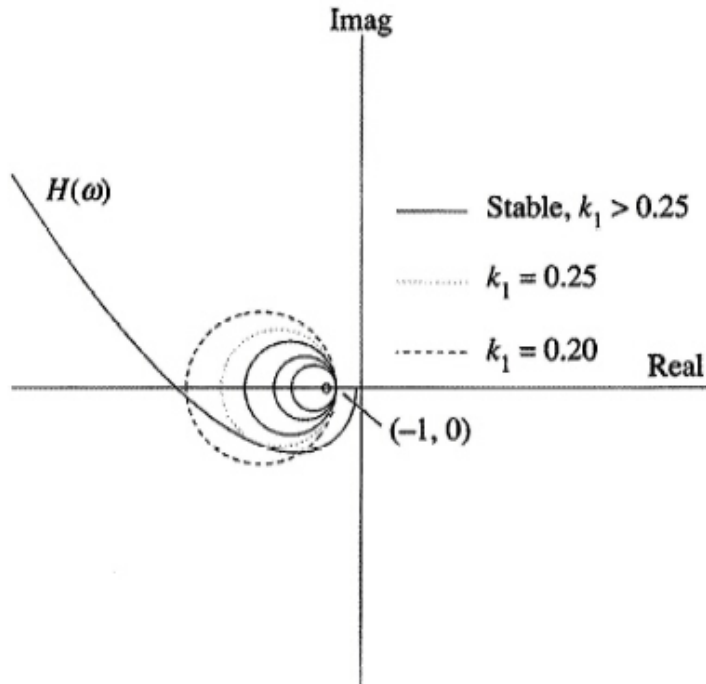


Figure 13.33
Circles defined for
varying values of
 k_1 , in
Example 13.14

The methods of equivalent gains and describing functions represent good techniques for gaining intuitive understanding of the performance of many nonlinear systems. The circle theorem is a rigorous technique which gives *sufficient* conditions for stability for systems having a single nonlinearity contained in a sector. Perhaps the most powerful approach to the study of stability of nonlinear systems is Lyapunov's second method.

13.1.6 Lyapunov's Second Method

Lyapunov's second method is a theoretical tool for analyzing the stability of nonlinear differential and difference equations. Lyapunov developed the theory to examine the stability of nonlinear differential equations. The work was presented to the control community in two papers by Kalman and Bertram who extended the theory to difference equations as found in discrete control systems. The most important feature of Lyapunov's second method is that it does not require the solutions of the system equations to be known, which is fortunate since, as noted earlier, solutions for nonlinear systems are rarely known. Although Lyapunov's second method does not require solving the system equations, it does require generation of a *Lyapunov function*, which, as we will see, can be very elusive.

The intuitive idea behind Lyapunov's second method is that a physical system can only store finite energy, and thus if we can show that energy is *always* being dissipated except at the equilibrium point, then the system must finally reach equilibrium when the energy is gone. The mathematical representation of the system "energy" is in the Lyapunov function. Since we are primarily dealing with discrete-time systems in this text,⁵ only the discrete-time definition of a Lyapunov function will be presented. $V(\mathbf{x})$ is a **Lyapunov function** for the system

$$\mathbf{x}(k+1) = \mathbf{f}(\mathbf{x}(k)) \quad \mathbf{f}(0) = 0 \quad (13.34)$$

if the following conditions hold ($V(\mathbf{x})$ is a scalar function):

⁵Although we consider continuous time plants, it is the stability of the overall discrete-time system we are interested in.

Lyapunov function

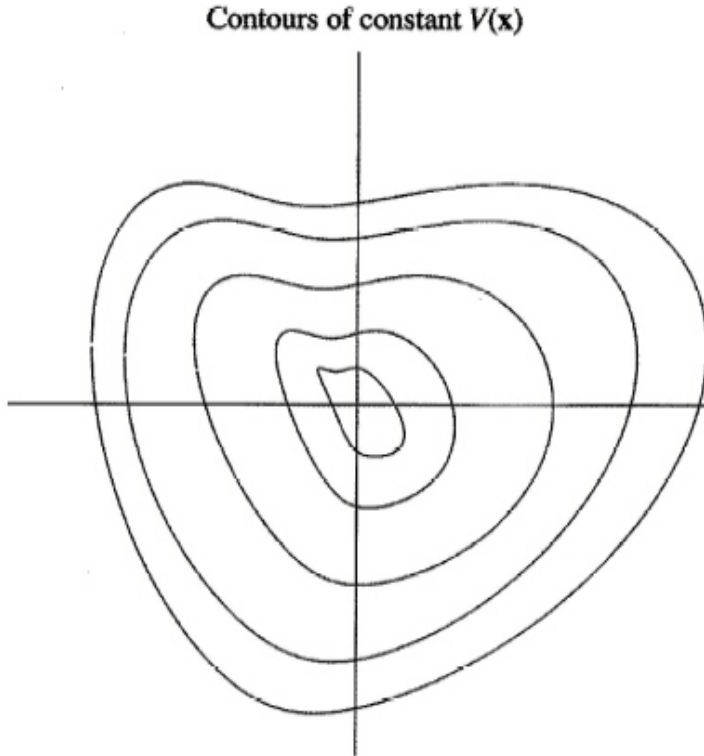


Figure 13.34
Contours of
 $V(x) = C_j$ for
several values of
 C_j

1. $V(\mathbf{x} = \mathbf{0}) = 0$, and $V(\mathbf{x})$ is continuous in \mathbf{x} .
2. $V(\mathbf{x})$ is positive definite, i.e. $V(\mathbf{x}) \geq 0$, with $V(\mathbf{x}) = 0$ only if $\mathbf{x} = \mathbf{0}$.
3. $\Delta V(\mathbf{x}) \triangleq V(\mathbf{f}(\mathbf{x})) - V(\mathbf{x})$ is negative definite, i.e., $V(\mathbf{f}(\mathbf{x})) - V(\mathbf{x}) \leq 0$ with $\Delta V(\mathbf{x}) = 0$ only if $\mathbf{x} = \mathbf{0}$.

Lyapunov's main theorem is that the equilibrium solution $\mathbf{x}(k) = \mathbf{0}$ for the system given by Eq. (13.34) is asymptotically stable (note that the system is not being forced) if there exists a Lyapunov function in \mathbf{x} . For *global* asymptotic stability, we need the additional condition

$$0 < \phi(\|\mathbf{x}\|) < V(\mathbf{x}) \quad (13.35)$$

where ϕ is any function of the norm of \mathbf{x} , such that

$$\lim_{\|\mathbf{x}\| \rightarrow \infty} \phi(\|\mathbf{x}\|) = \infty.$$

The stability result can be explained as follows: lines of constant $V(\mathbf{x})$ form closed regions around the point $\mathbf{x} = \mathbf{0}$ as shown in Fig. 13.34, and on those lines, the state trajectory will always move *into* the region. Since these regions approach the point $\mathbf{x} = \mathbf{0}$, the system state must come to rest at this point. Another way of looking at the Lyapunov function is as a nonlinear “meter” of size. The meter monitors all of the system states through what may be a highly nonlinear function and the meter indicates a monotonically decreasing value as a function of time. Since the system is known to be at rest when the Lyapunov function is zero, we know that the system will eventually be at rest when the meter reads zero.

A serious difficulty of this analysis technique is in finding a Lyapunov function for a given system. One common approach is to try to use an energy function for the system. If Eq. (13.34) represents a

physical system where energy must be lost with time, the energy function is a good candidate. While finding Lyapunov functions for continuous-time nonlinear systems is often very difficult, finding them for discrete-time nonlinear systems is even more challenging. It is at this point that most texts now show that a Lyapunov function of the form $V(\mathbf{x}) = \mathbf{x}^T P \mathbf{x}$ can be used to prove stability of a linear system. However, for the stability of a linear system it is much easier to solve for the location of the system poles. An example of the application of Lyapunov's second method to proving stability of a discrete-time system is cited in Section 13.3.2, but the derivation is quite complex. In addition to stability tests, Lyapunov theory can be an aid to the designer for choosing control alternatives for nonlinear systems by finding a control law which yields a Lyapunov function for the system.

Stability Based on a Lyapunov Function

Example 13.15

Use Lyapunov's second method to prove that the LQR design procedure derived in Chapter 9 always yields a stable system.

Solution. From the LQR design of Chapter 9 the steady state solution to the Riccati equation yields the following control law

$$u_k = -\mathbf{K}\mathbf{x} = -(\mathbf{Q}_2 + \mathbf{\Gamma}^T \mathbf{S}_\infty \mathbf{\Gamma})^{-1} \mathbf{\Gamma}^T \mathbf{S}_\infty \mathbf{\Phi} \mathbf{x}. \quad (13.36)$$

The problem is to prove using Lyapunov's second method that \mathbf{K} as defined above yields an asymptotically stable system

$$\mathbf{x}_{k+1} = (\mathbf{\Phi} - \mathbf{\Gamma} \mathbf{K}) \mathbf{x}_k. \quad (13.37)$$

Since the cost of this control is $\mathcal{J} = \mathbf{x}^T \mathbf{S}_\infty \mathbf{x} > 0$, we propose a Lyapunov function of

$$V(\mathbf{x}_k) = \mathbf{x}^T \mathbf{S}_\infty \mathbf{x}, \quad (13.38)$$

and thus we need to show $\Delta V(\mathbf{x})$ is negative definite (we already know \mathbf{S}_∞ is positive definite). Proceeding, we have

$$\begin{aligned} \Delta V(x) &= \mathbf{x}_{k+1}^T \mathbf{S}_\infty \mathbf{x}_{k+1} - \mathbf{x}_k^T \mathbf{S}_\infty \mathbf{x}_k \\ &= \mathbf{x}_k^T [\mathbf{\Phi} - \mathbf{\Gamma} \mathbf{K}]^T \mathbf{S}_\infty [\mathbf{\Phi} - \mathbf{\Gamma} \mathbf{K}] \mathbf{x}_k - \mathbf{x}_k^T \mathbf{S}_\infty \mathbf{x}_k \\ &= -\mathbf{x}_k^T [\mathbf{Q}_1 + \mathbf{K}^T \mathbf{Q}_2 \mathbf{K}] \mathbf{x}_k, \end{aligned}$$

where the steady state solution to the Riccati equation \mathbf{S}_∞ has been substituted into the Riccati equation to complete the last step, namely,

$$\mathbf{S}_\infty = [\mathbf{\Phi} - \mathbf{\Gamma} \mathbf{K}]^T \mathbf{S}_\infty [\mathbf{\Phi} - \mathbf{\Gamma} \mathbf{K}] + \mathbf{Q}_1 + \mathbf{K}^T \mathbf{Q}_2 \mathbf{K}. \quad (13.39)$$

Because $[\mathbf{Q}_1 + \mathbf{K}^T \mathbf{Q}_2 \mathbf{K}]$ is positive definite, $\Delta V(\mathbf{x})$ is negative definite and thus the closed-loop LQR controller is asymptotically stable.

13.2 Nonlinear Control Structures: Design

In the previous section we covered tools and techniques for the analysis and simulation of control systems containing nonlinearities. In this section, we will discuss the deliberate *introduction* of nonlinearities into the controller for performance which is improved over that of a simpler linear controller.

13.2.1 Large Signal Linearization: Inverse Nonlinearities

The simplest case of the introduction of nonlinearities into a control design is that of **inverse nonlinearities**. It is sometimes the case that a nonlinearity is reversible and can be undone. For example suppose the plant has an output that is measured by an optical sensor whose output is proportional to the square of the signal to be measured. Let the measurement y be given by $y = x_1^2$ where the state x_1 is generated by a linear system and is known to be always positive. A regulator could be designed

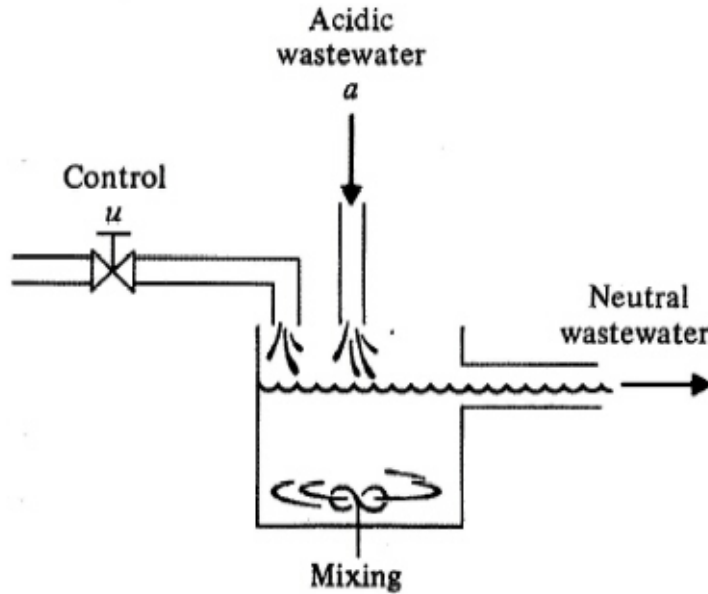


Figure 13.35
Schematic
diagram of a
wastewater
treatment system

with reasonable accuracy assuming that the excursions of the measured variable were kept rather small using the technique of linearization. A set point servomechanism for this system that required significant dynamic range would present the designer with serious difficulties however due to the nonlinearity. One fairly obvious technique would therefore be to undo the nonlinearity in the controller, i.e., control \sqrt{y} instead of y , thus turning the difficult design into a much simpler linear design. One of the most important features of digital control is that many functions such as the square root are now *easy* to perform, and given enough calculation time, perhaps very close to free. Significant improvements can be gained from the application of the inverse nonlinearities technique. Sometimes referred to as **linearizing control** or **large signal linearization**, the following are examples of what we shall refer to as inverse nonlinearity control, or INL control.

We will consider the treatment of acidic wastewater from a processing plant, the schematic for which is shown in Fig. 13.35. The objective is to add a base solution to the wastewater to neutralize the pH of the effluent. The acid and the base form a relatively harmless salt which will not harm the environment.

The model for this example is that of McAvoy, Hsu, and Lowenthal (1972), and Goodwin and Sin (1985). We start by defining the output of the system y as

$$y \triangleq [H^+] - [OH^-], \quad (13.40)$$

which is the concentration difference from neutrality. The objective is to control the output y of the system, with the nominal set point being $r = y = 0$ in the steady state. The actual measurement for this system is the pH, $\triangleq p$, of the effluent. The relationship between the measurement $p(t)$ and the variable y that we wish to control is given by

$$y = 10^{-p} - 10^p K_w, \quad (13.41)$$

where K_w is the equilibrium constant of water ($\approx 10^{-14}$ gram-ion/liter). Equation 13.41 can be derived with the following relationships $[OH^-][H^+] = K_w$ and $p = -\log[H^+]$. It is important to note that the first powerful advantage of using digital control in this case is in being able to transform the pH output measurement p into the variable we wish to control y , our first application of inverse nonlinearity. The model of the process is given by

$$V\dot{y} = F(a - y) - u(b + y), \quad (13.42)$$

Table 13.2

Parameter	Value	Units
a	0.001	moles/L
b	0.001	moles/L
F	0.100	L/sec
V	2.00	L
T	10.0	sec

where

- V = volume of the mixing tank [liters]
- F = rate of acid flow [liters/sec]
- a = concentration of the acid [gram-ions/liter]
- b = concentration of the base [gram-ions/liter]
- u = flow rate of the base (our control variable) [liters/sec]

Suppose that all of the parameters are fixed and known (we will examine aspects of this later). The initial objective is to build a regulator for the system given by Eq. (13.42). Before we propose a control structure, we need to examine the model and decide on some basic performance objectives.

The system of Eq. (13.42) is **bilinear**: The input is multiplied by the output

$$V\dot{y} = Fa - Fy - ub + uy.$$

As a first approach let us apply linearization to this system. To linearize, we must first define the nominal operating point

$$\begin{aligned} p_{nom} &= 7.00 \quad (\text{neutral}) \\ \Rightarrow y &= 0 \\ \dot{y} &= 0. \end{aligned}$$

We can calculate the nominal or steady state control input required by setting $y = 0$, and $\dot{y} = 0$ in Eq. (13.42), and solving for required u , $u = Fa/b$. As before, we take partial derivatives at the operating point to obtain

$$V\dot{y} = Fa - (F + Fa/b)y - bu. \quad (13.43)$$

This linearized model is a simple, stable, first-order system with a bias input Fa/b and a negative control gain. Any uncertainty in the bias input which can be approximately cancelled with feed forward would lead to a steady state regulator error. This provides us with the opportunity to employ an integral controller. Our fundamental performance objective is to set the time response of the system so that linear transients will die out in about 200 seconds. For this magnitude of time constant, a 10-second sample period ($T = 10.0$) should be more than sufficient (and as we shall see, provides plenty of time to calculate the control even with the most inexpensive control or signal processors). For illustrative purposes we will use the process constants defined in Table 13.2.

This yields the discrete time system given by Eq. (13.44)

$$y_{k+1} = 0.3679y_k - 0.00315u_k + 3.161 \times 10^{-5}d_k, \quad (13.44)$$

where d_k specifies a disturbance input with a nominal value of one (1.0) in units of Fa . To design an integral controller, we augment the order of the system by defining a new state w as

$$w_{k+1} = w_k + (y_r(k) - y(k))T, \quad (13.45)$$

which is simply the scaled integral of the command-response error. As pointed out in Chapter 8, the input command can be introduced in the process of state feedback into the control. The new discrete

time plant model is thus

$$\begin{bmatrix} y_{k+1} \\ w_{k+1} \end{bmatrix} = \begin{bmatrix} 0.3679 & 0 \\ -10.0 & 1 \end{bmatrix} \begin{bmatrix} y_k \\ w_k \end{bmatrix} + \begin{bmatrix} -0.00315 \\ 0 \end{bmatrix} u_k + \begin{bmatrix} 3.161 \times 10^{-5} \\ 0 \end{bmatrix} d_k + \begin{bmatrix} 0 \\ 10 \end{bmatrix} y_r(k), \quad (13.46)$$

for which we must design a control law. Given that the system is linearized we can just employ the techniques of Chapter 8 to place the system poles at desired locations. Computing the feedback gains given the pole locations is easy, the question is where should we place the poles? There are several ways to proceed, but we will take a short cut and place the poles according to the basics developed in Chapter 7 to achieve a rise time for the linear controller of 200 seconds. With $t_r = 200.0$ and a desired damping ratio ζ of about 0.7, the poles z_r should be placed approximately at

$$\mathbf{z}_r = \begin{bmatrix} 0.93706 + 0.06034j \\ 0.93706 - 0.06034j \end{bmatrix}, \quad (13.47)$$

using the following relationships: $\omega_d \approx \frac{1.8}{t_r}$ for rise time defined by 10% to 90% of unit step response, and

$$\begin{aligned} r &= e^{-\omega_d T \zeta} \\ \theta &= \omega_d T \sqrt{1 - \zeta^2}, \end{aligned}$$

where z_r is given by $re^{\pm j\theta}$. Using the `place` command, the feedback gains \mathbf{K} are found to be

$$\mathbf{K} = [160.70 \quad 0.24133]. \quad (13.48)$$

Starting from rest (steady state) at $y = 0.0001$, the responses of the linear controller with the linearized plant model as well as the linearly controlled nonlinear plant model are shown superimposed in Fig. 13.36. Note that the step response of the real system (nonlinear plant model) is degraded over that of the intended design (much slower).

Before proceeding it is important to discuss valve nonlinearity. A valve can only be fully open, fully closed, or somewhere in between. Thus the control u can only be positive (we cannot extract base solution from the mixing tank), and the maximum flow rate of the base is 2.0 liters per second. Hence our control is calculated as follows

$$u_k = \begin{cases} 0 & -\mathbf{K}\mathbf{x}_k < 0 \\ -\mathbf{K}\mathbf{x}_k & 0 < -\mathbf{K}\mathbf{x}_k < 2 \\ 2 & -\mathbf{K}\mathbf{x}_k > 2. \end{cases} \quad (13.49)$$

The stability analysis techniques of the previous section could be used to examine the effect of Eq. (13.49) on the INL controller. It would also be an interesting exercise to derive the effects of quantization on the measurement of p . Nonlinear functions will give sometimes unexpected or strange results when their arguments are quantized. These effects usually can be bounded by analysis and then simulated to verify performance.

We have already used inverse nonlinearity in the design by applying Eq. (13.41) to p to obtain the plant output y . Essentially we compensated for a nonlinearity in the output sensor. Next we wish to apply a linearizing technique to the control law which undoes the nonlinearity of the plant (in contrast to that of the measurement device). There is no exact way to do this except in rare cases where the nonlinearity does not appear in the continuous differential equation models of the plant. The state space description of the plant can be written as follows

$$V\dot{y} = -F(1+u)y + ub + Fa,$$

where the term $(1+u)$ can be taken as a variable coefficient in an otherwise linear differential equation. This system can be discretized for various values of u because in between sample times the

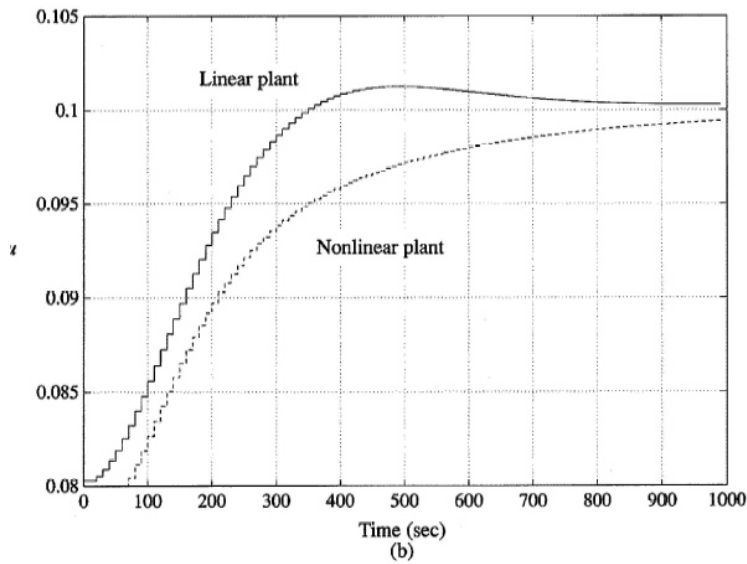
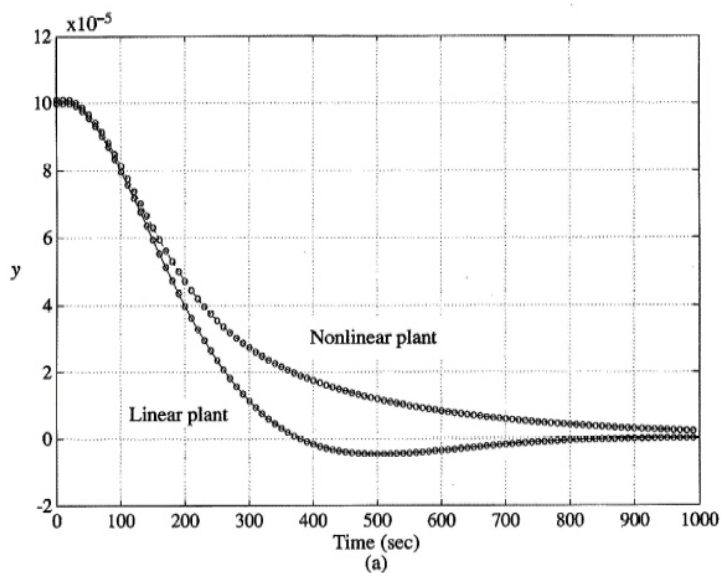


Figure 13.36
Response of the linear controller on both the linearized plant model and the true bilinear plant

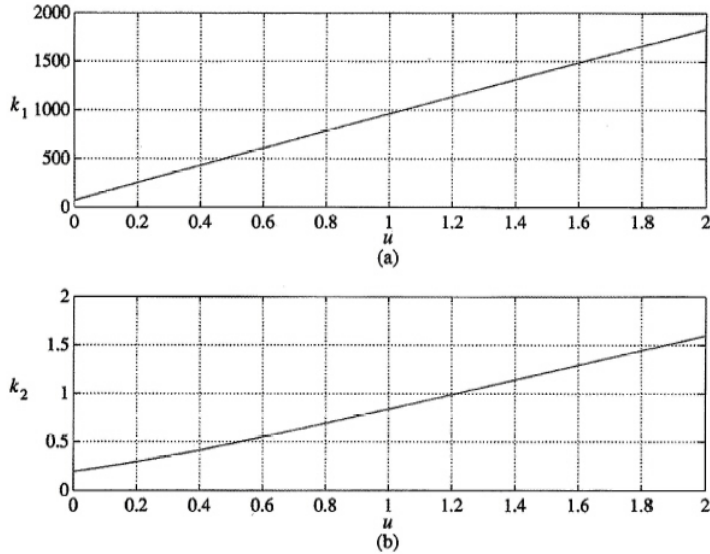


Figure 13.37 Control gains as a function of admissible control values. The value of the previous control u_{k-1} is used to determine the control gains used in calculating u_k

value of u is held constant. Thus it is possible to describe the system's behavior accurately from one sample to the next by using a discrete model which is a function of the applied control. The delayed control will be used to make the algorithm practical as we can't use the current value of the control to calculate the control gains, hence there is some error in our method. Essentially the INL control keeps the system matrix

$$\Phi_{\text{sys}} = \Phi_{ol}(u) - \Gamma_u(u)\mathbf{K}(u)$$

constant as a function of u . When the nonlinearity of the plant causes $\Phi_{ol}(u)$ to vary with u , the control gain $\mathbf{K}(u)$ is changed with a nonlinear control algorithm to make Φ_{sys} a constant matrix. Applying this technique is fairly simple: the state transition matrix is calculated for points u in $[0, 2]$, the feedback gains are then calculated as shown in Fig. 13.37, and then they are stored in a table from which the actual gains are interpolated during operation.

Fig. 13.38 shows a comparison between the linearized plant, constant \mathbf{K} , system response and the real nonlinear plant but using the INL (inverse nonlinearity) control algorithm. The INL controller gives an equivalent response much closer to the design target (linear control of idealized linear plant) as can be seen.

One point which must be made clear however is that the INL controlled system as just described contained several approximations. This means that although the results may look great in simulation, the potential exists for unexpected behavior because we have not shown that the system is stable under all conditions.⁶ Correlated and uncorrelated noise and modeling errors would have to be examined carefully to insure that the system continued to perform as intended. In this case, Fig. 13.39 shows the effects of process noise in the control input to the plant. Under many different examinations this INL controller produced excellent results, mainly because the control u_{k-1} is always a good approximation to u_k .

If the measurement for y is noisy and we use a state estimator, the model of the plant used in the estimator can be the nonlinear model as derived above, making the estimator much closer to the real plant than a linear model would be. Just as in the case of the control (without the delay), the estimator gain L (a scaler) would be a function of u so as to make the state transition matrix a constant value.

Another example will be given illustrating both INL in the controller as well as the state estimator. Figure 13.40 depicts the block diagram of an actuator consisting of a torque motor driven by a current source. We assume that the current source has limited output magnitude but that its voltage does not

⁶The issue is the approximation of the current control u_k as u_{k-1} . If the closed-loop system equations were totally linear including INL control, linear analysis can obviously prove stability despite how many nonlinear tricks were employed to make them linear.

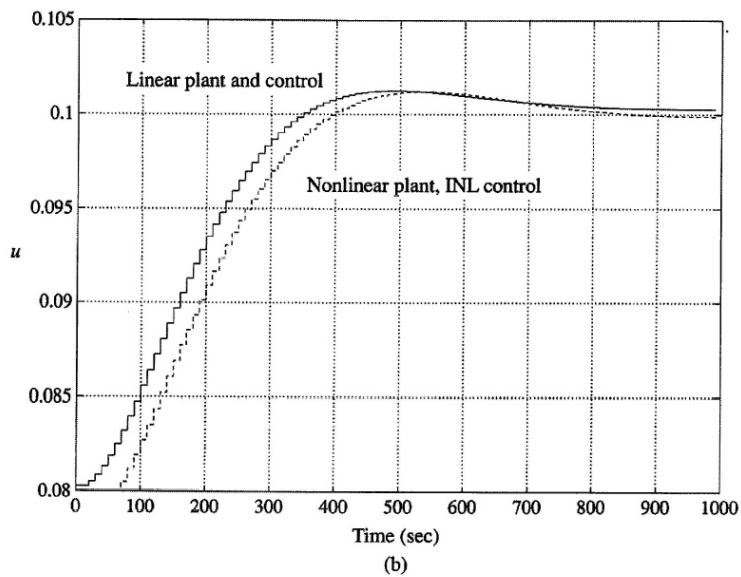
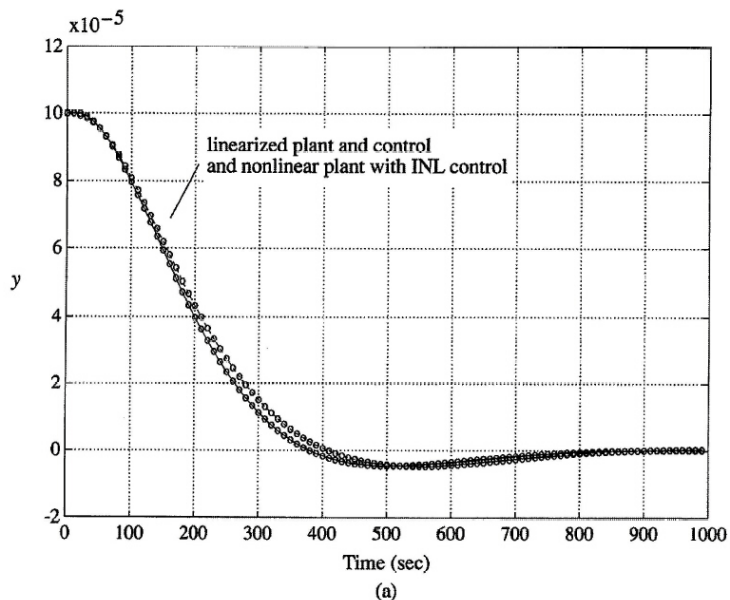
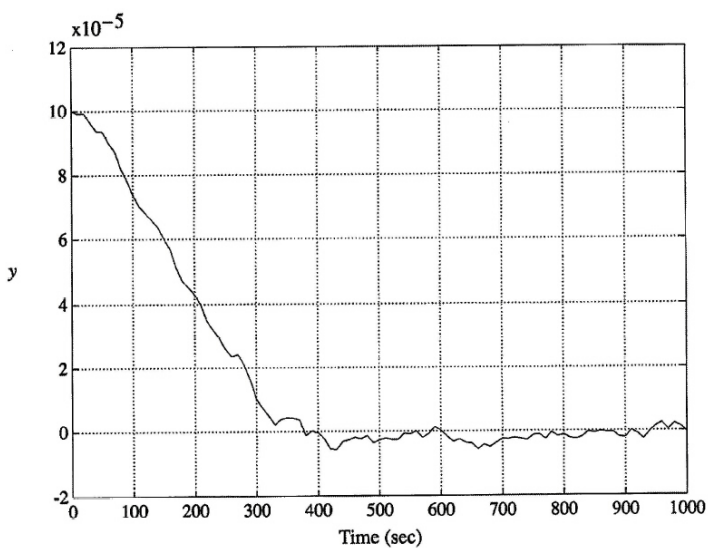
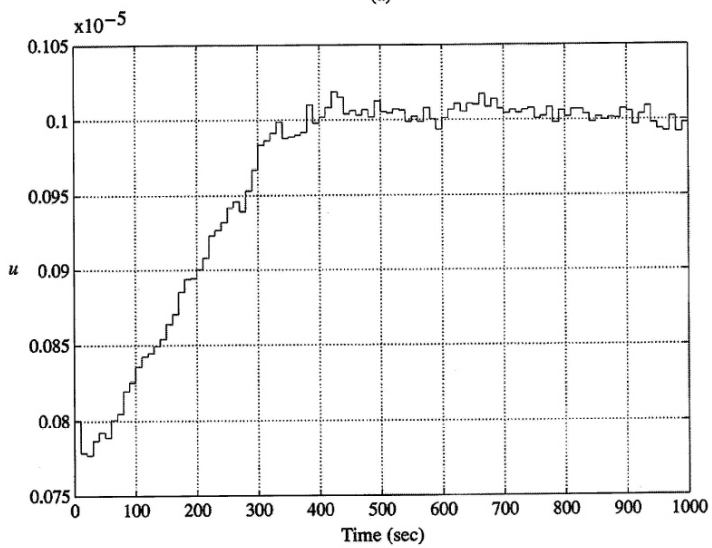


Figure 13.38 Comparison of linear control on linearized plant versus INL control on true nonlinear plant, showing that the INL control makes the overall system behave much like the idealized linear one



(a)



(b)

Figure 13.39
System operation in the presence of measurement noise (a) output response (b) control effort

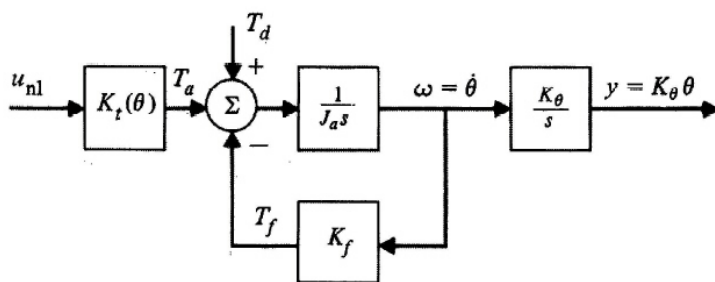


Figure 13.40
Block diagram of rotary actuator model for example of INL controllers. The control u_{nl} is from a unity gain power amplifier (configured as a current source) driven by a D/A converter

Table 13.3

Rotary actuator parameters. Note that the range of values for y will be K_θ times as large as that for θ

Parameter	Value	Units
$ \theta $	≤ 0.2	rad
$ u_{nl} $	≤ 1.0	amps
K_{t0}	-7.00	-
K_{t1}	8.00	-
K_{tnom}	0.3	N-m-amp ⁻¹
J_a	0.00012	N-m-rad ⁻¹
K_θ	1000	mrad-rad ⁻¹
K_f	0.001	N-sec

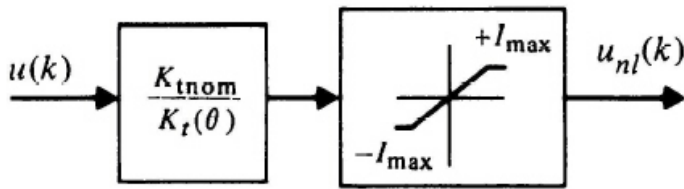


Figure 13.41
Calculation of the control which linearizes the plant. Note that the limited control authority $|u| \leq u_{\max} = I_{\max}$ is a model of the power amplifier

saturate. The applied control u_{nl} is from a D/A converter and is in units of armature current. It is the armature current command actually applied to the motor to produce a torque $T_a = u_{nl}K_t(\theta)$. The torque factor $K_t(\theta)$ is given by

$$K_t(\theta) = K_{tnom}(K_{t0} + K_{t1} \cos \theta), \quad (13.50)$$

which is nonlinear due to variation in the flux density along the magnetic gap of the motor. Table 13.3 contains the nominal motor parameters for the model of Fig. 13.40 and the definition of $K_t(\theta)$ given above. A linearized design would start with the assumption that

$$K_t = K_{tnom}(K_{t0} + K_{t1} \cos \theta_{nom})$$

is a constant in the neighborhood of the nominal angle of operation θ_{nom} . However, with the values given in Table 13.3 the torque factor varies 16% over the range of angles assumed by the servo, and thus using INL control and nonlinear estimation will prove advantageous.

The first step will be to undo the varying torque factor of the actuator as described by Eq. (13.50) and depicted in Fig. 13.41. Here again the method of table look-up will be employed to calculate the applied control as a function of the computed control, u , by the formula

$$\begin{aligned} u_{nl} &= I_{\max} \text{sat} \left(\frac{u K_{tnom}}{I_{\max} K_t(\theta)} \right) \\ &= I_{\max} \text{sat} \left(\frac{u}{I_{\max} \overline{K_t}(\theta)} \right), \end{aligned} \quad (13.51)$$

where $K_t(\theta) = K_{t0} + K_{t1} \cos(\theta)$. The computed control u defined in the usual sense of state feedback with a reference command input as $u \triangleq \mathbf{K}(y_r \mathbf{\Gamma}_{yr} - \hat{\mathbf{x}})$ where $\mathbf{\Gamma}_{yr}$ will be defined shortly. The nonlinear control u_{nl} is computed with the variable portion of $\mathbf{K}_r(\theta)$, *i.e.*, the nominal torque constant K_{tnom} is still effectively in the forward path.

By calculating the control this way the overall nonlinearity and plant combined will behave as if the plant were linear from input u as long as the current source is unsaturated. The control u we will use will be based on linear estimated state feedback. Before we can formulate the control we must estimate the unmeasured states.

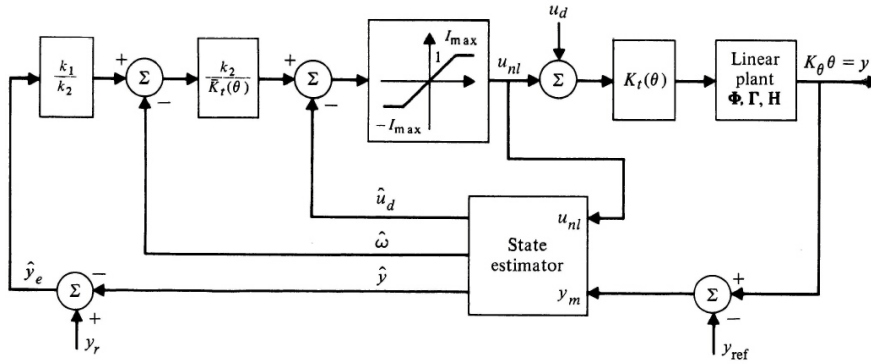


Figure 13.42
Block diagram of
the rotary
actuator
positioning
servomechanism
with an estimator

Both the rotational velocity ω and the disturbance input T_d are not measured and hence must be estimated. Since it is the control u which will be used to compensate for the effect of the disturbance torque T_d , we will estimate the bias torque along the lines discussed in Section 8.6.2, and call it u_d , or control disturbance. Estimating u_d will provide benefits as we shall see. In addition, we will estimate the measured variable, y , as well to provide some noise immunity at high frequencies. Thus the state of the estimator is

$$\hat{\mathbf{x}}(k) \triangleq (\hat{y} \quad \hat{\omega} \quad \hat{u}_d)^T.$$

If it were not for the saturation function in the current source we could assume a linear model for the plant (torque factor K_{tnom}) from the input u . However when the current source saturates the output model should include the estimated torque factor variation $K_t(\hat{y}/K_\theta)$. Thus we will build an estimator with the input u_{nl} and the variable torque factor. The complete system is shown in Fig. 13.42.

The complete state-space description of this system is comprised of a second-order plant model and a third-order estimator model. The uncontrollable input u_d is modeled as a state in the estimator so that the effect of the input can be accounted for in the model. Since it is uncontrollable, there is no sense in including it in the plant model, which is given by

$$\mathbf{F} = \begin{bmatrix} 0 & K_\theta \\ 0 & -K_f/J_a \end{bmatrix} \quad (13.52)$$

$$\mathbf{G} = [0 \quad K_{\text{tnom}}/J_a]^T \quad (13.53)$$

$$\mathbf{H} = [1 \quad 0], \quad (13.54)$$

with the plant state $[y \ \omega]^T$. The discrete time plant model is thus

$$\Phi = \begin{bmatrix} 1 & 0.1 \\ 0 & 1 \end{bmatrix} \quad (13.55)$$

$$\Gamma = [0.0125 \quad 0.25]^T, \quad (13.56)$$

using $T = 0.0001$ seconds. For the state estimator we will augment the state with the unknown bias input estimate \hat{u}_d so the estimator state is $\hat{\mathbf{x}} = [\hat{y} \ \hat{\omega} \ \hat{u}_d]^T$. Thus we have

$$\Phi_e = \begin{bmatrix} 1.0 & 0.1 & 0.0125 \\ 0 & 1.0 & 0.25 \\ 0 & 0 & 1.0 \end{bmatrix} \quad (13.57)$$

$$\Gamma_e = [0.0125 \quad 0.25 \quad 0]^T \quad (13.58)$$

$$\mathbf{H}_e = [1 \quad 0 \quad 0]. \quad (13.59)$$

Since \hat{u}_d is just the negative of the required steady state control, negative feedback of \hat{u}_d forms an integrator. Since the integrator output is saturated in software before being output to the DAC, this

structure constitutes an ideal **zero wind-up error integrator**. Note that the following must hold in the steady state

$$\mathcal{E}\{y - \hat{y}\} = 0,$$

where $\mathcal{E}\{(\cdot)\}$ is read “expected value of (\cdot) ”. Furthermore,

$$\mathcal{E}\{\hat{\omega}\} = 0 \quad \text{and} \quad \mathcal{E}\{u\} = -u_d,$$

which implies

$$\mathcal{E}\{k_1(y_r - y) - k_2\hat{\omega}\} = 0,$$

hence,

$$\mathcal{E}\{y_r - y\} = 0.$$

As long as $|u_d| < u_{\max}$, the positioning error is forced to a mean value of zero despite the value of u_d .

The equations representing this system, using a current estimator to minimize control delay, are

$$\begin{aligned} \hat{\mathbf{x}}_{k+1} &= \Phi_e \hat{\mathbf{x}}_k + \Gamma_e u_k + L_c y_{k+1} - L_c \mathbf{H}_e \bar{x}_{k+1} \\ &= \Phi_e \hat{\mathbf{x}}_k + \Gamma_e u_k + L_c y_{k+1} - L_c \mathbf{H}_e \Phi_e \hat{\mathbf{x}}_k - L_c \mathbf{H}_e \Gamma_e u_k \\ \hat{x}_{k+1} &= (\Phi_e - L_c \mathbf{H}_e \Phi_e) \hat{x}_k + (\Gamma_e - L_c \mathbf{H}_e \Gamma_e) u_k + L_c y_{k+1}. \end{aligned}$$

Defining $\mathbf{x}i \triangleq \hat{\mathbf{x}}_k - L_c y$, $\Gamma_{y_r} = \mathbf{H}_e^T$, $\mathbf{M} = (\mathbf{I} - L_c \mathbf{H}_e)$, and a control

$$u = \mathbf{K}(y_r \Gamma_{y_r} - \hat{\mathbf{x}}),$$

we can derive

$$\mathbf{x}i_{k+1} = \mathbf{M}(\Phi_e - \Gamma_e \mathbf{K}) \mathbf{x}i_k + \mathbf{M}(\Phi_e L_c \mathbf{H} - \Gamma_e \mathbf{K} L_c \mathbf{H}) x_k + \mathbf{M} \Gamma_e \mathbf{K} \Gamma_{y_r} y_r \quad (13.60)$$

for the state estimator, and the state equations governing the plant are

$$\mathbf{x}_{k+1} = (\Phi - \Gamma \mathbf{K} L_c \mathbf{H}) \mathbf{x}_k - \Gamma \mathbf{K} \mathbf{x}i + \Gamma \mathbf{K} \Gamma_{y_r} y_r(k). \quad (13.61)$$

Define $\mathbf{x}_s^T \triangleq [x^T \ \xi^T]$ and the complete closed loop system by the state equations

$$\mathbf{x}_s(k+1) = \Phi_s \mathbf{x}_s(k) + \Gamma_s y_r(k), \quad (13.62)$$

and the system output

$$y = \mathbf{H}_s \mathbf{x}_s, \quad (13.63)$$

where $\mathbf{H}_s = [1 \ 0 \ 0 \ 0 \ 0]$. Thus the complete system is of fifth order, and the closed-loop system matrices are given by

$$\Phi_s = \begin{bmatrix} \Phi - \Gamma \mathbf{K} L_c \mathbf{H} & -\Gamma \mathbf{K} \\ \mathbf{M}(\Phi_e L_c \mathbf{H} - \Gamma_e \mathbf{K} L_c \mathbf{H}) & \mathbf{M}(\Phi_e - \Gamma \mathbf{K}) \end{bmatrix}, \quad (13.64)$$

and

$$\Gamma_s = \begin{bmatrix} \Gamma \mathbf{K} \Gamma_{y_r} \\ \mathbf{M} \Gamma_e \mathbf{K} \Gamma_{y_r} \end{bmatrix}. \quad (13.65)$$

If we subtracted a plant output reference signal y_{ref} from the output before the plant output measurement

$$y_m \triangleq y - y_{ref},$$

the estimator position input would then be y_m instead of y . The reference input y_{ref} would add to the system state equations through an input matrix $\Gamma_{y_{ref}}$, adding an additional term to Eq. (13.62) of

$$\Gamma_{y_{ref}} y_{ref} = \begin{bmatrix} \Gamma \mathbf{K} L_c \\ \mathbf{M}(\Gamma_e \mathbf{K} - \Phi_e) L_c \end{bmatrix} y_{ref}. \quad (13.66)$$

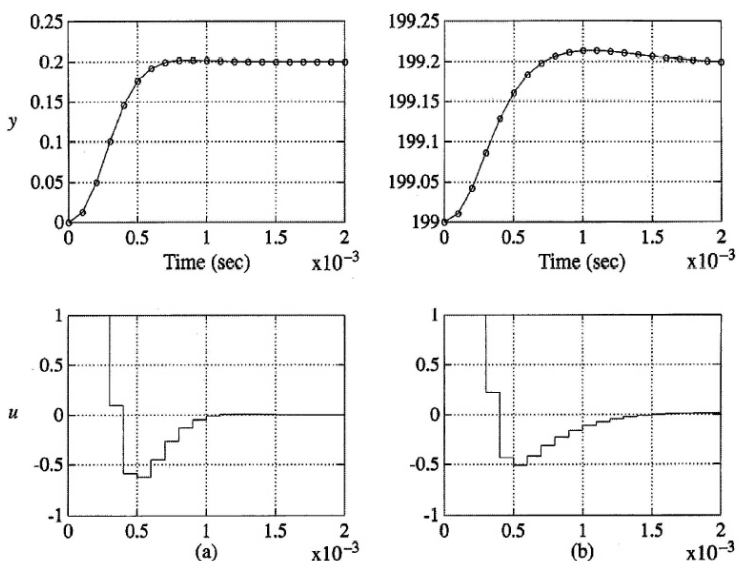


Figure 13.43
 Small step response of positioning servo with nonlinear torque factor and a linear controller, at two locations, near $y_r = 0$ and $y_r = 199$

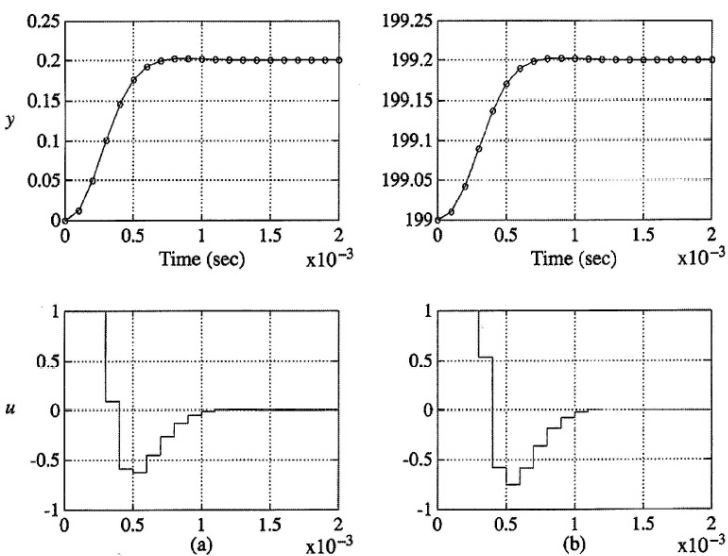


Figure 13.44
 Small step response of the positioning servo with nonlinear torque factor and an INL nonlinear controller, at two locations, near $y_r = 0$ and $y_r = 199$

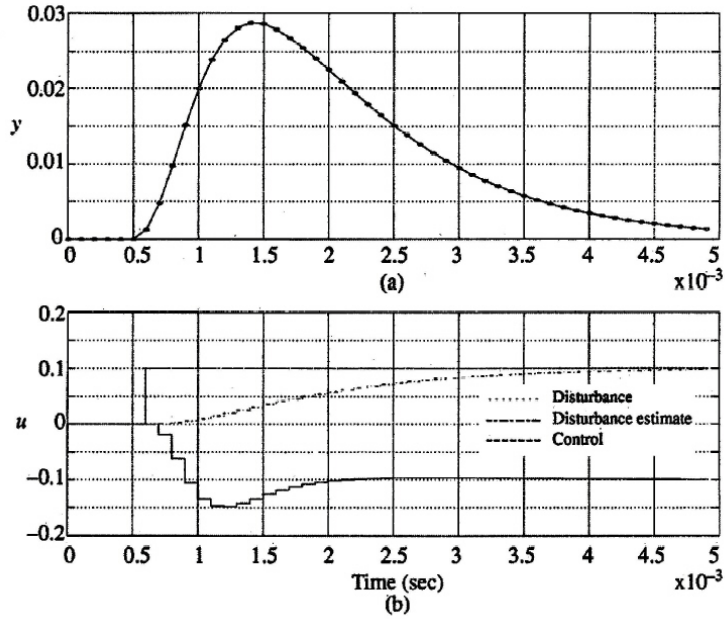


Figure 13.45
Response of the servo to a disturbance step

The linear control law and estimator gains used are given by

$$\mathbf{K} = [11.80 \quad 3.35 \quad 1], \quad (13.67)$$

and

$$\mathbf{L} = [0.728 \quad 1.848 \quad 0.493]^T. \quad (13.68)$$

It is interesting to compare the linear control of the nonlinear plant and INL control of the same plant. Fig. 13.43 shows the small step response of the system (zero disturbance u_d) at two locations, near $\theta = 0$ and $\theta = 0.20$ radians, for the linear controller, while Fig. 13.44 shows the same conditions under INL control. Note the difference between the two due to both changing plant and errors in the estimator model. By employing INL control as in Fig. 13.42, the unit step responses in the two locations are nearly identical.

For the INL design, there is no estimated disturbance because, unlike the linear state estimator, the INL design uses a model of the plant nonlinearity to match modeled torque against what is actually produced by the motor. In addition to a better state estimate, the INL design adjusts the control law to account for the changing plant gain produced by the varying torque factor. The resulting INL design produces a consistent response independent of position, both in the time domain and of course in the frequency domain where the closed-loop transfer function will remain constant versus actuator angle as a robustness advantage.

Bias torque disturbances are handled without causing a steady state position error as seen in Fig. 13.45. More important than a step response to a disturbance however, is the response of the servo to a bias torque such as hysteretic damping produced by the ball bearings in the torque motor. A nonlinear torque is produced which always opposes the direction of rotation, and is hysteretic in form. The control structure allows this bias torque to be continually estimated and compensated without resetting or holding any integrators as is sometimes done to eliminate the wind-up problem.

So far we have only examined the unit step command response of the servo at locations of extremes in the torque factor. With the saturation value of $I_{\max} = 1$, we would expect the effect of the saturation function to come into play for increasing values of command change. While a maximum position change of $\Delta y = 400$ is possible, simulation of the response of this system to such a command change quickly shows it to be disastrous because overshoot and settling time become extremely long compared to linear response. A very common problem in control systems is illustrated by this point:

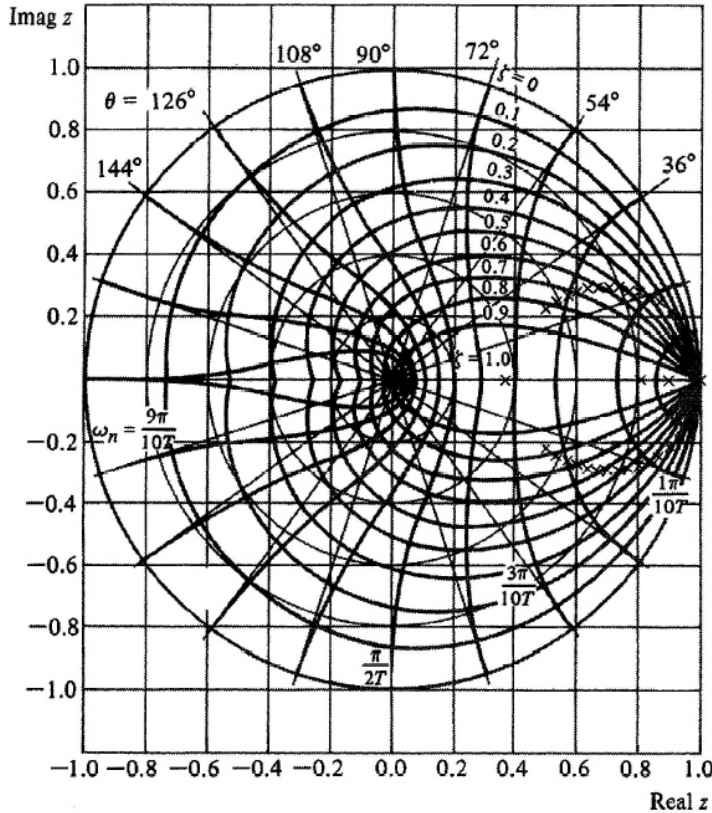


Figure 13.46
Root locus
plotted as
function of the
equivalent gain

Linear unit step response is not the final analysis in systems with saturation or any other nonlinearity. The method of equivalent gains given in Section 13.1.4 suggests that this system is always stable as can be seen in the equivalent gain root locus of this system plotted in Fig. 13.46. However, the roots become increasingly lightly damped and oscillatory with longer period as the command input increases. We will investigate methods of improving the response to large changes in command input in the next section.

Although the control structure developed in Example 13.20 was designed with all of the requirements we initially thought of, we neglected to include the caveat that the system had to accomplish all of this with a severe limitation on the available control authority. As illustrated in Fig. 13.47, it turns out that the saturation nonlinearity results in a coupling between usable bandwidth and input command magnitude. Figure 13.47 shows the response of our torque motor servomechanism for increasing input step magnitudes: The response degrades as input magnitude increases, as predicted by the equivalent gains root locus shown in Fig. 13.46. To avoid saturation using the linear control law $u = -\mathbf{K}\mathbf{x}$ for step inputs, we could approximate a constraint on k_1 of \mathbf{K} such that

$$k_1 \leq \frac{1}{2\|y_r\|^\infty}. \quad (13.69)$$

Since the bandwidth of the system is roughly proportional to k_1^2 , we are forced to limit the bandwidth inversely proportional to the square of the maximum input amplitude change (e.g., $+y_r$ to $-y_r$). Hence we must look for an alternate solution if we wish to maintain the small signal performance of the linear design and improve the large signal performance where we must take limited control authority into account, which brings us to time-optimal control.

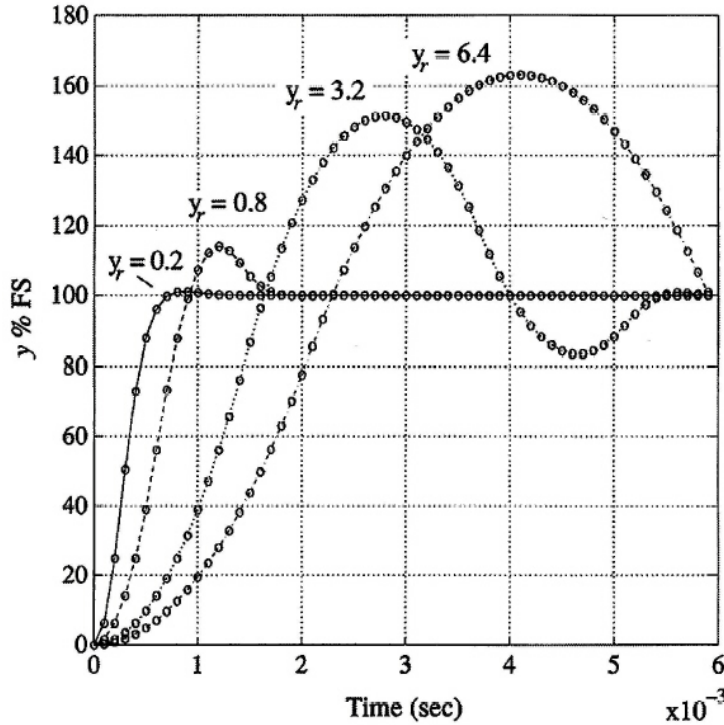


Figure 13.47
Response of the torque motor positioning servo for several size inputs. Note how the response degrades with increasing command change magnitude

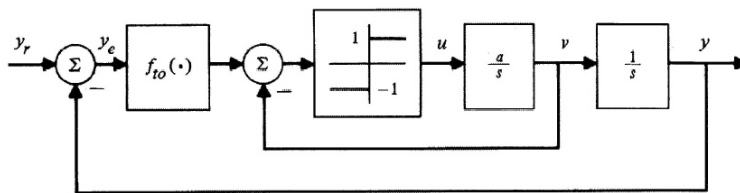


Figure 13.48
Continuous time-optimal controller for double integrator plant

13.2.2 Time-Optimal Servomechanisms

The subject of time-optimal control is very important in the study of nonlinear motion control systems. Many servomechanisms have at least one mode of operation in which it is advantageous to move the actuator quickly from one state to the next. A simple example of this might be the positioning servo for a robot arm. Another might be the positioning of a plotter pen in either axis. Discrete time-optimal control is possible but very difficult to implement, and it also suffers from some deficiencies which we will examine later. Fortunately an *extension* of practical continuous-time time-optimal control strategies to discrete-time controllers is possible. To examine the concepts behind a time-optimal nonlinear control technique we will focus on the proximate time-optimal servomechanism or PTOS developed by Workman (1987), and apply the PTOS control structure to the torque motor positioning servo.

Before introducing the discrete-time time-optimal controller, we will briefly review the structure of the continuous-time time-optimal control of a double integrator plant. Continuous-time PTOS will be also be discussed in preparation for the main illustration of a discrete-time PTOS.

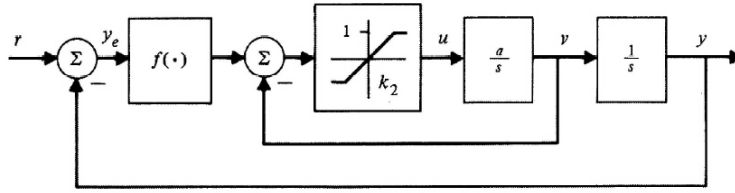


Figure 13.49
Continuous-time proximate time-optimal servomechanism (PTOS)

An Overview of Continuous Time-Optimal Control

Consider the time-optimal control system shown in Fig. 13.48. The plant consists of a double integrator driven by a limiter or saturation block. Given the limited control authority, the optimal control law is a nonlinear function of the distance to the target and the plant velocity. In Fig. 13.48 the control law is shown without specifying the nonlinear function $f_{to}(\cdot)$. The equations describing this system are derived in many texts, and are shown to be

$$\dot{y} = v \quad (13.70)$$

$$\dot{v} = a \operatorname{sgn}(f_{to}(y_e) - v) \quad (13.71)$$

$$f_{to}(y_e) = \operatorname{sgn}(y_e)(2a|y_e|)^{1/2}, \quad (13.72)$$

where

$$y_e \triangleq y_r - y.$$

In this form, it is helpful to define the move length L for later use as the position error at the receipt of a new reference (step) input $y_r(t)$

$$L \triangleq y_r(t_0) - y(t_0) = y_e(t_0).$$

The control law given by Eqs. (13.71)–(13.72) and shown in Fig. 13.48, although time-optimal, is not practical. Even the smallest system process or measurement noise will cause the control to “chatter” between the maximum and minimum values. Removing the infinite gain operators from the time-optimal controller gives the system a finite bandwidth, and hence is much more practical for most applications. It should be noted that in some cases, on–off control is the only alternative, in which case techniques such as deadzone and hysteresis are employed to minimize the chatter. When a linear region of control is possible, an effective alternative is available.

Continuous Proximate Time-Optimal Servomechanism⁷

A **proximate time-optimal servomechanism** (PTOS) is shown in Fig. 13.49. The function $f(\cdot)$ is a finite slope⁸ approximation to the switching function $f_{to}(\cdot)$ given by Eq. (13.72). The signum function of Eq. (13.71) has been replaced by the saturation function which, together with the gain factor k_2 , can be thought of as a finite slope approximation to the signum function. The equations which define the PTOS are

$$\dot{y} = v \quad (13.73)$$

$$\dot{v} = a \operatorname{sat}(k_2(f(y_e) - v)). \quad (13.74)$$

The function $f(\cdot)$ is given by

$$f(y_e) = \begin{cases} \frac{k_1}{k_2}(y_e) & \text{for } |y_e| \leq y_\ell \\ \operatorname{sgn}(y_e)[(2a\alpha|y_e|)^{1/2} - (1/k_2)] & \text{for } |y_e| > y_\ell, \end{cases} \quad (13.75)$$

⁷For more detail on the PTOS, see Workman (1987).

⁸The derivative of f_{to} is infinite at $y = 0$.

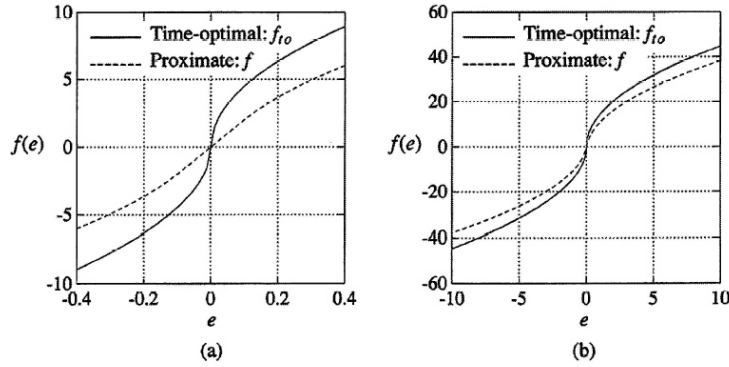


Figure 13.50
The function $f(\cdot)$ for two different ranges of position error,
(a) $|y_e| \leq 0.40$,
and
(b) $|y_e| \leq 10.0$

where the positive factor α is referred to as the acceleration discount factor and is less than 1.0 ($0 < \alpha < 1$). By discounting the available acceleration a to αa , we have a design that allows us to accommodate uncertainty in the plant acceleration factor at the cost of some increase in response time as we shall see. A close examination of Eq. (13.75) will show that it is close to the true time-optimal function f_{to} with an adjustable acceleration discount factor α . The linear portion of the curve connects the two disjoint halves of the nonlinear portion. To connect the nonlinear regions of $f(\cdot)$ such that $f(\cdot)$ and $f'(\cdot)$ remain continuous, we have a constraint relating the gains k_1 and k_2 and the size of the linear region y_ℓ

$$k_2 = \left(\frac{2k_1}{\alpha a} \right)^{1/2}, \quad (13.76)$$

and the size of the linear region is

$$y_\ell = \frac{1}{k_1}. \quad (13.77)$$

Computing the Switching Curve for PTOS

Example 13.16

Given the following parameters, determine the function $f(\cdot)$ for the PTOS:

Parameter	Value
k_1	10.0
α	0.80
a	100.0

Solution. First, using Eq. (13.76) we have

$$k_2 = \left(\frac{20.0}{80.0} \right)^{1/2} = 0.500,$$

and a linear region defined by $y_\ell = 0.10$ and thus the function $f(\cdot)$ is given by

$$f(y_e) = \begin{cases} 20.0y_e & \text{for } |y_e| \leq 0.10 \\ \text{sgn}(y_e)[(160.0|y_e|)^{1/2} - 2.0] & \text{for } |y_e| > 0.10 \end{cases}$$

This function is shown for two different ranges of y_e in Fig. 13.50.

By approximating the positioning time as the time it takes the position error to be within the linear region, we can define a percentage *increase* P in response time of a PTOS system over that of a minimum time control of the same plant

$$P \triangleq 100\% \left[\frac{1}{2} \left(\frac{1}{\sqrt{\alpha}} - 1 \right) \right]. \quad (13.78)$$

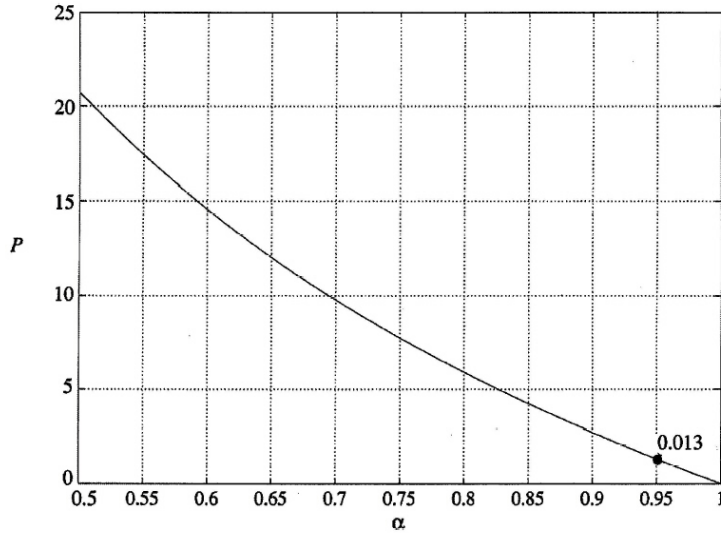


Figure 13.51
Percentage increase P in move time versus α . The point marked on the curve represents $P = 1.3\%$ for $\alpha = 0.95$

Note that the value of P is independent of the size of the step input (move length L), but to make sense, the move length L must be greater than the length of the linear region y_l . In fact, it should be clear that the linear region y_l is not arbitrarily chosen as $1/k_1$, rather it is related to the distance above which it is practical to move the actuator with a given desired system bandwidth. Although reasonable values of α are usually such that $\alpha \in [0.80 \ 0.99]$, P is plotted for a wide range of α in Fig. 13.51. From the figure, it is clear that a step response using PTOS and the $f(\cdot)$ derived in Example 13.17 is approximately 6% slower than a time-optimal system for the same size step.

A simulation of both the minimum-time controller and the PTOS system when the plant gain a is known is shown in Fig. 13.52. For the case shown, the PTOS system is 1.3% slower, but has much improved control behavior during regulation mode. In addition to the linear regulation, it has also been shown in Workman (1987) that PTOS has far better robustness properties to small changes in a , unmodeled dynamics, and disturbances acting on the plant.

Discrete-Time PTOS

Next, we will extend the continuous-time proximate time-optimal servomechanism (PTOS) to discrete-time control of a continuous-time double integrator plant driven by a zero-order hold. As in the continuous time case the states are defined as position and velocity. Assuming an insignificant calculation delay, we have the following discrete-time, state-space description of the plant

$$\mathbf{x} \triangleq [y \quad v]^T \quad (13.79)$$

$$\mathbf{x}(k+1) = \begin{bmatrix} 1 & T_s \\ 0 & 1 \end{bmatrix} \mathbf{x}(k) + \begin{bmatrix} aT_s^2/2 \\ aT_s \end{bmatrix} u(k). \quad (13.80)$$

The control structure is a discrete-time mapping of the same proximate time-optimal control law used in continuous time with some slightly different conditions on the function $f(\cdot)$ which will be discussed later. The mapped control law is then

$$u(k) = \text{sat}(k_2[f(y_e(k)) - v(k)]), \quad (13.81)$$

where the definition of y_e is the same as in the continuous time case. Quantization in the D/A and A/D converters will be assumed negligible, and the output $u(k)$ is input to the plant through a latching D/A converter, which has the same unit pulse response as the zero order hold function. A block diagram of this system is shown in Fig. 13.53.

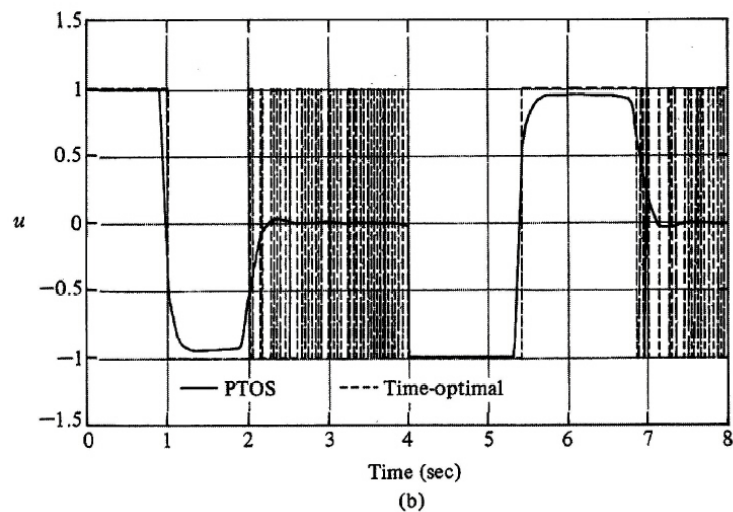
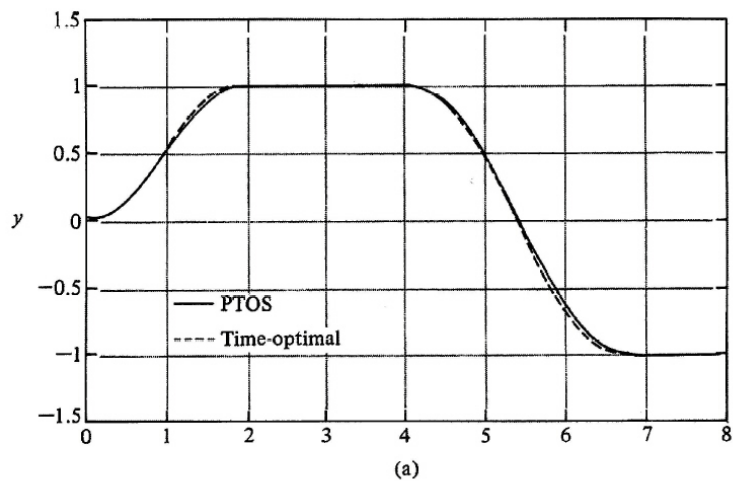


Figure 13.52
Variables y and u
for time-optimal
control and
PTOS

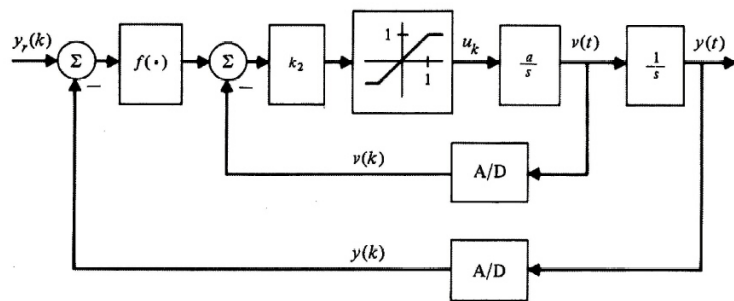


Figure 13.53
Discrete-time
proximate
time-optimal
servomechanism
(PTOS)

Key Approximation

The ideal time-optimal control of a discrete-time system suffers from the same difficulties as the continuous-time time-optimal control, including control chatter and extreme sensitivity to modeling errors and unmodeled dynamics. A valuable fact, however, permits us to extend the continuous-time PTOS to discrete-time systems: as the sampling rate increases, the true optimal discrete-time control tends to look identical to a sampled continuous-time control. This does not mean that the sampling rate must be high or higher than would otherwise be selected to make the approximation valid, indeed we will see that the required minimum sampling rate is lower than that usually chosen in control designs. By adjusting the acceleration discount factor α , the *practical* time-optimal controller in the PTOS will leave enough control margin during trajectory following that differences between continuous-time and discrete-time optimal control strategies are minimized. Control margin refers to the ability of the system to respond to small errors in modeling, or measurement, with small changes in control response. In the time-optimal system, the infinite gain operators provide no such margin for error.

An analysis of the mapping of an ideal time-optimal controller (continuous system) to a discrete system controller points out why the discrete time solution *cannot be the same as the continuous time one*. As an example, consider the *smallest* move length L for which the discrete time mapping would produce the exact continuous time response: the control signal is $+1$ for one sample, and -1 for the next. The total movement in y is then

$$y(2) - y(0) = aT_s^2. \quad (13.82)$$

Thus $L_{min} = aT_s^2$ is the smallest movement for which our discrete mapped controller will match the ideal continuous time controller (of course the terminal velocity must be zero). What happens when $L < L_{min}$? Clearly there is a problem mapping the continuous-time control to discrete-time. The ideal continuous time-optimal controller uses control values of ± 1 , but with that constraint it is not possible to reach $L < L_{min}$, or for that matter any arbitrary values of L . The reachable set of L 's for the **mapped** controller is given by

$$L^r = n^2 L_{min} \quad \text{for all integers } n. \quad (13.83)$$

The reason for the “quantized” values of reachable positions stems from the quantization in time along with the restriction that the control must be of magnitude one or zero. If we allow control values to range between ± 1 (as in the true discrete-time time-optimal control), then all positions are reachable. Hence the applicability of the practical PTOS, which by construction has a linear region of operation.

Sample Time Constraints

There are two constraints on the discrete-time PTOS which arise due to the sampling of the feedback signals and the zero-order hold on the control to the plant. Before stating these conditions, we need to define the *bandwidth* of the discrete-time PTOS while in the linear region of operation ($|y_e| \leq y_l$, and $|u| < 1$). From k_1 and k_2 , the closed loop bandwidth of the system (ω_n) is calculated as follows. In the linear region, the control is given by $u = -k_1 x_1 - k_2 x_2$. If this control is substituted into Eq. (13.79) the characteristic equation is given by $z^2 + p_1 z + p_2$ where $\sqrt{p_2} = r = e^{-\sigma T_s}$ and $p_1 = -2r \cos(\theta)$ where $\theta = \omega_d T_s$. The natural frequency, which approximates the bandwidth, is given by $w_n = \sqrt{(\sigma^2 + \omega_d^2)}$. For the

given system, the parameters are

$$\begin{aligned} k_2 &= \left(\frac{2k_1}{a\alpha} \right)^{1/2} \\ r^2 &= \frac{ak_1T_s^2}{2} + ak_2T_s - 2 \\ -2r\cos(\theta) &= \frac{ak_1T_s^2}{2} - ak_2T_s + 1. \end{aligned}$$

With these results, the closed-loop bandwidth is given by

$$\omega_d = \frac{1}{T_s} \left[\left(\arccos \left(\frac{p_1}{-2r} \right) \right)^2 + \left(\frac{\ln(p_2)}{2} \right)^2 \right]^2. \quad (13.84)$$

Also, we define the ratio of the sampling (radian) frequency to desired (radian) bandwidth as

$$N \triangleq \frac{\omega_s}{\omega_n} = \frac{f_s}{f_n}. \quad (13.85)$$

For most discrete-time servomechanisms, the value of N is greater than five. Some designers use the approximation:

$$N \approx 20\sqrt{1 - \zeta^2} \quad \text{for } \zeta < 1,$$

which for $\zeta = 0.707$ means $N \approx 14$.

It is shown in Workman (1987) that if

$$N > 6.3,$$

then it is possible to show that the system is stable, and also that the performance of the system is guaranteed, in that the control will not saturate during the deceleration phase to the target position.

Variable Output Gain and Control Authority

To generalize the form of the plant, we will include a variable saturation maximum value, m , and an output gain, k_y . The plant becomes

$$\mathbf{x} \triangleq [y \quad v]^T \quad (13.86)$$

$$\mathbf{x}(k+1) = \begin{bmatrix} 1 & k_y T_s \\ 0 & 1 \end{bmatrix} \mathbf{x}(k) + \begin{bmatrix} aT_s^2/2 \\ aT_s \end{bmatrix} u(k) \quad (13.87)$$

with a control

$$u_k = m \text{sat}(k_2(f(y_e) - v_k)/m). \quad (13.88)$$

The new set of design equations are as follows. Choose

$$k_2 = \left(\frac{2k_1 k_y}{a\alpha} \right)^{1/2} \quad (13.89)$$

and a linear region

$$y_\ell = \frac{m}{k_1}, \quad (13.90)$$

which will again make the function $f(\cdot)$ and $f'(\cdot)$ continuous. The function $f(\cdot)$ also changes. To accommodate m we have

$$f(y_e) = \begin{cases} \frac{k_1}{k_2} y_e & |y_e| \leq y_\ell \\ \text{sgn}(y_e) [((2ma\alpha k_y)|y_e|)^{1/2} - (m/k_2)] & |y_e| > y_\ell \end{cases} \quad (13.91)$$

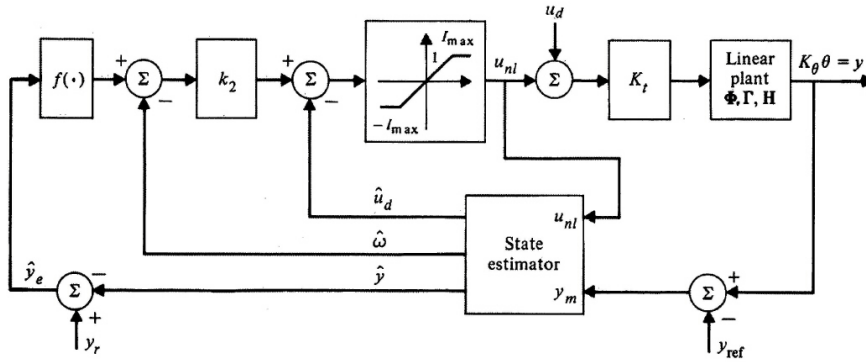


Figure 13.54
Velocity command function used in the PTOS

and again we must ensure that

$$N > 6.3.$$

Design of PTOS

Example 13.17

Apply PTOS to the rotary actuator angular position controller shown in Fig. 13.40.

Solution. To begin, we will assume that the torque factor K_t is a constant given by the smallest value over the desired control range, not a function of the actuator position θ , and that the actuator friction factor K_f is zero resulting in a double integrator plant. With these simplifying assumptions, the normalized responses of the linear control law developed earlier to a range of changes in command position are shown in Fig. 13.47. Because of the limited control authority, the response for larger move distances degrades severely. To use the PTOS structure, we substitute a nonlinear function $f(\cdot)$ derived from the actuator parameters for the k_1/k_2 gain block and let $\bar{K}_t(\theta) = 1$. Namely, the acceleration constant for the rotary actuator is given by

$$a = \frac{K_t(0.0)}{J_a} = 2500.0.$$

Choosing an acceleration discount factor α equal to 0.84, we can use the constraint on k_2 from Eq. (13.89) to determine

$$k_2 = \sqrt{\frac{2k_1 K_\theta}{\alpha a}} = \sqrt{0.9524k_1}, \tag{13.92}$$

where the gain K_θ is used for k_y . Equation (13.89) can also be used as a design constraint in a parameter optimization design to obtain the best value for k_1 and the estimator gains. The values chosen for this design are

$$\mathbf{K} = [11.80 \quad 3.3523 \quad 1],$$

and

$$\mathbf{L} = [0.7280 \quad 1.848 \quad 0.4933]^T.$$

The resulting velocity command function is thus

$$f(y_e) = \begin{cases} 3.520 y_e & |y_e| \leq 0.0847 \\ \text{sgn}(y_e)[(4.2|y_e|)^{1/2} - (.2983)] & |y_e| > 0.0847, \end{cases} \tag{13.93}$$

which is then used as shown in Fig. 13.54. Figure 13.55 shows the responses of the PTOS to a wide range of move angles, L . If we compare these responses to those of a linear controller as shown in Fig. 13.47, it is clear that the nonlinear control structure yields overall superior performance.

Consider Example 13.17 with a torque factor which is not constant but as described by Eq. (13.50). To employ PTOS on such a structure and include INL for plant gain normalization and

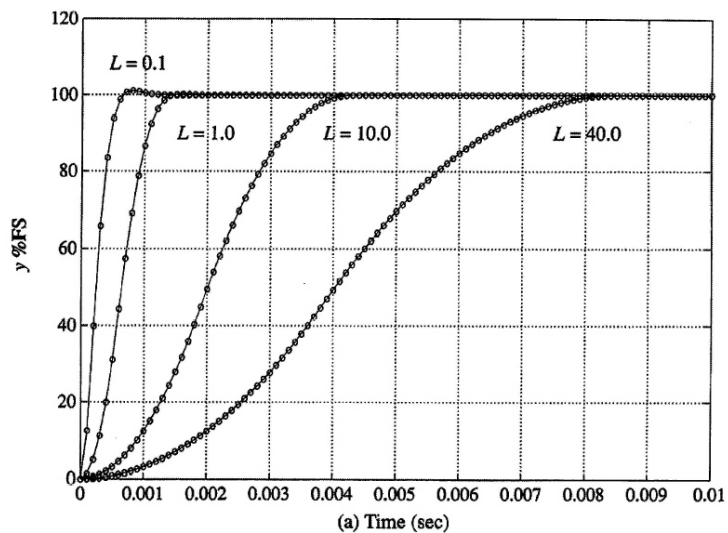
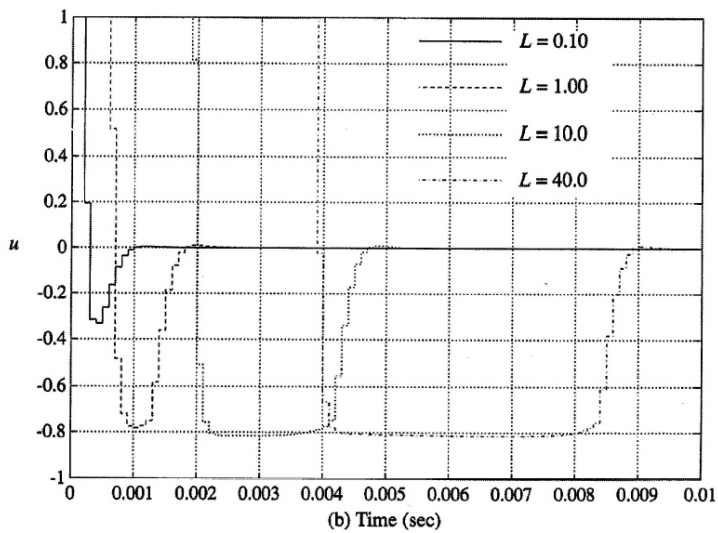


Figure 13.55
Normalized (to full scale) PTOS responses for a wide range of different step changes in command position input y (move angles L)



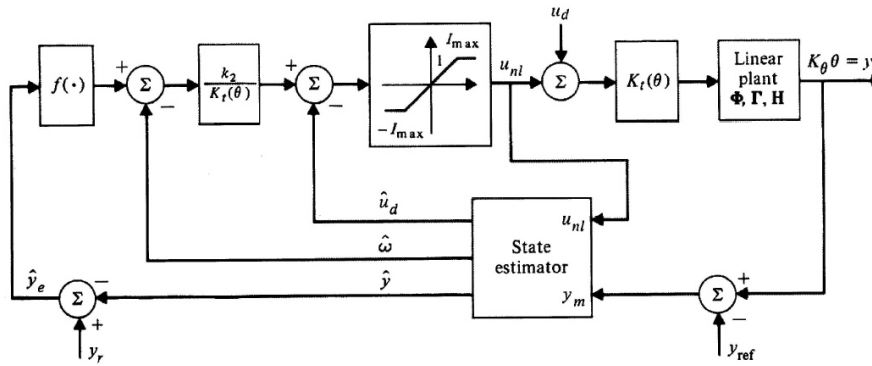


Figure 13.56
Block diagram of
the rotary
actuator PTOS
for the torque
motor example
with INL control

estimator model correction, the simple velocity function $f(\cdot)$ would have to assume the minimum available torque constant. Since this was done already in the generation of the velocity command function in Example 13.17, we can apply INL directly to it without changing Eq. (13.93). Both INL control and the PTOS for the plant of Example 13.20 are shown applied together in Fig. 13.56.

Since $K_r^{-1}(\theta)$ normalizes the plant gain versus θ , it is not necessary to vary k_1 as a function of θ . By using the minimum available torque constant we sacrifice 16% of the available plant acceleration capability near $\theta = 0$. To remedy this we would have to employ a much more complex control structure than PTOS. From Fig. 13.51, we can see that assuming even a 20% lower K_r than actual we would be sacrificing an upper bound of a 6% loss in response time performance. In reality, the performance loss will probably be more like an average of 3% because the plant is only capable of maximum acceleration at $\theta = 0$. If recovering the 3% average performance lost is worth the added complexity it may be worthwhile to develop the required velocity command function $f(y_e, \theta)$.

13.2.3 Extended PTOS for Flexible Structures

The PTOS controller discussed in the previous section focused on second-order plants, mainly double integrator or real-pole and an integrator type.⁹ Unfortunately, most servomechanisms contain flexible modes in the actuator or structure being controlled, yielding plants of higher order than the simple double integrator. On the other hand, these higher-order plants are often dominated by their double-integrator components (inertial response). When the flexible modes are high enough in frequency, the response of the plant to a PTOS control will be that of a rigid body with some small residue of flexible-mode motion in the output. It is often the case in servo design that the flexible modes are beyond the desired bandwidth of the closed-loop controller, but still should be accounted for in the *linear* part of the control law. The PTOS architecture has been extended to include such cases, and the extended architecture is referred to as XPTOS as shown in Fig. 13.57.

XPTOS Design Procedure

Design of the free parameters in the XPTOS structure is much like that for the PTOS. The linear portion of the control law is calculated using some technique which allows the constraint on k_2 to be taken into account. The model of the plant used in the state estimator must contain output and output derivative (position and velocity in a positioning servo) as two of the states. For example

$$\mathbf{x} = \begin{bmatrix} y \\ \dot{y} \\ x_{r,1} \\ \vdots \\ x_{r,n-2} \end{bmatrix}.$$

⁹Although not discussed, the PTOS architecture can be extended to second-order plants with complex poles.

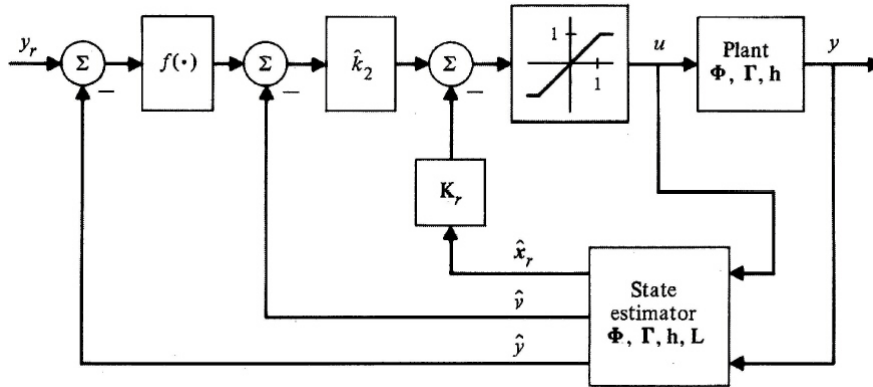


Figure 13.57
Extended proximate time-optimal servo (XPTOS). The residual states \hat{x}_r are flexible mode states

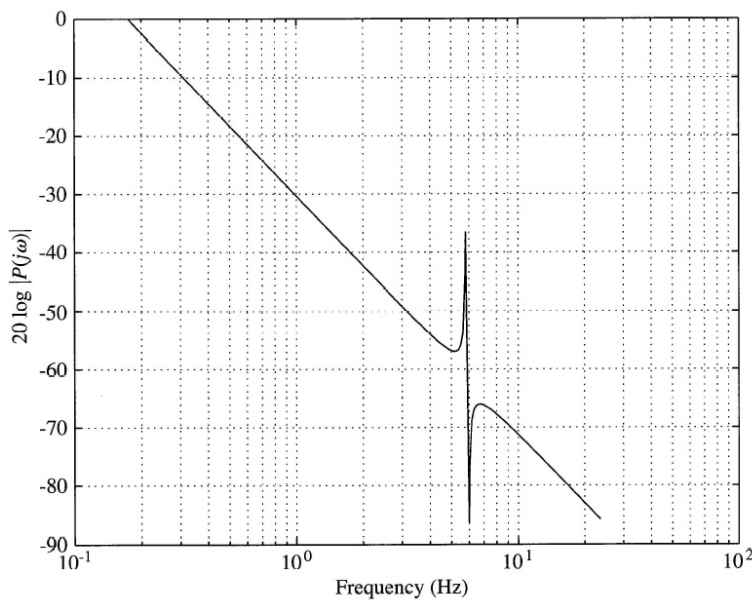


Figure 13.58
Frequency response of a double integrator plant with a lightly damped flexible mode at 6 Hz. Frequency response of a double integrator plant with a lightly damped flexible mode at 6 Hz, sampled at $T_s = 0.02$ seconds

With this state definition, the feedback gain vector \mathbf{K} is defined as

$$\mathbf{K} \triangleq [k_1 \quad k_2 \quad K_r] .$$

The function $f(\cdot)$ is then designed as in the PTOS controller, but the constant α must be adjusted to accommodate the flexible modes. To provide control margin while decelerating toward the target, α is made smaller than that used if the flexible mode(s) were not present. In this manner the control is kept from saturating during deceleration, and the flexible modes are actively damped while the actuator is approaching the target. To decide the proper value for α , the system is simulated and α is adjusted until the system performance meets the goals. For extremely flexible systems, and/or systems where the control bandwidth is very close to the frequency of the flexible modes, some control saturation during deceleration might have to be allowed.

For illustration of the value of the XPTOS architecture, we will attempt a fast (proximate time-optimal) positioning of a double integrator plant with a significant flexible mode of vibration. The frequency response of the nominal plant is shown in Fig. 13.58. The flexible mode has a 10dB open-loop rise at a frequency only slightly above the desired closed-loop bandwidth or about 4.0 Hz. Gain stabilization is not feasible and without feedback from the flexible modes (K_r) the system would be

Table 13.4
Parameter Value Units

T_s	0.020	sec
α	0.95	
f_d	4.0	Hz
m	5.0	V
a	1.2	$m - sec^2 V^{-1}$
f_{rp}	5.8	Hz
f_{rz}	6.0	Hz
ζ_r	.002	
k_1	333	$V - m^{-1}$
k_2	24.17	$V - sec - m^{-1}$
k_y	1.0	$V - rad^{-1}$

unstable. The plant model is given by the transfer function

$$P(s) = \frac{s^2 + 2\zeta_r(2\pi f_{rz})s + (2\pi f_{rz})^2}{s^2 + 2\zeta_r(2\pi f_{rp})s + (2\pi f_{rp})^2} \left(\frac{f_{rp}}{f_{rz}}\right)^2 \frac{a}{s^2}. \quad (13.94)$$

The state model is given by

$$\mathbf{F} = \begin{bmatrix} 0 & 1 & 0 & 0 \\ 0 & 0 & 1 - \left(\frac{\omega_{rp}}{\omega_{rz}}\right)^2 & 2\zeta_r \left(\frac{\omega_{rp}}{\omega_{rz}} - \left(\frac{\omega_{rp}}{\omega_{rz}}\right)^2\right) \\ 0 & 0 & 0 & \omega_{rp} \\ 0 & 0 & -\omega_{rp} & -2\zeta_r \omega_{rp} \end{bmatrix}$$

$$\mathbf{G} = \begin{bmatrix} 0 & a \left(\frac{\omega_{rp}}{\omega_{rz}}\right)^2 & 0 & a\omega_{rp} \end{bmatrix}^T$$

$$\mathbf{H} = [1 \ 0 \ 0 \ 0].$$

The numbers for the example are given in Table 13.4.

Matrices of a discrete model based on a sample and zero-order hold sampled at 50 samples per second are

$$\Phi = \begin{bmatrix} 1.0 & .02 & 0 & 0 \\ 0 & 1 & .0012 & .0005 \\ 0 & 0 & 0.7462 & 0.6650 \\ 0 & 0 & -0.6650 & 0.7435 \end{bmatrix}$$

$$\Gamma = [0.0002 \ 0.0226 \ 0.3046 \ 0.7981]^T,$$

with \mathbf{H} as in the continuous model. We wish to derive a controller that gives the desired closed-loop bandwidth of approximately 4.0 Hz subject to the constraints given by Eq. (13.89). For simplicity we will assume state measurements are available although in practice a state estimator is surely required. Initially we are faced with the choice of α which must finally be chosen by simulation. So to begin, we choose $\alpha = 0.95$ and take a linear design corresponding to

$$K = [333 \ 24.17 \ 0.1307 \ 0.1785].$$

The function $f(\cdot)$ is thus

$$f(y_e) = \begin{cases} 13.78y_e & |y_e| \leq 0.015 \\ \text{sgn}(y_e) \left[\sqrt{(11.4|y_e|)} - 0.2069 \right] & |y_e| > 0.015. \end{cases} \quad (13.95)$$

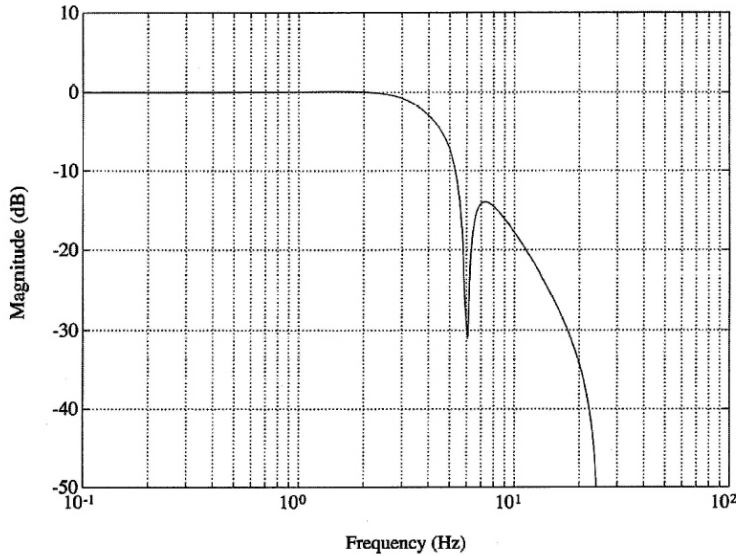


Figure 13.59
Closed-loop
frequency
response of the
XPTOS system
when the plant
has a single large
flexible mode at 6
Hz, sampled at
 $T_s = 0.02$ seconds

Initial simulations showed that $\alpha = 0.95$ was too aggressive with the flexible mode in the plant because the control saturated quite heavily during deceleration. By choosing a value of $\alpha = 0.80$, there is enough margin for the control of the flexible mode. The final PTOS function is

$$f(y_e) = \begin{cases} 12.64y_e & |y_e| \leq 0.015 \\ \text{sgn}(y_e) \left[\sqrt{9.6|y_e|} - 0.1898 \right] & |y_e| > 0.015. \end{cases}$$

The resulting closed-loop response is shown in Fig. 13.59. The system performance, shown in Fig. 13.60 for a move length of $L = 1$ is excellent. Note that during deceleration the control contains a component of the flexible mode frequency. Once the 6-Hz component has decayed, the resulting control magnitude is approximately 4 which corresponds to $m\alpha$.

Arrival at the target is of critical importance in high accuracy positioning servos, and a close examination of the positioning error for this system is shown with an expanded scale in Fig. 13.61. The tuned system has excellent performance, as long as the response time increase of about 6% can be tolerated.

13.2.4 Introduction to Adaptive Control

Parameter variations in the plant of a control system can have severe impact on performance and stability. For this reason, control system designers have long desired a control algorithm which somehow automatically redesigns itself as the plant changes. This is the subject of adaptive control. There are several reasonable definitions for the term “Adaptive.” It is the opinion of the authors that when a control system’s signal *paths* change, as opposed to the signals, the control system is adaptive. Thus, simple feedback of any signal is not adaptive, because the feedback law doesn’t change. It is worthwhile to note that there is always a lively discussion among control engineers about the definition of adaptive control. One definition is that an adaptive controller is any control system that is designed from an adaptive viewpoint. Another is that adaptive control is any control system which monitors its performance and makes adjustments to improve that performance. Åström (Åström and Wittenmark, 1988) defines adaptive control as a control system comprised of a fast (controller) loop, and a slow (control adjustment) loop. In any case, the definition of the term adaptive is to “modify according to changing circumstances”. Almost all adaptive control systems do modify themselves under changing circumstances, the issues left to discuss become, “what are the changing circumstances to be accounted for?” and “how do we modify the control algorithm in light of the changes?”

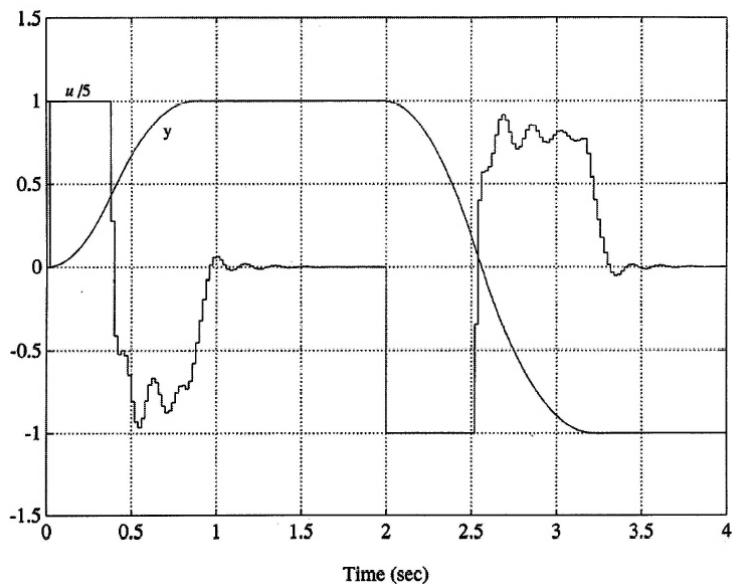


Figure 13.60
XPTOS
responses for
 $L = 1$. Plant is a
double integrator
with a large
flexible mode at 6
Hz, sampled at
 $T_s = 0.02$ seconds

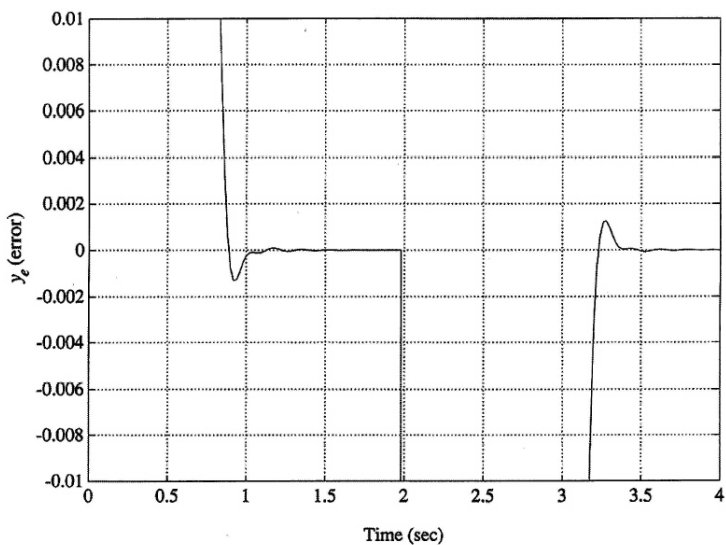


Figure 13.61
XPTOS error
responses for
 $L = 1$ of a double-
integration plant
with a large
flexible mode of
6 Hz, sampled at
 $T_s = 0.02$ seconds

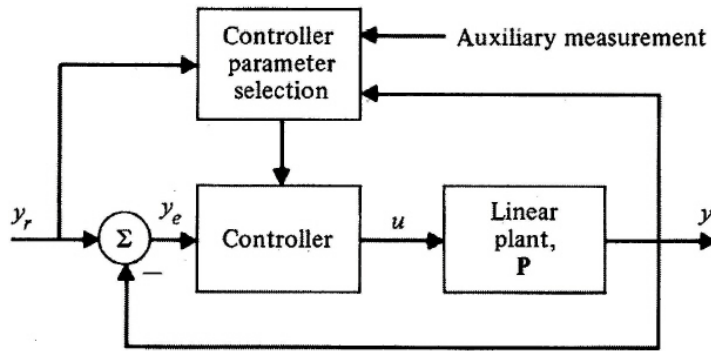


Figure 13.62
Structure of the
“gain scheduled”
Controller

Use of Adaptive Control

To design a control system, the designer must define four basic things:

1. A model of the plant to be controlled and the range of its validity.
2. The nominal value of the model parameters and their expected deviation.
3. The performance objectives.
4. The constraints on the design, such as the cost of control action, control authority limits, and the intended cost of the controller.

Accounting for the second item in the list can be costly in cases of large plant variation. If a fixed-parameter automatic control system is used, the parameter variation directly affects the capability of the design to meet the performance specifications under all operating conditions. If an adaptive controller is used, the parameter variations are accounted for at the price of increased complexity of the controller and therefore cost of implementing the design.¹⁰ It is this cost versus performance trade-off which must be examined carefully in choosing the control structure. Adaptive control is certainly more complex than fixed-parameter control, and carries with it more complex failure mechanisms. In addition, adaptive control is both time-varying and nonlinear, increasing the difficulty of stability and performance analysis. Thus, the decision to use adaptive control should be made very carefully. It is the increased complexity of adaptive controllers and the corresponding implementation difficulties which led to perhaps more obvious and simple adaptive controllers, such as gain scheduling.

Gain Scheduling

Gain scheduling, as shown in Fig. 13.62, is a process by which one of several different control algorithms is chosen based on some operating condition(s), and is thus adaptive (the signal paths change). Since the control algorithms are designed off-line with *a priori* information, the main burdens of gain scheduling are identifying the proper control design to be used and effecting a smooth transfer from one design to another during system operation. Effectively, the design is broken into *regions* of operation, and in each, a fixed control design is used. Simulation is used to examine the transition from one region to another. It should be noted that often the question of stability is circumvented by having very few regions and ensuring that the controller will pass from one to another without getting trapped at the boundary. It is reasoned that for a few regions that are switched between very *infrequently*, or a continuous set of parameters that are modified very slowly,¹¹ the

¹⁰Increasing the complexity of a software project increases the development costs, and in all but very rare instances will increase hardware costs.

¹¹Slowly in this context implies that control parameters are changed in small discrete amounts at a rate much slower than the slowest time constant of the closed loop system.

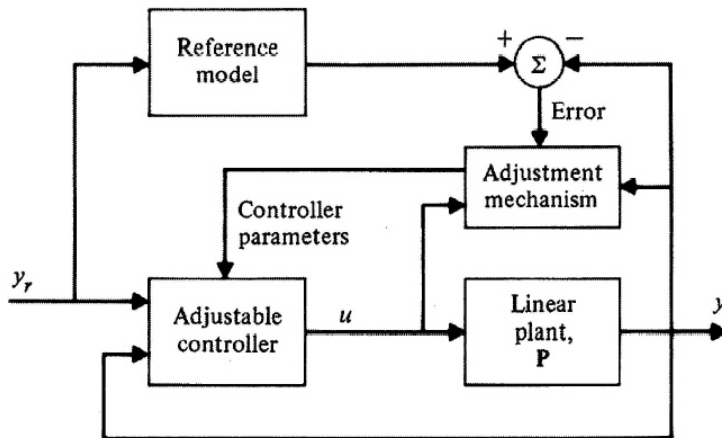


Figure 13.63
Model Reference
Adaptive Control
(MRAC)

system stability can be ensured by examining each of the linear control laws as if it were fixed. Thus gain scheduling is usually thought of (or defined) as dependent on some slowly varying parameter (relative to the control bandwidth). The method of *averaging* is a sophisticated concept often used to evaluate the stability of systems which have slowly varying parameters. Unfortunately, averaging analysis is beyond the scope of this text (see Anderson (1986)). In practice, stability analysis of gain-scheduled systems consists of close examination of system simulations. Proof of system stability is rarely sought after.

The linearized system dynamics of a robot arm with a load are given by

$$\frac{Y(z)}{U(z)} = \frac{k_h(1 - bz^{-1})}{(1 - z^{-1})(1 - az^{-1})},$$

until the load is dropped, at which point the system dynamics change to

$$\frac{Y(z)}{U(z)} = \frac{k_h^*(1 - b^*z^{-1})}{(1 - z^{-1})(1 - a^*z^{-1})}.$$

Using the technique of gain scheduling, the designer precomputes the control laws for both plants, \mathbf{K} and \mathbf{K}^* . When the controller microprocessor receives the command to drop the load (or makes the decision itself), the new control law \mathbf{K}^* is used instead of the old one.

Although gain scheduling is adaptive, it is perhaps the least sophisticated of the strategies of adaptive control. This is because a relatively small number of designs are done off-line and loaded into the controller as options that are subsequently chosen during operation as a function of some measured or computed condition. To be fair, gain scheduling is also the most widely used of all adaptive algorithms *by far*, and it can be very effective. For example, it is the predominant method of control used to handle the wide plant variations that occur in flight control systems. Aerodynamic models vary greatly with Mach number or dynamic pressure (function of velocity and air density), and avionic control systems usually schedule gains according to one of these variables, which can either be sensed or estimated. Gain scheduling begins to lose its appeal if the nature of the plant variation is either unpredictable, too variable, or too complex to handle by precomputing control laws and deciding when to use the appropriate one. In any of these cases, a more sophisticated technique is required whereby the control law is designed *on-line*.

Model Reference Adaptive Control (MRAC)

Model reference adaptive control, shown in Fig. 13.63, has a slightly different approach in that it modifies an existing control design to improve some calculated performance measure (error formulated as a desired system model output minus the actual system output). Direct MRAC updates the

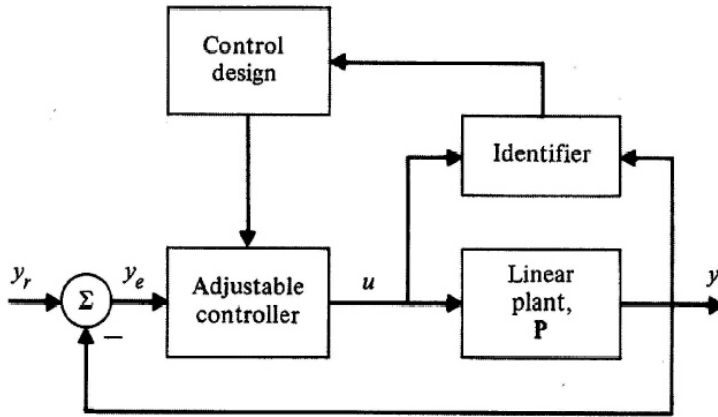


Figure 13.64
Structure of the
explicit
self-tuning
regulator

controller parameters directly, whereas indirect MRAC updates a reference model and the parameters of that model are then used in a design calculation to compute the controller parameters.

Self-Tuning Regulator (STR)

There are many versions and refinements of these ideas that make up the field of adaptive control. The self-tuning regulator originally developed by Åström and Wittenmark is the type of adaptive controller that will be studied in some detail. An excellent survey of the field of adaptive control was done by Åström.

Another approach to adaptive control is in identifying the important plant parameters (the plant model) *while the system is running*. Once the plant parameters are available from the identifier, they are used to redesign the control algorithm according to some design rule as in Fig. 13.64 (explicit self-tuning regulator). Alternately, instead of identifying the plant parameters explicitly, it is possible to formulate the control structure such that the controller parameters which lead to a desired closed-loop system are identified directly (implicit self-tuning regulator). It has been shown that self-tuning regulators and model reference adaptive control can be identical, depending on the underlying design methods.

Explicit Self-Tuning Regulator: Model

Although many different model structures are possible, a minimal state space realization is preferred because of the tremendous volume of design and simulation tools which are available for design in the state space. Most parameter estimation routines are based on a specific model structure, so to be compatible one must choose a common structure. A typical structure is that of an auto regressive moving average (ARMA) model, and as discussed in Chapter 8, the ARMA model parameters can be found using off-line or on-line techniques. The specific parameter estimation algorithms chosen are a function of many considerations including processing power, measurement and process noise, and desired convergence rates.

An ARMA description of an n th order plant with input u and output y is

$$y(k) = -a_1y(k-1) - \cdots - a_ny(k-n) + b_0u(k) + \cdots + b_nu(k-n). \quad (13.96)$$

If no direct control feedforward term exists as in most physical systems, the coefficient b_0 in Eq. (13.96) is zero. The coefficients of the differential equation given by Eq. (13.96) will be used to define a **parameter vector** θ as follows

$$\theta^T \triangleq [a_1 \quad \cdots \quad a_n \quad b_0 \quad \cdots \quad b_n]. \quad (13.97)$$

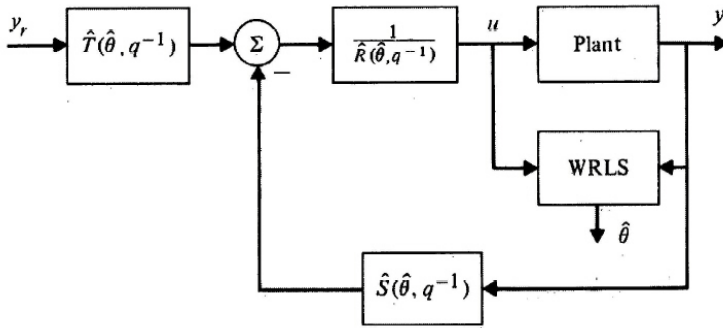


Figure 13.65
Self-tuning regulator (STR) block diagram. Note that the dependence of \hat{S} , \hat{R} , and \hat{T} on the estimated plant parameters is shown explicitly rather than showing them as a function of time

Where appropriate, b_0 will be dropped from the parameter vector leaving $2n$ parameters. If we define a vector of past outputs and past (plus present if b_0 is not 0) controls, as

$$\phi_k^T \triangleq [-y_{k-1} \quad \cdots \quad -y_{k-n} \quad u_k \quad \cdots \quad u_{k-n}], \quad (13.98)$$

then we can write the current output as

$$y(k) = \theta^T \phi_k. \quad (13.99)$$

Equation (13.98) is commonly referred to as the regression vector or vector of regressors. In **polynomial operator form** the plant model is expressed as

$$A(q^{-1})y = B(q^{-1})u, \quad (13.100)$$

which is just a shorthand notation for Eq. (13.96), where q^{-1} is the unit delay operator, for example

$$A(q^{-1})y = y(k) + a_1y(k-1) + \cdots + a_ny(k-n) \quad (13.101)$$

and

$$B(q^{-1})u = b_0u(k) + \cdots + b_nu(k-n).$$

Thus A and B are polynomial operators which characterize the plant. Because z^{-1} represents the z -transform, it is technically incorrect to use it as a delay operator on a system with time-varying coefficients where the z -transform does not apply. Although q^{-1} is used as the delay operator in most literature (and this chapter), it should be just as clear if z^{-1} were used.

Explicit Self-Tuning Regulator: Control Design

There are many ways of specifying the performance objectives of the plant, including input-output bandwidth, step response, phase margin, gain margin, and pole locations. The design method is usually a function of the design objectives. If transformations can be made between various forms of design objectives, then almost any design method can be chosen.

For adaptive control we are interested in a design method which can be accomplished on-line. On-line operation mandates a trade-off between computational complexity or burden and ultimate performance. Any design method chosen must use the information identified from input-output data from the plant, and compute some controller parameters to obtain a desired closed loop behavior. The self-tuning regulator shown in Fig. 13.65 uses weighted recursive least squares (WRLS) (see Chapter 12) to identify the plant parameters and adjust the polynomials S , T , and R which make up the controller.

A powerful design method is that of pole placement. The power of the method lies in the fact that *all* methods essentially just place the poles of the system (zeros cannot be placed with state feedback), thus the (linear) control laws derived by any design technique can be implemented with pole placement. One deficiency in the pole placement design technique is that it assumes that you

know where to put the poles. It could be said that deciding *where* to put the poles is the design, and that pole placement is really an implementation step. In adaptive control, pole placement provides a computationally efficient way of updating the control parameters once the plant parameters are known, assuming the pole locations are decided upon in advance. If the pole locations are to be chosen on-line with a technique such as LQR design, the computational burden climbs astronomically. Therefore, the design step usually consists of designing a control law to place the closed-loop system poles at predetermined locations, and/or at locations which are a simple function of the identified plant parameters. Pole placement is then essentially specifying the desired relationship between command-input and controlled-output as

$$A_d y = B_d y_r, \quad (13.102)$$

where A_d and B_d represent the *desired* closed-loop polynomial operators and y_r is the desired response or reference command. The transfer function of the desired system would be

$$\frac{Y(\omega)}{Y_r(\omega)} = \frac{B_d(q = e^{j\omega T_s})}{A_d(q = e^{j\omega T_s})}, \quad (13.103)$$

where T_s is the sampling time. In shorthand notation we have

$$\frac{Y(\omega)}{Y_r(\omega)} = \frac{B_d(\omega)}{A_d(\omega)} \quad (13.104)$$

$$G_{cl}(\omega) = \frac{Y(\omega)}{Y_r(\omega)}. \quad (13.105)$$

Equation 13.103 is important for several reasons. Perhaps most importantly its numerator should usually contain the zeros of the plant (zeros of $B(q^{-1})$), because achieving a transfer function $G_{cl}(\omega)$ that does not contain some or all of the zeros in $B(q^{-1})$ with Eq. (13.106) implies the zeros are cancelled by poles of the system (roots of A_d). Cancelling roots that are not well inside the unit circle is a bad idea for two reasons: first, the cancellation can never be done exactly and second, the cancellation will occur in only the transfer function G_{cl} (and those which differ from it by a *constant* factor). Thus, if the controller attempts to cancel unstable roots of $B(q^{-1})$ this would destabilize the system because the residues of the unstable modes cannot be made exactly zero. Also, stable roots which are nearly cancelled in the transfer function G_{cl} would not be cancelled in other transfer functions, such as the ones relating disturbance forces to the output of the system. If the stable roots nearly cancelled in G_{cl} represent an eigenresponse much slower than the rest of the system, the eigenresponse will be excited to a much higher extent by, for example, disturbance forces as opposed to the reference command input. This has the unwanted effect of producing extraordinarily slow responses to disturbance forces.

The zeros of A_d can be chosen *a priori*, or according to a simple function of plant parameters such as radial pole projection to optimize overall closed-loop performance for the expected set of plants.

The basic self-tuning regulator is shown in Fig. 13.65. The following equations define the overall system (see Åström (1995)). Define $A_d(q^{-1})$ as the desired closed-loop characteristic polynomial. By the certainty equivalence principle, it follows that

$$A_d(q^{-1}) = A_m(q^{-1})A_e(q^{-1}), \quad (13.106)$$

where A_e is the desired characteristic polynomial of the state estimator and A_m is the desired closed-loop characteristic polynomial if full state feedback were used without the estimator. If the model of the plant in the state estimator represents the plant exactly, and there is no noise in the system, then for perfect estimator initial conditions the closed-loop transfer function of the system is fully adequate to describe all plant responses. The closed-loop transfer function under these ideal conditions is

$$G_{cl}(\omega) = \frac{B(\omega)A_e(\omega)}{A_m(\omega)A_e(\omega)}. \quad (13.107)$$

STR Algorithm

The **estimated parameter vector** $\hat{\theta}$ at time index k is defined as

$$\hat{\theta}^T(k) \triangleq [\hat{a}_1(k) \quad \cdots \quad \hat{a}_n(k) \quad \hat{b}_1(k) \quad \cdots \quad \hat{b}_n(k)], \quad (13.108)$$

with b_0 constrained to be zero. It is θ we wish to identify.

Identification: Using weighted recursive least squares (WRLS) we have

$$\hat{\theta}(k+1) = \hat{\theta}(k) + \left[\frac{P(k-1)\phi(k)}{a^{-1} + \phi^T(k)P(k-1)\phi(k)} \right] (y(k) - \phi^T(k)\hat{\theta}(k)) \quad (13.109)$$

$$P(k) = \frac{1}{\gamma}P(k-1) - \frac{1}{\gamma} \left[\frac{P(k-1)\phi(k)\phi^T(k)P(k-1)}{a^{-1} + \phi^T(k)P(k-1)\phi(k)} \right], \quad (13.110)$$

where $\gamma = 1$, $a = 1$ for RLS (unweighted) and $0 < \gamma < 1$, $a = 1 - \gamma$ for exponentially weighted RLS (WRLS). From $\hat{\theta}(k)$ we form $\hat{A}(k, q^{-1})$, $\hat{B}(k, q^{-1})$ where the coefficients of \hat{A} and \hat{B} are \hat{a}_i and \hat{b}_i , respectively.

Control Law: In keeping with the desire to leave plant zeros in the closed-loop transfer function (no cancellations), we select $B_m = \hat{B}$. We select A_m and A_e from desired closed-loop and state estimator characteristic polynomials, and from

$$\hat{A}(k, q^{-1})\hat{R}(k, q^{-1}) + q^{-1}\hat{B}(k, q^{-1})\hat{S}(k, q^{-1}) = A_m(q^{-1})A_e(q^{-1}), \quad (13.111)$$

solve for $\hat{R}(k, q^{-1})$, $\hat{S}(k, q^{-1})$ and finally calculate $\hat{T}(k, q^{-1})$ from

$$\hat{T}(k, q^{-1}) = [A_m(1)/\hat{B}(k, 1)]A_e(q^{-1}). \quad (13.112)$$

The control signal $u(k)$ is given by

$$\hat{R}(k, q^{-1})u(k) = -\hat{S}(k, q^{-1})y(k) + \hat{T}(k, q^{-1})y_r(k), \quad (13.113)$$

which completes the STR algorithm.

Equation (13.111) is referred to as the ‘‘Diophantine equation’’ and has been studied extensively. The difficulties which arise in solving Eq. (13.111) for $\hat{R}(k, q^{-1})$, $\hat{S}(k, q^{-1})$, $\hat{T}(k, q^{-1})$ include nonuniqueness of the solution and singularities which occur when the estimated plant polynomials $\hat{A}(k, q^{-1})$, and $\hat{B}(k, q^{-1})$ contain common or numerically close factors. In Eq. (13.113) $y_r(k)$ is the unfiltered input reference, as seen in Fig. 13.65. The local convergence proof for this can be found in Goodwin (1984). While global stability of this algorithm is possible, proof of global stability requires **persistence of excitation**. Persistent excitation (PE) refers to the condition of providing the identification routine with enough information about the plant dynamics that the parameter estimates converge to the correct solution. Without PE, the parameter estimates can drift which, of course, causes the resulting controller to be different from the desired controller, and sometimes even unstable. One of the difficulties of losing PE is referred to as **probing**: The system will usually destabilize, and the resulting wild control and plant output action becomes temporarily PE (exciting on a finite interval of time), causing a reconvergence of the plant parameter estimates and hence the controller, thus stabilizing the system. Clearly this can be a vicious cycle in the absence of corrective action. The specific persistent excitation condition is a function of the parameter estimation routine. Excitation measures for various estimation algorithms are also given in Goodwin (1984). A common one for RLS is found in Chapter 12.

Here we shall examine the design of a simple adaptive controller using the explicit or indirect STR. Consider a continuous time transfer function relating the position of a motor armature to the input current

$$G(s) = \frac{Y(s)}{U(s)} = \frac{1}{s(s+1)}, \quad (13.114)$$

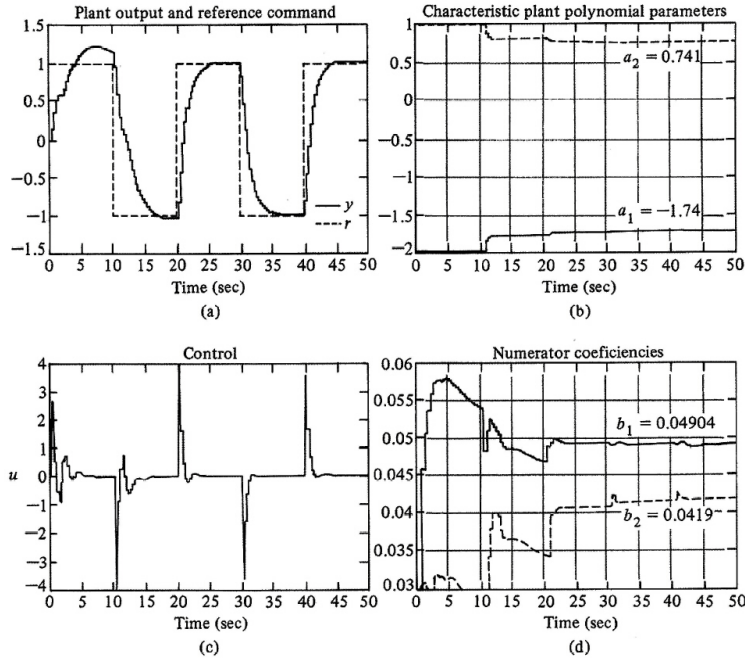


Figure 13.66 Simulation of the self-tuning regulator of Example 13.18. Note the improving command tracking as the parameter estimates converge for the plant (a) command and output response (b) estimated parameters a_1 and a_2 (c) control response (d) estimated parameters b_1 and b_2

which corresponds to the actual parameters of a physical plant. Since we are doing adaptive control, the plant must have a large variance in its parameters, in which case our nominal control design will be designed for the nominal plant. Sampled at $T = 0.330$ seconds, the discrete transfer function is

$$G(q^{-1}) = \frac{b_1 q^{-1} + b_2 q^{-2}}{1 + a_1 q^{-1} + a_2 q^{-2}} \tag{13.115}$$

$$= \frac{0.0489 q^{-1} + 0.0438 q^{-2}}{1 - 1.7189 q^{-1} + 0.7189 q^{-2}} \tag{13.116}$$

$$= \frac{0.0489 q^{-1} (1 + 0.8957 q^{-1})}{(1 - q^{-1})(1 - 0.7374 q^{-1})}, \tag{13.117}$$

which clearly has a zero at -0.8957 , along with poles at 1 and 0.7374 . Design an STR controller for this plant.

Solution. The nominal plant, from which we design the initial control gains, is given by

$$G(q^{-1}) = \frac{\bar{b}_1 q^{-1} + \bar{b}_2 q^{-2}}{1 + \bar{a}_1 q^{-1} + \bar{a}_2 q^{-2}} \tag{13.118}$$

$$= \frac{0.03 q^{-1} + 0.03 q^{-2}}{1 - 2.0 q^{-1} + 1.0 q^{-2}} \tag{13.119}$$

$$= \frac{0.03 q^{-1} (1 + q^{-1})}{(1 - q^{-1})^2}. \tag{13.120}$$

Let us choose the closed-loop system poles to give a settling time of about 12 samples, and also choose them to be real. This yields

$$A_m = (1 - 0.60 q^{-1})^2. \tag{13.121}$$

As stated

$$B_m = \hat{B}. \tag{13.122}$$

Next, we must choose the estimator poles. We will select faster poles, but keep some small amount of noise filtering in the system

$$A_e = (1 - 0.40 q^{-1})^2.$$

With these choices, we can use the pole placement technique to design the controller polynomials S , T , and R with a numerical routine which solves the Diophantine equation with inputs \hat{A} , \hat{B} , A_m , and A_e . The estimated

plant parameters come from an estimation routine such as weighted recursive least squares. For the nominal plant conditions given, and the actual plant, the simulation of the adaptive controller shown in Fig. 13.66 demonstrates the operation of the STR. The value of $\gamma = 0.90$ was used in the WRLS routine. To provide the excitation necessary for the parameter identification routine an alternating position set-point command was provided (period of 20 seconds). Note the original output response is poor, but improves once the parameter estimates converge. As mentioned in Chapter 7, it is possible to construct S , T , and R to give integral control, which would be desired in most designs having such a variable plant.

Controller versus Regulator

The STR is a system based on a linear control law, aimed at setting the poles of the overall system to achieve the desired **regulator** characteristics. The contradiction is that the regulator operation environment usually does not provide the richness of excitation or a signal-to-noise ratio that permits identification. This is because the job of the state regulator is to *keep* things constant or quiescent. If there were no disturbances, the input and output to the plant would be **constant**. Hence during regulator operation, the size of the control is proportional to the size of the disturbance, and ideally the output variation is small. Hence under disturbance rejection conditions, the signal-to-noise ratio is rarely more than 0 dB! Thus for many adaptive control systems, set-point changes are used to provide a signal environment in which the ID algorithm will work well. In addition, set-point changes provide clear demonstration of the system's transient response. If we define a controller or servomechanism as usually following changing input commands, and a regulator as maintaining a constant set-point, the STR would be better referred to as a self-tuning controller or STC. Some of the difficulties associated with regulation can be overcome if an external excitation signal is applied while the self-tuning regulator is tuning.

Most control systems are not linear over large set-point changes. Among the many possibilities, the control usually saturates. Saturation of the control effort is only now being considered in the proofs of stability for self-tuning controllers. Hence in the standard STC we have a structure which assumes a wholly linear control system [once the polynomials $S(q^{-1})$, $T(q^{-1})$, and $R(q^{-1})$ are fixed for the identified plant parameters $\hat{\theta}_a$]. Clearly as we place the poles in locations requiring arbitrarily fast (and perhaps reasonable) time responses the control effort will grow large in amplitude, thus increasing the probability that the system will use values of control effort that are not practical. To implement most nonlinear control laws requires measurement or estimation of a particular set of plant state variables. Since the STC structure does not allow for much choice of the system state, an alternate structure for the STC must be developed.

GSTOC: General Self-Tuning Observer Controller

In this section we will define a general self-tuning observer-controller (GSTOC) algorithm for adaptive control. Rather than a polynomial form, the GSTOC is a structure based on a state estimator with state feedback.

1. Identify the model parameters and formulate a state space model of the plant $\{\Phi_{pp}, \Gamma_{pp}, \mathbf{h}_{pp}\}$.
2. Design a state estimator, obtaining \mathbf{L}_{pp} .
3. Design a control law, obtaining \mathbf{K}_{pp} .

Note that this very general algorithm does not specify which methods are to be used to identify the plant model, or to choose the closed-loop estimator or control gains.

The algorithm for the GSTOC is a strong function of the states chosen to model the plant. In Fig. 13.67 the plant is shown as having a model of $\{\Phi, \Gamma, \mathbf{h}\}$ which is a function of the true plant parameters θ . The form of the model has not been specified, and some forms have advantages over others. The physical model is one which originates from an application of basic physics, and will be denoted with the p-subscript such as $\{\Phi_p, \Gamma_p, \mathbf{h}_p\}$, with the state vector \mathbf{x}_p . The important thing

GSTOC algorithm

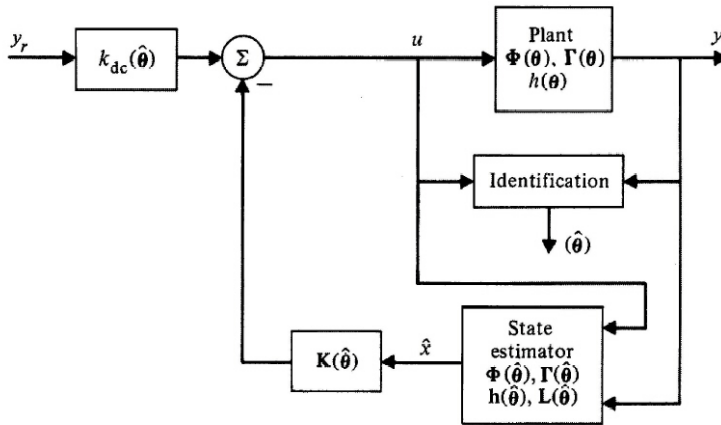


Figure 13.67 Self-tuning observer controller. Both the state estimator poles and the closed-loop system poles are placed based on the model parameters, $(\hat{\theta})$ obtained from the identification scheme. Note k_{dc} is necessary to insure proper DC gain

about the physical model is that the elements of the state vector \mathbf{x}_p have a physical meaning, such as velocities, positions, pressures, temperatures, etc. The practical value of physical model states is that it is straightforward to build test conditions on those states for control purposes. If another form is used, say the controller canonical form, the states are a linear combination of the physical states. For example, a particular state variable may be related to the physical states in that it is velocity plus position plus acceleration. This amalgam of physical states unnecessarily complicates the control designer's task. If, for example, it is desired to sense and limit the acceleration, the transformation back to the physical states would have to be formed and executed anyway. So in many cases it is best to formulate the system model using the physical states. In addition, the ARMA model is the most sensitive model from a coefficient round-off standpoint. Either cascade or parallel models generally have much better numerical properties, especially with increasing order.

If the identification is based on an ARMA model of the plant, then the transformation to the physical states is not simple in most cases. It usually requires a transformation matrix $T \in \mathbf{R}^{n \times n}$ that has no exploitable structure. Since different physical plants rarely share a fixed or regular structure, a general transformation from physical form to a canonical form is not possible. Of course it is possible to derive a transformation for a specific minimal physical model to a canonical form, but there is no guarantee that any exploitable structure will exist in the transform that would reduce the computational complexity below that of matrix multiplication (of order n^3).

Issues in Adaptive Control

Adaptive control receives much attention in the research community. Among the primary difficulties in analysis of adaptive control systems is the time varying and nonlinear nature of the state equations of an adaptive system. Additionally, many algorithms require large amounts of computation, limiting their use to the most expensive systems, which focuses attention on finding practical methods with less computational burden. Another key difficulty, although not specific to adaptive control, is accurate plant identification under closed-loop control. Many advances have been made in proving stability under certain (sometimes limited) conditions. However, stability is *not* performance, and not much ground has been gained in proving performance bounds. A lot could be said about the various issues in adaptive control, but the reader is encouraged to read some of the references for this chapter to learn more. Below is a partial list of issues in adaptive control.

Stability with:

1. No known information.
2. Known plant order.
3. Unmodeled dynamics.

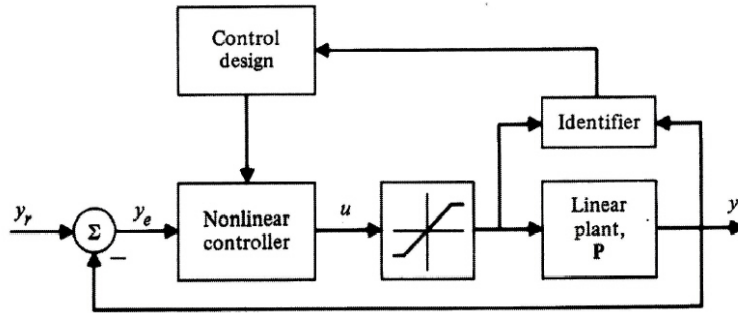


Figure 13.68
Structure of the adaptive nonlinear controller. Although the saturation block is not required, it is usually present in the control to any real plant and thus provides an excellent example of a system that can perform better with a nonlinear controller

4. Disturbances, noise.
5. Unknown high frequency phase.
6. Plant zeros outside unit circle (not stably invertible).
7. Limited control authority.
8. Plant poles outside the unit circle.
9. Various degrees of plant excitation.

Performance Issues:

1. Convergence rate.
2. Comparison versus fixed control law.
3. Robustness enhancement.

Of course the list above varies a bit from STR to MRAC. While the STR can handle plant zeros outside the unit circle, the MRAC runs into stability difficulties. Unlike continuous-time systems which rarely have right-half-plane zeros, discretized plants *very often* have zeros outside the unit circle. In fact, this has been proven guaranteed for pole-zero excess greater than one, and fast enough sampling rates. In addition, incorporating nonlinear control design such as time-optimal control is difficult with the MRAC while it is easily accomplished with an STR (see APTOS in next section).

Adaptive nonlinear control provides for adjustment of a nonlinear control law instead of the linear control law assumed in standard adaptive control. A block diagram of an adaptive nonlinear controller is shown in Fig. 13.68. Although this is but one of hundreds of possible examples, the ideas are illustrated well by extending the nonlinear controller of Example 13.17 to include an adaptive feature.

As an example of adaptive nonlinear control we will adjust the PTOS controller developed in Section 13.3.2 and the plant will be the familiar double integrator. Although PTOS is robust to deviations in the model, performance improvements can be achieved by *adapting* PTOS (APTOS) to changes in the plant.

We will propose and analyze a simple one parameter identifier in the APTOS structure as an example of adaptive nonlinear control. In terms of polynomials in the unit delay operator q^{-1} , the input-output relationship of the double integrator plant is

$$(q^{-1} + q^{-2})u = \left(\frac{2}{a_{nom}T_s^2} \right) (1 - q^{-1})^2 y,$$

where a_{nom} represents the nominal or expected value of the plant gain a . Normalizing the estimated parameter \hat{a}_n in this way is a convenient way to organize the equations. The estimated parameter

is then $\hat{a} = \hat{a}_n a_{nom}$. If the estimated parameter is exactly equal to the expected nominal value, then $\hat{a}_n = 1.0$ ($\hat{a} = a_{nom}$). If the estimated value of a is 15 percent larger than a_{nom} , then $\hat{a} = 1.15$. When the parameter estimator has converged ($\hat{a} = a$), $a = \hat{a}_n a_{nom}$. If the measured data are $\{ u, y, t = 0, T_s, 2T_s, \dots \}$ then we can form an equation error as follows

$$\varepsilon \triangleq z - \hat{a}_n \phi, \quad (13.123)$$

where

$$z = \left(\frac{2}{a_{nom} T_s^2} \right) (1 - q^{-1})^2 y \quad (13.124)$$

$$\phi = (q^{-1} + q^{-2})u. \quad (13.125)$$

Consider the LMS identifier (see Chapter 12) for the *normalized* plant gain \hat{a}

$$\hat{a}_{k+1} = \hat{a}_k + g\phi\varepsilon. \quad (13.126)$$

With this identifier and some PE conditions (satisfied by changes in the input reference command r), it is possible to adjust the design of the closed-loop PTOS controller so it can adapt to changes in the acceleration constant of the plant. In the implementation, the parameter estimate is *not* updated when the system is in regulation mode, which prevents parameter drift due to lack of persistent excitation. After a countable number of input command changes, the system is tuned.

In this case, update of the control law is simple in that only a single parameter is identified. The parameter \hat{a} will simply scale the acceleration gain used to calculate the velocity trajectory, as well as the other design parameters which are a function of a . Specifically, we have the following adjustments to make

$$\hat{k}_1 = \frac{k_1}{\hat{a}} \quad (13.127)$$

$$\hat{k}_2 = \frac{k_2}{\hat{a}} \quad (13.128)$$

$$\hat{y}_l = \frac{1}{\hat{k}_1}, \quad (13.129)$$

and based on these parameters the velocity trajectory $f(\cdot)$ is

$$f(y_e) = \begin{cases} \frac{k_1}{k_2}(y_e) & \text{for } |y_e| \leq \hat{y}_l \\ \text{sgn}(y_e)[(2a_{nom}\hat{a}\alpha|y_e|)^{1/2} - \frac{1}{\hat{k}_2}] & \text{for } |y_e| > \hat{y}_l. \end{cases} \quad (13.130)$$

Hence in this single unknown parameter case, the adjustment of the control algorithm is fairly straightforward. When multiple parameters are identified the trajectory is far more complex than that given by Eq. (13.130). For cases other than the double integrator, explicit calculation of the function $f(\cdot)$ also becomes impractical.

Next we will examine the performance of the simple APTOS system during adaptation. Adaptation under ideal conditions is shown in Fig. 13.69. As is seen in the figure, the closed-loop system clearly approaches that of the tuned PTOS controller. Overshoot in the first command change responses is due to the initial overestimate of the plant acceleration gain capability. Position overshoot is in effect amplified in the control signal, so to judge the final degree of overshoot it is easier to look at the control signal. The control is shown in the same plot as the plant position output, and has been scaled by a factor of ten.

Generating a Table for $f(\cdot)$

In the discrete time case, an alternative for finding the desired velocity as a function of position error exists: generate a table for values of $f(\cdot)$ versus the argument. Given a position error value

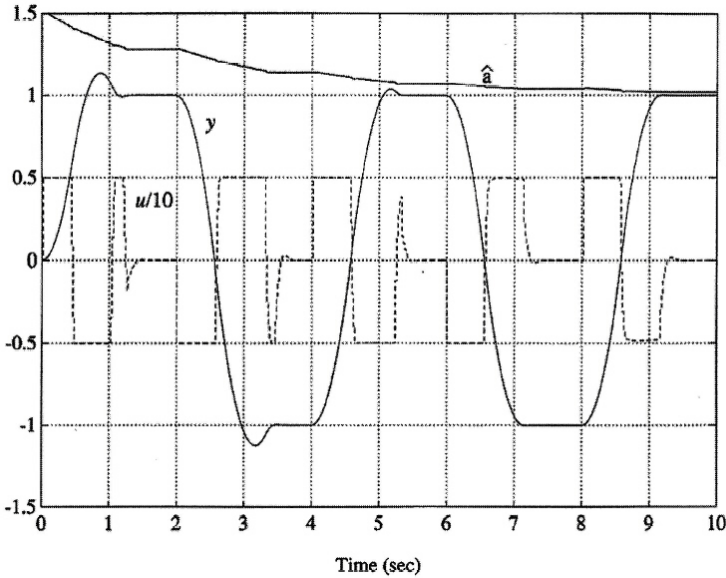


Figure 13.69
APTOS transient
behavior to an
initial error in
parameter
estimate of 50%

$y_e(k)$, many methods are available for obtaining the corresponding value of $f(y_e(k))$ from the table of stored values. Closest entry or various types of interpolation can be employed. The resolution of the data stored in the table can be variable as well (Workman, 1982). Whatever the technique, we must discuss *how* the values in the table are generated in the first place, and how this can alleviate the problem of computing $f(\cdot)$.

Backwards in Time

The trajectory of a plant that leads to the origin can be derived by starting at the origin, applying the desired control while trajectory following, and simulating the system *backwards* in time. In discrete time this process is simply an iteration on the inverse system. If the plant is described by

$$\mathbf{x}_{k+1} = \Phi \mathbf{x}_k + \Gamma u_k \quad (13.131)$$

$$y = \mathbf{h}\mathbf{x}, \quad (13.132)$$

then the inverse system is given by

$$\mathbf{x}_k = \Phi^{-1} \mathbf{x}_{k+1} - \Phi^{-1} \Gamma u_k \quad (13.133)$$

$$y = \mathbf{h}\mathbf{x}. \quad (13.134)$$

Now stepping Eq. (13.133) from a final condition, with the desired deceleration control history, will generate the state trajectory that leads to the origin. Of course to be of use in the PTOS architecture it is necessary that the position and velocity states be available in the state \mathbf{x} . If the plant is identified using a second-order WRLS algorithm, then the resulting ARMA parameters must be used to derive the state space representation in terms of these states.

Computing a State Transformation for PTOS

Example 13.19

Assume a constrained (one of the system poles is at $z = 1$) identification is done on a second-order plant. The form of the constrained result is as follows

$$x_o(k+1) = \begin{bmatrix} 1+a_2 & 1 \\ -a_2 & 0 \end{bmatrix} x_o(k) + \begin{bmatrix} b_1 \\ b_2 \end{bmatrix} u(k), \quad (13.135)$$

and the output is given by the first state

$$y = \begin{bmatrix} 1 & 0 \end{bmatrix} x_o. \quad (13.136)$$

Equation 13.135 is an observer canonical form of a plant with a zero at $z = b_2/b_1$ and two poles, one at $z = 1$, and one at $z = a_2$. This corresponds to the discrete time model (sampling time of T seconds) of a continuous time plant given by a real-pole followed by an integrator. The state of the physical form of the model consists of position and velocity ($x_p = [y, v]^T$). The state space description in this form is

$$\mathbf{x}_p(k+1) = \begin{bmatrix} 1 & T \\ 0 & +a_2 \end{bmatrix} \mathbf{x}_p(k) + \begin{bmatrix} \frac{b_1}{T} \\ \frac{b_2 + b_1 a_2}{T} \end{bmatrix} u(k), \quad (13.137)$$

and again the output is given by the first state

$$y = \begin{bmatrix} 1 & 0 \end{bmatrix} x_p. \quad (13.138)$$

Complete the transformation from the observer form of Eq. (13.135) to the physical form of Eq. (13.137) and the inverse to be used to construct the PTOS curve. That is, find T_{po} so that $x_p = T_{po}x_{po}$.

Solution. The transformation matrix T_{po} from observer states to physical states is given by

$$T_{po} = \begin{bmatrix} 1 & 0 \\ \frac{a_2}{T} & \frac{1}{T} \end{bmatrix} \quad (13.139)$$

and

$$T_{po}^{-1} = T_{op} = \begin{bmatrix} 1 & 0 \\ -a_2 & T \end{bmatrix}. \quad (13.140)$$

Now after identification by WRLS, Φ_o and Φ_p are obtained by direct substitution of the ARMA parameters (θ)

$$\theta^T = [a_1 \quad a_2 \quad b_1 \quad b_2],$$

where the feedforward term b_0 is assumed to be zero and is not estimated (constrained to zero). Thus from the ARMA parameters we can derive the inverse physical system

$$x_p(k) = \begin{bmatrix} 1 & T/a_2 \\ 0 & -1/a_2 \end{bmatrix} x_p(k+1) + \begin{bmatrix} \frac{b_2}{a_2} \\ \left(\frac{b_2 + b_1 a_2}{a_2 T} \right) \end{bmatrix} u(k). \quad (13.141)$$

Now, whenever an updated set of ARMA parameters is available from the identification routine, the time-optimal trajectory can be generated by updating Eq. (13.141) with new parameters and iterating with a beginning terminal condition and a desired control. The results are stored in a table and used for the trajectory.

If the PTOS structure is used however, it is not the state we should store in the table. Rather, we should store a value for $f(\cdot)$ which would give us the trajectory generated by Eq. (13.141) when run forward in time with a PTOS controller. That is, in PTOS we have

$$u = k_2(f(y_e) - v), \quad (13.142)$$

so, given points on a trajectory (y, v), and the control used to generate it, we have

$$f(y_e) = v + u/k_2. \quad (13.143)$$

Note that if we generate the positive quadrant of the trajectory ($y_e > 0, f(y_e) > 0$), the control will be *negative* and Eq. (13.143) will actually cause the stored value of $f(y_e)$ to be smaller than the actual trajectory the system will follow. As the velocity loop gain increases, the velocity error will decrease, and the modification of Eq. (13.143) will become smaller. Also, to allow for control margin in deceleration we should incorporate an acceleration discount factor in Eq. (13.141). This is trivial in that it is accomplished by reducing the value of u used to generate $f(\cdot)$. For a maximum control of m we have

$$u = \alpha m. \quad (13.144)$$

Table 13.5RNS algorithm for the computation of the control law parameters P that minimize $C(P)$

-
0. $k \leftarrow 0$.
 1. $P \leftarrow P^0$, select initial parameters.
 2. $C^* \leftarrow \infty$.
 3. $k = k + 1$, calculate cost function $C(P)$.
 4. If $C(P) > C^*$, go to 7.
 5. $P^* \leftarrow P$.
 6. $C^* \leftarrow C(P)$.
 7. If $k > k_{max}$ go to step 10.
 8. Select new $P \leftarrow P^*[1 + \text{rand}(\cdot)\rho]$.
 9. Go to step 3.
 10. Write output files.
 11. Done.
-

Thus an explicit formulation of the desired velocity function is not required in the discrete-time case. This is a key benefit, since most servomechanisms include either friction or back-emf (see Fig. 13.40), which make explicit calculations difficult, and implementation nearly impossible.

Section 13.2.1 contains some of the basic ideas used in adaptive nonlinear control. Adjusting nonlinear control algorithms based on plant parameters that are identified while the controller is operating is the fundamental concept. Adaptive nonlinear control is sometimes used in the field of robotics,¹² where the plant is always highly nonlinear and the control algorithm is usually some form of INL controller such as computed torque; adaptive control is used to adjust for variations in plant parameters such as payload inertia or varying plant characteristics such as friction, motor torque constant, bias forces, and gains.

13.3 Design with Nonlinear Cost Functions

We have already covered LQR, LQG, and pole-placement in Chapters 8 and 9. Other techniques based on nonlinear cost functions are available that augment the aforementioned design tools. Essentially the quadratic case, although nonlinear, is used because it is mathematically tractable. The results are proven to be optimal in a *quadratic* sense. The question always arises, “Is that the proper quantity to optimize?” All too often the answer is negative. But in that case the theory leaves us high and dry, at least for the most part. A very useful technique is that of random neighborhood search (RNS) based on a nonlinear cost functional. This method is a type of Monte Carlo procedure with an improved technique for choosing parameters.

13.3.1 Random Neighborhood Search

The technique here is very simple: Formulate the desired properties of the control system as a cost function, and search in a Monte Carlo fashion for the controller parameters which best minimize the cost. But only search the region in parameter space centered on a point which has the lowest known cost. Defining the cost as C and the controller (free) parameters P the algorithm is given by Table 13.5. The size of the search region centered about the current optimum point is up to the engineer using the program, as is the relative weighting of various terms which comprise the cost function.

Up to now we have not specified the nature of the cost function. It clearly is not the familiar quadratic one, or we would use the LQR design techniques of Chapter 9. Let us use an example to

¹²Robot dynamics are extremely complicated. A good reference in the context of adaptive control is given in Craig (1986).

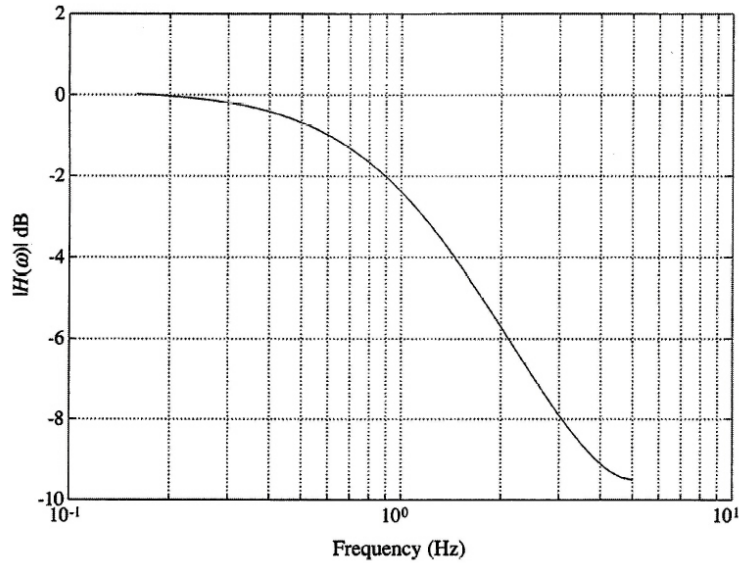


Figure 13.70
Frequency
response after
optimization

illustrate the RNS design algorithm. Consider the system described by the transfer function

$$H(z) = \frac{az^{-1}}{1 - bz^{-1}} \quad (13.145)$$

Suppose that we want to find the parameters $P = (a, b)$ to minimize the cost function $C(P)$. This will be a highly nonlinear problem if the cost is in terms of more classical measures of system performance, for example

$$C = W_{BW} |f_{BW} - 1| + W_{DC} |H(0) - 1.00|, \quad (13.146)$$

where

$H(e^{j\omega T})$ = system transfer function

$T = 0.01$, sampling interval, sec.

f_{BW} = is the lowest frequency where $20 \log |H(e^{j2\pi f_{BW} T})| < -2.5$

W_{BW} = weighting on bandwidth error

W_{DC} = weighting on zero-frequency gain error.

Although it would be much simpler to determine P analytically in this case, in more realistic cases it is extremely difficult if not impossible to minimize C in any way but numerically. Proceeding, we build a program which implements the algorithm in Table 13.5 and search for P to minimize C given by Eq. (13.146). The results of the parameter search are shown in Fig. 13.70 and Fig. 13.71 and tabulated in Table 13.6.

One of the most interesting features of this algorithm is that the field of search is sufficiently wide that it will not get stuck as a gradient algorithm might for complex cost functions with a multitude of local minima. The field of search for each intermediate point $P = (a_i, b_i)$ is in this case (two parameters) a square with the four corners defined by $((1 \pm \rho)a_i, (1 \pm \rho)b_i)$. Clearly the rate of convergence and the solution which is optimal is affected by the relative weighting factors put on the various components of the cost function, in this case the DC gain error as well as the bandwidth error. A high weighting (W_{DC}) on the DC gain error would tend to follow a trajectory in the parameter space given by $a = 1 - b$. High emphasis on the bandwidth would yield $b \rightarrow 0.5$ much more rapidly but concurrently with $a \rightarrow 0.5$.

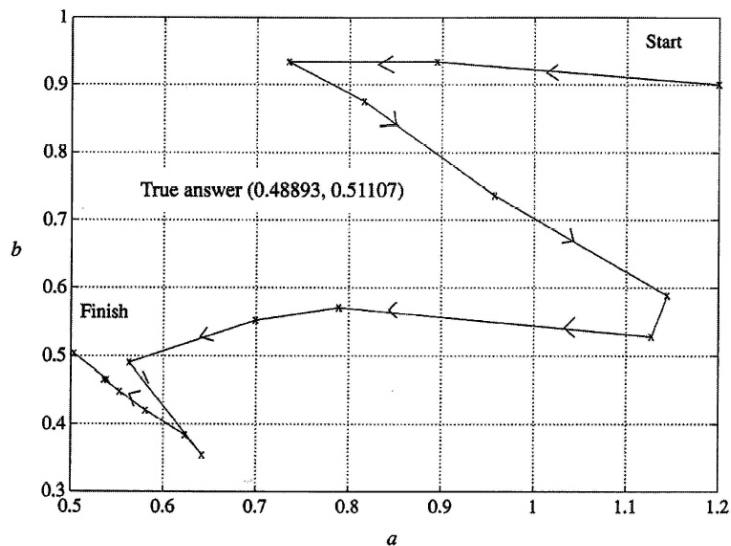


Figure 13.71
Successful parameter moves during the RNS optimization

Table 13.6

Performance measures and parameters before and after optimization with RNS routine (50 iterations with $\rho = 0.30$)

Parameter/Masurement	Initial Value	Optimized Value
a	1.200	0.505
b	0.900	0.485
$H(0)$	12.00	1.002
f_{BW}	3.700	1.099
C	489.5	2.505
T		0.10
W_{BW}		10.0
W_{DC}		20.0

Table 13.7
Desired performance goals for torque motor positioning servo

Performance Measure	+ Symbol in Value	Units	Eq. (13.148)
Bandwidth	1000.	Hertz	f_{BW}
Minimum damping	0.750	ζ_{\min}	
Minimum phase margin	45.0	degrees	pm
Peaking of H_{yyr}	4.00	dB	$peak$
Maximum time constant	900.0	microseconds	$\bar{\tau}$
Sum of time constants	1.80	milliseconds	$\Sigma\tau$
Attenuation at 4 kHz	22	dB	$20\log_{10}(H_{ol}(2\pi 4000))$
Gain margin	20.	dB	g_m

The advantage of this algorithm is in the specification of the cost function C . Since there are many obvious arguments against using RNS in this problem (primarily that the problem can be solved by inspection), a more complicated example will be used to compare and contrast the benefits of RNS against LQR.

We will now compare two different techniques to design the torque motor servo as given in Fig. 13.42 in Section 13.2.1. Since the structure of the problem has already been chosen, we would now like to choose the free parameters to achieve the design objectives. Using the LQR approach to the design problem, we choose to minimize the cost function

$$\mathcal{J} = \frac{1}{2} \sum_{k=0}^N [\mathbf{x}_k^T \mathbf{Q}_1 \mathbf{x}_k + \mathbf{u}_k^T \mathbf{Q}_2 \mathbf{u}_k]. \quad (13.147)$$

This method requires that values of \mathbf{Q}_1 and \mathbf{Q}_2 must be selected. In Chapter 9 we discussed the derivation of the optimal control law gains \mathbf{K} for which $\mathbf{u} = -\mathbf{K}\mathbf{x}$ given \mathbf{Q}_1 and \mathbf{Q}_2 , and gave guidelines for selection of the \mathbf{Q} 's. Control designers do not usually think in terms of \mathbf{Q}_1 and \mathbf{Q}_2 in determining performance. Indeed, most control engineers think in terms of more classical measures of performance such as command response, disturbance response, bandwidth, and sensitivity to parameter uncertainty. Also, when control engineers are given specifications, it is usually the classical performance measures that are given.¹³ The reality is that often \mathbf{Q}_1 and \mathbf{Q}_2 are chosen, the classical performance measures of the resulting system are computed, and then \mathbf{Q}_1 and \mathbf{Q}_2 are changed to affect desired changes in the classical performance measures. Of course, once the desired performance is achieved, the design can be claimed to be optimal in the sense that it minimizes Eq. (13.147). In fact minimizing Eq. (13.147) was not the original goal, but rather we wanted to minimize a classical cost function such as Eq. (13.146).

In order to proceed with the RNS design, it is first necessary to define the design goals. We will summarize the performance of the positioning servo with some classical measures. Because of uncertainty in the plant dynamics above 2 kHz, we will limit the closed-loop–3 dB bandwidth from the command input to plant position to 1 kHz. To minimize system sensitivity, we will also constrain the damping ratio of each mode to be at least 0.550, the decay envelope of each mode to be at least as fast as 900 microseconds, and the sum of all time constants to be less than 1.8 milliseconds. To minimize amplification of mid-band disturbances in the position reference and noise input y_{ref} , we will limit the peaking in the closed-loop transfer function from y_{ref} to y to 4 dB. We would also like to ensure that a detrimental set of mechanical plant resonances which are near 4 kHz are attenuated by at least 22 dB. These requirements are summarized in Table 13.7.

¹³Sometimes control engineers are given detailed specifications, but they often have a significant role in developing these specifications.

A cost function C which represents the desired goals in Table 13.7 can be defined as follows

$$\begin{aligned}
C = & W_{BW} |f_{BW} - 1000| - W_{\zeta} \text{rect}(\zeta_{\min} - 0.750) \\
& - W_{pm} \text{rect}(pm - 45.0) + W_{peak} \text{rect}(peak - 4.00) \\
& + W_{\tau_{\max}} \text{rect}(\bar{\tau} - 1.0 \times 10^{-3}) + W_{\tau_{\text{sum}}} \text{rect}(\Sigma_{\tau} - 1.8 \times 10^{-3}) \\
& + W_{4kHz} \text{rect}(22.0 + 20. \log_{10}(H_{ol}(2\pi 4000.))) \\
& + W_{gm} \text{rect}(20.0 - g_m) + W_{peakhe} \text{rect}(peakhe - 4.5) \\
& + W_{peakyr} \text{rect}(peakyr - 1.0), \tag{13.148}
\end{aligned}$$

with the following definitions: the closed-loop transfer function from reference input y_r to output y is

$$H_{yy_r}(\omega) = \frac{Y(\omega)}{Y_r(\omega)},$$

from position reference (and/or noise) input y_{ref} is

$$H_{yy_{ref}}(\omega) = \frac{Y(\omega)}{Y_{ref}(\omega)},$$

and bandwidth is taken as the first -3 dB point of the appropriate transfer function. The function “rect” is best described as a linear diode, or rectifier according to the equation

$$\text{rect}(x) \triangleq \begin{cases} x & x \geq 0 \\ 0 & x < 0. \end{cases}$$

The design found using a 500 run RNS method starting from a stable pole placement design is (note this is not a unique solution)

$$\mathbf{K} = [11.80 \quad 3.232 \quad 1.000]. \tag{13.149}$$

For a PTOS controller (see Section 13.2.2), we can easily place a constraint on k_2 such that

$$k_2 = \left(\frac{2k_1 K_{\theta}}{\alpha a} \right)^{1/2}.$$

With $\alpha = 0.840$, and an a given by $K_t(0)/J_a$, we have the following slightly different \mathbf{K}

$$\mathbf{K} = [11.80 \quad 3.3523 \quad 1.000], \tag{13.150}$$

which was used in Section 13.2.2. The estimator gains found by the RNS run were

$$\mathbf{L} = [0.7280 \quad 1.8477 \quad 0.4933]^T. \tag{13.151}$$

The results are summarized in Table 13.8 and Fig. 13.72.

It is important to note that there exists an *inverse* control problem, that is, for some \mathbf{K} , there may exist at least one set of \mathbf{Q}_1 and \mathbf{Q}_2 for which \mathbf{K} is the optimal control law to minimize Eq. (13.147). Therefore, using the INS method might produce an LQR optimal control law, but we aren't sure what \mathbf{Q}_1 and \mathbf{Q}_2 are for that K . Is this important? If so, either one should use the LQR approach to design or develop the necessary theory to generate an optimal analytical solution to minimize C without numerical iteration. Along these lines, a technique for linear controller design in terms of classical measures of performance has been worked out by Boyd and co-workers (Boyd, 1988). The technique uses the parameterization method of Youla, shows that the performance measure is convex in the parameters of the controller as defined, and invokes powerful numerical means to compute the optimal solution. One disadvantage of using this approach is that it may produce a controller of high order, from which the designer might wish to use some approximation or model reduction technique. When coupled with other design techniques, Boyd's method is a powerful tool that shows great promise.

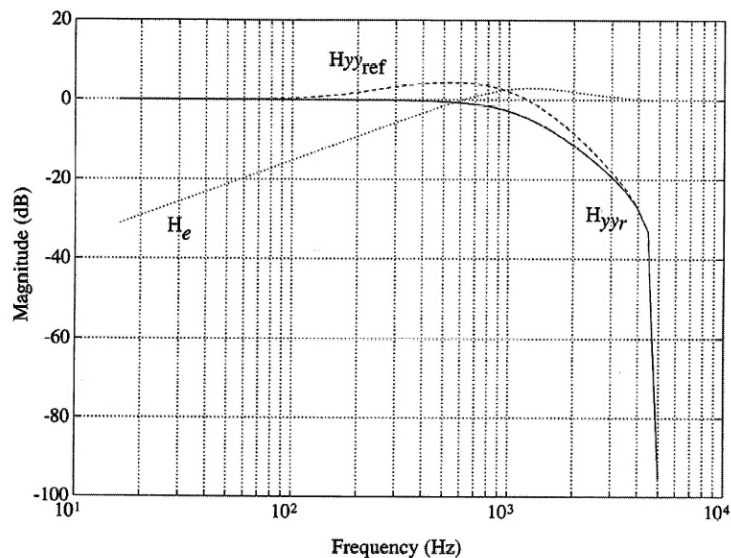


Figure 13.72
Frequency response after optimization

Table 13.8

Performance measures and parameters before and after optimization with RNS routine for (500 iterations, $\rho = 0.30$)

Parameter/Measurement	Initial Value	Optimized Value
L^T	[0.6089 2.193 1.232]	[0.7280 1.8477 0.4933]
K	[2.9612 1.4372 1.000]	[11.80 3.3523 1.000]
Σ_τ	1992. μ secs	1833. μ secs
$\bar{\tau}$	513. μ secs	920. μ secs
f_{BW}	512. Hz	961 Hz
$20 \cdot \log_{10}(H_{ol}(2\pi 4000))$	38.0 dB	27.4 dB
g_m	19.76	15.10 dB
ζ_{min}	0.650	0.812
$peak$	8.12 dB	4.269 dB
T		0.10 mSec
W_{BW}		0.01
W_{pm}		0.20
W_{peak}		3.30
W_ζ		10.0
W_{taumax}		10000.
W_{tausum}		10000.
W_{peakhe}		3.3
W_{peakyr}		3.3
W_{4khz}		0.33
W_{gm}		0.33

In either LQR or RNS design, it is difficult to imagine dispensing with the design engineer. In the case of LQR, the design engineer must iterate on \mathbf{Q}_1 and \mathbf{Q}_2 , and α if pincers is used (see Chapter 9). A lot of judgement and practical intuition goes into the iterative steps. With RNS, the cost function is much more clearly put in terms of performance specifications, but *convergence* and optimal control laws are not guaranteed. In addition, when constructing the cost function C , there is no guarantee what the minimum value of C will be. Of course the *structure* of the controller determines what is achievable: integral control, model reduction, current versus predictor estimation are all important factors in achieving performance objectives, and neither RNS nor LQR control synthesis alternatives explicitly make those choices.

13.4 Summary

In this chapter topics on the analysis and design of nonlinear control systems are presented. The main points in the analysis are

- The describing function is a heuristic approach to analysis based on the frequency response.
- The describing function will usually give good estimates of the amplitude and frequency of steady-state oscillations known as a limit cycle.
- For nonlinear characteristics that have no memory, the equivalent gain method can be used with the root locus to give the same results as the describing function.
- A sufficient condition for stability is given by the circle criterion.
- A comprehensive stability theory is given by the second method of Lyapunov.

The main points covered on the design of nonlinear control systems are

- Many nonlinear systems can be made linear for control by the use of an inverse nonlinearity.
- Time-optimal control is an effective objective for many motion control problems.
- A stable almost time-optimal controller can be constructed as the PTOS controller.
- A digital PTOS can be designed and shown to be stable if limitations on the sample period are observed.
- The PTOS controller can be made adaptive by including the estimation of key parameters.
- The PTOS controller can be heuristically extended to control higher-order dynamic systems.
- The self-tuning regulator is a general adaptive controller for linear systems with slowly varying parameters that is widely used in the process industries.

13.5 Problems

13.1 Using linearization, design a Type 0 control system (the function $f(r, v, y)$) for the following plant

$$\begin{aligned}\dot{x}_1 &= 30x_2 \\ \dot{x}_2 &= 75w \\ w &= \arctan u \\ u &= f(r, v, y)\end{aligned}$$

where the output $y = x_1$ is to track a random reference input. The state variable x_2 is the plant velocity. The system should have a settling time no more than 0.10 seconds, and no more than 10% overshoot. The normal operating point is at $y = 0$. Use a sample time of $T = 0.01$ sec.

- 13.2 Simulate the system you designed in Problem 1. For what range of input step magnitudes does the system meet the 10% overshoot requirement? Can you design the system to accept larger step inputs without violating the 10% overshoot constraint?
- 13.3 Assuming that the nominal set-point for problem 1 is again $y = \text{constant}$, but that a disturbance is present in the plant input, $d = -0.500$, redesign the controller using linearization for the same specifications. The plant equations become

$$\begin{aligned}\dot{x}_1 &= x_2 \\ \dot{x}_2 &= w - 0.500 \\ w &= \frac{2}{\pi} \arctan u \\ u &= f(r, v, y).\end{aligned}$$

Simulate the system you design. For what range of input step magnitudes does the system meet the 10% overshoot requirement? What happened to the controller gains? Why?

- 13.4 Show that the describing function of the signum function with a deadzone is

$$D(A) = \begin{cases} \frac{4m}{\pi} \sqrt{1 - \left(\frac{d}{A}\right)^2} & A > d \\ 0 & A < d \end{cases}$$

where the deadzone is centered around zero and is of width $2d$ ($\pm d$), and the magnitude of the nonzero part of the input-output relationship is m . What is the range of equivalent gains for the signum function with deadzone?

- 13.5 Calculate the describing function of the quantizer (hint: use the previous problem to construct the input-output relationship for the quantizer). What is the range of equivalent gains for the quantizer? What sector does the quantizer nonlinearity lie in?
- 13.6 Calculate the describing function of the truncation function, $y = q \text{int}(x/q)$. The function $\text{int}(x)$ is the largest integer smaller than x .
- 13.7 Explain using the method of equivalent gains why truncation of a servo error signal e as above will almost surely lead to an unstable system at $e = 0$. What sector does the truncation nonlinearity lie in?
- 13.8 What is the equivalent gain of the deadzone nonlinearity versus the input amplitude to it? The input-output relationship of the deadzone function is

$$y = \text{DZ}(x) \triangleq \begin{cases} 0 & |x| \leq d \\ K(x-d) & x > d \\ K(x+d) & x < -d. \end{cases}$$

- 13.9 The accompanying figure shows a discrete-time phase-locked-loop (PLL) in which a deadzone having $K = 1$ (see previous problem) has been inadvertently added to the voltage controlled oscillator. Use equivalent gains to determine if the deadzone will cause the PLL to have a limit-cycle. Assume another pole (a factor $(1 - 0.5z^{-1})$ in the compensator denominator) is present in the phase discriminator. Would the system behave differently?

10.00

- 13.10 Given positive constants c_1 and c_2 , let $y = f(x) = c_1x + c_2 \sin x$

- (a) What sector is the function $f(\cdot)$ in?
- (b) Sketch the region specified by the circle theorem which should be avoided to guarantee stability of a linear plant $P(z)$ with $f(\cdot)$ in the feedback path.

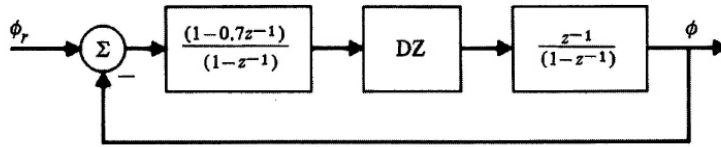


Figure 13.73
Block diagram of
a phase-locked
loop

13.11 Using linearization, derive a linearized model of the PLL with the deadzone nonlinearity (as given above in Problem 8) in the VCO, at the $[0\ 0]$ state with zero input phase.

13.12 Using the linearized model of the wastewater pH control example

- Find pole locations which indeed give a 0 to 100% rise time of 200 seconds with no more than 5% overshoot.
- Will the speed of the controller have an effect on the validity of the linearized model? Consider control amplitudes.
- Using a finite control authority, reconsider (b).

13.13 Calculate the describing function $D(A)$ of

(a) $y = x^{2n-1}$ for $n = 1, 2, 3, \dots$

(b) Show¹⁴ that the describing function $N(A)$ of an arbitrary odd polynomial with coefficients b_n

$$y = b_1x + b_3x^3 + b_5x^5 + \dots + b_{2n-1}x^{2n-1} \quad \text{for } n = 1, 2, 3, \dots$$

where x is the input to the polynomial and y is the output, is given by

$$N(A) = b_1 + \frac{3}{4}b_3A^2 + \frac{5}{8}b_5A^4 + \frac{3}{64}b_7A^6 + \dots$$

where the input is $x = A \sin \omega t$.

13.14 Using the polynomial describing function above and the series expansion of the arctangent function, calculate the describing function for the arctangent nonlinearity with input x and output y , $y = \frac{2}{\pi} \arctan x$. Use the range of x given by $|x| \leq 1$.

13.15 What sector is the arctangent function of Problem 1 in? According to the method of equivalent gains, is the control system designed for Problem 1 stable?

13.16 Find the best parameters m and k for the modified saturation function that best fits the input-output relationship for the arctangent nonlinearity of Problem 1.

- Simulate the control system of Problem 1 using the modified saturation nonlinearity found above.
- For what size step inputs does the system respond with less than 10% overshoot.
- Plot the describing function of the arctangent nonlinearity from the previous problem and that of the saturation function. From this analysis, which nonlinearity gives a wider range of inputs while remaining within the overshoot criterion? Does this match the simulation?
- If the plant contained a disturbance input of 0.5 and the arctangent nonlinearity was replaced by the saturation nonlinearity, would you have to redesign the controller to maintain small signal response characteristics? Why?

¹⁴From Ogata.

- 13.17 Assume a measurement of the input–output relationship of a memoryless nonlinearity is available.
- Suggest a technique for quantitatively calculating the describing function.
 - In the language of your choice, write a program to plot $N(A)$ given a table of data characterizing the nonlinearity.
 - Check your program with the saturation nonlinearity.
 - Use your program to calculate the describing function for the arctangent function. Is it easier to run the program or do the calculation to obtain a closed–form solution?
 - Can you make your program work for nonlinearities with memory? Try a signum function with hysteresis.
- 13.18 Redesign the controller design of Problem 3 so that it is Type 1.
- Use the describing function for the saturation nonlinearity to examine the stability of the Type 1 controller. Is the system always stable?
 - Repeat using the method of equivalent gains: is the Type 1 control system designed in the last problem always stable? For what range of u is the system stable?
 - Use simulation to estimate the range of step inputs for which the system is stable.
- 13.19 Can you think of some realizable control system which has an infinite control authority? Describe it.
- 13.20 Use the circle theorem to determine the stability of the torque motor positioning servo of Fig. 13.40 and Fig. 13.42 using linear state estimator feedback (*without* INL control). Use the control and estimator gains given in the example.
- 13.21 For the wastewater pH control problem, calculate the open-loop system matrix for three values of control, 0, 1, and 2. Calculate the gains $\mathbf{K}(u)$ for each of these three controls that maintain the system roots at the locations given by \mathbf{z}_r in Eq. (13.47).
- 13.22 In the wastewater pH control example, calculate the effect of quantizing the measurement p on the calculated variable y from Eq. (13.41). Would it be better to measure y directly? If so, can you think of a reason why it might be difficult to measure y given $p \in (0, 14)$? Simulate the system and show the effect of quantization on various step responses. Is it clear from the error statistics that the system is nonlinear? Why?
- 13.23 Consider the wastewater pH control example. Use equivalent gains to examine the effect of control saturation on the stability of the INL controller, assuming that the error in using the delayed control u_{k-1} is negligible.
- 13.24 Show that the inclusion of the control bias estimator in the torque motor example yields a closed-loop system which is Type 1.
- 13.25 Design an alternative controller structure for the torque motor servo using an explicit integration of the error $r - \hat{y}$ as was used in the wastewater pH controller. Is it reasonable to drop the estimate of u_d ? What if the integration were $r - y$?
- 13.26 Using MATLAB or equivalent, do an equivalent gains analysis of the torque motor servo example to examine the variable torque factor $K_t(\theta)$, with and without the INL controller, i.e., plot the root locus versus θ or y . Can you determine a method to quantify the effect of the approximation of θ being a constant during the sampling interval? Hint: examine the error produced by the approximation, bound it, and do a root locus.

Table 13.9
Plant parameters for the gain scheduling example

Parameter	With Load	Without Load
k_h	1.44	1.94
a	0.90	0.70
b	-0.90	-0.50

- 13.27 For the system of Problem 1, derive a *linearizing* controller for some range of control errors e . What is the maximum range of u for which you could make the system appear perfectly linear? Assuming u is output from a digital processor via a 12-bit DAC, and we desire a quantization level q of 0.006885 units, what is the maximum value of w ?
- 13.28 Using a state estimator, do a design for the wastewater pH controller assuming an unknown input bias u_d to the system. Eliminate the wind-up problem in the same way as that done for the torque motor servo. Show a block diagram of your controller. Add INL to the controller and to the state estimator.
- 13.29 Assume that the torque factor in the torque motor servo of Fig. 13.40 is a function of ambient temperature T_a and actuator power dissipation (because of flux density degradation with increasing magnet temperature), according to

$$K_t(\theta, T_m) = K_{tnom}(T_m) (K_{t0} + K_{t1} \cos(\theta)),$$

where

$$K_{tnom}(T_m) = (1 + \beta[T_a - T_m])K_{tnom},$$

with $T_a = 25^\circ\text{C}$, $\beta = 0.000758$, and the heat flow equation relating input energy u^2 and ambient temperature T_a to magnet temperature T_m is given by

$$\dot{T}_m = -0.1T_m + 0.1T_a + 13.2u^2$$

with magnet temperature in units of degrees Celsius. Can you suggest a way to use gain scheduling and apply INL control at the same time? Assume that a measurement of T_a is available.

- Design the complete system using T_m directly.
 - If a measurement of T_m is not available, find \hat{T}_m with an open-loop model and use this estimate in (a).
 - Given the time constant for magnet heating (10 seconds), and a sample rate of $T_s = 10^{-4}$ seconds, what is the discrete feedback constant used to give this relatively long time constant? Given the low bandwidth of this model, suggest an alternative sample rate which yields more reasonable model coefficients. How could this be implemented?
 - Simulate (a) and (b). Examine the effects of measurement error in the ambient temperature T_a on the controller. Based on your results, would you recommend buying a sensor to measure the ambient temperature?
- 13.30 What is the maximum steady state value for u in the problem above? Assume that the maximum safe steady state temperature T_a is 200°C . Can you suggest a scheme to protect the actuator from higher power dissipation? If the ambient ranges from 20° to 40°C , how important is knowing T_a ? What is the error if we assume T_a is a nominal 25°C ? To be safe, show that we should assume $T_a = 40^\circ\text{C}$.
- 13.31 For the gain scheduling example, use the parameters in Table 13.9 to design a control law to maintain constant eigenvalues of $z = .866e^{\pm 11j}$.

- 13.32 Simulate the gain-scheduled system of the last problem and examine behavior before and after dropping the payload. Assume the payload is dropped at a sampling instant.
- 13.33 For the torque motor servomechanism of Fig. 13.40, do an equivalent gains analysis of the closed-loop system assuming the input to the estimator is *not* saturated along with the control. Is the system always stable?

Chapter 14

Design of a Disk Drive Servo: A Case Study

Perspective on the Design Process

To illustrate many of the concepts developed in this book, the design of a disk drive head positioning servomechanism provides an excellent case study. In most textbook examples, the problems are *highly* simplified for pedagogy: Too much detail often obscures the underlying point. Indeed, most of this text has followed this principle and many of the individual problems of this case study are used to illustrate various parts of the design process in earlier chapters. However, for a final design example we will not spare all of the detail but will present some of the difficult realities of a real problem. The problem requires constructing models of the plant, the actuator, and the sensor and verifying these models with simulations. Next comes determining the specifications both for the components and for the entire system. Following the problem formulation comes the design of a small-signal linear controller and finally the design is completed with a nonlinear controller for handling large signal behavior. The last step is testing the design in simulation for its performance in the presence of varying parameters before constructing a prototype and testing performance by experiment. We begin the case study by giving a description of the disk drive which will serve to set the stage for the specification development in our design, and this too will be in more depth than in our typical examples.

Chapter Overview

A general discussion of disk drives and current performance specifications are given in Section 14.1. In Section 14.2 the several components that comprise the disk drive servo are described and models given. The specific performance specifications for the servo case study are given in Section 14.3. Finally, the details of the design are presented in Section 14.4. As with earlier chapters, this ends with a set of problems designed to enhance the learning process.

14.1 Overview of Disk Drives

Disk drives serve as an important data storage medium for data processing systems. In a disk drive, rotating disks, sputtered with a thin magnetic layer or recording medium, are written with data in concentric circles or **tracks**. Data is written by a **head** which is a small horseshoe-shaped electromagnet with a very thin gap. Remaining positioned only microinches above the recording medium on an air bearing surface (ABS) (often referred to as a **slider**), the energized electromagnet produces a strong magnetic field in the air gap which magnetically polarizes the recording medium, an operation called **writing**. Once polarized, the recording medium remains so until rewritten. Hence, disk drives are **nonvolatile** storage. Besides being connected to a high speed bipolar current source for writing, a

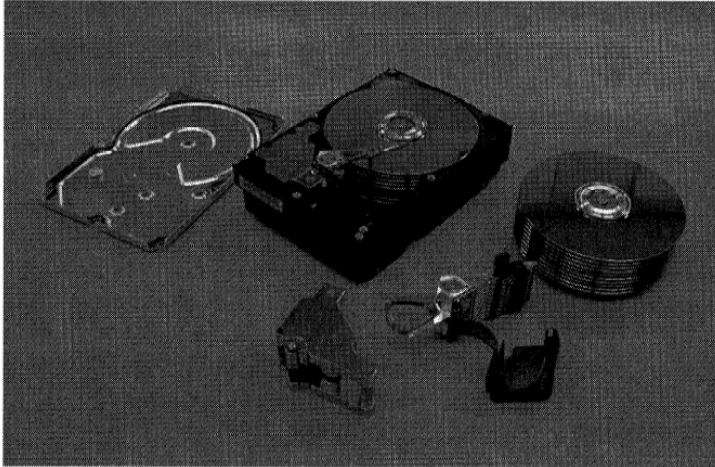


Figure 14.1
Picture of an IBM 18 GB disk drive and some of the constituent pieces: a) spindle motors and disk stack, b) rotary actuator, c) magnet structure

read head (sometimes the same element as the write head) is also connected to a high gain preamplifier, the output of which is fed to a **read detector** which converts the analog information signal read from the disk surface into detected digital data. The width (in the direction of a disk radius) of the write gap determines the **track width**, which in today's rigid (as opposed to floppy) disk drives is usually less than 120 microinches or 3 microns. (A micron is 10^{-6} meters.) Track density is the reciprocal of the track width. A 100-microinch track corresponds to 10,000 tracks per inch (TPI). To determine the storage capacity of a disk drive, we need to define the **bit density**: the number of bits which can be stored along a unit distance of a track, usually quoted in bits per inch (BPI) or bits per millimeter. The highest density used (inner radius of the disk, or innermost track), it usually ranges from 100,000 to 200,000 BPI in today's (1997) machines. **Area density** is the product of BPI and TPI, and ranges from 500 to 2,000 million bits per square inch (0.5 to 2 gigabits per square inch). Finally, to calculate storage capacity we multiply area density times the available surface area for each disk **surface**. Since disks range from 2.5 inches in diameter to 5.25 inches, and the number of disks in a particular drive range from 1 to 12, drive storage capacities range from 1 gigabyte to 36 gigabytes per head-disk assembly (HDA). A picture of an IBM 18 GB HDA containing ten 3.5-inch disks is shown in Fig. 14.1. Disk rotation rate and bit density together determine the **data rate** of the disk drive. Typical data rates range from 5 to 25 megabytes per second. Unlike digital tape storage which accesses information sequentially on the tape, new information can be accessed directly regardless of the information currently being read from the disk. For this reason, the disk drive is referred to as a **direct access storage device** (DASD, pronounced **daz-dee**). In fact, in disk drives with more than one disk surface, the heads are positioned in unison such that a track defines a **cylinder** corresponding to N tracks of total data for N heads. A cylinder of data is thus N times the total track capacity. Because switching from one head to another is an electrical function (the actuator barely moves), the data in a cylinder can be accessed very quickly.

The recording heads are moved with an actuator across the disk surface to reach each track. A head positioning servomechanism is a control system which positions the read/write heads (mounted on the actuator) in a disk drive over a desired track with minimum statistical deviation from the track center (subject to control magnitude constraints) and repositions the heads from one track to another in minimum time within the constraints imposed by the intended cost of the machine. A schematic of the servo is shown in Fig. 14.2. A storage controller sends commands and receives status from the servo system.

For computer system performance reasons, it is desirable to reach any track as quickly as possible with the actuator. Once the actuator is regulating the position of the heads at the desired track, the smaller the variation of the position of the heads from the true track center, the closer the tracks can be put together (higher track density), and the lower the soft error rate of the recording channel

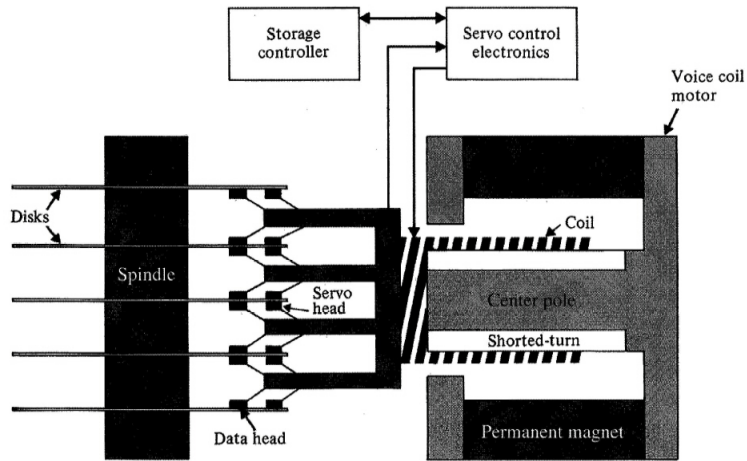


Figure 14.2
Schematic diagram of the head positioning servomechanism. Cross-section of disk stack, spindle, head-arm assembly, and voice coil motor are shown with storage controller and servomechanism control

Characteristic	Value ²	Units	Value	Units
Storage capacity per HDA	18	gigabytes		
Track density	10,000	TPI	393.7	TPmM ³
Bit density	130,000	BPI ⁴	5118.11	BPmM
Data bandwidth	1.1	inches	28	millimeters
Access time	8	msec		
Single track access time	1.5	msec		
Approximate 3σ data-head TMR ⁵	15	microinches	0.375	microns

Table 14.1
Some basic characteristics of a high performance 3.5" half-high form factor disk drive

(typically 1 bit error in 10^8 or 10^9 bytes read¹). The servo must operate with finite control authority, and in the presence of position reference noise, uncertain high-frequency actuator dynamics, sensor noise, many sensor nonlinearities, no absolute position reference during most operations and nonzero saturation recovery time in the power amplifier. In addition to all this, the servo must also be robust in the presence of actuator parameters that vary from 1) motor to motor, 2) stroke to stroke, 3) temperature changes, and 4) age. In short, the disk drive servo represents a typical mass-produced servomechanism.

14.1.1 High Performance Disk Drive Servo Profile

To put matters in perspective, a list of critical performance parameters for the IBM 18GB 3.5" disk drive example will be discussed.

The list of performance specifications in Table 14.1 illustrates the challenge to the disk drive servo designer. The actuator moves over a 28 millimeter stroke, and when track-following the position error is maintained to a statistical deviation of less than one-half micron (3σ). Thus the 3σ deviation of the servo head from its track center is on the order of one "line width" in state-of-the-art IC technologies. Perhaps a better physical perspective can be obtained by putting it another way: The 3σ deviation is approximately 1/400th the width of a human hair.

For the 18 GB disk drive, the access time specification of Table 14.1 translates into accelerations of approximately $50g$'s, or 50 times the acceleration due to gravity. The actuator is a rotary actuator so rotary accelerations should be considered instead of linear ones. The single track access time is the time it takes the servo to move the heads one track (forward or reverse) and is an important

¹Without error correction.

parameter in that designers of operating systems and data base systems select data access methods to minimize the amount and distance of seeking,⁶ hence many seeks are of the one-track variety. To compute an effective access time for purely randomly distributed data, the **weighted average access time** (WAAT) is calculated. The WAAT is calculated assuming equal probability of seeking to any track at any time. If the time it takes to do a j -track seek is denoted τ_j , the WAAT⁷ ($\bar{\tau}_a$) is

$$\bar{\tau}_a \triangleq \sum_{j=1}^{j=N-1} 2 \frac{N-j}{N(N-1)} \tau_j \quad (14.1)$$

where N denotes the total number of tracks available to the customer. Optimal control strategies such as PTOS as described in Chapter 13 are used to achieve the access time objective. The access performance of the servo only pays off if the position regulation at the end of a seek is immediate, that is, does not suffer a large position error transient near the target due to the effect of the seek. This fact implies “bumpless” transfer from the minimum time controller to the minimum variance controller, something accomplished using a nonlinear control structure such as PTOS (see Chapter 13).

Meeting the minimum-time and the minimum-variance objectives with smooth handover is a challenge that becomes even tougher in the face of varying plant parameters. Since high-end DASD are usually manufactured in numbers upward of one million units, maintaining the guaranteed performance across all machines is a difficult task, usually requiring a very conservative design. Design conservatism has two drawbacks, it costs money and, if fixed-design control is used, it causes machines with good hardware to perform more like those with poorer hardware. Fixed-design controllers degrade performance to provide system tolerance to poor hardware, and therefore, some adaptive techniques will also be examined as part of our design.

14.1.2 The Disk-Drive Servo

A nonlinear model showing the major components for a disk-drive servo plant is shown in Fig. 14.3. The position to be controlled is represented by y , and the control input is u . Disturbance forces acting on the actuator are represented by the input f_d . A position reference input y_{ref} is used to indicate the center of the track being followed.

When linearized, this model is of order

$$n_p = (2 + n_{ac} + n_{vc} + n_{pa} + n_{pes} + n_{hda}).$$

During track-following operation when the signals are small, the model is easily linearized. Components of both Coulomb friction and stiction in $k_v(v, x)$ are usually rendered insignificant by the natural dither in the system provided by track motion and servo surface⁸ noise. The model shown in Fig. 14.3 is extremely complex, and is simplified for analysis and design except on occasions where high order effects are being investigated via simulation.

The complete model may be of order 40, so design can be complicated and even simulation can be terribly time consuming. When the accuracy of the required simulation is not stringent, the order of the model is reduced to perhaps 3 by considering only the rigid-body dynamics, greatly simplifying the simulation task. Table 14.2 is a summary of typical data on model complexity. Once the analytical structure is in place, complexities such as noise, nonlinearities, and additional dynamics will be examined carefully.

²Although the practice is slowly changing to use metric units, most disk drive parameters are still given in English units, and are given in both forms here for reference.

³Tracks Per milliMeter, Bits Per milliMeter.

⁴Bits per inch.

⁵Track Misregistration: statistical measure of the position error between the data heads and the center of their respective tracks.

⁶A seek is a change of track address.

⁷No-motion or 0-track seeks are not included in the standard definition of the weighted average access time, although under operating conditions no-motion seeks are very common.

⁸The servo surface is that on which a read head reads position reference information.

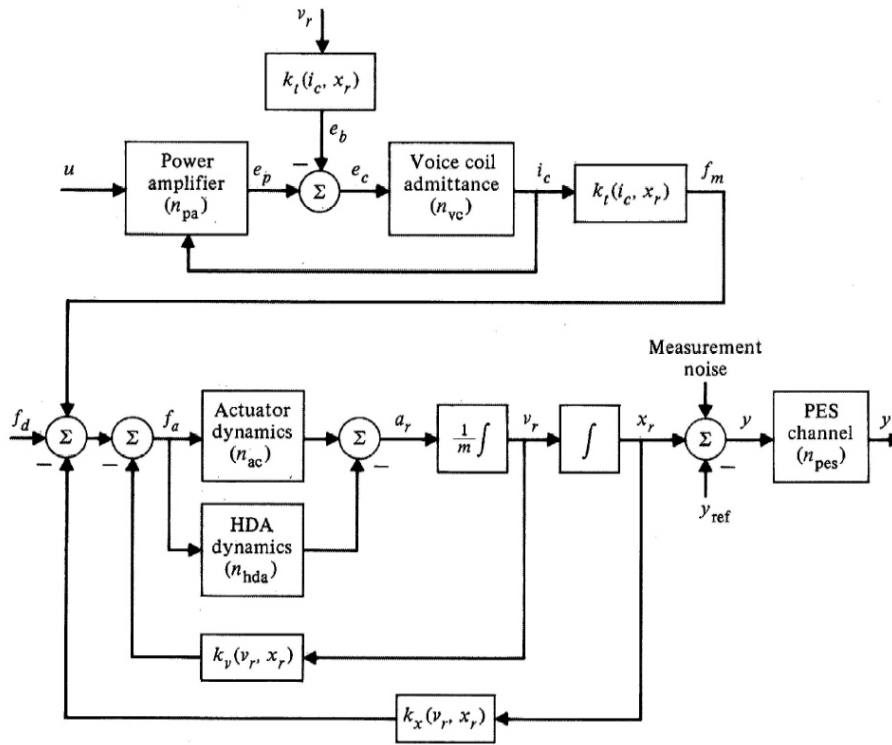


Figure 14.3 High order, fairly complete model of DASD servo plant. The Position Error Signal Channel is a measurement channel, and the Head-Disk Assembly (HDA) dynamics include the disks, spindle, and basic structural hardware that integrates all of the components (baseplate)

Model Component	Nonlinearity Type	Linearized Order	Nominal Order
Power amplifier	Saturation	$n_{pa} : 0$	0
Voice coil	Hysteresis, saturation	$n_{vc} : 2 - 5$	2
Actuator	Materials damping	$n_{ac} : 0 - 30$	0
HDA	Materials damping, rotation	$n_{hda} : 0 - 30$	0
PES meas. channel	Transfer curve	$n_{pes} : 0$	0
Velocity damping	Static and Coulomb friction	$k_v(v, x) : 0$	0
Position feedback	Hysteresis	$k_x(v, x) : 0$	0

Table 14.2 Model components and associated nonlinearity types, linearized dynamic order, and nominal order (simple model)

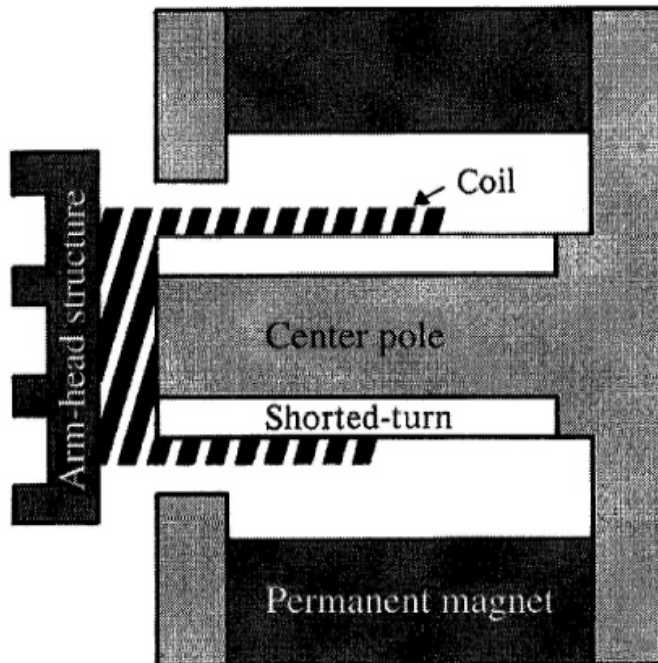


Figure 14.4
Schematic of a voice coil motor. The coil is attached to a structure on which the read/write heads are mounted

14.2 Components and Models

14.2.1 Voice Coil Motors

In disk drives containing linear actuators, or actuators which move in one direction (in and out along a disk radius), the motor is often referred to as a *voice coil* motor (VCM) because of its similarity to a loudspeaker. Most linear actuators are of the moving-coil type: A coil of wire is rigidly attached to the structure to be moved and suspended in a magnetic field created by permanent magnets as shown in Fig. 14.4.

When a current is passed through the coil, a force is produced which tends to accelerate it radially inward or outward, depending on the direction of the current. The force produced is a function of the current i_c and the position of the coil in the field x_r .

$$f_m = k_t(i_c, x_r) \quad (14.2)$$

A reasonable first-order approximation of this relationship is given by

$$f_m = k_t i_c \quad (14.3)$$

where k_t is a linearized nominal value of $k_t(i_c, x_r)$. Current in the coil is often referred to as the **prime mover**. Some disk drives, especially small ones (disk diameters less than or equal to 5.25 inches), use rotary actuators. In a rotary actuator, the heads are mounted on the end of arms which pivot about an axis which is parallel to the disk spindle. Torque is produced by current in much the same manner as the VCM, but the coil is an armature of a rotary motor, like that of a torque-motor. Rotary actuators are simple, inexpensive, and provide compact packaging opportunities, but are usually considered inferior from two standpoints: first, the head gap does not remain parallel to a disk radius as a function of angle of rotation⁹ (track location), and second, the unwanted dynamics

⁹This is often referred to as head *skew*, and is detrimental in that the apparent width of the head changes as a function of the skew angle and hence track location. Also, the skew of the air bearing surface produces a variation of the head fly-height, a particularly sensitive recording parameter.

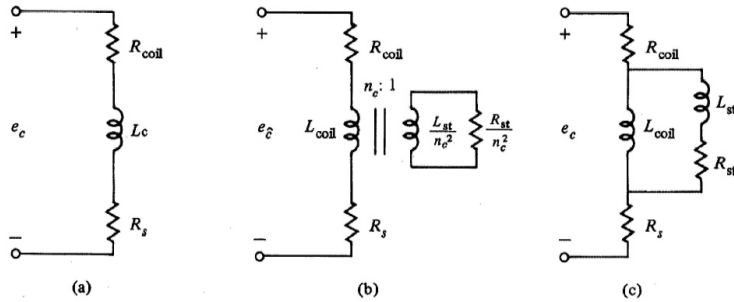


Figure 14.5
Electrical circuit of a typical linear actuator, without the shorted turn (a), and (b) including the shorted turn caused by mutual inductance between the center pole and the voice coil

of a rotary actuator are usually lower in frequency thereby limiting the control system bandwidth relative to that obtainable with a linear actuator. Depending on the performance and cost objectives, either a rotary or a linear actuator might prove better than its counterpart.

Either type of actuator requires current in the coil to produce a force. The voice coil admittance shown in Fig. 14.5 is the relationship from coil voltage to coil current. Coils always have an associated inductance and resistance, the time constant of which is far from negligible. To complicate matters somewhat, the coil generates a voltage when moving in the magnetic field (Lenz's law), and in metric units the back-electro-motive-force or back emf e_b that is generated is just

$$e_b = k_t(i_c, x_r)v_r \quad (14.4)$$

where v_r is the coil velocity. An electrical schematic of the voice coil is shown in part (a) of Fig. 14.5. For this case, the voice coil admittance is

$$\frac{I_c(s)}{E_c(s)} = \frac{1/R_c}{sL_c/R_c + 1} \quad (14.5)$$

From Fig. 14.5 it should be clear that $e_c \triangleq e_p - e_b$, or that the effective coil voltage is the applied voltage from the power amplifier minus that produced by the generator effect of the coil moving in the magnetic field. Also, as shown in Fig. 14.5, we have defined the effective coil resistance R_c as the actual coil resistance plus the current sense resistance R_s , or $R_c \triangleq R_{coil} + R_s$.

14.2.2 Shorted Turn

Typical voice coil time constants range from 1 to 10 milliseconds, an amount which is far too long for reasons which shall become clear. In 1908, the RCA corporation was granted a patent on a feature which helped to solve this long-time constant problem for loudspeakers, the **shorted turn**. As shown in part (a) of Fig. 14.5, the circuit representing the coil with a voltage drive is a series inductance and resistance, the time constant of which is L_c/R_c . To produce high force or torque factors (k_t in Eq. (14.4)), the magnetic field of the motor must be made as high as possible. Achieving large magnetic fields using permanent magnets is done with significant amounts of steel in the magnetic circuit. Both a blessing and a curse, the permeability of this steel is extremely high when not fully magnetically saturated,¹⁰ which produces a large inductance L_c and thus a large time constant L_c/R_c . Many tradeoffs can be made regarding the resistance, power handling capability, volume, and mass of the moving coil, all of which usually yield an unsatisfactory electrical time constant. Fortunately, the shorted turn can be of assistance. Shown in Fig. 14.4, the linear motor has a center pole which the coil surrounds. Mutual inductance between the center pole and the coil produces a transformer effect as shown in Fig. 14.5, but because the resistivity of the center pole material is fairly high, the reflected impedance of the center pole is very high relative to R_{coil} and thus is negligible. The idea of the shorted turn is to replace the surface layer of the center pole with a very low resistivity

¹⁰Saturating the magnetic material in the VCM reduces inductance, but must be done with care as it can cause large stray leakage fields to emanate from the VCM.

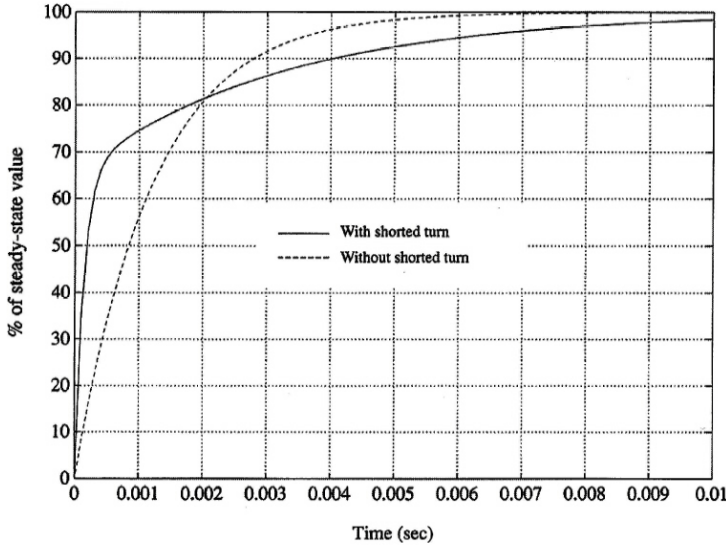


Figure 14.6
Voltage step response of coil current, in terms of percent of steady state value, with and without a shorted turn

material such as gold or low oxygen content copper. Now the transformer action has a significant and advantageous effect on the electrical circuit because the reflected impedance of the shorted turn can be smaller than R_{coil} .

As can be calculated from part (b) of Fig. 14.5, the shorted turn inductance allows a fraction of the current ($R_s/(R_s + R_c)$) to flow quickly into the coil if the value of $(L_{st} \parallel L_c)/(R_c + R_{st})$ is much smaller than L_c/R_c . The voice coil admittance with the shorted turn is

$$\frac{I_c(s)}{E_c(s)} = \frac{1}{R_c} \frac{\tau_z s + 1}{\tau_{p1} \tau_{p2} s^2 + (\tau_{p1} + \tau_z) s + 1} \quad (14.6)$$

where

$$\tau_z = \frac{L_c + L_{st}}{R_{st}} \quad (14.7)$$

$$\tau_{p1} = \frac{L_c}{R_c} \quad (14.8)$$

$$\tau_{p2} = \frac{L_{st}}{R_{st}}. \quad (14.9)$$

The voice coil parameters for the plant in this design are shown in Table 14.3. A step response of coil current to an input voltage is shown (no back emf), in percent of final steady state value in Fig. 14.6. As can be seen by Fig. 14.6, the steady state value of coil current for a given input voltage is not affected by the shorted turn. In either case the steady state current is simply given by

$$I_{ss} = \frac{e_{max}}{R_{coil} + R_s} = \frac{e_{max}}{R_c}. \quad (14.10)$$

Since voice coil current is the prime mover, the power amplifier shown in Fig. 14.7 is configured as a *current source*. In this manner, the dynamics of the plant between input to the power amplifier u and voice coil current i_c are not important, which simplifies the model and design procedure. This technique is used fairly often in control system design, and for that matter in all engineering: Break the problem into smaller parts. By designing a power amplifier which serves as a current source, the overall design is simplified.

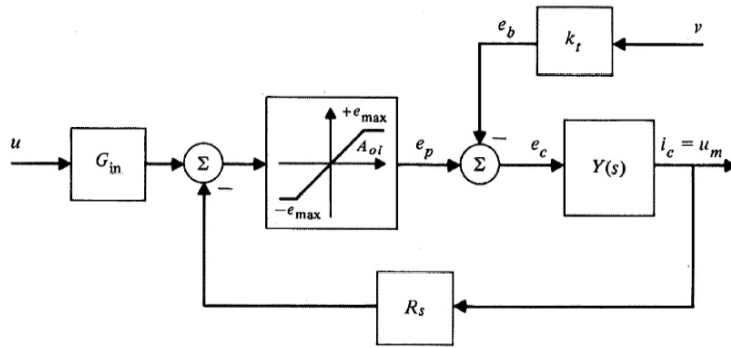


Figure 14.7
Schematic of power-current source with voice coil load. Back emf e_b is subtracted from the power amplifier output

14.2.3 Power Amplifier Saturation

A simplified schematic diagram of a power current source with a voice coil motor load is shown in Fig. 14.7. If the voltage output e_p of the power amplifier remains less than e_{max} (the supply value minus some small transistor saturation drop), it will continue to behave as a current source. However, when the current demand u exceeds that which is physically possible given the finite power supply voltage, the current source fails to behave as such. Instead, during voltage saturation it behaves as a voltage source of constant value, and the corresponding coil current i_c now will show the effects of the back emf e_b and the voice coil admittance. During seeking, especially longer seeks (greater than 10 tracks), the power amplifier will be called upon to deliver the maximum available current to the voice coil, in which case the amplifier will saturate. We will have to take power amplifier saturation into account in our design. The astute reader will note that this saturating power amplifier situation is not as straightforward as simple saturation: the saturation is in a dynamic continuous feedback loop which makes prediction of the saturation behavior very difficult. Small changes in command input to the power current source can cause short term saturation. Saturation depends on the back emf generated by the voice coil and thus the actuator velocity. To solve this problem, we will *measure* the coil current rather than trying to model the highly nonlinear system in the state estimator. For simplicity, we will assume the power amplifier gain is unity ($G_{in} = R_s$ in Fig. 14.7), and the measured coil current will be referred to as u_m . When the power amplifier can respond to the input without saturation, $u_m = u$ is a good approximation.

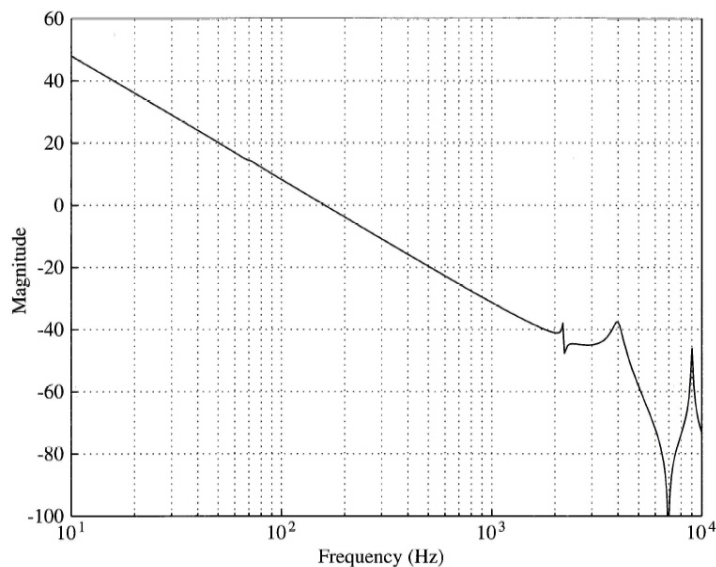
14.2.4 Actuator and HDA Dynamics

The actuator and HDA structures of course are not perfectly rigid. Their flexibility gives them dynamic behavior that must be accounted for in the design of a servomechanism which positions the actuator in the HDA. Although there are perhaps hundreds of flexible modes, or **resonances**, in the total system, much of the character can be defined by considering only three or four modes. This is because many modes have an insignificant amplitude or are too high in frequency to be of interest (*i.e.*, they don't appreciably affect the design). In our case, we will consider a four-mode system, three modes of higher frequency nature (> 1 kHz) due to the actuator and one mode of lower frequency (< 100 Hz) due to interaction between the HDA and the vibration isolating shock mounts¹¹ between the magnet structure and the base casting which supports the spindle. The frequency response of our actuator, in terms of current input and position output, is shown in Fig. 14.8.

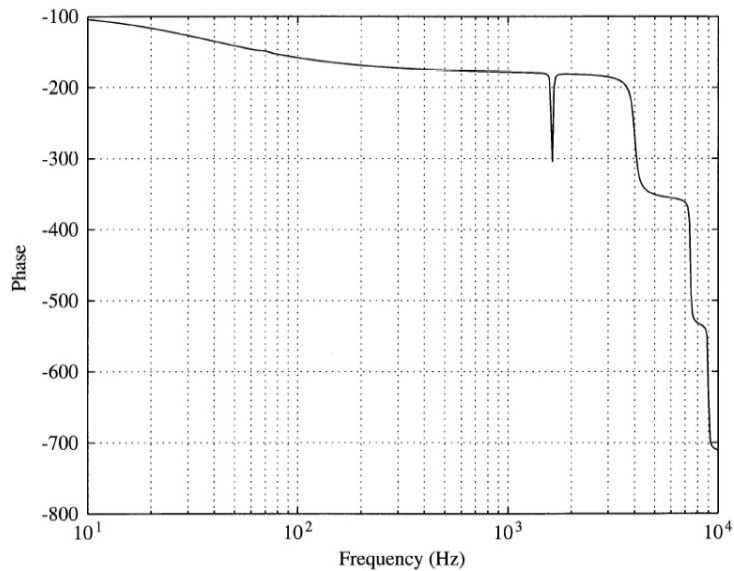
A linear state-space model for the HDA, along the lines of that shown in Fig. 14.3 with four resonant terms is given by Eqs. (14.11)–(14.14).

$$\dot{\mathbf{x}}(t) = \mathbf{F}\mathbf{x}(t) + \mathbf{G}u(t) \quad (14.11)$$

¹¹The voice coil motor magnet structure in most systems is mounted on vibration isolators or *shock mounts*. Reaction forces from the VCM act on the HDA, which in turn acts on the HDA shock mounts that physically support the disk drive.



(a)



(b)

Figure 14.8 Magnitude and phase response of the actuator used in our case design. Although there is a flexible mode at 70 Hz due to VCM isolators, it is small and hard to see on this scale. Note the real pole introduced by the coefficient of viscous drag in the actuator

and the output $y = \mathbf{H}\mathbf{x}$. The matrices \mathbf{F} and \mathbf{G} are given by

$$\mathbf{F} = \begin{bmatrix} 0 & k_y & 0 & 0 & 0 & 0 & 0 & 0 & 0 & 0 & 0 \\ 0 & k_{fric}/m & k_v b_1 & k_v b_2 & k_v b_3 & k_v b_4 & k_v b_5 & k_v b_6 & k_v b_7 & k_v b_8 & 0 \\ 0 & 0 & 0 & 0 & \omega_1 & 0 & 0 & 0 & 0 & 0 & 0 \\ 0 & 0 & -\omega_1 & -2\zeta_1 \omega_1 & 0 & 0 & 0 & 0 & 0 & 0 & 0 \\ 0 & 0 & 0 & 0 & 0 & \omega_2 & 0 & 0 & 0 & 0 & 0 \\ 0 & 0 & 0 & 0 & -\omega_2 & -2\zeta_2 \omega_2 & 0 & 0 & 0 & 0 & 0 \\ 0 & 0 & 0 & 0 & 0 & 0 & 0 & \omega_3 & 0 & 0 & 0 \\ 0 & 0 & 0 & 0 & 0 & 0 & -\omega_3 & -2\zeta_3 \omega_3 & 0 & 0 & 0 \\ 0 & 0 & 0 & 0 & 0 & 0 & 0 & 0 & 0 & \omega_4 & 0 \\ 0 & 0 & 0 & 0 & 0 & 0 & 0 & 0 & -\omega_4 & -2\zeta_4 \omega_4 & 0 \end{bmatrix} \quad (14.12)$$

and

$$\mathbf{G} = \begin{bmatrix} 0 \\ 0 \\ 0 \\ \omega_1 \\ 0 \\ \omega_2 \\ 0 \\ \omega_3 \\ 0 \\ \omega_4 \end{bmatrix} \quad (14.13)$$

and

$$\mathbf{H} = [1 \ 0 \ 0 \ 0 \ 0 \ 0 \ 0 \ 0 \ 0 \ 0 \ 0] \quad (14.14)$$

where $k_v = k_t/m$ is a normalization factor such that the maximum acceleration of the plant is always given by $k_v i_c$. During the linear mode of operation, the current of the power current source will be considered ideal, e.g., the current in the coil follows the input to the power amplifier exactly ($u_m = u$). Also, our design will use the familiar zero-order hold to provide the control signal to the power amplifier by employing a latching D/A. The D/A output is scaled such that the control can saturate the power amplifier and will thus use most of the available power from the servo power supply to accelerate the actuator during a seek. The parameters defining the plant for our case study will be given shortly.

14.2.5 Position Measurement Sensor

Most DASD servomechanisms employ what is referred to as a **dedicated** servo: One of the heads mounted on the actuator structure is dedicated to reading position information from its associated disk surface. Known as the **servo surface**, the disk is written at the time of manufacture with position information. Ideally, each data head would be able to report its position to the control system, allowing the servo to faithfully position that head when it is selected by the recording channel for reading or writing. Such a scheme is referred to as an **embedded servo** because the position information is embedded in the read back signal for each head, along with the normal data signal. If time-division multiplexing is used to embed the servo position information among customer data, the servo is referred to as a **sector servo** because small sectors of each track spaced evenly around the circumference are written at the time of manufacture with servo position information. Unfortunately, sector servo impacts system performance parameters by interrupting data flow, lowering the average data rate, and adding to the position settling time when switching from one head to another, a phenomenon often referred to as **loss of cylinder mode**. In the sector servo design, there is a conflict between the requirement for fast sampling for the servo and the fact that each sector reduces the available space for customer data. It is for this reason that current technology often favors the use of dedicated servos. A limitation of the dedicated servo design is the finite accuracy with which the data heads in a stack can be positioned over their respective tracks since many mechanical, thermal,

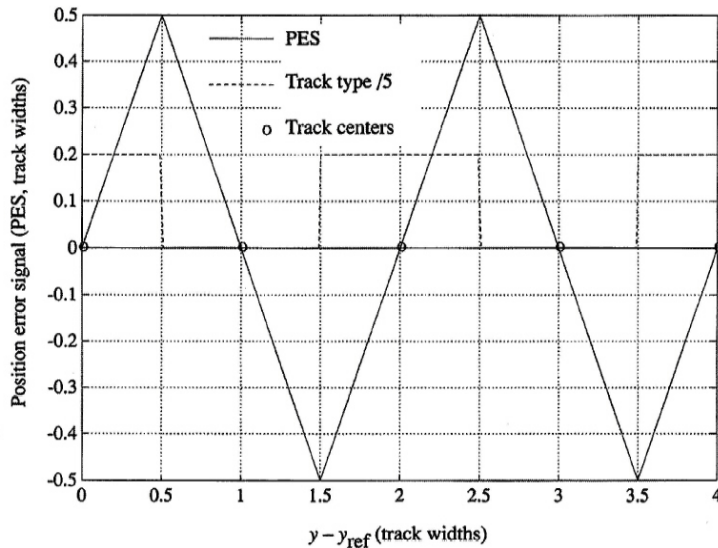


Figure 14.9
Position measurement versus relative position error $y - y_{ref}$. This measurement signal is often referred to as the position error signal (PES) because it is the error signal, not absolute position

and vibrational sources of positioning difference exist between the data heads and the servo head which is located on a separate surface. Our design will be for a dedicated servo. Although many manufacturing and performance differences exist in different designs, the design described here will be applicable to other methods of position measurement.

In a dedicated servo, the servo surface is written with information that, upon demodulation, yields a position error signal: The measurement is the position of the servo head relative to the servo disk. In addition, the measurement is actually relative to the **nearest track center**. In other words, the signal read back from the head positioned at a constant radius is proportional to the nearest track center, not to its position on the entire disk, because the information read back does not contain a track address.¹² There is at least some additional information: A one or two bit address is written onto each track. With one additional bit, the position signal contains the error relative to the nearest track center, plus a digital logic signal indicating whether the head is over an *even* or an *odd* numbered track, as shown in Fig. 14.9. In a quadrature type PES channel, we know which of four different types of tracks the head is positioned over, because two signals are demodulated that are in spatial quadrature with respect to each other, as shown in Fig. 14.10. At the innermost and outermost cylinders, a special pattern is written which is detected by the PES channel and sent to the controller, indicating that either the inner- or outermost cylinder has been detected. From this information, we must construct an absolute position measurement for the servo so that we can seek and find a particular track with high reliability. When we design the state estimator we will see how this is accomplished. Although we will plot PES versus time instead of position, in the equations for the system and the measured value of $y - y_{ref}$ we will neglect the PES “modulation” of the measurement.

14.2.6 Runout

Besides seeking from one track to another, the servo we are designing must follow the track motion once on track, and keep the error as small as possible. Two primary sources of track motion exist, apparent and real. To understand how we could measure an apparent track motion, we must remember that the signals used to compute position are written onto the servo disk surface. In the process of servo-writing, the head that writes the signals cannot be kept perfectly still, and therefore the servo tracks are not perfect circles. In addition, the servo surface contains defects and irregularities of many types, all of which cause the position reference to appear as though it was not

¹²It is impractical to encode track address in each servo track for many reasons. One of the most important is that it cannot be reliably read when the head is traveling at any significant radial velocity.

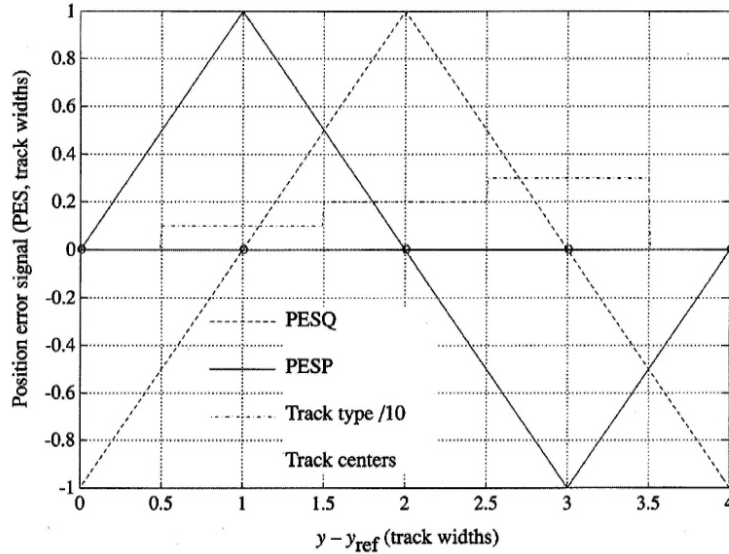


Figure 14.10 Primary and quadrature position measurement versus relative position error $r - y - y_r$. Here the PES channel delivers two signals, each used as the position reference on alternate tracks, with slope correction. Note there are four track types, numbered 0-3, which can be decoded from the signal

written on a perfect circle. This apparent track motion will cause the servo to move the servo head in an attempt to reduce the position error to zero, and thus will result in real actuator motion. If the path the servo head follows every time is the same, there is no harm done with respect to the reading process *on the track being followed* as long as the track was never written over for any reason. However, adjacent tracks will tend to be squeezed by the wandering head, a process which is only detrimental when writing data. Writing off the perfect circle causes the head to write on the adjacent track's data, at least to an extent, which in turn causes a loss of signal amplitude. If enough data is written over, the damage can be severe enough to cause a **hard error**, in that the customer data is lost and not recoverable with an error correction code. Servo writing produces **repeatable runout (RRO)**, in that the runout stays locked to the disk rotation (both frequency and phase). It is worthwhile to note that the RRO can be heavily influenced by disk surface defects that are of extremely high bandwidth. To keep high bandwidth surface noise repeatable, the sampling clock *must* be locked to the disk rotation rate, with extremely low time jitter to ensure that a sample is always taken at the same physical location on the disk. If the sample clock is asynchronous to the disk rotation, the nonrepeatable runout (NRRO) will be much larger and the track misregistration (TMR) of the servo will be increased. Another mechanism besides asynchronous sampling can cause RRO to increase the NRRO: saturation. If a repeatable disk defect is large enough to saturate the power amplifier, then the servo response becomes variable instead of repeatable, hence an increase in NRRO.

So far, we have only discussed apparent motion. Real repeatable motion occurs in many circumstances, such as if the servo disk slips its center point after being servo written. This would cause a large amount of RRO at the rotation frequency of the spindle. Such motion must be followed with high fidelity. Nonrepeatable runout is a product of disk drive vibrations and electrical noise in the measurement channel. Many sources exist for the vibration, including the spindle motor, spindle bearings, air movement in the HDA, the actuator itself, and force disturbances such as closing covers. Even earthquakes are a consideration for disk drives operating in Japan where their occurrence is quite frequent! Both NRRO and RRO must be reduced as much as possible, within the control authority and bandwidth limitations imposed by the servo and the actuator we are trying to control. For the most part, we can model both NRRO and RRO as signals that i) add directly to the position measurement (in the form of y_{ref}), ii) have energy decreasing with increasing frequency, and iii) have amplitude distributions which are roughly Gaussian (usually truncated). Thus the simple model of the input y_{ref} is given by

$$y_{ref} \sim N\left(0, \sqrt{\sigma_{nrro}^2 + \sigma_{rro}^2}\right). \quad (14.15)$$

Parameter	Description	Value	Units	Tolerance
m	moving mass of actuator	0.200	kilograms	$\pm 3.0\%$
k_t	force constant	20.0	Newtons-amp ⁻¹	$\pm 10.0\%$
k_y	position measurement gain	10000.	volts- M^{-1}	$\pm 5.0\%$
R_{coil}	coil resistance	8.00	ohms	$\pm 20.0\%$
n_c	number of turns in the voice coil	150	turns	± 2
R_s	sense resistance for power amp	0.250	ohms	$\pm 1.0\%$
R_{st}	shorted-turn resistance ¹³	5.00	ohms	+0, -6.0%
L_{coil}	coil inductance	0.010	henrys	+0, -15.0%
L_{st}	shorted-turn inductance	0.0020	henrys	+0, -15.0%
e_{max}	saturated power amp voltage	34.0	volts	-0, +5.0%
k_{fric}	viscous friction coefficient	2.51	N-sec- M^{-1}	$\pm 7.5\%$
RPM	disk rotation rate	3623	revs-min ⁻¹	$\pm 3.0\%$
t_w	track width	12.50	microns	$\pm 1.0\%$
x_s	actuator stroke length	0.028	meters	$\pm 0.10\%$

Table 14.3

Plant parameters and tolerances for the case design

Parameter	Description	Distribution	Mean	Standard Deviation
RRO	repeatable runout	Gaussian	0	$\sigma_{rro} = 0.25$
NRRO	nonrepeatable runout	Gaussian	0	$\sigma_{nrro} = 0.125$

Table 14.4

Statistical parameters for repeatable and nonrepeatable runout, before servo rejection. Although RRO contains pseudorandom noise (it repeats every revolution), it usually contains significant sinusoidal components at harmonics of the rotational frequency

Refinements of this simple model include frequency shaping due to bearings and structural resonances, as well as a high harmonic content with a fundamental frequency due to disk rotation. One useful simulation technique is to experimentally measure either time domain NRRO and RRO waveforms or their spectral content and use either of them as input to system simulation models. Measurements must usually be done with some form of closed loop system and corrected with the appropriate system transfer function to obtain the desired open loop runout components.

14.3 Design Specifications

Before the design of the controller can begin, it is necessary to identify the specific parameters of the components to be used and to give particular quantities to the several performance specifications that the design is required to meet. We begin with the parameters.

14.3.1 Plant Parameters for Case Study Design

For our specific design case, we will use the parameters in Tables 14.3–14.5. These “givens” are normally part of the engineering problem, *i.e.*, what are the plant requirements to meet a set of goals? In this design case, we will assume the parameters given are the best we can expect within the cost constraints, and therefore our job is to make the best use of the plant that we can. If it was desired to improve a certain performance parameter, some changes in the plant would probably have to be negotiated with mechanical engineers and management.

14.3.2 Goals and Objectives

Setting performance goals must be done after there is an understanding of the basic plant to be controlled. In previous sections, we outlined motor forces, coil time constants, physical parameters such as track width, and actuator dynamics. All of these combine to determine what goals are practical for this design. Presumably, cost and packaging requirements, such as weight and space or form factor, have already been taken into account in arriving at the designs which lead to the parameters given. It is now the job of the control engineer to use this plant to the utmost given the cost constraints.

¹³Reflected into the primary circuit by the number of turns in the coil squared, or n_c^2 .

Parameter	Description	Value	Units	Tolerance
ω_1	resonance: VCM isolator	$2\pi 70$	rad-sec ⁻¹	±5.0%
ω_2	resonance: head suspension	$2\pi 2200$	rad-sec ⁻¹	±10.0%
ω_3	resonance: actuator arm carrier	$2\pi 4000$	rad-sec ⁻¹	±5.0%
ω_4	resonance: coil structure	$2\pi 9000$	rad-sec ⁻¹	±5.0%
b_1	first resonance coupling	-0.00575	–	±7%
b_2	first resonance coupling	0.0000115	sec ⁻¹	±7%
b_3	second resonance coupling	0.0230	–	±10%
b_4	second resonance coupling	0.00	sec ⁻¹	±7%
b_5	third resonance coupling	0.8185	–	±5%
b_6	third resonance coupling	0.0	sec ⁻¹	±10%
b_7	fourth resonance coupling	0.1642	–	±5%
b_8	fourth resonance coupling	0.0273	sec ⁻¹	±10%
ζ_1	first resonance damping	0.05	–	±10%
ζ_2	second resonance damping	0.005	–	±40%
ζ_3	third resonance damping	0.05	–	±40%
ζ_4	fourth resonance damping	0.005	–	±50%

Table 14.5
Dynamic
(resonance) plant
parameters and
tolerances for the
case design

For this design, we'll assume the control computer is a typical digital signal processor (DSP), with a cycle time of 100 nanoseconds and a 16-bit word length. The position error signal (PES) channel has two signals in quadrature so we'll need two A/D channels including sample-and-holds for position measurement. Because of saturation, we'll also *measure* the coil current induced by the control u_k , which will require another input channel. As mentioned previously, the power amplifier will be driven by a dedicated D/A converter. Some associated circuitry, including the command and status registers, will all be contained in an interface chip. Unless some of the A/D and D/A function is integrated, this could wind up being an expensive design. Some microprocessors are available with room for application specific integrated circuitry (so called ASICs) which could be used for analog I/O because of the small number of pins required.

In the following discussion, we will refer to the open loop, closed loop, and error transfer functions of our servomechanism, $H_{cl}(s)$, $H_{ol}(s)$, and $H_e(s)$, with the following definitions:

$$H_{cl} = \frac{Y(s)}{Y_{ref}(s)} \quad (14.16)$$

$$H_{ol} = \frac{Y(s)}{(Y_{ref}(s) - Y(s))} \quad (14.17)$$

and

$$H_e = \frac{(Y_{ref}(s) - Y(s))}{Y_{ref}(s)} \quad (14.18)$$

The suspension resonance of our actuator is at approximately 2200 Hz, and because it varies quite a bit in frequency and damping, we will make the system gain stable at this resonant frequency. This limits our system closed-loop bandwidth to about 1 kHz because we'll need about 10 dB of gain margin from the open-loop base line (transfer function without resonances). If we have a gain of -3 dB at 1 kHz, one octave higher in frequency the two-pole slope will give us another -12 dB, yielding approximately 15 dB of gain margin at 2000 Hz. Given this bandwidth, it would be difficult to obtain a maximum time constant smaller than 500 microseconds. This is because the open-loop crossover frequency will be at about 500 Hz (roughly half of closed-loop bandwidth), and to get some reasonable phase margin (say 45 degrees) will require a lead compensation zero at about 200 Hz. The zero will have a closed-loop pole close to it based on root locus considerations. A pole at 200 Hz will yield a time constant of 830 microseconds. Hence we shouldn't look for a transient arrival time of less than 1–2 milliseconds. For a one-track position move, the system will probably be dominated by its linear response, and hence we will have a seek time goal of 2 milliseconds.

How about longer seeks? To compute the approximate move time of this system for intermediate length seeks, we can use the shorted-turn current and the motor parameters to calculate accelerations.

Shorted-turn current refers to current through the low inductance path of the circuit, shown in Fig. 14.5, which is used instead of the maximum steady state current because the long time constant of the motor is longer than the seek time, and hence is not available to us for control.¹⁴ If the maximum shorted-turn current I_{st} is given by

$$I_{st} = I_{ss} \frac{R_{coil}}{R_{coil} + R_{st}}, \quad (14.19)$$

where $I_{ss} = e_{max}/R_c$, then the maximum available current for intermediate length seeks is approximately

$$I_{st} = 4.12 \times 0.635 = 2.6 \text{ amps.} \quad (14.20)$$

Using this current and twice the time it takes to move half the distance at a constant acceleration, we can derive the approximate time it takes to do a j -track seek

$$t_j \approx 2\sqrt{j t_w / a_{max}} + t_{settle} \quad (14.21)$$

where

$$a_{max} = \frac{k_t I_{st}}{m} \quad (14.22)$$

Using the parameters from Table 14.3, we get

$$t_j \approx 0.439\sqrt{j} + 1.5 \text{ milliseconds.} \quad (14.23)$$

Using Eq. (14.16) and Eq. (14.23), we obtain an average access time of approximately 15.0 milliseconds (using a 1.5 millisecond settling time).

So far we have covered one-track seek time and WAAT. From a computer system point of view, these are two of the main servo parameters. In addition, average **latency** is a key parameter. Latency refers to the rotational delay incurred after arriving on track until the data location being sought is found. Average latency is approximately half the rotational period. Although the servo does not directly determine the rotational frequency of the disks, the maximum RPM is related to the ability of the servo to follow disturbances at the harmonics of the rotational frequency. The first harmonics are very important, and the servo error transfer function magnitude at those frequencies must be large enough to yield a sufficiently small closed-loop NRRO. Since the rotational frequency of this drive is 3623 RPM or 60.4 Hz, we will tentatively set our error transfer function goal to be -30 dB at this frequency. Likewise, we will get approximately a 12 dB per octave rise in gain in this frequency range, so we'll set the error transfer function gain at this frequency to be about -15 dB, with a 0 dB gain at about 400 Hz.

Achieving the 1 kHz closed-loop bandwidth and gain stabilizing the plant resonances will require at least an 8–10 kHz sampling rate. Because there is a plant resonance at 9 kHz, it is desirable not to have this frequency alias into the passband of the servo. Considering our DSP cycle time of 100 nanoseconds, we will set our initial sampling frequency at 15 kHz, corresponding to a sample time of 66 microseconds (660 processor instructions/sample). This will place the alias of the 9 kHz resonance at 6 kHz, well above the servo bandwidth. After the first pass design is complete, we can revisit this choice.

14.4 Disk Servo Design

So far we have specified closed-loop bandwidth, access time, settling time, one-track seek time, and several error transfer function gains. We must choose a control structure that will allow us to meet these goals. Almost all disk file servos with linear or rotary actuators (not stepping motors) use a PTOS- or XPTOS-like structure (see Chapter 13), whether continuous or sampled data. One common alternative includes **mode switching**, wherein the controller switches from a bang-bang time-optimal mode of operation to a linear controller near the target track. Although the performance

¹⁴It is for this reason we would like I_{st} to be as large a fraction of I_{ss} as possible. This is accomplished by minimizing both L_{st} and R_{st} so that the fast time constant is not degraded.

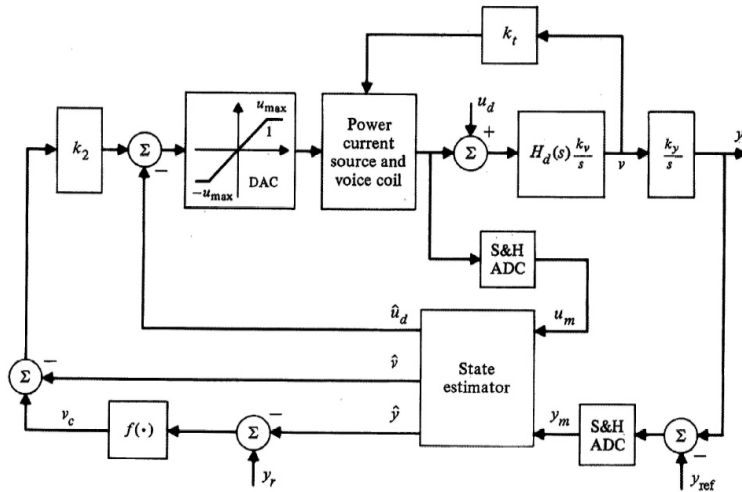


Figure 14.11 Disk-drive servomechanism. Command input y_r contains the desired track address while y_{ref} is the track-center reference

of mode switching systems can be excellent, they tend to be more sensitive to initial conditions, plant parameter variations, and noise. To meet the combined access time and regulation requirements we will choose an XRTOS structure. Because actuator friction and cable forces are non-zero and highly variable, we will estimate the bias forces on the actuator as a state variable.

14.4.1 Design of the Linear Response

To begin, we will assume the motor parameters are known constants as given in Table 14.3. The block diagram of our disk servo is given in Fig. 14.11. For simplicity, we have modeled the resonance characteristics with the transfer function

$$H_d(s) = \sum_{j=1}^4 \frac{b_{2j}\omega_j s + b_{2j-1}\omega_j^2}{s^2 + 2\zeta\omega_j s + \omega_j^2}$$

which is a parallel combination of four quadratic terms in normal mode canonical form. The values given in Table 14.5 were determined by experimental fitting of the frequency response. Because of the large variations in the plant resonances, we will gain-stabilize them and assume that the structure is rigid for the control design. For the same reason we will not try to model resonances in the state estimator. In terms of Fig. 14.11, we assume that $H_d(s) = 1$.¹⁵ The resonances will be included in simulating the final system response. Although there is an unknown constant disturbance input u_d caused by external effects such as the force from the cables attached to the coil assembly, we will not include it in the plant model for control design because it is uncontrollable. The rigid body model is

$$\begin{aligned} \mathbf{F}_{rb} &= \begin{bmatrix} 0 & k_y \\ 0 & -k_{fric}/m \end{bmatrix} \\ \mathbf{G}_{rb} &= \begin{bmatrix} 0 & k_v \end{bmatrix}^T \\ \mathbf{H}_{rb} &= \begin{bmatrix} 1 & 0 \end{bmatrix} \end{aligned} \tag{14.24}$$

where $k_v = k_t/m$ is the acceleration constant, and the plant state is $[y \ v]^T$. With a sampling interval of $T = 66 \times 10^{-6}$, the discrete time plant model based on the rigid body plant model is then

$$\begin{aligned} \Phi_{rb} &= \begin{bmatrix} 1 & 0.6597 \\ 0 & 0.9992 \end{bmatrix} \\ \Gamma_{rb} &= \begin{bmatrix} 0.0022 & 0.0066 \end{bmatrix}^T \end{aligned} \tag{14.25}$$

¹⁵Note that $H_d(0) = 1$.

assuming no calculation delay is being modeled. We can expect to incur some calculation delay in the actual implementation and modification of the system to include this factor is suggested as problem. For the state estimator we will augment the state with the unknown bias input estimate \hat{u}_d so the estimator state is $\hat{\mathbf{x}} = [\hat{y} \ \hat{v} \ \hat{u}_d]^T$ and the plant output, y , is the estimator input. Thus we have

$$\begin{aligned}\Phi_e &= \begin{bmatrix} 1 & 0.6597 & 0.0022 \\ 0 & 0.9992 & 0.0066 \\ 0 & 0 & 1.0 \end{bmatrix} \\ \Gamma_e &= [0.0022 \ 0.0066 \ 0]^T \\ \mathbf{H}_e &= [1 \ 0 \ 0].\end{aligned}\quad (14.26)$$

For the complete system model we will use a current estimator based on Eq. (14.26), along with a full order model of the plant including its resonances. The transfer function $H_d(s)$ represents the discrete time flexible modes. The plant matrices are

$$\Phi = \begin{bmatrix} 1.0 & 0.6597 & 0 & 0 & 0.0000 & 0.0000 & 0.0014 \\ 0 & 0.9992 & 0.0 & 0.0 & 0.0001 & 0.0001 & 0.0034 \\ 0 & 0 & 0.9996 & 0.0290 & 0 & 0 & 0 \\ 0 & 0 & -0.0290 & 0.9967 & 0 & 0 & 0 \\ 0 & 0 & 0 & 0 & 0.6131 & 0.7873 & 0 \\ 0 & 0 & 0 & 0 & -0.7873 & 0.6052 & 0 \\ 0 & 0 & 0 & 0 & 0 & 0 & -0.0330 \\ 0 & 0 & 0 & 0 & 0 & 0 & -0.9182 \\ 0 & 0 & 0 & 0 & 0 & 0 & 0 \\ 0 & 0 & 0 & 0 & 0 & 0 & 0 \\ 0.0008 & 0.0001 & .0002 \\ 0.0034 & -0.0002 & 0.0005 \\ 0 & 0 & 0 \\ 0 & 0 & 0 \\ 0 & 0 & 0 \\ 0 & 0 & 0 \\ 0.9182 & 0 & 0 \\ -0.1249 & 0 & 0 \\ 0 & -0.8180 & -0.5465 \\ 0 & -0.5465 & -0.8125 \end{bmatrix}\quad (14.27)$$

$$\Gamma = \begin{bmatrix} 0.0007 \\ 0.0034 \\ 0.0004 \\ 0.0290 \\ 0.3869 \\ 0.7873 \\ 1.0330 \\ 0.9182 \\ 1.8180 \\ -0.5465 \end{bmatrix}\quad (14.28)$$

and

$$\mathbf{H} = [1 \ 0 \ 0 \ 0 \ 0 \ 0 \ 0 \ 0 \ 0 \ 0 \ 0].\quad (14.29)$$

The equations representing this system, using a current estimator to minimize control delay, can be derived for the state estimator as follows

$$\begin{aligned}\hat{\mathbf{x}}_{k+1} &= \Phi_e \hat{\mathbf{x}}_k + \Gamma_e u_k + \mathbf{L}_c y_{k+1} - \mathbf{L}_c \mathbf{H}_e \hat{\mathbf{x}}_{k+1} \\ &= \Phi_e \hat{\mathbf{x}}_k + \Gamma_e u_k + \mathbf{L}_c y_{k+1} - \mathbf{L}_c \mathbf{H}_e \Phi_e \hat{\mathbf{x}}_k - \mathbf{L}_c \mathbf{H}_e \Gamma_e u_k \\ \hat{\mathbf{x}}_{k+1} &= (\Phi_e - \mathbf{L}_c \mathbf{H}_e \Phi_e) \hat{\mathbf{x}}_k + (\Gamma_e - \mathbf{L}_c \mathbf{H}_e \Gamma_e) u_k + \mathbf{L}_c y_{k+1}.\end{aligned}\quad (14.30)$$

Defining

$$\xi = \hat{\mathbf{x}}_k - \mathbf{L}_c y, \Gamma_{y_r} = \mathbf{H}_e^T, \mathbf{M} = (\mathbf{I} - \mathbf{L}_c \mathbf{H}_e),$$

and a control $u = \mathbf{K}(y_r \Gamma_{y_r} - \hat{\mathbf{x}})$ we can derive the following

$$\xi_{k+1} = \mathbf{M}(\Phi_e - \Gamma_e \mathbf{K}) \xi_k + \mathbf{M}(\Phi_e \mathbf{L}_c \mathbf{H} - \Gamma_e \mathbf{K} \mathbf{L}_c \mathbf{H}) \mathbf{x}_k + \mathbf{M} \Gamma_e \mathbf{K} \Gamma_{y_r} y_r \quad (14.31)$$

for the state estimator, and the state equation governing the plant is

$$\mathbf{x}_{k+1} = (\Phi - \Gamma \mathbf{K} \mathbf{L}_c \mathbf{H}) \mathbf{x}_k - \Gamma \mathbf{K} \xi + \Gamma \mathbf{K} \Gamma_{y_r} y_r(k). \quad (14.32)$$

Defining $\mathbf{x}_s^T = [\mathbf{x}^T \xi^T]$ and the complete closed-loop system by the state equations

$$\mathbf{x}_s(k+1) = \Phi_s \mathbf{x}_s(k) + \Gamma_s y_r(k) \quad (14.33)$$

and the system output equation $y = \mathbf{H}_s \mathbf{x}_s$ where

$$\mathbf{H}_s = [1 \ 0 \ 0 \ 0 \ 0 \ 0 \ 0 \ 0 \ 0 \ 0 \ 0 \ 0 \ 0 \ 0].$$

Thus the complete system is of thirteenth order, and the system matrices are given by

$$\Phi_s = \begin{bmatrix} \Phi - \Gamma \mathbf{K} \mathbf{L}_c \mathbf{H} & -\Gamma \mathbf{K} \\ \mathbf{M}(\Phi_e \mathbf{L}_c \mathbf{H} - \Gamma_e \mathbf{K} \mathbf{L}_c \mathbf{H}) & \mathbf{M}(\Phi_e - \Gamma \mathbf{K}) \end{bmatrix}. \quad (14.34)$$

and

$$\Gamma_s = \begin{bmatrix} \Gamma \mathbf{K} \Gamma_{y_r} \\ \mathbf{M} \Gamma_e \mathbf{K} \Gamma_{y_r} \end{bmatrix}. \quad (14.35)$$

Subtracting a plant output reference signal y_{ref} from the output before the plant output measurement, $y_m = y - y_{ref}$ the estimator position input is then y_m instead of y . The reference input y_{ref} would add to the system state equations through an input matrix $\Gamma_{y_{ref}}$, adding an additional term to Eq. (14.33) of

$$\Gamma_{y_{ref}} y_{ref} = \begin{bmatrix} \Gamma \mathbf{K} \mathbf{L}_c \\ \mathbf{M}(\Gamma_e \mathbf{K} - \Phi_e) \mathbf{L}_c \end{bmatrix} y_{ref}.$$

14.4.2 Design by Random Numerical Search

Note that the system matrices derived above are valid for any order plant model, including either the rigid-body plant or the flexible-body plant model. For the control law and state estimator gains, we will use the random numerical search (RNS) technique of Chapter 13, and the rigid-body plant model. The reason for this is that our control law is being designed to attenuate the flexible dynamics. In essence we will design a rigid-body controller that will allow us to neglect the higher-order flexible modes of the plant. Decay envelopes and root locations of the flexible modes are therefore not under our control. Instead we are attempting a design that minimizes the energy that will be seen in the output from these flexible modes. With the large variations in the flexible modes, a control strategy that attempts to actively damp the flexible modes would require some form of adaptive control. Typically mechanical structures change damping and stiffness (resonant frequency) with temperature and age making controllers tuned at time of manufacture impractical. In addition, serviceability of a system suffers for manufacturing-tuned controllers because arbitrary controllers cannot replace defective ones in the field without being “tuned.”

Because of uncertainty in the plant dynamics above 2 kHz, we decided to limit the closed-loop -3 dB bandwidth from the command input to plant position input to 1 kHz. To minimize system sensitivity, we will also constrain the damping ratio of each mode to be at least 0.65, the decay envelope of each mode to be at least as fast as 1.5 milliseconds, and the sum of all time constants to be less than 3.0 milliseconds. To minimize amplification of midband disturbances in the position reference and noise input y_{ref} , we will limit the peaking in the closed-loop transfer function from y_{ref} to y to 4 dB, or $20 \log \|H_{y_r}(s)\|_\infty < 4$ dB. We would also like to ensure that plant resonances which are near 4 kHz are attenuated by at least 22 dB. These requirements are summarized in Table 14.6.

Performance Measure	Value + Eq. (14.36)	Units	Symbol in
Bandwidth of H_{cl}	1000.	Hertz	f_{BW}
Minimum damping	0.650	ζ_{min}	
Minimum phase margin	45.0	degrees	pm
Peaking of H_{cl}	3.00	dB	$peak$
Peaking of H_e	4.00	dB	$peak$
Maximum time constant	1.50	microseconds	$\bar{\tau}$
Sum of time constants	3.00	milliseconds	$\Sigma\tau$
Attenuation at 60 Hz	30	dB	$20 \cdot \log_{10}(H_e(2\pi 60))$
Attenuation at 1.6 kHz	10	dB	$20 \cdot \log_{10}(H_{ol}(2\pi 1600))$
Attenuation at 4 kHz	22	dB	$20 \cdot \log_{10}(H_{ol}(2\pi 4000))$
Gain margin	20.	dB	gm

Table 14.6
Desired performance goals for disk drive head positioning servo

A cost function C that represents the desired goals in Table 14.6 can be defined as follows

$$\begin{aligned}
C = & W_{BW} |f_{BW} - 1000| + W_{\zeta} \text{soft}(0.65 - \zeta_{min}) + \\
& W_{pm} \text{soft}(45.0 - pm) + W_{peak} \text{soft}(peak - 4.00) + \\
& W_{\tau_{max}} \text{soft}(\bar{\tau} - 1.0 \times 10^{-3}) + W_{\tau_{sum}} \text{soft}(\Sigma\tau - 1.8 \times 10^{-3}) + \\
& W_{60hz} \text{soft}(22.0 + 20 \log_{10}[H_e(2\pi 60.)]) + \\
& W_{1600hz} \text{soft}(22.0 + 20 \log_{10}[H_{ol}(2\pi 1600.)]) + \\
& W_{4khz} \text{soft}(22.0 + 20 \log_{10}[H_{ol}(2\pi 4000.)]) + \\
& W_{gm} \text{soft}(20.0 - gm)
\end{aligned} \tag{14.36}$$

where the function “soft” is best described as a linear diode, or

$$\text{soft}(x) = \begin{cases} x & x \geq 0 \\ 0 & x < 0. \end{cases}$$

The design found using an RNS method (750 runs) starting from a stable pole placement design for the fifth-order system (using the rigid-body plant model and third-order state estimator) is given by

$$\mathbf{K} = [17.9142 \quad 71.5426 \quad 1.000] \tag{14.37}$$

subject to the constraint on k_2 from PTOS, $k_2 = \left(\frac{2k_1 k_y}{\alpha k_v}\right)^{1/2}$, with $\alpha = 0.70$ and $k_v = k_t/m$ given in Table 14.3 of parameters. The state estimator gain matrix is

$$\mathbf{L}_c = [1.039 \quad 0.1534 \quad -4.5574]^T. \tag{14.38}$$

The acceleration discount factor α was chosen assuming we could only make use of the shorted turn current I_{st} . Using the worst case parameters from the table, we get a safe value for α of 0.70. Performance parameters and weighting factors used in the RNS optimization are given in Table 14.7. For the base fifth-order design, the frequency response is shown in Fig. 14.12.

In addition, we can see from the same analysis that the open-loop envelopes plotted show that in some cases the system is phase stable. Because the resonance coupling parameters and damping ratios were stressed in the nominal cases for a conservative design, we will live with the cases shown that are phase stable. If the designer felt that this is not unlikely, and that the phase margin for this resonance was not enough, the design would have to be re-optimized, perhaps with more weighting on the attenuation at 4 kHz. A pole constellation for the Monte Carlo analysis is shown in Fig. 14.15.

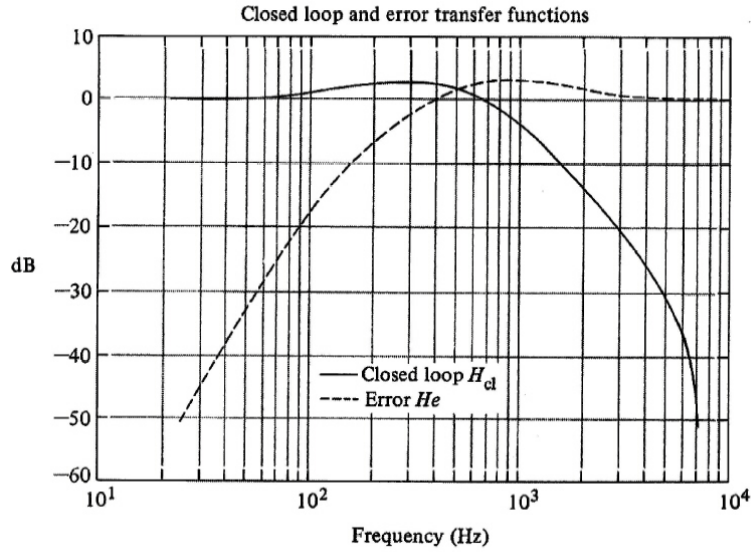


Figure 14.12
Frequency response after RNS optimization

Parameter	Optimized Value	Weighting Factor
\mathbf{L}_c^T	[1.039 0.1534 - 4.5574]	
\mathbf{K}	[17.9142 71.5096 1.0]	
Σ_τ	3.14 milliseconds	$W_{\tau_{sum}}$ 10000
$\bar{\tau}$	1.47 milliseconds	$W_{\tau_{max}}$ 10000
f_{BW}	959 Hz	W_{BW} 0.01
$20 \cdot \log_{10}(H_e(2\pi 60))$	-29.0dB	W_{60hz} 0.25
$20 \cdot \log_{10}(H_{ol}(2\pi 1600))$	-13.0dB	W_{1600hz} 1.0
$20 \cdot \log_{10}(H_{ol}(2\pi 4000))$	-25.5dB	W_{4khz} 0.33
g_m	18.5dB	W_{g_m} 0.33
ζ_{min}	0.707	W_ζ 10.0
$peak$	2.72dB	W_{peak} 3.30

Table 14.7
Performance measures after optimization with weighting factors shown for a random numerical search routine after 750 iterations with $\rho = 0.30$

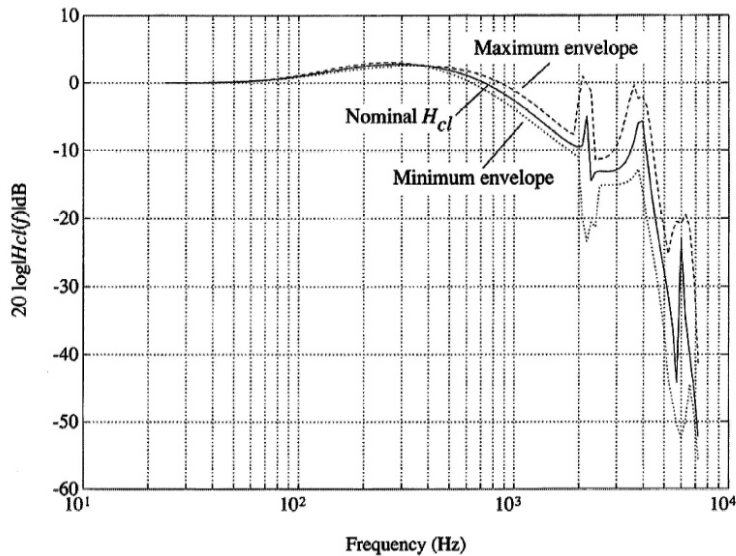
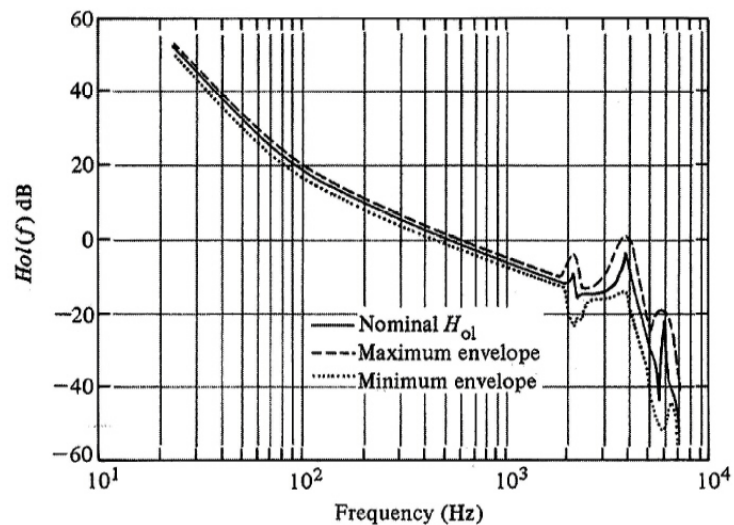
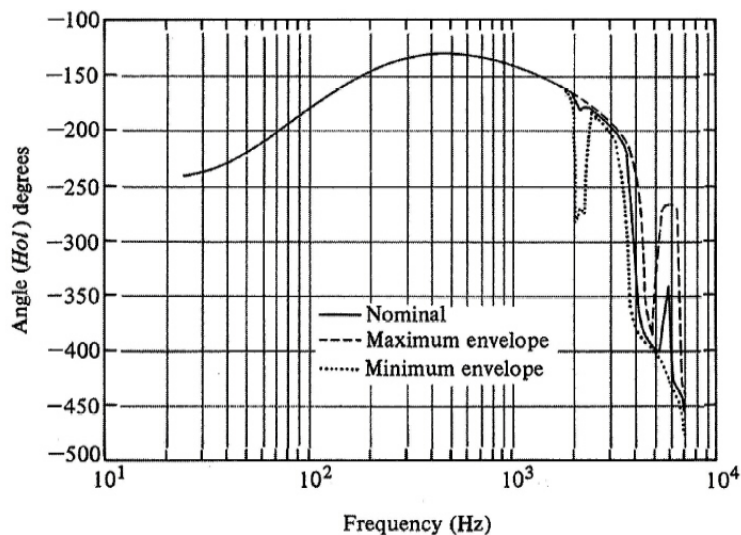


Figure 14.13
Monte Carlo analysis of closed-loop response H_{cl} for 250 sample systems



(a)



(b)

Figure 14.14
 Monte Carlo analysis of open loop response H_{cl} for 250 sample systems.
 (a) Nominal magnitude and envelope,
 (b) nominal phase and envelope

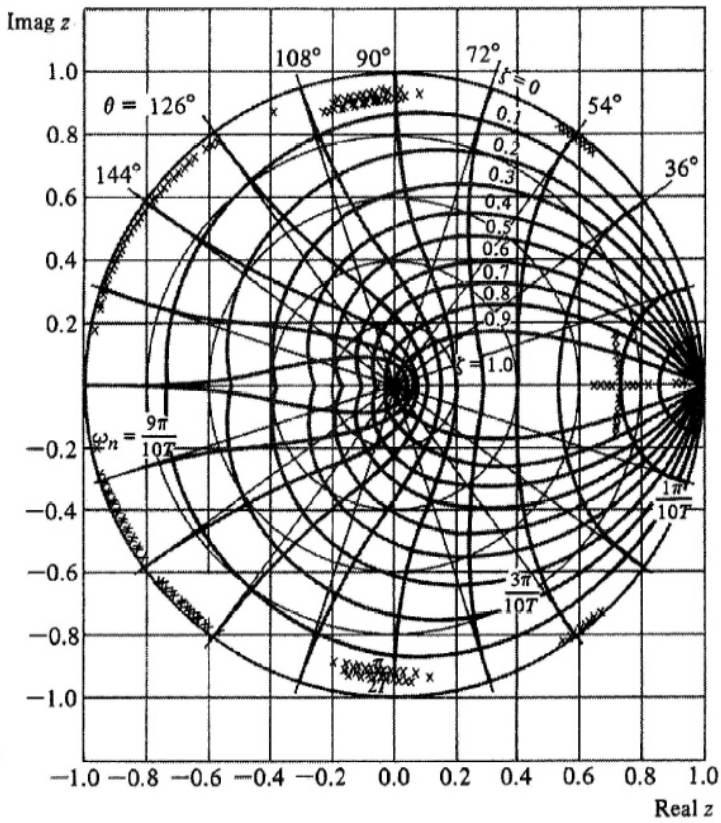


Figure 14.15
Root constellation for the 250 sample systems of the Monte Carlo analysis

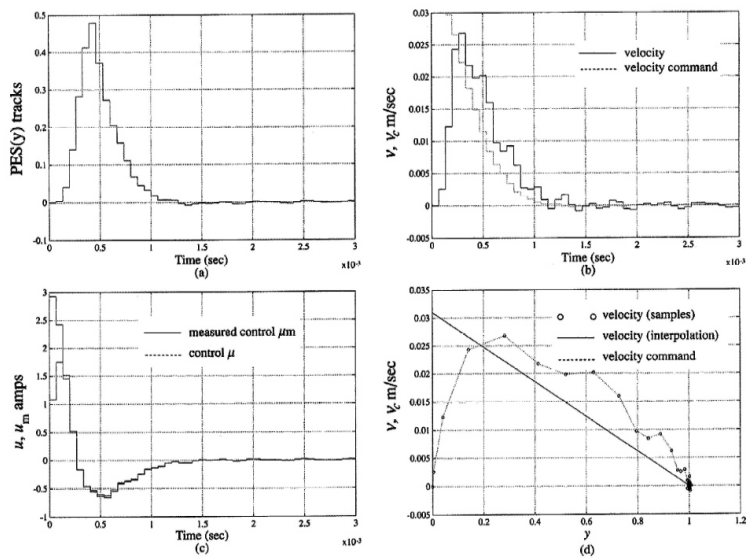


Figure 14.16
One track seek waveforms. Instead of plotting position, the PES is plotted in units of tracks. Note the arrival time is approximately one millisecond

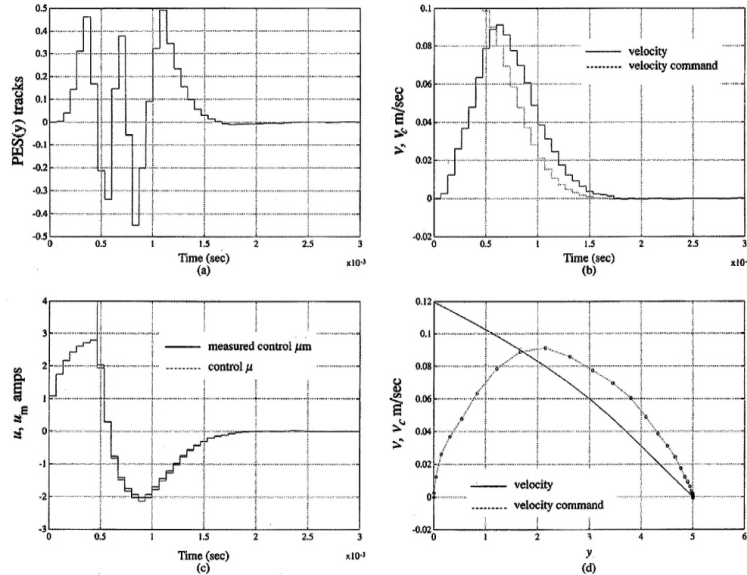


Figure 14.17
Five track seek waveforms. Note the arrival time is less than that for the one-track seek, approximately one-half millisecond

14.4.3 Time-Domain Response of XPTOS Structure

Critical to the performance of the servo is the time-domain response. Most important because of its frequency of occurrence is the one-track seek. Shown in Fig. 14.16, the one-track seek is indeed completed in 2.0 milliseconds, which was our design goal. In fact, it is finished early enough so that there should be some margin for variation of parameters and still remain below the target. One interesting feature of Fig. 14.16 can be seen in the phase plane plot: A straight line interpolation of the sampled velocity is probably not too accurate. Because of the 9 kHz resonance, the true continuous plant output has some intersample ripple. However, since the position output is fairly smooth, the effect is not of great importance. Also of interest is the fact that the one-track seek does not use maximum control, at least from the D/A converter point of view. In fact, it's maximum is 2.0, only half the maximum D/A output value. Note however that the *measured* control does not respond to the command perfectly. Voice coil time constants prohibit the power amplifier from following the command input with high fidelity for the first three samples, but after that the command and the measured value correspond fairly well. If we did not measure the true control, the state estimator would have significant estimator errors due to the difference between the control command and the current actually achieved in the coil. This error would become far worse on longer seeks when the power amplifier spends more time in saturation.

Next we'll examine a five-track seek, as shown in Fig. 14.17. Now the PES waveform in the plot shows four track crossings before arrival at the final track. Although the seek is finished in 2 milliseconds, there is little room for parameter variation. However, allowing 1 millisecond for variation of parameters, we can safely say that the system finishes the five-track seek in 3 milliseconds. Measured current, or control u_m , is markedly different from the command current (control u) during the acceleration phase of the seek. In this plot the effects of the VCM time constants are clear. Note that in the phase plane plot the relative effect of the high frequency plant dynamics is much smaller than in the one-track seek.

Examination of Eq. (A.22) shows that a rough approximation of the WAAT is the time it takes to accomplish a seek of length $N/3$, where N is the total number of tracks. For a stroke of 28 millimeters at 12.5 microns per track, this corresponds to a 3666 track seek. Shown in Fig. 14.18, the seek takes approximately 13 milliseconds to complete. A 13 millisecond average access time corresponds well to the goal of 15 milliseconds we set for the design. Several other features are worthy of note in Fig. 14.18. First, the PES plot no longer shows track crossings. With a sample time of 66 microseconds, the servo will be crossing as many as 5.3 tracks per sample interval per meter per second. This can be derived from looking at the state transition matrix Φ_e or Φ_s for the

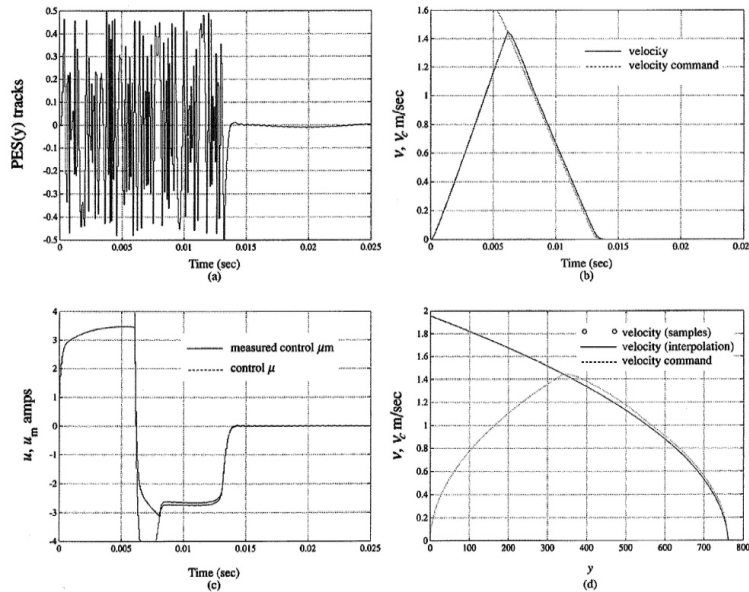


Figure 14.18
 Seek waveforms for one third stroke move, or 3666 tracks. This length seek roughly corresponds to the weighted average access time, which is approximately 13.0 milliseconds

way in which velocity updates the position. Thus, at the peak velocity the position will change approximately 8 tracks in a single sample interval for this length seek. Another point of interest is the current waveform. Note that the current never comes close to the commanded current during the acceleration phase of the seek. Also, during deceleration, the control saturates in an effort to make the plant follow the velocity command v_c from the function $f(\cdot)$. Without the voice coil poles the current could instantaneously respond to the control, and with them the response is sluggish, so the velocity overshoots the phase plane trajectory. In deriving the PTOS architecture, the power amplifier is assumed a perfect current source, and is not sluggish. But the parameter α allows the velocity trajectory to be less aggressive than the ideal plant could follow, and thus the system is robust to “unmodeled” dynamics such as those of the voice coil. Although theoretically possible, implementation of a fourth order trajectory to account for the two voice coil motor poles (instead of the second order trajectory $f(\cdot)$) is difficult.

Note also in Fig. 14.18 that the control comes out of saturation at some point fairly early in the deceleration phase. Because the control is unsaturated, the system is under feedback control. Remaining under control is important to ensure that the arrival to the target track takes place without overshoot.

Looking carefully at the position arrival to the target track in Fig. 14.18, a small and slowly varying offset from track center can be seen. Attributable to the low frequency resonance caused by the reaction forces of the magnet structure through the isolators to the HDA baseplate, this resonance response is about 4 microinches peak to peak. For our design, nothing can be done about this resonance. However, if the resonance varies slowly enough in time, an adaptive or self-tuning approach can be of great assistance. Essentially, a model of this structural resonance would be included in the state estimator, and adjusted to track the true resonance at start-up times. Feedback of the two states (second-order model) is then added directly into the control, as in the XPTOS structure. Adaptive control is required here because small variations in plant parameters relative to the model yield quickly degrading performance. For this design, a couple of microinches of transient NRRO (the vibration will eventually cease) is small enough to be neglected. However, as the ratio of moving mass to fixed mass and access time both decrease, the effect of this resonance can become devastating. Several patents have been issued on techniques using external accelerometers on the baseplate to provide feedback into the control to reduce the error caused by this effect.

Finally, we will examine the longest length seek. Shown in Fig. 14.19, the seek is complete in approximately 23 milliseconds. Although the peak velocity is 2.5 meters per second, it is common to saturate the command velocity to limit this peak velocity. One reason to limit the peak velocity

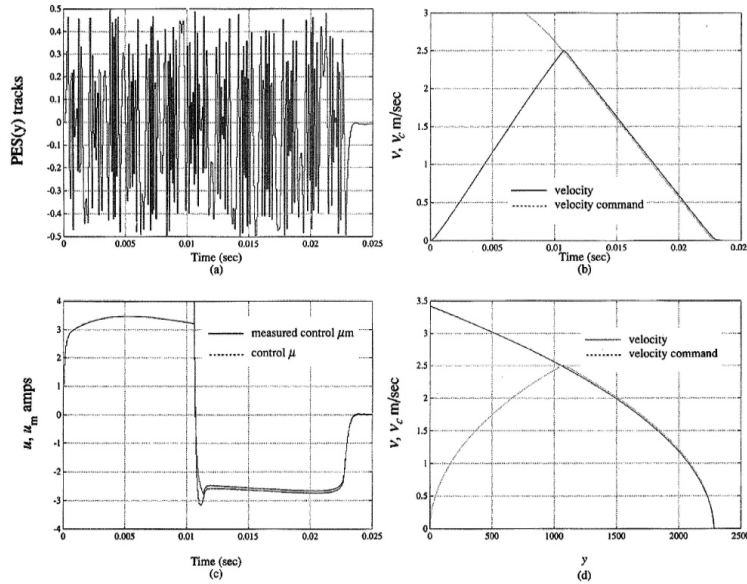


Figure 14.19
Maximum length seek waveforms, 11,000 tracks. Note that the back emf generated by the coil helps the power current source to reverse the direction of current in the coil. During acceleration the back emf caused the current to begin to decrease

is to limit the track crossing frequency. At 2.5 meters per second, the track crossing frequency is approximately 80 kHz, and the PES circuit filter bandwidth has to be at least this high to generate position error signals with reasonable fidelity. A quadrature PES channel can be used to lower the required bandwidth by a factor of two, to 40 kHz. Although somewhat better, a bandwidth of 40 kHz will allow quite a bit of aliasing to take place with a 15 kHz sampling frequency. One alternative is to filter the PES with a lower bandwidth filter after arriving on track, thus limiting the aliased noise. Increasing track density exacerbates this problem, so some new ideas in PES signal modulation and demodulation must be explored.

14.4.4 Implementation Considerations

Although we have discussed some of the implementation details in the previous section on design, we will cover some of the final details necessary to write the DSP program code, either high level or assembly language. We have yet to specify the variables, the order of computation, and the word length for each. To specify the variables, we will examine the state estimator computations and the control calculation.

For the state estimator, we have a prediction phase and a time update phase. Since we are measuring the control (u_m), it is not available for the prediction phase. Equation (14.39) is the normal prediction equation for the current estimator

$$\hat{\mathbf{x}}_{k+1} = \Phi_e \hat{\mathbf{x}}_k + \Gamma_e u(k). \quad (14.39)$$

We are measuring the current i_c at time $k + \Delta$ ($u_m = i_c(k + \Delta)$), where Δ is smaller than but close to the sample time T . By waiting as long as possible after the control output is sent to the D/A to sample the coil current i_c , we will give the power amplifier time to settle to the desired value if it can. When saturated, the output may be quite different than the desired control (this is why we're measuring it). For high accuracy, we could assume an average *effective* control of $(u_m(k-1) + u_m(k))/2$ when the measured current differs greatly from the intended value of $u(k)$. For now we'll just use the measured control u_m as input to our state estimator. When the digitized $u_m(k)$ is available, we can complete the prediction update according to Eq. (14.39).

$$\hat{\mathbf{x}}_{k+1} = \Phi_e \hat{\mathbf{x}}_k + \Gamma_e u_m(k) \quad (14.40)$$

With the state transition matrices given by Eqs. (14.27)–(14.29), the scalar update equations are done

-
1. Set track-type to 0. $y_m \leftarrow -p$
 2. If $(p > q$ and $p > -q)$: track-type = 1, $y_m \leftarrow q$
 3. If $(p > q$ and $p < -q)$: track-type = 2, $y_m \leftarrow p$
 4. If $(p < q$ and $p > -q)$: track-type = 3, $y_m \leftarrow -q$
 5. $y_m \leftarrow y_m + \text{track} - \text{type} \times t_w$
-

Table 14.8
Method for
constructing the
measurement y_m
from the digitized
 p and q
waveforms

in two steps, the first of which is

$$\bar{x}_1^0(k+1) = \hat{x}_1(k) + 0.6597\hat{x}_2(k) \quad (14.41)$$

$$\bar{x}_2^0(k+1) = \hat{x}_2(k) \quad (14.42)$$

$$\bar{x}_3(k+1) = \hat{x}_3(k) \quad (14.43)$$

where $\bar{x}_1^0(k+1)$ and $\bar{x}_2^0(k+1)$ are intermediate values of the final predictions. Since $\bar{x}_3^0(k+1)$ does not depend on u_m , it can be updated immediately. When the control u_m is available, we compute

$$\bar{x}_1(k+1) = \bar{x}_1^0(k+1) + 0.0022u_m(k) \quad (14.44)$$

$$\bar{x}_2(k+1) = \bar{x}_2^0(k+1) + 0.0066u_m(k). \quad (14.45)$$

By splitting the prediction into two parts, we can wait until the last possible instant before converting u_m and still be ready for the next sample interrupt. When the next conversion complete signal interrupts the processor, we will be directed to the main control calculation routine.

Although not explicitly shown in Fig. 14.11, the calculation of y_m will take two A/D conversions to convert both the primary and quadrature channels of our position error channel. Because of the cost of A/D conversions, we will do them in series instead of in parallel. Our A/D conversions will signal the processor when conversion is complete by special hardware interrupt that immediately directs the processor to the correct interrupt routine. Special analog circuitry can be employed to furnish a single A/D converter input with the correct waveform (p or q), along with the two digital track-type bits to the processor. However, besides the cost, some opportunity for error detection is lost by implementing the construction of y_m in analog circuitry. Defining the digitized PES waveforms as $p(k)$ and $q(k)$, the signal y_m is computed from Table 14.8.

Once the measurement y_m has been constructed, we can proceed with the estimator time update. The prediction error is computed first: $e = \bar{x}_1 - y_m$. Next the estimates are calculated

$$\begin{aligned} \hat{x}_1 &= \bar{x}_1(k+1) + 1.039e \\ \hat{x}_2 &= \bar{x}_2(k+1) + 0.1534e \\ \hat{x}_3 &= \bar{x}_3(k+1) + -4.5574e. \end{aligned} \quad (14.46)$$

Now that the state estimates are available we can calculate the control. First, compute the current position error, $y_e = y_r - \hat{x}_1$. Now we must compute the velocity command v_c . Computation of $f(\cdot)$ directly is very time consuming. As an alternative, we can fit the trajectory with a simple polynomial or use table lookup. When $y_e \leq y_l$, the velocity command is just a linear function of the position error $v_c = 0.0311y_e$. With a maximum control of 4.0, the linear region distance y_l (on either side of zero) is 1.3605 tracks. For table lookup, if $y_e > 1.3605$, we call a routine which finds v_c given y_e as an input. The rest of the control is calculated as follows

$$\begin{aligned} v_e &= v_c - \hat{v} \\ u &= \text{sat}(k_2 v_e - \hat{u}_d) \\ \hat{v} &= \hat{x}_2 \\ \hat{u}_d &= \hat{x}_3. \end{aligned} \quad (14.47)$$

Equations (14.46) and (14.47) represent the entire control algorithm. Because of the nonlinearity, it is difficult to precompute much of the control algorithm. Although some improvement can be made by using the predicted position for precomputing the velocity trajectory, we will assume we cannot do any precomputation of u .

Variable	Min	Max	Units	Resolution	Word Length
\bar{x}_1, \hat{x}_1	0	12000	tracks	$1/2^{14}$	2
$\bar{x}_2, \hat{x}_2, v_c, v_e$	-2.6	2.6	m/sec	0.0001	2
$\bar{x}_3, \hat{x}_3, u, u_m, u_d$	-4.2	4.2	amps	0.0002	2
y_e	-12000	12000	tracks	$1/2^{14}$	1
e	-2	2	tracks	$1/2^{14}$	1

Table 14.9
Minimum and maximum range, approximate quantization level of interest, and required word length (16 bit words)

Scaling

To choose scale factors and word lengths, it is necessary to determine the range of each variable in our system, along with an approximate value for the smallest quantity of interest for the variable. Table 14.9 contains a summary of the variables, their ranges, and the word length required.

14.5 Summary

In this chapter, we have presented a case study of design using a high performance disk drive servo. Although many details of the design process were presented, many more remain, including component selection and detailed programming of the control computer or DSP. Most of these points are dependent on the technology and budget of the project and difficult to make relevant as part of the control design process. The main points are:

- A real problem is often very complex, containing many details that are not essential to be considered in a first-pass design.
- Each component needs to be analyzed to evaluate its contribution to the overall design.
- The linear control-observer structure described in earlier chapters gives a good start but numerical search can significantly improve the design.
- The XPTOS structure is a practical approach for high-performance motion control to account for large signal performance.

14.6 Problems

- 14.1 For the following system, design a control system to place the nominal closed-loop poles of the system such that the flexible mode is well damped and the time response of the system settles to a step in 5 milliseconds. Next, generate the frequency-response envelope using the Monte Carlo technique. Are all systems in the set stable?

$$\begin{aligned}
 T &= \mathcal{N}(0.001, 0.00001), \\
 b &= \text{uniform}(0.001, 0.00001), \\
 \zeta &= \text{uniform}(0.0005, 0.005), \\
 \omega_r &= \mathcal{N}(1200, 150), \\
 G &= \mathcal{N}(1.00, 0.04),
 \end{aligned}$$

where T is the sampling rate, and the continuous plant transfer function is given by

$$H_p(s) = \frac{G(s+b)\omega_r^2}{s^2(s^2 + 2\zeta\omega_r s + \omega_r^2)}.$$

- 14.2 For the system of Problem 14.1, outline a technique by which the open-loop gain of the system could be adaptively adjusted at start-up time.

- (a) What would the expected range of adaptation be?
- (b) Redo the Monte Carlo analysis assuming that the variation in G is compensated for (assume its variation is 0).
- (c) Is it worth compensating for changes in G of 4%?

14.3 Given a plant with the state-space description

$$\Phi = \begin{bmatrix} 1 & 0.0002 & 0.00003 \\ 0 & 1 & 0.1726 \\ 0 & 0 & 1 \end{bmatrix}$$

$$\Gamma = \begin{bmatrix} 0.00003 \\ 0.1726 \\ 0 \end{bmatrix}$$

$$H = [1 \ 0 \ 0]$$

where the sample time is $T_s = 0.0001$. Assume the time it takes to compute and output the control is $\lambda = 10^{-5}$ sec.

- (a) Design a linear feedback control that gives a bandwidth of approximately 1000 Hz, with the maximum time constant no greater than 1.0 milliseconds, for a reference input r (feedback $\mathbf{K}(\mathbf{H}^T r - \mathbf{x})$).
- (b) What is the order of the plant model used to design the control law?
- (c) Assuming the plant states to be measured, where does the delayed control that is to be fed back come from? What if the control is saturated first?
- (d) Do a root locus of your design versus an actual λ in the range of 8 to 15 microseconds. Is the design sensitive to variable control delay?
- (e) For the variation in λ given in part (d), what range of phase margin does the system have?

14.4 For the plant given in Problem 14.3, assume the sensor for the plant output y has a static gain error tolerance of $\pm 5\%$ (including zero frequency).

- (a) Given that the feedback law is constructed as in Problem 14.3, what is the best control accuracy achievable?
- (b) How should the system be changed if the desired static accuracy is to be no worse than 1%?

14.5 Redesign¹⁶ the disk drive servo to account for a calculation delay of $\lambda = 40 \mu\text{sec}$.

- (a) Will the same control law work? Why not?
- (b) Is there any advantage in feeding back the delayed control into the control law?
- (c) Plot frequency responses and time responses for your system.
- (d) Do a Monte Carlo analysis of your design. Is it manufacturable? (Use the same tolerances used in the case study, but add the tolerance on λ and set it to the sample time tolerance.

14.6 For the case study design, draw the block diagram for INL (see Chapter 13) control given the following variation in k_t versus y : $k_t(y) = 15 \cdot (1 - |y - 1130.0|/11300)$, where, as before, y is in tracks and the total stroke of the actuator covers 2240 tracks.

- (a) What are your new control and state estimator gains given the same design objectives?

¹⁶This and the remaining problems are very involved and require a computer design tool such as MATLAB, along with a significant amount of time.

- (b) By calculating only one gain factor versus stroke, show that you can maintain fixed pole locations for the complete system.
 - (c) Design a velocity trajectory for this system. What has to change?
 - (d) Do a time-domain simulation of this system. Plot waveforms as in the case design.
- 14.7 For the case study design, assume that the second resonant frequency is well known (fixed parameters). Add a model of this mode to the state estimator and redesign the state estimator and the control law to damp this mode, and obtain a 1600-Hz closed-loop bandwidth.

Appendix A

Examples

In this appendix we describe five control problems which are used to illustrate the analysis and design techniques developed in the text. These are collected here in order to permit references to them at a number of places in the text without the need to repeat the derivation of the model or discuss the specifications each time the example is used.

A.1 Single-Axis Satellite Attitude Control

Satellites often require attitude control for proper orientation of antennas and sensors with respect to the earth. Figure A.1 shows a communications satellite with a three-axis attitude-control system. To gain insight into the three-axis problem we often consider one axis at a time. Figure A.2 depicts this case where motion is allowed only about an axis perpendicular to the page. The equations of motion of the system are given by

$$I\ddot{\theta} = M_C + M_D, \quad (\text{A.1})$$

where I is the moment of inertia of the satellite about its mass center, M_C is the control torque applied by the thrusters, M_D are the disturbance torques, and θ is the angle of the satellite axis with respect to an “inertial” reference. The inertial reference must have no angular acceleration. Normalizing, we define

$$u = M_C/I, \quad w_d = M_D/I \quad (\text{A.2})$$

and obtain

$$\ddot{\theta} = u + w_d. \quad (\text{A.3})$$

Taking the Laplace transform

$$\theta(s) = \frac{1}{s^2} [u(s) + w_d(s)], \quad (\text{A.4})$$

which becomes, with no disturbance

$$\frac{\theta(s)}{u(s)} = \frac{1}{s^2} = G_1(s). \quad (\text{A.5})$$

In the discrete case with u being applied through a zero-order hold, we can use the methods of Chapter 4 to obtain the discrete transfer function

$$\begin{aligned} G_1(z) &= \frac{\theta(z)}{u(z)} \\ &= \frac{T^2}{2} \frac{(z+1)}{(z-1)^2}. \end{aligned} \quad (\text{A.6})$$

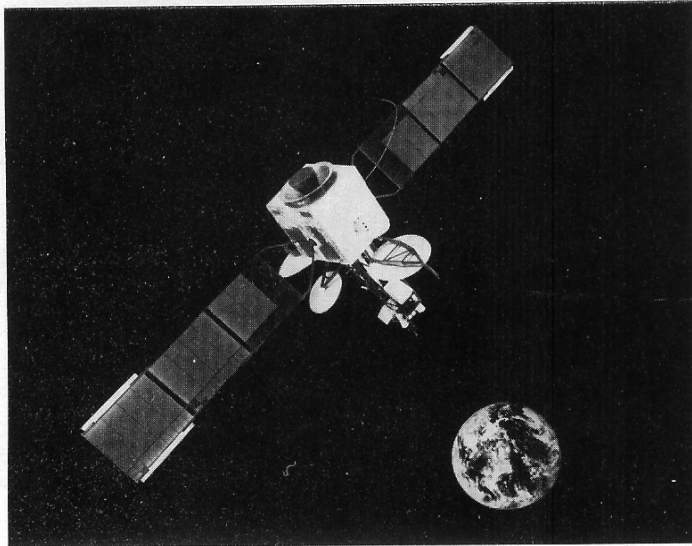


Figure A.1
Communications satellite (courtesy Space Systems-Loral)

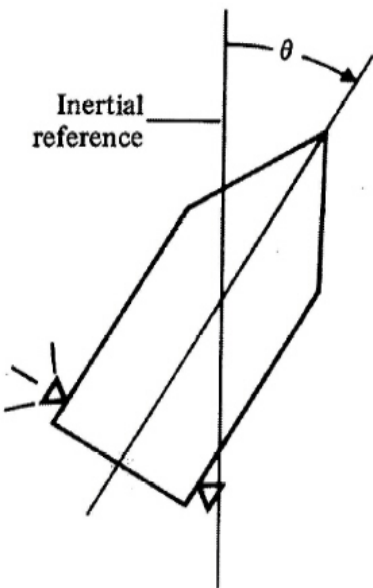


Figure A.2
Satellite-control schematic



Figure A.3
Satellite tracking
antenna
(courtesy Space
Systems-Loral)

A.2 A Servomechanism for Antenna Azimuth Control

It is desired to control the elevation of an antenna designed to track a satellite as shown in Fig. A.3. The antenna and drive parts have a moment of inertia J and damping B arising to some extent from bearing and aerodynamic friction, but mostly from the back emf of the DC-drive motor. A schematic is shown in Fig. A.4.

The equation of motion is

$$J\ddot{\theta} + B\dot{\theta} = T_c + T_d, \quad (\text{A.7})$$

where T_c is the net torque from the drive motor and T_d is the disturbance torque due to wind. If we define

$$B/J = a, \quad u = T_c/B, \quad w_d = T_d/B,$$

the equation reduces to

$$\frac{1}{a}\ddot{\theta} + \dot{\theta} = u + w_d. \quad (\text{A.8})$$

Transformed, it is

$$\theta(s) = \frac{1}{s(s/a + 1)} [u(s) + w_d(s)] \quad (\text{A.9})$$

or, with no disturbances,

$$\frac{\theta(s)}{u(s)} = \frac{1}{s(s/a + 1)} = G_2(s). \quad (\text{A.10})$$

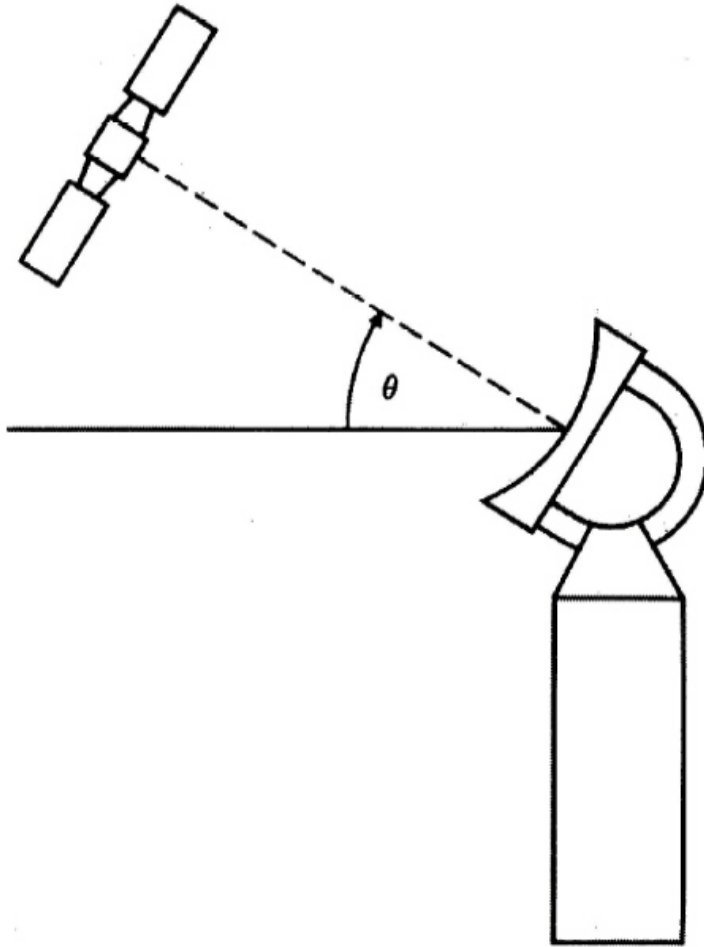


Figure A.4
Schematic
diagram of
antenna

The discrete case with $u(k)$ applied through a zero-order hold yields

$$G_2(z) = \frac{\theta(z)}{u(z)} = K \frac{(z+b)}{(z-1)(z-e^{-aT})}, \quad (\text{A.11})$$

where

$$K = \frac{aT - 1 + e^{aT}}{a}, \quad b = \frac{1 - e^{-aT} - aTe^{-aT}}{aT - 1 + e^{-aT}}.$$

The model given by Eq. (A.7) is only a linear approximation to the true motion, of course. In reality there are many nonlinear effects that must be considered in the final design. To give some ideas of these considerations, we present the major features of the angle, θ_s , of the satellite to be followed and of the servomechanism that must be designed to achieve the tracking.

The general shape of $\theta_s(t)$ and its velocity and acceleration are sketched in Fig. A.5. The peak values of velocity and acceleration depend critically on the altitude of the satellite above the earth and on the elevation above the horizon of the orbit seen from the antenna. An orbit of 200 miles above the earth that passes at an elevation above the antenna of 86° requires a maximum azimuth rate of 0.34 rad/sec (about $20^\circ/\text{sec}$). For the purpose of setting the tracking accuracy and gains, a reasonable assumption is that the antenna should be capable of following this peak velocity in the steady state with acceptable error.

The size of the allowable tracking error is determined by the antenna properties. The purpose, of course, is to permit acceptable communication signals to be received by the antenna electronics. For this, we must consider the dependence of signal amplitude on pointing error. A sketch of a typical pattern is shown in Fig. A.6. The beam width $\Delta\theta$ is the range of tracking error permissible if acceptable communications are to be achieved. Typical values of the beam width can vary from a few degrees (0.1 rad) to less than one degree (0.01 rad). The total error will be composed mainly of tracking errors due to θ_s motion, wind-gust errors, and random errors caused by noise in the measurement of satellite position. A reasonable allowance is to permit tracking errors of 10% of the beam width and an equal contribution from wind gusts. For a beam width of 0.1 rad, then, we allow a tracking error of 0.01 rad, from which it follows that $K_v = 1$ (if $\dot{\theta}_{\max} = 0.01$ rad/sec). For a 60-ft. tracking antenna, a typical beam width is 0.01 rad, and if 0.34 rad/sec must be followed, the velocity constant for a 10% error (0.001 rad) is $K_v = 0.34/0.001 = 340$. For a velocity constant of this magnitude, a conversion to a Type 2 system with two poles at $z = 1$ is probably required.

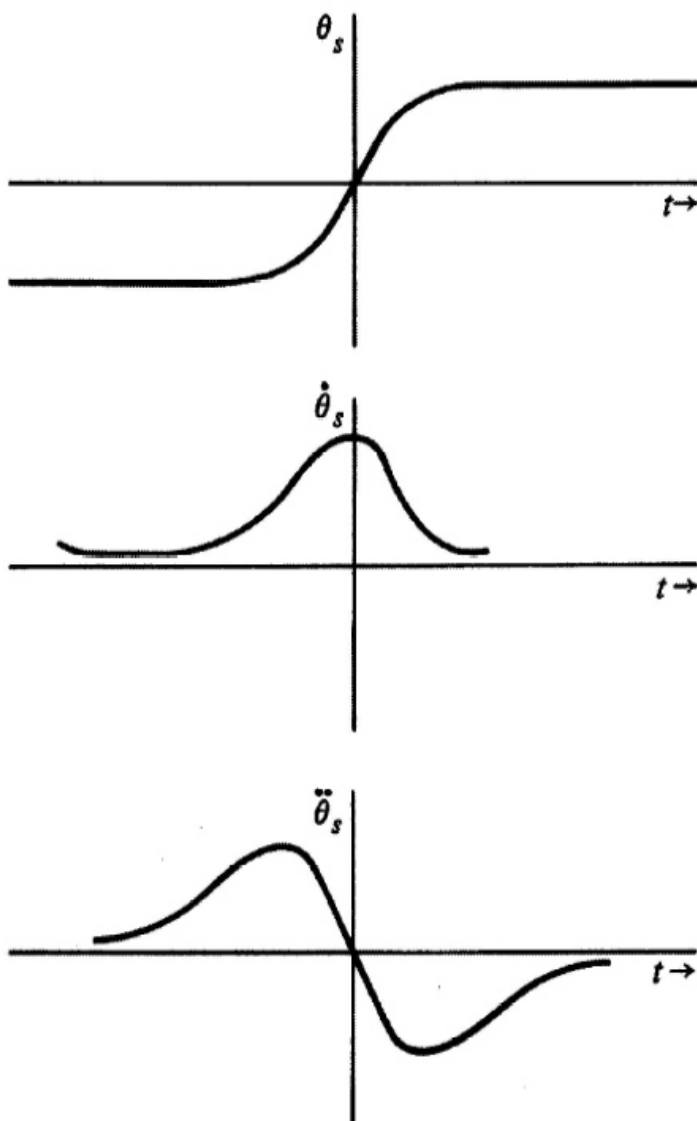
In addition to considerations of tracking error, the designer must take into account the fact that the drive motor has finite torque and power capability. In selecting the drive motor, one must keep in mind that the total torque must be capable of meeting the acceleration demands of tracking, overcoming the wind torque, and overcoming the static friction of the drive-train gears and antenna mount. The power of the motor must be able to supply this torque at the maximum tracking velocity.

A.3 Temperature Control of Fluid in a Tank

The temperature of a tank of fluid with a constant flow rate in and out is to be controlled by adjusting the temperature of the incoming fluid. The temperature of the incoming fluid is controlled by a mixing valve that adjusts the relative amounts of hot and cold supplies of the fluid (Fig. A.7). Because of the distance between the valve and the point of discharge into the tank, there is a time delay between the application of a change in the mixing valve and the discharge of the flow with the changed temperature into the tank.

The differential equation governing the tank temperature is

$$\dot{T}_e = \frac{1}{cM}(q_{\text{in}} - q_{\text{out}}), \quad (\text{A.12})$$

**Figure A.5**

General shape of the command angle and its first two derivatives, which the tracking antenna must follow

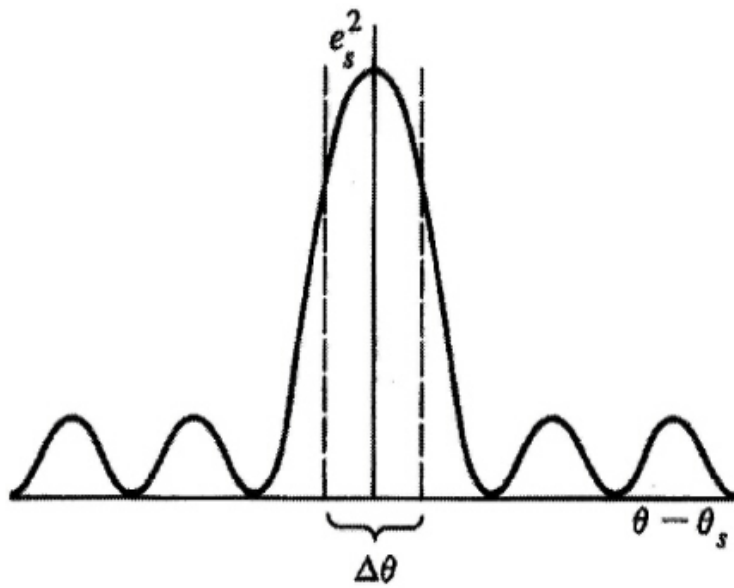


Figure A.6
Plot of signal power received as a function of tracking error

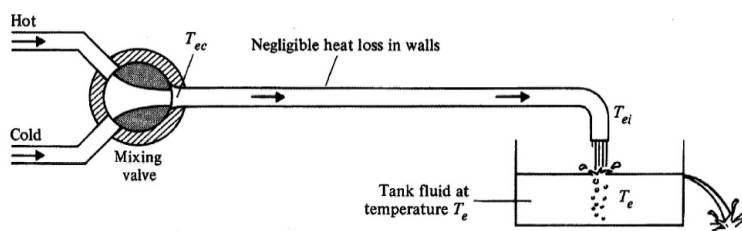


Figure A.7
Tank temperature control

where

$$\begin{aligned}
 T_e &= \text{tank temperature,} \\
 c &= \text{specific heat of the fluid,} \\
 M &= \text{fluid mass contained in the tank,} \\
 q_{\text{in}} &= c\dot{m}_{\text{in}}T_{ei}, \\
 q_{\text{out}} &= c\dot{m}_{\text{out}}T_e, \\
 \dot{m} &= \text{mass flow rate } (= \dot{m}_{\text{in}} = \dot{m}_{\text{out}}), \text{ and} \\
 T_{ei} &= \text{temperature of fluid entering tank;}
 \end{aligned}$$

but the temperature at the input to the tank at time t is the control temperature τ_d sec in the past, which can be expressed as

$$T_{ei}(t) = T_{ec}(t - \tau_d), \quad (\text{A.13})$$

where

$$\begin{aligned}
 \tau_d &= \text{delay time, and} \\
 T_{ec} &= \text{temperature of fluid immediately after the control valve and directly} \\
 &\quad \text{controllable by the valve.}
 \end{aligned}$$

Combining constants, we obtain

$$\dot{T}_e(t) + aT_e(t) = aT_{ec}(t - \tau_d), \quad (\text{A.14})$$

where

$$a = \dot{m}/M,$$

which, transformed, becomes

$$\frac{T_e(s)}{T_{ec}(s)} = \frac{e^{-\tau_d s}}{s/a + 1} = G_3(s). \quad (\text{A.15})$$

To form the discrete transfer function of G_3 preceded by a zero-order hold, we must compute

$$G_3(z) = \mathcal{Z} \left\{ \frac{1 - e^{-Ts}}{s} \frac{e^{-\tau_d s}}{s/a + 1} \right\}.$$

We assume that $\tau_d = lT - mT$, $0 \leq m < 1$. Then

$$\begin{aligned}
 G_3(z) &= \mathcal{Z} \left\{ \frac{1 - e^{-Ts}}{s} \frac{e^{-lTs} e^{mTs}}{s/a + 1} \right\} \\
 &= (1 - z^{-1})z^{-l} \mathcal{Z} \left\{ \frac{e^{mTs}}{s(s/a + 1)} \right\} \\
 &= (1 - z^{-1})z^{-l} \mathcal{Z} \left\{ \frac{e^{mTs}}{s} - \frac{e^{mTs}}{s + a} \right\} \\
 &= \frac{z-1}{z} \frac{1}{z^l} \mathcal{Z} \{ 1(t + mT) - e^{-a(t+mT)} 1(t + mT) \} \\
 &= \frac{z-1}{z} \frac{1}{z^l} \left\{ \frac{z}{z-1} - \frac{e^{-amT} z}{z - e^{-aT}} \right\} \\
 &= \frac{1}{z^l} \frac{(1 - e^{-amT})z + e^{-amT} - e^{-aT}}{z - e^{-aT}} \\
 &= \frac{1 - e^{-amT}}{z^l} \frac{z + \alpha}{z - e^{-aT}}; \\
 \alpha &= \frac{e^{-amT} - e^{-aT}}{1 - e^{-amT}}. \quad (\text{A.16})
 \end{aligned}$$

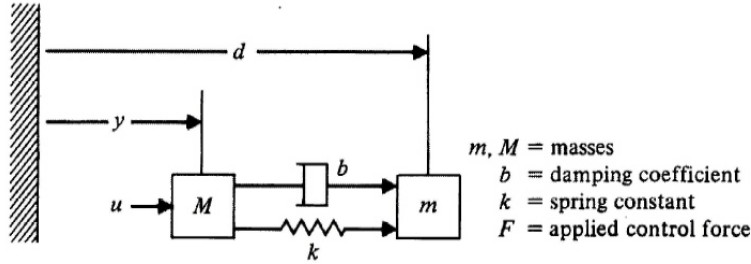


Figure A.8
Double-mass
spring system

From Eq. (A.16) it is easy to see that the zero location, $-\alpha$, varies from $\alpha = \infty$ at $m = 0$ to $\alpha = 0$ as $m \rightarrow 1$ and that $G_3(1) = 1.0$ for all a, m , and l .

For the specific values of $\tau_d = 1.5$, $T = 1$, $a = 1$, Eq. (A.16) reduces to ($l = 2$, $m = \frac{1}{2}$)

$$G_3(z) = \frac{z + 0.6065}{z^2(z - 0.3679)}.$$

A.4 Control Through a Flexible Structure

Many controlled systems have some structural flexibility in some portion of the system. The spacecraft of Fig. A.1 may not be perfectly rigid, the angle tracker of Fig. A.3 may have some flexibility between the angle observed by the antenna and the angle of the base, and almost any mechanical system such as a robot arm or a disk drive read/write head assembly would exhibit some degree of structural flexibility.

Conceptually, these systems are equivalent to the double mass–spring device shown in Fig. A.8. The equations of motion are

$$\begin{aligned} M\ddot{y} + (\dot{y} - \dot{d})b + (y - d)k &= u, \\ m\ddot{d} + (\dot{d} - \dot{y})b + (d - y)k &= 0, \end{aligned} \quad (\text{A.17})$$

which, when transformed, become,

$$\begin{bmatrix} Ms^2 + bs + k & -(bs + k) \\ -(bs + k) & ms^2 + bs + k \end{bmatrix} \begin{bmatrix} y(s) \\ d(s) \end{bmatrix} = \begin{bmatrix} 1 \\ 0 \end{bmatrix} u(s). \quad (\text{A.18})$$

Two transfer functions are of interest: one between u and d , the other between u and y . The first represents the case where there is structural flexibility between the sensor and the actuator, a situation called the noncolocated case. The second represents the colocated case where the sensor is placed on the same rigid body as the actuator, but there exists a mechanical oscillation elsewhere in the system that is coupled to the mass to which the actuator and sensor are attached.

Using Eq. (A.18) we can obtain both transfer functions

$$\frac{d(s)}{u(s)} = \frac{1}{M} \frac{\left(\frac{b}{m}s + \frac{k}{m}\right)}{s^2 \left[s^2 + \left(1 + \frac{m}{M}\right) \left(\frac{b}{m}s + \frac{k}{m}\right) \right]}, \quad (\text{A.19})$$

which becomes for the typical case with very low damping

$$\frac{d(s)}{u(s)} \cong \frac{1}{M} \frac{k/m}{s^2 \left[s^2 + \left(1 + \frac{m}{M}\right) \left(\frac{b}{m}s + \frac{k}{m}\right) \right]} = G_4(s) \quad (\text{A.20})$$

and

$$\frac{y(s)}{u(s)} = \frac{1}{M} \frac{\left(s^2 + \frac{b}{m}s + \frac{k}{m}\right)}{s^2 \left[s^2 + \left(1 + \frac{m}{M}\right) \left(\frac{b}{m}s + \frac{k}{m}\right) \right]} = G_5(s). \quad (\text{A.21})$$

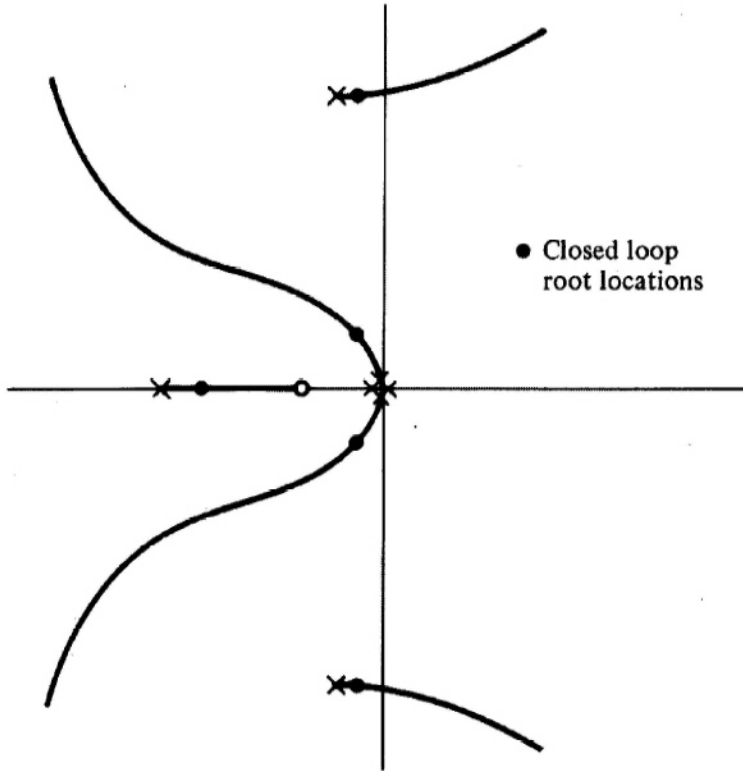


Figure A.9
 Root locus for double mass-spring system with flexibility between sensor and actuator. The noncollocated case

For $m/M \ll 1$, Eq. (A.21) indicates that the system dynamics are essentially $1/s^2$, but there are poles and zeros at the structural bending-mode frequency that almost cancel each other. A small value of m/M in this simplified example represents the fact that the flexibility is not a dominant response to the control input u and $1/s^2$ is a good model for many such problems.

Equation (A.20) always has the $1/s^2$ (“rigid-body”) poles plus the resonance poles without the neighboring zeros of Eq. (A.21). The noncollocated case is the harder one to control for if a lead compensation is used to stabilize Eq. (A.20), the structural mode is destabilized, as shown in the root locus of Fig. A.9, and depending on the feedback gain and original structural damping, the structural mode could well be driven unstable.

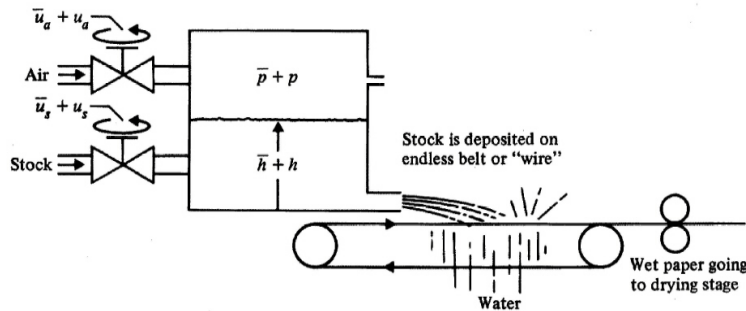


Figure A.10
 Pressurized flow box

A.5 Control of a Pressurized Flow Box

This example is multivariable because it has two control variables and two measurable states. The basic function of the system is to keep the paper-stock flow out the bottom opening (slice) (Fig. A.10) at a consistent rate. The differential equations of motion are¹

$$\begin{bmatrix} \dot{H} \\ \dot{h} \\ \dot{u}_a \end{bmatrix} = \begin{bmatrix} -0.2 & +0.1 & +1 \\ -0.05 & 0 & 0 \\ 0 & 0 & -1 \end{bmatrix} \begin{bmatrix} H \\ h \\ u_a \end{bmatrix} + \begin{bmatrix} 0 & 1 \\ 0 & 0.7 \\ 1 & 0 \end{bmatrix} \begin{bmatrix} u_c \\ u_s \end{bmatrix}, \quad (\text{A.22})$$

where

$H = h + p/\rho_s g =$ total head perturbation,

$p =$ air pressure,

$\bar{p} =$ mean air pressure,

$h =$ stock-level perturbation,

$u_a =$ perturbation in air-valve opening,

$u_c =$ command value to air valve, and

$u_s =$ perturbation in stock-valve opening.

Note from Eq. (A.22) that there is two-way coupling between the two outputs, H and h , and that u_s affects both states; therefore, it is difficult to decouple the system so as to influence either H or h alone with a single control. The third equation in Eq. (A.22) represents dynamics of the air-valve actuator, which is such that u_a does not respond instantaneously to an air command u_c . The transfer functions between u_c and u_s and H and h are

$$G_6(s) = \frac{1}{\Delta(s)} \begin{bmatrix} s & (s+1)(s+0.07) \\ -0.05 & 0.7(s+1)(s+0.13) \end{bmatrix}$$

where $\Delta(s) = (s+1)(s+0.1707)(s+0.02929)$.

¹These numbers are mainly contrived and might not correspond to any real head box, alive or dead.

Appendix B

Tables

B.1 Properties of z -Transforms

Let $\mathcal{F}_i(s)$ be the Laplace transform of $f_i(t)$ and $F_i(z)$ be the z -transform of $f_i(kT)$

Number	Laplace Transform	Samples	z -Transform	Comment
—	$\mathcal{F}_i(s)$	$f_i(kT)$	$F_i(z)$	
1	$\alpha\mathcal{F}_1(s) + \beta\mathcal{F}_2(s)$	$\alpha f_1(kT) + \beta f_2(kT)$	$\alpha F_1(z) + \beta F_2(z)$	The z -transform is linear
2	$\mathcal{F}_1(e^{Ts})\mathcal{F}_2(s)$	$\sum_{\ell=-\infty}^{\infty} f_1(\ell T)f_2(kT - \ell T)$	$F_1(z)F_2(z)$	Discrete convolution corresponds to product of z -transforms
3	$e^{+nTs}\mathcal{F}(s)$	$f(kT + nT)$	$z^n F(z)$	Shift in time
4	$\mathcal{F}(s + a)$	$e^{-akT} f(kT)$	$F(e^{aT}z)$	Shift in frequency
5	—	$\lim_{k \rightarrow \infty} f(kT)$	$\lim_{z \rightarrow 1} (z - 1)F(z)$	If all poles of $(z - 1)F(z)$ are inside the unit circle and $F(z)$ converges for $1 \leq z $
6	$\mathcal{F}(s/\omega_n)$	$f(\omega_n kT)$	$F(z; \omega_n T)$	Time and frequency scaling
7	—	$f_1(kT)f_2(kT)$	$\frac{1}{2\pi j} \oint_{c_3} F_1(\zeta)F_2(z/\zeta) \frac{d\zeta}{\zeta}$	Time product
8	$\mathcal{F}_3(s) = \mathcal{F}_1(s)\mathcal{F}_2(s)$	$\int_{-\infty}^{\infty} f_1(\tau)f_2(kT - \tau)d\tau$	$F_3(z)$	Continuous convolution does <i>not</i> correspond to product of z -transforms

B.2 Table of z -Transforms

$\mathcal{F}(s)$ is the Laplace transform of $f(t)$ and $F(z)$ is the z -transform of $f(kT)$. Unless otherwise noted, $f(t) = 0, t < 0$ and the region of convergence of $F(z)$ is outside a circle $r < |z|$ such that all poles of $F(z)$ are inside r .

Number	$\mathcal{F}(s)$	$f(kT)$	$F(z)$
1	—	$1, k = 0; 0, k \neq 0$	1
2	—	$1, k = m; 0, k \neq m$	z^{-m}
3	$\frac{1}{s}$	$1(kT)$	$\frac{z}{z-1}$
4	$\frac{1}{s^2}$	kT	$\frac{Tz}{(z-1)^2}$
5	$\frac{1}{s^3}$	$\frac{1}{2!}(kT)^2$	$\frac{T^2}{2} \frac{z(z+1)}{(z-1)^3}$
6	$\frac{1}{s^4}$	$\frac{1}{3!}(kT)^3$	$\frac{T^3}{6} \frac{z(z^2+4z+1)}{(z-1)^4}$
7	$\frac{1}{s^m}$	$\lim_{a \rightarrow 0} \frac{(-1)^{m-1}}{(m-1)!} \frac{\partial^{m-1}}{\partial a^{m-1}} e^{-akT}$	$\lim_{a \rightarrow 0} \frac{(-1)^{m-1}}{(m-1)!} \frac{\partial^{m-1}}{\partial a^{m-1}} \frac{z}{z - e^{-aT}}$
8	$\frac{1}{s+a}$	e^{-akT}	$\frac{z}{z - e^{-aT}}$
9	$\frac{1}{(s+a)^2}$	$kT e^{-akT}$	$\frac{Tz e^{-aT}}{(z - e^{-aT})^2}$
10	$\frac{1}{(s+a)^3}$	$\frac{1}{2} (kT)^2 e^{-akT}$	$\frac{T^2}{2} e^{-aT} \frac{z(z + e^{-aT})}{(z - e^{-aT})^3}$
11	$\frac{1}{(s+a)^m}$	$\frac{(-1)^{m-1}}{(m-1)!} \frac{\partial^{m-1}}{\partial a^{m-1}} (e^{-akT})$	$\frac{(-1)^{m-1}}{(m-1)!} \frac{\partial^{m-1}}{\partial a^{m-1}} \frac{z}{z - e^{-aT}}$
12	$\frac{a}{s(s+a)}$	$1 - e^{-akT}$	$\frac{z(1 - e^{-aT})}{(z-1)(z - e^{-aT})}$

(continues on next page)

Number	$\mathcal{F}(s)$	$f(kT)$	$F(z)$
13	$\frac{a}{s^2(s+a)}$	$\frac{1}{a}(akT - 1 + e^{-akT})$	$\frac{z[(aT - 1 + e^{-aT})z + (1 - e^{-aT} - aTe^{-aT})]}{a(z-1)^2(z - e^{-aT})}$
14	$\frac{b-a}{(s+a)(s+b)}$	$(e^{-akT} - e^{-bkT})$	$\frac{(e^{-aT} - e^{-bT})z}{(z - e^{-aT})(z - e^{-bT})}$
15	$\frac{s}{(s+a)^2}$	$(1 - akT)e^{-akT}$	$\frac{z[z - e^{-aT}(1 + aT)]}{(z - e^{-aT})^2}$
16	$\frac{a^2}{s(s+a)^2}$	$1 - e^{-akT}(1 + akT)$	$\frac{z[z(1 - e^{-aT} - aTe^{-aT}) + e^{-2aT} - e^{-aT} + aTe^{-aT}]}{(z-1)(z - e^{-aT})^2}$
17	$\frac{(b-a)s}{(s+a)(s+b)}$	$be^{-bkT} - ae^{-akT}$	$\frac{z[z(b-a) - (be^{-aT} - ae^{-bT})]}{(z - e^{-aT})(z - e^{-bT})}$
18	$\frac{a}{s^2 + a^2}$	$\sin akT$	$\frac{z \sin aT}{z^2 - (2 \cos aT)z + 1}$
19	$\frac{s}{s^2 + a^2}$	$\cos akT$	$\frac{z(z - \cos aT)}{z^2 - (2 \cos aT)z + 1}$
20	$\frac{s+a}{(s+a)^2 + b^2}$	$e^{-akT} \cos bkT$	$\frac{z(z - e^{-aT} \cos bT)}{z^2 - 2e^{-aT}(\cos bT)z + e^{-2aT}}$
21	$\frac{b}{(s+a)^2 + b^2}$	$e^{-akT} \sin bkT$	$\frac{ze^{-aT} \sin bT}{z^2 - 2e^{-aT}(\cos bT)z + e^{-2aT}}$
22	$\frac{a^2 + b^2}{s((s+a)^2 + b^2)}$	$1 - e^{-akT} \left(\cos bkT + \frac{a}{b} \sin bkT \right)$	$\frac{z(Az + B)}{(z-1)(z^2 - 2e^{-aT}(\cos bT)z + e^{-2aT})}$ $A = 1 - e^{-aT} \cos bT - \frac{a}{b} e^{-aT} \sin bT$ $B = e^{-2aT} + \frac{a}{b} e^{-aT} \sin bT - e^{-aT} \cos bT$

Appendix C

A Few Results from Matrix Analysis

Although we assume the reader has some acquaintance with linear equations and determinants, there are a few results of a more advanced character that even elementary control-system theory requires, and these are collected here for reference in the text. For further study, a good choice is Strang (1976).

C.1 Determinants and the Matrix Inverse

The determinant of a product of two square matrices is the product of their determinants

$$\det(\mathbf{AB}) = \det \mathbf{A} \det \mathbf{B}. \quad (\text{C.1})$$

If a matrix is diagonal, then the determinant is the product of the elements on the diagonal.

If the matrix is partitioned with square elements on the main diagonal, then an extension of this result applies, namely,

$$\det \begin{bmatrix} \mathbf{A} & \mathbf{0} \\ \mathbf{B} & \mathbf{C} \end{bmatrix} = \det \mathbf{A} \det \mathbf{C}, \quad \text{if } \mathbf{A} \text{ and } \mathbf{C} \text{ are square submatrices.} \quad (\text{C.2})$$

Suppose \mathbf{A} is a matrix of dimensions $m \times n$ and \mathbf{B} is of dimension $n \times m$. Let \mathbf{I}_m and \mathbf{I}_n be the identity matrices of size $m \times m$ and $n \times n$, respectively. Then

$$\det[\mathbf{I}_n + \mathbf{BA}] = \det[\mathbf{I}_m + \mathbf{AB}]. \quad (\text{C.3})$$

To show this result, we consider the determinant of the matrix product

$$\det \begin{bmatrix} \mathbf{I}_m & \mathbf{0} \\ \mathbf{B} & \mathbf{I}_n \end{bmatrix} \begin{bmatrix} \mathbf{I}_m & \mathbf{A} \\ -\mathbf{B} & \mathbf{I}_n \end{bmatrix} = \det \begin{bmatrix} \mathbf{I}_m & \mathbf{A} \\ \mathbf{0} & \mathbf{I}_n + \mathbf{BA} \end{bmatrix} = \det[\mathbf{I}_n + \mathbf{BA}].$$

But this is also equal to

$$\det \begin{bmatrix} \mathbf{I}_m & -\mathbf{A} \\ \mathbf{0} & \mathbf{I}_n \end{bmatrix} \begin{bmatrix} \mathbf{I}_m & \mathbf{A} \\ -\mathbf{B} & \mathbf{I}_n \end{bmatrix} = \det \begin{bmatrix} \mathbf{I}_m + \mathbf{AB} & \mathbf{0} \\ -\mathbf{B} & \mathbf{I}_n \end{bmatrix} = \det[\mathbf{I}_m + \mathbf{AB}],$$

and therefore these two determinants are equal to each other, which is Eq. (C.3).

If the determinant of a matrix \mathbf{A} is not zero, then we can define a related matrix \mathbf{A}^{-1} , called “ \mathbf{A} inverse,” which has the property that

$$\mathbf{AA}^{-1} = \mathbf{A}^{-1}\mathbf{A} = \mathbf{I}. \quad (\text{C.4})$$

According to property Eq. (C.1) we have

$$\det \mathbf{AA}^{-1} = \det \mathbf{A} \cdot \det \mathbf{A}^{-1} = 1,$$

or

$$\det \mathbf{A}^{-1} = \frac{1}{\det \mathbf{A}}.$$

It can be shown that there is an $n \times n$ matrix called the **adjugate** of \mathbf{A} with elements composed of sums of products of the elements of \mathbf{A}^{-1} and having the property that

$$\mathbf{A} \cdot \text{adj } \mathbf{A} = \det \mathbf{A} \cdot \mathbf{I}. \quad (\text{C.5})$$

Thus, if the determinant of \mathbf{A} is not zero, the inverse of \mathbf{A} is given by

$$\mathbf{A}^{-1} = \frac{\text{adj } \mathbf{A}}{\det \mathbf{A}}.$$

A famous and useful formula for the inverse of a combination of matrices has come to be called the **matrix inversion lemma** in the control literature. It arises in the development of recursive algorithms for estimation, as found in Chapter 9. The formula is as follows: If $\det \mathbf{A}$, $\det \mathbf{C}$, and $\det (\mathbf{A} + \mathbf{BCD})$ are different from zero, then we have the matrix inversion lemma:

$$(\mathbf{A} + \mathbf{BCD})^{-1} = \mathbf{A}^{-1} - \mathbf{A}^{-1} \mathbf{B} (\mathbf{C}^{-1} + \mathbf{DA}^{-1} \mathbf{B})^{-1} \mathbf{DA}^{-1}. \quad (\text{C.6})$$

The truth of Eq. (C.6) is readily confirmed if we multiply both sides by $\mathbf{A} + \mathbf{BCD}$ to obtain

$$\begin{aligned} \mathbf{I} &= \mathbf{I} + \mathbf{BCDA}^{-1} - \mathbf{B} (\mathbf{C}^{-1} + \mathbf{DA}^{-1} \mathbf{B})^{-1} \mathbf{DA}^{-1} \\ &\quad - \mathbf{BCDA}^{-1} \mathbf{B} (\mathbf{C}^{-1} + \mathbf{DA}^{-1} \mathbf{B})^{-1} \mathbf{DA}^{-1} \\ &= \mathbf{I} + \mathbf{BCDA}^{-1} - [\mathbf{B} + \mathbf{BCDA}^{-1} \mathbf{B}] (\mathbf{C}^{-1} + \mathbf{DA}^{-1} \mathbf{B})^{-1} \mathbf{DA}^{-1}. \end{aligned}$$

If we subtract \mathbf{I} from both sides and factor \mathbf{BC} from the left on the third term, we find

$$\mathbf{0} = \mathbf{BCDA}^{-1} - \mathbf{BC} [\mathbf{C}^{-1} + \mathbf{DA}^{-1} \mathbf{B}] (\mathbf{C}^{-1} + \mathbf{DA}^{-1} \mathbf{B})^{-1} \mathbf{DA}^{-1},$$

which is

$$\mathbf{0} = \mathbf{0}, \quad \text{which was to be demonstrated.}$$

C.2 Eigenvalues and Eigenvectors

We consider the discrete dynamic system

$$\mathbf{x}_{k+1} = \mathbf{\Phi} \mathbf{x}_k, \quad (\text{C.7})$$

where, for purposes of illustration, we will let

$$\mathbf{\Phi} = \begin{bmatrix} \frac{5}{6} & -\frac{1}{6} \\ 1 & 0 \end{bmatrix}. \quad (\text{C.8})$$

If we assume that it is possible for this system to have a motion given by a geometric series such as z^k , we can assume that there is a vector \mathbf{v} so that \mathbf{x}_k can be written

$$\mathbf{x}_k = \mathbf{v} z^k. \quad (\text{C.9})$$

Substituting Eq. (C.9) into Eq. (C.7), we must find the vector \mathbf{v} and the number z such that

$$\mathbf{v} z^{k+1} = \mathbf{\Phi} \mathbf{v} z^k,$$

or, multiplying by z^{-k} yields

$$\mathbf{v} z = \mathbf{\Phi} \mathbf{v}. \quad (\text{C.10})$$

¹If \mathbf{A}^{ij} is the $(n-1) \times (n-1)$ matrix (minor) found by deleting row i and column j from \mathbf{A} , then the entry in row i and column j of the adj \mathbf{A} is $(-1)^{i+j} \det \mathbf{A}^{ji}$.

If we collect both the terms of Eq. (C.10) on the left, we find

$$(z\mathbf{I} - \Phi)\mathbf{v} = \mathbf{0}. \quad (\text{C.11})$$

These linear equations have a solution for a nontrivial \mathbf{v} if and only if the determinant of the coefficient matrix is zero. This determinant is a polynomial of degree n in z (Φ is an $n \times n$ matrix) called the **characteristic polynomial** of Φ , and values of z for which the characteristic polynomial is zero are roots of the characteristic equation and are called **eigenvalues** of Φ . For example, for the matrix given in Eq. (C.8) the characteristic polynomial is

$$\det \left\{ \begin{bmatrix} z & 0 \\ 0 & z \end{bmatrix} - \begin{bmatrix} \frac{5}{6} & -\frac{1}{6} \\ 1 & 0 \end{bmatrix} \right\}.$$

Adding the two matrices, we find

$$\det \left\{ \begin{bmatrix} z - \frac{5}{6} & +\frac{1}{6} \\ -1 & z \end{bmatrix} \right\},$$

which can be evaluated to give

$$z(z - \frac{5}{6}) + \frac{1}{6} = (z - \frac{1}{2})(z - \frac{1}{3}). \quad (\text{C.12})$$

Thus the characteristic roots of this Φ are $\frac{1}{2}$ and $\frac{1}{3}$. Associated with these characteristic roots are solutions to Eq. (C.11) for vectors \mathbf{v} , called the **characteristic** or **eigenvectors**. If we let $z = \frac{1}{2}$, then Eq. (C.11) requires

$$\left\{ \begin{bmatrix} \frac{1}{2} & 0 \\ 0 & \frac{1}{2} \end{bmatrix} - \begin{bmatrix} \frac{5}{6} & -\frac{1}{6} \\ 1 & 0 \end{bmatrix} \right\} \begin{bmatrix} v_{11} \\ v_{21} \end{bmatrix} = \begin{bmatrix} 0 \\ 0 \end{bmatrix}. \quad (\text{C.13})$$

Adding the matrices, we find that these equations become

$$\begin{bmatrix} -\frac{1}{3} & \frac{1}{6} \\ -1 & \frac{1}{2} \end{bmatrix} \begin{bmatrix} v_{11} \\ v_{21} \end{bmatrix} = \begin{bmatrix} 0 \\ 0 \end{bmatrix}. \quad (\text{C.14})$$

Equations (C.14) are satisfied by any v_{11} and v_{21} such that

$$v_{21} = 2v_{11},$$

from which we conclude that the eigenvector corresponding to $z_1 = 1/2$ is given by

$$\mathbf{v}_1 = \begin{bmatrix} a \\ 2a \end{bmatrix}. \quad (\text{C.15})$$

We can arbitrarily select the scale factor a in Eq. (C.15). Some prefer to make the length² of eigenvectors equal to one. Here we make the largest component of \mathbf{v} have unit magnitude. Thus the scaled \mathbf{v}_1 is

$$\mathbf{v}_1 = \begin{bmatrix} \frac{1}{2} \\ 1 \end{bmatrix}. \quad (\text{C.16})$$

In similar fashion, the eigenvector \mathbf{v}_2 associated with $z_2 = 1/3$ can be computed to be

$$\mathbf{v}_2 = \begin{bmatrix} \frac{1}{3} \\ 1 \end{bmatrix}.$$

Note that even if all elements of Φ are real, it is possible for characteristic values and characteristic vectors to be complex.

²Usually we define the length of a vector as the square root of the sum of squares of its components or, if $\|\mathbf{v}\|$ is the symbol for length, then $\|\mathbf{v}\|^2 = \mathbf{v}^T \mathbf{v}$. If \mathbf{v} is complex, as will happen if z_i is complex, then we must take a conjugate, and we define $\|\mathbf{v}\|^2 = (\mathbf{v}^*)^T \mathbf{v}$, where \mathbf{v}^* is the complex conjugate of \mathbf{v} .

C.3 Similarity Transformations

If we make a change of variables in Eq. (C.7) according to $\mathbf{x} = \mathbf{T}\mathbf{x}$, where \mathbf{T} is an $n \times n$ matrix, then we start with the equations

$$\mathbf{x}_{k+1} = \Phi \mathbf{x}_k,$$

and, substituting for \mathbf{x} , we have

$$\mathbf{T}\mathbf{x}_{k+1} = \Phi \mathbf{T}\mathbf{x}_k.$$

Then, if we multiply on the left by \mathbf{T}^{-1} , we get the equation in \mathbf{x} ,

$$\mathbf{x}_{k+1} = \mathbf{T}^{-1} \Phi \mathbf{T} \mathbf{x}_k. \quad (\text{C.17})$$

If we define the new system matrix as Ψ , then the new states satisfy the equations

$$\mathbf{x}_{k+1} = \Psi \mathbf{x}_k,$$

where

$$\Psi = \mathbf{T}^{-1} \Phi \mathbf{T}. \quad (\text{C.18})$$

If we now seek the characteristic polynomial of Ψ , we find

$$\det[z\mathbf{I} - \Psi] = \det[z\mathbf{I} - \mathbf{T}^{-1} \Phi \mathbf{T}].$$

Because $\mathbf{T}^{-1} \mathbf{T} = \mathbf{I}$, we can write this polynomial as

$$\det[z\mathbf{T}^{-1} \mathbf{T} - \mathbf{T}^{-1} \Phi \mathbf{T}],$$

and the \mathbf{T}^{-1} and \mathbf{T} can be factored out on the left and right to give

$$\det[\mathbf{T}^{-1} [z\mathbf{I} - \Phi] \mathbf{T}].$$

Now, using property Eq. (C.1) for the determinant, we compute

$$\det \mathbf{T}^{-1} \cdot \det [z\mathbf{I} - \Phi] \cdot \det \mathbf{T},$$

which, by the equation following Eq. (C.4), gives us the final result

$$\det [z\mathbf{I} - \Psi] = \det [z\mathbf{I} - \Phi]. \quad (\text{C.19})$$

From Eq. (C.19) we see that Ψ and Φ have the same characteristic polynomials. The matrices are said to be “similar,” and the transformation Eq. (C.18) is a similarity transformation.

A case of a similarity transformation of particular interest is one for which the resulting matrix Ψ is diagonal. As an attempt to find such a matrix, suppose we *assume* that Ψ is diagonal and write the transformation \mathbf{T} in terms of its columns, \mathbf{t}_i . Then Eq. (C.18) can be expressed as

$$\begin{aligned} \mathbf{T}\Psi &= \Phi \mathbf{T}, \\ [\mathbf{t}_1 \ \mathbf{t}_2 \ \dots \ \mathbf{t}_n] \Psi &= \Phi [\mathbf{t}_1 \ \mathbf{t}_2 \ \dots \ \mathbf{t}_n] \\ &= [\Phi \mathbf{t}_1 \ \Phi \mathbf{t}_2 \ \dots \ \Phi \mathbf{t}_n]. \end{aligned} \quad (\text{C.20})$$

If we *assume* that Ψ is diagonal with elements $\lambda_1, \lambda_2, \dots, \lambda_n$, then Eq. (C.20) can be written as

$$[\mathbf{t}_1 \ \mathbf{t}_2 \ \dots \ \mathbf{t}_n] \begin{bmatrix} \lambda_1 & 0 & \dots & 0 \\ 0 & \lambda_2 & \dots & 0 \\ 0 & & & \\ \cdot & & & \\ \cdot & \ddots & & \\ \cdot & & & +\lambda_n \end{bmatrix} = [\Phi \mathbf{t}_1 \ \Phi \mathbf{t}_2 \ \dots \ \Phi \mathbf{t}_n].$$

Multiplying the matrices on the left, we find

$$[\lambda_1 \mathbf{t}_1 \lambda_2 \mathbf{t}_2 \cdots \lambda_n \mathbf{t}_n] = [\Phi \mathbf{t}_1 \cdots \Phi \mathbf{t}_n]. \quad (\text{C.21})$$

Because the two sides of Eq. (C.21) are equal, they must match up column by column, and we can write the equation for column j as

$$\lambda_j \mathbf{t}_j = \Phi \mathbf{t}_j. \quad (\text{C.22})$$

Comparing Eq. (C.22) with Eq. (C.10), we see that \mathbf{t}_j is an eigenvector of Φ and λ_j is an eigenvalue. We conclude that if the transformation \mathbf{T} converts Φ into a diagonal matrix Ψ , then the columns of \mathbf{T} must be eigenvectors of Φ and the diagonal elements of Ψ are the eigenvalues of Φ [which are also the eigenvalues of Ψ , by Eq. (C.19)]. It turns out that if the eigenvalues of Φ are distinct, then there are exactly n eigenvectors and they are independent; that is, we can construct a nonsingular transformation \mathbf{T} from the n eigenvectors.

In the example given above, we would have

$$\mathbf{T} = \begin{bmatrix} \frac{1}{2} & \frac{1}{3} \\ 1 & 1 \end{bmatrix},$$

for which

$$\mathbf{T}^{-1} = \begin{bmatrix} 6 & -2 \\ -6 & 3 \end{bmatrix},$$

and the new diagonal system matrix is

$$\begin{aligned} \mathbf{T}^{-1} \Phi \mathbf{T} &= \begin{bmatrix} 6 & -2 \\ -6 & 3 \end{bmatrix} \begin{bmatrix} \frac{5}{6} & -\frac{1}{6} \\ 1 & 0 \end{bmatrix} \begin{bmatrix} \frac{1}{2} & \frac{1}{3} \\ 1 & 1 \end{bmatrix} \\ &= \begin{bmatrix} 3 & -1 \\ -2 & 1 \end{bmatrix} \begin{bmatrix} \frac{1}{2} & \frac{1}{3} \\ 1 & 1 \end{bmatrix} \\ &= \begin{bmatrix} \frac{1}{2} & 0 \\ 0 & \frac{1}{3} \end{bmatrix} \end{aligned}$$

as advertised! If the elements of Φ are real and an eigenvalue is complex, say $\lambda_1 = \alpha + j\beta$, then the conjugate, $\lambda_1^* = \alpha - j\beta$, is also an eigenvalue because the characteristic polynomial has real coefficients. In such a case, the respective eigenvectors will be conjugate. If $\mathbf{v}_1 = \mathbf{r} + j\mathbf{i}$, then $\mathbf{v}_2 = \mathbf{v}_1^* = \mathbf{r} - j\mathbf{i}$, where \mathbf{r} and \mathbf{i} are matrices of real elements representing the real and imaginary parts of the eigenvectors. In such cases, it is common practice to use the real matrices \mathbf{r} and $-\mathbf{i}$ as columns of the transformation matrix \mathbf{T} rather than go through the complex arithmetic required to deal directly with \mathbf{v}_1 and \mathbf{v}_1^* . The resulting transformed equations are not diagonal, but rather the corresponding variables appear in the coupled equations

$$\dot{\eta} = \alpha\eta - \beta v, \quad \dot{v} = \beta\eta + \alpha v. \quad (\text{C.23})$$

C.4 The Cayley-Hamilton Theorem

A very useful property of a matrix Φ follows from consideration of the inverse of $z\mathbf{I} - \Phi$. As we saw in Eq. (C.5), we can write

$$(z\mathbf{I} - \Phi) \text{adj}(z\mathbf{I} - \Phi) = \mathbf{I} \det(z\mathbf{I} - \Phi). \quad (\text{C.24})$$

The coefficient of \mathbf{I} on the right-hand side of Eq. (C.24) is the characteristic polynomial of Φ , which we can write as

$$a(z) = z^n + a_1 z^{n-1} + a_2 z^{n-2} + \cdots + a_n.$$

The adjugate of $z\mathbf{I} - \Phi$, on the other hand, is a *matrix* of polynomials in z , found from the determinants of the minors of $z\mathbf{I} - \Phi$. If we collect the constant matrix coefficients of the powers of z , it is clear that we can write

$$\text{adj}(z\mathbf{I} - \Phi) = \mathbf{B}_1 z^{n-1} + \mathbf{B}_2 z^{n-2} + \cdots + \mathbf{B}_n,$$

and Eq. (C.24) becomes a polynomial equation with matrix coefficients. Written out, it is

$$[z\mathbf{I} - \mathbf{\Phi}][\mathbf{B}_1 z^{n-1} + \mathbf{B}_2 z^{n-2} + \cdots + \mathbf{B}_n] = z^n \mathbf{I} + a_1 z^{n-1} \mathbf{I} + \cdots + a_n \mathbf{I}. \quad (\text{C.25})$$

If we now multiply the two matrices on the left and equate coefficients of equal powers of z , we find

$$\begin{aligned} \mathbf{B}_1 &= \mathbf{I}, \\ \mathbf{B}_2 &= \mathbf{\Phi}\mathbf{B}_1 + a_1 \mathbf{I} = \mathbf{\Phi} + a_1 \mathbf{I}, \\ \mathbf{B}_3 &= \mathbf{\Phi}\mathbf{B}_2 + a_2 \mathbf{I} = \mathbf{\Phi}^2 + a_1 \mathbf{\Phi} + a_2 \mathbf{I}, \\ &\vdots \\ \mathbf{B}_n &= \mathbf{\Phi}\mathbf{B}_{n-1} + a_{n-1} \mathbf{I} = \mathbf{\Phi}^{n-1} + a_1 \mathbf{\Phi}^{n-2} + \cdots + a_{n-1} \mathbf{I}, \\ 0 &= \mathbf{\Phi}\mathbf{B}_n + a_n \mathbf{I} = \mathbf{\Phi}^n + a_1 \mathbf{\Phi}^{n-1} + a_2 \mathbf{\Phi}^{n-1} + \cdots + a_n \mathbf{I}. \end{aligned} \quad (\text{C.26})$$

Equation (C.26) is a statement that the matrix obtained when matrix $\mathbf{\Phi}$ is substituted for z in the characteristic polynomial, $a(z)$, is exactly zero! In other words, we have the Cayley-Hamilton theorem according to which

$$a(\mathbf{\Phi}) = 0. \quad (\text{C.27})$$

Appendix D

Summary of Facts from the Theory of Probability and Stochastic Processes

D.1 Random Variables

We begin with a space of experiments, Ω , whose outcomes are called ω and depend on chance. Over the space Ω and its subsets Ω_i we define a probability function P ,¹ which assigns a positive number between 0 and 1 to each countable combination of subsets in Ω to which an outcome (or “event”) can belong. P has the properties that the probability of *some* outcome is certain, in which case it is assigned the value 1

$$P(\Omega) = 1,$$

and the probability of an outcome that may result from events Ω_i, Ω_j , which have no common points (the intersection of Ω_i and Ω_j is empty) is the sum of the probabilities of Ω_i and Ω_j

$$P\{\Omega_i \cup \Omega_j\} = P(\Omega_i) + P(\Omega_j).$$

In addition to the function P we define a **random variable** $x(\omega)$, which maps Ω into the real line such that to each outcome ω in Ω we associate a value x , and the probability that a chance experiment maps into a value x that is less than or equal to the constant a is²

$$\Pr(x \leq a) = F_x(a). \quad (\text{D.1})$$

The function $F_x(\xi)$ is called the **distribution function** of the random variable. If F_x is a smooth function,³ we define its derivative $f_x(\xi)$ as the **density function**, which has the property

$$\Pr\{a \leq x \leq b\} = \int_a^b f_x(\xi) d\xi. \quad (\text{D.2})$$

Because the whole space Ω maps into the line somewhere, we have

$$\int_{-\infty}^{\infty} f_x(\xi) d\xi = 1. \quad (\text{D.3})$$

Two common density functions that we shall have reason to use are the **uniform density** and the **normal** or **Gaussian density**. A random variable having a uniform density has zero probability of having any value outside a finite range between lower limit ℓ and upper limit u , $\ell \leq x \leq u$, and f_x is constant inside this range. Because of Eq. (D.3), the constant is $1/(u - \ell)$. A sketch of the uniform density is given in Fig. D.1.

¹See Parzen (1962).

² $\Pr\{\cdot\}$ is meant to be read “the probability that $\{\cdot\}$.”

³Using the impulse, we can include simple discontinuities, as must be done if a specific value of x has nonzero probability.

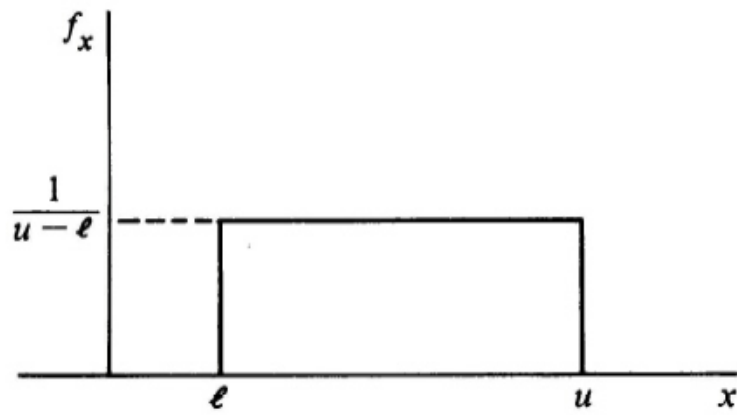


Figure D.1
Sketch of the uniform density function

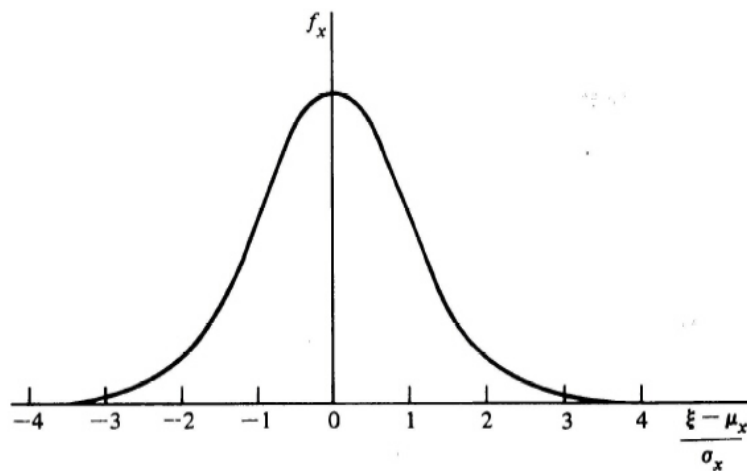


Figure D.2
Sketch of the normal density function

The normal density function is given by the equation

$$f_x(\xi) = \frac{1}{\sqrt{2\pi}\sigma_x} \exp\left(-\frac{1}{2} \frac{(\xi - \mu_x)^2}{\sigma_x^2}\right) \quad (\text{D.4})$$

and shown in the sketch in Fig. D.2.

The importance of the normal density derives mainly from the following facts:

1. The distribution of a random variable based on events which themselves consist of a sum of a large number of independent⁴ random events is accurately approximated by the normal law. Such a distribution describes electrical noise caused by thermal motions of a large number of particles as in a resistor, for example.
2. If two random variables have (jointly) normal distributions, then their sum also has a normal distribution. (As an extension of this second point, if the input to a linear system is normal, then the distribution of its output is also normal.)

D.2 Expectation

By the very nature of variables whose values are dependent on chance, we cannot discuss a formula for the calculation of values of x . To describe a random variable, we instead discuss average values such as the arithmetic mean or the average power. Such concepts are contained in the idea of **expectation**. The expected value of a function g of a random variable whose density is f_x is defined as

$$\begin{aligned} \mathcal{E}\{g(x)\} &= \int_{-\infty}^{\infty} g(\xi) f_x(\xi) d\xi \\ &= \overline{g(x)}. \end{aligned} \quad (\text{D.5})$$

Important special cases are the mean, variance, and mean square. If $g(x) = x$, then we have the mean, namely

$$\mathcal{E}(x) = \int_{-\infty}^{\infty} \xi f_x(\xi) d\xi = \bar{x} = \mu_x. \quad (\text{D.6})$$

For the uniform distribution, the mean is given by

$$\begin{aligned} \bar{x} &= \int_{-\infty}^{\infty} \xi f_x(\xi) d\xi \\ &= \int_{\ell}^u \left[\frac{1}{u-\ell} \right] d\xi = \frac{1}{u-\ell} \left[\frac{\xi^2}{2} \Big|_{\ell}^u \right] \\ &= \frac{1}{u-\ell} \left[\frac{u^2}{2} - \frac{\ell^2}{2} \right] = \frac{u+\ell}{2}. \end{aligned} \quad (\text{D.7})$$

Because the probability density function has the intuitive properties of a histogram of relative frequency of occurrence of a particular x , we see that the mean, like an arithmetic mean, is a weighted average of the random variable values.

If $g(x)$ in Eq. (D.5) is $g = (x - \bar{x})^2$, then the expected value is the average of the square of the variation of the variable from the mean; this number is called the **variance** of x , written $\text{var } x$. For

⁴The technical definition of “independent” will be given shortly.

the uniform density we compute

$$\begin{aligned}
 \mathcal{E}(x - \bar{x})^2 &= \text{var } x \\
 &= \int_{-\infty}^{\infty} (\xi - \bar{x})^2 f_x(\xi) d\xi \\
 &= \int_{\ell}^u (\xi - \bar{x})^2 \frac{1}{u - \ell} d\xi \\
 &= \frac{1}{u - \ell} \left[\frac{(\xi - \bar{x})^3}{3} \Big|_{\ell}^u \right] \\
 &= \frac{1}{u - \ell} \left\{ \frac{(u - \bar{x})^3}{3} - \frac{(\ell - \bar{x})^3}{3} \right\}.
 \end{aligned}$$

Substituting Eq. (D.7) for \bar{x} , we find

$$\mathcal{E}(x - \bar{x})^2 = \frac{1}{3(u - \ell)} \left\{ \left(\frac{u - \ell}{2} \right)^3 - \left(\frac{\ell - u}{2} \right)^3 \right\},$$

and, simplifying, we get

$$\text{var } x = \frac{(u - \ell)^2}{12}. \quad (\text{D.8})$$

The square root of the variance is called the **standard deviation** and given the symbol σ . Thus, for the uniform density

$$\sigma_x^2 = \frac{(u - \ell)^2}{12}. \quad (\text{D.9})$$

If we let $g(x)$ be simply x^2 , then we compute by Eq. (D.5) the mean-square value $\overline{x^2}$. However, consider an expanded expression for the variance, and let the mean value of x be μ

$$\begin{aligned}
 \text{var } x &= \int_{-\infty}^{\infty} (\xi - \mu)^2 f_x(\xi) d\xi \\
 &= \int_{-\infty}^{\infty} (\xi^2 - 2\xi\mu + \mu^2) f_x(\xi) d\xi \\
 &= \overline{x^2} - 2\mu^2 + \mu^2 \\
 &= \overline{x^2} - \mu^2.
 \end{aligned}$$

Thus we find

$$\overline{x^2} = \text{var } x + \mu^2.$$

For the uniform density, the mean-square value is, therefore

$$\overline{x^2} = \frac{(u - \ell)^2}{12} + \left(\frac{u + \ell}{2} \right)^2.$$

The integration is more complicated in the case of the normal density, but the definitions are the same; namely, if x has the normal density given by Eq. (D.4), then

$$\bar{x} = \int_{-\infty}^{\infty} \xi f_x(\xi) d\xi = \mu_x \quad (\text{D.10a})$$

and

$$\begin{aligned}
 \mathcal{E}(x - \mu_x)^2 &= \int_{-\infty}^{\infty} (\xi - \mu_x)^2 f_x(\xi) d\xi \\
 \text{var } x &= \sigma_x^2. \quad (\text{D.10b})
 \end{aligned}$$

Note that the mean and standard deviation already appear as parameters of the density given by Eq. (D.4). Because these two parameters completely describe the normal density, it is standard to say that a random variable with normal density having mean μ and standard deviation σ is distributed according to the $N(\mu, \sigma)$ law.

D.3 More Than One Random Variable

Frequently the random experiment has an outcome that is mapped into several random variables, say x_1, x_2, \dots, x_n or, organized as a column matrix

$$\mathbf{x} = (x_1 x_2 \dots x_n)^T.$$

For this collection we define the probability that

$$x_1 \leq a_1, x_2 \leq a_2, \dots, x_n \leq a_n$$

as

$$\Pr\{\mathbf{x} \leq \mathbf{a}\}$$

and let this be the distribution $F_{\mathbf{x}}(\xi)$ with vector argument. The corresponding density $f_{\mathbf{x}}(\xi)$ is a function such that the probability that \mathbf{x} is in a box with sides a_i and b_i is given by

$$\Pr\{\mathbf{a} < \mathbf{x} \leq \mathbf{b}\} = \int_{a_1}^{b_1} \dots \int_{a_n}^{b_n} f_{\mathbf{x}}(\xi_1, \dots, \xi_n) d\xi_1 \dots d\xi_n. \quad (\text{D.11})$$

The mean of the vector is a vector of the means

$$\mathcal{E}\{\mathbf{x}\} = \boldsymbol{\mu}_{\mathbf{x}} = (\mu_{x_1} \mu_{x_2} \dots \mu_{x_n})^T, \quad (\text{D.12})$$

and likewise the deviation of the random variables from the mean-value vector is measured by a matrix of terms called the **covariance matrix**, $\text{cov } \mathbf{x}$, defined as

$$\text{cov } \mathbf{x} = \mathcal{E}\{(\mathbf{x} - \boldsymbol{\mu}_{\mathbf{x}})(\mathbf{x} - \boldsymbol{\mu}_{\mathbf{x}})^T\} = \mathbf{R}_{\mathbf{xx}}. \quad (\text{D.13})$$

Thus $\text{cov } \mathbf{x}$ is a matrix with the element in row i and column j given by

$$\mathcal{E}\{(x_i - \mu_{x_i})(x_j - \mu_{x_j})\}.$$

Often the symbol $\mathbf{R}_{\mathbf{x}}$ will be used for the covariance matrix of a random vector \mathbf{x} . In an obvious way we can extend Eq. (D.13) to include the case of different random vectors \mathbf{x} and \mathbf{y} with mean vectors $\boldsymbol{\mu}_{\mathbf{x}}$ and $\boldsymbol{\mu}_{\mathbf{y}}$. We define the covariance of \mathbf{x} and \mathbf{y} as

$$\text{cov}(\mathbf{x}, \mathbf{y}) = \mathcal{E}\{(\mathbf{x} - \boldsymbol{\mu}_{\mathbf{x}})(\mathbf{y} - \boldsymbol{\mu}_{\mathbf{y}})^T\} = \mathbf{R}_{\mathbf{xy}}. \quad (\text{D.14})$$

Consider now the special case of two random variables x and y having distribution $F_{x,y}(\xi, \eta)$ and (joint) density $f_{x,y}(\xi, \eta)$. Because the probability that y has any value is the integral from $-\infty$ to $+\infty$ over η , the density of x is given by

$$f_x(\xi) = \int_{-\infty}^{\infty} f_{x,y}(\xi, \eta) d\eta. \quad (\text{D.15})$$

If $f_{x,y}$ is such that

$$f_{x,y}(\xi, \eta) = f_x(\xi) f_y(\eta), \quad (\text{D.16})$$

we say that x and y are **independent**.

It often happens that we know a particular value of one random variable, such as the output y of a dynamic system, and we wish to estimate the value of a related variable, such as the state x . A useful function for this situation is the **conditional density**, defined as the density of x given that the value of y is η and is defined as

$$f_{x|y}(\xi | \eta) = \frac{f_{x,y}(\xi, \eta)}{f_y(\eta)}. \quad (\text{D.17})$$

Note that, from Eqs. (D.15) and (D.16), if x and y are independent, then

$$f_{x|y}(\xi | \eta) = f_x(\xi). \quad (\text{D.18})$$

The most important multivariable probability density is the normal or Gaussian law given by

$$f_{\mathbf{x}}(\boldsymbol{\xi}) = [(2\pi)^n |\mathbf{R}_{\mathbf{x}}|]^{-1/2} \exp\left[-\frac{1}{2}(\mathbf{x}i - \boldsymbol{\mu}_{\mathbf{x}})^T \mathbf{R}_{\mathbf{x}}^{-1}(\mathbf{x}i - \boldsymbol{\mu}_{\mathbf{x}})\right], \quad (\text{D.19})$$

where $|\mathbf{R}_{\mathbf{x}}|$ is the determinant of the matrix $\mathbf{R}_{\mathbf{x}}$.

For the multivariable normal law, we can compute the mean

$$\mathcal{E}\{\mathbf{x}\} = \boldsymbol{\mu}_{\mathbf{x}},$$

and the covariance matrix

$$\mathcal{E}\{(\mathbf{x} - \boldsymbol{\mu}_{\mathbf{x}})(\mathbf{x} - \boldsymbol{\mu}_{\mathbf{x}})^T\} = \mathbf{R}_{\mathbf{x}}.$$

Like the scalar normal density, the multivariable law is described entirely by the two parameters $\boldsymbol{\mu}$ and \mathbf{R} , the difference being that the multivariable case is described by matrix parameters rather than scalar parameters. In Eq. (D.19) we require the inverse of $\mathbf{R}_{\mathbf{x}}$ and have thus implicitly assumed that this covariance matrix is nonsingular. [See Parzen (1962) for a discussion of the case when $\mathbf{R}_{\mathbf{x}}$ is singular.]

D.4 Stochastic Processes

In a study of dynamic systems, it is natural to have random variables that evolve in time much as the states and control inputs evolve. However, with random time variables it is not possible to compute z -transforms in the usual way; and furthermore, because specific values of the variables have little value, we need formulas to describe how the means and covariances evolve in time. A random variable that evolves in time is called a **stochastic process**, and here we consider only discrete time.

Suppose we deal first with a stochastic process $w(k)$, where w is a scalar distributed according to the density $f_w(N)$. Note that the density function depends on the time of occurrence of the random variable. If a variable has statistical properties (such as f_w) that are independent of the origin of time, then we say the process is **stationary**. Considering values of the process at distinct times, we have separate random variables, and we define the covariance of the process w as

$$R_w(j, k) = \mathcal{E}(w(j) - \bar{w}(j))(w(k) - \bar{w}(k)). \quad (\text{D.20})$$

If the process is stationary, then the covariance in Eq. (D.20) depends only on the magnitude of the difference in observation times, $k - j$, and we often will write $R_w(j, k) = R_w(k - j)$ and drop the second argument. Because a stochastic process is both random and time dependent, we can imagine averages that are computed over the time variable as well as the averages defined in Section D.2. For example, for a stationary process $w(n)$ we can define the mean as

$$\tilde{w}(k) = \lim_{N \rightarrow \infty} \frac{1}{2N+1} \sum_{n=-N}^N w(n+k), \quad (\text{D.21})$$

and the second-order mean or autocorrelation

$$\begin{aligned} & \mathcal{E}\{(w(j) - \tilde{w})(w(k) - \tilde{w}(k))\} = \\ & \lim_{N \rightarrow \infty} \frac{1}{2N+1} \sum_{n=-N}^N \{(w(n+j) - \tilde{w}(j))(w(n+k) - \tilde{w}(k))\}. \end{aligned} \quad (\text{D.22})$$

For a stationary process, the time average in Eq. (D.21) is usually equal to the distribution average, and likewise the second-order average in Eq. (D.22) is the same as the covariance in Eq. (D.20). Processes for which time averages give the same limits as distribution averages are called **ergodic**.

A very useful aid to understanding the properties of stationary stochastic processes is found by considering the response of a linear stationary system to a stationary input process. Suppose we let the input be w , a stationary scalar process with zero mean and covariance $R_w(j)$, and suppose we

take the output to be $y(k)$. We let the unit-pulse response from w to y be $h(j)$. Thus from standard analysis (see Chapter 4), we have

$$y(j) = \sum_{k=-\infty}^{\infty} h(k)w(j-k), \quad (\text{D.23})$$

and the covariance of $y(j)$ with $y(j+\ell)$ is

$$\begin{aligned} R_y(\ell) &= \mathcal{E}y(j+\ell)y(j) \\ &= \mathcal{E} \left\{ \sum_{k=-\infty}^{\infty} h(k)w(j+\ell-k) \right\} \left\{ \sum_{n=-\infty}^{\infty} h(n)w(j-n) \right\}. \end{aligned} \quad (\text{D.24})$$

Because the system unit-pulse response, $h(k)$, is not random, both $h(k)$ and $h(n)$ can be removed from the integral implied by the \mathcal{E} operation, with the result

$$R_y(\ell) = \sum_{k=-\infty}^{\infty} h(k) \sum_{n=-\infty}^{\infty} h(n) \mathcal{E}\{w(j+\ell-k)w(j-n)\}. \quad (\text{D.25})$$

The expectation in Eq. (D.25) is now recognized as $R_w(\ell-k+n)$, and substituting this expression in Eq. (D.25), we find

$$R_y(\ell) = \sum_{k=-\infty}^{\infty} h(k) \sum_{n=-\infty}^{\infty} h(n) R_w(\ell-k+n). \quad (\text{D.26})$$

Equation (D.26) is not especially enlightening, but the z -transform of it is. We proceed with several simple steps as follows

$$\begin{aligned} z\{R_y(\ell)\} &= \sum_{\ell=-\infty}^{\infty} R_y(\ell)z^{-\ell} \\ &= \sum_{\ell=-\infty}^{\infty} \sum_{k=-\infty}^{\infty} h(k) \sum_{n=-\infty}^{\infty} h(n) R_w(\ell-k+n) z^{-\ell}. \end{aligned}$$

Exchanging the order, because $h(k)$ and $h(n)$ do not depend on ℓ , we have

$$z\{R_y(\ell)\} = \sum_{k=-\infty}^{\infty} h(k) \sum_{n=-\infty}^{\infty} h(n) \sum_{\ell=-\infty}^{\infty} R_w(\ell-k+n) z^{-\ell}.$$

Now we let $m = \ell - k + n$ in the last sum, leading to

$$z\{R_y(\ell)\} = \sum_{k=-\infty}^{\infty} h(k) \sum_{n=-\infty}^{\infty} h(n) \sum_{m=-\infty}^{\infty} R_w(m) z^{-(m+k-n)}.$$

Finally we use the fact that $z^{-(m+k-n)} = z^{-m}z^{-k}z^n$ and distribute these terms to the corresponding sums with the result

$$\begin{aligned} z\{R_y(\ell)\} &= \sum_{k=-\infty}^{\infty} h(k)z^{-k} \sum_{n=-\infty}^{\infty} h(n)z^n \sum_{m=-\infty}^{\infty} R_w(m)z^{-m} \\ &= S_y(z). \end{aligned} \quad (\text{D.27})$$

For reasons soon to be clear, we call the z -transform of R_y the **spectrum of y** and use the symbol $S_y(z)$, and similarly for w and S_w . With these symbols and recognition that the z -transform of the unit-pulse response is the system-transfer function, $H(z)$, Eq. (D.27) becomes

$$S_y(z) = H(z)H(z^{-1})S_w(z). \quad (\text{D.28})$$

To give an interpretation of Eq. (D.28) we make two observations. First note that $R_y(0) = \mathcal{E}(y^2)$ is the mean-square value or power in the y -process. By the inverse transform integral, we have

$$\begin{aligned}\overline{y^2} &= R_y(0) \\ &= \frac{1}{2\pi j} \oint S_y(z) \frac{dz}{z} \\ &= \frac{1}{2\pi j} \oint H(z)H(z^{-1})S_w(z) \frac{dz}{z}.\end{aligned}\quad (\text{D.29})$$

Now, as a second step, we suppose that $H(z)$ is the transfer function of a very narrow bandpass filter centered at ω_0 , so that $H(z)H(z^{-1})$ is $|H(e^{j\omega_0 T})|^2$ and is nearly zero except at ω_0 . Then the integral in Eq. (D.29) can be approximated by assuming that $S_w(z)$ is nearly constant at the value $S_w(e^{j\omega_0 T})$, where $|H|^2$ is nonzero and can thus be removed from the integral. The result is

$$\begin{aligned}\overline{y^2} &= S_w(e^{j\omega_0 T}) \frac{1}{2\pi j} \oint H(z)H(z^{-1}) \frac{dz}{z} \\ &= S_w(e^{j\omega_0 T})K.\end{aligned}\quad (\text{D.30})$$

In Eq. (D.30) we have defined the integral as a constant dependent on the exact area of the narrow-band characteristic of $H(z)$. But now we can give good intuitive meaning to Eq. (D.30). The mean square of the output of a very-narrow-band filter is proportional to the S_w . If S_w is constant for all z , we say the process is white (after the spectrum of white light, which has equal intensity at all frequencies). Hence we call S_w the **power spectral density** of the w -process. Equation (D.28) is the fundamental formula for transform analysis of linear constant systems with stochastic inputs.

An alternative to transform analysis and Eq. (D.28) is transient analysis via the state-variable formulation, described in Section 4.3.3. In this case, we take the system equations to be

$$\begin{aligned}\mathbf{x}(k+1) &= \Phi\mathbf{x}(k) + \Gamma_1\mathbf{w}(k), \\ \mathbf{y}(k) &= \mathbf{H}\mathbf{x}(k).\end{aligned}\quad (\text{D.31})$$

We assume that the system starts at $k = 0$ with the initial value

$$\begin{aligned}\mathcal{E}\{\mathbf{x}(0)\} &= \mathbf{0}, \\ \mathcal{E}\{\mathbf{x}(0)\mathbf{x}^T(0)\} &= \mathbf{R}_{\mathbf{xx}}(0;0) \\ &= \mathbf{P}_{\mathbf{x}}(0),\end{aligned}$$

and that $\mathbf{w}(k)$ is a stationary process with covariance

$$\begin{aligned}\mathcal{E}\{\mathbf{w}(k)\mathbf{w}^T(k+j)\} &= \mathbf{0} \quad (j \neq 0) \\ &= \mathbf{R}_{\mathbf{w}} \quad (j = 0).\end{aligned}\quad (\text{D.32})$$

Note that by Eq. (D.27), $S_w(z) = \mathbf{R}_{\mathbf{w}}$, a constant, and hence \mathbf{w} is a white process. With these conditions, we can compute the evolution of $\mathbf{P}_{\mathbf{x}}$, the autocovariance of the state at time k . Thus

$$\begin{aligned}\mathcal{E}\{\mathbf{x}(k)\mathbf{x}^T(k)\} &= \mathbf{R}_{\mathbf{xx}}(k;k) \\ &= \mathbf{P}_{\mathbf{x}}(k),\end{aligned}$$

and

$$\begin{aligned}\mathcal{E}\{\mathbf{x}(k+1)\mathbf{x}^T(k+1)\} &= \mathbf{P}_{\mathbf{x}}(k+1) \\ &= \mathcal{E}\{(\Phi\mathbf{x}(k) + \Gamma_1\mathbf{w}(k))(\Phi\mathbf{x}(k) + \Gamma_1\mathbf{w}(k))^T\} \\ &= \Phi\mathcal{E}\{\mathbf{x}(k)\mathbf{x}^T(k)\}\Phi^T + \Phi\mathcal{E}\{\mathbf{x}(k)\mathbf{w}^T(k)\}\Gamma_1^T \\ &\quad + \Gamma_1\mathcal{E}\{\mathbf{w}(k)\mathbf{x}^T(k)\}\Phi^T + \Gamma_1\mathcal{E}\{\mathbf{w}(k)\mathbf{w}^T(k)\}\Gamma_1^T.\end{aligned}\quad (\text{D.33})$$

Because the center two terms in Eq. (D.33) are zero by Eq. (D.32)⁵ we reduce Eq. (D.33) to

$$\begin{aligned}\mathbf{P}_x(k+1) &= \mathbf{\Phi}\mathbf{P}_x(k)\mathbf{\Phi}^T + \mathbf{\Gamma}_1\mathbf{R}_w\mathbf{\Gamma}_1^T, \\ \mathbf{P}_x(0) &= \text{a given matrix initial condition.}\end{aligned}\tag{D.34}$$

Equation (D.34) is the fundamental equation for the time-domain analysis of discrete systems with stochastic inputs. Note that Eq. (D.34) represents a nonstationary situation because the covariance of $\mathbf{x}(k)$ depends on the time k of the occurrence of \mathbf{x} . However, if all the characteristic roots of $\mathbf{\Phi}$ are inside the unit circle, then the effects of the initial condition, $\mathbf{P}_x(0)$, gradually diminish, and \mathbf{P}_x approaches a stationary value. This value is given by the solution to the (Lyapunov) equation

$$\mathbf{P}_x = \mathbf{\Phi}\mathbf{P}_x\mathbf{\Phi}^T + \mathbf{\Gamma}_1\mathbf{R}_w\mathbf{\Gamma}_1^T.\tag{D.35}$$

⁵ $\mathbf{x}(k)$ is a combination of $w(0), w(1), \dots, w(k-1)$, all of which are uncorrelated with $w(k)$.

References

Abramovitch, D., R. Kosut, G. Franklin, "Adaptive Control with Saturating Inputs," *Proceedings of the 25th Conference on Decision and Control*, pp. 848–852, 1986.

Ackermann, J., "Der Entwurf Linearer Regelungssysteme in Zustandsraum," *Regelungstechnik und Prozessdatenverarbeitung*, **7**, pp. 297–300, 1972.

Al Saggaf, U.M., and Franklin, G.F., "On Model Reduction," *Proc. 25th Conference on Decision and Control*, Athens, Greece, 1986, pp. 1064–1069.

Alphas, A., and J.A. Feldman, "The Versatility of Digital Signal Processing Chips," *IEEE Spectrum*, **24**, pp. 40–45, 1987.

Amit, N., "Optimal Control of Multirate Digital Control Systems," Ph.D. thesis, Stanford University, July 1980.

Anderson, B.D.O., and J.B. Moore, *Optimal Filtering*, Prentice-Hall, Englewood Cliffs, N.J., 1979.

Ash, R.H., and G.R. Ash, "Numerical Computation of Root Loci Using the Newton-Raphson Technique," *IEEE Trans. on Auto. Contr.*, **AC-13**, 5, pp. 576–582, 1968.

Åström, K.J., *Introduction to Stochastic Control Theory*, Academic Press, New York, 1970.

Åström, K.J., "Theory and Applications of Adaptive Control." This paper is an expanded version of a plenary lecture given at the 8th IFAC Congress in Kyoto 1981., Lund Institute of Technology, Dept. of Automatic Control, Box 725, S-220 07 Lund, Sweden, 1981.

Åström, K.J., and T. Bohlin, "Numerical Identification of Linear Dynamical Systems from Normal Operating Records," *Theory of Self-Adaptive Control Systems*. P. Hammond, ed., Plenum Press, New York, 1966.

Åström, K.J., and P.E. Eykhoff, "System Identification—A Survey," *Automatica*, **7**, pp. 123–162, 1971.

Åström, K.J., and B. Wittenmark, "On Self Tuning Regulators," *Automatica*, **9**, pp. 185–189, 1973.

Åström, K.J., and B. Wittenmark, *Computer Controlled Systems, Theory and Design*, Prentice-Hall, Englewood Cliffs, N.J., 1984.

Åström, K.J., and B. Wittenmark, *Adaptive Control*, Addison-Wesley, Reading, Mass., 1988.

Athans, M., "Special Issue on the Linear-Quadratic-Gaussian Estimation and Control Problem," *IEEE Trans. on Aut. Contr.* **AC-16**, 6, 1971.

- Bai, E., and S.S. Sastry, *Global Stability Proofs for Continuous Time Indirect Adaptive Control Schemes*, College of Engineering, U.C. Berkeley, 94720, memorandum, March, 1986.
- Berg, M.C., N. Amit, and J.D. Powell, "Multirate Digital Control System Design," *IEEE Transactions on Automatic Control*, Vol. 33, No. 12, Dec. 1988.
- Berman, H., and R. Gran, "An Organized Approach to the Digital Autopilot Design Problem", *Journal of Aircraft*, **11**, July 1974, pp. 414–422.
- Bertram, J.E., "The Effect of Quantization in Sampled-Feedback Systems," *Trans. AIEE*, **77**, pt. 2, pp. 177–182, 1958.
- Blackman, R.B., *Linear Data-Smoothing and Prediction in Theory and Practice*, Addison-Wesley, Reading, Mass., 1965.
- Bode, H., *Network Analysis and Feedback Amplifier Design*, D. Van Nostrand, New York, 1945.
- Bracewell, R.N., *The Fourier Transform and Its Applications*, 2nd ed., McGraw-Hill, New York, 1978.
- Bryson, A.E., and Y.C. Ho, *Applied Optimal Control*, Halsted Press, Washington, D.C., 1975.
- Bryson, A.E., "Kalman Filter Divergence," *AIAA Journal of Guidance and Control*, January, 1978.
- Butterworth, S., "On the Theory of Filter Amplifiers," *Wireless Engineering*, **7**, pp. 536–541, 1930.
- Cannon, R.H., Jr., *Dynamics of Physical Systems*, McGraw-Hill, New York, 1967.
- Clark, R.N., *Introduction to Automatic Control Systems*, John Wiley, New York, 1962.
- Clary, J., *Robust Algorithms in Adaptive Control*, Ph.D. thesis, Stanford University, 1984.
- Daniels, R.W., *Approximation Methods for Electronic Filter Design*, McGraw-Hill, New York, 1974.
- D'Azzo, J.J., and C.H. Houpis, *Linear Control Systems Analysis and Design*, McGraw-Hill, New York, 1975.
- Dorf, R.C., *Modern Control Systems*, Addison-Wesley, Reading, Mass., 1980.
- Emami-Naeini, A., and G.F. Franklin, "Zero Assignment in the Multivariable Robust Servomechanism," *Proceedings of the IEEE Conference on Decision and Control*, pp. 891–893, December, 1982.
- Evans, W.R., "Control System Synthesis by Root Locus Method," *AIEE Trans.*, **69**, pt. 2, pp. 66–69, 1950.
- Fekete, N., "Model-Based Air-Fuel Control of a Lean Multi-cylinder Engine", Ph.D. Dissertation, Dept of Mechanical Engineering, Stanford Univ., February 1995.
- Fortmann, T.E., and K.L. Hitz, *An Introduction to Linear Control Systems*, Marcel Dekker, New York, 1977.
- Franklin, G.F., and J.D. Powell, "A Digital Control Lab Course," *IEEE Control Systems Magazine*, April 1989.

- Franklin, G.F., J.D. Powell, and A. Emami-Naeini, *Feedback Control of Dynamic Systems*, 8th Ed, Pearson, 2019.
- Golub, G., "Numerical Methods for Solving Linear Least Squares Problems," *Numer. Math.* **7**, pp. 206–216, 1965.
- Golub, G., and C. Van Loan, *Matrix Computations*, Johns Hopkins Press, Baltimore, Md., 1983.
- Goodwin, G.C., Ramadge, P.J. and Caines, P.E. "Discrete-Time Multivariable Adaptive Control," *IEEE Transactions on Automatic Control*, Vol. AC-25, No. 3, pp. 449–456, 1980.
- Goodwin G.C., and Sin, K.S. *Adaptive Filtering Prediction and Control*, Prentice-Hall, Englewood Cliffs, N.J., 1984.
- Gopinath, B., "On the Control of Linear Multiple Input-Output Systems," *Bell Sys. Tech. J.*, **50**, March 1971.
- Graham, D., and R.C. Lathrop, "The Synthesis of Optimum Response: Criteria and Standard Forms," *Trans. AIEE*, **72**, pt. 2, pp. 273–288, 1953.
- Hamming, R., *Numerical Methods for Scientists and Engineers*, McGraw-Hill, New York, 1962.
- Harvey, C.A., and G. Stein, "Quadratic Weights for Asymptotic Regulator Properties," *IEEE Trans. on Aut. Contr.*, **AC-23**, 3, 1978.
- Hirata, H., "Sample Rate Effects on Disturbance Rejection for Digital Control Systems," Ph.D. dissertation, Dept. Aero/Astro, Stanford University, 1989.
- Hnatek, E.R., *A User's Handbook of D/A and A/D Converters*, John Wiley, New York, 1976.
- Householder, A.S., *The Theory of Matrices in Numerical Analysis*, Blaisdell, Waltham, Mass., 1964.
- Hurewicz, W., *Theory of Servomechanisms*, Chapter 5, Radiation Laboratory Series, Vol. 25, McGraw-Hill, New York, 1947.
- James, H.M., N.B. Nichols, and R.S. Phillips, *Theory of Servomechanisms*, Radiation Laboratory Series, Vol 25, McGraw-Hill, New York, 1947.
- Jury, E.I., *Theory and Application of the z-transform Method*, J. Wiley, New York, 1964.
- Kailath, T., *A Course in Linear System Theory*, Prentice-Hall, Englewood Cliffs, N.J., 1979.
- Kailath, T., *Linear Systems*, Prentice-Hall, Englewood Cliffs, N.J., 1980.
- Källström, C., "Computing $\text{EXP}(A)$ and $\int \text{EXP}(As)ds$," *Report 7309*, Lund Institute of Technology, Division of Automatic Control, March, 1973.
- Kalman, R.E., "On the General Theory of Control Systems," *Proc. First International Congress of Automatic Control*, Moscow, 1960.
- Kalman, R. E., *Analysis and Design Principles of Second and Higher Order Saturating Servomechanisms*, *Trans. AIEE*, part II. vol. 74, pp. 294–310, 1955.
- Kalman, R.E., and T.S. Englar, "A User's Manual for the Automatic Synthesis Program," *NASA Contractor Report NASA CR-475*, June, 1966.

- Kalman, R.E., Y.C. Ho, and K.S. Narendra, "Controllability of Linear Dynamical Systems," *Contributions to Differential Equations*, Vol. 1, No. 2, Wiley, New York, 1961.
- Katz, P., and J.D. Powell, "Sample Rate Selection for Aircraft Digital Control," *AIAA Journal*, **13** (8), August 1975.
- Katz, P., "Selection of Sample Rate for Digital Control of Aircraft," Ph.D. thesis, Stanford University, September 1974.
- Kautsky, J., N.K. Nichols, and P. Van Dooren, "Robust Pole Assignment in Linear State Feedback," *Int. J. Control*, Vol. 41, No. 5, pp. 1129–1155, 1985.
- Kendal, M.C., and A. Stuart, *The Advanced Theory of Statistics*, Vol. 2, Griffin, London, 1961.
- Kirk, D. E., *Optimal Control Theory*, Prentice-Hall, Englewood Cliffs, N.J., 1970.
- Kochenburger, R. J., "A Frequency Response Method for Analysis and Synthesis of Contactor Servomechanisms," *Transactions of AIEE*, vol 69, pp. 270–284, 1950.
- Kranc, G.M., "Input-Output Analysis of Multirate Feedback Systems," *IRE Trans. on Automatic Control*, Vol. AC-3, pp. 21–28, 1957.
- Kuo, B.C., *Automatic Control Systems*, 3rd ed., Prentice-Hall, Englewood Cliffs, N.J., 1975.
- Kwakernaak, H., and R. Sivan, *Linear Optimal Control Systems*, Wiley, New York, 1972.
- La Salle, J., and S. Lefschetz, *Stability by Liapunov's Direct Method*, Academic Press, New York, 1961.
- Laub, A.J., A. Linnemann, and M. Wette, "Algorithms and Software for Pole Assignment by State Feedback," *Proceedings of IEEE Control Society 2nd Symposium on Computer Aided Control System Design*, Santa Barbara, Calif, March 13–15, 1985.
- Lefschetz, S., *Stability of Nonlinear Control Systems*, Academic Press, New York, 1975.
- Ljung, L., and T. Söderström, *Theory and Practice of Recursive Estimation*, MIT Press, Cambridge, Mass., 1983.
- Luenberger, D.G., *Introduction to Linear and Nonlinear Programming*, Addison-Wesley, Reading, Mass., 1973.
- Luenberger, D.G., "Observing the State of a Linear System," *IEEE Trans. Military Electr.* **MIL-8**, 1964.
- Mantey, P., "Eigenvalue Sensitivity and State Variable Selection," *IEEE Trans. on Aut. Contr.*, **AC-13**, 3, 1968.
- Mantey, P.E., and G.F. Franklin, "Comment on 'Digital Filter Design Techniques in the Frequency Domain'," *Proc. IEEE*, **55**, 12, pp. 2196–2197, 1967.
- Mason, S.J., "Feedback Theory: Further Properties of Signal Flowgraphs," *Proc. IRE*, **44**, pp. 970–976, 1956.
- Mayr, O., *The Origins of Feedback Control*, M.I.T. Press, Cambridge, Mass., 1970.

- Mendel, J.M., *Discrete Techniques of Parameter Estimation*, Marcel Dekker, New York, 1973.
- Moir, S., *Chemfet Sensors in Industrial Process Control*, Sensors, vol 5, pp. 39–45, 1988.
- Moler, C., and C. van Loan, “Nineteen Dubious Ways to Compute the Exponential of a Matrix,” *Siam Review*, **20**, 4, 1978.
- Morrison, R. L., “Microcomputers Invade the Linear World,” *IEEE Spectrum*, **15**, 7, pp. 38–41, 1978.
- Narendra, K. S., and J. H. Taylor, *Frequency Domain Criteria for Absolute Stability*, Academic Press, New York, 1978.
- Nyquist, H., “Regeneration Theory,” *Bell System Technical Journal*, **11**, pp. 126–147, 1932.
- Ogata, K., *Modern Control Engineering*, Prentice-Hall, Englewood Cliffs, N.J., 1970.
- Ogata, K., *Discrete-Time Control Systems*, Prentice-Hall, Englewood Cliffs, N.J., 1987.
- Oldenburger, R., *Optimal and Self-optimizing Control*, The MIT Press, Cambridge Mass., 1966.
- Parks, P. “Liapunov Redesign of Model Reference Adaptive Control Systems,” *IEEE Trans. on Automatic Control*, Vol. AC-11, No. 3, 1966.
- Parsons, E.K., “Efficient Sampling Rates for Digital Controllers and Pointing Systems with Digital Solid-State Detectors.” Ph.D. thesis, Stanford University, June 1982.
- Parzen, E., *Stochastic Processes*, Holden-Day, San Francisco, 1962.
- Pascoal A., R.L. Kosut, G.F. Franklin, D. Meldrem, and M.L. Workman, “Adaptive Time-Optimal Control of Flexible Structures,” *Proc. 1989 American Control Conference*, Pittsburg, PN, USA.
- Peled, U., and J.D. Powell, “The Effects of Prefilter Design on Sample Rate Selection in Digital Control Systems,” *Proceedings of AIAA G&C Conference*, Paper No. 78-1308, August 1978.
- Rabiner, L.R., and C.M. Rader, eds., *Digital Signal Processing*, IEEE Press, New York, 1972.
- Ragazzini, J.R., and G.F. Franklin, *Sample-Data Control Systems*, McGraw-Hill, New York, 1958.
- Rosenbrock, H.H., *State Space and Multivariable Theory*, Wiley, New York, 1970.
- Rosenbrock, H.H., and C. Storey, *Mathematics of Dynamical Systems*, Wiley, New York, 1970.
- Saucedo, R., and E.E. Shiring, *Introduction to Continuous and Digital Control Systems*, Macmillan, New York, 1968.
- Schmidt, L.A., “Designing Programmable Digital Filters for LSI Implementation,” *Hewlett-Packard Journal*, **29**, 13, 1978.
- Schmitz, E., *Experiments on the End-Point Position Control of a Very Flexible One-Link Manipulator*, Ph.D. thesis, Stanford University, 1985.
- Slaughter, J., “Quantization Errors in Digital Control Systems,” *IEEE Trans. Aut. Contr.*, **AC-9**, pp. 70–74, 1964.

- Sidman, M.D., *Adaptive Control of a Flexible Structure*, Ph.D. thesis, Stanford University, 1986.
- Sidman, M.D., and G.F. Franklin, "Adaptive Control of a Flexible Structure," *Proc. 2nd IFAC Workshop on Adaptive Control Signal Processing*, July 1986, Lund, Sweden, pp. 131–136.
- Söderström, T., L. Ljung, and I. Gustavsson, "A Comparative Study of Recursive Identification Methods," *Lund Report 7427*, December 1974.
- Stengel, R.F., *Stochastic Optimal Control*, Wiley, New York, 1986.
- Stephens, H.C., and M.L. Workman, "Position Error Signal Modulator/De-modulator," U.S. Patent 4,575,776, 1986.
- Strang, G., *Introduction to Applied Mathematics*, Wellesley Cambridge Press, 1986.
- Strang, G., *Linear Algebra and Its Applications*, Academic Press, New York, 1976.
- Terman, F.E., *Radio Engineering*, McGraw-Hill, New York, 1932.
- Trankle, T.L., and A.E. Bryson, "Control Logic to Track Outputs of a Command Generator," *Journal of Guidance and Control*, March-April, 1978.
- Truxal, J.G., *Automatic Feedback Control System Synthesis*, McGraw-Hill, New York, 1955.
- Tummala, R., and G. Rymaszewski, "Microelectronics Packaging Handbook," Van Nostrand-Reinhold, 1988
- Tustin, A., "A Method of Analyzing the Behavior of Linear Systems in Terms of Time Series," *JIEE (London)*, **94**, pt. IIA, pp. 130–142, 1947.
- Van Loan, C.F., "Computing Integrals Involving the Matrix Exponential," *IEEE Trans. of Automatic Control*, Vol. AC-23, No. 3, June 1978.
- Van Valkenburg, M.E., *Analog Filter Design*, Holt, Rinehart, and Winston, New York, 1982.
- Vaughn, D.R., "A Nonrecursive Algebraic Solution for the Discrete Riccati Equation," *IEEE Trans. Aut. Contr.*, **AC-15**, 5, October 1970.
- Vidyasagar, M., *Nonlinear Systems Analysis*, Prentice-Hall, Englewood Cliffs, N.J., 1978.
- Viersma, T.J., *Analysis, Synthesis and Design of Hydraulic Servosystems and Pipelines*, Elsevier, Amsterdam, 1980
- Whitbeck, R.F., and D.G.J. Didaleusky, "Multirate Digital Control Systems with Simulation Applications", Vol. I, II, III, U.S. Air Force Technical Report No. AFWAL-TR-80-3031, Systems Technology, Inc., Hawthorne, Calif. 1980.
- Whitbeck, R.F., D.G.J. Didaleusky, and L.G. Hofmann, "Frequency Response of Digitally Controlled Systems", *AIAA Journal of Guidance and Control*, Vol.4, No. 4, July–August, 1981.
- Whitbeck, R.F., and L.G. Hofmann, "Digital Control Law Synthesis in the W Domain," *J. of Guidance and Control*, Vol. 1, No. 5, pp. 319–326, 1978.
- Widrow, B., "A Study of Rough Amplitude Quantization by Means of Nyquist Sampling Theory," *IRE Trans. on Circuit Theory*, **CT-3**, 4, pp. 266–276, 1956.

Wiener, N., *Interpolation, Extrapolation and Smoothing of Stationary Time Series*, Wiley, New York, 1948.

Wilde, D.J., and C.S. Beightler, *Foundations of Optimization*, Prentice-Hall, Englewood Cliffs, N.J., 1967.

Woodson, H.H., and J.R. Melcher, *Electromechanical Dynamics: Part I, Discrete Systems*, Wiley, New York, 1968.

Workman, M. L., *Magnetic Recording, vol II: Computer Data Storage*, Chapter 2: Data Storage on Rigid Disks, edited by D. Mee and E. Daniels, McGraw Hill, New York, 1988.

Workman, M. L., *Adaptive Proximate Time-Optimal Servomechanisms*, Ph.D. thesis, Stanford University, 1987.

Workman, M.L., *U.S. Patent No. 4,679,103: Digital Servo Control System for a Data Recording Disk File*, IBM Corporation, San Jose, Calif., 1987.

Workman, M.L., R.L. Kosut, and G.F. Franklin, "Adaptive Proximate Time-Optimal Control: Continuous Time Case," *Proceedings of the Automatic Control Conference*, pp. 589–594, 1987.

Workman, M.L., R.L. Kosut, and G.F. Franklin, "Adaptive Proximate Time-Optimal Control: Discrete Time Case," *Proceedings of the Conference on Decision and Control*, pp. 1548–1553, 1987.

Workman, M.L., "Sliding Mask Variable Resolution Velocity Trajectory for a Data Recording Disk File," U.S. Patent 4,486,797, 1984.

Zames, G., "On the Input-Output Stability of Time-Varying Nonlinear Feedback Systems, Part II: Conditions Involving Circles in the Frequency Plane and Sector Nonlinearities," *IEEE Trans. Auto. Control*, vol AC-11, pp. 465–476, 1966.

Index of MATLAB Functions

Starred functions are part of the Digital Controls Toolbox, freely available online at www.elliskaglepress.com

rlocfind, 22
ss, 9
tf, 9
zpk, 9
acker, 33, 36, 225, 232, 234
bode, 25, 31, 103
c2d, 83, 89, 222, 227
connect, 171
ctrb, 275
d2c, 367
damp, 35, 49
disrw*, 312, 356
dlqr, 297, 321
dlyap, 340, 356
eig, 35, 84
feedback, 22, 47, 227
impulse, 13, 100
initial, 227
jdequiv*, 299
kalman, 36, 310, 326
loglog, 103
lqrd, 299
lqr, 34
lsim, 11, 256
lyap, 356
margin, 49
nyquist, 190
obsv, 276
place, 33, 225, 232
qss*, 337
qwc*, 336
refi*, 246
ripple, 183
roots, 35
semilogx, 103
set, 140
ssdata, 83, 227
ss, 140, 222
step, 11, 13, 22, 47, 100
tf, 62
tzero, 84
zgrid, 98

Index

- s*-plane design, 130
- s*-plane to *z*-plane, 97, 174
- z*-transform
 - modified, 84
- Ackermann's formula
 - control, 225
 - estimator, 231, 234, 236
- actuator delay, 268
- adaptive control, 481
 - gain scheduling, 483
 - model reference, 484
 - self-tuning regulator, 485
- adjoint equations, 287
- Aizermann's conjecture, 451
- aliasing, 4, 124
- Amit, N., 367
- analog prefilter, 364
- analog-to-digital converter, 2, 44
- Anderson and Moore, 309
- antenna control, 540
- antialiasing filters, 125, 364
- ARMA model, 387
- Åström and Wittenmark, 364
- autocorrelation, 384

- backward rectangular rule, 46, 53, 59, 148
- bandwidth, 24, 201, 206
- batch least squares, 304
- bending modes, 358
- Berg, M., 367
- Berman and Gran, 355
- Bertram bound, 335
- bias
 - estimation, 259
 - identification, 400, 404
- BIBO stability, 71
- bilinear transform, 150
- bit density, 509
- Block diagrams, 11
- BLUE, 400, 401
- Bode, 24, 183
 - gain-phase relationship, 28, 200
- Bode plot, 24, 183
 - gain margin, 28, 190
 - phase margin, 28, 190
- break points, 26
- Bryson, 309
- Bryson's rules, 313
- Bryson, A. and Ho, Y.-C., 288, 309
- Butterworth filter, 152

- CACSD, 1, 5, 9
- canonical form
 - cascade, 68
 - control, 64, 224
 - direct, 68
 - observer, 66
- Cayley-Hamilton theorem, 556
- characteristic equation, 17, 58
- characteristic equation, 178
- chirp, 380
- circle criterion, 451
- Clary's method, 382
- clock, 2
- colocated, 281, 546
- colored noise, 309
- combined discrete and continuous, 3
- command input, 244
- compensation, 31
 - emulation, 167
 - frequency response, 183
 - root locus, 174
 - state-space, 37, 239
- compensator, 239
- complementary sensitivity, 17, 198
- conditional probability, 562
- consistent estimate, 398
- constant-coefficient difference equation, 57
- control law, 33, 222
- controllability, 33, 225, 271
 - matrix, 226
- convolution, 70
- correlated noise, 309
- cost equivalents, 298

- cost function, 34, 283, 287
 - discrete equivalent, 298
- covariance, 302, 562
- cross-correlation, 384
- cross-power spectrum, 384
- crossover frequency, 28, 200
- cruise-control, 216
- current estimator, 228, 232
- cycle delay, 62, 205

- damping ratio, 12, 97
- DC gain, 106
- deadbeat, 281
- decoupling, 283, 328
- delay, 76, 265, 354
 - model, 265
 - $T/2$, 48, 128, 172
- derivative control, 18
- describing functions, 436
 - hysteresis, 439
 - limit cycle analysis, 441
 - quantizer, 444
 - saturation, 437
 - stability analysis, 441
- determinant, 552
- DFT, 103, 378
- difference equation, 56
- difference equations, 46
- Digital Control Toolbox, 5
- digital filters, 4, 146
- digital signal, 3
- digital-to-analog converter, 2
- direct design, 174
- discrete design, 165
- discrete equivalent noise, 311
- discrete equivalents, 59, 146
 - backward rule, 59, 150
 - design by, 168
 - forward rule, 59, 150
 - trapezoid rule, 59, 150
- discrete signal, 45
- discrete signals, 2
- discrete transfer function, 60, 130
- disk drive, 252, 263, 280, 331
- distribution function, 558
- disturbance
 - estimation, 253, 256
 - modeling, 258
 - rejection, 1, 256, 355
- dither, 347
- divergent filter, 309
- double mass-spring, 226, 281, 297, 359, 368, 546
- duality, 310

- dynamic range, 6

- eigenvalue, 553
- eigenvector, 553
 - decomposition, 292
- Emami-Naeini and Franklin, 249
- embedded servo, 518
- emulation, 3, 44, 147, 301
 - design by, 165, 167
 - equivalent cost, 300
- engine control, 268
- engine speed governor, 268
- equivalent gains, 346
- equivalent s -plane, 97
- ergodic, 384
- error
 - equation, 389
 - output, 390
 - prediction, 390
- error constants, 166, 204
 - Truxal's rule, 177
- estimation
 - accuracy, 302
 - of bias, 259
- estimator, 32, 222
 - compared with classical, 251
 - current, 228, 232
 - design, 228
 - error equation, 230
 - prediction, 228
 - reduced order, 235
- Euler's method, 45, 59, 147
- Euler-Lagrange equations, 292
- event-based, 2
- excavator control, 217
- expectation, 302, 560
- exponential response, 93

- Fast Fourier Transform, 103
- feedforward, 246, 247, 259, 322
- Fekete, 268
- FFT, 103
- Fibonacci numbers, 57
- final value theorem, 11, 106
 - discrete, 176
- first-order hold, 158
- flexible structure, 546
- FOH, 158
- forward rectangular rule, 46, 59, 147
- four disk system, 412
- Fourier Transform, 103
- free running, 2
- frequency response, 24, 102
 - design, 183
 - design by, 166

- specifications, 24, 196, 198
- stability, 27
- z -transform, 185
- gain margin, 28, 190
- gain scheduling, 483
- Gaussian distribution, 558
- Gopinath, B., 235
- gradient, 91
- Hamiltonian
 - control, 292
 - estimation, 310
- Hamming window, 384
- hidden oscillations, 125, 179
- Hirata, 360
- ideal low-pass filter, 126
- identification, 5, 374
 - bias, 400, 404
 - Clary's method, 382
 - equation error, 388
 - known factors, 382
 - one-frequency-at-a-time, 378
 - output error, 390
 - prediction error, 390
- impulse response, 11
- independence, 562
- integral control, 18, 247, 253, 322
- intersample ripple, 125, 179
- inverse nonlinearities, 455
- inverse z -transform, 109
- Jacobian, 91
- Jury stability test, 73
- Kalman and Bertram, 367
- Kalman filter, 307
 - analog, 313
 - constant gain, 309
- Katz, 359, 361
- Kautsky, 226
- Kranc, 139, 367
- Kwakernaak and Sivan, 313, 356
- lag compensation, 31
- Lagrange multipliers, 287
- Laplace transform, 9
- latency, 183
- lead compensation, 31
- least squares
 - batch, 304
 - biased, 404
 - estimate, 302, 391
 - recursive, 304
- likelihood function, 405
- limit cycle, 344
- linear quadratic Gaussian, 310
- linear quadratic regulator, 34, 292
- linearity, 71
- linearization, 90, 375, 428
- log-likelihood function, 406
- LQG, 310
- LQR, 34, 292
- Luenberger observer, 235
- Lyapunov equation, 340, 356, 566
- Lyapunov function, 453
- Lyapunov's second method, 453
- magnetic levitation, 215
- magnetic tape drive, 318
- magnitude, 24
- Mason's rule, 63
- MATLAB, 5
- matrix inverse, 552
 - lemma, 553
- maximum likelihood estimation, 405
- Mayr, 5
- measurement noise, 306, 364
- MIMO, 32, 221, 283
- model
 - nonparametric, 374
 - parametric, 374
- modern control theory, 4
- modified z -transform, 84
- Moler, 82, 88
- multirate sampling, 367
- multivariable design, 313
- NASTRAN, 433
- noise, 311
 - discrete equivalent, 311
 - measurement, 306
 - process, 306
- non-minimum phase, 201
- noncausal, 70
- noncollocated, 546
- noncollocated, 281
- nonlinearity, 89
- normal distribution, 405, 558
- normal equations, 393
- notch filter, 281
- numerical integration, 44, 147, 427
 - rectangular rules, 148
 - trapezoid rule, 148
 - Tustin's method, 150
- Nyquist
 - frequency, 125
 - stability criterion, 186

- observability, 36, 231, 271
 - matrix, 232
- observer, 32, 222
 - Luenberger, 235
- observer canonical form, 66
- oil-mass resonance, 217
- one-frequency-at-a-time, 378
- optimal control, 34, 283
 - time-varying, 286
- optimal estimation, 36, 301
 - steady-state, 309
- output error, 250, 375
- overshoot, 15

- paper machine, 315
- parameter errors, 196, 360
- parametric identification, 374, 386
- Parsons, 300
- partial fraction expansion, 23
- peak overshoot, 24
- Peled, 365
- persistently exciting, 488
- phase, 24
- phase margin, 28, 48, 172, 190, 191
- PID control
 - continuous, 18
 - discrete, 49
- pincer procedure, 314
- pole placement, 4, 33, 223, 243
 - control law, 223, 226
 - estimator, 232, 239
- pole selection
 - estimator, 231
- poles, 11, 62
 - cancellation, 255
 - selection, 227, 239, 244
- power spectral density, 311, 565
- power spectrum, 384
- prediction error, 375
- prediction estimator, 228
- prefilters, 364
- pressurized flow box, 548
- prewarping, 151
- process noise, 36, 306, 311
- proportional control, 18
- PTOS, 470
 - discrete-time, 472
 - extended, 478
- pulse response, 68

- quantization, 3, 334, 358
 - models, 335
 - random, 341
 - steady-state error, 337
 - variance, 339
 - worst-case error, 335
- quantized signal, 3

- radial projection, 243
- Ragazzini and Franklin, 367
- Ragazzini's method, 208
- random neighborhood search, 496
- random variables, 558
- reciprocal root properties, 293
- rectangular rules, 147
 - stability, 150
- recurrence equation, 56
- recursive least squares, 304, 305, 394
- reduced order estimators, 235
- reference input, 1, 37, 244
 - effect on zeros, 249
 - following, 262
- refi.m, 322
- regulation, 1
- regulator, 221, 292
 - design, 238
- representation
 - fixed point, 333
 - floating point, 334
 - quantization, 334
 - round-off, 334
- resolution, 6
- resonances, 358
- resonant peak, 24
- Riccati equation, 289
 - algebraic, 292
- ripple, 4, 139
- rise time, 15, 24
- robust, 1, 167
 - design, 362
- robust design, 362
- root locus, 19
 - computer-aided, 21
 - continuous, 18
 - design by, 165
 - discrete, 174
 - symmetric, 294, 311
- root selection, 226
 - estimator, 231, 239
- root sensitivity, 343
- round-off error, 333
 - stochastic analysis, 338
- round-off of parameters, 342
- Routh, 73
- runout, 519

- sample and hold, 120
- sample period, 2, 45
- sample rate, 45
 - lower bound, 353

- selection, 167, 352
- sampled-data system, 2
 - block diagram analysis, 130
 - definition, 119
- sampling theorem, 4, 125, 353
- satellite attitude control, 78, 538
- scaling in the z -plane, 106
- sector analysis, 448
- sensitivity, 1, 17, 193, 360
 - complementary, 198
 - constraints, 201
 - function, 193
 - integral, 200
 - performance, 195
 - reduction, 362
 - stability robustness, 198
- sensor, 2
 - delay, 265
 - noise, 36, 313, 364
- separation principle, 238, 361
- settling time, 15
- shorted turn, 514
- Sidman, M. D., 412
- similarity transformations, 555
- simulation, 425
- smoothness, 353
- specifications
 - s -plane, 166
 - z -plane, 174
 - frequency domain, 24, 190
 - sensitivity, 193
 - time-domain, 15, 166
- spectral density, 565
- spectral estimation, 383
- stability, 12, 27, 71
 - augmentation, 362
 - BIBO, 71
 - margins, 27, 190
 - Nyquist's criterion, 186
 - robustness, 196
 - Routh's criterion, 73
- standard deviation, 561
- state, 9
- state space, 4, 78
 - continuous design, 32
 - equivalents, 156
- state-variable form, 8
- stationarity, 71
- steady-state error, 17, 26, 166, 204
- Stengel, 309
- step response, 13
- stochastic least squares, 397
- stochastic process, 563
- successive loop closure, 367
- sweep method, 288
- symmetric root locus, 294, 311
- system identification, 374
- system type, 17
 - discrete, 176
- $T/2$ delay, 48
- temperature control, 542
- tethered satellite, 217
- time constant, 12
- time correlation, 309
- time delay, 76, 235, 265, 354, 542
- time shift, 106
- time-optimal control, 469
- time-varying optimal, 286
- track density, 509
- Trankle and Bryson, 245
- transfer function, 9, 60
- transform methods, 4, 165
- trapezoid rule, 59, 156
- truncation, 334
- Truxal's rule, 177
- Tustin's method, 150
 - prewarping, 151
 - state space formula, 156
- type 0, 17, 176
- type 1, 17, 166, 176
- undamped natural frequency, 12
- uniform distribution, 558
- unit pulse, 92
- unit step, 92
- Van Loan, 82, 88, 299
- variance, 405, 560
- variation of parameters, 81
- vector gain margin, 193
- velocity constant, 17, 166, 176
 - Bode frequency response, 204
- voice coil motor, 513
- warping, 151
- weighted average access time, 511
- weighted least squares, 304
- weighting matrices, 287
 - selection, 313
- Whitbeck and Didaleusky, 367
- white noise, 311
- worst steady-state error, 337
- worst-case error bound, 335
- z -plane
 - damping, 97
 - design, 165
- z -transform, 4, 60

- exponential response, 93
- properties, 105, 549
 - convolution, 105
 - final value , 106
 - inverse, 107
 - linearity, 105
 - scaling, 106
 - time shift, 106
- table of, 550
- unit pulse, 92
 - unit step, 92
- zero placement, 249
- zero-order hold (ZOH), 45, 73, 122
 - delay, 128
 - equivalent, 158
 - frequency response, 128
- zero-pole matching, 156
- zeros, 11, 62
 - effect of, 98